DEEP-SEA RESEARCH PART II

Topical Studies in Oceanography

Special Issue: Understanding Ecosystem Processes in the Eastern Bering Sea III

Guest Editors: Carin J. Ashjian, H. Rodger Harvey, Michael W. Lomas, Jeffrey M. Napp, Michael F. Sigler, Phyllis J. Stabeno and Thomas I. Van Pelt

Volume 109, 2014

CONTENTS

Introductory Article

M.W. Lomas and P.J. Stabeno — 1 — An introduction to the Bering Sea Project: Volume III

Special Issue Articles

C. Ladd — 5 — Seasonal and interannual variability of the Bering Slope Current

V. Luchin and G. Panteleev — 14 — Thermal regimes in the Chukchi Sea from 1941 to 2008

W. Cheng, E. Curchitser, C. Ladd, P. Stabeno and M. Wang — 27 — Influences of sea ice on the Eastern Bering Sea: NCAR CESM simulations and comparison with observations

M.E. Sullivan, N.B. Kachel, C.W. Mordy, S.A. Salo and P.J. Stabeno — 39 — Sea ice and water column structure on the eastern Bering Sea shelf

B.A. Stauffer, J.I. Goes, K.T. McKee, H. do Rosario Gomes and P.J. Stabeno — 57 — Comparison of spring-time phytoplankton community composition in two cold years from the western Gulf of Alaska into the southeastern Bering Sea

M.F. Sigler, P.J. Stabeno, L.B. Eisner, J.M. Napp and F.J. Mueter — 71 — Spring and fall phytoplankton blooms in a productive subarctic ecosystem, the eastern Bering Sea, during 1995–2011

J.I. Goes, H. do Rosario Gomes, E.M. Haugen, K.T. McKee, E.J. D'Sa, A.M. Chekalyuk, D.K. Stoecker, P.J. Stabeno, S.-I. Saitoh and R.N. Sambrotto — 84 — Fluorescence, pigment and microscopic characterization of Bering Sea phytoplankton community structure and photosynthetic competency in the presence of a Cold Pool during summer

L.V. Morales, J. Granger, B.X. Chang, M.G. Prokopenko, B. Plessen, R. Gradinger and D.M. Sigman — 100 — Elevated $^{15}N/^{14}N$ in particulate organic matter, zooplankton, and diatom frustule-bound nitrogen in the ice-covered water column of the Bering Sea eastern shelf

(*Continued on inside back cover*)

For a full and complete Guide for Authors, please go to http://www.elsevier.com/locate/dsr2.

0967-0645(201411)109:C;1-G

109

DEEP-SEA RESEARCH II Vol. 109 (2014) 1–300

BERING SEA ECOSYSTEM PROCESSES

ELSEVIER

Volume 109 November 2014 ISSN 0967-0645

DEEP-SEA RESEARCH PART II

Understanding Ecosystem Processes in the Eastern Bering Sea III

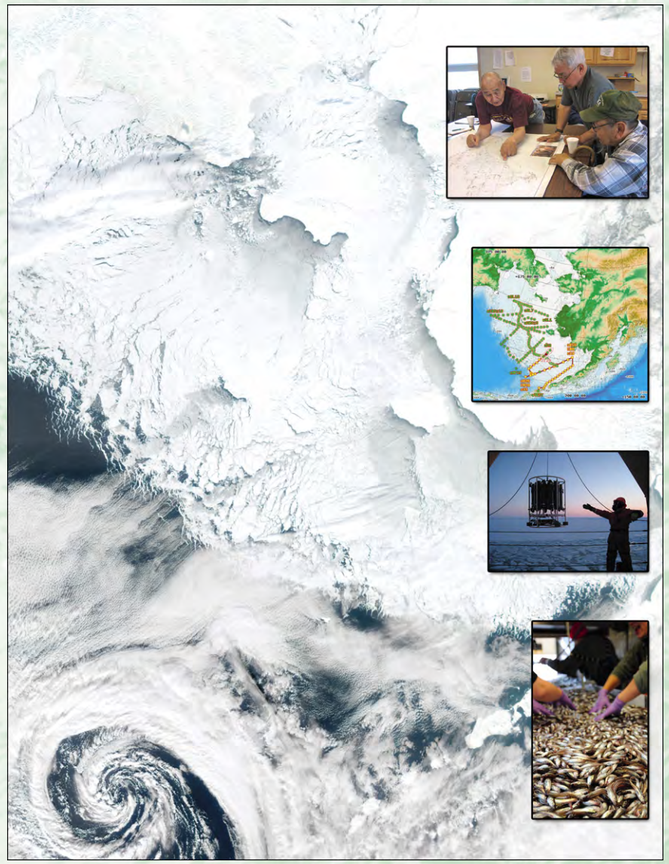

www.elsevier.com/locate/dsr2

DEEP-SEA RESEARCH II

http://www.elsevier.com/locate/dsr2

Publication information: *Deep-Sea Research II* (ISSN 0967-0645). For 2014, volumes 99–110 (12 issues) are scheduled for publication. Subscription prices are available upon request from the Publisher or from the Elsevier Customer Service Department nearest you or from this journal's website (http://www.elsevier.com/locate/dsr2). Further information is available on this journal and other Elsevier products through Elsevier's website (http://www.elsevier.com). Subscriptions are accepted on a prepaid basis only and are entered on a calendar year basis. Issues are sent by standard mail (surface within Europe, air delivery outside Europe). Priority rates are available upon request. Claims for missing issues should be made within six months of the date of dispatch.

Orders, claims, and journal inquiries: please contact the Elsevier Customer Service Department nearest you:

St. Louis: Elsevier Customer Service Department, 3251 Riverport Lane, Maryland Heights, MO 63043, USA; phone: (877) 8397126 [toll free within the USA]; (+1) (314) 4478878 [outside the USA]; fax: (+1) (314) 4478077; e-mail: JournalCustomerService-usa@elsevier.com

Oxford: Elsevier Customer Service Department, The Boulevard, Langford Lane, Kidlington, Oxford OX5 1GB, UK; phone: (+44) (1865) 843434; fax: (+44) (1865) 843970; e-mail: JournalsCustomerServiceEMEA@elsevier.com

Tokyo: Elsevier Customer Service Department, 4F Higashi-Azabu, 1-Chome Bldg, 1-9-15 Higashi-Azabu, Minato-ku, Tokyo 106-0044, Japan; phone: (+81) (3) 5561 5037; fax: (+81) (3) 5561 5047; e-mail: JournalsCustomerServiceJapan@elsevier.com

Singapore: Elsevier Customer Service Department, 3 Killiney Road, #08-01 Winsland House I, Singapore 239519; phone: (+65) 63490222; fax: (+65) 67331510; e-mail: JournalsCustomerServiceAPAC@elsevier.com

Author inquiries: For inquiries relating to the submission of articles (including electronic submission) please visit this journal's homepage at http://www.elsevier.com/locate/dsr2. For detailed instructions on the preparation of electronic artwork, please visit http://www.elsevier.com/artworkinstructions. Contact details for questions arising after acceptance of an article, especially those relating to proofs, will be provided by the publisher. You can track accepted articles at http://www.elsevier.com/trackarticle. You can also check our Author FAQs at http://www.elsevier.com/authorFAQ and/or contact Customer Support via http://support.elsevier.com.

Printed by Henry Ling Ltd., Dorchester, United Kingdom

The paper used in this publication meets the requirements of ANSI/NISO Z39.48-1992 (Permanence of Paper)

Cover Image: Background is a MODIS True Color satellite image showing seasonal sea ice extent on 28 February, 2008, with image centered on the eastern Bering Sea shelf area, bounded by St. Lawrence Island and Bering Strait to the north, the Aleutian Islands chain to the south, Chukotka (Russian Federation) to the west, and mainland Alaska (US) to the east. Inset images from top to bottom: Elders of the Native Village of Savoonga, facilitated by the late Caleb Pungowiyi, discuss local and traditional knowledge of St. Lawrence Island marine resources (photo by T. Van Pelt); station map from the summer 2010 BEST-BSIERP Bering Sea Project research cruise (TN250) on the R/V *Thomas G. Thompson* (map courtesy EOL/NCAR); retrieving the CTD and Niskin rosette aboard the USCGC *Healy* (cruise 09-01), northern Bering Sea, March 2009 (photo by T. Van Pelt); scientists sorting age-0 walleye pollock and Pacific cod aboard the NOAA Ship *Oscar Dyson* (photo courtesy of L. DeCicco).

Volume 109, 2014

(*Continued from outside back cover*)

J.N. Cross, J.T. Mathis, M.W. Lomas, S.B. Moran, M.S. Baumann, D.H. Shull, C.W. Mordy, M.L. Ostendorf, N.R. Bates, P.J. Stabeno and J.M. Grebmeier — 112 — Integrated assessment of the carbon budget in the southeastern Bering Sea

J.T. Mathis, J.N. Cross, N. Monacci, R.A. Feely and P. Stabeno — 125 — Evidence of prolonged aragonite undersaturations in the bottom waters of the southern Bering Sea shelf from autonomous sensors

D.K. Stoecker, A.C. Weigel, D.A. Stockwell and M.W. Lomas — 134 — Microzooplankton: Abundance, biomass and contribution to chlorophyll in the Eastern Bering Sea in summer

D.K. Stoecker, A. Weigel and J.I. Goes — 145 — Microzooplankton grazing in the Eastern Bering Sea in summer

L.B. Eisner, J.M. Napp, K.L. Mier, A.I. Pinchuk and A.G. Andrews III — 157 — Climate-mediated changes in zooplankton community structure for the eastern Bering Sea

W.W. Strasburger, N. Hillgruber, A.I. Pinchuk and F.J. Mueter — 172 — Feeding ecology of age-0 walleye pollock (*Gadus chalcogrammus*) and Pacific cod (*Gadus macrocephalus*) in the southeastern Bering Sea

L. De Forest, J.T. Duffy-Anderson, R.A. Heintz, A.C. Matarese, E.C. Siddon, T.I. Smart and I.B. Spies — 181 — Taxonomy of the early life stages of arrowtooth flounder (*Atheresthes stomias*) and Kamchatka flounder (*A. evermanni*) in the eastern Bering Sea, with notes on distribution and condition

C.D. Vestfals, L. Ciannelli, J.T. Duffy-Anderson and C. Ladd — 190 — Effects of seasonal and interannual variability in along-shelf and cross-shelf transport on groundfish recruitment in the eastern Bering Sea

S.K. Neidetcher, T.P. Hurst, L. Ciannelli and E.A. Logerwell — 204 — Spawning phenology and geography of Aleutian Islands and eastern Bering Sea Pacific cod (*Gadus macrocephalus*)

M.R. Baker and A.B. Hollowed — 215 — Delineating ecological regions in marine systems: Integrating physical structure and community composition to inform spatial management in the eastern Bering Sea

N.M. Jones, B.A. Hoover, S.A. Heppell and K.J. Kuletz — 241 — A cross-shelf gradient in $\delta^{15}N$ stable isotope values of krill and pollock indicates seabird foraging patterns in the Bering Sea

H.M. Renner, B.A. Drummond, A.-M. Benson and R. Paredes — 251 — Reproductive success of kittiwakes and murres in sequential stages of the nesting period: Relationships with diet and oceanography

G.L. Hunt Jr., M. Renner and K. Kuletz — 266 — Seasonal variation in the cross-shelf distribution of seabirds in the southeastern Bering Sea

K.J. Kuletz, M. Renner, E.A. Labunski and G.L. Hunt Jr. — 282 — Changes in the distribution and abundance of albatrosses in the eastern Bering Sea: 1975–2010

M. Renner and H.P. Huntington — 293 — Connecting subsistence harvest and marine ecology: A cluster analysis of communities by fishing and hunting patterns

Abstracted/indexed in *BIOBASE, BIOSIS databases/Zoological Records, CAB International, Chemical Abstracts Service, Current Awareness in Biological Sciences, Current Contents ASCA/Engineering Technology & Applied Science/Science Citation Index/SCISEARCH Data, Current Contents/Agriculture, Biology & Environmental Sciences, Current Contents/Physics, Chemical, & Earth Sciences, Engineering Index, Environmental Periodicals Bibliograph, Bib & Index, INSPEC Data/Cam Sci Abstr, Marine Literature Review, Meteorological and Geoastrophysical Abstracts, Oceanbase, Oceanographic Literature Review, Research Alert, Scisearch.* Also covered in the abstract and citation database *SCOPUS®*. Full text available on *ScienceDirect®*.

DEEP-SEA RESEARCH
PART II

Topical Studies in Oceanography

Understanding Ecosystem Processes in the Eastern Bering Sea III

Guest Editors:

Carin J. Ashjian
Woods Hole Oceanographic Institution, Woods Hole, Massachusetts, USA

H. Rodger Harvey
Ocean, Earth, and Atmospheric Sciences, Old Dominion University, Norfolk, Virginia, USA

Michael W. Lomas
Bigelow Laboratory for Ocean Sciences, East Boothbay, Maine, USA

Jeffrey M. Napp
Alaska Fisheries Science Center, NOAA, Seattle, Washington, USA

Michael F. Sigler
Alaska Fisheries Science Center, NOAA, Juneau, Alaska, USA

Phyllis J. Stabeno
Pacific Marine Environmental Laboratory, NOAA, Seattle, Washington, USA

Thomas I. Van Pelt
North Pacific Research Board, Anchorage, Alaska, USA

ELSEVIER

Amsterdam • Boston • London • New York • Oxford • Paris • Philadelphia • San Diego • St. Louis

STATEMENT POLICY

Deep-Sea Research Part II: Topical Studies in Oceanography Publishes the topical issues arising from the many international and interdisciplinary projects which are undertaken.

Shorter research papers are welcomed for *Deep-Sea Research Part I: Oceanographic Research Papers*. Acceptable topics for papers include:

(1) the results of original scientific research
(2) theoretical work of evident oceanographic applicability
(3) the solution of some instrumental or laboratory problem with evidence of its successful use, and
(4) applications of oceanography.

Papers dealing with research on continental shelves (water depths shallower than 100–200 m) in most cases should be submitted to our sister journal *Continental Shelf Research*.

Progress reports and review articles may be invited by the Editor but these are generally more appropriate for *Progress in Oceanography*.

Funding body agreements and policies
Elsevier has established agreements and developed policies to allow authors whose articles appear in journals published by Elsevier to comply with potential manuscript archiving requirements as specified as conditions of their grant awards. To learn more about existing agreements and policies please visit http://www.elsevier.com/fundingbodies.

Abstracted/indexed in *BIOBASE, BIOSIS databases/Zoological Records, CAB International, Chemical Abstracts Service, Current Awareness in Biological Sciences, Current Contents ASCA/Engineering Technology & Applied Science/Science Citation Index/SCISEARCH Data, Current Contents/Agriculture, Biology & Environmental Sciences, Current Contents/Physics, Chemical, & Earth Sciences, Engineering Index, Environmental Periodicals Bibliograph, Bib & Index, INSPEC Data/Cam Sci Abstr, Marine Literature Review, Meteorological and Geoastrophysical Abstracts, Oceanbase, Oceanographic Literature Review, Research Alert, Scisearch.* Also covered in the abstract and citation database *SCOPUS*®. Full text available on *ScienceDirect*®.

Deep-Sea Research II 109 (2014) 1–4

Contents lists available at ScienceDirect

Deep-Sea Research II

journal homepage: www.elsevier.com/locate/dsr2

Introduction

An introduction to the Bering Sea Project: Volume III

1. Introduction

The Bering Sea is sensitive to spatial and temporal changes in the seasonal ice cover that acts as a major organizing factor and driver of the ecosystem. During winter, atmospheric forcing, latitude, and ocean circulation combine to produce a massive expanse of seasonal ice, which in cold years can cover the eastern Bering Sea shelf from Bering Strait to the Alaska Peninsula. In spring, the retreating ice, long daylight hours, and nutrient-rich ocean waters result in intense marine productivity. This burst of spring production, together with more episodic summer and early fall production, provides the energy that ultimately sustains nearly half of the US annual commercial fish landings as well as providing food and cultural value to thousands of Bering Sea coastal and island residents. However, predicted major changes in ice cover in the coming decades (Overland et al., 2012) have intensified concern over the future of this economically and culturally important region.

In response to ongoing observations of environmental changes in this critical region, the North Pacific Research Board (NPRB) and the National Science Foundation (NSF) partnered to support a major ecosystem-scale study of how climate change affects the Bering Sea ecosystem, from physics and chemistry to lower trophic level organisms (e.g. plankton) to humans. The "Bering Sea Project" integrated two research programs, the NSF-funded Bering Ecosystem Study (BEST) and the NPRB-funded Bering Sea Integrated Ecosystem Research Program (BSIERP), and included substantial in-kind contributions from the National Oceanic and Atmospheric Administration and the US Fish and Wildlife Service. Over the six-year program, the Bering Sea Project has provided new insights into the functioning of the eastern Bering Sea ecosystem, particularly in the north-central domain (~59–62°N) where data sets and temporal coverage had previously been sparse.

The previous two Bering Sea Project special issues in Deep-Sea Research II, volumes 65–70 published in 2012 and volume 94 published in 2013, primarily present papers that describe new information on this ecosystem and how change will affect individual species, trophic levels, or guilds. Those papers placed new data in their historical context, assessed implications for the future of the Bering Sea ecosystem and generally addressed one or more of the core program hypotheses that guided the field program and ongoing synthesis activities. These hypotheses include: (1) physical forcing, including climate, affects food availability; (2) ocean conditions structure trophic relationships through bottom-up processes; (3) ecosystem controls are dynamic; (4) location matters; and (5) commercial and subsistence fisheries reflect climate. This third special issue continues to address the core hypotheses, but has a greater focus on mid-level synthetic activities, which advance our understanding of the ecosystem as an integrated whole and how it might respond to changes in climate. In the following paragraphs we provide some context and brief summaries of each of the papers appearing in this 3rd Bering Sea Project special issue, grouped by broad topic or trophic level.

2. Ocean physics

The Bering Sea shelf varies both spatially and temporally. While the most distinct differences in shelf regions are in the cross-shelf domains (coastal, middle and outer), papers in the first special issue documented a division at 59–60°N between the northern and southern shelves (Stabeno et al., 2012a). The northern shelf is colder, with weaker tides and vertical stratification to which temperature and salinity contribute equally; by contrast, the southern shelf is warmer, with stronger tides, and is vertically stratified mainly by temperature. One of the drivers of the differences between the north and south is that ice persists for approximately two months longer on the northern than on the southern shelf (Stabeno et al., 2012b). In this third issue, Sullivan et al. (2014) investigated the impact of melting ice and found that the southern Bering Sea was cooled and freshened by melting ice as it is first advected southward in winter, while the northern Bering Sea is freshened in spring when the ice melts during its retreat. This difference results in the presence of a low-salinity pool on the northern shelf. The presence or absence of sea ice on the southern shelf in March and April determines whether a given year is warmer or colder than the long-term average. After the first two special issues, an open question remained of how comparable the years defined as "warm" and "cold" in the southern Bering Sea were to those in the north. Panteleev and Luchin (2014) found that there was no correlation between northern and southern cold/warm years. Both papers reinforce the marked differences between the northern and southern shelves.

Winter and spring sea ice is a defining characteristic on the Bering Sea shelf, determining such diverse variables as ocean temperatures through the following summer, the extent of the cold pool, and timing of the spring bloom. Temperature and stratification are key predictors that structure the Bering Sea ecosystem (Baker and Hollowed, 2014). The timing of ice retreat is a primary indicator of the temperature of the southern shelf during the following summer and thus defines warm and cold years (Stabeno et al., 2012b). While the northern shelf is expected to maintain extensive ice for the foreseeable future, the southern shelf is extremely sensitive to changes in the timing of ice retreat. Cheng et al. (2014) predicts that, as a result of climate change, a northward shift of ice extent by ~2° latitude in the next 40 years

http://dx.doi.org/10.1016/j.dsr2.2014.09.004

is to be expected. This loss of sea ice on the southern shelf will result in a warmer southern shelf.

3. Phytoplankton and primary production

The seasonal presence or absence of sea ice in the southeastern Bering Sea, just as for physics, appears to have a marked impact on the diversity and function of the lower trophic levels. For example, in an analysis of the mooring chlorophyll fluorescence time-series, Sigler et al. (2014) observed that the timing of the open water spring bloom was dependent upon stratification. This pattern of physical control, tied to the presence or absence of sea ice, leads to a variable time period between the fall blooms in one year and the spring bloom in the subsequent year and is hypothesized to have important implications for the flow of energy to mesozooplankton in the spring (Morales et al., 2014; Sigler et al., 2014) and for 'refueling' in the fall. Sigler et al. (2014) also suggest that the presence or absence of sea ice impacts the magnitude of the spring bloom, where ice algal production may reduce the nutrient content of the upper water column by consumption and rapid export to the benthos, thus leading to lower chlorophyll and primary production in the subsequent open-water spring bloom and summer period. The lower chlorophyll values may not necessarily lead to lower net primary production, as reductions in the mean cell size of the phytoplankton population and warmer summer temperatures leading to enhanced nutrient recycling may offset reduced total chlorophyll in some regions as observed by Stauffer et al. (2014). A further complication in chlorophyll production is spatial variability in nutrient limitation, which would tend to favor smaller cell size.

Previous papers in the Bering Sea special issue series have highlighted the importance of material exported to the benthos versus retention of that material to be recycled in the upper water column (e.g., Baumann et al., 2013; Moran et al., 2012). In this special issue, Cross et al. (2014) show that the pattern of benthic-pelagic coupling varies across the shelf, with more material exported horizontally to the deep ocean basin from the outer domains, whereas in the middle domain, most organic matter is locally exported to the benthos. The extensive export of material to the benthos effectively removes nutrients from the upper water column and can lead to nutrient limitation in the phytoplankton, thus favoring growth of small cells (Goes et al., 2014), with further cumulative effects for both small and large grazing zooplankton and microzooplankton. The retention of organic matter in shelf sediments deprives the upper water column of nutrients, but leads to significant remineralization at depth. This in turn results in an increase in carbon dioxide and the acidification of deep waters as observed by Mathis et al. (2014), which may ultimately have a negative effect on benthic (and pelagic) communities despite the increased supply of organic matter.

4. Zooplankton

One of the more important findings in the second special issue was the importance of microzooplankton to the ecosystem (Sherr et al., 2013). Microzooplankton biomass increases seasonally, and at least part of that increase is linked to the variability of mesozooplankton grazing control on microzooplankton during winter and spring. In contrast to experimental grazing observations, Morales et al. (2014), present stable isotope data that suggests mesozooplankton preferentially graze on diatoms and other primary producers, and that there is little to no evidence of grazing at more than one trophic level. This apparent lack of grazing control leads to increased microzooplankton biomass from spring to summer, consistent with the findings of Stoecker et al. (2014b) who observed that microzooplankton biomass was equal to or greater than phytoplankton biomass. Furthermore, Stoecker et al. (2014a), measured that these high microzooplankton biomass stocks consume from ~60% to in excess of 100% of daily phytoplankton production along an cross-shelf transect. The impact of this near complete consumption of net primary production in summer on the growth of mesozooplankton through summer or fall is unknown. It is also unknown if this seasonal pattern of microzooplankton grazing and biomass accumulation is different in warm years, since these observations were all made in cold years. Clear changes in the relative abundance of small and large mesozooplankton in the fall have been observed between warm and cold years by Eisner et al. (2014), with large mesozooplankton increasing dramatically in abundance from warm to cold years. These changes did not occur abruptly at the end of the warm period, and built as the influence of sea ice and cold temperatures persisted. The change began one year earlier in the northern Bering Sea compared to the southeastern Bering Sea.

5. Fish

Walleye pollock (*Gadus chalcogrammus*) and Pacific cod (*G. macrocephalus*) are two of the largest and most valuable fisheries in the Bering Sea. Both species responded negatively to the warm period (2000–2005), with reduced recruitment resulting in a decrease of ~40% in annual walleye pollock quota in 2008–2010. It has been hypothesized that in cold years, euphausiid and copepod populations increased, resulting in a richer available prey resource that better prepared the pollock for winter (Heintz et al., 2013; Stabeno et al., 2012b). Strasburger et al. (2014) found that, while they have similar early life histories, in the cold years pollock and cod larvae begin to divide prey resources as they age rather than competing for the same prey. While their study focused on cold years, the authors suggest that during warm years with reduced prey abundance and prey of lower energetic quality, the two species may compete for the same limited resources, thus contributing to decrease in recruitment of both species during these years.

Other mechanisms, such as the successful transport of eggs and larvae to suitable nursery grounds, can also influence the recruitment of these fish species. Warm and cold years were associated with significantly different currents on the middle shelf (Stabeno et al., 2012b). In addition, Ladd (2014) observed that annual and interannual variability exists in the Bering Slope Current (BSC), with a stronger BSC in the winter months. Vestfals et al. (2014) found that the recruitment of groundfish was significantly correlated with both transport in the BSC and also onshelf flow. This was especially true for Pacific cod, but other species such as halibut (*Hippoglossus stenolepis*) also benefited from increased onshelf flow in the Bering Sea shelf canyons. Studying the spawning phenology of Pacific cod, Neidetcher et al. (2014) found interannual variations in the timing of spawning of up to 10 days between years (2005–2007). This is similar to Bering Sea Project results for pollock spawning between warm and cold periods reported by Smart et al. (2012). Such relatively small changes in timing could interact with the temporal changes in transport to impact the survival of eggs and larvae.

Arrowtooth flounder (*Atheresthes stomias*) and Kamchatka flounder (*A. evermanni*) have similar predation impacts and are prey to similar organisms in the Bering Sea. Directed fishing efforts on both species have increased in recent years and both species must be correctly separated and recorded in catch data, however juveniles cannot be easily distinguished. De Forest et al. (2014) developed a genetic technique to distinguish between the larvae

and early juveniles of Arrowtooth flounder and Kamchatka flounder using mtDNA cytochrome oxidase subunit I. Larvae of Arrowtooth and Kamchatka flounder were found to have similar distributions in the eastern Bering Sea, but juveniles have slightly different distributions with juvenile Kamchatka flounder closer to the shelf break and in deeper water. The larvae of the two flounder also showed a divergence in nutritional quality that suggested a separation in their diets and ecological niches, but there was no difference in lipid content as a measure of energy content between the species by the juvenile stages.

6. Seabirds

The spatial distributions of seabirds and temporal changes in population size have been linked to a wide variety of marine phenomena at spatial scales from ocean basins to small-scale tidal fronts. A central theme of these studies has been the relationship between seabird foraging behavior and prey abundance, density and type, and consequent impacts on chick rearing and survivorship, changes in total populations and population centers of abundance. Renner et al. (2014), using a 36-year record of seabird abundance on the Pribilof Islands, found that breeding success was most closely related to the prior years success. This retrospective analysis found that chick survival was enhanced when chicks were fed fish rather than crustacean zooplankton, and was further enhanced when fed coastal fish species rather than oceanic species. However, long-term changes in population numbers were more closely related to the overall condition of the adults, highlighting a need to focus on non-breeding season foraging behavior to understand population dynamics. This is additionally highlighted by changes in the distributional patterns of albatrosses, which breed elsewhere but forage in the Bering Sea in their summer non-breeding season. Kuletz et al. (2014) examined the distribution of three albatross species within the Bering Sea, and found that centers of distribution of black-footed (*Phoebastria nigripes*) and short-tailed (*P. albatrus*) albatross have moved northward, while the Laysan albatross (*P. immutabilis*) has moved southward. This southward move was primarily due to increased abundance along the Aleutian Islands, although they were also found farther north in recent years. These changes are hypothesized to be related to the distribution and abundance of their primary prey (squid), rather than due to changes in climate.

There are two main feeding strategies in seabirds - surface foragers and pursuit divers. To better understand the distribution of seabirds that fit in each feeding category, Hunt et al. (2014) clustered seabird distributions by the depth range over which they fed to determine if they defined ecological domains. Indeed, birds aggregated into bathymetric bins (shallow, mid, deep) except in winter, when the ocean is less stratified and the shelf frontal structures weaker or non-existent. This analysis provided strong evidence for topographic anchoring of feeding regions (e.g., tied to fronts), which explained the seasonal movements of some seabird population distributions, and suggested that seabird populations were more attuned to movements of surface water masses than depth per se. Jones et al. (2014), studying the $\delta^{15}N$ signature of both seabirds and prey items (juvenile pollock and krill), found strong relationships between $\delta^{15}N$ values in both predator and prey, implying that food source and feeding strategy could be inferred from $\delta^{15}N$ values. The isotopic data suggested that thick-billed murres (*Uria lomvia*) foraged in specific locations where food quality and abundance were high, whereas black-legged kittiwakes (*Rissa tridactyla*) tended to be more opportunistic. Use of isotopic methods, which inherently integrate over a longer period of an organism's lifespan, may be useful in understanding behavior and condition of adults during the non-breeding season, a key period identified by Renner et al. (2014).

7. Subsistence harvest

In addition to providing ~40% of the US catch of fish and shellfish, the Bering Sea provides ~11 million kg of fish, marine mammals and birds to support Alaskan natives and others living along the coastline and on the islands of the Bering Sea. Subsistence harvests provide a significant portion of the food consumed by Alaskan Native communities. Using a cluster analysis approach, Renner and Huntington (2014) found that the type of food harvested by different coastal communities split along geographic lines, reflecting food availability. For instance, in the villages in the northern Bering Sea and in the Chukchi and Beaufort Seas, harvest is dominated by marine mammals, while the harvest in villages in the southern Bering Sea is dominated by fish and other seafood. These harvest characteristics are similar to ecoregions defined on biological patterns Sigler et al. (2011). Changes in subsistence harvest could be used monitor changes in individual species within regional ecosystems forced by climate change.

8. Conclusion

The common thread through the Bering Sea Project has been the central hypotheses: (1) Physical forcing and its modification by climate affects food availability; (2) Ocean conditions structure trophic relationships through bottom-up processes; (3) Ecosystem controls are dynamic; (4) Location matters and; (5) Commercial and subsistence fisheries reflect climate. In this 3rd special issue, manuscripts begin to explore warm versus cold comparisons through synthesis of other datasets with those generated by the Bering Sea project, or interpreting other datasets (e.g., mooring datasets) in the context of the broader ecology of the Bering Sea. These synthetic activities are focusing both within trophic levels as well as among trophic levels and provide a basis to understand the ecosystem in a more mechanistic way. In the concluding paragraph of the Introduction to the first special issue, Weise et al. (2012) stated, “As more analyses are completed, integration across program components will increase and advance our understanding accordingly.“ With this issue, we are realizing that goal.

Acknowledgments

This third special issue and broader program has greatly benefited from the contributions of Tom van Pelt and the additional members of the scientific advisory board of the Bering Sea Program (Carin Ashjian, Rodger Harvey, Jeff Napp and Mike Sigler). This arcticle is NPRB publication 501, Bering Sea Project publication 143 and PMEL publication 4171.

References

Baker, M.R., Hollowed, A.B., 2014. Delineating ecological regions in the North Pacific: identifying biophysical drivers of community composition. Deep Sea Res. II 109, 215–240. http://dx.doi.org/10.1016/j.dsr2.2014.03.001.

Baumann, M., Moran, S., Kelly, R., Lomas, M., Shull, D., 2013. ^{234}Th balance and implications for seasonal particle retention in the eastern Bering Sea. Deep Sea Res. II 94, 7–21.

Cheng, W., Curchitser, E., Ladd, C., Stabeno, P.J., Wang, M., 2014. Influences of sea ice on the Eastern Bering Sea: NCAR CESM simulations and comparison with observations. Deep Sea Res. II 109, 27–38. http://dx.doi.org/10.1016/j.dsr2.2014.03.002.

Cross, J., Mathis, J.T., Lomas, M.W., Moran, S.B., Baumann, M., Shull, D., Mordy, C.W., Ostendorf, M.L., Bates, N.R., Stabeno, P.J., Grebmeier, J.M., 2014. Integrated

assessment of the carbon budget in the southeastern Bering Sea. Deep Sea Res. II 109, 112–124. http://dx.doi.org/10.1016/j.dsr2.2014.03.003.
De Forest, L.G., Duffy-Anderson, J.T., Heintz, R.A., Matarese, A.C., Siddon, E.C., Smart, T.I., Spies, I.B., 2014. Current knowledge on the ecology and taxonomy of the early life stages of arrowtooth (Atheresthes stomias) and Kamchatka flounder (A. evermanni) in the eastern Bering Sea. Deep Sea Res. II 109, 181–189. http://dx.doi.org/10.1016/j.dsr2.2014.05.005.
Eisner, L.B., Napp, J.M., Mier, K.L., Pinchuk, A.I., Andrews, A.G.I., 2014. Climate-mediated changes in zooplankton community structure for the eastern Bering Sea. Deep Sea Res. II 109, 157–171. http://dx.doi.org/10.1016/j.dsr2.2014.03.004.
Goes, J.I., Gomes, H.R., Haugen, E.M., Mckee, K.T., D'a, E.J., Chekalyuk, A.M., Stoecker, D.K., Stabeno, P., Saitoh, S.-I., Sambrotto, R.N., 2014. Fluorescence, pigment and microscopic characterization of Bering Sea phytoplankton community structure and photosynthetic competency in the presence of a Cold Pool during summer. Deep Sea Res. II 109, 84–99. http://dx.doi.org/10.1016/j.dsr2.2013.12.004.
Heintz, R.A., Siddon, E.C., Farley, E.V., Napp, J.M., 2013. Correlation between recruitment and fall condition of age-0 pollock (Theragra chalcogramma) from the eastern Bering Sea under varying climate conditions. Deep Sea Res. II 96, 150–156.
Hunt, G.L.J., Renner, M., Kuletz, K.J., 2014. Seasonal variation in the cross-shelf distribution of seabirds in the southeastern Bering Sea. Deep Sea Res. II 109, 266–281. http://dx.doi.org/10.1016/j.dsr2.2013.08.011.
Jones, N.M., Hoover, B.A., Heppell, S.A., Kuletz, K.J., 2014. A cross-shelf gradient in δ15N stable isotope values of krill and pollock indicates seabird foraging patterns in the Bering Sea. Deep Sea Res. II 109, 241–250. http://dx.doi.org/10.1016/j.dsr2.2014.04.008.
Kuletz, K.J., Renner, M., Labunski, E.A., Hunt, G.L., Jr.,, 2014. Changes in the distribution and abundance of Eastern Bering Sea Albatrosses: 1975–2010. Deep Sea Res. II 109, 282–292. http://dx.doi.org/10.1016/j.dsr2.2014.05.006.
Ladd, C., 2014. Seasonal and interannual variability of the Bering Slope Current. Deep Sea Res. II 109, 5–13. http://dx.doi.org/10.1016/j.dsr2.2013.12.005.
Mathis, J.T.C., J.N., Monacci, N., Stabeno, P.J., 2014. Evidence of prolonged aragonite undersaturations in the bottom waters of the Bering Sea shelf from autonomous sensors. Deep Sea Res. II 109, 125–133. http://dx.doi.org/10.1016/j.dsr2.2013.07.019.
Morales, L.V., Granger, J., Chang, B.X., Prokopenko, M., Plessen, B., Gradinger, R., Sigman, D.M., 2014. Elevated 15N/14N in particulate organic matter, zooplankton, and diatom frustule-bound nitrogen in the ice-covered water column of the Bering sea eastern shelf. Deep Sea Res. II 109, 100–111. http://dx.doi.org/10.1016/j.dsr2.2014.05.008.
Moran, S.B., Lomas, M.W., Kelly, R.P., Prokopenko, M., Granger, J., Gradinger, R., Iken, K., Mathis, J.T., 2012. Seasonal succession of net primary productivity, particulate organic carbon export, and autotrophic community composition in the eastern Bering Sea. Deep Sea Res. II 65-70, 84–97.
Neidetcher, S.K., Hurst, T., Ciannelli, L., Logerwell, E., 2014. Spawning Phenology and Geography of Pacific cod (Gadus macrocephalus). Deep Sea Res. II 109, 204–214. http://dx.doi.org/10.1016/j.dsr2.2013.12.006.
Overland, J.E., Wang, M., Wood, K.R., Percival, D.B., Bond, N.A., 2012. Recent Bering sea warm and cold events in a 95-year context. Deep Sea Res 65-70, 6–13.
Panteleev, G., Luchin, V., 2014. climatological study of the thermal regimes of the Chukchi Sea circulation, which is correlate with the Bering Strait flow. Deep Sea Res. II 109, 14–26. http://dx.doi.org/10.1016/j.dsr2.2014.05.007.
Renner, H.M., Drummond, B.A., Benson, A.-M., Paredes, R., 2014. Reproductive success of kittiwakes and murres in sequential stages of the nesting period: Relationships with diet and oceanography. Deep Sea Res. II 109, 251–265. http://dx.doi.org/10.1016/j.dsr2.2014.03.006.
Renner, M., Huntington, H., 2014. Connecting subsistence harvest and marine ecology: a cluster analysis of communities by fishing and hunting patterns. Deep Sea Res. II 109, 293–299. http://dx.doi.org/10.1016/j.dsr2.2014.03.005.
Sherr, E.B., Sherr, B.F., Ross, C., 2013. Microzooplankton grazing impact in the Bering Sea during spring sea ice conditions. Deep Sea Res. II 94, 57–67.
Sigler, M.F., Renner, M., Danielson, S.L., Eisner, L.B., Lauth, R.R., Kuletz, K.J., Logerwell, E.A., Hunt Jr., G.L., 2011. Fluxes, fins, and feathers: relationships among the Bering, Chukchi, and Beaufort Seas in a time of climate change. Oceanography 24 (3), 250–265. http://dx.doi.org/10.5670/oceanog.2011.77.
Sigler, M.F., Stabeno, P.J., Eisner, L.B., Napp, J.M., Mueter, F.J., 2014. Spring and fall phytoplankton blooms in a productive subarctic ecosystem, the eastern Bering Sea, during 1995–2011. Deep Sea Res. II 109, 71–83. http://dx.doi.org/10.1016/j.dsr2.2013.12.007.
Smart, T.I., Duffy-Anderson, J.T., Horne, J.K., 2012. Alternating temperature states influence walleye pollock (Theragra chalcogramma) early life stages in the southeastern Bering Sea. Mar. Ecol. Prog. Ser. 455, 257–267.
Stabeno, P., Farley, E., Kachel, N., Moore, S., Mordy, C., Napp, J., Overland, J., Pinchuk, A., Sigler, M., 2012a. A comparison of the physics, chemistry and biology of the northeastern and southeastern Bering Sea Shelf. Deep Sea Res. II 65-70, 14–30.
Stabeno, P., Moore, S., Napp, J., Sigler, M., Zerbini, A., 2012b. Comparison of warm and cold years on the southeastern Bering Sea shelf. Deep Sea Res. II 65-70, 31–45.
Stauffer, B.A., Goes, J.I., Mckee, K.T., Gomes, H.R., Stabeno, P.J., 2014. Comparison of spring-time phytoplankton community composition in two cold years from the western Gulf of Alaska into the southeastern Bering Sea. Deep Sea Res. II 109, 57–70. http://dx.doi.org/10.1016/j.dsr2.2014.03.007.
Stoecker, D.K., Weigel, A., Goes, J.I., 2014a. Microzooplankton grazing in the Eastern Bering Sea in summer. Deep Sea Res. II 109, 145–156. http://dx.doi.org/10.1016/j.dsr2.2013.09.017.
Stoecker, D.K., Weigel, A.C., Stockwell, D.A., Lomas, M.W., 2014b. Microzooplankton: Abundance, biomass and contribution to chlorophyll in the Eastern Bering Sea in summer. Deep Sea Res. II 109, 134–144. http://dx.doi.org/10.1016/j.dsr2.2013.09.007.
Strasburger, W.W., Hillgruber, N., Pinchuk, A.I., Mueter, F., 2014. Feeding ecology of age-0 walleye pollock (Gadus chalcogramma) and Pacific cod (Gadus macrocephalus) in the southeastern Bering Sea. Deep Sea Res. II 109, 172–180. http://dx.doi.org/10.1016/j.dsr2.2013.10.007.
Sullivan, M.E., Salo, S.A., Stabeno, P.J., Mordy, C.W., 2014. The influence of sea ice on seasonal water column changes on the eastern Bering Sea Shelf. Deep Sea Res. II 109, 39–56. http://dx.doi.org/10.1016/j.dsr2.2014.05.009.
Vestfals, C.D., Ciannelli, L., Duffy-Anderson, J.T., Ladd, C., 2014. Effects of seasonal and interannual variability of along-shelf and cross-shelf transport on groundfish recruitment in the eastern Bering Sea. Deep Sea Res. II 109, 190–203. http://dx.doi.org/10.1016/j.dsr2.2013.09.026.
Weise, F.K., Wiseman, Jr., W.J., van Pelt, T.I., 2012. Bering sea linkages. Deep Sea Res 65-70, 2–5.

Michael W. Lomas *
Bigelow Laboratory for Ocean Sciences, East Boothbay, ME 04544, USA

Phyllis J. Stabeno
Pacific Marine Environmental Laboratory, NOAA, Seattle WA 98115, USA

Available online 19 September 2014

* Corresponding author.

Deep-Sea Research II 109 (2014) 5–13

Contents lists available at ScienceDirect

Deep-Sea Research II

journal homepage: www.elsevier.com/locate/dsr2

Seasonal and interannual variability of the Bering Slope Current

Carol Ladd *

Pacific Marine Environmental Laboratory, NOAA, 7600 Sand Point Way, Seattle, WA 98115-6349, USA

ARTICLE INFO

Available online 17 December 2013

Keywords:
Bering Sea
Slope currents
Satellite altimetry
Surface topography

ABSTRACT

Time series of sea-surface height anomalies derived from satellite altimeters and absolute dynamic topography are used to examine variability in the geostrophic surface currents in the Eastern Bering Sea. The data suggest that the primary source of water to the eastern boundary currents of the Bering Sea is flow from the North Pacific through Amukta Pass, an Aleutian pass located at ~172°W. The Aleutian North Slope Current (ANSC) is strongest and most variable in the winter months. Upon turning the corner to feed the Bering Slope Current (BSC), the ANSC bifurcates, resulting in a westward flow at ~54°N in addition to the northwestward flowing BSC. This westward countercurrent has not been previously observed. In the winter, the BSC flows strongly to the northwest and is located near the shelf-break. During the rest of the year, the mean flow is broadly northwestward, but weaker and farther from the shelf break. A continuous northwestward-flowing current is rarely observed in the altimetry data except during winter months, as it is overwhelmed by mesoscale variability. The strength of the BSC in winter is correlated with the Multivariate ENSO Index and the North Pacific Index on interannual timescales.

Published by Elsevier Ltd.

1. Introduction

The mean cyclonic gyre circulation in the Bering Sea (Fig. 1) comprises the southward flowing Kamchatka Current along the western boundary (Favorite et al., 1976; Panteleev et al., 2006; Sayles et al., 1979), the eastward flowing Aleutian North Slope Current (ANSC) north of the Aleutian Islands (Reed and Stabeno, 1999; Stabeno et al., 2009), and the north-westward flowing Bering Slope Current (BSC) along the eastern shelf-break (Johnson et al., 2004; Kinder et al., 1975). The near-surface circulation of the Bering Sea has been estimated using satellite-tracked drifters (Stabeno and Reed, 1994), while the subsurface flow has been estimated from hydrographic surveys (Cokelet et al., 1996; Kinder et al., 1975; Reed et al., 1993; Schumacher and Reed, 1992), moorings (Schumacher and Reed, 1992), and profiling float data (Johnson et al., 2004). Most recently, Panteleev et al. (2012) estimated Bering Sea circulation from a dataset derived from a combination of satellite altimetry and *in situ* data. They noted significant lagged correlations between transports in the Alaskan Stream, the BSC, and the Kamchatka Current, suggesting continuity of flow around the Bering Sea basin.

From limited current meter data, Schumacher and Reed (1992) observed northwestward flow in the BSC with speeds of 5–15 cm s^{-1} aligned with the large-scale bathymetry. They noted seasonal changes in kinetic energy, but stated that the net flow was not seasonal or strongly related to local wind forcing. On the other hand, a modeling study found a strong seasonal cycle in the BSC with strong flow close to the shelf-break during winter and weaker flow displaced off-shelf during the summer (Overland et al., 1994).

Further complicating the analysis of variability is the ubiquitous presence of eddies in the Eastern Bering Sea basin. Eddies in this region exhibit scales of 10–200 km horizontally (Paluszkiewicz and Niebauer, 1984; Stabeno et al., 1999) and >1000 m vertically (Mizobata et al., 2008; Roden, 1995). Cokelet et al. (1996) examined the Rossby numbers of eddies in the Bering Sea and found them to be small enough for geostrophy to hold with negligible inertial effects. In the BSC, the highest eddy kinetic energy values are observed near the canyons that incise the Eastern Bering Sea shelf break (Ladd et al., 2012; Okkonen, 2001). Altimetry data suggests that eddy kinetic energy in the BSC is highest in spring and summer, and weaker in fall/winter (Ladd et al., 2012; Okkonen, 2001). The seasonal cycle is probably due to a combination of propagation of energy from inflow through the Aleutian passes, and enhanced baroclinic instability during the summer due to stronger stratification (Mizobata et al., 2008). Interannual variability in eddy kinetic energy in the region is correlated with the winter North Pacific Index (NPI) (Ladd et al., 2012) and the Pacific Decadal Oscillation (Panteleev et al., 2012). The NPI is associated with wind stress curl patterns and simultaneous spin-up of the subpolar and subtropical gyres in the North Pacific (Ishi and Hanawa, 2005), suggesting that a strong Bering Sea gyre circulation during the preceding winter leads to increased eddy activity in the spring (Ladd et al., 2012).

Altimetry data have been very useful for examining eddy activity in the Bering Sea (*e.g.* Ladd et al., 2012; Mizobata and Saitoh, 2004; Okkonen, 2001). These data can also be used to examine variability of

* Tel.: +1 206 526 6024; fax: +1 206 526 6485.
E-mail address: carol.ladd@noaa.gov

0967-0645/$ - see front matter Published by Elsevier Ltd.
http://dx.doi.org/10.1016/j.dsr2.2013.12.005

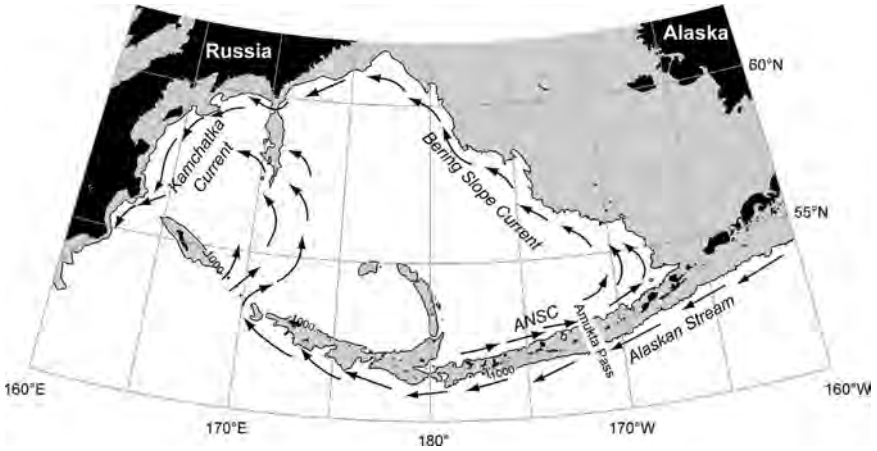

Fig. 1. Schematic of Bering Sea currents. Gray shading denotes regions with depth < 1000 m.

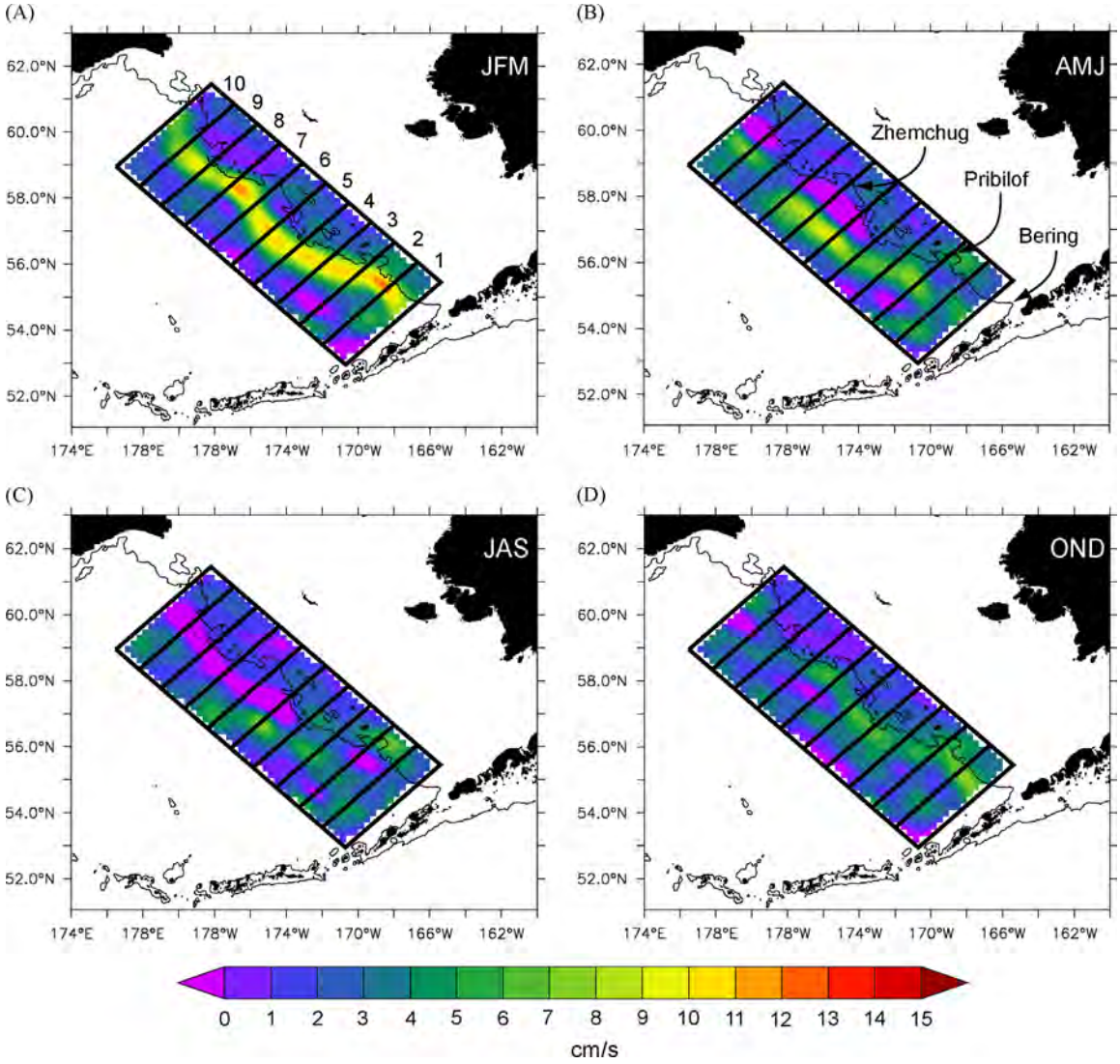

Fig. 2. Climatology of along-shelf component of velocity (cm s^{-1}) created by averaging 20 years of ADT data over 3-month periods: (A) January–March, (B) April–June, (C) July–September, and (D) October–December. Positive values denote speed in northwestward direction (317°) while negative values (light purple) denote speed in the southeastward direction (137°). The subregions discussed in the text are outlined. Canyons are noted in panel (b). Black contour denotes 200 m isobath (shelf-break).

the surface currents. Our focus will be on examining variability of the currents in the Eastern Bering Sea, particularly the ANSC and the BSC.

2. Data

2.1. Satellite altimetry

Gridded sea surface height anomalies (SSHA) were downloaded from Archiving, Validation and Interpretation of Satellite Oceanographic data (AVISO). These anomalies, relative to the mean sea surface height over 1993–1999 (SSALTO/DUACS, 2012), allow analysis of variability of geostrophic surface currents. AVISO applies an optimal interpolation methodology to merge data from multiple altimeters (Le Traon et al., 1998; SSALTO/DUACS, 2012) and produces two versions of the merged gridded datasets, "ref" and "upd". The "ref" dataset consists of delayed-mode, merged data from two satellite missions and has stable temporal sampling. The "upd" dataset merges data from up to four satellites at a given time. While the inclusion of data from additional satellites results in improved spatial and temporal resolution, the quality of the time series is not temporally stable (SSALTO/DUACS, 2012). Because our focus is on temporal variability, we use the "ref" dataset here. The AVISO product has 7 day temporal resolution and 1/3° spatial resolution (Ducet et al., 2000; Le Traon and Dibarboure, 1999). To examine complete years, we restrict our analysis to altimetry data in the period 1993–2012 (20 years).

To examine the mean flow and seasonal cycle, gridded absolute geostrophic surface currents derived from absolute dynamic topography (ADT) for 1993–2012 were also downloaded from AVISO. ADT is the sum of SSHA and mean dynamic topography, where the latter is the mean sea surface height minus the geoid. The mean dynamic topography used here is CNES-CLS09 derived by Rio et al. (2011). This dataset was created using the CLS01 altimetric mean sea surface and a recent geoid model computed from 4.5 years of Gravity Recovery and Climate Experiment (GRACE) data, combined with *in situ* measurements (including all profiles from the Argo array) (Rio et al., 2011).To examine seasonality, climatologies were created by averaging the 20 years of ADT data into four seasons: January–March, April–June, July–September, October–December. Deviations from the seasonal means were used to compute variance ellipses, representing the magnitude and direction of seasonal velocity variability (Preisendorfer, 1988).

The shelf-break of the Eastern Bering Sea runs more than 1000 km in extent from the southeast corner to the northern boundary. To examine spatial and temporal variability in the BSC, we divide this large region into 10 smaller regions (Fig. 2), numbered from 1 (southeast) to 10 (northwest). To represent the current in the along-shelf direction, we use the component of velocity oriented 317°/137° from north averaged into seasons. In each sub-region, the maximum of this seasonally averaged component of flow defines the strength and position of the current.

Seasonal heating produces changes in sea surface height (SSH), η_{steric}, due to the thermal expansion or contraction of the water column. Spatial gradients in η_{steric} will give rise to geostrophic currents but these currents will be confined to the region above the shallow seasonal thermocline (Gill and Niller, 1973; Kelly et al., 1999). Average monthly change in η_{steric} can be calculated from average monthly net heat fluxes:

$$\frac{\partial \eta}{\partial t} = \frac{\alpha Q_{net}}{\rho_0 c_p},$$

where Q_{net} is the net heat flux (sum of latent and sensible heat flux, and shortwave and longwave radiation), α is the coefficient of thermal expansion, ρ_0 is the average water density and c_p is the specific heat of seawater. Using monthly average climatological Q_{net} from the National Centers for Environmental Prediction, we examined seasonality in the SSH difference (ΔSSH) at 57°N across the BSC (176°W to 173°W). The change in η_{steric} per month is of order 10^{-2} cm while changes in the total ΔSSH range from 0.4 cm (difference between July and August) to 13.9 cm (difference between January and December) per month. Thus, seasonal changes in the steric height across the BSC do not significantly influence the seasonality of the BSC calculated from the ADT.

2.2. In situ data

Fourteen surveys across the ANSC and the BSC were used by Stabeno et al. (2009) to derive geostrophic transport referenced to 1500 m. Two additional surveys have been completed since then, and those surveys are included here for a total of 16 surveys. Out of these 16 surveys, two pairs were sampled within a month of each other. Thus, assuming an integral timescale longer than a month, we use $n=14$ for statistical significance testing. These data illustrate high temporal variability caused largely by eddies in the region. High correlation between the two currents demonstrate the connectivity of the flow from the ANSC to the BSC (Stabeno et al., 2009). (See Fig. 4 for location of the two transects.)

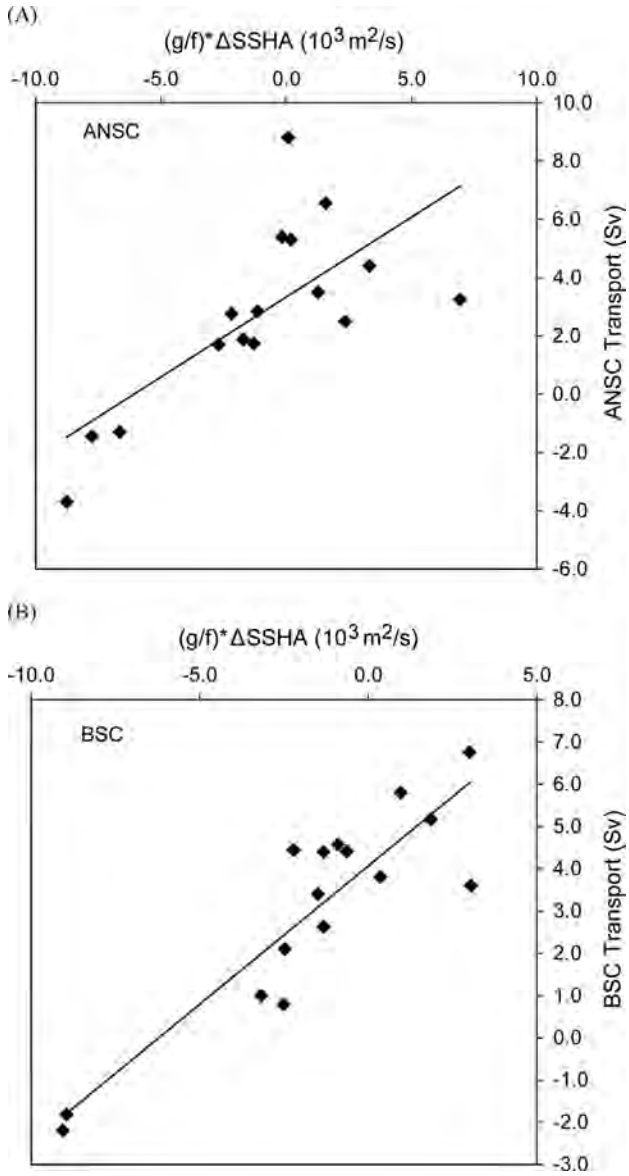

Fig. 3. Scatterplots showing correlation between surface transports calculated from SSHA and geostrophic transports from Stabeno et al. (2009) and 2 more recent estimates. (A) ANSC transport and (B) BSC transport. Regression lines are overlaid.

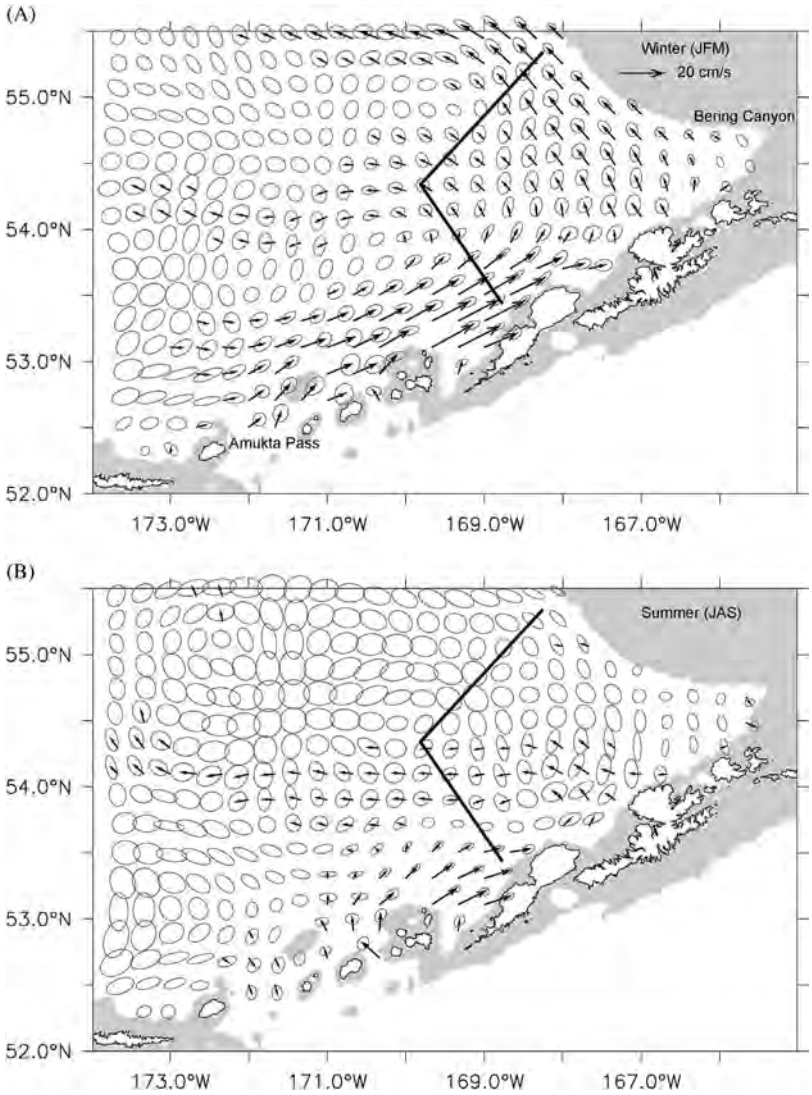

Fig. 4. Surface velocity variance (ellipses) and mean velocities (vectors) derived from ADT for (A) winter (January–March) and (B) summer (July–September). Only velocities that are significant at 95% confidence limits are plotted. A scale arrow representing 20 cm s^{-1} is shown in upper right. Variance ellipses are scaled so that if the mean vector reaches outside the ellipse, it is significant. Location of transects used to derive volume transport are denoted by thick lines.

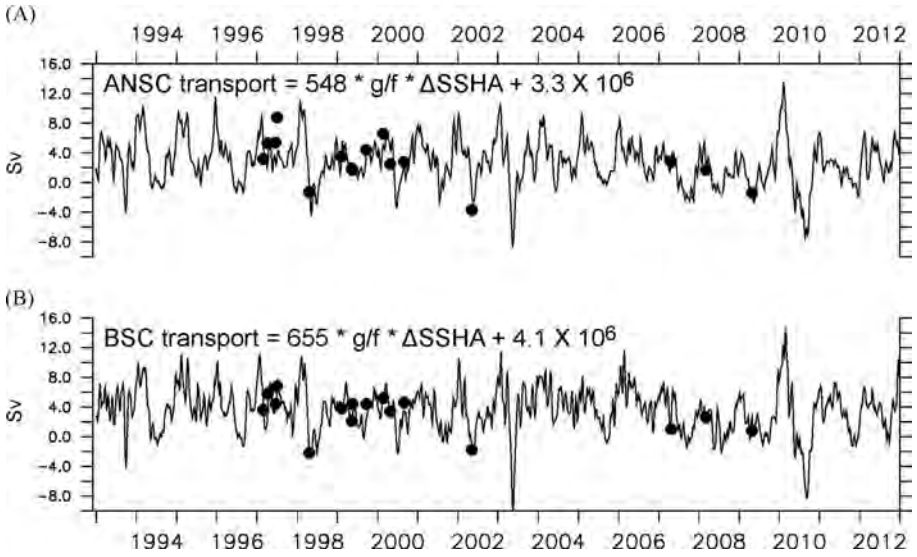

Fig. 5. Volume transport (Sv) along the (A) ANSC transect and (B) BSC transect derived from regression equations discussed in text. Black dots denote geostrophic transports calculated from *in situ* observations (including two more recent realizations not included in Stabeno et al. (2009)).

To examine how well surface currents derived from altimetry data correspond to the geostrophic transport calculated from hydrographic data, we interpolated SSHA to the dates and geographical endpoint positions of the *in situ* surveys and calculated the surface transport anomalies across the sections from the following relationship (Kelly et al., 1999):

$$\text{surface transport} = \frac{g}{f}\Delta SSHA.$$

In both currents, surface transports calculated from SSHA were significantly correlated ($n=14$, $P<0.005$, two-tailed significance test) with geostrophic transports referenced to 1500 m (Fig. 3), suggesting that even with temporal and spatial smoothing inherent in the altimetry dataset, surface transport anomalies reflect variability in volume transport observed via *in situ* data. The BSC exhibited a higher correlation coefficient ($R=0.90$) than the ANSC ($R=0.72$), not surprising given the smaller spatial scales of the ANSC (Stabeno et al., 1999).

Assuming a system characterized by an active upper layer and a quiescent lower layer, $\Delta SSHA$ is proportional to the transport of the upper layer (Kelly et al., 1999). Thus to first order, regression equations relating *in situ* transports and $\Delta SSHA$ allow estimates of the effective depth of the upper layer and the mean transport. In addition, assuming stationarity, applying the regression equations to the altimetry data allows examination of the entire time series of volume transports. The resulting regression equations are

$$\text{ANSC Transport} = 548\frac{g}{f}\Delta SSHA + 3.3 \times 10^6$$

$$\text{BSC Transport} = 655\frac{g}{f}\Delta SSHA + 4.1 \times 10^6$$

suggesting an effective upper layer depth of 548 m in the ANSC and 655 m in the BSC with mean transports of 3.3 Sv (1 Sv$=10^6$ m^3 s^{-1}) and 4.1 Sv, respectively. For comparison, mean transport estimated by Stabeno et al. (2009) for the 14 transects was 3.1 ± 3.1 Sv for the ANSC and 3.3 ± 2.6 Sv for the BSC and Johnson et al. (2004) estimated transport of 3.5 ± 1.1 Sv for the upper layer (1000 m) of the BSC. It should be noted that because of seasonality in stratification, the effective upper layer depth would be expected to vary seasonally. The *in situ* transects used in calculating the regressions were primarily (12 of the 16) taken during the spring (February–May) and the regressions are likely biased to spring conditions.

3. Results

3.1. Aleutian North Slope Current

The ANSC flows eastward along the north side of the Aleutian Islands, turning the corner in the southeast corner of the basin to

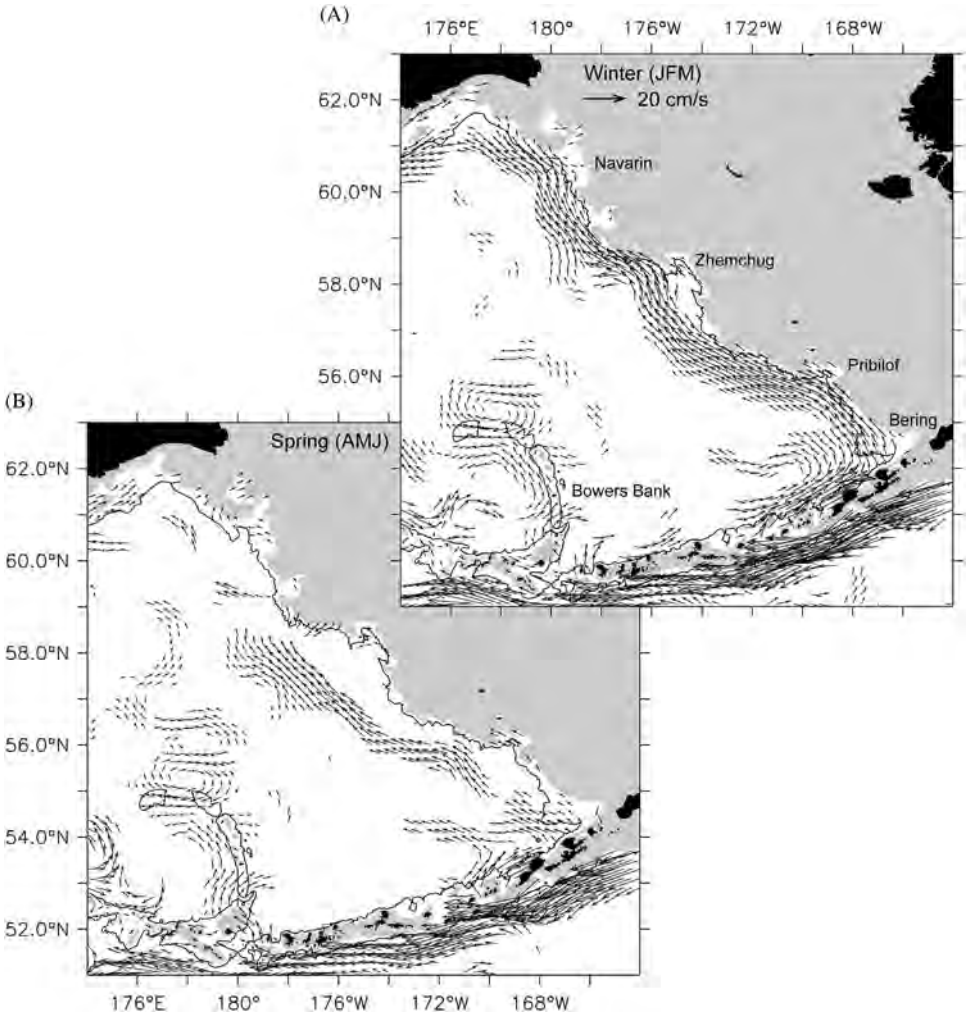

Fig. 6. Seasonal surface current climatology derived from ADT as in Fig. 4. A scale arrow representing 20 cm s^{-1} is shown in panel (A). Only velocities that are significant at 95% confidence limits are plotted. Velocities in water shallower than 200 m isobath are not shown. The 1000 m isobath is overlaid.

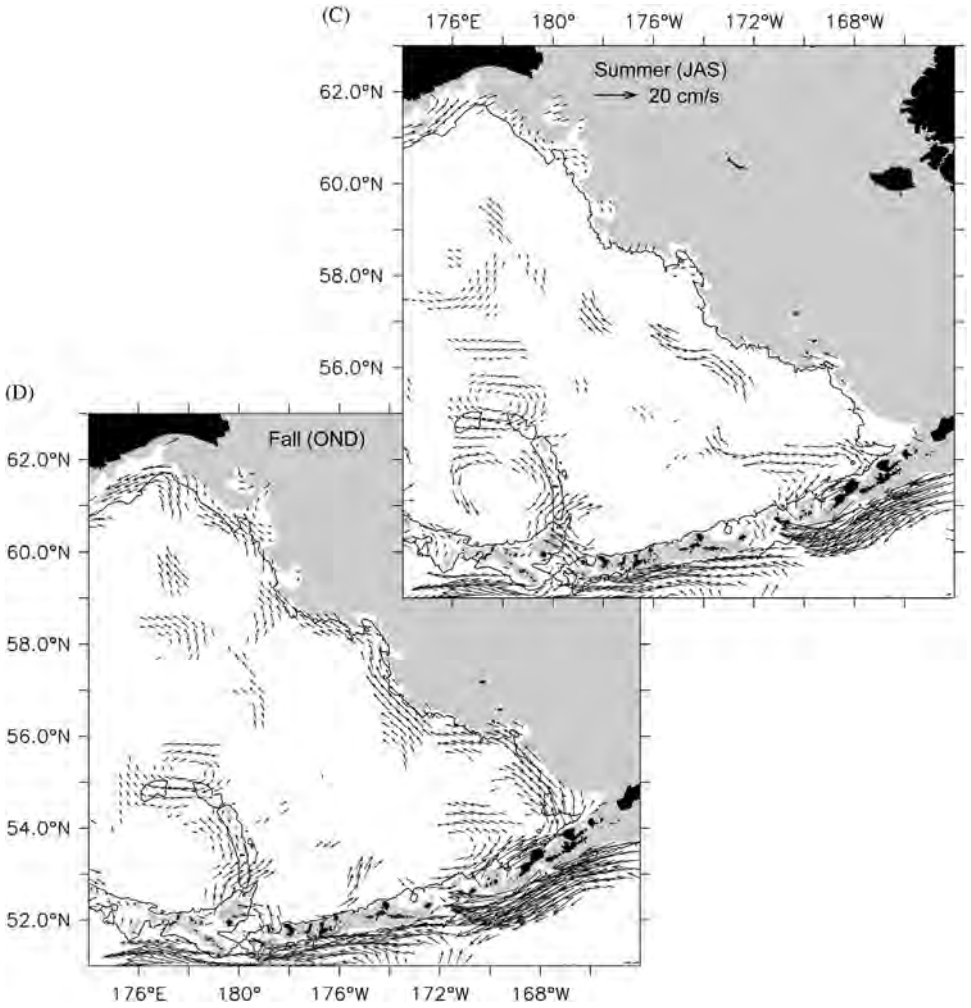

Fig. 6. (*continued*)

Table 1
Transports (Sv) across ANSC and BSC transects shown in Fig. 4 derived from regression equations applied to SSHA time series.

	1993–2012				Winter (JFM)		Spring (AMJ)		Summer (JAS)		Fall (OND)	
	Mean	S.D.	Max	Min	Mean	S.D.	Mean	S.D.	Mean	S.D.	Mean	S.D.
ANSC	2.8	3.0	13.6	−8.8	5.3	2.6	1.8	2.8	1.0	2.3	3.0	2.3
BSC	3.6	3.0	14.6	−10.1	6.0	2.5	3.0	2.9	1.9	2.8	3.6	2.2

feed the BSC. The January–March data show a strong ANSC (Fig. 4) east of ~172°W (the approximate longitude of Amukta Pass), supporting previous evidence suggesting that Amukta Pass is the primary source of ANSC flow (Stabeno et al., 2009; Stabeno et al., 1999). West of Amukta Pass, mean ANSC velocities are not significant. The northeastward flowing ANSC reaches into Bering Canyon during the winter while the mean flow over Bering Canyon is insignificant during the summer. A bifurcation is apparent in the southeast corner of the basin with some of the ANSC flow turning offshelf to flow westward at ~54°N. This countercurrent is significant in both summer and winter and has not been previously described. Neither satellite-tracked Argos drifters drogued at 40 m (Stabeno and Reed, 1994) or Argo floats (Johnson et al., 2004) suggest such a countercurrent but the data is relatively sparse and variability is high. During the summer (July–September), ANSC currents are weaker and more tightly confined to the Aleutian Islands. Variability in the ANSC is also stronger in the winter than the summer (see size of variance ellipses; Fig. 4), while variance in the basin (away from the shelf) is higher in summer.

While the regressions calculated above have their limitations (*i.e.* location of the transect may not be the best location for examining the individual currents, seasonal bias mentioned above), to first order, they allow an examination of the temporal variability of volume transport in the two currents (Fig. 5). Mean transport across the ANSC transect is estimated as 2.8 ± 0.8 Sv (95% confidence interval) with a maximum of 13.6 Sv occurring in February 2010 and a minimum of −8.8 Sv (southwestward flow) in May 2003 (Table 1). The seasonal cycle exhibits a maximum transport of 5.9 ± 1.5 Sv in January and minimum of 0.8 ± 1.1 Sv in August.

Table 2
Winter (January–March) averaged BSC surface speeds (cm s^{-1}) in sub-regions discussed in text and displayed in Fig. 2. Standard Deviation (S.D.) is a measure of the interannual variability in the winter averaged BSC speed. Correlation coefficients (R) with the MEI and NPI are listed along with associated p-value (in parentheses). Significant correlations ($p < 0.05$) are bold. P-values are calculated assuming $n=20$ independent winter averages.

Sub-region	Mean	S.D.	MEI correlation (p-value)	NPI correlation (p-value)
1	14.0	3.4	**0.52 (0.018)**	**−0.51 (0.023)**
2	14.8	3.6	**0.65 (0.002)**	**−0.67 (0.001)**
3	15.2	2.7	**0.60 (0.005)**	**−0.62 (0.004)**
4	14.3	4.0	**0.78 (0.000)**	**−0.72 (0.000)**
5	14.5	4.0	**0.52 (0.019)**	**−0.56 (0.011)**
6	15.3	4.2	**0.45 (0.044)**	**−0.49 (0.027)**
7	14.0	3.3	0.43 (0.056)	**−0.54 (0.013)**
8	12.8	3.0	0.20 (0.390)	−0.40 (0.082)
9	13.3	3.1	0.18 (0.438)	−0.41 (0.072)
10	13.2	3.7	0.08 (0.734)	−0.26 (0.265)

3.2. Bering Slope Current

Seasonality in the BSC is pronounced with stronger flow close to the shelf-break during the winter and weaker flow positioned farther west (off-shelf) during the rest of the year. The BSC is strongest in the winter months (January–March) with average speeds greater than 10 cm s^{-1} (Figs. 2A, 6A and Table 2). A significant current follows the 1000 m isobath along almost the entire extent of the eastern shelf-break. The only places the BSC departs from the 1000 m isobath is near Zhemchug Canyon where the isobath cuts deeply into the canyon and at the northern extent where the current turns toward the west at ~61°N, roughly 100 km south of the 1000 m isobath.

In April–September, the BSC is weaker and positioned farther west, away from the shelf-break (Figs. 2B,C and 6B,C). Velocities are only significant south of ~58.5°N (Fig. 6B,C), consistent with the hypothesis that the BSC turns off-shelf to flow westward across the Bering Sea at that latitude (Stabeno and Reed, 1994). The westward shift of the BSC to a position farther from the shelf-break is most apparent near Zhemchug Canyon (57–58°N) where eddy energy is particularly strong in the spring (Ladd et al., 2012). By October–December, the BSC strengthens and moves back toward the east in closer proximity to the shelf-break (Figs. 2D and 6D). During this season, the BSC stays closer to the 1000 m isobath over the entire extent of the current, flowing into Zhemchug Canyon and turning to feed the Kamchatka Current at almost 62°N.

As discussed in Section 2.1, we represent BSC speed by the spatial maximum (in each sub-region) of the seasonally averaged component of flow in the along-shelf direction (317°). Average winter (JFM) BSC speeds in the southernmost 7 regions (Fig. 2) are greater than 14.0 cm s^{-1}, while north of there (regions 8–10), BSC speeds drop to less than 13.3 cm s^{-1} (Table 2), a statistically significant difference. The slower current north of ~58.5°N suggests that even during the winter, some of the BSC water turns off-shelf to flow westward across the Bering Sea at that latitude.

Using the regression equation from Fig. 3, mean transport across the BSC transect in the southeast corner of the basin is estimated as 3.6 ± 0.8 Sv (95% confidence interval) with a maximum of 14.6 Sv occurring in February 2010 and a minimum of −10.1 Sv (flow in southeastward direction) in May 2003 (Table 1). While the reversed direction of transport observed in May 2003 in both the BSC and the ANSC was due to a strong anticyclonic eddy in the region, the high transport in both currents in February 2010 appears to be due to enhanced gyre-scale circulation. Flow in the Alaskan Stream was also very strong at this time. The seasonal cycle exhibits a maximum transport of 6.5 ± 1.2 Sv in January and minimum of 1.5 ± 1.7 Sv in September. Variability is maximum in May and minimum in November.

3.2.1. Interannual variability

As an estimate of the surface current speeds of the BSC, time series (3-month averages) of maximum along-shelf component of velocity in each of the 10 regions were generated. Position of the current was calculated by finding the longitude where the maximum occurred in each region. Each season was examined separately.

Winter BSC speeds are significantly correlated with the multivariate ENSO index (MEI; (Wolter and Timlin, 1993, 1998)) and the North Pacific Index (NPI; (Trenberth and Hurrell, 1994)) in regions 1–7 (Table 2). In regions 8–10, correlations are weaker and not significant, again suggesting a discontinuity in the BSC at ~58.5°N. The highest correlations are calculated for region 4 (NPI: $R=-0.72$, $P=0.0003$; MEI: $R=0.78$, $P=0.0000$), between Pribilof and Zhemchug Canyons, probably due to smaller eddy kinetic energy there (Ladd et al., 2012). Winter BSC speed in region 4 averaged over 1993–2012 was 14.3 cm s^{-1}. Peak BSC speeds occurred in 1998, 2003, and 2010 (Fig. 7), all years with both a positive MEI (El Niño years) and a strong negative NPI (strong Aleutian Low). Maximum winter averaged BSC speed in region 4 occurred during the very strong El Niño of 1998 (23.9 cm s^{-1}); minimum occurred in 2012 (9.0 cm s^{-1}). Correlations between seasonal BSC speeds and the winter MEI and NPI are weaker in the other seasons (but still significant in the southernmost two regions in spring).

The mean position of the BSC is farthest east (closest to the shelf-break) during the winter (Fig. 2). In region 4, the mean longitude during winter is 173.0°W ± 0.4° (95% confidence interval), while in summer, the mean longitude is 173.3°W ± 0.4°, not significantly different. In region 7, on the other hand, mean longitude is 176.5°W ± 0.2° (winter) and 177.5°W ± 0.4° (summer), a significant difference. While the position of the current can change by up to 4° of longitude (~240 km) from year to year, the variability is not coherent between subregions, suggesting that mesoscale variability is likely responsible for interannual shifts in BSC position. Correlations of BSC position with climate indices (NPI, MEI) are insignificant.

4. Discussion

Geostrophic surface currents derived from satellite altimetry data are used to examine variability of the BSC along the Eastern Bering Sea shelf-break. Schematic representations of the circulation of the Bering Sea show the BSC as a continuous northwestward current. It is

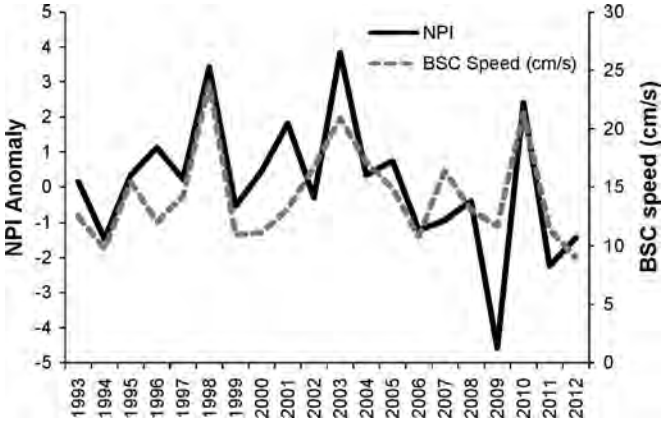

Fig. 7. November–March NPI anomaly (reversed for clarity; dark line) and January–March BSC speed (cm s^{-1}) in region 4 (~56.5°N; light gray).

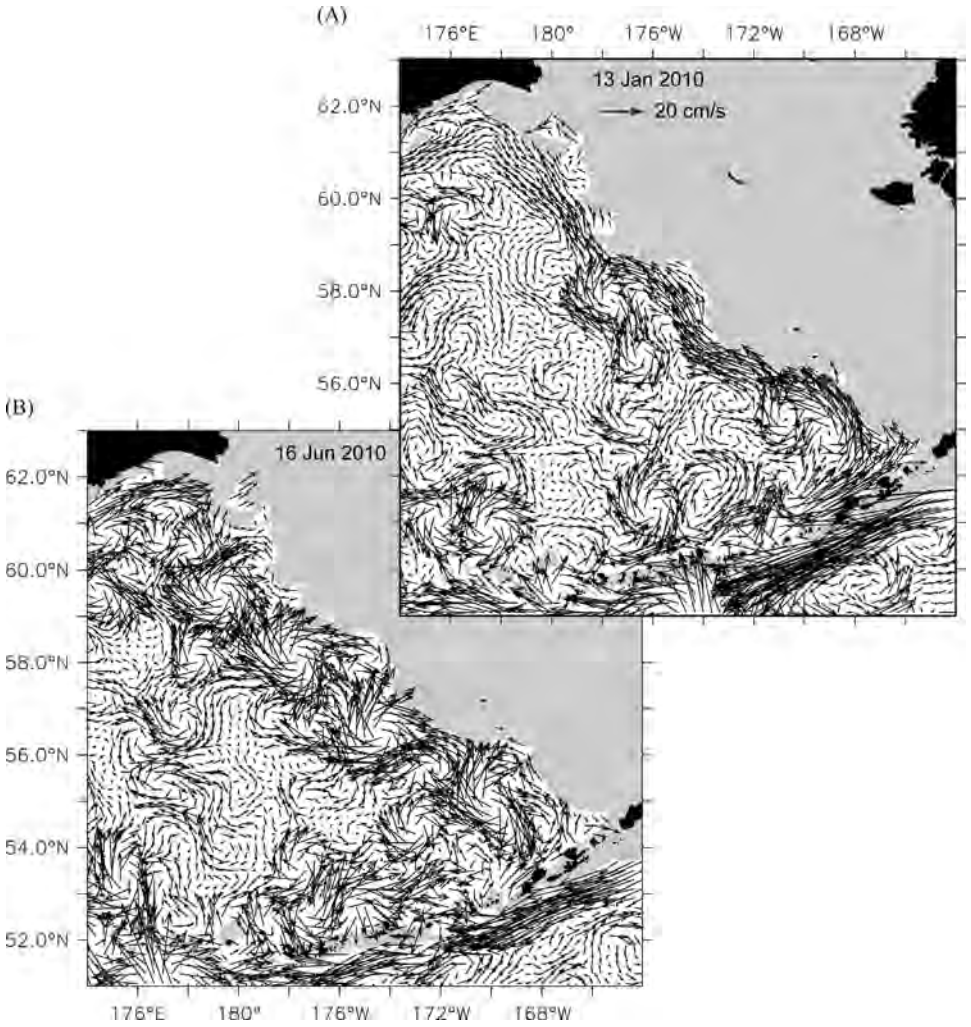

Fig. 8. Geostrophic surface currents for (A) 13 January 2010 and (B) 16 June 2010 are shown as an example of instantaneous snapshots.

important to note that, outside of the winter months, mesoscale eddies overwhelm the current and it is not a continuous, cohesive feature (*i.e.* Fig. 8). Thus, tracers, biota, nutrients, *etc.* being advected by the current would be more likely to move in the cross-shelf direction (into the basin or onto the shelf) during the summer months.

Flow from the Pacific to the Bering Sea primarily through Amukta Pass (~172°W in the Aleutian Islands) provides the source waters for the ANSC, which in turn feeds the BSC. The seasonality of the source through Amukta Pass, as well as a strong seasonal cycle in mesoscale eddy energy (Ladd et al., 2012; Okkonen, 2001), results in a strong seasonal cycle in the BSC strength and position. The transport through Amukta Pass is strongest in the winter months (Ladd and Stabeno, 2009), leading to stronger ANSC flow that reaches farther east (impinging on Bering Canyon) before turning the corner to become the BSC. The position of the BSC along its entire length is also farther east, closer to the shelf-break, during winter than during the summer months. Thus, the influence of the ANSC/BSC system on flow over Bering Canyon and the shelf-break is likely stronger in winter.

Several commercially important flatfish and rockfish species spawn in the deep water near the shelf-break in the Eastern Bering Sea, and the larvae are transported across the shelf-break to reach nursery areas on the shelf. Ocean currents and the associated drift pathways have been shown to be important for flatfish recruitment in the Bering Sea (Sohn et al., 2010; Vestfals et al., 2014; Wilderbuer et al., 2002). For example, Greenland halibut eggs hatch in winter in deep water and larvae rise through the water column as they develop. It is likely that the canyons along the Bering Sea shelf-break are important spawning locations and conduits for transport onto the shelf (Sohn et al., 2010). Thus, seasonality of BSC position and the intrusion of the ANSC/BSC system into Bering Canyon is likely important for flatfish life history and recruitment.

A compilation of drifter data (that does not resolve the seasonal cycle) suggests that the BSC separates from the shelf-break to form westward flow near 58.5°N and is not a continuous current north of that point (Stabeno and Reed, 1994). Panteleev et al. (2011) suggest that the BSC turns toward the east at 61°N, 178°W. The altimetry data also suggests that the BSC weakens north of ~58.5°N. However, during the winter, the BSC flows northwest as far north as ~61°N (although weaker) before turning the corner to feed the Kamchatka Current (Figs. 2 and 6). During the summer, there is no evidence of a BSC along the eastern shelf-break north of ~58.5°N and the connection between the BSC and the Kamchatka Current appears to occur farther south than during the winter. Thus, the strength of the bifurcation of the BSC appears to be seasonally modulated.

Strong interannual variability in the strength of the BSC is correlated with the North Pacific Index (NPI) and Multivariate ENSO Index (MEI). Thus, variation in transport could be one mechanism by which climate influences fish recruitment. The NPI is associated with wind stress curl patterns and simultaneous spin-up of the subpolar and subtropical gyres in the North Pacific (Ishi and Hanawa, 2005) suggesting that interannual variability of the BSC

is wind-driven. Years with particularly high BSC speeds tend to be El Niño years. A modeling study found that connections between El Niño and ocean circulation in the Gulf of Alaska are largely driven by local winds and runoff (teleconnections) as opposed to Kelvin wave propagation (Hermann et al., 2009). This is likely to be the case in the Bering Sea as well. Relationships between climate indices and circulation derived from altimetry could be used to extend time series to periods prior to the altimetry record.

4.1. Conclusions

Satellite altimeters have been observing the sea surface height of the World Ocean for over 20 years. These data have been used here to examine variability in the boundary currents of the Eastern Bering Sea. Schumacher and Alexander (1999) hypothesized that a decrease in inflow from the North Pacific to the Bering Sea may occur due to global warming. The resulting reduction in the strength of the BSC would affect the ecosystems of the eastern Bering Sea by influencing the formation of eddies and the transport of nutrients and biota. Alternatively, Panteleev et al. (2012) found a significant positive trend in eddy activity from 1993 through 2010 suggesting that the large-scale circulation may be spinning up. While we do not observe such trends (either increasing or decreasing) in the 20 year record examined here, it is imperative that we continue to monitor the currents of the Eastern Bering Sea.

Acknowledgments

Discussions with P. Stabeno and A. Hermann are appreciated. The altimeter products were produced by Ssalto/Duacs and distributed by AVISO with support from CNES (http://www.aviso.oceanobs.com/duacs/). Two anonymous reviews and a review and discussions with Seth Danielson resulted in a much improved paper. Support from NSF (Grant number 1107250) is gratefully acknowledged. This research is contribution EcoFOCI-0795 to NOAA's Ecosystems and Fisheries-Oceanography Coordinated Investigations and PMEL contribution 3973. This is BEST-BSIERP Bering Sea Project publication number 121.

References

Cokelet, E.D., Schall, M.L., Dougherty, D.M., 1996. ADCP-referenced geostrophic circulation in the Bering Sea Basin. J. Phys. Oceanogr. 26, 1113–1128.
Ducet, N., Le Traon, P.Y., Reverdin, G., 2000. Global high-resolution mapping of ocean circulation from TOPEX/Poseidon and ERS-1 and-2. J. Geophys. Res. – Oceans 105, 19477–19498.
Favorite, F., Dodimead, A.J., Nasu, K., 1976. Oceanography of the Subarctic Pacific Region, 1960–71. International North Pacific Fisheries Commission. Bulletin 33, p. 187.
Gill, A.E., Niller, P.P., 1973. The theory of the seasonal variability in the ocean. Deep Sea Res. Oceanogr. Abstracts 20, 141–177, http://dx.doi.org/10.1016/0011-7471(73)90049-1.
Hermann, A.J., Curchitser, E.N., Haidvogel, D.B., Dobbins, E.L., 2009. A comparison of remote *vs* local influence of El Niño on the coastal circulation of the Northeast Pacific. Deep-Sea Res. II 56, 2427–2443, http://dx.doi.org/10.1016/j.dsr2.2009.02.005.
Ishi, Y., Hanawa, K., 2005. Large-scale variabilities of wintertime wind stress curl field in the North Pacific and their relation to atmospheric teleconnection patterns. Geophys. Res. Lett. 32, L10607, http://dx.doi.org/10.1029/2004gl022330.
Johnson, G.C., Stabeno, P.J., Riser, S.C., 2004. The Bering Slope Current system revisited. J. Phys. Oceanogr. 34, 384–398.
Kelly, K.A., Singh, S., Huang, R.X., 1999. Seasonal variations of sea surface height in the Gulf Stream region. J. Phys. Oceanogr. 29, 313–327. (10.1175/1520-0485(1999)029 < 0313:svossh > 2.0.co;2).
Kinder, T.H., Coachman, L.K., Galt, J.A., 1975. The Bering Slope Current system. J. Phys. Oceanogr. 5, 231–244.
Ladd, C., Stabeno, P.J., 2009. Freshwater transport from the Pacific to the Bering Sea through Amukta Pass. Geophys. Res. Lett. 36, L14608, http://dx.doi.org/10.1029/2009GL039095.
Ladd, C., Stabeno, P.J., O'Hern, J.E., 2012. Observations of a Pribilof eddy. Deep-Sea Res. I 66, 67–76, http://dx.doi.org/10.1016/j.dsr.2012.04.003.
Le Traon, P.Y., Dibarboure, G., 1999. Mesoscale mapping capabilities of multi-satellite altimeter missions. J. Atmos. Oceanic Technol. 16, 1208–1223.
Le Traon, P.Y., Nadal, F., Ducet, N., 1998. An improved mapping method of multi-satellite altimeter data. J. Atmos. Oceanic Technol. 15, 522–534.
Mizobata, K., Saitoh, S.-I., Wang, J., 2008. Interannual variability of summer biochemical enhancement in relation to mesoscale eddies at the shelf break in the vicinity of the Pribilof Islands, Bering Sea. Deep-Sea Res. II 55, 1717–1728.
Mizobata, K., Saitoh, S., 2004. Variability of Bering Sea eddies and primary productivity along the shelf edge during 1998–2000 using satellite multisensor remote sensing. J. Mar. Syst. 50, 101–111, http://dx.doi.org/10.1016/j.jmarsys.2003.09.014.
Okkonen, S.R., 2001. Altimeter observations of the Bering Slope Current eddy field. J. Geophys. Res. – Oceans 106, 2465–2476.
Overland, J.E., Spillane, M.C., Hurlburt, H.E., Wallcraft, A.J., 1994. A numerical study of the circulation of the Bering Sea Basin and exchange with the North Pacific Ocean. J. Phys. Oceanogr. 24, 736–758.
Paluszkiewicz, T., Niebauer, H.J., 1984. Satellite observations of circulation in the Eastern Bering Sea. J. Geophys. Res. 89, 3663–3678, http://dx.doi.org/10.1029/JC089iC03p03663.
Panteleev, G., Yaremchuk, M., Luchin, V., Nechaev, D., Kukuchi, T., 2012. Variability of the Bering Sea circulation in the period 1992–2010. J. Oceanogr. 68, 485–496, http://dx.doi.org/10.1007/s10872-012-0113-0.
Panteleev, G., Yaremchuk, M., Stabeno, P.J., Luchin, V., Nechaev, D.A., Kikuchi, T., 2011. Dynamic topography of the Bering Sea. J. Geophys. Res. – Oceans 116, C05017, http://dx.doi.org/10.1029/2010jc006354.
Panteleev, G.G., Stabeno, P., Luchin, V.A., Nechaev, D.A., Ikeda, M., 2006. Summer transport estimates of the Kamchatka Current derived as a variational inverse of hydrophysical and surface drifter data. Geophys. Res. Lett. 33, L09609, http://dx.doi.org/10.1029/2005GL024974.
Preisendorfer, R.W., 1988. Principal Component Analysis in Meteorology and Oceanography. Elsevier, New York.
Reed, R.K., Khen, G.V., Stabeno, P.J., Verkhunov, A.V., 1993. Water properties and flow over the deep Bering Sea Basin, summer 1991. Deep. Sea Res. 40, 2325–2334.
Reed, R.K., Stabeno, P.J., 1999. The Aleutian North Slope Current. In: Loughlin, T.R., Ohtani, K. (Eds.), Dynamics of the Bering Sea. University of Alaska Sea Grant, Fairbanks, pp. 177–191.
Rio, M.H., Guinehut, S., Larnicol, G., 2011. New CNES-CLS09 global mean dynamic topography computed from the combination of GRACE data, altimetry, and *in situ* measurements. J. Geophys. Res. – Oceans 116, C07018, http://dx.doi.org/10.1029/2010jc006505.
Roden, G.I., 1995. Aleutian Basin of the Bering Sea: thermohaline, oxygen, nutrient, and current structure in July 1993. J. Geophys. Res. – Oceans 100, 13539–13554, http://dx.doi.org/10.1029/95JC01291.
Sayles, M.A., Aagaard, K., Coachman, L.K., 1979. Oceanographic Atlas of the Bering Sea Basin. University of Washington Press, Seattle & London.
Schumacher, J.D., Alexander, V., 1999. Variability and role of the physical environment in the Bering Sea ecosystem. In: Loughlin, T.R., Ohtani, K. (Eds.), Dynamics of the Bering Sea. Univ. Alaska Sea Grant. Fairbanks, pp. 147–160.
Schumacher, J.D., Reed, R.K., 1992. Characteristics of currents over the continental slope of the eastern Bering Sea. J. Geophys. Res. – Oceans 97, 9423–9433.
Sohn, D., Ciannelli, L., Duffy-Anderson, J.T., 2010. Distribution and drift pathways of Greenland halibut (*Reinhardtius hippoglossoides*) during early life stages in the eastern Bering Sea and Aleutian Islands. Fish. Oceanogr. 19, 339–353, http://dx.doi.org/10.1111/j.1365-2419.2010.00549.x.
SSALTO/DUACS, 2012. SSALTO/DUACS User Handbook: (M)SLA and (M)ADT Near-Real Time and Delayed Time Products. Ramonville St-Agne. France, p. 59.
Stabeno, P.J., Ladd, C., Reed, R.K., 2009. Observations of the Aleutian North Slope Current, Bering Sea, 1996–2001. J. Geophys. Res. – Oceans 114, C05015, http://dx.doi.org/10.1029/2007JC004705.
Stabeno, P.J., Reed, R.K., 1994. Circulation in the Bering Sea basin observed by satellite-tracked drifters: 1986–1993. J. Phys. Oceanogr. 24, 848–854.
Stabeno, P.J., Schumacher, J.D., Ohtani, K., 1999. The physical oceanography of the Bering Sea. In: Loughlin, T.R., Ohtani, K. (Eds.), Dynamics of the Bering Sea. Univ Alaska Sea Grant, Fairbanks, pp. 1–28.
Trenberth, K.E., Hurrell, J.W., 1994. Decadal atmosphere–ocean variations in the Pacific. Clim. Dyn. 9, 303–319.
Vestfals, C.D., Ciannelli, L., Duffy-Anderson, J.T., Ladd, C., 2014. Effects of seasonal and interannual variability in along-shelf and cross-shelf transport on ground-fish recruitment in the eastern Bering Sea. Deep-Sea Res. II 109, 190–203, http://dx.doi.org/10.1016/j.dsr2.2013.09.026.
Wilderbuer, T.K., Hollowed, A.B., Ingraham, W.J., Spencer, P.D., Conners, M.E., Bond, N.A., Walters, G.E., 2002. Flatfish recruitment response to decadal climatic variability and ocean conditions in the eastern Bering Sea. Prog. Oceanogr. 55, 235–247.
Wolter, K., Timlin, M.S., 1993. Monitoring ENSO in COADS with a seasonally adjusted principal component index. In: Proceedings of the 17th Climate Diagnostics Workshop. NOAA/N MC/CAC. NSSL. Oklahoma Clim. Survey. CIMMS and the School of Meteor. Univ. of Oklahoma. Norman, OK, pp. 52–57.
Wolter, K., Timlin, M.S., 1998. Measuring the strength of ENSO – how does 1997/98 rank? Weather 53, 315–324.

Deep-Sea Research II 109 (2014) 14–26

Contents lists available at ScienceDirect

Deep-Sea Research II

journal homepage: www.elsevier.com/locate/dsr2

Thermal regimes in the Chukchi Sea from 1941 to 2008

Vladimir Luchin [a], Gleb Panteleev [b,c,*]

[a] V.I.Il'ichev Pacific Oceanological Institute, Far Eastern Branch, Russian Academy of Sciences (POI FEB RAS), 43 Baltiyskaya Street, Vladivostok 690041, Russia
[b] International Arctic Research Center, University of Alaska, 930 Koyukuk Dr., P.O. Box 757340, Fairbanks, AK 99775, USA
[c] National Research Tomsk Polytechnic University, Tomsk, Russia

ARTICLE INFO

Available online 2 July 2014

Keywords:
Chukchi sea
Thermal regimes
Interannual variability
4Dvar data assimilation

ABSTRACT

The summer (June–October) temperature observations in the surface (0 m) and subsurface (20 m-bottom) Chukchi Sea layers collected from 1941 to 2008 have been analyzed using the self-consistent data recovery procedure based on correlation analysis and iterative empirical orthogonal function (EOF) decomposition. The analysis of the surface and subsurface EOFs identified "cold", "normal", and "warm" thermal states with variability of 2–3 years, and also 4–7 years. We found that the Chukchi Sea water temperature has gradually increased since 1941. Warming in the surface layer since 1941 has been minimal in the Bering Strait (0.012 °C yr^{-1}, total 0.8 °C) and maximal in Long Strait (0.030–0.036 °C yr^{-1}, total 2.0–2.4 °C). In the subsurface layer, temperatures have increased about half as much; minimal (0.0030–0.0075 °C yr^{-1}, total 0.2–0.5 °C) in Long Strait and rather uniform (0.010–0.015 °C yr^{-1}, total 0.7–1.0 °C) for the remaining Chukchi Sea. Analysis of the satellite sea-surface height anomaly data shows that during the "warm" periods there is a stronger flow through the Bering Strait and intensification of the northwestward currents in the central Chukchi Sea. Extensive correlation analysis shows that the thermal state of the Chukchi Sea agrees well with the flow of Pacific water through the Bering Strait and by an increase of the global atmospheric temperature. In addition, typical circulation during "warm" and "cold" periods was reconstructed using four-dimensional variational (4Dvar) data assimilation into the ocean model, and estimates of volume and heat fluxes in the Chukchi Sea during "cold" and "warm" periods were derived which are consistent with EOF and correlation analyses.

1. Introduction

The shallow Chukchi Sea (CS) (Fig. 1) is located between the Arctic and Pacific oceans. Because of this location, CS thermal conditions are defined by the large-scale atmospheric and oceanic processes, which occur in both oceans. The Chukchi Sea is covered by ice for most of the year. According to long-term observations, the concentration of ice in the Chukchi Sea begins to decrease in June, and reaches its minimum in August–September. At that point, ice begins increasing again, and by November–December, new ice completely covers the Chukchi Sea. There is also significant interannual variability in ice cover in the Chukchi Sea in summer. During the warmest years, about 80–85% of the Chukchi Sea can be free of ice, though ice can cover up to 90% of the CS during the coldest periods (Plotnikov and Pustoshnova, 2012).

Large-scale ice, ocean, and atmosphere variability in the Arctic Ocean have been analyzed in many publications (e.g. Bjorgo et al., 1997; Comiso, 2002; Parkinson et al., 1999; Rothrock et al., 1999; Stroeve et al., 2007; Tucker et al., 2001; Wadhams and Davis, 2000). It was also shown that interannual variability as well as atmosphere and ice cover in the Arctic Ocean exhibit both a linear trend and oscillation with a period of 10, 20, and 50–60 years (e.g., Raspopov et al., 2004; Frolov et al., 2007). Several mechanisms were discussed. In particular, Empirical Orthogonal Function (EOF) analysis of the atmospheric pressure showed that the first (the Arctic Oscillation, AO) and second (the Dipole Oscillation, DO) components are associated for the observed diminishing of ice cover and ice thickness (e.g. Proshutinsky and Johnson, 1997; Wang et al., 2009). Meanwhile, the observed changes in ice cover are also related to global warming (Thompson and Wallace, 1998) and the culmination of an ice/ocean – albedo positive feedback (Ikeda et al., 2003; Wang et al., 2005). These large-scale factors obviously affect CS as well, though intense flow through the Bering Strait also applies strong additional forcing to the CS state (e.g., Coachman et al., 1975; Woodgate et al., 2005a, 2005b).

The flow of Pacific water through the Bering Strait brings to the Arctic Ocean about one-third of the total freshwater inflow to the Arctic Ocean (Serreze et al., 2006) and can melt out $1–2 \times 10^6$ km^2 of the one meter thick ice there (Beszczynska-Möller et al., 2011; Woodgate et al., 2010). For this reason, the Bering Strait flow has significant impact on the thermochaline and biological condition

* Corresponding author at: International Arctic Research Center, University of Alaska, 930 Koyukuk Dr., P.O. Box 757340, Fairbanks, AK 99775, USA.
E-mail addresses: vluchin@poi.dvo.ru (V. Luchin), gleb@iarc.uaf.edu (G. Panteleev).

http://dx.doi.org/10.1016/j.dsr2.2014.05.007
0967-0645/

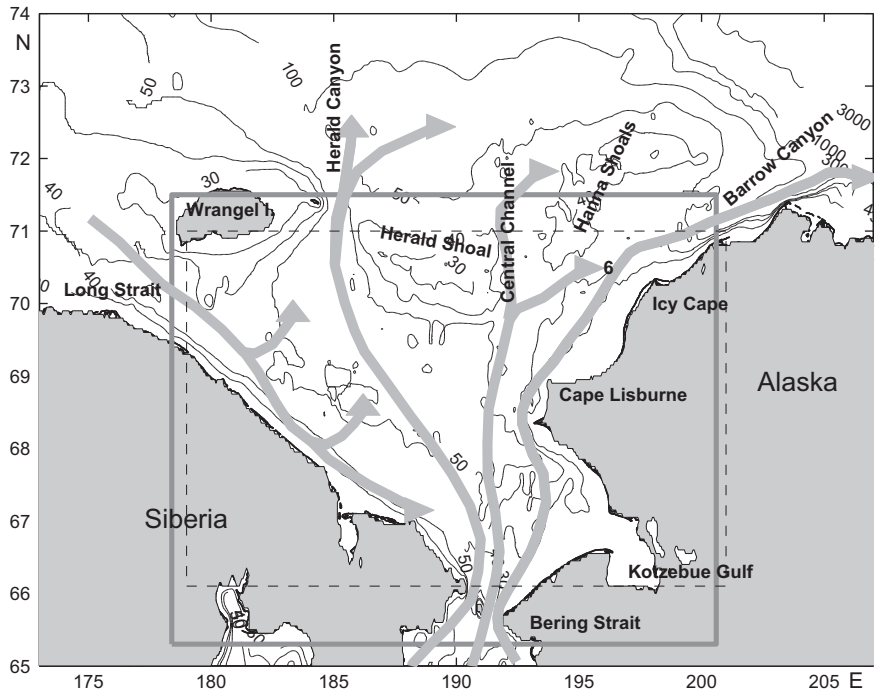

Fig. 1. Bottom topography in the CS. Thin dashed and solid thick lines designate the domains for EOF analysis and numerical modeling. Thick gray lines designate the schematic of local circulation.

in the entire Western Arctic Ocean (e.g., Killworth and Smith, 1984; Shimada et al., 2001; Steele et al., 2004; Walsh et al., 1989; Aagaard and Carmack, 1989) and plays an important role in the global freshwater cycle (e.g., Aagaard and Carmack, 1989; Wijffels et al., 1992; Woodgate and Aagaard, 2005), and possibly even the world climate (De Boer and Nof, 2004).

According to Aagaard et al. (2006), the observed warming and freshening of the upper halocline in the Pacific sector of the Arctic Ocean is the result of the penetration of Atlantic and Pacific water into the Arctic Ocean. Further, the salinity of Pacific water entering into the deep Arctic Ocean is defined by processes in the deep regions of the Bering Sea, Eastern Bering Sea shelf and Chukchi Sea.

Due to geographical proximity (close geographical locations), thermohaline structures in the Northern Bering and Chukchi Seas are formed by very similar processes. These include the persistence of northward flow in both regions, similarity in the seasonal cycle, and processes of ice formation in the winter polynyas located in the Gulf of Anadyr and along the Alaskan Coast between Cape Lisburne and Cape Barrow (Aagaard et al., 1981; Cavaleri and Martin, 1994; Gladyshev, Khen, 1999; Hu et al., 2011; Itoh et al., 2012; Schumacher et al., 1983).

It has also been shown that oceanic processes in the CS and Northern Bering Sea are regulated externally by the sea-level gradient between the Pacific and Atlantic oceans and by wind (e.g. Coachman and Aagaard, 1966; Shtokman, 1957). It is generally hypothesized that this gradient is of steric origin (Coachman et al., 1975; Stigebrandt, 1984) due to evaporation and precipitation rates that differ between the Pacific Ocean (precipitation prevails over evaporation and sea level is elevated) and the Atlantic Ocean (evaporation dominates precipitation and sea level is reduced). This sea-level gradient is believed to drive the mean northward flow of approximately $0.8–1.0\times10^6$ m^3 s^{-1} from the Bering Sea towards the Arctic Ocean. The schematic of the Chukchi Sea circulation is shown in Fig. 1. The inflow of $\sim0.9\times10^6$ m^3 s^{-1} through the Bering Strait generates three branches through the Herald and Barrow Canyons, and the Central Channel. On average, there is also a weak ($\sim0.1\times10^6$ m^3 s^{-1}) inflow through the Long Strait, though this flow can vary significantly—from 1×10^6 m^3 s^{-1} inflow to 1×10^6 m^3 s^{-1} outflow (Münchow et al., 1999; Panteleev et al., 2010).

Basic understanding of CS dynamics has improved since earlier studies in the 1950s, 1960s, and 1970s (Coachman et al., 1975; Gudkovich, 1961, 1962; Shtokman, 1957) due to both observational (Aagaard et al., 1985; Weingartner et al., 2005; Woodgate et al., 2005a) and modeling studies (Nihoul et al., 1993; Overland and Roach, 1987; Panteleev et al., 2010; Proshutinsky, 1986; Proshutinsky et al., 1995; Spall, 2007; Spaulding et al., 1987; Winsor and Chapman, 2004). In particular, it was shown that local wind significantly modifies the Bering Strait inflow at time scales from synoptic to inter-annual, sometimes blocking it completely or even reversing it (see Aagaard et al., 1985; Panteleev et al., 2010; Roach et al., 1995; Woodgate et al., 2005a). It was also shown that bottom topography is responsible for the three branches of Pacific water that transit the CS; the Alaskan Coastal Current and the Central and Herald outflows (Coachman and Aagaard, 1966; Coachman et al., 1975; Weingartner et al., 1998; Woodgate et al., 2005a). Synoptic and seasonal variability are regulated by the wind and sea ice conditions.

It is well known that warm Pacific water defines CS thermal conditions (Carmack, 1986; Coachman and Aagaard, 1974; Coachman et al., 1975; Codispoti, 1979; Fedorova and Yankina, 1963; Overland and Roach, 1987; Proshutinsky, 1986; Wilson and Wallace, 1990; Woodgate et al., 2005a, 2005b). Fedorova and Yankina (1963) estimated that Pacific water brings heat which, averaged annually, is enough to melt approximately 50% of the entire winter sea-ice area in the CS. Another example of this influence was given by Woodgate et al. (2006), who showed that the increase of Bering Strait heat input alone between 2001 and 2004 could have melted 640,000 km^2 of one-meter-thick ice.

During the 2001–2007, there has been a gradual increase of heat flow through the Bering Strait (Woodgate et al., 2006, 2010) and a corresponding decrease of the observed ice thickness (Steele et al., 2004; Woodgate et al., 2010). According to

Woodgate et al. (2010), mean annual temperature in the Bering Strait increased from −0.4 °C to +0.4 °C between 2001 and 2007. Thus, heat flux through the Bering Strait ($\sim$5.0–5.7 $\times 10^{20}$ J yr^{-1}) in 2007 was comparable to the annual shortwave radiation flux in the CS, and according to Woodgate et al. (2010), this heat was sufficient to melt one-third of the total ice that was lost from the Arctic Ocean during the summer. However, this estimate does not take into account the possible heat loss to the atmosphere.

The interannual variability of CS hydrophysical parameters has been analyzed in a number of publications (e.g. Coachman and Aagaard, 1988; Fedorova and Yankina, 1963; Nikiforov and Shpayher, 1980; Roach et al., 1995; Shpayher and Fedorova, 1978; Shpayher et al., 1968; Wang et al., 2010; Woodgate et al., 2006, 2010). These studies, however, are based on the analysis of observations collected during variable time periods, from several years (e.g. Shimada et al., 2006) to 1–3 decades (e.g. Coachman and Aagaard, 1988; Fedorova and Yankina, 1963; Roach et al., 1995; Shpayher and Fedorova, 1978; Wang et al., 2010; Woodgate et al., 2006, 2010), or on data sets that do not cover the entire CS (e.g. Luchin and Semiletov, 2005).

In this study we analyze CS thermal conditions using all available *in situ* temperature data collected from 1941 to 2008. In the next section we describe the data sets and the EOF approach used for analysis. The results of the EOF decomposition and identification of climatological thermal regimes are presented in Section 3. In Section 4 we provide the correlation analysis between CS thermal conditions and several parameters that represent variability in the ocean and atmosphere. In Section 5 we describe the results of the four-dimensional reconstruction of CS circulation during "warm" and "cold" periods. Section 6 summarizes our results.

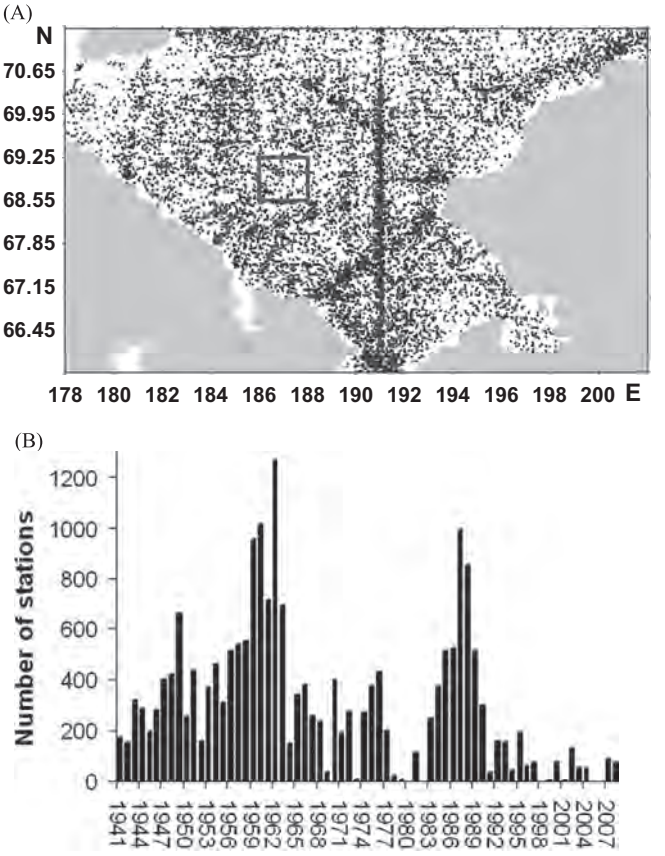

Fig. 2. (A) Spatial and (B) temporal distributions of CS temperature observations 1941–2008. Black square (186–188°E, 68.55–69.25°N) shows the spatial scale of the utilized bin.

2. Data and data analysis

For our study we utilized 20,369 temperature profiles collected in the CS between 1941 and 2008 (Fig. 2). Most of the data were from the World Ocean database developed at the Russian Research Institute of Hydrometeorological Information (http://esimo.ru/meta/datasets/index.jsp) and from the international Word Ocean Database 2009 (WOD09) (http://www.nodc.noaa.gov/OC5/WOD09/pr_wod09.html). The distribution of these CS data is highly unequal in both time and space (Fig. 2).

Using this database we formed two arrays of oceanographic observations. The first array includes surface (0 m) observations during July–September and defines CS thermal conditions during the period of maximum summer ocean heating (16,154 stations). The second array includes all subsurface (20 m below the surface to the bottom) June–October observations (18,926 stations). We intentionally apply two different temporal windows because summer atmospheric heating is the major factor that defines the thermal state of the surface layer, and including surface data sampled in early June and late October may contaminate this effect in years with insufficient observations during the summer period. The subsurface layer is more inertial and applying the larger temporal window allowed us to use a larger volume of data and to fill some gaps in the obtained time series.

Initial data preprocessing included quality control and vertical interpolation of the available temperature profiles. Subsequent analysis included several steps. First, we averaged temperature over the horizontal 2° longitude × 0.7° latitude (83 km × 78 km) bins and calculated three-dimensional mean climatological (1941–2008) temperature distributions for each month (June–October). Second, we calculated the temperature anomalies with respect to the obtained monthly climatological temperature for available temperature profiles and averaged them over each 2° longitude × 0.7° latitude (83 km × 78 km) bin. Thus, we formed a monthly anomaly array for each month (June–October) from 1941 to 2008. Finally, taking into account that large-scale thermal processes occur on a temporal scale of several months or more, we calculated the mean annual anomalies for July–September (June–October) for the surface (subsurface) layers, respectively. The obtained annual anomalies averaged for the July–September (June–October) for the surface (subsurface) layers were utilized for EOF analysis described below.

Due to irregular data distribution, the obtained time series of the temperature anomalies have a large number of gaps in approximately 40% of the bins. To fill these gaps we applied a self-consistent procedure of data recovery based on correlation analysis and iterative EOF decomposition of the available data previously utilized for the analysis of the thermal regimes and for ice hindcast/forecast in the Okhotsk Sea (Luchin and Zhigalov, 2006; Plotnikov, 1988).

The procedure of the data gap filling includes two steps. First we formed the time series of the temperature anomaly for each 2° longitude × 0.7° latitude (83 km × 78 km) bin and calculated the correlation coefficients $R_{i,j}$ between jth bin and all other bins. We also estimated the corresponding confidence level $T_{i,j} = R_{i,j}\sqrt{(N_{i,j}-2)/(1-R_{i,j}^2)}$, where $N_{i,j}$ is the number of overlapping elements in the temperature time series in ith and jth bins (i.e., $N_{i,j}=N_i \cap N_j$). If $T_{i,j}$ was greater than the critical value of the t-test (Hazewinkel, 2001), the corresponding time series were used to recover missing values in the time series Y in the jth bin using the values of the time series X from other bins, through the standard linear regression equation

$$Y_i = A_0 + A_1 * X_i, A_0 = \overline{Y} - A_1 * \overline{X}, A_1 = ((\overline{X * Y}) - (\overline{X}) * (\overline{Y}))/((\overline{X^2} - (\overline{X})^2),$$

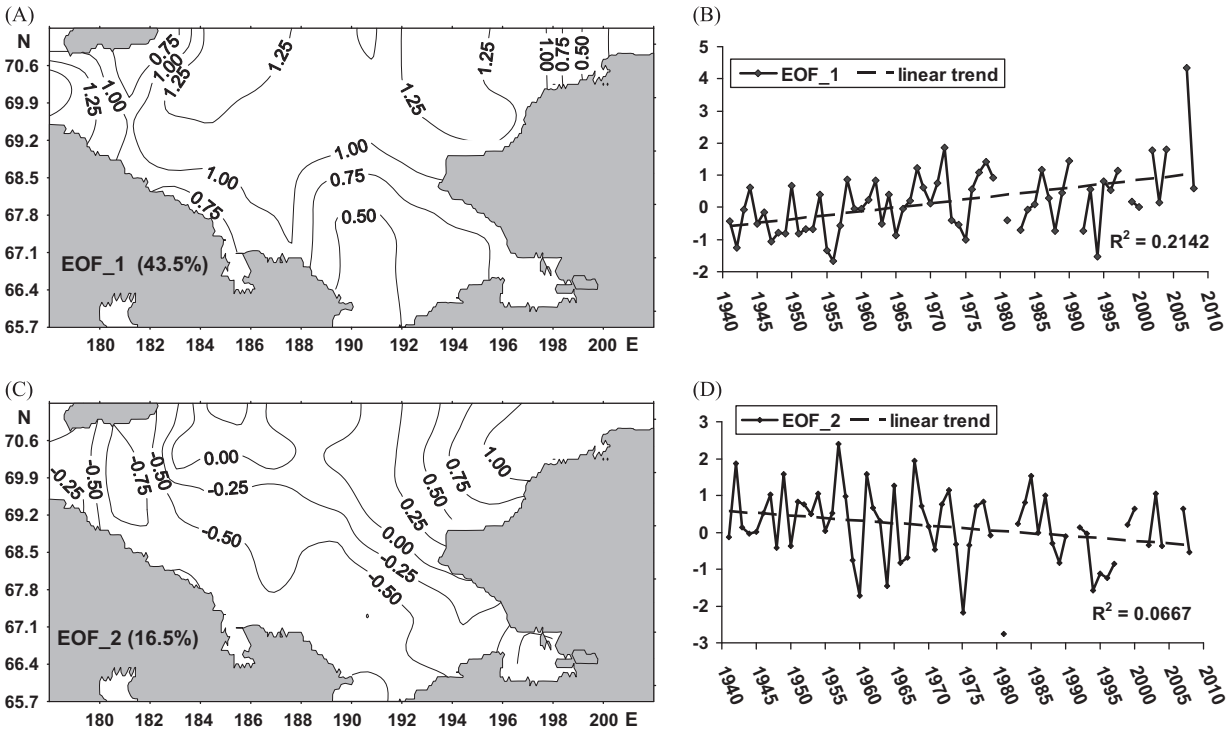

Fig. 3. Spatial distribution and temporal amplitude of the first (A, B) and second (C, D) EOFs of the surface (0 m) CS water temperature anomaly decompositions. Percentages in parentheses indicate the amount of inter-annual variability described by the corresponding EOF.

where overbars designate time averaging. Finally, missing values from time series Y are defined as $Y_m = \sum Y_i * F_i / \sum F_i$, where $F_i = T_i / \Sigma T_i$. The summation in the last formulas included the 4 bins for the surface and 5 bins for the subsurface with the highest correlation. The number of utilized bins were defined empirically through the bootstrapping procedure.

After the first step approximately 7% of the gaps remained; in order to fill these gaps we applied an additional recovering procedure based on iterative EOF decomposition and recovery (Beckers and Rixen, 2003). At the beginning of this procedure the gaps are filled with 0 values; after EOF decomposition the gap values are recovered using several vectors obtained from the EOF decomposition. Using the conventional bootstrapping procedure, we found that the first four EOFs usually produce the best recovery. The procedure of EOF decomposition and gap re-filling is repeated until convergence.

Figs. 3 and 4 show spatial and temporal distribution of the first and second EOFs of the temperature for the surface (0 m) and subsurface temperature averaged between 20 m and the bottom. In the surface layer, the first and second EOFs describe, respectively, 43.5% and 16.5% of the temporal variability (Fig. 3A and C). Fig. 3A shows that the first EOF describes synchronic cooling or heating of CS surface water with minimum amplitude in the Bering Strait and near Barrow Canyon. In most of the CS, the EOF amplitude gradually increases toward the northern regions.

In the subsurface layer, the first and second EOFs describe, respectively, 33.3% and 14.8% of the temporal variability (Fig. 4A and C). The spatial distribution of the first subsurface EOF is rather uniform for most of the CS with minima in Long Strait and Barrow Canyon.

The second EOFs for the surface and subsurface layers exhibit typical anti-symmetric (dipole) patterns (Figs. 3C and 4C). This pattern may describe the inter-annual anti-correlation between the eastern and western parts of the CS, but it could also be an artifact due to orthogonality of the EOF modes (Dommenget and Latif, 2002).

The visual similarity between surface and subsurface EOFs (Figs. 3A and 4A) and high temporal correlation of 0.62 between the first modes of the surface and subsurface EOFs, suggest that the temperature in both layers was controlled by similar physical processes. However, there are some differences in the location of the surface and subsurface maxima and minima. The difference is especially significant in Bering Strait (Long Strait), where the surface EOF has a local minimum (maximum), while the subsurface EOF in these regions exhibits the reverse (Figs. 3A and 4A). This difference could be caused by the following.

First, highly variable and intensive currents exist in the Bering Strait, promoting enhanced vertical and horizontal mixing. Vertical mixing between subsurface and surface layers decreases the temperature of the surface layer and minimizes the range of inter-annual variability. The spatial velocity gradients in the other parts of the CS are much weaker (e.g. Panteleev et al., 2010), and we suggest that less intensive vertical and horizontal mixing processes occur in these regions.

Second, surface thermal conditions in the Long Strait are mostly defined either by advection from the East Siberian Sea or Pacific water flow from the Bering Strait. For this reason, the temperature in the Long Strait varies from 0 to 2 °C, if advection from East Siberian Sea dominates, or 2–4 °C, if Pacific water reaches the Long Strait (Luchin and Semiletov, 2005). This results in significant interannual variability in surface water temperature in the Long Strait (Fig. 3A). In the subsurface layer, the Long Strait is usually occupied by very cold (below 0 °C) water (e.g., Fig. 6 from Panteleev et al., 2010) and for this reason, subsurface EOF has a local minimum here, indicating depressed interannual variability (Fig. 4A).

The temporal evolution of surface and subsurface layer temperatures (Figs. 3B and 4B) exhibits a positive trend, which is consistent with the overall warming of the CS. The spatial variability of the first EOF (Fig. 3A) indicates that surface warming is minimal in the Bering Strait (0.012 °C yr^{-1}, total 0.8 °C), while strong maxima are seen in the northern CS and in Long Strait

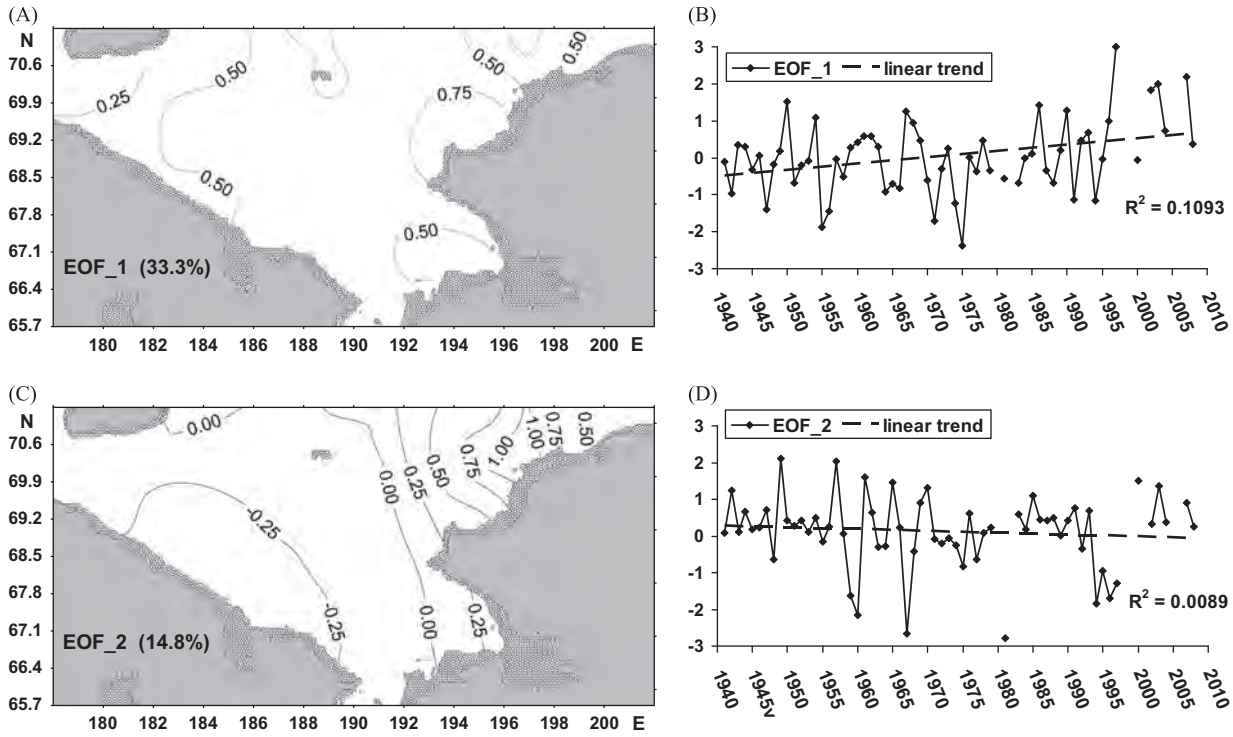

Fig. 4. Spatial distribution and temporal amplitude of the first (A, B) and second (C, D) EOFs of the sub-surface (20 m bottom) CS water temperature anomaly decompositions. Percentages in parentheses show the amount of inter-annual variability described by the corresponding EOF.

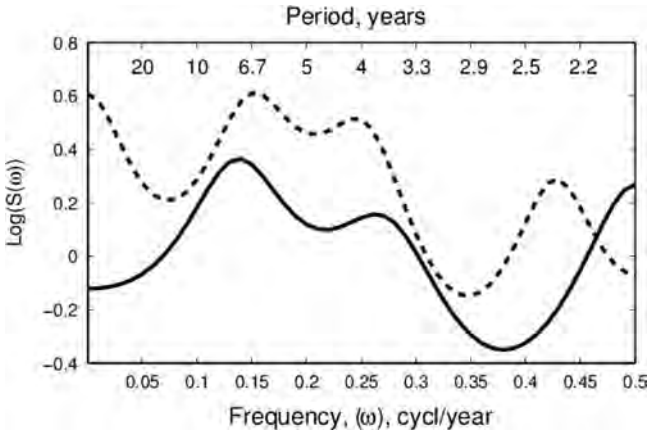

Fig. 5. The frequency spectrum of the first EOFs for the surface (solid line) and subsurface (dashed line) layers. The inverse frequency ($1/\omega$) gives the period in years.

($0.030–0.036\ ^{\circ}C\ yr^{-1}$, total 2.0–2.4 °C). In the subsurface layer, the temperature increase is only half as great; it is minimal (0.0030–$0.0075\ ^{\circ}C\ yr^{-1}$, total 0.2–0.5 °C) in Long Strait and rather uniform ($0.010–0.015\ ^{\circ}C\ yr^{-1}$, total 0.7–1.0 °C) in the remaining CS. The frequency spectra of the first EOF modes are shown in Fig. 5. Relative maximum surface EOF energy occurs at a period of 2 and over a period of 3.5–7 years, while maximum variability of the subsurface EOF occurs over periods of 2–3 and approximately 3.5–6.7 years.

Spatial maps of the second EOFs in the surface and subsurface have similar distributions and are highly correlated in time ($R_{corr}=0.73$). This can be related to the variability of local barotropic currents and in particular to the periodic intensification of total transport through Herald or Barrow canyons. These hypotheses, however, must be viewed with caution because EOF analysis is based on pure statistical assumptions and does not take dynamics into account; dynamics can be significant for the relatively small CS, where topography controls a significant part of the local circulation. First EOFs (Figs. 3A and 4A) describe two to three times more inter-annual variability than second EOFs (Figs. 3C and 4C). Therefore, we will concentrate our attention on the analysis of the first surface and subsurface EOFs.

3. Thermal regimes in the Chukchi Sea

The thermal state for each year can be classified in accordance with the amplitude of the first EOFs. We find it reasonable to subdivide CS thermal conditions into five basic categories: "extreme cold," "extreme warm," "cold," "warm," and "normal," following the algorithm described by Eliseeva and Yuzbashev (1998). The time series of the first EOFs can be used as follows. First we remove the temporal trend, calculate mean de-trended temperature for each year, corresponding standard deviations σ and temperature anomalies ΔT for each year, defined as a difference for each particular year and mean de-trended temperature during 1941–2008. Then, the criterias for "normal," "cold," and "warm" states could be, respectively, defined as $|\Delta T| < 0.674\sigma$, $-2\sigma < \Delta T < -0.674\sigma$, and $0.674\sigma < \Delta T < 2\sigma$. The criteria for the "extreme cold" and "extreme warm" are, respectively, $\Delta T < -2\sigma$ and $2\sigma < \Delta T$.

The results of this classification for the surface and subsurface layers are shown in Table 1. Note that removing the trend was necessary for analyzing thermal condition in the Chukchi Sea and its variability with periods of less than 10 years.

Analysis of Table 1 shows that usually the thermal condition of the subsurface layer coincided with, or at least was very close, to the thermal condition of the surface layer. We found only three years (1971, 1997, and 2003) when thermal conditions in the surface and subsurface layers differed significantly. Francis et al. (2011) analyzed the variability of CS wave conditions and identified several extremely strong storms in 1997 and 2003.

We hypothesize that these events could have mixed relatively warm surface water with the colder subsurface layer, increasing (decreasing) the temperature of the subsurface (surface) layer. It is not clear why the surface and subsurface layers were so different in 1971.

Using the results of the classification in Table 1, we recovered the typical temperature distributions for the "cold," "normal," and "warm" years, extracting temperature profiles from the database for the corresponding group of years and averaging them for the surface and subsurface layers. As a result, we obtained the six temperature distributions shown in Figs. 6 and 7. According to these results, large-scale surface and subsurface water temperatures exhibit similar variability during "cold," "normal," and "warm" years. The most typical feature of this variability is the spread of the warm and cold waters in both layers under different climatological states. Taking into account that in the "warm" state, more than 80% of the CS measures higher than 4 °C in the surface and 1 °C in the subsurface layers, and that the similarity in the spatial position between surface 4 °C and subsurface 1 °C isotherms, we will consider these isotherms as a boundary between warm and cold water in the surface and subsurface layers. As seen in Figs. 6 and 7, the 4 °C isotherm in the surface layer and the 1 °C isotherm in the subsurface layer mark the boundaries between warm and cold waters. The basic difference between the three typical states is the size of the region occupied by the water with temperature >4 °C (1 °C) in surface (subsurface) layers. During "cold" years, the warm water area is minimal and the warm water spreads mostly along the Alaskan coast. During the "warm" years, we observe warm water in almost the entire CS with the exception of the western part near Long Strait.

Atmospheric heating mostly affects the surface layer, so it is logical to use the temperature distribution in the quasi-isolated subsurface layer in order to analyze the spread of Pacific water in the CS. Analyzing Fig. 7, we suggest that during "cold" years the warm Pacific water from the Bering Strait spreads along the Alaskan coast and through Herald Canyon. Negative temperatures in Barrow Canyon and Long Strait may indicate the significant decrease or even absence of Pacific water in these regions (Fig. 7A).

During "warm" years (Figs. 6 and 7c), we suggest that the flow of Pacific water along the Alaskan coast towards Barrow Canyon is more intense than in "cold" years. We also observe significant areas around the Herald Canyon occupied by warm waters in both surface and subsurface layers, suggesting more intensive northward flow in this region. In Long Strait the warm water occupies the surface layer, indicating that Pacific water may reach this region as well. During "normal" years (Figs. 6B and 7B), the Pacific water is still present in both the Herald and Barrow Canyons, but absent in the Long Strait, suggesting that this flow is negligible.

There are two basic causes of a different temperature distribution in "cold" and "warm" years: (1) variation of the Pacific water flow through Bering Strait, and (2) interannual variability in atmospheric heat flux. To analyze the relative impact of these factors we plot the difference in temperature between "warm" and "cold" years (Fig. 8).

Fig. 8A indicates that the surface difference is approximately 2–3 °C in the western CS and 4–5 °C in the northeastern regions. Interestingly, the highest difference, 6 °C, was found in the subsurface layer between Alaskan coast and Hanna Shoal, indicating that the thermal state of the subsurface layer in "warm" years is extremely different from the thermal state in "cold" periods. Both distributions illustrated in Fig. 8 show a small temperature difference (<1 °C) in the Bering Strait.

Atmospheric forcing occurs on a scale of about 1000–2000 km (e.g., Serreze et al., 1993; Serreze and Barrett, 2008). Therefore, the interannual variability of atmospheric forcing should provide more-or-less uniform heating/cooling over the entire CS, but this is not evident in Fig. 8. Thus, we can conclude that the variability of Pacific water flow is the major factor that explains the temperature difference between "cold" and "warm" years.

Table 1
Typical CS thermal conditions from 1941 to 2008. Standard font identifies years when a similar thermal state existed in the surface and subsurface layers. Bold font indicates years when thermal conditions in surface and subsurface differed significantly, i.e. belong to the two non-adjacent states (e.g. "cold" and "warm"). **E_W**—Extreme warm, **W**—Warm, **N**—Normal, **C**—Cold, **E_C**—Extreme cold years.

Years	Surface	Subsurface	Years	Surface	Subsurface
1941	N	N	1975	C	E_C
1942	C	N	1976	N	N
1943	N	W	1977	W	N
1944	W	W	1978	W	N
1945	N	N	1979	N	N
1946	N	N	1980	No data	No data
1947	C	C	1981	C	C
1948	N	N	1982	No data	No data
1949	N	N	1983	C	C
1950	W	W	1984	N	N
1951	N	N	1985	N	N
1952	N	N	1986	W	W
1953	N	N	1987	N	N
1954	W	W	1988	C	C
1955	C	C	1989	N	N
1956	C	C	1990	W	W
1957	N	N	1991	No data	C
1958	W	N	1992	C	N
1959	N	N	1993	N	N
1960	N	N	1994	E_C	C
1961	N	W	1995	N	N
1962	W	W	1996	N	N
1963	N	N	1997	**N**	**E_W**
1964	N	C	1998	No data	No data
1965	C	N	1999	C	No data
1966	N	C	2000	C	N
1967	N	W	2001	No data	No data
1968	W	W	2002	W	W
1969	N	N	2003	**C**	**W**
1970	N	N	2004	W	N
1971	**W**	**C**	2005	No data	No data
1972	W	N	2006	No data	No data
1973	N	N	2007	E_W	W
1974	C	C	2008	N	N

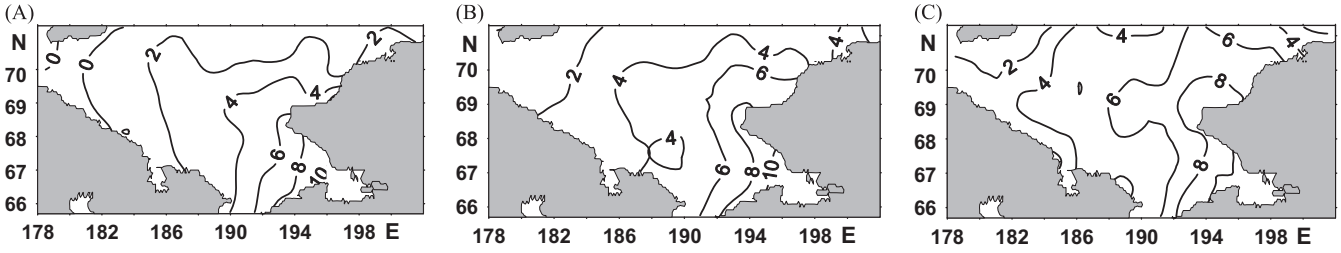

Fig. 6. Typical temperature distribution (°C) during (A) "cold", (B), "normal", and (C) "warm" years at the surface.

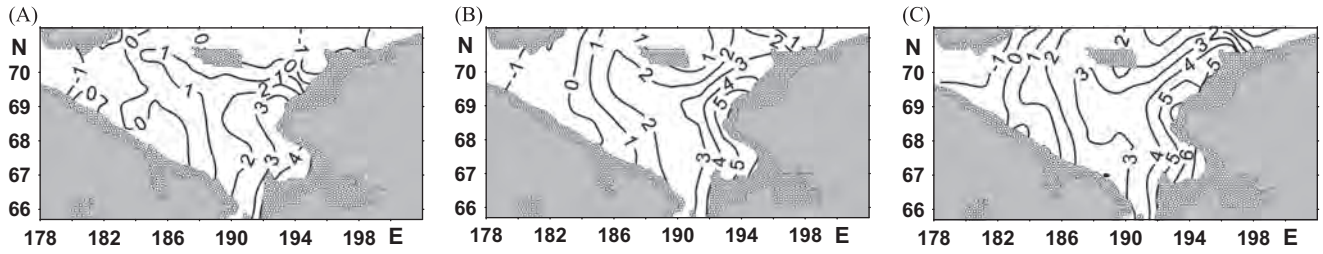

Fig. 7. Typical temperature distribution (°C) during (A) "cold", (B), "normal", and (C) "warm" years at 30 m depth.

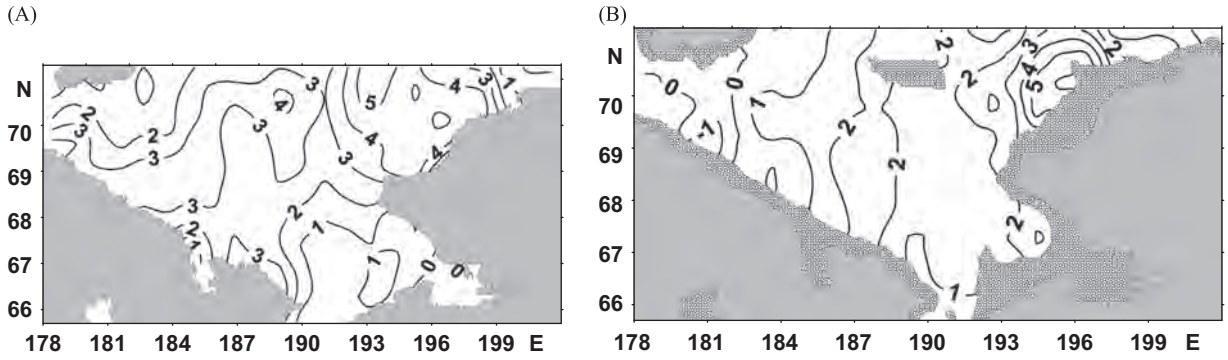

Fig. 8. Difference between mean temperature (°C) in "warm" and "cold" years (A) at the surface and (B) at 30 m depth.

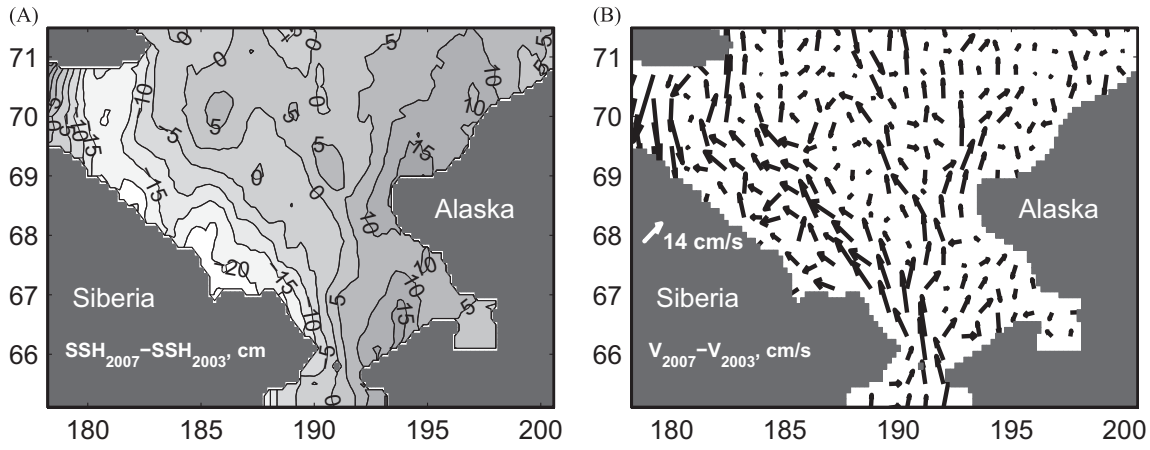

Fig. 9. Difference (A) between mean CS sea surface height (SSH) distribution in 2007 (extreme "warm" year) and 2003 (cold year) and (B) corresponding near-surface geostrophic currents.

The temperature maps in Figs. 6–8 indicate only qualitative differences between "cold" and "warm" year circulation. In order to obtain a quantitative estimate we averaged available Envisat satellite along-track sea-level anomaly (SLA) observations (www.aviso.oceanobs.com) for the ice-free regions during 2007 (a "warm" year) and 2003 (a "cold" year), and calculated mean SLA distributions for these two years. The difference between the 2007 SLA and the 2003 SLA is shown in Fig. 9A. This map can also be viewed as a difference between two absolute sea surface heights (SSHs) between the chosen years.

Taking into account geostrophic momentum balance in the CS (Panteleev et al., 2010; Proshutinsky, 1986; Spaulding et al., 1987) we estimated the difference between 2007 and 2003 geostrophic circulations (Fig. 9B). This analysis indicates a 2007 increase in northward flow of 10–15 cm s^{-1} in almost all CS regions relative to 2003. This strong current would allow Pacific water to flow from the Bering Strait to Long Strait in approximately 70–80 days. Approximately the same time would be needed for water to flow from the Bering Strait to Herald and Barrow Canyons. The estimate of the circulation difference between 2007 and 2003 is in good agreement with the difference in temperature fields during "cold" and "warm" years (Figs. 6 and 7). Thus, Fig. 9 can be viewed as an estimate of the difference in circulation between "warm" and "cold" years in the CS. It is necessary to note that satellite observation near the coast usually include significant errors due to spatial and resolution inaccuracy in our knowledge of the Geoid and effects of the coastal currents. This may explain unrealistic currents in the Long Strait (Fig. 9B).

4. Correlation analysis

The derived time series of EOF amplitudes (Figs. 3B and 4B) were used to identify significant correlations between CS thermal conditions and important parameters describing ice, ocean, and atmosphere conditions in the Pacific and Arctic oceans. In particular, we analyzed correlations between first (summer) EOFs (Figs. 3B and 4B) and the following parameters:

(1) Global Mean Land Ocean Temperature (GMLOT) for 1948–2008 from http://www.esrl.noaa.gov/psd/data/climateindices/.
(2) Atmospheric temperature at 1000 mb in the Southern CS (ATSCS) for 1958–1997 from http://www.esrl.noaa.gov/psd/cgi-bin/data/timeseries/timeseries1.pl. These time series were derived from NCEP/NCAR reanalysis for the area 65–67.5°N and 187.5–192.5°E.
(3) *in situ* observations of the Atmospheric Temperature in the Anadyr (ATA) for 1941–2008. http://cdiac.ornl.gov/ftp/russia_daily/Russia_stations/25563.txt.
(4) Ice Conditions (% of ice cover) in the CS (ICCS) and Northern Bering Sea (ICNBS) for 1950–2008 and 1960–2008, respectively. These ice data were obtained from the historical archives of the Russian Hydrometeorologycal Service (1950–1991) and from National Oceanic and Atmospheric Administration (NOAA) and Russian satellites (1992–2008).
(5) *in situ* observations from moorings of the near-bottom temperature (WTNB), salinity (WSNB), and volume transport (WVT) in the Bering Strait for 1990–2003 (Woodgate et al., 2006, 2010). The time series for these observations are available since 1990 but have several gaps.
(6) Pacific North American (PNA) and AO indexes for 1950–2008 from www.esrl.noaa.gov/psd/data/climateindices.
(7) The first mode of the EOF decomposition of the Water Temperature anomaly in the Bering Sea (WTBS) from May to August at 50 m for 1950–2001 (Luchin and Sokolov, 2007)
(8) The Meridional Wind component near the Bering Strait (MWBS) at 1000 mb for 1948–2008 (http://www.esrl.noaa.gov/psd/cgi-bin/data/timeseries/timeseries1.pl). The time series were derived from NCEP/NCAR reanalysis for the area 65–67.5°N and 187.5–192.5°E.
(9) Surface temperature in the Bering Strait (SST_BS) for 1948–2008 from http://www.esrl.noaa.gov/psd/cgi-bin/data/timeseries/timeseries1.pl. The time series were derived from NCEP/NCAR Reanalysis for the region 65.7–67.6°N, 187.5–193.1°E.

We suggest the analysis of the correlation between derived EOFs and the indices described above may clarify the relationship between the thermal state of the CS and (a) global processes (e.g., GMLOT); (b) ocean–atmosphere processes in the Northern Hemisphere (e.g., PNA); (c) local ocean–atmosphere processes in the CS and surrounding areas (ATSCS, ATA, ICCS, ICNBS, WTNB, WSNB, WVT, WTBS, MWBS, SST_BS).

Monthly estimates of the outlined parameters were averaged for spring (March–May) and summer (July–September). The estimates of the correlation between the averaged values and the time series of the first (summer) EOFs are shown in Table 2. The critical correlation coefficients were estimated as $R_{crit}=\tanh(t*\sigma_z)$, where $\sigma_z=(n-3)^{-0.5}$, where n is the length of the overlapping time series, and t is the critical point of the Student's t-distribution for the 95% level (Anderson, 1971).

According to Table 2, GMLOT is the only factor that is significantly correlated with both (summer) EOFs and for both periods of our interest (spring and summer). Note that the significant correlations are the result of the trend in the EOFs time series (Figs. 3B and 4B). After de-trending, the correlations significantly decrease and the only significant correlation (−0.3) that remains is the correlation between subsurface (summer) EOFs and spring GMLOT (Table 2).

In spring, ATSCS and ATA correlate with subsurface (summer) EOF (correlations=0.37 and 0.45) while the corresponding correlations with surface (summer) EOF are low (correlations=0.19 and 0.26). This is the consequence of accumulation of the cold and saline water in the subsurface layer during winter. In summer, this subsurface water still remains in a large part of the CS. In summer, both surface and, to a lesser degree, subsurface (summer) EOFs significantly correlate with ATSCS (correlations=0.73 and 0.44, respectively). These correlations indicate the surface water is warmed more by the atmosphere than the subsurface water, probably due to strong summer thermocline. Summer EOFs are also anti-correlated with local ice concentration (ICCS; correlations=−0.70 and −0.64), indicating intensive heat exchange between ocean and atmosphere, and corresponding ice melting. Note that the discussed correlations between summer indices (ATSCS, ATA, and ICCS) and both (summer) EOFs are mostly a result of the interannual variability (Table 2).

We did not find any significant correlations between spring WTNB and surface/subsurface (summer) EOFs, probably due to the relatively short period of available observations and the 100% ice concentration. It is not surprising that during the summer the WTNB and subsurface (summer) temperature EOFs are well correlated (0.77). There is no correlation, however, between summer WTNB and surface (summer) EOF, probably because ocean temperature at the surface is also affected by atmospheric heating and the strong summer thermocline in the CS (Coachman et al., 1975), which does not allow intensive vertical mixing.

Interestingly, during the spring, WSNB significantly anti-correlates with the subsurface (summer) EOF (−0.82) and does not correlate with surface EOF (−0.44). This result agrees well with winter processes on the Northern Bering Sea Shelf, where ice formation in the local polynyas generate high salinity and cold water near the bottom (Aagaard et al., 1981; Cavaleri and Martin, 1994; Gladyshev and Khen, 1999; Schumacher et al., 1983). It was found that annual productivity of the dense and salty water in the Anadyr Polynya ranges from 0.1 to 0.23×10^6 m^3 s^{-1} (Cavaleri and Martin, 1994). Dense and salty water from the Gulf of Anadyr reaches the Bering Strait approximately 90–100 days after the beginning of the formation in early winter (Gladyshev and Khen, 1999). A similar result was reported by Woodgate et al. (2006, 2010), who revealed the maximum near bottom salinity in the Bering Strait between March and May.

It is necessary to note the significant (0.45) correlation between subsurface thermal conditions in the Chukchi and Bering Seas. The interannual variability at 50 m in the Bering Sea is strongly controlled by intensive winter cooling (Azumaya and Ohtani, 1995; Luchin et al., 2002; Luchin and Sokolov, 2007). It is well known that Bering Strait currents strongly correlate with local winds (Aagaard et al., 1985; Coachman and Aagaard, 1966; Panteleev et al., 2010; Roach et al., 1995; Shtokman, 1957; Woodgate et al., 2005a). Therefore, taking into account that the first subsurface (summer) EOF mode correlates well with the MWBS (0.49) during the spring (March–May), we suggest that the physical mechanism responsible for the correlation between subsurface layers in the Chukchi and Bering seas is the subsurface transport through the Bering Strait. Luchin and Sokolov (2007) also revealed the high correlation (~0.8) between ICNBC and WTBS. Therefore the correlations described above suggest that during the late winter and spring of the "warm" years, relatively warm Pacific water accumulates in the Northern Bering Sea and enters into the Chuckhi Sea. In addition, due to Pacific water flow in the Northern Bering Sea, there is a decrease in ice formation and relative freshening of the bottom water.

The situation changes in summer, when surface Pacific water entering into the Chukchi Sea is warmer and more saline than Chukchi surface water. Due to enhanced vertical mixing in the Bering Strait the vertical gradients of temperature and salinity decrease.

As a result, WSNB and surface (summer) EOF correlate well (0.70). The correlation between (summer) EOFs and WVT is similar to the correlation with WSNB: WVT correlates significantly only with subsurface/surface (summer) EOFs during the spring/summer

Table 2
Correlations between first EOFs (surface layer and subsurface layer) and several indexes/parameters describing dynamic and thermal atmospheric and ocean states. Bold fonts highlight the correlations that are larger than the corresponding critical values.

Parameters	Period of averaging (months)	Trend were not removed		Trends removed	
		EOF-1 (surface layer)	EOF-1 (sub-surface layer)	EOF-1 (surface layer)	EOF-1 (sub-surface layer)
		(critical correlation coefficients are shown in brackets)			
1. Global Mean Lan/Ocean Temperature (**GMLOT**)	(03–05)	**0.43** (*0.27*)	**0.47** (*0.27*)	−0.11 (*0.27*)	−**0.30** (*0.27*)
	(07–09)	**0.36** (*0.27*)	**0.37** (*0.27*)	−0.01 (*0.27*)	−0.07 (*0.27*)
2. Atmospheric temperature at 1000 mb in the Southern CS (**ATSCS**)	(03–05)	0.19 (*0.33*)	**0.37** (*0.33*)	0.16 (*0.33*)	**0.42** (*0.33*)
	(07–09)	**0.73** (*0.33*)	**0.44** (*0.33*)	**0.72** (*0.33*)	0.29 (*0.33*)
3. *in situ* observations of the Atmospheric Temperature in the Anadyr (**ATA**)	(03–05)	0.26 (*0.26*)	**0.45** (*0.26*)	0.17 (*0.26*)	**0.38** (*0.26*)
	(07–09)	**0.47** (*0.26*)	0.26 (*0.26*)	**0.35** (*0.26*)	0.14 (0.26)
4. Ice conditions (% of ice cover) in the CS (**ICCS**)	(03–05)	100% ice	100% ice	100% ice	100% ice
	(07–09)	−**0.70** (*0.28*)	−**0.64** (*0.28*)	−**0.64** (*0.28*)	−**0.58** (*0.28*)
5. Ice conditions (% of ice cover) in the Northern Bering Sea (**ICNBS**)	(03–05)	−0.11 (*0.32*)	−**0.47** (*0.32*)	−0.06 (*0.32*)	−**0.43** (*0.32*)
	(07–09)	0% ice	0% ice	0% ice	0% ice
6. *in situ* observations from moorings of the Bering Strait (according to R. Woodgate)					
(A) Near-bottom temperature (**WTNB**)	(03–05)	−0.37 (*0.61*)	0.32 (*0.61*)	−0.39 (*0.61*)	0.30 (*0.61*)
	(07–09)	0.25 (*0.61*)	**0.77** (*0.61*)	0.19 (*0.61*)	**0.77** (*0.61*)
(B) Near-bottom salinity (**WSNB**)	(03–05)	−0.44 (*0.67*)	−**0.82** (*0.67*)	−0.45 (*0.67*)	−**0.82** (*0.67*)
	(07–09)	**0.70** (*0.67*)	0.31 (*0.67*)	0.66 (*0.67*)	0.30 (*0.67*)
(C) Volume transport (**WVT**)	(03–05)	0.64 (*0.75*)	**0.81** (*0.75*)	0.62 (*0.75*)	**0.81** (*0.75*)
	(07–09)	**0.75** (*0.75*)	0.10 (*0.75*)	0.72 (*0.75*)	0.08 (*0.75*)
7. Pacific North American (**PNA**)	(03–05)	−0.06 (*0.28*)	−0.08 (*0.28*)	−0.14 (*0.28*)	−0.13 (*0.28*)
	(07–09)	**0.50** (*0.28*)	**0.29** (*0.28*)	**0.52** (*0.28*)	**0.30** (*0.28*)
8. Arctic Oscillation **(AO)**	(03–05)	**0.30** (*0.28*)	**0.35** (*0.28*)	0.21 (*0.28*)	−**0.39** (*0.28*)
	(07–09)	−**0.29** (*0.28*)	−0.21 (*0.28*)	**0.29** (*0.28*)	−0.28 (*0.28*)
9. The first mode of the EOF decomposition of the Water Temperature anomaly in the Bering Sea **(WTBS)**	(05–08)	0.10 (0.29)	**0.45** (0.29)	0.15 (0.29)	**0.49** (0.29)
10. The Meridional Wind component near the Bering Strait **(MWBS)**	(03–05)	0.24 (0.27)	**0.49** (0.27)	0.23 (0.27)	**0.49** (0.27)
	(07–09)	0.14 (0.27)	0.22 (0.27)	0.12 (0.27)	0.23 (0.27)
11. Sea surface temperature in the Bering Strait (**SST_BS**)	(07–09)	**0.65** (0.27)	**0.36** (0.27)	**0.55** (0.27)	0.23 (0.27)

(correlations = 0.81 and 0.75, respectively). This probably indicates that transport of relatively warm and salty Pacific water through the Bering Strait plays a preconditioning role in the formation of warm CS conditions during the summer–fall season.

We compared our results (Table 1) with the classification of "warm," "cold," "normal" years for the southeastern Bering Sea shelf proposed by Stabeno et al. (2012). It was found that from the overlapping 16-year period, both classifications agree only in 3 years for the surface and 4 years for the subsurface layers. One possible reason for the weak correlation between classifications may be the statistical structure of the interannual variability of the temperature anomaly described by Luchin et al. (2002). According to Fig. 5 from Luchin et al. (2002), the spatial distribution of the first temperature EOF at 30 m has a maximum near the Cape of Navarin, while in the Eastern Bering Sea Shelf first temperature EOF is approximately half as large. Also, the second EOF from Luchin et al. (2002; Fig. 5), is negative in the Northwestern Bering Sea and positive in the Southeastern Bering Sea shelf, indicating that variability of temperature in these regions is controlled by different processes.

The correlations identified between (summer) EOFs and the several important climatological indexes for the Northern Hemisphere were found to be rather low. Table 2 shows that only surface (summer) EOF is moderately correlated with the PNA index during the summer (0.50). Therefore, we suggest that thermal conditions in the CS are mostly defined by local thermal and dynamical ocean and atmosphere processes (such as ATSCS, ATA, ICCS, ICNBS, WTNB, WSNB, WVT, WTBS, MWBS, SST_BS), rather than by global climatological variability in the Northern Hemisphere (e.g., GMLOT, AO). This agrees well with the results described by Shpayher and Fedorova (1978) and Woodgate et al. (2006, 2010).

5. Variational analysis of the Chukchi Sea circulation during "warm" and "cold" years

In this section we describe the results of the reconstruction of CS circulation during typical "warm" and "cold" years derived through applying the four dimensional variational (4Dvar) data assimilation approach (Wunsch, 1996). This approach allows the circulation to be reconstructed via assimilating all available data into the ocean model. It has proved to be a useful and efficient tool in numerous ocean circulation studies (e.g., Awaji et al., 2003; Panteleev et al., 2006, 2010; Wunsch, 1996).

In the present study we employ a 4Dvar inversion based on the Semi-Implicit Ocean Model (SIOM) previously utilized to reconstruct CS circulation for a 1-year period (Panteleev et al., 2010). The grid of the SIOM model has a horizontal resolution of 10 km with 15 unequally-spaced vertical levels ranging between 2.5 m near surface and 10–20 m near ocean bottom. The time step of the model is 2.4 h. The SIOM model was configured for the domain shown in Fig. 1. The temporal period of model integration was 3 months (July 15–October 15), which roughly corresponds to the ice-free period in the CS. The details of the data assimilation approach can be found in Panteleev et al. (2010).

5.1. Data

The following data were utilized to reconstruct CS circulations:

(a) Temperature and salinity data were extracted from our database. The profiles were selected for the "warm" and "cold" years according to the classification scheme shown in Table 1 and additionally sub-sampled for each particular month (July, August, September, and October). The vertical profiles were

averaged within each model box, and monthly mean temperature and salinity data and their variances were used for the reconstruction.

(b) Near surface wind fields, and heat and salt flux data assimilated into the model are taken from monthly mean National Centers for Environmental Prediction (NCEP) reanalysis (www.cdc.noaa.gov/cdc/data.ncep.reanalysis.derived.html) for the "warm" and "cold" years (Table 1). Significant errors in the NCEP/National Center for Atmospheric Research (NCAR) forcing were noticed by Ladd and Bond (2002). Therefore, we used wind stress, and heat and salt flux data with relatively high error variances (up to 40% of their spatial and temporal variability in the CS).

(c) The estimates of the monthly Bering Strait transports for the "warm" and "cold" states were derived from available Bering Strait observations (Woodgate et al., 2005a, 2005b) and averaged over the ensemble of the "warm" and "cold" years. We found, on average, that monthly Bering Strait transports during the "warm" state are approximately 0.20–0.25×10^6 m^3 s^{-1} larger than the estimates for the "cold" period. Similarly to Panteleev et al. (2010), a 0.2×10^6 m^3 s^{-1} variance for the obtained estimates of monthly Bering Strait transport was used.

5.2. Reconstructed circulations during the "warm" and "cold" states

The reconstructed velocity fields at 7.5 m during the "cold" and "warm" years averaged for the period of model integration are shown in Fig. 10, which clearly indicates enhanced northwestward flow through the central CS toward Herald Channel during "warm" years. Another interesting result obtained through the 4Dvar reconstruction is the difference in Siberian Coastal Current (SCC) circulation in Long Strait versus along the Siberian Coast. Our results indicate eastward flow through the southern part of Long Strait in "warm" years (Fig. 10A). Most of this flow recirculates toward the north, but a small portion flows along the Siberian coast and reaches the Bering Strait. During "cold" years the Long Strait current changes its direction and flows westward. As illustrated in Fig. 10B, this current originates as a small branch of the flow entering the CS from the Bering Strait.

The SCC is strongly affected by baroclinic forcing, as implied by freshwater impact along the Siberian coast (Pavlov et al., 1996; Sverdrup, 1929; Weingartner et al., 1999; Yankovsky and Chapman, 1997). Therefore, we hypothesize that during "warm" years the more intensive snow melting causes an enhanced freshwater discharge from all Siberian rivers. This freshwater flux forms an intensive baroclinic coastal current, and continuously supports it along the entire Siberian coast; it may reach the Bering Strait. During "cold" years, the freshwater flux along the Siberian coast is depressed and the flow in Long Strait is predominantly controlled by the inflow through the Bering Strait, local topography, and wind pattern. Of course, anomalous wind modifies coastal circulation, and for particular years, wind effects may have stronger control on the coastal current (e.g., Münchow et al., 1999).

Table 3 presents the averaged volume transports and heat fluxes calculated with respect to -1.9 °C through the Bering and Long Straits and the two sections shown in Fig. 10 during "warm" and "cold" periods. The difference of 0.26×10^6 m^3 s^{-1} between "warm" and "cold" transport in the Bering Strait (27% of the total transport during "cold" years) is constrained by the estimates of Bering Strait transport utilized in the cost function minimized during the data assimilation procedure. Interestingly, the corresponding difference in heat flux is about 10×10^{12} J s^{-1}, almost 50% larger than total heat flux during "cold" years.

The difference in transports and heat fluxes through Long Strait in "warm" vs. "cold" years are 0.85×10^6 m^3 s^{-1} and 5.5×10^{12} J s^{-1}, respectively. There are no direct observations of the total Long Strait transport. Meanwhile, according to the reconstruction of CS circulation between October 1990 and October 1991 (Panteleev et al., 2010), an inflow of approximately 0.3×10^6 m^3 s^{-1} entered the CS during October 1990 (a "warm" year in the surface and subsurface layers, see Table 1) and a weak outflow of $0.05–0.1\times10^6$ m^3 s^{-1} exited the CS during August–September 1991 (a "cold" year in the subsurface layer, see Table 1).

Table 3
Volume transports (bold, 10^6 m^3 s^{-1}) and heat fluxes (italic, 10^{12} J s^{-1}) through the Bering and Long straits and the two sections designated by solid (1) and dashed (2) lines in Fig. 10.

State	Bering Strait	Long Strait	Sections	
			1	2
Warm	**1.22**/*32.05*	**−0.59**/*−3.55*	**1.24**/*27.03*	**0.32**/*13.14*
Cold	**0.96**/*22.0*	**0.26**/*2.0*	**0.39**/*5.90*	**0.23**/*6.34*

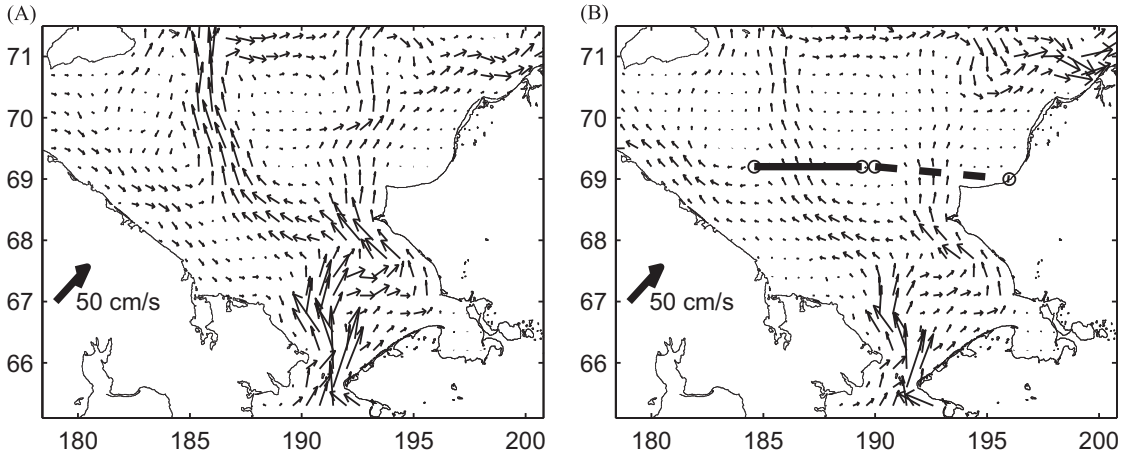

Fig. 10. Mean velocity at 7.5 m in the CS during (A) "warm" and (B) "cold" years. Transects used to quantify volume transport and heat flux through Herald Canyon (solid) and along Alaskan coast (dashed) are shown in (B).

These results were obtained through the assimilation of temperature, salinity, and velocity data from 11 moorings into the ocean model using the 4Dvar data assimilation approach. Three of these moorings were deployed in the Bering Strait, two in the Herald Canyon, one in the Barrow Canyon, five in the central part of the CS, and one in the northern part of the Long Strait. Despite the fact that only one mooring was in the Long Strait, the unprecedented number of velocity observations and dynamical constraints of the utilized ocean model allowed accurate estimation of flows through all boundaries of the CS, including the Long Strait.

It is necessary to note that we do not have any Long Strait transport observations during August–September 1990, when the impact of the coastal freshwater should have been stronger. Also, 1990 was not a "very warm" year (see Figs. 3B and 4B); noting this the results of CS circulation reconstruction for 1990–1991 seem to be in reasonable agreement with the obtained estimates of Long Strait transport climatological variability. We hypothesize that the difference in the transport through the Long Strait can be explained by more intensive freshwater discharge along the Siberian coast caused by snow melting and riverine discharge during "warm" years.

Weingartner et al. (1999) analyzed the temperature/salinity and shipboard acoustic Doppler current profiler data obtained between 1992 and 1995 and estimated SCC transport into the CS to be 0.1×10^6 m^3 s^{-1}. Note that, as shown in Table 1, the years from 1992 to 1995 ranged from "extremely cold" to "normal," so this estimate of the SCC may underestimate the mean (or "normal") climatological transport through Long Strait. If we suggest that SCC transport during the "normal" period equals the mean between "cold" and "warm" transports (i.e. 0.17×10^6 m^3 s^{-1} into the CS), we may conclude that derived estimates of Long Strait transport are realistic.

The two right-hand columns of Table 3 present the volume and heat transports through the two sections shown in Fig. 10B. Interestingly, during the "warm" years the transport through Section 1 (Herald Branch, Table 3 and Fig. 10B) is almost four times larger than transport through Section 2, while during "cold" years the ratio between these transports is approximately 1.69. The difference between heat fluxes is much greater. During "cold" years heat flux along the Alaskan coast (Section 2) is slightly smaller than the heat flux through the Herald Canyon, while during "warm" years, the heat flux through the central CS is twice as large as the corresponding flux along the Alaskan coast. Thus, the obtained estimates of volume and heat fluxes agree very well with results of the EOF and correlation analyses.

6. Conclusions

We present an analysis of CS thermal conditions during 1941–2008 using all available *in situ* observations and self-consistent EOF decomposition. We found that the first EOF explains approximately 43.5% and 33.3% of the variability in the surface and subsurface layers, respectively. The retrieved time series of the first mode of EOF decomposition were used to identify typical "normal", "warm", and "cold" CS states. We found that during "cold" years the flow of "warm" Pacific water through the Bering Strait is depressed and most Pacific water flows along the Alaskan coast and outflows through Barrow Canyon, while during "warm" years the Pacific water spreads widely along the Siberian coast and extensive transport of Pacific water occurs through Herald Channel. We also found that satellite observations of the SSH anomaly in 2007 ("extreme warm") and 2003 ("cold") years agree reasonably well with these results (Fig. 9).

Our EOF analysis identifies significant warming of the CS surface water during the last 68 years. The warming is greatest in the northern CS and near Long Strait (0.030–0.036 °C yr^{-1}, total 2.0–2.4 °C) and smallest in the Bering Strait (0.012 °C yr^{-1}, 0.8 °C). In the subsurface layer, the temperature increase is about half as large and is fairly uniform with the exception of regions near Long Strait, suggesting that the global warming of the atmospheric temperature and the inter-annual variability of Pacific water flow through Bering Strait are the most important factors controlling the CS thermal condition. The correlation analysis that was conducted between the temporal evolution of the identified EOF patterns and several important parameters that describe ice, ocean, and atmosphere conditions in the Pacific Arctic agrees well with these conclusions.

The spectral analysis of the EOF modes shows peaks at 2–3 years and 3.5–7 years. We failed to find significant correlations between derived EOFs and known climatological indexes (AO, PNA, etc.), indicating that the thermal state variability is probably not fully described by the variability of the atmospheric forcing, with other mechanisms also controlling local dynamics. One possible mechanism supporting the dominance of local factors on the thermal state of the CS and surrounding regions was proposed by Shimada et al. (2006), who explained the observed decrease in ice concentration in the Pacific Arctic. They suggested that an increase in Pacific water flow to the Canadian Arctic during the summer delays the processes of ice formation in the southern part of the Canadian Arctic. This intensifies anticyclonic wind forcing and increases flux of Pacific Water into the Canadian Basin. The latter causes the observed tremendous changes in ice covering the Pacific Arctic. Meanwhile, several well-separated peaks in the EOF spectra (Fig. 5) indicate that there are probably several important mechanisms responsible for interannual CS variability. We hypothesize that these mechanisms include the complicated ice–ocean–atmosphere interaction and may be related to the Pacific water inflow through either Barrow or Herald Canyons. The physical mechanisms responsible for the peaks in the EOF spectra can be identified in future through the reconstructing the circulation in the CS and/or the Pacific sector of the Arctic Ocean for a multiple-year period using the variational data assimilation approach (e.g. Panteleev et al., 2010).

The reconstructed velocity fields at 7.5 m (Fig. 10) during "cold" and "warm" years clearly indicate enhanced northwestward flow through the central CS toward Herald Channel during "warm" years. Another interesting result obtained via 4Dvar reconstruction is the difference in the circulation in Long Strait. During "warm" years our results indicate intensive eastward flow through southern Long Strait (Fig. 10A). Most of this flow recirculates toward the north, but a small portion flows along the Siberian coast and reaches the Bering Strait. During "cold" years the Long Strait current changes its direction and flows westward. These scenarios do not include the anomalous variability of the zonal wind over the CS that significantly influences the flow through Long Strait (Münchow et al., 1999).

Using the results of the 4Dvar reconstruction we estimated the volume and heat transports in the CS and quantified the large increase of volume and heat transport through the central CS during "warm" periods over that in "cold" years. Our estimates of the mean climatological fluxes through Long Strait are in good agreement with previous estimates and suggest extremely high interannual variability of the flow through the Long Strait.

The described results of 4Dvar circulation reconstruction during "warm" and "cold" years are not final in the sense that these results do not include error estimates. Therefore, we did not take into account other important features of CS circulation during the different regimes. In the future, we plan to accomplish a more accurate analysis of CS circulation, and include reconstruction of the circulation during the "normal" state, estimation of the errors through the inversion of the Hessian matrix in the reduced space

(e.g. Panteleev et al., 2011), and more detailed analysis of the circulations.

Acknowledgments

This study was supported by Grant 09-III-A-07-321 from the Far Eastern Branch of the Russian Academy of Sciences, mega-Grant of the Russian Government no. 2013-220-04-157 and an 828 award from the North Pacific Research Board. BEST-BSIERP Bering Sea Project publication no. 135. Gleb Panteleev was also supported by the Japan Agency for Marine–Earth Science and Technology through their sponsorship of research activities at the International Arctic Research Center and by National Science Foundation, United States awards 1107925 and 120374. We are very grateful to Phyllis Stabeno and three anonymous reviewers for their extremely helpful reviews and valuable suggestions.

References

Aagaard, K., Carmack, E.C., 1989. The role of sea ice and other fresh water in the Arctic circulation. J. Geophys. Res. 94 (C10), 14,485–14,498.
Aagaard, K., Coachman, L.K., Carmack, E.C., 1981. On the halocline of the Arctic Ocean. Deep-Sea Res. 28, 529–545.
Aagaard, K., Shumacher, J.D., Roach, A.T., 1985. On the wind driven flow through Bering Strait. J. Geophys. Res. 90 (C4), 7213–7221, http://dx.doi.org/10.1029/JC090iC04p07213.
Aagaard, K., Weingartner, T.J., Danielson, S.L., Woodgate, R.A., Johnson, G.C., Whitledge, T.E., 2006. Some controls on flow and salinity in Bering Strait. Geophys. Res. Lett. 33, L19602, http://dx.doi.org/10.1029/2006GL026612.
Anderson, T.W., 1971. The Statistical Analysis of Time Series. Wiley p. 704.
Azumaya, T., Ohtani, K., 1995. Effect of winter meteorological conditions on the formation of the cold bottom water in the eastern Bering Sea shelf. J. Oceanogr. 51, 665–680.
Awaji, T., Masuda, S., Ishikawa, Y., Sugiura, N., Toyoda, T., Nakamura, T., 2003. State estimation of the North pacific Ocean by a four-dimensional variational data assimilation experiment. J. Oceanogr. 59, 931–943.
Beckers, J.-M., Rixen, M., 2003. EOF calculations and data filling from incomplete oceanographic data sets. J. Atmos. Ocean. Technol. 20, 1839–1856.
Beszczynska-Mıller, A., Woodgate, R.A., Lee, C., Melling, H., Karcher, M., 2011. A synthesis of exchanges through the main oceanic gateways to the Arctic Ocean. Oceanography 24 (3), 82–99, http://dx.doi.org/10.5670/oceanog.2011.59.
Bjorgo, E., Johannessen, O.M., Miles, M.W., 1997. Analysis of merged SSMR-SSMI time series of Arctic and Antarctic sea ice parameters 1978–1995. Geophys. Res. Lett. 24, 413–416.
Carmack, E.C., 1986. Circulation and mixing in ice-covered waters. In: Untersteiner, N. (Ed.), The Geophysics of Sea Ice. Plenum, pp. 641–712.
Cavaleri, D.J, Martin, S., 1994. The contribution of Alaskan, Siberian, and Canadian coastal polynyas to the cold halocline layer of the Arctic Ocean. J. Geophys. Res. 99 (C9), 18,343–18,362.
Coachman, L.K., Aagaard, K., 1966. On the water exchange through Bering Strait. Limnol. Oceanogr. II (I), 44–59.
Coachman, L.K., Aagaard, K., 1974. Physical oceanography of Arctic and Subarctic seas. In: Nelson, H., Herman, Y. (Eds.), Marine Geology and Oceanography of the Arctic Sea. Springer-Verlag, pp. 1–72.
Coachman, L.K., Aagaard, K., 1988. Transports through Bering Strait: annual and interannual variability. J. Geophys. Res. 93, 15,535–15,540.
Coachman, L.K., Aagaard, K., Tripp, R.B., 1975. Bering Strait: The Regional Physical Oceanography. University of Washington Press p. 172.
Codispoti, L., 1979. Arctic Ocean processes in relation to the dissolved silicon content of the Atlantic. Mar. Sci. Commun. 5, 361–381.
Comiso, J.C., 2002. A rapidly declining Arctic perennial ice cover. Geophys. Res. Lett. 29, 1956, http://dx.doi.org/10.1029/2002GL015650.
De Boer, A.M., Nof, D., 2004. The exhaust valve of the North Atlantic. J. Clim. 17 (3), 417–422.
Dommenget, D., Latif, M., 2002. A cautionary note on the interpretation of EOFs. J. Clim. 15, 216–225.
Eliseeva, I.I., Yuzbashev, M.M., 1998. The General Theory of Statistics. Finance and Statistics Press p. 368 (in Russian).
Fedorova, Z.P., Yankina, Z.S., 1963. Supply of Pacific water through the northern Bering Strait. Trudy AANII 3 (5), 21–44.
Francis, O., Panteleev, G., Atkinson, D., 2011. Ocean wave conditions in the Chukchi Sea from satellite and in situ observations. Geophys. Res. Lett. 38, L24610, http://dx.doi.org/10.1029/2011GL049839.
Frolov, I.Ye., Gudkovich, Z.M., Karklin, V.P., 2007. Long-term variability of sea ice in the Eurasian arctic. In: Remote Sensing of Sea Ice in the Northern Sea Route, Section 7.1. Praxis Publishing Ltd, pp. 398–409.
Gladyshev, S.V., Khen, G.V., 1999. Transformation of the brine bottom waters of the gulf of Anadyr in summer–fall 1995. Meteorol. Gidrol. 6, 66–74.
Gudkovich, Z.M., 1961. Nature of Pacific current in the Bering Strait and causes of its intensity and seasonal variability. Okeanologiya 1, 35–48.
Gudkovich, Z.M., 1962. On the nature of the Pacific current in Bering Strait and the causes of its seasonal variations. Deep-Sea Res. 9, 507–510.
Hu, H., Wang, J., Wang, D.-R., 2011. A model-data study of the 1999 St. Lawrence Island polynya in the Bering Sea. J. Geophys. Res. 116, C12018, http://dx.doi.org/10.1029/2011JC007309.
Ikeda, M., Wang, J., Makshtas, A., 2003. Importance of clouds to the decaying trend in the Arctic ice cover. J. Meteorol. Soc. Jpn. 81, 179–189.
Itoh, Motoyo, Shimada, Koji, Kamoshida, Takashi, McLaughlin, Fiona, Carmack, Eddy, Nishino, Shigeto, 2012. Interannual variability of Pacific Winter Water inflow through Barrow Canyon from 2000 to 2006. J. Oceanogr. 68, 575–592, http://dx.doi.org/10.1007/s10872-012-0120-1.
Killworth, P.D., Smith, J.M., 1984. A one-and-a-half dimensional model for the Arctic halocline. Deep-Sea Res. 31, 271–293.
Ladd, C., Bond, N., 2002. Evaluation of the NCEP/NCAR reanalysis in the NE Pacific and at the Bering Sea. J. Geophys. Res. 107 (C10), http://dx.doi.org/10.1029/2001JC001157.
Luchin, V.A., Semiletov, I.P., 2005. Interannual variability of water temperature in the Chukchi Sea. Proc. Russ. Acad. Sci. Earth Sci. 405A (9), 1419–1422 (in Russian).
Luchin, V.A., Semiletov, I.P., Weller, G.E., 2002. Changes in the Bering Sea region: atmosphere–ice–water system in the second half of the twentieth century. Prog. Oceanogr. 55 (1–2), 23–44.
Luchin, V.A., Sokolov, O.V., 2007. Interannual variability and forecast of the thermal condition in the upper layer in the Bering Sea. Izv. TINRO 151, 312–337.
Luchin, V.A., Zhigalov, I.A., 2006. Types of water temperature distribution in active layer of the Okhotsk Sea and possibility of its prediction. Izv. TINRO 147, 183–204.
Münchow, A., Weingartner, T.J., Cooper, L.W., 1999. The summer hydrography and surface circulation of the East Siberian Shelf Sea. J. Phys. Oceanogr. 29, 2167–2182.
Nihoul, J.C. J., Adam, P., Brasseur, P., Deleersnijder, E., Djenidi, S., Haus, J., 1993. Three dimensional general circulation model of the northern Bering Sea's summer ecohydrodynamics. Cont. Shelf Res. 13, 509–542, http://dx.doi.org/10.1016/0278-4343(93)90093-D.
Nikiforov, Ye. G., Shpayher, A.O., 1980. Features of the Formation of Hydrological Regime Large-scale Variations in the Arctic Ocean. Gidrometeoizdat, Leningrad p. 269 (in Russian).
Overland, J.E., Roach, A.T., 1987. Northward flow in the Bering and Chukchi Seas. J. Geoph. Res 92, 7097–7105.
Panteleev, G., Nechaev, D., Ikeda, M, 2006. Reconstruction of summer Barents Sea circulation from climatological data. Atmos.–Ocean 44 (2), 111–132.
Panteleev, G., Nechaev, D.A., Proshutinsky, A., Woodgate, R., Zhang, J., 2010. Reconstruction and analysis of the Chukchi Sea circulation in 1990–1991. J. Geophys. Res. 115, C08023, http://dx.doi.org/10.1029/2009JC005453.
Panteleev, G., Yaremchuk, M., Stabeno, P., Luchin, V., Nechaev, D., Kikuchi, T., 2011. Dynamic topography of the Bering Sea. J. Geophys. Res., 116, http://dx.doi.org/10.1029/2010JC006354.
Parkinson, C.L., Cavalieri, D.J., Gloersen, P., Zwally, H.J., Comiso, J.C., 1999. Arctic Sea ice extent, areas, and trends, 1978–1996. J. Geophys. Res. 104 (C9), 20,837–20,856.
Pavlov, V.K., Timokhov, L.A., Basjajov, G.A., Kulakov, M.Y., Kurazhov, V.K., Pavlov, P. V., Pivovarov, S.V., Stanovoy, V.V., 1996. Hydrometeorological regime of the Kara, Laptev and East Siberian seas. Technical Memorandum APL-UW TM. Applied Physics Labortory, University of Washington, Seattle, pp. 1–96.
Plotnikov, V.V., 1988. Use of multipurpose optimization algorithms in solving problems of sea ice prediction. Meteorol. Gidrol. 8, 57–66.
Plotnikov, V.V., Pustoshnova, V.I., 2012. Variability and Conjugacy of Ice Conditions in the System of East Arctic Seas (the Laptev, East Siberian, and Chukchi Seas). Meteorol. Gidrol. 37 (7), 468–476.
Proshutinsky, A., 1986. Calculation surge fluctuations in the level and circulation of water of the Chukchi Sea. Meteorol. Gidrol. 1, 54–61.
Proshutinsky, A.Y., Johnson, M.A., 1997. Two circulation regimes of the wind driven Arctic Ocean. J. Geophys. Res. 102 (C6), 12,493–12,514.
Proshutinsky, A., Proshutinsky, T., Weingartner, T., 1995. Northern Sea Route Reconnaissance Report: Climatology of Environmental Conditions Affecting Commercial Navigation along the Northern Sea Route. U.S. Army Corps of Engineers, 196 pp.
Raspopov, O.M., Dergachev, V.A., KolstrÖm, T., 2004. Hale cyclicity of polar activity and its relation to climate variability. Sol. Phys. 224, 455–463.
Roach, A.T., Aagaard, K., Pease, C.H., Salo, S.A., Weingartner, T., Pavlov, V., Kulakov, M., 1995. Direct measurements of transport and water properties through the Bering Strait. J. Geophys. Res. C9, 18,443–18,457.
Rothrock, D.A., Yu, Y., Maykut, G.A., 1999. Thinning of the Arctic sea-ice cover. Geophys. Res. Lett. 26, 3469–3472.
Serreze, M.C., Box., J.E, Barry, R.G, Walsh, J.E, 1993. Characteristics of Arctic synoptic activity 1952–1989. Meteorol. Atmos. Phys. 51, 147–164.
Serreze, M.C., Barrett, A.P., Slater, A.G., Woodgate, R.A., Aagaard, K., Lammers, R.B., Steele, M., Moritz, R., Meredith, M., Lee, C.M., 2006. The large-scale freshwater cycle of the Arctic. J. Geophys. Res. 111, C11010, http://dx.doi.org/10.1029/2005JC003424.
Serreze, M.C., Barrett, A.P, 2008. The summer cyclone maximum over the Central Arctic Ocean. J. Clim. 21, 1048–1065.
Shimada, K., Carmack, E.C., Hatakeyama, K., Takizawa, T., 2001. Varieties of shallow temperature maximum waters in the western Canadian Basin of the Arctic Ocean. Geophys. Res. Lett. 28, 3441–3444.

Shimada, K., Kamoshida, T., Itoh, M., Nishino, S., Carmack, E., McLaughlin, F., Zimmermann, S., Proshutinsky, A., 2006. Pacific Ocean inflow: influence on catastrophic reduction of sea ice cover in the Arctic Ocean. Geophys. Res. Lett. 33, L08605, http://dx.doi.org/10.1029/2005GL025624.

Shpayher, A.O., Fedorova, Z.P., 1978. Interannual variability of hydrological conditions of the Russia Siberian shelf seas. Proc. AARI 349, 16–25 (in Russian).

Shpayher, A.O., Federova, Z.P., Yankina, Z.S., 1968. Variability of thermal conditions of the Chukchi Sea in the last decades. Probl. Arct. Antarct. Reg. 29, 19–28.

Shtokman, V.B., 1957. Influence of wind on currents in the Bering Strait and causes of their high velocities and predominant northern direction. Trans. Inst. Okeanolog Akad. Nauk SSSR 25, 171–197.

Spall, M., 2007. Circulation and water mass transformation in a model of the Chukchi Sea. J. Geophys. Res. 112, C05025, http://dx.doi.org/10.1029/2005JC003364.

Spaulding, M., Isaji, T., Mendelsohn, D., Turner, A.C., 1987. Numerical simulation of wind-driven flow through Bering Strait. J. Phys. Oceanogr. 17, 1799–1816.

Stabeno, P.J., Kachel, N.B., Moore, S.E., Napp, J.M., Sigler, M., Yamaguchi, A., Zerbini, A.N., 2012. Comparison of warm and cold years on the southeastern Bering Sea shelf and some implications for the ecosystem. Deep-Sea Res. II 65–70, http://dx.doi.org/10.1016/j.dsr2.2012.02.020, 31–45.

Steele, M., Morison, J., Ermold, W., Rigor, I., Ortmeyer, M., Shimada, K., 2004. Circulation of summer Pacific halocline water in the Arctic Ocean. J. Geophys. Res. 109, C02027, http://dx.doi.org/10.1029/2003JC002009.

Stigebrandt, A., 1984. The North Pacific: a global – scale estuary. J. Phys. Oceanogr. 14, 464–470.

Stroeve, J.C., Holland, M.M., Meier, W., Scambos, T., Serreze, M., 2007. Arctic sea ice decline: faster than forecast. Geophys. Res. Lett. 34, L09501, http://dx.doi.org/10.1029/2007GL029703.

Schumacher, J.D., Aagaard, K., Pease, C.H., Tripp, R.B., 1983. Effects of a shelf polynya on flow and water properties in the Northern Bering Sea. J. Geophys. Res. 88 (C5), 2723–2732.

Student test. In: Hazewinkel, M. (Ed.), Encyclopedia of Mathematics. Springer (978-1-55608-010-4).

Sverdrup, H.U., 1929. The waters on the North-Siberian Shelf. In: The Norwegian North Polar Expedition with the "Maud" 1918–1925, Scientific Results, vol. 4(2). Geophysical Institute, Bergen, Norway p. 131.

Thompson, D.W. J., Wallace, J.M., 1998. The Arctic Oscillation signature in the wintertime geopotential height and temperature fields. Geophys. Res. Lett. 25, 1297–1300.

Tucker III, W.B., Weatherly, J.W., Eppler, D.T., Farmer, D., Bentley, D.L., 2001. Evidence for the rapid thinning of sea ice in the western Arctic Ocean at the end of the 1980s. Geophys. Res. Lett. 28, 2851–2854.

Wadhams, P., Davis, N.R., 2000. Further evidence of ice thinning in the Arctic Ocean. Geophys. Res. Lett. 27, 3973–3976.

Walsh, J.J., McRoy, C.P., Blackburn, T.H., Coachman, L.K., Goering, J.J., Henriksen, K., Andersen, P., Nihoul, J.J., Parker, P.L., Springer, A.M., et al., 1989. The role of Bering Strait in the carbon/nitrogen fluxes of polar marine ecosystems. In: Rey, L., Alexander, V., Brill, E.J. (Eds.), Proceedings of the Sixth Conference of the Comitй Arctique International. I. Ecosystems of Northern Seas, Leiden, Netherlands, pp. 90–120.

Wang, J., Ikeda, M., Zhang, S., Gerdes, R., 2005. Linking the Northern Hemisphere sea ice reduction trend and the quasi-decadal Arctic Sea Ice Oscillation. Clim. Dyn. 24, 115–130, http://dx.doi.org/10.1007/s00382-004-0454-5.

Wang, J., Woodgate, R.A., Weingartner, T., Lindsay, R., 2010. The 2007 Bering Strait oceanic heat flux and anomalous Arctic sea-ice retreat. Geophys. Res. Lett. 37, L01602, http://dx.doi.org/10.1029/2009GL041621.

Wang, J., Zhang, J., Watanabe, E., Ikeda, M., Mizobata, K., Walsh, J.E., Bai, X., Wu, B., 2009. Is the dipole anomaly a major driver to record lows in Arctic summer sea ice extent? Geophys. Res. Lett. 36, L05706, http://dx.doi.org/10.1029/2008GL036706.

Weingartner, T.J., Aagaard, K., Woodgate, R., Danielson, S., Sasaki, Y., Cavalieri, D., 2005. Circulation on the north central Chukchi Sea shelf. Deep-Sea Res. II 52, 3150–3174, http://dx.doi.org/10.1016/j.dsr2.2005.10.015.

Weingartner, T.J., Cavalieri, D.J., Aagaard, K., Sasaki, Y., 1998. Circulation, dense water formation and outflow on the northeast Chukchi Sea shelf. J. Geophys. Res. 103 (C4), 7647–7662.

Weingartner, T., Danielson, S., Sasaki, Y., Pavlov, V., Kulakov, M., 1999. The Siberian Coastal Current: a wind- and buoyancy-forced Arctic coastal current. J. Geophys. Res: Oceans (1978–2012) 104 (C12) 29697–29713, http://dx.doi.org/10.1029/1999JC900161.

Wijffels, S.E., Schmitt, R.W., Bryden, H.L., Stigebrandt, A., 1992. Transport of freshwater by the oceans. J. Phys. Oceanogr. 22, 155–162.

Wilson, C., Wallace, D., 1990. Using the nutrient ratio NO/PO as a tracer of continental shelf waters in the central Arctic. J. Geophys. Res. 95, 22,193–22,208.

Winsor, P., Chapman, D.C., 2004. Pathways of Pacific water across the Chukchi Sea: a numerical model study. J. Geophys. Res. 109, C03002, http://dx.doi.org/10.1029/2003JC001962.

Woodgate, R.A., Aagaard, K., 2005. Revising the Bering Strait freshwater flux into the Arctic Ocean. Geophys. Res. Lett. 32, L02602, http://dx.doi.org/10.1029/2004GL021747.

Woodgate, R.A., Aagaard, K., Weingartner, T.J., 2005a. Monthly temperature, salinity, and transport variability of the Bering Strait throughflow. Geophys. Res. Lett. 32, L04601, http://dx.doi.org/10.1029/2004GL021880.

Woodgate, R.A., Aagaard, K., Weingartner, T.J., 2005b. A year in the physical oceanography of the Chukchi Sea: moored measurements from autumn 1990–1991. Deep-Sea Res. II 52, 3116–3149, http://dx.doi.org/10.1016/j.dsr2.2005.10.016.

Woodgate, R.A., Aagaard, K., Weingartner, T.J., 2006. Interannual changes in the Bering Strait fluxes of volume, heat and freshwater between 1991 and 2004. Geophys. Res. Lett. 33, L15609, http://dx.doi.org/10.1029/2006GL026931.

Woodgate, R.A., Weingartner, T., Lindsay, R., 2010. The 2007 Bering Strait oceanic heat flux and anomalous Arctic sea-ice retreat. Geophys. Res. Lett. 37, L01602, http://dx.doi.org/10.1029/2009GL041621.

Wunsch, C., 1996. The Ocean Circulation Inverse Problem. Cambridge University Press p. 442.

Yankovsky, A.E., Chapman, D.C., 1997. A simple theory for the fate of buoyant coastal discharges. J. Phys. Oceanogr. 27, 1386–1401.

Deep-Sea Research II 109 (2014) 27–38

Contents lists available at ScienceDirect

Deep-Sea Research II

journal homepage: www.elsevier.com/locate/dsr2

Influences of sea ice on the Eastern Bering Sea: NCAR CESM simulations and comparison with observations

Wei Cheng [a,c,*], Enrique Curchitser [b], Carol Ladd [c], Phyllis Stabeno [c], Muyin Wang [a,c]

[a] Joint Institute for the Study of the Atmosphere and Ocean, University of Washington, 3737 Brooklyn Ave NE, Box 355672, Seattle, WA 98105-5672, USA
[b] Institute of Marine and Coastal Sciences, Rutgers University, 71 Dudley Rd., New Brunswick, NJ 08901, USA
[c] Pacific Marine Environmental Laboratory, NOAA, 7600 Sand Point Way NE, Seattle, WA 98115, USA

ARTICLE INFO

Available online 19 March 2014

Keywords:
Bering Sea
Sea ice
Numerical models
Ocean temperature
Salinity

ABSTRACT

We examine the influences of sea ice on the Eastern Bering Sea (EBS) regional oceanography on seasonal and inter-annual time scales using the National Center for Atmospheric Research-Community Earth System Model (NCAR CESM) simulations, comparing the modeling results with satellite and *in situ* observations when possible. While the modeled mean seasonal cycle of ice cover in the EBS middle shelf is generally within the uncertainty range of satellite observations, in the northern domain (north of 59°N), the simulation reaches its annual maximum in April instead of in March, as observed by satellite remote sensing; modeled ice reduction in late spring in the region is also slower than observations. Despite this bias, the simulation captures the observed seasonal transit of freshwater from the north to the south via ice advection; en route, the sea ice melts, cooling and freshening the local water column. On inter-annual time scales, modeling results suggest that extensive ice cover persisting into spring in the central EBS leads to cold anomalies in the bottom water, especially on the middle and inner shelves of the southern domain. The corresponding salinity anomalies are positive in the northern coastal domain, and weak but negative in the southern middle shelf. The associated 10-m ocean current anomalies are southward on the shelf and directed offshore in the slope region. Comparing years 1961–2005 versus years 2005–2050, the Probability Distribution Function of ice cover on the EBS middle shelf shifts northward by ~2° latitude.

1. Introduction

The Bering Sea is part of North Pacific Subarctic and is bounded to the north by Bering Strait, which connects the Bering Sea with the Arctic Ocean, and to the south by the Aleutian Island chain (Fig. 1). The Eastern Bering Sea (EBS) shelf is wide (~500 km) and flat (with depth less than 180 m). As early as November, sea ice begins forming in the northern EBS, and under the prevailing wind conditions, is transported southward 700–1000 km, and in years with extensive sea ice, the ice can cover much of the EBS shelf. Maximum ice extent typically occurs in March, but it can occur as early as February or as late as April (Stabeno et al., 2012a). During melting season, sea ice retreats and by June the Bering Sea is usually ice free. Sea ice extent in the EBS is highly variable on inter-annual scales, but thus far, shows no significant trends since the beginning of the satellite record in 1979 (Brown et al., 2011).

The seasonal changes of sea ice profoundly influence the physical oceanography of the EBS and its ecosystem. During extensive ice years, with sea ice persisting on the southern shelf after mid-March, the water column over the southern shelf (south of 60°N) tends to be colder (~3 °C) and fresher than during years with little ice (Stabeno et al., 2010, 2012b; Ladd and Stabeno, 2012; Sullivan et al., 2014). The timing of ice retreat also influences the timing of the spring phytoplankton bloom (Sigler et al., 2014), zooplankton species composition, and fish recruitment. For instance, a period of limited ice over the southern shelf (2001–2005) was characterized by fewer large crustacean zooplankton the following summer (Stabeno et al., 2012a). As a result the young of the year walleye pollock (*Theragra chalcogramma*) had less lipids and failed to survive the following winter (Heintz, personal communication), resulting in very low recruitment (Stabeno et al., 2012b).

The EBS shelf is divided into three domains (Coachman, 1986). During the summer, the inner or coastal domain (water depth < 50 m) is characterized as well mixed or weakly stratified, while the middle domain (50–100 m) has well defined two-layer structure with a wind mixed surface layer and tidally mixed bottom layer. The outer domain (100–180 m) is more oceanic,

* Corresponding author at: Joint Institute for the Study of the Atmosphere and Ocean, University of Washington, 3737 Brooklyn Ave NE, Box 355672, Seattle, WA 98105-5672 USA. Tel.: +1 206 526 4581; fax: +1 206 526 6485.
E-mail address: wei.cheng@noaa.gov (W. Cheng).

http://dx.doi.org/10.1016/j.dsr2.2014.03.002
0967-0645/

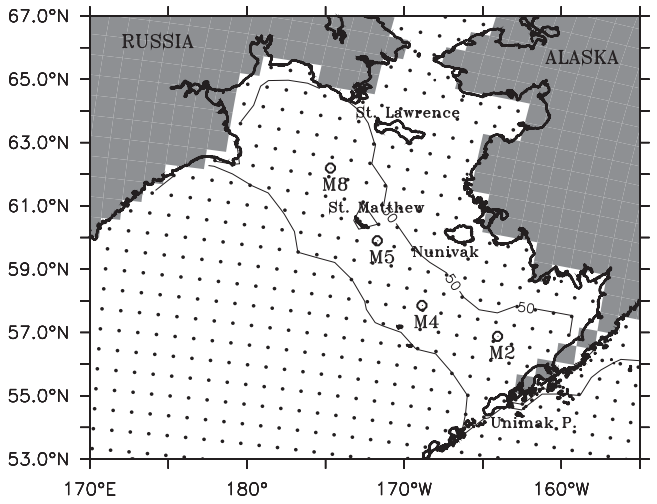

Fig. 1. Study area. The circles mark the ocean moorings in the Eastern Bering Sea shelf used in this study and their names. Gray (white) area is land (ocean) in the CESM model, and the dots indicate ocean grid points. Note that St. Lawrence, St Matthew, and Nunivak Islands are not represented by the CESM grid. Thin black lines indicate the 50-m and 200-m ocean depth in CESM.

with a well-mixed surface layer and bottom layer separated by an intermediate layer. In the middle domain, the influence of winter/spring sea ice persists through the following summer. As part of a biophysical observing network on the EBS shelf, four moorings in the middle domain (M2, M4, M5 and M8) (Fig. 1) provide long time series (10–19 years) of temperature and salinity data (e.g. Stabeno et al., 2010, 2012a, 2012b; Sigler et al., 2014; Sullivan et al., 2014).

Sea ice and ocean variability in the EBS have been studied in regional ocean–ice circulation models. These models are often driven by "observed" atmospheric states of the recent past, hence the name "hindcast". For example, a regional hindcast simulation of the northeast Pacific from year 1969 to 2005 is shown to have the most skills in reproducing inter-annual variability of ice concentration in the EBS and subsurface ocean (60 m) temperature anomalies (Danielson et al., 2011a). Zhang et al. (2010) argue that a substantial inter-annual variability of the Bering Sea ice cover is controlled by changes in the wind-driven advection and melting at the ice edge, again using a regional model of the northern hemisphere north of 39°N. Another class of numerical models used to study the ocean and sea ice is climate models. Climate models include all components of the earth's system—atmosphere, land, ocean, sea ice, and simulate the interactions among them.

The purpose of this study is to examine the impacts of sea ice on the EBS shelf water properties, using output from a global climate model, the NCAR-CESM (National Center for Atmospheric Research-Community Earth System Model), and compare model output with *in situ* (primarily data from moorings) and satellite observations. NCAR-CESM is a well-known global climate model but to the best of our knowledge, its simulation in the EBS has not been examined. We will examine sea ice variability on seasonal, inter-annual, and decadal time scales. Pan-Arctic sea ice is projected to decline in the future under Greenhouse Gas (GHG) forcing but there are large uncertainties (Wang and Overland, 2009). Climate signals associated with GHGs and aerosol forcing are not spatially uniform. For instance, since 2007, winter/spring sea ice extent has been well above average in the EBS even though the summer minimum ice extent in the Arctic has reached record minimums (Stroeve et al., 2007; Stabeno et al., 2012a, 2012b; Brown and Arrigo, 2012).

The paper is organized as follows. In Section 2 we describe the satellite sea ice concentration and the mooring data used in this study; we also introduce the global climate model and the model output, and describe methodology briefly. Spatiotemporal variability of sea ice simulated by the model and influences of sea ice on the upper ocean are examined, and compared with observations in Section 3. In Section 4 we summarize major findings from this study and discuss the implications of these results on the EBS ecosystem.

2. Data and methods

2.1. Satellite and mooring data

Ice concentration maps are derived using data from the Bootstrap algorithm files of daily ice concentration downloaded from the National Snow and Ice Data Center (NSIDC), available at sidads.colorado.edu/pub/DATASETS/nsidc0079_gsfc_bootstrap_seaice/final-gsfc/north/daily/. The files use data from the Scanning Multichannel Microwave Radiometer (SMMR) aboard the Nimbus-7 satellite or the Special Sensor Microwave/Imager (SSM/I) aboard Defense Meteorological Satellite Program (DMSP) satellites (Comiso, 2000), depending on the year. We used data from years 1987 to 2005.

To examine how the ice cover varies along the EBS middle shelf, a 100 km by 100 km box was defined centered on each of four biophysical moorings (M2, M4, M5, and M8, see Fig. 1) that have been maintained by NOAA since the 1990s. Percent of ice cover from satellite was averaged over these 100 km by 100 km regions and a monthly climatology was calculated.

The four moorings used in this study are described in detail in Stabeno et al. (2012a and 2012b). In general, they are subsurface moorings (except M2 in the summer which is a surface mooring) made of chain. Each mooring measures temperature, and salinity throughout the water column and chlorophyll fluorescence at ~11 m.

2.2. Numerical model

The NCAR-CESM is a global coupled ocean–sea ice–atmosphere–land model (Gent et al., 2011) participating in the IPCC (Intergovernmental Panel on Climate Change) assessment reports. Specific formulations of the sea ice model used in CESM are summarized in Holland et al. (2012). CCSM4 (the version of CESM used in up-to-now publications) simulated Arctic ice extent seasonal cycle in the 20th century follows observations closely (Jahn et al., 2012). Arctic sea ice simulated by CCSM4 in the 21st century has also been investigated in a number of studies (e.g., Vavrus et al., 2012).

The particular configuration of the CESM used in this study has 0.9° latitude by 1.25° longitude resolution for the atmosphere and land components, and nominal 1° horizontal resolution (it is ~60 km in the Bering Sea region) for the ocean and sea-ice components. The external climate forcing factors (including natural and anthropogenic components) vary with time. We used two types of model output. First, the monthly averaged ocean and sea ice states from the CESM "historical" and "RCP" (Representative Concentration Pathways) simulations were downloaded from NCAR data mass storage. The "historical" simulations were initialized from a spun-up state of the climate system under pre-industrial GHGs forcings, and cover years 1850–2005 (we only used output from 1961 onward), while the "RCP" simulations were initialized from the climate state of the model at the end of the "historical" simulations, and cover years 2006–2100 and beyond (Gent et al., 2011). The GHGs concentration and aerosol load in historical runs are based on observations, while those in the RCP runs are projections from different emission scenarios. RCP runs

are named by the magnitude of atmosphere radiative forcing in W/m^2 by the end of 21st century, and four forcing scenarios are available: RCP2.6, RCP4.5, RCP6.0, and RC8.5. We use results from the RCP6.0 forcing (radiative forcing stabilizes at 6.0 W/m^2 by year 2100), which is considered a medium emission scenario.

In addition to using the monthly mean archives of the CESM simulations, we also carried out a CESM RCP6.0 run with daily sea ice and ocean output from December 1, 2016 to June 30, 2017. We use the daily output to compare with the mooring data, assessing the CESM's performance in simulating ice formation processes and influences of sea ice on the EBS. Since the CESM is a coupled climate model, the ocean, atmosphere, and sea ice states are internally generated by the model. For example, in CESM simulations, river runoff and surface E−P (evaporation minus precipitation) are both part of the solution and surface forcing driving the ocean; simulated runoff and surface E−P are added to the top ocean (or sea ice if ice is presented) grid through virtual salinity flux formulae. Because of nonlinearity of the climate system, model realizations have no direct correspondence to the "clock time" in observations, which is one particular realization of the climate system. That said, the GHG and aerosol forcings in the CESM are specified according to observations in the "historical" runs (for the period 1850–2005). Mooring observations last from the 1990 s to now, spanning the model "historical" (1850–2005) and "RCP" (2006–2100) periods. We chose to run year 2017 for daily output for two reasons. First, 2017 is closer to the present time than years before 2005; secondly, the monthly mean ice cover at the mooring sites in this year is representative of extensive ice years at these locations in the late 20th century simulations.

To study the inter-annual variability of sea ice and its impact on the EBS shelf, we calculated Empirical Orthogonal Functions (EOF) of physical parameters from March of 1987–2005 using the CESM monthly output. Shelf-water properties and circulation averaged over "high" and "low" ice years are also computed and the contrast between them is examined. The "high" and "low" ice years are defined as follows: if modeled March ice cover during the period 1961–2005 at the M5 location is beyond one standard deviation (STD) of the ice cover time series, it is either a "high" ice year (>1 STD) or a "low" ice year (<-1 STD).

3. Results

3.1. Sea ice mean seasonal cycle

Monthly mean climatology (defined over the period 1987–2005) of sea ice cover was computed from the CESM "historical" simulation and compared with the satellite data. Satellite data (thin black lines in Fig. 2) show a gradual increase in ice cover from December through March (growth in December is small), with the ice cover reaching its maximum in March on the middle shelf regardless of latitude. After March, ice cover decreases rapidly. At the southern two sites (M2 and M4), ice cover is reduced to zero by May. Farther north, an additional month is required for complete loss of sea ice (June at M5 and M8). The magnitude of the 95% confidence interval suggests that ice cover is more variable at the central location (M5) than location farther north (M8).

While the simulations show the same general seasonal evolution as the observations and the confidence intervals of both data overlap over a large portion of the seasonal cycle, there are marked differences in timing and magnitude. The CESM captures the March maximum at the southern two sites (Fig. 2, M2 and M4); at the northern sites (M5 and M8), CESM reaches annual maximum ice cover in April, a month later than observed. The simulation generally underestimates ice cover at all four locations leading up to the March maximum and overestimates ice cover after April at M5 and M8, where complete loss of ice occurs

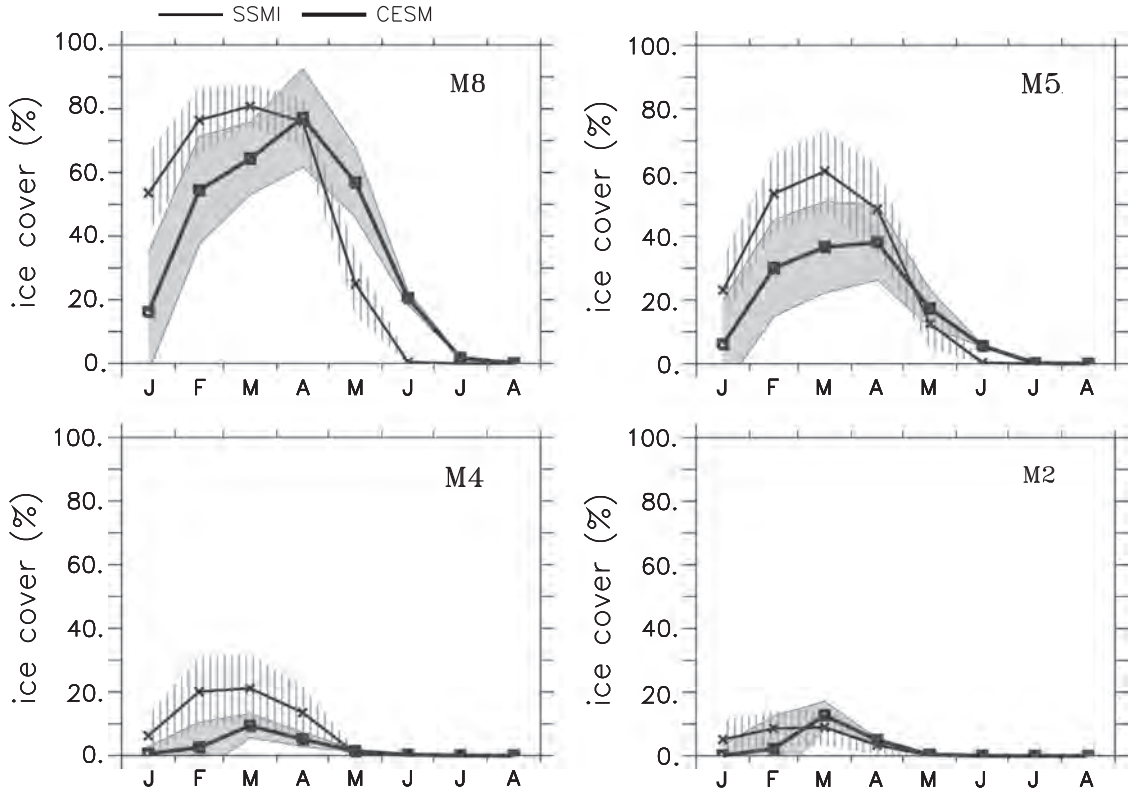

Fig. 2. Monthly climatology (averaged over years 1987–2005) of sea ice cover at the mooring sites from the CESM simulation (thick black) and satellite data (thin black). Names of the moorings are marked on each panel. Vertical shading indicates the 95% confidence limit.

one month later than observed. The magnitude of the inter-annual variability in the seasonal cycle of ice cover is mostly captured by CESM except at the M4 location where the model underestimates it.

The modeled spatial pattern of ice cover in March, is qualitatively similar to observations (Fig. 3). The biggest discrepancy is that the simulated ice cover gradient is weaker than observations, especially in the western part of the domain. The model results show significant ice cover off the 200-meter shelf break in the northern Bering Sea, where sea ice is constrained to the shelf in satellite observations. In addition, in the southeast corner of the EBS shelf, the influence of warm inflow from the Pacific likely results in less ice north of the Alaska Peninsula in the satellite observations (Stabeno et al., 2002, Fig. 3 upper panel). Due to coarse spatial resolution, the CESM is not expected to reproduce such regional features.

3.2. Ice formation: dynamic versus thermodynamic processes

Processes governing sea ice areal extent changes in the CESM can be summarized by the following equation:

$$\frac{\partial A}{\partial t} = -\nabla \cdot (\vec{u} A) + \psi + f$$

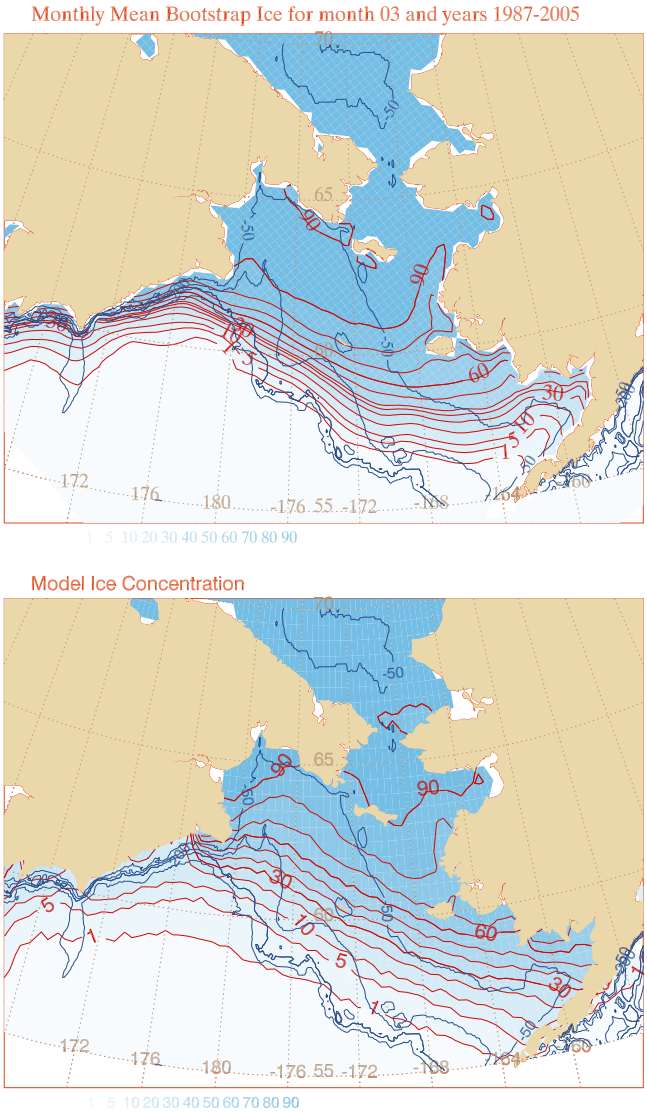

Fig. 3. Multi-year (1987–2005) mean March sea ice cover (percentage) from satellite observations (upper panel) and the CESM simulation (lower panel).

where A is the factional area covered by sea ice, $\vec{u}$ is the horizontal ice velocity, $\nabla = (\partial/\partial x, \partial/\partial y)$, ψ is a ridging/rafting redistribution function, and f represents local thermodynamic melting (when $f<0$) or freezing (when $f>0$). Combination of the 1st two terms on the right hand side is the dynamic contribution. For simplicity, we call it "advection" because that is the dominant process in our study region.

Not surprisingly, ice cover changes seasonally in different locations due to different processes. At M8, ice cover increases rapidly in the first half of January due to advection (Fig. 4a, dotted line), after which ice advection stabilize or decrease the ice cover slightly until late April, while local freezing contributes to a slow ice cover increase (dashed line in Fig. 4a). Ice cover at M8 begins to decrease at the end of April because of a combination of advection, which dominate at the beginning of the decrease, and a gradual thermodynamic melting which lasts into mid-May. At M2 and M5, winter ice growth is a result of advection offset by local melting (Fig. 4b and c). Temporary freezing at M5 occurred during early February (indicated by the upward slope of the dashed line in Fig. 4b), but did not overcome the accumulated thermodynamic melting at the site. At the peak of seasonal ice cover, the magnitudes of the time integral of dynamic and thermodynamic effects increase from north to south, indicating that the lower latitude regions experience stronger dynamic accumulation as well as greater melting. Freezing is only important in the northernmost region from January through April. Modeled ice reduction in late winter/early spring at the M2 and M5 sites is primarily due to advection.

Spatially, south of the Siberian coast and along the northern Bering Sea inner shelf, local freezing (Fig. 5a) is largely offset by advection out of the region (Fig. 5b). These regions are known polynya formation regions (Niebauer, 1998). The balance is reversed in the offshore locations along the ice edge, where advection into the region is canceled by local ice melt. In other

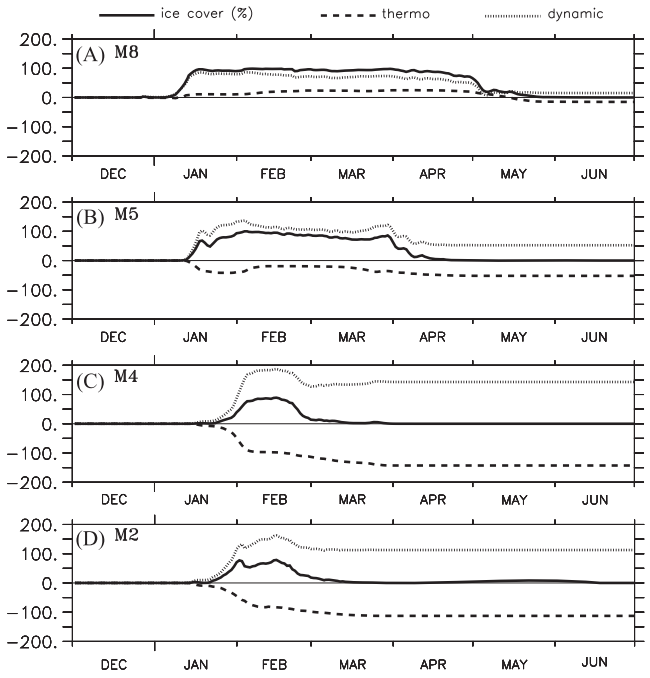

Fig. 4. Modeled time integrals of sea ice growth rate starting from ice-free December 1st: $A(t) = \int_{T_0}^{t} (\partial A/\partial t)\, dt$, $T_0 = Dec1$, where A is the fractional ice cover (percent), t is time. Panels (a)–(d) correspond to mooring sites M8, M5, M4, and M2 respectively. Furthermore, $\partial A/\partial t$ (and therefore $A(t)$) is decomposed into dynamic or primarily advection (dotted lines) and thermodynamic (dashed lines) contributions (see Section 3.2 for the definition of each contribution). Solid lines show model output of daily ice cover.

words, in the CESM sea ice is thermodynamically formed in the northern domain along the coast, transported southward and offshore, and subsequently melts in the warmer ambient environment. This is the well-known "freshwater conveyor" effect of seasonal sea ice on the Bering Sea shelf (Pease, 1980). During this seasonal transit, the largest ice-ocean exchanges in heat and freshwater occur at the ice edge (Fig. 5c and d).

Ice growth and retreat have strong inter-annual variability, which are influenced by the wind. To illustrate this, EOFs of March ice advective growth/loss, ice thermodynamic freezing/melting, and wind stress are calculated and compared with one another. The spatial pattern of the wind stress 1st EOF mode (Fig. 6a) is similar to the southwestward mean wind stress in this region. The corresponding principal component (black line on Fig. 6b) fluctuates between negative and positive values, suggesting this mode is associated with a fluctuation in the strength of the northeasterly winds on inter-annual time scales. The wind stress principal component is highly correlated with principal components of ice cover changes due to thermodynamics and advection (Fig. 6b): the correlation coefficients between the three principal components range between 0.80 and 0.97. When the northeasterly winds are strong, more sea ice is advected into the central middle shelf (Fig. 6c), where it melts (Fig. 6d); at the same time, freezing and removal by advection are enhanced in the northern and coastal regions. The situation reverses under weak northeasterly winds. The strong coupling between ice advection and melting is observed in the EBS (Sullivan et al., 2014) and shown in the regional model of Zhang et al. (2010), and is captured by the CESM simulation.

Next we examine relationships between sea ice formation and ice-ocean heat and freshwater exchanges in the CESM. As latitude increases, modeled seasonal ice cover starts earlier and ends later (Fig. 7). At all sites and throughout the cold season, the modeled ocean under ice cover loses heat to sea ice (black line in Fig. 7a). This is because temperature of the ocean surface layer in CESM is always at or above sea water freezing point (Fig. 8): when the ocean temperature drops below freezing point, sea water freezes and the resulting latent heat release brings it back to freezing point. In comparison, temperature of the ice bottom is at the freezing point. Therefore, both sensible heat flux and ice melting extract heat from the ocean, and their combined effect is larger than heat release to the ocean during freezing. In the southern domain (M2), ocean-to-ice heat loss is strongly influenced by ice advection and subsequent melting: the lag-zero correlation coefficients between the heat loss and ice cover increase due to advection and melting is 0.52 and 0.97, respectively, both are statistically significant at the 95% confidence level (Fig. 7a). Ocean to ice heat loss at the central domain (M5) is again highly correlated ($r^2=0.31$) with ice cover change due to advection (Fig. 7a).

The freshwater flux (units: meter per unit time) to the ocean under sea ice in CEMS includes the flux from ice and snow melt at

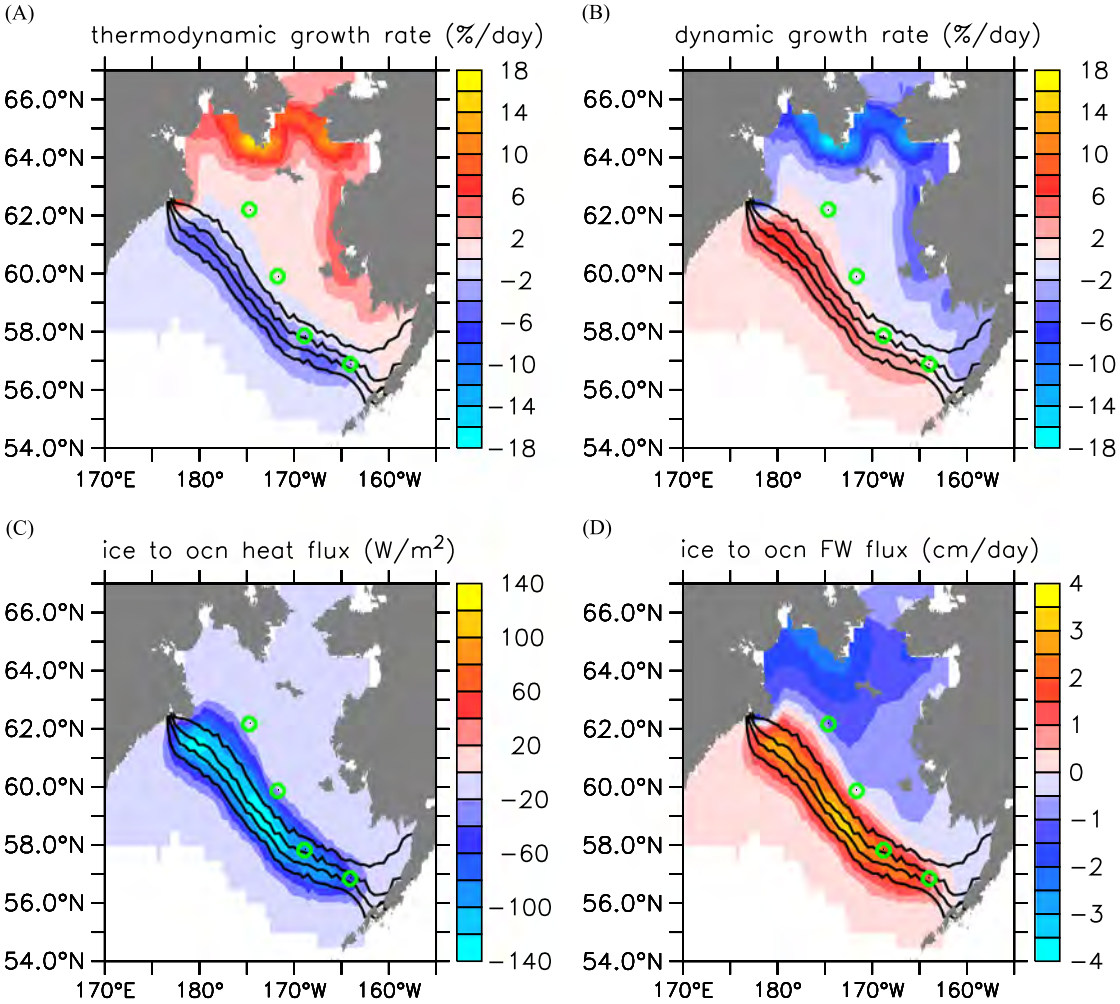

Fig. 5. Spatial patterns of ice cover growth rate (units: percent/day) from (a) thermodynamics and (b) dynamics or primarily advection contributions (see Section 3.2 for the definition of each contribution). Ice to ocean (c) heat (W/m^2) and (d) freshwater (cm/day) fluxes. White areas are ice-free. Positive values in (c) and (d) mean flux into the ocean. Black contours mark the 80%, 60%, 40%, and 20% ice cover. February averages of the model year in Fig. 4 are shown. Circles mark the mooring locations.

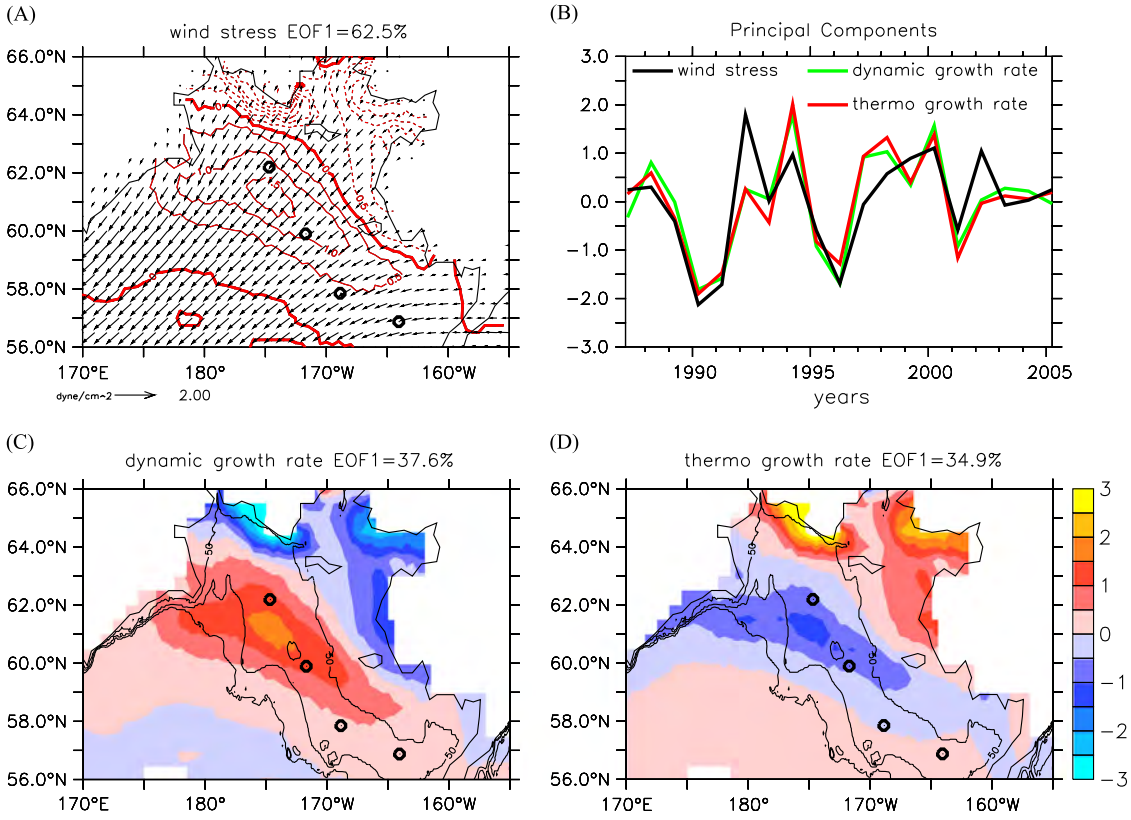

Fig. 6. (a) EOF1 of March wind stress. (b) Corresponding principal components of the EOF patterns shown in (a), (c), and (d). EOF1 of March ice cover growth rate due to (c) dynamics or advection and (d) thermodynamics. Shading contours of (c) are overlaid in (a). Thin black lines on (c) and (d) denote the 50 m, 100 m, and 200 m ocean depths. CESM March output from years 1987 to 2005 are used for this analysis. Percentage of variance explained by EOF1 is marked on (a), (c), and (d).

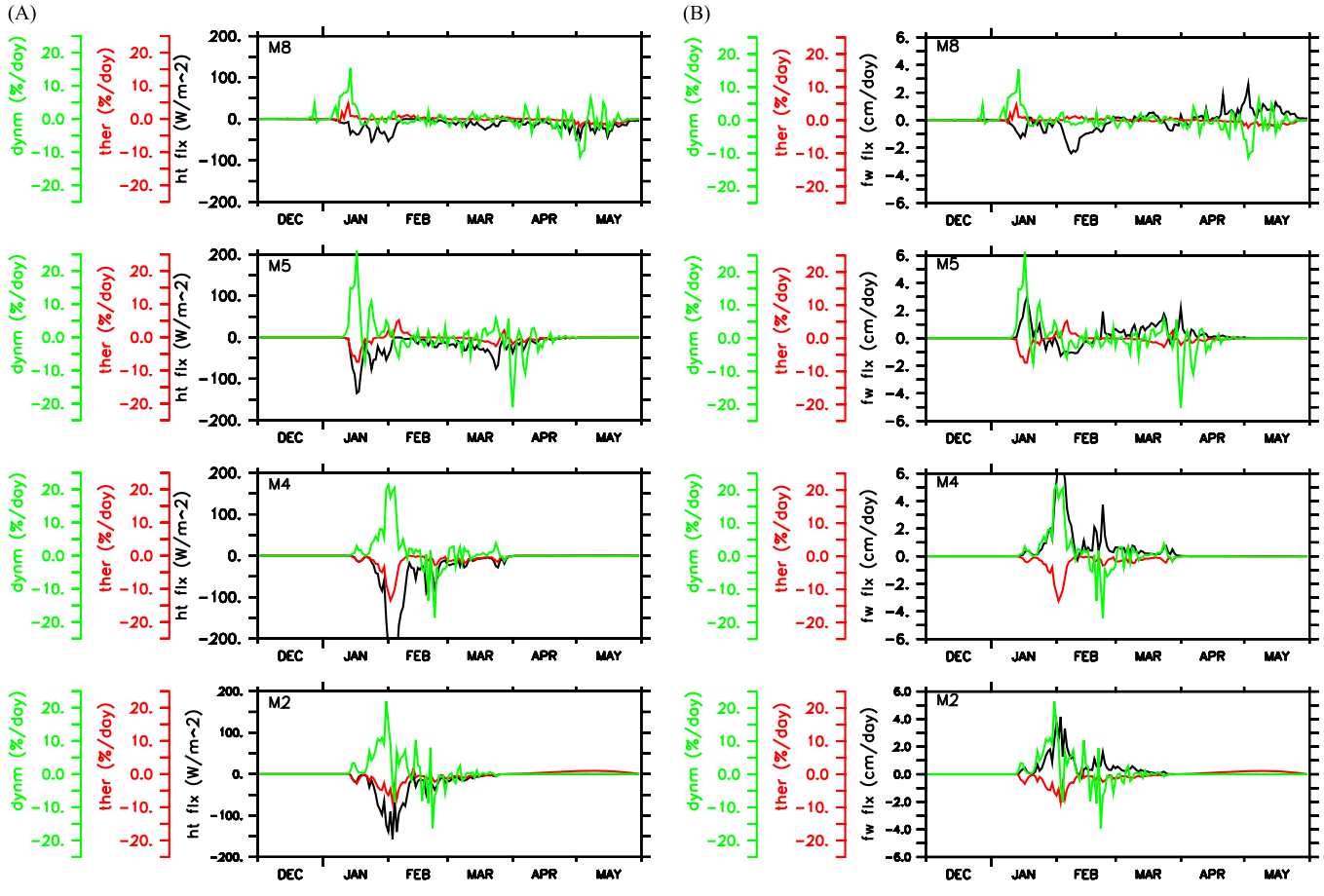

Fig. 7. Red (green) lines indicate modeled daily ice cover growth rate due to thermodynamics (dynamics or advection) at the mooring locations, while black lines show the corresponding ice to ocean (a) heat, (b) freshwater fluxes, where positive values mean flux into the ocean. (For interpretation of the references to color in this figure legend, the reader is referred to the web version of this article.)

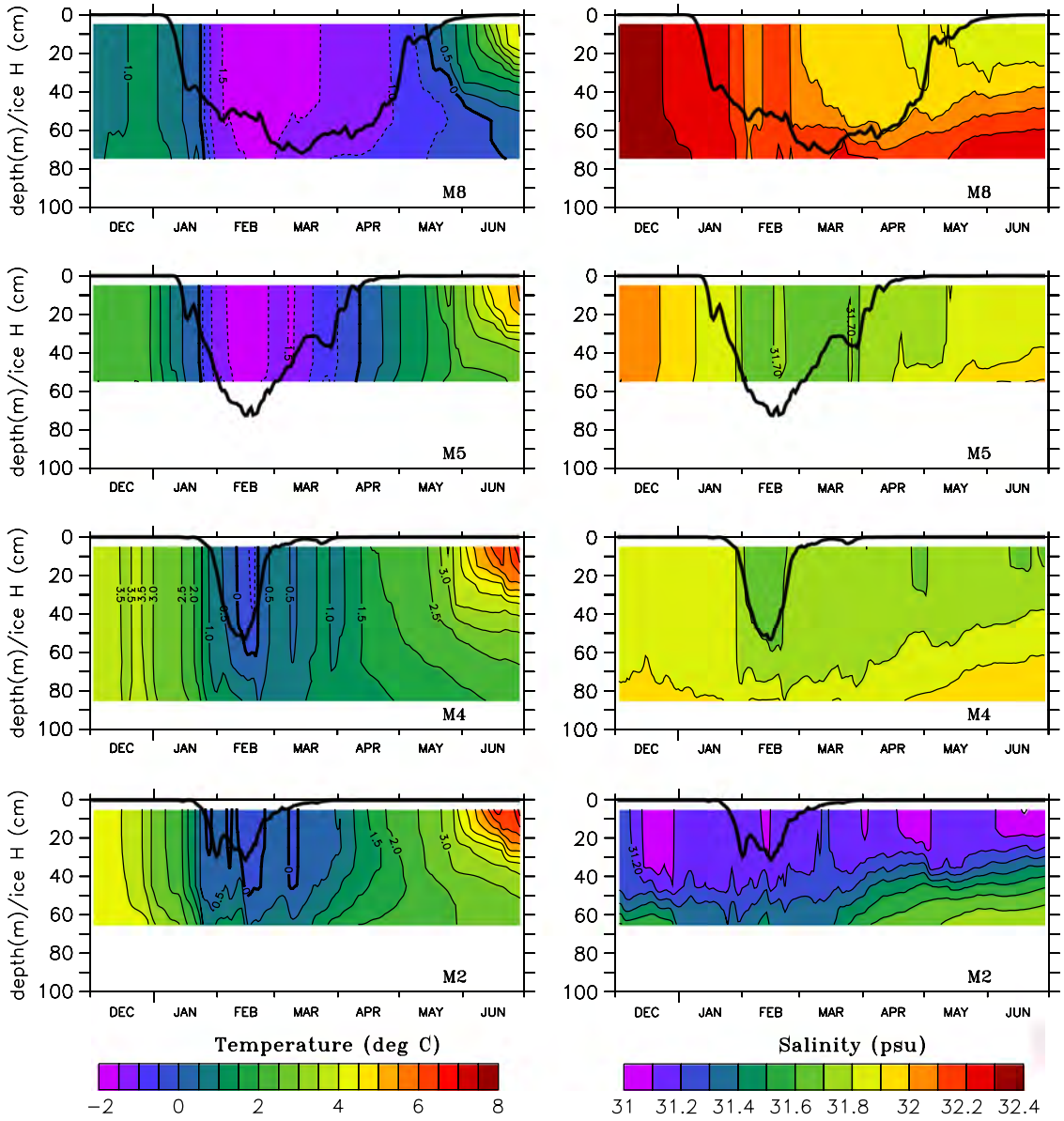

Fig. 8. Modeled daily ocean temperature (left panels) and salinity (right panels) as a function of depth (0–100 m) and time at the mooring locations. The thick black lines show ice thickness (cm) in those locations.

the surface, ice melt at the ice-water interface, and lateral ice and snow melt. At all locations, the modeled ocean gains (loses) freshwater whenever ice melts (forms) (Fig. 7b). In the southern domain (M2), freshening of the ocean by ice melting is evident throughout the cold season. In the central domain (M5), the ocean loses freshwater in February during freezing but the integral effect over the cold season is to freshen the ocean. At M8, the ocean loses freshwater at the beginning of the season during freezing and gains freshwater during ice melting. The net freshwater flux at M8 averaged over the whole ice-covered season is relatively small (-4.9 cm/day), compared to $+30.2$ cm/day at M5 and $+48.6$ cm/day at M2. Ice growth due to advection (green lines in Fig. 7b) plays an implicit role in ice-ocean freshwater exchange through its influence on thermodynamic formation (Fig. 5).

3.3. *Influences on the ocean: intra-seasonal and inter-annual time scales*

The upper ocean properties in the EBS are influenced by arrival and retreat of sea ice on intra-seasonal time scales. At M5 and M8, the water column in CESM is vertically well mixed at the beginning of the winter (December) as a result of wind mixing (Fig. 8). Absence of stratification at these locations is maintained through spring under significant ice cover, similar to observations at the moorings (Sullivan et al., 2014). The water column at M8 cools slightly (<1 °C) with ice arrival in the first half of January. At M5 the water column cools by ~ 3 °C from January to March due to aforementioned heat loss to sea ice (Section 3.2), and to atmosphere under fractional ice cover. In comparison, multi-year mooring observations show little cooling at M8, and an averaged cooling of 2.9 °C (ranges between 1.8 °C and 3.6 °C) at M5 after ice arrival (Sullivan et al., 2014, their Table 3). Concomitantly, modeled water column at the M8 location shows little change in salinity associated with ice arrival; at the M5 location, it freshens by ~ 0.3 psu as the ice thickness increases. Freshening at M5 is caused, in part, by arrival and subsequent melting of sea ice (Figs. 4 and 7b). In comparison, mooring data indicate a mean freshening of ~ 0.5 psu (ranges between 0.5–0.9 psu) at M5 with the arrival of ice, and very little freshening at M8 with the first arrival of ice. Both moorings have substantial freshening

associated with the retreat of ice in the late spring (Sullivan et al., 2014, their Table 4).

At M2, differences between the modeled and observed water column structures are greater. In December, the modeled water column is stratified near the bottom, albeit weakly, especially in salinity (Fig. 8, bottom panels). In observations, during years with little or no ice over the mooring, the water column is well mixed usually by November (Table 2 in Sullivan et al., 2014). During years in which ice is extensive over the southern domain, the ice often arrives when the water column is well mixed, but above freezing. The ice cools and freshens the surface waters, but the near bottom waters remain warm and salty for several weeks before the water column becomes well mixed. CESM simulates cooling and freshening at M2 after ice arrival, similarly to observations, but stratification below 40 m persists in the model. The modeled ocean stratification increases following ice thickness reduction at all mooring locations (Fig. 8), consistent with that stratification in the mooring measurements usually begins after ice concentrations have decreased (Sullivan et al., 2014).

The modeled near-surface ocean gradually cools beginning in fall (not shown). In the model, as in observations, cooling at M8 and M5 continues under significant ice coverage (Fig. 8, in late January), until the temperature reaches the freezing point. The quasi-steady thermal ocean lasted a couple months at M8, but only briefly at M5 (mid February). At the modeled M8 location, significant warming of the ocean does not occur until late April when sea ice begins to decrease (Fig. 8). Modeled ocean at the M5 location begins warming in February, prior to the rapid sea ice reduction; at the M2 location warming begins in February along with the ice retreat. In observations, warming generally begins in March at M8, and the water column can warm through advection during the winter months especially at the southern moorings M2 and M4 (Stabeno et al., 2010, 2012a; Sullivan et al., 2014).

The modeled seasonal evolution of near-surface salinity differs from north to south (Fig. 8). Modeled salinity at the mooring locations usually reaches an annual minimum in September (not shown), after which, salinity increases until December. After the ice arrival, modeled salinity at M8 generally decreases, and the freshening trend continues throughout the season (from December to May), although it is also punctuated by episodes of salinity increase. At M5, salinity decreases from January to early February, along with ice increase. Salinity then exhibits relatively weak

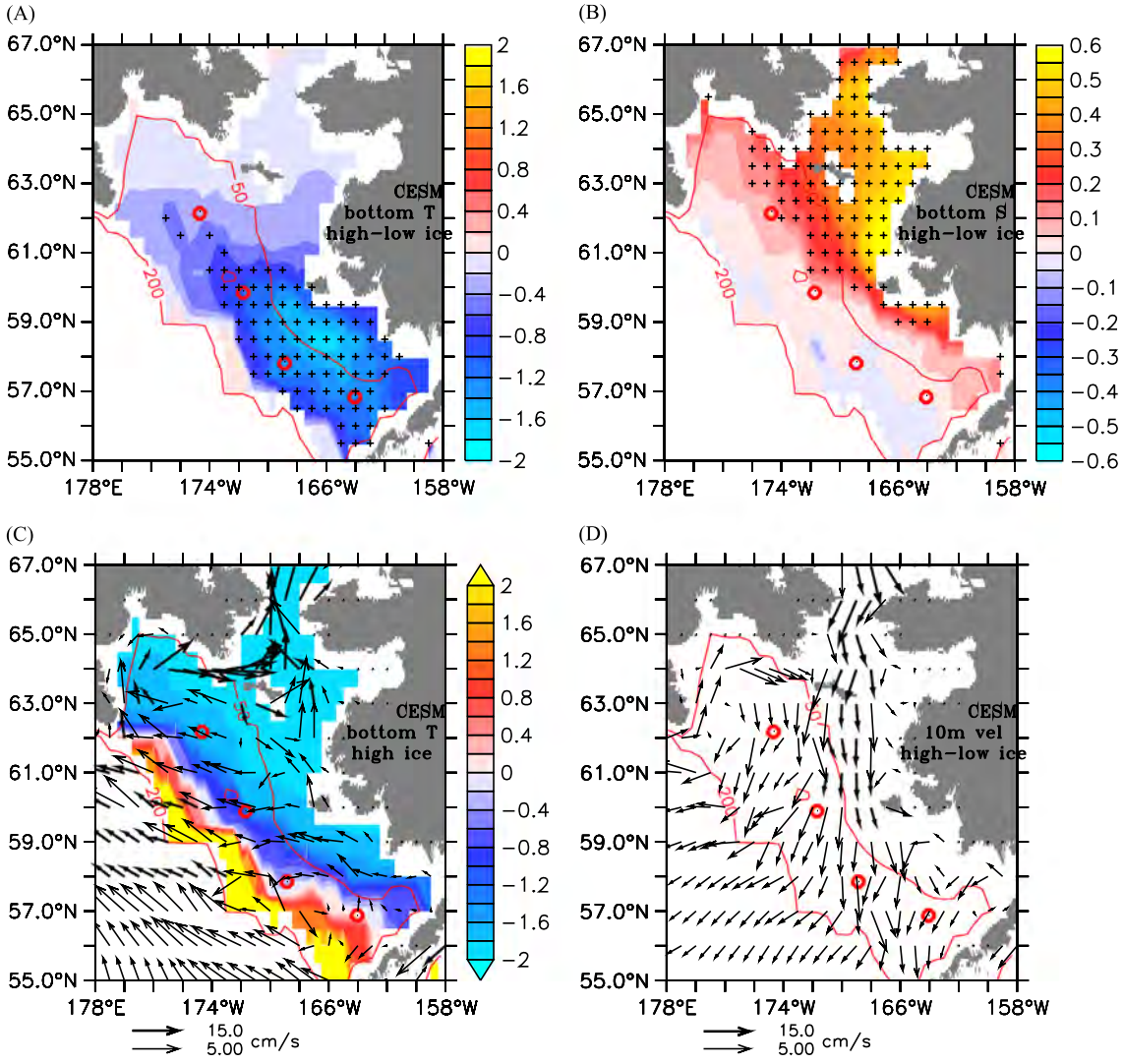

Fig. 9. Modeled March Eastern Bering Sea shelf anomalies of (a) bottom temperature (°C), (b) bottom salinity (psu), and (d) 10 m velocity. Anomalies are defined as the composite mean over high ice years minus that over low ice years (see text for the definitions of high and low ice years). Crosses in (a) and (b) mark where the anomalies are significant at the 95% confidence level. For reference, high ice years' composite mean of March bottom temperature (shade) and 10-m velocity (vector) are shown in (c). Thin red lines in all panels mark the 50 m and 200 m ocean depth. Note the vectors in (c) and (d) use two scales. (For interpretation of the references to color in this figure legend, the reader is referred to the web version of this article.)

changes from late February to mid-March, followed by a slight increase from mid-March to mid-April before stabilizing. At M2, large synoptic scale variability is seen in the modeled salinity. In comparison, moored salinity at M2 and M4 begins to increase in October because of increased cross shelf flux and continues until the arrival of ice, at which time the water column begins to freshen. Throughout the cold season, salinity can vary as a result of advection and ice balance. At M8, most of the freshening in the mooring data occurs with the retreat of ice in the spring, with a layer of fresher water dominating the surface mixed layer throughout the summer. Brine rejection is rarely seen at the mooring sites.

On inter-annual time scales, cold bottom temperature in high ice years results in cool anomalies over the shelf (Fig. 9). The strongest anomaly occurs in the southern domain (Fig. 9a); concomitantly, a large part of the inner and middle shelf exhibits positive salinity anomalies (Fig. 9b). Spatially, the gradient in the temperature anomalies is strongest in the north-south direction, while the salinity anomaly has the strongest gradient in the onshore-offshore direction. As expected, in this subarctic sea, the bottom density anomaly (not shown) is dominantly controlled by salinity. The anomalous ocean circulation associated with extensive ice cover is southward on the shelf except in the Gulf of Anadyr (Fig. 9d), and the largest anomalies are located in the northern coastal domain. The anomalous circulation in the slope region (200 m < depth < 2000 m) is directed offshore.

3.4. Decadal changes: "historical" versus "RCP" simulations

We compare modeled March ice cover at the mooring sites between two periods: 1961–2005 versus 2006–2050 (Fig. 2). During the earlier period, the average ice cover at M2 and M4 is usually < 50% while ice cover at M8 is usually > 50%, with ice cover at M5 fluctuating between low and high conditions on inter-annual time scales (Fig. 10, left panels). Ice cover at all locations in the later period (Fig. 10, right panels) is reduced relative to the earlier period. M2 and M4 are mostly ice-free in the later period, only occasionally having significant ice cover. In the earlier period, the probability distribution functions (PDF) of ice cover at M2 and M4 show high occurrence of low ice cover events, while the PDF at M8 has high occurrence of high ice cover events; the PDF at M5 is approximately flat among all categories (Fig. 11, left panels). In the later period, the PDF at M5 has high occurrence of low ice cover events, while the PDF at M8 is more or less flat among all categories (Fig. 11, right panels). In this sense, the PDF at M8 in the later period is similar to the PDF at M5 in the earlier period.

4. Summary and discussions

In terms of the seasonal cycle of sea ice cover in the EBS, the biggest discrepancies between CESM simulations and satellite observations are the delayed onset of the annual maxima (by a month) and slower spring melting in the northern Bering Sea in the simulation (Fig. 2). One possible reason for the slower spring melting in the model could be that the simulation maintains weak stratification of the water column under the ice (Fig. 8), while observations show that the water column is well mixed throughout the winter. The EBS shelf loses heat and gains freshwater during the melting season. If the ocean layer receiving these fluxes is too shallow due to stratification, this cooling and freshening of the surface layer would be too strong. A cooled ocean slows down further melting, causing a negative feedback on ice melting. An anomalously fresh surface layer further increases water column stability. In addition, an initial delay in ice retreat allows ice to remain into the period when spring winds are weakening, further

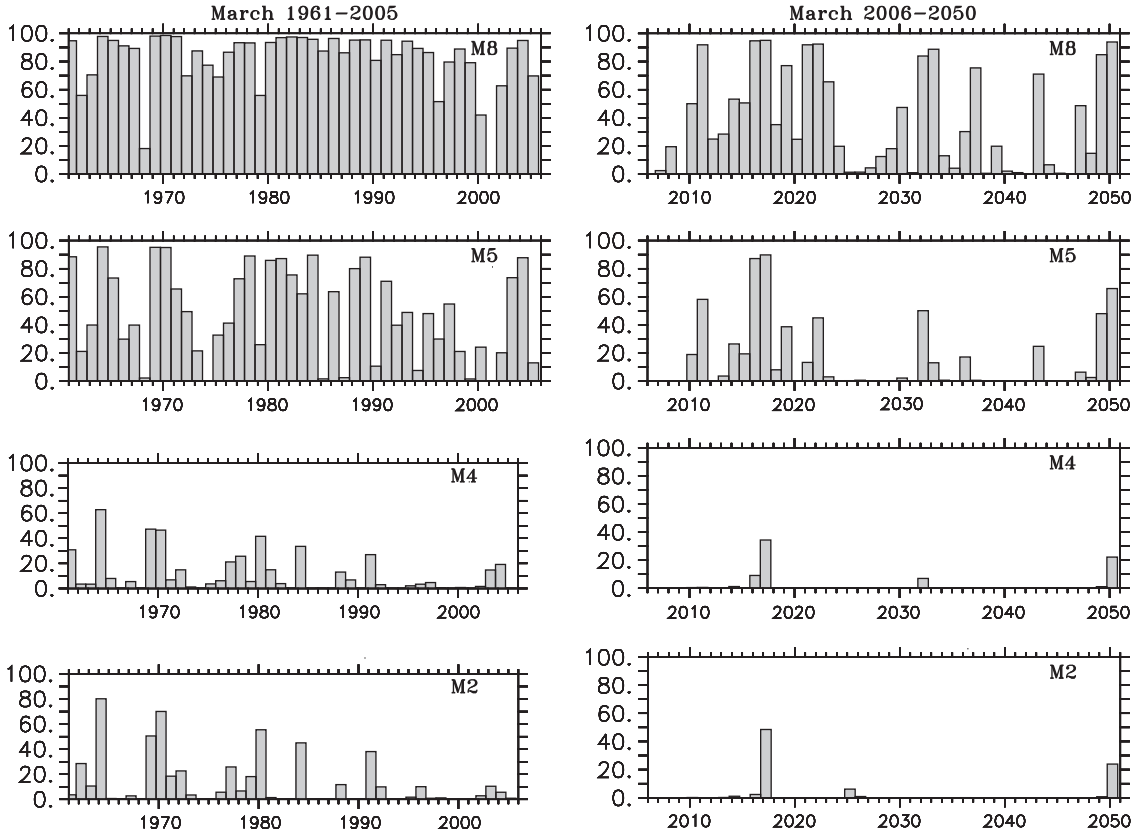

Fig. 10. CESM simulaitons of March ice cover (percentage) at the mooring locations in "historical" time (years 1961–2005, left panels) and "RCP" projections (years 2006–2050, right panels).

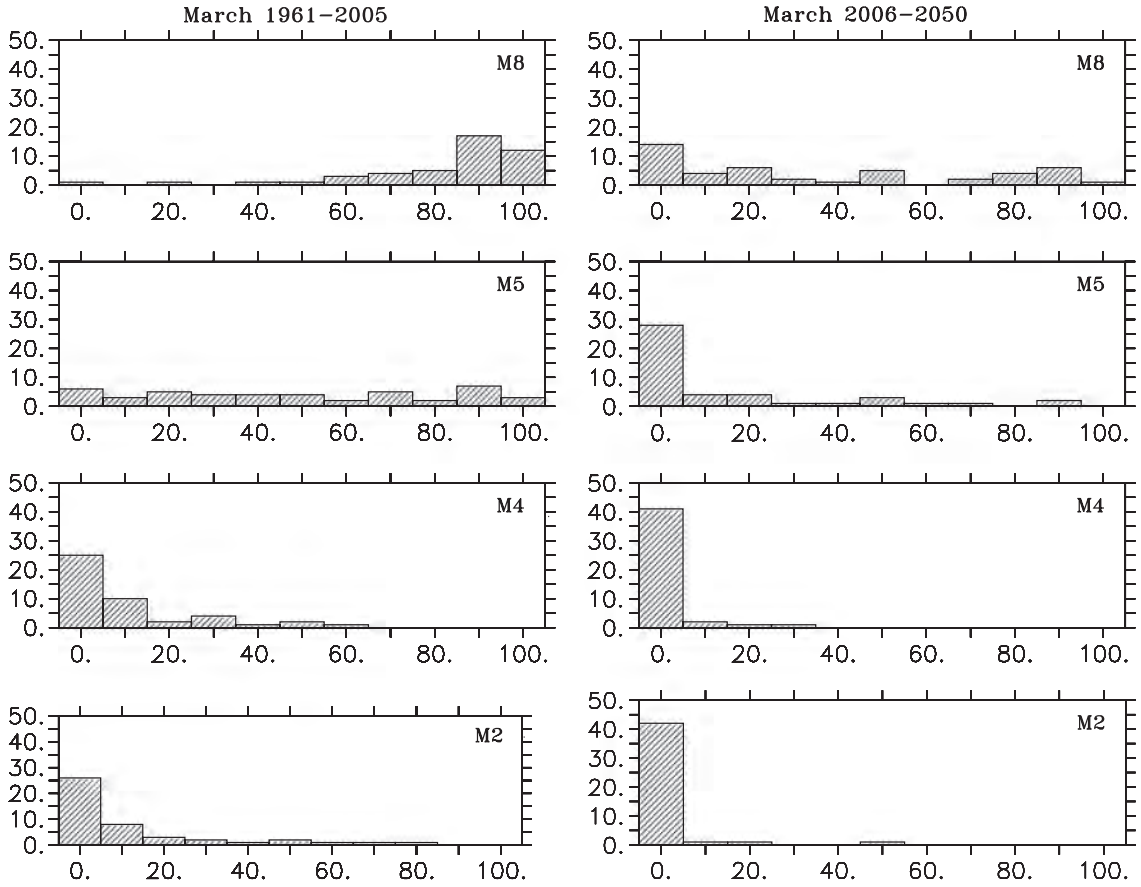

Fig. 11. Probability distribution functions (PDFs) of the CESM simulated March ice cover at the mooring locations. Left panels are from the "historical" simulations (years 1961–2005), and right panels are from the "RCP" simulations (years 2006–2050).

delaying ice break-up and melt. These feedbacks may contribute to the slower melting in the model than in observations.

Modeled seasonal ice advance in the EBS is consistent with the "freshwater conveyor" conceptual model suggested by observations (Pease, 1980). During winter months, sea ice in the model is formed in the northern coastal domain and transported southward and offshore; subsequently sea ice melts in the warmer ambient water (Fig. 5). Based on the CESM simulations, locations of the long-term monitoring moorings M2 and M4 are in the winter melting regime while M8 is within the winter freezing zone; the location of M5 is in a transition zone where both freezing and melting can take place during winter. This representation by the model is consistent with *in situ* observations.

Modeled inter-annual variability in ice advection and thermodynamic formation rates are larger at M8 and M5 locations than farther south (Fig. 6). On the other hand, inter-annual variability in spring ice retreat timing is higher in the southeastern Bering Sea than in the northern Bering Sea (Brown and Arrigo, 2013). Hence, the northern and southern EBSs are both subject to strong inter-annual variability but in different sea ice processes: in the north, variability is associated with the ice formation rate, while in the south, it is associated with the timing of ice retreat.

At all mooring sites and throughout the cold season, modeled heat flux at the ice-ocean interface is from the ocean to the ice while freshwater flux can be either into the ocean (during melting) or out of the ocean (brine rejection during freezing) (Fig. 7). Ice formation in the EBS in nature is influenced by island polynyas. St. Lawrence Island, to the north of M8, and to a lesser extent St. Matthew Island to the north of M5, are associated with important polynyas. Although the St. Lawrence polynya only contributes a small fraction (2.8%) of the total potential ice production in the whole Bering Sea (Hu et al., 2011), the associated brine production can perturb the local salt budget, while its effects on shelf-wide salt budget could be less significant (Danielson et al., 2006). Nonetheless, CESM does not resolve either polynya. Thus, the model underestimates oceanic responses to island polynya formation (Grebmeier and Cooper, 1995).

With these caveats, CESM simulations suggest that higher spring ice concentration in the central EBS leads to positive salinity anomalies (relative to years with less spring ice concentration) on a large part of the bottom water (Fig. 9b). The positive salinity anomaly is strongest in the northern coastal domain, while anomalies are weakly negative in the southern end of the middle- and outer-shelf (Fig. 9b). Correspondingly, bottom water on the shelf has cold anomalies in high ice years relative to low ice years (Fig. 9a), and the anomalies are strongest in the southern domain. Both temperature and salinity anomalies persist from spring into summer (not shown), similar to the persistency in the regional model of Zhang et al. (2012).

The modeled temperature anomalies resemble to some degree the observed southern Bering Sea bottom temperature variability on inter-annual time scales associated with sea ice variations (e.g., Stabeno et al., 2012b). The modeled temperature and salinity anomaly patterns differ regionally (Fig. 9a versus Fig. 9b). This result supports the conclusion by Danielson et al. (2011b) that inter-annual thermal and haline variability over the central Bering Sea shelf are largely uncoupled. The underlying physical mechanisms such as the role of surface forcing (including surface E − P and runoff) and/or lateral advection for these anomalies in the CESM simulations are the subjects of our future investigations.

According to the CESM simulations, surface ocean circulation on the shelf is anomalously southward during high ice years, and

directed off shore in the slope region (Fig. 9d). The southward circulation anomalies on the shelf are consistent with the southward wind anomalies (Fig. 6). Such wind anomalies are also expected to cause the Anadyr current to flow stronger in the on-shelf direction toward Bering Strait (Danielson et al., 2012), a feature reproduced by the CESM. Deeper ocean (depth >30 m) circulation anomalies remain southward on the shelf but slightly northwestward in the slope region (not shown), enhancing the northward flowing Bering Slope Current along the shelf break. The strength of the Bering Slope Current is correlated with the multivariate ENSO index and North Pacific Index on inter-annual time scales (e.g., Ladd, 2014), and these climate indices have been shown to influence the EBS surface wind and sea ice variability (Niebauer, 1998).

Over a 45-year time span (between period 1: 1961–2005 and period 2: 2006–2050), the EBS ice concentration PDF have shifted northward by 2°. PDF of Ice concentration at M8 in the later period is more or less flat, similar to PDF of ice concentration at M5 in the earlier period, while PDF at M5 in the later period becomes similar to PDF at M2 and M4 in the earlier period. Satellite observations thus far have not detected significant trend in the Bering Sea ice cover (Brown et al., 2011), but we expect the situation to change as climate forcing continues and longer observations become available.

Sea ice has profound effects on the EBS primary production (Hunt et al., 2002; Stabeno et al., 2010; Brown and Arrigo, 2013; Sigler et al., 2014), zooplankton community structure (Hunt et al., 2002; Coyle et al., 2011; Eisner et al., 2014), and upper trophic level species (e.g., Wyllie-Echeverria and Wooster, 1998; Mueter and Litzow, 2008). Timing of ice retreat determines timing of the spring bloom. Over the southern shelf, if ice is presented after mid-March, an early ice-associated bloom occurs; otherwise the spring bloom usually occurs in May (Stabeno et al., 2001; Hunt et al., 2002).

Lower water temperatures associated with more sea ice reduce the energy required for zooplankton overwinter survival, resulting in increased spawning biomass and production (Sigler et al., 2014). In addition, the distribution of low bottom temperatures associated with sea ice (the cold pool) determine available habitat for some fish species (Hollowed et al., 2012). Conversely, warmer temperatures increase metabolic requirements, leading to food limitation. This could result in reduced net primary production (Lomas et al., 2012), leading to poor overwinter survival of zooplankton (Coyle et al., 2011).

In addition to influences on temperature and salinity, ice melt results in input of ice algae to the water column, and ice algae provides an early source of food for zooplankton growth and spawning (Sigler et al., 2014). Thus, the "freshwater conveyor" associated with seasonal sea ice in the EBS can also be thought of as conveyor belt for ice algae, and possibly zooplankton. The balances between ice advection and ice formation/melt are important to the ecosystem, and understanding what processes controls the seasonal to inter-annual variability in these balances will have important implications. Our results reiterate that surface winds in the EBS should be closely monitored because of their strong influence on ice advection and formation.

Global climate models are more often used to study global and basin scale processes; their applications on regional scales are less common. However, marine ecosystem responses to changing environment tend to operate on regional scales, and we rely on climate models for future projections. Thus, understanding how climate models work on all scales is critically important to our ability to predict future changes in the physical environment and marine ecosystems. The new insight found in this study is that the CESM, with its limited horizontal resolution, is able to reproduce many aspects of the observed seasonal sea ice advance/retreat in the EBS and its inter-annual variability driven by surface wind, and shows similar processes to those found in higher resolution regional models (Danielson et al., 2011a; Zhang et al., 2010, 2012).

This may seem surprising at first. However, first, CESM includes a state-of-art sea ice model with multiple thickness distribution functions and is shown to simulate the Arctic sea ice very well (e.g., Jahn et al., 2012). Secondly, the seasonal advance and retreat of sea ice in the EBS is strongly influenced by surface wind and hence large scale atmospheric patterns, which climate models simulate reasonably well. In addition, while the CESM horizontal resolution is coarse, the EBS shelf is wide and shallow; the CESM simulated Bering Strait throughflow (1 ± 0.05 Sv) and ice flux (270 ± 39 km^3/year), both were computed from the daily model output, are close to observations (Woodgate et al., 2005; Travers 2012, master thesis, its Table 3.4), indicating that the model is able to capture the dynamic balance between the Bering Sea, the Arctic, and remote forcings (Aagaard et al., 2006). Our next step is to investigate the Bering Sea ice–ocean system in a coupled biophysical ocean–ice circulation model. This class of models can afford higher spatial resolution and is driven by "observed" atmospheric forcing, and is readily comparable to real time observations. Combining knowledge gained from different models and observations should ultimately improve our understanding of the system.

Acknowledgments

We thank W. Floering, C. Dewitt and S. McKeever for maintaining, deploying and recovering the instruments on the mooring, and D. Kachel, and P. Proctor for data processing. Support from NPRB and NOAA's North Pacific Climate Regimes and Ecosystem Productivity (NPCREP) program is gratefully acknowledged. The CESM project is supported by the National Science Foundation and the Office of Science (BER) of the U.S. Department of Energy. Computing resources were provided by the Climate Simulation Laboratory at NCAR's Computational and Information Systems Laboratory (CISL), sponsored by the National Science Foundation and other agencies. This publication is partially funded by the Joint Institute for the Study of the Atmosphere and Ocean (JISAO) under NOAA Cooperative Agreement NA10OAR4320148, Contribution no. 2093. This is contribution FOCI-0806 to the Ecosystems & Fisheries Oceanography Coordinated Investigations, No. 3995 to NOAA/Pacific Marine Environmental Laboratory. This is the BEST-BSIERP Bering Sea Project publication number 129, NPRB publication number 473.

References

Aagaard, K., Weingartner, T.J., Danielson, S.L., Woodgate, R.A., Johnson, G.C., Whitledge, T.E., 2006. Some controls on flow and salinity in Bering Strait. Geophys. Res. Lett. 33 (19), http://dx.doi.org/10.1029/2006GL026612.

Brown, Z.W., van Dijken, G.L., Arrigo, K.R., 2011. A reassessment of primary production and environmental change in the Bering Sea. J. Geophys. Res.: Oceans 116 (C8), http://dx.doi.org/10.1029/2010JC006766.

Brown, Z.W., Arrigo, K.R., 2012. Contrasting trends in sea ice and primary production in the Bering Sea and Arctic Ocean. ICES J. Mar. Sci. 69, 1180–1193, http://dx.doi.org/10.1093/icesjms/fss113.

Brown, Z.W., Arrigo, K.R., 2013. Sea ice impacts on spring bloom dynamics and net primary production in the Eastern Bering Sea. J. Geophys. Res: Oceans 118 (1), 43, http://dx.doi.org/10.1029/2012JC008034.

Coachman, L.K., 1986. Circulation, water masses and fluxes on the southeastern Bering Sea shelf. Cont. Shelf Res. 5 (1–2), 23–108.

Comiso, J.C., 2000. updated 2012, Bootstrap Sea Ice Concentrations from Nimbus-7 SMMR and DMSP SSM/I-SSMIS. Version 2. Final-GSFC, northern hemisphere, Boulder. NASA DAAC at the National Snow and Ice Data Center, Colorado USA

Coyle, K.O., Eisner, L.B., Mueter, F.J., Pinchuk, A.I., Janout, M.A., Cieciel, K.D., Farley, E. V., Andrews, A.G., 2011. Climate change in the southeastern Bering Sea: impacts on pollock stocks and implications for the oscillating control hypothesis. Fish. Oceanogr. 20, 139–156, http://dx.doi.org/10.1111/j.1365-2419.2011.00574.x.

Danielson, S., Aagaard, K., Weingartner, T., Martin, S., Winsor, P., Gawarkiewicz, G., Quadfasel, D., 2006. The St. Lawrence polynya and the Bering shelf circulation:

New observations and a model comparison. J. Geophys. Res.: Oceans 111 (C9), http://dx.doi.org/10.1029/2005JC003268.
Danielson, S., Curchitser, E., Hedstrom, K., Weingartner, T., Stabeno, P., 2011a. On ocean and sea ice modes of variability in the Bering Sea. J. Geophys. Res.: Oceans 116 (C12), http://dx.doi.org/10.1029/2011JC007389.
Danielson, S., Eisner, L., Weingartner, T., Aagaard, K., 2011b. Thermal and haline variability over the central Bering Sea shelf: seasonal and inter-annual perspectives. Cont. Shelf Res. 31 (6), 539–554, http://dx.doi.org/10.1016/j.csr.2010.12.010.
Danielson, S., Hedstrom, K., Aagaard, K., Weingartner, T., Curchitser, E., 2012. Wind-induced reorganization of the Bering Shelf circulation. Geophys. Res. Lett. 39 (8) http://dx.doi.org.com.
Eisner, L.B., Napp, J.M., Mier, K.L., Pinchuk, A.I., Andrews, A.G., 2014. Climate-mediated changes in zooplankton community structure for the eastern Bering Sea. Deep-Sea Res. II 109, 157–171, http://dx.doi.org/10.1016/j.dsr2.2014.03.004.
Gent, P.R., Danabasoglu, G., Donner, L.J., Holland, M.M., Hunke, E.C., Jayne, S.R., Lawrence, D.M., Neale, R.B., Rasch, P.J., Vertenstein, M., Worley, P.H., Yang, Z.-L., Zhang, M., 2011. The Community Climate System Model version 4. J. Climate 24, 4973–4991, http://dx.doi.org/10.1175/2011JCLI4083.1.
Grebmeier, J.M., Cooper, L.W., 1995. Influence of the St. Lawrence Island Polynya upon the Bering Sea benthos. J. Geophys. Res: Oceans 100 (C3), 4439–4460, http://dx.doi.org/10.1029/94JC02198.
Holland, M.M., Bailey, D.A., Briegleb, B.P., Light, B., Hunke, E., 2012. Improved sea ice shortwave radiation physics in CCSM4: the impact of melt ponds and aerosols on Arctic Sea Ice. J. Climate 25, 1413–1430, http://dx.doi.org/10.1175/JCLI-D-11-00078.1.
Hollowed, A.B., Barbeaux, S.J., Cokelet, E.D., Farley, E., Kotwicki, S., Ressler, P.H., Spital, C., Wilson, C.D., 2012. Effects of climate variations on pelagic ocean habitats and their role in structuring forage fish distributions in the Bering Sea. Deep-Sea Res. II 65–70, 230–250 http://dx.doi.org.com.
Hu, H., Wang, J., Wang, D.-R., 2011. A model-data study of the 1999 St. Lawrence Island polynya in the Bering Sea. J. Geophys. Res.: Oceans 116 (C12), http://dx.doi.org/10.1029/2011JC007309.
Hunt Jr., G.L., Stabeno, P., Walters, G., Sinclair, E., Brodeur, R.D., Napp, J.M., Bond, N.A., 2002. Climate change and control of the southeastern Bering Sea pelagic ecosystem. Deep-Sea Res. II 49, 5821–5853.
Jahn, A., Bailey, D.A., Bitz, C.M., Holland, M.M., Hunke, E.C., Kay, J.E., Lipscomb, W.H., Maslanik, J.A., Pollak, D., Sterling, K., Strœve, J., 2012. Late 20th century simulation of Arctic Sea ice and ocean properties in the CCSM4. J. Climate 25, 1431–1452, http://dx.doi.org/10.1175/JCLI-D-11-00201.1.
Ladd, C.A., Stabeno, P.J., 2012. Stratification on the Eastern Bering Sea shelf revisited. Deep-Sea Res. II 65–70, 72–83.
Ladd, C., 2014. Seasonal and interannual variability of the Bering Slope Current. Deep-Sea Res. II 109, 5–13, http://dx.doi.org/10.1016/j.dsr2.2013.12.005.
Lomas, M.W., Moran, S.B., Casey, J.R., Bell, D.W., Tiahlo, M., Whitefield, J., Kelly, R.P., Mathis, J.T., Cokelet, E.D., 2012. Spatial and seasonal variability of primary production on the Eastern Bering Sea shelf. Deep-Sea Res. II 65–70, 126–140.
Mueter, F.J., Litzow, M.A., 2008. Sea ice retreat alerts the biogeography of the Bering Sea continental shelf. Ecol. Appl. 18, 309–320.
Niebauer, H.J., 1998. Variability in Bering Sea ice cover as affected by a regime shift in the North Pacific in the period 1947–1996. J. Geophys. Res.: Oceans 103 (C12), 27717–27737, http://dx.doi.org/10.1029/98JC02499.
Pease, C.H., 1980. Eastern Bering Sea ice processes. Mon. Weather Rev. 108 (12), 2015–2023.
Sigler, M.F., Stabeno, P.J., Eisner, L.B., Napp, J.M., Mueter, F.J., 2014. Spring and fall phytoplankton blooms in a productive subarctic ecosystem, the eastern Bering Sea, during 1995–2011. Deep-Sea Res. II 109, 71–83, http://dx.doi.org/10.1016/j.dsr2.2013.12.007.
Stabeno, P.J., Bond, N.A., Kachel, N.B., Salo, S.A., Schumacher, J.D., 2001. On the temporal variability of the physical environment over the south-eastern Bering Sea. Fish. Oceanogr. 10, 81–98.
Stabeno, P., Reed, R., Napp, J., 2002. Transport through Unimak Pass, Alaska. Deep Sea Res. II: Top. Stud. Oceanogr. 49 (26), 5919–5930, http://dx.doi.org/10.1016/S0967-0645(02)00326-0.
Stabeno, P.J., Napp, J., Mordy, C., Whitledge, T., 2010. Factors influencing physical structure and lower trophic levels of the eastern Bering Sea shelf in 2005: sea ice, tides and winds. Prog. Oceanogr. 85 (3–4), 180–196.
Stabeno, P.J., Farley Jr., E.V., Kachel, N.B., Moore, S., Mordy, C.W., Napp, J.M., Overland, J.E., Pinchuk, A.I., Sigler, M.F., 2012a. A comparison of the physics of the northern and southern shelves of the eastern Bering Sea and some implications for the ecosystem. Deep-Sea Res. II 65–70, 14–30.
Stabeno, P.J., Kachel, N.B., Moore, S.E., Napp, J.M., Sigler, M., Yamaguchi, A., Zerbini, A.N., 2012b. Comparison of warm and cold years on the southeastern Bering Sea shelf and some implications for the ecosystem. Deep-Sea Res. II 65–70, 31–45.
Stroeve, J., Holland, M.M., Meier, W., Scambos, T., Serreze, M., 2007. Arctic sea ice decline: faster than forecast. Geophys. Res. Lett. 34, L09501, http://dx.doi.org/10.1029/2007GL029703.
Sullivan, M., Mordy, C., Salo, S., Stabeno, P., 2014. The influence of sea ice on seasonal water column changes on the eastern Bering Sea shelf. Deep-Sea Res. II 109, 39–86.
Vavrus, S.J., Holland, M.M., Jahn, A., Bailey, D.A., Blazey, B.A., 2012. 21st-century arctic climate change in CCSM4. J. Climate 25, 2696–2710, http://dx.doi.org/10.1175/JCLI-D-11-00220.1.
Wang, M., Overland, J.E., 2009. A sea ice free summer Arctic within 30 years? Geophys. Res. Lett. 36, L07502, http://dx.doi.org/10.1029/2009GL037820.
Woodgate, R.A., Aagaard, K., Weingartner, T.J., 2005. Monthly temperature, salinity, and transport variability of the Bering Strait through flow. Geophys. Res. Lett. 32 (4), http://dx.doi.org/10.1029/2004GL021880.
Wyllie-Echeverria, T., Wooster, W.S., 1998. Year-to-year variations in Bering Sea ice cover and some consequences for fish distributions. Fish. Oceanogr. 7, 159–170.
Zhang, J., Woodgate, R., Moritz, R., 2010. Sea ice response to atmospheric and oceanic Forcing in the Bering Sea. J. Phys. Oceanogr. 40 (8), 1729–1747, http://dx.doi.org/10.1175/2010JPO4323.1.
Zhang, J., Woodgate, R., Mangiameli, S., 2012. Towards seasonal prediction of the distribution and extent of cold bottom waters on the Bering Sea shelf. Deep Sea Res. II: Top. Stud. Oceanogr. 65–70, 58–71, http://dx.doi.org/10.1016/j.dsr2.2012.02.023.

Deep-Sea Research II 109 (2014) 39–56

Contents lists available at ScienceDirect

Deep-Sea Research II

journal homepage: www.elsevier.com/locate/dsr2

Sea ice and water column structure on the eastern Bering Sea shelf

Margaret E. Sullivan [a,b,*], Nancy B. Kachel [a,b], Calvin W. Mordy [a,b], Sigrid A. Salo [b], Phyllis J. Stabeno [b]

[a] Joint Institute for the Study of the Atmosphere and Ocean, University of Washington, 3737 Brooklyn Ave NE, Box 355672, Seattle, WA 98105-5672, USA
[b] Pacific Marine Environmental Laboratory, NOAA, 7600 Sand Point Way NE, Seattle, WA 98115, USA

ARTICLE INFO

Available online 30 June 2014

Keywords:
Bering Sea
Sea ice
Ocean temperature
Salinity
Ocean currents
Stratification
Ice melt

ABSTRACT

Seasonal sea ice is a defining characteristic of the eastern Bering Sea shelf, and plays a critical role in determining the vertical structure of temperature and salinity over this shelf. Ice movement relative to local winds, ice composition, and the impact of both arrival and retreat of ice on the water column at four mooring sites over the middle shelf are examined. Ice forms primarily in coastal regions and is advected over the southern and outer shelves. Ice drift from satellite data for two representative years, 2003 and 2007, was ~2% of local NCEP wind speed and oriented 44° to the right of the winds (r^2=0.25). Measurements from 30 ice cores collected in 2006–2009 gave an average salinity of 5.62 ± 0.88, and an average nitrate concentration of 0.99 ± 0.83 μM. Time series data collected at the biophysical moorings in the Bering Sea (1995–2012) were used to explore the evolution of the water column under ice. At the northern mooring, M8, the water column had mixed and cooled to ~−1 °C prior to the arrival of ice. Little melt occurred after ice arrival. At the other three moorings, the ocean temperature was 2–4 °C when ice arrived, resulting in extensive melt. Melting ice freshened and cooled the upper water column, resulting in stratification, which persisted for 10–25 days. Wind-induced water-column mixing occurred more slowly under the ice than in ice-free waters. An estimated 1.4 m of ice melted with the first arrival of ice at the three southern moorings where the latent heat of fusion accounted for approximately half the observed cooling. During ice retreat, there appeared to be little ice melt around the southern two moorings, but an estimated 0.8 m at M5 and M8. The extent of ice melt sets up the water column for the following summer.

1. Introduction

Situated between the North Pacific and the Arctic Ocean, the eastern Bering Sea shelf is ice-free in summer. Ice begins to form along the coast in the northern Bering Sea as early as November (Pease, 1980). During subsequent months, the sea ice is advected southward with maximum ice extent typically occurring in March or April (Stabeno et al., 2012b). In extensive ice years, sea ice can advance more than 1000 km, which, prior to the extensive melting now occurring in the Arctic Ocean, was the largest ice advance in any arctic or subarctic region (Niebauer, 1998). Sea ice typically begins to retreat in late winter or early spring, and the Bering Sea is again ice-free by late June.

Pease (1980) describes the expansion of ice into the southern Bering Sea middle shelf as a conveyor belt in which ice forms in polynyas in the northern Bering Sea, and is advected southward by winds. These polynyas are most common on the southward- and westward-facing coastlines due to prevailing northerly winds in winter, but can also form off northward- and westward-facing coastlines when winds are southerly (Niebauer and Schell, 1993; Niebauer et al., 1999). The St. Lawrence polynya occurs along the southern coast of St. Lawrence Island, and is a dominant ice-producing feature (Danielson et al., 2006; Drucker et al., 2003; Schumacher et al., 1983; Stringer and Groves, 1991), with ice advected primarily toward the south and southwest (McNutt, 1981). The leading edge of the ice melts as it encounters warmer ocean temperatures in the south or along the shelf break (McNutt, 1981; Zhang et al., 2010).

The eastern Bering Sea continental shelf is broad (>500 km), less than 180 m deep, and extends more than 1200 km south from Bering Strait to the Aleutian Islands. The shelf is divided into inner (water depth <50 m), middle (~50–100 m), and outer (~100–180 m) domains (Coachman, 1986), which are separated by transition zones or fronts (Kachel et al., 2002; Schumacher et al., 1979; Stabeno et al., 2001). Ice typically appears first in the coastal

* Corresponding author at: Pacific Marine Environmental Laboratory, NOAA, 7600 Sand Point Way NE, Seattle, WA 98115, USA. Tel.: +1 206 526 6185; fax: +1 206 526 6485.
E-mail address: msulliva@u.washington.edu (M.E. Sullivan).

http://dx.doi.org/10.1016/j.dsr2.2014.05.009
0967-0645/

domain, and latest in the outer domain. On average, sea ice covers the middle shelf north of 58°N for five months each year, with ice persisting, on average, for less than one month on the shelf south of 57°N (Stabeno et al., 2012a).

North–south differences in timing of ice retreat and advance, together with a north (weaker)–south (stronger) gradient in tidal energy, result in distinct differences in the water-column structure on the northern and southern shelves during the summer (Stabeno et al., 2012a). The northern shelf, with a more extensive and persistent ice cover, remains cold until solar input warms the ocean, initiates ice melt, and sets up summer stratification. This results in a warmer, fresher surface layer overlaying a colder, saltier bottom layer separated by a ~10 m interface. The cold bottom layer (<2 °C) over the middle shelf, known as the cold pool, remains largely well mixed due to the tides and persists through the summer. In contrast, in the south, ice retreat typically occurs in March or April with southerly winds; these winds are usually still strong enough to mix the water column (Stabeno et al., 2010). The water column becomes thermally stratified when winds weaken and solar insolation increases (Stabeno et al., 2007). In years with extensive ice in March or April, the bottom temperatures in ice-covered areas in the south are <2 °C, and part of the cold pool (Stabeno et al., 2012b; Wyllie-Echeverria and Wooster, 1998). During years when the sea ice does not extend onto the southern shelf, the bottom temperatures remain above 2 °C, and the cold pool exists only over the northern shelf (Stabeno et al., 2012a, 2012b).

The presence or absence of sea ice impacts spatial and temporal variability of biological production across the shelf and slope (Sigler et al., 2014; Stabeno et al., 2012a, 2012b). Constituents of sea ice, including iron and phytoplankton, are advected southward, and influence the amount and fate of spring production (Aguilar-Islas et al., 2008; Schandelmeier and Alexander, 1981). In addition, sea ice impacts the timing of the spring phytoplankton bloom, with an under-ice bloom occurring if ice is present after mid-March, and an open-water bloom occurring in May or June if no ice is present after mid-March (Brown and Arrigo, 2013; Sigler et al., 2014; Stabeno et al., 2012a). Vertical stratification of the water column is important to support under-ice phytoplankton blooms (Alexander and Niebauer, 1981; Mundy et al., 2009). The southern extent of the cold pool and the timing of spring primary production influence the food chain and higher trophic level predator–prey relationships for the following 6–8 months (Sigler et al., 2014), and over longer time scales (Mueter and Litzow, 2008).

The purpose of this paper is to examine the impact of sea ice on the vertical structure of the water column. Measurements from satellites, ice cores and four long-term biophysical moorings distributed along the 70-m isobath from 56.9°N to 62°N are used to determine the rate and direction of ice movement, the arrival of ice at moorings, and the extent of ice melt and resulting stratification at each of the mooring sites (Fig. 1). First, calculations of the rate and direction of ice movement in the region using satellite images are shown. Next, the characteristics of 30 ice cores collected from 2006 to 2009 are presented. Using time series of temperature, salinity and currents from the biophysical moorings (M2, M4, M5 and M8; Fig. 1), the impact of sea ice on the water column structure is examined. Using selected time series from the ~42 yearly records, the thickness of the ice melted at the mooring sites is estimated.

2. Methods

2.1. Satellite data

Satellite measurements of ocean color and sea surface temperature (SST) were obtained using Moderate Resolution Imaging Spectroradiometer (MODIS) data files from the ocean color website at NASA (http://oceancolor.gsfc.nasa.gov). SeaDAS, a NASA image-analysis package, was used to map true-color and SST images. Individual ice floes were identified in a series of true-color images and tracked from one image to another until they were no longer recognizable (Holt et al., 1992; Leberl et al., 1983). Ocean color and SST observations cannot be made through clouds, severely limiting the number of MODIS images conducive to floe-tracking over a stormy Bering Sea. In addition, increased cloud cover is associated with southerly winds, so the set of tracked floes were biased against times when southerly winds were prevalent. This limited the analysis to years with a sufficient number of consecutive days clear enough to follow a floe, and to large floes in regions where horizontal shear was weak enough that floes remained intact.

For 2002–2011, ice concentration data from the Advanced Microwave Scanning Radiometer-Earth Observing System (AMSR_E) sensor aboard the MODIS Aqua satellite were downloaded from the National Snow and Ice Data Center website (http://nsidc.org/data/amsre/; Cavalieri et al., 2003). Ice concentrations from the NASA Special Sensor Microwave Imager (http://nsidc.org/data/docs/daac/ssmi_instrument.gd.html; Maslanik and Stroeve, 1999) were used for fall 1994–2002 to extend the time span prior to the start date of AMSR-E data. Daily-mean ice concentration values were used in this paper. The data were used to calculate mean daily ice concentrations within boxes centered on the four moorings (M2, M4, M5, and M8 in Fig. 1). The grid size of the ice data is approximately 12.5 km × 12.5 km. Following Stabeno et al. (2012a) we used 100 km × 100 km boxes.

2.2. Wind stress and winds

The National Center for Environmental Prediction – Department of Energy Reanalysis 2 (NCEP-2) uses a state-of-the-art analysis/forecast system to perform data assimilation with data ranging from January 1979 to August 2012 (http://www.cpc.ncep.noaa.gov/products/wesley/reanalysis2/; Kanamitsu et al., 2002), and is an update to the National Center for Atmospheric Research (NCEP/NCAR) reanalysis. Six-hourly wind and wind-stress data were extracted from the NCEP-2 at the grid points nearest to the four mooring locations. These data were obtained from the website maintained by NOAA Earth System Research Laboratory, Physical Sciences Division in Boulder, Colorado, USA (http://www.esrl.noaa.gov/psd/). NCEP-2 winds are well correlated with observed winds in the Bering Sea (Ladd and Bond, 2002).

QuikSCAT wind data were downloaded from the Jet Propulsion Laboratory, Physical Oceanography Distributed Active Archive Center (http://podaac.jpl.nasa.gov). Scatterometer winds are derived from ripple patterns on the surface of the ocean, and are therefore limited to ice-free areas. Although the instrument sees through clouds, measurements are affected by heavy rain. The records identify pixels where rain was suspected, and these records were excluded from our analysis. Grid spacing for QuikSCAT winds is 12.5 km (0.25° longitude), and the data were binned into 2° bins for regional plots.

2.3. Ice core measurements

During four springs (2006–2009), a total of 30 ice cores were collected from floes distributed over the eastern Bering Sea shelf by NOAA and University of Washington scientists (Fig. 1B). In 2006, sampling was conducted from the R/V *Thomas* G. *Thompson* (Cruise TN193). The *Thompson* is not an icebreaker and thus, sampling was restricted to the ice edge. Cruises in 2007–2009 were conducted on the icebreaker U.S.C.G.C. *Healy* as part of the

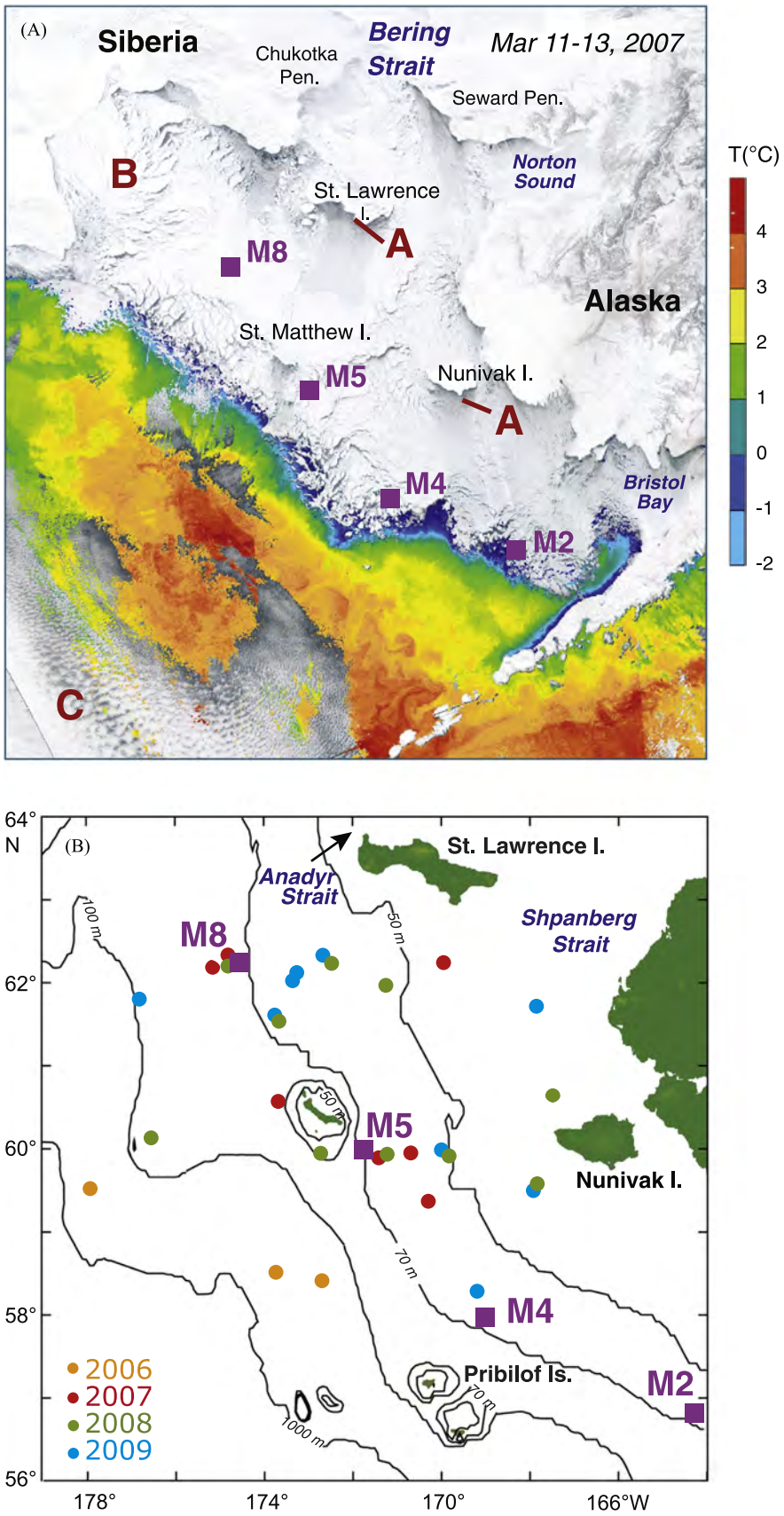

Fig. 1. (A) A MODIS True-Color image combined with MODIS sea surface temperature in the Eastern Bering Sea for March 11–13, 2007. The large red letters indicate: A, polynyas; B, heavy ice; and C, cloud cover. (B) Shelf map showing distribution of ice sampling sites in each year (2006–2009) and bathymetry. The four mooring locations (M2, M4, M5, and M8) and geographic names are also indicated in both panels.

Table 1
Ice stations, 2006–2009, with mean data values for each core. Arithmetic mean and standard deviation from data points are listed at the bottom. The ice thickness value for 2007 ice-station #2 was excluded from the mean thickness.

Date	Ice station	Snow depth (cm)	Ice thickness (cm)	Air temp. (°C)	Mean salinity	Mean temp. (°C)	Mean ice density (10^3 kg m^{-3})	Mean nitrate (μM)	Chl *a*, trad. (μg/l)
29-April-06	01 (D3)	2	50	−5.5	4.86	−1.72	0.89	0.4	1.69
30-April-06	02 (D4)	4	37	−5.9	7.23	−2.48	0.85	0.5	1.59
3-May-06	03 (E3)	27	100	−2.6	6.00	−1.58	0.97	2.2	2.78
17-April-07	1	1	51	−9.8	5.83	−3.75	0.91	0.3	35.06
19-April-07	2	–	>329	–	4.05	−4.14	0.89	1.1	–
21-April-07	3	2	30	−1.0	–	−2.00	–	0.2	–
24-April-07	4	3	73	−1.2	5.79	−1.46	0.91	1.2	4.48
30-April-07	5	2	64	–	4.74	−1.39	0.89	0.4	18.24
6-May-07	6	2	62	−1.0	5.26	−1.43	0.90	0.1	42.92
7-May-07	7	0	69	2.6	4.00	−0.10	0.82	3.1	20.65
3-April-08	1	10	44	0.9	6.57	−2.23	0.93	1.2	–
4-April-08	2	43	92	−10.0	5.64	−3.44	0.89	1.1	5.99
6-April-08	4	8	55	−5.3	5.77	−2.56	0.89	1.1	–
8-April-08	5	8	41	−13.8	5.86	−3.20	0.92	3.5	–
8-April-08	5a	6	40	–	5.44	−3.25	0.91	1.5	–
12-April-08	6	4	76	−8.0	7.24	−2.86	0.83	1.0	18.02
15-April-08	8	17	85	–	–	−2.73	–	0.3	2.84
16-April-08	9	11	59	−1.1	–	−2.38	–	0.8	2.65
28-April-08	10	5	41	−2.5	6.34	−2.10	0.88	0.2	–
29-April-08	11	7	69	−4.0	6.04	−2.19	0.85	0.7	9.51
30-April-08	12	5	71	−3.0	5.29	−2.13	0.88	2.1	13.66
5-April-09	1	4	73	1.5	5.70	−2.97	0.92	1.5	14.17
7-April-09	2	17	87	−0.2	5.05	−3.09	0.89	0.3	5.14
14-April-09	3	5	93	−10.6	6.39	−5.46	0.91	0.5	13.44
16-April-09	4	9	43	−4.2	7.21	−4.35	0.92	1.2	34.04
18-April-09	5	28	87	−5.3	4.59	−1.60	0.92	0.7	8.81
20-April-09	6	30	86	−3.6	5.63	−2.56	0.88	0.4	9.25
1-May-09	8	16	64	–	–	−1.76	–	1.4	34.25
2-May-09	9	4	42	−0.2	4.70	−0.60	0.84	0.3	13.56
3-May-09	10	21	127	−0.6	5.04	−1.78	0.86	0.3	3.80
Mean		10	66	−3.8	5.62	−2.44	0.89	0.99	12.76
Std. deviation		10	23	4.1	0.88	1.11	0.03	0.83	30.49

Bering Sea Project (http://bsierp.nprb.org/). This permitted sampling deep into the pack-ice.

Floes were chosen for accessibility and for ease of data collection. Sampling was biased against ice that was too thin to walk on or highly rafted, and to times when air temperature was above −15 °C. All samples were taken in spring when both melting and refreezing were prevalent. In 2006, the three ice-sampling stations were located along the ice edge in the outer domain. The 27 stations sampled in 2007–2009 were located within the ice field over the middle and inner domains (Fig. 1B; Table 1).

At most sites, air temperature, freeboard, ice thickness, and snow cover were recorded; geographic coordinates were recorded at the beginning and end of each site visit using a GPS unit. All cores were obtained using a Kovacs[1] Mark-II, 9-cm diameter, 1.15-meter-long ice corer driven by an attachable gas engine. Cores were positioned on a black plastic surface, then measured and photographed. Top and bottom conditions and banding were noted. Small holes were drilled and temperatures were recorded every 10 cm along the core using either an Oakton Acorn or an Omega thermometer. All cores were sliced into 10-cm sections and double-bagged for later analysis. On the ship, sections from each core were thawed in the dark. The melt-water volume was measured and then sub-sampled to measure salinity and nutrient concentrations. Salinities were processed at sea using a salinometer referenced against IAPSO standard water. Ice density was determined from the dimensions of each ice core, and the volume of the ice melt.

[1] Use of trade names does not constitute an endorsement by NOAA.

Samples for nutrient analysis were filtered using a syringe with 0.45 μm cellulose acetate membranes, and collected in 30 ml acid-washed, high-density polyethelene bottles after being rinsed three times with sample water. Samples were analyzed shipboard within 12 hours of collection. Nitrate and nitrite concentrations were determined using a combination of analytical components from Alpkem, Perstorp, and Technicon. WOCE-JGOFS standardization and analysis procedures specified by Gordon et al. (1994) were followed, including reagent preparation, calibration of labware, preparation of primary and secondary standards, and corrections for blanks and refractive index.

For determination of chlorophyll and phaeopigment content, a second core was taken at the sites. One liter of filtered sea water was added to sections of ice to prevent cell lysis during melting. Sub-samples (~250 ml) were filtered though Whatman GF/C filters, and the filters were frozen at −80 °C, for later analysis. Pigments were extracted in cold 90% acetone in the dark for 24 hours and values determined using a calibrated fluorometer according to the acidification method (Strickland and Parsons, 1968).

2.4. Moorings

Four biophysical mooring sites (M2, M4, M5, and M8) are the cardinal locations of the Bering Sea biophysical observing network (Fig. 1). When possible, the moorings are recovered and redeployed twice a year, once in the spring (April/May) and again in the late summer or early fall (September/October). During years with extensive ice, moorings at M8 and sometimes at M5 are only recovered/deployed in September. Moorings at M2 have been maintained almost continually since 1995, while moorings have

been deployed at M4 since 1996 (continuously since 2000), at M5 since 2005, and at M8 since 2004. At the writing of this manuscript, these moorings provided 42 fall-through-spring sets of time series describing water-column conditions.

Data collected by instruments on the moorings included temperature (miniature temperature recorders, SeaBird SBE-37 and SBE-39) and salinity (SBE-37). Currents were measured using an upward-looking, bottom-mounted, 300 or 600 kHz Teledyne RD Instruments Acoustic Doppler Current Profiler (ADCP) deployed within 500 m of the main mooring. All instruments were calibrated prior to deployment, and the data were processed according to manufacturers' specifications. The main mooring "line" at each site was chain and the instruments were mounted in-line in metal frames. Such construction is necessary to reduce the chances of losing the mooring due to sea ice and heavy fishing pressure in the region.

Sampling intervals varied among the different instruments and ranged from 10 to 60 min. Small data gaps (<1 day) were filled using linear interpolation or spectral methods. Unless otherwise noted, data presented here have been filtered using a 35-hour, cosine squared, tapered Lanczos filter to remove semidiurnal and diurnal tidal signals, and re-sampled to 6-hour intervals. Daily mean currents were calculated from the low-pass-filtered data, and thus do not include tides.

The top instrument at each mooring was at a depth between 1 and 20 m. When the mixed layer was deeper than the depth of the top instrument, the data from the top instrument could be reliably extrapolated to the surface (Stabeno et al., 2007). However, when the top instrument was below ~20 m and the ice had retreated from the mooring in the spring, the mixed layer was usually shallower than the top instrument and near-surface temperatures estimates were not reliable.

2.5. Calculation of volume of ice melt

Estimates of magnitude of ice melt can be made at the mooring sites from the change in salinity in the water column using the following equation:

$$h_w S_i + (H - h_w) S_w = H S_f \quad (1)$$

or

$$h_w = H(S_w - S_f)\,(S_w - S_i)^{-1} \quad (2)$$

where h_w is the thickness of water resulting from ice melt, S_i is the salinity of the ice, H is the depth of the upper mixed layer (which may be the whole water column), S_w is the initial salinity of the water column and S_f is the final salinity of the water column. This is an approximation since an introduced piece of ice does not melt completely, but rather the ice is advected over the water with only a portion of it melting at that location. When the water reaches the freezing point, there is no further net melting of the ice.

The thickness of the ice melted, h_i, was calculated using $h_i = h_w \rho_w / \rho_i$, where ρ_w is the density of water and ρ_i is the density of ice. Using the value of h_w calculated from salinity, the change in temperature of the water column per unit area due to latent heat can be calculated using the following equation:

$$\Delta T \text{ per unit area} = L \rho_i h_i (C_w \rho_w (H - h_w))^{-1} \quad (3)$$

where L is the latent heat of fusion of sea ice, C_w is the specific heat capacity of seawater, and T is temperature. This calculation is an approximation that includes several assumptions, primarily that there is no advection or there are no horizontal gradients. While it is impossible to completely avoid advection and gradients in these data sets, care must be taken in selecting examples to limit these influences.

3. Results and discussion

3.1. Satellite floe-tracking and winds

Ice in the Bering Sea can be broadly characterized using true-color satellite imagery from which polynyas (dark shadows leeward of the coastline), thin ice (gray, often seaward of the open water of the polynya), and thicker ice (white) can be identified (Fig. 1A). Ice conditions, including the location of polynyas and the direction and extent of ice advance, can change rapidly and are largely forced by winds (Fig. 2). For example, in late February 2003, northeasterly winds near Siberia and easterly winds off the Alaskan coast reduced the ice concentration near Siberia, St. Lawrence Island, and the Alaskan coast (Fig. 2A). Nine days later, southerly winds over the eastern shelf resulted in ice edge retreat in the east and compression of the ice along those coastlines (Fig. 2B). In mid-March, northerly winds opened polynyas in the north, advanced the ice edge, and increased the ice concentration at the ice edge (Fig. 2C).

Floe trajectories obtained from true-color satellite images are shown for 2003 and 2007 (Fig. 3), a warm and a cold year, respectively (Stabeno et al., 2012b). These trajectories are primarily from advancing ice. While many floes could only be tracked for a few days, several were tracked for 1–2 weeks while they moved southward more than 100 km. The maps from both years show a corridor in which ice floes moved from the shelf north and east of St. Lawrence Island through Shpanberg Strait, with more westward ice motion in 2003 than 2007 as floes moved beyond Shpanberg Strait. These observations are similar to the conveyor belt corridor observations of Pease (1980). With southerly winds, ice produced from a polynya north of Nunivak Island could also contribute to the conveyor belt corridor (Figs. 2 and 3A). South of the Chukotka Peninsula, floes moved eastward with prevailing currents (Danielson et al., 2006), and those nearest the coast continued north through Anadyr Strait. A few floes originating southwest of St. Lawrence were tracked to M8 (Fig. 3).

These floe trajectories were used to infer the origin of ice in each of the four mooring areas (Figs. 1 and 3). The ice at M8 originated from the conveyor belt, from the polynya south of St. Lawrence Island (McNutt, 1981; Schumacher et al., 1983), and occasionally from Anadyr Strait (Schumacher et al., 1983). The M4 and M5 sites were directly influenced by ice from the conveyor belt corridor (Muench and Ahlnas, 1976; Pease, 1980). The area around M2 was outside the dominant influence of the conveyor belt corridor, and was subject to ice formed in polynyas to the south of Nunivak Island and along the northern Bristol Bay coast during northerly or northeasterly winds.

Tracked floes, which had typical speeds of 0.1–0.3 m s^{-1}, were influenced by both winds and currents. These findings are comparable to earlier observations (McNutt, 1981; Muench and Ahlnas, 1976; Shapiro and Burns, 1975; Weeks and Weller, 1984), as well as results from a recent ice model (Zhang et al., 2010), but slower than the 0.5 m s^{-1} average reported by Pease (1980) and the 0.45 m s^{-1} average reported by Macklin et al. (1984). Ice drift was compared to NCEP-2 winds interpolated in space and time, and found to be ~2% of local wind speed ($n=440$) and oriented 44° to the right of the wind direction with an R-squared value of 0.25, which is higher than the findings of Macklin et al. (1984).

While wind largely controlled the movement of sea ice (Figs. 2 and 3), the timing of storms was also important. The influence of wind events on ice formation varied dependent upon the season. Northerly winds during active freeze-up (January into March) created more ice than similar winds would have generated during warming (mid-April to May). Nonetheless, northerly winds later in the season could prolong ice cover by continuing to transport ice southward. For example, in the winter of

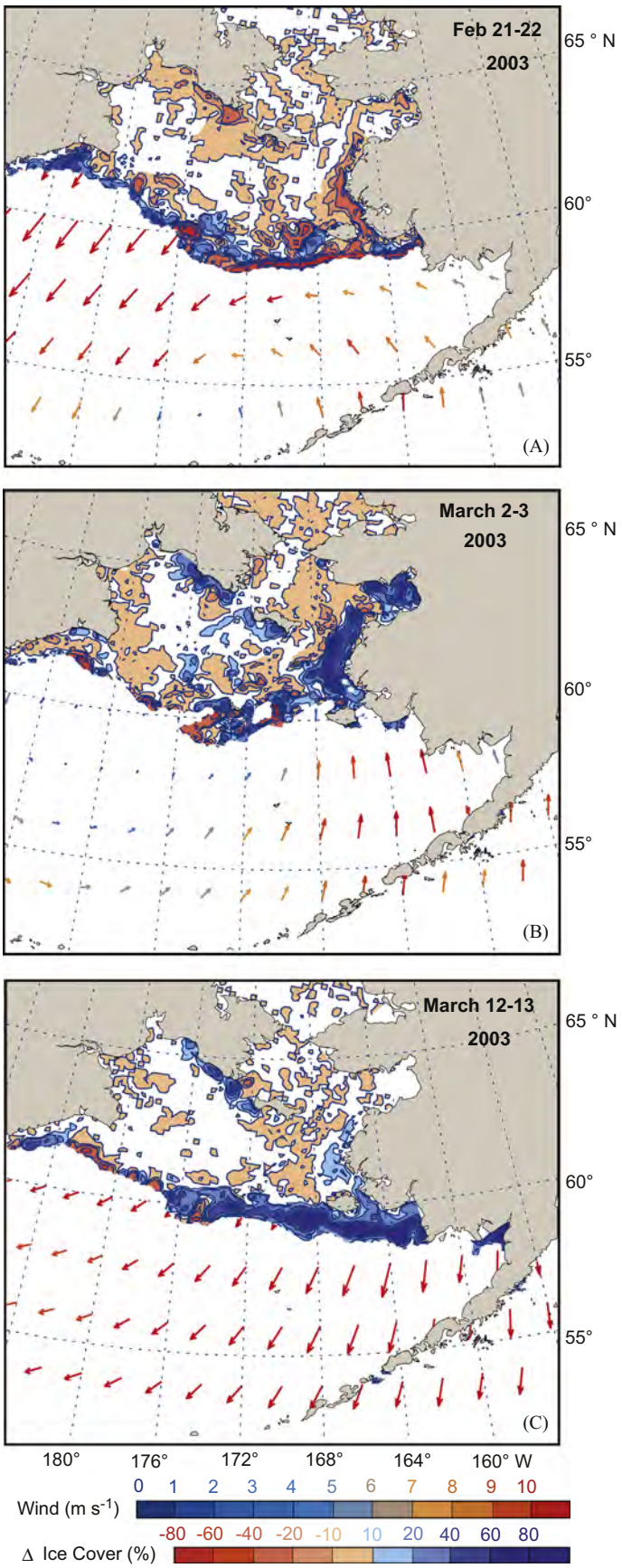

Fig. 2. Change in ice concentration (color filled) and associated 2-day mean QuikSCAT winds (vectors) are shown for three time periods: (A) February 21–22, 2003; (B) March 2–3, 2003; and (C) March 12–13, 2003.

2005–2006, northerly winds in December and January (Fig. 4A) pushed the ice to its most southern extent in late January, despite a water-column temperature of ~2.8 °C. The next episode of sustained northerly winds occurred in mid-April (initial water temperature of 0.5 °C), and although the ice advanced at this time, the ice edge did not regain its earlier position due to warmer water temperatures. At the beginning of April, the water column warmed from −1 °C to >0 °C. In contrast, during the winter of 2006–2007, there were several storms in December and January (Fig. 4B), but the longest period of northerly winds was during March and April. Sea ice reached its maximum southern extent in late March (Rodionov et al., 2007). The water column cooled in early March (from 1.1 °C to −1.7 °C) and did not begin warming until the ice began retreating.

3.2. Sea-ice cores

Thirty ice stations were sampled on the eastern Bering Sea shelf in April and early May on four cruises between 2006 and 2009 (Fig. 1B). Ice thickness ranged from 37 to 127 cm with a single outlier of >329 cm of rafted ice at an inner domain station (Table 1). Mean ice thickness was calculated excluding this outlier. Surface water from nearby hydrographic casts over these four years had mean salinity of 31.9, mean temperature of −1.7, and mean nitrate concentration of 10.2 μM. Salinities in the ice were low (mean 5.62 ± 0.88, Table 1), reflecting brine rejection during ice formation and brine drainage. There was considerable variability in the shapes of the salinity profiles (Fig. 5C). Some salinity profiles showed the well-defined C-shape (e.g.,left-most curve, Fig. 5C) of marginal ice zones and young ice (Eicken, 2003; Malmgren, 1927). Another common pattern was a double C-shape, often a result of rafting. Mean ice density of $0.89 \pm 0.03 \times 10^3$ kg m^{-3} is in agreement with Table 1 summary in Timco and Frederking (1996). Nutrient concentrations were low in the ice cores (mean nitrate 0.99 ± 0.83 μM), suggesting that ice was not a conveyor of macro nutrients in the Bering Sea. Melting sea ice, however, did provide a significant contribution of iron to the water column (Aguilar-Islas et al., 2008).

Horizontal banding was evident in the ice cores, and often, dark coloration occurred at the ice–water interface (Fig. 5). Some banding was correlated with elevated chlorophyll-*a* and phaeopigments, while in other cores the banding appeared to be sediment. Highest chlorophyll concentrations were most commonly found in the bottom section of each ice core. For example, in 2009, bottom chlorophyll was as high as 208.6 μg l^{-1} (ranging from 2.2 to 208.6), compared to the mean concentration of 4.0 ± 5.5 μg l^{-1} found across the rest of the 2009 core slices. Mean snow depth on floes was variable, but generally less than 10 cm (Table 1).

3.3. Influence of sea ice on the water column

Typically, the depth-averaged water-column temperature reaches a maximum in September (Stabeno et al., 2012a, 2012b), when the mixed layer begins to deepen. In examining the 18 years of data at M2, the depth-averaged temperature was approximately the same in August as in September. Temperature data from August were used to represent maximum summer near-surface temperature prior to autumn wind mixing (Table 2). The highest mean August near-surface temperature was 12.5 °C (M2, 2002, a warm year) and the lowest monthly mean bottom temperature was −1.7 °C (M8, 2009, a cold year). The differences between monthly mean surface and bottom temperatures in August ranged from 5.2 to 10.8 °C.

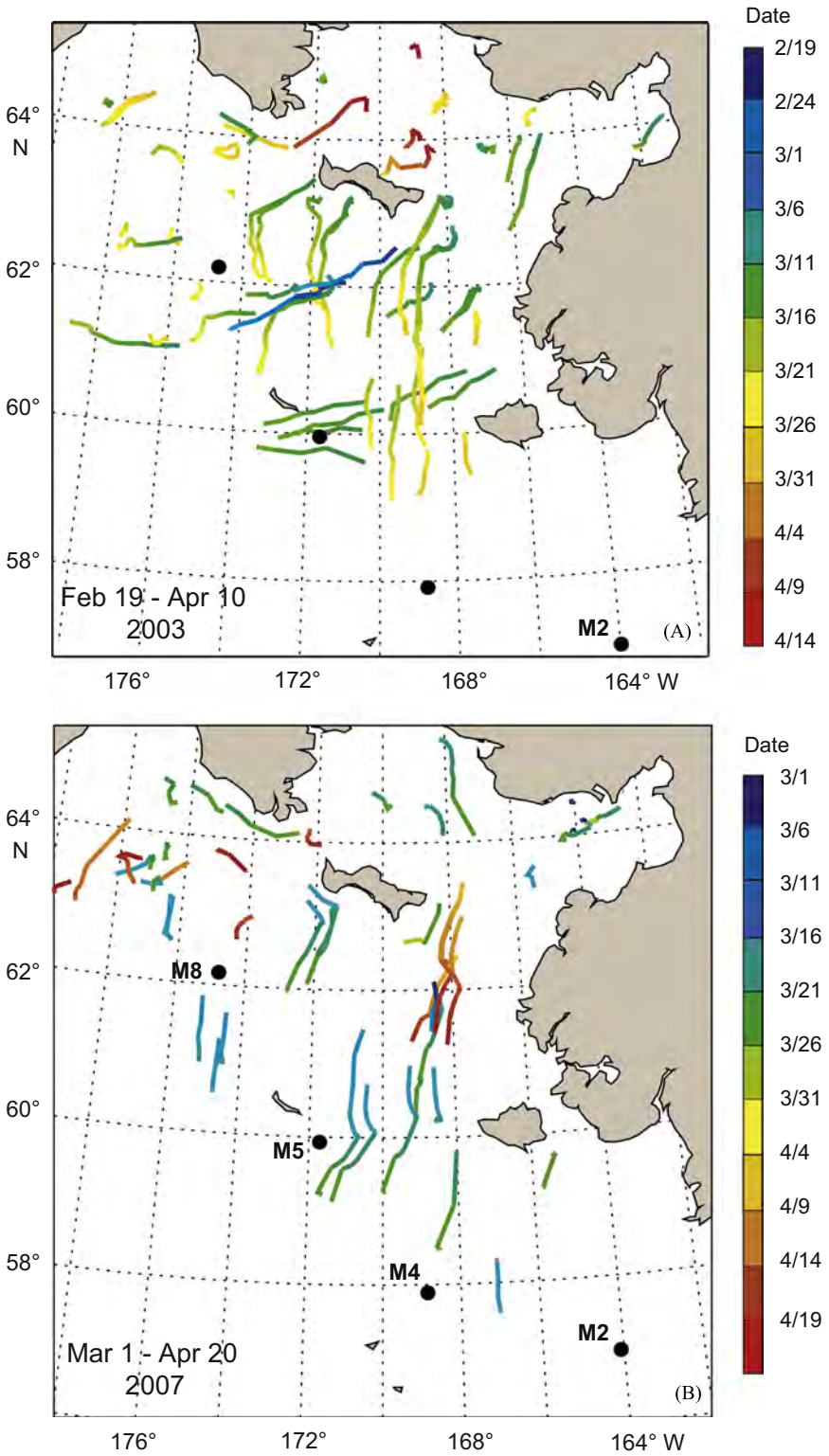

Fig. 3. Ice floe trajectories tracked using MODIS True Color images are shown for two years: (A) February 19–April 15, 2003 and (B) March 1–April 20, 2007. The color bars indicate the dates of observations. See color bar at right of plots for dates. Mooring locations are also indicated.

The time at which the water column became well mixed varied from north to south (Table 2), with M8 remaining stratified the longest of the four mooring sites. At M8 during summer, both temperature and salinity contribute equally to density stratification, while at the southern moorings density stratification is controlled by temperature (Ladd and Stabeno, 2012; Stabeno et al., 2010). Since the vertical differences in temperature are similar north-to-south, the stratification is almost twice as strong at M8 than at the other mooring sites (Ladd and Stabeno, 2012; Stabeno et al., 2010, 2012a), thus delaying mixing there.

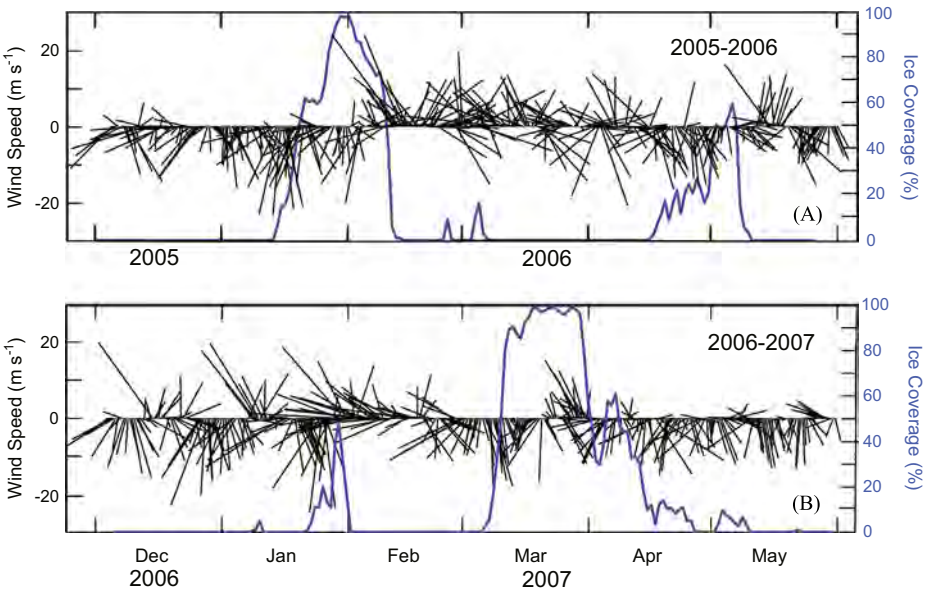

Fig. 4. Wind vector plots, from 6-hourly NCEP-2 Reanalysis data centered at mooring site M4, for the cold seasons of (A) 2005–2006 and (B) 2006–2007. Northward is upward. Ice extent in the 100-km × 100-km box around M4 is also shown.

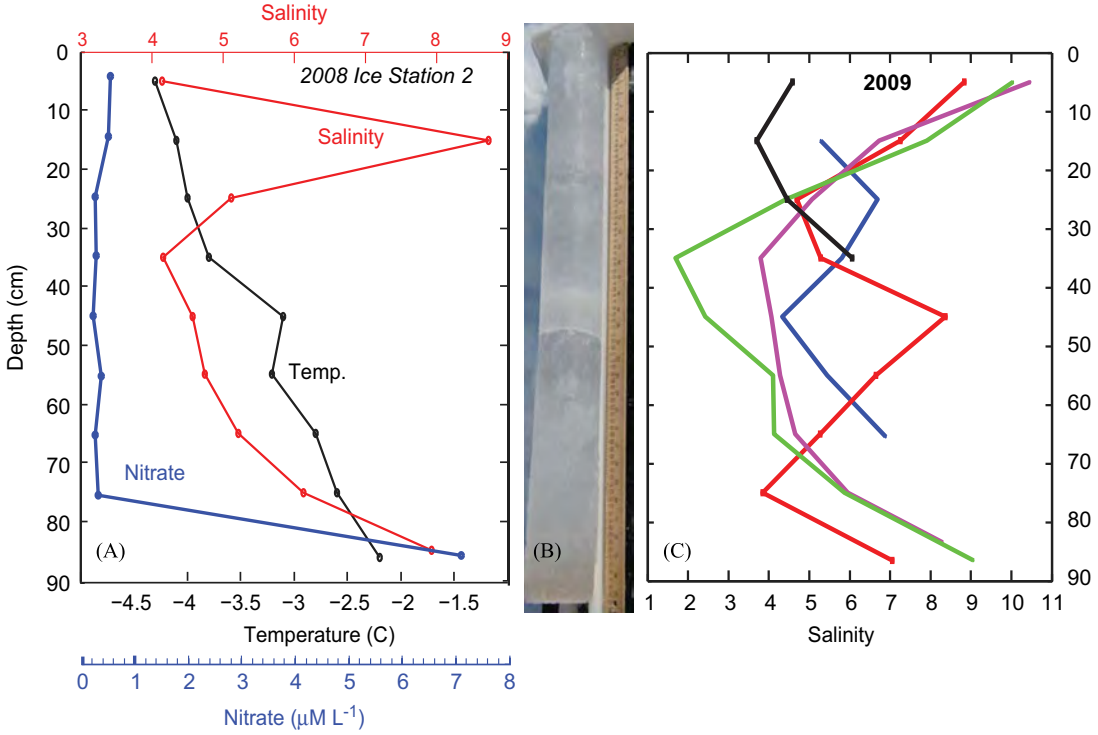

Fig. 5. (A) Vertical profiles of temperature, salinity, and nitrate from an ice core collected at Ice Station 2 in 2008 (Table 1). (B) Ice core photograph from same station. (C) Selected vertical profiles of salinity from 2009 ice cores shown in various shades. (The web version of this article contains a colorized version of this figure.)

While there is considerable information on the timing and characteristics of ice retreat and melting (Alexander and Niebauer, 1981; Hunt and Stabeno, 2002; Stabeno et al., 1998, 2012b), less is known about the short-term response of the water column to melting sea ice. Instruments at each of the four biophysical moorings in the Bering Sea measured temperature, salinity, and currents in the water column as ice was advected over the moorings. In total, there were 42 sets of data showing the water-column response to the ice. Several patterns were evident in the time series at the various moorings. To explore these patterns, seven examples were selected (two from M2, three from M4, and one each from M5 and M8).

3.3.1. *No ice (example: M2, fall 2004-spring 2005)*

From 1995 to the present, there was little (< 20%) or no ice present for five years of observations at M2 and two years at M4. In October 2004, the water column at M2 was cooling and mixing

Table 2
Statistics and information from the four Bering Sea shelf moorings. The location of the moorings and the years during which they were deployed are given on the left. Mixing information includes the range of time, and average date, at which the water column became well mixed with a temperature difference of <0.02 °C. The years during which areal sea ice concentration was $<20\%$ for the entire cold season were 1996, 2001, 2003–2005 at M2, and 2001 and 2005 at M4. Mooring sites M5 and M8 always had ice present during the cold season. Numbers in parentheses indicate the means for all years during which each mooring was deployed. All other numbers are for the time period 2005–2011.

Mooring	Mean August temp. 2005–2011 (all years)		Fall water column mixing date and temperature		Minimum temp. 2005–2011 (all years) (°C)
	Surface (°C)	Bottom (°C)	Date range (mean)	Temperature 2005–2011 (all years) (°C)	
M2					
56.9°N, 164.1°W	10.1 ± 1.4	1.4 ± 1.5	10/21–12/4	3.6 ± 2.1	-1.7 ± 0.11
1995–2011	(10.4 ± 1.4)	(2.0 ± 1.3)	(Nov. 9)	(4.1 ± 1.5)	(-0.6 ± 1.9)
M4					
57.9°N, 168.9°W	9.4 ± 1.0	1.2 ± 1.4	10/18–11/24	3.4 ± 1.9	-1.7 ± 0.04
1996, 1999–2011	(9.7 ± 1.2)	(2.2 ± 1.5)	(Nov. 1)	(4.4 ± 1.7)	(-1.1 ± 1.1)
M5					
59.9°N, 171.7°W	8.9 ± 1.0	-0.8 ± 0.7	10/16–12/21	1.7 ± 0.9	-1.7 ± 0.02
2005–2011			(Nov. 20)		
M8					
62.2°N, 174.7°W	5.0 ± 2.7	-1.5 ± 0.1	12/4–1/25	-1.0 ± 0.6	-1.8 ± 0.05
2005–2011			(Dec. 19)		

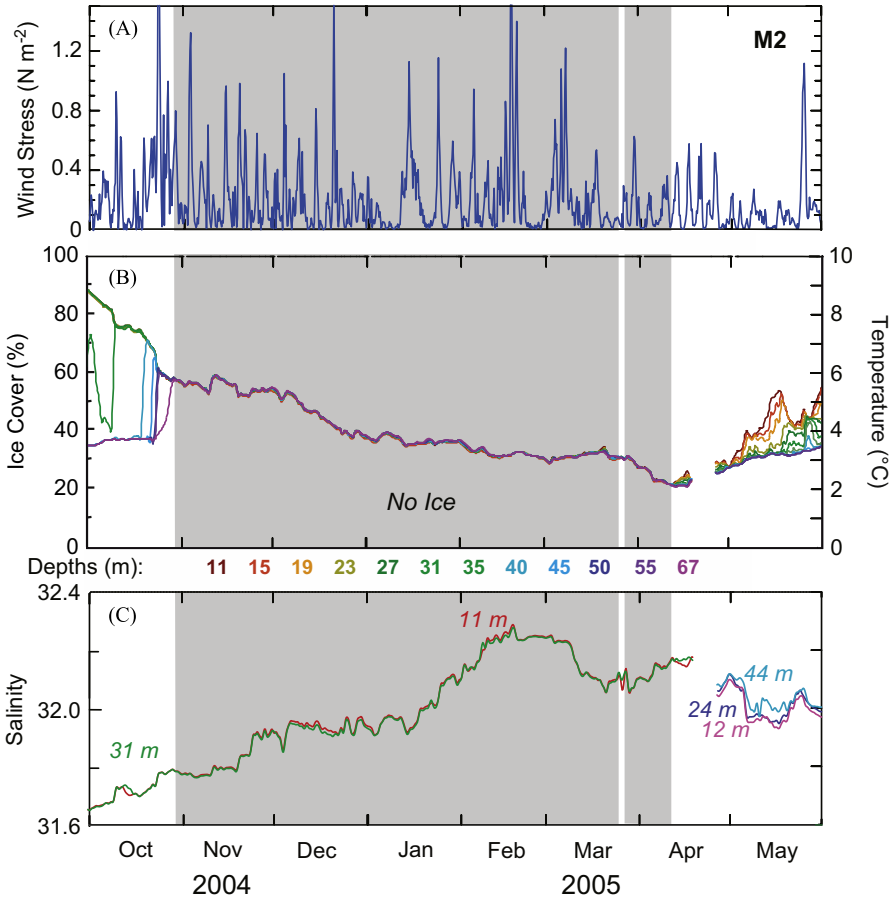

Fig. 6. Time series from M2 showing (A) wind stress, (B) temperature at 12 depths distributed through the water column, and (C) salinity at four depths. The breaks in the time series (B and C) occurred when the winter mooring was replace by the summer mooring. The gray shading indicates times when the water column was well mixed. There was no ice cover at M2 during this period. Temperature depths in (B) are shown below the panel as colored numbers.

(Fig. 6). From a mean August surface temperature of 12.5 °C and mean bottom temperature of 3.2 °C (not shown), the water column became well mixed at 5.7 °C at the end of October. The mean wind stress during the fall of 2004 ($0.23\ \mathrm{N\ m^{-2}}$) was not substantially stronger than the long-term (1995–2012) mean ($0.20\ \mathrm{N\ m^{-2}}$). The water column remained well-mixed through the winter until April 8, with the bottom temperature reaching a minimum of ~2.0 °C in mid-April. Minimum water-column temperature in January 2005 was anomalously high, and was surpassed by only two other warm years: January 2001 (3.0 °C) and January 2003 (3.4 °C). All three years were within an unusually warm period, 2001–2005 (Stabeno et al., 2012b). At M2, mean minimum winter

temperature from 1995 to 2011 was -0.6 ± 1.9 °C, while the mean for the nine years excluding this warm window (2001–2005) was -1.7 ± 0.1 °C (Table 2). Salinity increased from ~31.7 in early October to ~32.3 in mid-February, most likely from advection of more saline water from the outer shelf and slope (Sullivan et al., 2008).

3.3.2. A single ice event (example: M2, winter–spring 2007)

During the winter and spring 2007, ice was present near M2 for approximately one month (Fig. 7). During this period, winds were moderate, with isolated storms interspersed with periods of weak winds. The water column became well mixed (defined as when the vertical temperature difference was <0.04 °C, and the salinity difference was <0.02) at 3.6 °C in mid November, 2006 (not shown). Ice arrived in the vicinity of the mooring on March 2, and four days later, as the ice coverage reached ~20%, the water column began to stratify with colder, fresher water overlying warmer, saltier water. The top 39 m of the water column cooled to the freezing point (−1.7 °C) by mid-March and ice melt decreased the surface salinity by ~0.5. The water column remained stratified for ~20 days. There were four moderate storms during the ice period (Fig. 7A, 1–4). The first storm (March 6–9) coincided with the arrival of the ice; the second (March 18–22) occurred during a period of >90% ice cover; and the third (March 25–27) occurred during a period of decreasing ice. The second storm coincided with a slight mixing at 39–44 m, and the third event resulted in the total mixing of the water column. The primary cause of the greater mixing associated with the third storm, which was only slightly stronger than the second, was likely reduced ice cover. Less areal ice cover permitted more rapid movement of ice floes and also greater direct energy transfer between the atmosphere and the water. Internal waves generated elsewhere can also contribute to mixing, but is beyond the scope of this paper (Martini et al., 2013; Muench et al., 1983).

The duration and ice concentration at M2 in 2007 (Fig. 7) typified ice coverage in the south. Ice cover at M2 was more variable, had lower areal concentration and persisted for shorter periods of time than at the other three mooring areas (Stabeno et al., 2012a). M2 was outside the direct path of the ice conveyor belt corridor, and it was likely that ice near M2 arrived from Nunivak Island and the coastal polynya to the east. Over the 17-year period (late winter 1995 to spring 2011), single winter ice events occurred 6 times at M2 (lasting 20–83 days) and 7 times at M4 (lasting 11–121 days).

3.3.3. Multiple ice events with incomplete mixing (example: M4, winter–spring 2011)

During some years, ice was intermittent, with ice advancing and retreating several times during the cold season (December–May). The winter and spring of 2011 illustrated this pattern at M4.

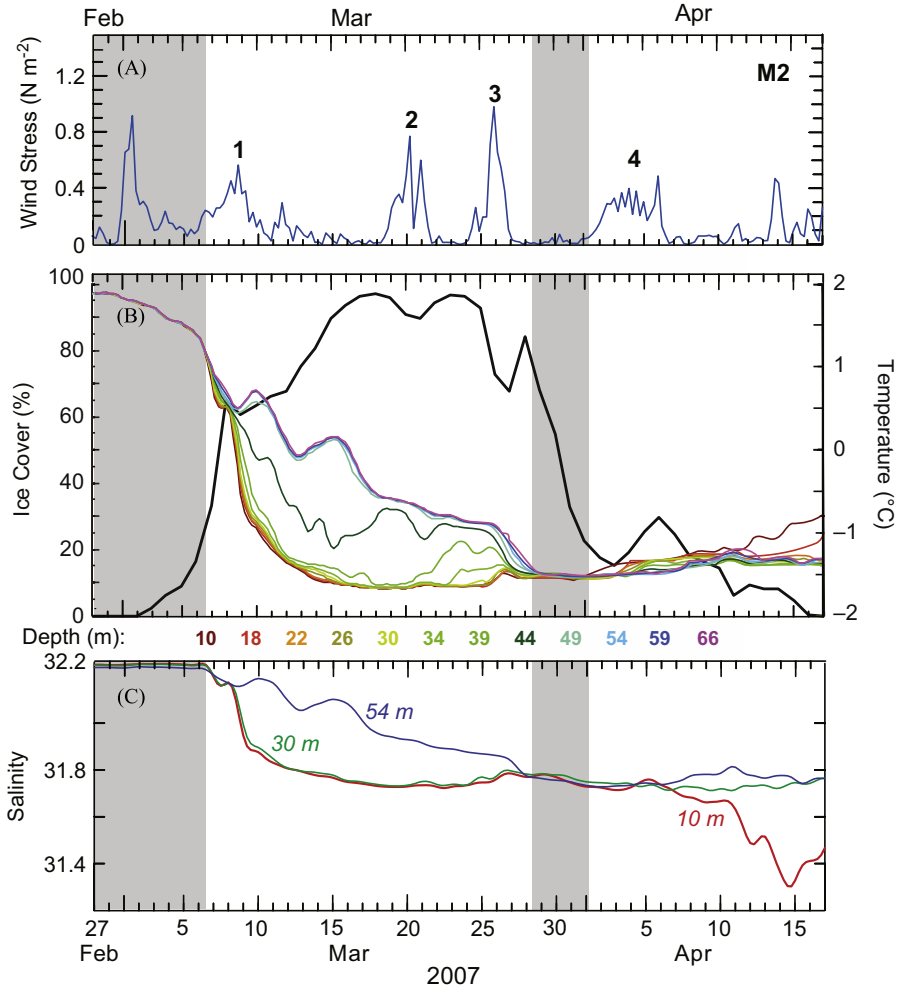

Fig. 7. Time series from M2, February 27–April 17, 2007, showing (A) wind stress, (B) temperature at 12 depths distributed through the water column and the percent areal ice cover (black line) in the 100-km × 100-km box around M2, and (C) salinity at three depths. The gray shading indicates times when the water column was well mixed. Temperature depths in (B) are shown below the panel as colored numbers.

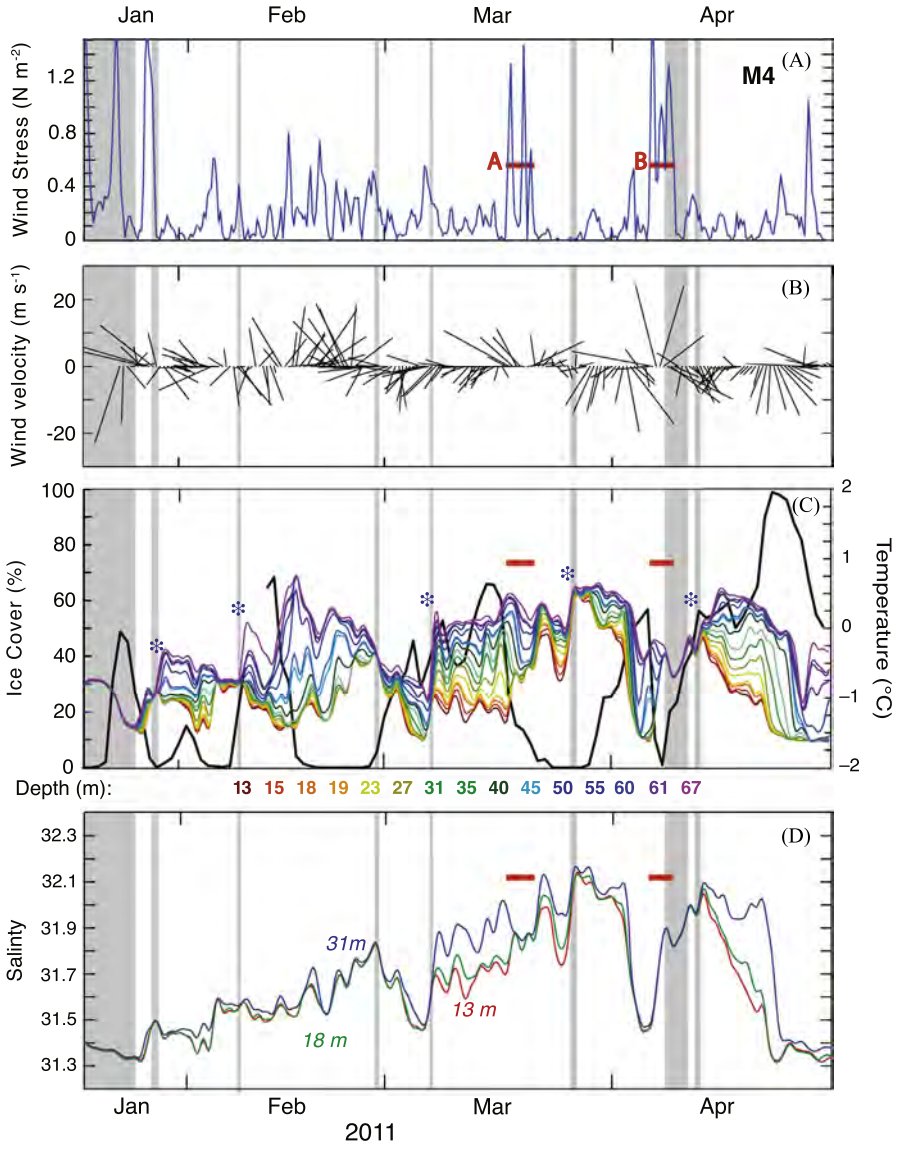

Fig. 8. Time series from M4, January 19–May 1, 2011, showing (A) 6-hourly wind stress, (B) 12-hourly wind velocity, (C) temperature at 16 depths distributed through the water column and the percent areal ice cover (black line) in the 100-km × 100-km box around M4, and (D) salinity at three depths. The gray shading indicates times when the water column was well mixed. Asterisks (*) indicate periods of increased temperature and salinity, likely a result of advection. Two storms are indicated in each panel by a red bar. Temperature depths in (B) are shown below the panel as colored numbers.

The water column became well mixed at ~1.7 °C in late November 2010 (not shown) and was still well mixed when northerly winds forced the ice over the mooring on January 20 (Fig. 8). Strong winds kept the water column well mixed as the ice cooled and freshened the water. The ice persisted for approximately one week and then retreated under southeasterly winds. Following this initial ice advance and retreat, the winds remained variable, forcing four major ice events over the next three months. As expected, periods of northerly or northeasterly winds resulted in ice advancing, while periods of southerly winds resulted in ice retreat. Maximum areal ice concentration remained below 70%, except for the final ice event in late April.

While variable, salinity (especially at 31 m) generally increased from January into late March despite the melting ice evidenced by the cooling of the surface waters. Large freshening events (> 0.3) of the complete water column occurred (e.g., early March, early April), but freshening of surface waters (from ice melt) occurred more often. The greatest decrease in salinity (0.6) occurred in late April when ice concentrations approached 100%. The temperature time series showed recurring, albeit weak, stratification (< 1.5 °C difference between top and bottom), interspersed with well-mixed periods (Fig. 8, gray shading). The cooling and freshening of the upper 20–27 m of water with the advent of ice was similar to the event described at M2 in 2007 (Fig. 7). The water column began mixing after each ice retreat and was usually well mixed before the next arrival of ice, only to become stratified again. The two wind events (A and B in Fig. 8A) were similar in magnitude. The winds during the first storm mixed the water column, but not completely (Fig. 8C; ~1 °C in temperature, 0.3 in salinity). During the second storm, the water column mixed completely. Wind mixing became most effective in both cases when ice concentration fell below 30%.

The bottom temperatures often warmed after mixing episodes (Fig. 8C), consistent with advection. Similarly the 0.7 increase in salinity from mid-January through late March also indicated advection. Mean winter currents at M4 are southward (Stabeno et al., 2010). Currents, which flow north along the 100-m isobath, can circle around St. Paul Island (Sullivan et al., 2008) and advect warmer, more saline water onto the middle-shelf near M4.

Multiple instances of ice advance and retreat were not uncommon at the three southern moorings. They occurred in: 4 of 17 years at M2; 1 of 17 years at M4; and 3 of 17 years at M5. The example discussed here (Fig. 8) had the highest occurrence of these events across the dataset. This example, with its series of advances and retreats, has served as a good illustration of how wind and/or advection influence water-column structure.

3.3.4. *A cold year with persistent ice (example: M4, winter–spring 2008)*

During 2007–2008 (both cold years, Stabeno et al., 2012b), the water column became well mixed on November 15 at 2.8 °C and cooled to −0.4 °C by January 13 (not shown). Ice reached the area in early February coincident with strong winds (Fig. 9). The water column was well mixed for 3–4 days in early February, and then became stratified as winds weakened and ice concentration increased to >20%. The ice-covered water column became well mixed again in late February and remained well mixed or weakly stratified until late March. Once again, there are strong indications that advection played a role in stratifying the water column. In both early February and late March there was a marked increase in temperature and salinity below 40 m, while the temperature and salinity in the upper water column remained relatively constant. Low-pass-filtered, near-bottom currents during the February event were $>10\ \mathrm{cm\ s^{-1}}$ from the south. During the March event, currents were variable and relatively weak ($<10\ \mathrm{cm\ s^{-1}}$; Fig. 9D and E).

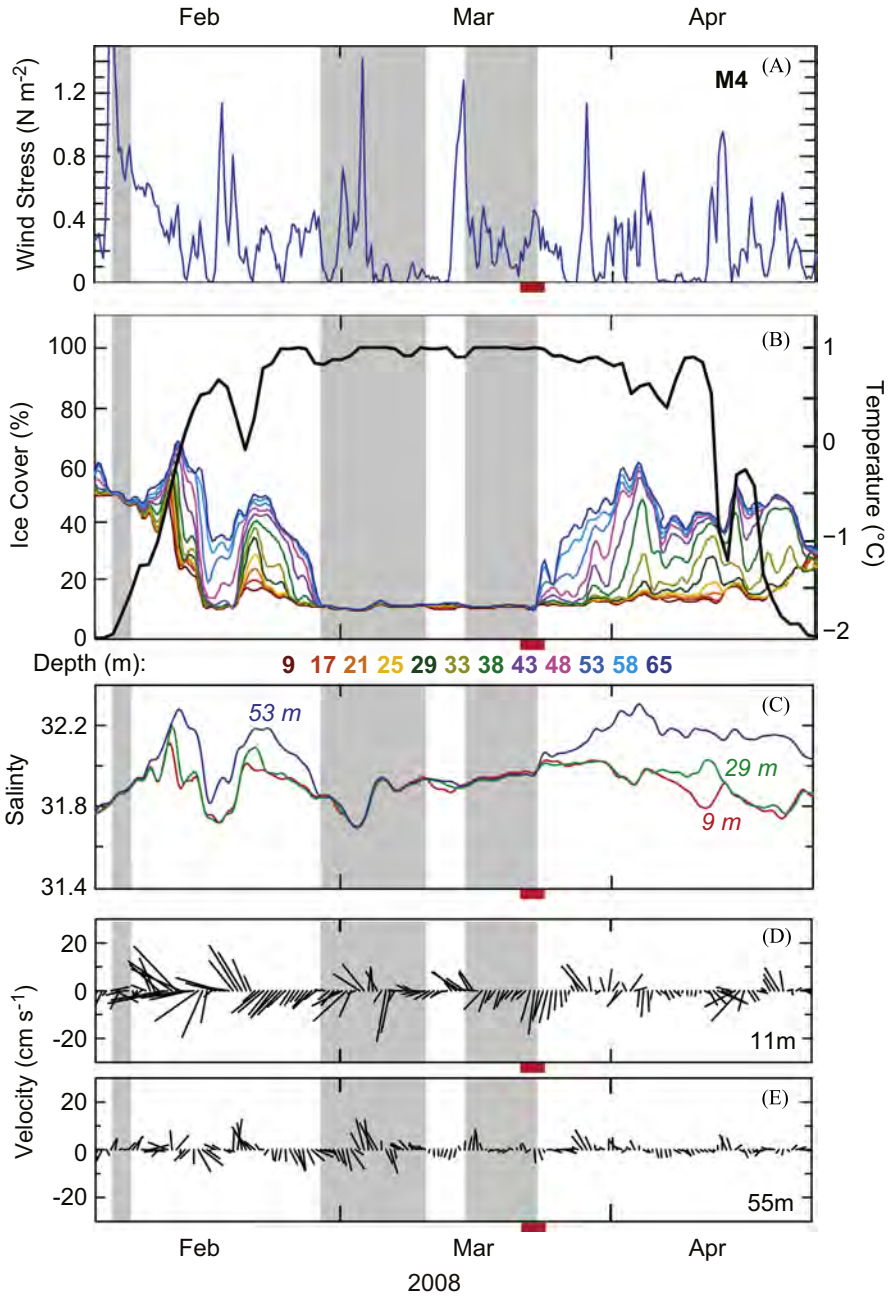

Fig. 9. Time series from M4, February 2–April 24, 2008, showing (A) wind stress, (B) temperature at 12 depths distributed through the water column and the percent areal ice cover (black line) in the 100-km × 100-km box around M4, and (C) salinity at three depths. Low-pass-filtered currents are shown at (D) 11 m and (E) 55 m. The gray shading indicates times when the water column was well mixed. The red bar at the bottom of each panel represents the time period shown in Fig. 10. Temperature depths in (B) are shown below the panel as colored numbers.

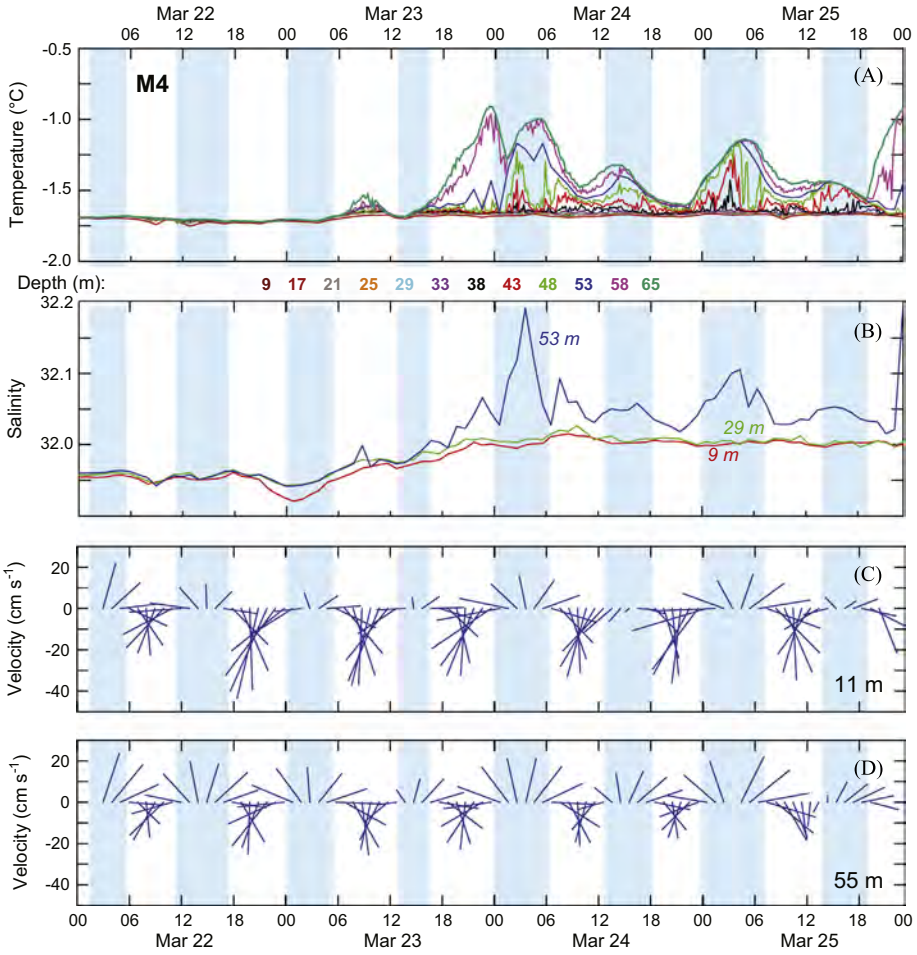

Fig. 10. A zoomed-in section from Fig. 9 (red bars) shows March 2008 hourly time series at M4 of (A) temperature at 12 depths, (B) hourly salinity at three depths, and hourly current velocity at (C) 11 m and (D) 55 m. The blue shading indicates periods when the bottom currents have a northward component. Northward is upward. Temperature depths in (A) are shown below the panel as colored numbers.

While the daily mean currents were relatively weak in mid-March (Fig. 9), the tidal currents were strong, resulting in flows exceeding 40 cm s^{-1} (Fig. 10). The first and second increases in bottom temperature and salinity occurred when the currents began to turn eastward. Once the boundary (front) between the warmer, more saline bottom water and the cooler, fresher bottom water passed the mooring, the relationship between the events and the direction of the current became complex, because bottom frontal structures are often not straight lines. The low-pass-filtered data showed a relatively steady increase in stratification in late March (Fig. 9B and C), but the unfiltered data showed that the increase in stratification occurred as a series of events related to the tidal currents. That the surface temperatures remained near freezing is not surprising since there was ~100% ice cover in the 100-km × 100-km box around M4, keeping the upper water column cold with low salinity.

3.3.5. Two ice events, one stratified and one well mixed (example: M5, 2005–2006)

During the cold season of 2005–2006 extensive ice arrived at M5 in December and finally departed in early June. Four periods of strong ice retreat occurred over this time (Fig. 11). The water column became fully mixed in early November at ~3.1 °C (not shown), and remained so until mid-December when ice cover reached ~30%. Two distinct periods of >90% ice concentration occurred. During the first ice event, late December through late February, the winds were relatively weak for the first 6 weeks and strengthened for the last 2 weeks. In contrast, during the second ice event, the winds were stronger during the first 5 weeks and weaker during the last 2–3 weeks. Ice, combined with low wind stress during the first ice event, cooled and freshened only the upper water column (upper 24–42 m) without greatly impacting the deeper water. A sharp increase in bottom salinity in early February and the accompanying increase in temperature were likely due to advection. Areal ice concentration fell to <30% in late February, and under the influence of relatively strong winds, the water mixed. The storms on February 12 with >50% ice cover had little impact mixing the water column, while a week later after the ice began retreating, winds of similar magnitude readily mixed the water column. A second large influx of ice occurred in mid-March. In sharp contrast to the first event, the water column remained largely well mixed through two months of 60–90% ice concentration. During this time, the temperature (~−1.8 °C) and the salinity (~31.8) remained relatively constant. That the water-column temperature was at the freezing point with constant salinity supports the conclusion that there was little net ice melt during the second ice event.

M5, similar to M4, was solidly within the ice conveyor belt (Fig. 1). Ice cover was often 80–100%, either steadily retaining a high concentration of ice all season, or partially retreating for a periods of days to weeks and returning to a high concentration. For the fall 1994-spring 2011 period, AMSR_E ice concentrations at M5 showed five years with

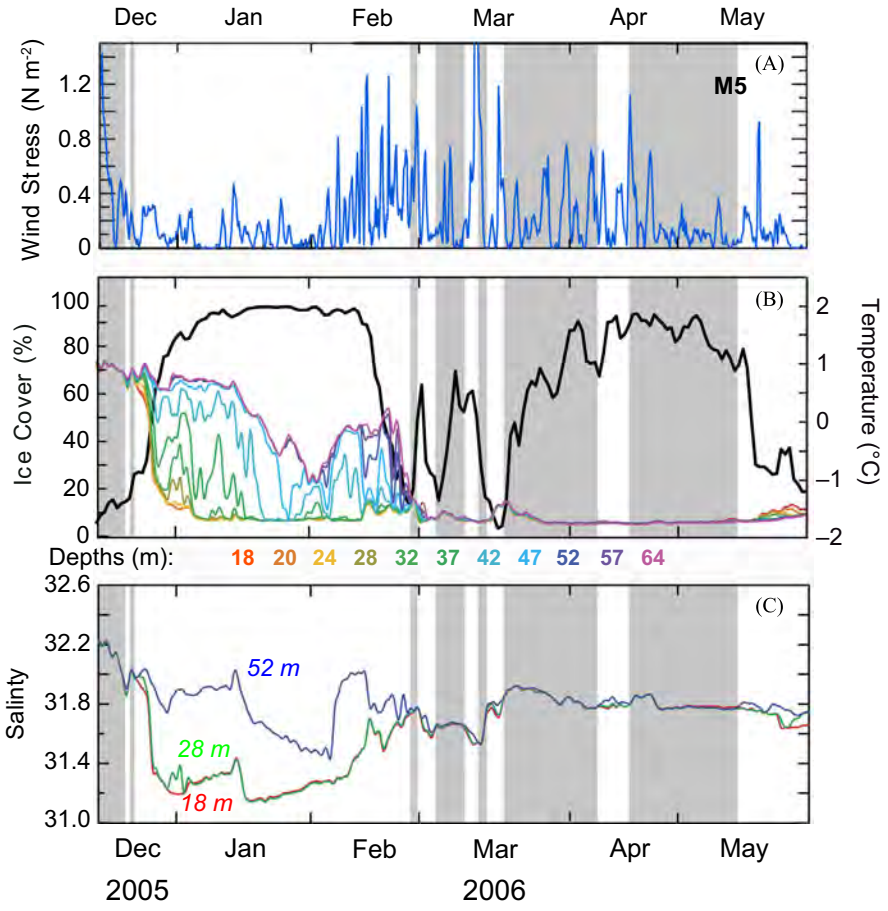

Fig. 11. Time series from M5, December 14, 2005–May 31, 2006, showing (A) wind stress, (B) temperature at 11 depths distributed through the water column and the percent areal ice cover (black line) in the 100-km × 100-km box around M5, and (C) salinity at three depths. The gray shading indicates times when the water column was well mixed. Temperature depths in (B) are shown below the panel as colored numbers.

a single ice event, and 10 years with multiple ice events. As such, the cold season of 2005–2006 was fairly typical at M5.

3.3.6. *Months of ~100% ice cover (example: M8, 2008–2009)*

M8 is the farthest north of the four moorings (Fig. 1) and representative of the northern shelf (Stabeno et al., 2012a). The water column at M8 from 2005 to 2011 mixed notably later (early December to late January) and at colder temperatures (average −1.0 °C) than at M2, M4, or M5 (Table 2). The average minimum winter temperature over those years was −1.8 °C, which was colder than at the southern moorings as a result of higher salinity. In 2008 the water column became well mixed at −0.1 °C in early December (Fig. 12). Sea ice arrived in late December and stratified the water column for a few days until the water column cooled to < −1.7 °C. The high areal ice cover (>90%) and a well-mixed or weakly stratified water column persisted for ~165 days. Surface water began to warm and stratify ahead of the May ice melt, and ice concentration was <20% by the end of May 2009.

The patterns of strong pre-ice cooling, minimal ice melt, minimal decrease in water temperature, and areal ice concentrations >80% for more than four months were typical at M8. The duration of ice cover (Fig. 12) was typical for the period (1995–2011) for the northern shelf. Over the 17-year period, ice around M8 was present an average of 127 days, with the longest single, near-100% ice concentration event lasting 189 days in 2005–2006. Twelve of the 17 years examined had only one ice event (80–100% coverage) during the cold season, and the remaining five years had two ice events.

3.4. *Estimating the magnitude of ice melt and its direct influence on temperature*

The thickness of the total ice melt can be estimated using the time series from the moorings and Eqs. (2) and (3). The largest problem with selecting data for this calculation was advection. Care was made in selecting examples where freshening was well defined and advection did not play an important role in modifying the water column. Of the 42 sets of winter and spring data (1995–2012), 15 sets were suitable for this calculation (Table 3). For each of these data sets the water column was well mixed at the time of ice arrival; the water column (or at least the upper layer) cooled to the freezing point within a month of ice arrival, and there was measurable cooling and freshening of the water column. Advection did not appear to influence the system in these selected instances.

Among the 14 annual examples (two sets from M2, 2009 were combined together to provide total cooling for that year) most were from the southern moorings, with only three from M5 and none from M8. The lack of examples from M8 was due primarily to

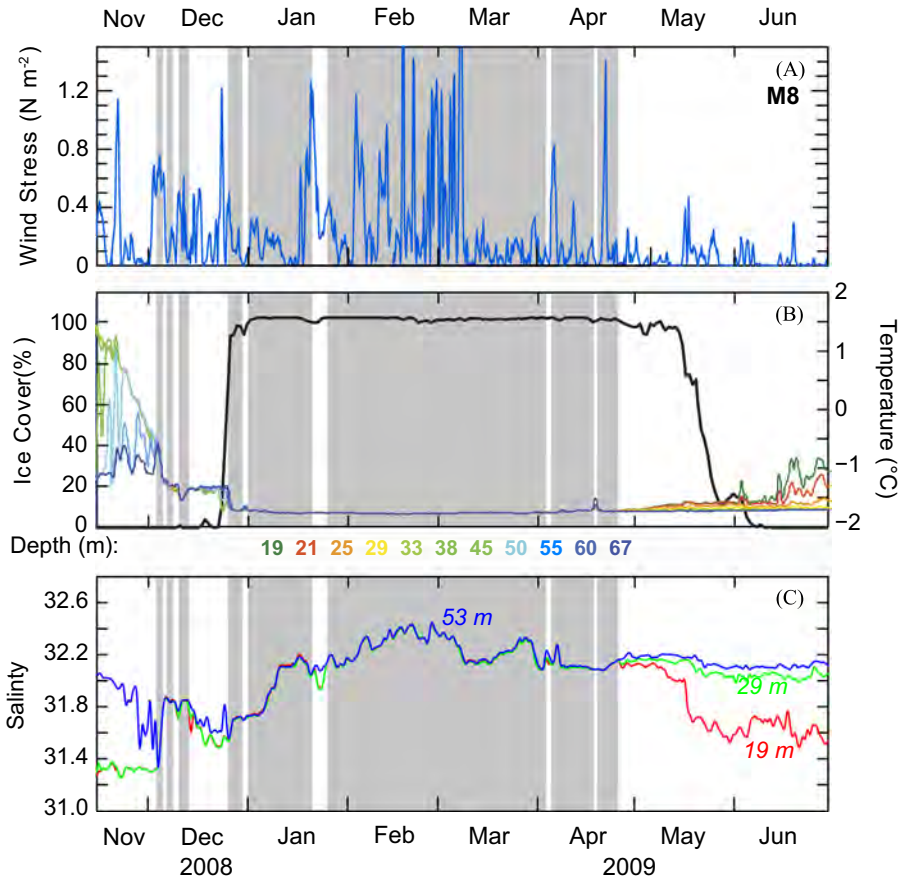

Fig. 12. Time series from M8, November 15, 2008–June 30, 2009, showing (A) wind stress, (B) temperature at 11 depths distributed through the water column and the percent areal ice cover (black line) in the 100-km × 100-km box around M8, and (C) salinity at three depths. The gray shading indicates times when the water column was well mixed. Temperature depths in (B) are shown below the panel as colored numbers.

Table 3
Observations and calculations of the impact of melting ice on the water column. T_w (S_w) is the depth-averaged temperature (salinity) of the water column when the ice arrives. ΔT (ΔS) is the average change in temperature (salinity) in the part of the water column that was modified by melting ice. H is depth of the water column cooled (usually the entire water column), h_i is the thickness of ice melted as calculated from changes in salinity, and h_w is the equivalent depth of water melted. ΔT_L is the change in temperature due to latent heat of fusion and the final column is the fraction of the observed cooling that is caused by the latent heat of fusion. Note that 2009 at M2 had two distinct melting events (a and b), which were combined together (2009t).

Mooring – year	T_w (°C)	ΔT (°C)	S_w	ΔS	H (m)	h_w (m)	h_i (m)	ΔT_L (°C)	$\Delta T_L/\Delta T$
M2–1998	2.0	3.4	31.95	0.45	25	0.43	0.51	1.17	0.34
2000	1.1	2.9	31.94	0.55	70	1.48	1.75	1.42	0.49
2006	2.6	4.3	32.12	0.71	27	0.73	0.86	1.82	0.43
2007	1.2	2.8	32.30	0.50	70	1.33	1.57	1.27	0.45
2009t		3.1		0.35	70	0.95	1.11	0.91	0.29
a	*2.2*	*2.0*	*32.00*	*0.20*	*70*	*0.54*	*0.63*	*0.52*	*0.26*
b	*−0.6*	*1.1*	*31.92*	*0.15*	*70*	*0.41*	*0.48*	*0.39*	*0.35*
2012	0.8	2.5	31.94	0.32	70	0.86	1.02	0.83	0.33
M4–2004	1.2	2.2	32.24	0.34	70	0.91	1.07	0.87	0.40
2006	2.5	3.8	32.38	0.65	70	1.72	2.03	1.65	0.43
2007	0.7	2.4	32.18	0.46	70	1.23	1.45	1.18	0.49
2009	1.6	3.5	32.11	0.45	70	1.21	1.42	1.15	0.33
2012	0.2	1.9	31.96	0.34	70	0.92	1.08	0.88	0.46
M5–2006	0.9	2.6	32.20	0.92	32	1.12	1.32	2.35	0.90
2007	2.0	3.6	32.20	0.50	70	1.34	1.57	1.28	0.36
2010	−0.1	1.8	31.55	0.70	70	1.92	2.25	1.83	1.00
Mean		2.9		0.52		1.15	1.36	1.33	0.48

the water column being already at or near the freezing point when ice first appeared at that mooring site and any stratification resulting from the arrival of ice was minimal and short lived.

From each of the examples, the average initial salinity (S_w) and initial ocean temperature (T_w) were determined (Table 3). After the arrival of ice, the water column often became stratified and then re-mixed to a depth of H. Usually it mixed to the bottom, but in certain instances only the surface was mixed before the retreat of ice. The changes in salinity and temperature of this mixed layer were calculated. Using Eq. (2) and an ice salinity of 6 (Table 1), h_w was calculated. Using the mean density (0.89×10^3 kg m^{-3}) from Table 1 the thickness (h_i) of ice melted was estimated for each data set, giving a mean thickness of 1.3 m. At −1.7 °C and a salinity of 6, the latent heat of fusion of sea ice (L) is 65 cal g^{-1} (2.72×10^5 J kg^{-1}; Weeks and Weller, 1984). Using Eq. (3), the change in temperature due to the latent heat of fusion (ΔT_L) was calculated for each example (Table 3). In these examples where care was taken to eliminate advection, the latent heat of fusion accounted for an estimated 26–100% of total observed cooling. On average, almost half of the cooling of the water column was due solely to ice melt; the remainder was from air–sea interaction either directly or through the ice.

A similar estimate can be made when ice melted in place in the spring (Table 4). At the southern two moorings most ice retreated through advection rather than by melting, as evidenced by the lack of freshening. At the northern two moorings, however, there was often a sharp decrease in salinity associated with loss of sea ice.

Table 4
Statistics for the amount of ice that melts at moorings sites when the ice retreats. Column headings are the same as in Table 3.

Mooring – year	ΔS	H	S_w	h_w	h_i
M5 – 2007	0.7	25	31.5	0.69	0.81
2008	0.7	25	31.4	0.69	0.81
2010	1.3	25	31.3	1.28	1.51
2011	0.3	30	31.4	0.35	0.42
2012	0.9	25	31.4	0.89	1.04
M8 – 2006	0.2	35	32.4	0.27	0.31
2008	0.7	32	32.8	0.84	0.98
Mean	0.7	28	31.7	0.71	0.84

This decrease in salinity resulted in a fresher surface layer with an average depth of 28 m (Table 4). This lower-salinity layer persists at M8 throughout the summer season (Stabeno et al., 2012a). The estimated amount of melted ice ranged from 0.31 m to 1.51 m (from Eq. (2)), with an average of 0.84 m.

In winter, the arrival of ice freshened and cooled the southern shelf, while in spring, the retreat of ice freshened the northern shelf. These calculations of ice melt are probably underestimates because ice melt resulting from the advection of warmer water is not included, and minimal changes in temperature and salinity are not considered. In addition, the estimate that 1.4 m of ice melted applies only to the middle domain. Once the water column reaches the freezing point, ice continues to be transported over the water column without modifying it. The ice eventually melts at the leading edge, which is often on the outer domain or over the slope.

4. Summary and conclusions

Winds are the primary driver in the formation and advection of sea ice on the Bering Sea shelf. The winds were primarily from the north, resulting in the creation of polynyas along the leeward coasts, and transport of sea ice south- or southwestward over the Bering Sea shelf. Variability in the winds resulted in sudden changes in the distribution and areal concentration of the ice during the cold season. The wind-driven conveyor belt of Pease (1980) originated north-northeast of St. Lawrence Island fanning south and westward over the shelf. This main corridor provided ice primarily to the areas around moorings M4 and M5. The St. Lawrence polynya and the region around Anadyr Strait contributed ice to the area around M8. Finally, the Alaskan coastal polynyas in Bristol Bay and south of Nunivak Island were the primary suppliers of sea ice in the vicinity of M2.

The moorings extend along the 70-m isobath of the middle shelf, with M8 on the northern shelf, M5 in the transition zone between north and south, and M2 and M4 on the southern shelf. Thus, examining data from these moorings gives insight on how the middle shelf responded spatially and temporally to ice melt. Over the southern part of the middle shelf (south of ~59 °N; Stabeno et al., 2012a), the ice melt occurred primarily when the ice was advected southward. Approximately 1.4 m of ice melted, freshening the water column and reducing the concentration of nutrients. Over the northern part of the middle shelf, as represented by M8, there was little ice melt during the initial arrival of ice. Most of the melt at this site occurred when the ice edge retreated. Ice melt during retreat left behind a fresher surface layer, which persisted at M8 through the summer. This increased the strength of stratification and likely contributed to the delay of the fall mixing of the water column on the northern shelf by ~1.3 months, relative to M2 (Table 2). The transition zone at M5 had substantial ice melt during both ice advance and retreat (a total ~2.1 m; Tables 3 and 4).

Typically, when ice first arrived, the water column (or the surface mixed layer) cooled and freshened, and remained well mixed. Once the areal ice cover exceeded 20–25%, the melting ice stratified the water column, with a fresher, colder layer overlaying warmer, more saline water. This surface layer was usually > 20 m deep. The vertical stratification usually was relatively weak, $\Delta\sigma_t = \sim 0.18$ kg m^{-3} (using mean temperature and salinity values from Table 3 of −1.7 °C and 31.7, respectively, for surface layer, and 1.3 °C and 32.2, respectively, for bottom layer), but persisted for 10–25 days. Storms quickly re-mixed the water column when ice retreated (e.g., Fig. 8), but even under ice, the water column eventually became well mixed (e.g., Figs. 7, 9 and 10). Advection can play a role in the stratification of the water column, particularly in the vicinity of the ice edge front.

Without sea ice, the water column at M2 and M4 usually cooled by ~4 °C to ~2 °C, whereas in years with extensive ice, the water column cooled on average > 6 °C to −1.7 °C (Stabeno et al., 2012b). Multiple consecutive cold (warm) years modified this pattern, making the depth-averaged summer temperatures colder (warmer). Average cooling in a series of cold years was ~5.5 °C, while average cooling in a series of warm years was ~4.5 °C (from Fig. 4A in Stabeno et al., 2012b). For comparison, greater cooling (~7.5 °C) occurred in a transition between a warm and a cold year. The greater cooling during cold years compared to warm years came from two sources. First, the air temperature during years with extensive ice was colder than years with little or no ice; thus, cooling due to sensible heat flux was greater in those years. The second source of cooling was the latent heat flux due to ice melt. The cooling from the estimated melting of 1.4 m of ice accounted for approximately half the observed cooling of the water column. In sharp contrast, on the northern shelf near M8, the water column cooled to ~−1 °C before ice arrived (Table 2). Ice arrival further cooled water temperatures to ~−1.8 °C with little ice melt.

This discussion of sea-ice melt applies to the middle shelf domain, and not to the coastal or outer shelf domains. In the coastal domain, ice is formed and shore fast ice and rafting are common. The water column is typically well mixed by tides. In the outer shelf domain advection dominates and intrusions of warmer, more saline slope water are common (e.g., Coachman, 1986; Stabeno and van Meurs, 1999; Sullivan et al., 2008). The water column is deeper (> 100 m) and not well mixed even in the winter (Stabeno et al., 1998).

A few inferences can be made about how the coastal and outer domains may respond to ice melt. Probably little ice is melted in the coastal domain until ice retreat at the end of the cold season. The coastal domain, with its weak alongshore flow, retains the signature of lower salinity through the summer as a result of ice melt (Danielson et al., 2012; Kachel et al., 2002) and river runoff (Roden, 1967). With the breakdown of the Inner Front in late summer, this low-salinity signature spreads out over the shelf (Ladd and Stabeno, 2012). The signature of ice melt on the outer domain is ephemeral; it does not persist through the summer because of the persistent alongshore currents and onshore intrusions of more saline, nutrient rich water (Stabeno et al., 2010).

It is becoming evident that the presence or absence of sea ice in spring is the single most important component determining the physical and biological structure of the Eastern Bering Sea shelf ecosystem, not only in the winter and spring when it is present, but also during the warm season (Hunt and Stabeno, 2002; Hunt et al., 2010; Stabeno et al., 2010, 2012a, 2012b). The southward advance of sea ice early in the season transports fresher water, which melts at the ice edge, reducing the salinity of the middle shelf by ~0.4 (Table 3). In contrast, late in the cold season, ice retreat transports fresher water northward, where ice melt provides approximately one half of the summer stratification on the northern shelf (Ladd and Stabeno, 2012; Stabeno et al., 2012a). The

low concentrations of nitrate in the sea ice do not greatly affect nitrate concentrations in the water column as the ice melts. However, significant amounts of iron in the sea ice (Aguilar-Islas et al., 2008) do contribute to the production along the slope. Notable concentrations of chlorophyll-*a* were found in bottom sections of the ice cores at the ice–seawater interface. These ice algae provide an early concentrated food source (Mock and Gradinger, 2000; Niemi et al., 2011) for zooplankton (Durbin and Casas, 2013; O'Brien, 1987; Runge and Ingram 1991), and are also exported to the ocean floor, supporting the benthic ecosystem (Cooper et al., 2013). While chlorophyll-*a* is transported by the ice toward the ice edge, it is not known if the ice also transports large amounts of zooplankton, which feed on the ice algae. The absence of ice over the southern shelf during consecutive warm years (2001–2005) likely contributed, directly or indirectly, to a drop in populations of large crustacean zooplankton (e.g., *Calanus marshallae*, *Thysanoessa raschii*) and a resultant reduction in the pollock fishery (Coyle et al., 2008; Hunt et al., 2010; Stabeno et al., 2012b).

Acknowledgments

We thank the officers and crews of the NOAA ships *Miller Freeman* and *Oscar Dyson*, U.S. Coast Guard Cutter *Healy*, and R/V *Thomas G. Thompson* for the invaluable assistance in making these oceanographic measurements. Special thanks go to the personnel who collected the ice cores including E. Cokelet, D. Kachel, P. Proctor, and J. Cross, and to members of the National Marine Mammal Lab during the 2006 ice cruise. We thank W. Floering, C. Dewitt, and S. McKeever for maintaining, deploying, and recovering the instruments on the mooring; D. Kachel and P. Proctor for processing the mooring and shipboard measurements; P. Proctor for nutrient analysis on some samples; and A. Hermann for comparison of ice drift data to interpolated NCEP winds. Graphics were provided by K. Birchfield. This research was funded by Grants from The North Pacific Research Board (Grant B52) and the National Science Foundation (Grants 0732430, 1107250, and 0813985), and with support from NOAA's North Pacific Climate Regimes and Ecosystem Productivity (NPCREP) program. This publication was partially funded by the University of Washington Joint Institute for the Study of the Atmosphere and Ocean (JISAO) under NOAA Cooperative Agreements NA17RJ1232 and NA10OAR4320148, and is contribution EcoFOCI-0802 to NOAA's Ecosystems and Fisheries-Oceanography Coordinated Investigations, contribution 2157 to JISAO, contribution 3975 to NOAA's Pacific Marine Environmental Laboratory, BEST-BSIERP Bering Sea Project publication number 137, and NPRB publication number 482. The findings and conclusions in this paper are those of the authors and do not necessarily represent the views of NOAA's Oceanic and Atmospheric Research.

References

Aguilar-Islas, A.M., Rember, R.D, Mordy, C.W., Wu, J., 2008. Sea ice-derived dissolved iron and its potential influence on the spring algal bloom in the Bering Sea. Geophys. Res. Lett. 35, L24601. http://dx.doi.org/10.1029/2008GL035736.

Alexander, V., Niebauer, H.J., 1981. Oceanography of the eastern Bering Sea ice-edge zone in spring. Limnol. Oceanogr. 26 (6), 1111–1125.

Brown, Z.W., Arrigo, K.R., 2013. Sea ice impacts on spring bloom dynamics and net primary production in the Eastern Bering Sea. J. Geophys. Res. 118, 43–62. http://dx.doi.org/10.1029/2012JC008034.

Cavalieri, D.J., Markus, T., Comiso, J.C., 2003. AMSR-E/Aqua Daily L3 12.5 km Brightness Temperature, Sea Ice Concentration, & Snow Depth Polar Grids, Version 2. 2002–2011. NASA DAAC at the National Snow and Ice Data Center, Boulder, Colorado, USA. ⟨http:/nsidc.org/data/amsre/⟩.

Coachman, L.K., 1986. Circulation, water masses and fluxes on the southeastern Bering Sea shelf. Cont. Shelf Res. 5 (1–2), 23–108.

Cooper, L.W., Sexson, M.G., Grebmeier, J.M., Gradinger, R., Mordy, C.W., Lovvorn, J.R., 2013. Linkages between sea-ice coverage, pelagic–benthic coupling, and the distribution of spectacled eiders: observations in March 2008, 2009 and 2010, northern Bering Sea. Deep-Sea Res. II 94, 31–43.

Coyle, K.O., Pinchuk, A.I., Eisner, L.B., Napp, J.M., 2008. Zooplankton species composition, abundance and biomass on the eastern Bering Sea shelf during summer: the potential role of water column stability and nutrients in structuring the zooplankton community. Deep-Sea Res. II 55, 1755–1791.

Danielson, S., Aagaard, K., Weingartner, T., Martin, S., Winsor, P., Gawarkiewicz, G., Quadfasel, D., 2006. The St. Lawrence polynya and the Bering shelf circulation: new observations that test the models. J. Geophys. Res. 111, C09023. http://dx.doi.org/10.1029/2005JC003268.

Danielson, S., Hedstrom, K., Aagaard, K., Weingartner, T., Curchitser, E., 2012. Wind-induced reorganization of the Bering Shelf circulation. Geophys. Res. Lett. 39 (8). http://dx.doi.org/10.1029/2012GL051231.

Drucker, R., Martin, S., Moritz, R., 2003. Observations of ice thickness and frazil ice in the St. Lawrence Island polynya from satellite imagery, upward looking sonar, and salinity/temperature moorings. J. Geophys. Res. 108 (C5), 3149. http://dx.doi.org/10.1029/2001JC001213.

Durbin, E.G., Casas, C.C., 2013. Early reproduction by *Calanus glacialis* in the Northern Bering Sea: the role of ice algae as revealed by molecular analysis. J. Plankton Res. http://dx.doi.org/10.1093/plankt/fbt121.

Eicken, H., 2003. From the microscopic to the macroscopic to the regional scale: growth, microstructure and properties of sea ice. In: Thomas, D.N., Dieckmann, G.S. (Eds.), Sea Ice – An Introduction to its Physics, Biology, Chemistry and Geology. Blackwells Scientific Ltd., London, pp. 22–81.

Gordon, L.I., Jennings Jr., J.C., Ross, A.A., Krest, J.M., 1994. A suggested protocol for continuous flow automated analysis of seawater nutrients (phosphate, nitrate, nitrite and silicic acid) in the WOCE Hydrographic Program and the Joint Global Ocean Fluxes Study. WHP Operations and Methods. WOCE Hydrographic Program Office, Methods Manual 91-1, November.

Holt, B., Rothrock, D.A., Kwok, R., 1992. Determination of sea ice motion from satellite images. In: Carsey, F.D. (Ed.), Microwave Remote Sensing of Sea Ice, Geophys. Monogr. Ser. 68. AGU, Washington, D.C., pp. 343–354. http://dx.doi.org/10.1029/GM068p0343.

Hunt Jr., G.L., Allen, B.M., Angliss, R.P., Baker, T., Bond, N., Buck, G., Byrd, G.V., Coyle, K.O., Devol, A., Eggers, D.M., Eisner, L., Feely, R.A., Fitzgerald, S., Fritz, L.W., Gritsay, E.V., Ladd, C., Lewis, W., Mathis, J., Mordy, C.W., Mueter, F., Napp, J., Sherr, E., Shull, D., Stabeno, P., Stepanenko, M.A., Strom, S., Whitledge, T.E., 2010. Status and trends of the Bering Sea region, 2003–2008. In: McKinnell, S.M., Dagg, M.J. (Eds.), Marine Ecosystems of the North Pacific Ocean, 2003–2008, 4. PICES Special Publication, pp. 196–267.

Hunt Jr., G.L., Stabeno, P.J., 2002. Climate change and the control of energy flow in the southeastern Bering Sea. Prog. Oceanogr. 55 (1–2), 5–22, http://www.pices.int/publications/special_publications/NPESR/2010/NPESR_2010.aspx.

Kachel, N.B., Hunt Jr., G.L., Salo, S.A., Schumacher, J.D., Stabeno, P.J., Whitledge, T.E., 2002. Characteristics and variability of the inner front of the southeastern Bering Sea. Deep-Sea Res. II 49 (26), 5889–5909.

Kanamitsu, M., Ebisuzaki, W., Woollen, J., Yang, S.-K., Hnilo, J.J., Fiorino, M., Potter, G.L., 2002. NCEP-DOE AMIP-II Reanalysis (R-2). Bull. Am. Meteor. Soc. 83, 1631–1643.

Ladd, C., Bond, N.A., 2002. Evaluation of the NCEP/NCAR reanalysis in the NE Pacific and the Bering Sea. J. Geophys. Res. 107 (C10), 3158. http://dx.doi.org/10.1029/2001JC001157.

Ladd, C., Stabeno, P.J., 2012. Stratification on the Eastern Bering Sea shelf revisited. Deep-Sea Res. II 65–70, 72–83.

Leberl, F., Raggam, J., Elachi, C., Campbell, W.J., 1983. Sea ice motion measurements from SEASAT SAR images. J. Geophys. Res. 88 (C3), 1915–1928. http://dx.doi.org/10.1029/JC088iC03p01915.

Macklin, S.A., Pease, C.H., Reynolds, R.M., 1984. Bering Air-Sea-Ice Study (BASICS), February and March 1981. NOAA Tech Memo ERL PMEL-52, 104 pp.

Malmgren, F., 1927. On the properties of sea ice, Norwegian North polar expedition with the "Maud" 1918–1925. Sci. Results 1 (5), 67.

Martini, K.I., Alford, M.H., Kunze, E., Kelly, S.M., Nash, J.D., 2013. Internal bores and breaking internal tides on the oregon continental slope. J. Phys. Oceanogr. 43, 120–139. http://dx.doi.org/10.1175/JPO-D-12-030.1.

Maslanik, J., Stroeve, J., 1999. Near-Real-Time DMSP SSM/I-SSMIS Daily Polar Gridded Sea Ice Concentrations. 1994–2002 (Updated daily). NASA DAAC at the National Snow and Ice Data Center, Boulder, Colorado, USA. ⟨http:/nsidc.org/data/docs/daac/ssmi_instrument.gd.html⟩.

McNutt, S.L., 1981. Remote sensing analysis of ice growth and distribution in the Eastern Bering Sea. In: Hood, D.W., Calder, J.A. (Eds.), Eastern Bering Sea Shelf: Oceanography and Resources, Vol. 1. USDOC/NOAA/OMPA, pp. 141–165 (Chapter 10), http://www.biodiversitylibrary.org/bibliography/61718#/summary; http://dx.doi.org/10.5962/bhl.title.61718; http://www.pmel.noaa.gov/pubs/docs/Eastern_Bering_2.10.pdf.

Mock, T., Gradinger, R., 2000. Changes in photosynthetic carbon allocation in algal assemblages of Arctic sea ice with decreasing nutrient concentrations and irradiance. Mar. Ecol. Prog. Ser. 202, 1–11.

Muench, R.D., Ahlnas, K., 1976. Ice movement and distribution in the Bering Sea from March to June 1974. J. Geophys. Res. 81, 4469–4476.

Muench, R.D., LeBlond, P.H, Hachmeister, L.E., 1983. On some possible interactions between internal waves and sea ice in the marginal ice zone. J. Geophys. Res. 88, 2819–2826.

Mueter, F.J., Litzow, M.A., 2008. Sea ice retreat alters the biogeography of the Bering Sea continental shelf. Ecol. Appl. 18, 309–320. http://dx.doi.org/10.1890/07-0564.1.

Mundy, C.J., Gosselin, M., Ehn, J., Gratton, Y., Rossnagel, A., Barber, D.G., Martin, J., Tremblay, J.-É., Palmer, M., Arrigo, K.R., Darnis, G., Fortier, L., Else, B., Papakyriakou, T., 2009. Contribution of under-ice primary production to an ice-edge upwelling phytoplankton bloom in the Canadian Beaufort Sea. Geophys. Res. Lett. 36, L17601. http://dx.doi.org/10.1029/2009GL038837.

Niebauer, H.J., 1998. Variability in Bering Sea ice cover as affected by a regime shift in the North Pacific in the period 1947–1996. J. Geophys. Res. 103 (C12), 27,717–27,737.

Niebauer, H.J., Bond, N.A., Yakunin, L.P., Plotnikov, V.V., 1999. An update on the climatology and sea ice of the Bering Sea. In: Loughlin, T.R., Ohtani, K. (Eds.), The Bering Sea: A Summary of Physical, Chemical and Biological Characteristics and a Synopsis of Research. North Pacific Marine Science Organization, PICES, Alaska Sea Grant, pp. 29–60.

Niebauer, H.J., Schell, D.M., 1993. Physical environment of the Bering Sea population. In: Burns, J.J., Montague, J.J., Cowles, C.J. (Eds.), The Bowhead Whale. The Society for Marine Mammalogy Special Pub. No. 2, Seattle, Washington, pp. 23–43.

Niemi, A., Michel, C., Hille, K., Poulin, M., 2011. Protist assemblages in winter sea ice: setting the stage for the spring ice algal bloom. Polar Biol. 34, 1803–1817.

O'Brien, D.P., 1987. Direct observations of the behavior of *Euphausia superba* and *Euphausia crystallorophias* (Crustacea: Euphausiacea) under pack ice during the Antarctic spring of 1985. J. Crustacean Biol. 7, 437–448.

Pease, C.H., 1980. Eastern Bering Sea ice processes. Mon. Weather Rev. 108 (12), 2015–2023.

Roden, G.I., 1967. On river discharge into the northeastern Pacific Ocean and the Bering Sea. J. Geophys Res. 72 (22), 5613–5629. http://dx.doi.org/10.1029/JZ072i022p05613.

Rodionov, S.N., Bond, N.A., Overland, J.E., 2007. The Aleutian Low, storm tracks, and winter climate variability in the Bering Sea. Deep-Sea Res. II 54, 2560–2577.

Runge, J.A., Ingram, R.G., 1991. Under-ice feeding and diel migration by the planktonic copepods *Calanus glacialis* and *Pseudocalanus minutus* in relation to the ice algal production cycle in Southeastern Hudson Bay, Canada. Mar. Biol. 108, 217–225.

Schandelmeier, L., Alexander, V., 1981. An analysis of the influence of ice on spring phytoplankton population structure in the southeast Bering Sea. Limnol. Oceanogr. 26 (5), 935–943.

Schumacher, J.D., Aagaard, K., Pease, C.H., Tripp, R.B., 1983. Effects of a shelf polynya on flow and water properties in the Northern Bering Sea. J. Geophys. Res. 88, 2723–2732.

Schumacher, J.D., Kinder, T.H., Pashinski, D.J., Charnell, R.L., 1979. A structural front over the continental shelf of the eastern Bering Sea. J. Phys. Oceanogr. 9 (1), 79–87.

Shapiro, L.H., Burns, J.J., 1975. Satellite observations of sea ice movement in the Bering Strait region. In: Weller, G., Bowling, S.A. (Eds.), Climate of the Arctic. Twenty-fourth Alaska Science Conference. Geophysical Institute, University of Alaska, Fairbanks, Fairbanks, Alaska, pp. 379–386 (15–17 August, 1973).

Sigler, M.F., Stabeno, P.J., Eisner, L.B., Napp, J.M., Mueter, F.J., 2014. Spring and fall phytoplankton blooms in a productive subarctic ecosystem, the eastern Bering Sea, during 1995–2011. Deep-Sea Res. II 109, 71–83.

Stabeno, P.J., Bond, N.A., Kachel, N.B., Salo, S.A., 2007. On the recent warming of the southeastern Bering Sea shelf. Deep-Sea Res. II 54, 2599–2618.

Stabeno, P.J., Bond, N.A., Kachel, N.B., Salo, S.A., Schumacher, J.D., 2001. On the temporal variability of the physical environment over the southeastern Bering Sea. Fish. Oceanogr. 10 (1), 81–98.

Stabeno, P.J., Farley Jr., E.V., Kachel, N.B., Moore, S., Mordy, C.W., Napp, J.M., Overland, J.E., Pinchuk, A.I., Sigler, M.F., 2012a. A comparison of the physics of the northern and southern shelves of the eastern Bering Sea and some implications for the ecosystem. Deep-Sea Res. II 65–70, 14–30.

Stabeno, P.J., Kachel, N.B., Moore, S.E., Napp, J.M., Sigler, M., Yamaguchi, A., Zerbini, A.N., 2012b. Comparison of warm and cold years on the southeastern Bering Sea shelf and some implications for the ecosystem. Deep-Sea Res. II 65–70, 31–45.

Stabeno, P.J., Napp, J., Mordy, C., Whitledge, T., 2010. Factors influencing physical structure and lower trophic levels of the eastern Bering Sea shelf in 2005: Sea ice, tides and winds. Prog. Oceanogr. 85 (3–4), 180–196.

Stabeno, P.J., Schumacher, J.D., Davis, R.F., Napp, J.M., 1998. Under-ice observations of water column temperature, salinity and spring phytoplankton dynamics: eastern Bering Sea shelf. J. Mar. Res. 56 (1), 239–255.

Stabeno, P.J., van Meurs, P., 1999. Evidence of episodic on-shelf flow in the southeastern Bering Sea. J. Geophys. Res. 104 (C12), 29,715–29,720. http://dx.doi.org/10.1029/1999JC900242.

Strickland, J.D.H., Parsons, T.R., 1968. A Practical Handbook of Seawater Analysis, first ed. Bull. 167, Fish. Res. Bd Can., Ottawa p. 293.

Stringer, W.J., Groves, J.E., 1991. Location and areal extent of polynyas in the Bering and Chukchi seas. Arctic 44, 164–171.

Sullivan, M.E., Kachel, N.B., Mordy, C.W., Stabeno, P.J., 2008. The Pribilof Islands: temperature, salinity and nitrate during summer 2004. Deep-Sea Res. II 55 (16–17), 1729–1737. http://dx.doi.org/10.1016/j.dsr2.2008.03.004.

Timco, G.W., Frederking, R.M.W., 1996. A review of sea ice density. Cold Reg. Sci. Technol. 24 (1), 1–6.

Weeks, W.F., Weller, G., 1984. Offshore oil in the Alaskan Arctic. Science 225, 371–378.

Wyllie-Echeverria, T., Wooster, W.S., 1998. Year to year variations in Bering Sea ice cover and some consequences for fish distributions. Fish. Oceanogr. 7, 159–170.

Zhang, J., Woodgate, R., Moritz, R., 2010. Sea ice response to atmospheric and oceanic forcing in the Bering Sea. J. Phys. Oceanogr. 40 (8), 1729–1747.

Deep-Sea Research II 109 (2014) 57–70

Contents lists available at ScienceDirect

Deep-Sea Research II

journal homepage: www.elsevier.com/locate/dsr2

Comparison of spring-time phytoplankton community composition in two cold years from the western Gulf of Alaska into the southeastern Bering Sea

Beth A. Stauffer [a,*], Joaquim I. Goes [a], Kali T. McKee [a], Helga do Rosario Gomes [a], Phyllis J. Stabeno [b]

[a] Lamont-Doherty Earth Observatory of Columbia University, Department of Biology and Paleo Environment, 61 Route 9W, Palisades, NY 10964, USA
[b] Pacific Marine Environmental Laboratory, NOAA, 7600 Sand Point Way NE, Seattle, WA 98115, USA

ARTICLE INFO

Available online 19 March 2014

Keywords:
Community composition
Phytoplankton
Climatic changes
Food webs
Marine ecology

ABSTRACT

The Bering Sea is a highly productive ecosystem providing the main oceanographic connection between the North Pacific and Arctic oceans. The atmospheric connection with the Arctic Ocean leads to seasonal sea ice formation in the Bering Sea, the areal extent and timing of retreat of which have important implications for primary productivity and phytoplankton community composition in this region. Hydrographic data from cruises and satellite sea ice and sea surface temperature data in spring 2011 and 2012 suggest classification of these years as relatively warmer and colder years, respectively. Locations in the western Gulf of Alaska (Pavlof Bay), at the north end of an eastern pass through the Aleutian Islands (Unimak Pass), and on the continental shelf of the Bering Sea (M2) were visited in both years. Stratification was apparent on the shelf in 2012, while the water column was comparatively well-mixed at other locations in both years. Phytoplankton biomass was highest in 2011 overall and specifically on the shelf in both years, while minimal biomass was measured within the well-mixed Unimak Pass in 2012. Surface phytoplankton size distributions included substantial contributions of picoplankton ($<3\,\mu m$) in 2011 (21–35%), while micro- (20–200 μm) and nanoplankton (3–20 μm) comprised 79% and 95% of biomass in Pavlof Bay and at M2, respectively, in 2012. Analyses of similarity revealed spatial variability in the phytoplankton assemblages within each year (2011: $R=0.588$, $p<0.004$; 2012: $R=0.646$, $p<0.004$). Additionally, between-year variability had a strong and significant effect on differences between assemblages across all locations ($R=0.579$, $p<0.0003$), likely masking differences between sites when years were grouped ($R=0.134$, $p<0.079$). These differences were likely driven by the dominance (up to 75% in Unimak Pass) of the colonial prymnesiophyte *Phaeocystis* sp. at all sites in 2011, resulting in reduced community diversity, compared to more widespread abundance of large diatoms of the genera *Thalassiosira*, *Thalassiothrix*, and *Chaetoceros* in 2012. The current study shows that within-regime differences in phytoplankton community composition between years can be almost as great as that between locations with vastly different oceanographic settings. High between- and multi-year variability may combine with a potential overall decline in sea ice in the Bering Sea to produce significant changes in the productive base of the food web with potential cascading effects on higher, economically and ecologically important trophic levels.

1. Introduction

The Bering Sea provides the major connection between the North Pacific and Arctic oceans. The area of the Bering Sea is almost evenly divided between shallow waters of the continental shelf (<200 m) and deeper waters (>200 m) southwest of the continental slope (Hunt et al., 2010), and its physics have been well discussed in other sources (e.g. Stabeno et al., 2001, 2012a, 2002, 1999). Through geostrophic transport, water enters the eastern Bering Sea from the North Pacific through a series of passes along the Aleutian Island chain. Unimak Pass is one of the shallow ($<$ 80 m) eastern passes through which warm, low-salinity, southward-flowing waters of the Alaska Coastal Current (ACC) first enter the Bering Sea, constituting the only major connection between the shelves of the North Pacific Ocean and Bering Sea (Stabeno et al., 2002; Ladd and Stabeno, 2012). Unimak Pass also allows for advection of zooplankton populations (Longhurst, 1998)

* Corresponding author. Present address: 2013-2014 AAAS Science & Technology Policy Fellow at U.S. Environmental Protection Agency, 1200 Pennsylvania Ave, NW, Washington DC 20460, USA. Tel.: +1 202 564 1401; fax: +1 845 365 8150.
E-mail address: stauffer@ldeo.columbia.edu (B.A. Stauffer).

http://dx.doi.org/10.1016/j.dsr2.2014.03.007
0967-0645/

and some nutrients (Stabeno et al., 2002) onto the shelf. Circulation within the Bering Sea is dominated by a cyclonic gyre, and waters exit the sea via geostrophic flow northward through the Bering Strait into the Arctic Ocean or southward though the Kamchatka Strait into the western North Pacific Ocean (Stabeno et al., 1999; Hunt et al., 2010).

The oceanography of the Bering Sea is strongly influenced by the in- and outflow of waters of differing origins and by atmospheric coupling with the Arctic Ocean (Hunt et al., 2010; Brown and Arrigo, 2012). Wind direction is largely a function of the location and magnitude of the Aleutian Low and shows variability on interannual, multi-year, and multi-decadal time scales (Jin et al., 2009; Overland et al., 2012). Wind direction has significant implications for the Bering Sea, with warm periods (e.g. 2001–2005) dominated by spring wind anomalies out of the south, and cool periods (e.g. 2007–2010) dominated by spring wind anomalies originating in the northwest (Hunt et al., 2010; Brown and Arrigo, 2012; Stabeno et al., 2012b). Warm years are characterized by higher than average sea temperatures, low sea ice area, decreased sea ice extent, and early retreat of ice, relative to cool years (Stabeno et al., 2012b). The date of ice retreat, in combination with water column stabilization by solar heating and cessation of winter storm activity, directly affects the timing of the spring phytoplankton bloom especially in the southeastern Bering Sea sea-shelf which supports a large portion of the food web (Hunt et al., 2002; Sigler et al., 2014).

The implications of warm years on primary production and the spring bloom are multidimensional. The spring bloom of phytoplankton requires stratification of the water column; in cool years the bloom occurs in cold water (-1.5–$2\ ^{\circ}C$) as sea ice melts, while in warm years the bloom is delayed until solar heating stratifies the water column and, as a result, occurs in warm (5–8 °C) waters (Stabeno et al., 2012b). There tends to be a generally positive response of net primary production with sea surface temperature (Hare et al., 2007; Mueter et al., 2009; Hunt et al., 2010); the effects of temperature on composition of the phytoplankton community, however, are less clear. Cells $>5\ \mu m$ in size have generally comprised the bulk of the standing stocks (Lomas et al., 2012), and early work in the Bering Sea documented distinct spring-time ice edge and shelf break communities dominated by large diatoms (Schandelmeier and Alexander, 1981). Furthermore, recent evidence suggests a shift within the phytoplankton community towards smaller cells (Noiri et al., 2005; Hare et al., 2007; Fujiwara et al., 2011) and reduced microzooplankton grazing of the spring bloom (Strom and Fredrickson, 2008) in warm years. This combination of smaller cells and lower microzooplankton grazing has been suggested to lead to observed reductions in the abundance of large zooplankton, including the copepod *Calanus marshallae* in warmer years (Hunt et al., 2008, 2011; Lomas et al., 2012; Stabeno et al., 2012b). More generally, shifts in diversity and community structure have been shown to significantly affect stability and functioning in complex aquatic food webs via a combination of direct and indirect effects (Downing and Leibold, 2002; Narwani and Mazumder, 2012). Unfortunately, community composition remains a parameter that is difficult to measure remotely (e.g. via satellite) or with in situ instrumentation (e.g. on moorings) with the result that trends in phytoplankton community structure in environments such as the Bering Sea are still rather poorly understood.

The effects of multi-year variability between warm and cold conditions on the Bering Sea ecosystem have been investigated for several decades, largely motivated by the economic role of the region as a major producer of seafood for the United States and its direct connection to the rapidly changing Arctic ecosystem (Stroeve et al., 2007; Brown and Arrigo, 2012; Overland et al., 2012). The Bering Sea generates approximately 40% of the United States finfish and shellfish landings in the U.S., employs a large population of fishers, processors, and distributors, and supports subsistence for over 50,000 local residents, many of whom are Alaskan natives (Stabeno et al., 2012b). Hunt et al. (2002) proposed an Oscillating Control Hypothesis, suggesting bottom-up or top-down control of fisheries in cold or warm regimes, respectively, largely as a result of changes in the timing of the spring phytoplankton bloom, differential temperature-regulated zooplankton production, and impacts of secondary production on survival and recruitment of piscivorous fish. This hypothesis has been revised since its original inception to incorporate evidence for a lack of large zooplankton in warm years (Hunt et al., 2008; Lomas et al., 2012; Stabeno et al., 2012b), despite increased primary production (Hunt et al., 2011). However, the effects of changes in the community composition of primary producers on these dynamics remain largely unknown.

Climate-driven trends in sea ice decline have been documented in the Arctic Ocean (e.g. Stroeve et al., 2007); however, the impacts of climate change on sea ice and temperature in the Bering Sea remain somewhat obscured. Satellite-based observations of sea ice do not indicate a long-term decline in the last six decades (Brown and Arrigo, 2012), while model-based predictions suggest a potential air temperature increase and severely reduced sea ice extent in the Bering Sea by 2050 (Wang et al., 2012). Continued high variability and the potential for long-term change in temperatures and sea ice extent may have significant implications for the dynamics of the spring bloom, affecting the composition of phytoplankton communities with potentially significant effects on the food web of the Bering Sea. However, such information is still rare.

The current study compares spring-time phytoplankton communities from the western Gulf of Alaska, through Unimak Pass, and into the southeastern Bering Sea shelf during a relatively warm (2011) and cold (2012) year. These years follow the documented cold years of 2007–2010 and fall within the range of conditions described by Stabeno et al. (2012b), namely increased ice extent and cooler temperatures, suggesting that 2011 and 2012 likely also fall within this cold regime. Given the importance that the timing, magnitude, and composition of spring blooms in the Bering Sea have on the greater ecosystem, the current study's focus on within-regime variability provides important insights into the significantly different communities that even small changes in environmental conditions can affect. With variability in environmental conditions, especially sea ice coverage in the southern Bering Sea, expected to increase with continued climate change (Stabeno et al., 2012a), an understanding of the potential effects on community structure of primary producers is of great importance.

2. Methods

2.1. Remote sensing

Sea surface temperature (SST) data for the region was accessed for the day of 15 May in each year through the Group for High Resolution Sea Surface Temperature (GHRSST; http://podaac.jpl.nasa.gov/GHRSST). The GHRSST global level 4 analysis is produced daily on a 0.25° grid at the NOAA National Climatic Data Center and employs optimal interpolation (OI) using data from the 4 km Advanced Very High Resolution Radiometer (AVHRR) Pathfinder Version 5 time series and in situ ship and buoy observations. Sea ice extent data were obtained from the National Snow & Ice Data Center (http://nsidc.org/data/seaice_index/archives/) and regional estimates of areal extent (m^2), excluding data north of the Bering Strait, were calculated in ArcMap (v. 10, Esri). Rates of sea-ice

retreat for each year were calculated as the difference between subsequent monthly averaged areas, relative to the time period (m^2 $month^{-1}$). Aqua MODIS chlorophyll (Chl *a*) data were accessed through the NASA website (http://oceancolor.gsfc.nasa.gov/) as monthly composites for May 2011 and May 2012. Net primary production data were accessed from the Oregon State University Ocean Productivity website (http://www.science.oregonstate.edu/ocean.productivity/standard.product.php) as monthly composites based on the Vertically Generalized Production Model (VGPM; Behrenfeld and Falkowski, 1997). Mean summer rates of primary production data (g C m^{-2} d^{-1}) were calculated based on an average of the monthly estimates for May through August for 2011 and 2012.

2.2. Water column data

2.2.1. Physical water column

Several stations were occupied during the cruises of 2011 and 2012. However, due to extensive ice conditions in 2012, the focal areas of the two cruises were significantly different. As a consequence only three of the several stations occupied in both 2011 and 2012 overlapped: Pavlof Bay (henceforth 'Pavlof'), a small bay in the Gulf of Alaska on the eastern side of the Alaskan Peninsula; Unimak Pass (henceforth 'Unimak'), a shallow, narrow coastal pass allowing for exchange of Alaska Coastal Current water with relatively nutrient-rich waters originating from the Bering Canyon (Stabeno et al., 2002; Mordy et al., 2005); and M2, along the 70 m isobath towards the edge of the broad continental shelf (Table 1). The M2 location is so-named after the long-term biophysical mooring maintained by the NOAA Eco-FOCI program at this site (http://www.ecofoci.noaa.gov). These stations, while spatially diverse, represent the flow of water containing nutrients and zooplankton through one of the major Aleutian passes (Unimak) connecting the western Gulf of Alaska (Pavlof) and the shelf of the southeastern Bering Sea (M2). Additionally, interannual variability in sea ice extent is most pronounced in this southern region of the Bering Sea, and changes in environmental conditions, primary production, and trophic interactions in the southern Bering Sea are thought to have significant implications for the ecosystem and organisms further north (Stabeno et al., 2012a).

Water column profiles at these stations were obtained using a 911plus/917plus conductivity, temperature, depth (CTD) sensor (Sea-Bird®) outfitted with additional sensors for dissolved oxygen (SBE 43, Sea-Bird), WETstar chlorophyll fluorescence (WetLabs®), and photosynthetically active radiation (Biospherical/Licor®). Data were processed according to Sea-Bird-recommended protocols and binned to 1 m intervals. Samples for dissolved inorganic-phosphate, silicate, nitrate, nitrite, and ammonium were collected from the Niskin bottles as part of the Eco-FOCI project in 2011 and 2012. Samples were collected in 25 ml acid-washed polyethylene bottles following triple rinsing with sample seawater, and kept frozen at −80 °C until analysis. Analyses were run by continuous flow analysis according the World Ocean Circulation Experiment (WOCE) protocol of (Gordon et al., 1993). Nutrient concentrations were not available from the 2011 or 2012 cruises or from any historic Eco-FOCI cruises for the Pavlof Bay location in the Gulf of Alaska (D. Kachel, personal communication).

Table 1
Station locations and cruise sampling dates in 2011 and 2012.

Station	Latitude (°N)	Longitude (°W)	Date sampled	
			2011	2012
Pavlof Bay	55.18	161.69	17 May	28 April
Unimak Pass	54.94	165.00	27 May	29 April
M2	56.86	164.06	18 May	8 May

2.2.2. Phytoplankton biomass

Discrete water samples were collected via Niskin bottle just below the surface, at the subsurface chlorophyll maximum (SCM), and 1% light level, as determined from the vertical profiles. Size-fractionated Chl *a* samples were obtained by gravity filtration of whole water through 200 and 20 μm Nitex mesh and 47 mm polycarbonate membranes with 3 μm pore size (Whatman®). Whole and size-fractionated water was then filtered onto 25 mm glass fiber filters (Whatman®) and stored at −20 °C until analysis. Chl *a* samples were extracted in 90% acetone overnight at −20 °C and run on a lab fluorometer (Turner Designs Trilogy®) before and after acidification with 10% HCl, according to the protocol of Parsons et al. (1984).

2.3. Plankton assemblages

2.3.1. Assemblage composition

Samples for assemblage analysis were stored in the dark and kept cool until analysis by an onboard imagine particle analyzer (FlowCAM; Fluid Imaging Technologies®). A 4X objective (UPlan FLN, Olympus®) and 300 μm field-of-view flow cell were used. Approximately 10 ml and 25 ml were run through the system in 2011 and 2012, respectively, and cells were counted and imaged on Auto Image mode with a peristaltic pump rate of approximately 0.32–0.44 ml min^{-1} (according to manufacturer specifications). Cells were classified into at least genus-level using the Visual Spreadsheet program (Fluid Imaging®) following removal of images of bubbles, duplicate particles, and obvious debris. In Auto Image mode, the FlowCAM images only a portion of the volume passed through the system. The volume imaged is a function of the total number of particles imaged, field of view dimensions, depth of the flow cell, and total number of frames that were collected. The estimated volume imaged was on average 1.66 and 3.81 ml in 2011 and 2012, respectively. In order to minimize issues associated with volume estimation error, plankton counts were used in subsequent analyses as relative abundances for each sample.

2.3.2. Statistical analyses

The Shannon index of diversity (H'), which depends on both richness and evenness of taxa (Shannon, 1948), was calculated based on relative abundances determined from FlowCAM analyses, and differences between years at each site were determined using a t-test. Differences between plankton assemblages were further examined using the Bray-Curtis coefficient of dissimilarity within the multivariate statistical software package PRIMER v.6® (Clarke and Warwick, 2001). Relative abundances were square-root transformed to reduce the influence of highly represented genera/classes and the tendency for a few well-represented taxa to drive the similarity analyses (Bray and Curtis, 1957; Clarke and Warwick, 2001). Similarity matrices between samples based on the Bray-Curtis coefficient were further used in hierarchical cluster analysis with similarity profile permutation tests (SIMPROF) to examine if dissimilarities among the assemblages were statistically significant. Community similarities were graphically represented using non-metric multidimensional scaling (MDS), a technique which allows for 2-dimensional representation of communities differentiated in multidimensional space (Clarke and Warwick, 2001). The distribution of communities on the MDS diagram is indicative of their similarities, with more similar communities grouping together. MDS diagrams are typically presented in two dimensions, which are most easily understood. The real data, however, exist in more than two dimensions. As a result, the distances

between each pair of objects in an MDS diagram may contain slight inaccuracies, and the sum of those inaccuracies is referred to as the stress (Sturrock and Rocha, 2000). This stress value increases with added samples and variables (in our case, taxa) and decreases as more dimensions are added for representation of the relationships between communities. Typically a value ≤ 0.1 is considered a good ordination of the data (Clarke, 1993).

Finally, differences between communities were further investigated using one-way permutation-based analyses of similarity (ANOSIM), to differentiate variability between years from that between locations (Clarke and Gorley, 2006). ANOSIM is a non-parametric, modified version of the Mantel test and is distribution-free (Clarke, 1993). The magnitude of the ANOSIM R statistic can be used as a measure of the strength of the difference between two groups (Clarke and Gorley, 2006), thus allowing assignment of relative intensities of the effects of year or location on community variability.

3. Results

3.1. Physical environment

3.1.1. Sea surface temperature and sea ice

Spring sea surface temperature (SST) in the Bering Sea and adjacent Gulf of Alaska was, on average, warmer in 2011 than 2012 (Fig. 1). By mid-May 2011, only the northernmost region of the Bering Sea was still below 0 °C, the area around M2 was approximately 1.01 °C, and much of the larger region had warmed to 0–2 °C (Fig. 1A). In mid-May 2012, however, much of the Bering Sea, including the area around M2 was still < 0 °C (Fig. 1C). Conversely, the western Bering Sea was characterized by temperatures up to 1.5 °C warmer in 2012 than in 2011 (Fig. 1). Sea ice covered a much larger area of the Bering Sea in March–June 2012 than during the same months in 2011 (Fig. 2). From March through May, the areal extent of sea ice in 2012 was up to two times greater than for the same months in 2011 and >8 times higher in June 2012 than in June 2011 (Table 2). Rates of ice retreat varied from 2.3×10^8 to 1.29×10^{10} m^2 month^{-1} in 2011, with the fastest rates from April to May (Table 1). Ice continued to accumulate in 2012 through March, and retreated at rates of 1.50×10^{10} to 2.07×10^{10} m^2 month^{-1} in April and May 2012 (Table 2).

3.1.2. Hydrography

In the western Gulf of Alaska, which is less directly affected by sea ice than the Bering Sea, temperatures at Pavlof ranged from 3.2–4.1 °C in 2011 and 1.3–2.2 °C in 2012 (Fig. 3A). Salinity was also slightly lower at Pavlof in 2011 (range: 31.5–31.7) relative to 2012 (31.7–31.9; Fig. 3B), and lower concentrations of dissolved oxygen were measured in 2011 (max: 7.8 ml L^{-1}) than in 2012 when surface dissolved oxygen concentrations reached a maximum of 9.9 ml L^{-1} (Fig. 3C). Temperatures at Unimak were almost one degree warmer than Pavlof, ranging from 4.5 to 5.1 °C at the surface in 2011, while temperatures remained within 1.3–1.5 °C in 2012 (Fig. 3E). Salinity was slightly higher at Unimak in 2011 (32.0–32.2) than in 2012 (31.8–32.0) and did not vary significantly with depth in either year (Fig. 3F). Dissolved oxygen concentrations at Unimak were comparable between years and largely uniform throughout the water column, with surface concentrations approximately 8.1 and 7.8 ml L^{-1} in 2011 and 2012, respectively (Fig. 3G).

On the shelf of the southeastern Bering Sea, temperatures at M2 ranged from -1.0 °C at the surface to -0.5 °C at depth in 2012, 2 degrees cooler than surface temperatures of 2.1 °C in 2011 (Fig. 3I). Some evidence of weak thermal stratification was apparent in 2011 (Fig. 3J). Salinities ranged from 31.6 at the surface to 31.9 at depth in 2011, with a slight halocline apparent around 36 m (Fig. 3J). In contrast, salinity reached a minimum of 31.0 at the surface in 2012 and showed a distinct halocline from 16 to 26 m depth (Fig. 3J). Dissolved oxygen varied with depth between 9.6 and 9.9 ml L^{-1} at the surface to 7.3–7.4 ml L^{-1} at depth (Fig. 3K) and an oxycline was evident at depths approximately corresponding to the halocline in each year.

3.1.3. Dissolved nutrients

Samples for nutrient analyses were not collected at the Pavlof location in either year. However, comparison of Unimak and M2 locations alone yields interesting differences between the Aleutian Islands pass and continental shelf in nutrient composition and concentration. Phosphate concentrations at Unimak increased slightly with depth, from 0.6 μg kg^{-1} at the surface to 0.95 μg kg^{-1} at 90 m in 2011 and 1.2–1.4 μg kg^{-1} in 2012 (Fig. 4A). In contrast, phosphate at M2 was depleted in near-surface waters above the halocline in 2011 (0.5 μg kg^{-1}), suggesting some degree of utilization prior to the sampling date, and increased to 1.5 μg kg^{-1} with depth (Fig. 4A). Phosphate was generally higher and more uniform with depth in 2012, with concentrations of approximately 1.5 μg kg^{-1} near surface and at 70 m (Fig. 4A). Distributions of silicate with depth in 2011 and 2012 largely corresponded to those of phosphate described above. Silicate concentrations were somewhat depleted at the surface but otherwise increased only marginally with depth at Unimak in 2011 (15.3–19.8 μg kg^{-1}) and 2012 (19.7–26.7 μg kg^{-1}) and decreased slightly with depth at M2 in 2012 (32.2–31.6 μg kg^{-1}; Fig. 4B). In 2011, however, near-surface silicate concentrations at M2 reached a

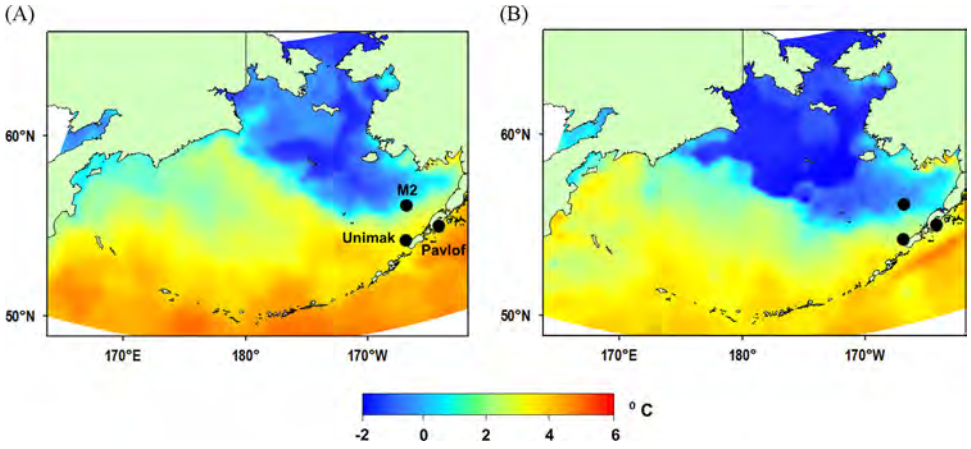

Fig. 1. Sea surface temperature (°C) in the Bering Sea on 15 May 2011 (A) and 2012 (B). Overlapping stations in both years at Pavlof, Unimak, and M2 are indicated by black circles and labels. White areas indicate no available data.

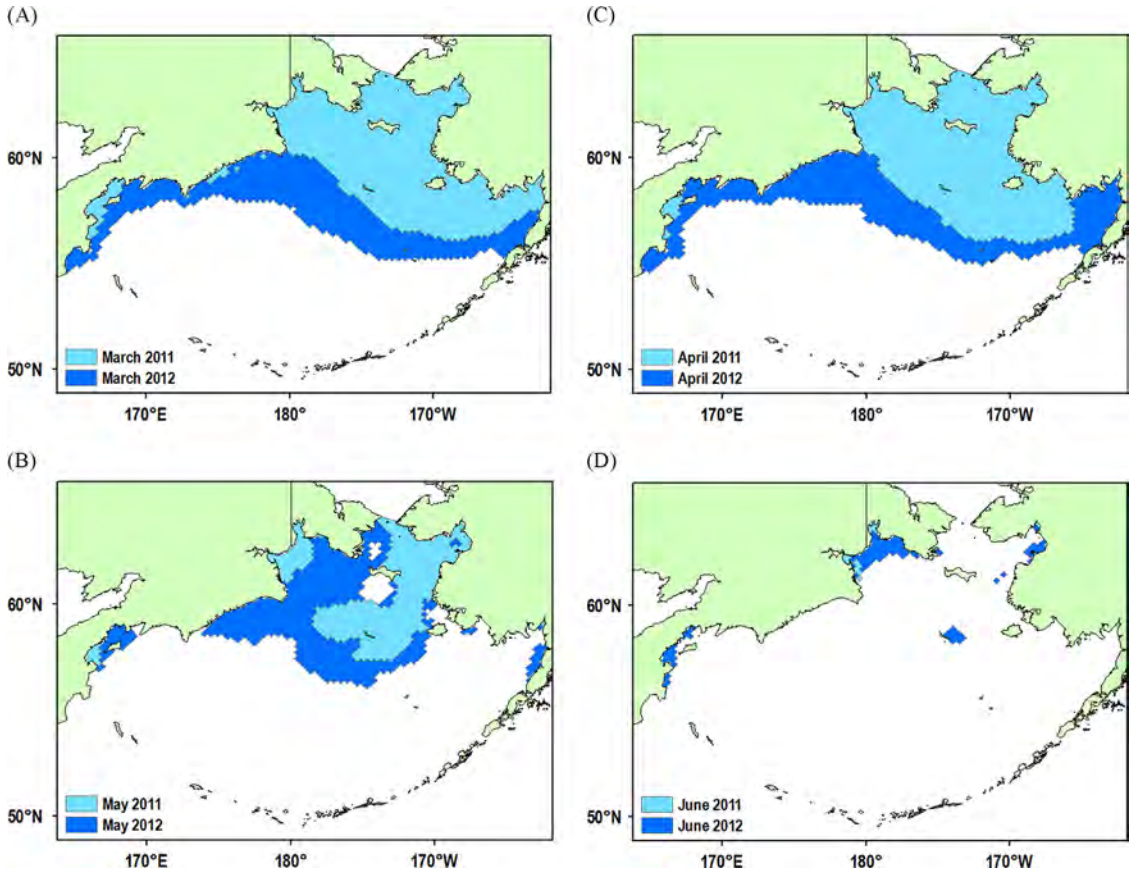

Fig. 2. Sea ice coverage in 2011 (light blue) and 2012 (dark blue) for months of (A) March, (B) April, (C) May, and (D) June. (For interpretation of the references to color in this figure caption, the reader is referred to the web version of this paper.)

Table 2
Sea ice area (m^2) and monthly averaged retreat rate (m^2 $month^{-1}$) in the Bering Sea, March–June 2011 and 2012. Area and retreat rate were calculated from National Sea Ice Data Center monthly averages for the region. A positive retreat rate means accumulation of sea ice over that time period.

	2011	2012
Sea Ice Area		
March	7.04×10^{11}	1.16×10^{12}
April	6.97×10^{11}	1.16×10^{12}
May	3.10×10^{11}	7.12×10^{11}
June	8.75×10^{9}	7.06×10^{10}
Retreat rate		
March–April	-2.30×10^{8}	$8.11E \times 10^{7}$
April–May	-1.29×10^{10}	-1.50×10^{10}
May–June	-9.72×10^{9}	-2.07×10^{10}

minimum of 0.8 μg kg^{-1} at the shallowest depth sampled but increased to 27.2 μg kg^{-1} at 68 m depth (Fig. 4B).

Nitrate concentrations were higher throughout the water column at both locations in 2012, measuring 11.3 and 13.1 μg kg^{-1} near-surface at Unimak and M2, respectively (Fig. 4C), suggesting a potentially common source of new nitrogen. In 2011, nitrate was much lower throughout the water column at Unimak, ranging from only 1.8 to 6.3 at 90 m (Fig. 4C). Near-surface nitrate reduction (0.8 μg kg^{-1}) was apparent at M2 in 2011, yet concentrations increased to 10.7–12.0 μg kg^{-1} with depth (Fig. 4C). M2 nitrite and ammonium concentrations in 2011 followed comparable patterns, varying from 0.03 and 0.8 μg kg^{-1} at 30 m to 0.30 and 2.5 μg kg^{-1} at 70 m, respectively (Fig. 4D and E). In contrast, nitrite concentrations were relatively low (0.08–0.14 μg kg^{-1}) and uniform throughout the water column at M2 in 2011 and at Unimak in both years, (Fig. 4D). Ammonium also was relatively low at Unimak both years, with concentrations ranging from 0.8 to 2.5 μg kg^{-1} and 2.0 to 1.5 μg kg^{-1} from surface to depth in 2011 and 2012, respectively (Fig. 4E). M2 ammonium concentrations in 2012 were relatively uniform throughout the water column and, at 3.3–3.5 μg kg^{-1}, the highest seen in this dataset (Fig. 4E).

3.2. Phytoplankton

3.2.1. Chl a

Remote sensing data showed higher surface Chl *a* concentrations in the eastern Bering Sea and the Gulf Alaska contiguous to the Aleutian Islands in May 2011(Fig. 5A) than in May 2012 (Fig. 5B). However, it should be noted that Chl *a* was much higher in the western Bering Sea in 2012 when temperatures in this region were also increased, indicative of the propensity for a high level of regional variability in oceanography and biological processes attributable to the strength and the location of the Aleutian Low Pressure region over the Bering Sea (Saitoh et al., 2002). Overall Chl *a* was also higher throughout the water column of the three sites sampled in 2011 (Fig. 3). Minor subsurface chlorophyll maxima (SCM) of 16.9 and 12.0 μg L^{-1} were observed at Pavlof in 2011 and 2012 (Fig. 3D), while Chl *a* was more uniformly distributed throughout the water column in both years at Unimak (Fig. 3H). Unimak Chl *a* concentrations varied between 23.8 μg L^{-1} at 20 m and 8.7 μg L^{-1} at 90 m in 2011, while concentrations in 2012 were $\leq$ 1.7 μg L^{-1} throughout the water column (Fig. 3H). The highest biomass in this dataset was observed in 2011 at M2, where a broad SCM centered around 20 m contained Chl *a* at concentrations of 36.7 μg L^{-1} (Fig. 3L). A well-defined SCM up to 21.5 μg L^{-1} was also evident at M2 in 2012 centered around 20 m (Fig. 3L).

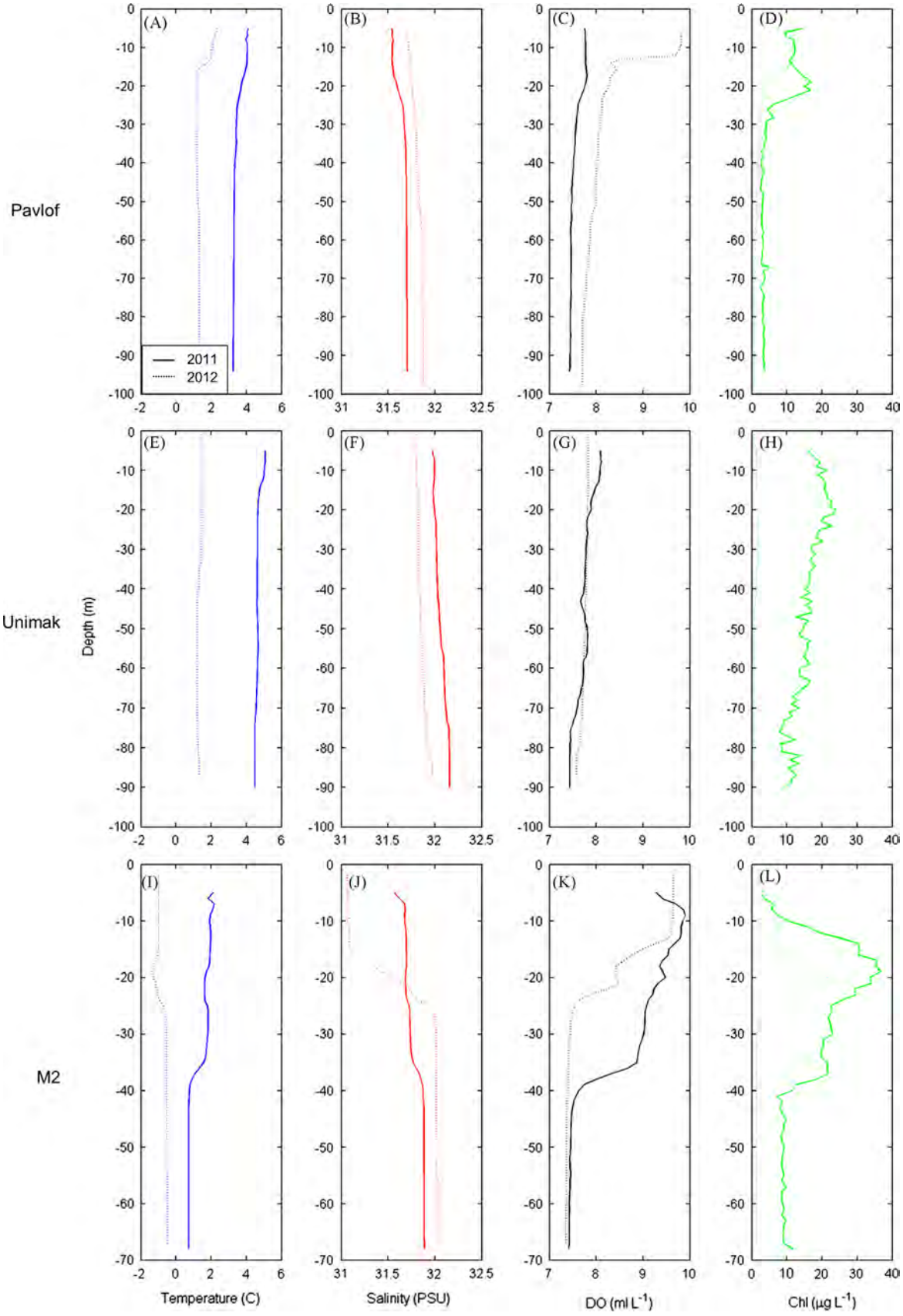

Fig. 3. Depth profiles of (A) temperature, (B) salinity, (C) dissolved oxygen, and (D) chlorophyll fluorescence in 2011 (solid lines) and 2012 (dotted lines). Data from Pavlof (top row), Unimak (middle row), and M2 (bottom row) are shown.

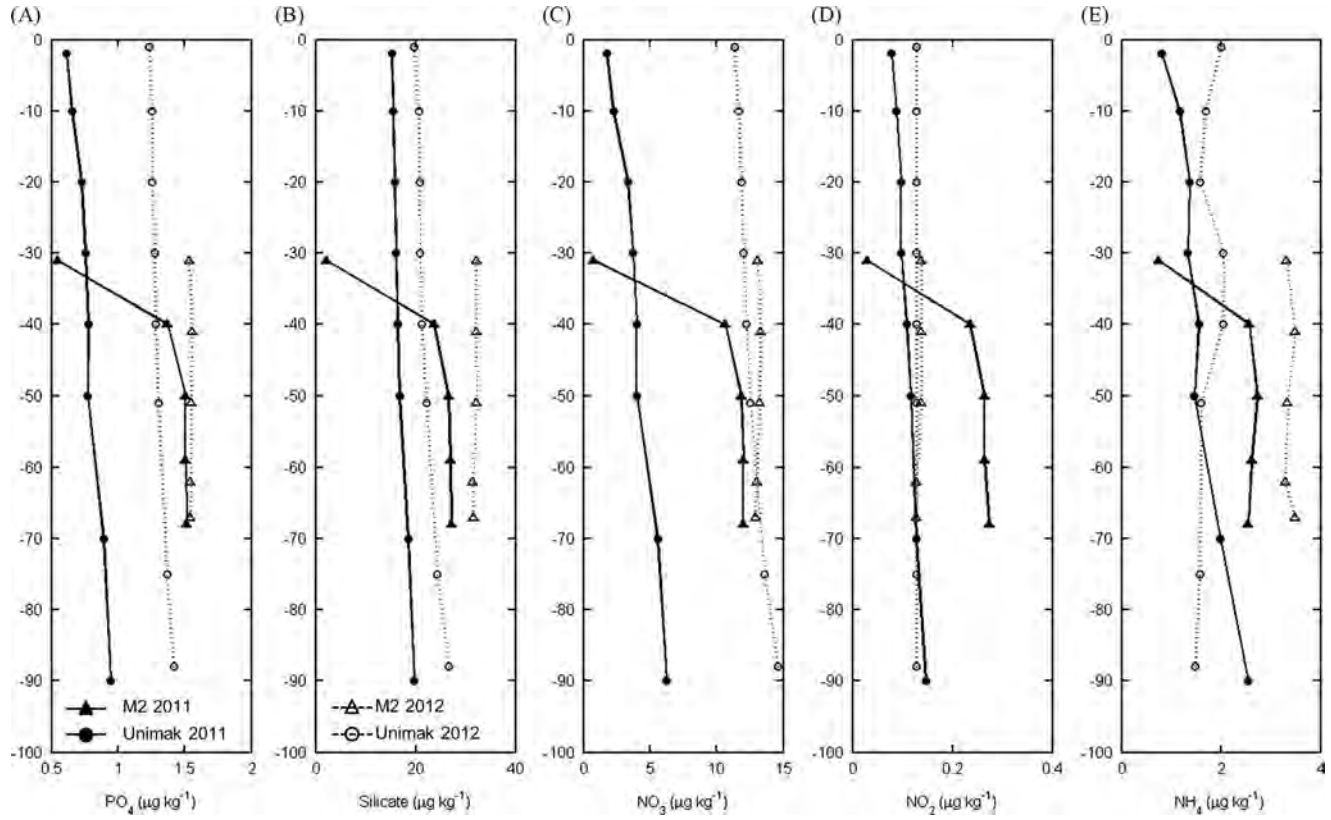

Fig. 4. Depth profiles of (A) phosphate, (B) silicate, (C) nitrate, (D) nitrite, and (E) ammonium in 2011 (solid lines, filled symbols) and 2012 (dotted lines, open symbols). Data are shown for Unimak (circles) and M2 (triangles). Data was not available from Pavlof in either year.

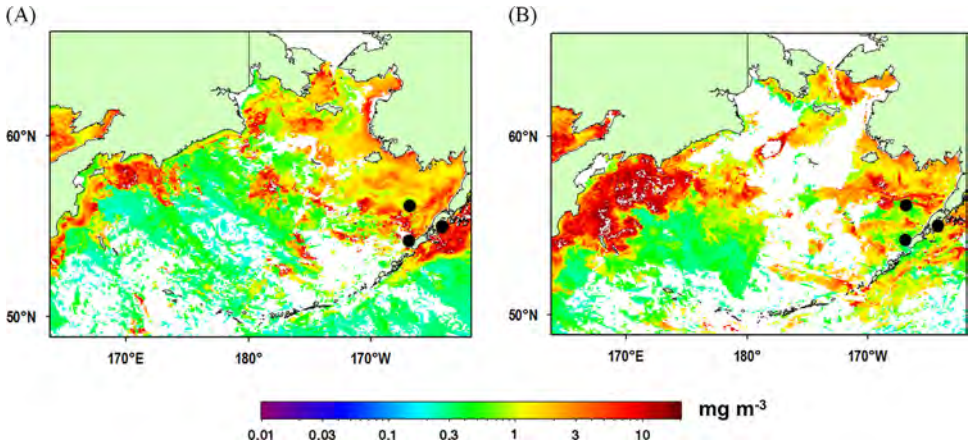

Fig. 5. Surface chlorophyll (mg m^3) in (A) May 2011 and (B) 2012. Overlapping stations in both years are indicated by black circles. White areas indicate no available data.

Phytoplankton >200 μm in size and microplankton (20–200 μm) comprised $>50\%$ of total Chl *a* in 2011 at all sites and depths and at Pavlof in 2012 (Fig. 6). In contrast, cells >200 μm in size and nanoplankton (3–20 μm) were dominant at all depths at Unimak in 2012, with a substantial contribution ($>$ 40%) from picoplankton (<3 μm). Finally, the M2 surface and SCM communities in 2012 were dominated by microplankton (2–200 μm) and nanoplankton ($\sim$95% together), while picoplankton comprised $\sim$8% of total Chl *a* at depth in 2012 (Fig. 6). Chl *a* size fractions were significantly different between years (t-test; $p<0.01$) at Pavlof (micro- and picoplankton) and Unimak (micro-, nano-, and picoplankton). Differences in size fractionated Chl *a* at M2 were not statistically significant.

Overall higher Chl *a* in 2011 in the eastern Bering Sea indicated by ship-based (Fig. 3) and synoptic May data (Fig. 5) appeared to correspond to an appreciable difference between years in overall rates of net summer primary productivity (NPP) as measured by satellite (Fig. 7). Mean rates of summer NPP from May through August were highest near the coasts and along the "Green Belt" region (Springer et al., 1996) in 2011, and rates of NPP at M2 and Unimak stations were 0.10–0.25 g C m^{-2} d^{-1} higher in 2011 than in 2012 (Fig. 7A). Conversely, increased NPP in the western Gulf of Alaska and through the Bering Strait was observed for this time period in 2012, with an increase of 0.29 g C m^{-2} d^{-1} from 2011 rates at

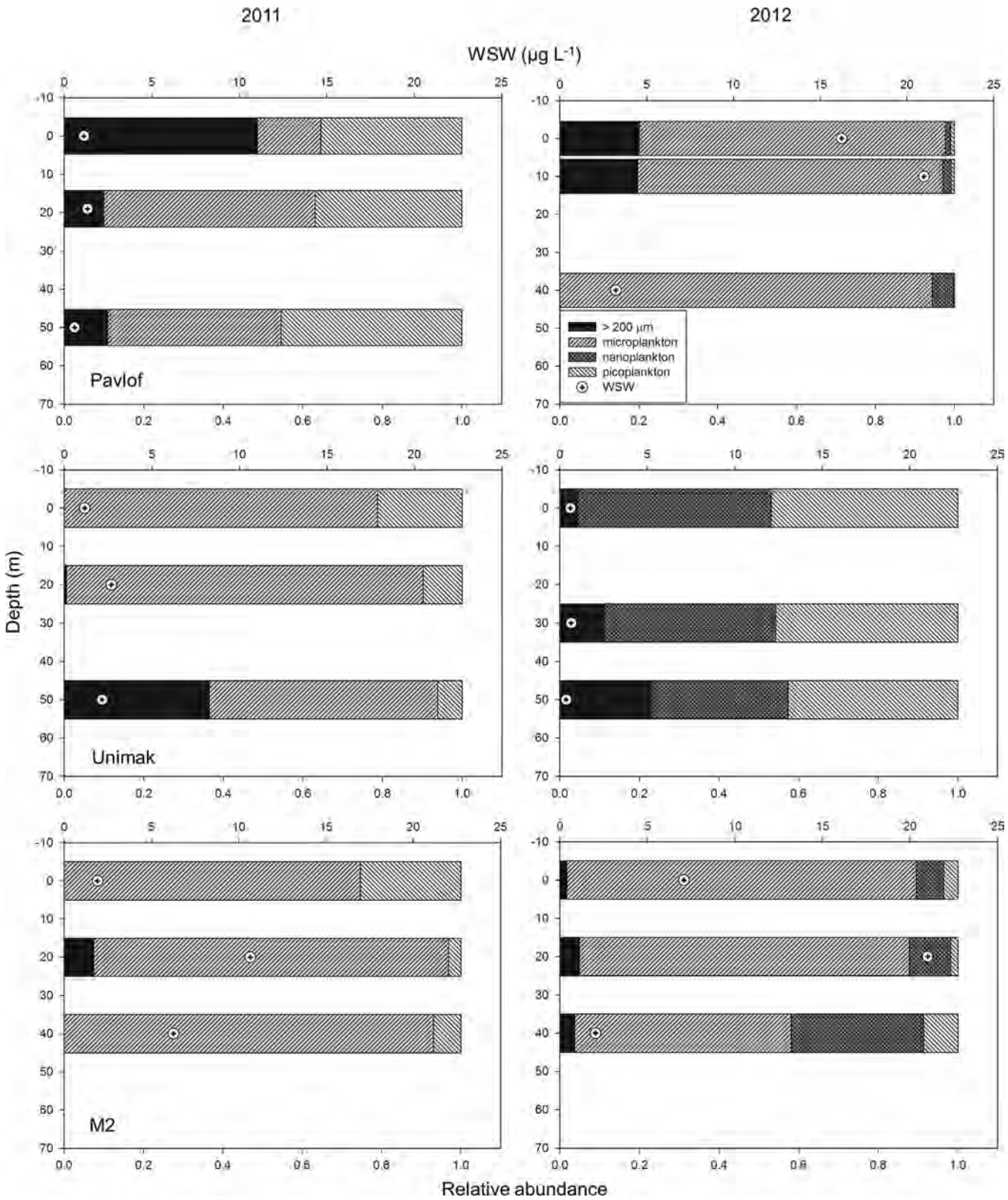

Fig. 6. Whole seawater and size fractionated chlorophyll from Pavlof (top row), Unimak (middle row), and M2 (bottom row) in 2011 (left) and 2012 (right). Samples were fractionated from whole seawater (WSW, circle) and size classes corresponding to > 200 µm (black), microplankton (20–200 µm; gray), nanoplankton (3–20 µm; dark gray) and picoplankton (< 3 µm; light gray) were discriminated. Significant differences ($p < 0.05$) were detected between years in the micro- and picoplankton size fractions at Pavlof and in the micro-, nano-, and picoplankton fractions at Unimak (see Results).

Pavlof (Fig. 7B). This increased NPP is consistent with maximum surface dissolved oxygen concentrations at Pavlof in 2012 (Fig. 3C).

3.2.2. Plankton assemblages

The composition of plankton assemblages varied greatly between 2011 and 2012 at the majority of locations (Table 3).

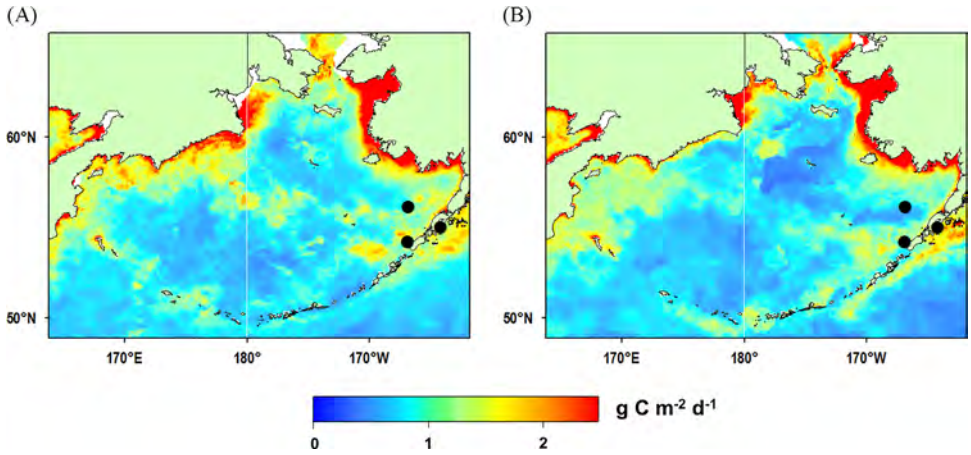

Fig. 7. Mean rates of primary productivity (g C m^{-2} d^{-1}) averaged from May through August in (A) 2011 and (B) 2012. Overlapping stations in both years are indicated by black circles. White areas indicate no available data.

Table 3
Dominant plankton taxa in the western Gulf of Alaska and eastern Bering Sea in 2011 and 2012. The relative abundances of taxa contributing ≥ 1% to the total community across all times and locations or to a single community at Pavlof, Unimak, or M2 locations are presented. Relative abundances for surface (Surf), subsurface chlorophyll maximum (SCM), and 1% light level (Deep) at each station. '–' indicates that the taxa was not detected.

	Total	Pavlof						Unimak						M2					
		2011			2012			2011			2012			2011			2012		
		Surf	SCM	Deep	Surf	SCM	Deep	Surf	SCM	Deep	Surf	SCM	Deep	Surf	SCM	Deep	Surf	SCM	Deep
Phaeocystis	29.3	11.9	54.6	100	1.48	0.49	11.6	71.3	74.5	79.3	5.88	–	–	46.8	44.3	16.2	5.10	2.51	1.30
Thalassiosira	19.9	–	–	–	40.9	51.9	50.9	–	–	–	–	10.0	–	6.33	–	26.5	69.0	53.6	49.6
Pseudonitzschia	7.91	56.7	29.1	–	0.91	1.65	1.73	3.59	8.51	3.72	11.8	10.0	8.33	1.27	2.46	1.47	1.09	–	–
Thalassiothrix	7.25	–	–	–	0.23	0.49	–	–	–	0.53	–	60.0	66. 7	–	–	–	2.43	0.12	–
Chaetoceros decipiens	4.46	1.49	–	–	0.80	3.95	1.73	4.19	6.38	2.13	–	–	8.33	19.0	13.9	16.2	2.07	0.06	–
Chaetoceros socialis	3.58	–	–	–	30.1	19.9	11.0	–	–	–	–	–	–	–	–	–	2.55	0.78	–
Nitzschia	2.61	–	–	–	–	0.16	0.58	–	–	2.13	–	–	–	10.1	17.2	14.7	0.12	1.91	–
Strombidium	2.58	22.4	5.45	–	–	0.49	–	4.19	3.19	1.06	5.88	–	–	1.27	–	1.47	0.49	0.06	0.43
Coscinodiscus	2.36	2.99	–	–	10.5	8.07	2.31	2.99	2.13	1.06	–	–	–	–	4.10	4.41	0.97	0.78	2.17
Navicula	2.26	–	–	–	2.17	2.64	6.36	–	–	–	–	10.0	–	–	–	–	6.32	7.05	6.09
Putative *Cryptophyte*	1.72	–	–	–	–	0.82	–	7.78	4.26	3.19	–	–	–	5.06	5.74	–	0.12	–	3.91
Skeletonema	1.48	–	–	–	0.68	–	0.58	–	–	–	–	–	–	5.06	7.38	5.88	3.16	1.26	2.61
Dactyliosolen	1.46	–	–	–	–	–	–	–	–	–	–	–	–	–	–	–	–	17.2	9.13
Euglenid	1.37	–	–	–	0.57	–	0.58	–	–	–	23.5	–	–	–	–	–	–	–	–
Laboea	1.14	–	7.27	–	0.11	–	–	–	–	–	11.8	–	–	1.27	–	–	0.12	–	–
Small pennate diatom	1.09	–	–	–	–	–	–	–	–	–	–	–	–	–	–	–	1.82	5.26	12.6
Oligotrich ciliate	1.04	–	–	–	0.11	0.16	–	–	–	–	–	–	16. 7	–	–	–	–	0.90	0.87
Eucampia	0.98	–	–	–	–	–	–	–	–	–	17.8	–	–	–	–	–	–	–	–
Gyrodinium	0.94	–	–	–	2.05	2.47	2.31	3.59	–	0.53	–	–	–	3.80	0.82	–	0.24	0.60	0.43
Odontella	0.89	–	–	–	1.03	1.98	2.89	–	–	–	–	10.0	–	–	–	–	–	0.18	–
Chaetoceros didymus	0.80	–	–	–	0.11	0.16	2.31	–	–	–	11.8	–	–	–	–	–	0.12	–	–
Fragillariopsis	0.68	–	–	–	–	–	0.58	–	–	–	–	–	–	–	–	–	2.55	2.09	6.96
Protoperidinium	0.55	–	–	–	0.11	0.66	–	–	–	–	–	–	–	–	–	8.82	0.12	0.18	–
Rhizosolenia	0.55	–	–	–	0.23	–	–	–	–	2.66	5.88	–	–	–	–	–	–	1.08	–

The prymnesiophyte *Phaeocystis* sp. was numerically dominant at most depths at all three locations in 2011, constituting on average 55.4% of the community in that year (Table 3). This small colonial haptophyte constituted ≤5.10% of the community in any sample from 2012, a year which instead was dominated by diatoms including *Thalassiosira* spp. and *Thalassiothrix* spp., contributing up to 69.0% and 66.7%, respectively, to depth-specific assemblages in 2012 (Table 3). Chain-forming *Pseudonitzschia* spp. were abundant at Pavlof (29.0–56.7%) in 2011 and Unimak in both 2011 (up to 8.51%) and 2012 (up to 11.8%; Table 3). However, *Pseudonitzschia* spp. were rarely observed in 2012 at Pavlof and M2, in favor of centric diatoms *Chaetoceros socialis* (11.0–30.1%) and *Coscinodiscus* sp. (2.31–10.5%) at Pavlof; euglenids (23.5%) and *Eucampia* sp. (17.8%) at the surface and small oligotrich ciliates at depth (16.7%) at Unimak; and diatoms *Navicula* spp. and *Dactyliosolen* spp. at the M2 SCM (7.05% and 17.15%, respectively; Table 3). Abundance diatom species at M2 in 2011 also included *Chaetoceros decipiens* (≤19%), *Nitzschia* spp. (≤17.2%), and *Skeletonema* (≤7.38%). Putative cryptophytes were observed in 2011 at relative abundances of 7.78% and 5.74% in the Unimak surface and M2 SCM assemblages, respectively; they constituted <4% of the assemblage at any of the sites in 2012 and were otherwise not distinguishable by FlowCAM imaging that year (Table 3).

Finally, it is worth noting that assemblages varied at each location with depth. For example, *Pseudonitzschia* spp. comprised 29.1% and 56.7% of the surface and SCM Pavlof communities, respectively, in 2011 but were not detected in deep samples at that same site (Table 3). Furthermore, oligotrich ciliates in the genus *Strombidium* were abundant in surface samples at Pavlof in 2011 and Unimak in 2012 but were largely absent from other depths at

those locations (Table 3), while *Odontella* sp. comprised 10% of the SCM community at Unimak in 2012 and were otherwise not detected in surface or deep samples at that site (Table 3).

These differences in richness and evenness of taxa were also manifest as differences in diversity of the microplankton community between locations and years. Mean diversity (H') averaged across the three depths significantly increased from 2011 to 2012 from 1.067 to 2.694 at Pavlof ($p < 0.04$) and from 2.179 to 2.772 at M2 ($p < 0.002$; Table 4). This increased diversity is likely a reflection of an increased number of taxa observed in the 2012 samples across depths at these locations and overall reduced dominance of a single taxonomic group (Table 3). In contrast, a slight decrease in diversity was observed at Unimak (Table 4).

While differences in diversity have implications for food webs, these effects are often driven by differences in community composition (Downing and Leibold, 2002; Narwani and Mazumder, 2012). Multivariate statistical analyses of plankton assemblages revealed distinct microplankton communities between years and between locations within each year (Fig. 8). Multidimensional scaling (MDS) of each depth-resolved community from the 2011 and 2012 stations ($N = 18$) revealed broad levels of similarity (45%) among Unimak, M2, and subsurface Pavlof assemblages in 2011 (Group A); Pavlof and M2 assemblages in 2012 (Group B); and subsurface Unimak assemblages in 2012 (Group C; Fig. 8). These groups were statistically different from one another ($p < 0.05$) using the permutation-based SIMPROF test (Clarke and Gorley, 2006). In 2011, microplankton assemblages at the three depths at Unimak were 55% similar and statistically distinct ($p < 0.05$) from the equally similar depth-resolved assemblages at M2 (Group A; Fig. 8). In 2012, microplankton assemblages at the three depths at Pavlof were 55% similar and statistically distinct ($p < 0.05$) from the depth-resolved M2 assemblages in that year (Group B; Fig. 8). Subsurface Pavlof assemblages in 2011, while 45% similar to other 2011 assemblages, were significantly different from the surface assemblage at this site. Surface Unimak assemblages in 2012 and surface Pavlof assemblages in 2011 were also distinct from all others ($p < 0.05$; Fig. 8). Finally, the MDS stress, which indicates goodness of fit of the multidimensional data in 2-dimensional space was low (≤ 0.1) and less than the 1% cutoff stress level for an 18-object MDS (Sturrock and Rocha, 2000), suggesting that Fig. 8 is a good representation of the relationships between phytoplankton assemblages.

Differences between assemblages were further tested using a series of non-parametric one-way analyses of similarity (ANOSIM), which quantified the effects of year and location on assemblage similarities. As a rank-based test, the magnitude of the ANOSIM test statistic (R) is indicative of the relative strength of the differences between two groups (Clarke and Gorley, 2006) and therefore can be compared across analyses. Assemblages were significantly different between years ($R = 0.579$, $p < 0.0003$) and to a lesser extent between locations ($p < 0.079$; Table 3). Assemblages within each year were also very different between locations ($p < 0.004$), most notably between M2 and Unimak in 2011 ($R = 0.809$) and between Pavlof and M2 in 2012 ($R = 0.963$; Table 5). Based on the magnitude of the R test statistic, spatial variability within each year ($R = 0.588$, 0.646) appeared to play an only slightly stronger role than variability between years ($R = 0.579$) in the overall variability between assemblages (Table 5). Variability between locations in each year was often driven by stronger differences between Gulf of Alaska/Aleutian Islands locations (Pavlof, Unimak) and the Bering Sea shelf (M2).

Table 4
Test statistics (t), degrees of freedom (df) and significance levels (p) for t-tests of Shannon diversity index (H') at Pavlof, Unimak, and M2 locations in 2011 and 2012.

Location	Mean H'		t	df	p
	2011	2012			
Pavlof	1.067	2.694	−3.001	4	0.040*
Unimak	1.915	1.657	0.852	4	0.442
M2	2.179	2.772	−7.535	4	0.002*

* Significant differences ($p < 0.05$) between 2011 and 2012 means.

4. Discussion

4.1. Within-regime sea ice and temperature variability

The Bering Sea is characterized by large interannual, multi-year, and decadal scale variability in sea ice extent and SST (Jin et al., 2009; Brown et al., 2011; Overland et al., 2012; Stabeno et al.,

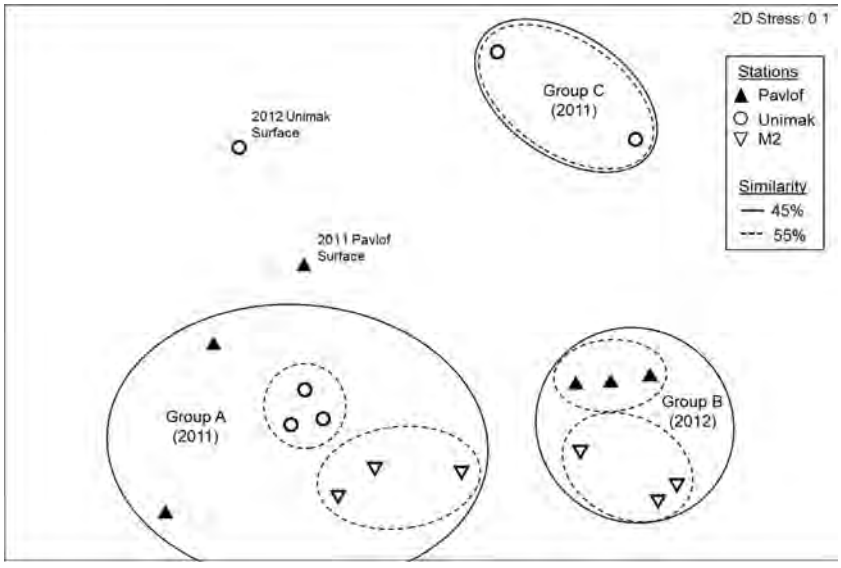

Fig. 8. Non-metric multidimensional scaling (MDS) plot of surface, subsurface chlorophyll maximum, and deep microplankton communities at Pavlof (filled triangles), Unimak (open circles), and M2 (open triangle) in 2011 and 2012. Microplankton relative abundances in each sample were square-root transformed, and community similarities were determined by resemblance based on Bray Curtis coefficients. The distance between points represents the level of similarity in microplankton community composition, and solid and dotted contour lines enclose communities that are 45% and 55% similar to each other, respectively. Samples included within groups A, B, and C are significantly similar to each other at a 45% level. Stress = 0.1.

Table 5
Test statistics (R) and significance levels (p) for analyses of similarity (ANOSIM) of phytoplankton communities at Pavlof, Unimak, and M2 locations in 2011 and 2012. Four one-way analyses were completed for effects of the factors year, location, and location in each year specifically. Pair-wise site comparisons are included for analyses of location.

Factor	R	p
Year	0.579	0.0003*
Location, both years	0.134	0.079
Pavlof-M2	0.104	0.169
Pavlof-Unimak	−0.035	0.558
M2-Unimak	0.333	0.017
Location, 2011	0.588	0.004*
Pavlof-M2	0.704	0.1
Pavlof-Unimak	0.333	0.1
M2-Unimak	0.809	0.1
Location, 2012	0.646	0.004*
Pavlof-M2	0.963	0.1
Pavlof-Unimak	0.556	0.1
M2-Unimak	0.63	0.1

* Significant results ($p < 0.05$).

2012a; 2012b). Notable warm (2000–2005) and cold (2007–2010) periods from the past decades are thought to represent major excursions from average conditions in the Bering Sea and to be dominated by sub-decadal variability (Overland et al., 2012), while the multi-decadal Pacific Decadal Oscillation is also apparent in long-term trends (Jin et al., 2009). Contrary to compelling evidence for long-term warming and reductions in sea ice in the Arctic Ocean in the last several decades, questions of evidence for long-term warming of the Bering Sea and potential ecosystem impacts remain (Brown and Arrigo, 2012). What is apparent however, is that large interannual and multi-year variability in the environment of the Bering Sea have significant implications for the food webs and fisheries sustainability in this productive ecosystem (Hunt et al., 2010, 2011; Stabeno et al., 2012b).

Data from cruises conducted in spring 2011 and 2012 from the western Gulf of Alaska into the southeastern Bering Sea offered an excellent opportunity to contrast the environmental conditions and plankton assemblages in the region during a relatively warmer (2011) and colder (2012) spring within a single (cold) regime. Characterization of 2011 as a relatively warmer year than 2012 is supported by lower than average monthly sea ice extent in 2011 compared to continued sea ice accumulation into April in 2012 (Table 1, Fig. 2) and overall warmer temperatures in 2011 both at the surface in mid-May (Fig. 1) and throughout the water column at all sites (Fig. 3). While the temporal overlap of the cruises was imperfect, the M2 station was sampled only 10 days earlier in 2012 while Pavlof and Unimak were sampled 19 and 28 days apart, respectively. These data also yield insights into the transition between the Gulf of Alaska and Bering Sea, which, via advection, can provide a significant community of zooplankton as well as nutrients to the Bering Sea shelf (Stabeno et al., 2002; Mordy et al., 2005).

4.2. Hydrographic variability

Differences in salinity between 2011 and 2012 were largely limited to M2, where the continued influence of sea ice in the shelf region in April–May 2012 was apparent as significant freshening and cooling of surface waters on the shelf (Fig. 3). Stratification at M2, which was weaker in 2011 as a result of earlier sea ice retreat from the region that year, likely led to the formation of subsurface maxima of chlorophyll and dissolved oxygen saturation in the euphotic zone in both years. In contrast, bidirectional tidal flow through Unimak Pass kept the phytoplankton biomass relatively well-mixed in that location in both years. Overall, the highest Chl *a* concentrations were observed in 2011 via both in situ fluorescence (Fig. 3) and remote sensing (Fig. 5), and NPP was generally higher in the eastern Bering Sea in 2011 (Fig. 7). These results are consistent with documented direct relationships of increasing productivity with warming of the surface ocean in this region (Hare et al., 2007; Mueter et al., 2009; Hunt et al., 2010). However, NPP in the western Gulf of Alaska was higher in 2012, despite generally cooler temperatures that year, suggesting different processes, potentially related to nutrient limitation (e.g. Fiechter et al., 2009; Stabeno et al., 2004), controlling productivity in this adjacent sea. Across both years, Chl *a* and NPP were also elevated along the 70 m isobath of the continental shelf adjacent to the highly productive 'Green Belt' region of the eastern Bering Sea (Springer et al., 1996). Phytoplankton biomass and productivity also showed distinct patterns of variability in the eastern and western regions of the Bering Sea, consistent with previous observations of a see-saw effect on regional variability (Saitoh et al., 2002).

The nutrient concentrations in 2011 and 2012 offer insight into the status of the spring bloom in each year and potential for nutrient transport into the Bering Sea from the Gulf of Alaska. Overall, nutrients were available at higher concentrations throughout the water column in 2012, suggesting that significant drawdown, especially of nitrate, had not yet occurred by late April–early May. Phosphate, silicate, nitrite, and ammonium were available at higher concentrations at M2 than at Unimak in both years, again consistent with the shelf region as one of high nutrient availability and productivity (Springer et al., 1996) and negligible spring-time nutrient input from ACC waters via the Aleutian passes (Stabeno et al., 2002; Mordy et al., 2005; Cooper et al., 2012). Slight drawdown of nitrate, phosphate and silicate at Unimak in 2011 suggested increased phytoplankton utilization at this location in late May–early June 2011, while more substantial drawdown at M2 of all measured nutrients indicated a spring bloom fully underway (Lomas et al., 2012). Mooring data from M2 indeed shows a preceding bloom event in 2011 approximately one month before the cruise sampling date (Sigler et al., 2014). However, a significant response of the acoustically measured consumer community (e.g. zooplankton and fishes) did not occur until after the cruise sampling date at this location. Similarly, the consumer response at M2 in 2012 occurred just following the phytoplankton community captured by the 2012 cruise in that year as well. These trends suggest that the phytoplankton communities captured on each cruise were those that more directly impacted higher trophic levels compared to earlier bloom communities.

4.3. Within-regime phytoplankton community variability

Size distribution of the phytoplankton community varied across years and locations, driven largely by numerical dominance of the colonial prymnesiophyte *Phaeocystis* spp. in 2011, which comprised > 50% of the surface plankton assemblage at all three locations (Table 3). *Phaeocystis* spp. is capable of forming colonies up to 2000 μm in size, and so they were likely captured in more than one size fraction of chlorophyll, including the > 200 μm fraction, in 2011. Putative cryptophytes (conservatively identified based on morphology and size) were also common in 2011 but largely undetected in 2012 consistent with recent observations of an increase in their relative abundance in warmer waters (Goes et al., 2014). Dominance of nanoplankton over microplankton during the relatively warmer spring of 2011 is consistent with previously reported changes in spring-time plankton communities with increased SST (Lomas and Glibert, 1999; Noiri et al., 2005; Hare et al., 2007; Fujiwara et al., 2011) and with a general

transition towards nanoplankton in summer assemblages (Fujiki et al., 2009; Fujiwara et al., 2011; Goes et al., 2014).

In contrast, phytoplankton assemblages dominated by larger cells in the diatom genera *Thalassiosira*, *Thalassiothrix*, *Chaetoceros*, and *Nitzschia*, in the relatively cooler spring of 2012 more closely resemble species composition reported in other studies (Schandelmeier and Alexander, 1981; Springer et al., 1996). Sea ice extent was still substantial during the April–May 2012 cruise (Fig. 2), and active retreat from the southeastern Bering Sea is thought to release iron into the surface waters (Aguilar-Islas et al., 2008), also potentially favoring growth of large diatoms with relatively high iron demands. As such, the dominant taxa in 2012 represent more cold-adapted, ice-associated species that thrive once iron limitation becomes minimal (Noiri et al., 2005).

It should be noted that, as a result of the low magnification used for FlowCAM analyses, smaller cells (e.g. non-colonial nanoplankton) were potentially excluded, though their abundances were captured in the size-fractionated chlorophyll analyses. *Phaeocystis* spp. was often captured as entire colonies or parts thereof, suggesting that its observed numerical dominance in 2011 is likely an underestimation of the true number of cells of this genus in the samples and that large colonies were included in the larger size fractions of Chl *a* instead of the nanoplankton fractions. These inconsistencies between size-fractionated estimations of biomass and microscopically derived characterizations of community composition suggest a valuable contribution of both approaches to continued studies of such complex communities.

Diversity in aquatic ecosystems has been shown to significantly impact functioning and stability of complex food webs through a combination of direct and indirect effects which have been largely attributed to changes in species composition (Downing and Leibold, 2002; Narwani and Mazumder, 2012). Conservative estimates of diversity of the phytoplankton assemblages averaged over depth in the Gulf of Alaska and on the Bering Sea shelf were higher in 2012 than in 2011, likely driven by a switch from widespread dominance of a single taxonomic group in 2011 to higher taxonomic richness and more even distributions of taxa in 2012. Additionally, overall low diversity at Unimak in both years, combined with high rates of water flow through this pass, suggests this location as a transitional area in which the forces driving diversity are in flux relative to the more stable Gulf of Alaska and Bering Sea shelf locations. Combined with the low phytoplankton biomass observed at Unimak in 2012, low levels of diversity at Unimak also have implications for feeding, growth, and survival of consumer populations during their advection from the Gulf of Alaska into the Bering Sea (Longhurst, 1998).

Given the important role species composition can play in the functioning and stability of food webs, it is therefore necessary to characterize phytoplankton assemblages beyond traditional measures of biomass. Multidimensional scaling (MDS) analyses revealed that assemblages were most different between the two years, reflecting the fundamental differences between dominant phytoplankton groups during the warm spring of 2011 and the colder, more typical spring of 2012. Hare et al. (2007) documented a shift from diatom to nanoplankton dominance in manipulated communities exposed to a temperature increase of $+4.7\ ^{\circ}C$ above ambient, while Noiri et al. (2005) similarly observed a shift from larger cells to nanoplankton in treatments incubated with a $5\ ^{\circ}C$ increase in temperature. This shift in dominance to smaller cells has been hypothesized to arise from differential nutrient (especially nitrate) uptake kinetics in nano- versus microplankton (Hare et al., 2007); specifically, large diatoms ($>20\ \mu m$) account for a disproportionate amount of the uptake of nitrate in cool, nutrient-rich waters and this uptake does not readily saturate (Lomas and Glibert, 1999). In contrast, nitrate uptake saturates at lower concentrations in warmer, nutrient-poor waters due to physiological stress caused by nutrient depletion (Lomas et al., 2012). In the meantime, smaller cells typically have higher adaptability to nutrient depletion due to higher surface area: volume ratios, and colonial *Phaeocystis* spp., specifically, has been shown to maintain high productivity under low nutrient conditions (Tungaraza et al., 2003). The potential for small cells to thrive under conditions of nutrient depletion is reflected in the current study, where small cells ($<3\ \mu m$) accounted for 25% of the overall Chl *a* in 2011 in highly productive surface waters of M2 with nitrate concentrations $<1\ \mu mol\ kg^{-1}$.

A high degree of spatial variability in the transition from the western Gulf of Alaska onto the Bering Sea shelf was also apparent within each year, with two notable outliers: surface assemblages from Unimak in 2012 and from Pavlof in 2011. Overall biomass was low in Unimak in 2012, and as a result the assemblage was dominated by a few taxa that were uncommon in other samples (euglenids, *Eucampia* sp., *Chaetoceros didymus*). Very few cells were detected and classified from this site overall, so these unique taxa, present at relatively low abundances, had a significant impact on the resemblance of this assemblage to others both at Unimak and beyond. Similarly, the 2011 Pavlof surface assemblage was strongly dominated ($>50\%$) by taxa that contributed on average $<8\%$ to all other assemblages. The significant difference of these surface communities to their deeper counterparts suggests more variability in surface assemblages than at depth, insights that are consistent with trends in community composition and diversity with depth in a shallow tropical lake (Hubble and Harper, 2002) and differences in protistan assemblages with depth in the eastern North Pacific (Schnetzer et al., 2011). These results also provide support for the continued study of complex ecosystems such as the Bering Sea by methods capable of resolving depth-specific trends and characterizing composition of phytoplankton communities in addition to synoptic views of biomass and productivity provided by remotely sensed parameters. More importantly, zooplankton are known to feed on subsurface maxima and thin layers of phytoplankton when subsurface biomass constitutes a significant fraction of the whole water column (Benoit-Bird et al., 2010; Greer et al., 2013), as was the case at M2 in both years. As a result, differences in species composition with depth, as have been documented in the current study, may have significant implications for our understanding of the trophic relationship and transport of carbon between phytoplankton and their consumers in the Bering Sea.

Water mass characteristics at the three locations sampled in the current study transition from warm, nutrient-poor ACC water entering Pavlof Bay to a highly variable mixture of ACC- and cooler, nutrient-rich Bering Canyon-derived water in Unimak Pass, and finally to nutrient-replete, sea ice-influenced waters on the continental shelf near M2. Spatial differences in phytoplankton community composition within each year were strongest between M2 and the two non-shelf stations, Pavlof and Unimak, consistent with previously observed differences between spring communities near the Aleutian and Pribilof Islands (Schandelmeier and Alexander, 1981) and likely attributable to these spatially distinct water masses. However, the current study also indicates that temporal variability between years within a single climatic regime has an effect almost equal to spatial variability on structuring the phytoplankton communities along this gradient.

4.4. Implications for the Bering Sea ecosystem

The Bering Sea is responsible for a large portion of finfish and shellfish landings in the United States and is economically and societally important for the local communities (Stabeno et al., 2012b). As a result, the dynamics of sea ice, water temperature, the timing and composition of spring blooms, and implications for the

food web in the southeastern Bering Sea have been the focus of research for several decades. Several studies have found fewer large crustacean zooplankton (e.g. *C. marshallae*) on the shelf during warm years, while smaller copepods and euphausids have not responded as quickly to temperature (Hunt et al., 2011; Lomas et al., 2012; Stabeno et al., 2012b). Lomas et al. (2012) theorized that larger zooplankton were more abundant in cooler years due to the presence of large diatoms, which are an excellent food choice compared to smaller nanoplankton. This suggests that larger zooplankton would have been more abundant in 2012 in the current study, given the relative dominance of large chain-forming diatoms and despite overall higher levels of phytoplankton biomass and rates of production in 2011. Instead, dominance of *Phaeocystis* spp. in 2011 may have led to fewer large copepods in the warmer year. This negative effect is likely due to both the overall smaller size distribution of this species and evidence that *Phaeocystis* spp. is a poor food item for most copepods, resulting in lower grazing rates (Nejstgaard et al., 2007), reduced fecundity (Turner et al., 2002), and increased grazing on microzooplankton (Hansen et al., 1993).

Lower than average grazing by microzooplankton, which have been shown to consume the bulk of the spring bloom, has also been observed during warm years (Strom and Fredrickson, 2008). This decoupling of production from consumption can further impact abundance and fecundity of zooplankton populations due to year-round feeding of copepods on microzooplankton (Lomas et al., 2012). Additionally, Pacific cod and walleye Pollock recruitment in the eastern Bering Sea have been negatively correlated with increasing temperature (Mueter et al., 2009) despite an overall positive correlation of fish recruitment with SST. The underlying mechanism is theorized to be a function of zooplankton populations: years with fewer large, lipid-rich zooplankton negatively impact age 0 walleye Pollock, resulting in increased predation and subsequent weak recruitment of year 1 juveniles (Hunt et al., 2002, 2011). Effects of changing phytoplankton community composition on zooplankton feeding, growth, reproduction, and recruitment therefore have the potential for far-reaching consequences for higher, ecologically and commercially important organisms.

These trophic pathways and feedbacks represent very real implications for the effects of reduced sea ice extent or rapid retreat in warm years and ensuing changes in plankton community composition. Using an atmosphere–ocean general circulation model, Wang et al. (2012) predicted a 42% reduction in spring sea ice extent relative to the 1980–1999 mean and largely ice free Decembers by 2050. Overland et al. (2012) utilized nearly a century of historical data to predict continuing positive and negative excursions lasting for multiple years in the future, but with poor predictability of when such events may occur and for how long they will last. Considering the role of the Bering Sea ecosystem as a conduit between the north Pacific and Arctic Ocean and the economically and ecologically important fisheries contained within its basin, potential future increases in SST and reduction in ice extent, even within single climatic regimes, will have important consequences for the phytoplankton community and, as a result, the entire ecosystem.

Acknowledgments

This is BEST-BSIERP publication number *130*. This work was supported by the National Aeronautics and Space Administration (Grants # NNX10AP10G and NNX11AP28G), and space aboard the *R/V Oscar Dyson* was generously provided by the National Oceanic and Atmospheric Administration in concert with the Eco-FOCI project. The authors thank K. Keebler for field assistance, J.M. Rose for helpful discussions of multivariate statistical analyses, the crew of the R/V *Oscar Dyson* for general cruise support, and D. Kachel, C. Mordy, P. Proctor, and other members of the Eco-FOCI group for helpful conversations on hydrographic data processing, nutrient data, and general support at sea.

References

Aguilar-Islas, A.M., Rember, R., Mordy, C.W., Wu, J., 2008. Sea ice-derived dissolved iron and its potential influence on the spring algal bloom in the Bering Sea. Geophys. Res. Lett. 35, L24601.

Behrenfeld, M.J., Falkowski, P.G., 1997. Photosynthetic rates derived from satellite-based chlorophyll concentration. Limnol. Oceanogr. 42, 1–20.

Benoit-Bird, K.J., Moline, M.A., Waluk, C.M., Robbins, I.C., 2010. Integrated measurements of acoustical and optical thin layers I: Vertical scales of association. Cont. Shelf Res. 30, 17–28.

Bray, J.R., Curtis, J.T., 1957. An ordination of the upland forest communities of southern Wisconsin. Ecol. Monogr. 27, 325–349.

Brown, Z.W., Arrigo, K.R., 2012. Contrasting trends in sea ice and primary production in the Bering Sea and Arctic Ocean. ICES J. Mar. Sci. 69, 1180–1193.

Brown, Z.W., van Dijken, G.L., Arrigo, K.R., 2011. A reassessment of primary production and environmental change in the Bering Sea. J. Geophys. Res. – Oceans, 116.

Clarke, K.R., 1993. Non-parametric multivariate analyses of changes in community structure. Aust. J. Ecol. 18, 117–143.

Clarke, K.R., Gorley, R.N., 2006. PRIMER v6: User Manual/Tutorial. PRIMER-E, Plymouth.

Clarke, K.R., Warwick, R.M., 2001. Change in Marine Communities: An Approach to Statistical Analysis and Interpretation, 2nd edition UK:PRIMER-E, Plymouth.

Cooper, L.W., Janout, M.A., Frey, K.E., Pirtle-Levy, R., Guarinello, M.L., Grebmeier, J. M., Lovvorn, J.R., 2012. The relationship between sea ice break-up, water mass variation, chlorophyll biomass, and sedimentation in the northern Bering Sea. Deep Sea Res. II: Top. Stud. Oceanogr. 65–70, 141–162.

Downing, A.L., Leibold, M.A., 2002. Ecosystem consequences of species richness and composition in pond food webs. Nature 416, 837–841.

Fiechter, J., Moore, A.M., Edwards, C.A., Bruland, K.W., Di Lorenzo, E., Lewis, C.V.W., Powell, T.M., Curchitser, E.N., Hedstrom, K., 2009. Modeling iron limitation of primary production in the coastal Gulf of Alaska. Deep Sea Res. II: Top. Stud. Oceanogr. 56, 2503–2519.

Fujiki, T., Matsumoto, K., Honda, M.C., Kawakami, H., Watanabe, S., 2009. Phytoplankton composition in the subarctic North Pacific during autumn 2005. J. Plankton Res. 31, 179–191.

Fujiwara, A., Hirawake, T., Suzuki, K., Saitoh, S.I., 2011. Remote sensing of size structure of phytoplankton communities using optical properties of the Chukchi and Bering Sea shelf region. Biogeosciences 8, 3567–3580.

Goes, J.I., Gomes, H.D.R., Haugen, E., Mckee, K., D'sa, E., Chekalyuk, A.M., Stoecker, D., Stabeno, P., Saitoh, S., Sambrotto, R., 2014. Bering Sea phytoplankton community structure and photosynthetic competency in the presence of a Cold Pool during summer. Deep Sea Res. II: Topical Studies in Oceanography 109, 84–99, http://dx.doi.org/10.1016/j.dsr2.2013.12.004.

Gordon, L.I., Joe C. Jennings, J., Ross, A.A., Krest., J.M., 1993. A suggested protocol for continuous flow automated analysis of seawater nutrients (phosphate, nitrate, nitrite and silicic acid). In: The WOCE Hydrographic Program and the Joint Global Ocean Fluxes Study.

Greer, A.T., Cowen, R.K., Guigand, C.M., Mcmanus, M.A., Sevadjian, J.C., Timmerman, A.H.V., 2013. Relationships between phytoplankton thin layers and the fine-scale vertical distributions of two trophic levels of zooplankton. J. Plankton Res. 35, 939–956.

Hansen, F.C., Reckermann, M., Klein Breteler, W.C.M., Riegman, R., 1993. *Phaeocystis* blooming enhanced by copepod predation on protozoa: evidence from incubation experiments. Mar. Ecol. Prog. Ser., 102

Hare, C., Leblanc, K., DiTullio, G., Kudela, R., Zhang, Y., Lee, P., Riseman, S., Hutchins, D., 2007. Consequences of increased temperature and CO_2 for phytoplankton community structure in the Bering Sea. Mar. Ecol. Prog. Ser. 352, 9–16.

Hubble, D.S., Harper, D.M., 2002. Phytoplankton community structure and succession in the water column of Lake Naivasha, Kenya: a shallow tropical lake. Hydrobiologia 488, 89–98.

Hunt, G.L., Coyle, K.O., Eisner, L.B., Farley, E.V., Heintz, R.A., Mueter, F., Napp, J.M., Overland, J.E., Ressler, P.H., Salo, S., Stabeno, P.J., 2011. Climate impacts on eastern Bering Sea food webs: a synthesis of new data and an assessment of the oscillating control hypothesis. ICES J. Mar. Sci. 68, 1230–1243.

Hunt Jr, G.L., Allen, B.M., Angliss, R.P., Baker, T., Bond, N., Buck, G., Byrd, G.V., Coyle, K.O., Devol, A., Eggers, D.M., Eisner, L., Feely, R., Fitzgerald, S., Fritz, L.W., Gritsay, E.V., Ladd, C., Lewis, W.M.J., Mordy, C.W., Mueter, F., Napp, J., Sherr, E., Shull, D., Stabeno, P., Stepanenko, M.A., Strom, S., Whitledge, T.E., 2010. Status and trends of the Bering Sea region, 2003–2008. In: McKinnell, S.M., Dagg, M.J. (Eds.), Marine Ecosystems of the North Pacific Ocean, 2003–2008, 4. PICES Special Publication, pp. 196–267.

Hunt, G.L., Stabeno, P., Walters, G., Sinclair, E., Brodeur, R.D., Napp, J.M., Bond, N.A., 2002. Climate change and control of the southeastern Bering Sea pelagic ecosystem. Deep Sea Res. II: Top. Stud. Oceanogr. 49, 5821–5853.

Hunt, G.L., Stabeno, P.J., Strom, S., Napp, J.M., 2008. Patterns of spatial and temporal variation in the marine ecosystem of the southeastern Bering Sea, with special

reference to the Pribilof Domain. Deep Sea Res. II: Top. Stud. Oceanogr. 55, 1919–1944.
Jin, M.B., Deal, C., Wang, J., McRoy, C.P., 2009. Response of lower trophic level production to long-term climate change in the southeastern Bering Sea. J. Geophys. Res. – Oceans, 114.
Ladd, C., Stabeno, P.J., 2012. Stratification on the Eastern Bering Sea shelf revisited. Deep Sea Res. II: Top. Stud. Oceanogr. 65–70, 72–83.
Lomas, M.W., Glibert, P.M., 1999. Temperature regulation of nitrate uptake: a novel hypothesis about nitrate uptake and reduction in cool-water diatoms. Limnol. Oceanogr. 44, 556–572.
Lomas, M.W., Moran, S.B., Casey, J.R., Bell, D.W., Tiahlo, M., Whitefield, J., Kelly, R.P., Mathis, J.T., Cokelet, E.D., 2012. Spatial and seasonal variability of primary production on the Eastern Bering Sea shelf. Deep Sea Res. II: Top. Stud. Oceanogr. 65–70, 126–140.
Longhurst, A.R., 1998. Ecological Geography of the Sea. Academic Press, San Diego, CA.
Mordy, C.W., Stabeno, P.J., Ladd, C., Zeeman, S., Wisegarver, D.P., Salo, S.A., Hunt, G. L., 2005. Nutrients and primary production along the eastern Aleutian Island Archipelago. Fish. Oceanogr. 14, 55–76.
Mueter, F.J., Broms, C., Drinkwater, K.F., Friedland, K.D., Hare, J.A., Hunt, G.L., Melle, W., Taylor, M., 2009. Ecosystem responses to recent oceanographic variability in high-latitude Northern Hemisphere ecosystems. Prog. Oceanogr. 81, 93–110.
Narwani, A., Mazumder, A., 2012. Bottom-up effects of species diversity on the functioning and stability of food webs. J. Anim. Ecol. 81, 701–713.
Nejstgaard, J.C., Tang, K.W., Steinke, M., Dutz, J., Koski, M., Antajan, E., Long, J.D., 2007. Zooplankton grazing on *Phaeocystis*: a quantitative review and future challenges. Biogeochemistry 83, 147–172.
Noiri, Y., Kudo, I., Kiyosawa, H., Nishioka, J., Tsuda, A., 2005. Influence of iron and temperature on growth, nutrient utilization ratios and phytoplankton species composition in the western subarctic Pacific Ocean during the SEEDS experiment. Prog. Oceanogr. 64, 149–166.
Overland, J.E., Wang, M., Wood, K.R., Percival, D.B., Bond, N.A., 2012. Recent Bering Sea warm and cold events in a 95-year context. Deep Sea Res. II: Top. Stud. Oceanogr. 65–70, 6–13.
Parsons, T.R., Maita, Y., Lalli, C.M., 1984. A Manual of Chemical and Biological Methods for Seawater Analysis. Pergamon Press, Inc., New York.
Saitoh, S.-i., Iida, T., Sasaoka, K., 2002. A description of temporal and spatial variability in the Bering Sea spring phytoplankton blooms (1997–1999) using satelite multi-sensor remote sensing. Prog. Oceanogr. 55, 131–146.
Schandelmeier, L., Alexander, V., 1981. An analysis of the influence of ice on spring phytoplankton population structure in the southeast Bering Sea. Limnol. Oceanogr. 26, 935–943.
Schnetzer, A., Moorthi, S.D., Countway, P.D., Gast, R.J., Gilg, I.C., Caron, D.A., 2011. Depth matters: Microbial eukaryote diversity and community structure in the eastern North Pacific revealed through environmental gene libraries. Deep Sea Res. I 58, 16–26.
Shannon, C.E., 1948. A mathematical theory of communication. Bell Syst. Tech. J. 27 (379–423), 623–656.
Sigler, M.F., Stabeno, P.J., Eisner, L.B., Napp, J.M., Mueter, F.J., 2014. Spring and fall phytoplankton blooms in a productive subarctic ecosystem, the eastern Bering Sea, during 1995–2011. Deep Sea Res. II 109, 71–83, http://dx.doi.org/10.1016/j.dsr2.2013.12.007.
Springer, A.M., McRoy, C.P., Flint, M.V., 1996. The Bering Sea Green Belt: shelf-edge processes and ecosystem production. Fish. Oceanogr. 5, 205–223.
Stabeno, P.J., Bond, N.A., Kachel, N.B., Salo, S.A., Schumacher, J.D., 2001. On the temporal variability of the physical environment over the south-eastern Bering Sea. Fisheries Oceanogr 10, 81–98.
Stabeno, P.J., Bond, N.A., Hermann, A.J., Kachel, N.B., Mordy, C.W., Overland, J.E., 2004. Meteorology and oceanography of the Northern Gulf of Alaska. Cont. Shelf Res. 24, 859–897.
Stabeno, P.J., Farley Jr, E.V., Kachel, N.B., Moore, S., Mordy, C.W., Napp, J.M., Overland, J.E., Pinchuk, A.I., Sigler, M.F., 2012a. A comparison of the physics of the northern and southern shelves of the eastern Bering Sea and some implications for the ecosystem. Deep Sea Res. II: Top. Stud. Oceanogr. 65–70, 14–30.
Stabeno, P.J., Kachel, N.B., Moore, S.E., Napp, J.M., Sigler, M., Yamaguchi, A., Zerbini, A.N., 2012b. Comparison of warm and cold years on the southeastern Bering Sea shelf and some implications for the ecosystem. Deep Sea Res. II: Top. Stud. Oceanogr. 65–70, 31–45.
Stabeno, P.J., Reed, R.K., Napp, J.M., 2002. Transport through Unimak Pass, Alaska. Deep Sea Res. II: Top. Stud. Oceanogr. 49, 5919–5930.
Stabeno, P.J., Schumacher, J.D., Ohtani, K., 1999. The physical oceanography of the Bering Sea: a summary of physical, chemical, and biological characteristics, and a synopsis of research on the Bering Sea. In: Loughlin, T.R., Ohtani, K. (Eds.), Dynamics of the Bering Sea: A Summary of Physical, Chemical, and Biological Characteristics, and a Synopsis of Research on the Bering Sea. Alaska Sea Grant College Program, Fairbanks, pp. 1–28
Stroeve, J., Holland, M.M., Meier, W., Scambos, T., Serreze, M., 2007. Arctic sea ice decline: faster than forecast. Geophys. Res. Lett. 34, L09501.
Strom, S.L., Fredrickson, K.A., 2008. Intense stratification leads to phytoplankton nutrient limitation and reduced microzooplankton grazing in the southeastern Bering Sea. Deep Sea Res. II: Top. Stud. Oceanogr. 55, 1761–1774.
Sturrock, K., Rocha, J., 2000. A multidimensional scaling stress evaluation table. Field Methods 12, 49–60.
Tungaraza, C., Rousseau, V., Brion, N., Lancelot, C., Gichuki, J., Baeyens, W., Goeyens, L., 2003. Contrasting nitrogen uptake by diatom and *Phaeocystis*-dominated phytoplankton assemblages in the North Sea. J. Exp. Mar. Biol. Ecol. 292, 19–41.
Turner, J.T., Ianora, A., Esposito, F., Carotenuto, Y., Miralto, A., 2002. Zooplankton feeding ecology: does a diet of *Phaeocystis* support good copepod grazing, survival, egg production and egg hatching success? J. Plankton Res. 24, 1185–1195.
Wang, M., Overland, J.E., Stabeno, P., 2012. Future climate of the Bering and Chukchi Seas projected by global climate models. Deep Sea Res. II: Top. Stud. Oceanogr. 65–70, 46–57.

Deep-Sea Research II 109 (2014) 71–83

Contents lists available at ScienceDirect

Deep-Sea Research II

journal homepage: www.elsevier.com/locate/dsr2

Spring and fall phytoplankton blooms in a productive subarctic ecosystem, the eastern Bering Sea, during 1995–2011

Michael F. Sigler [a,*], Phyllis J. Stabeno [b,1], Lisa B. Eisner [c,2], Jeffrey M. Napp [c,3], Franz J. Mueter [d,4]

[a] Alaska Fisheries Science Center, National Marine Fisheries Service, National Oceanic and Atmospheric Administration, 17109 Pt. Lena Loop Rd., Juneau, AK 99801, USA
[b] Pacific Marine Environmental Laboratory, Oceans and Atmospheric Research, National Oceanic and Atmospheric Administration, 7600 Sand Point Way NE, Seattle, WA 98115-0070, USA
[c] Alaska Fisheries Science Center, National Marine Fisheries Service, National Oceanic and Atmospheric Administration, 7600 Sand Point Way NE, Seattle, WA 98115-0070, USA
[d] University of Alaska Fairbanks, Juneau Center for Fisheries and Oceans, 17309 Pt. Lena Loop Rd., Juneau, AK 99801, USA

ARTICLE INFO

Available online 27 December 2013

Keywords:
Phytoplankton bloom
Spring
Fall
Bering Sea
Climate
Zooplankton

ABSTRACT

The timing and magnitude of phytoplankton blooms in subarctic ecosystems often strongly influence the amount of energy that is transferred through subsequent trophic pathways. In the eastern Bering Sea, spring bloom timing has been linked to ice retreat timing and production of zooplankton and fish. A large part of the eastern Bering Sea shelf (~500 km wide) is ice-covered during winter and spring. Four oceanographic moorings have been deployed along the 70-m depth contour of the eastern Bering Sea shelf with the southern location occupied annually since 1995, the two northern locations since 2004 and the remaining location since 2001. Chlorophyll *a* fluorescence data from the four moorings provide 37 realizations of a spring bloom and 33 realizations of a fall bloom. We found that in the eastern Bering Sea: if ice was present after mid-March, spring bloom timing was related to ice retreat timing ($p < 0.001$, df = 1, 24); if ice was absent or retreated before mid-March, a spring bloom usually occurred in May or early June (average day 148, SE = 3.5, $n = 11$). A fall bloom also commonly occurred, usually in late September (average day 274, SE = 4.2, $n = 33$), and its timing was not significantly related to the timing of storms ($p = 0.88$, df = 1, 27) or fall water column overturn ($p = 0.49$, df = 1, 27). The magnitudes of the spring and fall blooms were correlated ($p = 0.011$, df = 28). The interval between the spring and fall blooms varied between four to six months depending on year and location. We present a hypothesis to explain how the large crustacean zooplankton taxa *Calanus* spp. likely respond to variation in the interval between blooms (spring to fall and fall to spring).

Published by Elsevier Ltd.

1. Introduction

The timing and magnitude of phytoplankton blooms in subarctic ecosystems often strongly influence the amount of energy transferred through subsequent trophic pathways. In the southeastern Bering Sea, spring bloom timing has been linked to production of large crustacean zooplankton and walleye pollock (*Gadus chalcogrammus*) (Hunt et al., 2002, 2011; Coyle et al., 2011); if ice is present after mid-March, an early ice-associated bloom occurs there; otherwise a spring bloom usually occurs in May (Hunt et al., 2002; Stabeno et al., 2001). Although spring bloom timing is well-characterized in the southeastern part of the shelf (Brown and Arrigo, 2011, 2013; Hunt et al., 2002, 2011; Rho and Whitledge, 2007; Stabeno et al., 2001), less is known about the spring bloom elsewhere in the eastern Bering Sea (Brown and Arrigo, 2013), as well as the characteristics of the fall bloom (Rho and Whitledge, 2007).

The eastern Bering Sea is dominated by a broad continental shelf (~500 km wide), a large part of which is ice-covered during winter, with the maximum extent varying >100 km among years. In ice-covered areas, the seasonal cycle of primary production begins with ice algae (primarily large diatoms), which begin to grow in the spring when light level becomes adequate. Ice algae are adapted to lower light levels than pelagic phytoplankton (Kirst and Wiencke, 1995) and grow within the ice and at the ice–water

* Corresponding author. Tel.: +1 907 789 6037; fax: +1 907 789 6094.
E-mail addresses: mike.sigler@noaa.gov (M.F. Sigler), phyllis.stabeno@noaa.gov (P.J. Stabeno), lisa.eisner@noaa.gov (L.B. Eisner), jeff.napp@noaa.gov (J.M. Napp), fmueter@alaska.edu (F.J. Mueter).
[1] Tel.: +1 206 526 6453.
[2] Tel.: +1 206 526 4060.
[3] Tel.: +1 206 526 4148.
[4] Tel.: +1 907 790 5448.

0967-0645/$ - see front matter Published by Elsevier Ltd.
http://dx.doi.org/10.1016/j.dsr2.2013.12.007

interface depending on the amount of overlying snow cover. Ice algae begin to grow in mid-February in the Bering Sea (R. Gradinger, University of Alaska, Fairbanks, pers. comm.) and may provide an early concentrated food source (chlorophyll *a* maximum $\sim 300\ \mu g\ l^{-1}$; Mock and Gradinger, 2000; Niemi et al., 2011) for zooplankton (e.g. O'Brien, 1987; Runge and Ingram, 1991). Sea ice algae that are not grazed can seed the spring phytoplankton bloom or may aggregate and sink out of the upper water column (Tremblay et al., 1989, Riebesell et al., 1991; Haecky et al., 1998; Fortier et al., 2002) with seeding more likely if the release from ice is not followed by a strong mixing event that breaks down stratification (Jin et al., 2007). Sedimentation of ice algae occurs during and immediately after growth of water column phytoplankton starts over the Bering Sea middle shelf (R. Gradinger, University of Alaska, Fairbanks, pers. comm.). Ice algae net growth within the ice typically is terminated during ice melt in late spring or early summer.

Phytoplankton in the Bering Sea exhibit net growth in the spring once the water becomes stratified and the mixed layer is shallower than the critical depth (*sensu* Sverdrup, 1953). Prior to this, phytoplankton are considered to be light-limited, but have adequate nutrients due to the advection of nutrient rich slope water onto the shelf during the previous winter, which is mixed throughout the water column (Niebauer et al., 1995); nutrient recycling on the shelf also is important (Granger et al., 2011). The phytoplankton spring bloom typically ends when the surface nutrient supply is exhausted and phytoplankton growth becomes nutrient limited (typically below 1 μM nitrate). Grazing pressure from mesozooplankton and microzooplankton also increases as the spring progresses, which can reduce the net accumulation of phytoplankton standing stocks.

In the summer, phytoplankton concentration in the surface mixed layer is typically low due to nutrient limitation and continued grazing pressure. Episodic wind events can break down stratification and mix nutrients and viable phytoplankton cells to the surface during this period (Sambrotto et al., 1986; Stabeno et al., 2010; Mordy et al., 2012). During fall, increased frequency and intensity of storms and overall cooling of the water column reduces stratification and deepens the mixed layer so that nutrients are mixed to the surface to fuel fall phytoplankton blooms. The fall bloom ends when phytoplankton become light limited, due to decreased day length and deepening of the mixed layer. Pelagic–benthic coupling (Grebmeier et al., 2006) and luxury nutrient consumption by diatoms near the sediment interface may also be important (Droop, 1973), since the Bering Sea shelf is a shallow shelf system with 1% light levels located 10–20 m below the pycnocline (Mordy et al., 2012). Phytoplankton present in the water column during late fall, when ice begins to form, can be incorporated into the ice with large diatom cells preferentially selected (Gradinger and Ikavalko, 1998; Niemi et al., 2011). Ice algal cells may grow slowly during winter when light levels are very low (Melnikov, 1998) and then begin to grow faster when light increases in spring.

In this paper we focus on the middle domain of the eastern Bering Sea shelf where four oceanographic moorings have been located. The measurements on the moorings include temperature and chlorophyll *a* fluorescence. In summer, the middle domain is strongly stratified into two layers, with a wind-mixed upper layer and a tidally-mixed lower layer. The middle domain typically extends from the 50 m isobath to the 100 m isobath, and is bounded by oceanic fronts or transition zones (Iverson et al., 1979). In winter, the middle domain is usually well mixed and cold, with a large part (> 50%) ice-covered. These four oceanographic moorings provide the longest, daily record of in situ oceanographic measurements in the eastern Bering Sea. This paper is the first examination of the chlorophyll *a* fluorescence data, excepting previous analyses of the spring bloom at the southernmost mooring (Hunt et al., 2002, 2011; Stabeno et al., 2001). In this paper our objectives are to: characterize spring and fall blooms over the eastern Bering Sea middle shelf; relate their timing and strength to physical characteristics including spring ice retreat and fall overturn; and discuss some implications of these results for one of the large crustacean zooplankton taxa characteristic of that domain (*Calanus* spp.).

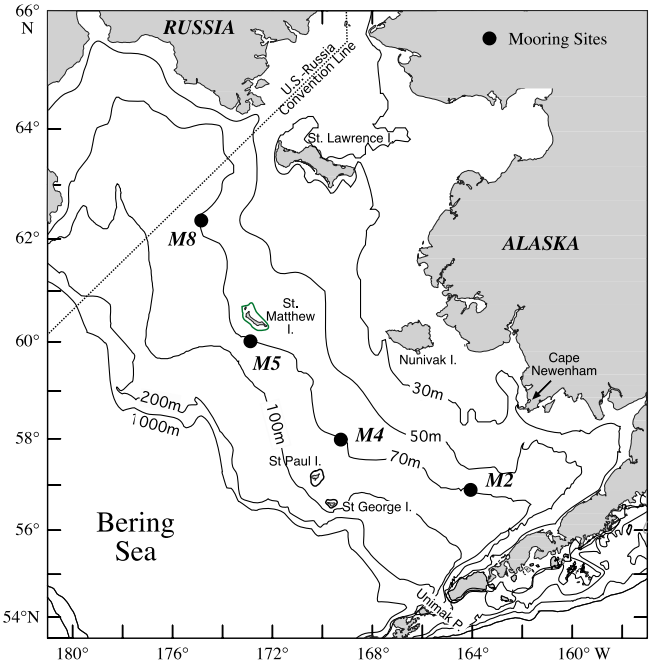

Fig. 1. Study area and mooring locations.

2. Data and methods

2.1. Moorings

Four oceanographic moorings have been deployed along the 70-m depth contour of the eastern Bering Sea shelf with two southern locations sampled almost continually since 1995 (M2) and 1999 (M4), and two northern locations since 2004 (M8) and 2005 (M5) (Fig. 1). Prior to 2005, moorings were recovered and redeployed twice a year, once in the spring (April/May) and again in the late summer or early fall (September/October). Since 2006, there has been extensive ice on the northern shelf in spring and M8 (and sometimes M5) has only been recovered and redeployed once a year in August or September. Data collected by instruments on the moorings included temperature (miniature temperature recorders, SeaBird[5] SBE-37 and SBE-39) and chlorophyll *a* fluorescence (WET Labs DLSB ECO Fluorometer). A transition to fluorometer sensors with wipers that sharply reduced fouling occurred during 2001–2004. Data were collected at least hourly. During autumn, winter, and early spring, the shallowest instrument was at 11 m at M2 and M4, at 15 m at M5 and at 20 m at M8. During late spring to early autumn (the ice-free period), the mooring at M2 included a surface toroid measuring temperature at a depth of 1 m, and the upper instrument at M4 was at 11 m, as was the upper instrument at M5 and M8 if a summer mooring was deployed. For consistency, our analyses focus on data recorded at

[5] Use of trade names does not constitute an endorsement by NOAA.

11 m (or the shallowest instrument at M5 and M8 during autumn, winter and early spring). This standardization is reasonable because for parallel data sets collected at both 1 and 11 m at M2 and M4, the data recorded at 11 m captured 96% of variability recorded at 1 m (Stabeno et al., 2007). At these mooring locations, the water column is well-mixed during winter and develops a 15–35 m wind-mixed layer once stratification develops during spring (Stabeno et al., 2007). Farther north, at M8 and possibly M5, the spring bloom can occupy a narrower depth range and slowly sink, so that identified maximum Chlorophyll *a* fluorescence values and timings are approximate.

Additional chlorophyll data were collected when the moorings were deployed and recovered and were used for quality control of the chlorophyll *a* fluorescence data collected by mooring instruments. Chlorophyll *a* fluorescence measurements were made with a Seabird SBE 911 *plus* system with chlorophyll *a* fluorescence sensors (WET Labs WETStar). Data were recorded during the downcast, with a descent rate of usually 15 m min^{-1} to a depth of 35 m, and 30 m min^{-1} below that. Water samples for extracted chlorophyll *a* were collected during CTD casts, filtered through glass fiber filters (nominal pore size 0.7 μm), and then frozen at −80 °C until analysis. Frozen chlorophyll *a* samples were analyzed with a calibrated benchtop Turner TD-700 fluorometer using standard acidification methods (Parsons et al., 1984).

Conversion of in vivo chlorophyll *a* fluorescence (volts) to chlorophyll *a* concentration (μg l^{-1}) was performed for both the moored and CTD chlorophyll *a* fluorescence sensors using relationships provided by the manufacturer for each instrument during annual service. We did not attempt to create a relation between mooring chlorophyll *a* fluorescence and extracted chlorophyll *a* from water samples due to the limited number of water samples at deployment and recovery of the moorings and the difficulty of matching the timing and location of the water samples and mooring measurements. The chlorophyll *a* estimates based on the fluorescence sensors were compared to the chlorophyll *a* water samples collected during CTD casts for quality control of the mooring-based measurements; when unusual (>40 μg l^{-1}) values of chlorophyll *a* occurred or isolated spikes occurred, these measurements were suspect and so were excluded from the analysis. Less than 1% of data were excluded based on this criterion. The mooring-based measurements were also reviewed for measurement drift due to fouling and when drift occurred, these measurements were excluded from the analysis. Drift was assessed based on a consistent rise in the recorded fluorescence; this assessment sometimes excluded up to two to three months of data. Typically drift did not occur during winter and was more common during summer, which was mostly eliminated for instruments with wipers.

2.2. Sea ice

Two sources of sea-ice data were used. The first source was the National Ice Center (NIC), with data available from 1972 to 2005; the second source was the Advanced Microwave Scanning Radiometer EOS (AMSR), with data available from 2002 to 2012 (Spreen et al., 2008). These two data sets provide data over the entire period (1972–2012) for which high-quality data on sea-ice extent and areal concentration are available. We downloaded data available from the NIC website (⟨http://www.natice.noaa.gov⟩) for our study period (1995–2005) which were interpolated to a 0.25 degree grid. NIC data are derived from a variety of sources including the Advanced Very High Resolution Radiometer (AVHRR) aboard the Polar Orbiting Environmental Satellites (POES). AMSR data consist of daily ice concentration at 12.5 km resolution, which are available from the National Snow and Ice Data Center (NSIDC; ⟨http://nsidc.org⟩). To examine how the ice cover varies along the 70-m isobath, a 100 km by 100 km box was defined around each of our biophysical moorings (M2, M4, M5, and M8) maintained by NOAA. AMSR and NIC data overlap during the four-year period 2002-2005, during which time they have very similar values (M2, Stabeno et al., 2012b). To span the period 1972–2012, we used both NIC and AMSR data, using the average value in the overlap years to derive the annual cycle of percent ice cover for each mooring location.

2.3. Wind

Winds were estimated using daily data from the National Centers for Environmental Prediction (NCEP)/National Center for Atmospheric Research (NCAR) Reanalysis (Kalnay et al., 1996). We follow the procedure used in Bond and Adams (2002) to specify particular elements of the atmospheric forcing on a daily basis for selected periods and interpolated wind velocity to the locations of four moorings (Fig. 1). The daily winds from the reanalysis are reliable in this region based on a comparison to independent buoy measurements from 1995 to 2000 (Ladd and Bond, 2002).

2.4. Data analysis

Ice cover for each mooring and year was examined to determine if ice was present at any time that winter or spring and if present, when the ice retreated for the last time. Ice retreat was considered to have occurred when ice cover fell below 15% for the last time during that spring. The temperature records for each mooring and year were examined to determine: (1) when the ocean began warming following ice retreat; and (2) when fall overturn occurred. When ice was present the temperature was approximately −1.7 °C. Warming was considered to have started when the near surface temperature rose above −1 °C for the last time that spring. Fall overturn was considered to have occurred once temperature (at 11 m) fell 2 °C below the summer maximum.

We also considered basing timing of the fall overturn on timing of mixed layer depth deepening. Unfortunately, the mooring data at M5 and M8 were inadequate to do this. We tested whether timing of mixed layer depth deepening and fall temperature drop were related, which would support using fall temperature drop as a measure of stratification breakdown and the resultant nutrient replenishment that could support a fall bloom. We found that they are related (Fig. 2) (Pearson′s product-moment correlation = 0.61, df = 20, $p = 0.002$). The relationship was highly significant for M4 (Pearson′s product-moment correlation = 0.95, df = 6, $p < 0.001$) and not significant for M2 (Pearson′s product-moment correlation = 0.50, df = 12, $p = 0.07$), but the latter relationship was strongly influenced by one data point. In 1997, the mixed layer depth deepened about 40 days after the temperature dropped, which is later than usual and may have occurred because winds were weak that late summer and early fall. If this data point is excluded, the relationship for M2 is much better (Pearson′s product-moment correlation = 0.76, df = 11, $p = 0.003$).

The average wind speed records by calendar day and location were examined to determine when the first stormy period occurred after day 210 (ca. July 27). The wind data were divided into 10-day periods; if daily average wind was greater than 11 m s^{-1} for half or more of the ten-day period, then this period was defined as stormy (Sullivan et al., 2014).

Chlorophyll *a* values for each mooring and year were examined to determine the time and magnitude of the maximum value in spring and fall. These records were plotted and the times and magnitudes of the spring and fall blooms were assigned (Appendix Fig. 1). Each year, the spring bloom was assigned to the maximum value before day 180 (ca. June 27) and the fall bloom was assigned to the maximum value after day 210 (ca. July 27). In some years the data record was discontinuous and the maximum value could not

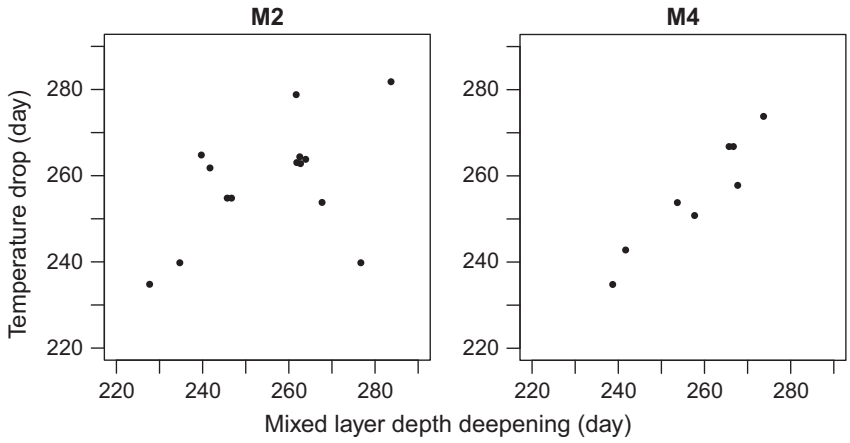

Fig. 2. The relationship of mixed layer depth deepening (day) and temperature drop (day) for moorings M2 and M4. The mooring data at M5 and M8 were inadequate to compute mixed layer deepening.

be determined (e.g., spring bloom at M2 in 1996 and the fall bloom at M4 in 1996). The values are tabled in Appendix Table 1.

2.5. Comparison to shelf-wide patterns for chlorophyll *a*

Satellite ocean color data were examined to understand the spatial pattern of chlorophyll *a* over the middle shelf. In particular, we wanted to find out whether it was reasonable to assume chlorophyll *a* values derived from the mooring fluorescence data were representative of chlorophyll *a* values over a much larger area. To do so, we retrieved eight-day composite Level-3 SeaWiFS and MODIS-Aqua chlorophyll *a* data at 9-km spatial resolution using the Giovanni online data system, developed and maintained by the NASA Goddard Earth Sciences Data and Information Services Center (Acker and Leptoukh, 2007). Data for a rectangular region (54–66°N and 157–180°W) that encompasses the eastern Bering Sea shelf were extracted from the global coverage datasets (units: mg m^{-3}). Open ocean values (offshore of the 500 m isobaths) and nearshore values (inshore of 10 m isobaths) were excluded. We compared eight full years of overlap between the two data sets (2003–2010) based on correlations and absolute differences (bias) of the logarithmically transformed data on a pixel-by-pixel basis. Estimates from the two satellites were strongly correlated ($r=0.65$) and bias was found to be negligible (median bias <0.01, 88% of 1.4 million paired observations had absolute bias <0.05). The SeaWiFS data from 1998–2002 were combined with the MODIS-Aqua data from 2003–2011 to produce the longest possible continuous time series of remotely-sensed chlorophyll *a* data. Finally, we correlated eight-day composites of the mooring chlorophyll *a* data with 8-day remotely-sensed chlorophyll *a* data for all non-missing pairs on a pixel-by-pixel basis to produce correlation maps for each of the four moorings.

2.6. Zooplankton metabolism

We examined some implications of these results for a large crustacean zooplankton taxa characteristic of that domain (*Calanus* spp.).The effect of temperature on the respiration of late stage *Calanus* spp. was approximated from literature values. To estimate respiration rates, we used a Q_{10} of 2.77 and nitrogen-specific respiration of *Calanus finmarchicus* (130 μmol O_2 gN^{-1} h^{-1}; Saumweber and Durbin, 2006), average bottom temperatures in cold and warm years (−1.8 and 2 °C, respectively; Stabeno et al., 2012a), wet weight measurements on preserved *Calanus* spp. C5 obtained from the eastern Bering Sea during August and September (1.82×10^{-3} g), and literature values for the relationship of dry to wet weight (15%) and nitrogen to dry weight (8%) for copepods.

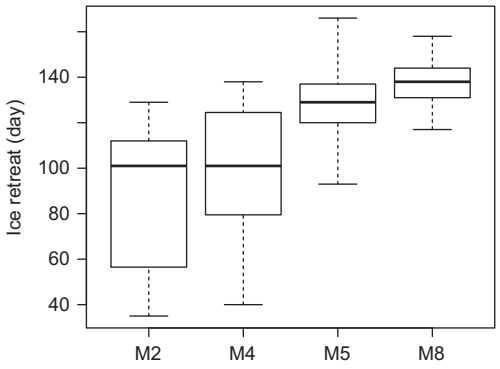

Fig. 3. A boxplot of ice retreat (day) by mooring. The box extends from the first quartile to the third quartile, the heavy line dividing the box is the median and the whiskers are the smallest and largest values. The number of years with ice present were 12 (M2), 15 (M4), 17 (M5) and 17 (M8).

3. Results

3.1. Spring

Ice was present for about two out of three years at M2 (12 of 17), nearly all years at M4 (15 of 17), and all years at M5 and M8 (17 of 17). When ice was present, retreat was significantly (ANOVA, $p<0.001$, df=3, 57) earlier in the south (mean M2: Day 88; M4: 99; M5: 130; M8: 138) (Fig. 3). In some years when ice was present, retreat occurred before mid-March (M2 during 1998, 2000, 2002, 2006 and M4 during 2000 and 2002) (Appendix Table 1). Ice was absent at M2 during 1996, 2001 and 2003–2005 and at M4 during 2001 and 2005. Ice presence reduced ocean temperature below −1 °C in all cases, but one (ice was present at M2 in 2002, but for only 11 days, and minimum temperature was −0.1 °C).

The timing of warming (near-surface temperature > −1 °C) was strongly correlated with the timing of ice retreat (Pearson's $r=0.96$, df=40, $p<0.001$). The interval between ice retreat and warming was longer in the north (M2 warming averaged Day 100; M4: 110; M5: 153; M8: 181, corresponding to intervals for M2 of 12 days; M4: 11; M5: 23; M8: 43).

The spring bloom usually reached only one peak (34 of 37 cases) (Appendix Fig. 1), so that the maximum value and when the maximum value occurred are reasonable measures of the magnitude and timing of the spring bloom. Double rather than single spring peaks occurred at M2 in 2003 and 2011 and at M4 in 1997. The maximum was distinct from the other values at M4 in 1997; the jump was too high for accumulation of biomass due to either

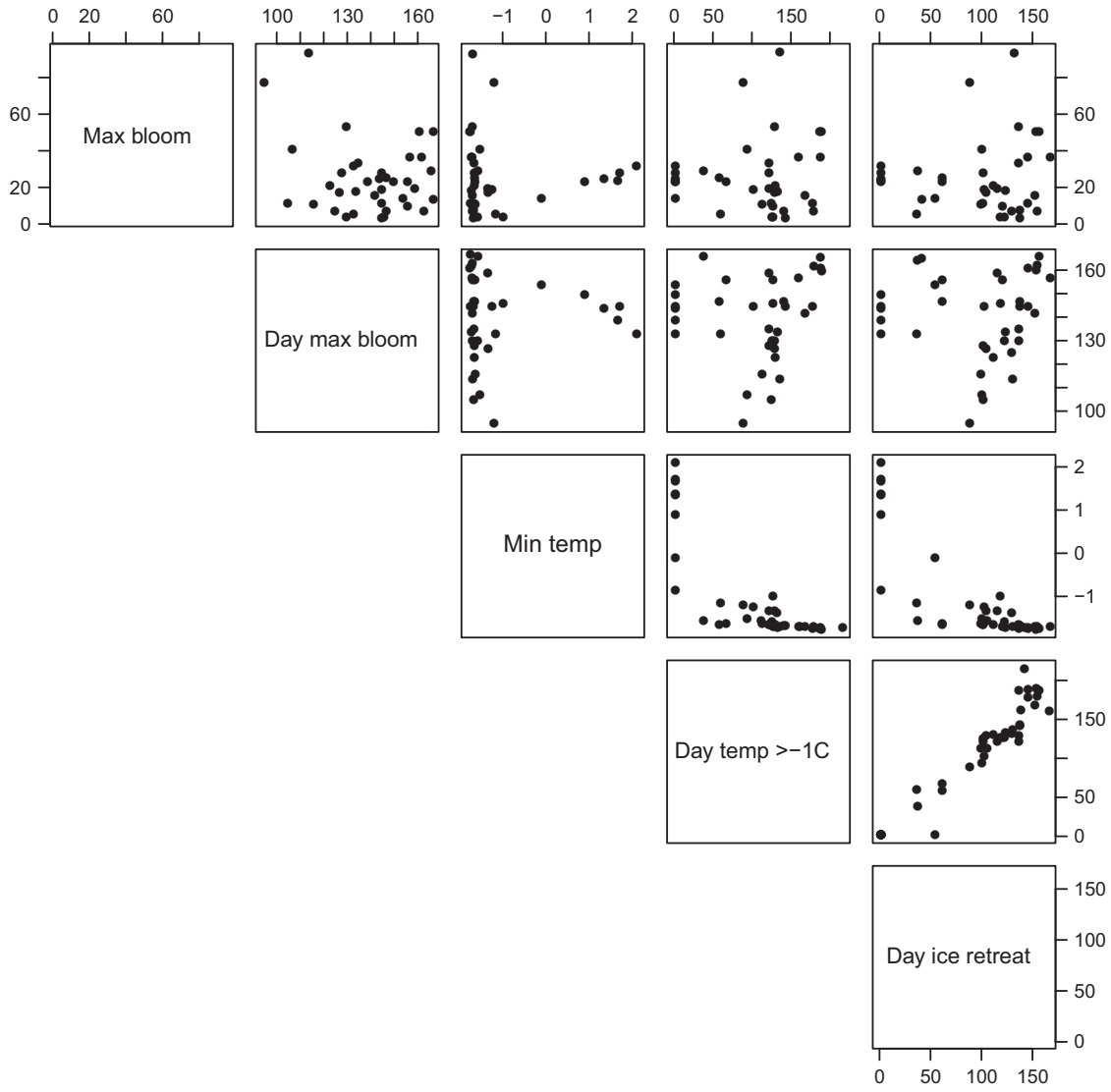

Fig. 4. Scatterplots of maximum spring bloom magnitude (μg Chl l^{-1}), spring bloom timing (day), minimum winter–spring temperature (day), day temperature rose above −1 °C and day ice cover fell below 15%. If ice was absent that year, then the ice retreat day is zero.

continued growth or reduced grazing and instead may be due to advection of a different water mass.

During years when ice was absent (or was present, but retreated before mid-March), the spring bloom maximum occurred in late May to early June (average day 148, SE=3.5, n=11) (Fig. 4, panel row 2, column 5). This pattern occurred for M2 and M4 but not M5 or M8 where ice always was present after mid-March (Fig. 5). There was no statistically significant difference in timing of the spring bloom maximum in years when ice was absent (average day 141) and when ice was present, but retreated before mid-March (average day 153) (two-way t-test, df=9, p=0.10). During years when ice was absent or retreated before mid-March, spring bloom maximum averaged 19 μg Chl l^{-1} (log-transformed, SE=1.2, n=11) (Fig. 4, panel row 1, column 5). There was no statistically significant difference in spring bloom maximum in years when ice was absent (average 25 μg Chl l^{-1}) and when ice retreated before mid-March (average 15 μg Chl l^{-1}) (log-transformed, two-way t-test, df=9, p=0.14).

In contrast to the late May to early June timing of the spring bloom in years when ice was absent or retreated early, if ice was present after mid-March (day 75), an ice-associated bloom occurred between early April and mid-June and the bloom timing was related to ice retreat timing (Fig. 4, panel row 2, column 5), regardless of mooring (Fig. 5). Later blooms occurred when ice retreat was later (linear regression, y-intercept=53, slope=0.66, df=1, 24, $p<0.001$) (Fig. 6). This relationship implies that bloom day is 119 when ice retreat occurs on day 100, 152 when ice retreat occurs on day 150, and 172 when ice retreat occurs on day 180. There was no statistically significant difference in spring bloom magnitude whether ice was absent or present, but retreated before mid-March (average 19 μg Chl l^{-1}) or ice was present after mid-March (average 17 μg Chl l^{-1}) (log-transformed, two-way t-test, df=35, p=0.70); the overall average spring bloom magnitude was 17 μg Chl l^{-1} (log-transformed, SE=1.2, n=37).

3.2. Fall

Fall overturn timing was similar among moorings on average (M2 mean was Day 259; M4: 261; M5: 259; M8: 268 (ANOVA, df=3, 34, p=0.49)), but was more variable at M2 and M4 (Fig. 7). Sometimes an early major storm prompted early fall overturn; on five occasions when overturn was earlier than usual (approximately day 240 versus a range of 250–280), the day of the first

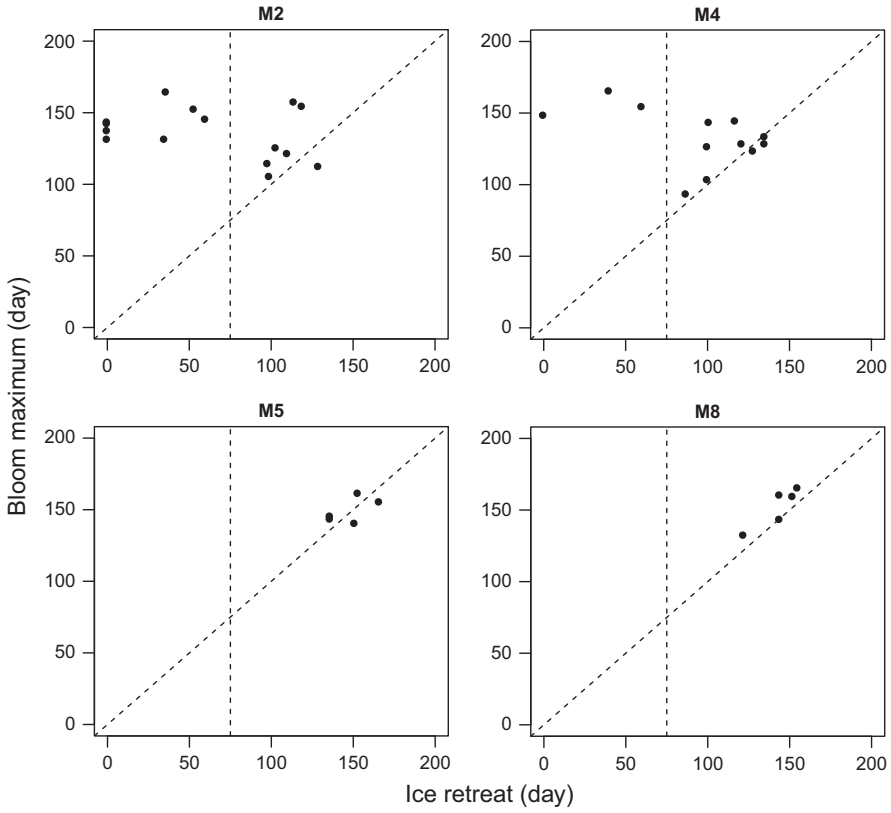

Fig. 5. Scatterplots of spring bloom maximum (day) versus ice retreat (day) by mooring. If ice was absent that year, then the ice retreat date is zero. The diagonal dashed line is the 1:1 line to compare timings of spring bloom and ice retreat. The vertical dashed line is March 15.

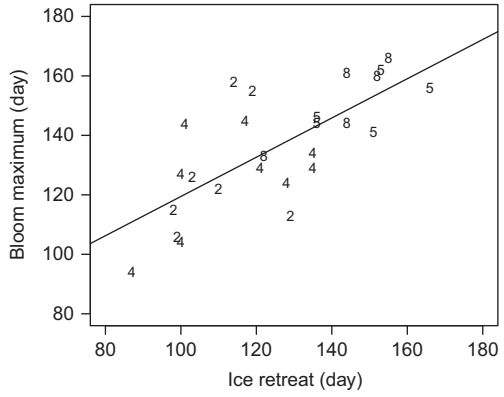

Fig. 6. Scatterplot of the observed (number) and fitted (line, based on simple linear regression, y-intercept = 53, slope = 0.66, df = 1, 24, $p < 0.001$) values of spring bloom maximum (day) versus ice retreat (day) for all moorings when ice was present after March 15. The number indicates mooring number.

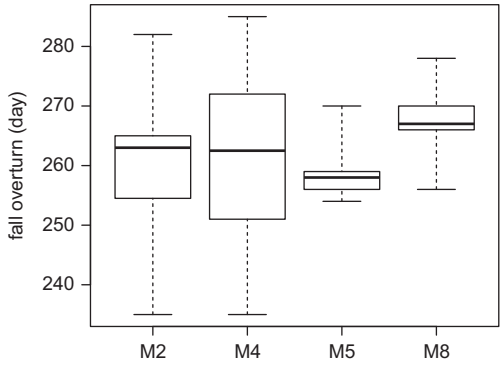

Fig. 7. A boxplot of fall overturn (day) by mooring. The box extends from the first quartile to the third quartile, the heavy line dividing the box is the median and the whiskers are the smallest and largest values. The numbers of years when fall overturn could be determined were 15 (M2), 10 (M4), 16 (M5) and 7 (M8).

major storm was earlier than usual (about day 240 versus a range of 240–320) (Fig. 8, panel row 4, column 5).

The fall bloom usually reached only one peak (30 of 33 cases) (Appendix Fig. 1), so that the maximum value and when the maximum value occurred are reasonable measures of the magnitude and timing of the fall bloom. Double rather than single fall blooms occurred at M2 once (1998) and M4 twice (2004, 2007). In six cases (1996 M4, 2002 M2, 2005 M4, 2007 M2, 2009 M5, 2010 M8), only the descending limb of the fall fluorescence data is available due to instrument failure, hence the fall bloom peak is uncertain and no values for magnitude or timing were assigned.

There was no significant relationship between fall overturn timing and fall bloom timing (linear regression, df = 1, 27, $p = 0.88$) (Fig. 8, panel row 2, column 4) or fall bloom magnitude (linear regression, log-transform, df = 1, 27, $p = 0.49$) (Fig. 8, panel row 1, column 4).

Fall bloom timing was similar among moorings (M2 mean: Day 276; M4: 277; M5: 258; M8: 281) (ANOVA, $p = 0.32$, df = 3, 29) (Fig. 9). Fall bloom magnitude also was similar among moorings (ANOVA, log-transform, $p = 0.93$, df = 3, 30) (Fig. 9). On average, the fall bloom occurred on day 274 (late September) (SE = 4.2, $n = 33$) with an average chlorophyll value of 8 μg Chl l^{-1} (SE = 1.2, $n = 34$).

The magnitudes of the spring and fall blooms were correlated (Pearson's $r = 0.46$, df = 28, $p = 0.011$, log-transformed values) (Fig. 10).

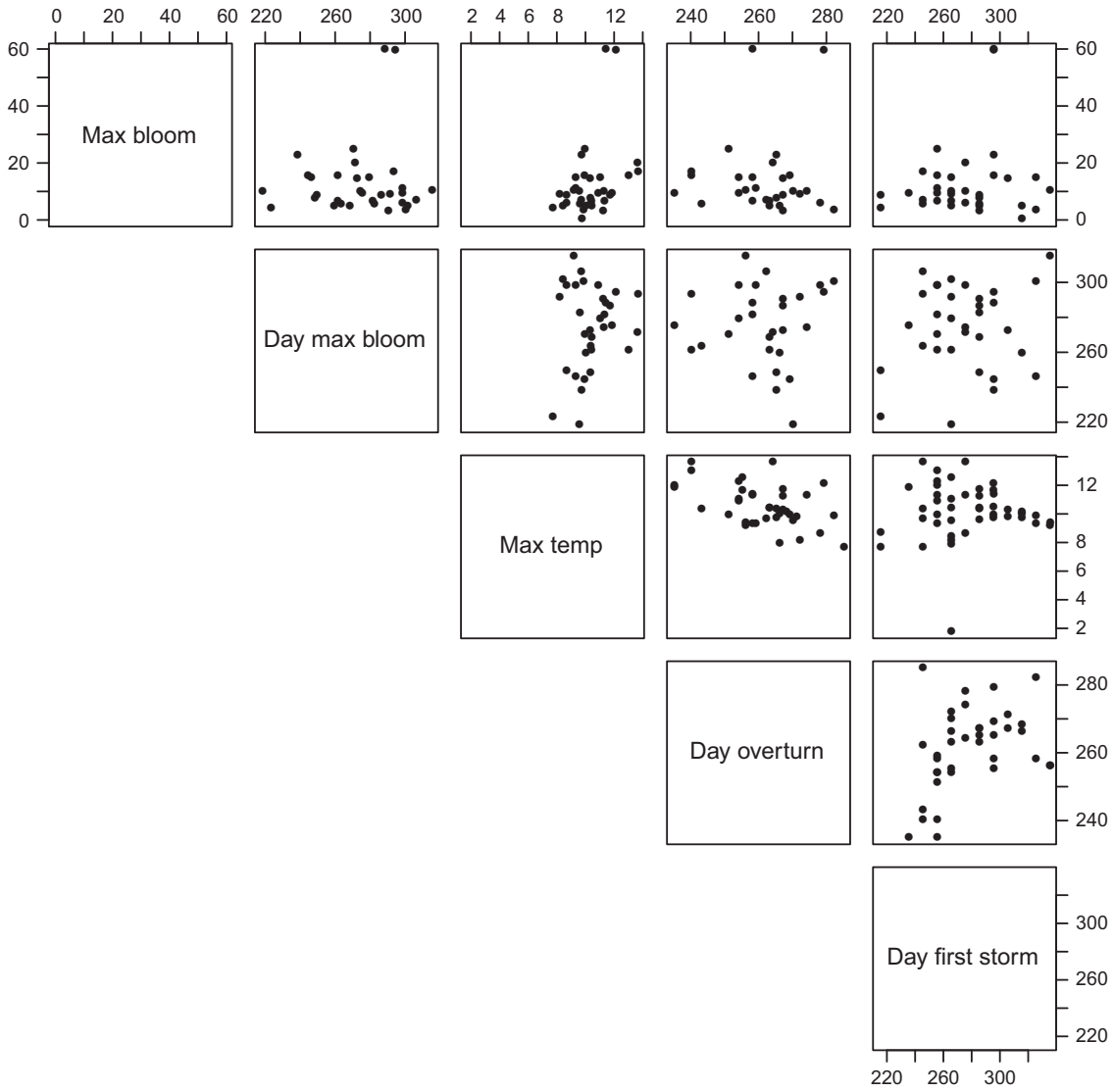

Fig. 8. Scatterplots of maximum fall bloom magnitude (μg Chl l^{-1}), fall bloom timing (day), maximum summer–fall temperature (°C), fall overturn (day) and first storm (day).

The interval of time between the spring and fall blooms ranged from about 4–6 months, with longer intervals occurring for earlier spring blooms (linear regression, intercept = 294, slope = −1.16, df = 1, 27, $p < 0.001$) (Fig. 11).

3.3. Comparison to shelf-wide patterns

Eight-day composites of chlorophyll *a* values at both M2 and M4 were moderately to strongly correlated with remotely-sensed chlorophyll *a* values over broad regions of the eastern shelf (Appendix Fig. 2), including the middle shelf in the southeast and most of the northern Bering Sea except Norton Sound. In contrast, chlorophyll *a* values at M5 were positively correlated with remotely-sensed values over much of the shelf north of about 60°N, but negatively correlated with remotely-sensed values to the south of M5. Chlorophyll *a* values at M8 were positively correlated with remotely-sensed values over the northwestern part of the shelf and much of the outer shelf and negatively correlated with remotely-sensed values on much of the inner shelf. These negative correlations are likely due to differences in bloom timing.

4. Discussion

4.1. Spring

We found that in the eastern Bering Sea: if ice was present after mid-March, spring bloom timing was related to ice retreat timing; if ice was absent or retreats before mid-March, a spring bloom usually occurred in May or early June. Our findings generally match Brown and Arrigo (2013) based on their satellite-based observations (see exception below), as well as those of Hunt et al. (2002, 2011) and Stabeno et al. (2001). In general, ice-associated phytoplankton blooms are observed near the retreating ice edge on shipboard surveys and in ocean color data, due to melting ice increasing the stability of the water column (Alexander and Niebauer, 1981; Niebauer et al., 1995; Hunt et al., 2010; Brown et al., 2011). While the spring bloom usually moves northward as the eastern Bering Sea becomes ice free, sometimes ice melts in the north before disappearing farther south and a spring bloom occurs in the northern ice-free area before it occurs in the south if light levels are sufficient. For example in 2010, the northern Bering Sea melted earlier than in the south leaving an area of persistent ice between M2 and M4. Percent ice cover also influences whether

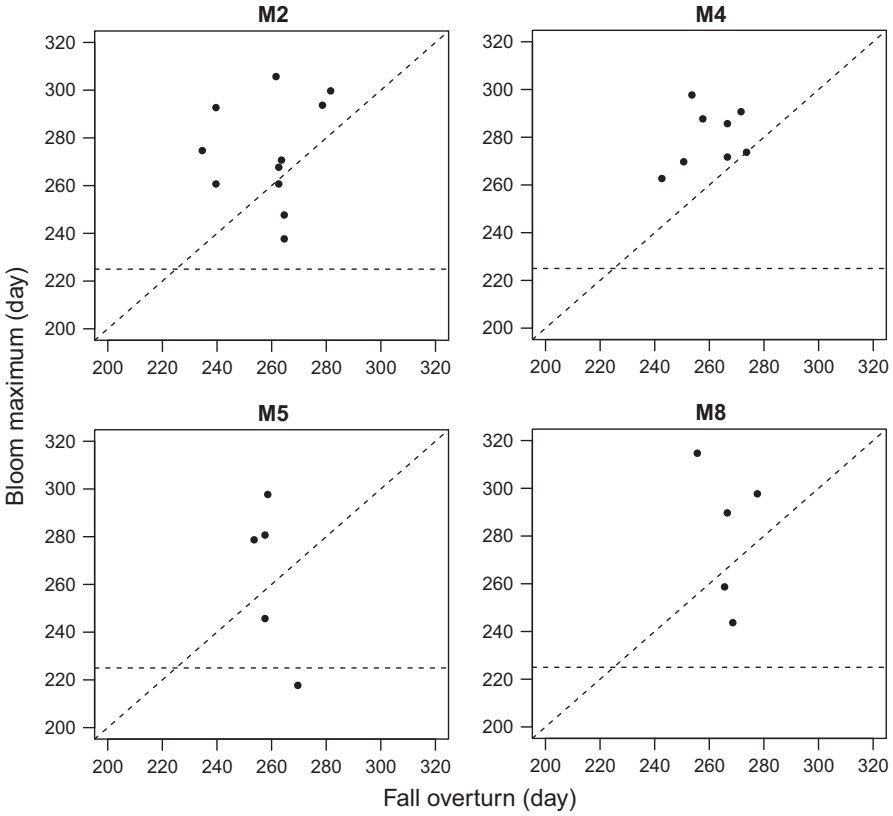

Fig. 9. Scatterplots of fall bloom maximum (day) versus fall overturn (day) by mooring. The diagonal dashed line is the 1:1 line to compare timings of fall bloom maximum and fall overturn. The horizontal dashed line is August 15.

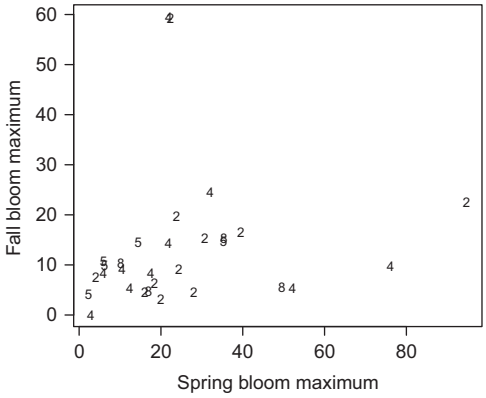

Fig. 10. Scatterplot of maximum spring bloom magnitude ($\mu g\ Chl\ l^{-1}$) and maximum fall bloom magnitude. The number indicates mooring number.

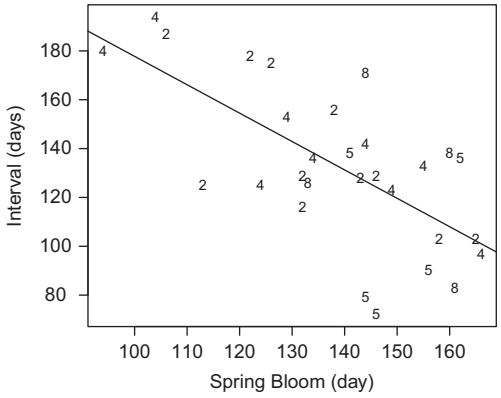

Fig. 11. Scatterplot of observed (number) and fitted (line, based on linear regression, intercept = 294, slope = − 1.16, df = 1, 27, $p < 0.001$) values for all moorings. The *y*-axis is the interval between the spring and fall bloom maximum (days). The *x*-axis is the spring bloom maximum (day). The number indicates mooring number.

or not ice-associated blooms occur by modulating both light and stratification (Sullivan et al., 2014).

The relationship between the timing of the spring bloom and ice retreat when ice retreat occurred after mid-March was statistically significant for the eastern Bering Sea (pooled data from the north and south; Fig. 6), which contradicts Brown and Arrigo (2013), who concluded that ice retreat timing was a good predictor of spring bloom timing for only the northern Bering Sea. The different conclusions for the southeastern Bering Sea likely resulted from how the two data sets were analyzed. Brown and Arrigo (2013) classified their data into four regions corresponding to M2, M4, M5 and M8 (i.e., similar geographic grouping to our approach). In one analysis, Brown and Arrigo (2013) regressed spring bloom timing versus ice retreat timing and found significant relationships for the northern, but not southeastern Bering Sea. In a second analysis, they classified the southeastern Bering Sea data based on whether or not ice retreat occurred before (early) or after (late) the mean ice retreat date for the two regions (M2 and M4) and whether the bloom occurred within (ice-edge bloom) or after (open-water bloom). Open-water blooms were defined as those occurring 20 days or more after ice retreat. They found no significant difference in mean timing between open-water blooms of early retreat (or ice free) years and ice-edge blooms of late retreat years.

Like their first analysis, we regressed spring bloom timing versus ice retreat timing, but instead classified the data into two groups: ice absent or ice retreat before March 15; and ice retreat after March 15 following Hunt et al. (2002, 2011). Mid-March was chosen as the time when sufficient light becomes available for a

phytoplankton bloom in the southeastern Bering Sea (Hunt et al., 2002). We pooled all mooring data for years when ice was present after mid-March (Fig. 6) to test whether ice retreat and the spring bloom move northward as the season progresses. We suspect that if the Brown and Arrigo (2013) data set were similarly analyzed (regress bloom timing versus ice retreat timing when ice retreat occurred after mid-March), our results would match and both data sets would support the conclusions that the spring bloom occurs later when the ice retreats later in both the northern and southeastern Bering Sea and that the bloom generally moves northward as the shelf becomes ice free.

The present work corrects and clarifies the relationship of spring bloom timing and ice retreat timing reported by Hunt et al. (2002) for the southeastern Bering Sea. Their conclusion of late ice retreats with early ice-related blooms oversimplifies the data; while supported by early ice-related blooms for 1995, 1997 and 1999, later ice-related blooms occurred for 1975 and 1976 (Hunt et al., 2002, their Fig. 7). There is some evidence that there were early blooms under the ice in these two years, but the data are not very reliable. With more years of data, Hunt et al. (2011) observed that because ice can remain in the southeastern Bering Sea until May or rarely June, the calendar date of an ice-associated bloom could be later than that of an open-water bloom (i.e., if the ice retreat is late, the spring bloom also is late).

In addition to ice retreat timing, wind patterns can affect spring bloom timing. Short-lived surface pulses of chlorophyll *a* can occur with early ice retreat during a temporary relaxation of winds without significant stratification (Brown and Arrigo, 2013; Stabeno et al., 2010) and precede the larger primary bloom in May or early June. When ice retreat occurs after mid-March in the southeastern Bering Sea, a very early bloom can occur when strong winds advect ice which melts in place during a temporary relaxation of winds (Brown and Arrigo, 2013; Stockwell et al., 2001). This scenario matched the two earliest spring blooms we observed in the southeastern Bering Sea (1997 at M2; 2003 at M4, Appendix Table 1). An open-water bloom subsequent to the ice-related spring bloom also can occur after a strong mixing event. This occurred in 1997, when a strong ice associated bloom in April was followed by a very strong storm in late May that resulted in an open water bloom.

We summarize these findings on spring bloom timing and ice retreat timing (ours; Brown and Arrigo, 2013; Hunt et al., 2002, 2011) as follows. If ice retreats after mid-March, an ice-associated bloom occurs; this pattern applies throughout the eastern Bering Sea. If the ice retreats early (before mid-March), there is no ice-associated bloom because sunlight is insufficient to initiate an ice-associated bloom. To date, early ice retreat occurs only in the southeastern Bering Sea and not in the northern Bering Sea; this pattern of persistent ice in the northern Bering Sea is expected to continue into the foreseeable future (Stabeno et al., 2012a). An open-water bloom occurs if ice retreats before March 15 or ice is absent; this pattern applies only in the southeastern Bering Sea.

We anticipated that spring blooms for late retreat years would be lower in magnitude due to consumption of nutrients by ice algae prior to the spring bloom maximum; ice algae growth and the spring phytoplankton bloom together can create a prolonged period of production or two distinct spring blooms (Niebauer et al., 1995; Stabeno et al., 2001). The timing of the maximum chlorophyll *a* value usually coincided with that of ice retreat, suggesting that these values represent both ice algae and phytoplankton. We found some evidence that ice algae production reduces the subsequent value of maximum chlorophyll *a*. The spring bloom maximum averaged 25 (μg chlorophyll *a* l^{-1}) when ice was absent, 15 when ice retreated before mid-March and 17 when ice retreated after mid-March. Although not significant, these differences imply that the phytoplankton spring bloom magnitude may be higher when ice and ice algae are absent. Further analyses are needed to understand this potential difference; these analyses would consider reductions in loss terms (grazing or sinking), measurements of nutrient draw-down and differences in the physical resupply of nutrients from off the shelf.

Another analysis found a similar effect; modeled net primary production (NPP) for open-water blooms of early retreat years were $>70\%$ more productive than the ice-edge blooms of late retreat years (Brown and Arrigo, 2013). Although not directly comparable to our analysis (NPP is time-integrated production whereas maximum chlorophyll *a* is standing stock at a single time point), their similarity implies that phytoplankton spring blooms may be stronger when ice and ice algae are absent. Further analyses are needed to understand this potential difference in NPP; these analyses would consider the temperature effect on phytoplankton growth rates, which was modeled in the NPP estimates, and under or within ice production during years with late ice retreat, which was not quantified (Brown and Arrigo, 2013).

4.2. Fall

A fall bloom commonly occurred in both the northern and southeastern Bering Sea, on average in late September. Winds at M2, M4, M5, and M8 are significantly correlated (Stabeno et al., 2010), which will tend to synchronize fall blooms, as was observed. However bloom timing was not significantly related to either storm or fall overturn timing. The lack of a significant effect was unexpected; however a timing effect for the fall bloom may be difficult to detect because timing is affected by several interacting factors including wind strength, stratification, fall cooling and light level. For example, fall overturn requires strong winds, but once cooling begins in late September and early October, less wind energy is necessary to overturn the ocean. A fall bloom also depends on sufficient light, introduction of nutrients from below the pycnocline, short periods of stabilization that allow phytoplankton to remain in the sunlit waters and grow, and may be influenced by zooplankton grazing.

The timing of fall overturn at M2 and M4 was much more variable than at M5 and M8 which may be due to north–south differences in stratification. In the south, stratification is almost completely controlled by temperature, while in the north it is equally controlled by temperature and salinity so variations in temperature have more effect on stratification in the south than in the north (Ladd and Stabeno, 2012). This contrast implies that the southeastern Bering Sea is more sensitive to the timing of fall cooling than the northern Bering Sea.

Our mooring data and previous middle-shelf observations (Rho and Whitledge, 2007; Brown et al., 2011) indicated that the magnitudes of fall blooms were weaker than spring blooms on average. It may be that nutrient supply rates are limiting (e.g., storm mixing) and/or the accumulation of chlorophyll *a* is limited by grazing. For instance, if the lower layer has 20 μM of nitrate and the surface mixed layer is 20 m deep and depleted of nitrate, which are typical conditions during summer, then deepening the mixed layer by 5 m will result in only 4 μM of nitrate, compared to 18 μM available for consumption in the top 20 m of water column in spring. In addition, variations in chlorophyll *a* reflect the result of multiple processes including phytoplankton growth, grazing, sinking, and advection. Chlorophyll *a* will not increase until cell growth exceeds losses by grazing and other factors. While grazing impact has been measured for spring (Cooney and Coyle, 1982; Sherr et al., 2013), grazing impact has not been measured for fall, so comparing grazing pressure on spring and fall blooms is not possible. Finally, phytoplankton physiological status and species composition can impact bloom intensity.

Broad-scale sampling of the eastern Bering Sea shelf found that late summer and early fall chlorophyll *a* values were higher during warm years compared to cold years (Eisner et al., 2012). Ocean color data for 1998–2007 in the Bering Sea also show that annual mean chlorophyll *a* and total primary production were higher in warm years than cold years (Brown et al., 2011; Mueter et al., 2009). We used the warm-average-cold year classification of Stabeno et al. (2012b) to classify our fall bloom data. Likewise we found that fall bloom magnitude was stronger in warm (average = 12.3 μg Chl l^{-1}, log-transform) versus cold (6.3) and average (8.6) years, but the differences were not statistically significant (ANOVA, log-transform, df = 2, 31, $p = 0.32$).

4.3. Spring/fall comparisons

Spring and fall bloom magnitudes were related, implying that a common factor influences spring and fall primary production (e.g., overwinter replenishment of nutrients). The fall bloom may be linked to the spring bloom by the fraction of spring bloom organic matter that sinks to the benthos, is remineralized and ultimately reintroduced to the euphotic zone during convection in the fall (M. Lomas, Bigelow Laboratory for Ocean Sciences, pers. comm.). In addition, this relationship likely amplifies secondary production during good years (both spring and fall blooms tend to be strong) and vice versa, bad years (both spring and fall blooms tend to be weak). An analysis of nutrient information, comparing spring–fall differences by year, would help us to understand the mechanism for this relationship.

The fall bloom occurred in late September on average, and the timing was less variable than for the spring bloom (varies over ~60 day compared to ~120 day period) regardless of location, so the spring–fall interval largely depends on spring bloom timing. In the northern Bering Sea, where ice is present every year and on average retreats in late May (Fig. 5), the interval typically lasted four months (Fig. 11). The interval also typically lasted four months in the southeastern Bering Sea in years when ice was absent or retreated before March 15. In contrast, the interval lasted up to six months in the southeastern Bering Sea in years when ice was present after March 15, but retreated soon thereafter.

4.4. The representativeness of the fluorescence data

Distinct spring and fall blooms occurred at these moorings located in the middle domain with the spring bloom stronger than the fall bloom. Likewise, a bimodal spring–fall pattern was found for net primary production for the middle domain with spring stronger than fall for both satellite-based (Brown et al., 2011) and temporally and spatially scattered in situ measurements (Rho and Whitledge, 2007). During the summer interval between the spring and fall blooms, we found that chlorophyll *a* fluorescence was low in the middle domain, similar to Goes et al. (2014). We also found that the mooring estimates of chlorophyll *a* were consistently correlated with satellite estimates of chlorophyll *a* in the middle domain at the same approximate latitude (Appendix Fig. 2). This pattern implies that the mooring information represents conditions of the middle domain over a range of ca. 150–200 km.

The bimodal spring–fall pattern was replicated for the inner domain except that spring and fall bloom magnitudes appear similar for satellite-based measurements (Brown et al., 2011). In contrast, the fall bloom was less distinct for the outer domain (Rho and Whitledge 2007; Brown et al., 2011). These patterns imply that bloom patterns differ somewhat among the inner, middle and outer domains, and that the mooring information do not well represent the oceanographic conditions of the inner (influence of the coastal current, river runoff, and tidal and wind mixing) or outer domains (influence of slope, episodic on-shelf flow and upwelling). The broad-scale data collected during the late summer BASIS sampling also indicates that chlorophyll *a* concentrations and phytoplankton particle size (large $>=10$ um and small <10 um) varied among shelf domains (Eisner et al., 2012). The relatively high concentrations found in the outer domain were primarily comprised of small taxa ($<$ 25% large); chlorophyll *a* concentrations on average were lower in the middle domain during these surveys, but when increases in chlorophyll *a* were observed (usually near M4), there was a higher proportion of large taxa (40–70% large). Besides phytoplankton, mixotrophic ciliates (a taxonomic group of microzooplankton that also photosynthesize) also can contribute to total chlorophyll *a* measurements in summer (Stoecker et al., 2014). Mesozooplankton and microzooplankton concentrations and taxonomic composition also vary cross-shelf (Eisner, 2014; Stoecker et al., 2014), which may cause variations in grazing and thus phytoplankton concentration among domains.

4.5. Biological implications

4.5.1. Lower trophic levels

Spring bloom timing predictably varied between early April and mid-June depending on ice presence/absence and ice retreat timing. Thus the secondary community (zooplankton species) that benefits will depend on how close timing of their spring energy-intensive needs such as reproduction and awakening from winter diapause matches the timing of the spring bloom. Species that require an early pulse of energy will benefit from years when ice is present, but retreats in late March (conditions that tend to result in early April phytoplankton bloom). In contrast, species with a phenology timed for a late energy pulse will benefit from years with no ice (conditions that tend to result in a late May to early June bloom).

These observations also imply that climate, through its connection to the production, transport, and dissipation of sea ice, has the potential to affect the success of zooplankton populations and the strength of coupling between primary production and higher trophic levels. For example, the large crustacean zooplankton taxa *Calanus* spp. may benefit in years when ice is present after March 15, but retreats relatively early. Baier and Napp (2003) observed that spring *Calanus* spp. concentrations in the southeastern Bering Sea were higher in cold years than in warm years, and that these individuals likely metamorphosed from naupliar to copepodite stages during the early spring bloom. They hypothesized that metamorphosis was a recruitment bottleneck and that an early spring bloom benefits copepodite recruitment. The spring bloom occurs during April in years when ice is present, but retreats relatively early, which may promote strong recruitment of copepodites. In addition, a cold winter with ice present likely reduces metabolism and lipid utilization by *Calanus* spp. and thus may promote winter survival (Coyle et al., 2011).

Recruitment of *Calanus* spp. on the eastern Bering Sea shelf is complicated, involving many different processes. Life history strategies of large crustacean zooplankton (LCZ) in the eastern Bering Sea may be able to take advantage of the oscillations between warm and cold periods, regardless of whether or not there are stanzas of multiple years of the same conditions (Overland et al., 2012). The timing of reproductive events for the *Calanus* congener *Calanus glacialis* varies between different physical and biological environments of the Arctic (Daase et al., 2013). The following scenarios were developed as a working hypothesis to explain some of the present observations and to serve as a guide for future research. In these scenarios, we simplified *Calanus* spp. life history into four major steps: spawning, metamorphosis, accumulation of depot lipids and overwintering. These scenarios make the following assumptions: (1) the timing of spawning by

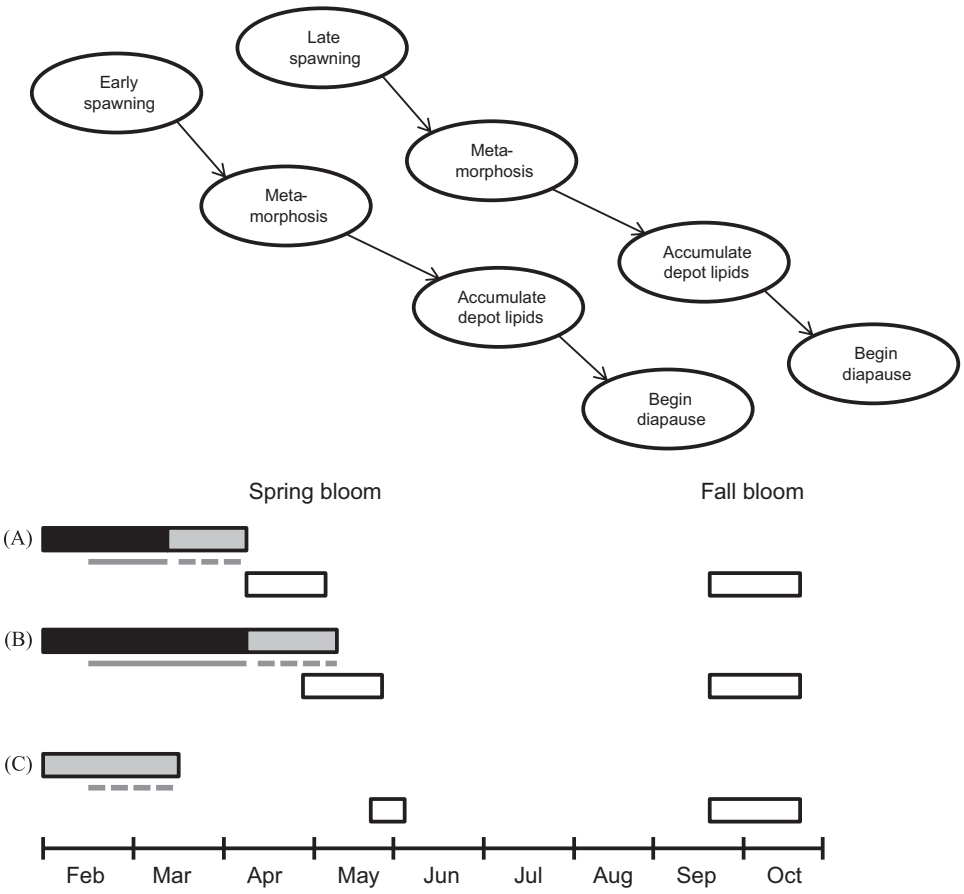

Fig. 12. Timing of *Calanus* spp. reproduction relative to the presence of ice and ice algae, and the spring and fall blooms. The *Calanus* spp. life history is simplified and the timings are approximate. Black is the period of ice cover; gray is the 50th percentiles for the timing of ice retreat. White rectangles are the 50th percentile dates for bloom maximum in the spring and fall. Ice algae blooms occur during ice cover (solid gray line) and ice retreat (dashed gray line) and begin as early as mid-February (R. Gradinger, personal comm.). A – a cold icy year, with ice retreat shortly after March 15; B – a cold icy year with ice retreat after April 14; C – no ice after March 15.

Calanus spp. is protracted (from February to May) (Baier and Napp, 2003 and references therein) and the longer that conditions are suitable, the more total eggs each individual will produce (E. Durbin, U. Rhode Island, pers. comm.); (2) early-spawned individuals enter diapause before late-spawned individuals; and (3) overwinter respiration is a function of temperature (Saumweber and Durbin, 2006). The working hypothesis does not address the role of advection of individuals into or out of the area.

Case A. Cold/Ice-Replete Years with Early Ice Retreat (Fig. 12). We hypothesize that access to under ice algae (beginning as early as mid February) increases egg production rates of early spawning *Calanus* spp. (Runge and Ingram, 1991). Metamorphosis to the copepodite stage benefits from an early ice retreat and spring bloom production (Baier and Napp, 2003). Summer accumulation of depot lipids is dependent on summer primary and microzooplankton production (Sambrotto et al., 1986; Sherr et al., 2013; Stoecker et al., 2014). Overwintering for individuals spawned in late winter begins relatively early and these individuals may not be able to take advantage of the fall bloom. The ability of individuals (C5 copepodites) to survive the following winter benefits from low respiration rates ($R_{C5\ copepodite}$ = 5.66 μm 0_2 d^{-1} at −1.8 °C (see methods)) resulting from cold bottom temperatures. Reproductive output during the following year(s) is maximized when there are subsequent ice-replete years and under ice algae.

Case B. Cold/Ice-Replete Years with Late Ice Retreat. In this scenario, both early and late spawning by *Calanus* spp. females benefits, as reproduction timing coincides with either the ice algae or the spring bloom. The nauplii and copepodites from late spawning would likely develop post-spring bloom (i.e., metamorphosis is not coincident with the spring bloom), and would depend upon summer primary and microzooplankton production to grow and accumulate depot lipids. The onset of overwintering occurs latest for the late-spawned progeny which may take advantage of the fall bloom to accumulate additional lipids before entering diapause. The ability to survive the overwintering period benefits from the cold bottom temperatures present in late fall through early spring.

Case C. Warm/Ice-Deplete Years. Egg production by early spawning of *Calanus* is reduced by the absence or short duration of sea ice and under ice algae. The timing of the spring bloom is late; it benefits late spawning of *Calanus* spp. females. The late spring bloom may coincide with metamorphosis of the early-spawned nauplii to copepodites, but is mismatched with the metamorphosis from the late spawners. Growth and development are dependent upon summer primary and microzooplankton production. Diapause that is delayed until after the fall bloom benefits late spawners. Warm bottom temperatures result in higher respiration rates – 47% higher daily respiration than during cold years ($R_{C5\ copepodite}$ = 8.34 μm 0_2 d^{-1} at 2.0 °C). The impact on lipid reserves is exacerbated if the period without food (beginning of diapause to the following spring bloom) is longer in warm years relative to cold. Thus we hypothesize that survival of *Calanus* spp. over a warm winter is low relative to a cold winter. Predation losses would also likely be higher in warm winters at a given predator abundance due to higher metabolism and food requirements of fishes. Absence of sea ice for a second year results in low reproductive output by the early spawners, and a decrease in the population.

5. Conclusions

- In the eastern Bering Sea: if ice is present after mid-March, spring bloom timing is related to ice retreat timing; if ice is absent or retreats before mid-March, a spring bloom usually occurs in May or early June.
- Spring and fall bloom magnitudes are related, implying that a common factor influences spring and fall primary production.
- We hypothesize that large crustacean zooplankton such as *Calanus* spp. benefit from cold, icy winters in the southeastern Bering Sea because ice algae or ice associated phytoplankton blooms provide an early spring food source and respiration rates are lower during cold winters.

Acknowledgments

We thank D. Kachel for data analysis, S. Salo for providing the ice data and W. Floering and C. Dewitt for deploying and recovering the moorings. We thank the officers and crews of the NOAA ships *Miller Freeman* and *Oscar Dyson* for their invaluable assistance in deploying and recovering the moorings. We thank Zach Brown, Rolf Gradinger, Mike Lomas and one anonymous reviewer whose comments improved our manuscript. The research was generously supported by the North Pacific Research Board and NOAA's North Pacific Climate Regimes and Ecosystem Productivity (NPCREP) and Fisheries Oceanography Coordinated Investigations programs. This is BEST-BSIERP publication no. 122 and NPRB publication no. 459. This is contribution FOCI-B807 to the Ecosystems & Fisheries Oceanography Coordinated Investigations and 3953 to the Pacific Marine Environmental Laboratory. The findings and conclusions in this paper are those of the authors and do not necessarily represent the views of NOAA's National Marine Fisheries Service or Oceans and Atmospheric Research.

Appendix A. Supplementary material

Supplementary data associated with this article can be found in the online version at http://dx.doi.org/10.1016/j.dsr2.2013.12.007.

References

Acker, J.G., Leptoukh, G., 2007. Online analysis enhances use of NASA Earth science data. Eos, Trans. Am. Geophys. Union 88 (2), 14.

Alexander, V., Niebauer, H.J., 1981. Oceanography of the eastern Bering Sea ice edge zone in spring. Limnol. Oceanogr. 26, 1111–1125.

Baier, C.T., Napp, J.M., 2003. Climate-induced variability in *Calanus marshallae* populations. J. Plankton Res. 25, 771–782.

Bond, N.A., Adams, J.M., 2002. Atmospheric forcing of the southeast Bering Sea Shelf during 1995–99 in the context of a 40-year historical record. Deep-Sea Res. II 49, 5869–5887.

Brown, Z.W., Arrigo, K.R., 2013. Sea ice impacts on spring bloom dynamics and net primary production in the eastern Bering Sea. J. Geophys. Res. 118, 1–20, http://dx.doi.org/10.1029/2012JC008034.

Brown, Z.W., van Dijken, G.L., Arrigo, K.R., 2011. A reassessment of primary production and environmental change in the Bering Sea. J. Geophys. Res. 116, C08014, http://dx.doi.org/10.1029/2010JC006766.

Cooney, R.T., Coyle, K.O., 1982. Trophic implications of cross-shelf copepod distributions in the southeastern Bering Sea. Mar. Biol. 70, 187–196.

Coyle, K.O., Eisner, L.B., Mueter, F.J., Pinchuk, A.I., Janout, M.A., Cieciel, K.D., Farley, E.V., Andrews, A.G., 2011. Climate change in the southeastern Bering Sea: impacts on pollock stocks and implications for the Oscillating Control Hypothesis. Fish. Oceanogr. 20, 139–156.

Daase, M., Falk-Petersen, S., Varpe, Ø., Darnis, G., Søreide, J.E., Wold, A., Leu, E., Berge, J., Philippe, B., Fortier, L., 2013. Timing of reproductive events in the marine copepod *Calanus glacialis*: a pan-Arctic perspective. Can. J. Fish. Aquat. Sci. 70, 1–14.

Droop, M.R., 1973. Some thoughts on nutrient limitation in algae. J. Phycol. 9 (3), 264–272.

Eisner, L.B., Cieciel, K., Gann, J. 2012. Phytoplankton biomass and size structure during late summer to early fall in the eastern Bering Sea. In: Zador, S. (Ed.), Ecosystem Considerations 2012, Stock Assessment and Fishery Evaluation Report, North Pacific Fisheries Management Council, 605 W 4th Ave, Suite 306, Anchorage, AK. ⟨http://www.afsc.noaa.gov/REFM/docs/2012/ecosystem.pdf⟩.

Eisner, L.B., Napp, J.M., Mier, K.L., Pinchuk, A.I., Andrews, A.G., 2014. Climate-mediated changes in zooplankton community structure for the eastern Bering Sea. Deep Sea Res. II 109, 157–171, http://dx.doi.org/10.1016/j.dsr2.2014.03.004.

Fortier, M., Fortier, L., Michel, C., Legendre, L., 2002. Climatic and biological forcing of the vertical flux of biogenic particles under seasonal Arctic sea ice. Mar. Ecol. Prog. Ser. 225, 1–16.

Goes, J.I., Gomes, H.R., Haugen, E., McKee, K., D'Sa, E., Chekalyuk, A.M., Stoecker, D., Stabeno, P., Saitoh, S., Sambrotto, R., 2014. Fluorescence, pigment and microscopic characterization of Bering Sea phytoplankton community structure and photosynthetic competency in the presence of a cold pool during summer. Deep-Sea Res. II 109, 84–99, http://dx.doi.org/10.1016/j.dsr2.2013.12.004.

Gradinger, R., Ikavalko, J., 1998. Organism incorporation into newly forming Arctic sea ice in the Greenland Sea. J. Plankton Res. 20, 871–886.

Granger, J., Prokopenko, M.G., Sigman, D.M., Mordy, C.W., Morse, Z.M., Morales, L.V., Sambrotto, R.N., Plessen, B., 2011. Coupled nitrification-denitrification in sediment of the eastern Bering Sea shelf leads to ^{15}N enrichment of fixed N in shelf waters. J. Geophys. Res.: Oceans (1978–2012) 116 (C11), 1–18, http://dx.doi.org/10.1029/2010JC006751.

Grebmeier, J.M., Cooper, L.W., Feder, H.M., Sirenko, B.I., 2006. Ecosystem dynamics of the Pacific-influenced northern Bering and Chukchi Seas in the Amerasian Arctic. Prog. Oceanogr. 71, 331–361.

Haecky, P., Jonsson, S., Andersson, A., 1998. Influence of sea ice on the composition of the spring phytoplankton bloom in the northern Baltic Sea. Polar Biol. 20, 1–8.

Hunt, G.L, Allen, B.M., Angliss, R.P., Baker, T., Bond, N., Buck, G., et al., 2010. Status and trends of the Bering Sea region, 2003–2008, pp. 196–267. In: McKinnell, S.M., Dagg, M.J. (Eds.), Marine Ecosystems of the North Pacific Ocean, 2003–2008, 4. PICES Special Publication 4, 393 p.

Hunt, G.L., Coyle, K.O., Eisner, L.B., Farley, E.V., Heintz, R.A., Mueter, F.J., Napp, J.M., Overland, J.E., Ressler, P.H., Salo, S., Stabeno, P.J., 2011. Climate impacts on eastern Bering Sea foodwebs: a synthesis of new data and an assessment of the Oscillating Control Hypothesis. ICES J. Mar. Sci. 68, 1230–1243.

Hunt, G.L., Stabeno, P.J., Walters, G., Sinclair, E., Brodeur, R.D., Napp, J.M., Bond, N.A., 2002. Climate change and control of the southeastern Bering Sea pelagic ecosystem. Deep-Sea Res. II 49, 5821–5853.

Iverson, R.L., Coachman, L.K., Cooney, R.T., English, T.S., Goering, J.J., Hunt Jr., G.L., McCauley, M.C., McRoy, C.P., Reeburg, W.S., Whitledge, T.E., 1979. Ecological significance of fronts in the southeastern Bering Sea. In: Livingston, R.J. (Ed.), Ecological Processes in Coastal and Marine Systems. Plenum Press, pp. 437–466.

Jin, M., Deal, C., Wang, J., Alexander, V., Gradinger, R., Saitoh, S., Iida, T., Wan, Z., Stabeno, P., 2007. Ice-associated phytoplankton blooms in the southeastern Bering Sea. Geophys. Res. Lett. 34, L06612, http://dx.doi.org/10.1029/2006GL028849.

Kalnay, E., Kanamitsu, M., Kistler, R., Collins, W., Deaven, D., Gandin, L., Iredell, M., Saha, S., White, G., Woollen, J., Zhu, Y., Leetmaa, A., Joseph, D., 1996. The NCEP/NCAR 40-year reanalysis project. Bull. Am. Meteorolog. Soc. 77 (3), 437–471.

Kirst, G.O., Wiencke, C., 1995. Ecophysiology of polar algae. J. Phycol. 31, 181–199, http://dx.doi.org/10.1111/j.0022-3646.1995.00181.x.

Ladd, C., Bond, N.A., 2002. Evaluation of the NCEP-NCAR Reanalysis in the northeast Pacific and Bering Sea. J. Geophys. Res. 107, 3158, http://dx.doi.org/10.1029/2001JC001157.

Ladd, C., Stabeno, P.J., 2012. Stratification on the Eastern Bering Sea shelf revisited. Deep Sea Res. II 65, 72–83.

Melnikov, I.A., 1998. Winter production of sea ice algae in the western Weddell Sea. J. Mar. Syst. 17, 195–205.

Mock, T., Gradinger, R., 2000. Changes in photosynthetic carbon allocation in algal assemblages of Arctic sea ice with decreasing nutrient concentrations and irradiance. Mar. Ecol. Prog. Ser. 202, 1–11.

Mordy, C.W., Cokelet, E.D., Ladd, C., Menzia, F.A., Proctor, P., Stabeno, P.J., Wisegarver, E., 2012. Net community production on the middle shelf of the eastern Bering Sea. Deep Sea Res. II 65, 110–125.

Mueter, F.J., Broms, C., Drinkwater, K.F., Friedland, K.D., Hare, J.A., Hunt, G.L., Melle, W., Taylor, M., 2009. Ecosystem responses to recent oceanographic variability in high-latitude Northern Hemisphere ecosystems. Prog. Oceanogr. 81, 93–110.

Niebauer, H.J., Alexander, V., Henrichs, S.M., 1995. A time-series study of the spring bloom at the Bering Sea ice edge I: physical processes, chlorophyll and nutrient chemistry. Continental Shelf Res. 15, 1859–1877.

Niemi, A., Michel, C., Hille, K., Poulin, M., 2011. Protist assemblages in winter sea ice: setting the stage for the spring ice algal bloom. Polar Biol. 34, 1803–1817.

O'Brien, D.P., 1987. Direct observations of the behavior of *Euphausia superba* and *Euphausia crystallorophias* (Crustacea: Euphausiacea) under pack ice during the Antarctic spring of 1985. J. Crustacean Biol. 7, 437–448.

Overland, J.E., Wang, M., Wood, K.R., Percival, D.B., Bond, N.A., 2012. Recent Bering Sea warm and cold events in a 95-year context. Deep-Sea Res. II 65–70, 6–13.

Parsons, T.R., Maita, Y., Lalli, C.M., 1984. A Manual of Biological and Chemical Methods for Seawater Analysis. Pergamon Press, Oxford p. 173.

Rho, T., Whitledge, T.E., 2007. Characteristics of seasonal and spatial variations of primary production over the southeastern Bering Sea shelf. Continental Shelf Res. 27, 2556–2569.

Riebesell, U., Schloss, I., Smetacek, V., 1991. Aggregation of algae form melting ice: implications for seeding and sedimentation. Polar Biol. 11, 239–248.

Runge, J.A., Ingram, R.G., 1991. Under-ice feeding and diel migration by the planktonic copepods *Calanus glacialis* and *Pseudocalanus minutus* in relation to the ice algal production cycle in southeastern Hudson Bay. Can. Mar. Biol. 108, 217–225.

Sambrotto, R.N., Niebauer, H.J., Goering, J.J., Iverson, R.L., 1986. Relationships among vertical mixing nitrate uptake and phytoplankton growth during the spring bloom in the southeast Bering Sea middle shelf. Continental Shelf Res. 5, 161–198.

Saumweber, W.J., Durbin, E.G., 2006. Estimating potential diapause duration in *Calanus finmarchicus*. Deep-Sea Res. II 53, 2597–2617.

Sherr, E.B., Sherr, B.F., Ross, C., 2013. Microzooplankton grazing impact in the Bering Sea during spring sea ice conditions. Deep-Sea Res. II 94, 57–67 http://dx.doi.org/10.1016/j.dsr2.2013.03.019.

Spreen, G., Kaleschke, L., Heygster, G., 2008. Sea ice remote sensing using AMSR-E 89 GHz channels. J. Geophys. Res. 113 (C2), C02.

Stabeno, P.J., Bond, N.A., Kachel, N.B., Salo, S.A., 2007. On the recent warming of the Southeastern Bering Sea Shelf. Deep-Sea Res. II 54, 2599–2618.

Stabeno, P.J., Bond, N.A., Kachel, N.B., Salo, S.A., Schumacher, J.D., 2001. On the temporal variability of the physical environment over the southeastern Bering Sea. Fish. Oceanogr. 10, 81–98.

Stabeno, P.J., Farley, E., Kachel, N.B., Moore, S.E., Mordy, C.W., Napp, J.M., Overland, J.E., Pinchuk, A.I., Sigler, M.F., 2012a. A comparison of the physics of the northern and southern shelves of the eastern Bering Sea and some implications to the ecosystem. Deep-Sea Res. II 65-70, 14–30, http://dx.doi.org/10.1016/j.dsr2.2012.02.019.

Stabeno, P.J., Kachel, N.B., Moore, S.E., Napp, J.M., Sigler, M.F., Yamaguchi, A., Zerbini, A.N., 2012b. Comparison of warm and cold years on the southeastern Bering Sea shelf and some implications to the ecosystem. Deep-Sea Res. II 65-70, 31–45, http://dx.doi.org/10.1016/j.dsr2.2012.02.020.

Stabeno, P.J., Napp, J., Mordy, C., Whitledge, T., 2010. Factors influencing physical structure and lower trophic levels of the eastern Bering Sea shelf in 2005: Sea ice, tides and winds. Prog. Oceanogr. 85 (3–4), 180–196.

Stockwell, D.A., Whitledge, T.E., Zeeman, S.I., Coyle, K.O., Napp, J.M., Brodeur, R.D., Pinchuk, A.I., Hunt, G.L., 2001. Anomalous conditions in the south-eastern Bering Sea, 1997: nutrients, phytoplankton and zooplankton. Fish. Oceanogr. 10 (1), 99–116.

Stoecker, D.K., Weigel, A.C., Stockwell, D.A., Lomas, M.W., 2014. Microzooplankton: abundance, biomass and contribution to chlorophyll in the eastern Bering Sea in summer. Deep-Sea Res. II 109, 134–144, http://dx.doi.org/10.1016/j.dsr2.2013.09.007.

Sullivan, M.E., Mordy, C.W., Salo, S.A., Stabeno, P.J., 2014. The influence of sea ice on seasonal water column changes on the southeastern Bering Sea Shelf. Deep-Sea Res. II 109, 39–56, http://dx.doi.org/10.1016/j.dsr2.2014.05.009.

Sverdrup, H.U., 1953. On conditions for the vernal blooming of phytoplankton. J. Cons. Perm. Int. Explor. Mer 18, 287–295.

Tremblay, C., Runge, J., Legendre, L., 1989. Grazing and sedimentation of ice algae during and immediately after a bloom at the ice–water interface. Mar. Ecol. Prog. Ser. 56, 291–300.

Deep-Sea Research II 109 (2014) 84–99

Contents lists available at ScienceDirect

Deep-Sea Research II

journal homepage: www.elsevier.com/locate/dsr2

Fluorescence, pigment and microscopic characterization of Bering Sea phytoplankton community structure and photosynthetic competency in the presence of a Cold Pool during summer

Joaquim I. Goes [a,*], Helga do Rosario Gomes [a], Elin M. Haugen [b], Kali T. McKee [a], Eurico J. D'Sa [c], Alexander M. Chekalyuk [a], Diane K. Stoecker [d], Phyllis J. Stabeno [e], Sei-Ichi Saitoh [f], Raymond N. Sambrotto [a]

[a] Lamont Doherty Earth Observatory, Columbia University, Palisades, New York, NY 10964, USA
[b] Bigelow Laboratory for Ocean Sciences, East Boothbay Harbor, Maine, ME 04544, USA
[c] Department of Oceanography and Coastal Sciences, Louisiana State University, Baton Rouge, LA 70803, USA
[d] University of Maryland Center for Environmental Science, Horn Point Laboratory, Cambridge, MD 21613, USA
[e] NOAA Pacific Marine Environmental Laboratory, 7600 Sand Point Way NE, Seattle, Washington, WA 98115-0070, USA
[f] Graduate School of Fisheries Sciences, Hokkaido University, 3-1-1 Minato-cho Hakodate, Hokkaido 041-8611, Japan

ARTICLE INFO

Available online 17 December 2013

Keywords:
Bering Sea
Phytoplankton
Taxonomy
Diversity
Sea-ice
Salinity
Temperature
Nutrients

ABSTRACT

Spectral fluorescence measurements of phytoplankton chlorophyll *a* (Chl *a*), phytoplankton phycobilipigments and variable fluorescence (Fv/Fm), are utilized with High Performance Liquid Chromatography (HPLC) estimates of phytoplankton pigments and microscopic cells counts to construct a comprehensive picture of summer-time phytoplankton communities and their photosynthetic competency in the eastern Bering Sea shelf. Although the Bering Sea was ice-free during our study, the exceptionally cold winter that preceded the summer of 2008 when our cruise took place, facilitated the formation of a "Cold Pool" ($<2\,^{\circ}C$) and its entrapment at depth in the northern middle shelf. The presence of a strong pycnocline over the entire middle and outer shelves restricted inorganic nutrient fluxes into the surface waters resulting in phytoplankton populations that were photo-physiologically stressed due to nutrient limitation. Elevated Chl *a* concentrations recorded in the Green Belt along the shelf edge of the Bering Sea, were due to *Phaeocystis pouchetii* and nano-sized cryptophytes. Although inorganic nutrients were not limiting in the Green Belt, Fv/Fm values were low in all probability due to iron limitation. Phytoplankton communities in the low biomass surface waters of the middle shelf were comprised of prasinophytes, haptophytes, cryptophytes and diatoms. In the northern part of the middle shelf, a sinking bloom made up of the centric diatoms *Chaeotoceros socialis*, *Thalassiosira nordenskioeldii* and *Porosira glacialis* was located above the Cold Pool. The high biomass associated with this senescent bloom and its accretion above the pycnocline, suggests that the Cold Pool acts as a barrier, preventing sinking phytoplankton from reaching the bottom where they can become available to benthic organisms. We further posit that if summer-time storms are not energetic enough and the Cold Pool is not eroded, its presence facilitates the transfer of the large spring phytoplankton bloom to the pelagic ecosystem.

1. Introduction

The eastern Bering Sea shelf is one of the most productive marine ecosystems in the world. From an ecosystem perspective, its most defining feature is its highly productive phytoplankton bloom which forms in spring and supports extraordinarily rich stocks of fish, migratory marine birds and mammals (Hunt et al., 2011). Sea food landings from the Bering Sea are extremely large and have been estimated to account for more than 10% of the world's and about 55% of the U.S. annual seafood harvest (NOAA, 2013).

As with most high-latitude oceanic regions, sea-ice is a key component of the Bering Sea shelf ecosystem. It provides the seed population for the spring bloom and is also responsible for introduction of dissolved iron into the water column which is especially beneficial to the Fe limited High Nutrient Low Chlorophyll (HNLC) waters of the offshore Bering Sea (Aguilar-Islas et al., 2007). Sea-ice also has a huge impact on the upper ocean circulation processes (Zhang et al., 2012) that aid in the advection of nutrients on to the shelf, and in the release of freshwater from

* Corresponding author.
E-mail address: jig@ldeo.columbia.edu (J.I. Goes).

0967-0645/$ - see front matter © 2013 Elsevier Ltd. All rights reserved.
http://dx.doi.org/10.1016/j.dsr2.2013.12.004

sea-ice which affects the static stability of the surface ocean and the formation of thermal structures and fronts on the eastern Bering Sea shelf (Kachel et al., 2002). These fronts which start developing in spring, create three distinct hydro-chemical domains, i.e. the inner-shelf, the middle-shelf and the outer-shelf that have been widely used in describing various aspects of the ecosystem of the eastern Bering Sea shelf (Coachman, 1986; Kachel et al., 2002; Sullivan et al., 2008). Phytoplankton growth over the eastern Bering Sea shelf is restricted to an extremely short season, and generally begins when sea-ice begins to retreat. Although growth occurs over a limited period, it is rapid, and greatly favored by increased stability of the water column induced by sea-ice melt water during cold years and thermal stratification during warm years. With the increase in solar radiation, spring-time phytoplankton are able to take advantage of extremely high concentrations of inorganic nutrients to form massive blooms over the wide expanse of the eastern Bering Sea shelf. In cold years, with significant sea-ice after mid-March, there can be two blooms, an early bloom in March–April, and a second bloom in May or June (Stabeno et al., 2010, 2012a) that can result from storm-driven injections of new nitrogen into the upper-water column (Sambrotto et al., 1986). This largely sea-ice dependent explosive growth of phytoplankton strips the entire Bering Sea shelf water column of all its nutrients in a short time. Since nutrient replenishment by vertical transport from the deep is severely constrained by a strong halocline (Aagaard et al., 1981; Woodgate et al., 2005), further biomass accumulation of phytoplankton in summer, especially in the southeastern Bering Sea is generally restricted (Whitledge et al., 1986; Rho et al., 2005). Summer phytoplankton population photosynthesis and growth are thus largely dependent on cross-shelf advective processes including mesoscale eddies that introduce nutrients on to the shelf (Springer et al., 1996; Mizobata and Saitoh, 2004; Okkonen et al., 2004).

While the areal extent and rate of retreat of sea-ice are important determinants of the magnitude of spring phytoplankton blooms, they can also influence environmental conditions that develop over the Bering Sea shelf in the following summer, such as the formation of the Cold Pool (Zhang et al., 2012; Stabeno et al., 2012a,b) and the degree of stratification (Ladd and Stabeno, 2012). The formation of the Cold Pool or bottom waters with temperatures $<2\ ^{\circ}C$, is tied to the process of stratification which begins in April or May. Once the water column over the middle shelf of the Bering Sea begins to stratify, the warmer surface waters insulate the bottom water layer from warming as the season progresses. The temperature of the bottom layer depends on sea-ice conditions in winter and the temperature of the water column at the onset of stratification in spring (Stabeno et al., 2002, 2007). In cold years (with extensive sea-ice through April), temperatures in the bottom layer or the Cold Pool usually remain below 2 °C throughout summer.

Sea-ice conditions over the Bering Sea are extremely sensitive to small changes in wind velocities and air temperatures. Since the Bering Sea comes under the influence of storms and climatic patterns such as ENSO (Overland et al., 2012), PDO, NAO and the AO (Overland et al., 1999), sea-ice conditions can vary greatly over seasonal, annual, interannual and decadal cycles (Stabeno et al., 2001) and influence phytoplankton communities and the food chain of the Bering Sea. A turning point in the cyclical pattern of Bering Sea sea-ice behavior (Stabeno and Overland, 2001; Overland and Stabeno, 2004) was the onset of the El-Niño in 1997 which had a huge impact on the ecosystem. Following this event, the Bering Sea experienced a rapid melt back of its sea-ice (Stabeno et al., 2001). Anomalous cloud-free conditions, increased solar heating, decreased onshore transport of slope water and reduced number of energetic storms (Stabeno et al., 2001) all acting in consonance during that year, contributed to the formation of a warm ($\sim$12 °C) and stable water column on the shelf in which few nutrients remained to support diatoms (Egge and Aksnes, 1992). These conditions caused a dramatic switch in phytoplankton populations, with profound effects on the rest of the food chain (Baduini et al., 2001; Stockwell et al., 2001). Diatoms were replaced by coccolithophore (i.e. *Emiliana huxleyi*) blooms, which occupied almost the entire continental shelf of the Southeastern Bering Sea (Broerse et al., 2003). The warming ($\sim$3 °C) trend persisted into the 2000s and was marked by significant decreases in sea-ice concentrations, ice duration, maximum ice extent and large crustacean zooplankton. This warm period was followed from 2008 to 2011 by a series of cold years, characterized by high ice extent, increases in large copepods and euphausiids, and improved recruitment of pollock and cod (Stabeno et al., 2012a,b). No comparable information is available on phytoplankton communities that would have taken place during the transition from a warm to a cold year. Such information is essential if we are to understand the influence of changing sea-ice patterns on the primary producers and the production pathways of organic matter which support the valuable fisheries of this extensive high-latitude continental shelf (Moran et al., 2012; Lomas et al., 2012).

Here we use high-resolution fluorescence-based estimates of phytoplankton chlorophyll *a* (Chl *a*), three spectral types of phycoerythrin (PE) and phytoplankton photosynthetic competency, coupled with microscopy and High Performance Liquid Chromatography (HPLC) measurements of diagnostic pigment biomarkers of phytoplankton groups for detailed characterization of phytoplankton community structure during the summer of 2008 which was characterized by the presence of a Cold Pool. Hydrographic and chemical data obtained during the cruise are utilized to describe the data in relation to the environmental conditions, in particular, in relation to the Cold Pool that prevailed during the summer of 2008.

This study was part of a NASA supported International Polar Year study on the impacts of sea-ice changes on the bio-optical properties of high-latitude oceans, and allowed us to participate in a Bering Sea Ecosystem Study-Bering Sea Integrated Ecosystem Research Program (BEST/BSIERP) cruise in the summer of 2008. Although there was no sea-ice during our study, residual effects of the cold winter were obvious from the presence of a Cold Pool and remnants of low salinity surface water in the northern regions of the eastern Bering Sea shelf. The ecological role of the Cold Pool is significant for higher trophic organisms and fisheries (Stabeno et al., 2012a). While it can obstruct cross shelf migration of subarctic fish (Kotwicki et al., 2005; Ciannelli and Bailey, 2005), it can act as a corridor for migration of Arctic species to the southeastern shelf (Stabeno et al., 2012a,b). The Cold Pool can possibly affect cross shore transport of nutrients, but its overall impacts on biomass and composition of phytoplankton within and outside of the pool remain unknown.

2. Materials and methods

The data presented in this study were collected on board the US Coast Guard Cutter *Healy* from the 1st to 31st July 2008. The cruise was part of the BEST/BSIERP study of the Bering Sea, a partnership project between the US National Science Foundation and the North Pacific Research Board, Alaska. Continuous hydrographic profiles were obtained at 177 oceanographic stations along a cruise track shown in Fig. 1, using a Sea-Bird Electronics® Conductivity–Temperature–Depth (CTD) rosette fitted with 12×30 l Niskin bottles. The cruise track in Fig. 1 is overlaid on 16 marine regions recently delineated by the BEST/BSIERP research community based on a large

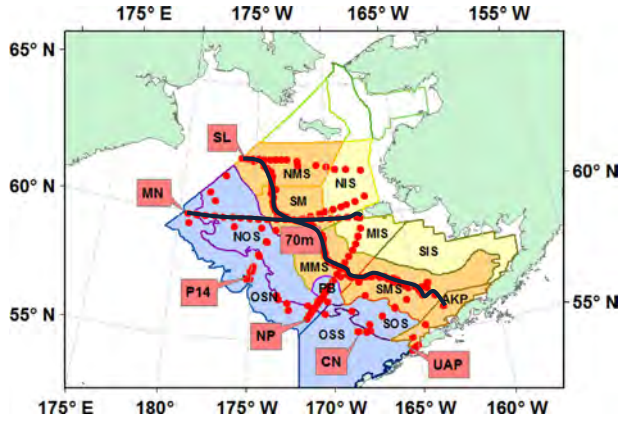

Fig. 1. Cruise track showing CTD station positions along various hydrographic lines occupied during BEST/BSIERP summer cruise of 2008 on board the US Coast Guard Cutter *Healy*. Stations have been overlaid on the 16 marine regions recently defined by the BSIERP community. A list of full form of the abbreviations for the 16 regions and the rationale for their dilineation is available in Ortiz et al. (2012). Thick lines have been overlaid to show the north–south 70 m isobath transect and the east–west MN transect.

set of observations of the oceanography, bathymetry, benthic fauna, fish, seabird and marine mammal distribution (Ortiz et al., 2012).

Samples for inorganic nutrients (SiO_3, NO_3+NO_2 and PO_4) were collected directly from Niskin bottles and analyzed immediately on board using a Lachat® QuikChem 8000 flow-injection analyzer (Gordon et al., 1993).

Samples for biological measurements were obtained from six depths, five in the euphotic column that included one from the deep chlorophyll maximum (DCM) and the sixth from below the euphotic depth.

For estimating phytoplankton Chl *a*, 250–500 ml of seawater from each of the six depths was filtered in triplicate onto 25 mm Whatman® GF/F filters, which were then placed in 90% acetone overnight at −20 °C for extraction. The pigment was analyzed fluorometrically on-board in a Turner Designs® TD700 fluorometer (Knap et al., 1994). In addition, another set of similarly collected samples at 46 stations was used to estimate a wide spectrum of pigments such as Chl *a*, *b*, *c* and carotenoids using HPLC (Van Heukelem and Thomas, 2001; Hooker et al., 2005). Seawater samples (1–2 l) in duplicate from three depths (surface, DCM and below the euphotic zone) were filtered in duplicate onto 25 mm Whatman® GF/F filters and stored at 80 °C until analysis. These pigments serve as diagnostic markers of phytoplankton taxa which means that the composition of the phytoplankton community can be evaluated at the same time that Chl *a* is accurately quantified as a proxy for total biomass estimates.

Phytoplankton taxonomic structure was studied using pigment biomarkers and the matrix factorization program CHEMTAX (Mackey et al., 1996, 1998). Rather than use simple ratios of marker pigments to identify phytoplankton groups, CHEMTAX uses a steepest descent algorithm to fit a matrix of expected pigment ratios for several taxa, to one consisting of the actual pigment ratios from unknown samples. In order to apply CHEMTAX, the heterogeneous data were first binned into three subsets, surface (0–2 m), mid-depth (10–33 m) and bottom (34–75 m). Pigment data (Chl *c*3, Chl *c*2, peridinin, 190-butanoyloxyfucoxanthin, fucoxanthin, prasinoxanthin, violaxanthin, 190-hexanoyloxyfucoxanthin, alloxanthin, zeaxanthin, lutein and Chl *b*) from each of these depth bins were then converted into pigment/Chl *a* ratios. Cluster analysis (Bray Curtis similarity) using PRIMER® ver. 6.1.13 was then performed on $\log(X+1)$ transformed pigment ratios to separate clusters with linkage distances greater than 70%. CHEMTAX was then applied to the pigment data from each of these clusters to obtain the contribution of eight phytoplankton groups to bulk Chl *a*. These included diatoms, dinoflagellates, chlorophytes, cryptophytes, prasinophytes, haptophyte-6 (indicating *E. huxleyi*), hapytophyte-8 (indicating *Phaeocystis pouchetii*) and cyanobacteria. The initial ratio matrix was from Table 6.1 in Higgins et al. (2011). From this initial matrix 29 artificial ratios were randomly generated within a certain range (Wright, personal communication). CHEMTAX was applied to these initial 30 matrices. The output of the matrix with the smallest RMS error was used to generate another 29 artificial ratios that were once again utilized in the subsequent runs which continued until the RMS error became more or less constant. The RMS error values obtained for the surface, mid-depth and bottom were 0.076, 0.045 and 0.042, respectively.

For microscopic identification and enumeration of phytoplankton, samples were collected in 100 ml screw top hard plastic bottles from 3 depths and at 27 stations (coincident with HPLC pigment analysis). Samples were fixed with 1% alkaline Lugol's iodine and preserved in 1.5% buffered formaldehyde solution. The samples were stored under dark and cool conditions and analyzed microscopically within a month of return from the cruise. Phytoplankton cells were allowed to settle overnight in an Ultermohl counting chamber and then counted using a Nikon® inverted microscope at 200× and 400× magnifications. The smallest cells enumerated were ~5 μm in diameter. Identification was based on standard taxonomic keys (Tomas, 1997). Cryptophytes were identified by epifluorescence microscopy using their yellow-orange fluorescence signatures (Booth, 1993; MacIssac and Stockner, 1993).

In addition to the above measurements, seawater samples from 6 depths were analyzed with the recently developed Advanced Laser Fluorometer (ALF) (Chekalyuk and Hafez, 2008). Samples were collected directly from the Niskin samplers into 500 ml acid-washed amber glass bottles, and stored for about 30 min in the dark at about 5 °C close to the average seawater temperature of our study area to minimize the impacts of non-photochemical quenching before analysis. Dark adaptation allows all of the PSII reaction centers and electron acceptor molecules of phytoplankton to become fully oxidized and hence available for photochemistry.

The ALF combines high-resolution spectral measurements of blue (405 nm) and green (532 nm) laser-stimulated fluorescence with spectral deconvolution techniques to quantify fluorescence of Chl *a*, PE and Chromophoric Dissolved Organic Matter (CDOM) (Chekalyuk and Hafez, 2008; Chekalyuk et al., 2012). All fluorescence values were normalized to water Raman spectra and with the exception of Chl *a* have been expressed as relative fluorescence units (RFU). RFU values for Chl *a* were converted into mg m^{-3} as described below. The ALF measurements with the blue laser excitation were used for estimating Chl *a* (peak at 679 nm), CDOM (peak at 508 nm) and variable fluorescence (Fv/Fm), whereas the fluorescence measurements with the green laser were used for detection and spectral discrimination of three group-specific types of PE fluorescence. These include PE-1 (peak at 565 nm fluorescence) from blue water or oligotrophic cyanobacteria with high phycourobilin/phycoerythrobilin (PUB/PEB) ratios, PE-2 (peak at 578 nm fluorescence) from green water cyanobacteria with low-PUB/PEB ratios that usually thrive in coastal mesohaline waters, and PE-3 (peak at 590 nm fluorescence) attributable to eukaryotic photoautotrophic cryptophytes (Chekalyuk and Hafez, 2008; Chekalyuk et al., 2012).

Between stations, the ALF was connected to the ship's uncontaminated seawater flow-through system, allowing for continuous in-water fluorescence measurements from approximately 3 m below the surface. With the exception of a few breaks for reconditioning, the ALF was operated over the entire cruise track

(Fig. 1), providing almost 95,000 near-real time fluorescence measurements of Chl *a*, CDOM, PE-1, PE-2, PE-3 and Fv/Fm.

For converting Raman-normalized ALF Chl *a* fluorescence measurements into mg m^{-3} units of Chl *a* concentration, we utilized separate conversion procedures, one for the discrete depth samples and one for the underway flow-through fluorescence measurements. Equation $y=0.347x^2+2.377x$ derived from a least square regression between the ALF in vivo Chl *a* fluorescence and HPLC measurements of Chl *a* concentration (see above; $N=111$; $R^2=0.91$) were used to convert Raman-normalized Chl *a* fluorescence into Chl *a* concentration (mg m^{-3}). It may be noted that the intercept was forced to zero during the regression analysis (based on the assumption that zero Chl *a* should result in zero fluorescence). The regression analysis without forcing the intercept to zero results in the intercept value 0.053 and the equation $y=0.370x^2+2.257x+0.053$; $R^2=0.907$, which corresponds to Chl *a* concentration 0.053 μg l^{-1}, or 0.3% ($=0.053/21=0.0025$) of the range of variability in Chl *a* concentration in the data set that we analyzed. The non-linear relationship that we observed between ALF Chl a fluorescence and HPLC Chl *a* was likely caused by the stronger pigment packaging effect in large diatom cells that dominated the high-Chl *a* samples at depth and in the northern region. Such a non-linear relationship between Chl *a* fluorescence and concentration has been reported in earlier publications (e.g., Chekalyuk et al., 2012)

The ALF underway in vivo Chl *a* fluorescence and variable fluorescence (Fv/Fm) measurements, particularly those obtained during the day were affected by solar-induced non-photochemical quenching (NPQ). To eliminate the NPQ effect on the accuracy of Chl *a* assessments from the underway fluorescence measurements, we used the NPQ-invariant ratios of Raman-normalized Chl *a* fluorescence to Fv/Fm (Chekalyuk and Hafez, 2011). The conversion equation $y=0.052x^2+0.609x$, which was derived from regression analysis between these units and HPLC measurements of Chl *a* concentration in the seawater samples ($N=111$; $r^2=0.83$), was used for calculation of Chl *a* concentration from the ALF underway fluorescence measurements.

A statistically significant relationship ($r^2=0.86$, $n=136$, $p<0.001$) was also obtained between the Raman corrected PE-3 fluorescence intensities and CHEMTAX-derived estimates of cryptophyte biomass. Fluorescence signatures of PE-1 and PE-2 derived by the ALF were relatively low throughout the study period. Although no comparable data on green and blue water cyanobacterial populations was available, PE-1 and PE-2 fluorescence measurements are known to provide good estimates of blue water and green-water cyanobacteria (Chekalyuk et al., 2012; Goes et al., in press). The ALF measurements of variable fluorescence, Fv/Fm reported below were adjusted for non-Chl *a* background fluorescence as per procedures described in detail in Chekalyuk and Hafez (2008).

2.1. Inorganic nutrients and dissolved iron amendment experiments

In order to investigate the roles of inorganic nutrients and dissolved iron as potentially important regulators of summer-time phytoplankton growth in waters above the Bering Sea shelf (Whitledge et al., 1986; Rho et al., 2005) and in the waters of the outer shelf (Aguilar-Islas et al., 2007), respectively, we undertook two iorganic nutrient/dissolved iron enrichment experiments, one with phytoplankton from a shelf station (NP-11) and the other with phytoplankton from an outer shelf or offshore station (P14-4). At the shelf station, inorganic NO_3 and NO_2 concentrations were below limits of detection and inorganic PO_4 and SiO_3 were 0.42, and 7.4 μM, respectively. At P14-4, inorganic NO_3, NO_2, PO_4 and SiO_3 concentrations were 3.62, 0.09, 0.69 and 3.13 μM, respectively. Dissolved iron concentrations were not measured by us, but typical dissolved-Fe concentrations at this time of the year can vary between 0.5 and 4 nmol l^{-1} on the shelf, and below detection limits offshore (Aguilar-Islas et al., 2007 and references cited therein).

For our experiments, surface seawater samples were carefully collected in acid cleaned, trace-metal free cubitainers using a Zodiac. In the first experiment, subsamples of water from outer shelf station P14-4 were transferred into 24 trace-metal free acid cleaned polyethylene bags, 8 of which were spiked with 1.5 nmol l^{-1} concentrations of dissolved iron, and another 8 with 2 μM of NO_3. A third subset of eight bags with no amendments served as controls. In the second experiment at the on-shelf station NP-11, seawater was transferred into 16 acid-cleaned bags and spiked with 2.7 μM of inorganic NO_3 and 2 μM of PO_4. Incubations of the control and treatments were undertaken in an on-deck incubator in which ambient sea-surface temperatures were maintained with running surface seawater.

During Expt 1, 4 bags from each of the treatments and the controls were collected on Day 3 and Day 6 for measurements of Chl *a* (mg m^{-3}) and at the end of Day 1 and Day 3 in Expt. 2.

A one-way Student *t*-test was used to assess if changes in Chl *a* within treatments were statistically significant over time of incubation whereas a one-way ANOVA (Holm-Sidak test) was used for assessing differences among treatments. The latter analysis was restricted to samples drawn at the end of the experiments. All statistical tests were performed using Sigmaplot 11®.

3. Results

3.1. Hydrographic conditions

In this section, we present an overview of the hydrographic conditions of the eastern Bering Sea in the summer of 2008 using the 16 sub-regions delineated in Ortiz et al. (2012). Additional details of the hydrographic conditions in the Bering Sea during the summer of 2008 are available in Cross et al. (2012); Stabeno et al. (2012a), Moran et al. (2012) and Lomas et al. (2012).

Our data synthesis yielded several noteworthy features which include: (1) sea surface water temperatures in excess of 6 °C at the surface with the exception of the cold water (1–2 °C) patch on the southeastern side of the Priblof Islands (PB) waters and another (~4 °C) patch around Nunivak Island (Fig. 2A), (2) a patch of low salinity in the northern middle shelf (NMS) and around St. Michael (SM) Island (Fig. 2B and D), (3) warmer waters over the entire outer shelf (OS) with signs of encroachment of outer shelf and slope waters on to the southern middle (SMS) and inner shelf (SMS) and (4) a Cold Pool distinctly seen in the spatial map at 45 m, north of 59.5°N (Fig. 2C). This Cold Pool encompassed the NMS and SM.

The Cold Pool is also clearly visible in the N-S hydrographic section along the 70 m isobath (Figs. 1 and 3A and B). Although the vertical section of the 70 m isobath shows an uniformly warm surface layer (Fig. 3A), two major frontal regions were visible at depth, the first around 57.5°N with ~2 °C waters southwards and the second at 59.5°N separating the <2 °C Cold Pool waters in the north from the warmer southern (>4 °C) waters. Thus the cross shelf fronts divided the deeper layer of the middle shelf into three broad regions, the southern, the central and the northern regions. Salinity values were clearly higher in the Cold Pool (Fig. 3B), but above the Cold Pool, an entrapped parcel of low salinity waters was observed in the upper 20 m possibly from spring-time residual melt water or from river runoff.

The distinct hydrographic conditions seen across the shelf are best explained by temperature and salinity profiles along cruise

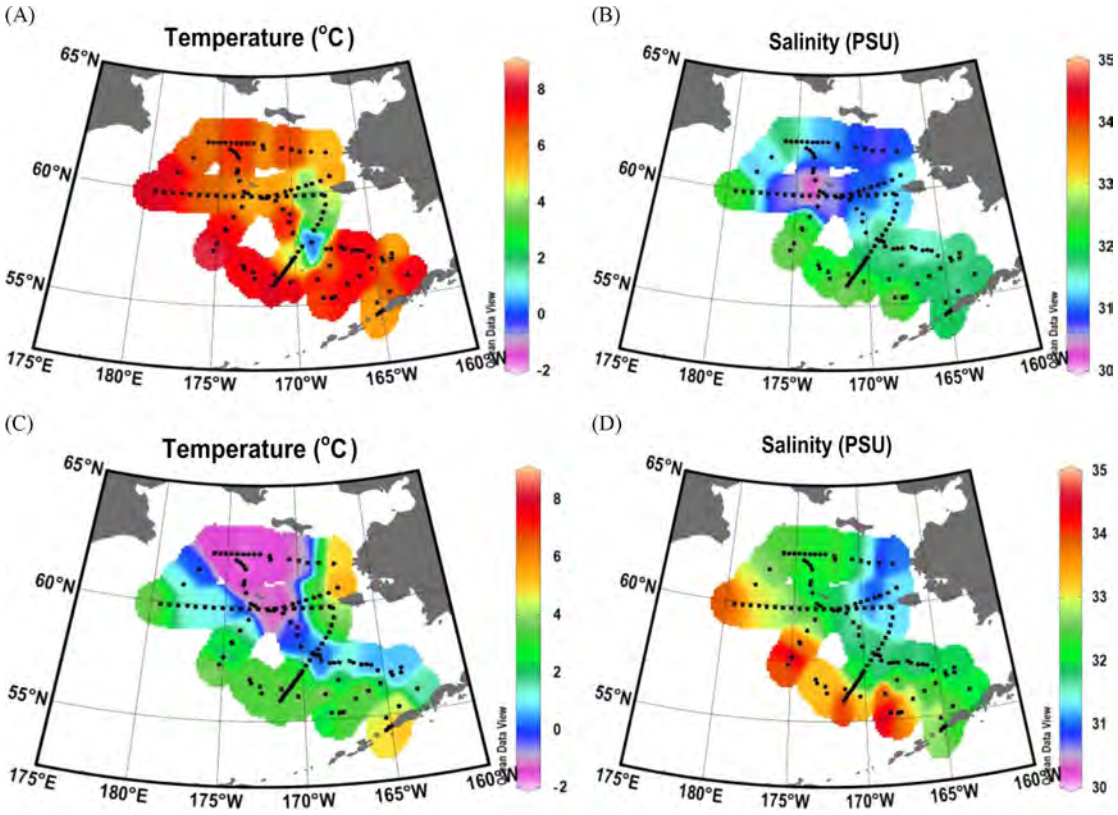

Fig. 2. Spatial distribution of surface (A and C) temperature (°C) and (B and D) salinity (PSU) at the surface and at 35 m over the study area.

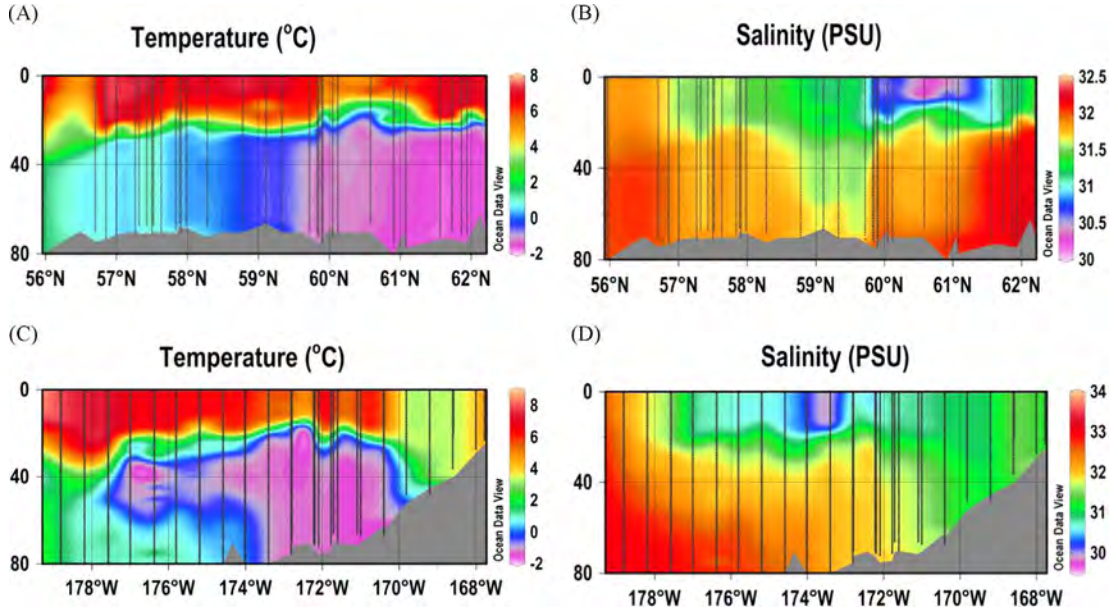

Fig. 3. Vertical sections of (A and C) temperature (°C) and (B and D) salinity (PSU) along the 70 m isobath and the MN line.

line MN (Figs. 1 and 3C and D) which we chose because it represents a section across the shelf where (1) the Cold Pool (located between 178° and 170°W in the middle shelf and extending to the outer shelf) was very prominent and (2) the three well known cross-shelf hydrographic domains, viz. the inner (IS), middle (MS) and the outer (OS) shelves were clearly distinguishable by fronts along the 50 m (inner front), 80 m (central front) and along the100 m (outer front) isobaths, respectively. The latter front separated the outer shelf from the offshore high salinity waters. Other noteworthy features that were evident include (1) the three layered structure of the outer shelf, (2) the highly stratified two layered water column of the middle shelf and (3) the coastal tidally well mixed waters eastwards of 170°W.

3.2. *Inorganic nutrient distribution*

Sea surface inorganic nutrients (PO_4–P, SiO_3, NO_3–N and NH_4–N) were clearly much lower in the eastern Bering Sea shelf

than offshore (Fig. 4A and D). This was particularly true in the southern inner and middle shelves (SIS and SMS). An east–west gradient in nutrients visible at the surface was also evident at 35 m, except for NH_4–N which formed a narrow, high-concentration band along the entire length of the 70 m isobath (Fig. 5A and D). Offshore, NH_4–N concentrations were much lower,

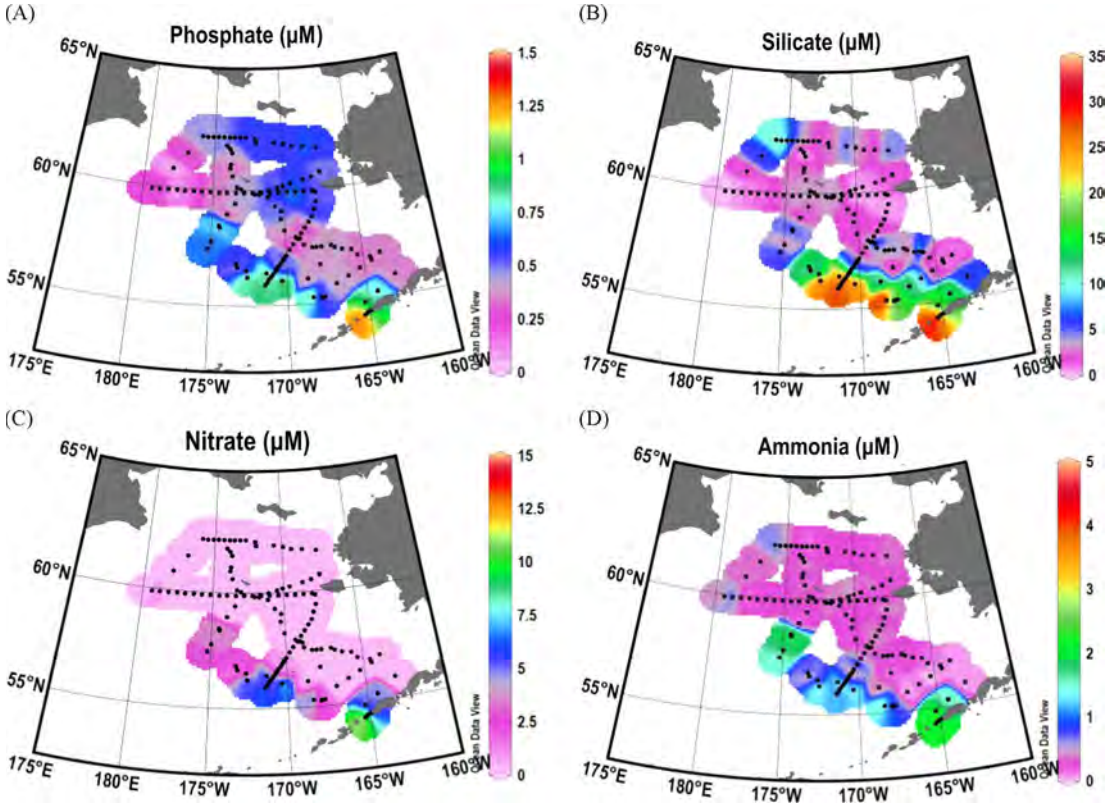

Fig. 4. Spatial distribution of (A) phosphate, (B) silicate, (C) nitrate and (D) ammonia (all expressed in μM) at the surface over the study area.

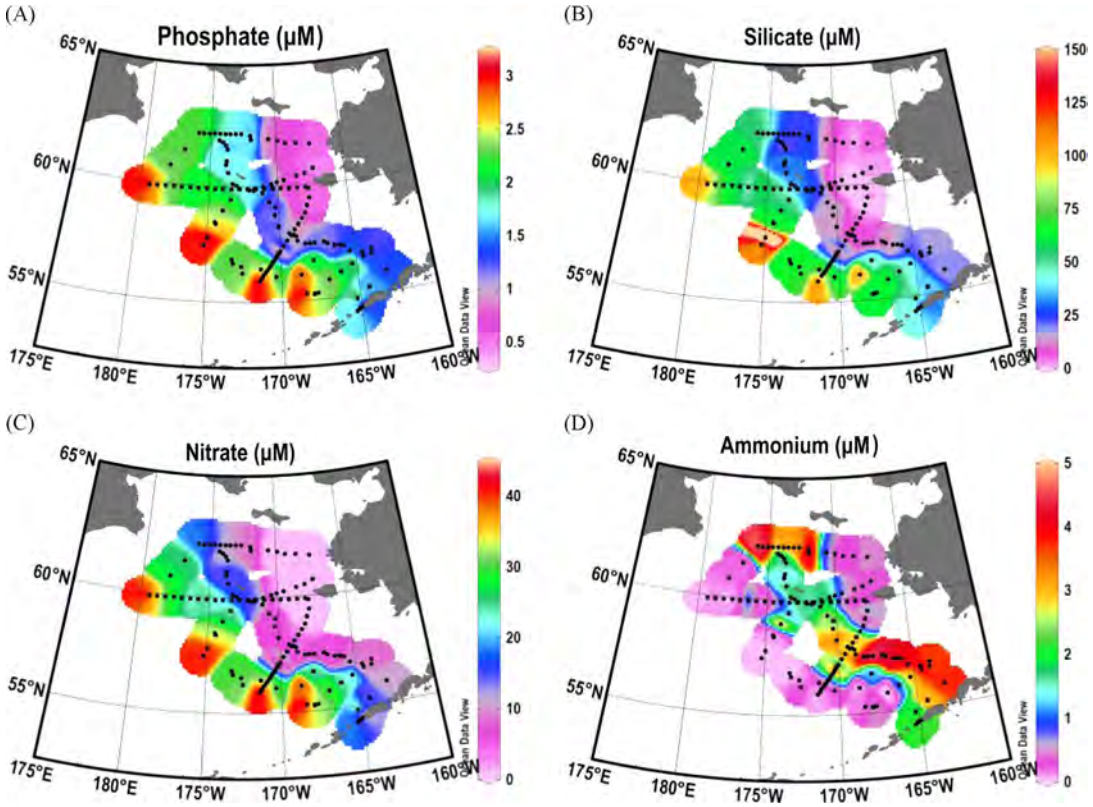

Fig. 5. Spatial distribution of (A) phosphate, (B) silicate, (C) nitrate and (D) ammonia (all expressed in μM) at 35 m over the study area.

indicating the highly localized nature of the regenerative and nitrification processes along the shelf break.

The N–S section along the 70 m isobath showed near depletion of inorganic nutrients in the first 20 m of the water column along the entire section (Fig. 6A and D). Below this layer, nutrient distribution confirmed that the middle shelf had three regions each with distinct concentrations. Nutrient concentrations within the Cold Pool in the north were much higher with the exception of NH_4–N, whose concentrations tended to be higher southwards (Fig. 6D). The lowest nutrient concentrations were observed in the central section of the middle shelf.

The MN section (Fig. 7A and D) shows the east–west or cross-shelf gradient in nutrient distribution with low concentrations throughout the water column in the inner shelf, and a prominent two layered structure in the middle shelf. In the Cold Pool, nutrient concentrations were extremely high, but abruptly transitioned to extremely low levels in the upper surface layer (0–30 m) above the halocline. Overall nutrient concentrations (PO_4–P, NO_3–N and SiO_3), were much higher offshore than in the adjacent outer shelf. The prominent band of NH_4–N seen along the shelf break region could be seen as a plume whose origins could be traced to the shallow outer shelf region. Onshore advection of nutrients was not evident along this section but it was much more prominent in the SOS, SMS along sections CN and NP (Fig. 1, data not shown) and westwards of the PB region.

3.3. *Spatial fluorescence patterns*

The high resolution underway fluorescence data collected by the ALF provides a comprehensive picture of the spatial patterns of sea surface Chl *a* (expressed as mg m^{-3}), phycobilipigments and Fv/Fm (Fig. 8A and E) which would not have been possible with discrete sampling alone. In general, the ALF dataset showed that surface Chl *a* concentrations were very low throughout the eastern Bering Sea shelf but confirmed the elevated Chl *a* in the Green Belt (Fig. 8A), a persistent band of high phytoplankton biomass and productivity observed along the shelf edge of the Bering Sea (Springer et al., 1996; Aguilar-Islas et al., 2007). Moderately high

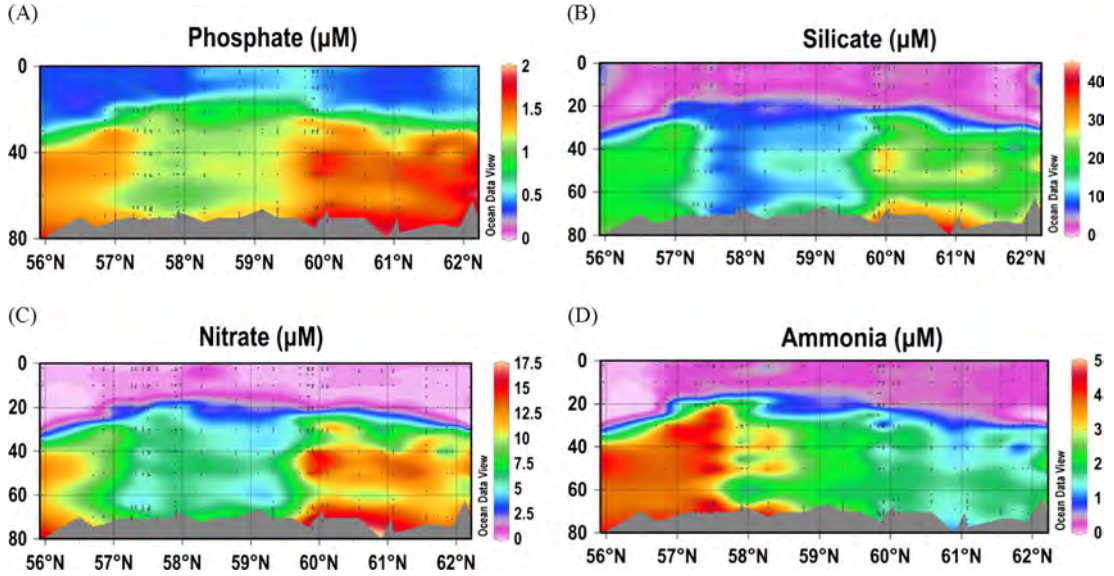

Fig. 6. Vertical sections of (A) phosphate, (B) silicate, (C) nitrate and (D) ammonia (all expressed in µM) along the 70 m isobath.

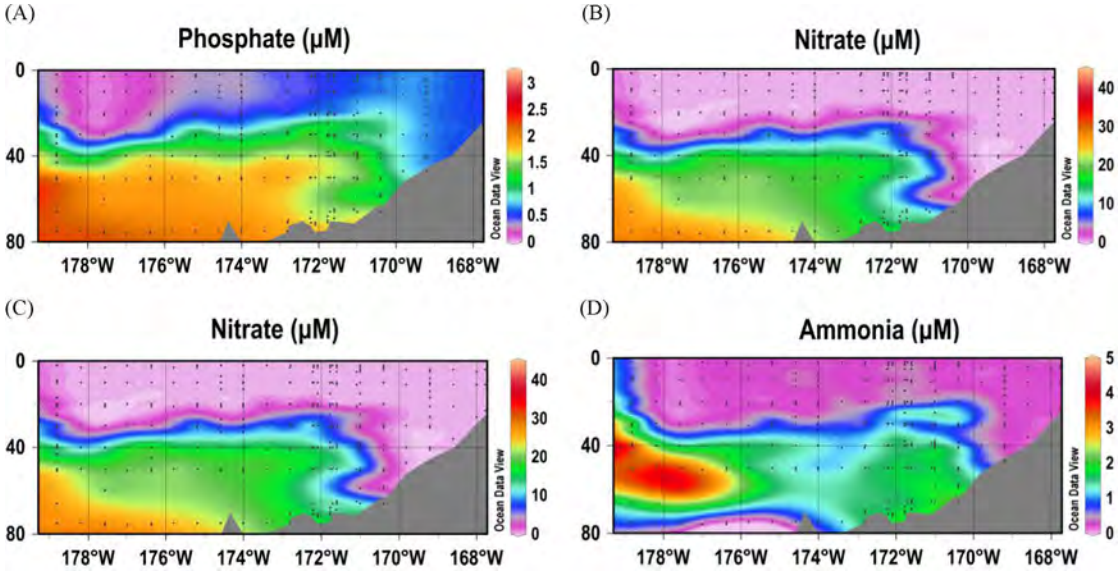

Fig. 7. Vertical sections of (A) phosphate, (B) silicate, (C) nitrate and (D) ammonia (all expressed in µM) along the MN line.

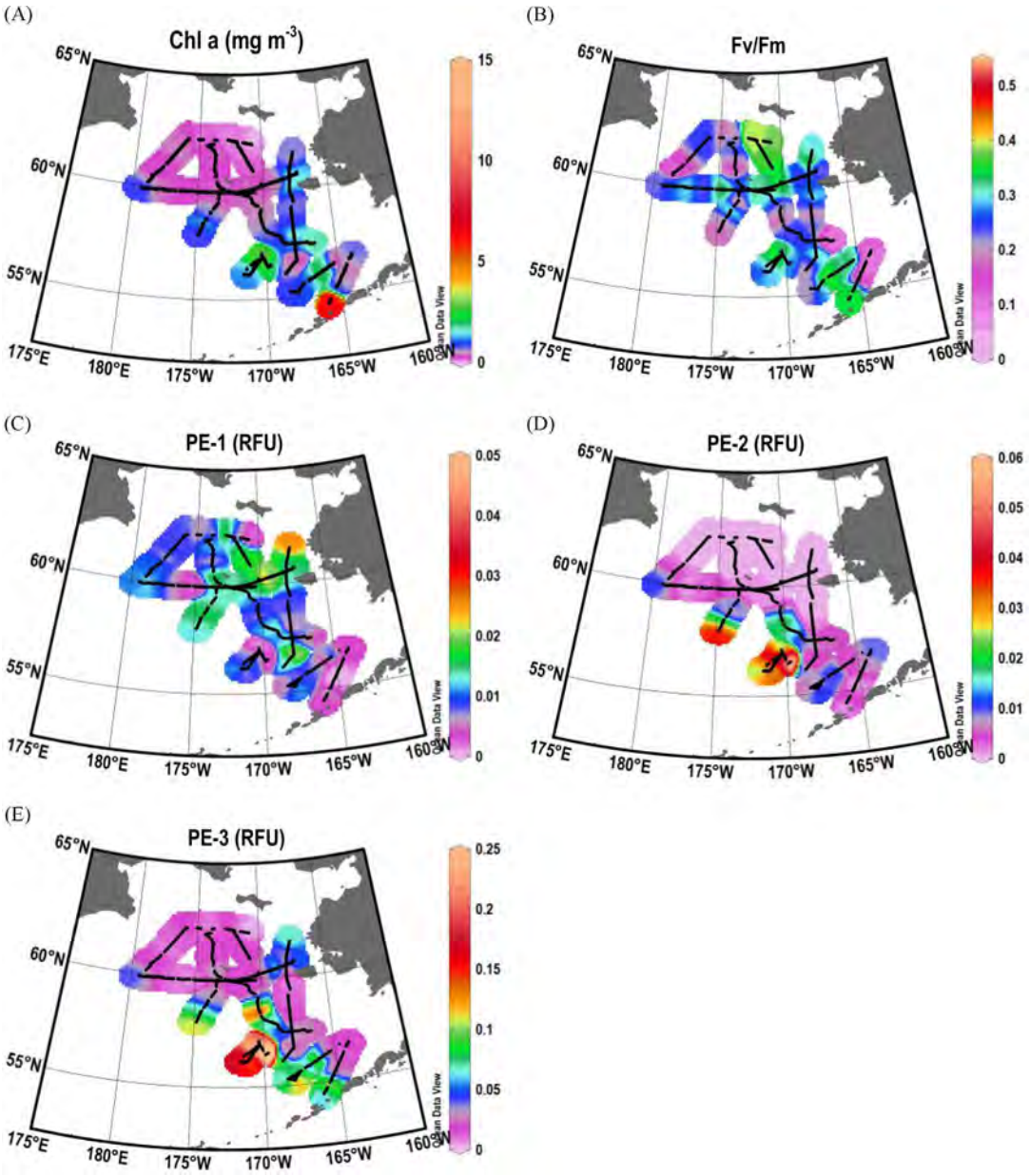

Fig. 8. Spatial patterns (A) Chl *a*, (B) Fv/Fm, (C) PE-1, (D) PE-2 and (E) PE-3 fluorescence in surface waters. (All values except Fv/Fm are expressed in relative fluorescence units, RFU.)

Chl *a* was observed in the southern outer shelf (SOS), in the low salinity NIS and the NMS regions, and in the region around PB. Fv/Fm (Fig. 8B), showed photo-physiologically active phytoplankton in the NIS and Alaskan Peninsula (AKP). Elsewhere over the entire shelf, including in the Green Belt, Fv/Fm values were low indicating that phytoplankton populations in the surface waters of the eastern Bering Sea shelf and offshore were stressed.

Of the three phycobilipigment types recorded by the ALF (Fig. 8C and E), PE-3 pigment type associated with cryptophytes had the highest fluorescence (Fig. 8C). PE-3 fluorescence was highest in the Green Belt region and in the low salinity pool in the NIS. Similarly, PE-1 fluorescence was higher in the Green Belt and in the low salinity waters of the NIS. On the other hand, PE-2 fluorescence was remarkably low over the entire shelf, with the exception of the region around the PB islands and in the Green Belt.

At depth, the highest Chl *a* concentrations were observed in the NIS and in the SM regions (Fig. 9A). As observed at the surface, Fv/Fm values were low throughout except in the low salinity waters in NIS and close to the PB and the Aleutian Islands (Fig. 9B). In general the distribution patterns of all three PE pigments at depth (Fig. 9C and E) mirrored the distribution patterns at the surface, but were much lower.

Along the 70 m isobath, Chl *a* values were low throughout, with the exception of a subsurface maxima located at 35 m above the Cold Pool (Fig 10A). High Fv/Fm values were coincident with the location of the subsurface Chl *a* maximum between 60.5 and 61.5°N (Fig. 10B). PE-1 fluorescence values were very low throughout the section although comparatively higher values were observed at the surface (Fig.10C). Both PE-2 and PE-3 fluorescence values were higher in the south. In addition however, subsurface patches of high Chl a were recorded around 61°N (Fig. 10D and E).

The cross-shelf MN section showed only one large region of high Chl *a* biomass at around 35 m in the middle shelf straddling the upper end of the Cold Pool. Other than that, phytoplankton biomass in the upper 20 m was very low (Fig. 11A). Offshore,

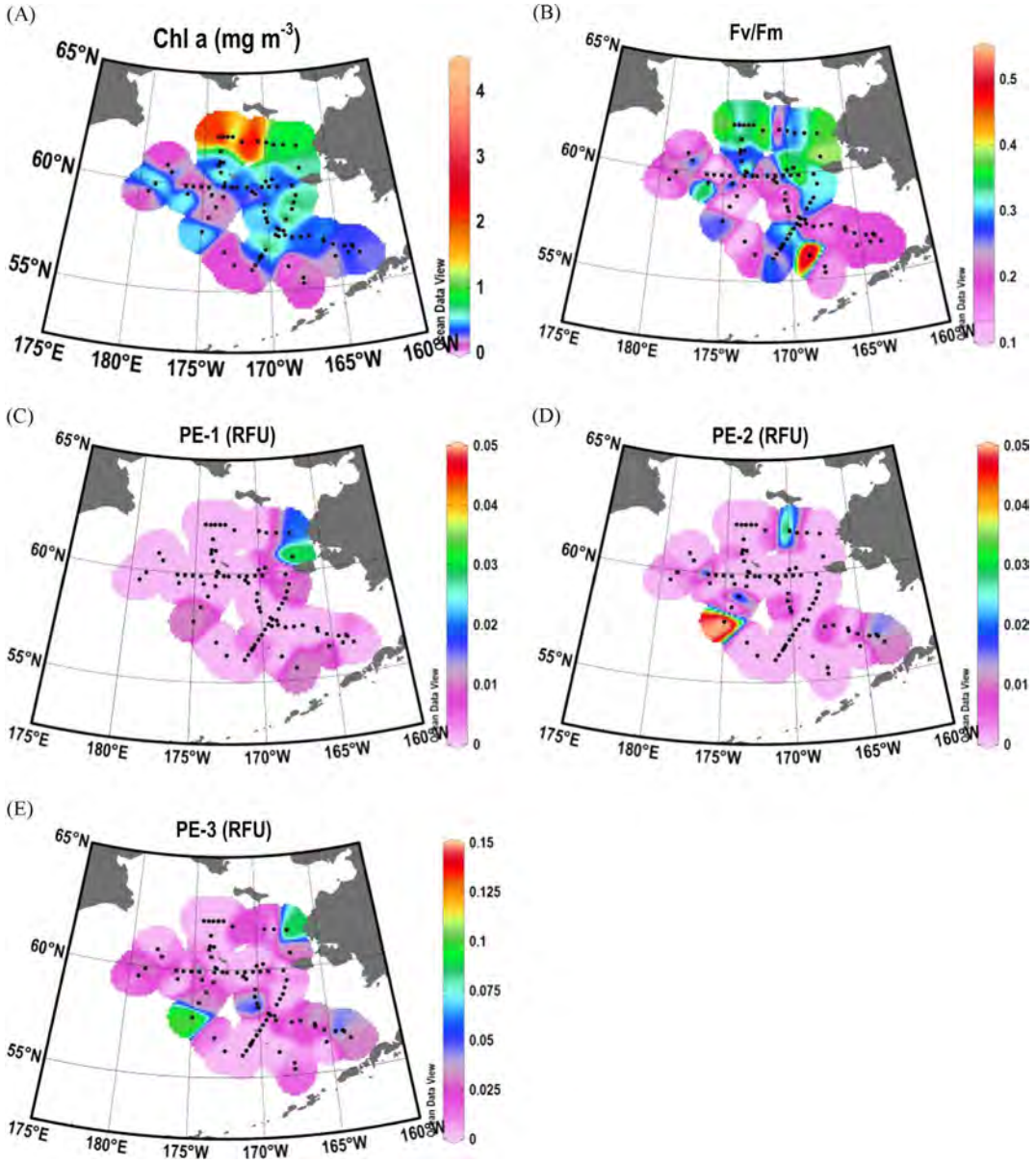

Fig. 9. Spatial patterns of (A) Chl *a*, (B) Fv/Fm, (C) PE-1, (D) PE-2 and (E) PE-3 fluorescence at 35 m in the water column. (All values except Fv/Fm are expressed in relative fluorescence units, RFU.)

moderately high Chl *a* was seen at the surface and at about 35 m. Variable fluorescence values were low along this entire section except for the higher values in the low salinity waters of the inner shelf (Fig. 11B) where PE-1 fluorescence was also high (Fig. 11C). Highest PE-2 values were recorded at the subsurface (40 m) above the Cold Pool and coincident with the high Chl *a* fluorescence (Fig. 11D). PE-3 fluorescence distribution patterns along the MN line (Fig. 11E) resembled in part the distribution patterns of Chl *a* fluorescence with the exception of a surface high in the inner shelf.

3.4. CHEMTAX based phytoplankton groups

CHEMTAX analyses of marker pigments showed a very mixed population of phytoplankton in the upper stratified layer (Fig. 12A). Offshore, haptophytes were significant components of the offshore phytoplankton population followed by cryptophytes and prasinophytes. The Green Belt was dominated by these three groups. These observations are consistent with the high PE-3 fluorescence values recorded in the Green Belt. Diatoms were highest in the NMS region and near the Aleutian Island chain, but in the low salinity waters of the NMS and SM, haptophytes were significant.

In contrast, at depth (35 m), diatoms accounted for over 90% of the population of the northern inner and middle shelves, but in the northern offshore region (OSN), haptophytes made up for a sizeable proportion of the population (Fig. 12B). The southern middle shelf was made up of a mixed population of cryptophytes, prasinophytes and diatoms.

The results of the spatial distribution patterns of the major phytoplankton groups based on CHEMTAX analysis of the pigment data (Fig. 12A and B) mirror the patterns of phytoplankton groups determined from the microscopic data (Fig 13A and F). Both centric and pennate diatoms were highest (1.6×10^4 and 1×10^3 cells l^{-1}, respectively) at depth in the NMS and SM regions where Chl *a* concentrations were low (Fig 13A and B), whereas the haptophyte, *Phaeocystis pouchettii* and cryptophytes were highest (1.3×10^4 and 4.2×10^3 cells l^{-1}, respectively) in the Green Belt

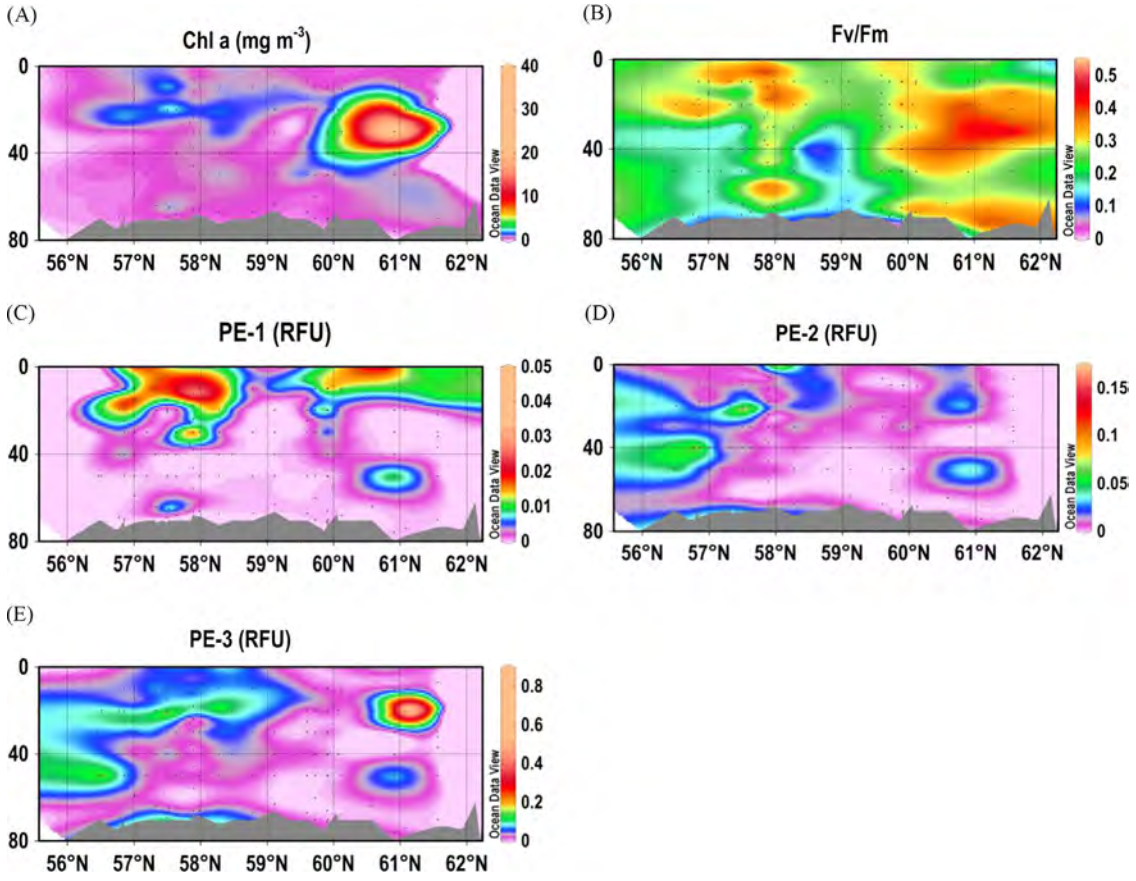

Fig. 10. Vertical sections of (A) Chl *a*, (B) Fv/Fm, (C) PE-1, (D) PE-2 and (E) PE-3 fluorescence along the 70 m isobath.

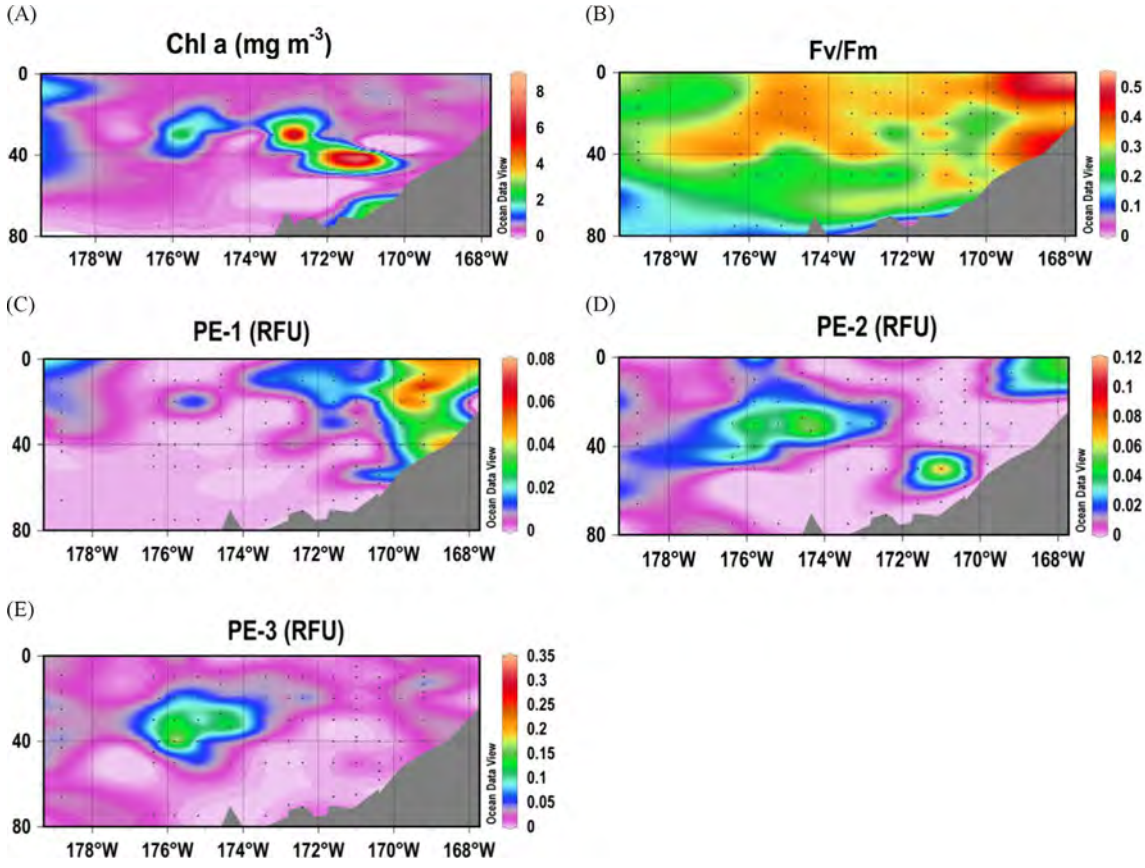

Fig. 11. Vertical sections of (A) Chl *a*, (B) Fv/Fm, (C) PE-1, (D) PE-2 and (E) PE-3 fluorescence along the MN line.

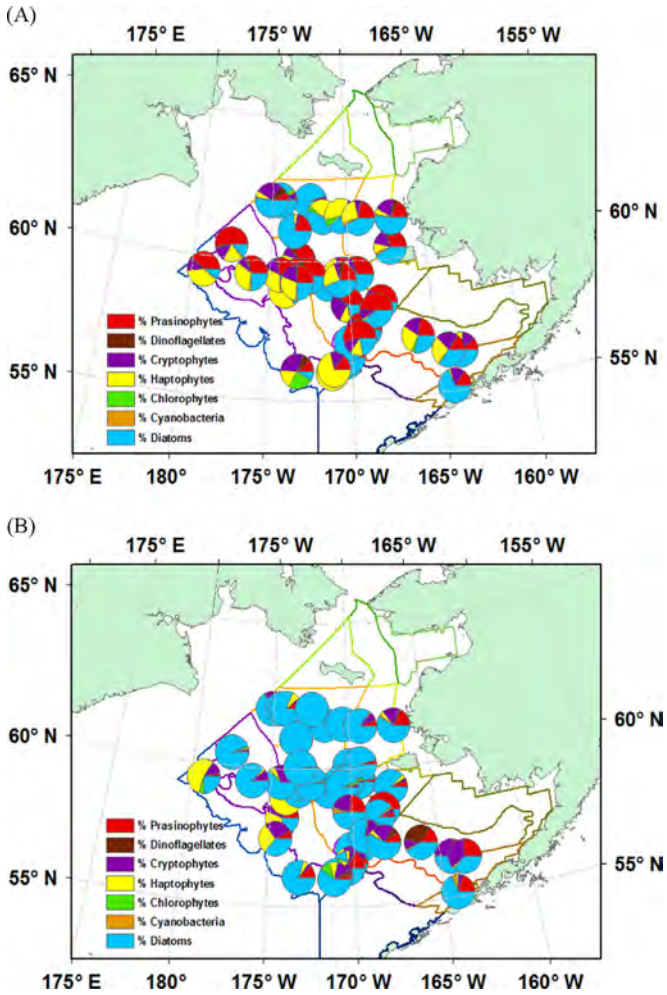

Fig. 12. Spatial patterns of HPLC/CHEMTAX derived groups of phytoplankton at (A) the surface and (B) 35 m in the water column over the study area.

around PB, OS and OSS (Fig. 13C and D). Counts of both the pigmented and heterotrophic dinoflagellates were low ($<2.2\times10^3$ and 0.75×10^2 cells l^{-1}) throughout the southeastern Bering Sea (Fig. 13E and F).

Along the N–S 70 m isobath, diatom concentrations were low throughout the surface layers (Fig. 14A) but at the subsurface, a diatom-rich patch with Chl *a* concentrations of about 15 mg m^{-3} was observed around 30–35 m located prominently above the Cold Pool between 58.3 and 62.3°N. In contrast, cryptophytes with Chl *a* concentrations of about 0.5 mg m^{-3} were seen just below the surface in the southern part of the transect between 56 and 59°N (Fig. 14B). Haptophytes were present all along the transect except between 57 and 59.5°N where prasinophytes dominated (Fig. 14C and D). The highest biomass of dinoflagellates was located to the south (Fig. 14E) of the transect where cryptophytes were also present, whereas the biomass of chlorophytes although low mimicked that of diatom where their maximum biomass at depth coincided with depths where the highest biomass of diatoms was measured.

The MN cross-shelf section of phytoplankton groups shows that the high Chl *a* patch recorded by the ALF (Fig. 11A) comprised mainly of diatoms (Fig. 15A). Elsewhere along this transect diatom concentrations were very low, in particular at the surface. Cryptophytes and haptophytes accounted for the second largest fraction of total phytoplankton biomass (Fig. 15B and C). Although their biomass was not high, cryptophytes were seen mainly offshore just above the Cold Pool. Concentrations of haptophytes were also high offshore but confined to a narrow band to the east. Prasinophytes were uniformly distributed in the upper 25 m along the MN section but their concentrations were low throughout (Fig. 15D). The biomass of dinoflagellates was highest offshore and at depth (Fig. 15E), whereas the highest biomass of chlorophytes (Fig. 15F) was coincident with that of the diatom patch (Fig. 15A).

3.5. Phytoplankton species counts and community structure

Phytoplankton species identified microscopically from samples collected from 2 depths and at 27 stations are listed in Table 1. These stations cover a broad region of the eastern Bering Sea shelf. The sinking phytoplankton bloom located above the Cold Pool was dominated by the centric diatoms *Chaetoceros socialis* (0.4–1.8×10^7 cells l^{-1}) as well as *Chaetoceros curvisetus* and *Thalassiosira nordenskioeldii*. These three species formed resting spores as they settled out of the shallow photic zone. A developing bloom of *Leptocylindrus danicus* and *Porosira glacialis* was observed in the NOS, NMS and SM regions where low salinity waters prevailed. Pennate diatoms such as *Pseudo-nitzschia* spp., *Thalassionema nitzschoides* and *Fragilariopsis* spp. were also observed in the SM and NMS regions in smaller numbers (<150 cells l^{-1}) at the surface but much higher numbers (<1200 cells l^{-1}) at depth. In the inner shelf region, the chrysophyte *Dinobryon balticum* was observed in greater numbers. In the Green Belt, region the haptophyte *P. pouchetii* and cryptophytes dominated, confirming results from CHEMTAX and the ALF (for cryptophytes). Cryptophyte numbers were highest ($0.6–1.9\times10^6$ l^{-1}) in the shelf break region as well as near the PB island once again consistent with the HPLC and ALF observations.

3.6. Inorganic nutrients and dissolved iron amendment experiments

The results of the inorganic nutrients and the dissolved iron amendment experiments are presented in Fig. 16A and B. Summertime phytoplankton from the Bering Sea shelf clearly responded positively (one way *t*-test, $p<0.001$) to inorganic NO_3 as evident from the over 3-fold increase in Chl *a* 72 h after the amendment. On the other hand, no increase in Chl *a* but a significant decrease (one way *t*-test, $p<0.01$) was observed in the incubation bags amended with inorganic PO_4 (Fig. 16A).

At the outer shelf station, a significant increase in Chl *a* concentrations above that recorded for the controls was observed (one-way ANOVA, $p<0.01$) in samples amended with both dissolved iron and inorganic NO_3, but the increase was clearly significantly higher (one-way ANOVA, $p<0.001$) in the former indicating the importance of dissolved iron as a regulator of phytoplankton growth offshore (Fig. 16B).

4. Discussion

Hydrological and chemical measurements revealed the highly stratified nature of the Bering Sea during the summer of 2008, which would have prevented nutrient replenishment of the euphotic zone. As a consequence phytoplankton biomass levels were low over the entire eastern Bering Sea shelf on account of inorganic nitrate limitation consistent with our nutrient amendment experiment at the on-shelf station. There were three exceptions to this overall picture, the first was in the NIS where moderately high Chl *a* (1–1.5 mg m^{-3}) was associated with low salinity and low temperature, possibly from recent sea-ice melt and/or river discharge. Near to the coast, the well mixed low-salinity waters were rich in CDOM (Naik et al., 2010) suggesting their riverine origin and also, rich in PE-1 and PE-2 suggesting an increased presence of cyanophytes, perhaps *Synechococcus* spp.,

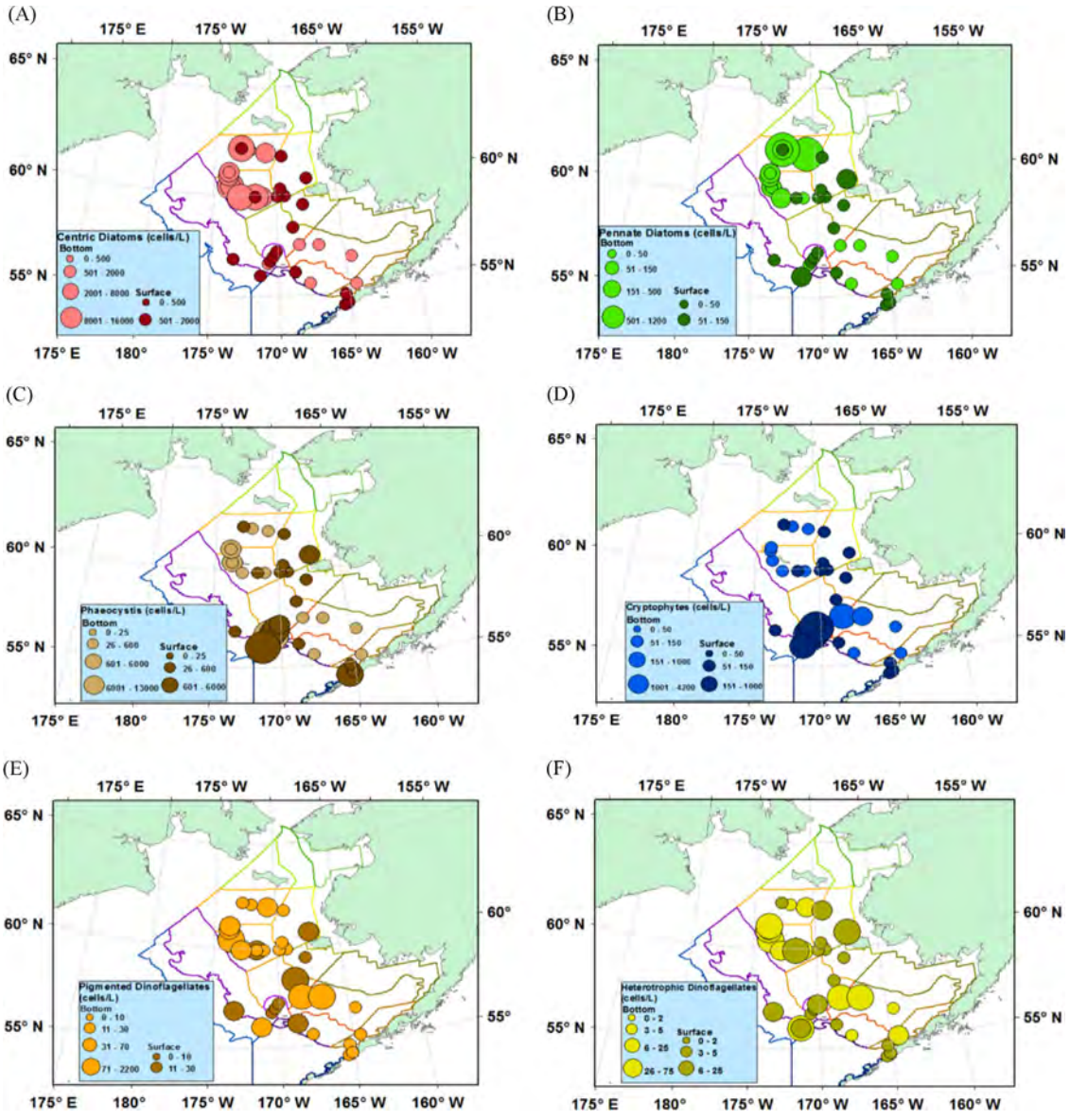

Fig. 13. Spatial patterns of (A) centric diatoms, (B) pennate diatoms, (C) *Phaeocystis*, (D) cryptophytes, (E) pigmented dinoflagellates and (F) heterotrophic dinoflagellates determined microscopically in samples from the surface and from the deep chlorophyll maxima (bottom). All values have been expressed as cells l^{-1}.

which we did not enumerate in this study. Although river discharge into the Bering Sea is associated with moderate nutrient concentrations (Guo et al., 2004), its influence offshore on phytoplankton biomass could be important in summer, when the inner shelf waters are highly nutrient deficient. Away from the coast, the low salinity waters were confined to an isolated cold patch, suggesting that the origin of this water was possibly from sea-ice melt. Moderately high phytoplankton Chl *a* and cell counts associated with this entrapped water parcel were likely the result of enhanced stability afforded by these waters to phytoplankton allowing them to remain in the upper well lit water column. Fv/Fm values recorded in these waters were quite high, evidence that phytoplankton within this water parcel were photosynthetically active, consistent with observations of higher growth rates observed by Stoecker et al. (2014). One possibility is that phytoplankton were benefiting from potentially elevated levels of iron and nutrients known to be released during sea-ice melt back (Aguilar-Islas et al., 2008). A little further offshore the haptophytes, *P. pouchetii* and some cryptophytes made up for a large fraction of the total Chl *a* biomass, possibly because these species were able to function better under the low nutrient conditions at the sea surface or they (in particular *P. pouchetii*) were not the preferred food source for micrograzers.

The other two regions where phytoplankton concentrations were moderately higher than elsewhere on the shelf were the PB, the Alaskan Peninsula (AKP) and the SMS, where there was evidence of cross-shelf advection of nutrients. As is typical in summer, the entire eastern Bering Sea shelf resembled a classical nitrate-limited, iron-replete system in which phytoplankton can be easily stimulated by an influx of new nutrients (Aguilar-Islas et al., 2007). This was evident from the low Fv/Fm over the entire southern and middle shelf region as well as from our on-board nutrient amendment experiments with shelf waters where a >3-fold increase in Chl *a* was observed within 3 days of inorganic NO3 (2.7 μM) additions (Fig. 16A). Offshore, particularly in the northern outer shelf (NOS) region, although inorganic NO_3 concentrations were not limiting (NO_3 ~3.5 μM), Chl *a* concentrations were very low possibly due to iron limitation. The low Fv/Fm values recorded suggested that these were high nutrient low chlorophyll (HNLC) waters, in which phytoplankton photosynthesis and growth were iron limited.

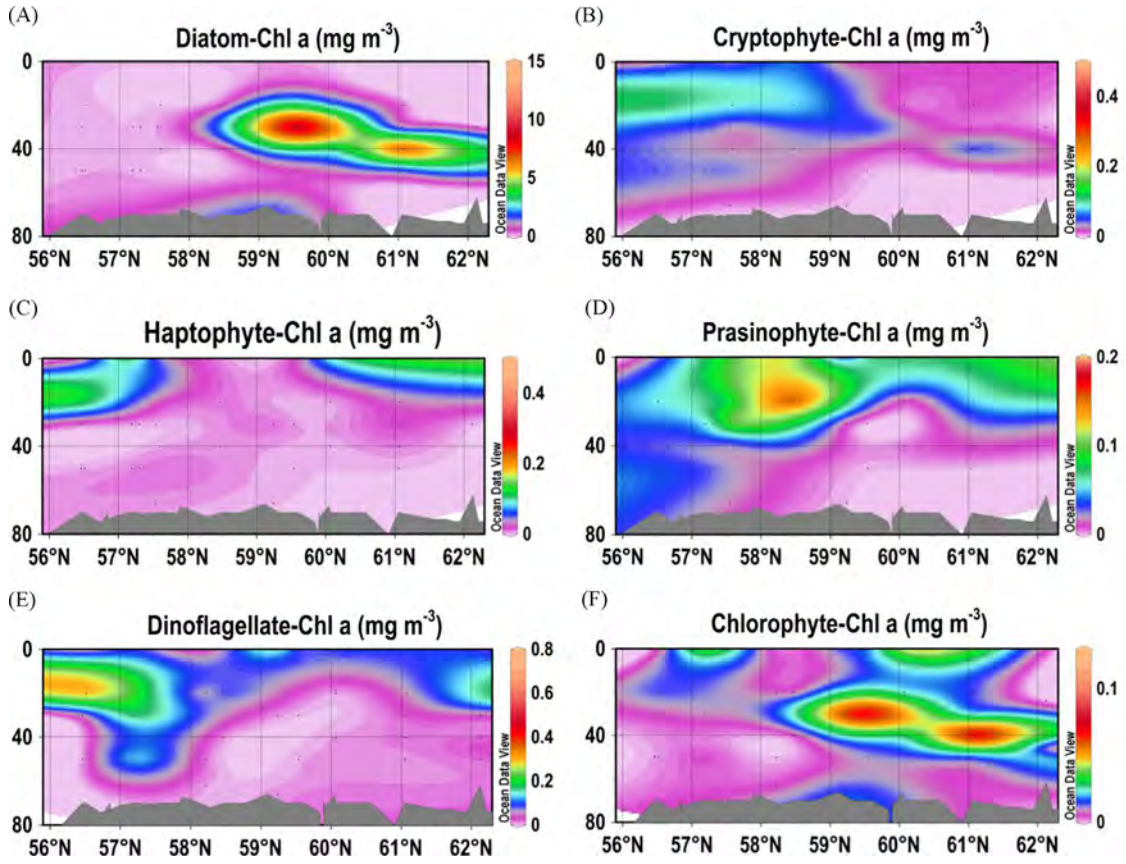

Fig. 14. Vertical sections of HPLC/CHEMTAX derived biomass attributable to (A) diatoms, (B) cryptophytes, (C) haptophytes, (D) prasinophytes, (E) dinoflagellates and (F) chlorophytes along the 70 m isobath.

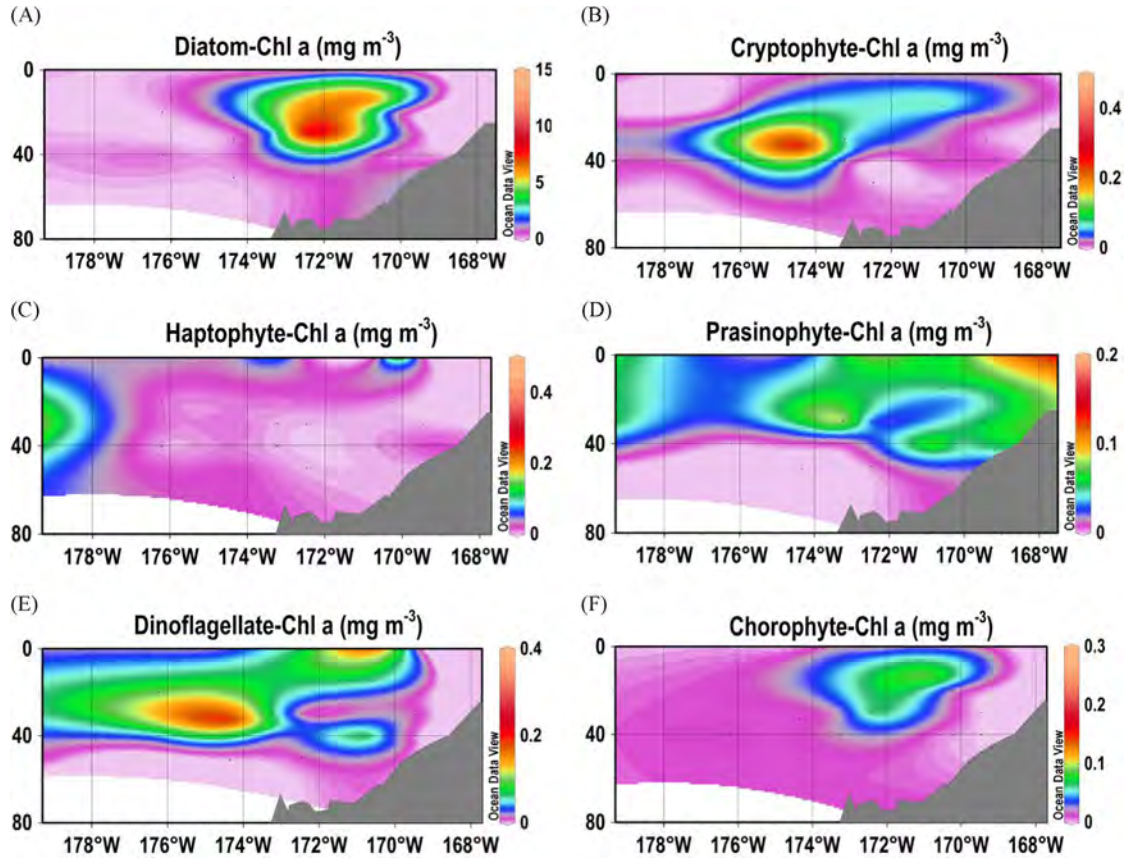

Fig. 15. Vertical sections of HPLC/CHEMTAX derived biomass attributable to (A) diatoms, (B) cryptophytes, (C) haptophytes, (D) prasinophytes, (E) dinoflagellates and (F) chlorophytes along the MN line.

Table 1
List of phytoplankton species observed in the eastern Bering Sea during the summer of 2008.

Centric diatoms
Attheya septentrionalis
Bacterosira sp.
Bacterosira bathyomphala
Biddulphia sp.
Chaetoceros compressus
C. concavicornis
C. constrictus
C. convolutus
C. curvisetus
C. laciniosus
C. septentrionalis
C. socialis
C. subtilis var. *abnormis*
Chaetoceros spp.
Corethron criophilum
Coscinodiscus sp.
Lauderia spp.
Leptocylindrus danicus
Melosira sp.
Paralia sulcata
Porosira glacialis
Proboscia alata
Rhizosolenia hebetata var semispina
T. anguste-lineata
T. nordenskioeldii
Thalassiosira spp.
Unidentified centric diatoms

Pennate diatoms
Fragilariopsis sp.
Gyrosigma fasciola
Navicula cf *bicapitata*
Navicula cf *distans*
Navicula sp.
Navicula sp.
Nitzschia closterium
Pleurosigma sp.
Pseudo-nitzschia spp.
Thalassionema nitzschoides
Tropidoneis sp.
Unidentified pennate diatom

Heterotrophic dinoflagellates
Gyrodinium spp.
Protoperidinium bipes
Protoperidinium spp.
Torodinium sp.
Unidentified heterotrophic dinoflagellates

Phototrophic dinoflagellates
Amphidinium sp.
Dinophysis acuta
Dinophysis rotundata
Gymnodinium spp.
Heterocapsa triquetra
Oxytoxum sp.
Prorocentrum minimum
Protoperidinium minuscula
Unidentified dinoflagellate

Cryptophytes
Unidentified

Chrysophyte
Dinobryon balticum

Euglenophyte
Eutreptia sp.

Haptophytes
Phaeocystis pouchetii

Silicoflagellate
Dictyocha speculum
Mesodinium sp.
Unidentified coccoids
Unidentified phytoflagellates
Unidentified cyanobacterial filaments
cf. *Tribonema* sp.

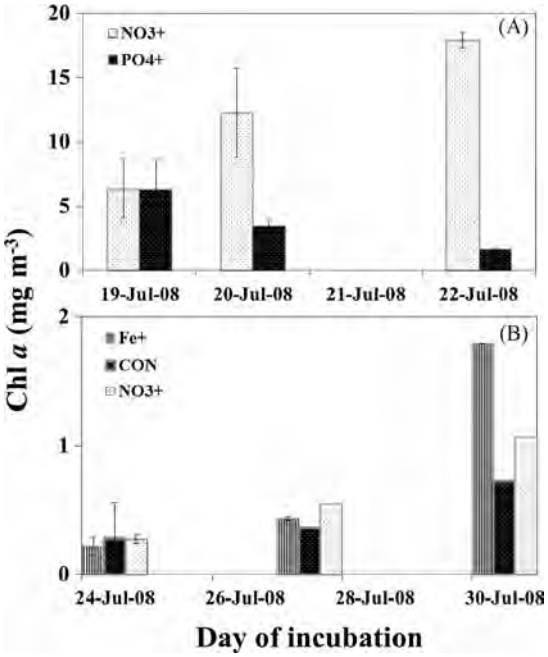

Fig. 16. Results of inorganic nutrient and dissolved iron experiments showing changes in Chl *a* at (A) on shelf station NP-11 and (B) at the outer shelf station St. P14-4.

Dissolved iron amendment experiments (Fig. 16B) revealed an 8-fold increase in Chl *a* by Day 6 consistent with the previous suggestions (Aguilar-Islas et al., 2007) of iron-limitation in the outer shelf waters of the Bering Sea. No such increase was observed in incubation bags amended with inorganic NO_3.

Diatoms, haptophytes, cryptophytes and prasinophytes made up a large portion of the population at the surface, but haptophytes were conspicuously absent at depth. They were also absent at the surface around PB, where diatoms dominated in all possibility due to increased sedimentary iron mobilization from the shallow shelf (Aguilar-Islas, et al., 2007). Notably Fv/Fm values and phytoplankton growth rates were higher here (Stoecker et al., 2014).

Chlorophyll *a* concentrations both at the surface and at depth were highest in the Green Belt which extended from across the entire shelf break region and into the off-shelf north (OSN) regions in association with the north-westward moving Bering Shelf current (Wang et al., 2012). Several studies (Mizobata and Saitoh, 2004; Okkonen et al., 2004) have shown that the high biomass of the Green Belt is sustained by eddies that promote cross shelf advective mixing of waters from the offshore region into the outer shelf domains. In summer, in particular, eddies tend to propagate north-westward along the shelf edge. As they are anticyclonic (Mizobata and Saitoh, 2004; Okkonen et al., 2004) they carry with them nutrient-rich upwelled water around their periphery (Mizobata et al., 2006). When cross-shelf advection due to eddies is strong, it can lead to an increase in the width of the Green Belt (Okkonen et al., 2004). Microscopic and pigment measurements, indicate the overall dominance of *P. pouchetii* in the Green Belt, observations similar to those of Springer et al. (1996) and Suzuki et al. (2002). Goering and Iverson (1981) and Flint et al. (2002) suggest that the dominance of *P. pouchetii* in the outer shelf and shelf-edge region is the result of a top-down effect in which the abundance of diatoms is controlled by preferential grazing on diatoms by herbivorous mesozooplankton. Primary productivity in the Green Belt was extremely high during the summer of 2008 (Lomas et al., 2012) but concomitant export fluxes measured using floating sediment traps (Moran et al., 2012) indicated low e-ratios

in the Green Belt as compared to the mid-shelf region. The role of *P. pouchetii* in the primary production budget and food web of the Green Belt thus remains unclear. It has been suggested that *P. pouchetii* blooms might support a greater development of microbial food webs and nutrient recycling. In general, gelatinous colonies of *Phaeocystis* spp. are not efficiently grazed by zooplankton and have slow sinking rates, (Springer et al., 1996; Nejstgaard et al., 2007). By providing substrates for the development of bacteria and heterotrophic nanoplankton, their major contribution would be sustenance of an active microbial food web in the shelf break region of the Bering Sea.

The Cold Pool in the middle shelf during our study and the warmer surface layer contributed to the development of a strong pycnocline that separated a pool of nutrient-rich water at depth from the otherwise nutrient depleted surface waters above.

In summer the layer below the pycnocline can become an important source of nutrients when they are introduced into surface shelf waters by post-spring bloom storms (Sambrotto et al., 1986; Stabeno et al., 2002) or by frontal processes (Kachel et al., 2002). Summer concentrations of nutrients within this pool depend on nutrient utilization especially at depth, when the spring bloom begins to form (Stockwell et al., 2001). A nutrient-depleted subsurface pool can result when considerable new production occurs at depth during the spring (Stockwell et al., 2001). Nutrient distribution patterns along the 70 m isobath showed that there was substantial nutrient depletion at depth between 58° and 60°N. North of this region, stratification resulting from the late retreat of sea-ice, coupled with an absence of strong winds, isolated the Cold Pool before nutrients could be utilized. With the freshly sinking bloom straddling its surface, it appears that the Cold Pool acts as a barrier for the sinking material, preventing it from reaching the bottom where it can be available for benthic organisms. During cold summers devoid of energetic storms like the summer that we encountered, we hypothesize that the Cold Pool reduces carbon export to depth, instead making it more accessible to pelagic organisms rather than benthic organisms. This idea is consistent with the observations of Coyle et al. (2011), Hunt et al. (2008), Lomas et al. (2012) and Stabeno et al. (2012a,b) who cite an increase in numbers of the largest copepod *Calanus marshallae* (a vital food source for commercially important fisheries of the Bering Sea) in the middle shelf during the cold years of 2008 and 2009 that followed the warm spell in the Bering Sea.

Based on the hydrographic and the chemical measurements, we suggest that the Cold Pool together with freshwater from sea-ice melt and from coastal riverine discharge together, obstruct cross shelf advection of offshore water on to the shelf, effectively isolating surface waters of the northern Bering Sea shelf, and preventing replenishment with new nutrients. The paucity of nutrients in the upper layer of the two layered middle shelf waters was in all likelihood responsible for the termination of the diatom bloom. The presence of cryptophytes and chlorophytes in the sinking bloom and the relative increase in prasinophytes at the sea surface suggest a pattern of succession of phytoplankton that is consistent with a transition from colder nutrient rich waters to warmer nutrient impoverished waters (Baduini et al., 2001; Stockwell et al., 2001). In general, nutrient poor waters at the surface were associated with cryptophytes, haptophytes and prasinophytes which accounted for a significant fraction of the low phytoplankton biomass.

5. Conclusions

In summer, the eastern Bering Sea shelf is a classic high iron low nutrient region which is not capable of supporting active phytoplankton growth. The Green Belt in contrast was richer and its higher biomass was made up largely of *P. pouchetii* and cryptophytes whose presence could have been aided by preferential grazing on diatoms, and whose sustained growth was most likely supported by eddy-driven upwelling of new nutrients. These populations were however photo-physiologically stressed possibly due to iron limitation. In the middle shelf, diatoms which made up for a large fraction of phytoplankton in subsurface waters appeared to be remnants of the spring bloom. The presence of the sinking diatom bloom right above the Cold Pool leads us to suggest, that this hydrographic feature when present, is an impediment for the transfer of organic matter to the benthic community. We posit that if the Cold Pool is not eroded by summer storms, its major ecological role is that it serves as a conduit for the transfer of organic matter to pelagic communities.

Acknowledgments

This study is being funded by NASA grants NNX11AP28G and NNX10AP10G. We are grateful to the National Science Foundation and to the North Pacific Research Board for permission to join the BEST/BSIERP multi-disciplinary cruises. Hydrological and chemical data utilized in this study was collected by NOAA, PMEL. We are especially grateful to William Floering of the NOAA, Pacific Marine Environmental Laboratory and to Calvin Mordy of the Joint Institute for the Study of the Atmosphere, University of Washington for their help during the cruise. This is BEST-BSIERP Bering Sea Project publication number 119 and Lamont Doherty Earth Observatory, Columbia University publication number 7752.

References

Aagaard, K., Coachman, L.K., Carmack, E., 1981. On the halocline of the Arctic Ocean. Deep Sea Res. I 28, 529–545.
Aguilar-Islas, A.M., Rember, R., Mordy, C.W., Wu., J., 2008. Sea-ice-derived dissolved iron and its potential influence on the spring algal bloom in the Bering Sea. Geophys. Res. Lett. 35, L24601.
Aguilar-Islas, A.M., Hurst, M.P., Buck, K.N., Sohst, B., Smith, G.J., Lohan, M.C., Bruland, K.W., 2007. Micro- and macronutrients in the southeastern Bering Sea: insight into iron- replete and iron-depleted regimes. Progr. Oceanogr. 73, 99–126.
Baduini, C.L., Hyrenbach, K.D., Coyle, K.O., Pinchuk, A., Mendenhall, V., Hunt, G.L., 2001. Mass mortality of short-tailed shearwaters in the south-eastern Bering Sea during summer 1997. Fish. Oceanogr. 10, 117–130.
Booth, B.C., 1993. Estimating cell concentration and biomass of autotrophic plankton using microscopy. In: Kemp, P.F., Sherr, B.F., Sherr, E.B., Cole, J.J. (Eds.), Handbook of Methods in Aquatic Microbial Ecology. Lewis Publ., Boca Raton, pp. 199–205.
Broerse, A.T.C., Tyrrell, T., Young, J.R., Poulton, A.J., Merico, A., Balch, W.M., Miller, P.I., 2003. The cause of bright waters in the Bering Sea in winter. Cont. Shelf Res. 23, 1579–1596.
Chekalyuk, A., Hafez, M.A., 2008. Advanced laser fluorometry of natural aquatic environments. Limnol. Oceanogr. Methods 6, 591.
Chekalyuk, A., Hafez, M.A., 2011. Photo-physiological variability in phytoplankton chlorophyll fluorescence and assessment of chlorophyll concentration. Opt. Exp. 19, 22643–22658.
Chekalyuk, A.M., Landry, M.R., Goericke, R., Taylor, A.G., Hafez, M.A., 2012. Laser fluorescence analysis of phytoplankton across a frontal zone in the California Current ecosystem. J. Plankton Res. 34, 761–777.
Ciannelli, L., Bailey, K.M., 2005. Landscape dynamics and resulting species interactions: The cod-capelin system in the southeastern Bering Sea. Mar. Ecol. Progr. Ser. 291, 227–236.
Coachman, L.K., 1986. Circulation, water masses, and fluxes on the southeastern Bering Sea shelf. Cont. Shelf Res. 5, 23–108.
Coyle, K.O., Eisner, L.B., Mueter, F.J., Pinchuk, A.I., Janout, M.A., Cieciel, K.D., Farley, E. V., Andrews, A.G., 2011. Climate change in the southeastern Bering Sea: impacts on pollock stocks and implications for the oscillating control hypothesis. Fish. Oceanogr. 20, 139–156.
Cross, J.N., Mathis, J.T., Bates, N.R., 2012. Hydrographic controls on net community production and total organic carbon distributions in the eastern Bering Sea. Deep Sea Res. II, 98–109.
Egge, J.K., Aksnes, D.L., 1992. Silicate as regulating nutrient in phytoplankton competition. Mar. Ecol. Prog. Ser. 83, 281–289.
Flint, M.V., Sukhanova, I.N., Kopylov, A.I., Poyarkov, S.G., Whitledge, T.E., 2002. Plankton distribution associated with frontal zones in the vicinity of the Pribilof Islands. Deep Sea Res. II 49, 6069–6093.

Goering, J.J., Iverson, R.L., 1981. Phytoplankton distribution on the southeastern Bering Sea shelf. East. Bering Sea Shelf Oceanogr. Resources 2, 933–946.
Goes, J.I., Gomes, H.R. Chekalyuk, A., Carpenter, E.J., Montoya, J.P., Coles, V.J., Yager, P.L., Berelson, W.M., Capone, D., Foster, R.A., Steinberg, D.K., Hafez, M. Influence of the Amazon River discharge on the biogeography of phytoplankton communities in the western tropical north Atlantic Ocean. Prog. Oceanogr., http://dx.doi.org/10.1016/j.pocean.2013.07.010, in press.
Gordon, L.I., Joe, C. Jennings, J., Ross, A.A., Krest, J.M., 1993. A suggested protocol for continuous flow automated analysis of seawater nutrients (phosphate, nitrate, nitrite and silicic acid) in the WOCE Hydrographic Program and the Joint Global Ocean Fluxes Study. In: WOCE Operations Manual, Vol. 3: The Observational Program, Section 3.2: WOCE Hydrographic Programme, Part 3.1.3: WHP Operations and Methods. WHP Office Report WHPO 91-1; WOCE Report No. 68/91, November 1994, Revision 1, Woods Hole, MA, USA, 52.
Guo, L., Tanaka, T., Wang, D., Tanaka, N., Murata, A., 2004. Distributions, speciation and stable isotope composition of organic matter in the southeastern Bering Sea. Mar. Chem. 91, 211–226.
Higgins, H.W., Wright, S.W., Schlüter, L., 2011. Quantitative interpretation of chemotaxonomic pigment data. In: Roy, S., Llewellyn, C.A., Johnsen, G., Egeland, E.S. (Eds.), Phytoplankton Pigments in Oceanography, Cambridge University Press, Cambridge, UK, pp. 257–301.
Hooker, S.B., Heukelem, L.V., Thomas, C.S., Claustre, H., Ras, J., Barlow, R., Sessions, H., Schluter, L., Perl, J., Trees, C., Stuart, V., Head, E., Clementson, L., Fishwick, J., Llewellyn, C., Aiken, J., 2005. The Second SeaWiFS HPLC Analysis Round Robin Experiment (SeaHARRE-2), NASA TM/2005-212785. NASA Goddard Space Flight Center, Greenbelt, MD.
Hunt, G.L., Stabeno, P.J., Strom, S., Napp, J.M., 2008. Patterns of spatial and temporal variation in the marine ecosystem of the southeastern Bering Sea, with special reference to the Pribilof Domain. Deep Sea Res. II 55, 1919–1944.
Hunt, G.L., Coyle, K.O., Eisner, L.B., Farley, E.V., Heintz, R.A., Mueter, F., Napp, J.M., Overland, J.E., Ressler, P.H., Salo, S., Stabeno, P.J., 2011. Climate impacts on eastern Bering Sea foodwebs: a synthesis of new data and an assessment of the Oscillating Control Hypothesis. ICES. J. Mar. Sci. J. Cons. 68, 1230–1243.
Kachel, N.B., Hunt Jr, G.L., Salo, S.A., Schumacher, J.D., Stabeno, P.J., Whitledge, T.E., 2002. Characteristics and variability of the inner front of the southeastern Bering Sea. Deep Sea Res. II 49, 5889–5909.
Knap, A., Michaels, A., Close, A., Ducklow, H., Dickson, A., 1994. Protocols for the Joint Global Ocean Flux Study (JGOFS) Core Measurements. JGOFS Report 19, p. 170.
Kotwicki, S., Buckley, T.W., Honkalehto, T., Walters, G., 2005. Variation in the distribution of walleye pollock (*Theragra chalcogramma*) with temperature and implications for seasonal migration. Fish. Bull. 103, 574–587.
Ladd, C., Stabeno, P.J., 2012. Stratification on the Eastern Bering Sea shelf revisited. Deep Sea Res. II 65–70, 72–83.
Lomas, M.W., Moran, S.B., Casey, J.R., Bell, D.W., Tiahlo, M., Whitefield, J., Kelly, R.P., Mathis, J.T., Cokelet, E.D., 2012. Spatial and seasonal variability of primary production on the Eastern Bering Sea shelf. Deep Sea Res., 126–140.
MacIssac, E.A., Stockner, J.G., 1993. Enumeration of phototrophic picoplankton by autofluorescence microscopy. In: Kemp, P.F., Cole, J.J., Sherr, B.F., Sherr, E.B. (Eds.), Handbook of Methodology in Aquatic Microbial Ecology. Lewis Publishers, Boca Raton, Florida, USA, pp. 187–197.
Mackey, D.J., Higgins, H.W., Mackey, M.D., Holdsworth, D., 1998. Algal class abundances in the western equatorial Pacific: estimation from HPLC measurements of chloroplast pigments using CHEMTAX. Deep Sea Res. I 45, 1441–1468.
Mackey, M.D., Mackey, D.J., Higgins, H.W., Wright, S.W., 1996. CHEMTAX – a program for estimating class abundances from chemical markers: application to HPLC measurements of phytoplankton. Mar. Ecol. Prog. Ser. 144, 265–283.
Mizobata, K., Saitoh, S., 2004. Variability of Bering Sea eddies and primary productivity along the shelf edge during 1998–2000 using satellite multisensor remote sensing. J. Mar. Syst. 50, 101–111.
Mizobata, K., Wang, J., Saitoh, S., 2006. Eddy-induced cross-slope exchange maintaining summer high productivity of the Bering Sea shelf break. J. Geophys. Res. 111, C10017.
Moran, S.B., Lomas, M.W., Kelly, R.P., Gradinger, R., Iken, K., Mathis, J.T., 2012. Seasonal succession of net primary productivity, particulate organic carbon export, and autotrophic community composition in the eastern Bering Sea. Deep Sea Res. II 65, 84–97.
Naik, P., D'Sa, E.J., Goes, J.I., Gomes, H.R., 2010. Assessment of particulate absorption properties in the southeastern Bering Sea from in-situ and remote sensing data. J. Appl. Remote Sens. 4, 043561.
Nejstgaard, J.C., Tang, K.W., Steinke, M., Dutz, J., Koski, M., Antajan, E., Long, J.D., 2007. Zooplankton grazing on *Phaeocystis*: a quantitative review and future challenges. Biogeochemistry 83, 147–172.
NOAA, 2013. Fisheries of the United States of 2012. In: Lowther, A. (Ed.), National Marine Fisheries Service, Office of Science and Technology. Silver Spring, Maryland, USA, p. 129.
Okkonen, S.R., Schmidt, G.M., Cokelet, E.D., Stabeno, P.J., 2004. Satellite and hydrographic observations of the Bering Sea 'Green Belt'. Deep Sea Res. II 51, 1033–1051.
Ortiz, I., Weise, F., Greig, A., 2012. Marine Regions Boundary Data for the Bering Sea Shelf and Slope. UCAR/NCAR – EOL/Computing, Data, and Software Facility. 10.5065/D6DF6P6C.
Overland, J.E., Salo, S., Adams, J.M., 1999. Salinity signature of the Pacific Decadal Oscillation. Geophys. Res. Lett. 26, 1337–1340.
Overland, J.E., Stabeno, P.J., 2004. Is the climate of the Bering Sea warming and affecting the ecosystem. Eos Trans. AGU 85, 309.
Overland, J.E., Wang, M., Wood, K.R., Percival, D.B., Bond, N.A., 2012. Recent Bering Sea warm and cold events in a 95-year context. Deep Sea Res. II 65–70, 6–13.
Rho, T., Whitledge, T.E., Goering, J.J., 2005. Interannual variations of nutrients and primary production over the southeastern Bering Sea shelf during the spring of 1997, 1998, and 1999. Oceanology 45 (376-390), 376–390.
Sambrotto, R.N., Niebauer, H.J., Goering, J.J., Iverson, R.L., 1986. Relationships among vertical mixing, nitrate uptake, and phytoplankton growth during the spring bloom in the southeast Bering Sea middle shelf. Cont. Shelf Res. 5, 161–198.
Springer, A.M., McRoy, C.P., Flint, M.V., 1996. The Bering Sea Green Belt: shelf-edge processes and ecosystem production. Fish. Oceanogr. 5, 205–223.
Stabeno, P.J., Kachel, N.B., Sullivan, M., Whitledge, T.E., 2002. Variability of physical and chemical characteristics along the 70-m isobath of the southeastern Bering Sea. Deep Sea Res. II 49, 5931–5943.
Stabeno, P.J., Bond, N.A., Salo, S.A., 2007. On the recent warming of the southeastern Bering Sea shelf. Deep-Sea Res. II 54, 2599–2618.
Stabeno, P., Napp, J., Mordy, C., Whitledge, T., 2010. Factors influencing physical structure and lower trophic levels of the eastern Bering Sea shelf in 2005: Sea-ice, tides and winds. Prog. Oceanogr. 85, 180–196.
Stabeno, P.J., Bond, N.A., Kachel, N.B., Salo, S.A., Schumacher, J.D., 2001. On the temporal variability of the physical environment over the south-eastern Bering Sea. Fish. Oceanogr. 10, 81–98.
Stabeno, P.J., Farley Jr, E.V., Kachel, N.B., Moore, S., Mordy, C.W., Napp, J.M., Overland, J.E., Pinchuk, A.I., Sigler, M.F., 2012a. A comparison of the physics of the northern and southern shelves of the eastern Bering Sea and some implications for the ecosystem. Deep Sea Res. II 65–70, 14–30.
Stabeno, P.J., Kachel, N.B., Moore, S.E., Napp, J.M., Sigler, M., Yamaguchi, A., Zerbini, A.N., 2012b. Comparison of warm and cold years on the southeastern Bering Sea shelf and some implications for the ecosystem. Deep Sea Res. II 65–70, 31–45.
Stabeno, P.J., Overland, J.E., 2001. Bering Sea shifts toward an earlier spring transition. Eos Trans. AGU, 82; , pp. 317–321.
Stockwell, D.A., Whitledge, T.E., Zeeman, S.I., Coyle, K.O., Napp, J.M., Brodeur, R.D., Pinchuk, A.I., Hunt, G.L., 2001. Anomalous conditions in the south-eastern Bering Sea, 1997: nutrients, phytoplankton and zooplankton. Fish. Oceanogr. 10, 99–116.
Stoecker, D., Weigel, A., Goes, J.I., 2014. Microzooplankton grazing in the eastern Bering Sea in summer. Deep Sea Res. II 109, 145–156, http://dx.doi.org/10.1016/j.dsr2.2013.09.017.
Sullivan, M.E., Kachel, N.B., Mordy, C.W., Stabeno, P.J., 2008. The Pribilof Islands: temperature, salinity and nitrate during summer 2004. Deep Sea Res. II 55, 1729–1737.
Suzuki, K., Minami, C., Liu, H., Saino, T., 2002. Temporal and spatial patterns of chemotaxonomic algal pigments in the subarctic Pacific and the Bering Sea during the early summer of 1999. Deep Sea Res. II 49, 5685–5704.
Tomas, C.R., 1997. Identifying Marine Phytoplankton. Academic Press, New York.
Van Heukelem, L., Thomas, C.S., 2001. Computer-assisted high-performance liquid chromatography method development with applications to the isolation and analysis of phytoplankton pigments. J. Chromatogr. A 910, 31–49.
Wang, M., Overland, J.E., Stabeno, P., 2012. Future climate of the Bering and Chukchi Seas projected by global climate models. Deep Sea Res. II 65–70, 46–57.
Whitledge, T.E., Reeburgh, W.S., Walsh, J.J., 1986. Seasonal inorganic nitrogen distributions and dynamics in the southeastern Bering Sea. Cont. Shelf Res. 5, 109–132.
Woodgate, R.A., Aagaard, K., Weingartner, T.J., 2005. Monthly temperature, salinity, and transport variability of the Bering Strait through flow. Geophys. Res. Lett. 32, L04601.
Zhang, J., Woodgate, R., Mangiameli, S., 2012. Towards seasonal prediction of the distribution and extent of cold bottom waters on the Bering Sea shelf. Deep Sea Res. II 65–70, 58–71.

Deep-Sea Research II 109 (2014) 100–111

Contents lists available at ScienceDirect

Deep-Sea Research II

journal homepage: www.elsevier.com/locate/dsr2

Elevated $^{15}N/^{14}N$ in particulate organic matter, zooplankton, and diatom frustule-bound nitrogen in the ice-covered water column of the Bering Sea eastern shelf

Laura V. Morales [a,*,1], Julie Granger [a,2], Bonnie X. Chang [a], Maria G. Prokopenko [b], Birgit Plessen [c], Rolf Gradinger [d], Daniel M. Sigman [a]

[a] Geosciences Department, Princeton University, Guyot Hall, Washington Road, Princeton, NJ 08544, USA
[b] Department of Earth Sciences, University of Southern California, 3651 Trousdale Parkway, Los Angeles, CA 90089-0704, USA
[c] Geoforschungszentrum Potsdam, Telegrafenberg, C 327, Potsdam D-14473, Germany
[d] University of Alaska Fairbanks, School of Fisheries and Ocean Sciences, 245 O'Neill Building, Fairbanks, AK 99775, USA

ARTICLE INFO

Available online 20 May 2014

Keywords:
Nitrogen isotopes
Particulate organic matter
Diatom-bound N
Zooplankton
Ammonium
Sea ice
Bering Sea shelf
Trophic

ABSTRACT

We conducted a survey of the natural abundance $^{15}N/^{14}N$ ratio ($\delta^{15}N$) of particulate organic matter (POM), diatom frustule-bound nitrogen ($\delta^{15}N_{DB}$), and zooplankton from water column material collected with net tows across the eastern Bering Sea shelf in late winter of 2007 and 2008, to investigate the N dynamics of primary and secondary production in relation to the presence of seasonal sea ice. The data reveal a pattern of increasing $\delta^{15}N$ northward and eastward (POM: 2.1–14.7‰; frustule-bound N: 4.9–20.7‰; zooplankton: 6.4–18.0‰), with POM $\delta^{15}N$ reaching ~9‰ higher than that of water-column nitrate. Higher $\delta^{15}N$ in each of these plankton fractions was largely associated with stations covered by sea ice. POM $\delta^{15}N$ collected concurrently from within sea ice was not sufficiently ^{15}N-enriched to explain the elevated water-column values. Rather, the $\delta^{15}N$ of water-column POM under sea ice appears to derive from the assimilation of ammonium released from shelf sediments. Water-column ammonium $\delta^{15}N$ was between 28‰ and 63‰, most likely due to partial nitrification in the sediment and overlying water column. The high $\delta^{15}N$ of this ammonium is effectively transmitted to phytoplankton under sea ice because light limitation from the ice cover delays the springtime nitrate assimilation that yields algal biomass with a lower $\delta^{15}N$. Despite this seasonal explanation, published $\delta^{15}N$ data from sediment traps, summertime zooplankton, and surface sediment indicate that a shoreward and northward $\delta^{15}N$ increase – albeit of a weaker magnitude – is perennial, suggesting that the $\delta^{15}N$ of the total annual fixed N supply (including both ammonium and nitrate) also increases shoreward and northward. This requires that the partial nitrification of ammonium underlying the spatial pattern in $\delta^{15}N$ is at least partly coupled to denitrification in the sediments that preferentially removes ^{14}N, causing the total fixed N reservoir on the shelf to evolve toward higher $\delta^{15}N$. Shelf geometry and the consequent benthic–pelagic coupling of N cycling thus seem to underlie the spatial pattern in the mean annual $\delta^{15}N$ of plankton, while sea-ice cover causes the high $\delta^{15}N$ of ammonium on the shelf to be most strongly reflected by the production occurring in the winter and early spring. Our results provide a basis for tracing the geographic and seasonal origins and trophic transfer of N in the Bering shelf ecosystem.

1. Introduction

The continental shelf region accounts for 50% of the Bering Sea's area and an even greater proportion of the region's annual primary production (Springer et al., 1996; Rho and Whitledge, 2007). Phytoplankton blooms occurring in late spring/early summer under open water conditions comprise the bulk of primary production over the eastern shelf region (Rho and Whitledge, 2007). This springtime production is dependent on an annual cycle of consumption and subsequent replenishment of nutrients available in the shelf water column.

* Corresponding author. Tel.: +1 530 752 2667.
E-mail addresses: lvmorales@ucdavis.edu (L.V. Morales), julie.granger@uconn.edu (J. Granger), bonniec@princeton.edu (B.X. Chang), prokopen@usc.edu (M.G. Prokopenko), birgit.plessen@gfz-potsdam.de (B. Plessen), rrgradinger@alaska.edu (R. Gradinger), sigman@princeton.edu (D.M. Sigman).
[1] Present address: Plant Sciences, Mail Stop-1, University of California, Davis, CA 95616, USA.
[2] Present address: Department of Marine Sciences, University of Connecticut, 1080 Shennecossett Road, Groton, CT 06340, USA.

http://dx.doi.org/10.1016/j.dsr2.2014.05.008
0967-0645/

Nitrate is the dominant N species in winter shelf waters (e.g., Granger et al., 2011), and is responsible for fueling most of the spring production. Spring phytoplankton growth depletes nitrate from the mixed layer of the eastern Bering shelf, and new inorganic nitrogen is only occasionally brought to the surface by rare summer storms (Sambrotto et al., 1986; Walsh and McRoy, 1986; Whitledge et al., 1986). Nutrient recharge of surface shelf waters starts in fall and peaks in winter (Whitledge et al., 1986), when effective horizontal and vertical transport of nutrients across the southeastern shelf is possible due to the weakening of hydrographic fronts, elimination of vertical stratification of the water column, and increasing wind strength (Coachman, 1986; Stabeno et al., 2002).

Two sources resupply inorganic nitrogen to the shelf surface waters: (1) nitrate-rich waters from the open Bering basin and (2) nitrogen (ammonia and nitrate) remobilized from shelf sediments. Nitrate-laden water from the Bering basin is transported shoreward across the shelf break along the base of the water column (Coachman and Walsh, 1981; Coachman, 1986; Stabeno et al., 2002). Wind and tidal mixing vertically redistribute this nutrient-rich water to the surface. Although off-shelf exchange appears to be the main form of nutrient recharge on the shelf, it is believed that the influence of this horizontal nutrient transport diminishes rapidly away from the shelf break (Coachman and Walsh, 1981; Coachman, 1986). Instead, nitrogen remobilized (both as nitrate and ammonium) and vertically redistributed directly from the shelf sediments appears to be more important for nutrient recharge on the inner and middle shelf areas (Whitledge et al., 1986; Rowe and Phoel, 1992; Granger et al., 2011, 2013).

Although the bulk of primary production occurs in spring, algae remain active on the shelf during winter. However, we know little about the nutrient consumption of primary producers outside of the late spring and summer productive seasons. Conditions for algal growth in winter are very different from those in other seasons, not only because nutrients are more abundant and light is less available but also because a large expanse of the inner (depth: 0–50 m) and middle (depth: 50–100 m) shelf and parts of the outer (depth:100 − ~200 m) shelf experience ice cover for a significant time period. Starting in fall, ice moves from the northern shelf polynyas and accumulates as far south as 54–56°N in February–March before starting its northward retreat (Stabeno et al., 2007a). The sea ice cover alters the salinity, temperature, nutrient distribution (Stabeno et al., 2010, 2012) and availability of light to primary producers (Gradinger, 2009; Lee et al., 2010), creating a growth environment for phytoplankton distinct from that of open water regions of the shelf.

The sea ice environment provides three potential habitats for winter algal growth: (1) the under-ice water column, (2) the bottom surface of the ice floes (Horner, 1985; Sukhanova et al., 1999), and (3) the interstitial spaces and brine channels within the ice column (Gradinger, 1999; Mock and Gradinger, 1999). Access to nutrients and light varies among these three habitats, best summarized as a gradient of potentially reduced nutrient availability but increased light levels upwards from the water column to the ice surface. Phytoplankton growing in the ice-covered water column have access to ambient inorganic water column nutrient pools, but experience significantly lower light levels than those in open-water conditions (Gradinger, 2009). Algae using the bottom of the ice as a growth substrate are protected from being mixed out of the euphotic zone and can benefit from increased light exposure while still accessing water column nutrients. However, boundary layer conditions at the ice surface potentially restrict access to nutrients by bottom-ice algae. Algae growing within the interstitial spaces of the ice column may benefit from the greatest light exposure, but they depend on nutrients incorporated during ice formation and occasionally imported from the water column such as during brine convective events (Notz and Worster, 2009).

The unique growth environments created by the sea ice are likely to have notable effects on the nutrient consumption dynamics and, consequently, on the C and N isotopic composition of organic matter originating from algal production on the ice-covered shelf. Studies in both the Arctic and Antarctic have shown that C and N isotope ratios ($\delta^{13}C$ and $\delta^{15}N$) of ice-associated algal material can be very elevated relative to particulate organic matter (POM) from the ice-free water column (Rau et al., 1991; Hobson et al., 1995). Elevated $\delta^{13}C$ and $\delta^{15}N$ of ice-derived POM likely derive from the semi-closed environment within the ice and its effects on the physical and biological dynamics of both C and N pools (Rau et al., 1991; Rysgaard and Glud, 2004; Rysgaard et al., 2008; Munro et al., 2010; Cozzi and Cantoni, 2011). Such findings suggest that the $\delta^{13}C$ and $\delta^{15}N$ of organic material on the ice-covered Bering shelf could provide a tracer of the relative contribution of ice-derived organic matter to shelf production. Additionally, the decreased light availability in the water column due to sea ice cover also curtails metabolic rates of phytoplankton C and N assimilation (Lee et al., 2010; Yun et al., 2012). This energetic restriction may be manifested as an increased reliance on ammonium relative to nitrate for N nutrition (e.g., Lee et al., 2010; Yun et al., 2012). A recent study suggested that on the eastern Bering shelf, ammonium and nitrate have substantially different $\delta^{15}N$, with ammonium enriched in ^{15}N relative to nitrate (Granger et al., 2011). Hence, the $\delta^{15}N$ of organic material on the shelf may also provide an indicator that sea ice cover affects which form of nitrogen is primarily consumed by phytoplankton in the water column.

To elucidate the N dynamics of production on the ice-covered shelf, we surveyed the $\delta^{15}N$ of three fractions of organic matter (phytoplankton-$\delta^{15}N_{POM}$; diatom frustule-bound N-$\delta^{15}N_{DB}$; zooplankton-$\delta^{15}N_{Zoo}$) isolated from net tows in the late winter to early spring over the eastern Bering Sea shelf. We investigated the regional distribution of organic matter $\delta^{15}N$ with a focus on identifying geographic patterns and the potential influence of sea ice on the $\delta^{15}N$ signal of primary ($\delta^{15}N_{POM}$ and $\delta^{15}N_{DB}$) and secondary production ($\delta^{15}N_{Zoo}$). Specifically, we investigated whether: 1) the $\delta^{15}N$ of POM produced under ice cover differs from that produced in open water conditions and 2) if the characteristic $\delta^{15}N$ signal of ice-associated production is transmitted to zooplankton consumers ($\delta^{15}N_{Zoo}$). Having identified a spatial pattern in organic matter $\delta^{15}N$, we sought to distinguish whether it was caused by the contribution of within-ice algal production to water column POM, or by differences in phytoplankton consumption of isotopically distinct inorganic N sources across the shelf. We additionally measured the $\delta^{13}C$ of zooplankton as a supplementary way of assessing the importance of ice productivity as a zooplankton food source. Our interpretation of the distribution of $\delta^{15}N$ of organic matter is discussed in the context of the N and C isotopes of within-ice algal production and the $\delta^{15}N$ of the inorganic nitrogen sources (nitrate and ammonium) available on the shelf.

2. Materials and methods

2.1. Study area and data sources

We collected samples and data over the eastern Bering shelf aboard the USCG Healy during spring 2007 (April 10–May 12, *HLY-07-01*) and 2008 (March 31–May 6, *HLY-08-02*) as part of the Bering Sea Ecosystem Study (BEST) (Fig. 1). Sea ice was present over the shelf during both sampling seasons and ice extent differed between years, with ice covering most of the shelf region in 2008 (Fig. S1).

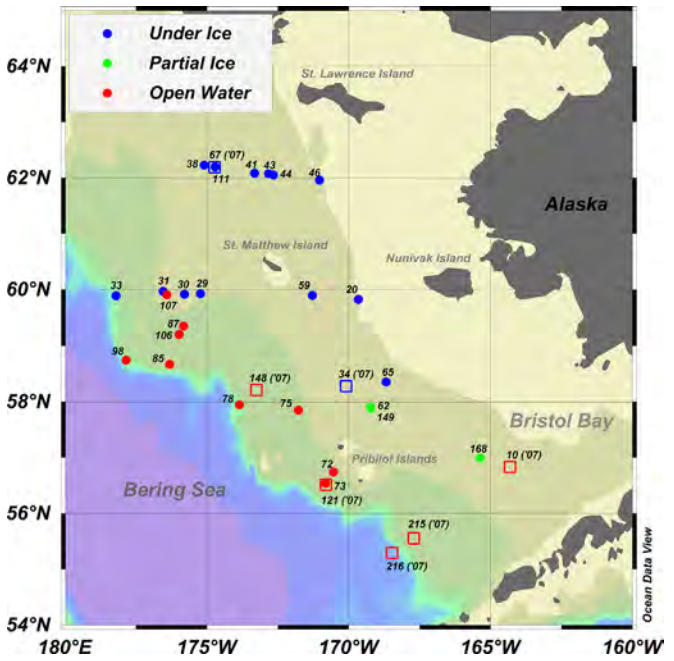

Fig. 1. Map of study area. Location of net tow sampling stations in April 2007 and 2008. Square symbols indicate stations visited in 2007 and round symbols in 2008. Map generated with Ocean Data View (Schlitzer, 2012).

Phytoplankton and zooplankton were collected at discrete stations with single net tows of the upper 30 m of water with a 153 μm mesh net in 2007 (7 stations) and a 53 μm mesh net in 2008 (25 stations). Samples were stored frozen at −20 °C in Nalgene bottles on-board the ship and kept frozen until analysis. Additionally, at 11 stations in 2008, a hand-held net (53 μm mesh) was used to collect zooplankton, from which a few individuals were picked out, rinsed, identified on-board and frozen individually. In the lab, specific fractions (bulk phytoplankton, zooplankton, diatom frustules) of the net tows were prepared and analyzed for natural abundance N isotope ratios and N content (Section 2.2). Individually sorted zooplankton were analyzed separately for the stable isotope ratios of both C and N.

Additional information required for analysis and interpretation of the isotopic data generated for this study was acquired from the BEST Data Archive. Observational reports and images of sea ice collected during the BEST cruises were used to classify the relative sea surface ice cover at each net tow station (HLY-07-01ScienceCrew, 2007; Sambrotto/LDEO, 2007; Ashjian/LDEO, 2008; Gradinger et al., 2008). Depth-specific measurements of water column nitrate, ammonium, chlorophyll-*a*, and O_2 were obtained from hydrocast data (Napp, 2007; Stabeno et al., 2007b, 2008; Lomas/BIOS, 2008). The natural abundance N isotope composition of water column nitrate at corresponding hydrographic stations was measured by Granger et al. (2011) and is also documented in the BEST data archive (Sigman and Granger, 2011). We also compared the organic matter fractions measured for this study with $\delta^{15}N$ and $\delta^{13}C$ measurements of ice-core and water column POM >0.8 μm (Gradinger et al., 2012; Iken et al., 2012a).

2.2. Net tow material preparation

2.2.1. Physical separation of bulk net tow samples

Net tow material was thawed at room temperature and sorted sequentially through 600 μm-, 425 μm-, and 250 μm-mesh size brass sieves. The smallest size material (<250 μm) was collected into 15 or 50 mL polypropylene centrifuge tubes. Some of this material was preserved with a 2% acidified formalin solution in filtered seawater (1:1 37% formaldehyde and glacial acetic acid) and archived for plankton identification. Genus and species classifications reported here are as published in Tomas (1996).

The remaining <250 μm material was centrifuged for 15 min at 4000 rpm to concentrate the phytoplankton fraction of POM (henceforth referred to as POM). Approximately 0.5 mL of this concentrate was transferred to an acid washed 2 mL centrifuge tube and oven-dried at 80 °C for N isotope-ratio analysis. The remainder of each sample filtrate was separated into 15 mL aliquots to undergo chemical cleaning in preparation for diatom-bound N isotope-ratio analysis (Section 2.2.2).

The zooplankton retained by the sequential-mesh size sieves were picked out, briefly rinsed with UV oxidized deionized water (DIW), and bottled together per sampling station in combusted 4 mL screw-top glass vials. This pooled zooplankton fraction consisted primarily of copepods and a few euphausiids. Samples were dried at 60 °C for N isotope-ratio analysis.

2.2.2. Chemical cleaning for diatom frustule N analysis

Organic N exclusively associated with diatom frustules was isolated from the phytoplankton POM fraction using a cleaning technique developed for fresh diatom material (Morales et al., 2013), with a modification to remove mineral particles present in these samples. Briefly, the cleaning consists of five steps: (1) an initial freeze–thaw cycle and a sodium dodecyl sulfate detergent rinse, (2) density separation to isolate the mineral fraction, consisting of centrifugation in sodium polytungstate solution (ρ=2.15 g/mL) (Sigman et al., 1999), (3) preliminary oxidative cleaning with potassium permanganate, (4) intermediate oxidative cleaning with dilute perchloric acid ($HClO_4$), and (5) final oxidative cleaning with concentrated (70%) perchloric acid. For a few stations processed before we became aware of the presence of an interfering mineral fraction, the density separation with polytungstate (step 2) was performed after the entire cleaning sequence because we had processed all the material and lacked sufficient material to start anew. To rinse off any N contaminant introduced by this step, we repeated a round of concentrated perchloric acid oxidation after the density separation. After the complete treatment, samples were dried for N isotopic analysis of the organic matter that is found within the diatom frustule walls ('diatom-bound N') and is thus protected from the cleaning protocol by the siliceous biomineral matrix.

2.3. Bulk POM and zooplankton N content and isotope analysis

Dried POM (<250 μm) samples (Section 2.2.1) were ground, and 0.6–1.0 mg of material placed in pre-combusted tin capsules for N isotopic analysis. Whole zooplankton pooled fractions retained on progressive sieves were packed into pre-combusted tin capsules for N isotope analysis. Similarly, individual zooplankton picked on-board were packed individually into tin capsules for simultaneous C and N isotope analysis. We did not extract lipids from zooplankton samples; however, according to paired comparison at three stations, mean copepod and euphausiid $\delta^{15}N$ and $\delta^{13}C$ values were not significantly different from lipid-extracted samples (Iken et al., 2012b). The N content and isotopic composition of the N and C in the POM and zooplankton were measured with on-line Dumas combustion. Analyses were performed at the GeoForschungsZentrum (Potsdam, Germany) using an NC2500 Carlo Erba elemental analyzer coupled with a ConFlow III interface to a Thermo-Fisher DELTA+XL stable isotope mass spectrometer. Isotope ratios are expressed in delta notation ($\delta^{15}N=[(^{15}N/^{14}N)_{sample}/(^{15}N/^{14}N)_{standard}-1]\times 1000$ and $\delta^{13}C=[(^{13}C/^{12}C)_{sample}/(^{13}C/^{12}C)_{standard}-1]\times 1000$), where atmospheric N_2 and PeeDee Belemnite are the universal reference materials for $\delta^{15}N$ and $\delta^{13}C$, respectively. Isotopic reference materials used for calibration were IAEA-N1 and IAEA-N2 for $\delta^{15}N$ and USGS24 and IAEA CH-7 for

$\delta^{13}C$. Instrumental precision as evaluated by repeated measures of isotopic standards was 0.2‰ for both $\delta^{15}N$ and $\delta^{13}C$. Two to three replicates of POM and pooled zooplankton were run per station. The average deviation of replicate samples measured for $\delta^{15}N$ was <0.4‰ for POM and <1.0‰ for pooled zooplankton.

2.4. Diatom frustule-bound N content and isotopic analysis

Diatom frustule-bound N content and $\delta^{15}N$ of the chemically cleaned samples were determined using the persulfate-denitrifier method developed for the isotopic analysis of sedimentary diatom-bound N (Robinson et al., 2004). Approximately 5–7 mg of the POM fraction (Section 2.2.1) was digested with a potassium persulfate reagent solution (POR) (1.5 M NaOH and 0.22 M $K_2S_2O_8$) to oxidize all organic N within the diatom frustules to NO_3^- (Robinson et al., 2004). Resulting nitrate concentrations were determined by conversion of sample NO_3^- to NO using a heated vanadium (III) solution and detected by chemiluminescence on a Teledyne 200E Chemiluminescence NO_x analyzer (Braman and Hendrix, 1989). Analysis of $\delta^{15}N$ was performed using the 'denitrifier method' (Sigman et al., 2001). Adequate sample volume to yield 10 or 20 nmol of N was injected into a bacterial suspension and converted to N_2O through bacterially mediated reduction. This N_2O product was analyzed for $\delta^{15}N$ using a modified Thermo-Finnigan GasBench II and Delta Plus gas-chromatographer and mass spectrometer (Casciotti et al., 2002), with IAEA-N3 nitrate isotopic reference material as a standard. Instrumental precision for $\delta^{15}N$, evaluated with repeated measures of the isotopic standard, was <0.2‰.

To minimize N contamination, all glassware, plasticware, septa and caps used in analysis were acid washed with 10% HCl, soaked in deionized water (with the exception of polyethylene centrifuge tubes and 4 mL borosolicate vials), and dried in a clean oven. Glassware was further combusted for 3 h at 500 °C to ensure incineration of any organic contaminants.

Blank contribution from contaminants and from the persulfate oxidation reagent (POR) was typically ≤ 1 μm N, representing as much as 15% of the total N, but typically only ~6%. Each batch of samples oxidized and measured was corrected for the contribution of the POR blank to the measured $\delta^{15}N$ by concurrently measuring a dilution-series of an in-house amino acid standard of known isotopic composition.

At most stations, only enough material to perform one cleaning was available, so we could not produce chemical treatment replicates. Nevertheless, at all stations we measured two samples of the cleaned material for frustule-bound $\delta^{15}N$ ($\delta^{15}N_{db}$) using different POR batches. The average deviation of these replicate $\delta^{15}N_{db}$ samples was <0.6‰, which includes both methodological and natural variability.

2.5. Measurement of water column $\delta^{15}N_{NH_4^+}$

The N isotopic composition of water column ammonium ($\delta^{15}N_{NH_4^+}$) at six stations visited in 2008 was determined using the method developed by Zhang et al. (2007). NH_4^+ was oxidized to nitrite (NO_2^-) with sodium hypobromite. NO_2^- was subsequently reduced to nitrous oxide (N_2O) by sodium azide buffered to pH 4–5 by 100% acetic acid. The isotopic composition of the resultant N_2O was then analyzed on a Thermo GasBench II Delta V gas chromatograph isotope ratio mass spectrometer coupled to an automated purge-and-trap system (Casciotti et al., 2002), using IAEA N1 and IAEA N2 as reference materials for calibration. Measurement error for replicate batch analyses is typically ~1‰ for samples with ≥ 2 μM ammonium.

2.6. Classification of relative ice cover

Hydrographic stations were classified into 3 categories of ice surface cover: under ice, partial ice, and open water. These were determined from photographs taken every 15 min by the *USS Healy's* AloftCon camera near the time of sampling and verified with observational reports as well as cruise notes from 2008. Stations were classified as 'under ice' if images showed >50–100% ice cover at sampling times, 'partial ice' cover if there was >20–50% ice cover and 'open water' from 0% to 20% ice coverage. Only three stations were classified as partially ice covered, and were included with under ice stations for most analyses.

2.7. Data analysis and statistics

The average $\delta^{15}N$ of replicate diatom samples cleaned individually was taken as the true diatom-bound N $\delta^{15}N$ ($\delta^{15}N_{db}$) and used for analysis. Replicates of bulk POM and zooplankton sieved from the net tow at each station were also averaged, and station average $\delta^{15}N$ was used for all comparisons. The $\delta^{15}N$ and $\delta^{13}C$ measurements of the zooplankton individually sorted on-board are presented per individual, but station averages of chaetognaths, copepods, and euphausiids were used for comparisons between taxonomic groups.

Correlation analysis among $\delta^{15}N_{POM}$, $\delta^{15}N_{Zoo}$ and $\delta^{15}N_{DB}$ was performed with reduced major axis (RMA) linear regressions, accounting for analytical error in both the *x* and *y* measurements. The regression coefficients and 95% confidence intervals of their slopes and intercepts were calculated using RMA regression software available at ⟨http://www.bio.sdsu.edu/pub/andy/rma.html⟩ (Bohonak, 2004). Pearson's correlation coefficient (*r*) and *p*-values are also reported.

3. Results

3.1. Plankton community composition (53–250 μm)

Diatoms were the dominant phytoplankton component in our 53–250 μm POM fraction recovered from the net tows. We observed flagellates and dinoflagellates only occasionally in our samples, and small copepods and other microzooplankton almost never. Consistent with our observations, diatoms frequently represented >80% of the autotrophic microplankton (diatoms, flagellates, and dinoflagellates) biomass in the upper 30 m of the water column at the stations sampled here (Lomas, 2008). Twelve diatom genera were represented in the net tow assemblage of the samples (Table S1). We coarsely assessed diatom species dominance/co-dominance within our samples, designating the most visually abundant species as dominant for that station's sample. In general, stations under ice cover were more species rich with respect to diatoms than open water stations (mean ± SD: 4.1 ± 1.2 vs. 3.5 ± 1.6 species; N.S.) and there were more species present in ice covered stations altogether (Table S1). *Fragilariopsis* species were most commonly identified as the dominant genus at ice covered stations, whereas *Chaetoceros* species were frequently dominant at open water stations (Fig. S2). The second most abundant genuses were Coscinodiscus at ice-covered stations and Thalassiosira at open water stations.

Seven taxonomic groups were collected and identified in the zooplankton samples on-board: amphipods, chaetognaths, copepods, decapods, euphausiids, gastropods, and mysids. Three of these groups, chaetognaths, euphausiids, and copepods, were collected from all of the sampling stations. In our samples, no relation was observed between zooplankton species composition and the degree of sea ice cover.

3.2. Nitrogen and carbon isotopic composition

The stable N isotopic composition of the bulk POM (53–250 μm), diatom frustule-bound N and net tow zooplankton ranged widely. $\delta^{15}N_{POM}$ ranged from 2.1‰ to 14.7‰ with nitrogen content ranging from 0.4% to 5.0% N dry wt. Similarly, $\delta^{15}N_{DB}$ ranged from 4.9‰ to 20.7‰ (N content: 3.8–20.2 μmol/g opal). We detected no patterns in the $\delta^{15}N_{DB}$ or $\delta^{15}N_{POM}$ signal at individual stations associated with the identity of the dominant diatom species or genus. Zooplankton $\delta^{15}N$ ranged from 6.7‰ to 16.2‰ (N content: 4.7–15.6% dry wt.). The $\delta^{15}N$ of individually sorted zooplankton similarly ranged from 6.4‰ to 18.0‰. Chaetognath $\delta^{15}N$ was 10.3‰ to 17.3‰ which is between 0‰ and 6‰ higher than paired values of euphausiids and copepods at the same station (mean difference ± SD: 3.7 ± 1.5‰) (Table S2). The $\delta^{13}C$ measured for individual zooplankton ranged from −24.5‰ to −15.7‰. The $\delta^{13}C$ of euphausiids was 8.7–12.5‰, ranging 0–3.5‰ higher than that of copepods and chaetognaths from the same station (mean difference ± SD: 0.8 ± 1.1‰).

3.3. Isotopic relationships among POM, zooplankton, and diatom-bound N

Overall, the three fractions of organic matter showed consistent $\delta^{15}N$ relationships throughout the eastern Bering shelf. $\delta^{15}N_{DB}$ was positively correlated to $\delta^{15}N_{POM}$ ($r=0.65$, $p<0.0003$, RMA slope = 0.8 ± 0.2 [95% confidence limits]), and zooplankton $\delta^{15}N$ was positively correlated to both $\delta^{15}N_{POM}$ and $\delta^{15}N_{DB}$ ($r=0.76$, $p<0.000001$, RMA slope = 0.69 ± 0.18 [95% confidence limits] and $r=0.63$, $p<0.0002$, RMA slope = 0.58 ± 0.18 [95% confidence limits]) (Fig. 2). In most cases $\delta^{15}N_{DB}$ was greater than the corresponding $\delta^{15}N_{POM}$, with an average offset of 3.5 ± 3.9‰ (mean ± SD). Net tow zooplankton $\delta^{15}N$ was on average 2.6 ± 2.5‰ (mean ± SD) higher than $\delta^{15}N_{POM}$ from the same station. $\delta^{15}N_{Zoo}$ was neither consistently higher nor lower than $\delta^{15}N_{DB}$.

3.4. Spatial patterns in $\delta^{15}N$

POM $\delta^{15}N$ values increased from the outer shelf towards the inner shelf domain, a pattern mirrored by both diatom frustule-bound and zooplankton $\delta^{15}N$ across the shelf (Fig. 3). The shoreward increase in $\delta^{15}N$ of all N fractions also appeared to co-vary with the general extent of sea ice (Figs. 3 and S1). Stations under ice cover at the time of sampling exhibited higher $\delta^{15}N_{POM}$, $\delta^{15}N_{DB}$, and $\delta^{15}N_{Zoo}$ than stations in open waters. Stations with ice cover had both greater ranges and higher maximum values for $\delta^{15}N$ ($\delta^{15}N_{POM}$: 3.8–14.7‰; $\delta^{15}N_{DB}$: 5.4–20.7‰; $\delta^{15}N_{Zoo}$: 9.6–16.2‰) compared to open water stations ($\delta^{15}N_{POM}$: 2.1–7.9‰; $\delta^{15}N_{DB}$: 4.8–12.7‰; $\delta^{15}N_{Zoo}$: 6.7–12.5‰). Ice-covered stations were largely located on the middle and inner shelf, except for a group of four stations under ice cover on the outer shelf west of St. Matthew's Island (Stns. 29–33). These four stations and two others on the northern middle shelf (Stns. 38 &111) had the lowest $\delta^{15}N_{POM}$, $\delta^{15}N_{DB}$, and $\delta^{15}N_{Zoo}$ values among ice covered stations, overlapping with the highest values at open-water stations (Figs. 2 and 3).

$\delta^{15}N_{Zoo}$ was consistently higher for all zooplankton types at stations under ice cover (Fig. 4), regardless of differences among taxonomic groups (Section 3.2). Corresponding measurements of $\delta^{13}C$ suggest that euphausiids from ice-covered stations tended to have $\delta^{13}C$ 1–2‰ higher than at open-water stations; however, this spatial pattern was not evident for the other taxonomic groups (chaetognaths and copepods). For those groups, $\delta^{13}C$ showed no distinctions of individuals among taxonomic groups or with respect to ice cover, regardless of corresponding $\delta^{15}N$. Copepods showed a broad overlap in $\delta^{13}C$ of individuals from ice covered and open water stations, despite a clear distinction in $\delta^{15}N$.

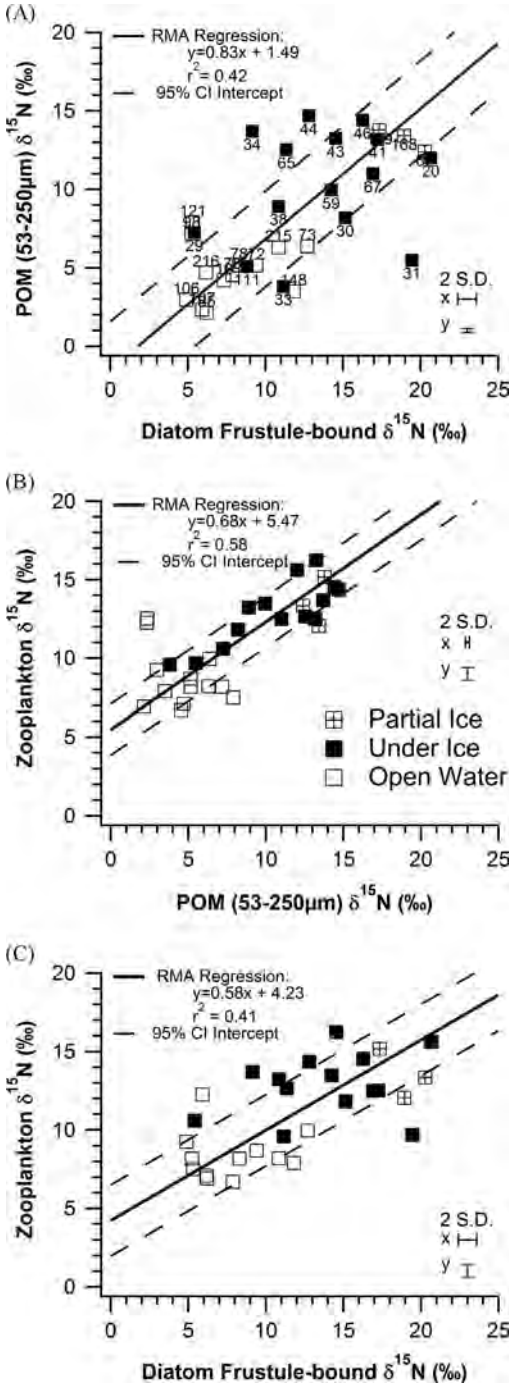

Fig. 2. Relationships between the $\delta^{15}N$ of POM fractions. RMA regressions of (A) diatom-bound N vs. bulk POM (53–250 μm) $\delta^{15}N$, (B) bulk POM (53–250 μm) N vs. zooplankton $\delta^{15}N$, and (C) diatom frustule-bound N vs. zooplankton $\delta^{15}N$.

3.5. $\delta^{15}N$ of water column ammonium

$\delta^{15}N_{NH_4^+}$ at 10 m depth in the water column measured at six of the hydrographic stations surveyed ranged from 28‰ to 63‰ (Table 1). The ammonium concentration at this depth ranged from ~0.1 to 2.9 μM among the six stations. At two stations, very high $\delta^{15}N_{NH_4^+}$ was measured (61‰ and 63‰); one of these stations was the only one characterized by significant plankton growth (Stn. 106). Entire depth profiles of $\delta^{15}N_{NH_4^+}$ and ammonium concentration were measured at only two ice-covered stations (Stns. 65 and 138), and revealed no apparent depth-dependence for either measure (Fig. S3).

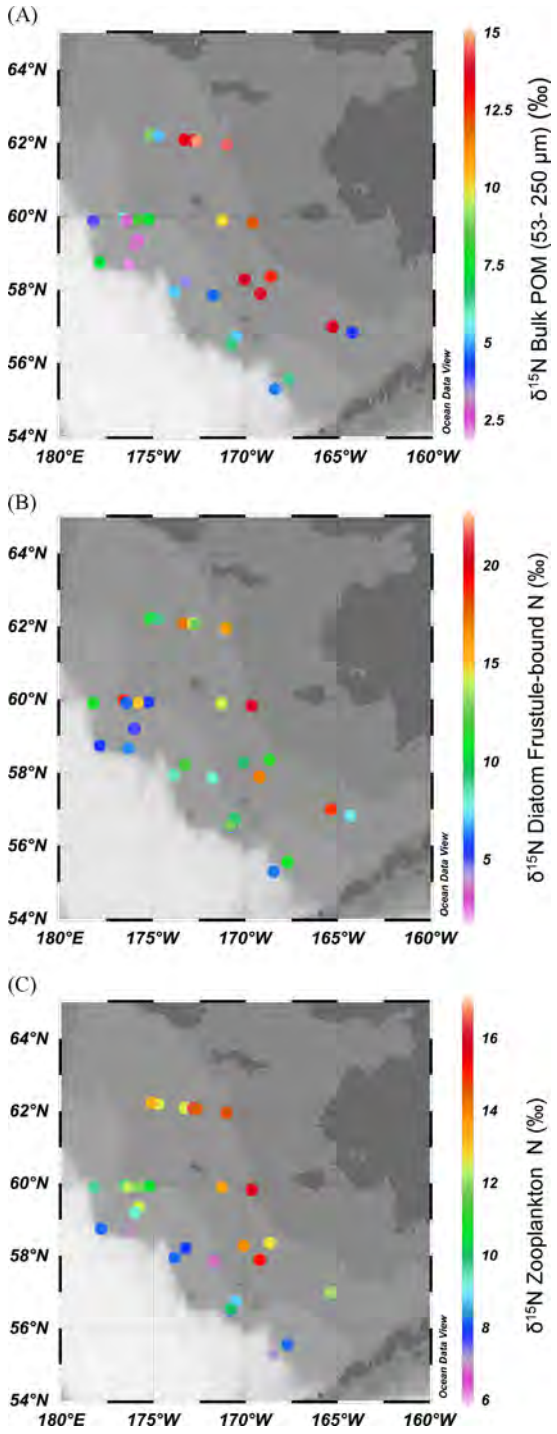

Fig. 3. Spatial distribution of organic matter $\delta^{15}N$. Spatial distribution of values of $\delta^{15}N$ of (A) bulk POM (53–250 μm), (B) diatom frustule-bound N, and (C) net tow zooplankton from 2007–2008. Maps generated with Ocean Data View (Schlitzer, 2012).

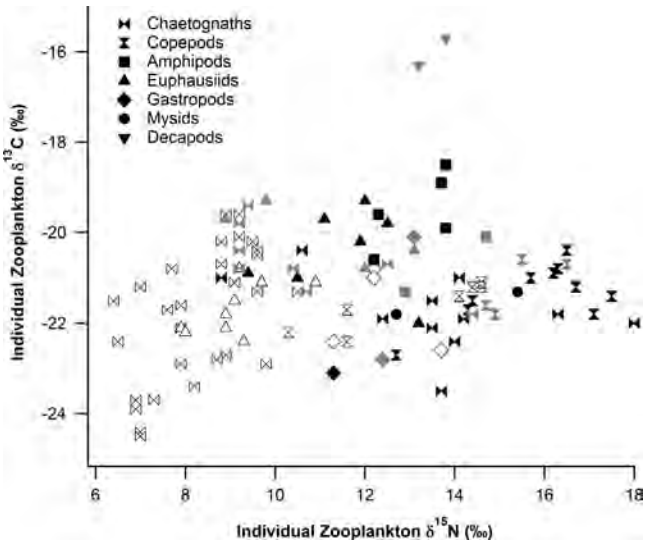

Fig. 4. C and N isotopic ratios of individual zooplankton. $\delta^{13}C$ vs. $\delta^{15}N$ of individually picked net tow zooplankton from April 2008. Symbol fill indicates station ice cover at the time of sampling. Open symbols: open water stations; filled symbols: under ice (black) or partial ice stations (gray). Symbol shape indicates taxonomic group.

4. Discussion

4.1. Significance of the $\delta^{15}N$ correlations among organic matter fractions

The $\delta^{15}N$ signals of late winter production on the eastern Bering shelf showed a strong increase eastward and northward that coincided with the transition from open water to ice-covered regions. Both primary producers ($\delta^{15}N_{DB}$, $\delta^{15}N_{POM}$) and consumers ($\delta^{15}N_{Zoo}$) exhibited the same trend of increase, with a range of 10–15‰ (Fig. 3). The concordance between the three signals suggests mechanistic relationships among them.

We included the $\delta^{15}N_{DB}$ as a measure of the phytoplankton $\delta^{15}N$ signal that is not influenced by the non-phytoplankton material in POM and as a way to assess whether the autotrophic portion of the $\delta^{15}N_{POM}$ signal involves diatoms, which are critical for higher trophic levels. Both $\delta^{15}N_{POM}$ and $\delta^{15}N_{DB}$ exhibited parallel patterns, despite the likely inclusion of detrital material, bacteria, fecal pellets, microzooplankton, and smaller non-diatom phytoplankton in the bulk POM fraction (53–250 μm). These additional components could cause deviation in the $\delta^{15}N$ of POM from that of the organic matter exclusively associated with the diatom frustules. The agreement between these stable isotope signals is not driven by the inclusion of the diatom-bound N in the POM N-pool per se, as diatom-bound N represented an insignificant fraction of the bulk PON (on the order of $\leq 0.001\%$). Instead, to the extent that the diatom frustule-bound $\delta^{15}N$ parallels that of the diatom biomass, the agreement between $\delta^{15}N_{DB}$ and $\delta^{15}N_{POM}$ may reflect the fact that diatoms make up the bulk of the POM fraction analyzed, although it is possible (in fact, likely) that the $\delta^{15}N$ of diatoms and other phytoplankton are strongly correlated. Diatoms typically dominate the phytoplankton biomass on the ice covered regions Bering shelf (Sukhanova et al., 1999; Moran et al., 2012), and our microscope observations and independently generated counts (Lomas, 2008) confirm this was true for the stations presented here. The mean difference between bulk $\delta^{15}N_{POM}$ and $\delta^{15}N_{DB}$ observed in this study (mean ± SD: 2.6 ± 2.5‰) is on the whole consistent with inferences from deep sea sediment $\delta^{15}N_{DB}$ that the $\delta^{15}N$ of diatom-bound N is on average ~3‰ higher than the $\delta^{15}N$ of the bulk biomass of the diatoms (Robinson et al., 2005; Brunelle et al., 2007; Robinson and Sigman, 2008).

Regardless of whether the POM fraction we measured was primarily composed of diatom or non-diatom primary production it was directly consumed by the mesozooplankton, as evident from the $\delta^{15}N_{Zoo}$. The differences between the $\delta^{15}N$ of the zooplankton from net tows and the 53–250 μm POM were ~3‰, consistent with the ^{15}N enrichment per trophic level typical in marine ecosystems (Minagawa and Wada, 1984; Hobson and Welch, 1992; Michener and Kaufman, 2007) (Fig. 2B), and suggest the predominance of primary consumption among the pooled zooplankton samples. Indeed, since the zooplankton fraction isolated

Table 1
The $\delta^{15}N$ and concentrations of ammonium and nitrate at the upper 10 m of seawater for select hydrographic stations in April 2008.

Station	Lat. (°N)	Lon. (°W)	Hydrographic domain	Chl *a* (μg/L)	$\delta^{15}N_{NO_3}$ (‰ vs. air)	$[NO_3^-]$ (μM)	$\delta^{15}N_{NH_4}$ (‰ vs. air)	$[NH_4^+]$ (μM)
50	61.767	168.469	Inner	1.20	–	6.5	33	2.6
51	61.720	167.832	Inner	0.45	4.0	5.5	29	2.4
54	60.399	168.630	Inner	0.28	2.9	2.8	28	2.4
65	58.366	168.704	Middle	0.31	5.5	7.4	63	2.9
138	58.952	170.312	Middle	0.25	5.3	4.6	38	2.3
106	59.202	175.978	Outer	13.74	–	14.6	61[a]	~0.1

[a] Measurement error is likely > 1‰ given the low ammonium concentration; nevertheless, $\delta^{15}N$ of the blanks was ~ −10‰, such that the elevated $\delta^{15}N_{NH_4}$ value is robust.

from net tows was primarily copepods and euphausiids, we would expect it to reflect only one trophic level of ^{15}N enrichment from the primary producers. The robustness of the correlation between $\delta^{15}N_{Zoo}$ and $\delta^{15}N_{POM}$ is remarkable given that consumer signals are integrated over a large temporal and spatial scale, and it indicates that the shelf-wide patterns in the $\delta^{15}N$ of primary producers propagate to first level consumers. This underlying spatial pattern may be useful in dietary and foraging studies of animals at higher trophic levels present on the eastern Bering shelf. This point will be addressed below.

4.2. Origins of the spatial isotopic patterns in organic matter

The eastern Bering shelf is characterized by three different hydrographic domains, inner, middle, and outer, whose seaward boundaries are defined by fronts roughly coincident with the 50-, 100-, and 200-m isobaths (Fig. 1) (Kinder and Schumacher, 1981; Coachman, 1986; Overland et al., 1999; Mathis et al., 2010). Each hydrographic domain exhibits different physical and biogeochemical characteristics. In winter to early spring, the water column of the ice-covered inner and middle domains is well mixed to the bottom due to convection from ice brines, and the outer shelf has a surface wind-mixed layer and a tidally mixed bottom layer contiguous with waters beyond the shelf break (Kinder and Schumacher, 1981). Bottom water nitrate concentrations, equivalent to surface nitrate concentrations at the start of the growing season, were ~23 μM at the outer-, 12 μM at the middle-, and 3 μM at the inner-shelf regions (see Granger et al., 2011). The $\delta^{15}N$ of dissolved nitrate across these domains showed a decreasing shoreward trend: ~6.5‰, ~5.5‰, and ~4.5‰ at the outer, middle and inner shelf, respectively (Granger et al., 2011). Thus, the high $\delta^{15}N$ of plankton inshore does not reflect a parallel ^{15}N enrichment of the ambient water column nitrate.

Similarly, the ^{15}N enrichment of plankton inshore is not explained by the isotopic fractionation that accompanies partial consumption of the nitrate pool, which would generate phytoplankton with signatures more ^{15}N-*deplete* than the source nitrate. Assuming an average value of 5‰ for the isotope effect of phytoplankton nitrate assimilation (Sigman et al., 2009) and closed system Rayleigh dynamics (Mariotti et al., 1981), the $\delta^{15}N$ expected for phytoplankton assimilating nitrate can be calculated from the initial $\delta^{15}N$ and concentration of nitrate at each domain (Fig. 5A). At the outer shelf, the $\delta^{15}N_{POM}$ at open water stations generally followed the $\delta^{15}N$ of the integrated product predicted by the Rayleigh model for nitrate consumption, except for a few stations at the high end of the ambient nitrate concentrations observed. Surface nitrate concentrations at the outer shelf ranged from 21 μM to nil, and were matched by increasing $\delta^{15}N$ of nitrate, from 7‰ to 16‰. This is consistent with isotope discrimination during nitrate assimilation by phytoplankton, as nitrate depletion and increasing $\delta^{15}N_{POM}$ were also associated with coincident increases in chlorophyll-*a* concentrations (Fig. 5A).

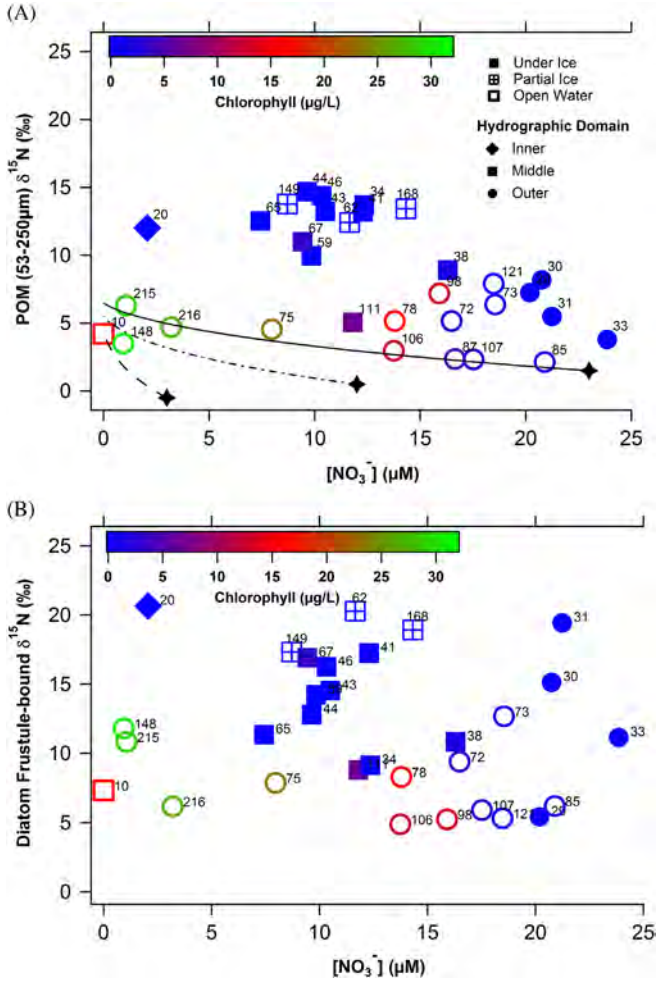

Fig. 5. POM and diatom frustule-bound $\delta^{15}N$ vs. seawater nitrate concentration. (A) $\delta^{15}N$ of POM as a function of $[NO_3^-]$ at the surface (5 m depth), per chlorophyll concentration (μg/L). The plotted lines represent the expected $\delta^{15}N$ of POM produced by phytoplankton growth on ambient nitrate, based on the integrated product Rayleigh model with a prescribed isotope effect of 5‰ at the outer shelf domain (solid line), the middle shelf domain (dash–dot line), and the inner shelf domain (dashed line). The initial $[NO_3^-]$ and $\delta^{15}N_{NO_3}$ correspond to mean values observed in the respective domains (Granger et al., 2011) (See Section 4.2). Black stars indicate initial points of the Rayleigh models. (B) The diatom-bound $\delta^{15}N$ as a function of $[NO_3^-]$ at the surface (5 m depth) per chlorophyll concentration (μg/L).

In contrast, at ice-covered stations, particularly those on the inner and middle shelf, $\delta^{15}N_{POM}$ values did not follow trends expected from Rayleigh distillation during nitrate assimilation by phytoplankton (Fig. 5A). The $\delta^{15}N_{POM}$ was systematically 5–10‰ greater than expected for the integrated product of nitrate assimilation. Stations under ice cover generally had low chlorophyll-*a* at the surface (Fig. 5A) and showed no apparent depletion of ambient nitrate, indicating little growth on nitrate. The only

exception was station 111 on the middle shelf, which had higher chlorophyll concentrations from a nascent marginal ice bloom, and at which $\delta^{15}N_{POM}$ was also closer to that predicted from nitrate assimilation.

Diatom-bound $\delta^{15}N$ showed the same general trend as that of $\delta^{15}N_{POM}$ (Fig. 5B), albeit with substantial scatter, which may be attributed to the possible presence in our samples of diatom frustules that were grown *ex-situ* but transported to the sites by ice-floes. This shared variation in $\delta^{15}N$ rules out the possibility that the $\delta^{15}N_{POM}$ variation is driven by isotopic alteration during degradation of senescent phytoplankton material, as such degradation would not affect the $\delta^{15}N$ of frustule-bound N. Rather, the frustule-bound data confirm that the $\delta^{15}N$ variation is driven by biomass production. Altogether, values of $\delta^{15}N_{POM}$ and $\delta^{15}N_{DB}$ in relation to surface nitrate and chlorophyll-*a* concentrations suggest that, while the $\delta^{15}N$ of POM at open water stations is consistent with phytoplankton growth on ambient nitrate, the $\delta^{15}N$ of POM collected at ice-covered stations appears inconsistent with nitrate as the primary N source. Algae at ice-covered stations must therefore fulfill their nutritional needs with an N pool that is distinct from water column nitrate, one with a much higher $\delta^{15}N$.

4.3. Sources of high-$\delta^{15}N$ nitrogen for late winter primary production

Together, the $\delta^{15}N$ signals of diatom-bound N, POM, and zooplankton observed over the shelf suggest that primary production at ice-covered stations in early spring is fueled by an N pool other than water column NO_3^-. Such high $\delta^{15}N$ requires an N source with substantially higher $\delta^{15}N$ than that of nitrate, one that is either more important for phytoplankton's N nutrition as one goes northward and shoreward, and/or is increasingly ^{15}N-enriched inshore. We consider two candidate N sources distinct from water column NO_3^- to explain the elevated $\delta^{15}N$ of primary production and its spatial pattern: (1) an internal N pool within sea ice and (2) NH_4^+ in the water column regenerated from shelf sediments, a pool that persists during winter.

Most of the stations with high $\delta^{15}N$ of organic matter were under ice during sampling. There was little photosynthetic activity in the water column, and the POM collected at these stations could largely derive from ice algal production released into the water column. These 'within-ice' algae are trapped in the ice during its formation (Horner, 1985; Dieckmann et al., 1991; Gradinger, 1999). Ice algae can drain through brine channels and accumulate at a concentrated ~5 cm band at the ice bottom, experiencing accelerated growth given sufficient light (Horner, 1985). Phytoplankton within the ice grow in a closed/semi-closed system with respect to the available nutrient pool; continued production depends on internal nutrient recycling and exchange with the water column, and the degree of the latter can vary with the physical characteristics of the ice and location of phytoplankton growth in the ice column (McMinn et al., 1999; Fripiat et al., 2007). The dissolved inorganic nitrogen (DIN) incorporated into the ice is from the water column such that its $\delta^{15}N$ is expected to reflect that of DIN in the water column, at least initially. However, the ice column can host biological processes such as denitrification and anammox (Rysgaard and Glud, 2004; Rysgaard et al., 2008) that would lead to ^{15}N enrichment in the ambient N pools. In addition, volatilization of NH_3 could also lead to ^{15}N enrichment of the N pools within sea ice (Rau et al., 1991). Similarly, the dissolved C pool within sea ice can become ^{13}C-enriched relative to the DIC pool in surrounding seawater due to the combined effects of CO_2 degassing from ice and high degrees of DIC consumption by algae (Papadimitriou et al., 2004; Munro et al., 2010). These conditions can lead to elevation of both $\delta^{13}C$ and $\delta^{15}N$ in POM derived from algal growth within ice, and POM elevated in $\delta^{13}C$ and/or $\delta^{15}N$ has been documented in Arctic and Antarctic sea ice (Rau et al., 1991; Hobson et al., 1995; Tamelander et al., 2008; Pineault et al. 2013).

POM (> 0.8 μm) isolated from the bottom 10 cm of sea ice by Gradinger et al. (2012) during the 2008 cruise had $\delta^{15}N$ ranging from 4.8‰ to 12.2‰.While most of the $\delta^{15}N$ values of sea ice POM were elevated relative to seawater nitrate, the majority were too low to explain the $\delta^{15}N_{POM}$ and $\delta^{15}N_{DB}$ values observed at most ice covered stations. Ice $\delta^{15}N$ POM values at 10 of the 12 ice stations were ≤ 7.6‰ (Gradinger et al., 2012), notably lower than the $\delta^{15}N$ of POM (53–250 μm) observed in the water column at the majority of ice-covered stations (Fig. 2). Direct comparison at five corresponding stations revealed that ice POM $\delta^{15}N$ was as much as 9.6‰ lower than *in-situ* water column POM (53–250 μm). One plausible explanation for this difference is that the ice POM $\delta^{15}N$ measurements were of > 0.8 μm POM, whereas our net-collected POM represented only the > 53 μm size fraction. However a direct comparison of > 0.8 μm POM from ice and the water column at 9 of the ice covered stations indicated that ice POM was also up to 4.0‰ lower (Iken et al., 2012a), indicating that the difference we observed in $\delta^{15}N$ between ice and the water column POM was not entirely due to differences in the size fractions analyzed. This observation reinforces the idea that contribution by ice POM to the water column could not be responsible for the high $\delta^{15}N$ values observed in POM from the water column.

Additionally, the $\delta^{13}C$ values of water column POM (> 0.8 μm) (−25.1‰ to −22.7‰) (Iken et al., 2012a) were also consistently lower than sea ice POM (−22.6‰ to −13.3‰) (Gradinger et al. 2012), with the difference ranging between 1.1‰ and 11.4‰. Furthermore, sea ice POM $\delta^{13}C$ was higher than the $\delta^{13}C$ of individual copepods and euphausiids from ice covered areas (Fig. 4), not lower, as is expected if the zooplankton sampled were consuming only ice-derived POM. In contrast the $\delta^{13}C$ of water column POM (> 0.8 μm) was in fact lower than zooplankton $\delta^{13}C$, consistent with water column POM being at least part of the zooplankton food source. Therefore, we conclude that the contribution of ice-derived POM to the underlying water column POM and zooplankton nutrition was probably low at the time of sampling and is unable to account for the observed spatial patterns in $\delta^{15}N$ of the organic matter collected from the water column.

A second explanation for the elevated $\delta^{15}N$ we observe on the shelf is the consumption of NH_4^+ released from shelf sediments (Whitledge et al., 1986) (Fig. 6). Elevated $\delta^{15}N_{POM}$, $\delta^{15}N_{DB}$, and $\delta^{15}N_{Zoo}$ were mostly observed in the inner and middle hydrographic domains (Fig. 1). In both 2007 and 2008, ammonium concentrations on the shelf increased shoreward, from 0.5 to 4.0 μM in waters on the middle and inner shelves (Stabeno et al., 2007b, 2008; see Granger et al., 2011). The NH_4^+ in the water column at stations on the shelf proved to be exceptionally ^{15}N-enriched (Table 1). This likely derives from the benthic efflux of NH_4^+ that is ^{15}N-enriched due to coupled nitrification–denitrification and further heavy isotope discrimination of NH_4^+ by nitrification in the ice-covered water column (Granger et al., 2011).

Substantial N isotope discrimination can be associated with ammonium assimilation by phytoplankton, with an isotope effect (ε) as high as 25‰ (Pennock et al., 1996; Waser et al., 1998, 1999), producing phytoplankton with a $\delta^{15}N$ lower than that of its NH_4^+ source. However, this isotope effect is observed to decline sharply as ammonium concentration declines (Hoch et al., 1992; Pennock et al., 1996; Vo et al., 2013). In any case, given the extremely high $\delta^{15}N_{NH_4^+}$, upwards of 60‰ at some locations, isotope discrimination during ammonium assimilation would still give way to relatively high values of phytoplankton POM observed here.

Given the limited light energy available to the water column phytoplankton growth at ice-covered stations, it is plausible that

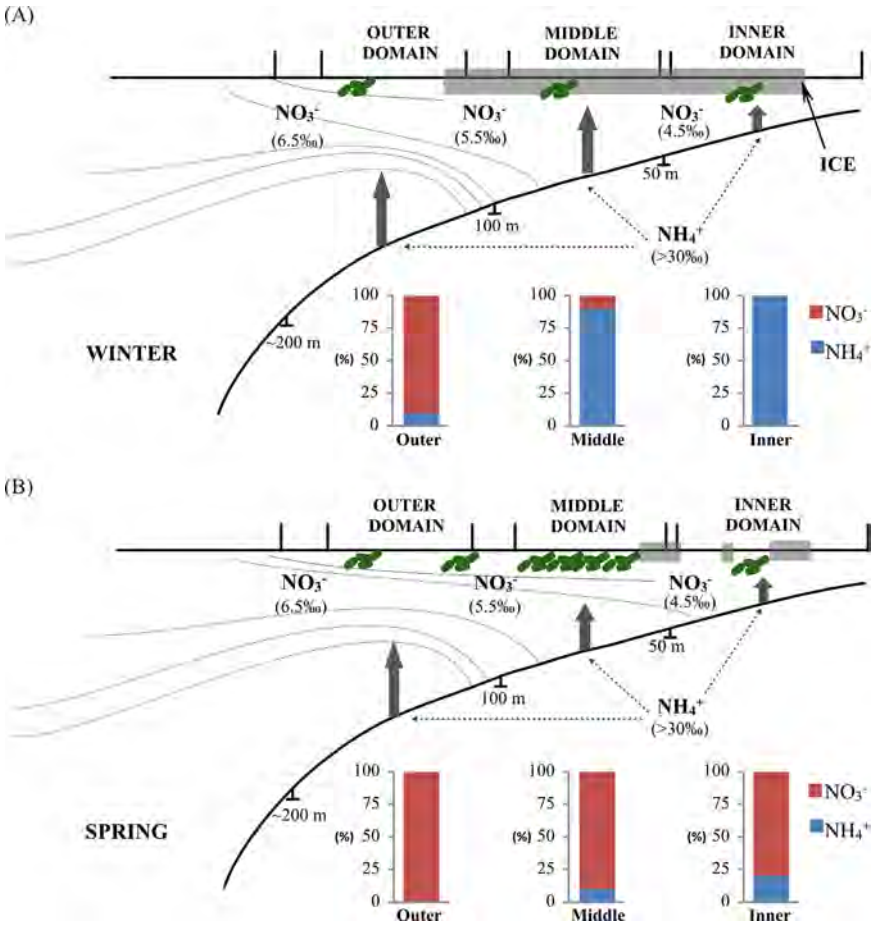

Fig. 6. Scheme of seasonal N dynamics on the eastern Bering Sea shelf. Water column stratification of a representative cross-section of the eastern Bering shelf and the proposed distribution of isotopically heavy NH_4^+ regenerated from the sediments under: (A) Late winter conditions: extensive ice cover present on the shelf and no stratification on the middle and inner shelves and (B) Late spring conditions: reduced ice cover on the shelf and 2-layer stratification in the middle shelf. Light gray lines indicate density isolines of the water column meant to be illustrative of typical seasonal stratification based on information from published studies (Kinder and Schumacher, 1981; Ladd and Stabeno, 2012). Hypothesized phytoplankton assimilation of ^{15}N-enriched ammonium relative to ambient nitrate uptake in the water column is illustrated below the corresponding shelf regions for both scenarios. Uptake of water column ammonium is prevalent on the middle and inner shelves in winter relative to nitrate consumption, but nitrate consumption is dominant in the spring over the entire shelf. $\delta^{15}N$ values of water column NO_3^- represent initial nitrate $\delta^{15}N$ and are taken from Granger et al. (2011).

they would rely on the ambient NH_4^+ pool rather than NO_3^- for N nutrition (Dortch, 1990). Moreover, the reliance of phytoplankton on ammonium should be more pronounced on the ice-covered inner and middle shelves, where ammonium concentrations were the highest and primary production the lowest. At the ambient NH_4^+ concentrations observed in these regions, ammonium inhibition of nitrate uptake and assimilation is possible, and would also be enhanced by the low light conditions (Dortch, 1990). On the outer shelf, the small contribution of ammonium to the total DIN pool should curtail its relative uptake by phytoplankton and its consequent influence on $\delta^{15}N_{POM}$.

As NO_3^- consumption becomes more dominant with increasing productivity throughout the shelf $\delta^{15}N_{POM}$ should subsequently decrease from the high value imposed by NH_4^+ assimilation, to converge on the $\delta^{15}N$ imposed by nitrate assimilation – a scenario that is consistent with our observations. This mechanism can adequately explain the early to late season shift in $\delta^{15}N_{POM}$ of two stations (Stn. 31 – 107 and 38 – 111), with late season values upon the inception of algal growth aligning closer to expectations from Rayleigh dynamics for nitrate assimilation (Fig. 5A). Thus, the algal consumption of ^{15}N-enriched NH_4^+ in the water column can adequately explain both the broad-scale shelf-wide spatial patterns we observed as well as temporal changes in $\delta^{15}N_{POM}$ of the ice-covered shelf in early spring.

4.4. Implications for inter-seasonal N dynamics on the shelf

Reported measurements of the $\delta^{15}N$ of organic material and zooplankton on the southeastern Bering shelf are consistent with the patterns observed here (Schell et al., 1998; Smith et al., 2002; Guo et al., 2004). Maximum $\delta^{15}N$ of material collected in sediment traps at the NOAA Mooring Station M2 on the middle shelf (56°53′N, 164°02′W) varied from 15‰ in spring down to 9‰ in summers (Smith et al., 2002). Similarly, suspended particulate organic material (SPOM; $>0.8\,\mu m$ POM filtered from water samples onto a glass fiber filter) and net plankton (NP; collected from net tows) sampled concurrently at this location in late spring had a comparable $\delta^{15}N$ range (6–15‰) (Smith et al., 2002). In contrast, the $\delta^{15}N$ of SPOM measured in early fall by Guo et al. (2004) spanned a lower range (4–9‰). Generally the values we observed on the ice-covered middle shelf are similar to the upper range of values reported previously for late spring, and distinctly higher than those reported for the fall, while at the outer shelf our $\delta^{15}N_{POM}$ values (2.1–8.2‰; Figs. 3 and 5A) are more similar to those reported in both summer and fall. Thus, our observations in the context of previously reported measurements intimate a late winter to summer decrease in the $\delta^{15}N$ of POM.

As in our study, both of the previous studies reported an increase in the $\delta^{15}N$ of organic material from the outer to the

inner shelf (Smith et al., 2002; Guo et al., 2004). A similar trend was also observed shelf-wide for zooplankton sampled in the fall, with $\delta^{15}N_{Zoo}$ increasing shoreward and northward across the shelf (copepods: 6–12‰; euphausiids: 8–10‰; chaetognaths: 10–16‰) (Schell et al., 1998). Although the data of Schell et al. (1998) mirror the relative spatial pattern in $\delta^{15}N_{Zoo}$ as reported here, we observe some markedly higher maximum $\delta^{15}N_{Zoo}$ values than the fall values reported by that study, particularly among individual euphausiids and copepods (Fig. 4). While the possibility of seasonal variability in the trophic structure cannot be definitively ruled out, this is best explained by the spring to fall $\delta^{15}N$ decrease in POM.

We have proposed that the differential algal consumption of the water column NH_4^+ regenerated from shelf sediments vs. water column nitrate can adequately account for the entire range of elevated $\delta^{15}N_{POM}$ of the ice-covered shelf in early spring, and that this can also explain the $\delta^{15}N_{POM}$ decrease from winter to spring and summer (Fig. 6). This explanation requires the high-$\delta^{15}N$ NH_4^+ in the water column to have increasing influence from the outer to the inner domain, consistent with its greater prevalence inshore. Moreover this mechanism would be most prominent in winter, when light limitation of algae by sea ice cover causes as stronger preference for ammonium. By itself, however, this mechanism cannot account for a similar cross-shelf gradient in POM and zooplankton in the early fall, when sea ice is absent, and at which time dissolved inorganic nitrogen ($DIN = NO_3^- + NH_4^+$) in surface waters is exhausted, so that $\delta^{15}N_{POM}$ should be that of the original pooled DIN.

Granger et al. (2011) proposed that DIN becomes ^{15}N-enriched inshore relative to the $\delta^{15}N$ of DIN at the continental slope due to net isotopic fractionation during coupled nitrification–denitrification, manifested as the benthic efflux of high-$\delta^{15}N$-ammonium to the water column. The shoreward and northward increase in zooplankton and POM $\delta^{15}N$ observed in late summer and fall (Schell et al., 1998; Smith et al., 2002; Guo et al., 2004) can then be explained as recording this shoreward and northward increase in DIN $\delta^{15}N$ imparted by benthic N loss. Thus we propose that the pattern of elevated $\delta^{15}N$ in organic matter inshore during winter is due to the reliance of sea ice-covered phytoplankton on high-$\delta^{15}N$ ammonium derived from sediments, while a less pronounced shoreward POM $\delta^{15}N$ increase is present in summer/fall as the biomass produced captures the weaker but still significant, shoreward increase in the $\delta^{15}N$ of the entire DIN pool. In summary the preferential removal of low-$\delta^{15}N$ DIN to benthic denitrification on the shelf appears to underlie the spatial pattern in $\delta^{15}N$ of organic matter on the eastern Bering shelf but sea ice cover modulates the seasonality of this signal by driving wintertime consumption of ammonium, the component of the DIN with the highest $\delta^{15}N$.

4.5. Implications for characterizing food webs on the eastern shelf

The year-round presence of a spatial gradient in the $\delta^{15}N$ of particulate organic matter and zooplankton whose magnitude exhibits a seasonality modulated by sea ice has important implications for the use of N isotopes to study the diets, foraging ecology, and habitat use of animals on the eastern Bering shelf. Our findings show that there is substantial, albeit predictable, spatial and temporal variability in the $\delta^{15}N$ of primary production available to primary consumers, which is likely to be reflected beyond the primary consumer level. Indeed a recent study of krill, pollock, and seabird $\delta^{15}N$ around the Pribilof Islands reveals that the cross-shelf gradient of $\delta^{15}N$ on the eastern Bering shelf is detectable at the scale of 10–100 km, exerting a multi-trophic influence that propagates all the way from zooplankton to top-tier seabird predators (Jones et al., 2014). Knowledge that the spatial gradient in $\delta^{15}N$ is adequately strong to be detectable at scales as fine as 10 km opens up the possibility of studying animal migration and detecting use of foraging areas not only on shelf vs. non-shelf areas and distant basins (e.g., Schell et al., 1989; Lee et al., 2005; Oppel and Powell, 2008), but also within sub-regions of the eastern Bering shelf.

Furthermore, the seasonal variation in $\delta^{15}N$ is also pertinent to interpreting the causes of variation in $\delta^{15}N$ observed for animals among seasons. Because there is some degree of temporal variation in the magnitude of the signal at locations under the influence of sea ice (i.e., inner and middle shelf locations), care must be taken to design studies that will allow researchers to distinguish whether seasonal fluctuations in the $\delta^{15}N$ of higher level consumers are due to changes in the trophic level consumed, in the spatial extent of foraging, or in temporal variations of the $\delta^{15}N$ at the base of the food-web (Newsome et al., 2010). For example, higher $\delta^{15}N$ in wintering salmon on the Bering shelf compared to summer values were attributed to consumption of prey at higher trophic levels, despite accompanying evidence of greater contribution of low-level consumers to stomach contents during winter (Fournier, 2011). Our results suggest that elevated wintertime $\delta^{15}N$ of salmon can be explained by the winter increase in the baseline $\delta^{15}N$ of prey on the ice-covered shelf, reaffirming the importance of accounting for $\delta^{15}N$ at the base of the food web when interpreting trophic structure (Vander Zanden and Rasmussen, 1999).

This study illustrates the indirect role of sea ice in modulating the $\delta^{15}N$ of primary producers in late winter, by creating conditions for light-limited growth reliant on ammonium in the water column. The origin of the distinct $\delta^{15}N$ signal of ammonium reflects the coupling of N cycling between the water column and benthos, and this coupling ultimately accounts for a ^{15}N enrichment of the total DIN pool inshore, which is reflected in biomass production regardless of season. This study thus provides a mechanistic basis to explain variations in the $\delta^{15}N$ of primary producers on the eastern shelf that will guide interpretations of trophic dynamics of the shelf ecosystem.

Acknowledgments

Funding for this project was provided by NSF grants ANT-0453680, ARC-0612198, and ARC-0732767, the John T. Bonner Senior Thesis Fund of the Princeton University Ecology and Evolutionary Biology Department, the Grand Challenges Program and the Wallbridge Fund, and the Round Table Thesis Fund of Princeton University Office of the Dean of Undergraduates. Thanks to Frank-Yi Wang, Jason Cutrera, Kritee, and Haojia Ren for technical and lab support; Danielle Schmitt, Katherine Shull, Shannon Tronick, the Bender Lab, and the Morel Lab for equipment use; and Alexander Pinchuk for zooplankton identification, Carin Ashjian, and the BEST 2007–2008 science crew and ship crews for all logistical and technical support in the field. We also thank three anonymous reviewers for improving the manuscript. Data from the BEST Data Archive was provided by NCAR.EOL under sponsorship of the National Science Foundation at DSRII-3652.xml. This is BEST–BSIERP Bering Sea Project Publication Number 140.

Appendix A. Supporting information

Supplementary data associated with this article can be found in the online version at http://dx.doi.org/10.1016/j.dsr2.2014.05.008.

References

Ashjian/LDEO, 2008. HLY-08-02 Aloftcon camera images. In: NCAR/EOL (Ed.), ⟨http://data.eol.ucar.edu/codiac/dss/id=102.021⟩.

Bohonak, A.J., 2004. RMA Software for reduced major axis regression, 1.17. ⟨http://www.bio.sdsu.edu/pub/andy/rma.html⟩.

Braman, R.S., Hendrix, S.A., 1989. Nanogram nitrite and nitrate determination in environmental and biological materials by vanadium(III) reduction with chemiluminescence detection. Anal. Chem. 61, 2715–2718.
Brunelle, B.G., Sigman, D.M., Cook, M.S., Keigwin, L.D., Haug, G.H., Plessen, B., Schettler, G., Jaccard, S.L., 2007. Evidence from diatom-bound nitrogen isotopes for subarctic Pacific stratification during the last ice age and a link to North Pacific denitrification changes. Paleoceanography 22, PA125.
Casciotti, K.L., Sigman, D.M., Hastings, M.G., Bohlke, J.K., Hilkert, A., 2002. Measurement of the oxygen isotopic composition of nitrate in seawater and freshwater using the denitrifier method. Anal. Chem. 74, 4905–4912.
Coachman, L.K., 1986. Circulation, water masses, and fluxes on the southeastern Bering Sea shelf. Cont. Shelf Res. 5, 23–108.
Coachman, L.K., Walsh, J.J., 1981. A diffusion model of cross-shelf exchange of nutrients in the southeastern Bering Sea. Deep-Sea Res. 28A, 819–846.
Cozzi, S., Cantoni, C., 2011. Stable isotope (d13C and d15N) composition of particulate organic matter, nutrients and dissolved organic matter during spring ice retreat at Terra Nova Bay. Antarct. Sci. 23, 43–56.
Dieckmann, G.S., Lange, M.A., Ackley, S.F., Jennings, J.C., 1991. The nutrient status in sea ice of the Weddell Sea during winter: effects of sea ice texture and algae. Polar Biol. 11, 449–456.
Dortch, Q., 1990. The interaction between ammonium and nitrate uptake in phytoplankton. Mar. Ecol. Prog. Ser. 61, 183–201.
Fournier, W.J., 2011. Seasonal and Interannual Variation in Food Habits and Growth of Chinook Salmon (*Oncorhynchus tshawytscha*) in the Bering Sea, School of Aquatic and Fishery Sciences. University of Washington p. 67.
Fripiat, F., Cardinal, D., Tison, J.L., Worby, A., 2007. Diatom-induced silicon isotopic fractionation in Antarctic sea ice. J. Geophys. Res. 112, G02001.
Gradinger, R., 1999. Vertical fine structure of the biomass and composition of algal communities in Arctic pack ice. Mar. Biol. 133, 745–754.
Gradinger, R., 2009. Sea-ice algae: major contributors to primary production and algal biomass in the Chukchi and Beaufort Seas during May/June 2002. Deep-Sea Res. II 56, 1201–1212.
Gradinger, R., Bluhm, B., Iken, K., Frey, L., 2008. Standard sea ice observation reports Healy Cruises HLY-08-01 and HLY-08-02. In: NCAR/EOL (Ed.), ⟨http://catalog.eol.ucar.edu/cgi-bin/best_hly-08-02/research/prod_browse?platform=ice_observations&prod=report&howmany=All&start=Start+Date&end=End+Date&submit=Get+Data⟩.
Gradinger, R., Iken, K., Bluhm, B., 2012. Particulate organic carbon and nitrogen concentrations and stable isotopes in Bering Sea ice. In: EOL/NCAR (Ed.), ⟨http://data.eol.ucar.edu/codiac/dss/id=102.267⟩.
Granger, J., Prokopenko, M.G., Mordy, C.W., Sigman, D.M., 2013. The proportion of remineralized nitrate on the ice-covered eastern Bering Sea shelf evidenced from the oxygen isotope ratio of nitrate. Global Biogeochem. Cycles 27, http://dx.doi.org/10.1002/gbc.20075.
Granger, J., Prokopenko, M.G., Sigman, D.M., Mordy, C.W., Morse, Z.M., Morales, L.V., Sambrotto, R.N., Plessen, B., 2011. Coupled nitrification–denitrification in sediment of the eastern Bering Sea shelf leads to ^{15}N enrichment of fixed N in shelf waters. J. Geophys. Res.: Oceans 116, C11006.
Guo, L., Tanaka, T., Wang, J., Tanaka, N., Murata, A., 2004. Distributions, speciation and stable isotope composition of organic matter in the southeastern Bering Sea. Mar. Chem. 91, 211–226.
HLY-07-01ScienceCrew, 2007. Standard sea ice observation reports Healy Cruises HLY-07-01 and HLY-07-02. In: NCAR/EOL (Ed.), ⟨http://catalog.eol.ucar.edu/cgi-bin/best/research/prod_browse?platform=ice_observations&prod=report&howmany=All&start=Start+Date&end=End+Date&submit=Get+Data⟩.
Hobson, K.A., Ambrose, W.G., Renaud, P.E., 1995. Sources of primary production, benthic–pelagic coupling, and trophic relationships within the Northeastern Water Polynya: insights from $\delta^{13}C$ and $\delta^{15}N$ analysis. Mar. Ecol. Prog. Ser. 128, 1–10.
Hobson, K.A., Welch, H.E., 1992. Determination of trophic relationships within a high Arctic marine food web using $\delta^{13}C$ and $\delta^{15}N$ analysis. Mar. Ecol. Prog. Ser. 84, 9–18.
Horner, R.A., 1985. Sea Ice Biota. CRC Press, Boca Raton p. 215.
Hoch, M.P., Fogel, M.L., Kirchman, D.L., 1992. Isotope fractionation associated with ammonium uptake by a marine bacterium. Limnol. Oceanogr. 37, 1447–1459.
Iken, K., Gradinger, R., Bluhm, B., 2012a. HLY-08-02 particulate organic matter (POM) isotopes. In: EOL/NCAR (Ed.), ⟨http://data.eol.ucar.edu/codiac/dss/id=102.269⟩.
Iken, K., Gradinger, R., Bluhm, B., 2012b. HLY-08-02 plankton isotopes. In: EOL/NCAR (Ed.), ⟨http://data.eol.ucar.edu/codiac/dss/id=102.271⟩.
Jones, N.M., Hoover, B.A., Heppell, S.A., Kuletz, K.J., 2014. A cross-shelf gradient in stable isotope values of krill and pollock indicates seabird foraging patterns in the Bering Sea. Deep-Sea Res. II 109, 241–250, http://dx.doi.org/10.1016/j.dsr2.2014.04.008.
Kinder, T.H., Schumacher, J.D., 1981. Hydrographic structure over the continental shelf of the southeastern Bering Sea. In: Hood, D.W., Calder, J.A. (Eds.), The Eastern Bering Sea Shelf, Oceanography and Resources. University of Washington, pp. 31–52.
Ladd, C., Stabeno, P.J., 2012. Stratification on the Eastern Bering Sea shelf revisited. Deep-Sea Res. II 65-70, 72–83.
Lee, S.H., Schell, D.M., McDonald, T.L., Richardson, W.J., 2005. Regional and seasonal feeding by bowhead whales *Balaena mysticetus* as indicated by stable isotope ratios. Mar. Ecol. Prog. Ser. 285, 271–287.
Lee, S.H., Stockwell, D., Whitledge, T.E., 2010. Uptake rates of dissolved inorganic carbon and nitrogen by under-ice phytoplankton in the Canada Basin in summer 2005. Polar Biol. 33, 1027–1036.
Lomas, M.W., 2008. Phytoplankton counts and carbon data. In: NCAR/EOL (Ed.), ⟨http://data.eol.ucar.edu/codiac/dss/id=102.163⟩.
Lomas/BIOS, 2008. Chlorophyll and primary production. In: NCAR/EOL (Ed.), ⟨http://data.eol.ucar.edu/codiac/dss/id=102.136⟩.
Mariotti, A., Germon, J.C., Hubert, P., Kaiser, P., Letolle, R., Tardieux, A., Tardieux, P., 1981. Experimental determination of nitrogen kinetic isotope fractionation: some principles; illustration for the denitrification and nitrification processes. Plant Soil 62, 413–430.
Mathis, J.T., Cross, J.N., Bates, N.R., Moran, S.B., Lomas, M.W., Mordy, C.W., Stabeno, P.J., 2010. Seasonal distribution of dissolved inorganic carbon and net community production on the Bering Sea shelf. Biogeosciences 7, 1769–1787.
McMinn, A., Skerratt, J., Trull, T., Ashworth, C., Lizotte, M., 1999. Nutrient stress gradient in the bottom 5 cm of fast ice, McMurdo Sound, Antarctica. Polar Biol. 21, 220–227.
Michener, R.H., Kaufman, L., 2007. Stable isotope ratios as tracers in marine food webs: an update. In: Michener, R.H., Lajtha, Kate (Eds.), Stable Isotopes in Ecology and Environmental Science. Blackwell Publishing Ltd, Massachussetts, USA, pp. 238–282.
Minagawa, M., Wada, E., 1984. Stepwise enrichment of ^{15}N along food-chains: further evidence and the relation between $\delta^{15}N$ and animal age. Geochim. Cosmochim. Acta 48, 1135–1140.
Mock, T., Gradinger, R., 1999. Determination of Arctic ice algal production with a new in situ incubation technique. Mar. Ecol. Prog. Ser. 177, 15–26.
Morales, L.V., Sigman, D.M., Horn, M.G., Robinson, R.S., 2013. Cleaning methods for the isotopic determination of diatom-bound nitrogen in non-fossil diatom frustules. Limnol. Oceanogr. Methods 11, 101–112.
Moran, S.B., Lomas, M.W., Kelly, R.P., Gradinger, R., Iken, K., Mathis, J.T., 2012. Seasonal succession of net primary productivity, particulate organic carbon export, and autotrophic community composition in the eastern Bering Sea. Deep-Sea Res. II 65-70, 84–87.
Munro, D.R., Dunbar, R.B., Mucciarone, D.A., Arrigo, K.R., Long, M.C., 2010. Stable isotope composition of dissolved inorganic carbon and particulate organic carbon in sea ice from the Ross Sea, Antarctica. J. Geophys. Res., 115.
Napp, J., 2007. Spring chlorophyll concentrations on the Eastern Bering Sea Shelf. In: NCAR/EOL (Ed.), ⟨http://data.eol.ucar.edu/codiac/dss/id=102.079⟩.
Newsome, S.D., Clementz, M.T., Koch, P.L., 2010. Using stable isotope biogeochemistry to study marine mammal ecology. Mar. Mamm. Sci. 26, 509–572.
Notz, D., Worster, M.G., 2009. Desalination processes of sea ice revisited. J. Geophys. Res.: Oceans, 114.
Oppel, S., Powell, A.N., 2008. Assigning king eiders to wintering regions in the Bering Sea using stable isotopes of feathers and claws. Mar. Ecol. Prog. Ser. 373, 149–156.
Overland, J.E., Salo, S.A., Kantha, L.H., Clayson, C.A., 1999. Thermal stratification and mixing on the Bering Sea shelf. In: Loughlin, T.R., Ohtani, K. (Eds.), Dynamics of the Bering Sea. University of Alaska Sea Grant College Program Report. University of Alaska Sea Grant College Program, Alaska, pp. 129–146.
Papadimitriou, S., Kennedy, H., Kattner, G., Dieckmann, G.S., Thomas, D.N., 2004. Experimental evidence for carbonate precipitation and CO_2 degassing during sea ice formation. Geochim. Cosmochim. Acta 68, 1749–1761.
Pennock, J.R., Velinsky, D.J., Ludlam, J.M., Sharp, J.H., Fogel, M.L., 1996. Isotopic fractionation of ammonium and nitrate during uptake by *Skeletonema costatum*: implications for $\delta^{15}N$ dynamics under bloom conditions. Limnol. Oceanogr. 41, 451–459.
Pineault, S., Tremblay, J.E., Gosselin, M., Thomas, H., Shadwick, E., 2013. The isotopic signature of particulate organic C and N in bottom ice: key influencing factors and applications for tracing the fate of ice-algae in the Arctic Ocean. J. Geophys. Res.: Oceans 118, 1–14.
Rau, G.H., Sullivan, C.W., Gordon, L.I., 1991. $\delta^{13}C$ and $\delta^{15}N$ variations in Weddell Sea particulate organic matter. Mar. Chem. 35, 355–369.
Rho, T., Whitledge, T.E., 2007. Characteristics of seasonal and spatial variations of primary production over the southeastern Bering Sea shelf. Cont. Shelf Res. 27, 2556–2569.
Robinson, R.S., Brunelle, B.G., Sigman, D.M., 2004. Revisiting nutrient utilization in the glacial Antarctic: evidence from a new method for diatom-bound N isotopic analysis. Paleoceanography, 19.
Robinson, R.S., Sigman, D.M., 2008. Nitrogen isotopic evidence for a poleward decrease in surface nitrate within the ice age Antarctic. Quat. Sci. Rev. 27, 1076–1090.
Robinson, R.S., Sigman, D.M., DiFiore, P.J., Rohde, M.M., Mashiotta, T.A., Lea, D.W., 2005. Diatom-bound N-15/N-14: new support for enhanced nutrient consumption in the ice age subantarctic. Paleoceanography, 20.
Rowe, G.T., Phoel, W.C., 1992. Nutrient regeneration and oxygen-demand in Bering Sea continental-shelf sediments. Cont. Shelf Res. 12, 439–449.
Rysgaard, S., Glud, R.N., 2004. Anaerobic N_2 production in Arctic sea ice. Limnol. Oceanogr. 49, 86–94.
Rysgaard, S., Glud, R.N., Sejr, M.K., Blicher, M.E., Stahl, H.J., 2008. Denitrification activity and oxygen dynamics in Arctic sea ice. Polar Biol. 31, 527–537.
Sambrotto/LDEO, 2007. HLY-07-01 Aloftcon camera images. In: NCAR/EOL (Ed.), ⟨http://data.eol.ucar.edu/codiac/dss/id=102.001⟩.
Sambrotto, R.N., Niebauer, H.J., Goering, J.J., Iverson, R.L., 1986. Relationships among vertical mixing, nitrate uptake, and phytoplankton growth during the spring bloom in the southeast Bering Sea middle shelf. Cont. Shelf Res. 5, 161–198.
Schell, D.M., Barnett, B.A., Vinette, K.A., 1998. Carbon and nitrogen isotope ratios in zooplankton of the Bering, Chukchi and Beaufort seas. Mar. Ecol. Prog. Ser. 162, 11–23.

Schell, D.M., Saupe, S.M., Haubenstock, N., 1989. Natural isotope abundances in bowhead whale (*Balaena mysticetus*) baleen: markers of agins and habitat usage. Ecol. Stud. 68, 260–269.

Schlitzer, R., 2012. Ocean Data View, ⟨http://odv.awi.de⟩.

Sigman, D.M., Altabet, M.A., Francois, R., McCorkle, D.C., Gaillard, J., 1999. The isotopic composition of diatom-bound nitrogen in Southern Ocean sediments. Paleoceanography 14, 118–134.

Sigman, D.M., Casciotti, K.L., Andreani, M., Barford, C., Galanter, M., Bohlke, J.K., 2001. A bacterial method for the nitrogen isotopic analysis of nitrate in seawater and freshwater. Anal. Chem. 73, 4145–4153.

Sigman, D.M., Granger, J., 2011. HLY-08-02 nitrate N and O natural abundance stable isotope ratios. In: NCAR/EOL (Ed.), ⟨http://data.eol.ucar.edu/codiac/dss/id=102.249⟩.

Sigman, D.M., Karsh, K.L., Casciotti, K.L., 2009. Nitrogen isotopes in the ocean. In: Steele, J.H., Thorpe, S.A., Turekian, K.K. (Eds.), Encyclopedia of Ocean Sciences, 2nd ed. Academic Press, New York, pp. 1884–1894.

Smith, S.L., Heinrichs, S.M., Rho, T., 2002. Stable C and N isotopic composition of sinking particles and zooplankton over the southeastern Bering Sea shelf. Deep-Sea Res. II 49, 6031–6050.

Springer, A.M., McRoy, C.P., Flint, M.V., 1996. The Bering Sea Green Belt: shelf-edge processes and ecosystem production. Fish Oceanogr 5, 205–223.

Stabeno, P., Napp, J., Mordy, C., Whitledge, T., 2010. Factors influencing physical structure and lower trophic levels of the eastern Bering Sea shelf in 2005: sea ice, tides and winds. Prog. Oceanogr. 85, 180–196.

Stabeno, P.J., Bond, N.A., Salo, S.A., 2007a. On the recent warming of the south-eastern Bering Sea shelf. Deep-Sea Res. II 54, 2599–2618.

Stabeno, P.J., Farley Jr, E.V., Kachel, N.B., Moore, S., Mordy, C.W., Napp, J.M., Overland, J.E., Pinchuk, A.I., Sigler, M.F., 2012. A comparison of the physics of the northern and southern shelves of the eastern Bering Sea and some implications for the ecosystem. Deep-Sea Res. II 65–70, 14–30.

Stabeno, P.J., Kachel, N.B., Sullivan, M., Whitledge, T.E., 2002. Variability of physical and chemical characteristics along the 70-m isobath of the southeastern Bering Sea. Deep-Sea Res. II 49, 5931–5943.

Stabeno, P.J., Sonnerup, R., Mordy, C.W., Whitledge, T.E., 2007b. HLY-07-01 CTD and Nutrient Data, in: NCAR/EOL (Ed.), ⟨http://data.eol.ucar.edu/codiac/dss/id=102.016⟩.

Stabeno, P.J., Sonnerup, R., Mordy, C.W., Whitledge, T.E., 2008. HLY-08-02 CTD data. In: NCAR/EOL (Ed.), ⟨http://data.eol.ucar.edu/codiac/dss/id=102.058⟩.

Sukhanova, I.N., Semina, H.J., Venttsel, M.V., 1999. Spatial distribution and temporal variability of phytoplankton in the Bering Sea. In: Loughlin, T.R., Ohtani, K. (Eds.), Dynamics of the Bering Sea. University of Alaska Sea Grant College Program Report. University of Alaska Sea Grant College Program, Alaska, pp. 453–483.

Tamelander, T., Reigstadt, M., Hop, H., Carroll, M.L., Wassman, P., 2008. Pelagic and sympagic contributions of organic matter to zooplankton and vertical export in the Barents Sea marginal ice zone. Deep-Sea Res. II 55, 2330–2339.

Tomas, C.R., 1996. Identifying Marine Diatoms and Dinoflagellates. Academic Press, San Diego.

Vander Zanden, M.J., Rasmussen, J.B., 1999. Primary consumer δ^{13}Cand δ^{15}N and the trophic position of aquatic consumers. Ecology 80, 1395–1404.

Vo, J., Inwood, W., Hayes, J.M., Kustu, S., 2013. Mechanism for nitrogen isotope fractionation during ammonium assimilation by *Escherichia coli* K12. Proc. Natl. Acad. Sci. USA 110, 8696–8701.

Walsh, J.J., McRoy, C.P., 1986. Ecosystem analysis in the southeastern Bering Sea. Cont. Shelf Res. 5, 259–288.

Waser, N.A., Yin, K.D., Yu, Z.M., Tada, K., Harrison, P.J., Turpin, D.H., Calvert, S.E., 1998. Nitrogen isotope fractionation during nitrate, ammonium and urea uptake by marine diatoms and coccolithophores under various conditions of N availability. Mar. Ecol. Prog. Ser. 169, 29–41.

Waser, N.A., Yu, Z.M., Yin, K.D., Nielsen, B., Harrison, P.J., Turpin, D.H., Calvert, S.E., 1999. Nitrogen isotopic fractionation during a simulated diatom spring bloom: importance of N-starvation in controlling fractionation. Mar. Ecol. Prog. Ser. 179, 291–296.

Whitledge, T.E., Reeburgh, W.S., Walsh, J.J., 1986. Seasonal inorganic nitrogen distributions and dynamics in the southeastern Bering Sea. Cont. Shelf Res. 5, 109–132.

Yun, M.S., Chung, K.H., Zimmermann, S., Zhao, J.P., Joo, H.M., Lee, S.H., 2012. Phytoplankton productivity and its response to higher light levels in the Canada Basin. Polar Biol. 35, 257–268.

Zhang, L., Altabet, M.A., Wu, T., Hadas, O., 2007. Sensitive measurement of NH_4^+ $^{15}N/^{14}N$ ($\delta^{15}NH_4^+$) at natural abundance levels in fresh and saltwaters. Anal. Chem. 79, 5297–5303.

Deep-Sea Research II 109 (2014) 112–124

Contents lists available at ScienceDirect

Deep-Sea Research II

journal homepage: www.elsevier.com/locate/dsr2

Integrated assessment of the carbon budget in the southeastern Bering Sea

Jessica N. Cross [a,b,*], Jeremy T. Mathis [b], Michael W. Lomas [c], S. Bradley Moran [d], Matthew S. Baumann [d], David H. Shull [e], Calvin W. Mordy [b,f], Morgan L. Ostendorf [f], Nicholas R. Bates [g], Phyllis J. Stabeno [b], Jacqueline M. Grebmeier [h]

[a] University of Alaska Fairbanks, School of Fisheries and Ocean Sciences, 245 O'Neill Building, Fairbanks, AK 99775, USA
[b] National Oceanic and Atmospheric Administration, Pacific Marine Environmental Laboratory, 7600 Sand Point Way, Seattle, WA 98115, USA
[c] Bigelow Laboratory for Ocean Sciences, 60 Bigelow Drive, East Boothbay, ME 04544, USA
[d] Graduate School of Oceanography, University of Rhode Island, Narragansett, RI 02992-1197, USA
[e] Department of Environmental Sciences, Huxley College of the Environment, Western Washington University, Bellingham, WA 98225-9181, USA
[f] Joint Institute for the Study of the Atmosphere and Ocean, University of Washington, P.O. Box 455672, 3737 Brooklyn Ave. NE, Seattle, WA 98105-5672, USA
[g] Bermuda Institute of Ocean Sciences, 17 Biological Lane, St. Georges, Bermuda GE01, USA
[h] Chesapeake Biological Laboratory, University of Maryland Center for Environmental Science, P.O. Box 38, Solomons, MD 20688, USA

ARTICLE INFO

Available online 19 March 2014

Keywords:
Bering Sea
Carbon budget
Biogeochemistry
Bering Ecosystem Study

ABSTRACT

During the primary field program for the Bering Ecosystem Study (2008–2010), independent seasonal estimates of net primary production (*NPP*), net community production (*NCP*), vertical export production (C_{exp}), and benthic carbon consumption (*BCC*) were used to construct a shelf-wide carbon budget for the southeastern Bering Sea. Here, we quantify the annual production, utilization, and transport of *NPP* for the southeastern shelf region of the Bering Sea (spatially partitioned into Outer, Middle, and Coastal Domains). We observed that approximately 25% and 30% of *NPP* on the shelf is exported horizontally from the Middle and Outer Domains, respectively. This horizontal transport was the dominant mode of carbon export in the Outer Domain, exceeding C_{exp} by more than 30 g C m^{-2} yr^{-1} (99 g C m^{-2} yr^{-1} compared to 67 g C m^{-2} yr^{-1}, respectively). In the Middle Domain, C_{exp} was more prominent than lateral transport (65 g C m^{-2} yr^{-1} and 46 g C m^{-2} yr^{-1}, respectively), and vertically exported carbon was more efficiently recycled in this Domain than in the Outer Domain (53% and 32% of C_{exp} respectively). In the Coastal Domain, lateral transport was a source of carbon to the bottom layer, with estimated input of carbon exceeding *NPP* by as much as 54 g C m^{-2} yr^{-1}. While the source of this additional carbon is unknown, one possible source is transport from the Middle Domain during wind events that induce coastal convergence. Overall, the combined carbon reservoir attributed to burial and transport in the Middle and Outer Domains is similar to a previous budget for this region (47%; Walsh and McRoy, 1986), although some qualitative differences are apparent. The data presented here indicate a more pelagic character in the Outer Domain relative to the Middle Domain, and that the Middle and Coastal Domain carbon budgets are balanced only when combined.

1. Introduction

The southeastern Bering Sea is one of the most productive shelf areas of the global ocean, with daily rates of net primary production (*NPP*) during ice edge blooms exceeding ~10 g C m^{-2} d^{-1} under optimal growth conditions (Niebauer et al., 1995; Lomas et al., 2012). The fate of this production has significant consequences for the attendant food web, and the energy provided by primary production sustains both pelagic and benthic commercial fisheries. However, varying physical and climatic conditions can favor energy accumulation in either the pelagic or the benthic compartments, with significant consequences for commercial populations (Hunt et al., 2002, 2011; Hunt and Stabeno, 2002). Remineralization of detrital production in the subsurface water column and underlying sediments results in the seasonal accumulation of carbon dioxide (CO_2) in bottom waters, sharply reducing seawater pH during the highly productive spring–summer period (Mathis et al., 2011a, b). This

* Corresponding author at: University of Alaska Fairbanks, School of Fisheries and Ocean Sciences, 245 O'Neill Building, Fairbanks, AK 99775, USA.
E-mail addresses: jncross@alaska.edu (J.N. Cross), jeremy.mathis@noaa.gov (J.T. Mathis), mlomas@bigelow.org (M.W. Lomas), sbmoran@mail.uri.edu (S.B. Moran), matthew.baumann@my.uri.edu (M.S. Baumann), david.shull@wwu.edu (D.H. Shull), mordy@uw.edu (C.W. Mordy), morgan.ostendorf@noaa.gov (M.L. Ostendorf), nick.bates@bios.edu (N.R. Bates), phyllis.stabeno@noaa.gov (P.J. Stabeno), jgrebmei@umces.edu (J.M. Grebmeier).

http://dx.doi.org/10.1016/j.dsr2.2014.03.003
0967-0645/

process increases the vulnerability to ocean acidification processes via the uptake of anthropogenic CO_2, and has been observed to result in undersaturation of important calcium carbonate ($CaCO_3$) minerals critical for shell-building organisms in both the Bering and Chukchi Seas (Bates et al., 2009; Mathis et al., 2011a, b; Cross et al., 2013).

Although it is clear that the balance of production and export is critical to understanding the functioning of the Bering Sea ecosystem, some portions of the carbon cycle remain poorly understood. For example, a paucity of data from near-coastal regions has resulted in limited and often conflicting patterns in temporal variability and the balance of primary production and export (e.g., Lomas et al., 2012; Moran et al., 2012). Other aspects of the carbon cycle have only recently gained attention, such as microzooplankton herbivory and surface bacterial remineralization loops (Moran et al., 2012; Olson and Strom, 2002; Sherr et al., 2013; Stoecker et al., 2014a,b). Recent physical and biogeochemical data has also provided some evidence that organic carbon losses due to lateral transport may be more complex than previously assumed (Danielson et al., 2012a, 2012b; Baumann et al., 2013a, 2013b).

In the last five years, oceanographic expeditions as part of the multidisciplinary Bering Sea Project provided an opportunity to evaluate independent estimates of the various rate and budget components of the Bering Sea shelf carbon cycle as a whole, and thereby to examine some of these unresolved carbon sinks. In this study, we provide a synthesis of net primary production (*NPP*), net community production (*NCP*), vertical export production (C_{exp}), and benthic carbon consumption (*BCC*) estimates to construct a budget for determining the fate of organic carbon production through heterotrophic utilization and transport across the southeastern Bering Sea shelf.

2. Methods

2.1. Sample collection

Physical, chemical, and biological measurements for the water column and sediments were collected as part of the Bering Sea Project during the following cruises: USCGC *Healy* during spring (April/May) of 2008 and 2009, and summer (July) of 2008; R/V *Knorr* in summer (June/July) of 2009; and R/V *Thomas G. Thompson* during late spring (May/June) and early summer (June/July) of 2010. Hydrographic (CTD) stations were occupied along two east–west transect lines (i.e., NP and CN lines) and one north–south transect along the 70 m isobath (i.e., 70 M) as well as in several regions of opportunity (Fig. 1). Biological and sediment studies were conducted at a subset of these stations. At the beginning of each spring cruise, sea ice cover was near 100% at all stations except for the southern stations of the 70 M line, which were sea-ice free when sampled during spring in all years. During spring of 2010, the timing of the occupation of some stations, as well as the spatial extent of sampling, was limited by the ice breaking capability of R/V *Thompson*. Some inshore stations were sampled later than usual during spring to allow for some sea ice melt. During summer observations, the entire Bering Sea shelf was sea-ice free for all years.

In order to facilitate a common spatial reference for the participants in the Bering Sea Project, the study region was divided into 16 standardized domains based on hydrographic structure, circulation patterns, and macrofaunal population distribution (Ortiz et al., 2012, Harvey and Sigler, 2013). Data included in this study were collected in Region 4, which we denote as the Southern Outer Domain; Regions 3 and 6, which we denote as the southern central domain; and Regions 2 and 7, which we denote as the Southern Coastal Domain (Fig. 1). Our domains comprise both

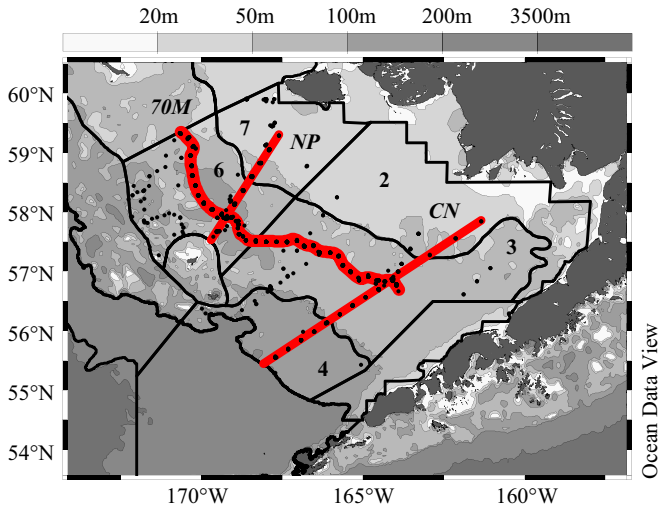

Fig. 1. A map of the southeastern Bering Sea shelf indicating sampling locations (dots) and major regions of the Bering Sea Shelf as defined by the Bering Sea Project (numbered regions delineated with dark black outlines). Bathymetry is shaded according to depth. Repeat hydrographic lines include the CN Line, the NP Line, and the 70 M Line.

the southern and the central portions of the eastern shelf according to the project definitions. However, a proviso to the definition of spatial domains is that the boundary between the southern and central shelves described by Ortiz et al. (2012) was included to distinguish the spatial area covered by historical groundfish surveys and has no hydrographic or biogeochemical context. In the absence of a strong boundary between the southern and central shelves, we combined these two areas in our synthesis effort. This study thus assumes that the northern boundary between the southeastern and northeastern portions of the shelves is a cross-shelf jet occurring in the vicinity of Nunivak Island (Danielson et al., 2011; Ortiz et al., 2012). Near the shelf break, biological regimes in the vicinity of the Pribilof Islands also led to the distinction of an elliptical domain (e.g., Cianelli et al., 2004; Hunt et al., 2008). Because of the unique processes occurring here, we have not included data collected in the Pribilof Domain (Region 5).

2.2. Sample analysis

2.2.1. Water column rate measurements

2.2.1.1. Net primary production (NPP). Samples for ^{14}C incubations were collected roughly every other day from depths approximately ~1.5%, ~5%, ~9%, ~17%, ~33%, ~55%, and ~100% light levels of surface incident photosynthetically active radiation (PAR) (Lomas et al., 2012). Light depths were determined by analysis of PAR profiles on the CTD downcast generated using an calibrated Biospherical Instruments PAR sensor. Net primary production (*NPP*) rates were calculated from the autotrophic incorporation of $NaH^{14}CO_3^-$ into particulate organic matter over a 24-h simulated in situ incubation using the ratio of added radiocarbon to total inorganic carbon present (Parsons et al., 1984; Lomas et al., 2012). Daily volumetric rates of *NPP* were integrated to the deepest sample depth (i.e., ~1.5% light level) and corrected for passive incorporation of $NaH^{14}CO_3^-$ using a dark control and the total added activity for the profile measured at the start of the incubation.

2.2.1.2. Net community production (NCP). *NCP* was measured using the seasonal drawdown of the photosynthetic reactants dissolved inorganic carbon (DIC; NCP_{DIC}) and total inorganic nitrogen

(nitrate+nitrite+ammonium or TIN; NCP_{TIN}) over the mixed layer depth (average=30 m). Samples for DIC were taken at every hydrographic station along the MN and NP lines and every other station along the 70 M line and analyzed according to the protocol of Mathis et al. (2010) and Cross et al. (2012) using the VINDTA 3C system (MARIANDA Inc.). These samples were calibrated using certified reference material provided by A.G. Dickson (Scripps Institute of Oceanography) and normalized to a deep water reference salinity of 35. *NCP* estimates were corrected for precipitation of carbonate minerals (e.g., Lee, 2001; Mathis et al., 2010).

Samples for nutrient analysis were syringe filtered using 0.45 μm cellulose acetate membranes, collected in 30-ml acid washed, high-density polyethylene bottles after three rinses, and analyzed shipboard within 1–12 h of collection. Nutrient analysis closely followed the WOCE-JGOFS standardization and analysis procedures specified by Gordon et al. (1994), including reagent preparation, calibration of lab ware, preparation of primary and secondary standards, and corrections for blanks and refractive index.

NCP_{DIC} values were taken from Mathis et al. (2010) and Cross et al. (2012) comprising measurements for both 2008 and 2009. Insufficient DIC observations in spring 2010 prevented the calculation of *NCP* for this year using inorganic carbon data. NCP_{TIN} calculations comprised data from all three years, and were performed as in Mordy et al. (2012), except that Mordy et al. only examined the middle shelf in 2008 and 2009, whereas we report NCP_{TIN} for all three years in each domain here. Data were converted from net nitrogen consumption to net carbon production via the Redfield Ratio (106C:16 N). While some older work has documented non-Redfield water column ratios of DIC:DIN, these perturbations were assumed to result from persistent denitrification processes, and did not necessarily imply non-Redfield phytoplankton uptake ratios (e.g., Codispoti et al., 1986). More recently, others have documented anomalous water column N:P ratios, resulting from increased phosphate demand during periods of rapid growth (Horak et al., 2013). Although unusually high phosphate content in particulate phytoplankton does not necessarily imply that C:N ratios should not conform to Redfield stoichiometry, some others have documented that low nitrate and high phosphate content relative to carbon content commonly co-occur in particulate phytoplankton (e.g., Martiny et al., 2013a, b). Here, we conform to the standard Redfield ratio, as utilized by Mordy et al. (2012).

2.2.1.3. POC export (C_{exp}). Vertical POC export (C_{exp}) flux was calculated using sediment trap POC mass, sediment trap ^{234}Th, and water column ^{234}Th/^{238}U disequilibrium, as described in Moran et al. (2012) and Baumann et al. (2013b). Surface tethered, free-floating sediment trap arrays were deployed in ice-free waters along the outer shelf and shelf break during spring and summer (n=spring and summer; 3 and 3 for 2008; 5 and 4 for 2009; 5 and 4 for 2010) (Baumann et al., 2013b). Briefly, sediment traps (4 per depth at depths of 25, 40, 50, 60 and 100 m) were filled with 0.4 μm pre-filtered, non-poisoned brine (S=~85‰) to isolate swimmers from settling material and deployed for ~1 d. Upon recovery and after settling, traps were siphoned to the seawater brine interface indicated by the discontinuity between layers. Traps were filtered onto a pre-combusted GF/F, sub-sampled (10 mm arc punch) for POC, and analyzed for ^{234}Th at sea.

Total (dissolved+particulate) ^{234}Th water column profiles were collected during each cruise throughout the shelf. ^{234}Th profiles were high resolution (~10 m) throughout the photic zone. Water column ^{234}Th samples were collected from CTD-rosette casts using the small volume (SV; 4 L) technique, in which ^{234}Th is extracted via co-precipitation with manganese oxide (MnO_2) (Benitez-Nelson et al., 2001; Buesseler et al., 2001). ^{234}Th contained on sediment trap and water column filter samples was quantified by the measurement of beta emissions of ^{234m}Pa (E_{max}=2.19 MeV; $t_{1/2}$=1.2 min) on a low-background beta detector (RISØ National Laboratory, Roskilde, Denmark; average detector efficiency: 44±3%). ^{238}U activities were calculated from salinity according to the relationship ^{238}U (dpm L^{-1})=salinity (‰)×0.0708 (Chen et al., 1986). The 10 mm arc punch POC subsamples were dried, fumed with HCl, dried and analyzed for POC on a Carlo Erba-440 Elemental Analyzer (Exeter Analytical, Inc., North Chelmsford, MA, USA) (Pike and Moran, 1997).

2.2.2. Sedimentary respiration rates and benthic carbon consumption (BCC)

Rates of sedimentary respiration were determined on intact sediment cores collected using an Ocean Instruments MC-800 eight-tube multicore. Up to three cores per station were incubated at near in situ temperatures for the determination of oxygen consumption rates. These were subcored using 8-cm diameter polycarbonate tubes. The cores were stored in the dark uncapped, for approximately 24 h, after which they were sealed with silicone stoppers equipped with magnetic stirrers and connected reservoirs containing bottom water from the same stations. Overlying water was sampled from each core over a period of 2–5 days and dissolved oxygen concentrations were determined using a fiber-optic oxygen microsensor (PreSens Microx TX3), calibrated before and after each reading. Oxygen fluxes were corrected using an empirical formula (y=1.125x+3.365, where y is the corrected flux and x is the uncorrected flux) for the slow diffusion of oxygen from the silicone stoppers used during incubations (Davenport et al., 2012). These fluxes were converted to benthic carbon consumption (*BCC*) via the revised Redfield ratio of carbon to oxygen (106 C:150 O_2; Anderson, 1995).

2.3. Carbon mass balance

While *NPP* and some carbon utilization and transport pathways were assessed through the Bering Sea Project as described above (*NPP*; *NCP*; C_{exp}; *BCC*), these parameters do not directly account for every aspect of the carbon cycle. However, these measurements do enable the calculation of the major carbon pathways and reservoirs; in particular, lateral carbon transport, heterotrophic respiration, and carbon accumulation in upper trophic level biomass. A generalized schematic of these sources and sinks are given in Fig. 2, separated into pelagic and benthic compartments.

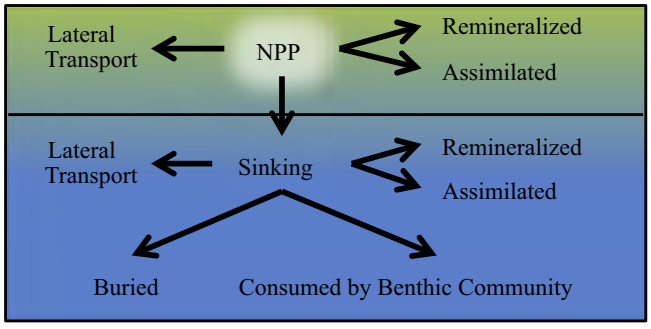

Fig. 2. Schematic showing the various budgetary components of the southeastern Bering Sea shelf carbon cycle. The pelagic compartment is shown in green and the benthic compartment is shown in blue. Arrows indicate sinks for the only organic carbon source parameterized in this budget, net primary production (*NPP*).

2.3.1. Surface layer heterotrophic respiration

There are two components to primary production: new production, which is composed of that portion of *NPP* that can be attributed to external nutrient inputs (typically nitrate); and regenerated production, which is driven predominantly by the re-assimilation of nutrients generated by the heterotrophic consumption of organic matter (typically ammonia and nitrite; Dugdale and Goering, 1967; Platt et al., 1977; Williams, 1993). By contrast, *NCP* measures the balance of *NPP* and heterotrophic (R_H) respiration processes across a given time period, such that $NCP = NPP - R_H$ (Williams, 1993). Often, *NCP* measurements assume that macronutrient limitation facilitates the rapid re-assimilation of any regenerated nutrients, such that *NCP* is conceptually equivalent to new production (e.g., Bates, 2006). Based on this assumption, the difference between *NPP* and *NCP* should be equal to regenerated production, with R_H occurring as a rapid intermediary step. During the early part of the production season, prior to the onset of nutrient limitation, we assume that there is some lag in this process, and that only late-season regenerated production is perfectly efficient. Over the entire production season, we assume that the difference between *NPP* and *NCP* can be partitioned evenly between regenerated production and heterotrophic respiration.

Outside of these theoretical definitions, measurement errors can also impact the magnitude of *T*; for example, sea-air CO_2 gas exchange and vertical diffusion have been shown to perturb NCP_{DIC} estimates by as much as 13% (Cross et al., 2012). This offset decreases NCP_{DIC} values, such that reported numbers can typically be considered conservative estimates. Here, a conservative estimate of NCP_{DIC} resulting from these offsets will also result in a conservative estimate of lateral transport (*T*).

2.3.2. Surface layer lateral transport

The offset between independent measurements of *NCP* by the drawdown of two separate photosynthetic reactants allowed for the calculation of carbon removal by lateral transport under the assumption of Redfield C and N production. Previous studies (e.g., Mathis et al., 2010; Cross et al., 2012; Mordy et al., 2012) have shown that NCP_{DIC} is generally greater than NCP_{TIN}. Errors in NCP_{DIC} due to diffusion, gas exchange, and natural offsets produced by variations in the phytoplankton C:N ratio (Sambrotto et al., personal communication) are not large enough to account for this imbalance. Instead, we propose that NCP_{DIC} and NCP_{TIN} are not equal due to the lateral movement of water with differing DIC:TIN ratios during the production season.

Because TIN is a limiting factor in primary production on the Bering Sea shelf and is typically depleted to near-zero levels by summer despite any spatial variation in spring TIN stocks, lateral transport does not strongly affect NCP_{TIN} calculations. In short, all TIN is utilized everywhere over the shelf, so the contribution of lateral transport to NCP_{TIN} estimates is difficult to observe. In contrast, non-limiting photosynthetic reactants like DIC are not uniformly depleted to a standard level, and lateral transport can alter NCP_{DIC} calculations. Further, the effect of lateral transport is magnified relative to TIN: Redfield production causes DIC to vary nearly ten times more strongly than nitrate, and resulting contributions of lateral transport to NCP_{DIC} are much more obvious. The amount of carbon exported by lateral transport (*T*) from the upper 30 m can therefore be estimated by the difference in *NCP* measured by seasonal DIC drawdown and TIN drawdown, such that $NCP_{DIC} - NCP_{TIN} = T$.

In the Outer Domain, a paucity of NCP_{TIN} data prevented the direct calculation of a transport term. However, Baumann et al. (2013a) estimate that ~30% of total ^{234}Th production in the water column is exported off-shelf from the Outer and Middle Domains. In the absence of discrete measurements, as an upper estimate we apply this 30% lateral mass transport loss factor to the Outer Domain.

2.3.3. Surface layer retained biomass

Direct measurement of export production allowed for the calculation of carbon retention at the surface layer by subtracting carbon losses from the initial *NPP* value, such that: $NPP - R_H - T - C_{exp}$ = surface layer retained biomass (*Bio*). Previous studies have shown that dissolved organic carbon (DOC) and lower trophic level particulate organic carbon (POC) do not accumulate in the surface layer (e.g., Cross et al., 2012; Baumann et al., 2013b). Therefore, any *NPP* unaccounted for by measured or assumed loss processes at the surface layer is likely not retained as part of the autotrophic carbon community, but rather is consumed and assimilated by higher trophic communities not included within the measured dissolved or particulate fractions.

2.3.4. Bottom layer carbon partitioning

We address the fate of exported carbon in bottom waters in two ways. First, we account for losses to benthic carbon consumption as directly measured by *BCC*. Second, we provide an upper estimate of carbon burial through a regional measurement of the thorium focusing factor (*FF*) as reported by Baumann et al. (2013a). The focusing factor describes the ratio of the inventory of ^{234}Th buried in the sediments relative to the water column deficit of ^{234}Th. While this is not a direct estimate of the carbon retention in the sediment, ^{234}Th is a particle reactive tracer, and can thus provide an upper-bound proxy for particulate carbon. By applying the percent focusing factor of ^{234}Th in the sediments to C_{exp}, we can provide a first-order, upper estimate of carbon burial (*B*). (Focusing factor estimates were not available for the Coastal Domain, which prevented the calculation of carbon burial in this region.) Additional losses of C_{exp} occur through heterotrophic consumption in the water column and bottom layer lateral transport. Some carbon will also be retained as accumulated biomass in higher trophic levels. However, we were not able to isolate these carbon reservoirs for bottom waters based on the available data.

3. Results

3.1. Net primary production

Twenty five seasonal estimates of *NPP* based on ^{14}C incubations integrated over the photic zone were available for the southeastern Bering Sea Shelf, although the timing and spatial orientation of these estimates varied widely. In particular, only one *NPP* profile was available for the Southern Outer Domain (Spring 2008). The Southern Middle Domain exhibited the best coverage, with 20 profiles spanning both seasons of all three years. The southern inner shelf was not sampled during 2008, while a spring profile is available for 2009 and both spring and summer profiles are available for 2010. In both spring and summer, *NPP* was much higher in the Middle Domain (118 ± 259 mmol C m^{-2} d^{-1} and 97 ± 153 mmol C m^{-2} d^{-1}, respectively) than in the Coastal Domain (7.5 ± 1.2 mmol C m^{-2} d^{-1} and 13.3 ± 8.2 mmol C m^{-2} d^{-1}). Spring *NPP* was slightly higher than summer *NPP* for the Middle Domain on average, while *NPP* for the Coastal Domain was 75% higher than in spring.

3.2. Net community production

Because *NCP* requires two seasonal occupations to calculate a single rate of drawdown of dissolved gases or nutrients, only one seasonal estimate is available as a directly measured value for each

year. However, most of the time period occurring between the seasonal occupations fell under the spring category. These *NCP* estimates are more a reflection of the seasonal drawdown of DIC and TIN integrated over the period of the spring bloom than the drawdown occurring over summer, and we denote these rates as typical of spring (Table 1).

Coverage of NCP_{DIC} over the shelf spanned all three domains. During spring of 2008 and 2009, DIC concentrations were nearly uniform throughout the water column and along each hydrographic section, indicating homogenized conditions typical of winter and preceding the spring bloom. DIC concentrations were drawn down as much as 176 μmol kg^{-1} by summer (Mathis et al., 2010; Cross et al., 2012), but varied spatially within each domain. At one station in the Southern Middle Domain, DIC concentrations in the upper 30 m were observed to increase between spring and summer. Some interannual variability was also observed. Coastal Domain NCP_{DIC} was higher in 2008 relative to 2009, while 2009 NCP_{DIC} was higher for the Middle and Outer Domains.

The greatest resolution for any single parameter in any single domain is provided by NCP_{TIN}. Approximately 33 seasonal profiles were available for the Southern Coastal Domain and nearly 200 for the Southern Middle Domain, although no seasonal estimates of NCP_{TIN} were available for the Southern Outer Domain. Additionally, this parameter represents the best temporal resolution of any other parameter in the dataset, with both spring and summer seasons sampled during all three years of the study.

Strong nutrient drawdown was observed between spring and summer station occupations, with substantial drawdown of bulk nutrient content integrated over the upper 30 m occurring by early to mid-May (e.g., year day 130; Fig. 3). The Middle Domain exhibited a much higher initial nutrient content (~200–500 mmol DIN m^{-2}) than the Coastal Domain (~50–250 mmol DIN m^{-2}). Additionally, low DIN concentrations were present in the water column through the summer season in the Middle Domain, while integrated values of DIN were substantially drawn down to <50 mmol DIN m^{-2} in the Coastal Domain. This spatial variation is typical of production in the Bering Sea. Limited macronutrient content (Sambrotto and Goering, 1983; Sambrotto et al., 1986; Whitledge et al., 1986; Springer and McRoy, 1993) but high micronutrient content (Aguilar-Islas et al., 2007; Hurst et al., 2010) of the Coastal Domain enables high rates of productivity in spring, but also facilitates faster and more complete drawdown of macronutrients. Prolonged productive periods are not typical of this domain relative to other areas of the shelf (Sambrotto et al., 1986; Whitledge et al., 1986; Springer and McRoy, 1993; Bond and Overland, 2005; Rho et al., 2005; Aguilar-Islas et al., 2007; Mathis et al., 2010). NCP_{TIN} was higher through the Southern Middle Domain than in the Southern Coastal Domain by a factor of two (20 ± 9 mmol C m^{-2} d^{-1} and 10 ± 3 mmol C m^{-2} d^{-1}, respectively; Table 1).

3.3. POC export

In total, 96 seasonal estimates of C_{exp} were made during the three years of this study. The C_{exp} rates given in Table 1 are an average of all three methods used to calculate this parameter, although some variability between the methods was observed. In general, sediment trap POC fluxes from open water deployments showed an increase in C_{exp} between spring and summer, while POC export estimated from ^{234}Th deficits generally decreased between the two seasons. Note that the sediment trap measurements of POC export were made only at the shelf-slope edge whereas POC export fluxes were determined from water column measurements of the ^{234}Th deficit (Baumann et al., 2013a) taken over the entire shelf. In areas where both sediment trap data and ^{234}Th profiles were taken at the same geographic locations, these different techniques agree to within a factor of 1.5–2 for POC export fluxes (Baumann et al., 2013b). In general, we observed that C_{exp} decreased by 15–25% between spring and summer (Table 1). The magnitude of this decrease increased towards the coast, indicating a stronger or more rapid seasonal cycle in the Coastal Domain than in the Middle and Outer Domains. Rates of C_{exp} were similar between the Outer and Middle Domains (22 ± 12 mmol C m^{-2} d^{-1} and 25 ± 11 mmol C m^{-2} d^{-1}, respectively), while C_{exp} was higher in the Coastal Domain (32 ± 8 mmol C m^{-2} d^{-1}), reflecting an increasing gradient towards the coast.

3.4. Benthic carbon consumption

Spring and summer estimates of benthic carbon consumption (*BCC*) were available for the Outer, Middle and Coastal Domains, comprising 26 total estimates. Most data were available for the central and Outer Domains, while only four samples were available for the Coastal Domain. In general, we observed that *BCC* increased towards the coast, although this gradient was much stronger during spring than during summer. Respiration rates were very similar across the entire shelf in the later production season, varying by 30% compared to the 75% variation observed in spring. A shelf-wide average shows that benthic respiration decreases between spring and summer, although there was some cross-shelf gradient in this parameter. Rates of *BCC* decreased strongly from spring to summer in the Coastal Domain (~45%; Table 1), while these increased in the Outer Domain by an equivalent margin (~51%; Table 1). Benthic respiration was very similar between spring and summer for the Middle Domain (7.9 ± 4 mmol C m^{-2} d^{-1} and 8.0 ± 4 mmol C m^{-2} d^{-1}). However, the high respiration rate observed in the Coastal Domain in spring increased the average spring respiration rate over the shelf, contributing to a bias in the shelf-wide average towards the pattern of production observed in the Coastal Domain. Relative to other parameters, however, an 18% change occurring between the two seasons was minimal.

Table 1
Carbon production, utilization, and transport (2008–2010). Independently measured seasonal rates of carbon production, utilization and transport for the three domains of the southern shelf between 2008 and 2010 in mmol C m^{-2} d^{-1}. *NPP* estimates of the southern Outer Domain were available only in summer, and include only one profile. *NCP* estimates were made between spring and summer. The measured rates are more heavily influenced by spring than summer dynamics, and are thus listed here as the spring rate. Subsequently, summer rates for *NCP* were not available. NCP_{TIN} was not measured in the southern Outer Domain. A focusing factor (*FF*) estimate from Baumann et al. (2013a) was not available for the Coastal Domain. Error listed is one standard deviation from the mean.

Parameter	Abbr.	Southern Outer Domain		Southern Middle Domain		Southern Coastal Domain	
		Spring	Summer	Spring	Summer	Spring	Summer
Net primary production	*NPP*	–	75.5 ± –	117.8 ± 259.3	96.7 ± 153.4	7.5 ± 1.2	13.3 ± 8.2
Net community production from DIC	NCP_{DIC}	45.0 ± 17.1	–	38.6 ± 33.5	–	15.8 ± 14.8	–
Net community production from TIN	NCP_{TIN}	–	–	20.2 ± 8.5	–	9.7 ± 2.8	–
Export production	C_{exp}	21.7 ± 12.1	22.4 ± 12.3	24.4 ± 11.3	19.9 ± 11.0	31.8 ± 7.6	23.8 ± 13.5
Focusing factor	*FF*	0.3 ± 0.1	0.2 ± 0.2	0.3 ± 0.1	0.2 ± 0.1	–	–
Benthic carbon consumption	*BCC*	4.1 ± 0.8	6.2 ± 2.5	7.9 ± 3.8	8.0 ± 4.1	16.0 ± 1.8	8.8 ± 3.5

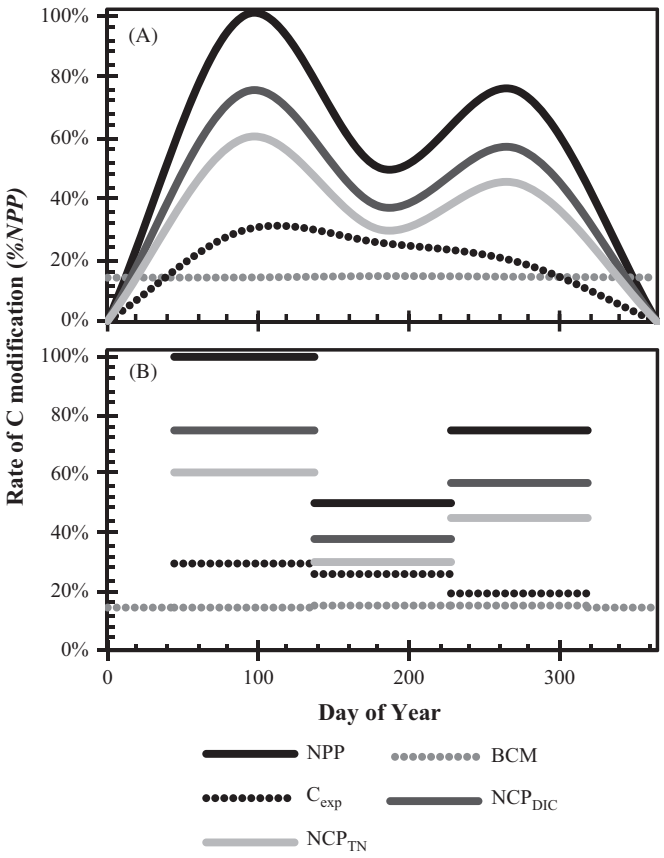

Fig. 3. The normalized rate of carbon modification occurring in each of the four seasons, relative to peak *NPP*, which occurs in spring, according to the generalized seasonal cycle determined through the literature record and our available measurements, as indicated in Table 1(A) and describing the possible annual extrapolation of seasonal measurements (B), which does not include any rate variations within a particular season.

4. Discussion

4.1. An annual model for the SE Bering Sea carbon cycle

Assuming that the SE Bering Sea carbon budget is imbalanced on the seasonal scale, it will be difficult to assess long-term (e.g., decadal) imbalances due to losses of carbon to lateral transport using a seasonal resolution. To eliminate seasonal imbalances resulting from natural biogeochemical processes, it is therefore necessary to assess the budget on the annual scale. However, previous work has discussed the challenges facing synthesis efforts of biogeochemical data sets due to the heterogeneity of processes that occur over short time and space scales on the Bering Sea shelf (e.g., Lomas et al., 2012). Spatiotemporal variability is difficult to resolve given widespread station locations, spatially extensive regional domains, and infrequent samplings. An attempt to define an annual cycle of carbon production and utilization over the shelf using observational data is therefore problematic at best. Despite obvious spatial and temporal limitations, numerous other studies have provided evidence for generalized patterns of carbon modification over the shelf (see Table 1). For example, the literature record shows evidence from multiple perspectives that *NPP* peaks in spring, decreases in summer, and increases in fall (e.g., Sambrotto et al., 1986; Springer et al., 1996; Rho and Whitledge, 2007; Lomas et al., 2012; Moran et al., 2012; Mordy et al., 2012), although with regional variability.

Applying these emergent patterns to the observational data collected here provides an opportunity not only to fill in the gaps in our observational data and permit an analysis of this group as a whole, but also to consider the Bering Sea from an annual perspective, and to test the validity of these annual patterns. Here, we approximate an annual carbon cycle by extrapolating seasonal measurements using previously observed or hypothesized patterns as a guide, and derive the resulting carbon mass balance. A detailed description of this approach and its application to this dataset is described in Supplemental Section 1, and an illustration of this extrapolation and a brief description are given below.

To extrapolate our seasonal data, we assumed that the year was comprised of four 91.25-day seasons. Data were partitioned into these seasons according to the timing of cruises and the physical and biogeochemical cycles described in Table 2. In Fig. 3A, we provide an illustration of the best generalized seasonal variation of our observed parameters presently allowed, normalized to the relative peak value for *NPP*. Data gaps were filled based on observed patterns, where possible, and otherwise using patterns observed in the literature.

As already mentioned, the literature record indicates that in general, primary production peaks in spring, decreases in summer, and increases again during fall storms, the breakdown of the seasonal thermocline and resulting convection that induce nutrient replenishment. Our observational data shows that *NPP* followed this pattern in the Middle Domain, but not in the Coastal Domain. Limited data prevented an observation of temporal patterns in Outer Domain *NPP* (see Table 1). Based on the consistency of the pattern of production in the literature, we chose to extrapolate Outer Domain data according to the Middle Domain pattern. Coastal Domain data was allowed to vary as observed in spring and summer, with fall production extrapolated as an average of the two. Patterns for NCP_{DIC} and NCP_{TIN} were not available across multiple seasons, and we thus assumed that they would follow the pattern for *NPP*.

According to the literature and our data (see Table 1), C_{exp} increases with *NPP* at the onset of production, and then decreases linearly through the summer and fall seasons. Our observations show that the Coastal Domain adhered to this pattern, but that C_{exp} in the Middle Domain was constant between spring and summer, and Outer Domain C_{exp} increased over this season. In both cases, fall rates of C_{exp} were assumed to decrease relative to summer, as has been observed in other areas (Buesseler, 1998). Due to a complete paucity of winter data, we assumed that previously well-established light and stratification constraints on primary production during this season resulted in negligible primary production (e.g., Sigler et al., 2014; Moran et al., 2012; Niebauer et al., 1990; Springer et al., 1996; Ladd and Stabeno, 2012), and therefore precluded subsequent carbon modification.

Where possible, the maximum amount of data were incorporated into this model to allow for naturally observed patterns, and seasonal variability that may differ between regions. For example, rates of *NPP* in active blooms were integrated over a 30-day period to minimize the effect of these extremely high rates over the entire season, with the remainder of *NPP* integrated over the remaining 61.25 days. Our data also indicate that benthic respiration varies very little on a seasonal scale, exhibiting a nearly constant background activity. During our spring surveys, most of the primary production had not reached the benthos although some respiration was evident (see Table 1; Section 3.4). We therefore incorporated this winter baseline rate of *BCC* into our model. Observations contradicting the average seasonal patterns for *NPP* and C_{exp} were also incorporated into the model, as previously described.

Without temporally continuous observations available for each parameter in a variety of locations within each domain, the illustration given in Fig. 3A is beyond the reach of the data collected. At present, we are unable to assess any variation in rate

across a season. Accordingly, our model of this seasonal cycle is given in Fig. 3B, representing a first-order approximation of the annual cycle of production as allowed by the data.

4.2. Annual mass balance

The annual mass balance of carbon production and utilization is given in Table 3 and visually represented in Fig. 4. *NPP*, our only listed carbon source, is given in black, while the various pelagic (green) and benthic (blue) sinks are indicated by the second series of bars. The benthic $R_H+T+Bio$ bulk term is indicated in white. The error given in each estimate in Table 3 is derived from the individual measurement error (Table 1). Standard compounding error was assumed for calculated variables, such that total standard error was equal to the square root of the sum of the squares of error terms for the variables included in the calculation.

In general, the carbon budgets for the Outer and Middle Domains were largely balanced even without distinguishing $R_H+T+Bio$ in the benthic compartment, although some differences were apparent in the internal partitioning of *NPP* between carbon sinks. In the Middle Domain, a greater proportion of *NPP* was exported vertically and remineralized more efficiently in the sedimentary compartment than in the Outer Domain. While surface layer lateral transport was similar between these two regions, lateral transport was larger than vertical transport as a sink for carbon in the Outer Domain than in the Middle Domain. In the Coastal Domain, very low estimates of *NPP* were exceeded by NCP_{DIC}, C_{exp} and *BCC*, indicating a large organic carbon deficit in this region.

4.3. The Outer and Middle Domains lose carbon

The lateral mass transport terms given in Table 3 correspond well to other recent calculations, indicating that the estimates presented here are reasonable. Baumann et al. (2013a) provided an estimate of off-shelf export of POC of 19 mmol C m^{-2} d^{-1}. An upper boundary to this estimate was also calculated by Baumann et al. (2013b) of 24 ± 35 mmol C m^{-2} d^{-1}. Extrapolating these estimates according to the same pattern of seasonal change we

Table 2
Seasonality in the eastern Bering Sea. A seasonal description of the physical characteristics of the shelf, also showing a breakdown of field activity. June–Aug.: Summer. Sept.–Nov.: Fall. Dec.–Feb.: Winter. Mar.–May: Spring. Data from bolded cruises were included in this carbon budget in the seasons listed. Ship and program names are abbreviated as follows: Eastern Bering Sea (EBS) Groundfish Survey; R/V *Knorr* (KN); R/V *Thompson* (TN); USCGC *Healy* (HLY); Bering-Aleutian Salmon International Survey (BASIS); NOAA Ship *Miller Freeman* (MF); USCGC *Polar Sea* (PSEA).

Mo.	Physical description	2007	2008	2009	2010
June	0% Ice cover; appearance of N/S transition in middle domain due to solar insolation; weaker currents[i,m]	EBS Groundfish Survey	EBS Groundfish Survey	**KN195 (6/14–7/13)**; EBS Groundfish Survey	**TN250 (6/16–7/14)**; EBS Groundfish Survey
July	Wind direction switches to northeastward; variable wind strength; weaker currents; euphotic zone, elevated chlorophyll fluorescence, and oxygen supersaturation deeper than pycnocline; loss of nutrients in bottom layer; majority small phytoplankton; *NPP* declines[c,k,m]	EBS Groundfish Survey	**HLY0803 (7/1–7/31)**; EBS Groundfish Survey	**KN195 (6/14–7/13)**; EBS Groundfish Survey	**TN250 (6/16–7/14);** EBS Groundfish Survey
Aug.	Maximum annual Stratification Index (SI; J/m^2; M2); variable wind strength; secondary freshet (glacial melt)[c,e,k]	BASIS Survey (8/15–10/8)			BASIS Survey (8/18–9/25)
Sept.	Maximum annual heat content; small fall bloom, incl. coccolithophores; wind direction E/SE; winds weak; deep mixing, remineralization, denitrification/anammox significant biogeochemical modifiers[d,h,l,k,l]	TN211 (9/25–10/11); BASIS Survey (8/15–10/8; 8/31–9/23); MF071 (9/17–9/30)	ME0823 (8/24–9/17); BASIS Survey (9/11–9/27)	MF0904b (9/22–10/13); BASIS Survey (8/26–9/14; 9/3–9/27)	BASIS Survey (8/18–9/25; 9/8–10/5)
Oct.	Stratification begins to erode; winds strengthen; flushing of central shelf begins[b,e,k]	TN211 (9/25–10/11); BASIS Survey (8/15–10/8)		MF0904b (9/22–10/13)	
Nov.	Ice formation begins; winds strong[k,l,m]				
Dec.	Ice covers northern shelf; winds strong; wind direction W/SW[k,l,m]				
Jan	Well-mixed water column (M4); winds strong; ice covers northern shelf; input of nutrient content to central shelf from Anadyr Water begins[c,k,m]				
Feb.	Winds strong; ice covers northern shelf[k,m]				
Mar.	Typical maximum ice extent; Winds strong; wind direction S/SW; under-ice bloom[j,k,m]		**HLY0801 (3/12–3/26)**	**HLY0901 (3/10–3/31)**	**PSEA 1001 (3/7–4/4)**
Apr.	Ice retreat begins; ice-edge bloom; winds begin to weaken; depth-averaged temperature minimum[e,k,m]	HLY0701 (4/11–5/11); MF0706 (4/18–5/6)	**HLY0802 (3/27–5/5)**	**HLY0902 (4/1–5/11)**	
May	Rapid ice ablation; light availability increases; stratification sets up firmly; primary freshet (snow melt); weaker currents; widespread spring bloom; majority large phytoplankton; maximum rate *NPP*[a,c,e,f,g,j]	HLY0702 (5/16–6/18)		**HLY0902 (4/1–5/11)**	**TN249 (5/9–6/14)**

[a] Brabets et al. (2000).
[b] Danielson et al. (2012b).
[c] Dornblaser and Striegl (2007).
[d] Iida et al. (2012).
[e] Ladd and Stabeno (2012).
[f] Lomas et al. (2012).
[g] Moran et al. (2012).
[h] Mordy et al. (2012).
[i] Sigler et al. (2014).
[j] Stabeno et al. (2001).
[k] Stabeno et al. (2007).
[l] Stabeno et al. (2012a).
[m] Stabeno et al. (2012b).

Table 3
Annual carbon budget for the Bering Sea shelf (2008–2010). The annual carbon budget mass balance for the three domains of the Bering Sea shelf based on the seasonal estimates from Table 2, in g C m^{-2} yr^{-1}. The abbreviation and measurement or calculation method for each parameter, as well as the water column layer over which it is valid, are also indicated. For measured parameters, the number of profiles contributing to the estimate is listed. For calculated parameters, the relative percent of *NPP* is also shown. The lateral transport term for the southern Outer Domain was calculated according to Baumann et al. (2013a). At bottom, remainder terms indicating percent loss of *NPP* to burial in the sediments or lateral mass transport were directly calculated by adding calculated burial and transport terms, and indirectly by accounting for all heterotrophic carbon requirements. The literature value for these estimates was calculated indirectly and taken from Walsh and McRoy (1986).

Parameter	Abbr.	Formula	Layer	Southern Outer Domain		Southern Middle Domain		Southern Coastal Domain	
Net primary production	*NPP*	Measured	Upper 30 m	331 ± –	*n*=1	172 ± 72	*n*=20	26 ± 15	*n*=4
Net community production from DIC	NCP_{DIC}	Measured	Upper 30 m	111 ± 42	*n*=22	95 ± 83	*n*=48	39 ± 36	*n*=14
Net community production from TIN	NCP_{TN}	Measured	Upper 30 m	–		50 ± 21	*n*=193	24 ± 7	*n*=33
Export production	C_{exp}	Measured	40 m	67 ± 20	*n*=55	65 ± 18	*n*=35	80 ± 17	*n*=6
Baumann focusing factor	*FF*	Measured	Sediment	0.28 ± 0.13	*n*=20	0.26 ± 0.10	*n*=27	–	
Benthic carbon consumption	*BCC*	Measured	Sediment	21 ± 6	*n*=11	35 ± 17	*n*=11	58 ± 11	*n*=4
Heterotrophic respiration	R_H	$0.5NPP - NCP_{AVG}$	Upper 30 m	110 ± 21	33% *NPP*	50 ± 42	29% *NPP*	−3 ± 12	−10% *NPP*
Lateral transport	*T*	$NCP_{DIC} - NCP_{TN}$	Upper 30 m	99 ± –	30% *NPP*	46 ± 85	26% *NPP*	15 ± 37	56% *NPP*
Carbon stored as biomass	*Bio*	$NPP - R_H - T - C_{exp}$	Upper 30 m	55 ± 29	17% *NPP*	12 ± 121	7% *NPP*	−66 ± 45	−253% *NPP*
Carbon burial	*B*	FF × C_{exp}	Sediment	19 ± 0	6% *NPP*	17 ± 0	10% *NPP*	–	
$R_H+T+Bio$	*R*	$C_{exp} - BCC - B$	Below 40 m	27 ± 21	8% *NPP*	13 ± 25	8% *NPP*	–	
Walsh remainder (indirect)		Literature	Full water column	49%		17% (0%)		–	
BEST remainder (direct)		$B+T$	Full water column	35%		36%		–	
BEST remainder (indirect)		$NPP - R_H - Bio - BCC$	Full water column	44%		44%		–	

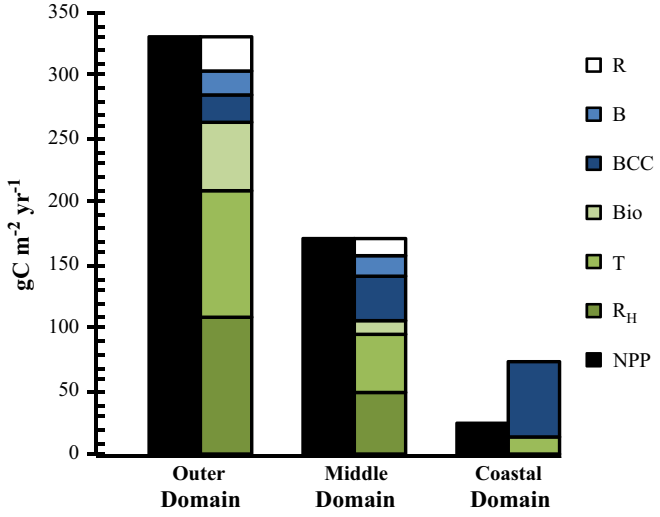

Fig. 4. Carbon production, utilization and transport by g C m^{-2} yr^{-1} by each of the measured and calculated processes listed in Table 3. Production terms are indicated in black and gray, surface water sinks are indicated in green, bottom water carbon sinks are indicated in blue, and the total value of the indistinguishable bottom layer carbon sinks (*R*, where $R=R_H+T+Bio$ below 40 m) is indicated in white. This visualization highlights the increasing disconnect between *NPP* and carbon losses towards the Outer Domain, and the dominance of known carbon sinks (*BCC*, *T*) in excess of *NPP* in the Coastal Domain.

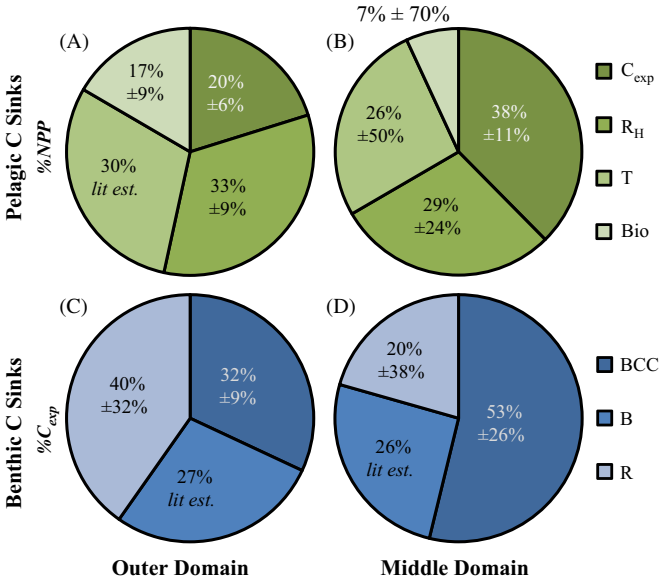

Fig. 5. Partitioning of the pelagic (A and B) sinks of *NPP* and benthic sinks of C_{exp} (C and D). Percent loss of carbon exported to 40 m in the Outer Domain (A and C) and the Middle Domain (B and D). Standard compounding error was assumed in the propagation of error terms from Table 3, except in cases where the values were estimated based on previous literature, indicated by *lit est*. In the benthic compartment, the *R* term is conceptually comprised of the bulk carbon modification by water column heterotrophy, carbon stored as biomass, and lateral transport. Partitioning between these sources was not possible with this dataset.

attributed to C_{exp} here, this gives a range of annual transport between 50 and 66 g C m^{-2} yr^{-1}. Our calculated *T* value for the Middle Domain is somewhat lower than these mass estimates. Given that *T* could not be calculated for the Outer Domain, we scaled *T* in this region as 30% of *NPP*, as was estimated by Baumann et al. (2013a). The discrete rate measurement range from Baumann et al. (2013b) is somewhat lower than what we projected in Table 3 for the Outer Domain. However, this range accounts only for westward lateral transport, while the estimate based on Baumann (2013a) we show in Table 3 accounts for lateral transport in any horizontal direction out of the domain.

Lateral mass transport as % *NPP* is similar in the Outer and Middle Domains (Fig. 5A and B). However, relative to other sinks for *NPP*, the significance of lateral mass transport is stronger in the Outer Domain than in the Middle Domain. In the Outer Domain, *T* occurs on approximately the same scale as R_H (Fig. 5A). Both of these terms are larger than C_{exp}, indicating that organic carbon consumption in the surface layer and lateral mass transport are much more significant than vertical export and bottom water consumption of organic matter. In the Middle Domain, C_{exp} is the largest sink for *NPP*, indicating that vertical mass transport is more significant than lateral mass transport (Fig. 5B).

The relative importance of transport carbon losses in the Outer Domain may also be exhibited in bottom waters. Nearly identical focusing factors (*FF*) result in similar percentages of C_{exp} lost to

burial (B) in each domain. Because BCC is so much stronger in the Middle Domain, a much smaller portion of C_{exp} is left over after utilization in this region (Fig. 5C and D). As noted earlier, this bottom water remainder (hereafter referred to as R) should conceptually be split between R_H, Bio, and T. The smaller R for the Middle Domain may result from an insignificant contribution of benthic T. Long residence times exhibited by bottom waters in the Middle Domain (Coachman, 1986; Danielson et al., 2012b; Stabeno et al., 2012b) likely decrease the relative importance of T for the R term. The water column in the Outer Domain is much deeper than that for the Middle Domain, and residence times of bottom water for the Outer Domain are much shorter (Coachman, 1986). Based on this evidence, it is possible that a larger portion of R in this domain will be comprised of carbon lost to lateral mass transport occurring in the bottom layer of this region, and that the relative magnitude of this sink for NPP may account for the larger R in this domain.

4.4. The Coastal Domain gains carbon from the Middle Domain

Measured carbon utilization is greater than carbon production in the Coastal Domain. It is unlikely that this offset results from errors in C_{exp}. While it is possible that C_{exp} values may be influenced by sediment resuspension, there is a 1.5–2 agreement between sediment trap particulate matter, implying that sediment resuspension may not be a significant concern (Moran et al., 2012; Baumann et al., 2013b). While a twofold difference cannot explain the entire deficit, this error may account for much of it. However, the concurrent observation of NCP_{DIC} and BCC values are also greater than NPP, indicating that multiple sinks are greater than the estimated observed sources. Two possible solutions remain to balance the carbon budget: poor annual extrapolation of production data, or lateral mass transport of carbon into the system unresolved by NCP_{DIC} and NCP_{TIN}.

Lomas et al. (2012) observed that the annual spring bloom may be somewhat delayed relative to the rest of the shelf, with peak production occurring later. We even observed this pattern on average in our seasonal data (see Table 1). According to our extrapolation for data with both seasons, this merely switches the spring and summer seasons in this productivity pattern, as estimates of fall production are the average of spring and summer values. For errors in extrapolation to cover the Coastal Domain carbon deficit, our fall extrapolations are also too low, indicating then that spring production increases linearly through summer and fall. However, some measurements included in our annual extrapolation of NPP were based on a single spring station occupation, which would have underestimated annual productivity that peaks in summer. Without the single-season occupation data, NPP in this region would still be lower than NCP_{DIC}, C_{exp}, and BCC, indicating again that that compounding errors in our fall NPP extrapolation would be the source for this offset. However, nutrient limitation in later seasons is well established in the Bering Sea, and it is unlikely that fall production—even that stimulated by nutrient replenishment from persistent storms—would overwhelm peak productivity levels in nutrient-replete seasons.

While we cannot rule out that the large difference between NPP and C_{exp} is an artifact of the compounding of error during our calculations, there is some potential that this offset is caused by a supply of externally produced organic carbon to the Coastal Domain. As we have suggested with regards to NCP_{DIC}, input of preconditioned waters may be altering BCC and C_{exp} by delivering organic matter produced in other areas. In the Coastal Domain, lateral mass transport may be a source of carbon to this region, rather than a sink. To balance the offset between NPP, surface carbon utilization, lateral mass transport, and C_{exp}, a minimum of 66 g C m^{-2} yr^{-1}, or 7.92 Tg yr^{-1} is required for input into the Southern Coastal Domain.

The most logical source of lateral mass transport of organic matter into the Coastal Domain are the Yukon and Kuskokwim Rivers, which contribute 234 km^3 of freshwater to the Coastal Domain annually (Mathis et al., 2011a). Previous work has indicated that the organic matter delivered to the shelf with these river waters can dramatically influence the carbon cycle of the Coastal Domain (Mathis et al., 2011a; Cross et al., 2012). River data from
the US Geological Survey (USGS) indicates the combined organic matter discharge from these rivers is approximately ~1.27 Tg C yr^{-1}. Even under the extremely improbable assumption that all of this organic matter is delivered to the Southern Coastal Domain, organic matter from rivers cannot provide an adequate supplement to support the observed benthic activity. Assuming an average total organic carbon (TOC) concentration of 65 μmol kg^{-1} in the waters entering the Bering Sea from the north Pacific and using a volume transport from Unimak Pass into the Coastal Domain of 0.042 Sv (Kinney et al., 2009), we see that this source of carbon contributes another ~1.1 Tg C yr^{-1}, a reservoir too small to cover the imbalance between C_{exp} and NPP.

An additional supply of organic matter to the Southern Coastal Domain may be the Southern Middle Domain. Our estimate of T for the Middle Domain indicates that ~8.74 Tg C yr^{-1} is exported laterally. This mass could easily support the benthic carbon demand occurring in the Coastal Domain. If the Middle Domain is the source of this excess organic matter, this would imply a significant focusing of dispersed production in this area similar to that observed over the northern shelf (Cooper et al., 2012). Recent work suggests that during years exhibiting cold winters such as 2008–2010, enhanced northward flow occurring over the shelf results from an increased density gradient over the shelf due to greater volumes of ice production and brine rejection (Danielson et al., 2012b). Under these conditions, northerly winds cause coastal convergence and upwelling near the shelf break. If the effects of the cross-shelf density gradient and upwelling reach all the way to the coast, this convergence could deposit Middle Domain productivity in the Coastal Domain under northerly wind conditions and account for the missing carbon supply, and indicates that the Middle and Coastal domains are balanced within 0.8 Tg C yr^{-1} when taken together.

4.5. Comparison with the previous Bering Sea carbon budget

Rates of primary production on the Bering Sea shelf have been estimated since the early 1960s (Ivenakov, 1961; Azova, 1964), and several comprehensive reviews of the literature have been conducted each decade since the 1990s (e.g., Springer et al., 1996; Hunt et al., 2002; Mathis et al., 2010; Lomas et al., 2012). Because of the importance of the regional fisheries these measurements are often discussed at an ecosystem level, with a particular emphasis on the energy provided to upper trophic levels and pelagic fish populations. The Processes and Resources of the Bering Sea (PROBES) Program developed a complete carbon budget based on the relative consumption of NPP by upper trophic levels. After accounting for heterotrophic energy requirements, Walsh and McRoy (1986) estimated that approximately 49% and 17% of annual NPP remained for transport and burial in the Outer and Middle Domains, respectively.

With the available data, it is possible to discretely calculate both a transport and a burial term for comparison. However, like the method of Walsh and McRoy (1986), this combined burial/transport remainder term can also be indirectly calculated by subtracting all heterotrophic carbon utilization terms (R_H, Bio, BCC) from NPP. For the BEST dataset, these indirect remainder terms are

higher than those calculated directly (Table 3). The difference between these two methods results from limited bottom water data, which prevents the partitioning of carbon between R_H, T, and *Bio* below 40 m. In the direct calculation of the remainder term, any potential transport in bottom waters is ignored, and therefore the term is likely underestimated; in the indirect calculation of the remainder term, bottom water R_H and stored biomass is ignored, resulting in an overestimation of the burial and transport term.

Of these two estimation methods, we suggest that the direct calculation is likely more accurate. Directly calculating the remainder term relies on fewer assumptions, and ignores only one carbon pool (bottom water T) while the indirect method ignores two (bottom water R_H and *Bio*). Considering that the transport velocities in bottom water are very small (Danielson et al., 2012a; Stabeno et al., 2012a,b), loss of carbon by lateral transport in bottom waters is likely also very small (e.g., Bacon et al., 1994), which substantially reduces the error generated by ignoring this term. In comparison, the carbon pools ignored by the indirect calculation of this remainder term are likely much larger. Water column respiration is nontrivial in bottom waters over the shelf (Mathis et al., 2011b), and the magnitude of the R_H term, as well as the biomass stored by a sedimentary community which respires over the entire year, are likely larger in scale than bottom water transport.

Both our directly and indirectly calculated remainder terms are on the same order as those calculated by Walsh and McRoy (1986). Given the uncertainties inherent in these extrapolations and the wider spatial area covered here relative to PROBES, this is likely to be the best possible comparison. However, there are also qualitative differences between our data and that reported by Walsh and McRoy in the partitioning of carbon implied by these remainder terms. Our directly calculated remainder term is slightly smaller for the Outer Domain (Table 3). The data presented here indicate a larger portion of productivity and less vertical export than Walsh and McRoy (1986) but also less storage of carbon as biomass. This implies that we observed a carbon sink not apparent in the Walsh and McRoy budget. A portion of this sink is accounted for by our addition of a carbon reservoir for heterotrophic respiration, and the strong surface remineralization loop we demonstrated here. Thus, while our remainder estimates may be lower than those calculated by Walsh and McRoy (1986), they also depict a more strongly pelagic system. This is illustrated in Fig. 5, where the relative magnitude of *NPP* compared to any benthic utilization or any pelagic utilization is very high. The extreme inherent variability in the Bering Sea make it extremely difficult to document small long-term changes (Lomas et al., 2012). However, it is possible that the system has undergone a shift to a more strongly pelagic state in recent decades.

In the Middle Domain, Walsh and McRoy (1986) argued that despite a small, indirectly calculated $B+T$ remainder, the carbon budget was likely balanced over this area. It was suggested that the remaining carbon was cycled through the bottom water and benthic system on the annual scale, and that the Middle Domain was a dominantly benthic carbon system. In fact, Fig. 5 indicates that carbon utilization and transport below 40 m is nearly twice as large for this domain than for the Outer Domain (C_{exp}=38% *NPP* and 20% *NPP* in the Middle and Outer Domains, respectively). Following vertical export of *NPP*, *BCC* by $\%C_{exp}$ is also much greater in the Middle Domain than in the Outer Domain (58% and 35%, respectively; Fig. 5). However, surface layer utilization still dominates the modification of *NPP* in the Middle Domain ($R_H+T+Bio$=62% *NPP*), indicating that while the Middle Domain may have a stronger connection between surface production and benthic heterotrophy than the Outer Domain, it is still a predominantly pelagic system. We also demonstrate a qualitative loss of *NPP* to lateral mass transport and carbon burial.

Walsh and McRoy (1986) did not publish a carbon budget for the Coastal Domain, and the subsequent Inner Shelf Transfer and Recycling Program (ISHTAR) focused more on the northern Bering Sea Shelf. Other previous work has indicated that the Coastal Domain of the northern shelf ($>60^{\circ}$N) can be net heterotrophic on the seasonal scale (Cross et al., 2012), although the same study, and others, indicated that the Southern Coastal Domain surface layer is net autotrophic on an annual scale (e.g., Mathis et al., 2010; Lomas et al., 2012). This carbon budget indicates that the Southern Coastal Domain may be net heterotrophic on the annual scale when integrating over the full water column. We also suggest that the Coastal Domain may be a focusing center for carbon lost to transport from the Middle Domain.

4.6. Additional questions

While this work represents a first order estimate of the carbon budget in the SE Bering Sea, further questions also remain with respect to specific carbon biogeochemical processes. Given the demonstrated importance of lateral carbon transport and the dominance of heterotrophic processes at the coast, a better parameterization of both of these terms is essential to improving our understanding of the biological and biogeochemical cycles. Given limited *NCP* data, our present model indicates that heterotrophic respiration in the surface layer maintains a constant ratio to *NPP* across the spring and summer seasons, although some variability has recently been inferred (Moran et al., 2012). Present efforts are focused on resolving the spatiotemporal variability of *f*-ratios and the role of regenerated production that may indicate a better parameterization for heterotrophic respiration in future models (Mordy, unpublished data; Prokopenko, unpublished data).

In the benthic compartment, our parameterization of benthic remineralization only accounts for aerobic pathways in the sediments. Other concurrent studies indicate that net denitrification over the entire Bering Sea shelf consumes 5.2–6.2 Tg C yr^{-1} (Horak et al., 2013). Our studies cover ~15% of the area of the Bering Sea shelf estimated by Horak et al. (2013), indicating that anaerobic respiration should account for 0.8–0.9 Tg C yr^{-1} over the southern Middle and Outer Domains. The combined R integrated over these domains is ~3 Tg C yr^{-1}. Correspondingly, the anaerobic signal estimated by Horak et al. (2013) accounts for ~25–30% of the combined Middle and Outer Domain R given in Table 3. Additional studies concerning the partitioning of R between anaerobic and aerobic sedimentary respiration, transport, and carbon stored as biomass could refine our understanding of bottom layer carbon cycling, especially in the Outer Domain where R accounts for nearly 40% of C_{exp} (Fig. 5).

While the carbon imbalance in the Coastal Domain prevented the partitioning of carbon pools in this region, a better understanding of respiration processes could be particularly important. Focused deposition of laterally transported carbon may support the benthic community of the coastal domain relative to the pelagic community. However, the resulting net heterotrophy in this region due to bacterial remineralization processes could also induce a strong vulnerability to ocean acidification. While we have sufficient data in this region to make some statements about the potential importance of laterally transported carbon to the Coastal Domain, it is clear that all carbon processes in this region require further study. Some of the conflicting temporal patterns in organic carbon production and the unbalanced budget may be resolved simply by better spatial and temporal resolution of data in this region.

Data gaps did not result in substantial carbon budgetary imbalances in the Outer Domain, but limited spatial coverage of *NPP* may have skewed our results. Although rates in the middle domain for both spring and summer were observed to be higher in

the Middle Domain, our annual extrapolation resulted in higher rates of *NPP* for the Outer Domain based on the single summer profile available for this region (Table 1). If a more highly resolved *NPP* value for the region were lower, this could adjust our surface layer carbon partitioning. Specifically, R_H and *Bio* would decrease, and C_{exp} and *T* would represent a larger proportion of *NPP* than indicated in Fig. 5. Qualitatively, this would enhance our assessment that the Outer Domain loses carbon to lateral transport on the annual scale.

Across all domains, a better understanding of fall and winter processes would provide a better basis for assembling a true annual carbon budget. Here, we have neglected water column autotrophy and heterotrophy in the winter season, although winter production (e.g., Miksis-Olds et al., 2013) and respiration (e.g., Cross et al., in review) have been observed in the Bering Sea. It has also been hypothesized that under-ice blooms during late winter and early spring may play a critical role in determining ecosystem dynamics in the following late spring and summer (Hunt and Stabeno, 2002; Sigler et al., 2014). Understanding the contribution of winter processes should be a focus of any future process studies and synthesis efforts in the Bering Sea.

5. Conclusions

During the multi-disciplinary, multi-year field program executed by the Bering Sea Project, independent sampling for net primary production (*NPP*), two types of net community production (*NCP*), export production (C_{exp}), and benthic carbon consumption (*BCC*) allowed us to improve upon the annual carbon budgets of the Outer and Middle Domains of the southeastern Bering Sea Shelf constructed over thirty years ago. From these discrete measurements, estimates of heterotrophic respiration (R_H), carbon stored as biomass (*Bio*), carbon burial in the sediments (*B*), and lateral mass transport (*T*) were calculated to develop a carbon mass balance.

Specifically, we observed that more carbon is lost laterally in the Outer Domain than is exported vertically. A more efficient coupling between pelagic production and benthic utilization in the Middle Domain indicated a more balanced carbon budget. Unlike the Middle and Outer Domains, a new insight is that lateral mass transport was a source of carbon to the Coastal Domain. While the source of the organic carbon necessary to balance benthic utilization with organic carbon supply requires further study, focused deposition of Middle Domain *NPP* lost to transport could account for this imbalance. Relative to previous carbon budgets that indirectly calculated a percentage of *NPP* lost to transport and burial, this dataset made it possible to directly calculate this sink. This direct method showed a similar, if somewhat smaller percentage of *NPP* lost to transport and burial in the Outer Domain (35% *NPP*, Table 3), and contradicted the previous assumption that the carbon budget was balanced in the Middle Domain by showing a 36% loss of *NPP* to transport and burial. However, taken in conjunction with the Coastal Domain, the combined carbon budget for both regions is fully balanced to within 1 Tg C yr^{-1}.

As environmental conditions continue to change, it will be important to monitor spatial variations in carbon cycle and to continue to pursue a better understanding of the Bering Sea carbon budget, particularly with regards to the Coastal Domain. Some of the differences between this budget and the Walsh budget may have arisen due to the strong variability characteristic of the Bering Sea ecosystem. While striving for complete spatial resolution on short temporal scales is likely untenable, periodic synthesis efforts like the construction of carbon budgets may help to address some broad longer-term variability. For example, under future warming scenarios, TOC inputs from rivers will likely increase due to increased melting of permafrost and enhanced soil drainage (Striegl et al., 2005) which could strengthen the supply of organic matter to the benthos and increase net heterotrophic processes for the Coastal Domain. Construction of carbon budgets could also help to assess expected changes in pelagic/benthic partitioning in the coming decades.

Acknowledgments

The authors thank the officers and crew of USCGC *Healy*, R/V *Knorr*, and R/V *Thomas G. Thompson*, as well as Scott Hiller of SIO, Steve Roberts of UCAR, and the hydrographic team from the National Oceanic and Atmospheric Administration for their work in tirelessly supporting our science during multiple cruises. We also thank Ray Sambrotto for the provision of unpublished data for reference during this work. Lastly, we thank the Science Advisory Board, the data management team, and our colleagues in the Bering Sea Project, supported by the National Science Foundation and the North Pacific Research Board. The synthesis presented in this paper was supported by the National Science Foundation Grants ARC-1107997 to JTM, ARC-0732359 and ARC-1106910 to MWL, ARC-0732680 to SBM, PLR-1107250 to CWM, and Grant NPRB-B56 to SBM from the North Pacific Research Board. Partial funding for this project was also provided by the Joint Institute for the Study of the Atmosphere and Ocean (JISAO) under NOAA Cooperative Agreement NA10OAR4320148. This work is contribution EcoFOCI-0808 to NOAA's Ecosystems and Fisheries-Oceanography Coordinated Investigations, contribution 2180 to JISAO, contribution 3914 to NOAA's Pacific Marine Environmental Laboratory, publication 124 of the BEST-BSIERP Bering Sea Project and publication 464 of the North Pacific Research Board.

Appendix A. Supporting information

Supplementary data associated with this article can be found in the online version at http://dx.doi.org/10.1016/j.dsr2.2014.03.003.

References

Aguilar-Islas, A.M., Hurst, M.P., Buck, K.N., Sohst, B., Smith, G.J., Lohan, M.C., et al., 2007. Micro- and macronutrients in the southeastern Bering Sea: insight into iron-replete and iron-depleted regimes. Prog. Oceanogr. 73, 99–126.

Anderson, L.A., 1995. On the hydrogen and oxygen content of marine phytoplankton. Deep Sea Res. I 42 (9), 1675–1680.

Azova, N.V., 1964. Primary productivity of the Pribilof–Bristol area of the Bering Sea. In: Moiseev, P.A. (Ed.), Soviet Fisheries Investigations in the Northeastern Pacific, Part III. Pishchevaya Promyshlennost Publishing, Moscow, pp. 149–154

Bacon, M.P., Belastock, R.A., Bothner, M.H., 1994. ^{210}Pb balance and implications for particle transport on the continental shelf, U.S. Middle Atlantic Bight. Deep Sea Res. II 41 (2–3), 511–535.

Bates, N.R., 2006. Air–sea CO_2 fluxes and the continental shelf pump of carbon in the Chukchi Sea adjacent to the Arctic Ocean. J. Geophys. Res. 111 (C10), C10013.

Bates, N.R., Mathis, J.T., Cooper, L.W., 2009. Ocean acidification and biologically induced seasonality of carbonate mineral saturation states in the western Arctic Ocean. J. Geophys. Res. 114, C11007.

Baumann, M.S., Moran, S.B., Kelly, R.P., Lomas, M.W., Shull, D.H., 2013a. ^{234}Th balance and implications for seasonal particle retention in the eastern Bering Sea. Deep Sea Res. II 94, 7–21.

Baumann, M.S., Moran, S.B., Kelly, R.P., Lomas, M.W., Bell, D.W., 2013b. Seasonal decoupling of organic carbon export and net primary production in relation to sea-ice at the shelf break of the eastern Bering Sea: implications for off-shelf carbon export. J. Geophys. Res. 118, 1–19.

Benitez-Nelson, C., Buesseler, K.O., Rutgers van der Loeff, M., Andrews, J., Ball, L., Crossin, G., et al., 2001. Testing a new small-volume technique for determining ^{234}Th in seawater. J. Radioanal. Nucl. Chem. 238 (3), 795–799.

Bond, N.A., Overland, J.E., 2005. The importance of episodic weather events to the ecosystem of the Bering Sea shelf. Fish. Oceanogr. 14, 97–111.

Brabets, T.P., Wang, B., Meade, R.H., 2000. Environmental and hydrologic overview of the Yukon River Basin, Alaska, and Canada. Water Resources Investigations Report No. 99-4204. USGS, Anchorage, AK (114 pp)

Buesseler, K.O., 1998. The decoupling of production and particulate export in the surface ocean. Glob. Biogeochem. Cycl. 12 (2), 297–310.

Buesseler, K.O., Benitez-Nelson, C., Rutgers van der Loeff, M., Andrews, J., Ball, L., Crossin, G., et al., 2001. An intercomparison of small- and large-volume techniques for ^{234}Th in seawater. Mar. Chem. 74, 15–28.
Chen, J.H., Edwards, R.L., Wasserberg, G.J., 1986. ^{234}U and ^{232}Th in seawater. Earth Planet. Sci. Lett. 80 (3–4), 241–251.
Cianelli, L., Robson, B.W., Francis, R.C., Aydin, K., Brodeur, R.D., 2004. Boundaries of open marine ecosystems: an application to the Pribilof Archipelago, southeast Bering Sea. Ecol. Appl. 14 (3), 942–953.
Coachman, L.K., 1986. Circulation, water masses, and fluxes on the southeastern Bering Sea shelf. Cont. Shelf Res. 5, 23–108.
Codispoti, L.A., Friederich, G.E., Hood, D.W., 1986. Variability in the inorganic carbon system over the southeastern Bering Sea shelf during spring 1980 and spring–summer 1981. Cont. Shelf Res. 5 (1–2), 133–160.
Cooper, L.W., Janout, M.A., Frey, K.E., Pirtle-Levy, R., Guarinello, M.L., Grebmeier, J. M., et al., 2012. The relationship between sea-ice break-up, water mass variation, chlorophyll biomass, and sedimentation in the northern Bering Sea. Deep Sea Res. II 65–70, 141–162.
Cross, J.N., Mathis, J.T., and Bates, N.R., 2012. Hydrographic controls on net community production and total organic carbon distributions in the eastern Bering Sea. Deep Sea Res. II., 65-70, 98-109. http://dx.doi.org/10.1016/j.dsr2.2012.02.003.
Cross, J.N., Mathis, J.T., Bates, N.R., Byrne, R.H., 2013. Conservative and non-conservative variations of total alkalinity on the southeastern Bering Sea shelf. Marine Chemistry 154, 100–112. http://dx.doi.org/10.1016/j.marchem.2013.05.012.
Cross, J.N., Mathis, J.T., Frey, K.E., Cosca, C.E., Danielson, S.L., Bates, N.R., Feely, R.A., Takahashi, R., and Evans, W. Sea-air CO_2 fluxes in the Bering Sea: New insights into late-season dynamics on an ice-covered continental shelf. Journal of Geophysical Research, in review.
Danielson, S., Eisner, L., Weingartner, T., Aagaard, K., 2011. Thermal and haline variability over the central Bering Sea shelf: seasonal and interannual perspectives. Cont. Shelf Res. 31 (6), 539–554.
Danielson, S., Hedstrom, K., Aagaard, K., Weingartner, T., Curchister, E., 2012a. Wind-induced reorganization of the Bering shelf circulation. Geophys. Res. Lett. 39 (8), L08601.
Danielson, S., Weingartner, T., Aagaard, K., Zhang, J., Woodgate, R., 2012b. Circulation on the central Bering Sea shelf, July 2008–July 2010. J. Geophys. Res. 117, C10003.
Davenport, E.S., Shull, D.H., Devol, A.H., 2012. Roles of sorption and tube-dwelling benthos in the cycling of phosphorus in Bering Sea sediments. Deep Sea Res. II 65–70, 163–172.
Dornblaser, M.M., Striegl, R.G., 2007. Nutrient (N, P) loads and yields at multiple scales and subbasin types in the Yukon River Basin, Alaska. J. Geophys. Res. 112, G04S57.
Dugdale, R.C., Goering, J.J., 1967. Uptake of new and regenerated forms of nitrogen in primary productivity. Limnol. Oceanogr. 12 (2), 196–206.
Gordon, L.L., Jennings Jr., J.C., Ross, A.A., Krest, J.M., 1994. A suggested protocol for continuous flow automated analysis of seawater nutrients (phosphate, nitrate, nitrite, and silicic acid). Methods Manual No. 91-1. WOCE Hydrographic Program Office, Corvallis, OR (55 pp)
Harvey, R.H., Sigler, M.F., 2013. An introduction to the Bering Sea Project: volume II. Deep Sea Res. II 94, 2–6.
Horak, R.E.A., Whitney, H., Shull, D.H., Mordy, C.W., Devol, A.H., 2013. The role of sediments in the Bering Sea shelf N cycle: insights from measurements of benthic denitrification and benthic DIN fluxes. Deep Sea Res. II 94, 95–105.
Hunt Jr., G.L., Stabeno, P.J., 2002. Climate change and the control of energy flow in the southeastern Bering Sea. Prog. Oceanogr. 55 (1–2), 5–22.
Hunt Jr., G.L., Stabeno, P.J., Walters, G., Sinclair, E., Brodeur, R.D., Napp, J.M., et al., 2002. Climate change and control of the southeastern Bering Sea pelagic ecosystem. Deep Sea Res. II 49, 5821–5853.
Hunt Jr., G.L., Stabeno, P.J., Strom, S., Napp, J.M., 2008. Patterns of spatial and temporal variation in the marine ecosystem of the southeastern Bering Sea with special reference to the Pribilof Domain. Deep Sea Res. II 55, 1919–1944.
Hunt Jr., G.L., Coyle, K., Eisner, L., Farley, E.V., Heintz, R.A., Mueter, F., et al., 2011. Climate impacts on eastern Bering Sea food webs: a synthesis of new data and an assessment of the Oscillating Control Hypothesis. ICES J. Mar. Sci. 68 (6), 1230–1243.
Hurst, M.P., Aguilar-Islas, A.M., Bruland, K.W., 2010. Iron in the southeastern Bering Sea: elevated leachable particulate Fe in shelf bottom waters as an important source for surface waters. Cont. Shelf Res. 30, 467–480.
Iida, T., Mizobata, K., Saitoh, S.-I., 2012. Interannual variability of coccolithophore *Emiliania huxleyi* blooms in response to changes in water column stability in the eastern Bering Sea. Cont. Shelf Res. 34, 7–17.
Ivenakov, V.N., 1961. Primary production in the Bering Sea. Transl. Inst. Oceanol. Acad. Sci. USSR 51, 36–56.
Kinney, C.J., Maslowski, W., Okkonen, S., 2009. On the processes controlling shelf–basin exchange and outer shelf dynamics in the Bering Sea. Deep Sea Res. II 56 (17), 1351–1362.
Ladd, C., Stabeno, P.J., 2012. Stratification on the Eastern Bering Sea shelf revisited. Deep Sea Res. II 65–70, 72–83.
Lee, K., 2001. Global net community production estimated from the annual cycle of surface water total dissolved inorganic carbon. Limnol. Oceangr. 46 (6), 1287–1297.
Lomas, M.W., Moran, S.B., Casey, J.R., Bell, D.W., Tiahlo, M., Whitefield, J., et al., 2012. Spatial and seasonal variability of primary production on the Eastern Bering Sea Shelf. Deep Sea Res. II 65–70, 126–140.
Martiny, A.C., Vrugt, J.A., Primeau, F.W., Lomas, M.W., 2013a. Regional variation in the particulate organic carbon to nitrogen ratio in the surface ocean. Glob. Biogeochem. Cycl. 27, 723–731.
Martiny, A.C., Pham, C.T.A., Primeau, F.W., Vrugt, J.A., Moore, J.K., Levin, S.A., et al., 2013b. Strong latitudinal patterns in the elemental ratios of marine plankton and organic matter. Nat. Geosci. Lett. 6, 279–283.
Mathis, J.T., Cross, J.N., Bates, N.R., Moran, S.B., Lomas, M.W., Stabeno, P.J., 2010. Seasonal distribution of dissolved inorganic carbon and net community production on the Bering Sea shelf. Biogeosciences 7, 1769–1787.
Mathis, J.T., Cross, J.N., Bates, N.R., 2011a. Coupling primary production and terrestrial runoff to ocean acidification and carbonate mineral suppression in the eastern Bering Sea. Journal of Geophysical Research 116, C02030. http://dx.doi.org/10.1029/2010JC006453.
Mathis, J.T., Cross, J.N., Bates, N.R., 2011b. The role of ocean acidification in systemic carbonate mineral suppression in the Bering Sea. Geophys. Res. Lett. 19, 1–6. http://dx.doi.org/10.1029/2011GL048884.
Miksis-Olds, J.L., Stabeno, P.J., Napp, J.M., Pinchuk, A.E., Nystuen, J.A., Warren, J.D., et al., 2013. Ecosystem response to a temporary sea ice retreat in the Bering Sea: winter 2009. Prog. Oceanogr. 111, 38–51.
Moran, S.B., Lomas, M.W., Kelly, R.P., Gradinger, R., Iken, K., Mathis, J.T., 2012. Seasonal succession of net primary productivity, particulate organic carbon export, and autotrophic community composition in the eastern Bering Sea. Deep Sea Res. II 65–70, 84–97.
Mordy, C.W., Cokelet, E.D., Ladd, C., Menzia, F.A., Proctor, P., Stabeno, P.J., et al., 2012. Net community production on the middle shelf of the eastern Bering Sea. Deep Sea Res. II 65–70, 110–125.
Niebauer, H.J., Alexander, V., Henrichs, S.M., 1995. A time-series study of the spring bloom at the Bering Sea ice edge I: physical processes, chlorophyll, and nutrient chemistry. Cont. Shelf Res. 15, 1859–1878.
Niebauer, H.J., Alexander, V., Henrichs, S., 1990. Physical and biological oceanographic interaction in the spring bloom at the Bering Sea marginal ice edge zone. J. Geophys. Res. 95 (C12), 22229–22241.
Olson, M., Strom, S., 2002. Phytoplankton growth, microzooplankton herbivory and community structure in the southeast Bering Sea: insight into the formation and temporal persistence of an *Emiliania huxleyi* bloom. Deep Sea Res. II 49 (26), 5969–5990.
Ortiz, I., Wiese, F., Grieg A., 2012. Marine regions of the eastern Bering Sea shelf. ⟨http:/bsierp.nprb.org/documents/BSIERP_Regions.doc⟩ (accessed June 2012).
Parsons, T., Maita, Y., Lalli, C., 1984. A Manual of Chemical and Biological Methods for Seawater Analysis. Pergamon Press, New York, NY p. 184
Pike, S.M., Moran, S.B., 1997. Use of Poretics® 0.7 μm pore size glass fiber filters for determination of particulate organic carbon and nitrogen in seawater and freshwater. Mar. Chem. 57 (3–4), 355–360.
Platt, T., Denman, D.L., Jassby, A.D., 1977. Modeling the productivity of phytoplankton. In: Goldberg, E.D. (Ed.), Ideas and Observations on Progress in the Study of the Sea. John Wiley, New York, NY, pp. 807–856
Rho, T., Whitledge, T.E., 2007. Characteristics of seasonal and spatial variations of primary production over the southeastern Bering Sea shelf. Cont. Shelf Res. 27, 2556–2569.
Rho, T., Whitledge, T.E., Goering, J.J., 2005. Interannual variations of nutrients and primary production over the southeastern Bering Sea shelf during the spring of 1997, 1998, and 1999. Oceanology (Engl. Transl.) 45, 376–390.
Sambrotto, R.N., Goering, J.J., 1983. Interannual variability of phytoplankton and zooplankton production on the southeast Bering Sea shelf. In: Wooster, W.S. (Ed.), From Year-to-Year: Interannual Variability of the Environment and Fisheries of the Gulf of Alaska and the Eastern Bering Sea. Washington State Sea Grant, Seattle, WA, pp. 161–177
Sambrotto, R.N., Niebauer, H.J., Goering, J.J., Iverson, R.I., 1986. Relationships among vertical mixing, nitrate uptake, and phytoplankton growth during the spring bloom in the southeast Bering Sea middle shelf. Cont. Shelf Res. 5, 161–198.
Sherr, E.B., Sherr, B.F., Ross, C., 2013. Microzooplankton grazing impact in the Bering Sea during spring sea-ice conditions. Deep Sea Res. II 94, 57–67.
Sigler, M.F., Stabeno, P.J., Eisner, L.B., Napp, J.M., Mueter, F.J., 2014. Spring and fall phytoplankton blooms in a productive subarctic ecosystem, the eastern Bering Sea, during 1995-2011. Deep Sea Res. II 109, 71–83, http://dx.doi.org/10.1016/j.dsr2.2013.12.007.
Springer, A.M., McRoy, C.P., 1993. The paradox of pelagic food webs in the northern Bering Sea III. Patterns of primary production. Cont. Shelf Res. 13, 575–599.
Springer, A.M., McRoy, C.P., Flint, M.V., 1996. The Bering Sea green belt: shelf-edge processes and ecosystem production. Fish. Oceanogr. 5 (3–4), 205–223.
Stabeno, P.J., Bond, N.A., Kachel, N.B., Salo, S.A., Schumacher, J.D., 2001. On the temporal variability of the physical environment over the southeastern Bering Sea. Fish. Oceanogr. 10, 81–98.
Stabeno, P.J., Bond, N.A., Salo, S.A., 2007. On the recent warming of the Bering Sea shelf. Deep Sea Res. II 54, 2599–2618.
Stabeno, P.J., Farley Jr., E.V., Kachel, N.B., Moore, S., Mordy, C.W., Napp, J.M., et al., 2012a. A comparison of the physics of the northern and southern shelves of the eastern Bering Sea and some implications for the ecosystem. Deep Sea Res. II 65–70, 14–30.
Stabeno, P.J., Kachel, N.B., Moore, S.E., Napp, J.M., Sigler, M., Yamaguchi, A., et al., 2012b. Comparison of warm and cold years on the southeastern Bering Sea shelf and some implications for the ecosystem. Deep Sea Res. II 65–70, 31–45.
Stoecker, D.K., Weigel, A.C., Goes, J.I., 2014a. Microzooplankton grazing in the Eastern Bering Sea in summer. Deep Sea Res. II 109, 145–156, http://dx.doi.org/10.1016/j.dsr2.2013.09.017.

Stoecker, D.K., Weigel, A.C., Stockwell, D.A., Lomas, M.W., 2014b. Microzooplankton: Abundance, biomass, and contribution to chlorophyll in the eastern Bering Sea in summer. Deep Sea Res. II 109, 134–144, http://dx.doi.org/10.1016/j.dsr2.2013.09.007.

Striegl, R.G., Aiken, G.R., Dornblaser, M.M., Raymond, P.A., Wickland, K.P., 2005. A decrease in discharge-normalized DOC export by the Yukon River during summer through autumn. Geophys. Res. Lett. 32, L21413.

Walsh, J.J., McRoy, C.P., 1986. Ecosystem analysis in the southeastern Bering Sea. Cont. Shelf Res. 5 (1–2), 259–288.

Whitledge, T.E., Reeburgh, W.S., Walsh, J.J., 1986. Seasonal inorganic nitrogen distributions and dynamics in the southeastern Bering Sea. Cont. Shelf Res. 5, 109–132.

Williams, P.J., 1993. On the definition of phytoplankton production terms. ICES Mar. Sci. Symp. 197, 9–19.

Deep-Sea Research II 109 (2014) 125–133

Contents lists available at ScienceDirect

Deep-Sea Research II

journal homepage: www.elsevier.com/locate/dsr2

Evidence of prolonged aragonite undersaturations in the bottom waters of the southern Bering Sea shelf from autonomous sensors

Jeremy T. Mathis [a,b,*], Jessica N. Cross [b], Natalie Monacci [b], Richard A. Feely [a], Phyllis Stabeno [a]

[a] NOAA—Pacific Marine Environment Lab, 7600 Sand Point Way, Seattle, WA 98115, United States
[b] University of Alaska Fairbanks, School of Fisheries and Ocean Sciences, 245 O'Neill BLDG, Fairbanks, AK 99775, USA

ARTICLE INFO

Available online 24 July 2013

Keywords:
Bering Sea
Carbon cycle
Ocean acidification
Carbonate mineral saturation state

ABSTRACT

The southeastern shelf of the Bering Sea is a dynamic area that experiences seasonal variability in primary production and remineralization of organic matter, both of which control the carbon biogeochemistry of the water column. Surface-water partial pressure of carbon dioxide (pCO_2) is greatly reduced in summer by biological production, which increases carbonate mineral saturation states (Ω). In contrast, the export of large quantities of organic matter from surface blooms drives an active remineralization loop that sharply increases pCO_2 near the bottom, lowering pH and suppressing Ω. New observations from moored biogeochemical sensors in 2011 showed that seasonal net community production lowers surface-water pCO_2, causing large gradients between the ocean and atmosphere that are sustained throughout the summer, confirming that these waters likely remain supersaturated with respect to aragonite throughout the open water season. On the other hand, moored sensors deployed near the bottom showed that pCO_2 levels exceed 500 μatm by early June and remain at these high levels well into the autumn months, indicating that the bottom waters are likely continuously undersaturated in aragonite for at least several months during each year. Only a small fraction of the increased pCO_2 can currently be attributed to the intrusion of anthropogenic CO_2 from the atmosphere, while the majority is due to natural respiration processes. The biological impacts, along with the timing and duration of these undersaturation events, could play a role in the development of larval and juvenile calcifiers in the region and will change as anthropogenic CO_2 concentrations continue to rise.

Published by Elsevier Ltd.

1. Introduction

The southeastern continental shelf of the Bering Sea is a region that has demonstrated remarkable variability in recent decades in response to climate forcing (Stabeno et al., 2007, 2012) and the areas of the Bering Sea that are being affected by these changes are expanding, with unknown consequences to higher trophic level organisms and commercial fisheries (Grebmeier et al., 2006). Many of the anthropogenically induced changes, such as ocean acidification (OA; e.g., Caldeira and Wickett, 2003), which have garnered international attention in recent years, are exacerbated in the Bering Sea due to its unique physical and biogeochemical processes (Mathis et al., 2011b). One area of particular concern is that the intensity and duration of these events will lead to the decrease of carbonate minerals saturation states which are critical for the production and maintenance of shells and tests in both pelagic and benthic calcifying organisms (e.g. Feely et al., 2008; Hauri et al., 2009; Ries et al., 2009; Barton et al., 2012; Bednaršek et al., 2012).

While the average pH of the global ocean has already decreased by ~0.1 over the two and half centuries since the Industrial Revolution due mostly to human emission of carbon dioxide (CO_2) (Feely et al., 2009), more rapid and seasonally intensified changes in pH have occurred in the Bering Sea due to unique circulation patterns in the north Pacific (Byrne et al., 2010), natural seasonal variations in freshwater inputs from rivers and ice melt, and coupling between pelagic and benthic carbon production and remineralization (Mathis et al., 2011a,b). Additionally, the hydrographic structure of the Bering Sea shelf may create conditions more favorable for the retention of the respiration reaction products in some areas, facilitating the seasonal accumulation of CO_2 and the reduction of saturation states. It is likely that these factors make the Bering Sea more sensitive to short-term future changes brought on by OA than many other coastal margins (Fabry et al., 2009).

Natural seasonal changes in the carbonate mineral saturation states are driven by the region's intense cycle of organic matter

* Corresponding author at: NOAA—Pacific Marine Environmental Lab, 7600 Sand Point Way, Seattle, WA 98115, United States. Tel.: +1 206 526 4809; fax: +1 206 526 6744.
E-mail address: jeremy.mathis@noaa.gov (J.T. Mathis).

0967-0645/$ - see front matter Published by Elsevier Ltd.
http://dx.doi.org/10.1016/j.dsr2.2013.07.019

production and export. Each spring, the northward retreat of sea ice from the Bering Sea shelf, stimulates extensive ice algae and phytoplankton blooms that are driven by the onset of stratification (Ladd and Stabeno, 2012). These blooms consume dissolved inorganic carbon (DIC) in the surface mixed layer (Mathis et al., 2010; Cross et al., 2012) and produce seasonally intensified quantities of organic matter during photosynthesis. Some uncoupling between the seasonally intense periods of primary production and pelagic grazing can occur (e.g., Springer et al., 1996; Mathis et al., 2011a), leading to high rates of export of ungrazed organic matter from the surface (e.g., Moran et al., 2012; Cross et al., 2012; Cross et al., 2014). The removal of DIC from the surface mixed layer causes a sharp increase in pH and carbonate mineral saturation states (Ω), while the export production that supports the biologically diverse benthic communities in southern Bering Sea leads to elevated rates of respiration and organic matter remineralization in bottom waters and sediments (Grebmeier and McRoy, 1989; Devol and Christensen, 1993). The resulting accumulation of DIC at depth in summer and fall causes a broad reduction in pH and reduces Ω for both calcite and aragonite (Mathis et al., 2011b). Thus, ocean biology tends to drive seasonally divergent trajectories for seawater chemistry (Bates et al., 2009), with primary production in the euphotic zone increasing Ω in the mixed layer while an accumulation of DIC in subsurface waters through remineralization causes a reduction in Ω (Mathis et al., 2011a).

Coupled with the natural seasonal variability exhibited by the system, anthropogenic CO_2 provides the additional reductions necessary to drive carbonate mineral undersaturations (Mathis et al., 2011b), leading to concerns about the commercial and subsistence viability of this ecosystem in response to rising CO_2 levels and increasing OA. Unlike much of the west coast of North America, where seasonal upwelling is the dominant driver of OA events (Feely et al., 2008; Gruber et al., 2012; Hauri et al., 2012), the wide continental shelf of the eastern Bering Sea behaves more like an estuarine system (e.g. Feely et al., 2010), where stratification and the biological pump are the dominant drivers of Ω.

Given the coarse temporal resolution of carbonate observations in the southeastern Bering Sea it has been impossible to quantify the timing of onset, the period of duration, and the peak intensity of these carbonate mineral undersaturation events until now. Here, we describe new data collected at the M2 mooring site (Fig. 1) in 2011 that provide new insights into the seasonal progression of CO_2 concentrations and carbonate biogeochemistry at the surface and near the bottom in this region.

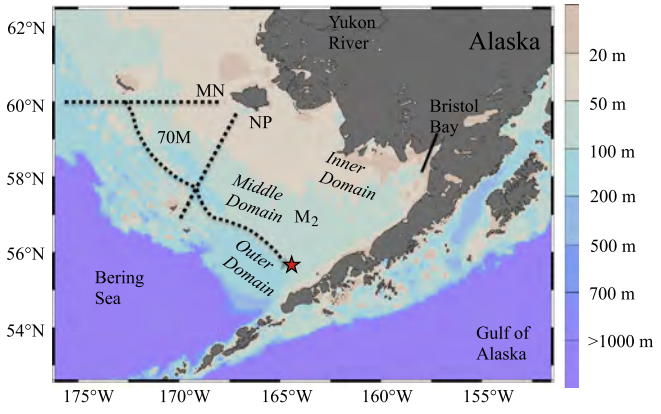

Fig. 1. Map of the southeastern Bering Sea showing the location of the M2 mooring. The black dashed lines (MN, NP and 70 M) show the location where discrete carbonate measurements were made in the water column in 2008–2010 to develop the relationships shown in Tables 1 and 2. The three major shelf domains are shown in italics.

2. Background

The southeastern Bering Sea sustains one of the most productive marine ecosystems in the ocean and supports an extraordinarily rich fishery that generates about 40% of all finfish and shellfish landings in the United States. It directly or indirectly provides over 25 million pounds of subsistence foods used by nearly 55,000 local residents, primarily Alaska Natives (Stabeno et al., 2012), particularly in small coastal communities.

The continental shelf near the M2 mooring is relatively wide (>500 km) compared to other coastal regions along the west coast of North America and is heavily influenced by the seasonal advance and retreat of sea ice, terrestrial discharge and interannual variability in the wind fields (Stabeno et al., 2010). Semi-permanent temperature fronts naturally divide the shelf into three along-shelf domains (Coachman, 1986; Kachel et al., 2002; Stabeno et al., 2012; Cross et al., 2013) with differing vertical structure. Wind forcing, tidal mixing, the seasonal advance and retreat of sea ice, terrestrial discharge, and bottom topography determine the location and strength of the fronts. The coastal domain extends from the western shores of Alaska out to roughly the 50 m isobath, where the Inner Front constitutes the boundary between the coastal domain and middle domain (Fig. 1). A well stratified, two-layer system exists in the middle domain during the ice-free months (April–October), where wind mixes the surface waters over a denser, tidally mixed bottom layer. A two-layer system is also present in the outer domain, although the transition between the surface and bottom layers is more gradual than in the middle domain.

The M2 mooring lies about half way through the middle domain, several hundred kilometers southwest of Bristol Bay (Fig. 1). Here, the water depth ranges from approximately 50 to 100 m, gradually deepening from east to west. In winter, the water column is generally well mixed with little to no gradient in temperature and salinity (Stafford et al., 2010). However, in summer the onset of seasonal ice melt and the contribution of moderate volumes of riverine discharge through the Inner Front create a well-defined two-layer structure. The surface layer is typically 20–30 m thick, with bottom waters underlying sharp gradients in temperature, inorganic nutrients and DIC concentrations (Mathis et al., 2010), and a weaker gradient in salinity (Stabeno et al., 2012; Ladd and Stabeno, 2012).

In spring, DIC concentrations in the middle domain near the M2 mooring range from ~2000 to 2050 μmoles kg^{-1} and are fairly uniform from the surface to the bottom (Mathis et al., 2010; Cross et al., 2012). In summer, as rates of net primary production (NPP) reach as high as 13 g C m^{-2} d^{-1} (Niebauer et al., 1995; Lomas et al., 2012; Cross et al., 2014) there is a pronounced gradient in DIC concentrations between the surface and bottom, with DIC accumulating at depth in response to remineralization of exported organic carbon produced at the surface. This remineralization increases the partial pressure of CO_2 (pCO_2) in bottom waters, which reduces carbonate mineral saturation states to a varying degree across the shelf. Over the northern part of the shelf, where bottom temperatures are the lowest and export production is the highest, an intense seasonal reduction in the aragonite saturation state has been observed in bottom waters, while Ω at the surface increase (Mathis et al., 2011a,b). The bottom water reduction of Ω aragonite corresponds to high apparent oxygen utilization (AOU) rates and elevated silicate concentrations, which are probably the result of both water column and sedimentary remineralization. The subsurface effects of remineralization can be especially significant during and after periods of peak production. These biologically driven, seasonally divergent trajectories of Ω, or the "Phytoplankton-Carbonate Saturation State" (PhyCaSS) Interaction, has also been observed in the Chukchi Sea (Bates et al., 2009;

Bates and Mathis, 2009), and is likely a typical feature of highly productive polar and sub-polar shelves.

Using data from seasonal, repeat hydrographic cruises in the Bering Sea from 2008 to 2010, Mathis et al. (2011b) determined that the current inventories of anthropogenic CO_2 (~35 μmoles kg^{-1}) in the Bering Sea could lead to a 0.2 reduction in the aragonite saturation state in the bottom waters where carbonate mineral undersaturations were observed. However, the paucity of fully resolved temporal data limited our understanding of how this process evolved with time. Several questions remained regarding when pCO_2 levels reach a point, where carbonate mineral undersaturation would occur, how long these levels of undersaturation would remain, and ultimately the intensity of these undersaturations events. To fill this data gap, we deployed OA sensors on the M2 mooring to better constrain the carbonate chemistry at the surface and at depth.

3. Methods

3.1. M2 mooring site

The Pacific Marine Environmental Laboratory (PMEL) and the Fisheries Oceanography Coordinated Investigations (FOCI) group began continuous monitoring at the M2 (Fig. 1) mooring site on the southeastern Bering Sea shelf in 1995. M2 is located on the 70-m isobath (Stabeno et al., 2010) southwest of Bristol Bay (Fig. 1). During the ice-free season (April/May–September/October), the M2 mooring array includes a surface toroid buoy with an aluminum tower. A subsurface mooring line is deployed during the winter season (October–April). Past instrumentation at the M2 site is documented in Ladd and Stabeno (2012) and Stabeno et al. (2007) and includes measurements of temperature, salinity, chlorophyll fluorescence, currents, and nitrate, with intermittent measurements of zooplankton biovolume and oxygen. Estimates of chlorophyll are calculated from the fluorescence using the factory calibrations.

3.2. OA instrumentation at M2

From May 2011 to October 2011, OA instrumentation was deployed at the surface buoy and approximately 3 m from the bottom at the M2 site. A Seabird Electronics package at a depth of 1 m sampled every 3 h to obtain measurements of temperature (°C), salinity, dissolved oxygen (DO; μmoles kg^{-1}), fluorescence (μg l^{-1}), and turbidity (% light transmission). A Sunburst Sensors Submersible Autonomous Moored Instrument for CO_2 (SAMI-CO_2) was also deployed at 1 m. The SAMI-CO_2 was calibrated over a range of 100–1500 μatm with a reported ±1 μatm precision (DeGrandpre et al., 1995), with most of the observed data falling within this range. At a 3-h sampling interval, the SAMI-CO_2 runs blanks every 28 cycles or every 3 days to test for instrument drift over the course of the deployment. A Sunburst Sensors Submersible Autonomous Moored Instrument for pH (SAMI-pH) was deployed at 1 m and near the bottom, but both sensors failed during the deployment and no pH data were recovered.

A bottom cage was deployed at a depth of 67 m, or roughly 3 m off the bottom. The cage included a seabird package measuring temperature (°C), salinity, and DO (μmoles kg^{-1}) as well as a SAMI-CO_2 sensor programmed to sample at longer intervals (18 h) than the surface instrument to conserve battery life in the colder bottom waters. The bottom SAMI-CO_2 sensor also ran routine blanks and was calibrated over a range of 100–1500 μatm with a reported ±1 μatm precision, with most of the recorded data falling within this range. Calibration casts, using a profiling, 911-plus CTD, were made during the mooring deployment (May 16, 2011) and retrieval (October 3, 2011), aboard the NOAA Ship *Oscar Dyson*.

Calibration samples for pCO_2 and DO were taken at the moored sensor depths at the surface and near the bottom. A modified version of the Winkler Titration method (Langdon, 2010) was used to calibrate the DO sensors on the Seabird packages. pCO_2 was calculated from dissolved inorganic carbon (DIC), total alkalinity (TA), temperature, and salinity using CO2SYS (version 1.05) and the thermodynamic model of Lewis and Wallace (1995). DIC and TA samples were collected as suggested by the Guide to Best Practices for Ocean CO_2 measurements (Dickson and Goyet, 1994) and were analyzed using a highly precise and accurate gas extraction/coulometric detection system (~0.02%, <2 μmoles kg^{-1}). The analytical system consists of a VINDTA 3C (Versatile Instrument for the Detection of Total Alkalinity) coupled to a CO_2 coulometer (model 5012; UIC Coulometrics). Routine analyses of Certified Reference Materials (CRMs, provided by A.G. Dickson, Scripps Institution of Oceanography) and repeat sampling ensured that the accuracy of the DIC/TA measurements was within 0.05% and was stable over time.

The complete seawater carbonic acid system (i.e., CO_2, $H_2CO_3^-$, HCO_3^-, CO_3^{2-}, H^+) can be calculated from two of the five measurable carbonate system parameters (i.e., DIC, TA, pCO_2, pH, and more recently CO_3^{2-}), along with temperature and salinity (Zeebe and Wolf-Gladrow, 2001; Dickson et al., 2007). The carbonic acid dissociation constants (pK_1 and pK_2) of Mehrbach et al. (1973), as refit by Dickson and Millero (1987), were used to calculate seawater pCO_2 and other carbonate parameters from the DIC/TA data obtained during the calibration casts, using the equations of Zeebe and Wolf-Gladrow (2001). In addition, the CO_2 solubility equations of Weiss (1974), and dissociation constants for borate and phosphate (Dickson et al., 2007), were used.

3.3. Empirical relationship between pCO_2 and Ω_{arg}

In order to fully constrain the carbonate system, two of the five parameters must be measured although currently, only two of these parameters (pCO_2 and pH) can be measured autonomously on moorings with any reliability. Unfortunately, during the M2 deployment in 2011, only the pCO_2 sensors returned good data, leaving us with only one of the two needed carbonate parameters. However, given our extensive sampling over the shelf in the preceding years we can estimate an approximate seasonal relationship between the carbonate mineral saturation state for aragonite (Ω_{arg}) and pCO_2 and to a lesser extent DO concentrations. Similar approaches have been employed along the west coast of North America and the Gulf of Alaska (Evans et al., 2013; Alin et al., 2012; Juranek et al., 2009), where multiple linear regressions (MLRs) have been used to determine Ω_{arg} from non-carbonate parameters (i.e. temperature, salinity, nitrate and DO), but here we use direct empirical relationships, rather than MLRs to estimate the seasonal changes in Ω_{arg}.

In order to develop empirical relationships between pCO_2/DO and Ω_{arg} for the southeastern Bering Sea, we synthesized data (over 1000 measurements) from seven Bering Sea Ecosystem Study (BEST) cruises (MN, NP and 70 M lines in Fig. 1) over the southern shelf where discrete carbonate system measurements were made (Tables 1 and 2; Fig. 2A and B). In addition to looking at the entire water column, we also developed empirical equations for just the surface mixed layer (0–30 m) and the subsurface layer (30 m to the bottom) in each season to determine any biases in discrete water masses. In the 3 years before the mooring deployment, pCO_2 ranged from <200 μatm at the surface to ~1500 μatm at depth over the course of the open water season (observations were made in May–September). DO concentrations ranged from

Table 1
The empirically derived relationships between pCO_2 and $\Omega_{arg.}$ from observations made over the southeastern Bering Sea shelf in 2008, 2009 and 2010. The regression equations were developed by fitting the data from different cruises in each year shown in Fig. 2A. The equation for the complete record was based on all the available data. The $\Omega=1$ column indicates the pCO_2 values (μatm) that were determined by solving the regression equations. The r^2 values indicate the fit of the curve for each dataset.

pCO_2 - $\Omega_{arg.}$ Relationships	Full Water Column			Surface (0 - 30 m)			Bottom (30 m - Bottom)		
	Regression Equations	$\Omega=1$ μatm	R^2	Regression Equations	$\Omega=1$ μatm	R^2	Regression Equations	$\Omega=1$ μatm	R^2
Spring 2008	$101.51x^{-0.752}$	466	0.91	$129.21x^{-0.794}$	456	0.96	$98.308x^{-0.745}$	473	0.89
Summer 2008	$126.7x^{-0.762}$	575	0.88	$79.449x^{-0.667}$	706	0.83	$80.159x^{-0.696}$	544	0.91
Spring 2009	$111.39x^{-0.77}$	455	0.91	$229.34x^{-0.892}$	443	0.96	$98.768x^{-0.749}$	460	0.90
Summer 2009	$262.97x^{-0.896}$	502	0.95	$239.96x^{-0.873}$	533	0.92	$150.73x^{-0.809}$	493	0.93
Fall 2009	$771.61x^{-1.053}$	552	0.93	$503.39x^{-0.977}$	583	0.84	$406.33x^{-0.957}$	532	0.87
Spring 2010	$126.23x^{-0.778}$	502	0.94	$130.45x^{-0.783}$	503	0.91	$101.82x^{-0.744}$	500	0.87
Summer 2010	$340.96x^{-0.942}$	488	0.90	$260.74x^{-0.889}$	522	0.84	$166.18x^{-0.829}$	477	0.85
Complete Record	$187.13x^{-0.84}$	507	0.88	$203.02x^{-0.849}$	522	0.82	$116.59x^{-0.767}$	495	0.89

Table 2
The empirically derived relationships between O_2 and $\Omega_{arg.}$ from observations made over the southeastern Bering Sea shelf in 2008, 2009 and 2010. The regression equations were developed by fitting the data from different cruises in each year shown in Fig. 2B. The equation for the complete record was based on all the available data. The $\Omega=1$ column indicates the O_2 values (μmoles kg^{-1}) that were determined by solving the regression equations. The r^2 values indicate the fit of the curve for each dataset.

O_2 - $\Omega_{arg.}$ Relationships	Full Water Column			Surface (0 - 30 m)			Bottom (30 m - Bottom)		
	Regression Equations	$\Omega=1$ μmol kg^{-1}	R^2	Regression Equations	$\Omega=1$ μmol kg^{-1}	R^2	Regression Equations	$\Omega=1$ μmol kg^{-1}	R^2
Spring 2008	$0.5124e^{0.0024x}$	279	0.62	$0.423e^{0.0029x}$	--	0.12	$0.5128e^{0.0024x}$	278	0.82
Summer 2008	$0.5285e^{0.0034x}$	188	0.43	$1.7707e^{0.0002x}$	--	0.00	$0.5286e^{0.003x}$	213	0.62
Spring 2009	$0.4671e^{0.0023x}$	331	0.57	$0.3118e^{0.0035x}$	--	0.09	$0.4699e^{0.0023x}$	328	0.71
Summer 2009	$0.3521e^{0.0042x}$	249	0.28	$5.377e^{-0.003x}$	--	0.03	$0.3996e^{0.0032x}$	287	0.42
Fall 2009	$0.2375e^{0.0058x}$	248	0.31	$1.5959e^{-0.0002x}$	--	0.00	$0.446e^{0.0027x}$	299	0.11
Spring 2010	$0.4836e^{0.0033x}$	220	0.62	$0.4815e^{0.0036x}$	--	0.17	$0.5759e^{0.0024x}$	230	0.62
Summer 2010	$0.5183e^{0.0032x}$	205	0.33	$2.3962e^{-0.0009x}$	--	0.01	$0.5286e^{0.0025x}$	255	0.52
Complete Record	$0.5173e^{0.0029x}$	227	0.31	$1.5441e^{0.00007x}$	--	0.00	$0.5069e^{0.0026x}$	261	0.48

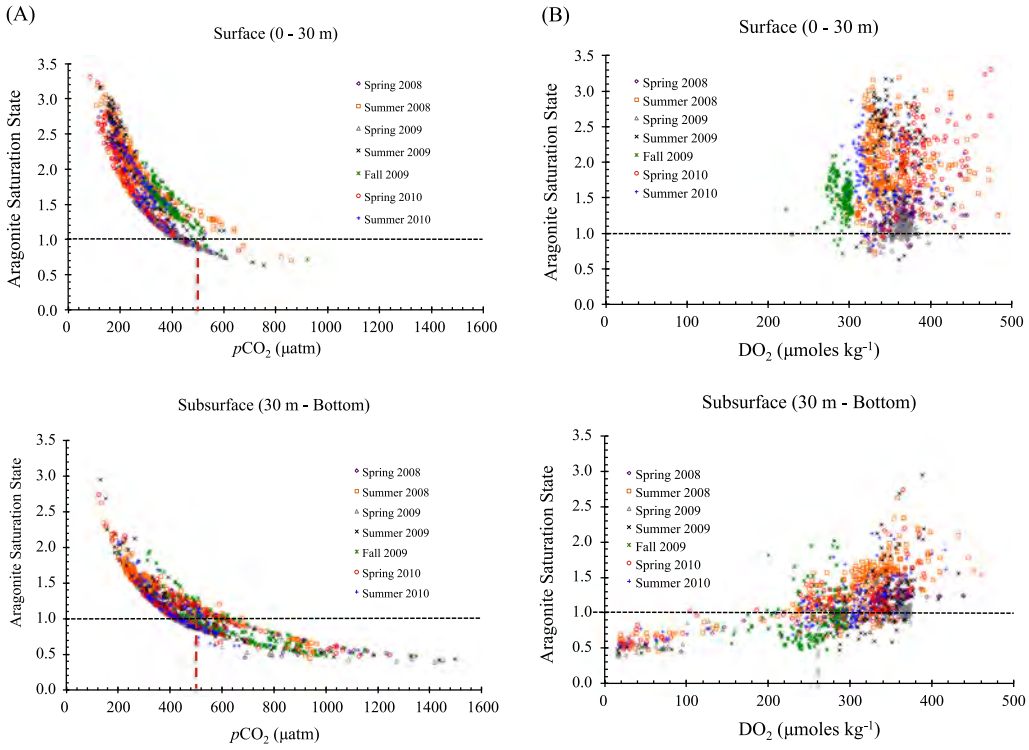

Fig. 2. (A) Empirical relationships between aragonite saturation state (Ω) and pCO_2 (μatm) developed for the surface mixed layer (top panel) and subsurface waters (bottom panel) for the southeastern Bering Sea from discrete data collected in 2008–2010. The dashed line indicates the saturation horizon ($\Omega=1$) for aragonite. Spring=April/May, summer=June/July, fall=September/October. The regression equation from each dataset is shown in Table 1. (B) Empirical relationships between aragonite saturation state (Ω) and DO concentrations (μmoles kg^{-1}) developed for the surface mixed layer (top panel) and subsurface waters (bottom panel) for the southeastern Bering Sea from discrete data collected in 2008–2010. The dashed line indicates the saturation horizon ($\Omega=1$) for aragonite. Spring=April/May, summer=June/July, fall=September/October. The regression equation from each dataset is shown in Table 2.

>50 μmoles kg^{-1} near the bottom to >450 μmoles kg^{-1} at the surface. The data show that when pCO_2 values reach approximately 500 μatm (Table 1), Ω_{arg} is at or below the saturation horizon ($\Omega_{arg}=1.0$; horizontal dashed line in Fig. 2A). Although the relationships between DO and Ω_{arg} are not as well-correlated (lower r^2 values), particularly at the surface, the threshold for aragonite undersaturation with respect to DO was ~225–260 μmoles kg^{-1} (Table 2; Fig. 2B). When pCO_2 values were less than 500 μatm and DO was greater than 260 μmoles kg^{-1} the data showed that Ω_{arg} was above the saturation horizon. These empirical relationships (Tables 1 and 2) were used to relate the moored observations of pCO_2/O_2 to Ω_{arg} to better understand the impacts of primary production and remineralization on the carbonate chemistry.

One caveat to our pCO_2–Ω_{arg} relationships is that we have to assume that the relationship between total alkalinity (TA) and DIC did not change between the 2008 and 2010 ship-based measurements and our mooring observations in 2011. A robust explanation of the conservative and non-conservative behavior of TA is given in Cross et al. (2013) but it was shown that a number of factors such as sea ice melt, riverine inputs, carbonate mineral dissolution and coccolith production can cause anomalies in TA concentrations relative to salinity over the shelf. All these drivers for the non-conservative behavior of TA were observed during our 2008–2011 measurements and are therefore captured in the calculated pCO_2 and Ω_{arg} values. Given these caveats, we feel confident that the pCO_2–Ω_{arg} relationship is valid for the discussion presented here.

4. Results and discussion

4.1. Surface observations

When the M2 mooring was deployed in mid-May 2011 sea ice had already retreated from the area and the ice edge was several hundred kilometers to the north. Surface water temperatures were still relatively cold (~2.5 °C), but some warming had occurred since the onset of ice melt. During the deployment of the mooring, surface water temperatures warmed considerably and reached a peak of 11 °C in mid-August before cooling began (Fig. 3). At the time of deployment, surface salinity was ~31.3, but increased to a maximum of ~31.9 a few weeks later likely due to flushing of ice melt waters out of the area. Starting in early July, salinity began to steadily decline, dropping to a minimum value of 31.1 in early September, likely due to the influence of freshwater discharge from the coast and the advection of ice melt water from farther north (Fig. 3).

Because the mooring was deployed in water that had been ice-free for at least a few weeks, the onset of the ice edge bloom was not observed. Chlorophyll concentrations ranged from 0 to 1.2 μ l^{-1} in the first few weeks of deployment, but later spiked to over 5.0 μg l^{-1} (early June; Fig. 3) with transmissivity dropping by 15% (Fig. 3). The increase in chlorophyll coincided with a period of increasing temperature and near constant salinity, which likely indicated the onset of temperature stratification often necessary to support a significant late spring open water phytoplankton bloom (Sigler et al., 2014). DO concentrations were elevated (>400 μmoles kg^{-1}) and oxygen was supersaturated at the surface at the time of the deployment, also indicating that primary production had already begun (Fig. 3). After the early June bloom, chlorophyll concentrations dropped quickly and remained fairly constant (~0–0.5 μ l^{-1}) until mid-August when a more gradual, less intense increase in chlorophyll occurred in conjunction with an increase in DO concentrations, indicating a late-season bloom which is common at M2 (Sigler et al., 2014). This gradual increase in chlorophyll and slow decrease in salinity could indicate advection of water from the Inner Front. The increase in chlorophyll in early September coincided with an increase in salinity and a slight decrease in temperature, and was associated with vertical mixing, which introduced nutrients into the surface mixed layer and thus stimulated a surge of primary production.

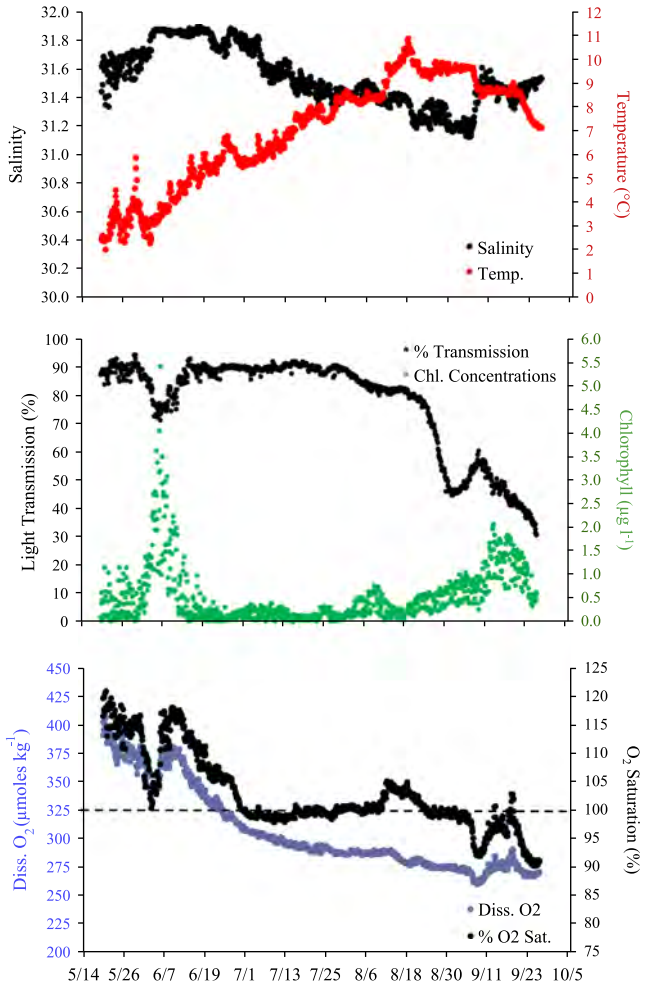

Fig. 3. Hydrographic mooring data from the surface (1 m depth) Seabird instrument package. The top panel shows temperature (°C) and salinity. The middle panel shows data from the transmissometer (% light transmission) and fluorometer (μg l^{-1}). The bottom panel shows dissolved oxygen concentration (μmoles kg^{-1}) and oxygen saturation (% saturation at in situ temperature).

As with DO concentrations, surface pCO_2 values at the time of deployment indicated that biological production had already occurred. Bates et al. (2011) showed that pCO_2 values under the sea ice of the eastern Bering Sea were near atmospheric concentrations (~390 μatm), which was certainly not the case at the time of the mooring deployment. In mid-May, pCO_2 values at the surface at M2 were ~150 μatm (red data in Fig. 4) or roughly 240 μatm lower than atmospheric values (black data in Fig. 4). This differential in air-sea pCO_2 (Δ pCO_2) values indicated the removal of several hundred μmoles kg^{-1} of DIC from the surface layer, which is consistent with the previous observations of DIC drawdown (Cross et al., 2012; Mathis et al., 2010; Codispoti et al., 1982) in the region. pCO_2 values increased fairly consistently at the surface throughout the deployment, with the exception of slight drawdowns occurring with the increases in chlorophyll values in early June and September (Fig. 3). The near constant increase in the pCO_2 is due to surface warming (Fig. 3) and air-sea fluxes that occurred over the course of the deployment, although values remained below atmospheric CO_2 concentrations for nearly all the deployments confirming that this part of the shelf provides

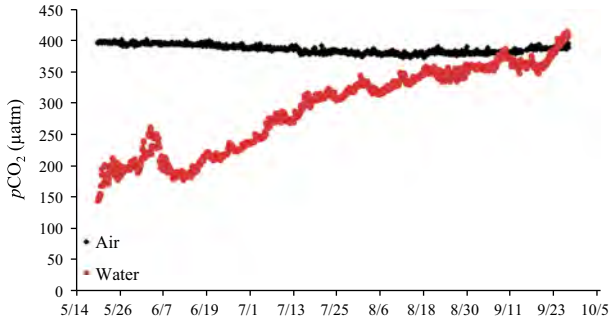

Fig. 4. Mooring data from the surface (1 m) pCO_2 (µatm) sensor (red points) as well as atmospheric pCO_2 values (black points).

a strong seasonal sink for atmospheric CO_2 (Bates et al., 2011; Cross et al., 2014) throughout the spring and summer.

Individual seasonal estimates from ship observations collected in 2008 showed that CO_2 fluxes into the surface layer ranged from −30 and 53 mmol C m^{-2} d^{-1} during spring and between −7 and −113 mmol C m^{-2} d^{-1} during summer (Bates et al., 2011). In general, fluxes were similar between the southern middle and southern coastal domains during spring (~20 mmol C m^{-2} d^{-1}). During summer, the influx of CO_2 to the surface layer increased strongly in the southern coastal domain (~59 mmol C m^{-2} d^{-1}) while influxes remained similar (16.5 mmol C m^{-2} d^{-1}) in the southern middle domain where M2 is located.

We used the Δ pCO_2 data along with daily averaged wind speed data from the M2 mooring to calculate air-sea exchange (F_{CO_2}; mmol m^{-2} d^{-1}) in 2011 using the following formula:

$$F_{CO_2} = K_{SST} \times K_{CO_2} \times \Delta pCO_2 \quad (1)$$

where K_{SST} is the gas transfer velocity (cm hr^{-1}), K_{CO_2} is the solubility of CO_2 (mmol m^{-3} µatm^{-1}) estimated by Weiss (1974), and ΔpCO_2 is the air-sea pCO_2 difference (µatm) between the atmosphere and surface water values at M2. Values of K_{SST} were determined from the quadratic wind speed dependency from Ho et al. (2011), such that

$$K_{SST} = (0.277 \times U^2) \times (Sc/600)^{-0.5} \quad (2)$$

where U is the daily averaged wind speed above the sea surface, and Sc is the Schmidt number for CO_2 at the in situ temperature. Wind speed was measured from sensors mounted on the tower of the M2 mooring approximately 3 m from the surface of the water and then corrected to 10 m.

During the first few weeks of the M2 deployment, F_{CO2} was fairly high (−15 to −125 mmol C m^{-2} d^{-1}) and consistent with seasonal ship-based estimates over this part of the shelf due to the large disequilibrium between the atmosphere and surface water pCO_2 values (Fig. 4) and relatively high, but variable wind speeds (2–12 m s^{-1}). However, by July, F_{CO_2} had decreased to −5 to −50 mmol C m^{-2} d^{-1} as surface pCO_2 values quickly increased and winds diminished. Both these factors sharply diminish air-sea gas exchange. Near the end of the deployment, surface water pCO_2 values exceeded atmospheric values (Fig. 4), even though surface temperatures had been decreasing for several weeks, which would have lowered surface water pCO_2. In late September, the surface waters at M2 became a weak source of CO_2 (+5 mmol C m^{-2} d^{-1}) to the atmosphere. This pattern has been previously observed over the northern shelf near the coast, resulting from the remineralization of allocthonous organic matter, likely derived from river discharge (Cross et al., 2012). While the trajectory of surface water pCO_2 values was still increasing at the time of the mooring recovery, it is unclear how high these values reached before the onset of sea ice and how much outgassing occurred.

4.2. Bottom water observations

Measurements from near the bottom at the M2 mooring site showed that temperature and salinity were much more uniform than at the surface during the duration of the deployment. Temperatures near the bottom warmed slightly from ~0.5 °C in mid-May to a maximum of 3 °C in early October (Fig. 5). Salinity showed very little variability, ranging from only 31.8 to 32.1 (Fig. 5). There was no chlorophyll sensor on the seabird package near the bottom, but transmissometer data showed a steep decrease in light transmission starting roughly at the same time as the sharp chlorophyll increase was observed at the surface (Fig. 5). The low light transmission continued from mid-June through the end of the deployment likely due to particle export from the surface (Moran et al., 2012) and some sediment resuspension.

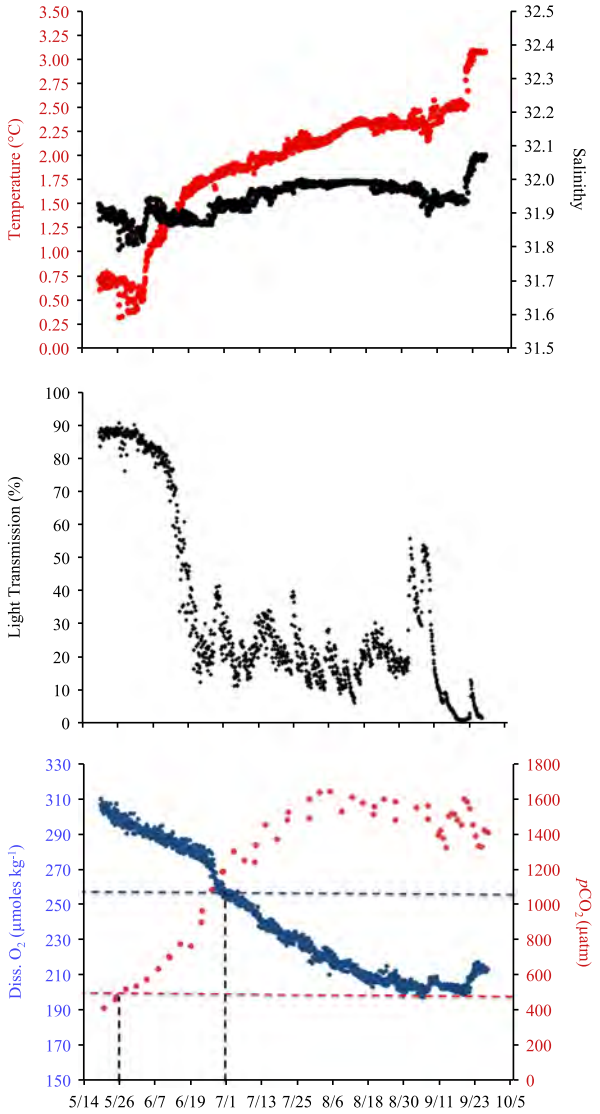

Fig. 5. Hydrographic mooring data from the near the bottom (67 m depth) Seabird instrument package. The top panel shows temperature (°C) and salinity. The middle panel shows transmissometer data (% light transmission). The bottom panel shows dissolved oxygen (blue) concentration (µmoles kg^{-1}) and pCO_2 (red) values (µatm). The black, dashed horizontal line shows the threshold of where pCO_2 values exceeded 500 µatm (Table 1) and the blue, dashed line indicates the DO threshold of 260 µmoles kg^{-1} (Table 2). The vertical lines show the approximate dates when the undersaturation threshold was reached.

DO concentrations near the bottom started at ~310 μmoles kg^{-1}, but decreased sharply and consistently during the deployment reaching a minimum value of ~200 μmoles kg^{-1} in September. pCO_2 values showed an inverse trend, starting at ~400 μatm and rising quickly to over 1400 μatm by the beginning of July, which was consistent with ship-based observations in 2008–2011. The combination of oxygen consumption and increased pCO_2 values is a clear indication of the remineralization of exported organic matter near the bottom. Although temperatures did warm slightly during the deployment, this would have only accounted for a ~50 μatm increase in pCO_2. The remaining increase (~950 μatm) had to have come from remineralization processes in the water column and underlying sediments, assuming that TA stayed relatively constant throughout the deployment. This seems likely given that salinity remained fairly constant and Cross et al. (2013) showed that most of the non-conservative processes that impact TA occur in the surface mixed layer. The only process that could have caused a non-conservative change in TA concentrations in bottom waters is carbonate mineral dissolution, which was evident in some northern locations over the shelf in summer and fall of 2008–2010 (Cross et al., 2013) where $CaCO_3$ Ω were very low (e.g., Ω_{arg}=0.51). Similar processes occurring at M2 could have added as much as 36 μmoles kg^{-1} of TA during the late summer and autumn months (Cross et al., 2013) to the bottom waters, which would have led to a ~450 μatm decrease in pCO_2 and mitigated the effects of respiration. However, $CaCO_3$ undersaturations were milder at M2, indicating slower dissolution processes. Perturbations to pCO_2 from TA generated by carbonate mineral dissolution were likely minimal in this area.

4.3. Assessing the carbonate chemistry

Using the pCO_2/O_2–Ω_{arg} relationships we can show that the surface waters at M2 likely remained supersaturated with respect to aragonite throughout the spring and summer months. When pCO_2 ranged from 150 to 400 μatm and DO concentrations were $>$ 260 μmoles kg^{-1} in 2008–2010, Ω_{arg} was between 3.5 and 1.2, which was likely what occurred during the M2 deployment as Ω_{arg} steadily decreased as air-sea gas exchange increased pCO_2 at the surface (Fig. 4) and DO concentrations returned to pre-bloom levels (Fig. 3). The only locations where aragonite was undersaturated at the surface in 2008–2010 was where there was a high concentration of sea ice melt or river runoff, both of which are low in TA (Mathis et al., 2011a) relative to marine waters. These locations all had salinities less than 30, which was not observed during the deployment at M2, although observations were not made at the time of ice retreat.

Although the 2011 results showed that Ω_{arg} is currently supersaturated in the surface waters near M2 this will likely not be the case by the end of this century. Anthropogenic CO_2 is accumulating in the ocean at rate of ~1.5–3.0 ppm yr^{-1} (Feely et al., 2009) so even as biological productivity lowers pCO_2 each spring, baseline levels of CO_2 in the surface waters of the Bering Sea will continue to rise. Because primary production in the eastern Bering Sea is nutrient limited, there will likely be no significant increase in productivity to offset the increasing CO_2 levels and increased stratification due to warming surface temperatures and increased freshwater discharge may actually lead to a reduction in primary production. In 2011, primary production lowered pCO_2 values to ~150 μatm, but with even a decade's worth of CO_2 accumulation at current emission rates minimum, post-bloom values would be closer to 165–180 μatm, excluding any further warming effect, which would also increase pCO_2. We can see from our 2011 observations that by the beginning of August, the surface water pCO_2 values at M2 were close to equilibrium with the atmosphere. By mid-century (2050), pCO_2 values at the surface will likely be greater than 450 μatm at the end of summer and ~500 μatm before the onset of sea ice assuming constant temperature and no change in TA. At that time, it is likely that localized aragonite undersaturation at the surface will begin to occur. By the end of the century (2100), if pCO_2 values exceed 700 μatm, aragonite will likely be undersaturated at the surface for most of the year with only short-term alleviations coming directly after the most intense periods of primary production.

On the other hand, the pCO_2/O_2–Ω_{arg} relationships showed that aragonite was already undersaturated near the bottom for at least 4 months (June–September) in 2011. It is unclear how long pCO_2 values stayed above 500 μatm and DO values stay below 260 μmoles kg^{-1}. Although there was a slight downward trend in pCO_2 between mid-August and October and we assume that values return to $<$ 500 μatm by the following spring as they did in previous years (Mathis et al., 2010), it may have taken several more months for the high pCO_2 water to dissipate either through vertical mixing, lateral transport or tidal flushing. Although only a relatively small portion of the current CO_2 loading (~150 ppm) in the bottom waters can be attributed to anthropogenic sources, the inventory will continue to increase as anthropogenic CO_2 concentrations increase, lengthening the duration and intensity of the undersaturation events.

The current bottom water carbonate mineral undersaturations and future surface undersaturations may have detrimental consequences for local calcifying organisms, but direct evidence from the environment is still lacking. Initial results of the experimental studies (Long et al., 2013a,b) indicate that OA may have a substantial negative effect on red king and Tanner crab stocks, particularly at the larval stages. Reduced survival at the larval stage is likely to reduce recruitment and subsequently affect the number of crabs available for commercial harvest. However, these early life stages do not currently coincide with undersaturation events, as they happen early in the year (January–June). More research on the effects of OA on other life history stages and the molecular response is necessary to fully understand the effects it will have on crab populations throughout the year as well as other benthic calcifying organisms.

The impacts of OA on pelagic calcifying and non-calcifying organisms in the southern Bering Sea is also unclear, but a new environmental study of pteropods in the Southern Ocean (Bednaršek et al., 2012) showed extensive shell dissolution when aragonite became undersaturated. Previous work has shown that pteropods can make up as much as 40% of the juvenile pink salmon diet (Aydin et al., 2005) so any disruptions to their stocks could have a cascading impact on the commercial salmon fishery. Another recent study of walleye pollock, also a commercially important fishery in the Bering Sea, showed that both juvenile and adult fish have a high tolerance for OA (Hurst et al., 2012). While there may not be a direct effect on certain pelagic finfish such as pollock because of limited impacts on growth and mortality, it is unknown how OA will affect the food supply of these fish or their behavior. Pollock rely heavily on copepods during early life-stages before shifting to euphausiids as their major prey source (Dwyer et al., 1987; Napp et al., 2001; Brodeur et al., 2002; Duffy-Anderson et al., 2002; Moss et al., 2009). The impacts of OA on these lower trophic level organisms have yet to be resolved (Fabry et al., 2008; Hendriks et al., 2010). Because of these uncertainties and the varying degrees of organismal responses, there will likely be winners and losers as OA continues to worsen in the Bering Sea.

5. Conclusions

Data from moored sensors deployed at the surface and near the bottom in the southeastern Bering Sea during the ice-free season of

2011 provided new insights into the seasonal cycling of carbonate biogeochemistry. Previous synoptic studies have shown that carbonate mineral saturation states are largely controlled by the timing, extent and location of primary production in the water column and the fate of the organic matter produced during these blooms. These findings were confirmed in 2011 as surface pCO_2 data during the open water season showed a substantial disequilibrium between the ocean and the atmosphere, particularly from mid-May to August where fluxes reached as high as -125 mmol C m^{-2} d^{-1}. Using empirical relationships between the pCO_2/O_2 and Ω_{arg}, we determined that Ω_{arg} is likely supersaturated at the surface throughout the year at the M2 site. During the open water months, there was a large range of Ω_{arg} as values peaked at ~3.5, but then quickly begin to decrease as air-sea exchange increased the pCO_2 and reduced Ω_{arg} to a minimum of ~1.2. The highest pCO_2 values (~410 μatm) observed during the mooring deployment correspond to lowest Ω_{arg} values, but they do not currently lead to aragonite undersaturation. However, pCO_2 values at the surface were trending upward at the time of sensor recovery and it is unclear how high surface pCO_2 reached prior to the onset of primary production the following spring. In addition, anthropogenic CO_2 is accumulating in these surface waters and will likely cause Ω_{arg} to become undersaturated at certain times of the year within the next few decades and perennially by the end of the century. This could have important consequences for pteropod populations, which are highly sensitive to Ω_{arg} and are a keystone species in the food web due to their prevalence as a food source for juvenile pink salmon.

Sensor data from near the bottom confirmed that extensive aragonite undersaturations occur over this part of the shelf due to the remineralization of exported organic matter from the surface. In 2011, the onset of aragonite undersaturations began in mid-June and persisted until the sensors were recovered at the beginning of October. This prolonged event was also notable due to its intensity, with pCO_2 rising above 1400 μatm, which is two times higher than the threshold where aragonite becomes undersaturated. It is unclear from the current data how long pCO_2 remained at these levels, but it seems safe to assume that aragonite was highly undersaturated for at least 4 months in 2011.

The sustained aragonite undersaturations could have profound implications for benthic calcifiers in the eastern Bering Sea. Currently, anthropogenic CO_2 is a relatively small contributor to the high pCO_2 values observed over the shelf and undersaturations have only been observed during late summer and fall months. However, as anthropogenic CO_2 continues to accumulate, the duration and intensity of undersaturation events will increase, exposing organisms to longer periods of potentially corrosive conditions.

The southeastern Bering Sea is an important area for both the local and national economies, with hundreds of millions of dollars in commercial species at risk due to increasing OA. Our results have shown that this area needs careful monitoring in the coming decades coupled with laboratory based experiments to determine the sensitivity of commercial organisms and keystone species in this sensitive and rapidly changing region.

Acknowledgments

The authors thank the officers and crew of the NOAA Fisheries Vessel Oscar Dyson for their efforts in supporting our work. We also thank the EcoFOCI group, especially Bill Floering from NOAA-PMEL for their efforts. The work presented in this paper was supported by the Alaska Ocean Observing System under NOAA awards A08NOS4730406 and NA11NOS0120020, the Cooperative Institute for Alaska Research with funds from NOAA under cooperative agreement NA08OAR4320751 with the University of Alaska, the National Science Foundation through award ARC-1107997 and the NOAA Ocean Acidification Program. Support for M2 was provided by PMEL's EcoFOCI program and by North Pacific Research Board, BSIERP Grant B-52. This is NPRB publication number 437 and BEST-BSIERP Bering Sea Project publication number 106.

References

Alin, S.R., Feely, R.A., Dickson, A.G., Hernández-Ayón, J.M., Juranek, L.W., Ohman, M.D., Goericke, R., 2012. Robust empirical relationships for estimating the carbonate system in the southern California Current System and application to CalCOFI hydrographic cruise data (2005–2011). J. Geophys. Res. 117 (C5), C05033, http://dx.doi.org/10.1029/2011JC007511.

Aydin, K.Y., McFarlane, G.A., King, J.R., Megrey, B.A., Myers, K.W., 2005. Linking oceanic food webs to coastal production and growth rates of Pacific salmon (Oncorhynchus spp.), using models on three scales. Deep-Sea Res. Part II: Top. Stud. Oceanogr. 52 (5 and 6), 757–780.

Barton, A., Hales, B., Waldbusser, G.G., Langdon, C., Feely, R.A., 2012. The Pacific oyster, Crassostrea gigas, shows negative correlation to naturally elevated carbon dioxide levels: implications for near-term ocean acidification effects. Limnol. Oceanogr. 57 (3), 698–710, http://dx.doi.org/10.4319/lo.2012.57.3.0698.

Bates, N.R., Mathis, J.T., 2009. The Arctic Ocean marine carbon cycle: evaluation of air-sea CO2 exchanges, ocean acidification impacts and potential feedbacks. Biogeosciences 6, 2433–2459, http://dx.doi.org/10.5194/bg-6-2433-2009.

Bates, N.R., Mathis, J.T., Cooper, L.W., 2009. Ocean acidification and biologically induced seasonality of carbonate mineral saturation states in the Arctic Ocean. J. Geophys. Res. 114, C11007, http://dx.doi.org/10.1029/2008JC004862.

Bates, N.R., Mathis, J.T., Jefferies, M.A., 2011. Air-sea CO2 fluxes on the Bering Sea shelf. Biogeosciences 8, 1237–1253.

Bednaršek, N., Tarling, G.A., Bakker, D.C.E., Fielding, S., Jones, E.M., Venables, H.J., Ward, P., Lézé, B., Feely, R.A., Murphy, E.J., 2012. Extensive dissolution of live pteropods in the Southern Ocean. Nature Geosci. 5, 881–885, http://dx.doi.org/10.1038/ngeo1635.

Brodeur, R.D., Wilson, M.T., Ciannelli, L., Doyle, M., Napp, J.M., 2002. Interannual and regional variability in distribution and ecology of juvenile pollock and their prey in frontal structures of the Bering Sea. Deep Sea Res. II 49 (26), 6051–6067.

Byrne, R.H., Meckling, S., Feely, R.A., Liu, Z., 2010. Direct observations of basin-wide acidification of the North Pacific Ocean. Geophys. Res. Lett. 37, L02601, http://dx.doi.org/10.1029/2009GL040999.

Caldeira, K., Wickett, M.E., 2003. Anthropogenic carbon and ocean pH. Nature 425 (6956), 365, http://dx.doi.org/10.1038/425365a.

Coachman, L.K., 1986. Circulation, water masses, and fluxes on the southeastern Bering Sea shelf. Cont. Shelf Res. 5, 23–108, http://dx.doi.org/10.1016/0278-4343(86)90011-7.

Codispoti, L.A., Friederich, G.E., Inverson, R.L., Hood, D.W., 1982. Temporal changes in the inorganic carbon system of the southeastern Bering Sea during spring 1980. Nature 296, 242–245, http://dx.doi.org/10.1038/296242a0.

Cross, J.N., Mathis, J.T., Bates, N.R., 2012. Hydrographic controls on net community production and total organic carbon distributions in the eastern Bering Sea. Deep Sea Res. II 65–70, 98–109, http://dx.doi.org/10.1016/j.dsr2.2012.02.003.

Cross, J.N., Mathis, J.T., Bates, N.R., Byrne, R.H., 2013. Conservative and nonconservative variations of alkalinity in the southeastern Bering Sea. Mar. Chem. 154, 100–112.

Cross, J.N., Mathis, J.T., Lomas, M.W., Moran, S.B., Baumann, M.S., Shull, D.H., Mordy, C.W., Bates, N.R., Stabeno, P.J., 2014. Integrated assessment of the carbon budget in the Southeastern Bering Sea: from the atmosphere to the sediments. Deep-Sea Res. II 109, 112–124.

DeGrandpre, M.D., Hammar, T.T., Smith, S.P., Sayles, F.L., 1995. In situ measurements of seawater pCO_2. Limnol. Oceanogr. 40 (5), 969–975.

Devol, A.H., Christensen, J.P., 1993. Benthic fluxes and nitrogen cycling in sediments of the continental margin of the eastern North Pacific. J. Mar. Res. 51, 345–372, http://dx.doi.org/10.1357/0022240933223765.

Dickson, A.G., C. Goyet (Eds.), 1994, Handbook of Methods for the Analysis of Various Parameters of the Carbon Dioxide System in Seawater, Version 2.0, Rep. ORNL/CDIAC-74, U.S. Dep. Of Energy, Washington, DC.

Dickson, A.G., Millero, F.J., 1987. A comparison of the equilibrium constants for the dissociation of carbonic acid in seawater media. Deep-Sea Res. 34, 1733–1743.

Dickson, A.G., Sabine, C.L., Christian, J.R., 2007. Guide to best practices for ocean CO2 measurements, Sidney, British Columbia, North Pacific Marine Science Organization. PICES Special Publication p. 3.

Duffy-Anderson, J.T., Bailey, K.M., Ciannelli, L., 2002. Consequences of a super-abundance of larval walleye pollock Theragra chalcogramma in the Gulf of Alaska in 1981. Mar. Ecol. Prog. Ser. 243, 179–190.

Dwyer, D.A., Bailey, K.M., Livingston, P.A., 1987. Feeding habits and daily ration of walleye pollock (Theragra chalcogramma) in the eastern Bering Sea, with special reference to cannibalism. Can. J. Fish. Aquat. Sci. 44 (11), 1972–1984, http://dx.doi.org/10.1139/f87-242.

Evans, W., Mathis, J.T., Winsor, P., Whitledge, T., Statscewich, H., 2013. A regression modeling approach for studying carbonate saturation states on the northern Gulf of Alaska shelf. J. Geophys. Res.: Oceans 118, 1–14, http://dx.doi.org/10.1029/2012JC008246. (2013).

Fabry, V.J., Seibel, B.A., Feely, R.A., Orr, J.C., 2008. Impacts of ocean acidification on marine fauna and ecosystem processes. ICES J. Mar. Sci. 65 (3), 414–432.

Fabry, V.J., McClintock, J.B., Mathis, J.T., Grebmeier, J.M., 2009. Ocean acidification at high latitudes: the Bellwether. Oceanography 22 (4), 160–171.
Feely, R.A., Sabine, C.L., Hernandez-Ayon, J.M., Ianson, D., Hales, B., 2008. Evidence for upwelling of corrosive "acidified" water onto the Continental Shelf. Science 320 (5882), 1490–1492, http://dx.doi.org/10.1126/science.1155676.
Feely, R.A., Doney, S.C., Cooley, S.R., 2009. Ocean acidification: present conditions and future changes in a high-CO_2 world. Oceanography 22 (4), 36–47.
Feely, R.A., Alin, S.R., Newton, J., Sabine, C.L., Warner, M., Devol, A., Krembs, C., Maloy, C., 2010. The combined effects of ocean acidification, mixing, and respiration on pH and carbonate saturation in an urbanized estuary. Estuar. Coast. Shelf Sci. 88, 442–449, http://dx.doi.org/10.1016/j.ecss.2010.05.004.
Grebmeier, J.M., McRoy, C.P., 1989. Pelagic–benthic coupling on the shelf of the northern Bering and Chukchi seas. Part III. Benthic food supply and carbon cycling. Mar. Ecol. Prog. Ser. 53, 79–91, http://dx.doi.org/10.3354/meps053079.
Grebmeier, J.M., Cooper, L.W., Feder, H.M., Sirenko, B.I., 2006. Ecosystem dynamics of the Pacific-influenced Northern Bering and Chukchi Seas in the Amerasian Arctic. Prog. Oceanogr. 71, 331–361.
Gruber, N., Hauri, C., Lachkar, Z., Loher, D., Frölicher, T.L., Plattner, G.K., 2012. Rapid progression of ocean acidification in the California Current System. Science 337 (6091), 220–223, http://dx.doi.org/10.1126/science.1216773.
Hauri, C., Gruber, N., Vogt, M., Doney, S.C., Feely, R.A., Lachkar, Z., Leinweber, A., McDonnell, A.M.P., Munnich, M., Plattner, G.-K., 2012. Spatiotemporal variability and long-term trends of ocean acidification in the California Current System. Biogeosci. Discus. 9, 10371–10428, http://dx.doi.org/10.5194/bgd-9-10371-2012.
Hauri, C., Gruber, N., Plattner, G.-K., Alin, S., Feely, R.A., Hales, B., Wheeler, P.A., 2009. Ocean acidification in the California Current System. Oceanography 22 (4), 60–71, http://dx.doi.org/10.5670/oceanog.2009.97.
Hendriks, I.E., Duarte, C.M., Alvarez, M., 2010. Vulnerability of marine biodiversity to ocean acidification: a meta-analysis. Estuarine Coastal Shelf Sci. 86 (2), 157–164.
Ho, D.T., Wanninkhof, R., Schlosser, P., Ullman, D.S., Hebert, D., Sullivan, K.F., 2011. Toward a universal relationship between wind speed and gas exchange: gas transfer velocities measured with 3He/SF6 during the Southern Ocean Gas Exchange Experiment. J. Geophys. Res. 116, C00F04, http://dx.doi.org/10.1029/2010JC006854.
Hurst, T., Fernandez, E., Mathis, J.T., Miller, J.A., Stinson, C.M., Ahgeak, E.F., 2012. Resiliency of juvenile walleye pollock to projected levels of ocean acidification. Aquat. Biol. 17, 247–259, http://dx.doi.org/10.3354/ab00483.
Juranek, L.W., Feely, R.A., Peterson, W.T., Alin, S.R., Hales, B., Lee, K., Sabine, C.L., Peterson, J., 2009. A novel method for determination of aragonite saturation state on the continental shelf of central Oregon using multi-parameter relationships with hydrographic data. Geophys. Res. Lett. 36, L24601, http://dx.doi.org/10.1029/2009GL040778.
Kachel, N.B., Hunt, G., Salo, S.A., Schumacher, J.D., Stabeno, P.J., Whitledge, T.E., 2002. Characteristics of the Inner Front of the south-eastern Bering Sea. Deep-Sea Res. Part II 49, 5889–5909, http://dx.doi.org/10.1016/S0967-0645(02)00324-7.
Ladd, C., Stabeno, P.J., 2012. Stratification on the Eastern Bering Sea shelf revisited. Deep-Sea Res. II 65-70, 72–83.
Langdon, C., 2010. Determination of dissolved oxygen in seawater by Winkler titration using the amperometric technique. In: Sloyan, B.M., Sabine, C. (Eds.), GO-SHIP Repeat Hydrography Manual: A Collection of Expert Reports and guidelines. IOC/IOCCP, Paris.
Lewis, E.R., D.W.R. Wallace (1995), Basic Programs for the CO2 System in Seawater. Report BNL-61827. Brookhaven Natl. Lab., Upton, NY.
Lomas, M.W., Moran, S.B., Casey, J.R., Bell, D.W., Tiahlo, M., Whitefield, J., Kelly, R.P., Mathis, J.T., Cokelet, E.D., 2012. Spatial and seasonal variability of primary production on the Eastern Bering Sea Shelf. Deep-Sea Res. II 65-70, 126–140.
Long, W.C., Swiney, K.M., FOY, R.J., 2013a. Effects of ocean acidification on the embryos and larvae of red king crab, Paralithodes camtschaticus. Mar. Pollut. Bull. 69, 38–47.
Long, W.C., Swiney, K.M., Harris, C., Page, H.N., Foy, R.J., 2013b. Effects of ocean acidification on juvenile red king crab (Paralithodes camtschaticus) and Tanner crab (Chionoecetes bairdi) growth, condition, calcification, and survival. PLoS ONE 8 (4), e60959, http://dx.doi.org/10.1371/journal.pone.0060959.
Mathis, J.T., Cross, J.N., Bates, N.R., Lomas, M.L., Moran, S.B., Mordy, C.W., Stabeno, P., 2010. Seasonal distribution of dissolved inorganic carbon and net community production on the Bering Sea Shelf. Biogeosciences 7, 1769–1787, http://dx.doi.org/10.5194/bg-7-1769-2010.
Mathis, J.T., Cross, J.N., Bates, N.R., 2011a. Coupling primary production and terrestrial runoff to ocean acidification and carbonate min- eral suppression in the eastern Bering Sea. J. Geophys. Res. 116, C02030, http://dx.doi.org/10.1029/2010JC006453.
Mathis, J.T., Cross, J.N., Bates, N.R., 2011b. The role of ocean acidification in systemic carbonate mineral suppression in the Bering Sea. Geophys. Res. Lett. 38, L19602, http://dx.doi.org/10.1029/2011GL048884.
Mehrbach, C., Culberson, C.H., Hawley, J.E., Pytkowicz, R.M., 1973. Measurement of the apparent dissociation constants of carbonic acid in seawater at atmospheric pressure. Limnol. Oceanogr. 18, 897–907.
Moran, S.B., Lomas, M.L., Kelly, R.P., Iken, K., Gradinger, R., Mathis, J.T., Propokenko, M., 2012. Sea-ice control of lower trophic carbon partitioning in the eastern Bering Sea. Deep-Sea Res. II , http://dx.doi.org/10.1016/j.dsr2.2012.02.011.
Moss, J.H., Farley, E.V., Feldmann, A.M., Ianelli, J.N., 2009. Spatial distribution, energetic status, and food habits of eastern Bering Sea Age-0 walleye pollock. Trans. Am. Fish. Soc. 138 (3).
Napp, J.M., Kendall, A.W., Schumacher, P., 2001. A synthesis of biological and physical processes affecting the feeding environment of larval walleye pollock (Theragra chalcogramma) in the eastern Bering Sea. Fish. Oceanogr. 9 (2), 147–162, http://dx.doi.org/10.1046/j.1365-2419.2000.00129.x.
Niebauer, H.J., Alexander, V., Henrichs, S.M., 1995. A time-series study of the spring bloom at the Bering Sea ice edge. I: physical processes, chlorophyll, and nutrient chemistry. Cont. Shelf Res. 15, 1859–1878.
Ries, J.B., Cohen, A.L., McCorkle, D.C., 2009. Marine calcifiers exhibit mixed responses to CO2-induced ocean acidification. Geology 37 (12), 1131–1134, http://dx.doi.org/10.1130/G30210A.1.
Sigler, M.F., Stabeno, P.J., Eisner, L.B., Napp, J.M., Mueter, F.J., 2014. Spring and fall phytoplankton blooms in a productive subarctic ecosystem, the eastern Bering Sea, during 1995–2011, 109, 71–83.
Springer, A.M., McRoy, C.P., Flint, M.V., 1996. The Bering Sea green belt: shelf-edge processes and ecosystem production. Fish. Oceanogr. 5, 205–223, http://dx.doi.org/10.1111/j.1365-2419.1996.tb00118.x.
Stabeno, P.J., Napp, J., Mordy, C., Whitledge, T., 2010. Factors influencing physical structure and lower trophic levels of the eastern Bering Sea shelf in 2005: sea ice, tides and winds. Prog. Oceanogr. 85 (3–4), 180–196.
Stafford, K.M., Moore, S.E., Stebeno, P.J., Holliday, D.V., Napp, J.M., Mellinger, D.K., 2010. Biophysical ocean observations in the southeastern Bering Sea. Geophys. Res. Lett. 37, L02606, http://dx.doi.org/10.1029/2009GL040724.
Stabeno, P.J., Bond, N.A., Salo, S.A., 2007. On the recent warming of the South-eastern Bering Sea shelf. Deep-Sea Res. II 54, 2599–2618.
Stabeno, P.J., Kachel, N.B., Moore, S.E., Napp, J.M., Sigler, M., Yamaguchi, A., Zerbini, A.N., 2012. Comparison of warm and cold years on the southeastern Bering Sea shelf and some implications for the ecosystem. Deep-Sea Res. II 65–70, 31–45, http://dx.doi.org/10.1016/j.dsr2.2012.02.020.
Weiss, R.F., 1974. Carbon dioxide in water and seawater: the solubility of a non-ideal gas. Mar. Chem. 2, 203–215.
Zeebe, R., Wolf-Gladrow, D., 2001. CO2 in seawater: equilibrium, kinetics, isotopes. Else. Oceanogr. Ser. 65, 2001.

Deep-Sea Research II 109 (2014) 134–144

Contents lists available at ScienceDirect

Deep-Sea Research II

journal homepage: www.elsevier.com/locate/dsr2

Microzooplankton: Abundance, biomass and contribution to chlorophyll in the Eastern Bering Sea in summer

Diane K. Stoecker [a,*], Alison C. Weigel [a], Dean A. Stockwell [b], Michael W. Lomas [c,1]

[a] University of Maryland Center for Environmental Science, Horn Point Laboratory, P.O. Box 775, Cambridge, MD 21613, USA
[b] Institute of Marine Science, University of Alaska Fairbanks, P.O. Box 757220, Fairbanks, AK 99775, USA
[c] Bermuda Institute of Ocean Sciences, 17 Biological Station, St. George's, GEO1, Bermuda

ARTICLE INFO

Available online 12 September 2013

Keywords:
Microzooplankton
Ciliates
Dinoflagellates
Mixotrophy
Bering Sea

ABSTRACT

Summer microzooplankton abundance and biomass were determined for three years, 2008, 2009, and 2010, during a four-year cold period in the eastern Bering Sea. Average microzooplankton densities ranged from 4×10^3 to 25×10^3 cells l^{-1} in the mixed layer. Microzooplankton biomass was 21–25 μg C l^{-1} in the mixed layer on the middle shelf (South and North Middle Domains), which has relatively low chlorophyll during summer stratification. However, microzooplankton biomass was about 1/2 that in the less stratified waters near the shelf break, greenbelt, and in the bloom waters in the Pribilof Island Domain. Although phytoplankton biomass was higher in deep chlorophyll maxima (DCM) than in surface waters on the shelf, microzooplankton biomass was generally not elevated in the DCM. High ratios (>1) of microzooplankton biomass to phytoplankton biomass were observed at chlorophyll *a* concentrations <1 μg l^{-1}. At times, average microzooplankton biomass was higher than the calculated phytoplankton biomass in the mixed layer in coastal (Inner Domain) and middle shelf (South and North Middle Domain) waters. A confounding factor in comparing microzooplankton and phytoplankton biomass was the contribution of plastid-retaining, mixotrophic, ciliates to chlorophyll *a*. On average, mixotrophic ciliates comprised 66% of the ciliate biomass, and in the North Middle Domain, on some cruises were estimated to have contributed over 50% of the chlorophyll *a* in the mixed layer. The 2008–2010 data suggest that extent of stratification, presence of localized blooms, and domain differences all have major influences on coupling of microzooplankton to phytoplankton stocks in summer in the eastern Bering Sea.

1. Introduction

We investigated the role of microzooplankton in Eastern Bering Sea food webs (Stoecker et al., 2013) as part of the Bering Sea Project, an integrated ecosystem investigation of top-down and bottom-up regulation of production on this extensive subarctic shelf (Harvey and Sigler, in press). The Eastern Bering Sea supports productive commercial and subsistence fisheries as well as major marine mammal and bird populations (Hunt et al., 2008, 2011). It is also highly sensitive to inter-annual and decadal-scale climate variability, with differences between warm, cold and average years reflected in secondary productivity and fish, bird, and mammal populations, particularly on the southern shelf (Aydin and Mueter, 2007; Hunt et al., 2002, 2011). The spatial extent of winter sea ice and the timing of sea ice retreat have a large impact on the timing and characteristics of the spring bloom and the ecology of the Bering Sea. Winter–spring conditions set up the shelf for the summer, influencing summer phytoplankton and zooplankton populations (Stabeno et al., 2012b). In addition, summer weather, particularly storms and wind mixing, break down stratification (Ladd and Stabeno, 2012) resulting in large, but ephemeral blooms (Sambrotto et al., 1986) that result in enhanced net community production (Mordy et al., 2012).

The Eastern Bering Sea Shelf is divided into six regions by its hydrography and bathymetry; north and south coastal (<50 m depth, North and South Inner Domains), north and south middle shelf (50–100 m; North and South Middle Domains), and outer shelf (100–200 m depth; North and South Outer Domains) (Coachman, 1986; Hunt et al., 2002; Lomas et al., 2012) (Fig. 1). The transitional area between the northern and southern domains corresponds to ~60° N; the MN line lies within the transitional area (Fig. 1) (Stabeno et al., 2010; Stabeno et al., 2012a). Each domain varies in physical forcing, biology, and susceptibility to climate change (Stabeno et al., 2012a). In summer, the south

* Corresponding author. Tel.: +1 410 221 8407; fax: +1 410 221 8490.
E-mail addresses: stoecker@umces.edu (D.K. Stoecker), dastockwell@alaska.edu (D.A. Stockwell), mlomas@bigelow.org (M.W. Lomas).
[1] Current address: Bigelow Laboratory for Ocean Sciences, 60 Bigelow Drive, East Boothbay, ME 04544, USA.

0967-0645/$ - see front matter © 2013 Elsevier Ltd. All rights reserved.
http://dx.doi.org/10.1016/j.dsr2.2013.09.007

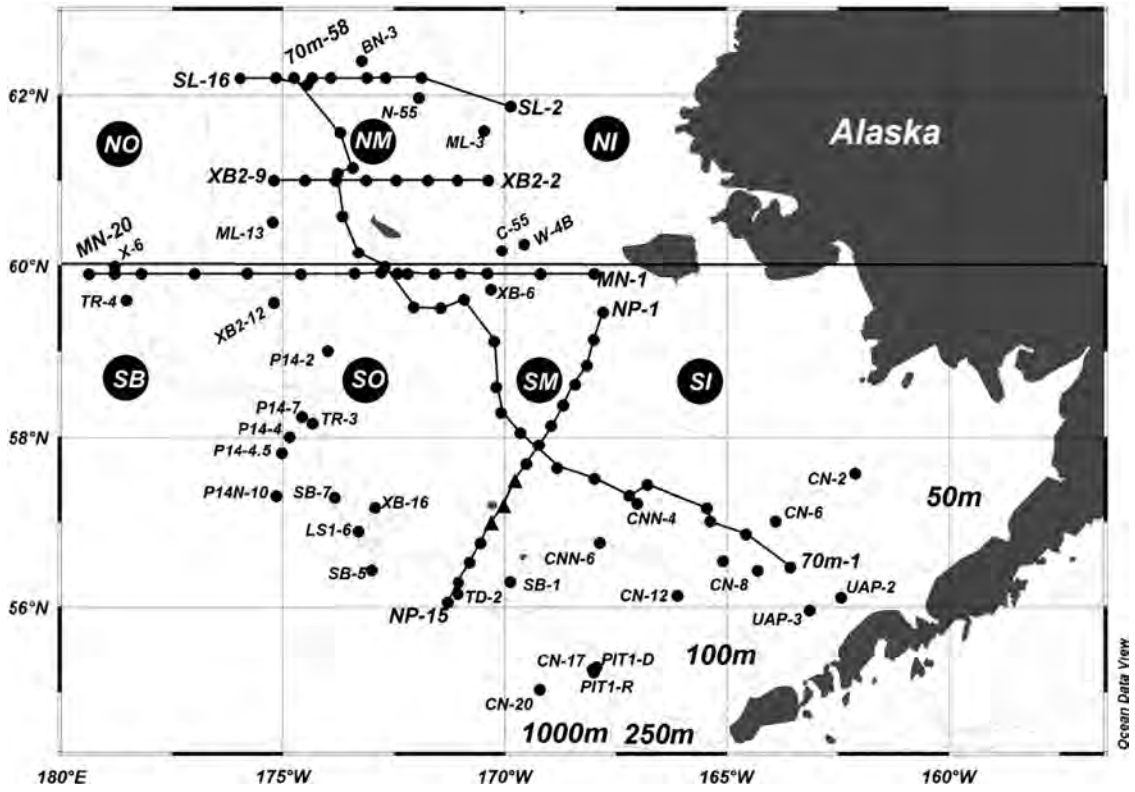

Fig. 1. The Eastern Bering Sea study region with the 50 m, 100 m, 250 m, and 1000 m isobaths indicated by gray lines and labeled. The solid line at 60° N denotes the North/South boundary. The solid circles with letters denote the major domains, North Outer (NO), North Middle (NM), North Inner (NI), South Outer (SO), South Middle (SM), and South Inner (SI) Domains and the Shelf Break (SB). Transect lines (70 m line, SL line, XB2 line, MN line and NP line) are indicated by solid lines and identified by the end member stations sampled. The three stations in the Pribilof Islands indicated by filled triangles, all other stations indicated by small filled circles. All stations were not sampled in all years (refer to Table 1).

middle shelf is a thermally stratified system with a wind mixed surface layer typically 20–30 m thick and a tidally mixed bottom layer. During summers 2008 and 2009 (cold years), net primary production (NPP) and chlorophyll values were highly variable, and most of the NPP was in the <5 μm fraction (Lomas et al. 2012). The middle shelf is separated from the inshore, shallow well-mixed coastal domain by the Inner Front, and from the offshore, outer domain by the Middle Transition Zone (Kachel et al., 2002; Stabeno et al. 2012a). In the southern inner or coastal domain, net primary production is very low in summer (Lomas et al., 2012). In the South Outer Domain, NPP is roughly similar to that in the Middle Domain (Lomas et al., 2012). The area around the Pribilof Islands on the southern shelf is a separate domain (Ciannelli et al., 2004). The Pribilof Domain is supplied with nutrient and plankton-rich water from the slope and outer shelf as well as being subject to tidal mixing; it can have new production and localized phytoplankton blooms in summer even when the rest of the south middle shelf is highly stratified (Hunt et al., 2008; Sambrotto et al., 2008). The Pribilof blooms are typically dominated by the >5 μm chlorophyll fraction. NPP was lower in the South Middle Domain than in the North Middle Domain in summer (Lomas et al., 2012).

The southern region is the most susceptible part of the Eastern Bering Sea to climate change due to inter-annual variation in the marginal ice zone (Stabeno et al., 2012a, 2012b). During 2007–2010 (cold years) the south middle shelf became well mixed after the retreat of sea ice, with thermal stratification starting in May (Stabeno et al., 2012b). The two-layer structure usually persists through October, however, the magnitude and extent of thermal stratification was not correlated with warm or cold years or spring sea ice extent on the southern shelf (Stabeno et al., 2012b). Wind mixing determines nutrient supply to the euphotic zone, and hence net community production (Mordy et al., 2012), during summer on the southern middle shelf.

On the northern shelf, the average amount of sea ice is greater and persists later in the year than in the south. Usually the North Middle Domain stratifies in summer due to combination of salinity and temperature (Stabeno et al., 2012a). Mixed layer water temperature in summer on the northern shelf is several degrees cooler than in the south. In contrast to the southern middle domain, subsurface phytoplankton blooms are common in summer on the northern middle shelf. The euphotic zone (~20–40 m deep) extends at least partially into the pycnocline (Stabeno et al., 2012a); phytoplankton growth may occur in the euphotic portions of the pycnocline. However, deep chlorophyll maxima resulting from sedimentation of surface blooms may also occur in the pycnocline and below.

Microzooplankton are an important link between primary production and higher trophic levels in polar and sub-polar as well as temperate and tropical waters (Levinsen and Nielsen, 2002; Calbet and Saiz, 2005; Campbell et al., 2009). In both warm and cold years and spring as well as summer, microzooplankton are major consumers of primary production in the Eastern Bering Sea (Liu et al., 2002; Olson and Strom, 2002; Strom and Fredrickson, 2008; Sherr et al., 2013; Stoecker et al., 2014). Microzooplankton are important prey for mesozooplankton, including large crustacean zooplankton such as euphausiids and copepods (e.g., *Calanus., Neocalanus,* and *Metridia* spp.) as well as for small crustacean zooplankton such as *Acartia*, *Pseudocalanus* and *Oithona* spp. (Gifford and Dagg, 1991; Levinsen and Nielsen, 2002; Campbell et al., 2009; Stoecker, 2013) and fish larvae (Fukami et al., 1999; Figueiredo et al., 2007; Montagnes et al., 2010). Crustacean zooplankton are food for larvae and juveniles of many important Bering Sea fish species including pollock

(Howell-Kübler et al., 1996; Coyle et al., 2008; Hunt et al., 2011). When chlorophyll is low and dominated by small phytoplankton, microzooplankton can be crucial to the survival and fecundity of mesozooplankton (Ohman and Runge, 1994). Microzooplankton are particularly important as a food for mesozooplankton after the spring bloom, during late spring and summer stratification (Ohman and Runge, 1994; Fileman et al., 2010).

Studies during both cold (1999) and warm (2004) years have shown that summer microzooplankton abundance and biomass in the Eastern Bering Sea shelf is relatively high and dominated by heterotrophic and mixotrophic dinoflagellates and ciliates. Most data are from the southern Bering shelf and the productive area around the Pribilof Islands (Olson and Strom, 2002; Strom and Fredrickson, 2008). However, relatively little information is available on variation in microzooplankton abundance and biomass across the shelf or on the shelf north of St. Matthew Island. No historical data were available on the association of microzooplankton with subsurface, high chlorophyll layers on the northern shelf.

We sampled microzooplankton in both the southern and northern shelf of the Eastern Bering Sea on approximately month long cruises in summers of 2008–2010. This was during a four year cold period with extensive sea ice cover in spring (Stabeno et al., 2012b). Our primary goal was to investigate summer microzooplankton abundance, biomass, and composition across domains. We were also interested in documenting the relative biomass of microzooplankton to phytoplankton in both the mixed layer and in the deep chlorophyll maxima because this ratio is an indicator of the potential importance of microzooplankton as food for mesozooplankton. The biomass of autotrophic and mixotrophic ciliates is often high in polar seas during summer (Putt, 1990; Simé-Ngando et al., 1992; Sorokin et al., 1996; Suzuki and Taniguchi, 1998; Levinsen and Nielsen, 1999; Montagnes et al., 2008). One of our goals was to determine if plastidic ciliates were important biomass components in the Eastern Bering Sea and to estimate their contribution to chlorophyll *a* in summer.

2. Materials and methods

2.1. Microzooplankton sampling and onboard observations

Samples for abundance and biomass estimates of microzooplankton (20–200 μm fraction) were collected on BEST/BSIERP summer cruises in 2008, 2009, and 2010 on the U.S.C.G. Healy, R/V Knorr and R/V T.G. Thompson, respectively. In 2008, the cruise was in July, but in 2009 and 2010 the cruise was earlier, from mid-June to mid-July (Table 1). Samples were collected from routine sampling stations along established transects including the cross shelf NP, MN and SL lines and south to north mid-shelf 70-m line (Fig. 1). In 2009 the XB2 transect was added to sample the greenbelt area. Mixed layer samples were routinely collected at a predetermined depth, usually 5 or 10 m. Microzooplankton samples were also collected during productivity casts from the depth of 55% of surface incident PAR irradiance that varied from 3–15 m depending upon the station (Lomas et al., 2012). In all cases this depth was within the surface mixed layer. Additional samples were obtained at stations with a pronounced deep chlorophyll *a* fluorescence maximum (DCM). The fluorescence maximum samples were from depths of 14 to 46 m. When multiple maxima were sampled, data are presented for the depth with the highest measured chlorophyll *a*.

Duplicate samples (250 ml) for microzooplankton were collected with 30 l Niskin bottles attached to a CTD and water samples were immediately preserved with 10% (final concentration) acid Lugol's solution (Guillard and Sieracki, 2005) in amber glass bottles on HY0803 in 2008 and with 5% (final concentration) acid Lugol's solution in 2009 (KN195-10) and 2010 (TN-250). Concentrations of acid Lugol's ranging from 0.6% to 20% have been used to fix and preserve microzooplankton (Stoecker et al., 1994; Gifford and Caron, 2000), with 5% used in investigations of Bering Sea microzooplankton by Olson and Strom (2002), Strom and Fredrickson (2008) and Sherr et al. (2013). In 2008, a 10 sample subset of samples was fixed with 2%, 5%, and 10% acid Lugol's solution. The mean ciliate abundance estimates were 6.7 ± 3.1, 6.0 ± 1.8 and 5.1 ± 3.0 cells ml^{-1} (mean $\pm$ standard deviation) with 2%, 5% and 10% acid Lugol's solution, respectively. The differences among treatments were not statistically significant (One Way ANOVA on square root transformed data, $p > 0.05$). The dinoflagellate abundance estimates were 5.2 ± 2.4, 5.9 ± 2.1 and 5.3 ± 2.90 cells ml^{-1} (mean $\pm$ standard deviation) with 2%, 5% and 10% acid Lugol's solution, respectively (One Way ANOVA, $p > 0.05$). Dinoflagellate average biomass estimates were 62.1 ± 41.2, 63.7 ± 32.9, 48.9 ± 29.0 (mean $\pm$ standard deviation) $\times 10^3$ μm^{-3} ml^{-1} with 2%, 5% and 10% acid Lugol's solution, respectively (One Way ANOVA, $p > 0.05$). Based on these data, we switched to 5% acid Lugol's in 2009 and 2010 since this concentration reduces cell shrinkage of ciliates compared to 10% (Stoecker et al., 1994) and matched the fixative concentration used on the spring cruises (Sherr et al., 2013). Lugol's fixed samples were stored in the dark until analysis at Horn Point Laboratory.

Onboard, we examined "fresh" samples from some stations, either live or fixed with 1% glutaraldehyde with transmitted light and/or epifluorescence microscopy in Utermöhl chambers on an inverted microscope. Our objective was to examine cells for the presence or absence of plastids and characterize the types of microzooplankton and microphytoplankton present. We determined which morphotypes of ciliates had plastids (i.e., were mixotrophs) and which were strictly heterotrophic.

Table 1
Number of microzooplankton samples by domain, cruise and layer (ML=mixed layer; DCM=chlorophyll max) on summer BEST/BSIERP cruises in Eastern Bering Sea in 2008 (HLY-08-03, July 3 to July 31), 2009 (KNORR 195-10, June 14 to July 13) and 2010 (TN-250, June 16 to July 14).

Domain	Layer	2008	2009	2010
South Outer	ML	6	8	6
South Middle	ML	10	13	15
	DCM	7	8	11
South Inner	ML	3	2	3
MN Transect	ML	6	13	9
North Middle	ML	8	15	9
	DCM	8	14	8
Pribilof Islands	ML	4	2	3
Shelf Break	ML	4	3	3

See Fig. 1 for station locations; not all stations sampled on all cruises.

2.2. Microzooplankton sample analysis

At Horn Point Laboratory we enumerated >20 μm protistan microzooplankton ($>\sim 15$ μm when fixed with acid Lugol's), using a Nikon Eclipse TE 2000-U inverted microscope, after settling 25 or 50 ml volumes overnight in Utermöhl chambers (Gifford and Caron, 2000). Our detection limit was ~ 40 cells l^{-1} with 25 ml settled samples and ~ 20 cells l^{-1} with 50 ml settled samples; 200–400 cells were enumerated per sample. A SPOT v 4.0 RT camera and SPOT diagnostic software were used to record images and to measure cells. Biovolumes were calculated from the measurements using appropriate geometric formulae. In accordance

with earlier microzooplankton studies in the Bering Sea (Olson and Strom, 2002; Strom and Fredrickson, 2008), all dinoflagellates within the designated size range were included in abundance and biomass estimates because most if not all photosynthetic dinoflagellates are also phagotrophic (Jeong et al., 2010).

The ciliates were placed in the following functional and taxonomic categories: (1) *Mesodinium rubrum (sym. Myrionecta rubra)*; this photoautotrophic ciliate consumes cryptophytes and other small prey. (2) Mixotrophic ciliates; these are non-loricate spirotrich ciliates (strombidiids) that graze on phytoplankton (usually nanophytoplankton), but have chlorophyll and are also photosynthetic. Only ciliates which we observed to have chlorophyll at sea and which we could recognize as the same morphospecies in the Lugol's fixed samples are included in this category. Thus, it is a minimum estimate of mixotrophic ciliates. (3) Non-loricate strictly heterotrophic spirotrich ciliates (this includes heterotrophic strombidiids and strobilidiids). This category may include a few mixotrophs that we were not able to recognize in the Lugol's fixed samples. The ciliates in this category are mostly grazers on phytoplankton. (4) Tintinnid ciliates. These were all heterotrophs. (5) Other=all other ciliates.

We used the "$C=0.19V$" conversion factor for ciliates fixed in 2% acid Lugol's solution from Putt and Stoecker (1989) for the samples fixed in 5% acid Lugol's solution. In a study of fixation methods, Stoecker et al. (1994) observed that the biovolume of ciliates fixed with 2% and 5% acid Lugol's was not statistically different; thus the Putt and Stoecker conversion can be applied. This conversion factor is commonly used for ciliates in 5% acid Lugol's (for example, in the studies of Bering Sea microzooplankton by Olson and Strom (2002), Strom and Fredrickson (2008), Sherr et al. (2013)). However, the biovolume of ciliates fixed in 10% are usually significantly lower than of cells fixed in 2% or 5% acid Lugol's solution (Stoecker et al., 1994). To correct for shrinkage in the 2008 samples fixed with 10% acid Lugol's solution we used a conversion factor of "$C=0.251V$"; this factor is based on Putt and Stoecker (1989) but corrected based on a comparison of cell shrinkage of preserved ciliates with 2% and 10% acid Lugol's solution (Stoecker et al., 1994). The tintinnids in our samples had transparent loricae, so we were able to observe and estimate their cell dimensions. We applied the same corrections factors for these cells as for non-loricate ciliates. We did not apply conversion factors based on lorica volume because this was unnecessary and estimates based on lorica volume often over-estimate ciliate biomass (Gilron and Lynn, 1989).

Dinoflagellates were categorized as thecate or non-thecate. Most of the dinoflagellates were non-thecate and we were not able to separate many of the smaller non-thecate dinoflagellates by morphotype in the Lugol's fixed samples and thus could not classify them as plastidic or non-plastidic. Therefore, we aggregated all dinoflagellates in one group. The dinoflagellates did not shrink differently in 5% and 10% acid Lugol's (refer to Section 2.1), so we used the dinoflagellate specific algorithm of Menden-Deuer and Lessard (2000) to estimate the biomass of morphotypes in both the 5% and 10% acid Lugol's samples. This procedure is the same as in other recent Bering Sea investigations of microzooplankton (Olson and Strom, 2002; Strom and Fredrickson, 2008; Sherr et al., 2013).

We also enumerated and sized other microzooplankton sized protist cells that could not be readily classified taxonomically or which were rare. These included unidentified heterotrophic microflagellates, testate amoebae, and the mixotrophic silicoflagellates. We did not include the colonial mixotrophic flagellate, *Dinobryon* spp., in our estimates because it did not preserve well in the Lugol's fixed samples. Biomasses of non-ciliate and non-dinoflagellate microzooplankton were estimated from biovolume using the general protist algorithm of Menden-Deuer and Lessard (2000). Metazoan microzooplankton (crustacea and rotifers) were rare compared to protists and are not included in our abundance and biomass estimates. Nanozooplankton were not included in our estimates. Estimation of microzooplankton abundance and biomass based on fixed samples can lead to an underestimation of both parameters compared to live counts with a FlowCAM (Jakobsen and Carstensen, 2011); thus our estimates should be considered minimum estimates of ciliate and dinoflagellate abundance and biomass.

2.3. Chlorophyll *a* and determination of phytoplankton biomass

For samples collected in conjunction with productivity casts, chlorophyll data available from the primary productivity study were used (Lomas et al., 2012). For other stations, we used chlorophyll data collected as part of core hydrographic measurements. At stations for which our sampling depth did not match the sampling depths for chlorophyll, we interpolated between depths when possible. We estimated phytoplankton biomass from chlorophyll *a* using an empirically determined Carbon to Chlorophyll *a* ratio of 50 (Lomas et al., 2012). Only data for stations and depths for which both microzooplankton and chlorophyll data were available were used in comparing microzooplankton and phytoplankton biomasses.

2.4. Estimation of mixotrophic ciliate contribution to chlorophyll *a*

We estimated the contribution of mixotrophic strombidiid ciliates to chlorophyll *a* l^{-1} by multiplying their biovolume l^{-1} by an average biovolume:Chl *a* factor specific to mixotrophic strombidiids. The conversion factor, 3.12 ($\pm$2.63) fg chl. *a* $(\mu m^3)^{-1}$, is the mean ($\pm$ standard deviation) chlorophyll density of five mixotrophic strombidiid species, *Laboea strobila* (Stoecker et al. 1988), *Strombidium capitatum*, *Strombidium conicum*, *Strombidium acutum*, and *Strombidium chlorophilum* (Stoecker et al. 1988/89; Stoecker et al., 2009). Assuming a *C*: volume conversion of $C=0.19V$ (Putt and Stoecker, 1989), mixotrophic ciliates have a *C*: Chl *a* ratio of ~62. Mixotrophic *Strombidium* spp. and *L. strobila* were the dominant plastid-containing ciliates in our samples as well as the taxa used to derive the conversion factors. We did not include *M. rubrum* in our estimates of ciliate contribution to chlorophyll because, compared to the mixotrophic strombidiids, this ciliate's contribution to biomass was very low.

2.5. Data analyses and statistics

We group stations by physical domain (Fig. 1) (Hunt et al., 2008; Lomas et al., 2012; Stabeno et al., 2012a) with the number of stations sampled in each domain each year (*N*) given in Table 1. Data for the MN line, a transitional area between the northern and southern shelves of the Eastern Bering Sea, do not belong in the other domains (Stabeno et al., 2012a) and are separate. Data are presented only for domains for which microzooplankton data were available for 2 or more stations in each year. Data are not available for all stations in all years and the distribution of data among domains varied from year to year. For example, the representation of Middle and Inner Shelf Domains was higher in 2010 than 2008 or 2009 (Table 1). Over-all yearly averages of abundance and biomass are influenced by station distribution. All statistical tests were run using Sigmaplot version 9.0. Two way Analysis of Variance (ANOVA) was used to test for differences in the microzooplankton abundance or biomass among domains by year. We applied standard transformations (log 10, square root or arcsin) when data did not meet assumptions for ANOVA. In cases in which the transformed data still did not meet the assumptions, one way ANOVAs were conducted on data for each domain

separately or a one way ANOVA on ranks was run using the combined data. Pair-wise multiple comparisons were made using the Holm–Sidak method. We used the Pearson Product Moment Correlation to examine association between microzooplankton abundance or biomass and chlorophyll *a*.

Data are archived at http://beringsea.eol.ucar.edu.

3. Results

3.1. Abundance and composition

During summers 2008–2010 the abundance of protistan microzooplankton was high in the Eastern Bering Sea (Table 2). Protistan microzooplankton occurred at average densities of 4×10^3 to 25×10^3 cells l^{-1} in the mixed layer on the shelf. Year and the year × domain interaction were significant sources of variation in microzooplankton abundance (Table 2). On the north middle shelf and along the MN transect, the mixed layer MZ abundance was higher in 2010 than in 2009 and higher in 2009 than in 2008 ($p<0.05$). On the south outer shelf, abundances were also higher in 2010 than in 2008 ($p<0.05$).

Ciliates and heterotrophic and mixotrophic dinoflagellates numerically dominated the microzooplankton, with other taxa contributing $<5\%$ to this assemblage. Ciliates ranged in average abundance in the mixed layer samples from 1.4×10^3 to 13.0×10^3 cells l^{-1} (Fig. 2A). Ciliate abundances were greater in 2010 than 2008 or 2009 ($p<0.05$) with the year × domain interaction significant. Abundances of dinoflagellates were greater in 2010 than 2008 and in 2009 than 2008 ($p<0.05$) with the year × domain interaction significant. In the South Outer Domain, South Inner Domain and along the MN transect, ciliates were more abundant in 2010 than 2008 or 2009 ($p<0.05$). In the North Middle Domain they were more abundant in 2009 and 2010 than in 2008 ($p<0.05$). Across years, domain was not a significant source of variation for abundance of ciliates ($p=0.416$) or dinoflagellates ($p=0.081$). Ciliates accounted for 30–53% of the microzooplankton in surface waters.

Over 95% of the ciliates were non-loricate spirotrich ciliates (mostly strombidiids and strobilidiids). The most common ciliates were mixotrophic strombidiids (*Strombidium* spp. and *L. strobilia*) with algal plastids. Mixotrophic ciliates were particularly prevalent in surface waters on the shelf where they numerically contributed 68–75% of the ciliate microzooplankton. The average abundance of mixotrophic ciliates was 0.4×10^3 to 7.7×10^3 cells l^{-1} (Fig. 2C). Mixotrophic ciliates were more abundant in 2010 than 2008 and more abundant in 2009 than 2008 with domain × year interaction

Table 2
Summer mixed layer microzooplankton abundance in the eastern Bering Sea (cells $\times10^3$ l^{-1}). Mean ± standard deviation.

Domain	2008	2009	2010
South Outer	5.23 ± 2.96	13.21 ± 7.99	24.85 ± 8.52
South Middle	12.57 ± 10.46	12.33 ± 3.71	16.50 ± 6.28
South Inner	6.82 ± 3.79	7.68 ± 2.57	24.58 ± 16.56
North Middle	3.96 ± 2.75	15.58 ± 5.32	24.40 ± 8.85
MN Transect	4.10 ± 2.68	11.35 ± 5.82	19.05 ± 8.07
Pribilofs	17.15 ± 5.92	9.10 ± 5.40	17.70 ± 6.96
Shelf Break	6.17 ± 3.77	8.44 ± 3.26	12.08 ± 6.17
2-WAY ANOVA			
Source of variation		df	*p*
Domain		6	0.230
Year		2	< 0.001
Interaction		12	0.001
Total		144	

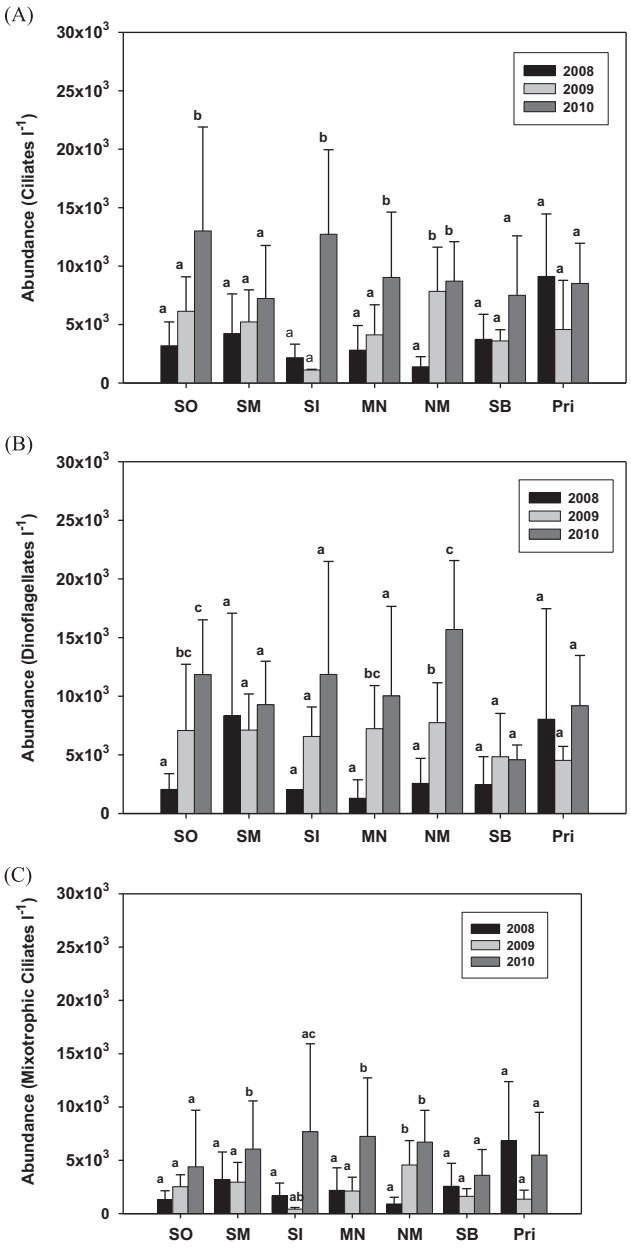

Fig. 2. Total ciliate abundance (A), heterotrophic/mixotrophic dinoflagellates abundance (B) and abundance of mixotrophic ciliates (C) in the mixed layer samples by domain/transect (SO = South Outer, SM = South Middle, SI = South Inner, MN = MN transect, NM = North Middle, SB = Shelf Break, Pri = Pribilof Islands) and year. Within a domain, different letters indicate significant differences among years ($p<0.05$). 2-Way ANOVA on square root (A and C) and log 10 transformed data (B); (df = 144).

significant ($p<0.05$). Similar to the total ciliates, mixotrophic ciliates were more abundant in 2009 and 2010 than in 2008 in the North Middle Domain (Fig. 2C). In the South Inner Domain mixotrophic ciliates were more abundant in 2010 than 2008 or 2009. Across years, domain was not a significant source of variation for abundance of mixotrophic ciliates ($p=0.326$). The primarily photosynthetic ciliate, *M. rubrum*, and tintinnid ciliates each made relatively minor (1–6%) numerical contributions to the ciliate assemblage.

Heterotrophic and mixotrophic dinoflagellates were co-dominant with the ciliates and ranged in abundance from 1.3×10^3 to 15.7×10^3 cells l^{-1} (Fig. 2B). In the South Outer Domain, dinoflagellates were more abundant in surface waters in 2009 and 2010 than in 2008 and along the MN transect and in the North Middle Domain

they tended to be more abundant in 2010 than in 2009 and 2008 ($p < 0.05$). Heterotrophic and mixotrophic dinoflagellates contributed an average of 45–67% of the microzooplankton in the mixed layer. The dinoflagellates were dominated by non-thecate heterotrophic dinoflagellates, with *Gyrodinium* and *Gyrodinium*-like species common. Thecate dinoflagellates such as the heterotrophic *Protoperidinium* spp. were rare.

3.2. Biomass and correlations with chlorophyll a

Average microzooplankton biomass in the mixed layer was 12–14 μg C l^{-1} in the South Outer Domain, at the shelf break station and at the Pribilof Island stations. Average microzooplankton biomass was 21–25 μg C l^{-1} on the shelf (Middle Domains, South Inner Domain) (Fig. 3). Biomass along the MN transect, which crossed from the inner to the middle and outer shelf between the south and north, and thus contained a mixture of domains, averaged 16 μg C l^{-1}. In the South Outer Domain, microzooplankton biomass was significantly higher in 2010 than 2008. Average microzooplankton biomass was similar for the three summer cruises for the South Middle Domain, MN transect, and Shelf Break. In the South Outer Domain, microzooplankton biomass was significantly higher in 2010 than 2008 (Fig. 3).

Microzooplankton biomass in the mixed layer was not correlated with chlorophyll *a* concentration (Pearson Product Moment Correlation, $N=132$, $p > 0.05$). High ratios (>1) of microzooplankton biomass to calculated phytoplankton biomass were observed at chlorophyll *a* concentrations of <1 μg Chl l^{-1} with ratios >2 observed occasionally observed at chlorophyll concentrations of <0.5 μg Chl l^{-1} (Fig. 4). Domain had a significant effect on the ratio of microzooplankton to phytoplankton biomass in the mixed layer during summer (Fig. 5). The ratio in the Middle Domains and along the MN transect was greater than in the South Outer Domain and the ratio in North Middle Domain was greater than at the Shelf Break (2-Way ANOVA). In the South Inner and North Middle Domains in summer 2008, average microzooplankton biomass in the mixed layer was greater than estimated phytoplankton biomass (Fig. 5). In the North and South Middle Domains and along the MN transect in summer 2010, microzooplankton biomass was greater than phytoplankton biomass in the mixed layer (Fig. 5). In summer 2009, compared to summer 2008 or 2010, the ratio of microzooplankton to phytoplankton biomass was low in North Middle Domain. In general, ratios were highest on the inner and middle shelf and lowest on the outer shelf and Shelf Break (Fig. 5). Overall,

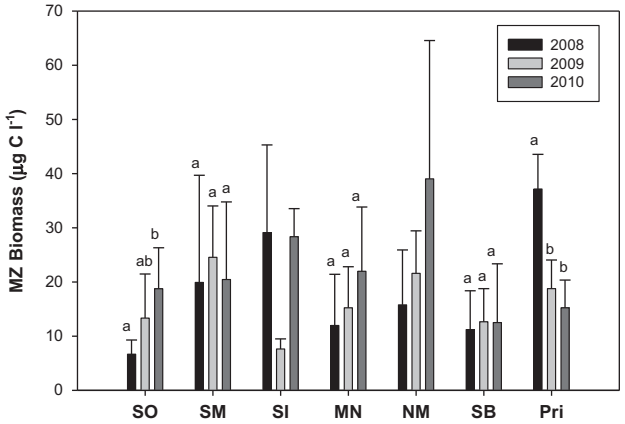

Fig. 3. Biomass of microzooplankton in the mixed layer samples by domain/transect. Regions and letters as in Fig. 2. 1-way ANOVAs tested the effect of year for each domain except SI and NM, for which the data did not meet assumptions for ANOVA.

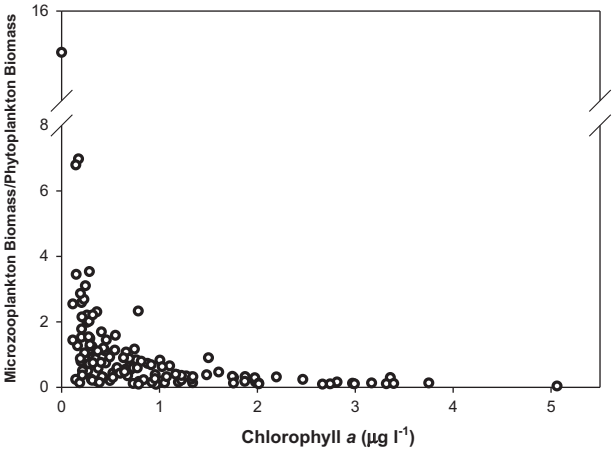

Fig. 4. Ratio of estimated microzooplankton biomass to phytoplankton biomass versus Chlorophyll *a* (Chl *a*) in mixed layer, Eastern Bering Sea summers 2008, 2009 and 2010. Data are from all samples for which there were both microzooplankton data and estimates of chlorophyll *a* ($N=132$). Log 10 (microzooplankton biomass/phytoplankton biomass) $= -0.477 - (0.871$ log 10 (chlorophyll *a*)); $p < 0.001$.

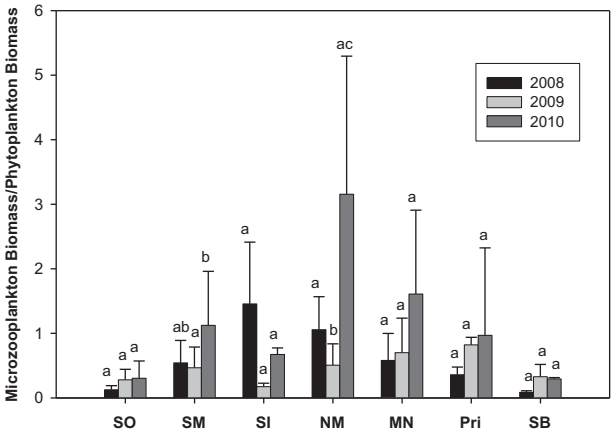

Fig.5. Ratio of estimated microzooplankton biomass to phytoplankton biomass in the mixed layer samples by domain/transect. Regions and letters as in Fig. 2.

the ratio of microzooplankton biomass to phytoplankton biomass was greater in 2010 than in 2008 or 2009 (Fig. 5).

The relative contribution of ciliates and dinoflagellates to microzooplankton biomass was roughly similar to their numerical contribution. Heterotrophic and mixotrophic dinoflagellates averaged 64% and ciliates 35% of microzooplankton biomass. Non-thecate heterotrophic dinoflagellates contributed almost all of the biomass in the dinoflagellate fraction. Among the ciliates, non-loricate choreotrich ciliates contributed 88% of the ciliate biomass and were dominated by mixotrophic species, contributing ~65% of the ciliate biomass. Other protistan taxa contributed $<5\%$ of the microzooplankton biomass at all stations.

3.3. Microzooplankton in the deep chlorophyll maxima (DCM)

On the middle shelf, there was often a pronounced deep chlorophyll maximum layer (DCM). POC: Chl *a* ratios are relatively constant with depth during the summer on the Eastern Bering Sea Shelf (Table 3 in Lomas et al., 2012); this indicates that the DCM corresponds to a maximum in phytoplankton biomass. In the South Middle Domain a DCM was observed at 41% of the stations and occurred at average depth of 24–26 m; in the North Middle Domain, a pronounced DCM was observed at 70% of the stations sampled and occurred at average depths of 30–34 m. The DCMs

Table 3
Microzooplankton biomass and composition in warm and cold years[a] and in years with high and low[b] summer stratification index in the Eastern Bering Sea.

Year	Temperature classification	Season	Summer stratification index	Biomass ($\mu g\ C\ l^{-1}$)	Composition	Ref.
1992	No data	Spring	No data	1–10 (Slope waters)	Dinoflagellates 48–54% of integrated biomass; remainder mostly ciliates	Howell-Kübler et al. (1996)
1999	Cold	Summer (*Emiliania huxleyi* bloom year)	Low	57 (18–164)	Dinoflagellates ~50%, ciliates ~50% of biomass	Olson and Strom (2002)
2004	Warm	Summer	High	38 (11–118) < 15 (M2, South Middle domain); Higher values in green belt, slope and Pribilof Domain	Heterotrophic dinoflagellates ~70% of biomass (included dinoflagellates < 20 μm); remainder mostly ciliates	Strom and Fredrickson (2008)
2008–2010	Cold	Spring (sea ice conditions)	Not applicable	11 ± 17 (non-bloom conditions) 23 ± 237 (bloom conditions)	Heterotrophic dinoflagellates 65–75% of biomass; remainder mostly ciliates	Sherr et al. 2013
2008–2010	Cold	Summer	Average	12–14 (outer and Pribilof Island domain and shelf break) 21–25 (middle and inner domains)	Heterotrophic and mixotrophic dinoflagellates 64% biomass; remainder mostly ciliates	This study

[a] Warm and cold years as defined by depth averaged water temperature (Stabeno et al., 2012a).
[b] SI=Stratification index at station M2 (middle south domain) in August. SI is compared to average values ± 1 SD in August (Ladd and Stabeno, 2012).

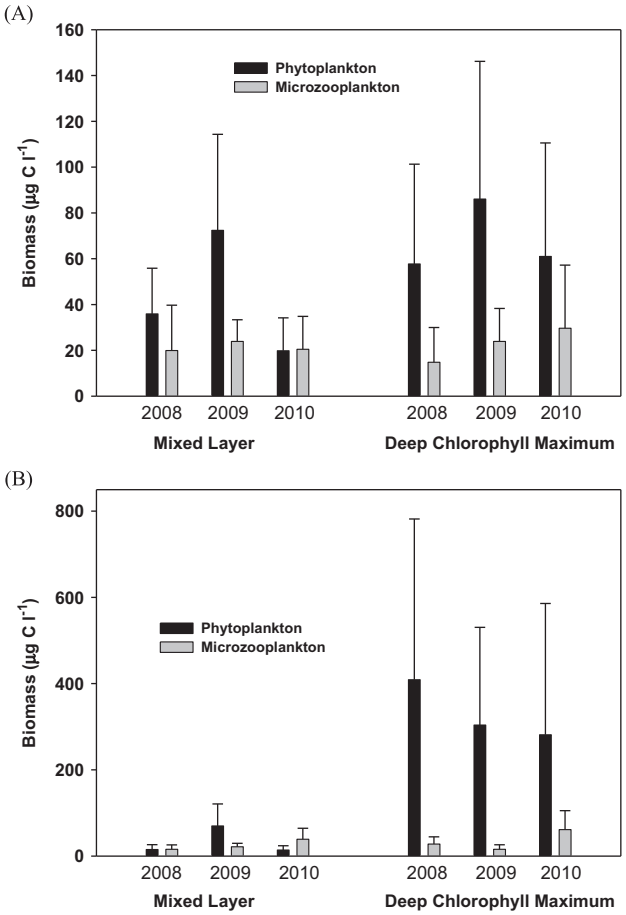

Fig. 6. Comparison of estimated biomass of microzooplankton and phytoplankton in the mixed layer and in the deep chlorophyll maximum (DCM) in (A) South Middle Domain, and (B) North Middle Domain. Note difference in *y*-axes between A and B. Mean ± Standard deviation.

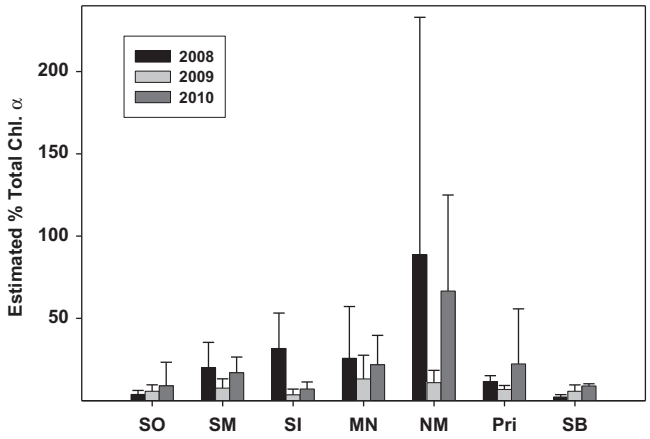

Fig. 7. Estimated contribution of mixotrophic ciliates to chlorophyll *a* in the mixed layer samples by domain/transect. Regions and letters as in Fig. 2.

were usually located at or below the base of the thermocline and were often rich in chain-forming diatoms. Although microphytoplankton were elevated in abundance in the DCM, microzooplankton were not (Fig. 6). There were no significant differences in microzooplankton biomass between the mixed layer and the DCM in the South or North Middle Domains (2-Way ANOVAs of year and layer; $p > 0.05$). As a result, the ratio of microzooplankton to phytoplankton biomass in the DCM was lower than the ratio in the corresponding mixed layer. In the South Middle Domain, the microzooplankton biomass ranged from an average of 33–103% in the mixed layer and 25–49% of phytoplankton biomass in the DCM depending on year (Fig. 6A). In the North Middle Domain, the microzooplankton biomass ranged from an average of 31–281% in the mixed layer and 5–2% in the DCM of phytoplankton biomass depending on year (Fig. 6B).

3.4. Estimated contribution of ciliates to chlorophyll a.

The estimated ciliate chlorophyll $a\ l^{-1}$ in the mixed layer was 0.09 (SD, 0.094), the median 0.07, and the range 0.00–0.49 (Fig. 7). Estimated ciliate chlorophyll was not correlated with total chlorophyll (Pearson Product Moment Correlation, $N=135$; $p > 0.05$). Estimated ciliate contribution to total chlorophyll was highly variable across years and domains (Fig. 7). In the North Middle Domain, the contribution was sometimes over 50%, with the estimated contribution greater in 2008 and 2010 than in 2009 when it was ~11%. In 2010, the contribution of ciliates to chlorophyll in the North Middle Domain was significantly higher

than in the South Middle Domain or South Outer Domain, all other comparisons were not statistically significant ($p > 0.05$).

4. Discussion

4.1. Confounding factors

Several factors confound the comparison of microzooplankton among seasons and years (Table 3). Timing of cruises is undoubtedly important. The Olson and Strom (2002) and Strom and Fredrickson (2008) data were from cruises in late July through August, about a month later than our cruises. Domains in the Eastern Bering Sea differ in their physics and biology as well as the timing of events (Hunt et al., 2008; Stabeno et al., 2012a; Eisner et al., 2014). The mix of stations sampled varied among studies and years, with some domains being better represented in some studies and years than others. For example, in 1999 and 2004, sampling was focused around the Pribilof Domain and the southern shelf (Olson and Strom, 2002; Strom and Fredrickson, 2008) whereas our investigation included the northern domains (Fig. 1). Even within our investigation, the cruise track and distribution of stations among domains varied from year to year (Table 1). The spring cruises focused on the marginal ice zone, with the distribution of stations depending on year-to-year variation in ice conditions (Sherr et al., 2013). In addition, although the methods were quite similar in all the studies (Table 3), there were differences in sampling schemes, fixation and counting procedures that may have influenced abundance and biomass estimates.

All three of our summer cruises were within an extended cold period with extensive sea ice in winter and spring (Stabeno et al., 2012b). However, there were year-to-year differences in the summer distribution and biomass of microzooplankton among our cruises. In 2009, the average ratio of microzooplankton to phytoplankton biomass in the mixed layer was low, particularly in the North Middle Domain. The contribution of mixotrophic ciliates to biomass was also relatively low in 2009. The average temperature for our mixed layer samples in the North Middle Domain was colder ($3.7 \pm 0.76^\circ$ C) in summer 2009 than in summer 2008 or ($6.3 \pm 0.51^\circ$ C) or 2010 ($5.9 \pm 0.22^\circ$ C). Although 2009 is classified as an average year in terms of the August stratification index, stratification set-up was unusually late (4 June) and breakdown early at M2 (station on south middle shelf) compared to most other years (Ladd and Stabeno, 2012). It appears that the typical summer microzooplankton assemblage, dominated by mixotrophic ciliates and heterotrophic dinoflagellates adapted to low chlorophyll, stratified waters, was not well developed by the time of our cruise in 2009 although this cruise had similar calendar dates to 2010.

Particularly in 2009 we noted small blooms of gelatinous colonial phytoplankton, *Phaeocystis pouchettii* and *Chaetoceros socialis,* on parts of the middle and outer shelf. These colonial phytoplankton are often poor food for microzooplankton (Nejstgaard et al., 2007). The presence of these bloom species may partially explain the relatively low ratio of microzooplankton to phytoplankton biomass in summer 2009. Strom and Fredrickson (2008) also noted that few large ciliates and dinoflagellates were present at high chlorophyll "green belt" stations. Localized mixing events and storms can lead to episodic blooms and relative low ratios of microzooplankton grazing to phytoplankton growth on the shelf (Stoecker et al., 2014).

4.2. Comparison between spring and summer

During spring sea ice conditions, microzooplankton biomass was more variable than during summer, particularly at bloom stations, however, average microzooplankton biomass during spring and summer were similar (Table 3). The ratio of microzooplankton to phytoplankton is higher in summer than in spring (Sherr et al., 2013). In spring, microzooplankton biomass was positively related to chlorophyll *a* (Sherr et al., 2013), but in summer we found no such relationship. In early spring, microzooplankton do not increase in abundance until phytoplankton populations are high enough to support their growth (Sherr and Sherr, 2009; Sherr et al., 2013). Although integrated rates of Net Primary Production (NPP) are lower in summer than in spring, estimated growth rates of phytoplankton are about twice as high in summer (Lomas et al., 2012; Moran et al., 2012); phytoplankton turn-over rapidly in summer and thus can support relatively high populations of microzooplankton for the observed chlorophyll *a* standing stock. Another factor that leads to persistence of high biomass of microzooplankton relative to phytoplankton after blooms is acquired phototrophy in mixotrophic ciliates (Dolan and Perez, 2000; Stoecker et al., 2009).

4.3. Comparisons among Domains

Summer microzooplankton abundance and biomass were surprisingly high in the low chlorophyll water found in the mixed layer over the middle shelf, with average estimates of microzooplankton biomass greater than in higher chlorophyll waters in the Pribilof Domain and at frontal and shelf break stations. In the North Middle Domain there was usually a well-developed DCM, but the biomass of microzooplankton was not usually elevated in the DCM relative to the mixed layer.

Both top down and bottom up factors may be responsible for the high biomass of microzooplankton in these relatively low chlorophyll waters. Top down control of microzooplankton may be low in summer in the mixed layer on the middle shelf, but data on copepod grazing on microzooplankton during the summer are lacking. In polar waters, copepod grazing can have a strong top-down impact on microzooplankton populations (Levinsen and Nielsen, 2002; Campbell et al., 2009).

Secondly, although phytoplankton biomass was higher at "bloom" stations in the Pribilof Domain and in the green belt and frontal areas, the phytoplankton may not have been as suitable a food for microzooplankton as the mixed populations of phytoflagellates and small diatoms on the middle shelf. Particularly in 2009, blooms of the colonial form of *P. pouchettii* were present at the high chlorophyll stations, including some Shelf Break, Pribiliof Island, South Outer, and North Middle Domain stations. The food value of *P. pouchettii*, particularly the colonies, is a subject of debate (reviewed in Nejstgaard et al., 2007). Although *P. pouchettii* is consumed by some microzooplankton, it may, in general, be a poor food for microzooplankton (Calbet et al., 2011 and references cited therein). Most microzooplankton may not be able to consume large colonies (Nejstgaard et al., 2007; Calbet et al., 2011), which dominated at some bloom stations. At other bloom stations, we observed *C. socialis*, a colonial gelatinous diatom that also may not be readily ingested by most microzooplankton.

Although phytoplankton were more abundant in DCMs than in the mixed layer above, microzooplankton usually were not more abundant in the DCM. In the North Middle Domain, sinking blooms of the centric diatoms *C. socialis*, *Thalassiosira nordenskioeldii* and *Porosira glacialis* were observed in 2009 (Goes et al., 2014). Similar sinking blooms were observed in this domain in 2010 and 2011. In Arctic waters, if a DCM is present, crustacean zooplankton are often concentrated in or just below the DCM (Saiz et al. 2013); this may result in high rates of predation on microzooplankton in the DCM. Many of the observed DCMs contained sinking microphytoplankton, including sea ice diatoms left-over from the spring and *Chaetoceros* and *Thalassiosira* chains that appeared to be in poor shape. Sinking blooms in Arctic waters

may be poor quality foods partially due to their low PUFA content (Mayzaud et al. 2013). Microzooplankton populations were not elevated in the DCM compared to the mixed layer, presumably due to top down control by crustacean zooplankton and/or low microzooplankton growth rates due to poor food quality and/or lower temperatures in the DCM than in the mixed layer (Campbell et al., 2009; Stabeno et al., 2012a; Rose et al., 2013).

4.4. Comparison between warm and cold years

The average biomass and composition of microzooplankton we found were within the ranges reported previously for microzooplankton in surface waters of the Eastern Bering Sea (Table 3). The average biomass of microzooplankton we observed appears to be somewhat lower than observed by Strom and Fredrickson (2008) during a warm year with a high stratification index (2004), however, differences in sampling locations confound this broad comparison by cruise averages. A higher proportion of their stations were in slope waters, the green belt or Pribilof Domain than in our study in which more sampling was on the middle shelf. If comparisons are by domain, the interpretation is different. In summer 2004, at the Middle South Domain station (M2), microzooplankton biomass was consistently $<15\ \mu g\ C\ l^{-1}$ (Strom and Fredrickson, 2008); this value is lower than the 21–25 $\mu g\ C\ l^{-1}$ that we observed in the Middle and Inner Domains during 2008–2010 (Table 3). In the summer of 1999, a cold year with low stratification, microzooplankton biomass estimates were perhaps slightly higher than for summer 2004, however the biomass ranges overlap (Table 3). There is no good evidence that microzooplankton biomass is higher in summers of "warm" than "cold" years. Although for the one warm year for which there are data on microzooplankton, summer stratification was also high (Table 3), over-all the strength of summer stratification is not correlated with "warm" or "cold" years as defined by depth averaged water temperature (Ladd and Stabeno, 2012). Domain, stratification, and timing of cruises in relationship to mixing events may have a greater effect on observed microzooplankton biomass and coupling to phytoplankton than temperature.

4.5. Contributions of mixotrophic ciliates to chlorophyll a

One of the surprising results of our cruises is the high abundance and biomass of mixotrophic strombidiid ciliates (*L. strobilia, Strombidium* spp.) and their estimated contribution to total chlorophyll. The primarily autotrophic ciliate, *M. rubrum* (*M. rubra*) was also present, but not abundant. On average, mixotrophic ciliates were 62% of ciliate abundance and 66% of estimated ciliate biomass in the mixed layer. Sorokin et al. (1996) estimated that in late spring-early summer, 30–40% of the ciliates on the shelf in the Western Bering Sea were mixotrophs; Booth et al. (1993) estimated that in the Western Sub-Arctic, 30–50% of the ciliates were mixotrophs. In the Subarctic Atlantic (Iceland, Greenland and Barents Seas), Putt (1990) observed that 58–65% of the ciliates in surface waters were mixotrophs. Likewise, in Disko Bay, Greenland, Levinsen et al. (2000) observed that 45–85% of the oligotrichous ciliates in surface waters in summer were mixotrophs. In summer, in stratified Sub-Arctic Seas, mixotrophic ciliates are generally very abundant and important components of the microzooplankton.

Calculation of estimated contribution of ciliates to chlorophyll is very sensitive to the factors used to estimate chlorophyll per unit biovolume. In the North Middle Domain, where chlorophyll levels were very low in the mixed layer in 2008 and 2010, average estimated contribution of mixotrophic ciliates to total chlorophyll was over 50% using the mean chlorophyll density of 3.12 − fg Chl *a* μm^{-3} calculated for mixotrophic ciliates (refer to Section 2.4). However, there is considerable variability among ciliate species in their chlorophyll density (standard deviation ± 2.63); depending on the mix of species present, the actual contribution of ciliates to chlorophyll in the Bering Sea may be considerably higher or lower. Putt (1990), based on determination of the chlorophyll content of ciliates collected at sea, estimated ciliates accounted for 4–15% of total chlorophyll *a* in summer in surface waters of the Nordic Seas. This is similar to our estimate of 5–14% for the South Shelf domains, but lower than our estimate of 22–35% for the more northern shelf (MN transect and North Middle Domain).

About 64% of the chlorophyll in the Bering Sea in summer is due to cells $<5\ \mu m$ in size (Lomas et al., 2012). Assuming 36% of the chlorophyll in the mixed layer in all domains is $>5\ \mu m$ and using the mean value for chlorophyll content of mixotrophic ciliates, the average contribution of ciliates to chlorophyll in the $>5\ \mu m$ size class ranges from 15% to 96%. It is clear that the contribution of ciliates to chlorophyll (and probably photosynthesis) (reviewed in Stoecker et al. (2009)), particularly in the size fraction that is readily accessible to crustacean zooplankton, is considerable, particularly in the northern domains. This also implies that bulk chlorophyll measurements overestimate the biomass of phytoplankton and that the ratios of microzooplankton biomass to chlorophyll *a* or phytoplankton biomass may be underestimates.

4.6. Importance of microzooplankton to crustacean zooplankton

Microzooplankton were included in Bering Sea Project because of their importance as a trophic link between primary production and crustacean zooplankton, which are important prey for fish, sea birds and some marine mammals (Coyle et al., 2008; Hunt et al., 2008; Stabeno et al., 2012b; Eisner et al., 2014; http://bsierp.nprb.org/focal/index.html). Crustacean zooplankton consume both phytoplankton and microzooplankton, but often have higher clearance rates for microzooplankton than phytoplankton, particularly when phytoplankton are not abundant and/or are small in size (Gifford and Dagg, 1991; Calbet and Saiz, 2005; Campbell et al., 2009). After the spring bloom, when phytoplankton are scarce, predation on microzooplankton can maintain fecundity of copepods (Ohman and Runge, 1994). Large, mixotrophic ciliates are particularly important as prey for copepods (Dutz and Peters, 2008) and young fish larvae (Figueiredo et al., 2007). Under these conditions, photosynthesis in ciliates may "boost" microbial food web efficiency and hence carbon availability to higher trophic levels (Stoecker et al., 2009). This may be important in stratified Bering Sea shelf waters where chlorophyll levels were relatively low (mean total Chl *a* $\sim 0.9\ \mu g\ l^{-1}$) and composed of small cells ($\sim$64% of chl *a* $<5\ \mu m$) in summer (Lomas et al., 2012). Crustacean zooplankton do not effectively graze cells $<5\ \mu m$ in size. Almost all cells larger than 15–20 μm in size in the mixed layer on the inner and middle shelf (with the exception of the Pribilof Domain) were microzooplankton. Estimated microzooplankton biomass in the mixed layer was 98% (SD 166%) of estimated phytoplankton biomass with a median value of 55% (Maximum 155%, Minimum 2%, $N=132$). In low chlorophyll surface waters, such as on the Bering Sea middle shelf in summer, about 50% of the diet of copepods is ciliates (Calbet and Saiz, 2005). Protistan microzooplankton are an important component of the diet of copepods in arctic and subarctic seas (Møller et al., 2006; Campbell et al., 2009).

4.7. Climate variability and the microzooplankton trophic link

One of the goals of the Bering Sea Project was to examine how climate induced changes in physical forcing through bottom-up processes will modify food availability at different trophic levels

(http://bsierp.nprb.org/focal/hypothesis.html). Climate and weather over the last thirty years are hypothesized to have influenced the ecology of the Eastern Bering Sea (Mathis et al., 2010; Overland et al., 2012; Stabeno et al., 2012b; Wang et al., 2012). The years of our study (2008–2011) were within a period of decreased annual variability and thus we could not directly compare microzooplankton abundance and biomass in warm and cold years as we had proposed since all three years were cold (Stabeno et al., 2012b). However, insight can be gained from comparing our data from 2008–2011 to warm periods. During the warm years of 1998 and 2001–2005, surface water temperatures on the southern middle shelf rose above 10° C during the summer, although during average and cold years surface waters temperatures remain below 10° C (Stabeno et al., 2012b).

Surface water temperatures can influence the timing and strength of stratification, which controls the availability of nutrients for phytoplankton growth and hence has a strong influence on new production, phytoplankton species composition, and perhaps the suitability of phytoplankton as food for microzooplankton (Sambrotto et al., 1986, 2008; Strom and Fredrickson, 2008; Mathis et al., 2010). During July and August of 2004, a warm year, intense stratification in the southeastern Bering Sea led to phytoplankton nutrient limitation and reduced microzooplankton grazing (Strom and Fredrickson, 2008). However, contrary to expectations, stratification index does not correlate with warm and cold years in the Eastern Bering Sea (Ladd and Stabeno, 2012). Weather and tides are important in controlling stratification. Advection of water onto the shelf and wind and tidal mixing make nutrients available to phytoplankton and can lead to localized blooms even during summer (Sambrotto et al., 1986, 2008).

However, in the Bering Sea Shelf, where surface water temperatures during cold and normal years are below 10° C even in summer, there might be a direct, positive effect of increased temperature on coupling between microzooplankton and phytoplankton growth. Based on a compendium of laboratory studies of cultured protists, Rose and Caron (2007) found that the maximum growth rate of herbivorous microzooplankton was lower than the maximum growth rates of phytoplankton below 10° C. If this relationship holds in natural communities, then the coupling of microzooplankton to phytoplankton would be expected to increase with increases in water temperature. However, Levinsen et al. (2000) found that in the Greenland Sea, net community growth and loss rates of ciliates and dinoflagellates were equal to or greater than of phytoplankton during the spring, even though water temperatures were sub-zero, indicating that temperature may not limit coupling between these trophic levels in Arctic ecosystems. Modeling of the general responses of microzooplankton herbivory to warming suggest that it may increase the ratio of microzoozooplankton grazing to phytoplankton growth under eutrophic, but not oligotrophic conditions (Chen et al., 2012). This indicates that stratification and mixing, by largely controlling nutrient availability, may control the coupling of microzooplankton and phytoplankton. Our knowledge of how climate variability will affect key phytoplankton groups, and their interactions with microzooplankton, is very limited, but it is clear that interactive effects of temperature, stratification/mixing and nutrients are important (Olson and Strom, 2002; Rose et al., 2009; Boyd et al., 2010).

5. Conclusions

a. Microzooplankton biomass equaled or exceeded summer phytoplankton biomass in the mixed layer in some domains. Microzooplankton were relatively more important in stratified shelf waters than in the green belt, Pribilof Island Domain or at the Shelf Break.
b. Mixotrophic strombidiid ciliates were the dominant component of the ciliate microzooplankton. They made important contributions to both microzooplankton biomass and chlorophyll, especially in the larger size classes.
c. Based on our data and previous investigations, the range of summer microzooplankton biomass was similar in warm and cold years, with differences among years obscured by differences among domains, derived in part by differences in mixing, nutrient supply and phytoplankton composition.

Acknowledgments

We thank the officers and crew of the U.S.C.G. Icebreaker Healy, R/V Knorr and R/V T.G. Thompson for their support and John Casey of BIOS, Dave Kachel of PMEL, Nancy Kachel of UW/JISAO, Jessica Cross of UAF for CTD sampling, advice and good cheer. We thank Kristin Blattner for excellent technical assistance during the first 2 years of the project. We thank Evelyn Sherr for helpful comments on an early draft of the manuscript. This research was supported primarily by NPRB project award B55 (DKS and ACW). This is BEST-BSIERP Bering Sea Project publication number 110, NBRB publication number 443, and UMCES contribution number.

References

Aydin, K., Mueter, F., 2007. The Bering Sea—a dynamic food web perspective. Deep Sea Res. II 54, 2501–2525.
Booth, B.C., Lewin, J., Postel, J.R., 1993. Temporal variation in the structure of autotrophic and heterotrophic communities in the Sub-Arctic Pacific. Prog. Oceanogr. 32, 57–99.
Boyd, P.W., Strzepek, R., Fu, F., Hutchins, D.A., 2010. Environmental control of open-ocean phytoplankton groups: now and in the future. Limnol. Oceanogr. 55, 1353–1376.
Calbet, A., Saiz, E., 2005. The ciliate-copepod link in marine ecosystems. Aquat. Microb. Ecol. 38, 157–167.
Calbet, A., Saiz, E., Almeda, R., Movilla, J.I., Alcarez, M., 2011. Low microzooplankton grazing rates in the Arctic Ocean during a *Phaeocystis pouchettii* Bloom (Summer 2007): fact or artifact of the dilution technique? J. Plankton Res. 33, 687–701.
Campbell, R.G., Sherr, E.B., Ashjian, C.J., Plourde, S., Sherr, B.F., Hill, V., Stockwell, D.A., 2009. Mesozooplankton prey preferences and grazing impact in the Western Arctic Ocean. Deep Sea Res. II 56, 1274–1289.
Chen, B.Z., Landry, M.R., Huang, B.Q., Liu, H.B., 2012. Does warming enhance the effect of microzooplankton grazing on marine phytoplankton in the ocean? Limnol. Oceanogr. 57, 519–526.
Ciannelli, L., Robson, B.W., Francis, R.C., Aydin, K., Brodeur., R.D., 2004. Boundaries of open marine ecosystems: an application to the Pribilof Archipelago, Southeast Bering Sea. Ecol. Appl. 14, 942–953.
Coachman, L.K, 1986. Circulation, water masses, and fluxes on the Southeastern Bering Sea shelf. Continental Shelf Res. 5, 23–108.
Coyle, K.O., Pinchuk, A.I., Eisner, L.B., Napp, J.M., 2008. Zooplankton species composition, abundance and biomass on the Eastern Bering Sea shelf during summer: The potential role of water-column stability and nutrients in structuring the zooplankton community. Deep-Sea Res. II 55, 1775–1791.
Dolan, J.R., Perez, M.T., 2000. Costs, benefits and characteristics of mixotrophy in marine oligotrichs. Freshwater Biol. 45, 227–238.
Dutz, J., Peters, J., 2008. Importance and nutritional value of large ciliates for the reproduction of *Acartia clausi* during the post spring-bloom period in the North Sea. Aquat. Microb. Ecol. 50, 261–277.
Eisner, L.B., Napp, J.M., Mier, K.K., Pinchuk, A.I., Andrews, III, A.G., 2014. Climate-mediated changes in zooplankton community structure for the Eastern Bering Sea. Deep-Sea Res. II 109, 157–171, http://dx.doi.org/10.1016/j.dsr2.2014.03.004.
Figueiredo, G.M., Nash, R.D.M., Montagnes, D.J.S., 2007. Do protozoa contribute significantly to the diet of larval fish in the Irish Sea? J. Mar. Biol. Assoc. UK 87, 843–850.
Fileman, E.S., Petropavlovsky, A., Harris, R.P., 2010. Grazing by the copepods *Calanus helgolandicus* and *Acartia clause* on the protozooplankton community at station L4 in the Western English Channel. J. Plankton Res. 32, 709–724.
Fukami, K., Watanabe, A., Fujita, S., Yamaoka, K., Nishijima, T., 1999. Predation on naked protozoan microzooplankton by fish larvae. Mar. Ecol. Prog. Ser. 185, 285–291.
Gifford, D.J., Caron, D.A., 2000. Sampling, preservation, enumeration and biomass of marine protozooplankton. In: Harris, R., Wiebe, P., Lenz, J., Skjoldal, H.R.,

Huntley, A. (Eds.), ICES Zooplankton Methodology Manual. Academic Press, San Diego, pp. 193–221. (Chapter 5).
Gifford, D.J., Dagg, M.J., 1991. The microzooplankton–mesozooplankton link: consumption of planktonic protozoa by the calanoid copepods *Acartia tonsa* Dana and *Neocalanus plumchrus* Murukawa. Mar. Microb. Food Webs 5, 161–177.
Gilron, G.L., Lynn, D.H., 1989. Assuming a 50% cell occupancy of the lorica overestimates tininnine ciliate biomass. Mar. Biol. 103, 413–416.
Guillard, R.R.L., Sieracki, M.S., 2005. Counting cells in cultures with the light microscope. In: Andersen, R.A. (Ed.), Algal Culturing Techniques. Elsevier Academic Press, Amsterdam, pp. 239–252. (Chapter 16).
Goes, J.I., Gomes, H.R., Haugen, E., McKee, K., D'Sa, E., Chekayuk, A.M., Stoecker, D., Stabeno, P., Seichi, S., Sambrotto, R., 2014. Community structure and photosynthetic competency of summer time phytoplankton during the formation of a Cold Pool in the Bering Sea. Deep Sea Res. II 109, 84–99, http://dx.doi.org/10.1016/j.dsr2.2013.12.004.
Harvey, H.R., Sigler, M.F., 2013. An introduction to the Bering Sea Project. Deep Sea Res. II, 94, 2–6.
Howell-Kübler, A.N., Lessard, E.J., Napp, J.M., 1996. Springtime microprotozoan abundance and biomass in the Southeastern Bering Sea and Shelikof Strait, Alaska. J. Plankton Res. 18, 731–745.
Hunt Jr., G.L., Coyle, K.O., Eisner, L.B., Farley, E.V., Heintz, R.A., Mueter, F., Napp, J.M., Overland, J.E., Ressler, P.H., Salo, S., Stabeno, P.J., 2011. Climate impacts on eastern Bering Sea food webs: a synthesis of new data and an assessment of the Oscillating Control Hypothesis. ICES J. Mar. Sci. 68, 1230–1243.
Hunt Jr., G.L., Stabeno, P., Strom, S., Napp, J.M., 2008. Patterns of spatial and temporal variation in the marine ecosystem of the Southeastern Bering sea, with special reference to the Pribilof Domain. Deep Sea Res. II 55, 1919–1944.
Hunt Jr., G.L., Stabeno, P., Walters, G., Sinclair, E., Brodeur, R.D., Napp, J.M., Bond, N.A., 2002. Climate change and control of the Southeastern Bering Sea pelagic ecosystem. Deep Sea Res. II 49, 5821–5853.
Jakobsen, H.H., Carstensen, J., 2011. FlowCAM: sizing cells and understanding the impact of size distributions on biovolume of planktonic community structure. Aquat. Microb. Ecol. 65, 75–87.
Jeong, H.J., Yoo, Y.D., Kim, J.S., Seong, K.A., Kand, N.S., Kim, T.H., 2010. Growth, feeding and ecological roles of the mixotrophic and heterotrophic dinoflagellates in marine planktonic food webs. Ocean. Sci. J. 45, 65–91.
Kachel, N.B., Hunt, G.L., Salo, S.A., Schumacher, J.D., Stabeno, P.J., Whitledge, T.E., 2002. Characteristics and variability of the inner front of the Southeastern Bering Sea. Deep Sea Res. II 49, 5889–5909.
Ladd, C., Stabeno, P.J., 2012. Stratification on the Eastern Bering Sea shelf revisited. Deep Sea Res. II 65–70, 72–83.
Levinsen, H., Nielsen, T.G., 1999. Plankton community structure and carbon cycling on the western coast of Greenland during the stratified summer situation. II. Heterotrophic dinoflagellates and ciliates. Aquat. Microb. Ecol. 16, 217–232.
Levinsen, H., Nielsen, T.G., 2002. The trophic role of marine pelagic ciliates and heterotrophic dinoflagellates in arctic and temperate coastal ecosystems: a cross-latitude comparison. Limnol. Oceanogr. 47, 427–439.
Levinsen, H., Nielsen, T.G., Hansen, B.W., 2000. Annual succession of marine pelagic protozoans in Disko Bay, West Greenland, with emphasis on winter dynamics. Mar. Ecol. Prog. Ser. 206, 119–134.
Liu, H., Suzuki, K., Saino, T., 2002. Phytoplankton growth and microzooplankton grazing in the subarctic Pacific Ocean and the Bering Sea during summer 1999. Deep Sea Res. I 49, 363–375.
Lomas, M.W., Moran, S.B., Casey, J.R., Bell, D.W., Tiahlo, M., Whitefield, J., Kelly, R.P., Mathis, J.T., Cokelet, E.D., 2012. Spatial and seasonal variability of primary production on the Eastern Bering Sea shelf. Deep-Sea Res. II 65-70, 126–140.
Mathis, J.T., Cross, J.N., Bates, N.R., Morman, S.B., Lomas, M.W., Mordy, C.W., Stabeno, P.J., 2010. Seasonal distribution of dissolved inorganic carbon and net community production on the Bering Sea shelf. Biogeosciences 7, 1769–1787.
Mayzaud, P., Boutoute, M., Noyon, M., Narcy, F., Gasparini, S., 2013. Lipid and fatty acids in naturally occurring particulate matter during spring and summer in a high arctic fjord (Kongsfjorden, Svalbard). Mar. Biol. 160, 383–398.
Menden-Deuer, S., Lessard, E.J., 2000. Carbon to volume relationships for dinoflagellates, diatoms, and other protist plankton. Limnol. Oceanogr. 45, 569–579.
Møller, E.F., Nielsen, T.G., Richardson, K., 2006. The zooplankton community in the Greenland Sea: composition and role in carbon turnover. Deep-Sea Res. I 53, 76–93.
Montagnes, D.J.S., Allen, J., Brown, L., Bulit, C., Davidson, R., Diaz-Avalos, C., Fielding, S., Heath, M., Holliday, N.P., Rasmussen, J., Sanders, R., Waniek, J.J., Wilson, D., 2008. Factors controlling the abundance and size distribution of the phototrophic ciliate *Myrionecta rubra* in open waters of the North Atlantic. J. Eukaryot. Microbiol. 55, 457–465.
Montagnes, D.J.S., Dower, J.F., Figueiredo, G.M., 2010. The protozooplankton–ichthyoplankton trophic link: an overlooked aspect of aquatic food webs. J. Eukaryot. Microbiol. 57, 223–228.
Moran, S.B., Lomas, M.W., Kelly, R.P., Gradinger, R., Iken, K., Mathis, J.T., 2012. Seasonal succession of net primary productivity, particulate organic carbon export and autotrophic community composition in the Eastern Bering Sea. Deep Sea Res. II 65–70, 84–97.
Mordy, C.W., Cokelet, E.D., Ladd, C., Menzia, F.A., Proctor, P., Stabeno, P.J., Wisegarver, E., 2012. Net community production on the middle shelf of the Eastern Bering Sea. Deep Sea Res. II 65–70, 110–125.
Nejstgaard, J., Tang, K., Steinke, M., Dutz, J., Koski, M., Antajan, E., Long, J.D., 2007. Zooplankton grazing on *Phaeocystis*: a quantitative review and future challenges. Biogeochemistry 83, 147–172.
Ohman, M.D., Runge, J.A., 1994. Sustained fecundity when phytoplankton resources are in short supply: omnivory by *Calanus finmarchicus* in the Gulf of St. Lawrence. Limnol. Oceanogr. 39, 21–36.
Olson, M.B., Strom, S.L., 2002. Phytoplankton growth, microzooplankton herbivory and community structure in the southeast Bering Sea: insight into the formation and temporal persistence of an *Emiliania huxleyi* bloom. Deep-Sea Res. II 49, 5969–5990.
Overland, J.E., Wang, M., Wood, K.R., Percival, D.B., Bond, N.A., 2012. Recent Bering Sea warm and cold events in a 95-year context. Deep Sea Res. II 65–70, 6–13.
Putt, M., 1990. Abundance, chlorophyll content and photosynthetic rates of ciliates in the Nordic Seas during summer. Deep-Sea Res. A 37, 1713–1731.
Putt, M., Stoecker, D.K., 1989. An experimentally determined carbon:volume ratio for marine "oligotrichous" ciliates from estuarine and coastal waters. Limnol. Oceanogr. 34, 1097–1103.
Rose, J.M., Caron, D.A., 2007. Does low temperature constrain the growth rates of heterotrophic protists? Evidence and implications for algal blooms in cold waters. Limnol. Oceanogr. 52, 886–895.
Rose, J.M., Feng, Y., Gobler, C.J., Gutierrez, R., Hare, C.E., LeBlanc, K., Hutchins, D.A., 2009. Effects of increased pCO_2 and temperature on the North Atlantic spring bloom. II. Microzooplankton abundance and grazing. Mar. Ecol. Prog. Ser. 388, 27–40.
Rose, J.M., Fitzpatrick, E., Wang, A., Gast, R., Caron, D.A., 2013. Low temperature constrains growth rates but not short-term ingestion rates of Antarctic ciliates. Polar Biol, http://dx.doi.org/10.1007/s00300-013-1291-y.
Sambrotto, R.N., Mordy, C., Zeeman, S.I., Stabeno, P.J., Macklin, S.A., 2008. Physical forcing and nutrient conditions associated with patterns of Chl a and phytoplankton productivity in the Southeastern Bering Sea during summer. Deep-Sea Res. II 55, 1745–1760.
Sambrotto, R.N., Niebauer, H.J., Goering, J.J., Iverson, R.L., 1986. Relationships among vertical mixing, nitrate uptake, and phytoplankton growth during the spring bloom in the Southeast Bering Sea middle shelf. Cont. Shelf Res. 5, 161–198.
Saiz, E., Calbet, A., Isari, S., Antó, M., Velasco, E.M., Almeda, R., Movilla, J., Alcarez, M., 2013. Zooplankton distribution and feeding in the Arctic Ocean during a *Phaeocystis pouchetii* bloom. Deep-Sea Res. I 72, 17–33.
Sherr, E.B., Sherr, B.F., 2009. Capacity of herbivorous protists to control initiation and development of mass phytoplankton blooms. Aquat. Microb. Ecol. 57, 253–262.
Sherr, E.B., Sherr, B.F., Ross, C., 2013. Microzooplankton grazing impact in the Bering Sea during spring sea ice conditions. Deep Sea Res. II 94, 57–67.
Simé-Ngando, T., Juniper, K., Vézina, A., 1992. Ciliated protozoan communities over Cobb Seamount: increase in biomass and spatial patchiness. Mar. Ecol. Prog. Ser. 89, 37–51.
Sorokin, Y.I., Sorokin, P.Y., Mamaeva, T.I., 1996. Density and distribution of bacterioplankton and planktonic ciliates in the Bering Sea and North Pacific. J. Plankton Res. 18, 1–16.
Stabeno, P.J., Farley Jr., E.V., Kachel, N.B., Moore, S., Mordy, C.W., Napp, J.M., Overland, J.E., Pinchuk, A.I., Sigler, M.F., 2012a. A comparison of the physics of the northern and southern shelves of the Eastern Bering Sea and some implications for the ecosystem. Deep Sea Res. II 65–70, 14–30.
Stabeno, P.J., Kachel, N.B., Moore, S.E., Napp, J.M., Sigler, M., Yamaguchi, A., Zerbini, A.N., 2012b. Comparison of warm and cold years on the southeastern Bering Sea shelf and some implications for the ecosystem. Deep Sea Res. II 65–70, 31–45.
Stabeno, P., Napp, J., Mordy, C., Whitledge, T., 2010. Factors influencing physical structure and lower trophic levels of the eastern Bering Sea shelf in 2005: sea ice, tides and winds. Prog. Oceanogr. 85, 180–196.
Stoecker, D.K., Silver, M.W., Michaels, A.E., Davis, L.H., 1988. Obligate mixotrophy in Laboea strobila, a ciliate which retains chloroplasts. Mar. Biol. 99, 415–423.
Stoecker, D.K., Silver, M.W., Michaels, A.E., Davis, L.H., 1988/1989. Enslavement of algal chloroplasts by four Strombidium spp. (Ciliophora, Oligotrichida). Mar. Microb. Food Webs 3, 79–100.
Stoecker, D.K., 2013. Predators of tintinnids. In: Dolan, J.R., Montagnes, D.J.S., Agatha, S., Coats, D.W., Stoecker, D.K. (Eds.), The Biology and Ecology of Tintinnid Ciliates: Models for Marine Plankton. John Wiley & Sons, Ltd., Oxford, pp. 123–144. (Chapter 5).
Stoecker, D.K., Gifford, D.J., Putt, M., 1994. Preservation of marine planktonic ciliates: losses and cell shrinkage during fixation. Mar. Ecol. Prog. Ser. 110, 293–299.
Stoecker, D.K., Johnson, M.D., de Vargas, C., Not, F., 2009. Acquired phototrophy in aquatic protists. Aquat. Microb. Ecol. 57, 279–310.
Stoecker, D.K., Weigel, A., Goes, J.I., 2014. Microzooplankton grazing in the eastern Bering Sea in summer. Deep-Sea Res. II 109, 145–156, http://dx.doi.org/10.1016/j.dsr2.2013.09. 017.
Strom, S.L., Fredrickson, K.A., 2008. Intense stratification leads to phytoplankton nutrient limitation and reduced microzooplankton grazing in the Southeastern Bering Sea. Deep Sea Res. II 55, 1761–1774.
Suzuki, T., Taniguchi, A., 1998. Standing crops and vertical distribution of four groups of marine planktonic ciliates in relation to phytoplankton chlorophyll *a*. Mar. Biol. 132, 375–382.
Wang, M., Overland, J.E., Stabeno, P., 2012. Future climate of the Bering and Chukchi Seas projected by global climate models. Deep-Sea Res. II 65–70, 46–57.

Deep-Sea Research II 109 (2014) 145–156

Contents lists available at ScienceDirect

Deep-Sea Research II

journal homepage: www.elsevier.com/locate/dsr2

Microzooplankton grazing in the Eastern Bering Sea in summer

Diane K. Stoecker [a,*], Alison Weigel [a], Joaquim I. Goes [b]

[a] University of Maryland Center for Environmental Science, Horn Point Laboratory, P.O. Box 775, Cambridge, MD 21613, USA
[b] 10 Marine Biology, Department of Marine Biology and Paleoenvironment, Lamont Doherty Earth Observatory at Columbia University, 61 Route 92, Palisades, NY 10964, USA

ARTICLE INFO

Available online 21 September 2013

Keywords:
Bering Sea
Microzooplankton grazing
Dilution method
Deep chlorophyll maximum
Fv/Fm

ABSTRACT

Dilution experiments to estimate microzooplankton grazing on phytoplankton were conducted during the summers of 2008, 2009, and 2010 in the Eastern Bering Sea as part of the BEST-BSIERP integrated ecosystem project. All three summers followed cold springs in the Bering Sea. Average microzooplankton grazing coefficients were relatively similar among regions, ranging from 0.16 to 0.34 d^{-1} in simulated *in situ* incubations with mixed-layer water collected from the depth of the 55% I_o isolume. In Off Shelf and Outer Shelf domains, microzooplankton consumed 67–78% of phytoplankton daily growth but in the Middle and Inner Shelf domains, microzooplankton grazing exceeded phytoplankton daily growth. Regional estimates of microzooplankton ingestion of phytoplankton carbon ranged from 4.4 to 11.0 μg C d^{-1}, with highest ingestion in the Off Shelf, Outer Shelf, and Alaska Peninsula regions and, lower ingestion in the Middle Shelf and Inner Shelf regions. On the northern Middle Shelf, a deep chlorophyll maximum (DCM) occurred at most stations. Grazing coefficients in the DCM were similar in magnitude to coefficients in the corresponding mixed layer. However, because of the higher phytoplankton biomass in the DCM, estimated microzooplankton ingestion and secondary production per liter were higher in the DCM than in the mixed layer. Measurements of photosynthetic quantum yields (Fv/Fm) in whole seawater and diluted treatments indicated that with some plankton assemblages, dilution had a negative effect on phytoplankton physiology and could have compromised their growth rates. This could have also resulted in an underestimation of microzooplankton grazing. Nevertheless, it is clear that microzooplankton grazing consumed most of the phytoplankton production in summer, and that microzooplankton were an important link in food webs supporting larger zooplankton and in carbon flow in the Eastern Bering Sea.

1. Introduction

The <200 μm fraction of zooplankton assemblages, which includes both microzooplankton and nanozooplankton, is an important link between primary producers and higher trophic levels in sub-polar and polar waters as well as in temperate and tropical waters (Levinsen and Nielsen, 2002; Calbet and Saiz, 2005; Campbell et al., 2009; Sherr et al., 2013). They are important grazers on pico, nano and microplankton, including large diatoms (Sherr et al., 2009, 2013). Previous studies have shown that the <200 μm fraction is the major consumer of primary production in summer in the Eastern Bering Sea (Liu et al., 2002; Olson and Strom, 2002; Strom and Fredrickson, 2008). In Arctic and sub-Arctic as well as temperate and tropical seas, microzooplankton are important prey for mesozooplankton, including both small and large crustacean zooplankton (Levinsen and Nielsen, 2002; Campbell et al., 2009) and hence are a significant component of the food web and carbon cycle.

Although microzooplankton can graze on large as well as small phytoplankton, including chain forming dinoflagellates (Strom et al., 2007; Sherr et al., 2013), their grazing rates, particularly microzooplankton biomass specific rates, can be influenced by phytoplankton species composition, physiological state and cell size (Olson and Strom, 2002; Strom and Fredrickson, 2008). In the Eastern Bering Sea, phytoplankton <5 μm comprise ~70% of the chlorophyll *a* in summer and autotrophic biomass is dominated by phytoflagellates (Lomas et al., 2012; Moran et al., 2012). Sporadic blooms of chain forming diatoms (mostly *Chaetoceros* and *Thalassiosira* spp.) and blooms of the solitary or colonial phytoflagellate *Phaeocystis pouchetti* occur in response to tidal and storm mixing or intrusion of deeper water onto the shelf (Sukhanova et al., 1999; Sambrotto et al., 2008). In late spring and summer, prolonged blooms of diatoms and *P. pouchetti* are associated with the shelf break and shelf partition fronts (Flint et al., 2002). During the anomalously warm and stratified spring of 1997, a bloom of the coccolithophorid, *Emiliana huxleyi*, developed on the southeastern shelf and during summers 1998–2000 the bloom was present (Stockwell et al., 2001; Merico et al., 2004). In summer, particularly on the northern shelf, a deep chlorophyll maximum (DCM) composed primarily of diatoms has often been encountered. It is

* Corresponding author. Tel.: +1 410 2218407; fax: +1 410 221 8490.
E-mail addresses: stoecker@umces.edu (D.K. Stoecker), jig@ideo.columbia.edu (J.I. Goes).

0967-0645/$ - see front matter © 2013 Elsevier Ltd. All rights reserved.
http://dx.doi.org/10.1016/j.dsr2.2013.09.017

not clear if the DCM is a resident low light population or physiologically inactive settled material (Moran et al., 2012; Stabeno et al., 2012a), and to what extent it is grazed by the <200 μm zooplankton.

Microzooplankton were sampled as part of the Bering Sea Project ecosystem study in the Eastern Bering Sea in summers of 2008, 2009, and 2010 (Stoecker et al., 2014), all part of a four year "cold" period characterized by extensive sea ice in spring (Stabeno et al., 2012b). Average summer microzooplankton (defined as ~20–200 μm size range) densities ranged from 4×10^3 to 25×10^3 cells l^{-1} in the mixed layer in stratified shelf waters but were about half that concentration in less stratified waters near the shelf break. High ratios (>1) of microzooplankton biomass to phytoplankton biomass were observed when chlorophyll concentrations were below 1 μg l^{-1} in the mixed layer (Stoecker et al., 2014). In coastal (inner domain) and Middle Shelf (middle domain) waters, the average biomass of microzooplankton in the mixed layer was often equal to or higher than that of phytoplankton. Microzooplankton were also found in the deep chlorophyll maxima (DCM) on the shelf; densities of microzooplankton in these high chlorophyll layers were usually similar to in the lower chlorophyll mixed layer. Microzooplankton abundance and biomass data from summers 2008–2010, along with results from previous studies during both "warm" and "cold" years in the Eastern Bering Sea (Liu et al., 2002; Olson and Strom, 2002; Strom and Fredrickson, 2008), indicate that summer microzooplankton population differences among domains are far greater than differences due to year-to-year variations in sea ice extent and water temperature (Stoecker et al., 2014).

Dilution grazing experiments were conducted with the <200 μm fraction of plankton in conjunction with microzooplankton sampling on the BEST-BSIERP summer cruises in 2008, 2009, and 2010. Although standard dilution experiments include grazing by both microzooplankton and nanozooplankton, they are commonly called "microzooplankton" dilution grazing experiments. Herein, this convention was followed. Prior to our study, summer data on grazing by microzooplankton in the Eastern Bering Sea were limited to the southern shelf and the productive waters around the Pribilof Islands (Olson and Strom, 2002; Hunt et al., 2008; Strom and Fredrickson, 2008). The primary goal was to conduct dilution grazing experiments across a spectrum of environments and to compare microzooplankton grazing among domains. One objective was to determine if grazing and its impact on phytoplankton correlated with the biomass of microzooplankton (Stoecker et al., 2014) and/or the dominance of certain phytoplankton taxa. Low grazing by the <200 μm fraction can occur during blooms of coccolithophorids (Olson and Strom, 2002) and *P. pouchetti* (reviewed in Nejstgaard et al. (2007)). Another objective was to determine if grazing by the <200 μm fraction was important in the DCM since this is a characteristic feature of the northern shelf in summer (Stabeno et al., 2012a).

2. Materials and methods

2.1. Sampling

Microzooplankton grazing experiments were conducted on Bering Sea Project summer cruises in 2008, 2009 and 2010 on the *USCG Healy* (HLY-08-03, July 3–July 31), R/V *Knorr* (KNORR 195-10, June 14 to July 13) and R/V *T.G. Thompson* 2010 (TN-250, June 16–July 14). The stations at which dilution grazing experiments were conducted are shown in

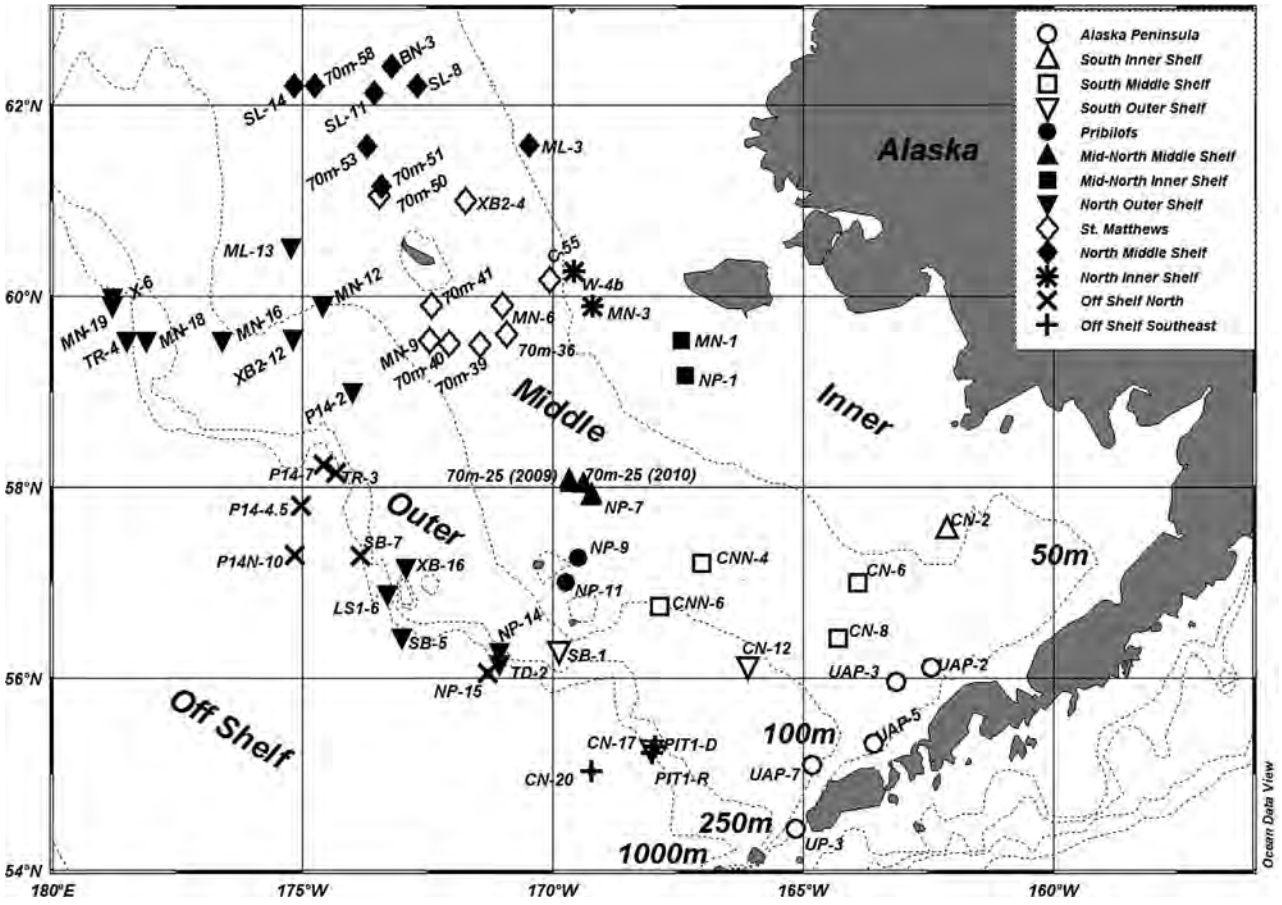

Fig. 1. Stations where dilution experiments were performed in the eastern Bering Sea during summers 2008, 2009, and 2010. Inner shelf (coastal), middle shelf, outer shelf and off shelf areas are indicated. Refer to Table 1 for list of stations, regions and experimental parameters; experiments were not performed at all stations in all years.

Fig. 1; the stations and depths of experiments for each year are given in Table 1. Stations are grouped by marine regions in the Bering Sea Project area as delineated by Ortiz et al. (2012). In most cases, dilution grazing experiments were undertaken in conjunction with the phytoplankton biomass and primary productivity casts with water collected from the depth of the 55% of surface PAR irradiance level (Lomas et al., 2012). At all stations the 55% irradiance level was in the surface mixed layer, with the sampling depth for mixed layer incubations ranging from 3 to 10 m (Table 1). In 2010 we also undertook microzooplankton grazing experiments using assemblages from the DCM which was located based on chlorophyll fluorescence profiles from the core CTD casts. Supporting information including water temperature, salinity, chlorophyll *a*, inorganic nutrients and irradiance were obtained from core program measurements or from the productivity casts (Lomas et al., 2012). Data are archived at http://beringsea.eol.ucar.edu.

2.2. Dilution experiments

Dilution grazing experiments are the only method available for estimating community grazing by the <200 μm fraction on the whole phytoplankton community. This method estimates phytoplankton growth rates (μ) and mortality of phytoplankton due to combined microzooplankton and nanoplankton grazing (g) (Landry, 1993). Dilution grazing experiments include all grazers ≤ 200 μm in size, including small heterotrophic and mixotrophic flagellates, as well as the larger ciliates and heterotrophic and mixotrophic dinoflagellates, but are commonly referred to as "microzooplankton" grazing experiments.

Pre-screened (<200 μm) whole seawater (WSW), containing natural assemblages of phytoplankton and microzooplankton, was diluted with filtered, particle free seawater (FSW) from the same sample. Dilution reduces microzooplankton encounter rates with phytoplankton prey; in highly dilute treatments net growth rate (NGR) of phytoplankton approach the intrinsic growth rate (μ). Phytoplankton mortality due to microzooplankton grazing was calculated as $\mu - \mathrm{NGR}$. A modified dilution method, the two-point method (Landry et al., 2008) was used because it is more efficient than the original method. The original and the two-point method were compared in grazing experiments conducted in the coastal Gulf of Alaska (Strom et al., 2006) and in the SE Bering Sea (Strom and Fredrickson, 2008) and were found to provide similar results.

In nutrient limited waters, which can occur in summer on the Bering Sea Shelf (Strom and Fredrickson, 2008), nutrient regeneration due to micrograzers can be important in supplying inorganic nutrients for phytoplankton growth. This would violate the first assumption of the dilution technique, that phytoplankton growth rate is not influenced by dilution (Landry, 1993). To circumvent this problem, inorganic nutrients can be added to all the bottles. However, then the estimated phytoplankton growth rates are no longer similar to *in situ* rates. In this situation, it is

Table 1
Dilution experiments, Eastern Bering Sea, summers 2008, 2009, and 2010. Stations are in following regions: Alaska Peninsula (AP), South Inner Shelf (SIS), South Middle Shelf (SMS), South Outer Shelf (SOS), Pribilof Islands (P), Mid North Middle Shelf (MNMS), Mid North Inner Shelf (MNIS), North Outer Shelf (NOS), St. Matthews (SM), North Middle Shelf (NMS), North Inner Shelf (NIS), Off Shelf North (OSN), and Off Shelf Southeast (OSSE). Station locations are shown in Fig. 1. Experiments with nutrient addition treatments are indicated as N=addition of nitrate, N*=addition of ammonium, N+P=addition of nitrate and phosphate. "B" indicates incubation in dark at ~0 °C. "CF" indicates experiment with a carbon filtration treatment. "F" indicates variable fluorescence measurements.

Region	Date	Station	Sample depth (m)	Water temp. (°C)		Region	Date	Station	Sample depth (m)	Water temp. (°C)	
AP	07/04/08	UP-3	5	5.39	N	**NOS**	07/05/10	ML-13	35	−1.07	B
AP	06/15/09	UAP-7	3	6.08		**NOS**	06/27/10	SB-5	4	5.44	N+P
AP	06/16/09	UAP-3	3	6.49		**NOS**	07/03/10	MN-16	7	5.36	B
AP	06/18/10	UAP-5	5	5.02		**NOS**	07/03/10	MN-18	26	1.65	N
AP	06/19/10	UAP-2	3	4.19	N+P	**SM**	07/10/08	C-55	4	5.41	N, F
SIS	06/17/09	CN-2	3	3.89		**SM**	07/23/08	MN-6	5	6.13	N, F
SMS	07/05/08	CN-6	7	5.12		**SM**	07/28/08	70m-36	5	6.75	
SMS	06/20/09	CNN-6	32	4.33		**SM**	07/06/09	XB2-4	4	3.92	
SMS	06/20/10	CN 8	7	3.24	N+P	**SM**	07/09/09	70m41	4	4.15	N+P
SMS	06/23/10	CNN 4	5	2.86	N+P	**SM**	06/30/10	70 m-40	5	4.59	N+P
SOS	06/21/10	CN 17	3	5.58		**SM**	07/02/10	MN-9	5	5.08	CF, B
SOS	06/18/09	CN-12	5	6.44		**SM**	07/09/10	70 m-50	36	−1.32	N+P
SOS	06/24/09	SB-1	5	6.16		**SM**	07/10/10	70 m-39	5	5.18	N
P	06/25/10	NP 9	6	3.77	N+P	**NMS**	07/12/08	SL-8	4	5.94	N, F
P	07/19/08	NP-11	3	4.26	N, F	**NMS**	07/26/08	SL-14	6	6.57	N, F
MNMS	07/14/08	NP-7	7	5.21	N, F	**NMS**	07/27/08	70m-53	7	6.77	
MNMS	06/22/09	NP-7	7	5.25	N*	**NMS**	07/08/09	70m58	10	3.30	N+P
MNMS	07/10/09	70m-25	6	4.67		**NMS**	07/06/10	ML-3	7	5.21	
MNMS	07/11/10	70m-25	3	6.53		**NMS**	07/07/10	SL 11	6	5.68	B
MNMS	07/11/10	70 m-25	28	-0.30	B	**NMS**	07/07/10	SL 11	33	−1.20	
MNIS	06/24/10	NP 1	4	3.62	N+P	**NMS**	07/08/10	BN-3	5	5.69	
MNIS	07/01/10	MN-1	5	3.52	N+P	**NMS**	07/08/10	BN-3	30	−1.22	
NOS	07/18/08	NP-14	5	7.41	N, F	**NMS**	07/09/10	70m-51	6	6.04	
NOS	07/15/08	NP-14	4	7.32	N, F	**NMS**	07/06/10	ML-3	7	5.21	N
NOS	07/20/08	LS1–6	5	7.47	N, F	**NIS**	07/09/08	MN-3	3	3.31	N
NOS	07/22/08	P14–2	7	7.07	N, F	**NIS**	07/11/08	W-4b	4	4.53	N, F
NOS	07/24/08	MN-12	7	6.24	N, F	**NIS**	07/01/09	MN-3	2	2.27	N*
NOS	07/25/08	MN-19	9	7.90	N, F	**OSN**	06/23/09	NP-15	4	6.40	N*
NOS	07/03/09	MN-19	10	6.03		**OSN**	06/26/09	P14-7	3	5.86	N+P
NOS	06/29/09	XB16	3	6.49	N*	**OSN**	06/28/10	P14N-10	10	5.77	N+P
NOS	07/04/09	X-6	2	5.50	N*	**OSN**	06/29/10	TR3	5	6.22	N
NOS	07/05/09	XB2–12	2	6.34		**OSN**	07/21/08	P14-4.5	7	7.72	N, F
NOS	06/26/10	TD2	4	5.86	N+P	**OSN**	06/25/09	SB-7	5	6.35	
NOS	06/27/10	SB-5	4	5.44	N+P	**OSSE**	06/19/09	CN-20	7	6.31	N
NOS	07/03/10	MN-16	7	5.36	N+P	**OSSE**	07/06/08	PIT-1	6	7.09	N
NOS	07/03/10	MN-18	26	1.65	B	**OSSE**	07/07/08	sta21	5	6.92	
NOS	07/04/10	TM4	35	1.67	B						
NOS	07/05/10	ML-13	3	5.97							

usual to run incubations with and without nutrient addition. *In situ* phytoplankton growth rate, μ, is estimated from the incubation without added nutrients and, if nutrient limitation is important, g can be determined from NGR and μ in the incubations with added nutrients.

To evaluate this, some, but not all, incubations were conducted with and without the addition of nutrients. In 2008, nutrient additions were 5 μM N as $NaNO_3$. Because inconsistent results were observed with the addition of nitrate alone, different nutrient additions were tried in subsequent years. In 2009, nutrient additions were as 5 μM N as NH_4Cl, and in 2010 nutrient additions were 5 μM N as $NaNO_3$ combined with 0.3 μM P as Na_2HPO_4. These additions are similar to those used by Strom and Fredrickson (2008) in earlier experiments in the Bering Sea which found no difference between N addition as NH_4Cl and $NaNO_3$.

All tubing, carboys, filter cartridges and incubation bottles were cleaned with 10% HCl, and rinsed three or more times with deionized water, and then rinsed with filtered seawater prior to use and between experiments (Landry, 1993). As mentioned earlier, in "mixed layer" experiments, water was collected with 30 L Niskin bottles on a CTD rosette from the depth corresponding to 55% surface irradiance level and in "DCM" experiments water was collected from the depth of chlorophyll fluorescence maximum. Seawater was gently siphoned (using silicone tubing) from Niskin bottles into black plastic covered polycarbonate carboys in the CTD bay. During siphoning, water was prescreened through a 200 μm Nitex mesh to remove larger zooplankton. This prescreened "whole seawater" (WSW) contained phytoplankton and microzooplankton, however when phytoplankton >200 μm (long diatom chains and large colonial phytoplankton) were present, the pre-screening removed them. Thus, the "WSW" contains a variable fraction of the total *in situ* chlorophyll. Filtered seawater (FSW) was prepared using gravity filtration and 0.2 μm pore size sterile Pall Capsule Filters. Treatments consisted of 100% WSW and diluted whole seawater. In early experiments 5% WSW was used for the diluted treatments (95% FSW), but in low chlorophyll waters it was difficult to obtain consistent chlorophyll measurements due to the low chlorophyll in the diluted treatment. A switch was made to 20% WSW (80% FSW and 20% WSW) when *in situ* chlorophyll levels were low. Silicon tubing was used to gently transfer, without bubbling, water (WSW or diluted seawater) from 20 l polycarbonate carboys to triplicate 1 l polycarbonate incubation bottles. If a nutrient addition series was included in an experiment, nutrient stock solution was added with a micropipette directly to triplicate WSW and diluted WSW incubation bottles.

At the beginning of each experiment, triplicate samples for chlorophyll (in effect, <200 μm chlorophyll because of the prescreening) were taken from the WSW and diluted seawater carboys. Samples for microzooplankton and *Phaeocystis* enumeration were siphoned directly from the Niskin bottles into 125 ml amber bottles and fixed with acid Lugol's solution as described (Stoecker et al., 2014). In mixed layer experiments (Table 1), the triplicate bottles for each treatment were incubated on deck in flowing sea-water with neutral density screening to approximate 55% surface irradiance. In DCM experiments, the bottles were incubated in the dark on ice in a cold room (Table 1). At the end of the incubations, chlorophyll samples were taken from each bottle. Chlorophyll samples were filtered onto 25 mm GF/F filters using gentle vacuum filtration, extracted in 90% acetone at -20 °C for 24 h, and then analyzed at sea with a pre-calibrated fluorometer (Turner Designs TD-700) (method modified from Parsons et al. (1984)). Total chlorophyll *a* for unscreened samples from the same stations and depths was available from the core measurements or from the primary production study (Lomas et al., 2012).

Chlorophyll *a* was used as a proxy for phytoplankton biomass. The intrinsic growth rate of phytoplankton (μ, d^{-1}) was calculated from the change in chlorophyll during incubations without and with added nutrients. Similarly, the net growth rate (NGR) of phytoplankton in the presence of microzooplankton grazing was calculated without and with added nutrients (Landry, 1993; Olson and Strom, 2002). Mortality due microzooplankton grazing, g, was calculated as $\mu - NGR$. The fraction of phytoplankton growth grazed per day was estimated as g/μ. Daily ingestion (I) of phytoplankton biomass ($\mu g\ C\ l^{-1}\ d^{-1}$) was estimated from chlorophyll consumption using a C:Chl ratio of 50 for the Bering Sea (Lomas et al., 2012) as $I=(\text{Chl a})(50)(g)$. Assuming a gross growth efficiency of 35% for strictly heterotrophic microzooplankton, secondary production based on herbivory was estimated (Landry and Calbet, 2004).

2.3. Variable fluorescence measurements

In several studies, insignificant grazing coefficients and/or statistically significant "negative" microzooplankton grazing rates have been reported from a proportion of the stations in the Bering Sea and also from other sub-Arctic and Arctic seas (Olson and Strom, 2002; Strom and Fredrickson, 2008; Calbet et al., 2011; Sherr et al., 2013). "Negative grazing" is impossible, but calculation of negative "g" results when the μ of phytoplankton in the diluted treatment is lower than in the WSW. Lower growth of phytoplankton in the diluted treatments than in the WSW is usually attributed to lack of regenerated nutrients due to low numbers of micrograzers in the diluted treatments. However, nutrient addition usually did not eliminate the effect in our experiments. To explore the possibility that dilution itself, or chemicals released from plankton into the dilution water during preparation of FSW, have a negative effect on phytoplankton, the ratio of variable to maximum fluorescence (Fv/Fm) of phytoplankton in the undiluted WSW and diluted treatments was determined. Fv/Fm ratio is a measure of the potential maximum quantum yield of PSII in phytoplankton. A decrease in the ratio of Fv/Fm is usually associated with a reduction in ability of the cells to photosynthesize. From an ecological perspective, a decrease in the Fv/Fm ratio has often been used as an indicator of physiological stress. Fv/Fm was measured after incubation of subsamples in the dark for ~1 h in a Automated Laser Fluorometer (ALF) (Chekalyuk and Hafez, 2008). A more detailed description of the instrument and the measurement protocols is available in Goes et al. (2014). Fv/Fm was measured in samples from the triplicate incubation bottles in the 100%WSW, 20%WSW, 100%WSW+nutrients, 20%WSW+nutrients treatments at the end of the 24 h incubations in mixed layer experiments at 14 stations in 2008 (Table 1). Samples were collected in 500 ml amber glass bottles, and stored in the dark for about 30 min, to minimize the impacts of non-photochemical quenching before analysis in the ALF.

2.4. Enumeration of P. pouchettii

The bloom forming phytoplankter *P. pouchettii* has been associated with inhibition of grazing in dilution experiments (Calbet et al., 2011). To determine if low grazing coefficients were associated with abundance of *Phaeocystis* cells, this phytoplankter was enumerated in whole water samples fixed with acid Lugol's (refer to Stoecker et al. (2014)) using a 1-ml capacity Sedgwick-Rafter counting chamber at 400× magnification. However, the actual density of *P. pouchettii* cells in the incubations must have been lower, because colonies >200 μm in size were removed by screening to remove copepods before setting up the dilution experiment incubations.

2.5. Statistical analyses

Analysis of variance (ANOVA) was used to test statistical significance ($p < 0.05$) of differences between the net growth rate of phytoplankton in the WSW and diluted treatments in an experiment. Significantly higher phytoplankton net growth rates in the diluted treatment than in the WSW treatment would indicate that grazing was significant. ANOVA was used to test for differences in coefficients from incubations with and without addition of nutrients, mixed layer versus DCM incubations, and among domains. Two-tailed *T*-tests were used to compare variable fluorescence measurements between diluted and undiluted treatments within an experiment. Pearson product-moment correlation tested for statistically significant associations between factors, with the square of the correlation coefficient, r^2, a measure of the variation in one variable determined by the variation in the other variable. If the data did not fulfill the assumptions for ANOVA, we applied appropriate transformations. ANOVA on ranks was used if data still did not meet the assumptions. Sigmaplot version 9.0 (Systat Software, Inc.) was used for all statistical analyses.

3. Results

3.1. Effect of nutrient additions

The results of paired dilution experiments conducted with and without the addition of nutrients were compared (Table 2). In calculating means and standard deviations, data from all paired incubations, whether or not grazing was statistically significant were included; "0" was substituted for negative "g" values in calculating means. In 2008, 21 comparative experiments were conducted, with and without the addition of 5 μM nitrogen as sodium nitrate. Mean phytoplankton growth rates (μ, d^{-1}) in the control (no nutrient addition) and nutrient addition treatments were similar, however grazing coefficients (g, d^{-1}) were significantly lower in the nutrient treatments (Table 2). In 2009, five comparative experiments were conducted in which the 5 μM nitrogen nutrient treatment was attained using ammonium chloride. The effects on phytoplankton growth and grazing were both non-significant (Table 2). In 2010, 15 experiments were conducted in which the nutrient treatment was addition of 5 μM nitrogen as sodium nitrate in combination with 0.35 μM phosphate as sodium phosphate. The nutrient treatment significantly increased mean phytoplankton growth but not estimation of microzooplankton grazing (Table 2). Nutrient additions are done to prevent greater nutrient limitation in diluted than in undiluted treatments in microzooplankton grazing experiments; greater nutrient limitation in diluted treatments would result in an underestimation of microzooplankton grazing (refer to Section 2.2) (Landry, 1993; Strom and Fredrickson, 2008). However, microzooplankton grazing coefficients were the same or lower with nutrient addition than without nutrient addition (Table 2), indicating that there was no reason to use data from the nutrient addition treatments to estimate microzooplankton grazing in our experiments. Based on these results, microzooplankton grazing is reported based upon the no addition dilution series. Olson and Strom (2002) also noted that nutrient enrichment sometime results in a decrease in phytoplankton growth rates in dilution experiments in the Bering Sea.

Table 2
Effect of nutrient additions (+Nuts) on phytoplankton growth (μ) and microzooplankton grazing (g) in dilution experiments, mixed layer, summer, Eastern Bering Sea 2008, 2009, 2010. Mean (SD).

Year	Number of experiments		Control	+Nuts[a]	Control vs. nuts [b]
2008	21	μ	0.31 (0.178)	0.31 (0.204)	ns
		g	0.24 (0.237)	0.11 (0.224)	*
2009	5	μ	0.17 (0.178)	0.18 (0.159)	ns
		g	0.12 (0.114)	0.08 (0.113)	ns
2010	15	μ	0.28 (0.157)	0.36 (0.165)	**
		g	0.21 (0.125)	0.21 (0.138)	ns

* $p \leq 0.05$.
** $p \leq 0.01$.
[a] 2008: 5 μM N as sodium nitrate; 2009: 5 μM N as NH_4Cl; 2010: 5 μM N as sodium nitrate +0.3 μM P as sodium phosphate.
[b] Repeated measures ANOVA: ns=non-significant.

3.2. Phytoplankton growth, microzooplankton grazing, ingestion and production in the mixed layer

The <200 μm fraction of the total chlorophyll ranged from an average of 69% at the Off Shelf, 79–90% at the Outer Shelf stations, 41–98% at the Middle Shelf stations, 77% at the Inner Shelf stations and 74% at the Alaska Peninsula stations (Table 3). Grazing coefficients were greater than "0" in 61% of the 59 dilution experiments conducted with mixed layer assemblages (Table 3). To avoid biasing the data against low growth and grazing rates, all coefficients were included, whether or not they were significant,

Table 3
Growth coefficients of phytoplankton (μ, d^{-1}) and microzooplankton grazing coefficients (g, d^{-1}), and roportion phytoplankton daily growth grazed by microzooplankton (g/μ). Mixed layer data for 2008, 2009, 2010 combined by region. Mean (SD). For g and μ, mean of all incubations without added nutrients, but "0" used for negative g.

Region	Chl a <200 μm (μg l^{-1})	% Chl a <200 μm	Incubation PAR (μE s^{-1} m^{-2})	μ	g	g/μ
Off Shelf						
Southeast (n=3, 1*)	0.77 (0.44)	nd	742 (300.1)	0.24 (0.16)	0.16 (0.16)	0.67
North (n=6, 4*)	0.60 (0.54)	69 (32)	278 (119.3)	0.30 (0.12)[a]	0.23 (0.09)[a]	0.77[a]
Outer Shelf						
South (n=3, 2*)	0.79 (0.22)	90 (14)	210 (151.6)	0.32 (0.20)	0.25 (0.15)	0.78
North (n=14, 9*)	0.89 (0.64)	79 (14)	328 (141.5)	0.25 (0.24)	0.19 (0.12)	0.76
Middle Shelf						
South (n=3, 2*)	0.38 (0.22)	98 (2)	517 (146)	0.27 (0.11)	0.24 (0.06)	0.89
Mid-North (n=4, 3*)	0.40 (0.35)	41 (49)	241 (41.0)	0.08 (0.62)	0.19 (0.20)	1.56
St. Matthews (n=8, 6*)	0.52 (0.52)	62 (1)	344 (184.5)	0.25 (0.15)	0.28 (0.22)	1.17
North (n=8, 4*)	0.33 (0.41)	97 (25)	440 (188.4)	0.24 (0.21)	0.34 (0.28)	1.42
Inner Shelf						
(South, Mid-North and North combined) (n=6, 3*)	0.47 (0.28)	77 (50)	263 (116.2)	0.19 (0.14)	0.22 (0.25)	1.16
AK Peninsula (n=4, 2*)	0.71 (0.47)	74 (30)	334	0.45 (0.23)	0.27 (0.22)	0.60

* Number of experiments in which g was statistically significant ($p < 0.05$).
[a] Calculated without one outlier replicate in one experiment. Nd=no data.

in our estimates of average rates. Exclusion of "0" or non-significant coefficients can inflate regional and global estimates of both phytoplankton growth and microzooplankton grazing (Landry and Calbet, 2005). However, negative grazing coefficients were replaced with "0" in averaging because negative grazing is not possible; calculation of a negative "g" occurs when phytoplankton net growth is lower in the diluted treatment than undiluted treatment, and there are several reasons for this phenomenon (refer to Section 3.4). In these instances, the phytoplankton growth rate in WSW was substituted for the rate in the diluted treatment.

If data from the Mid-North region are excluded, average phytoplankton growth coefficients were in the range of 0.19–0.45 d^{-1} (Table 3). The average phytoplankton growth coefficient for the mid-north Middle Shelf was low (Table 3) because of one experiment with a significant negative growth rate ($\mu = -0.80$); without this one experiment, the average of the regional growth rates was 0.37 d^{-1}. The average phytoplankton growth rate in the Alaska Peninsula region appeared to be higher than rates in the other areas, but differences among regions were not statistically significant (1-WAY ANOVA, $p > 0.05$). Likewise, estimates of average microzooplankton grazing were relatively similar across regions, ranging from 0.16 to 0.34 d^{-1} (Table 3) and differences among regions were not statistically significant (1-WAY ANOVA, $p > 0.05$). Correlations between μ or g and mixed layer water temperature, inorganic nutrients (phosphate, silicate, nitrate, ammonium) and estimated total PAR for incubations (data not shown) were not statistically significant (Pearson Product Moment Correlation; $p > 0.05$). Both microzooplankton grazing and phytoplankton growth coefficients correlated negatively with total chlorophyll *a*, but the coefficients of determination (r^2) were low (Fig. 2A and B). Microzooplankton grazing (< 200 μm fraction) was not correlated with the biomass of 20–200 μm ciliate and dinoflagellate microzooplankton ($p > 0.05$) (data not shown). Microzooplankton grazing was also not correlated with abundance of *Phaeocystis* cells ($p > 0.05$) (data not shown).

The proportion of phytoplankton growth grazed by the < 200 μm fraction was calculated as "g/μ" from the average "g" and "μ" for regions (Table 3). Estimates for individual incubations could not be made because of negative or zero coefficients. Estimated average proportion of phytoplankton growth in the < 200 μm fraction grazed by phytoplankton appeared to vary among regions (Fig. 3). In the Off Shelf and Outer Shelf regions, microzooplankton grazing consumed 67–78% of phytoplankton growth but on the Middle Shelf and Inner Shelf (with the exception of the south Middle Shelf) microzooplankton grazing coefficients were greater than phytoplankton growth rates in the mixed layer (Fig. 3 and Table 3).

Estimated phytoplankton carbon ingestion by microzooplankton was 11.0 μg carbon l^{-1} d^{-1} in the Alaska Peninsula region, 8.2 Off Shelf, 7.7 on the Outer Shelf, 4.7 on the Middle Shelf and 4.4 d^{-1} on the Inner Shelf, with differences among regions not statistically significant (1 Way ANOVA, $p > 0.05$) (Fig. 4). Assuming that all microzooplankton were strictly heterotrophic and a gross growth efficiency of 35%, the estimated secondary production of microzooplankton in the mixed layer was 3.8 μg carbon l^{-1} d^{-1}, 2.9, 2.7, 1.6, and 1.5 for the Alaska Peninsula, Off Shelf, Outer Shelf, Middle Shelf and Inner Shelf regions, respectively. However, because of the prevalence of mixotrophy among the ciliates, it is possible that average gross growth efficiently of the microzooplankton was higher and thus secondary production higher (Stoecker et al., 2014).

3.3. *Microzooplankton grazing, ingestion and production in the DCM*

Dilution grazing experiments were conducted with deep chlorophyll maximum assemblages at four stations in 2010, with DCM experiments paired with mixed layer incubations at the same station

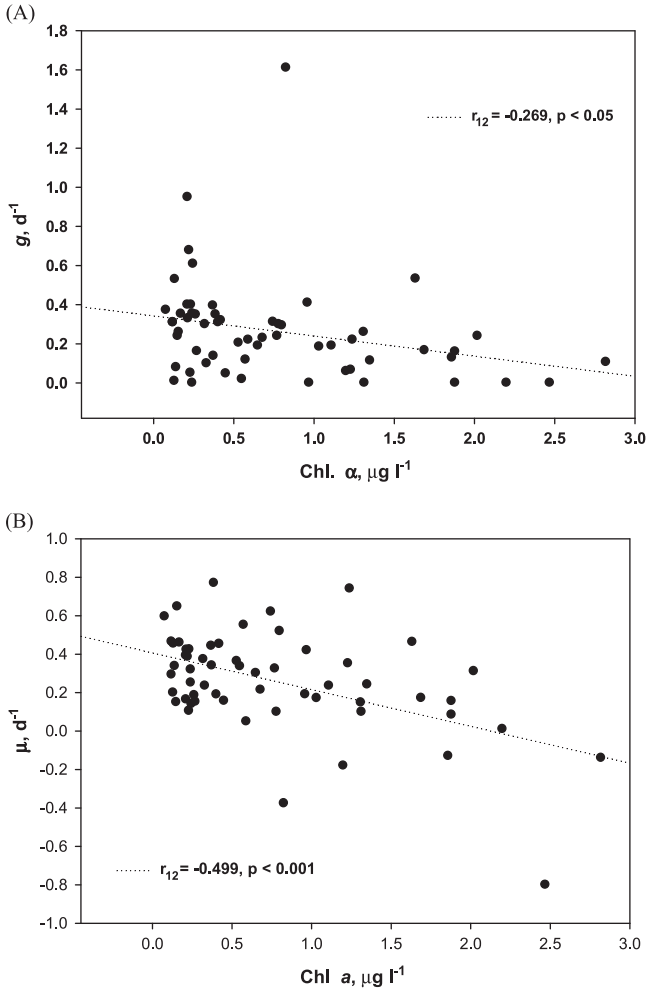

Fig. 2. Microzooplankton grazing coefficients (g, d^{-1}) (A) and phytoplankton growth (μ, d^{-1}) (B) vs. chlorophyll *a*, mixed layer, Eastern Bering Sea. Data for summers 2008, 2009 and 2010 were included; no nutrient addition treatments only. Product moment correlation coefficients (r_{12}) are shown as well as their statistical significance. The coefficient of determination, r^2, was 0.072 and 0.236 in A and B, respectively, indicating that variation in chlorophyll only determined a small proportion of the variation in grazing and phytoplankton growth coefficients.

(Table 4). Irradiance levels and water temperatures were low in the DCM; experiments were incubated in the dark on ice (~0 °C) in a cold room (Table 4). Incubation temperatures were 0.3–1.2 °C higher than *in situ* DCM water temperatures, which may have resulted in slightly elevated grazing. Grazing coefficients in the DCM ranged from ~0 to 0.70 d^{-1} and in two out of four DCM incubations, the grazing coefficients were significant ($p < 0.05$) (Table 4). It is interesting that in paired mixed layer and DCM incubations, the DCM grazing coefficients were similar in magnitude to the mixed layer coefficients (Table 4). However, because of the higher phytoplankton biomass in the DCM than in the mixed layer, the estimated ingestion of phytoplankton carbon by microzooplankton in the DCM was higher than in the mixed layer (Fig. 5). Assuming similar C:Chl ratios and gross growth efficiencies for microzooplankton in the mixed layer (refer to Section 3.2) and the DCM, microzooplankton production can be compared for the stations with statistically significant grazing in both layers (Table 4). At station SL-11, the calculated microzooplankton production in the mixed layer was 5.0 and in the DCM 13.2 μg C l^{-1} d^{-1}. At station BN-3, the calculated microzooplankton production in the mixed layer was 0.5 and in the DCM 3.1 μg C l^{-1} d^{-1}. (Production estimates were not made for experiments in which grazing was not statistical significant (Table 4).)

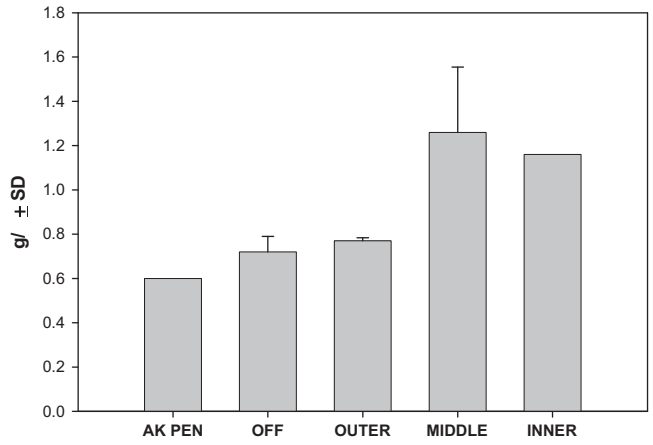

Fig. 3. Estimated fraction of phytoplankton daily growth consumed by microzooplankton grazing (g/μ) in the mixed layer, Eastern Bering Sea, summers 2008, 2009, 2010 (no nutrient addition treatments only). For each region, mean grazing (g) and growth (μ) coefficients (Table 3) were used to calculate a regional "g/u" (refer to Section 3.2). For each of the domains (OFF, OUTER, MIDDLE) with data for several regions (Table 3), the regional estimates were averaged to obtain a domain mean "g/μ". For the domain (AK PEN) with one region (Table 3) and for the domain (INNER) with data for only a few stations (Table 3), data from individual stations were used to calculate average g and u for the domain and then these averages were used to calculate the g/u for the domain. AK PEN=Alaska Peninsula region; OFF=off shelf; OUTER=outer shelf; MIDDLE=middle shelf; INNER=inner shelf or coastal. Data combined for summers 2008, 2009, and 2010. Error bars indicate standard deviation for OFF, OUTER, and MIDDLE domains.

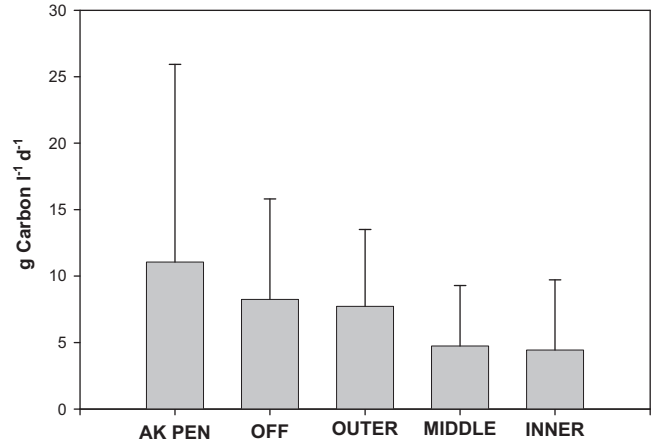

Fig. 4. Estimated microzooplankton ingestion of phytoplankton carbon in the mixed layer, Eastern Bering Sea, summers 2008, 2009, 2010. Estimates of ingestion from stations within a domain were averaged. AK PEN=Alaska Peninsula region; OFF=off shelf; OUTER=outer shelf; MIDDLE=middle shelf; INNER=inner shelf or coastal. Error bars indicate standard deviation.

Microzooplankton secondary production in the DCM on a per liter basis may be several fold higher than in the mixed layer.

3.4. Non-significant and "negative" grazing coefficients and Fv/Fm

In 39% of our dilution grazing experiments with mixed layer assemblages the grazing coefficients were not statistically significant ($p > 0.05$) and in 3% of our experiments grazing coefficients were statistically significant, but negative. Estimation of microzooplankton grazing in dilution experiments is based on the assumption that phytoplankton growth rate is the same in diluted and undiluted treatments. To determine if dilution was having a negative effect on the physiology of phytoplankton, and potentially on their growth rates, variable fluorescence (Fv/Fm) was measured in both the undiluted (WSW) and diluted (20% WSW) treatments at the end of paired incubations with and without added nitrate (Table 1). Fv/Fm was significantly lower (T-test, $p < 0.05$) in the diluted than undiluted treatments in eight out of 14 incubations without added nutrients and in seven out of 14 incubations with added nutrients (Table 5). Fv/Fm was significantly higher ($p < 0.05$) in the diluted treatments with than without added nitrate in three of the 14 experiments (data not shown). In only two experiments did this alleviate the negative effect of dilution on variable fluorescence of phytoplankton (Table 5). Low estimates of microzooplankton grazing coefficient were associated with experiments in which dilution had a large negative effect on Fv/Fm (Fig. 6).

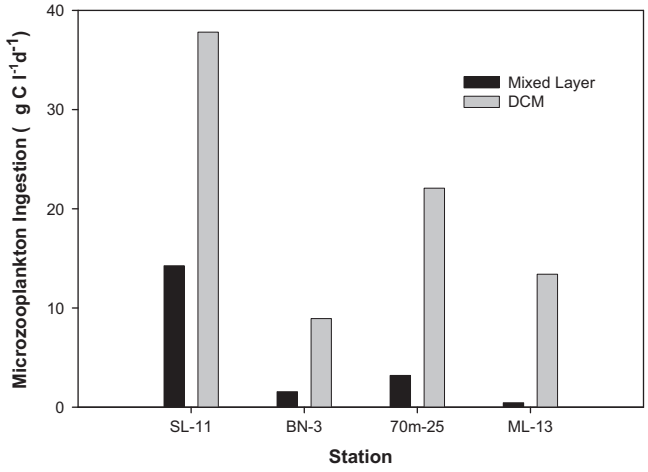

Fig. 5. Comparison of estimated microzooplankton ingestion of phytoplankton carbon, paired mixed layer and DCM experiments, Eastern Bering Sea, summer 2010.

Table 4
Paired deep chlorophyll maximum (DCM) and Mixed layer (ML) Dilution experiments, Middle Shelf, summer 2010. P-value indicates the statistical significance of the difference between the net growth rate of phytoplankton in the WSW and diluted treatment. ns=non-significant.

Domain (region)	Station	Sample depth (m)	Temp. (°C) In situ	Temp. (°C) Incub.	Avg. Incub. Irradiance μ E s^{-1} m^{-2}	Chlorophyll a (t_0) ($\mu g\ l^{-1}$)	μ	g	ANOVA p-value
Middle (10)	SL-11	6-ML	5.6	~6	347	0.30	0.16	0.95	< 0.001
		33-DCM	−1.2	~0	Dark	1.08	−1.03	0.70	< 0.001
Middle (10)	BN-3	5-ML	5.7	~6	524	0.10	0.29	0.31	< 0.01
		30-DCM	−1.2	~0	Dark	0.85	0.03	0.21	< 0.01
Middle(6)	70m-25	3-ML	6.5	~6	262	0.16	0.39	0.40	< 0.05
		28-DCM	−0.3	~0	Dark	1.84	−0.03	0.24	ns
Outer (8)	ML-13	3-ML	6.0	~6	330	0.11	0.34	0.08	ns
		35-DCM	−1.1	~0	Dark	5.36	0.04	0.05	ns

Table 5
Variable fluorescence (Fv/Fm) at the end of mixed layer dilution experiments in undiluted (WSW) and diluted (20% WSW) treatments without and with the addition of 0.05 μM N as sodium nitrate. All experiments conducted in summer 2008. $N=2$ or 3.

Station	Mean (SD), no nutrient addition		*T*-test	Mean (SD), nutrient addition		*T*-test
	WSW	20%WSW	*p*	WSW	20%WSW	*p*
C-55	0.345 (0.0071)	0.357 (0.0896)	ns	0.348 (0.031)	0.353 (0.459)	ns
W-4b	0.237 (0.0379)	0.263 (0.0752)	ns	0.245 (0.028)	0.283 (0.031)	ns
SL-8	0.350 (0.0433)	0.327 (0.0431)	ns	0.353 (0.040)	0.426 (0.087)	ns
NP-7	0.330 (0.0100)	0.232 (0.0126)	$p<0.05$	0.310 (0.010)	0.357 (0.041)	ns
NP-14	0.183 (0.1626)	0.198 (0.0775)	ns	0.317 (0.063)	0.270 (0.020)	ns
NP-14	0.263 (0.0115)	0.220 (0.0200)	$p<0.05$	0.268 (0.010)	0.267 (0.018)	ns
NP-11	0.341 (0.0136)	0.315 (0.0391)	ns	0.362 (0.007)	0.300 (0.025)	$p<0.05$
LS1-6	0.343 (0.0152)	0.278 (0.0202)	$p<0.05$	0.345 (0.008)	0.265 (0.007)	$p<0.05$
P14-4.5	0.253 (0.0144)	0.158 (0.0126)	$p<0.05$	0.268 (0.029)	0.183 (0.023)	$p<0.05$
P14-2	0.298 (0.0126)	0.233 (0.0252)	$p<0.05$	0.313 (0.005)	0.245 (0.022)	$p<0.05$
MN-6	0.280 (0.0173)	0.227 (0.0058)	$p<0.05$	0.307 (0.011)	0.247 (0.005)	$p<0.05$
MN-12	0.245 (0.0071)	0.153 (0.0153)	$p<0.05$	0.273 (0.028)	0.150 (0.014)	$p<0.05$
MN-19	0.250 (0.0173)	0.183 (0.0289)	$p<0.05$	0.240 (0.026)	0.163 (0.032)	$p<0.05$
SL-14	0.263 (0.0306)	0.210 (0.0346)	ns	0.283 (0.064)	0.233 (0.010)	ns

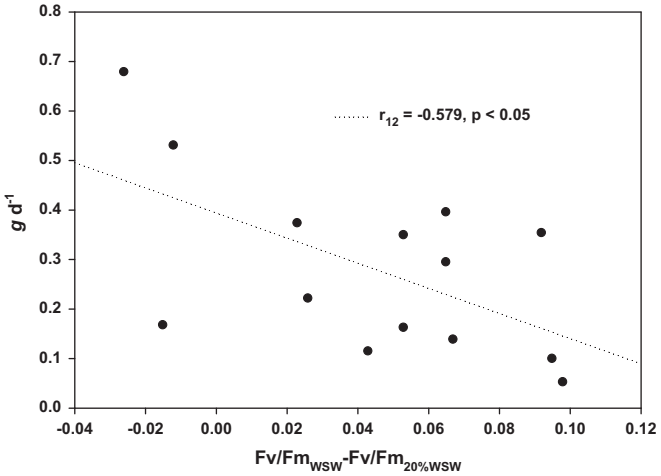

Fig. 6. Estimated microzooplankton grazing coefficients (g, d^{-1}) vs. the difference in variable fluorescence (Fv/Fm) between WSW and diluted treatments in an experiment. The product moment correlation coefficient (r_{12}) and its statistical significance are shown. Low grazing was associated with decreased Fv/Fm in the diluted compared to the whole seawater treatments. The coefficient of determination (r^2) was 0.335.

4. Discussion

During summers of 2008–2010, all "cold years" in the Eastern Bering Sea (Stabeno et al., 2012b), the over-all average mixed layer microzooplankton grazing coefficient was 0.26 d^{-1}, which is quite similar to the average coefficient of 0.29 d^{-1} observed on the SE shelf by Olson and Strom (2002) during summer 1999, another cold year (Table 6). In 2004, a "warm year" (Ladd and Stabeno, 2012), microzooplankton grazing was low on the SE Shelf (Strom and Fredrickson, 2008) (Table 6). The low grazing in 2004 was probably a response of microzooplankton to poor food quality caused by phytoplankton nutrient limitation due to intense stratification (Strom and Fredrickson, 2008), however "warm" years are not always associated with high stratification on the Bering Sea Shelf (Ladd and Stabeno, 2012), so it is unlikely that summer microzooplankton grazing is predictable from temperature alone. During 2004, phytoplankton growth rates responded strongly to addition of nutrients (Strom and Fredrickson, 2008) but increases in phytoplankton growth in response to nutrient additions were only observed in one year, 2010, in our study (Table 2). Contrary to expectations, nutrient addition sometimes resulted in lower estimates of phytoplankton growth and sometimes microzooplankton grazing. Possible inhibition of growth and grazing due to nutrient addition has been previously reported, but the reasons for inhibition are not understood (Gifford, 1988; Olson and Strom, 2002).

Average microzooplankton grazing coefficients during spring sea ice conditions are $<50\%$ of summer grazing coefficients (Table 6). The lower grazing coefficients in spring are probably due to a combination of factors including lower ratios of microzooplankton biomass to phytoplankton biomass in spring than in summer (Sherr et al., 2013; Stoecker et al., 2014), differences in size distribution and species composition of phytoplankton (Lomas et al., 2012) and lower water temperatures in spring (Rose and Caron, 2007; Rose et al., 2013).

It is interesting that both the growth rate of phytoplankton (μ) and microzooplankton grazing (g) was correlated negatively with total chlorophyll *a* in the mixed layer. Negative or no correlation of growth and grazing coefficients with chlorophyll have also been noted by Olson and Strom (2002), Strom et al. (2007), and Calbet et al. (2011) in northern seas in summer. This is consistent with domination of the phytoplankton by <5 μm cells, and a rate, rather than biomass, controlled production system dependent on nutrient recycling (Lomas et al., 2012). Based on primary production measurements, integrated phytoplankton growth rates (μ) averaged 0.42 d^{-1} (SD, 0.17) (Lomas et al., 2012), which is within the wide range of phytoplankton growth rates that we estimated in mixed layer dilution experiments (Table 6). In the north middle and inner domains, the biomass of microzooplankton to phytoplankton was high in summer (Stoecker et al., 2014), consistent with the high ratios of microzooplankton grazing to phytoplankton growth. A confounding factor in estimating phytoplankton growth and microzooplankton grazing from chlorophyll in dilution experiments on the Bering Sea Shelf is the high biomass of plastidic ciliates in summer (Stoecker et al., 2014). The incorporation of phytoplankton chloroplasts into ciliates may result in underestimation of microzooplankton grazing and an overestimate of "phytoplankton" biomass.

Comparison of the spatial distributions of phytoplankton growth, microzooplankton grazing, chlorophyll *a*, variable fluorescence, and phytoplankton composition from the HPLC (Goes et al., 2014) revealed similar patterns among some of the variables and identified the phytoplankton communities associated with different growth and grazing coefficients during summer 2008. High phytoplankton growth (μ, d^{-1}) and moderate microzooplankton grazing (g, d^{-1}) were measured on the north Middle Shelf, where diatom and cryptophytes patches, probably remnants of spring ice associated blooms, were observed (Fig. 7). Elevated phytoplankton

Table 6
Comparison of hydrographic conditions, phytoplankton growth coefficients and microzooplankton grazing coefficients from mixed layer dilution experiments conducted in the Bering Sea. Years classified as warm or cold, with high or low stratification index (Ladd and Stabeno, 2012; Stabeno et al., 2012b). Phytoplankton growth rates (μ) and MZ grazing rates (g) per day. Average with SD in parentheses, or range.

Cruise dates and hydrographic conditions in SE Bering Sea	Water (°C)	Growth	Grazing	Ref.
July 99: South Bering Sea (Off Shelf and Outer Shelf) (cold year)	5.3–7.7	0.2–0.6, 0.41 (n=5)	0.1–0.4, 0.27, (n=5)	Liu et al. (2002)
July–August 99; SE Bering Sea (cold year with low stratification index)	5.8–8.4	−0.7 to 0.6, 0.33 (n=13)	0.1–0.5, 0.29, (n=13)	Olson and Strom (2002)
July–August 04: SE Bering Sea (warm year with high stratification index)	9.3–13.4	0.0–1.0, 0.35 (n=18)	0.0–0.27, 0.13, (n=18)	Strom and Fredrickson (2008)
April–May, 2008, 2009, 2010-Non bloom, Eastern Bering Sea, ice edge (cold years)	−0.3 (1.4)	0.17 (0.14), n=17	0.08 (0.12), n=17	Sherr et al. (2013)
April–May, 2008, 2009, 2010-Bloom, Eastern Bering Sea, ice edge (cold years)	0.8 (1.7)	0.21 (0.12), n=21	0.09 (0.08), n=21	Sherr et al. (2013)
June–July, 2008, 2009, 2010-Eastern Bering Sea (cold years; low stratification index in 2008, stratification classification for 2009 & 2010 not yet available)	2.3–7.9	−0.8–0.8, 0.26, (n=61)	0.0–0.9, 0.26, (n=61)	This study

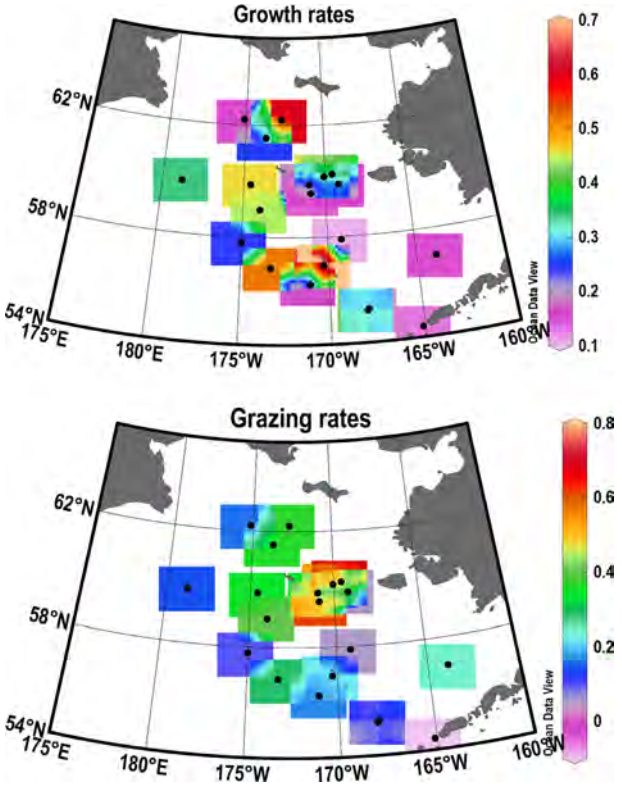

Fig. 7. Spatial distribution of phytoplankton growth (μ, d^{-1}) (upper panel) and microzooplankton grazing (g, d^{-1}) (lower panel) in the eastern Bering Sea, summer 2008.

growth and microzooplankton grazing were observed on the Middle Shelf near 60°N, at the border between the St. Matthews and north Inner Shelf regions. This area was characterized by relatively low surface chlorophyll *a* and moderate variable fluorescence. Diatom patches were observed to the east and haptophytes to the west of 170°W in this area. Phytoplankton growth and microzooplankton grazing were also relatively high on parts of the north Outer Shelf and Off Shelf north regions on the inner edge of the greenbelt. The greenbelt was characterized by low to moderate surface chlorophyll *a*, moderate variable fluorescence and dominance of phytoplankton biomass by cryptophytes and haptophytes. The Pribilof Island area was a hot spot for phytoplankton growth, with patches of both diatoms and haptophytes present, but microzooplankton grazing was moderate in this region. In contrast, the southeastern shelf and Peninsula area tended to have lower phytoplankton growth and microzooplankton grazing coefficients, although small flagellates, including cryptophytes and haptophytes, dominated (Goes et al., 2014).

In 2004, weak trophic coupling of phytoplankton growth to microzooplankton grazing was observed (Strom and Fredrickson, 2008), but strong coupling was observed in 1999 (Olson and Strom, 2002) and in summers of 2008, 2009, and 2010 (Table 6). On the shelf, microzooplankton grazing coefficients (g) often exceeded phytoplankton growth coefficients (μ) in the mixed layer, but g/μ was <1 in Alaska Peninsula, Off Shelf and Outer Shelf waters in summer (Table 3). On average, grazing is equivalent to phytoplankton growth in the sea (Banse, 1992), with ratios of g to μ exceeding 1 often found during the demise of blooms. For example, in the more southerly Gulf of Alaska, the ratio of microzooplankton grazing to phytoplankton growth on the Middle and Inner Shelf reaches a maximum in summer with $g/\mu > 1.0$ whereas in summer the ratio is lower on the Outer Shelf (Strom et al., 2007), similar to our observations in the Eastern Bering Sea. Another example is the Sea of Okhotsk, Liu et al. (2009) found that microzooplankton grazing (g) was about three times higher than phytoplankton growth (μ) in late summer in nutrient-depleted shelf waters whereas in the higher nutrient shelf break and strait waters, g/μ estimates were <0.5. Ratios of microzooplankton grazing to phytoplankton growth in excess of 1 may be a general, although transient, feature of highly stratified boreal and Arctic Shelf ecosystems in summer.

Large copepods, such as *Neocalanus* spp., *Calanus glacialis*, and *Metridia longa*, have a strong prey preference for microzooplankton, but are largely absent from the Middle and Inner Shelf waters in summer (Vidal and Smith, 1986; Gifford, 1993; Campbell et al., 2009; Hunt et al., 2008). A reduction in top down control of microzooplankton on the Eastern Bering Sea Shelf may be partially responsible for the high biomass of microzooplankton (Stoecker et al., 2014) and their high grazing impact on the Bering Sea Shelf in summer. A similar phenomenon occurs on the Gulf of Alaska Shelf, where summer populations of large copepods are low and large cell-size microzooplankton are very abundant due to diminished top down control (Strom et al., 2007).

Although the grazing impact of microzooplankton on phytoplankton growth (g/μ) was highest in Middle and Inner Shelf waters, estimated microzooplankton ingestion of phytoplankton carbon and secondary production of microzooplankton was highest in the Alaska Peninsula, Off Shelf and Outer Shelf waters. This was due to higher chlorophyll levels than on the Middle and Inner

Shelf. However, microzooplankton (20–200 μm) biomass in the Off Shelf and Outer Shelf regions was about half that in the inner and middle domains (Stoecker et al., 2014). One reason for this discrepancy may be that grazing by nanozooplankton (which are not included in the microzooplankton biomass estimates) makes a larger contribution to grazing in the higher chlorophyll regions. Nanozooplankton have been shown to be more abundant in frontal areas on the Outer Shelf and at the shelf break than in lower chlorophyll inner and middle domains in summer (Flint et al., 2002). The relatively low biomass of 20–200 μm microzooplankton (ciliates and large dinoflagellates) and high biomass of nanozooplankton in Peninsula, Off Shelf and Outer Shelf waters suggests a trophic cascade in which top down control of large microzooplankton by crustacean zooplankton releases nanozooplankton from grazing control. Conversely, large microzooplankton are probably relatively more abundant on the shelf in summer due to relaxation in top down control by large copepods which are mostly absent from the shelf in summer (Vidal and Smith, 1986; Hunt et al., 2008).

During the summer, the DCM in the northern domain can be well developed with >10 μg chlorophyll $a\,l^{-1}$ at some stations (Lomas et al., 2012; Goes et al., 2014). Thus, the processes within the DCM may be very important to carbon flux and trophic transfer. Microzooplankton biomass (Stoecker et al., 2014) was usually similar in the DCM to that in the mixed layer above. Although grazing coefficients were also roughly similar in the mixed layer and corresponding DCM, the calculated ingestion rates in the DCM were higher than in the mixed layer (Fig. 5). This difference might be partly due to differences in C:Chl *a* ratio in the mixed layer and in the DCM. The DCM samples ranged in depth from 26 to 35 m (Table 4), which was near or below the average depth of the 1% PAR isolume, 30 m (Lomas et al., 2012). Microalgae grown at low irradiances have lower C:Chl *a* than microalgae grown at higher irradiances; C:Chl *a* of ~25 is often observed in light limited phytoplankton (Geider 1987). Applying an average C:Chl. of 50 for the Bering Sea (Lomas et al., 2012) to the DCM might result in over-estimation of microzooplankton carbon ingestion by up to ~2 fold. If we assume that phytoplankton growth was low at these depths due to the low irradiance, the ratio of grazing to phytoplankton growth must have been very high. Microzooplankton grazing is often important in erosion of "plankton patches" (Menden-Deurer and Fredrickson, 2010).

If we assume that microzooplankton growth efficiency was similar in the mixed layer and DCM, the DCM may be an important site of microzooplankton production during summer, particularly on the northern shelf. The lack of accumulation of microzooplankton biomass in the DCM suggests that predation pressure on microzooplankton is high and thus that these layers may be important in trophic transfer to higher trophic levels. The impact of microzooplankton grazing on phytoplankton and export fluxes can be under-estimated if grazing near the base of the euphotic zone is not included (Landry et al., 2011).

The decrease in variable fluorescence during the incubations from some stations suggests that dilution had a negative impact on phytoplankton photosynthetic physiology and hence potentially growth rate. This effect was most evident at Off Shelf and Outer Shelf "bloom" locations. This effect was not simply due to N limitation alone in the diluted treatments; it occurred in control and, in most cases, the paired nitrate amended dilutions. One of the assumptions of the dilution method is that dilution does not change the growth rate of phytoplankton, and this assumption likely was violated in at least some dilution experiments. A decrease in phytoplankton growth rate with dilution would result in an underestimation of the grazing coefficients. This may partially account for the low or non- significant grazing coefficients. Low grazing rates of microzooplankton for the biomass of microzooplankton have previously been reported in the SE Bering Sea during intense summer stratification and nutrient limitation of phytoplankton (Strom and Fredrickson, 2008). Non-significant microzooplankton grazing coefficients have also been reported during the spring at both non-bloom and diatom bloom ice edge stations (Sherr et al., 2013). In addition to non-significant grazing coefficients, statistically significant negative rates occur. Negative dilution grazing results are usually not reported (Dolan and McKeon, 2005), or the negative coefficients treated as "0" (Strom and Fredrickson, 2008). Negative rates can only occur when the growth rate of phytoplankton, μ, is lower in the diluted treatment than in the whole seawater. In polar and subpolar ecosystems, non-significant and negative results in dilution experiments are common, particularly during *Phaeocystis* blooms (Calbet et al., 2011; Caron et al., 2000).

In culturing phytoplankton, a "lag" phase typically occurs after transfer of cells to new media, this has been ascribed to the time it takes cells to "ramp up" to better growth conditions, the "shock" of transfer and to lack of "conditioning factors" in the media. Perhaps something similar happens when phytoplankton are diluted with filtered seawater. Another possibility is that the mechanical stress involved in passage through filters results in release of "toxic" or "inhibitory" compounds into the filtered seawater used to make the dilutions. Strom and Fredrickson (2008) noted that release of diatom extracts from filters used to prepare filtered seawater may have inhibited growth of phytoplankton. During certain growth phases, *P. pouchetti* and many bloom forming diatoms produce cytotoxic aldehydes that are inhibitory to phytoplankton growth, including their own (Hansen and Eilertson, 2007; Paul et al., 2009). Mechanical stress can trigger the release of these compounds from cells (Hansen and Eilertson, 2007). We hypothesize that decreases in variable fluorescence and low or negative phytoplankton growth rates in diluted treatments could be due to presence of toxic aldehydes released from phytoplankton during preparation of filtered seawater. Preliminary results indicate that with some diatom and *Phaeocystis* blooms, treatment of filtered seawater with activated carbon to remove organic material prior to its use in dilution can reverse the negative effects on both "μ" and "g" (Stoecker and Nejstgaard, unpubl. data). However, contrary to expectation, grazing coefficients were not negatively correlated with abundance of *P. pouchetti* cells in the Bering Sea. Production of inhibitory compounds by *Phaeocystis* varies with life form and bloom stage (Nejstgaard et al., 2007), thus not all *Phaeocystis* cells will have the same impact on water chemistry. Furthermore, diatoms are also a source of cytotoxic aldehydes and are bloom dominants in the Bering Sea (Flint et al., 2002; Lomas et al., 2012). A simple relationship between one of these factors (*Phaeocystis* cells) and apparent low grazing coefficients is unlikely due to confounding factors.

Overestimation of microzooplankton grazing by the dilution technique may occur due to increases in microzooplankton populations because of the exclusion of mesozooplankton predators from the incubation bottles and starvation of microzooplankton in the diluted treatments (Dolan et al., 2000; Dolan and McKeon, 2005; Modigh and Franze, 2009). However, internal predation (microzooplankton predation on micro- and nanozooplankton) in incubations can lead to trophic cascades as well, decreasing grazing on phytoplankton (Stoecker and Evans, 1985; First et al., 2007, 2009). First et al. (2007) conducted dilution experiments in a range of temperate environments (coastal lagoons to offshore locations) and found that although microzooplankton biomass increased or decreased over time in most dilution experiments, adjusting for the actual grazer gradient did not significantly affect the estimated rates of microzooplankton grazing. In cold, subarctic waters the potential daily growth rate of microzooplankton is lower than in temperate waters and thus it is reasonable to

assume that changes in grazer density and the effect on grazing coefficients would also be lower than in the First et al. (2007) study in temperate waters.

To evaluate the potential increase of microzooplankton geometric mean biomass in our incubations, the increased microzooplankton biomass (C_t) at the end of incubations was calculated as the average microzooplankton biomass (C_o) for a domain (Stoecker et al., 2014) plus the estimated daily microzooplankton secondary production in that domain (Section 3.3). The geometric mean microzooplankton biomass, $\langle C\rangle$, during incubations was calculated as $\langle C\rangle=(C_t-C_o)/(\ln C_t-\ln C_o)$ (modified from Heinbokel (1978)). The average percent increase in microzooplankton biomass during an incubation was calculated as $((\langle C\rangle-C_o)\times 100)/C_o$). Using comparable domain data for biomass and secondary production, the potential elevation in microzooplankton biomass during the incubations was 3%, 4%, 10% and 11% in mixed layer dilution experiments conducted in the Inner Shelf, Middle Shelf, Outer Shelf, and shelf break/Off Shelf domains, respectively. Given the variability in estimated grazing typically found in dilution experiments, it seems unlikely that these relatively small potential increases in microzooplankton biomass would significantly influence estimates of microzooplankton grazing. In our experiments, it seems more likely that average microzooplankton grazing was underestimated, particularly in the Off Shelf and Outer Shelf waters, due to decreased phytoplankton growth in the diluted treatment in some incubations.

Whether or not grazing is underestimated or slightly over estimated, it is clear that microzooplankton grazing consumes most of phytoplankton production and that secondary production by microzooplankton is important. Most phytoplankton production is by <5 μm phytoplankton and thus passes through the microzooplankton link before it is available to crustacean zooplankton in summer. On the northern shelf, the DCM may often be a site of enhanced trophic transfer. Microzooplankton can comprise 49% or more of the food available to larger zooplankton on the Bering Sea Shelf in summer (Stoecker et al., 2014).

Acknowledgments

The authors thank the captain and crew of the *USCG Healy*, R/V *Knorr* and R/V *T.G. Thompson* for their assistance during the cruises. We thank Michael Lomas for advice and use of his fluorometer, Dean Stockwell and Michael Lomas for chlorophyll data, Carol Feierabend for enumerating *Phaeocystis* cells, Helga Gomes for help with the variable fluorescence measurements and Kristin Blattner for excellent technical assistance in 2008 and 2009. We thank Peter Lavrentyev for his thoughtful comments that improved the manuscript. DKS and AW were supported by Bering Sea Integrated Ecosystem Research Program (BSIERP) Project no. 55. JIG was supported by funding from the NASA. This is BEST-BSIERP Bering Sea Project publication no. 115, NPRB Publication no. 447 and UMCES Contribution no. 4807.

Reference

Banse, K., 1992. Grazing, temporal changes in phytoplankton concentrations, and the microbial loop in the open sea. In: Falkowski, P.G., Woods, A.D. (Eds.), Primary Productivity and Biogeochemical Cycles in the Sea. Plenum Press, New York, pp. 409–440.

Calbet, A., Saiz, E., 2005. The ciliate-copepod link in marine ecosystems. Aquat. Microb. Ecol. 38, 157–167.

Calbet, A., Saiz, E., Almeda, R., Movilla, J.I., Alcarez, M., 2011. Low microzooplankton grazing rates in the Arctic Ocean during a *Phaeocystis pouchetti* bloom (Summer 2007): fact or artifact of the dilution technique? J. Plankton Res. 33, 687–701.

Campbell, R.G., Sherr, E.B., Ashjian, C.J., Plourde, S., Sherr, B.F., Hill, V., Stockwell, D.A., 2009. Mesozooplankton prey preferences and grazing impact in the Western Arctic Ocean. Deep-Sea Res. II 56, 1274–1289.

Caron, D.A., Dennett, M.R., Lonsdale, D.J., et al., 2000. Microzooplankton herbivory in the Ross Sea, Antarctica. Deep-Sea Res. II 47, 3249–3272.

Chekalyuk, A., Hafez, M.A., 2008. Advanced laser fluorometry of natural aquatic environments. Limnol. Oceanogr., Methods 6, 591–609.

Dolan, J.R., McKeon, K., 2005. The reliability of grazing rate estimates from dilution experiments: have we over-estimated rates of organic carbon consumption by microzooplankton? Ocean Sci. 1, 1–7.

Dolan, J.R., Gallegos, C.L., Moigis, A., 2000. Dilution effects on microzooplankton in dilution grazing experiments. Mar. Ecol. Prog. Ser. 2000, 127–139.

First, M.R., Lavrentyev, P.J., Jochem, F.J., 2007. Patterns of microzooplankton growth in dilution experiments across a trophic gradient: Implications for herbivory studies. Mar. Biol. 151, 1929–1940.

First, M.R., Miller Jr., H.L., Lavrentyev, P.J., Pinckney, J.L., Burd, A.B., 2009. Effects of microzooplankton growth and trophic interactions on herbivory in coastal and offshore environments. Aquat. Microb. Ecol. 54, 255–267.

Flint, M.V., Sukhanova, I.N., Kopylov, A.I., Poyarkov, S.G., Whitledge, T.E., 2002. Plankton distribution associated with the frontal zones in the vicinity of the Pribilof Islands. Deep-Sea Res. II 49, 6069–6093.

Geider, R.J., 1987. Light and temperature dependence of the carbon to chlorophyll *a* ratio in microalgae and cyanobacteria: implications for physiology and growth of phytoplankton. New Phytol. 106, 1–34.

Gifford, D.J., 1988. Impact of grazing by microzooplankton in the northwest arm of Halifax Harbor, Nova Scotia. Mar. Ecol. Prog. Ser. 47, 249–258.

Gifford, D.J., 1993. Protozoa in the diets of *Neocalanus* spp. in the oceanic subarctic Pacific Ocean. Prog. Oceanogr. 32, 223–237.

Goes, J.I., Gomes, H., do, R., Haugen, E., McKee, K., D'Sa, E., Chekalyuk, A.M., Stoecker, D., Stabeno, P., Saitoh, S., Sambrotto, R., 2014. Fluorescence, pigment and microscopic characterization of Bering sea phytoplankton community structure and photosynthetic competency in the presence of a Cold Pool during summer. Deep Sea Res. II 109, 84–99, http://dx.doi.org/10.1016/j.dsr2.2013.12.004.

Hansen, E., Eilertson, H.C., 2007. Do the polyunsaturated aldehydes produced by *Phaeocystis pouchetti* (Hariot) Langerheim influence diatom growth during the spring bloom in Northern Norway? J. Plankton Res. 29, 87–96.

Heinbokel, J.F., 1978. Studies on the functional role of tintinnids in the southern California Bight. I. Grazing and growth rates in laboratory cultures. Mar. Biol. 47, 177–189.

Hunt Jr., G.L., Stabeno, P., Strom, S., Napp, J.M., 2008. Patterns of spatial and temporal variation in the marine ecosystem of the southeastern Bering sea, with special reference to the Pribilof Domain. Deep-Sea Res. II 55, 1919–1944.

Ladd, C., Stabeno, P.J., 2012. Stratification on the Eastern Bering Sea shelf revisited. Deep-Sea Res. II 65–70, 72–83.

Landry, M.L., 1993. Estimating rates of growth and grazing mortality of phytoplankton by the dilution method. In: Kemp, P.F., et al. (Eds.), Handbook of Methods in Aquatic Microbial Ecology. Lewis Publishers, Boca Raton, pp. 715–722.

Landry, M.R., Brown, S.L, Yoshimi, M.R., Selph, K.E., Bidigare, R.R., Yang, E.J., Simmons, M.P., 2008. Depth-stratified phytoplankton dynamics in Cyclone Opal, a subtropical mesoscale eddy. Deep-Sea Res. II 55, 1348–1359.

Landry, M.L., Calbet, A., 2004. Microzooplankton production in the oceans. ICES J. Mar. Sci. 61, 501–507.

Landry, M.L., Calbet, A., 2005. Reality checks on microbial food web interactions in dilution experiments: responses to the comments of Dolan and McKeon. Ocean Sci. 1, 39–44.

Landry, M.R., Selph, K.E., Yang, E.J., 2011. Decoupled phytoplankton growth and microzooplankton grazing in the deep euphotic zone of the eastern equatorial Pacific. Mar. Ecol. Prog. Ser. 421, 13–24.

Levinsen, H., Nielsen, T.G., 2002. The trophic role of marine pelagic ciliates and heterotrophic dinoflagellates in Arctic and temperate coastal ecosystems: a cross-latitude comparison. Limnol. Oceanogr. 47, 427–439.

Liu, H., Suzuki, K., Nishioka, J., Sohrin, R., Nakatsuka, T.,2009. Phytoplankton growth and microzooplankton grazing in the Sea of Okhotsk during late summer of 2006. Deep-Sea Res. I 56, 561–570.

Liu, H., Suzuki, K., Saino, T., 2002. Phytoplankton growth and microzooplankton grazing in the subarctic Pacific Ocean and the Bering Sea during summer 1999. Deep-Sea Res. I 49, 363–375.

Lomas, M.W., Moran, S.B., Casey, J.R., Bell, D.W., Tiahlo, M., Whitefield, J., Kelly, R.P., Mathis, J.T., Cokelet, E.D., 2012. Spatial and seasonal variability of primary production on the Eastern Bering Sea shelf. Deep-Sea Res. II 65–70, 126–140.

Menden-Deurer, S., Fredrickson, K., 2010. Structure-dependent, protistan grazing and its implication for the formation, maintenance and decline of plankton patches. Mar. Ecol. Prog. Ser. 420, 57–71.

Merico, A., Tyrrell, T., Lessard, E.J., Oguz, T., Stabeno, P.J., Zeeman, S.I., Whitledge, T.E., 2004. Modelling phytoplankton succession on the Bering Sea shelf: role of climate influences and trophic intractions in generating *Emiliamia huxleyi* blooms 1997–2000. Deep-Sea Res. I 51, 1803–1826.

Modigh, M., Franze, G., 2009. Changes in phytoplankton and microzooplankton populations during grazing experiments at a Mediterranean coastal site. J. Plankton Res. 31, 853–864.

Moran, S.B., Lomas, M.W., Kelly, R.P., Gradinger, R., Iken, K., Mathis, J.T., 2012. Seasonal succession of net primary productivity, particulate organic carbon export and autotrophic community composition in the eastern Bering Sea. Deep-Sea Res. II 65–70, 84–97.

Nejstgaard, J.C., Tang, K.W., Steinke, M., Dutz, J., Koski, M., Antajan, E., Long, J.D., 2007. Zooplankton grazing on *Phaeocystis*: a quantitative review and future challenges. Biogeochemistry 83, 147–172.

Olson, M.B., Strom, S.L., 2002. Phytoplankton growth, microzooplankton herbivory and community structure in the southeast Bering Sea: insight into the formation and temporal persistence of an *Emiliania huxleyi* bloom. Deep-Sea Res. II 49, 5969–5990.

Ortiz, Y., Weise, F., Greig, A., 2012. Marine regions boundary data for the Bering Sea shelf and slope. UCAR/NCAR—Earth Observing Laboratory/Computing, Data, and Software Facility. Dataset. doi:10.5065/D6DF6P6C.

Parsons, T., Maita, Y., Lalli, C., 1984. A Manual of Chemical and Biological Methods for Seawater Analysis. Pergamon Press, New York.

Paul, C., Barofsky, A., Vidoudez, C., Pohnert, G., 2009. Diatom exudates influence metabolism and cell growth of co-cultured diatom species. Mar. Ecol. Prog. Ser. 389, 61–70.

Rose, J.M., Caron, D.A., 2007. Does low temperature constrain the growth rates of heterotrophic protists? Evidence and implications for algal blooms in cold waters. Limnol. Oceanogr. 52, 886–895.

Rose, J.M., Fitzpatrick, E., Wang, A., Gast, R.J., Caron, D.A., 2013. Low temperature constrains growth rates but not short-term ingestion rates of Antarctic ciliates. Polar Biol. 36, 645–659.

Sambrotto, R.N., Mordy, C., Zeeman, S.I., Stabeno, P.J., Macklin, S.A., 2008. Physical forcing and nutrient conditions associated with patterns of Chl a and phytoplankton productivity in the southeastern Bering Sea during summer. Deep-Sea Res. II 55, 1745–1760.

Sherr, E.B., Sherr, B.F., Hartz, A.J., 2009. Microzooplankton grazing impact in the western Arctic Ocean. Deep-Sea Res. II 56, 1264–1273.

Sherr, E.B., Sherr, B.F., Ross, C., 2013. Microzooplankton grazing impact in the Bering Sea during spring sea ice conditions. Deep-Sea Res II 94, 57–67.

Stabeno, P.J., Farley Jr., E.V., Kachel, N.B., Moore, S., Mordy, C.W., Napp, J.M., Overland, J.E., Pinchuk, A.I., Sigler, M.F., 2012a. A comparison of the physics of the northern and southern shelves of the eastern Bering Sea and some implications for the ecosystem. Deep-Sea Res. II 65–70, 14–30.

Stabeno, P.J., Kachel, N.B., Moore, S.E., Napp, J.M., Sigler, M., Yamaguchi, A., Zerbini, A.N., 2012b. Comparison of warm and cold years on the southeastern Bering Sea shelf and some implications for the ecosystem. Deep-Sea Res. II 65–70, 31–45.

Stockwell, D.A., Whitledge, T.E., Zeeman, S.I., Coyle, K.O., Napp, J.M., Brodeur, R.D., Pinchuk, A.I., Hunt, G.L., 2001. Anomalous conditions in the south-eastern Bering Sea, 1997: nutrients, phytoplankton and zooplankton. Fish. Oceanogr. 10, 99–116.

Stoecker, D.K., Evans, G.T., 1985. Effects of protozoan herbivory and carnivory in a microplankton food web. Mar. Ecol. Prog. Ser. 25, 159–167.

Stoecker, D.K., Weigel, A., Stockwell, D., Lomas, M., 2014. Microzooplankton: Abundance, biomass and contribution to chlorophyll in the Eastern Bering Sea in summer. Deep-Sea Res 109, 134–144, http://dx.doi.org/10.1016/j.dsr2.2013.09.007.

Strom, S.L., Fredrickson, K.A., 2008. Intense stratification leads to phytoplankton nutrient limitation and reduced microzooplankton grazing in the southeastern Bering Sea. Deep-Sea Res. II 55, 1761–1774.

Strom, S.L., Macri, E.L., Olson, M.B., 2007. Microzooplankton grazing in the coastal Gulf of Alaska: variations in top-down control of phytoplankton. Limnol. Oceanogr. 52, 1480–1494.

Strom, S.L., Olson, M.B., Macri, E.L., Mordy, C.W., 2006. Cross-shelf gradients in phytoplankton community structure, nutrient utilization, and growth rate in the coastal Gulf of Alaska. Mar. Ecol. Prog. Ser. 328, 75–92.

Sukhanova, I.N., Semina, H.J., Venttsel, M.V., 1999. Spatial and temporal variability of phytoplankton in the Bering Sea. In: Loughlin, T.R., Ohtani, K. (Eds.), Dynamics of the Bering Sea. University of Alaska Sea Grant, Fairbanks, pp. 453–483.

Vidal, J., Smith, S., 1986. Biomass, growth, and development of populations of herbivorous zooplankton in the southeastern Bering Sea during spring. Deep-Sea Res. 33, 523–556.

Deep-Sea Research II 109 (2014) 157–171

Contents lists available at ScienceDirect

Deep-Sea Research II

journal homepage: www.elsevier.com/locate/dsr2

Climate-mediated changes in zooplankton community structure for the eastern Bering Sea

Lisa B. Eisner [a,*], Jeffrey M. Napp [a], Kathryn L. Mier [a], Alexei I. Pinchuk [b], Alexander G. Andrews III [c]

[a] NOAA-Fisheries, Alaska Fisheries Science Center, 7600 Sand Point Way NE, Seattle, WA 98115, United States
[b] University of Alaska Fairbanks, School of Fisheries and Ocean Sciences, 17101 Point Lena Loop Road, Juneau, AK 99801, United States
[c] NOAA-Fisheries, Alaska Fisheries Science Center, 17109 Point Lena Loop Road, Juneau, AK 99801, United States

ARTICLE INFO

Available online 19 March 2014

Keywords:
Zooplankton
Community structure
Climate change
Eastern Bering Sea

ABSTRACT

Zooplankton are critical to energy transfer between higher and lower trophic levels in the eastern Bering Sea ecosystem. Previous studies from the southeastern Bering Sea shelf documented substantial differences in zooplankton taxa in the Middle and Inner Shelf Domains between warm and cold years. Our investigation expands this analysis into the northern Bering Sea and the south Outer Domain, looking at zooplankton community structure during a period of climate-mediated, large-scale change. Elevated air temperatures in the early 2000s resulted in regional warming and low sea-ice extent in the southern shelf whereas the late 2000s were characterized by cold winters, extensive spring sea ice, and a well-developed pool of cold water over the entire Middle Domain. The abundance of large zooplankton taxa such as *Calanus* spp. (*C. marshallae* and *C. glacialis)*, and *Parasagitta elegans*, increased from warm to cold periods, while the abundance of gelatinous zooplankton (Cnidaria) and small taxa decreased. Biomass followed the same trends as abundance, except that the biomass of small taxa in the southeastern Bering Sea remained constant due to changes in abundance of small copepod taxa (increases in *Acartia* spp. and *Pseudocalanus* spp. and decreases in *Oithona* spp.). Statistically significant changes in zooplankton community structure and individual species were greatest in the Middle Domain, but were evident in all shelf domains, and in both the northern and southern portions of the eastern shelf. Changes in community structure did not occur abruptly during the transition from warm to cold, but seemed to begin gradually and build as the influence of the sea ice and cold water temperatures persisted. The change occurred one year earlier in the northern than the southern Middle Shelf. These and previous observations demonstrate that lower trophic levels within the eastern Bering Sea respond to climate-mediated changes on a variety of time scales, including those shorter than the commonly accepted quasi-decadal time periods. This lack of resilience or inertia at the lowest trophic levels affects production at higher trophic levels and must be considered in management strategy evaluations of living marine resources.

Published by Elsevier Ltd.

1. Introduction

In recent years, climate change in the western Arctic has led to rapid changes in the eastern Bering Sea shelf resulting in variations in seasonal sea ice coverage and water column temperatures, and these variations have affected the entire ecosystem (e.g. Napp and Hunt, 2001; Stabeno et al., 2012b). Zooplankters are essential prey for many fish, seabirds, and marine mammals, therefore there is considerable interest in changes in zooplankton abundance and how these changes may propagate through the food web and impact higher trophic levels (Coyle et al., 2011; Hunt et al., 2011). Many planktivorous fishes, seabirds, and marine mammals inhabit both the northeastern and southeastern Bering Sea during summer (e.g. Piatt and Springer, 2003; Friday et al., 2012; Hollowed et al., 2012; Stevenson and Lauth, 2012). Historical research documented variations in single species abundance and cross shelf patterns of zooplankton in the southeastern Bering Sea (Cooney and Coyle, 1982; Coyle and Pinchuk, 2002; Napp et al., 2002; Stabeno et al., 2010; Coyle et al., 2011; Stabeno et al., 2012a and b). However, there are few modern descriptions of the broad-scale distribution of eastern Bering Sea zooplankton, particularly for the northern Bering Sea (Motoda and Minoda, 1974; Coyle et al., 1996 and references therein). To better understand how climate variability and

* Corresponding author. Tel.: +1 206 526 4060.
E-mail addresses: Lisa.Eisner@NOAA.gov (L.B. Eisner), Jeff.Napp@NOAA.gov (J.M. Napp), Kathy.Mier@NOAA.gov (K.L. Mier), aipinchuk@alaska.edu (A.I. Pinchuk), Alex.Andrews@NOAA.gov (A.G. Andrews III).

http://dx.doi.org/10.1016/j.dsr2.2014.03.004
0967-0645/Published by Elsevier Ltd.

change are affecting the recruitment and broad-scale distributions of planktivores, we need a more thorough understanding of how climate and other forcing affects the production and distribution of zooplankton across the entire region.

The eastern Bering Sea is a large marine ecosystem characterized by a broad continental shelf >500 km wide and >1000 km long oriented in a north westerly direction from the Alaskan Peninsula in the south, to below St. Lawrence Island, approximately 63°N latitude, in the north. Near the northern boundary, the system shifts from a pelagic to benthic dominated system (e.g. Grebmeier et al., 2006; Stevenson and Lauth, 2012; Sigler et al., 2014). The shelf can be divided into regions or domains, each with their characteristic hydrography, circulation, and fauna (Iverson et al., 1979; Cooney and Coyle, 1982; Coachman, 1986; Kachel et al., 2002). Cross shelf domains are most distinct during summer and fall in the southeastern Bering Sea where there are three domains approximated by water depth: Outer (100–180 m), Middle (50–100 m) and Inner (<50 m). The Inner Domain is well mixed, the Middle Domain is stratified into two layers, and the Outer Domain is stratified, but with three layers. In addition to cross shelf variations, there are latitudinal variations in wind fields, water column properties, and most importantly, sea ice coverage (Stabeno et al., 2010, 2012a). The northeastern Bering Sea is ice covered every year; whereas coverage in the south historically varies by more than 100 km (Stabeno et al., 2012a). The cold pool (a layer of <2 °C water that resides on the shelf bottom), is formed as a result of winter cooling and mixing that most often precedes sea ice formation), and typically persists through the following summer. Its extent and magnitude varies with climatic conditions affecting the distribution of many upper trophic level organisms in the region (e.g. Wyllie-Echevarria and Wooster, 1998; Hollowed et al., 2012, Kotwicki and Lauth, 2013).

The goal of this manuscript is to describe the broad-scale spatial variations in large and small zooplankton community composition in the north and southeastern Bering Sea during warm and cold climate states. Additionally, we address several important questions regarding zooplankton ecology affected by changing climate conditions (see Table 1). The data for these analyses come from broad-scale surveys of zooplankton conducted by the Bering-Aleutian Salmon International Survey (BASIS) program at NOAA, and provide the opportunity to describe the spatial cross-shelf and latitudinal distribution of zooplankton for the entire eastern Bering Sea shelf. These surveys began in 1999 before the Bering Sea Project (Bering Sea Ecosystem Study [BEST] and Bering Sea Integrated Ecosystem Research Program [BSIERP]) was launched in 2007 (Wiese et al., 2012) and have continued into the present after the field components of BEST and BSIERP ended.

Table 1
Questions addressed in manuscript.

Q1	What are the spatial and temporal patterns of large and small zooplankton taxa in the eastern Bering Sea for 2003–2009?
Q2	How do the total abundances and biomasses of large and small zooplankton vary between warm and cold years for the southeastern and northeastern Bering Sea?
Q3a	Are the community compositions of large and small taxa different between warm and cold regimes within each domain?
b	When these communities differed between warm and cold regimes which taxa contributed most to the differences?
c	Did the observed differences in zooplankton community composition between regimes occur exactly during the break between low and high ice years?
d	Which taxa showed the largest variations among years?
Q4	For each domain, which environmental factors explained the greatest amount of variability in zooplankton community composition overall and between warm and cold regimes?

During the 2000s the region experienced different multi-year climate regimes (Stabeno et al., 2012b) above average sea water temperatures and very low sea ice coverage (2000–2005), a single year of average sea water temperatures and sea ice extent (2006), and cold years with extensive sea ice (2007–2009). Thus, in contrast to most regional scientific programs in the last 50 years whose timing or duration allowed limited sampling in a single ecosystem state, our dataset allows us to evaluate changes in the eastern Bering Sea shelf pelagic ecosystem during multiple thermal phases.

2. Methods

2.1. Survey station locations and oceanographic sample collection

From mid August to early October, 2003–2009, samples were collected in the eastern Bering Sea, at stations located from 54.5 to 63.0°N and 159.0 to 174.0°W, and spaced approximately 60 km apart (Cieciel et al., 2009; Farley and Moss, 2009; Fig. 1). Stations were divided into shelf regions for analyses using Eastern Bering Sea Marine Region designations based on oceanographic/hydrographic, fisheries, and oceanographic characteristics (Ortiz et al., 2012; Harvey and Sigler, 2013). We further grouped these regions into five major domains using approximately 60°N to split the shelf into south and north (Stabeno et al., 2010) and approximating cross-shelf domains defined by Coachman (1986) yielding: S Inner (<50 m bathymetry, marine regions 2 and 7), S Middle (50–100 m, regions 3 and 6), S Outer (100–200 m, region 4), N Inner ($<\sim40$ m, region11), and N Middle (~40–100 m, regions 9 and 10).

Vertical profiles of temperature, salinity, and chlorophyll a (Chla) fluorescence were collected at each station with a Sea-Bird[1] Model 25 or Model 9plus CTD. A rosette sampler was used to obtain discrete water samples for surface and bottom nutrients, total Chla (Whatman GF/F) and large size-fractionated Chla (>10 μm, Millipore Isopore polycarbonate membrane filters); all samples were stored frozen (−80 °C) for 6 months maximum and analyzed using standard procedures at shore-based facilities (Parsons et al., 1984; Gordon et al., 1993). Vertical profiles of Chla concentrations were derived from regressions between in vivo fluorescence and discrete Chla samples (mean $r^2=0.65$). Water column stability (energy required to mix the water column to 70 m, J m^{-3}) was calculated at each station from CTD temperature and salinity data (Simpson et al., 1977). Ice coverage (number of days of ice at each station during the prior winter) and timing of retreat (the last day of ice in spring) for a 60 km^2 square box centered on each station was obtained from the Advanced Microwave Scanning Radiometer (AMSR) on MODIS Aqua from the National Snow and Ice Data Center (NSIDC) (S. Salo, NOAA PMEL, personal comm.). We assumed no ice when concentrations dropped below 15%. Wind mixing data (wind velocity^3, u^{*3}) for August were obtained from National Centers for Environmental Prediction (NCEP) reanalysis data set (N. Bond, NOAA PMEL, personal comm.). Wind mixing data were averaged over a 2° latitude by 5° longitude box centered on a NOAA PMEL mooring at site M4 (57. 9°N, 168. 9°W; Stabeno et al., 2010). We assumed M4 winds approximated wind fields over our entire survey area, since winds at all four 70 m moorings in the northeast and southeast Bering Sea (M2, M4, M5 and M8) have shown strong coherence during recent years (Stabeno et al., 2010). Winter wind fields for the prior period (October–April) based on shelf-wide model results were used to estimate potential onshore and offshore flow, assuming that southeasterly winds

[1] Use of trade names does not signify an endorsement by the U.S. National Oceanic and Atmospheric Administration.

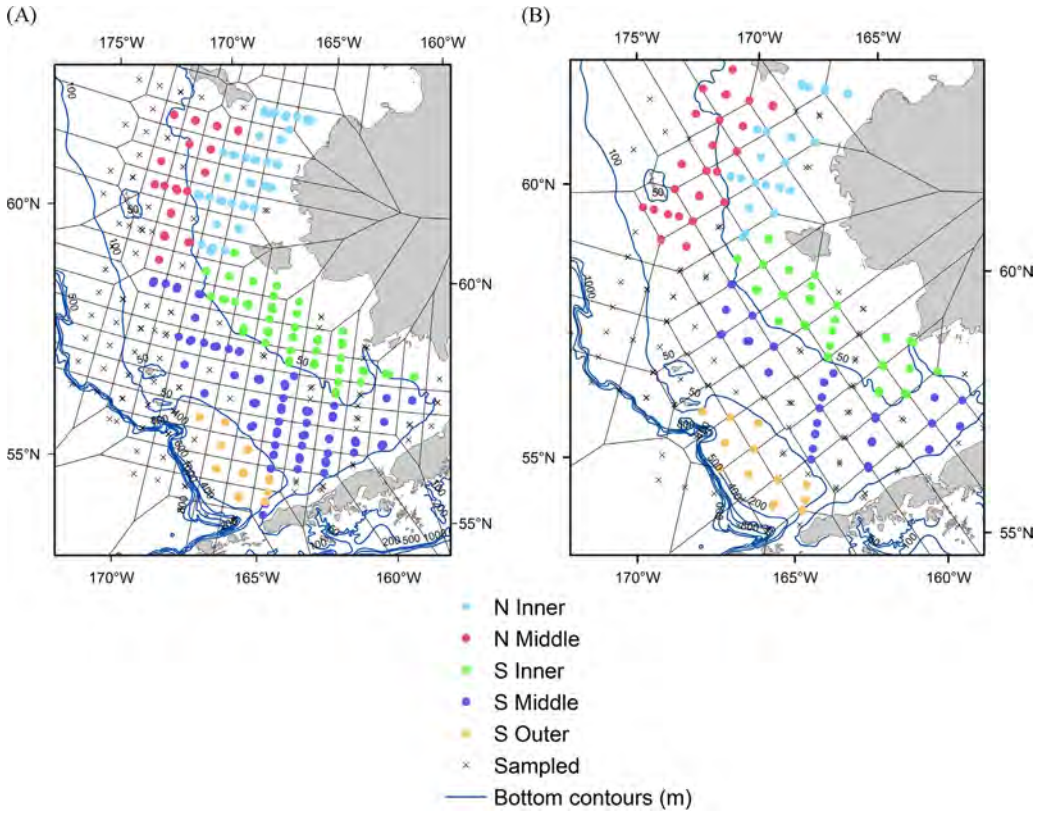

Fig. 1. Bering Sea study area showing stations used for analyses in each oceanographic shelf domain for: (A) large zooplankton and (B) small zooplankton. Black lines indicate spatial "blocks" which are Thiessen polygons around points. Blocks containing colored points (reduced data set) were visited at least two years during warm (2003–2005) and two years during cold (2006–2009) regimes; colors signify domain.

promote stronger onshore flows than northwesterly winds (Danielson et al., 2012).

2.2. Zooplankton sample collection and lab analysis

Zooplankton samples were collected and analyzed using methods described in Coyle et al. (2011). Briefly, small zooplankton assemblages were sampled at every other station with a 0.1 m^2 Juday net with 168 μm mesh (Volkov, 1984; Volkov et al., 2007). The net was towed vertically from within 5–10 m of the bottom (or maximum depth of 200 m) to the surface at about 1 m s^{-1}. Juday net samples were sieved into size fractions prior to counting on board ship (Volkov et al., 2007); however, data from all size fractions combined were used to quantify small zooplankton taxa. Large zooplankton assemblages were collected at every station with a 60 cm MARMAP-style bongo frame with a 505 μm mesh net. Oblique tows were conducted from the surface to within 5–10 m of the bottom, and volume filtered was measured with calibrated General Oceanics flowmeters. All samples were preserved in 5% formalin, buffered with seawater. Zooplankton collections from 2003 to 2004 were sorted at the Polish Plankton Sorting and Identification Center (Szczecin, Poland); collections from 2005 to 2009 were processed at the University of Alaska (Coyle et al., 2008). The lowest taxonomic level of sorting varied between labs, so we used the lowest taxonomic stage available across all years. Zooplankton tows were collected primarily during the daytime. Many euphausiids on the Bering Sea shelf stay within 1–2 m of the bottom during the day (Coyle and Pinchuk, 2002) and those in the water column are difficult to quantitatively capture with nets (e.g. Sameoto et al., 1993; Wiebe et al., 2004); therefore euphausiids were not included in our analyses. It is also possible that under representation of other diel migrants (e.g. *Metridia* spp.) occurred. The small volume filtered by Juday and bongo nets compared to larger nets (e.g. Multinet or MOCNESS) could have resulted in under sampling of relatively large and rare taxa. Accordingly, very large medusae such as *Chrysaora melanaster* were excluded since they were not quantitatively sampled by our bongo nets. Unidentified copepod nauplii were also excluded, although they were fairly numerous in the Juday net samples (~11% of total abundance). A total of 424 Juday and 717 bongo net samples were collected for all years combined.

2.3. Statistical analyses

Separate analyses were conducted for large (bongo samples) and small (Juday samples) zooplankton taxa. Zooplankton data were 4th root transformed (unless otherwise indicated) to down weight the contribution of dominant taxa to similarity/dissimilarity patterns (Clarke and Warwick, 2001). Initial analyses were conducted using both abundance (no. m^{-3}) and integrated abundance (no. m^{-2}) for comparisons among regions with large changes in bathymetry (Questions 1 and 2, Table 1). We found no substantial differences in the outcome when using number normalized by volume or area; therefore we chose to present abundances normalized by volume filtered (no. m^{-3}) to allow for comparisons with most prior studies on the eastern Bering Sea shelf which reported their abundance data normalized by volume filtered. Zooplankton biomass wet weights (g m^{-3}, Coyle et al., 2011) were used in Question 2 analyses. The warm regime was designated as 2003–2005 and the cold regime as 2006–2009 based on late summer/fall mean water column temperature anomalies for 2003–2009, estimated from CTD data collected during our surveys (cf. Stabeno et al., 2012b, which categorizes 2006 as a year of average temperatures and sea ice extent). For all

analyses, excluding those for Question 1, it was necessary to account for uneven sampling across years. Therefore, a reduced data set was used that included only station locations within equally spaced geographically partitioned regions (Blocks) that were sampled a minimum of two warm and two cold years (Fig. 1). Blocks were created in ArcMap/ArcInfo, 10.1 (ESRI, 2012) using Thiessen polygons, polygons constructed around stations by calculating the midline between each pair of adjacent stations (Thiessen and Alter, 1911; Gold, 1991). Blocks were approximately 60×60 km^2 for the large taxa (equivalent to the spacing of stations) and approximately 80×80 km^2 for the small (equivalent to the diagonal spacing of every other station). The small taxa required larger blocks due to sparser sampling. Separate analyses were conducted for each of the five major domains (S Middle, N Middle, S Inner, N Inner, S Outer) for Questions 3 and 4 analyses (Table 1).

Statistical analyses included cluster analysis, similarity percentage contribution of individual taxa (SIMPER), and permutational, multivariate analysis of variance (PERMANOVA) in the software package, PRIMER-E, version 6.1.15 with PERMANOVA+ version 1.0.5 (Clarke and Warwick, 2001; Clarke and Gorley, 2006; Anderson et al., 2008). All procedures used Bray–Curtis dissimilarities, a statistic commonly used to quantify the dissimilarity in composition between samples (Bray and Curtis, 1957). In our study, these procedures were used to evaluate variations in community composition (the relative abundances of zooplankton taxa). SIMPER calculates the average contribution of each taxon to the overall Bray–Curtis dissimilarity in community composition. PERMANOVA allows the use of distance measures, in our case, Bray–Curtis dissimilarity in community composition, to test for the significance of specific effects, similar to a multivariate ANOVA. The advantage of using a permutation test is that it does not require the data to follow a particular distribution and is therefore more robust than parametric statistics. This procedure also allows for the partitioning of the multivariate variation in abundance according to nested sampling designs and 2-way designs with interactions, as well as the addition of covariates, such as environmental variables (Anderson et al., 2008). Statistical procedures used for each of our research questions are detailed below.

(Q1) The taxonomic composition and distribution of zooplankton were evaluated qualitatively using abundance data from all stations and years. For grouping stations, we applied a hierarchical cluster analysis using group average linkage of Bray–Curtis dissimilarities among stations. We then used SIMPER analysis to determine the average percent contribution of each taxon in each station cluster. For grouping taxa, we applied a separate cluster analysis of Bray–Curtis dissimilarities using mean abundance (standardized untransformed data) of each taxon across station clusters. Standardization rather than transformation was necessary for grouping species since we were more interested in relative similarity/dissimilarity patterns rather than down weighting abundant species, which was necessary when grouping stations (Clarke and Warwick, 2001). Clusters were identified by drawing a line across branches on each dendrogram (one for station and one for taxa) determined by at least 50% similarity, length of branches (indicating stability of groups), a permutation procedure that objectively tests for grouping *a priori* (SIMPROF, Clarke and Warwick, 2001; Clarke and Gorley, 2006), and subjective biological interpretation of clusters. For the station cluster analysis, we designated station clusters as outliers if they contained less than 1% of the sampled stations.

(Q2) The total abundance and total biomass of all large and all small zooplankton in the north and south eastern Bering Sea for each year were estimated by summing the abundance or biomass of all taxa within each block and dividing by number of stations. The average abundance or biomass was computed over all blocks within each region, i.e. the south ($< 60^\circ$N, Inner, Middle and Outer Domains) and north (60–63°N, Inner and Middle Domains). Then, we estimated the mean and standard error (SE) of the 4th root transformed data, then back-transformed the data to estimate geometric means and SE of untransformed total abundance and biomass. To test for significant differences ($P < 0.05$) among years within each region, we applied ANOVA on 4th root transformed data, followed by Tukey pairwise comparisons.

(Q3a) To test for significant differences in zooplankton community composition between Regimes (warm vs. cold), a PERMANOVA was applied to all domains combined and then to each domain separately. In addition to the Regime effect, a geographic blocking factor (Block) was included as a random effect to account for the uneven sampling across years (defined above). Year was also included in the model as a random nested effect within Regime. Interactions among these effects were also included. A permutational dispersion (PERMDISP) analysis was applied to test for any significant dispersion effects between Regimes (Anderson et al., 2008). This is analogous to a univariate Levene test for homogeneity of variances in ANOVA and tests for differences in distances between the yearly centroids (center of points in multivariate space).

(Q3b) A 2-way (Regime and Block) SIMPER analysis was run to determine which zooplankton taxa contributed most to the differences between regimes for domains where significant differences were found between Regimes.

(Q3c) A PERMANOVA was applied to each domain to determine if zooplankton communities were significantly different for one or more years. In this case, Year was considered a fixed effect, and Block was considered a random effect accounting for spatial variability and the uneven sampling across years. To determine which consecutive years had significantly different community composition, pairwise multiple comparison tests were applied to consecutive years only. No Bonferroni correction was applied here as PERMANOVA provides exact tests, and a Bonferroni correction would be overly conservative in this case (Anderson et al., 2008).

(Q3d) The mean untransformed zooplankton abundances for the most common taxa (ones that jointly contributed to $\geq 97\%$ of the total untransformed abundance for all years combined) were calculated for the north and southeastern Bering Sea to determine which taxa contributed to the interannual variations in community structure and total abundance.

(Q4) A set of local environmental variables measured concurrently at the same stations as zooplankton abundance and regional variables measured yearly over the eastern Bering Sea were used to evaluate the conditions most often associated with variations in community composition (dependent variable), for warm vs. cold Regimes within each shelf domain. Variables were removed if they were correlated with other variables ($R > 0.8$) or were determined to be of lesser biological importance. The variables of interest were included as covariates (independent variables) in PERMANOVA tests for domains where significant differences were found between warm and cold years (based on results of Question 3a). The local covariates included temperature, Chla (a measure of phytoplankton biomass), nitrate, and ammonium measured at the surface (5 m) or above the mixed layer depth; stability over the top 70 m; integrated Chla and mean large size-fractionated Chla/total Chla over the top 50 m; day of ice retreat in spring prior to our late summer/ fall sampling; and temperature, salinity, and ammonium measured at the bottom or below the mixed layer depth. The regional covariate tested was the yearly winter (October–April) wind direction (% of time winds were from the SE and NW; Danielson et al., 2012). We also tested latitude and longitude to see if there were significant interannual geographic gradients within oceanographic domains.

We first removed the within year spatial variability by including a blocking factor (described previously). Then, each covariate

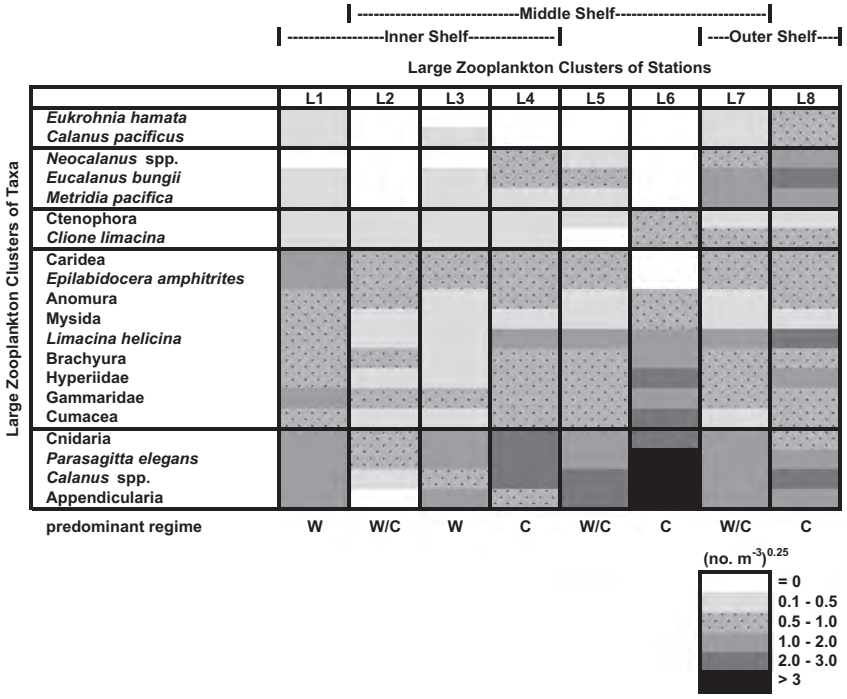

Fig. 2. Heat map of large zooplankton, summarizing station cluster analysis (x axis) and taxa cluster analysis (y axis). This figure indicates what taxa were prominent (or absent) in each station cluster. Each cell represents the average abundance of a specific taxon (scaled to 4th root transform) for each station cluster. Approximate domain designations are shown above station clusters. Designations at bottom indicate climate regime (W=warm; C=cold; W/C=both) when each station cluster was commonly observed. Horizontal lines separate clusters of taxa (indicating taxa which tended to co-occur over all years and domains combined).

was sequentially added using Type I sum of squares which tests for the significance of the addition of that variable with all prior covariates accounted for. The best fit model was chosen by including the most significant covariates in a particular order that gave the lowest mean square error. The Regime effect and interactions were included as the last covariates in the model. Whenever a Regime effect (added last) became insignificant ($P > 0.05$) compared to the Regime effect before adding environmental covariates ($P < 0.05$), we concluded that the environmental covariates were explaining at least some of the variability in community composition between warm and cold years. To examine yearly changes in temperature and sea ice variations we plotted surface and bottom temperature, day of sea ice retreat and number of days of ice coverage the prior winter, averaged over stations in the N and S Middle Domains.

3. Results

3.1. Spatial and temporal patterns of large and small zooplankton (Q1).

For large zooplankton, the multivariate analyses yielded eight station clusters (L1–L8, Figs. 2, 3). Station clusters show which stations had similar taxonomic compositions over the eastern Bering Sea shelf for all years combined. Taxa which contributed most to the identity of each station cluster (those that account for at least 80% of the total abundance within each station cluster) are listed in decreasing abundance for Clusters L1, L3, L4, and L8, described below. One pattern that stands out is the replacement of Middle Domain clusters during the transition from warm to cold years (Fig. 3). **Cluster L3** characterized by Cnidaria (gelatinous zooplankton dominated by *Aglantha digitale* in our study), *Parasagitta elegans* (Chaetognatha) and Appendicularia (Larvacea) extended over a broad area in the warm years, particularly 2003–2004, and was replaced in cold years by **Cluster L4** characterized by *Calanus* spp.[2] (Copepoda), Cnidaria and *P. elegans*. In addition, in warm years, there was a cluster confined primarily to the Inner Domain, **Cluster L1**, characterized by *P. elegans*, Cnidaria, *Epilabidocera amphitrites* (Copepoda) and Caridea (shrimp), but in cold years this group was observed less often. Latitudinal variations in the timing of changes were also seen, with increased coverage for **Cluster L4** in the northeastern Bering Sea in 2004–2005, and expansion southward and inshore into the Inner Domain in the following cold years. In contrast, in the Outer Domain, **Cluster L8** characterized by *Limacina helicina* (Pteropoda), *Calanus spp*., *Eucalanus bungii* (Copepoda), and *Metridia pacifica* (Copepoda), was observed during all years.

For small zooplankton, the analyses yielded nine station clusters (Figs. 4 and 5). Taxa which contributed most to the identity of each cluster are listed in decreasing abundance for Clusters S1, S4, S6, S7, S9, below. Similar to large taxa, in the Middle Domain there was one cluster with broad spatial coverage in warm years, **Cluster S4**, characterized by *Oithona* spp. (Copepoda), *Pseudocalanus spp*.(Copepoda), Echinodermata larvae, Polychaeta (annelid worms), molluscan Bivalvia larvae and Cirripedia (barnacle larvae), which was replaced in cold years by **Cluster S7**, characterized by *Pseudocalanus* spp., *Oithona* spp., *Acartia* spp. (Copepoda) and Polychaeta (Fig. 5), with fewer taxa making up the bulk of abundance in cold years. In the Inner Domain, a cluster with broad coverage in the southeastern Bering Sea, **Cluster S1**, characterized by *Oithona* spp., *Pseudocalanus* spp., larval Bivalvia, *Centropages abdominalis* (Copepoda), Polychaeta, *Acartia* spp., Echinodermata larvae and *Podon* sp. (Cladocera) was partially replaced in the coldest years, 2008–2009, by **Cluster S6**, characterized by *Pseudocalanus* spp. and *Acartia* spp. and *C. abdominalis*

[2] *Calanus* spp. referred to in this work is most likely a mixture of *C. marshallae* and *C. glacialis* based on recent genetic analyses by Campbell et al., personal comm. and J. Nelson (2009).

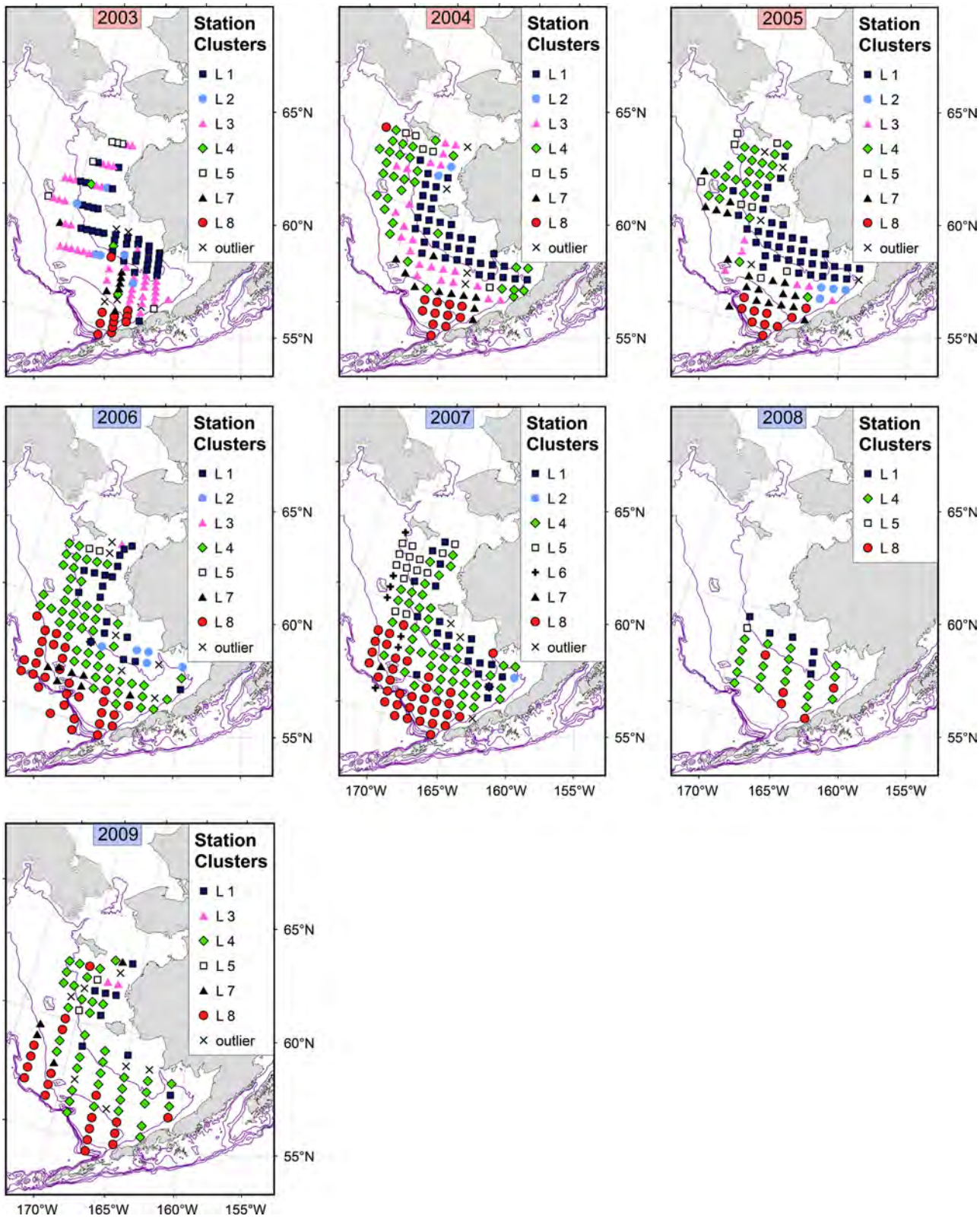

Fig. 3. Spatial variation of large zooplankton clusters for each year using 4th root transformed abundance data. Warm years highlighted with red and cold with blue. Refer to Fig. 2 to see taxa abundances for each cluster.

and by **Cluster S7**. Again, similar to the large taxa, in the Outer Domain there was one cluster common during all years, **Cluster S9**, characterized by *Oithona* spp., *Pseudocalanus* spp., *Metridia* spp. copepodites, *Acartia* spp., *Microcalanus* spp. (Copepoda), and Bivalvia larvae. Small taxa clusters did not show large north–south variations.

Each "taxa cluster" represents taxa that tended to co-occur at a station, based on analysis for all years and spatial areas combined (Figs. 2, 4, horizontal lines separate taxa clusters). Large zooplankton taxa that tended to co-occur included *Neocalanus* spp., *E. bungii*, *M. pacifica*; these are oceanic copepods resident in the

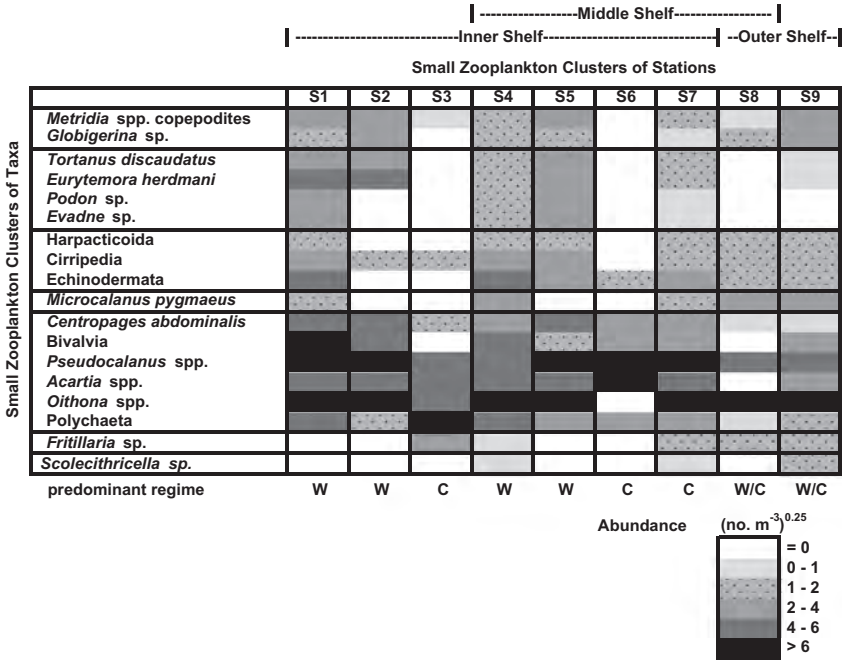

Fig. 4. Heat map of small zooplankton, summarizing station cluster analysis (*x* axis) and taxa cluster analysis (*y* axis). Refer to Fig. 2 for details.

Outer Domain or brought in from beyond the shelf break (Coyle and Pinchuk, 2002; Gibson et al., 2013). Other taxa that co-occurred were *P. elegans*, *Calanus* spp., and Appendicularia; all are common taxa with relatively high abundances in the Middle Domain (Coyle et al., 2008, 2011). Small taxa that tended to co-occur included *Evadne* sp. (Cladocera), *Podon* sp., *Eurytemora herdmani* (Copepoda), and *Tortanus discaudatus* (Copepoda), taxa typically neritic and common nearshore (Gieskes, 1971; Johnson, 1934; Kos, 1977); and *Oithona* spp., *Acartia* spp., *Pseudocalanus* spp., Polychaeta, Bivalvia larvae, and *C. abdominalis*, taxa that often reside in upper layers of the water column (Marlowe and Miller, 1975).

3.2. Total abundance and total biomass of large and small zooplankton during warm and cold regimes (Q2)

Trends in total abundance and biomass varied for large and small zooplankton and between the north and south eastern Bering Sea (Fig. 6). In the south, large zooplankton increased in abundance starting in 2007, peaked in 2008 and declined in 2009 (Fig. 6A), with abundances significantly higher in 2008 and 2009 than in prior years ($P<0.001$, ANOVA; $P<0.05$, Tukey pairwise comparisons). In contrast, small zooplankton steadily decreased in abundance from 2003 to 2009 with significantly higher abundances in warm years than in later cold years (2003, 2005 vs. 2008, 2009; and 2004 vs. 2009) ($P<0.001$, ANOVA; $P<0.05$, Tukey pairwise tests). In the north, total abundances of large zooplankton increased between 2004 and 2005 and decreased between 2007 and 2009 (Fig. 6B), with abundances significantly higher in 2007 than 2003, 2004 and 2009, and significantly higher in 2005 than 2004 ($P<0.001$, ANOVA; $P<0.05$, Tukey pairwise tests). Small zooplankton abundances in the north did not show clear trends with time (Fig. 6B), with no significant differences detected among years. The overall magnitude of large and small zooplankton abundances was similar in the north and south, except for the first three years (warm years) when small taxa were in higher abundance in the south than the north. Trends in biomass mirrored those in abundance except for small taxa in the south where despite the observed declines in abundance from 2003 to 2009, the biomass remained fairly constant (Fig. 6C, D). Statistical comparisons support these conclusions. The biomass of large taxa in the south was significantly higher in 2008 compared to prior years, and in 2009 compared to 2006 and 2007 ($P<0.001$, ANOVA; $P<0.05$, Tukey pairwise tests). In the north, biomass of large taxa was significantly higher in 2007 compared to 2009 ($P=0.02$, ANOVA; $P<0.05$, Tukey pairwise tests). The biomass of small taxa in both the south and north was not significantly different among years. It is also worth noting that in spite of high abundance of small taxa during the warm years, their biomass was similar to that of large taxa during the warm period in the south and during all years in the north (Fig. 6).

3.3. Statistical differences among assemblages, shelf domains, and years (Q3)

3.3.1. Zooplankton abundances between regimes by domain (Q3a)

We next evaluated if the observed differences in zooplankton assemblages between regimes were statistically significant for the five major shelf domains. For all domains combined, PERMANOVAs showed significant interactions between Regime and Domain ($P=0.012$, $P=0.001$, for large and small taxa, respectively), indicating that community structure varied by Regime depending on Domain. Therefore, each domain was evaluated separately for all further analyses. There were significant differences in the community structure between warm and cold regimes for all domains except the N Inner for large taxa and N Inner and S Outer for small taxa, after accounting for significant spatial block effects (Table 2). The strongest differences were observed in the S Middle and S Inner Domains.

3.3.2. Zooplankton taxa differences between warm and cold regimes (Q3b)

Large zooplankton taxa that substantially decreased in abundance (> 2-fold) during the transition from warm to cold regimes include Cnidaria, Gammaridae amphipods, Mysida, the neritic copepod *Epilabidocera amphitrites*, and the temperate copepod *Calanus pacificus* (Table 3). Taxa that substantially increased in

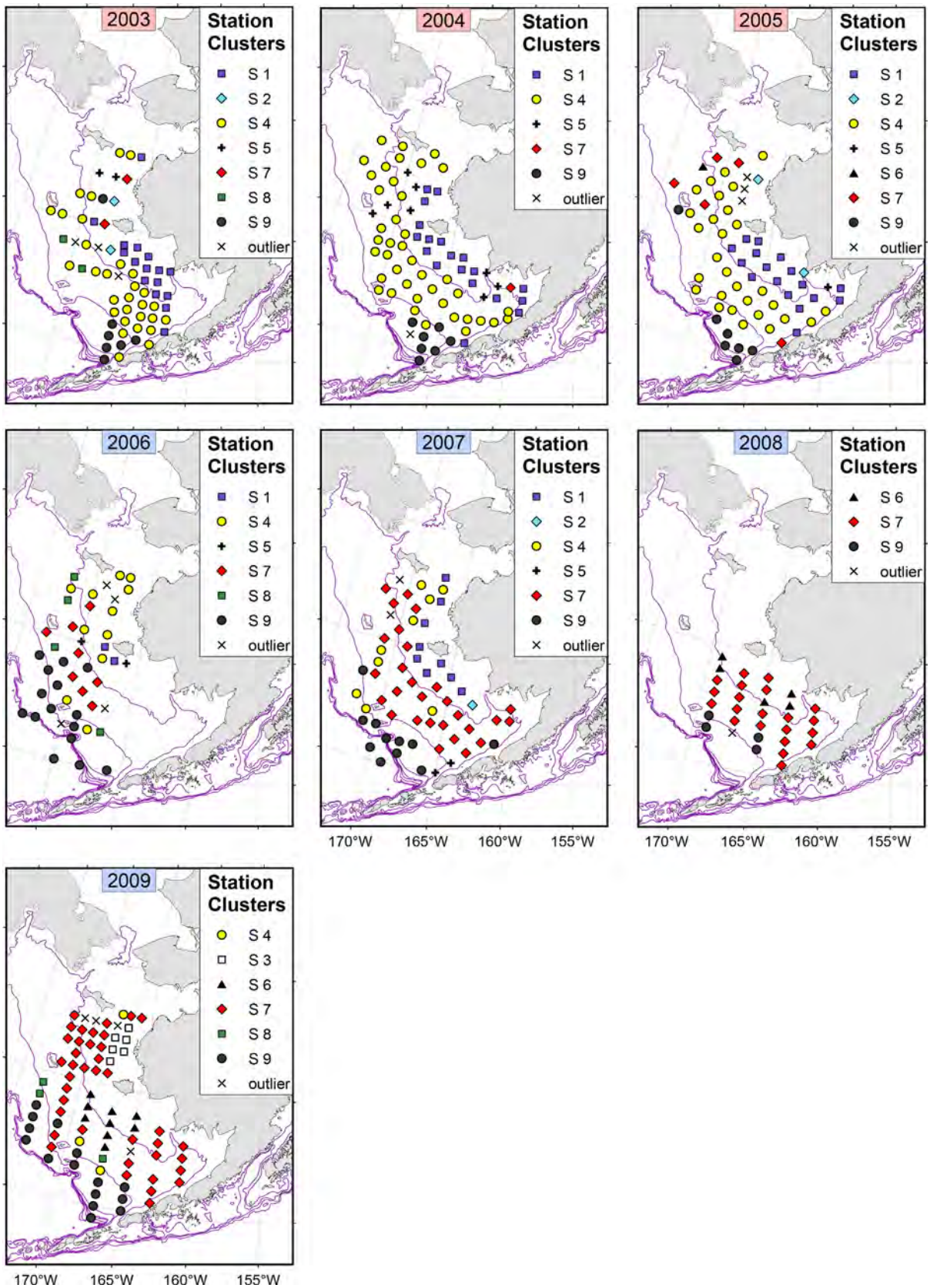

Fig. 5. Spatial variation of small zooplankton clusters by year using 4th root transformed abundance data. Warm years highlighted with red and cold with blue. Refer to Fig. 4 to see taxa abundances for each cluster.

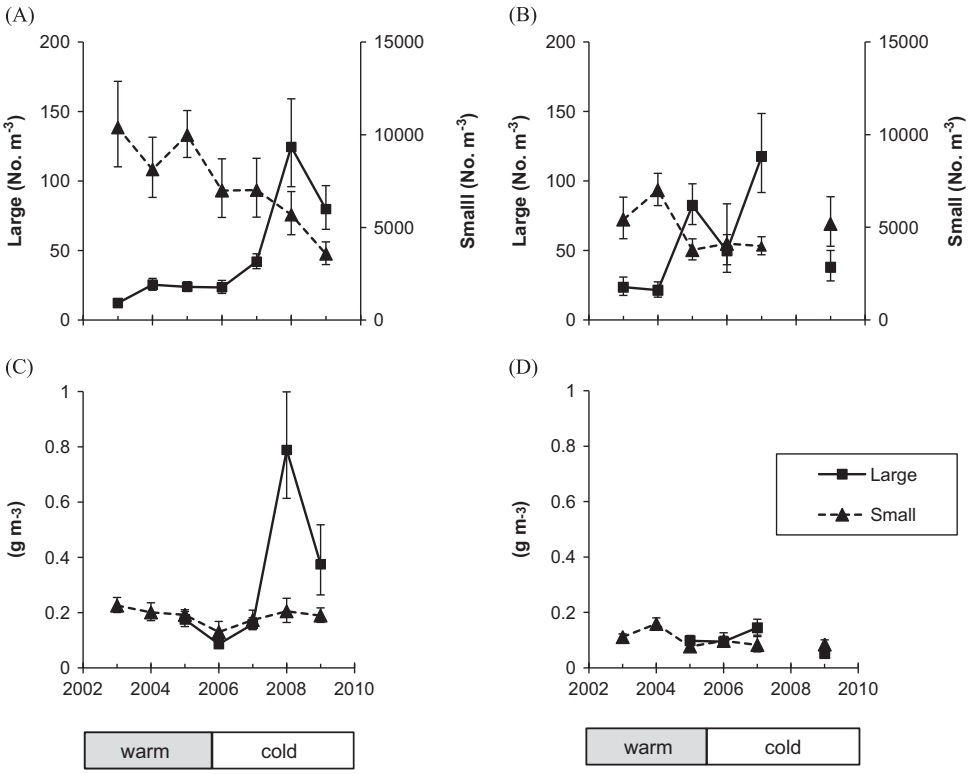

Fig. 6. Small and large zooplankton total mean abundance (no. m^{-3}) in the eastern Bering Sea in the (A) south (< ~60°N) and (B) north (~60–63°N), and total mean biomass (g m^{-3}) in the (C) south and (D) north. Geometric means and standard errors are shown. Bar indicates warm and cold regimes.

Table 2
PERMANOVA results (*P*-values from permutation test) for differences in community structure of large and small zooplankton taxa (abundance data) in the warm (2003–2005) vs. cold (2006–2009) years by domain (Fig. 1). Other effects in model are not shown (Block, Year (Regime), and interactions).

Domain	Large *P* (perm)	Small *P* (perm)
S Inner	0.002*	0.005*
S Middle	0.001*	0.001*
S Outer	0.008*	0.731
N Inner	0.152	0.438
N Middle	0.024*	0.029*

* Significant at $P < 0.05$.

abundance from warm and cold regimes include Anomuran and Brachyuran crab larvae, *Calanus* spp., *Parasagitta elegans*, the oceanic copepods *Neocalanus* spp. *Eucalanus bungii*, Hyperiidea amphipods and Cumacea. Taxa that showed both increases and decreases depending on domain include Appendicularia, Caridea decapods and *Limacina helicina*. *Calanus* spp. were the top contributor to changes in community composition between regimes (13–23% of total dissimilarity), particularly in the Middle Domain (both north and south). High contributions to dissimilarity (> 10%) were also seen for Caridea decapods in the S Inner, *P. elegans* and Appendicularia in the S Middle; *Limacina helicina* in the S Outer, and Appendicularia and Cnidaria in the N Middle Domains.

Most small zooplankton taxa decreased in abundance in the S Inner, S Middle and N Middle Domains from warm to cold years (Table 3). The only small taxa showing increases in cold years were *Acartia* spp. in all three domains, *Metridia* spp. copepodites and *Pseudocalanus* spp. in the S Middle Domain, and *Fritillaria* spp. (Appendicularia) in the N Middle Domain. *Oithona* spp. and larval bivalves had high contributions to dissimilarity in community composition between regimes for all three domains, with *Acartia* spp., Polychaeta, and Echinodermata larvae also important, particularly in the Middle Domain.

3.3.3. *Zooplankton abundances between consecutive years (Q3c and d)*

Next, we evaluated which consecutive years showed the greatest changes in community composition in each domain to determine if the differences between regimes occurred during our designated break point between warm to cold regimes (i.e. between 2005 and 2006) or if the changes in community composition took place over a period of years. We also evaluated which taxa showed the largest interannual variations in the south and north eastern Bering Sea.

For large and small zooplankton communities, most regions with the exception of the S Outer showed significant differences (based on pairwise multiple comparisons) between pairs of consecutive years (Table 4) indicating that interannual changes in community composition were observed over our entire study period, not just for the years when the temperature regime changed most rapidly from warm to cold (e.g. 2005–2007 in the south). For large zooplankton, the greatest interannual variations, in the south were seen by *Calanus* spp., which increased in cold years starting in 2007 (Fig. 7); while in the north, increases were due to Cnidaria in 2005 and 2007, and *Calanus* spp. starting in 2006. The small taxa that decreased in abundance from warm to cold years in the south were *Oithona* spp. and Bivalvia larvae, while in the north, *Oithona* spp. decreased only in 2005, 2007 and 2009 (Fig. 7). Small zooplankton composition in the north was most different in 2009, with higher levels of polychaetes and *Acartia* spp.; no data exist for 2008 to determine if this change was gradual. Overall, *L. helicina*, *M. pacifica*, *Pseudocalanus* spp., and Bivalvia larvae appear to be more abundant in the south, and *Cnidaria* and Polychaeta more abundant in the north. Some of the

Table 3
Percent contribution by large and small zooplankton taxa to differences (dissimilarity) between warm and cold years. Blue indicates >2 times back transformed abundance in cold than in warm years. Red indicates >2 times back transformed abundance in warm than in cold years.

Large Zooplankton	S Inner	S Middle	S Outer	N Middle	Small Zooplankton	S Inner	S Middle	N Middle
Cnidaria	9.0	6.0	5.2	11.4	***Oithona* spp.**	14.9	12.5	14.1
Gammaridae	8.3	6.5	2.9	7.4	**Bivalvia**	14.0	13.5	10.7
Mysida	7.0		3.3		**Echinodermata**	8.4	15.9	8.9
Epilabidocera amphitrites	8.2	4.1		6.2	**Polychaeta**	9.0	10.7	12.1
Calanus pacificus			3.8		**Cirripedia**	5.3	9.4	7.1
Appendicularia	7.6	10.5	6.6	12.7	***Centropages abdominalis***	7.0	6.5	8.8
Metridia pacifica			9.7		***Podon* sp.**	7.2		
Clione limacina		3.4	5.8		***Eurytemora herdmani***	6.4		
Caridea	10.2	3.6	2.9		***Tortanus discaudatus***	4.8		
Limacina helicina	4.1	6.4	12.9	6.7	***Metridia* spp. copepodites**		2.7	3.6
Cumacea	4.1			3.4	***Fritillaria* sp.**			4.2
Eucalanus bungii		3.0	9.1		***Pseudocalanus* spp.**	6.3	7.6	7.7
***Neocalanus* spp.**			7.3		***Acartia* spp.**	7.4	12.1	13.1
Parasagitta elegans	9.3	10.7	3.7	7.6				
Anomura	6.6	3.8		4.1				
Hyperiidae		5.8	6.3	6.9				
***Calanus* spp.**	13.4	22.5	8.8	17.0				
Brachyura	6.0	4.3	4.4	6.7				
Total %	93.6	90.5	92.6	90.1	Total %	90.6	90.8	90.2

Table 4
PERMANOVA results (*P*-values) showing differences in community composition for large and small zooplankton taxa (abundance data) by domain. *P*-values for at least one difference among years (All years) are followed by pairwise multiple comparisons for consecutive years.

Zooplankton		S Inner	S Middle	S Outer	N Inner	N Middle
Large						
All years		<0.001*	<0.001*	0.015*	<0.001*	<0.001*
2003	2004	0.005*	0.007*	0.382	0.290	0.157
2004	2005	<0.001*	<0.001*	0.084	0.001*	0.014*
2005	2006	<0.001*	<0.001*	0.364	0.026*	0.007*
2006	2007	0.001*	<0.001*	0.764	0.023*	0.002*
2007	2008	0.108	<0.001*			
2008	2009	0.043*	0.043*			
Small						
All years		<0.001*	<0.001*	0.011*	<0.001*	<0.001*
2003	2004	0.003*	0.296	0.743	0.028*	0.154
2004	2005	0.001*	0.045*	0.044*	0.026*	0.003*
2005	2006	0.160	0.031*	0.149	0.715	0.020*
2006	2007	0.438	0.084	0.243	0.734	0.133
2007	2008	0.038*	0.320	0.770		
2008	2009	0.087	0.057	0.204		

* $P<0.05$.

north–south variations can be explained by the lack of sampling in the Outer Domain in the northeastern Bering Sea.

3.4. Environmental factors contributing to observed differences in zooplankton community composition (Q4)

The interannual variations in zooplankton abundance and community composition appear to relate to changes in temperature and sea ice retreat in the eastern Bering Sea. Temperature above and below the mixed layer depth in the N and S Middle Domains showed a declining trend from 2003 to 2009, concurrent with increases in the date of ice retreat and duration of ice coverage (Fig. 8). The greatest difference in timing of ice retreat and ice coverage was found in the S Middle Domain, with increases seen from 2005 to 2008, which overlaps the increase in *Calanus* spp. (Figs. 7, 8). Decreases in surface and bottom temperatures coincided with decreases in small taxa such as *Oithona* spp. and increases in *Pseudocalanus* spp. and *Acartia* spp. in the S Inner and S Middle Domains. Temperature and small taxa abundance were lower in the north than the south (Figs. 7, 8). For large zooplankton taxa, models with environmental co-variates were constructed for the S Inner, S Middle, S Outer and N Middle Domains (where significant Regime effect was found). Environmental covariates were able to account for at least some of the variability in zooplankton community composition between regimes for all but the S Middle Domain, based on *P* values for Regime with and without environmental covariates (Table 5 vs. 2). Physical and geographic covariates explained the greatest amount of variability in large zooplankton community composition (Table 5). Temperature below the mixed layer depth was important in the N and S Middle Domains although temperature above the mixed layer depth, salinity below the mixed layer depth, ice retreat timing, latitude and longitude were also highly significant ($P<0.01$), depending on domain (Table 5). For small taxa, environmental covariates explained some of the variability in community composition between regimes in the S Inner, S Middle and N Middle Domains (Table 2 vs. 5). Similar to large taxa, physical covariates were highly significant, with temperature above and below the mixed layer depth important for the S Inner and S Middle Domains as well as stability for the S Middle Domain (Table 5). Overall, temperature explained the greatest amount of temporal variability in community structure, and was significant in models for all domains except the S Outer for large and the N Middle for small zooplankton. Most of the biologically related covariates, nutrients (ammonium and nitrate) at surface and bottom, surface Chla, percentage of large phytoplankton, and August wind mixing, were not significant.

4. Discussion

4.1. Overview

This study provides a rare look into how stanzas of warm and cold years affect the zooplankton community structure in both the

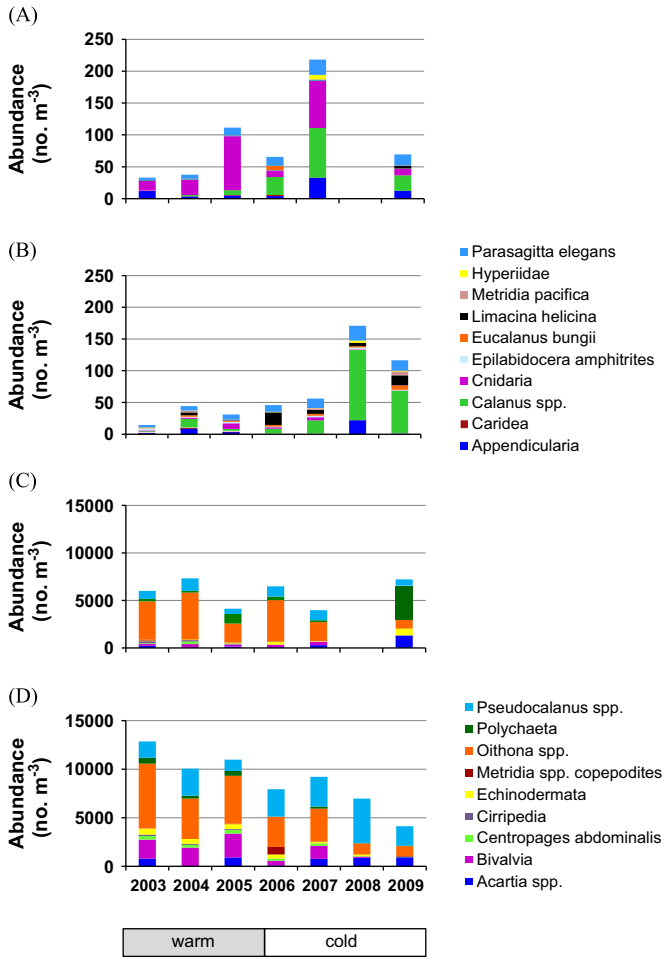

Fig. 7. Untransformed mean zooplankton abundances in the eastern Bering Sea for large taxa in the (A) south (< ~60°N) and (B) north (~60–63°N) and for small taxa in the (C) south and (D) north. Bar indicates warm and cold regimes.

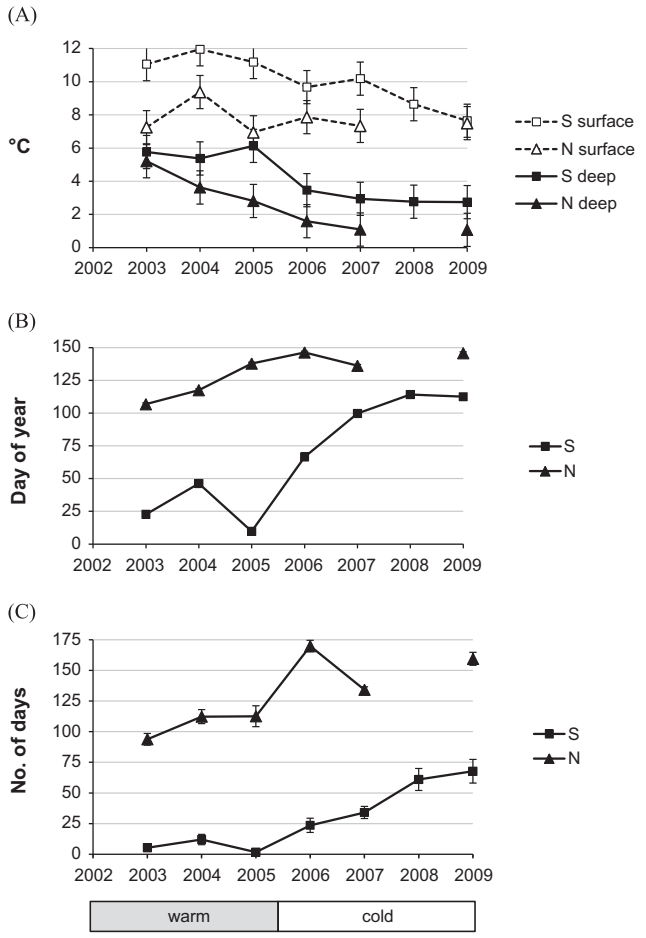

Fig. 8. (A) Mean temperature above (surface) and below (deep) the mixed layer depth during our surveys, (B) mean day of year for sea ice retreat during the prior spring, and (C) mean number of days of sea ice coverage during the prior winter, in the south (S) and north (N) Middle Domains. Standard errors are shown. Bar indicates warm and cold regimes.

north and south eastern Bering Sea and the environmental variables associated with these changes. Our analyses demonstrate the considerable cross-shelf variability in zooplankton communities as seen in prior studies (e.g. Cooney and Coyle, 1982), but also shows variability between assemblages in the north and south both in timing of changes in abundance of key taxa and total abundance and biomass. Water temperature showed the strongest relationship with large and small zooplankton community structure. We hypothesize that large taxa abundance has a direct or indirect relationship to bottom temperature (depending on taxa) and a direct relationship to the winter/spring southerly extent of sea ice (Baier and Napp, 2003); while small taxa abundance has a direct relationship to surface and bottom temperature. Ice algae and sea-ice related phytoplankton blooms in cold years may provide an early food source for large crustacean zooplankton on the southern shelf (Sigler et al., 2014). In contrast, lower temperatures may reduce temperature-dependent growth (e.g. Hirst and Lampitt, 1998), negatively impacting reproduction rates of small zooplankton with fewer cohorts produced during the growing season. However, temperature may also affect zooplankton survival, so multiple generations do not guarantee higher abundances. Possible exceptions to these conceptualized strategies for large and small taxa include increases in cold years of small copepods, *Pseudocalanus* spp. and *Acartia* spp., taxa shown to feed beneath the sea ice in Saroma-ko Lagoon, Japan (Saitoh and Hattori, 1997). Interestingly, *Metridia* spp. copepodites also increased in cold years even though adults did not: the mechanism is not known. The

Table 5
Results of best-fit PERMANOVA models using Type I (sequential) sum of squares showing *P*-values of environmental covariates for large and small zooplankton community composition. Order of inclusion in the model is shown in parentheses. An insignificant ($P > 0.05$) Regime (factor) indicates covariates explained some of the variability between regimes.

Variable	S Inner	S Middle	S Outer	N Middle
Large zooplankton				
Longitude	–	–	0.006 (1)*	–
Latitude	–	–	–	0.006 (1)*
Integrated Chla	0.012 (1)*	–	–	–
Winter wind direction	0.014 (2)*	–	–	–
S below MLD	–	0.001 (1)*	–	–
T below MLD	–	0.001 (2)*	–	0.001 (2)*
T above MLD	0.030 (3)*	0.001 (3)*	–	–
Ice retreat timing	–	–	0.006 (2)*	0.082 (3)*
Regime (factor)	0.079	0.001*	0.383	0.335
Small zooplankton				
Longitude	–	0.025 (4)*		0.020 (1)*
Latitude	–	–		0.042 (2)*
T below MLD	0.001 (1)*	0.003 (3)*		–
T above MLD	0.001 (2)*	0.001 (2)*		–
Ice retreat timing	–	–		0.202 (3)
Stability	–	0.001 (1)*		–
Regime (factor)	0.393	0.061		0.252

* Significant at $P < 0.05$.

observed changes in community composition were not abrupt, but showed gradual changes over a period of years, concordant with changes in sea ice and water temperature. Species-specific responses in cold years include both increases in omnivorous *Calanus* spp., *Neocalanus* spp., and in predators such as *P. elegans*, and decreases (with large interannual variability) in predatory Cnidaria (*A. digitale*).

4.2. Temporal and spatial patterns in community structure between regimes

Assemblages often were clustered together based on domain with separate groups of oceanic (e.g. *Neocalanus* spp., *Metridia pacifica*, *Eucalanus bungii*) and neritic taxa (*Podon sp*., *Evadne sp*., Polychaeta, Bivalvia larvae). These differences are attributed to, and maintained by, the presence of hydrographic fronts that separate the domains during summer and the consistency of hydrographic and biological processes that are inherent to the different domains (Iverson et al., 1979). The extension of a Middle Domain cluster into the Inner Domain in cold years for large zooplankton suggests that the Inner Front may not be as strong (or is more leaky) in cold years, possibly resulting in increased transport across the Inner Shelf. Alternatively, the Inner Front may be established later in the season in cold than in warm years allowing more time for Middle Domain taxa to become established in areas that eventually become the Inner Domain. Previous studies suggest the Inner Front was established later in the season during years with low sea surface temperatures (SSTs) (1998 and 1999), due to storminess and late ice retreat, than during a year with high SSTs (1997) (Kachel et al., 2002). Additionally, winter wind direction was a significant co-variate for large zooplankton in the S Inner Domain, suggesting the differences in wind fields may be related to onshore transport or timing of set up for the Inner Front (Kachel et al., 2002, Danielson et al., 2012). Inshore–offshore changes in centers of distribution within domains are also suggested by the importance of latitude or longitude in our best-fit models for small taxa within the N and S Middle Domains and large taxa within the N Middle and S Outer Domains.

The recent regime shifts influenced large and small zooplankton community structure over most shelf domains, but variations were greatest in the S Middle Domain, where the largest physical changes (e.g. sea ice retreat timing, temperature) were observed (Stabeno et al., 2012a). The high significance of surface temperature (and higher abundances) for small taxa in the south but not in the north may be because in the north, the Middle Domain summer surface temperature oscillated around 8 °C, whereas in the south, it declined from almost 12 °C in 2004 to below 8 °C in 2009. The surface layer may be where small taxa predominate, as found in the Gulf of Alaska (Marlowe and Miller, 1975).

North–south variations in Middle Domain zooplankton assemblages were also lower in cold years compared to a single warm year (2005) (Stabeno et al., 2012a). We found a similar result for 2005, but the other warm years (2003, 2004) showed much lower latitudinal variations in zooplankton assemblages. These differences may relate to interannual variability in the N–S strength of the temperature gradients. After the recent period of extended warming, even the north received heat so that in 2003 and 2004 the surface temperature gradients between the north and south were diminished. However, the north in 2005 was colder than in 2003–2004, while the south in 2005 was still warm (Danielson et al., 2011).

4.3. Interannual variations in total abundance and biomass

Total abundance and total biomass of zooplankton also varied by N–S region and regime. In the south, total abundances of large taxa were highest in cold years, and similarly total biomass for large zooplankton taxa increased 5–10 fold between 2005–2007 and 2008–2009. This is relevant to the feeding of small age-0 fishes, such as Walleye Pollock (*Gadus chalcogramma*, herein referred to as pollock). The improvement in age-0 pollock condition in cold years as evidenced by increased total energy content (kJ gm^{-1} wet weight) is attributed to the higher availability of large, lipid bearing zooplankton prey such as *Calanus* spp. and *Thysanoessa* spp. (Euphausiacea) in cold years (Coyle et al., 2011; Hunt et al., 2011; Heintz et al., 2013). *Calanus* spp., and *Neocalanus* spp. are also important prey for other forage fish such as juvenile Pacific salmon (*Oncorhynchus* spp.), Pacific Herring (*Clupea pallasi*) and Capelin (*Mallotus villosus*), planktivorous sea birds and endangered baleen whales such as the North Pacific Right Whale (*Eubalaena japonica*) (Russell et al., 1999; Springer et al., 2008; Sheffield-Guy et al., 2009; Coyle et al., 2011; Wade et al., 2011; Heintz et al., 2013). Therefore, decreases in large lipid-rich crustacean zooplankton in warm years may be detrimental to a variety of predators, not just pollock. In contrast to large taxa, biomass for small zooplankton in the southeastern Bering Sea was not different between regimes, even though abundances were lower in cold than warm years. This indicates that reductions in abundances of very small taxa such as *Oithona* spp. were compensated for by increases in abundances of larger taxa such as *Pseudocalanus* spp. and *Acartia* spp. Future work is needed to determine its impact on trophic transfer and production at higher trophic levels.

The northeastern Bering Sea did not follow the same pattern as the south. In the north, the abundance of large taxa increased 4-fold between 2004 and 2005, and in 2007 reached the same levels as observed in the south a year later (2008). Increases in the north were due to both Cnidaria and *Calanus* spp., while in the south they were due primarily to *Calanus* spp. Unlike in the south, total biomass for large zooplankton remained fairly constant in the north, even though taxonomic composition changed. The abundance and biomass of small taxa in the north declined slightly (not significantly) from 2004 to 2005, coincident with a drop in water temperature, and then remained at that level for the remainder of our time series.

Total zooplankton biomass (sum of the small and large taxa) was highest in the coldest years (2008–2009) in the south due to increases in large zooplankton biomass, but remained constant across all years in the north. Large and small taxa contributed equally to total biomass except in the south in 2008–2009, where the contribution to total biomass was 2–4 times higher for large compared to small taxa. This result for the southeastern Bering Sea was previously shown by Coyle et al. (2011), however biomass levels for the north and their relation to the south in warm and cold years is new. This suggests that as the climate warms, the total biomass available for higher trophic levels will decrease in the south, but may not change in the northeastern Bering Sea.

4.4. Proposed mechanisms driving variations in abundances of key taxa

Finally, to synthesize the information on changes in abundances and the environmental factors responsible for these changes between regimes and north–south regions, we describe potential mechanisms for some of the key herbivorous and predatory zooplankton taxa: *Calanus* spp., *Neocalanus* spp., *P. elegans* and *A. digitale* (Cnidaria).

Calanus spp. had the greatest impact on large zooplankton community structure between warm and cold regimes. Increases in *Calanus* spp. in cold years have been documented for the southeastern Bering Sea (Hunt et al., 2008; Coyle et al., 2011; Hunt et al., 2011; Stabeno et al., 2008, 2010, 2012b), but data were not available for the north. One proposed mechanism driving increases

in cold years in the south is that when ice algae are available there is an early source of food for *Calanus* spp. reproduction (Hunt et al., 2002; Baier and Napp, 2003; Durbin and Casas, 2013; Sigler et al., 2014). An early season ice-associated phytoplankton bloom can also provide a source of energy for metamorphosis and growth (Baier and Napp, 2003; Sigler et al., 2014). Lower winter water temperatures will also lower metabolic rates which allow *Calanus* spp. to reduce the energy required for survival. Therefore, a series of cold years may facilitate increases in spawning biomass and reproductive output resulting in a stronger year class (Sigler et al., 2014). A corollary of this is that warmer summer temperatures lead to increased food limitation due to increased metabolic requirements and reductions in net primary production (Lomas et al., 2012), which result in reductions in zooplankton lipid (energy) stores, poor overwinter survival, and fewer copepodites produced the following spring (Coyle et al., 2011).

In the southeastern Bering Sea, late summer abundance of *Calanus* spp. increased in 2007, the first year the majority of the S Middle Domain was ice covered, so the availability of an early spring algal food source, may have been important in this region. In the north, increases in ice coverage and retreat were seen from 2003 to 2006, but had a smaller range of variability than seen in the south. We do not yet understand what processes promoted increases in *Calanus* spp. in the northeastern Bering Sea starting in 2006; because this region was at least partially ice covered until mid-April in all years and presumably ice algae were available all years. Finally, because the *Calanus* spp. we sampled were a combination of *Calanus marshallae* and *Calanus glacialis*, changes in advection in the north and south of these different taxa may also be at play, and these two taxa may respond to changes in climate and temperature in different ways. *C. marshallae* was previously thought to be dominant in the southeastern Bering Sea, while *C. glacialis* dominated further northward in the Bering, Chukchi and Beaufort Seas (Frost, 1974). The highest abundances of *Calanus* spp. were observed in 2007 in the north and in 2008 in the south, a year after *Calanus* spp. began to increase in each region. This suggests that sequential years of cold conditions are advantageous to build large biomass of the species. Decreases in *Calanus* spp. in 2009 in the current study could be due to increases in predation from *Themisto libellula*, an arctic hyperid amphipod (Pinchuk et al., 2013).

Parasagitta elegans also increased in cold years with the largest abundances observed in 2007. *P. elegans* is a voracious predator of the early developmental stages of large and small copepods in the eastern Bering Sea (Baier and Terazaki, 2005), so this increase may be a response to increases in prey availability. On the southeastern shelf for 1995–1999, the most frequently consumed prey of *P. elegans* was *Calanus* nauplii in cold icy years when *Calanus* spp. were in higher abundance, with *Pseudocalanus* spp. predominantly consumed in relatively warmer years (Baier and Terazaki, 2005).

Neocalanus spp. overwinter off the shelf at depths of 200–2000 m (e.g. Miller et al., 1984). The newly hatched nauplii and copepodites ascend to the upper layer in late winter to early spring, where they complete their development by early summer (Vidal and Smith, 1986) and start to descend to deeper layers. Recent modeling suggests that wind is a primary factor controlling inter-annual variability in on-shelf transport of *Neocalanus* spp. (Gibson et al., 2013). Southeasterly winds, which prevailed during warm years, enhanced the on-shelf transport of oceanic zooplankton over the southern shelf, while northwesterly winds, more common in cold years, reduced onshore transport. This suggests that *Neocalanus* spp. abundance would be lower during cold years since it would be more difficult to move onto the southern shelf in spring (Danielson et al., 2012; Gibson et al., 2013). However, *Neocalanus* spp. abundance increased in cold years over the S Middle Domain in our data set and there was no significant difference in its abundance between warm and cold years over the Outer shelf. Thus, the explanation for variations in *Neocalanus* spp. abundance over the shelf is likely more complicated with multiple factors important (e.g. transport, food availability, predation).

Aglantha digitale, a small (10–40 mm long) hydromedusan jellyfish, was the most numerous Cnidarian collected in our bongo nets from 2005 to 2009, making up 93% (ranged 87–97% by year) of the total Cnidarian abundance. *A. digitale* is an ambush predator capable of retaining small, motile prey (Costello and Colin, 2002). This taxon has been shown to ingest adults and larvae of small copepods (*Oithona* spp., *Acartia* spp., *Pseudocalanus* spp., *Temora longicornis*), *Evadne* sp., *Oikopleura* spp., zooplankton eggs, veligers, tintinnids and dinoflagellates (Matsakis and Conover, 1991; Pages et al., 1996; Costello and Colin, 2002) with an estimated maximum prey size of 1.5 mm (Prudkovsky, 2006). Matsakis and Conover (1991) found that medusan carbon weight and total zooplankton carbon biomass varied reciprocally in studies in Bedford Basin, Nova Scotia. For the current study, in the northeastern Bering Sea with the exception of 2009, small copepod abundances tended to be higher when Cnidaria (*A. digitale* primarily) abundances were lower and vice versa (Fig. 7). Thus, predation by *A. digitale* on small copepods may be one factor to help explain these interannual changes in abundances. Higher numbers of Cnidarians in the northeastern Bering Sea may also partially account for lower numbers of small taxa in the north compared to the south. Average abundances of *A. digitale* and total copepods, respectively, were 42.5 m^{-3} and 3800 m^{-3} in the north and 4.3 m^{-3} and 6600 m^{-3} in the south, for 2005–2009 for the Inner and Middle Domains combined. If *A. digitale* consumes an average of 13.9 copepod prey per day (based on feeding experiments at 4 °C, Matsakis and Conover, 1991), then for the north and south respectively, they can consume 15% and 1% of the total copepod standing stock per day. In other studies, gelatinous zooplankton often consume $<10\%$ of prey resources, but can consume over 50% during episodic events (Matsakis and Conover, 1991 and references there in; Pages et al., 1996). We also found that *A. digitale* abundances were 63% and 72% higher in a warm year (2005) than in cold years (2006–2009) for the north and southeastern Bering Sea, respectively.

5. Conclusions

Changes in eastern Bering Sea zooplankton community composition in response to climate change will vary by oceanographic domain and by latitude, with larger effects predicted for the south compared to the northeastern Bering Sea. This impact will be stronger on large, than on small zooplankton community structure. Reductions in sea ice coverage and changes in ice retreat timing and subsequent decreases in food resources in the spring, increases in temperature and basal metabolic requirements, and potential changes in advection may be detrimental for large crustacean taxa such as *Calanus* spp. and *Neocalanus* spp. The negative impact of warming on large, lipid-rich zooplankton taxa is expected to propagate through the food web affecting commercial fisheries, seabirds, and protected species. In the eastern Bering Sea, statistical relationships between water temperature and recruitment of pollock have been used in combination with accepted climate change scenarios to project a future decrease in one of the world's largest fisheries (Ianelli et al., 2011; Mueter et al., 2011). Our work helps to elucidate the mechanisms behind that statistical relationship.

Alterations in the composition of small zooplankton assemblages from climate change may also contribute to anticipated effects at higher trophic levels. In the eastern Bering Sea, *Oithona* spp., dominant during the warm regime, decreased in abundance in the cold regime, while *Pseudocalanus* and *Acartia* spp. increased.

This species replacement had no net effect on the total biomass, but we speculate that it did affect trophic pathways, as *Pseudocalanus* and *Acartia* spp. are considered more favorable as food for other planktivores (e.g. *Oithona* spp. nauplii are under-represented in larval pollock stomachs). Accordingly under future warming scenarios, global food webs, which include humans, (*sensu* Rice and Garcia, 2011) may be impacted to a higher degree in regions that become ice-free compared to those which retain seasonal ice coverage.

Acknowledgments

We thank the captain and crews of the NOAA ship *Oscar Dyson*, and charter vessels, *Sea Storm*, *NW Explorer*, and *Epic Explorer*, for their years of hard work and diligence on our surveys. We are grateful for the assistance in field sampling, data processing and analysis from NOAA scientific staff and volunteers. In particular we would like to thank K. Cieciel, J. Gann and F. Van Tulder for sampling, processing and database maintenance of oceanographic data, M. Auburn-Cook, M. Courtney, A. Feldman, E. Farley, J. Murphy and B. Wing for the many years of survey participation and assistance with zooplankton collection and processing. We are deeply appreciative of the TINRO scientists, in particular N. Kuznetseva and A. Volkov, who conducted the onboard taxonomic analysis of Juday samples. We thank K. Coyle and his lab for assistance and guidance regarding zooplankton sampling and analysis, as well as the Polish Plankton Sorting and Identification Center for their contributions to the early part of this time series. K. Coyle also provided insightful comments on an earlier version of this manuscript. We greatly appreciate the helpful comments from the three anonymous reviewers and the journal editor, C. Ashjian. Funding was provided by the North Pacific Research Board, Bering Sea Fisherman's Association, Arctic-Yukon-Kuskokwim-Sustainable-Salmon-Initiative, and NOAA National Marine Fisheries Service including the Fisheries and the Environment (FATE) and the North Pacific Climate Regimes and Ecosystem Productivity (NPCREP) programs. This is contribution FOCI-0807 to NOAA's Ecosystems Fisheries Oceanography Coordinated Investigations, publication 123 for BEST/BSIERP and publication 460 for the North Pacific Research Board (NPRB).

References

Anderson, M.J., Gorley, R.N., Clarke, K.R., 2008. PERMANOVA+ for PRIMER: guide to software and statistical methods. PRIMER-E, Plymouth.

Baier, C.T., Napp, J.M., 2003. Climate-induced variability in *Calanus marshallae* populations. J. Plankton Res. 25, 771–782.

Baier, C.T., Terazaki, M., 2005. Interannual variability in a predator-prey interaction: climate, chaetognaths and copepods in the southeastern Bering Sea. J. Plankton Res 27 (11), 1113–1125.

Bray, J.R., Curtis, J.T., 1957. An ordination of the upland forest communities of Southern Wisconsin. Ecol. Monogr. 27, 325–349.

Cieciel, K., Farley, E.V., Eisner, L.B., 2009. Jellyfish and juvenile salmon associations with oceanographic characteristics during warm and cool years in the eastern Bering Sea. North Pac. Anadromous Fish Comm. Bull. 5, 209–224.

Clarke, K.R., Warwick, R.M., 2001. Change in Marine Communities: An Approach to Statistical Analysis and Interpretation, 2nd ed. PRIMER-E, Plymouth.

Clarke, K.R., Gorley, R.N., 2006. PRIMER v6: User Manual/Tutorial. PRIMER-E, Plymouth.

Coachman, L.K., 1986. Circulation, water masses and fluxes on the southeastern Bering Sea shelf. Cont. Shelf Res. 5, 23–108.

Cooney, R.T., Coyle, K.O., 1982. Trophic implications of cross-shelf copepod distributions in the southeastern Bering Sea. Mar. Biol. 70 (2), 187–196.

Costello, J.H., Colin, S.P., 2002. Prey resource use by coexistent hydromedusae from Friday Harbor, Washington. Limnol. Oceanogr. 47 (4), 934–942.

Coyle, K.O., Chavtur, V.G., Pinchuk, A.I., 1996. Zooplankton of the Bering Sea: A review of Russian-language literature. In: Mathisen, O., Coyle, K.O. (Eds.), Ecology of the Bering Sea: A review of Russian Literature, Alaska Sea Grant Program Report no. 96-01, University of Alaska, Fairbanks, pp. 97–133.

Coyle, K.O., Pinchuk, A.I., 2002. Climate-related differences in zooplankton density and growth on the inner shelf of the southeastern Bering Sea. Prog. Oceanogr. 55, 177–194.

Coyle, K.O., Pinchuk, A.I., Eisner, L.B., Napp, J.M., 2008. Zooplankton species composition, abundance and biomass on the eastern Bering Sea shelf during summer: the potential role of water column stability and nutrients in structuring the zooplankton community. Deep Sea Res. II 55, 1775–1791.

Coyle, K.O., Eisner, L.B., Mueter, F.J., Pinchuk, A.I., Janout, M.A., Cieciel, K.D., Farley, E.V., Andrews, A.G., 2011. Climate change in the southeastern Bering Sea: impacts on pollock stocks and implications for the oscillating control hypothesis. Fish Oceanogr. 20, 139–156.

Danielson, S., Eisner, L., Weingartner, T., Aagaard, K., 2011. Thermal and haline variability over the central Bering Sea shelf: seasonal and interannual perspectives. Cont. Shelf Res. 31, 539–554.

Danielson, S., Hedstrom, K., Aagaard, K., Weingartner, T., Curchitser, E., 2012. Wind-induced reorganization of the Bering shelf circulation. Geophys. Res. Lett. 39, L08601, http://dx.doi.org/10.1029/2012GL051231.

Durbin, E.G., Casas, M.C., 2013. Early reproduction by *Calanus glacialis* in the Northern Bering Sea: the role of ice algae as revealed by molecular analysis. J. Plankton Res, http://dx.doi.org/10.1093/plankt/fbt121.

ESRI, 2012. ArcGIS Desktop: Release 10.1. Redlands, CA: Environmental Systems Research Institute.

Farley, E.V., Moss, J.H., 2009. Growth rate potential of juvenile chum salmon on the eastern Bering Sea shelf: an assessment of salmon carrying capacity. N. Pac. Anadromous Fish Comm. Bull. 5, 265–277.

Friday, N.A., Waite, J.M., Moore, S.E., Zerbini, A.N., 2012. Cetacean distribution and abundance in relation to oceanographic domains on the eastern Bering Sea shelf: 1999–2004. Deep Sea Res. II 65–70, 260–272.

Frost, B.W., 1974. *Calanus marshallae*, a new species of Calanoid copepod closely allied to the sibling species *C. finmarchicus* and *C. glacialis*. Mar. Biol. 26, 77–99.

Gibson, G.A., Coyle, K.O., Hedstrom, K., Curchitser, E.N., 2013. A modeling study to explore on-shelf transport of oceanic zooplankton in the Eastern Bering Sea. J. Mar. Syst. 121, 47–64.

Gieskes, W.W.C., 1971. Ecology of the cladocera of the North Atlantic and the North Sea. Neth. J. Sea Res. 5 (3), 342–376.

Gold, C.M., 1991. Problems with handling spatial data—the Voronoi approach. CISM J. 45, 65–80.

Gordon, L.I., Jennings, J.C. Jr., Ross, A.A., Krest, J.M., 1993. A suggested protocol for continuous flow automated analysis of seawater nutrients (phosphate, nitrate, nitrite and silicic acid) in the WOCE Hydrographic Program and the Joint Global Ocean Fluxes Study. WOCE Hydrographic Program Office, Methods Manual WHPO 91-1, Oregon State University, Corvallis.

Grebmeier, J.M., Overland, J.E., Moore, S.E., Farley, E.V., Carmack, E.C., Cooper, L.W., Frey, K.E., Helle, J.H., McLaughlin, F.A., McNutt, S.L., 2006. A major ecosystem shift in the northern Bering Sea. Science 311 (5766), 1461–1464.

Harvey, H.R., Sigler, M.F., 2013. An introduction to the Bering Sea Project: volume II. Deep Sea Res. II (94), 2–6.

Heintz, R.A., Siddon, E.C., Farley Jr., E.V., Napp, J.M., 2013. Climate-related changes in the nutritional condition of young-of-the-year walleye pollock (*Theragra chalcogramma*) from the eastern Bering Sea. Deep Sea Res. II 94, 150–156.

Hirst, A.G., Lampitt, R.S., 1998. Towards a global model of in situ weight specific growth in marine planktonic copepods. Mar. Biol. 132, 247–257.

Hollowed, A.B., Barbeaux, S.J., Cokelet, E.D., Farley, E., Kotwicki, S., Ressler, P.H., Spital, C., Wilson, C.D., 2012. Effects of climate variations on pelagic ocean habitats and their role in structuring forage fish distributions in the Bering Sea. Deep Sea Res. II 65-70, 230–250.

Hunt Jr., G.L., Stabeno, P.J., Walters, G., Sinclair, E., Brodeur, R.D., Napp, J.M., Bond, N.A., 2002. Climate change and control of the southeastern Bering Sea pelagic ecosystem. Deep Sea Res. II 49, 5821–5853.

Hunt, G.L., Stabeno, P.J., Strom, S., Napp, J.M., 2008. Patterns of spatial and temporal variation in the marine ecosystem of the southeastern Bering Sea, with special reference to the Pribilof Domain. Deep Sea Res. II 55, 1919–1944.

Hunt Jr., G.L., Coyle, K.O., Eisner, L.B., Farley, E.V., Heintz, R., Mueter, F., Napp, J.M., Overland, J.E., Ressler, P.H., Salo, S., Stabeno, P.J., 2011. Climate impacts on eastern Bering Sea food webs: A synthesis of new data and an assessment of the oscillating control hypothesis. ICES J. Mar. Sci. 68, 1230–1243.

Ianelli, J.N, Hollowed, A.B., Haynie, A.C., Mueter, F.J., Bond, N.A., 2011. Evaluating management strategies for eastern Bering Sea walleye pollock (*Theragra chalcogramma*) in a changing environment. ICES J. Mar. Sci. 68 (6), 1297–1304.

Iverson, R.L., Coachman, L.K., Cooney, R.T., English, T.S., Goering, J.J., Hunt Jr., G.L., McCauley, M.C., McRoy, C.P., Reeburg, W.S., Whitledge, T.E., 1979. Ecological significance of fronts in the southeastern Bering Sea. In: Livingston, R.J. (Ed.), Ecological Processes in Coastal and Marine Systems. Plenum Press, pp. 437–466.

Johnson, M., 1934. The life history of the copepod *Tortanus discaudatus* (Thomspon and Scott). Biological Bull., Woods Hole 67, 182–200.

Kachel, N.B., Hunt Jr., G.L., Salo, S.A., Schumacher, J.D., Stabeno, P.J., Whitledge, T.E., 2002. Characteristics and variability of the inner front of the southeastern Bering Sea. Deep Sea Res. II 49 (26), 5889–5909.

Kos, M.S., 1977. Species of the genus *Eurytemora* (Copepoda, Calanoida) in the northern part of the Pacific Ocean: systematics, distribution, variability. Explor. Fauna Seas 20, 20–53.

Kotwicki, S., Lauth, R.R., 2013. Detecting temporal trends and environmentally-driven changes in the spatial distribution of groundfishes and crabs on the eastern Bering Sea shelf. Deep Sea Res. II 94, 231–243.

Lomas, M.W., Moran, S.B., Casey, J.R., Bell, D.W., Tiahlo, M., Whitefield, J., Kelly, R.P., Mathis, J.T., Cokelet, E.D., 2012. Spatial and seasonal variability of primary production on the Eastern Bering Sea shelf. Deep Sea Res II 65-70, 126–140.
Marlowe, C.J., Miller, C.B., 1975. Patterns of vertical distribution and migration of zooplankton at ocean Station "P". Limnol. Oceanogr. 20 (5), 824–844.
Matsakis, S., Conover, R.J., 1991. Abundance and feeding of medusae and their potential impact as predators on other zooplankton in Bedford Basin (Nova Scotia, Canada) during spring. Can. J. Fish. Aquat. Sci. 48 (8), 1419–1430.
Miller, C.B., Frost, B.W., Batchelder, H.P., Clemons, M.J., Conway, R.E., 1984. Life histories of large, grazing copepods in a subarctic ocean gyre: Neocalanus plumchrus, Neocalanus cristatus and Eucalanus bungii in the northeast Pacific. Prog. Oceanogr. 13, 201–243.
Motoda, S., Minoda, T., 1974. Plankton of the Bering Sea. In: Hood, D.W., Kelley, E.J. (Eds.), Oceanography of the Bering Sea with Emphasis on Renewable Resources. University of Alaska Press, pp. 207–241.
Mueter, F.J., Bond, N.A., Ianelli, J.N., Hollowed, A.B., 2011. Expected declines in recruitment of walleye pollock (*Theragra chalcogramma*) in the eastern Bering Sea under future climate change. ICES J. Mar. Sci. 68 (6), 1284–1296.
Napp, J.M., Hunt Jr., G.L., 2001. Anomalous conditions in the southeastern Bering Sea, 1997: linkages among climate, weather, ocean, and biology. Fish Oceanogr. 10, 61–68.
Napp, J.M., Baier, C.T., Brodeur, R.D., Coyle, K.O., Shiga, N., Mier, K., 2002. Interannual and decadal variability in zooplankton communities of the southeast Bering Sea shelf. Deep Sea Res. II 49, 5991–6008.
Ortiz, I, Weise, F., Greig, A., 2012. Marine Regions Boundary Data for the Bering Sea Shelf and Slope. UCAR/NCAR – Earth Observing Laboratory/Computing, data, and software facility. Dataset , http://dx.doi.org/10.5065/D6DF6P6C.
Pages, F., Gonzalez, H.E., Gonzalez, S.R., 1996. Diet of the gelatinous zooplankton in Hardangerfjord (Norway) and potential predatory impact by *Aglantha digitale* (trachymedusae). Mar. Ecol. Prog. Ser. 139 (1–3), 69–77.
Parsons, T.R., Maita, Y., Lalli, C.M., 1984. A Manual of Chemical and Biological Methods for Seawater Analysis. Pergamon Press, Oxford, England, p. 173.
Piatt, J.F., Springer, A.M., 2003. Advection, pelagic food webs and the biogeography of seabirds in *Beringia*. Mar. Ornithol. *31*, 141–154.
Pinchuk, A.I., Coyle, K.O., Farley, E.V., Renner, H.M., 2013. Emergence of the Arctic *Themisto libellula* (Amphipoda: Hyperiidae) on the southeastern Bering Sea shelf as a result of the recent cooling and their potential impact on pelagic food web. ICES J. Mar. Sci. 70 (6), 1244–1254.
Prudkovsky, A.A., 2006. Food selectivity in *Aglantha digitale* (Hydrozoa, Trachymedusae) in the White Sea. Zool. Zh. 85 (11), 1294–1302.
Rice, J.C., Garcia, S.M., 2011. Fisheries, food security, climate change, and biodiversity: characteristics of the sector and perspectives on emerging issues. ICES J. Mar. Sci. 68, 1343–1353.
Russell, R.W., Harrison, N.M., Hunt, G.J., 1999. Foraging at a front: Hydrography, zooplankton, and avian planktivory in the northern Bering Sea. Mar. Ecol. Prog. Ser. 182, 77–93.
Saitoh, H., Hattori, H., 1997. Diel vertical migration and feeding rhythm of copepods under sea ice at Saroma-ko Lagoon. J. Mar. Syst. 11, 191–203.
Sameoto, D., Cochrane, N., Herman, A., 1993. Convergence of acoustic, optical, and net-catch estimates of euphausiid abundance: Use of artificial light to reduce net avoidance. Can. J. Fish. Aquat. Sci. 50, 334–346.
Sheffield-Guy, L., Roby, D.D., Gall, A.E., Irons, D.B., Rose, I.C., 2009. The influence of diet and ocean conditions on productivity of auklets on St Lawrence Island, Alaska. Mar. Ornithol. 37 (3), 227–236.
Sigler, M.F., Stabeno, P.J., Eisner, L.B., Napp, J.M., Mueter, F.J., 2014. Spring and fall phytoplankton blooms in a productive subarctic ecosystem, the eastern Bering Sea, during 1995–2011. Deep-Sea Res. II 109, 71–83, http://dx.doi.org/10.1016/j.dsr2.2013.12.007.
Simpson, J.H., Hughes, D.G., Morris, N.C.G., 1977. The relation of seasonal stratification to tidal mixing on the continental shelf. Deep Sea Res. 24 (Suppl.), S327–S340.
Springer, A.M., Byrd, G.V., Iverson, S.J., 2008. Hot oceanography: planktivorous seabirds reveal ecosystem responses to warming of the Bering Sea. Mar. Ecol. Prog. Ser. 352, 289–297.
Stabeno, P.J., Kachel, N., Mordy, C., Righi, D., Dalo, S., 2008. An examination of the physical variability around the Pribilof Islands in 2004. Deep Sea Res. II 55 (16-17), 1701–1716.
Stabeno, P.J., Napp, J., Mordy, C., Whitledge, T., 2010. Factors influencing physical structure and lower trophic levels of the eastern Bering Sea shelf in 2005: sea ice, tides and winds. Prog. Oceanogr. 85 (3–4), 180–196.
Stabeno, P.J., Farley, E.V., Kachel, N., Moore, S., Mordy, C., Napp, J.M., Overland, J.E., Pinchuk, A.I., Sigler, M., 2012a. A comparison of the physics, of the northern and southern shelves of the eastern Bering Sea and some implications to the ecosystem. Deep Sea Res. II 65–70, 14–30.
Stabeno, P.J., Kachel, N.B., Moore, S.E., Napp, J.M., Sigler, M., Yamaguchi, A., Zerbini, A.N., 2012b. Comparison of warm and cold years on the southeastern Bering Sea shelf and some implications for the ecosystem. Deep Sea Res. II 65–70, 31–45.
Stevenson, D.E., Lauth, R.R., 2012. Latitudinal trends and temporal shifts in the catch composition of bottom trawls conducted on the eastern Bering Sea shelf. Deep Sea Res. II 65–70, 251–259.
Thiessen, A.J., Alter, J.C., 1911. Precipitation averages for large areas. Mon. Weather Rev. 39, 1082–1084.
Vidal, J., Smith, S.L., 1986. Biomass, growth, and development of populations of herbivorous zooplankton in the southeastern Bering Sea during spring. Deep Sea Res. 33, 523–556.
Volkov, A.F., 1984. Recommendations for Expedited Zooplankton Sample Processing at Sea. TINRO, Vladivostok p. 31 (in Russian).
Volkov, A.F., Efimkin, A.Y., Kuznetseva, N.A., 2007. Characteristics of the plankton community of the Bering Sea and several regions of the North Pacific in 2002–2006. Izv. TINRO 151, 338–364 (in Russian).
Wade, P.R., De Robertis, A., Hough, K., Booth, R, Kennedy, A., LeDuc, R., Munger, L., Napp, J., Shelden, K.E.W., Rankin, S., Vasquez, O., Wilson, C., 2011. Rare detections of North Pacific right whales in the Gulf of Alaska, with observations of their potential prey. Endang. Species Res. 13, 99–109.
Wiebe, P.H., Ashjian, C.J., Gallager, S.M., Davis, C.S., Lawson, G.L., Copley, N.J., 2004. Using a high-powered strobe light to increase the catch of Antarctic krill. Mar. Biol. 144, 493–502.
Wiese, F.K., Wiseman, W.J., van Pelt, T.I., 2012. Bering Sea linkages. Deep Sea Res. II 65–70, 2–5.
Wyllie-Echevarria, T., Wooster, W.S., 1998. Year-to-year variations in Bering Sea ice cover and some consequences for fish distributions. Fish. Oceanogr 7, 159–170.

Deep-Sea Research II 109 (2014) 172–180

Contents lists available at ScienceDirect

Deep-Sea Research II

journal homepage: www.elsevier.com/locate/dsr2

Feeding ecology of age-0 walleye pollock (*Gadus chalcogrammus*) and Pacific cod (*Gadus macrocephalus*) in the southeastern Bering Sea

Wesley W. Strasburger [a,b,*], Nicola Hillgruber [c,d], Alexei I. Pinchuk [c], Franz J. Mueter [c]

[a] Ted Stephens Marine Research Institute, Alaska Fisheries Science Center, NMFS, NOAA, 17109 Point Lena Loop Rd., Juneau, AK 99801, USA
[b] Department of Commerce, 17109 Point Lena Loop Rd., Juneau, AK 99801, USA
[c] School of Fisheries and Ocean Sciences, University of Alaska Fairbanks, 17101 Point Lena Loop Rd., Juneau, AK 99801, USA
[d] Thünen Institute of Fisheries Ecology, Wulfsdorfer Weg 204, 22926 Ahrensburg, Germany

ARTICLE INFO

Available online 10 October 2013

Keywords:
Walleye pollock
Pacific cod
Dietary composition
Feeding success
Southeastern Bering Sea
Larvae
Juveniles

ABSTRACT

Walleye pollock (*Gadus chalcogrammus*) and Pacific cod (*Gadus macrocephalus*) are of particular economic and ecological importance in the southeastern Bering Sea. The spatial and temporal overlap of early life stages of both species may explain their strongly correlated recruitment trends. Pelagic larvae and juveniles were collected during four research cruises in May, July and September of 2008, an exceptionally cold year, and their stomach contents were examined. Feeding success and diet composition of walleye pollock and Pacific cod were consistently different in spring, summer, and fall. Pacific cod larvae and juveniles always consumed larger and progressively fewer prey items per stomach than walleye pollock; this difference was particularly pronounced in the fall. Our data suggest that co-occurring early life stages of walleye pollock and Pacific cod were dividing prey resources rather than competing for them, at least during the exceptionally cold conditions in 2008 in the southeastern Bering Sea.

1. Introduction

Walleye pollock (*Gadus chalcogrammus*), hereafter called pollock, and Pacific cod (*Gadus macrocephalus*) are two of the largest and most valuable fisheries in the Bering Sea, with an annual harvest of 0.48–1.40 million metric tons (Ianelli et al., 2011) for pollock in the southeastern Bering Sea (SEBS) and 120,000–183,000 metric tons for Pacific cod in the eastern Bering Sea over the past decade (Thompson et al., 2011). These species are of ecological importance within the SEBS ecosystem (Aydin and Mueter, 2007), where they serve as prey for seabirds (Decker and Hunt, 1996), marine mammals (Sinclair et al., 1994) and other fishes, including older age-classes of pollock (Bailey, 1989). Both species are predatory, pollock consumes a variety of forage fishes (Coyle et al., 2011), while Pacific cod consume large amounts of commercially targeted crab species (Livingston, 1989; Urban, 2012). Thus, pollock and Pacific cod play a central role in the food web of the SEBS. A better understanding of the ecology of these two species and their interactions with different ecosystem components would enhance our ability to successfully model these populations via changing prey and prey quality as they are mediated by changing climatic conditions.

In the SEBS, pollock and Pacific cod exhibit similarities in early life history patterns, spatial distribution, and subsequent recruitment success (Bacheler et al., 2010; Duffy-Anderson et al., 2006; Hurst et al., 2012; Matarese et al., 2003; Mueter et al., 2011). Both species spawn from January to April (Bacheler et al., 2010; Shimada and Kimura, 1994) in relatively deep waters over the continental shelf, along the Alaska Peninsula, and near the Pribilof Islands (Bacheler et al., 2010; Fritz et al., 1993). Pollock eggs tend to be slightly positively buoyant and pelagic, while Pacific cod eggs tend to be negatively buoyant and demersal (Dunn and Materese, 1987). Post-hatch, both species rise to the epi-pelagic layer and share a similar horizontal distribution (Duffy-Anderson et al., 2006; Matarese et al., 2003). Specifically, both species have larval abundance maxima in the SEBS along the Alaska Peninsula and Aleutian Islands, particularly in and around Unimak Pass, as well as north of the Pribilof Islands (Matarese et al., 2003). During late spring and early summer, pelagic larvae and juveniles are concentrated in the upper mixed layer (10–40 m). By the fall, juvenile pollock disperse throughout the water column at standard lengths (SL) > 40 mm, while Pacific cod juveniles begin to settle out to a demersal lifestyle earlier in the year at > 35 mm SL (Bailey, 1989; Blackburn and Jackson, 1982; Ciannelli et al., 1998; Dunn and Materese, 1987; Nishiyama et al., 1986; Rugen and Materese, 1988).

* Corresponding author at: Ted Stephens Marine Research Institute, Alaska Fisheries Science Center, NMFS, NOAA, 17109 Point Lena Loop Rd., Juneau, AK 99801, USA. Tel.: +1 907 789 6009; fax: +1 907 789 6408.
E-mail addresses: wes.strasburger@noaa.gov (W.W. Strasburger), nhillgruber@alaska.edu (N. Hillgruber), aipinchuk@alaska.edu (A.I. Pinchuk), fmueter@alaska.edu (F.J. Mueter).

0967-0645/$ - see front matter © 2013 Elsevier Ltd. All rights reserved.
http://dx.doi.org/10.1016/j.dsr2.2013.10.007

Due to the spatial and temporal overlap of early pelagic life stages, and because of similarities in body size and shape, it is reasonable to assume that pollock and Pacific cod exploit similar prey resources, resulting in potential dietary overlap and the possibility for competition. Numerous studies have been conducted on the diet of larval and juvenile pollock in the SEBS, most of these diet studies focused either on larval fish in spring (Hillgruber et al., 1995; Nishiyama et al., 1986; Porter et al., 2005) or on juvenile stages later in the fall (Brodeur et al., 2000; Coyle et al., 2008, 2011; Moss et al., 2009; Schabetsberger et al., 2000, 2003). Published information regarding feeding success and dietary patterns of age-0 Pacific cod in the SEBS is limited, and is only available for juveniles later in their first year (Lee, 1985). Knowledge of early life stage feeding patterns in both species is of importance to better understand recruitment success, particularly in light of changing environmental conditions in the Arctic and sub-Arctic (Hunt et al., 2011).

The SEBS experiences oscillating temperature ranges (Mueter and Litzow, 2008; Overland and Stabeno, 2004) marked by variable sea ice conditions (i.e., extent, thickness, and time of retreat), water temperature, and stratification in this region (Stabeno et al., 2012). These changes in the physical environment influence the timing, duration, and magnitude of the spring bloom, as well as recruitment success, growth, and nutritional condition of the zooplankton community (Hunt and Stabeno, 2002; Hunt et al., 2002, 2011; Walsh and McRoy, 1986); which in turn affects larval and juvenile pollock and Pacific cod relying on the zooplankton community for prey (Coyle et al., 2011; Hunt et al., 2011; Moss et al., 2009). Seasonal sampling for this study was conducted in 2008, a year characterized by heavy sea ice cover, late ice retreat, and cold temperatures (Stabeno et al., 2012). The overall goal of this study was to examine and compare feeding success and dietary composition of both pollock and Pacific cod during their first year, and during cold conditions in the SEBS. The underlying hypothesis was that larvae and juveniles of these two species, which share ecological preferences, may feed on similar prey items and during cold conditions may both primarily consume large prey taxa (*Calanus marshallae/glacialis*, hereafter referred to as *Calanus* spp. and juvenile *Thysanoessa* spp.) which in turn may contribute to coincident strong cohorts. To test this hypothesis we

1) compared patterns of dietary composition of larvae and juveniles of these two gadoid species, and
2) compared measures of feeding success and dietary composition from the exceptionally cold growing season in 2008 to previous studies to evaluate environmental effects on recruitment potential.

2. Methods

2.1. Sample collection

This study was based on samples of early life history stages of pollock and Pacific cod that were acquired opportunistically from multiple projects (Table 1). The goal of sample acquisition was to obtain a good seasonal coverage of age-0 larval and juvenile stages of both species. Early life stages were obtained from sampling efforts in spring (May), summer (July), and fall (September) of 2008.

In spring of 2008, pre-flexion larvae were collected by the Alaska Fisheries Science Center, National Marine Fisheries Service participating in the Bering Sea Project (AFSC, NMFS; Fig. 1A). Fish larvae were collected with oblique 60 cm diameter Bongo tows (Table 1). Sampling was conducted 24 h a day; however, only two stations included in this study were sampled after dusk. After retrieval of the sampling gear, all fish larvae were removed from the codend and preserved in 5% buffered formalin-seawater solution. Six pollock and 8 Pacific cod larvae in these collections still retained a yolk-sac and were therefore considered to be not yet

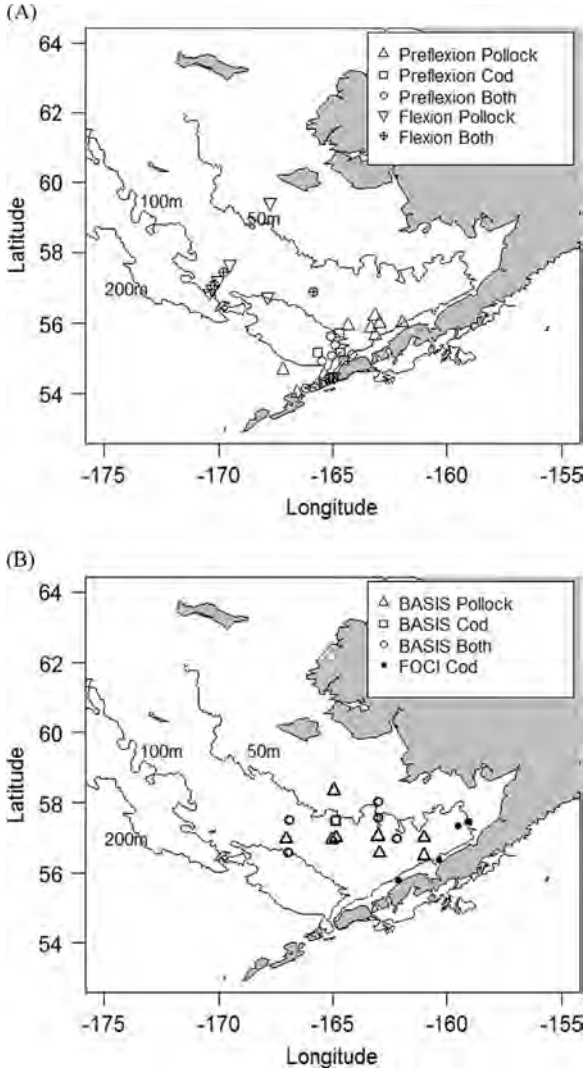

Fig. 1. Sampling sites for walleye pollock and Pacific cod used in this study. (A) Spring and mid-summer samples and (B) fall samples. See Table 1 for cruise details.

Table 1
Sample size (*N*) of walleye pollock and Pacific cod collected in 2008 by season (spring, summer, and fall), agency and/or project, sample gear, and mesh size. FOCI: Fisheries Oceanography Coordinated Investigations; NOAA AFSC: National Oceanic and Atmospheric Administration, Alaska Fisheries Science Center; BEST/BSIERP SFOS: Bering Ecosystem Studies/Bering Sea Integrated Ecosystem Research Project, School of Fisheries and Ocean Sciences; BASIS: Bering-Aleutian Salmon International Survey.

Season	Project/Agency	Gear	Mesh	Sample date range	Number of hauls (# of hauls with both pollock and cod)	Walleye pollock, *N* (size range, mm)	Pacific cod, *N* (size range, mm)
Spring	FOCI, NOAA AFSC	Bongo	500 μm	May 12–28	21 (7)	17 (3.2–7.4)	17 (3.0–7.6)
Summer	BEST-BSIERP SFOS	MOCNESS	500 μm	July 3–31	11 (4)	11 (4.4–22)	4 (9.1–16.4)
Fall	BASIS, NOAA AFSC	Rope Trawl	120 mm	September 9–27	14 (5)	13 (36.2–88)	6 (52.8–87)
Fall	FOCI, NOAA AFSC	Beam Trawl	7.0 mm	September 10–20	4 (0)	–	4 (65–87.2)

actively feeding. Consequently, these fish were excluded from all subsequent calculations of feeding success and diet composition.

In the summer of 2008, samples of pelagic flexion larvae were obtained by the University of Alaska Fairbanks, School of Fisheries and Ocean Sciences (UAF, SFOS) during a cooperative research cruise conducted as part of the Bering Ecosystem Study, National Science Foundation (BEST, NSF) and the Bering Sea Project, North Pacific Research Board (BSIERP, NPRB; Fig. 1A). Ichthyoplankton was collected using a 1 m^2 Multiple Opening/Closing Net and Environmental Sensing System (MOCNESS; Wiebe et al., 1976). The oblique MOCNESS tows provided depth-stratified samples in 20 m increments from a depth of 100 m, or near the bottom, to the surface. Sampling was conducted 24 h a day; however, no stations included in this study were sampled after dusk. After retrieval of the sampling gear, flexion larvae were preserved in 10% formalin seawater solution for further laboratory analysis.

In the fall of 2008, samples of pelagic juvenile pollock and Pacific cod were provided by the Bering Aleutian Salmon International Survey (BASIS), conducted by the Ted Stephens Marine Research Institute, National Oceanic and Atmospheric Administration (TSMRI, NOAA). Fish were collected with surface (0–20 m) and with midwater rope trawls (targeting acoustic signals; Fig. 1B). Sampling methods are described in more detail by Moss et al. (2009). All BASIS sampling occurred during daylight hours. After retrieval of the gear, fish were identified to species and fixed in 5% buffered formalin-seawater solution. Due to the low available sample size, demersal juvenile Pacific cod were also received from the Fisheries Oceanography Coordinated Investigations (FOCI) at the NOAA AFSC, NMFS (cruise number 3MF08; Fig. 1B); fish were collected with a beam trawl and recovered juveniles were frozen at sea for later processing.

The size range of fish processed for this study was similar across both species in every season with one exception (Table 1). The smallest juvenile Pacific cod (September) were larger than 50 mm TL, while the smallest pollock were just over 36 mm TL. However, only four juvenile pollock were smaller than 50 mm TL.

2.2. Laboratory analyses

All spring and summer fish were measured with calibrated micro-photographic software (Image Pro 3.0) to the nearest 0.1 mm SL, while fall samples were measured with a fish board to the nearest 0.1 mm TL. For each fish, the digestive tract was excised and the stomach was removed. Stomach fullness was visually estimated as: (1) empty, (2) traces, and (3–6) 25%, 50%, 75%, and 100% full (Adams et al., 2007). Stomach contents were gently removed and ingested prey items were examined with a LEICA MZ 16 stereo microscope and a LEICA DM LB2 compound microscope. Prey items were identified to the lowest taxonomic level and developmental stage possible. Total prey wet weight was determined by multiplying a mean prey taxon wet weight, obtained from zooplankton data collected from each respective cruise, by the number of that specific prey taxon in the gut. Spring zooplankton data did not include mean zooplankton wet weight estimates; therefore, volume estimates (%V as a substitute for %W) were calculated using established mensuration formulae (Napp et al., 1999). Published values of mean species and stage specific TL were used to estimate the mean TL of ingested prey.

2.3. Statistical analyses

For each season, cumulative prey curves were used to determine the number of stomachs needed to properly describe the dietary breadth of pollock and Pacific cod (Treloar et al., 2007); all stomachs were randomized 10,000 times to reduce the potential for bias due to sampling order and the mean number of new prey categories was plotted against the total number of stomachs analyzed. If the curve reached an asymptote, it was assumed that the minimum sample size needed to adequately describe the diet of pollock or Pacific cod had been met. Measures of feeding success for all stomachs were described as numerical feeding intensity (the total number of prey items per stomach), a fullness index (visually assigned values 1–6) (Adams et al., 2007), and feeding incidence (the proportion of fish with at least one ingested item) (Dauvin and Dodson, 1990). Mixed effects models using predator species as a fixed effect and location (station) as a random effect, and their respective null model (dropping the fixed species effect) were compared using a likelihood ratio test to identify significant differences in mean numerical feeding intensity, fullness, and prey size between predator species. Station means were used for all significance testing to avoid the issue of pseudo-replication. Fall numerical feeding intensity and spring and fall prey size data were log transformed to account for strong positive skew, while summer fullness and numerical feeding intensity data were square-root transformed to account for weak positive skew.

Prey composition was expressed as percent number (%*N*), percent of total prey volume (%*V*) or percent of total prey weight (%*W*), and percent frequency of occurrence (%FO) from all non-empty stomachs. Finally, the percentage index of relative importance (%IRI) was calculated from the previous indices (Cortés, 1997). Dietary comparisons were made with PRIMER Version 6 (Clarke and Gorley, 2006). Non-metric multi-dimensional scaling ordination (NMDS) was used to visualize significant dietary differences between species. This approach employed a Bray–Curtis similarity coefficient matrix applied to either square- or fourth-root transformed dietary data, depending on the degree of skewness. Kruskal's stress statistic 1 (Clarke and Gorley, 2006) was used to determine the best spatial representation of the samples. A stress of <0.2 was considered an acceptable fit (Clarke and Gorley, 2006). Multivariate one-way analysis of similarities (ANOSIM) was performed on the mean dietary composition within species at each station to investigate whether dietary composition differed significantly between species (Clarke and Gorley, 2006). ANOSIM reports a global R statistic that is analogous to an ANOVA *F* statistic and *p*-value. Similarity percentages (SIMPER) provides a measure of within species similarity and between species dissimilarity, and was used to isolate dietary categories that were significantly important, or contributed most to observed dissimilarities. The ANOSIM and SIMPER routines were performed on the mean diet of each predator species by station (Picquelle and Mier, 2011). Differences in dispersion, as a measure of diet variability, across groups were tested for significance using a permutation-based procedure (PERMDISP).

3. Results

3.1. Spring

In spring, 54 pollock at 17 stations and 47 Pacific cod at 17 stations were processed for dietary analysis. Cumulative prey curves of pre-flexion pollock and Pacific cod larvae reached an asymptote at approximately 45–50 and 35–40 stomachs, respectively. Twenty three prey types were pooled into 14 categories, 10 of these categories occurred in either pollock or Pacific cod stomachs.

In spite of their spatial and temporal co-occurrence in spring, larval stages of pollock and Pacific cod showed disparate patterns in feeding success and mean prey composition. Pre-flexion pollock larvae had an overall feeding incidence of 67.0%, while pre-flexion Pacific cod larvae reached 71.8%. Pacific cod larvae had a significantly higher mean prey volume of 0.5 ml (SE = 0.04) than pollock pre-flexion larvae with a mean prey volume of 0.3 ml (SE = 0.01; Table 2). Mean fullness score and numerical feeding intensity were

slightly higher in Pacific cod than in pollock, but not significantly so (Table 2).

The mean dietary composition (Table 3) between pre-flexion pollock and Pacific cod was significantly different (1-way ANOSIM; Table 4). SIMPER analysis attributed these differences primarily to a higher consumption of copepod eggs, late stage *M. pacifica* nauplii, and early *Calanus* spp. copepodites by Pacific cod, pollock were consuming higher numbers of smaller and younger naupliar stages, namely *M. pacifica* and *Pseudocalanus* spp. (Fig. 2). Pre-flexion pollock dietary composition had a mean similarity percentage of 18.3%, while the mean dietary composition was 16.4% similar within Pacific cod. While there was a mean dissimilarity of 88.7% between the two species, there was no significant difference in dietary dispersion between pollock and Pacific cod larvae in spring (PERMDISP; Table 4).

Table 2
Feeding intensity of age-0 walleye pollock and Pacific cod expressed as mean prey volume/size, visual fullness index scores, numerical feeding intensity (prey/stomach) and standard errors (SE) for all seasons with corresponding Chi-Square statistics, degrees of freedom (df) and *P*-values (*P*). Bold *P*-values indicate significant differences.

	Walleye pollock	Pacific cod	*Chi-Square*	df	*p*
Spring					
Prey volume (ml)	0.3 (0.01)	0.5 (0.04)	8.9	3,4	≤ **0.01**
Fullness (1–6)	2.7 (0.16)	3.3 (0.20)	2.6	3,4	0.11
Prey stomach^{-1}	1.8 (0.21)	2.0 (0.12)	2.7	3,4	0.10
Summer					
Prey size (mm)	0.9 (0.02)	1.7 (0.35)	24.7	3,4	≤ **0.001**
Fullness (1–6)	3.4 (0.11)	4.4 (0.98)	1.8	3,4	0.18
Prey stomach^{-1}	6.5 (0.50)	5.0 (1.83)	0.02	3,4	0.87
Fall					
Prey size (mm)	2.1 (0.04)	5.3 (0.17)	290.5	3,4	≤ **0.001**
Fullness (1–6)	3.9 (0.13)	4.3 (0.20)	3.2	3,4	0.07
Prey stomach^{-1}	74.7 (12.81)	11.4 (2.61)	42.5	3,4	≤ **0.001**

Table 3
Diet composition of walleye pollock and Pacific cod pre-flexion larvae as percent number (%*N*), percent volume (%V), percent frequency of occurrence (%FO), and percent index of relative importance (%IRI). "*N*" represents the sample size of all actively feeding larvae, excluding yolk-sac larvae, empty stomachs, and samples with no identifiable prey. NI-VI: naupliar stages, CI-VI: copepodite stages.

Prey items	**Spring pollock** (*N*=17)				**Spring cod** (*N*=17)			
	%N	*%V*	%FO	%IRI	*%N*	*%V*	%FO	%IRI
Copepod eggs	10.2	18.2	3.7	3.3	16.3	5.5	29.2	13.9
Calanus spp. NVI	0.0	0.0	0.0	0.0	2.0	1.7	4.2	0.3
Eucalanus spp. NIII	4.1	5.1	7.4	2.2	0.0	0.0	0.0	0.0
Metridia pacifica NII-III	14.3	2.2	14.8	7.8	6.1	0.2	8.3	1.2
Metridia pacifica NIV-VI	20.4	36.4	18.5	33.3	28.6	9.6	45.8	38.3
Oithona similis NV-VI	4.1	3.1	7.4	1.7	0.0	0.0	0.0	0.0
Pseudocalanus spp. NII-III	22.4	2.3	29.6	23.3	8.2	0.2	16.7	3.0
Pseudocalanus spp. NIV-VI	10.2	15.9	18.5	15.3	10.2	3.0	16.7	4.8
Calanus spp. CI-II	0.0	0.0	0.0	0.0	14.3	59.6	20.8	33.7
Metridia pacifica CIII	0.0	0.0	0.0	0.0	2.0	16.1	4.2	1.7
Microcalanus spp. CIV	2.0	2.1	3.7	0.5	0.0	0.0	0.0	0.0
Barnacle cyprids	4.1	4.8	1.9	4.1	0.0	0.0	0.0	0.0
Diatoms	8.2	9.9	5.6	8.5	8.2	1.7	4.2	1.7
Euphausiid calyptopis	0.0	0.0	0.0	0.0	4.1	2.3	8.3	1.2

Table 4
PRIMER ANOSIM and PERMDISP test results for comparing pollock and cod diets. ANOSIM results are presented as the Global *R* statistic (*R*) across all test groups and the resulting *P* value (*P*). PERMDISP results are presented as the Global *F* statistic (*F*) across all test groups, associated degrees of freedom (df1, 2). Bold values indicate significant differences.

	ANOSIM		**PERMDISP**			
	R	*P*	*F*	df1	df2	*P*
Spring						
Pollock vs cod	0.16	≤ **0.05**	2.07	1	49	> 0.05
Summer						
Pollock vs cod	0.40	≤ **0.01**	0.63	1	92	> 0.05
Fall						
Pollock vs cod	0.38	≤ **0.001**	14.34	1	99	≤ **0.001**

3.2. Summer

In summer, 113 flexion pollock larvae at 11 stations were processed for dietary analysis. The low sample size of Pacific cod flexion larvae in summer (5 fish at 4 stations), only allowed for restricted data analysis. Additionally, one Pacific cod larva contained no identifiable prey, effectively restricting the sample size to 4 station means, with each station consisting of only 1 individual. For pollock, the cumulative prey curve reached an asymptote at approximately 50 stomachs, while the cumulative prey curve for Pacific cod failed to reach an asymptote. Thirty five prey types, pooled into 17 categories were identified in the stomachs of flexion pollock and Pacific cod larvae; of these, 13 occurred in the diet of flexion pollock, 8 categories occurred in the diet of flexion Pacific cod larvae.

Despite the low sample size for Pacific cod flexion larvae, comparisons of mean feeding patterns between both species revealed notable differences. Specifically, prey size differed significantly with a mean of 1.7 mm (SE=0.35) for Pacific cod larvae in comparison to 0.9 mm (SE=0.02) for pollock larvae (Table 2). Pollock larvae had an overall feeding incidence of 79.6%, while 100% of Pacific cod were feeding. There were also slight differences in the mean fullness and numerical feeding intensity; however these differences were not statistically different.

The mean dietary composition between flexion pollock and Pacific cod larvae was significantly different (1-way ANOSIM; Table 4), and SIMPER analysis indicated that these differences were primarily due to Pacific cod consuming more early *Calanus* spp. and *Centropages abdominalis* copepodites. In contrast, pollock were consuming higher numbers of late *Acartia longiremis* copepodites, *Oithona similis* copepodites, and mid to adult stages of *Pseudocalanus* spp. (Table 5). Flexion pollock larvae had a mean dietary similarity of 22.3%, while Pacific cod had no within species

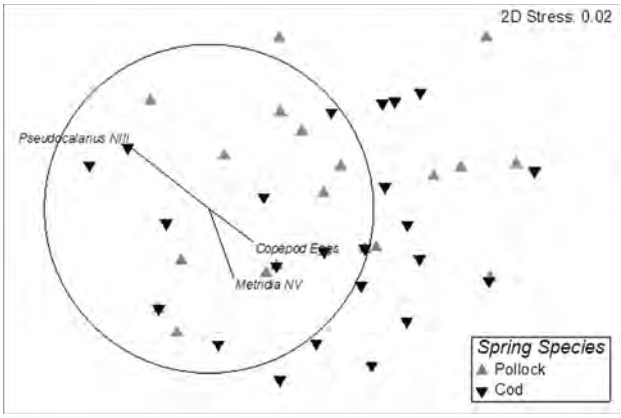

Fig. 2. Non-metric multidimensional scaling (NMDS) ordination of the dietary composition of pre-flexion walleye pollock and Pacific cod larvae collected in spring with Pearson correlation vectors from SIMPER identified prey categories. Two dimensional stress indicates how well the data can be represented in two dimensions (PRIMER: Kruskal stress formula 1).

Table 5
Diet composition of walleye pollock and Pacific cod flexion larvae as percent number (%*N*), percent volume (%*V*), percent frequency of occurrence (%FO), and percent index of relative importance (%IRI). "*N*" represents the sample size of all actively feeding larvae, excluding empty stomachs and samples with no identifiable prey. NII-VI: naupliar stages, CII-VI: copepodite stages.

Prey items	Summer pollock ($N=11$)				Summer cod ($N=4$)			
	%*N*	%*W*	%FO	%IRI	%*N*	%*W*	%FO	%IRI
Acartia spp. NIII	0.2	< 0.1	1.1	< 0.1	0.0	0.0	0.0	0.0
Calanoid nauplii	0.5	< 0.1	1.1	< 0.1	5.0	< 0.1	25.0	2.2
Pseudocalanus spp. NIV-VI	23.8	1.7	32.2	15.6	5.0	< 0.1	25.0	2.2
Acartia longiremis CIV-VI	18.7	12.1	37.8	22.1	0.0	0.0	0.0	0.0
Calanus spp. CIII	1.4	7.3	2.2	0.4	20.0	3.7	25.0	10.2
Calanus spp. CIV-VI	0.5	13.2	3.3	0.9	0.0	0.0	0.0	0.0
Centropages abdominalis CII	0.0	0.0	0.0	0.0	15.0	0.8	25.0	6.8
Centropages abdominalis CV	0.0	0.0	0.0	0.0	15.0	1.6	25.0	7.1
Metridia pacifica CIII-IV	1.5	0.7	2.2	0.1	0.0	0.0	0.0	0.0
Neocalanus spp. CII-IV	0.3	12.6	1.1	0.3	0.0	0.0	0.0	0.0
Neocalanus cristatus CV	0.0	0.0	0.0	0.0	5.0	74.9	25.0	34.5
Oithona similis CII-VI	12.4	2.3	24.4	6.8	0.0	0.0	0.0	0.0
Pseudocalanus spp. CII-III	16.3	5.3	28.9	11.9	0.0	0.0	0.0	0.0
Pseudocalanus spp. CIV-VI	22.5	38.9	35.6	41.4	30.0	1.8	50.0	27.4
Other copepodites	1.0	5.4	4.4	0.5	0.0	0.0	0.0	0.0
Themisto pacifica	0.0	0.0	0.0	0.0	5.0	17.2	25.0	9.6
Other	0.9	0.6	5.6	0.2	0.0	0.0	0.0	0.0

Table 6
Diet composition of walleye pollock and Pacific cod juveniles as percent number (%*N*), percent volume (%*V*), percent frequency of occurrence (%FO), and percent index of relative importance (%IRI). "*N*" represents the sample size of all actively feeding juveniles, excluding empty stomachs and samples with no identifiable prey. CIV-VI: copepodite stages.

Prey items	Fall pollock ($N=13$)				Fall cod ($N=10$)			
	%*N*	%*W*	%FO	%IRI	%*N*	%*W*	%FO	%IRI
Acartia longiremis CV	4.2	1.7	27.1	1.7	0.2	< 0.1	2.4	< 0.1
Acartia longiremis CVI	1.1	0.1	8.5	0.1	0.6	< 0.1	2.4	< 0.1
Calanus spp. CIV-VI	20.2	40.3	57.6	37.0	8.0	4.6	14.3	3.5
Centropages abdominalis CVI	2.5	0.4	8.5	0.3	0.2	< 0.1	2.4	< 0.1
Epilabidocera amphitrites CV-VI	1.5	1.4	13.6	0.4	1.5	0.4	7.1	0.3
Pseudocalanus spp. CV	5.8	0.4	20.3	1.3	0.4	< 0.1	4.8	< 0.1
Pseudocalanus spp. CVI	59.1	5.9	59.3	41.0	0.6	< 0.1	7.1	0.1
Euphausia pacifica	0.1	0.1	1.7	< 0.1	0.0	0.0	0.0	0.0
Thysanoessa spp.	1.8	27.1	35.6	8.6	44.9	69.9	64.3	74.7
Chionoecetes spp. megalopae	0.0	0.0	0.0	0.0	1.3	2.9	14.3	1.1
Themisto pacifica	0.2	1.7	11.9	0.2	3.4	7.2	16.7	3.4
Limacina helicina	0.1	< 0.1	5.1	< 0.1	32.3	0.5	14.3	9.1
Parasagitta elegans	2.6	20.8	37.3	9.3	6.3	14.4	19.0	7.7
Oikopleura spp.	0.4	< 0.1	1.7	< 0.1	0.2	< 0.1	2.4	< 0.1
Other	0.3	0.1	8.5	< 0.1	0.2	< 0.1	2.4	< 0.1

similarities. The mean dissimilarity between species was 93.6%. There was no significant difference in dietary dispersion between pollock and Pacific cod larvae (PERMDISP; Table 4), likely due to the low sample size of Pacific cod.

3.3. Fall

In the fall, 62 pollock at 13 stations and 42 Pacific cod at 10 stations were processed for dietary analysis. In the stomachs of juvenile pollock and Pacific cod, 21 prey types pooled into 15 categories were identified; of these, 14 occurred in the diet of either target species. The cumulative prey curves of juvenile pollock and Pacific cod juveniles reached an asymptote at around 20 and 36 stomachs, respectively.

In the fall, dietary patterns were more disparate between juvenile stages of pollock and Pacific cod than earlier in the year. Specifically, mean prey size and mean numerical feeding intensity were both significantly different (Table 2). Pacific cod had a higher mean prey size of 5.3 mm (SE = 0.17) and lower mean numerical feeding intensity of 11.4 (SE = 2.61) in comparison to pollock with a mean prey size of 2.1 mm (SE = 0.04) and a mean numerical feeding intensity of 74.7 (SE = 12.81). Mean fullness index score was slightly higher in Pacific cod than in pollock, but this difference was not significant (Table 2). Juvenile pollock had an overall feeding incidence of 95.2%, while 100% of Pacific cod juveniles were feeding.

Differences in feeding success were also apparent in mean dietary composition (1-way ANOSIM, Table 4), and these differences were primarily due to a higher consumption of late stages of calanoid copepodites by juvenile pollock (Table 6), while Pacific cod juveniles consumed higher numbers of larger crustaceans, such as juvenile stages of the euphausiid *Thysanoessa* spp., the sea snail *Limacina helicina*, and hyperiid amphipods (Fig. 3). The overall mean similarity within juvenile pollock dietary composition was 47.0% and 26.2% for Pacific cod. The mean dissimilarity between species dietary composition was 74.1%. In addition, dietary dispersion was significantly higher in juvenile Pacific cod than in pollock (PERMDISP; Table 4).

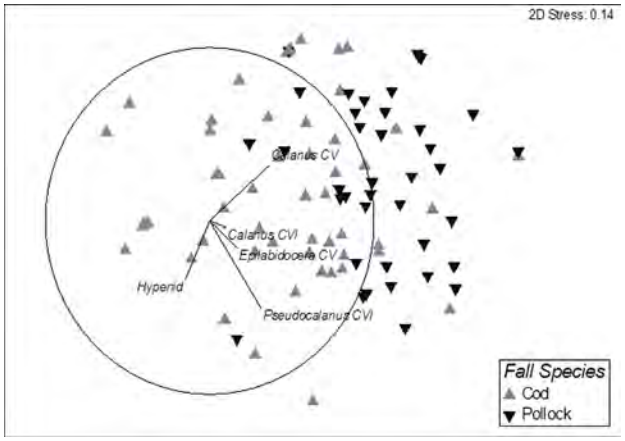

Fig. 3. Non-metric multidimensional scaling (NMDS) ordination depicting the dietary composition of fall-collected walleye pollock and Pacific cod juveniles. Vectors are the same as in Fig. 2.

4. Discussion

Despite sharing ecological preferences, temporal and spatial co-occurrence, and strong correlations in recruitment success (Bacheler et al., 2010; Duffy-Anderson et al., 2006; Hurst et al., 2012; Matarese et al., 2003; Mueter et al., 2011), patterns in feeding success and prey composition differed between all examined early life stages of pollock and Pacific cod during the cold conditions experienced in 2008. However, the number of samples included in this study was limited by availability from other research programs. Increased sampling, particularly from stations where both pollock and Pacific cod co-occurred, would have allowed investigations into sympatric vs. allopatric differences in feeding success and diet composition. Reduced sample sizes were either due to low feeding incidence in the spring, low catches of Pacific cod in the summer, or varying catches of either species in the fall. Further, when they were sampled simultaneously, the number captured or number available of one species was typically smaller than the other. Larger sample sizes with better spatial coverage would have allowed for meaningful two-way comparisons between interspecies size classes, regional domains, and sampling depth intervals; especially in the fall, when juvenile Pacific cod are beginning to settle out to a demersal lifestyle. Investigation into specific spatial domains would likely result in higher within species similarity percentages, and potentially higher between species similarity percentages. Additionally, prey field data were not sufficient to allow selectivity analysis in this study. Microzooplankton data from only two overlapping stations were available from the spring cruise, and the taxonomic resolution did not match this analysis. Summer zooplankton samples were selectively analyzed, and available data only overlapped with this study by approximately half. No zooplankton data were available from fall beam trawl samples or midwater trawl samples.

The diet of pre-flexion Pacific cod larvae in spring in the SEBS differed from that of pollock larvae due to higher consumption of copepod eggs, late calanoid nauplii, and an early inclusion of larger prey items including calanoid copepodites into their diet. A similar pattern was observed in pre-flexion Pacific cod larvae in Mutsu Bay, Japan (Takatsu et al., 2002). The large proportion of copepod eggs consumed by pre-flexion Pacific cod may have artificially inflated measures of fullness and feeding intensity, as pre-flexion pollock in the Gulf of Alaska were reported to display an inability to digest invertebrate eggs (Duffy-Anderson et al., 2002). Similar observations have been made for pre-flexion larval stages of other fish taxa (Conway et al., 1994; Hillgruber and Kloppmann, 2000; Redden and Daborn, 1991), and research has demonstrated that the ability of eggs to withstand digestion is largely a function of the invertebrate species providing the eggs (Conway et al., 1994; Redden and Daborn, 1991). Whether or not pre-flexion Pacific cod lack the ability to properly digest certain invertebrate eggs is currently not known, but may warrant further research. While no other published data on pre-flexion Pacific cod diet in the SEBS were available, the diet of larval Pacific cod ≤ 5 mm SL in March and April in Mutsu Bay, Japan, was restricted to mainly *Pseudocalanus* spp., *Oithona* spp., and *Metridia* spp. nauplii (Takatsu et al., 1995), larvae of 5–10 mm SL gradually incorporated more copepodite and adult stages of *Pseudocalanus* spp., *A. clausi*, and *Oithona* spp. into their diet.

Differences in dietary patterns between pollock and Pacific cod pelagic flexion larvae continued to be apparent with growth and as the year progressed. While no other studies from the Bering Sea were available for comparison, larval pollock from June of 1987 in the Gulf of Alaska demonstrated a similar dietary composition to their con-specifics in this study. Pollock diet in 1987 had high abundances of *Pseudocalanus* spp. and *Acartia* spp. copepodites and adults (Grover, 1990), though these larvae were larger (10–30 mm SL) than those examined in this study. The similarity in diet composition indicates that feeding patterns described here are typical for pollock flexion larvae at similar latitudes. In contrast, Pacific cod flexion larvae in this study relied most heavily on mid to late calanoid copepodite stages in the SEBS. It is important to remember that the dietary composition for Pacific cod in summer is represented by only 4 fish at 4 stations and a total of 20 identifiable prey items. Thus, results presented here are unlikely to properly describe the overall diet of Pacific cod flexion larvae, and likely overestimates the dietary value of the large copepod *Neocalanus cristatus* (Table 5). The values for %*W* and %IRI are very likely to be positively biased due to the comparatively large size of this calanoid copepod. However, even with a sample size of 4, Pacific cod were consuming prey items that did not occur in the diet of pollock larvae. Summer Bering Sea Pacific cod diet was similar to that in mid-August in nearshore waters of the Gulf of Alaska (Abookire et al., 2007), which was restricted to unidentified calanoid copepodites, while smaller larvae of 5–10 mm SL still concentrated numerically on copepod nauplii, but were incorporating calanoid copepodite stages as well. The range of ingested prey items in comparison to the range of fish size was similar to this study, thus suggesting a preference of Pacific cod flexion larvae for a larger average prey size than that of similar life stages and size classes of pollock at similar latitudes. Even though the number of Pacific cod larvae collected in the summer was low, the differences in mean dietary composition and mean prey size between the two species were still disparate enough to be statistically significant, suggesting a difference in dietary niche.

Differences in feeding patterns between pollock and Pacific cod were most pronounced in the fall. Pacific cod maintained a slightly higher level of feeding incidence, 100% compared to 95.2% in pollock juveniles. Mean prey size was significantly higher in Pacific cod juveniles, while pollock juveniles were consuming significantly higher numbers of smaller prey items. This is similar to results presented by Lee (1985), in which the length distributions for both predator species overlap with juvenile size ranges in the fall portion of this study. Pacific cod were also reported to have a heavier stomach lining than juvenile pollock of the same size, possibly providing a more robust containment for larger prey (Lee, 1985). Over the collection period from 1981–1983, Pacific cod consistently switched to larger prey items than pollock at around 50 mm TL (Lee, 1985). The smallest juvenile cod in this study were just above 50 mm TL and were already consuming large prey items. Conversely, juvenile pollock dietary composition gradually changed by slowly increasing the maximum prey size, but continuing to consume significant proportions of small calanoid

copepods until well past a total length of 50 mm; both in this study, and in Lee's findings. Additionally, Lee reported that the mean number of prey per stomach decreased with size in Pacific cod, but increased with size in pollock (Lee, 1985), as in our results. Juvenile pollock in Uchiura Bay, Hokkaido, did not switch to a larger prey until approximately 80 mm TL (Kamba, 1977), nearly twice the length at which Pacific cod displayed a similar switch in dietary preference. While the dietary breadth of both species was similar in spring and summer, there was a significant difference in fall, with juvenile Pacific cod utilizing a wider range of prey taxa. This may be a reflection of diverging life history patterns, with Pacific cod moving to a more demersal lifestyle. The mean dietary composition was also different, primarily due to an increased number of large crustacean-type prey items consumed by Pacific cod. This was similar to Pacific cod diet in Mutsu Bay, Japan, where summer juveniles were feeding on comparatively large prey items, such as gammarid amphipods and juvenile pollock (Takatsu et al., 2001). The dietary composition (*%W*) of juvenile pollock was predominantly large calanoid copepods and euphausiids, similar to results reported for cold conditions in Coyle et al. (2011). The diet of juvenile Pacific cod has similarities to the diet of age-0 Atlantic cod (*Gadus morhua*), both on the eastern coast of the United States, where they were found to be concentrating heavily on mysids, amphipods, and euphausiids at a TL < 100 mm (Link and Garrison, 2002), and in the North Sea where they were also concentrating on crustaceans, such as developmental stages of crab, at concentrations of up to 76% by number (Demain et al., 2011).While juvenile pollock diet focused on small copepods numerically (> 70%), these taxa only accounted for < 9% of the total dietary weight. Conversely, large calanoid copepods only accounted for < 23% of the total number of prey items, but for > 41% of the total dietary weight, with *Calanus* spp. occurring in nearly 60% of all juvenile pollock stomachs. Under warm conditions, with reduced numbers of large prey items, juvenile pollock would likely have to consume higher numbers of small copepods to satisfy their energetic demands.

The prevalent hypothesis predicting variability in pollock recruitment in the SEBS is the Oscillating Control Hypothesis, OCH (Hunt et al., 2002, revised in 2011). The revised OCH postulates bottom-up controls on pollock recruitment during warm periods, resulting in reduced recruitment success. Bottom-up control implies a lack of adequate prey resources, via a late phytoplankton bloom which is propagated throughout the zooplankton community, and positions overlapping populations for potential resource competition. Increased coeval (intra-cohort) cannibalism and overwinter starvation in pollock during warm years is thought to be due to a lack of quality prey items in the previous growing season; namely larger lipid-rich zooplankton taxa such as the copepod *Calanus* spp. and euphausiids (Coyle et al., 2011, Heintz et al., 2013).

Annual differences in feeding performance reported in the literature are likely the result of changes in the prey environment. For example, during the comparatively cold years of 2006–2009, median zooplankton biomass was more than twice that of the previous warm years of 2000–2005 (Stabeno et al., 2012), with an even larger increase in the biomass of large zooplankton species of 5–10 fold in the SEBS, the latter primarily due to an increase in the abundance of *Calanus* spp. (Eisner et al., 2014). Cold conditions have also been beneficial to the recruitment of *Chionoecetes opilio* in the SEBS (Marcello et al., 2012; Parada et al., 2010), a component of the diet of juvenile Pacific cod in this study. Also, there has been a distributional shift to the south of the Arctic hyperiid amphipod *Themisto libellula* since 2006 (Pinchuk et al., 2013). This species, which is primarily restricted to the Middle Domain of the eastern Bering Sea, has a high nutritional value due to its high lipid content (Noyon et al., 2011). Since the onset of the recent cold conditions, *T. libellula* has not only appeared in the eastern Bering Sea, but also in the diet of age-0 Pacific cod, where it was a substantial component by dietary weight (25–55%) within four years (Pinchuk et al., 2013). The absence of *T. libellula* in juvenile Pacific cod diet in this study may have been due to the low sample size of Pacific cod taken from within the cold pool. *Themisto libellula* is also thought to be a substantial predator on *Calanus* spp. with an estimated average predation impact of 35.8% of the standing stock of *Calanus* spp. per day and a maximum of 225% per day (Pinchuk et al., 2013). Thus, during cold conditions, it appears that not only are the diets of pollock and Pacific cod partitioned by size, but that Pacific cod may, to some extent, alleviate pressure on a preferred and energetically advantageous food source for pollock, while still obtaining energetically advantageous prey themselves.

During warm conditions, the absence of large, high-quality prey items in the Middle Domain results in sub-optimal prey resources for early life stages of Pacific cod and pollock (Coyle et al., 2011). These sub-optimal feeding conditions are reflected in a reduced total energetic content and reduced lipid content for age-0 pollock (Heintz et al., 2013). During warm years, age-0 pollock are displaced from the Outer to the Middle Domain (Smart et al., 2012), placing them in direct proximity to the center of abundance of age-0 Pacific cod (Hurst et al., 2012), thus enhancing the potential for competition due to greater spatial overlap between the two species. Other forage fish species, such as Pacific sandlance (*Ammodytes hexapterus*) and Pacific herring (*Clupea pallasii*), rely heavily on small copepods in the Gulf of Alaska (Purcell and Sturdevant, 2001). The dietary overlap between pollock, herring, and sandlance in that study ranged from 47–84%. Multiple species of gelatinous zooplankton were also relying heavily on small copepods, ranging from 40% numerically in *Pleurobrachia bachei* (Phylum: *Ctenophora*) to 60% by number in *Aurelia labiata* (Phylum: *Cnidaria*). Fluctuations in the zooplankton community in response to thermal conditions were most evident in the Middle Domain (Eisner et al., 2014). Thus, in warm years, survival of age-0 pollock may suffer from limited high-quality prey resources and higher rates of predation pressure from conspecifics in the form of cannibalism (Coyle et al., 2011) and from co-occurring age-0 Pacific cod (BASIS, unpublished data).

In the beginning of the production season, pollock exhibit low lipid and total energetic content, probably as a strategy of energy allocation towards somatic growth (Siddon et al., 2013). However, energy allocation patterns in pollock seem to change in late summer (July–September) from favoring somatic growth towards energy storage as a strategy to increase the probability of overwinter survival (Siddon et al., 2013). During warm conditions, total pollock energy densities nearing winter were an average of 35% less than those in cold years, accompanied by a threefold reduction in total lipid content (Heintz et al., 2013), Pacific cod seem to follow a similar pattern (Heintz, *pers. comm.*). It is likely that these changes in energy content are the result of the differences in the abundance of large and nutritious prey taxa during different thermal conditions (Coyle et al., 2011; Eisner et al., 2014; Heintz et al., 2013; Stabeno et al., 2012).

Trophic interactions between age-0 pollock and Pacific cod in the SEBS appear to be modulated by climate variability, with prey resource partitioning between the two species in cold years, and the potential for competition for sub-optimal prey resources during warm conditions (Coyle et al., 2011; Eisner et al., 2014). The latter may be further complicated by increased pollock mortality due to cannibalism and predation by Pacific cod. Additionally, age-0 pollock experience increased metabolic stress under warm conditions that result in fish that contain only 1/3 the lipid content than their cold condition counterparts (Heintz et al., 2013). These conditions may lead to poor nutritional status of juvenile stages of both species heading into the winter of their first year. Ultimately, these factors are likely to result in poor over-winter survival and subsequent recruitment success (Heintz and Vollenweider, 2010; Kooka and Yamamura, 2012).

Results presented here indicate temporally increasing prey partitioning throughout the first year, suggesting that co-occurring larval and juvenile stages of pollock and Pacific cod avoid competition during cold conditions in the SEBS. While Pacific cod consumed fewer, larger-bodied prey items, especially in the fall, juvenile pollock continued consuming increasing numbers of calanoid copepods, such as *Calanus* spp., *Pseudocalanus* spp., and *A. longiremis*. One potential explanation for the observed differences in prey size may be due to gape size, as morphological differences between Pacific cod and pollock at similar body sizes have been demonstrated (Lee, 1985). A positive relationship for gape size-prey size ratios have been demonstrated for different life stages of a number of marine species, including Atlantic cod (Puvanendran et al., 2004; Scharf et al., 2000). However, the observed partitioning of prey between the two species may be restricted if warmer temperatures lead to a decline in the abundance of large zooplankton species (Coyle et al., 2011; Eisner et al., 2014; Hunt et al., 2011; Stabeno et al., 2012), and consequently the diets of these two gadoid fishes may converge under warm conditions. During warm conditions age-0 Pacific cod may not only potentially compete with pollock, but may also consume pollock directly (Takatsu et al., 2002; BASIS, unpublished data). These scenarios, which could impact recruitment success, warrant further exploration, particularly under the expected warming of the sub-arctic waters of the southeastern Bering Sea (Mueter et al., 2011).

Acknowledgments

Funding for this research was provided by the Pollock Conservation Cooperative Research Center Grant no. G00005507 (PI: Dr. Nicola Hillgruber). This study would not have been possible without the generous donation of samples and data from colleagues of the Fisheries Oceanography Coordinated Investigations (FOCI) at the Alaska Fisheries Science Center, NMFS, the Bering Ecosystem Study (BEST, NSF) and the Bering Sea Integrated Ecosystem Research Project (BSIERP, NPRB) cooperatives, the University of Alaska Fairbanks, and the Bering-Aleutian Salmon International Survey (BASIS) program at the Ted Stevens Marine Research Institute (TSMRI), NOAA. I would also like to thank Elizabeth Siddon for numerous editorial suggestions, Dr. Sherry Tamone for the use of laboratory equipment, and Emily Fergusson for guidance in age-0 diet protocols and equipment. This is BEST-BSIERP Bering Sea Project publication no. 116, NPRB publication no. 450.

References

Abookire, A.A., Duffy-Anderson, J.T., Jump, C.M., 2007. Habitat association and diet of young-of-the-year Pacific cod (*Gadus macrocephalus*) near Kodiak, Alaska. Marine Biology 150, 713–726.

Adams, C.F., Pinchuk, A.I., Coyle, K.O., 2007. Seasonal changes in the diet composition and prey selection of walleye pollock (*Theragra chalcogramma*) in the northern Gulf of Alaska. Fisheries Research 84, 378–389.

Aydin, K., Mueter, F., 2007. The Bering Sea – a dynamic food web perspective. Deep-Sea Research II 54, 2501–2525.

Bacheler, N.M., Ciannelli, L., Bailey, K.M., Duffy-Anderson, J.T., 2010. Spatial and temporal patterns of walleye pollock (*Theragra chalcogramma*) spawning in the eastern Bering Sea inferred from egg and larval distributions. Fisheries Oceanography 19, 107–120.

Bailey, K.M., 1989. Interaction between the vertical distribution of juvenile walleye pollock *Theragra chalcogramma* in the eastern Bering Sea, and cannibalism. Marine Ecology Progress Series 53, 205–213.

Blackburn, J.E., Jackson, P.B., 1982. Seasonal Composition and Abundance of Juvenile and Adult Marine Finfish and Crab Species in the Nearshore Zone of Kodiak Islands' eastside during April 1978 through March 1979. Alaska Department of Fish and Game, Kodiak, Alaska. (Final Report 03-5-022-69).

Brodeur, R.D., Wilson, M.T., Ciannelli, L., 2000. Spatial and temporal variability in feeding and condition of age-0 walleye pollock (*Theragra chalcogramma*) in frontal regions of the Bering Sea. ICES Journal of Marine Science 57, 256–264.

Ciannelli, L., Brodeur, R.D., Buckley, T.W., 1998. Development and application of a bioenergetics model for juvenile walleye pollock. Journal of Fish Biology 52, 879–898.

Clarke, K.R., Gorley, R.N., 2006. PRIMER v6: User Manual/Tutorial. PRIMER-E, Plymouth.

Conway, D.V.P., McFadzen, I.R.B., Tranter, P.R.G., 1994. Digestion of copepod eggs by larval turbot *Scophthalmus maximus* and egg viability following gut passage. Marine Ecology Progress Series 106, 303–309.

Cortés, E., 1997. A critical review of methods of studying fish feeding based on analysis of stomach contents: application to elasmobranch fishes. Canadian Journal of Fisheries and Aquatic Sciences 54, 726–738.

Coyle, K.O., Eisner, L.B., Mueter, F.J., Pinchuk, A.I., Janout, M.A., Cieciel, K.D., Farley, E.V., Andrews, A.G., 2011. Climate change in the southeastern Bering Sea: impacts on pollock stocks and implications for the oscillating control hypothesis. Fisheries Oceanography 20, 139–156.

Coyle, K.O., Pinchuk, A.I., Eisner, L.B., Napp, J.M., 2008. Zooplankton species composition, abundance and biomass on the eastern Bering Sea shelf during summer: the potential role of water-column stability and nutrients in structuring the zooplankton community. Deep-Sea Research II 55, 1775–1791.

Dauvin, J.C., Dodson, J.J., 1990. Relationship between feeding incidence and vertical and longitudinal distribution of rainbow smelt larvae (*Osmerus mordax*) in a turbid well-mixed estuary. Marine Ecology Progress Series 60, 1–12.

Decker, M.B., Hunt, G.L., 1996. Foraging by murres (*Uria* spp.) at tidal fronts surrounding the Pribilof Islands, Alaska, USA. Marine Ecology Progress Series 139, 1–10.

Demain, D.K., Gallego, A., Jaworski, A., Priede, I.G., Jones, E.G., 2011. Diet and feeding niches of juvenile *Gadus morhua, Melanogrammus aegifinus,* and *Merlangius merlangus* durinig the settlement transition in the northern North Sea. Journal of Fish Biology 79, 89–111.

Duffy-Anderson, J.T., Bailey, K.M., Ciannelli, L., 2002. Consequences of a super-abundance of larval walleye pollock *Theragra chalcogramma* in the Gulf of Alaska in 1981. Marine Ecology Progress Series 243, 179–190.

Duffy-Anderson, J.T., Busby, M.S., Mier, K.L., Deliyanides, C.M., Stabeno, P.J., 2006. Spatial and temporal patterns in summer ichthyoplankton assemblages on the eastern Bering Sea shelf 1996–2000. Fisheries Oceanography 15, 80–94.

Dunn, J.R., Materese, A.C., 1987. A review of the early life history of Northeast Pacific gadoid fishes. Fisheries Research 5, 163–184.

Eisner, L.B., Napp, J.M., Mier, K.L., Pinchuk, A.I., Andrews, A.G., 2014. Climate-mediated Changes in Zooplankton Community Structure for the eastern Bering Sea. 109, 157–171, http://dx.doi.org/10.1016/j.dsr2.2014.03.004.

Fritz, L.W., Wespestad, V.G., Collie, J.S. 1993. Distribution and abundance trends of forage fishes in the Bering Sea and Gulf of Alaska. In: Is it food?: addressing marine mammal and sea bird declines. Workshop Summary, Alaska Sea Grant Rept. 93-01. University of Alaska, Fairbankspp, pp. 30–43.

Grover, J.J., 1990. Feeding ecology of late-larval and early juvenile walleye pollock, *Theragra chalcogramma*, from the Gulf of Alaska in 1987. Fishery Bulletin 88, 463–470.

Heintz, R.A., Siddon, E.C., Farley Jr., E.V., Napp, J.M., 2013. Correlation between recruitment and fall condition of age-0 pollock (*Theragra chalcogramma*) from the eastern Bering Sea under varying climate conditions. Deep-Sea Research II 94, 150–156.

Heintz, R.A., Vollenweider, J.J., 2010. Influence of size on the sources of energy consumed by overwintering walleye pollock (*Theragra chalcogramma*). Journal of Experimental Marine Biology and Ecology 393, 43–50.

Hillgruber, N., Kloppmann, M., 2000. Vertical distribution and feeding of larval blue whiting in turbulent waters of Porcupine Bank. Journal of Fish Biology 57, 1290–1311.

Hillgruber, N., Haldorson, L.J., Paul, A.J., 1995. Feeding selectivity of larval walleye pollock *Theragra chalcogramma* in the oceanic domain of the Bering Sea. Marine Ecology Progress Series 120, 1–10.

Hunt, G.L., Coyle, K.O., Eisner, L.B., Farley, E.V., Heintz, R.A., Mueter, F., Napp, J.M., Overland, J.E., Ressler, P.H., Salo, S., Stabeno, P.J., 2011. Climate impacts on eastern Bering Sea foodwebs: a synthesis of new data and an assessment of the Oscillating Control Hypothesis. ICES Journal of Marine Science 68, 1230–1243.

Hunt Jr., G.L., Stabeno, P.J., 2002. Climate change and the control of energy flow in the southeastern Bering Sea. Progress in Oceanography 55, 5–22.

Hunt Jr., G.L., Stabeno, P., Walters, G., Sinclair, E., Brodeur, R.D., Napp, J.M., Bond, N.A., 2002. Climate change and control of the southeastern Bering Sea pelagic ecosystem. Deep-Sea Research Part II 49, 5821–5853.

Hurst, T.P., Moss, J.H., Miller, J.A., 2012. Distributional patterns of 0-group Pacific cod (*Gadus macrocephalus*) in the eastern Bering Sea under variable recruitment and thermal conditions. ICES Journal of Marine Science 69, 163–174.

Ianelli, J.N., Barbeaux, S., Honkalehto, T., Kotwicki, S., Aydin, K., Williamson, N. 2011. Assessment of the walleye pollock stock in the eastern Bering Sea. In Stock Assessment and Fishery Evaluation Report for the Groundfish Resources of the Bering Sea/Aleutian Islands Regions, NOAA AFSC.

Kamba, M., 1977. Feeding Habits and Vertical Distribution of Walleye Pollock in Early Life Stage in Uchiura Bay, Hokkaido. Research Institute of North Pacific Fisheries, Hokkaido University Spec., pp. 156–189.

Kooka, K., Yamamura, O., 2012. Winter energy allocation and deficit of juvenile walleye pollock *Theragra chalcogramma* in the Doto area, northern Japan. Environmental Biology of Fishes 94, 389–402.

Lee, S.S. 1985. A Comparison of the Food Habits of Juvenile Pacific Cod and Walleye Pollock in the Southeast Bering Sea (M.S. Thesis), University of Alaska Fairbanks.

Link, J.S., Garrison, L.P., 2002. Trophic ecology of Atlantic cod *Gadus morhua* on the northeast US continental shelf. Marine Ecology Progress Series 227, 109–123.

Livingston, P.A., 1989. Interannual trends in Pacific cod, *Gadus macrocephalus*, predation on three commercially important crab species in the eastern Bering Sea. Fishery Bulletin 87, 807–827.

Marcello, L.A., Mueter, F.J., Dawe, E.G., Moriyasu, M., 2012. Effects of temperature and gadid predation on snow crab recruitment: comparisons between the Bering Sea and Atlantic Canada. Marine Ecology Progress Series 469, 249–261.
Matarese, A.C., Blood, D.M., Picquelle, S.J., Benson, J.L. 2003. Atlas of Abundance and Distribution Patterns of Ichthyoplankton from the Northeast Pacific Ocean and Bering Sea Ecosystems based on Research Conducted by the Alaska Fisheries Science Center (1972–1996). NOAA Professional Paper NMFS, 1. NOAA, Seattle. 281pp.
Moss, J.H., Farley, E.V., Feldmann, A.M., Ianelli, J.N., 2009. Spatial distribution, energetic status, and food habits of eastern Bering Sea age-0 walleye pollock. Transactions of the American Fisheries Society 138, 497–505.
Mueter, F.J., Litzow, M.A., 2008. Warming climate alters the demersal biogeography of a marginal ice sea. Ecological Applications 18, 309–320.
Mueter, F.J., Bond, N.A., Ianelli, J.N., Hollowed, A.B., 2011. Expected declines in recruitment of walleye pollock (*Theragra chalcogramma*) in the eastern Bering Sea under future climate change. ICES Journal of Marine Science 68, 1284–1296.
Napp, J.M., Mier, K., Cohen, M.K., 1999. Estimation of larval fish prey volume: mensuration formulae for copepod nauplii. Journal of Plankton Research 21, 1633–1642.
Nishiyama, T., Hirano, K., Haryu, T., 1986. The early life history and feeding habits of larval walleye pollock, *Theragra chalcogramma* (Pallas), in the southeastern Bering Sea. Bulletin of the International North Pacific Fisheries Commission 45, 177–227.
Noyon, M., Narcy, F., Gasparini, S., Mayzaud, P., 2011. Growth and lipid class composition of the Arctic pelagic amphipod *Themisto libellula*. Marine Biology 158, 883–892.
Overland, J.E., Stabeno, P.J., 2004. Is the climate of the Bering Sea warming and affecting the ecosystem? EOS Transactions of the American Geophysical Union 85, 309–316.
Parada, C., Armstrong, D.A., Ernst, B., Hinckley, S., Orensanz (Lobo), J.M., 2010. Spatial dynamics of snow crab (*Chinoecetes opilio*) in the eastern Bering Sea-Putting together the pieces of the puzzle. Bulletin of Marine Science 86, 413–437.
Picquelle, S.J., Mier, K.L., 2011. A practical guide to statistical methods for comparing means from two-stage sampling. Fisheries Research 107, 1–13.
Pinchuk, A.I., Coyle, K., Farley, E., Renner, H., 2013. Emergence of the Arctic *Themisto libellula* (Amphipoda: Hyperiidae) on the southeastern Bering Sea shelf as a result of the recent cooling and their potential impact on the pelagic food web. ICES Journal of Marine Science 70, 1244–1254.
Porter, S.M., Ciannelli, L., Hillgruber, N., Bailey, K.M., Chan, K.S., Canino, M.F., Haldorson, L.J., 2005. Analysis of factors influencing larval walleye pollock *Theragra chalcogramma* feeding in Alaskan waters. Marine Ecology Progress Series 302, 207–217.
Purcell, J.E., Sturdevant, M.V., 2001. Prey selection and dietary overlap among zooplanktiverous jellyfish and juvenile fishes in Prince William Sound, Alaska. Marine Ecology Progress Series 210, 67–83.
Puvanendran, V., Salies, K., Laurel, B., Brown, J.A., 2004. Size-dependent foraging of larval Atlantic cod (*Gadus morhua*). Canadian Journal of Zoology 82, 1380–1389.
Redden, A.M., Daborn, G.R., 1991. Viability of subitaneous copepod eggs following fish predation on egg-carrying copepods. Marine Ecology Progress Series 77, 307–310.
Rugen, W.C., Materese, A.C., 1988. Spatial and Temporal Distribution and Relative Abundance of Pacific cod (*Gadus macrocephalus*) Larvae in the Western Gulf of Alaska. National Marine Fisheries Service, Seattle, WA. (Northwest and Alaska Fisheries Science Center Processed Report 88-18).
Schabetsberger, R., Brodeur, R.D., Ciannelli, L., Napp, J.M., Swartzman, G.L., 2000. Diel vertical migration and interaction of zooplankton and juvenile walleye pollock (*Theragra chalcogramma*) at a frontal region near the Pribilof Islands, Bering Sea. ICES Journal of Marine Science 57, 1283–1295.
Schabetsberger, R., Sztatecsny, M., Drozdowski, G., Brodeur, R.D., Swartzman, G.L., Wilson, M.T., Winter, A.G., Napp, J.M., 2003. Size-dependent, spatial, and temporal variability of juvenile walleye pollock (*Theragra chalcogramma*) feeding at a structural front in the Southeast Bering Sea. Marine Ecology 24, 141–164.
Scharf, S.F., Juanes, F., Rountree, R.A., 2000. Predator size-prey size relationships of marine fish predators: interspecific variation and effects of ontogeny and body size on trophic-niche breadth. Marine Ecology Progress Series 208, 229–248.
Shimada, A.M., Kimura, D.K., 1994. Seasonal movements of Pacific cod, *Gadus macrocephalus*, in the eastern Bering Sea and adjacent waters based on tag-recapture data. Fishery Bulletin 92, 800–816.
Siddon, E.C., Heintz, R.A., Mueter, F.J., 2013. Conceptual model of energy allocation in walleye pollock (*Theragra chalcogramma*) from age-0 to age-1 in the south-eastern Bering Sea. Deep-Sea Research II 94, 140–149.
Sinclair, E.H., Loughlin, T., Pearcy, W., 1994. Prey selection by northern fur seal (*Callorhinus urinus*) in the eastern Bering Sea. Fishery Bulletin 92, 144–156.
Smart, T.I., Duffy-Anderson, J.T., Horne, J.K., Farley, E.V., Wilson, C.D., Napp, J.M., 2012. Influence of environment on walleye pollock eggs, larvae, and juveniles in the southeastern Bering Sea. Deep-Sea Research II 65–70, 196–207.
Stabeno, P.J., Kachel, N.B., Moore, S.E., Napp, J.M., Sigler, M., Yamaguchi, A., Zerbini, A.N., 2012. Comparison of warm and cold years on the southeastern Bering Sea shelf and some implications for the ecosystem. Deep-Sea Research II 65–70, 31–45.
Takatsu, T., Nakatani, T., Mutoh, T., Takahashi, T., 1995. Feeding habits of Pacific cod larvae and juveniles in Mutsu Bay, Japan. Fisheries Science 61, 415–422.
Takatsu, T., Yoshida, Y., Kooka, K., Sugimoto, K., Takahashi, T., 2001. Spatial and temporal distribution of Pacific cod *Gadus macrocephalus* juveniles in Mutsu Bay, Japan. Bulletin of the Japanese Society of Fisheries Oceanography 65, 6–14.
Takatsu, T., Toshikuni, N., Takanori, M., Kooka, K., Takahashi, T., 2002. Spatial distribution and feeding habits of Pacific cod (*Gadus macrocephalus*) larvae in Mutsu Bay, Japan. Fisheries Oceanography 11, 90–101.
Thompson, G.G., Ianelli, J.N., Lauth, R.R., 2011. Assessment of the Pacific Cod Stock in the Eastern Bering Sea and Aleutian Islands Area. Stock Assessment and Fishery Evaluation Report for the Groundfish Resources of the Bering Sea/Aleutian Islands Regions.
Treloar, M.A., Laurenson, L.J.B., Stevens, J.D., 2007. Dietary comparisons of six skate species (Rajidae) in southeastern Australian waters. Environmental Biology of Fishes 80, 181–196.
Urban, D., 2012. Food habits of Pacific cod and walleye pollock in the northern Gulf of Alaska. Marine Ecology Progress Series 469, 215–222.
Walsh, J.J., McRoy, C.P., 1986. Ecosystem analysis in the southeastern Bering Sea. Continental Shelf Research 5, 259–288.
Wiebe, P.H., Burt, K.H., Boyd, S.H., Morton, A.W., 1976. A multiple opening/closing net and environmental sensing system for sampling zooplankton. Journal of Marine Research 34, 313–326.

Deep-Sea Research II 109 (2014) 181–189

Contents lists available at ScienceDirect

Deep-Sea Research II

journal homepage: www.elsevier.com/locate/dsr2

Taxonomy of the early life stages of arrowtooth flounder (*Atheresthes stomias*) and Kamchatka flounder (*A. evermanni*) in the eastern Bering Sea, with notes on distribution and condition

Lisa De Forest [a,*], J.T. Duffy-Anderson [a], R.A. Heintz [b], A.C. Matarese [a], E.C. Siddon [b], T.I. Smart [a], I.B. Spies [a]

[a] Alaska Fisheries Science Center, National Marine Fisheries Service, National Oceanic and Atmospheric Administration, Seattle, WA 98115, USA
[b] Alaska Fisheries Science Center, Auke Bay Laboratories, National Marine Fisheries Service, National Oceanic and Atmospheric Administration, Juneau, AK 99801, USA

ARTICLE INFO

Available online 28 May 2014

Keywords:
Arrowtooth flounder
Kamchatka flounder
Atheresthes
Bering Sea

ABSTRACT

Arrowtooth flounder (*Atheresthes stomias*) and Kamchatka flounder (*A. evermanni*) are closely related flatfish species that co-occur in the eastern Bering Sea. As adults, arrowtooth flounder can be distinguished from Kamchatka flounder; however, larvae and early juveniles can only be indentified to the genus level due to morphological similarities. This has precluded studies of ecology for the early life stages of both species in the eastern Bering Sea. In this study, we developed a genetic technique to identify the larvae and early juveniles of the two species using mtDNA cytochrome oxidase subunit I (COI). Genetically identified specimens were then examined to determine a visual identification method based on pigment patterns and morphology. Specimens 6.0–12.0 mm SL and ≥ 18.0 mm SL can be identified to the species level, but species identification of individuals 12.1–17.9 mm SL by visual means alone remains elusive. The distribution of larvae (< 25.0 mm SL) of both arrowtooth flounder and Kamchatka flounder is similar in the eastern Bering Sea; however, juvenile (≥ 25.0 mm SL) Kamchatka flounder occur closer to the shelf break and in deeper water than juvenile arrowtooth flounder. Condition was determined for larvae and juveniles of each species by analyzing lipid content (%) and energy density (kJ/g dry mass). Kamchatka flounder larvae on average had higher lipid content than arrowtooth flounder larvae, but were also larger on average than arrowtooth flounder larvae in the summer. When corrected for length, both species had similar lipid content in the larval and juvenile stages.

Published by Elsevier Ltd.

1. Introduction

Arrowtooth flounder are large (max. size 86 cm total length), predatory flatfish that occur from off the coast of central California, north to the Bering Sea, and west to the Kamchatka Peninsula, Russia (Mecklenburg et al., 2002). Kamchatka flounder are similar in size, but occur primarily in the western Bering Sea with lesser occurrence in the eastern Bering Sea and along the Aleutian Islands (Mecklenburg et al., 2002). In the Bering Sea, arrowtooth flounder have been documented to feed primarily on juvenile and adult walleye pollock (*Gadus chalcogrammus*), euphausiids, and various shrimps (Yang and Livingston, 1986). They, in turn, are consumed by Alaska skates (*Bathyraja parmifera*) and sleeper sharks (*Somniosus pacificus*) as adults, and by Pacific cod (*Gadus macrocephalus*) and walleye pollock as juveniles (Spies et al., 2011). The diet of Kamchatka flounder is similar and often considered identical to arrowtooth flounder (Yang and Livingston, 1986). Both their predation impact and their role as prey for other organisms indicate that arrowtooth flounder and Kamchatka flounder are important constituents of the Bering Sea ecosystem (Aydin et al., 2007). The directed fishing effort for arrowtooth flounder has increased in recent years, as has the retention of adults caught in other commercial fisheries, possibly in response to an approximate eight-fold increase in adult arrowtooth flounder biomass in the Bering Sea since the early 1980s (Spies et al., 2011). Kamchatka flounder also experience some fishing pressure as directed commercial fishing has developed in recent years (Wilderbuer et al., 2011).

Despite their many similarities, these two species can be separated as adults by the number of gill rakers on the second upper gill arch (one in Kamchatka flounder, two to three in arrowtooth flounder) and the visibility of the dorsal-most eye from the blind side (top of eye is visible in arrowtooth flounder, no

* Corresponding author. Tel.: +1 206 526 4290.
E-mail address: Lisa.DeForest@noaa.gov (L. De Forest).

http://dx.doi.org/10.1016/j.dsr2.2014.05.005
0967-0645/Published by Elsevier Ltd.

part of eye visible in Kamchatka flounder) (Yang, 1988). Using electrophoretic examination of alleles at 32 different loci, Ranck et al. (1986) determined that arrowtooth flounder and Kamchatka flounder were two genetically-distinct species and, based on the distinct distributions of certain alleles, there was no hybridization between the two species. However, adults of arrowtooth flounder and Kamchatka flounder collected in scientific and commercial catches were often recorded as either all arrowtooth flounder or the genus *Atheresthes* (Yang and Livingston, 1986; Spies et al., 2011). In 1991, adult arrowtooth flounder and Kamchatka flounder individuals began to be separated as distinct species by the Alaska Fisheries Science Center (AFSC) Groundfish Assessment Program (Zimmerman and Goddard, 1996). As of summer 2011, fishing management regulations dictated that arrowtooth flounder and Kamchatka flounder must be separated and recorded as distinct species in commercial fishing hauls due to the emergence of a directed fishery for adult Kamchatka flounder (Wilderbuer et al., 2011).

While adults of both species have been well described, the early life stages in the eastern Bering Sea are less well known. High recruitment success has been suggested as one of the causes for the increase in population size of arrowtooth flounder in recent years (Spies et al., 2011). Understanding the early life stages of arrowtooth flounder is important to understanding recruitment and the first step is to identify and separate its early life stages from Kamchatka flounder. Our current study had the following objectives: (1) use genetic methods to identify larval and early juvenile *Atheresthes* collected in the eastern Bering Sea to species, (2) use the genetically identified individuals to develop a visual identification method that allows identification of historical and future samples, (3) describe the distribution and abundance of the early life stages of both arrowtooth flounder and Kamchatka flounder, and (4) examine condition as indicated by length adjusted dry mass, lipid content (%), and energy density of larvae and juveniles and to compare differences in nutritional quality between species.

2. Methods

2.1. Specimen collection

All specimens in this study were either collected directly at sea or were sorted from historical preserved samples collected on previous Alaska Fishery Science Center (AFSC) ichthyoplankton surveys. The specimens collected at sea were obtained on spring and summer cruises from 2006 to 2010 by scientists on AFSC, Bering Ecosystem Study (BEST), and Bering Sea Integrated Ecosystem Research Program (BSIERP) cruises (Table 1). Specimens were collected opportunistically, resulting in varied collection and preservation methods during the study. Methods of collection included using bongo nets (60 cm; 500 μm mesh), Multiple Opening/Closing Net and Environmental Sensing System (MOCNESS; 1 m^2 with 500 μm mesh; Wiebe et al., 1976), and surface and midwater trawls. Specimens removed from the bongo net were either placed directly into 100% non-denatured ethanol or into 5% formalin after an eyeball was removed. Sampling from the MOCNESS involved removing specimens only from the drogue net, which was open for the duration of the tow; all specimens were immediately frozen at −80 °C. The surface and midwater rope trawls sampled above and below the pycnocline; all specimens collected were immediately frozen at −80 °C. Specimens sorted from previously collected preserved samples were chosen from cruises occurring from 1994 to 2010 (Table 1). The samples were collected on previous AFSC ichthyoplankton surveys using 60-cm bongo nets, MOCNESS tows, Methot trawls (Methot, 1986), Tucker trawls (1 m^2 with 500 μm mesh; Tucker, 1951), and a modified bottom trawl (which samples the midwater). Sampling protocol during the cruises, along with sample handling and sorting, follows Matarese et al. (2003). All specimens used in this study were classified as either larvae (3.0–24.9 mm SL) or juveniles ($\geq$ 25.0 mm SL) (Matarese et al., 1989).

Table 1
Year and sampling date of cruises on which larval and juvenile *Atheresthes* specimens were collected. Number of specimens for each measurement is shown. Morphometric specimens not included in table, all 39 specimens measured were from the 7 May to 20 May 2009 cruise.

Year	Dates	Distribution	Genetics	Bioenergetics
1994	11 April–30 April	1		
	14 July–6 Sept	5		
	16 Sept–29 Sept	1		
1995	20 May–29 May	1		
1996	17 July–2 Aug	7		
	21 July–9 Aug	11		
	4 Sept–16 Sept	6		
1997	29 June–14 June	17		
	18 July–2 Aug	4		
	8 Sept–18 Sept	6		
1998	6 Sept–18 Sept	3		
1999	12 July–26 July	2		
	20 July–1 Aug	8		
	2 Sept–19 Sept	17		
2000	21 July–3 Aug	29		
2001	14 July–29 July	15		
2002	28 July–11 Aug	1		
2003	19 July–26 July	3		
2004	28 July–4 Aug	10		
2005	22 May–3 June	3		
	15 July–21 July	28		
2006	8 May–19 May		44	
	21 May–1 June	3		
	21 June–28 June	2		
2007	7 May–18 May		92	
	25 July–1 Aug	2		
2008	18 Feb–26 Feb	1708	16	
	19 Feb–28 Feb	6		
	12 May–21 May		26	
	24 May–30 May		4	
	3 July–17 July		7	7
2009	25 Feb–4 March	278	7	
	24 April–4 May	7		
	7 May–20 May		46	
	2 June–17 June	1		
	14 June–10 July	10	75	77
	2 Sept–30 Sept		9	20
2010	6 May–18 May		62	
	6 June–26 June	1		
	17 June–4 July	90	27	27
	30 June–17 July	6		
	16 Aug–26 Sept			59
Total		2292	415	190

2.2. Genetic identification

Genetic species identification was based on a restriction enzyme test (RFLP) that cut mitochondrial DNA at a specific nucleotide sequence within the cytochrome oxidase subunit I (COI) that is present in arrowtooth flounder but not Kamchatka flounder. The specific nucleotide sequence (GCTAGC) is a cut site for the restriction enzyme *Bmt*1 (New England Biolabs, Ipswich, MA). The cut site is fixed in arrowtooth flounder (i.e. base 329 Genbank accession number JQ353994.1) but not in Kamchatka flounder, where the sequence is ACTAGC (i.e. base 393 Genbank accession number KF386428.1). The test was based on an initial sequencing of three adult specimens from each species, followed by testing on 20 adult specimens of which the species identification was known. Fin tissue was used for DNA extraction in all

adults and was performed using Qiagen DNA extraction kits (Qiagen, Inc., Valencia, CA). For larval and early juveniles, a single eyeball (from either side of head) removed from either fresh, frozen, or 100% non-denatured ethanol preserved specimens was used for DNA extraction. The rest of the specimen body was placed back in its original preservative or, if frozen, photographed for future visual identification work.

Larval DNA was extracted from a single eyeball using a standard Chelex DNA extraction protocol. The eyeball was submerged in 150 µl of 10% (w/v) Chelex ® 100 resin (BIO-RAD Laboratories, Hercules, CA), heated to 60 °C for 20 min followed by 103 °C for 25 min. A 750 bp segment of COI was amplified using the following primers: COI_RajaF (5′–CCGCTTAACTCTCAGCCATC–3′) and COI_RajaR

(5′–TCAGGGTGACCAAAGAATCA–3′; Spies et al., 2006). Polymerase chain reactions (PCR) were conducted in a 10 µl volume, with approximately 100 ng DNA (1 µl taken from the Chelex supernatant), 10 mM Tris–HCl (pH 8.3), 50 mM KCl, 3.0 mM $MgCl_2$, 1.5 mM dNTPs, 0.5 pM of each primer, and 0.5 U Bioline Taq polymerase (Bioline USA, Inc., Boston, MA). PCR amplification using Chelex extractions can fail if the supernatant contains impurities such as proteins. Therefore, failed samples were repeated with a 1:10 or 1:100 dilution of the DNA, which typically resulted in success. The thermal cycling protocol consisted of 94 °C for 2 min, followed by 40 cycles of 94 °C (30 s), 57 °C (30 s), and 72 °C (30 s). DNA sequencing of amplified DNA from adult specimens was performed using COI_Raja primers at the University of Washington High Throughput Genomics Center (www.htseq.org).

Following PCR, DNA was digested using *Bmt1* according to manufacturer's instructions, in a total volume of 10:l with 2:l PCR product and 4 U of *Bmt1* at 37 °C for 1 h. Identification was based on either the presence of a single 750 bp fragment (Kamchatka flounder) or two fragments consisting of approximately 450 and 300 bp (arrowtooth flounder). This protocol was performed in a laboratory or at sea using an Agilent 2100 Bioanalyzer with a DNA 1000 kit (Agilent Technologies, Santa Clara, CA) and a BIO-RAD DNA Engine Thermalcycler.

2.3. Visual identification

Specimens identified using genetic methods were subsequently examined to develop a visual identification method based on morphological and pigmentation characters. Specimens were examined both with and without knowledge of their genetic identification to determine species-specific characters. Each specimen was critically evaluated with regards to morphology and pigment (such as the number of melanophores in a patch or the general shape and pattern of melanophore patches). Only specimens preserved in the same preservation medium were directly compared to minimize the identification of preservation artifacts as distinguishing species characters.

Morphometric measurements were taken from arrowtooth flounder and Kamchatka flounder larvae chosen from a single cruise. Only specimens initially preserved in formalin were used for morphometric measurements because the other preservation methods (100% ethanol and immediate freezing) shrink tissues and distort morphology. The following measurements were taken: standard length (SL), preanal length (tip of snout to anus), head length, snout length, eye diameter, and body depth (vertical measurement taken at pectoral fin; BD). The measurements were taken using a calibrated digital image analysis system consisting of a video camera attached to a stereo microscope and a computer with image analysis software. All measurements were recorded to the nearest 0.1 mm. A two sample *t*-test was used to identify statistically significant differences ($p < 0.05$) between each morphological measurement for the two species. Developmental stage terminology follows Kendall et al. (1984).

2.4. Distribution

Selected larval *Atheresthes* collected on previous AFSC cruises conducted from 1994 to 2010 (Table 1) were identified to the species level using pigmentation and morphological characters identified with the visual identification method. The locations of all specimens identified to species were mapped and a mean distribution based on abundance was calculated for each species using ArcGIS software.

2.5. Measures of condition

2.5.1. Biological sampling

Larval and juvenile *Atheresthes* were collected from five research surveys conducted in the summer and early fall from 2008 to 2010 (Table 1). All specimens were measured to the nearest 0.01 mm SL. Specimens < 30.0 mm SL were identified to species using the genetic methods previously described, while specimens > 30.0 mm SL were identified morphologically using the number of gill rakers on the upper arch of the second gill raker. All specimens had an eyeball removed, even if identified visually. Stomach contents were removed prior to chemical analysis.

2.5.2. Dry mass

Larvae were individually dried at 60 °C in a drying oven until their weight was stabilized. Juveniles were dried at 135 °C using a LECO Thermogravimetric Analyzer (TGA) 601 or 701, which provided percent moisture values used to convert wet mass to dry mass equivalents.

2.5.3. Estimation of lipid content (%)

For larvae, a sulfo-phospho-vanillin (SPV) colorimetric analysis (Van Handel, 1985) was performed to determine lipid content (%). Dried material was sonicated in 2:1 (by volume) chloroform: methanol solvent in glass centrifuge tubes for 60 min. Washes of 0.88% KCl and 1:1 (by volume) methanol:water were performed on the extracts as in the modified Folch extraction method (Vollenweider et al., 2011). Resulting chloroform extracts were evaporated in a LabConco RapidVap for 30 min at 40 °C and 250 mbar until reduced to approximately 1 ml in volume. Extracts were evaporated to dryness in 12 mm test tubes on a heating block at 75 °C and then allowed to cool. Concentrated sulfuric acid was added to the tubes prior to incubation at 100 °C for 10 min with subsequent cooling. The SPV reagent (1.2 mg/ml vanillin in 80% phosphoric acid) was added to each tube and allowed to develop for 10 min. Absorption was measured on an Agilent 8453 Spectrophotometer at 490 nm and extrapolated from species-specific calibration curves determined prior to analysis. For juveniles, lipid extraction was performed on dried material using a previously described method (Vollenweider et al., 2011) derived from the Folch extraction procedure.

2.5.4. Energy density

Energy density (kJ/g dry mass) was estimated using bomb calorimetry. Homogenized dry tissue was pressed into a pellet form and a Parr Instrument 6725 Semimicro Calorimeter with 6772 Precision Thermometer and 1109A Oxygen Bomb was used to measure the energy released from combustion of the sample pellets. The minimum pellet weight was set at 0.025 g of dry material based on the limits of instrument detection; individual larvae were composited within stations as needed to attain sufficient dry mass.

2.5.5. Statistical analysis

A general linear model was used to identify differences in the nutritional state of arrowtooth flounder and Kamchatka flounder. Lengths were compared by a nested analysis of variance (ANOVA) to account for differences in the numbers of fish collected. Species was the main factor with life stage nested in species and year nested in life stage. Post-hoc comparisons of species were conducted among the life stages using Bonferonni's adjusted t value. Analysis of covariance (ANCOVA) was employed to compare dry mass and lipid content between species. This approach permitted comparisons when length distributions differed between species and the responses covaried with length. The ANCOVA used species, year, and their interaction as main factors and length as covariate. Analyses were conducted separately for larvae and juveniles because the response variables were heteroscedastic when pooled across life stages. Variables were transformed prior to analysis using logarithms (base 10), and the assumption that both species had equivalent slopes was tested. Student's t was used to compare energy densities of larvae and juveniles.

3. Results

3.1. Genetics

The use of mtDNA COI restriction analysis proved successful in identifying all *Atheresthes* larvae and some early juveniles to species in the laboratory ($n=337$) and at sea ($n=78$). There were some discrepancies between the genetic identification and morphological identification of early juvenile specimens that were >37.0 mm SL. These discrepancies were present only in one set of specimens which were all collected and handled at the same time. It was decided that all specimens >30.0 mm would ultimately be identified morphologically using the reliable adult character of number of gill rakers on the second upper gill arc (1 gillraker in Kamchatka flounder and 2–3 gill rakers in arrowtooth flounder). Of the 415 total specimens, 165 were identified as arrowtooth flounder, 194 as Kamchatka flounder, and 56 failed to amplify properly resulting in an unknown identity. Size of specimens examined was 6.0–38.0 mm SL, with the majority of specimens 6.0–11.5 mm SL.

3.2. Visual identification

Visual examination of genetically-identified specimens was successful in determining key pigmentation differences between arrowtooth flounder and Kamchatka flounder larvae of 6.0–12.0 mm SL and ≥ 18.0 mm SL. These key pigmentation differences are size specific but not stage specific. Specimens 12.1–17.9 mm SL remain indistinguishable at this time because of the small sample size and a high degree of variation in pigmentation patterns.

Recently hatched Kamchatka flounder larvae (6.0–7.4 mm SL) can be distinguished from arrowtooth flounder of the same size by the presence of pigment dorsal to the gut at the anus and an anterior dorsal pigment patch located halfway between the anus and the caudal fin (Fig. 1A). Arrowtooth flounder begin to develop the same pigment patterns at about 7.5 mm SL, resulting in these characteristics no longer being able to be used.

Larvae of 7.5–12.0 mm SL can be identified by two characters. Kamchatka flounder larvae of 7.5–10.5 mm have pigment on the crown of the head, beginning as a few melanophores and developing to numerous melanophores that cover the entire crown of the head by approximately 9.0 mm SL (Fig. 1A). In general, arrowtooth flounder larvae do not begin to develop head pigment prior to 10.5 mm SL, however, a few individuals do develop one or two two small melanophores on the crown of the head beginning at approximately 8.5 mm SL (Fig. 1B). Thus, specimens 8.5–10.5 mm SL with only 1–3 melanophores on the head cannot be identified to species. In addition to crown pigment, the second character by which Kamchatka flounder larvae 7.5–12.0 mm SL can be identified is the pigment dorsal to the gut that starts at mid-gut and extends to the anus (Fig. 1A). Arrowtooth flounder larvae also have pigment dorsal to the gut, but it starts at $\frac{3}{4}$ gut length and extends to the anus. The combination of these two characters allows larvae 7.5–12.0 mm SL to be identified to species.

Few genetically identified specimens were larger than 12.0 mm SL. Identification methods for larger specimens began with the use of adult characters to identify specimens >25.0 mm SL. These identified specimens were then used as a guide to begin identifying smaller specimens. The adult characters used to determine the larger specimens was the number of gill rakers on the second upper gill arch: Kamchatka flounder have one gill raker, arrowtooth flounder have two or three. While these structures are not fully formed in specimens of 25.0–27.0 mm SL, fleshy protrusions that are the precursors to the gill rakers are evident. After numerous specimens were separated based on gill raker counts, a pattern in the dorsal pigment bands was seen to be different between the two species. The anterior dorsal patch on Kamchatka flounder is generally longer (>5 melanophores long) and the individual melanophores in the patch are close together, often touching and at times coalescing. Additionally, Kamchatka flounder develop melanophores between the anterior and posterior bands, which eventually connect the two bands at a smaller size than arrowtooth flounder (beginning as early as approximately 13.0 mm SL, but generally by 18.0 mm SL) (Fig. 1A). In contrast, arrowtooth flounder tend to have a short (<5 melanophores long) anterior dorsal band with melanophores that are widely spaced apart. Melanophores do not develop between the anterior and posterior dorsal bands until approximately 25.0 mm SL (Fig. 1B). The few large larvae and early juveniles used in the genetic technique confirmed the validity of these visual differences.

Morphological measurements were taken on 20 arrowtooth flounder larvae and 19 Kamchatka flounder larvae. Specimens ranged in length from 6.3 to 12.6 mm SL. Head length and eye diameter were not statistically different between the two species, but body depth and preanal length were. Larvae of Kamchatka flounder have a stouter body ($BD=12.0\pm1.1\%$ SL) than arrowtooth flounder larvae ($BD=9.8\pm1.4\%$ SL; $p<0.05$). In addition to a stouter body, Kamchatka flounder larvae also have a slightly longer preanal length than arrowtooth flounder larvae ($36.3\pm1.8\%$ SL vs. $35.1\pm1.8\%$ SL; $p<0.05$).

3.3. Distribution

Examining formalin-preserved specimens from previous AFSC cruises, a total of 1928 larvae and juveniles were identified to species using pigmentation and morphological characters identified above, with 364 individuals identified to genus because of ambiguous characters or damage. A total of 1315 arrowtooth flounder larvae and 480 Kamchatka flounder larvae were identified; 125 arrowtooth flounder juveniles and eight Kamchatka flounder juveniles were identified.

The majority of larval arrowtooth flounder and Kamchatka flounder were collected along the shelf break in the southeastern Bering Sea between Unimak and Umnak Pass (Fig. 2). There were also individuals collected farther north in Pribilof Canyon along the shelf break near deep water. The calculated mean distribution for both species is similar (Fig. 2).

Juveniles of both species were collected primarily north of where the majority of the larvae were collected. The calculated mean distribution of the two species showed that arrowtooth

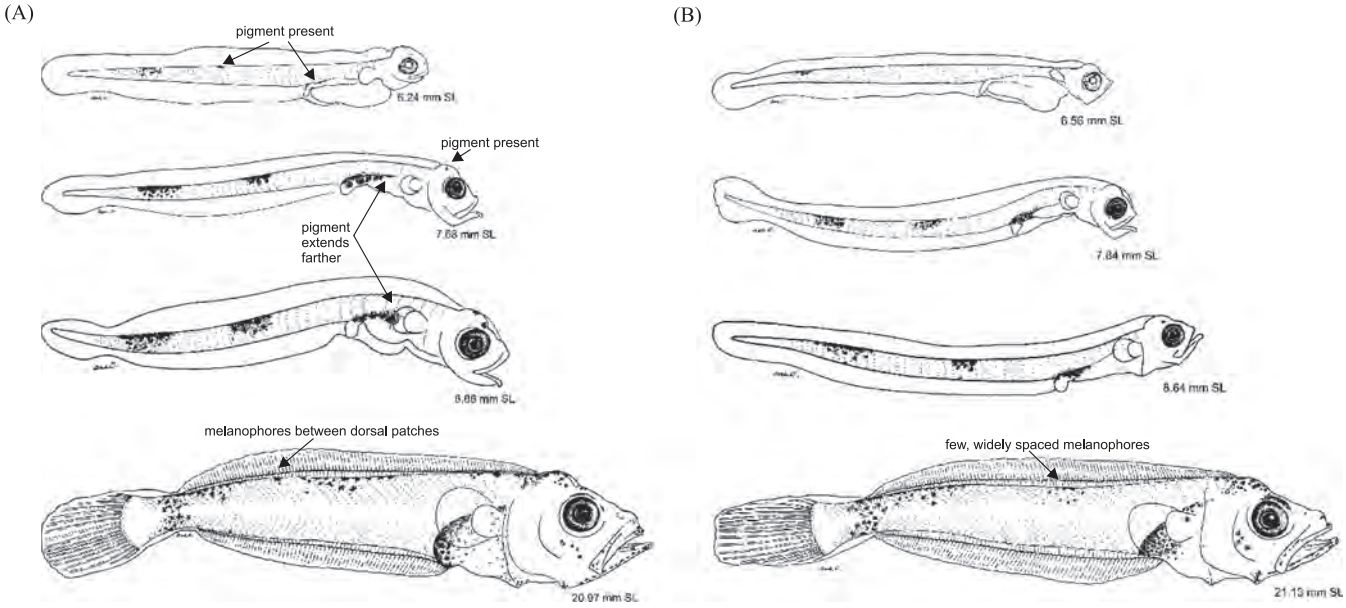

Fig. 1. Illustrations of eastern Bering Sea: (A) Kamchatka flounder (*Atheresthes evermanni*) and (B) arrowtooth flounder (*A. stomias*). Arrows point to key identifying characters between the two species. Illustrations by Ashlee Overdick.

flounder juveniles appear to be located farther east and over shallower waters than Kamchatka flounder juveniles, which have a mean distribution close to Pribilof Canyon and deeper water (Fig. 2). However, fewer Kamchatka flounder juveniles were collected and identified ($n=8$) than arrowtooth flounder juveniles ($n=125$), so caution should be used when interpreting this result.

3.4. Measures of condition

3.4.1. Biological sampling

Length analysis was restricted to larvae collected in 2009 and 2010 and juveniles collected in 2010. These were stages and years in which sufficient numbers of specimens were collected. No significant difference was found in the lengths of larvae or juveniles sampled in 2009 and 2010 ($F_{2.154}>0.77$, $p=0.466$), and larvae were significantly smaller than juveniles ($F_{2.154}>1000$, $p<0.001$). Pairwise comparisons of larvae and juveniles between the two species averaged across years indicated that Kamchatka flounder larvae averaged approximately 25% longer than arrowtooth flounder larvae ($t=4.6$, $p<0.001$), but no difference was detected among juveniles ($t=0.31$, $p=0.991$) (Table 2). Differences between the two sets of larvae therefore accounted for the overall difference detected between species ($F_{1.154}=6.71$, $p=0.010$).

3.4.2. Dry mass

The dry weights of larvae did not depend on year nor was there an interaction between year and species ($F_{1.96}<0.15$, $p>0.700$). However, larval arrowtooth flounder of a fixed length were approximately 25% lighter than similarly sized Kamchtaka flounder ($F_{1.96}=4.16$, $p=0.044$; Fig. 3A). No difference in dry mass was detected among juvenile specimens in 2010 ($F_{1.53}=1.68$, $p=0.20$; Fig. 3B). It was not possible to test for year effect due to an inadequate number of samples in 2008 and 2009.

3.4.3. Lipid content

In 2009 and 2010 the average lipid content of arrowtooth larvae was $7.5\pm0.3\%$ ($n=39$) of dry mass compared with $10.8\pm0.7\%$ for Kamchatka flounder larvae ($n=11$; Fig. 4A). While the lipid content of Kamchatka flounder larvae averaged approximately 30% more than that of arrowtooth flounder larvae, this difference was not significant after controlling for the differences in average length ($F_{1.45}=3.15$, $p=0.083$). Additionally, there was not an effect of year or interaction between year and species on larval lipid content ($F_{1.45}<2.37$, $p>0.130$). In 2010, there was no difference between juveniles ($F_{1.25}=0.03$, $p=0.857$). Arrowtooth flounder juveniles averaged $10.2\pm0.5\%$ lipid ($n=21$) in 2010 compared with $10.7\pm0.7\%$ ($n=7$) for Kamchatka flounder juveniles.

3.4.4. Energy density

Energy density in juveniles was only measured in 2010 and in larvae only in 2009. Only a few larvae could be measured because samples required compositing. Based on these limited sample comparisons, there was no statistically significant difference between the energy densities of the two species. Only six measurements of larval energy density were taken and the difference between species was not statistically significant ($t=1.06$, $p=0.366$) (Fig. 4B). Arrowtooth larvae averaged 19.2 ± 0.8 kJ/g dry mass; Kamchatka flounder larvae averaged 19.8 ± 0.7 kJ/g dry mass. Energy densities between juveniles of the two species were nearly identical ($t=1.19$, $p=0.244$), averaging 20.5 ± 0.2 kJ/g dry mass for arrowtooth flounder ($n=16$) and 20.8 ± 0.2 kJ/g dry mass for Kamchatka flounder ($n=12$).

4. Discussion

With the increasing population size of arrowtooth flounder and interest for increased directed fishing effort for both arrowtooth flounder and Kamchtaka flounder, there is a need to fully identify and study both species in all life stages for management and ecological purposes. Adults of arrowtooth flounder have been studied with regard to their distribution (Zimmerman and Goddard, 1996), predation effects on walleye pollock (Ianelli et al., 2009), and their role as prey for other organisms (Livingston and Jurado-Molina, 2000). The early life stages in the Gulf of

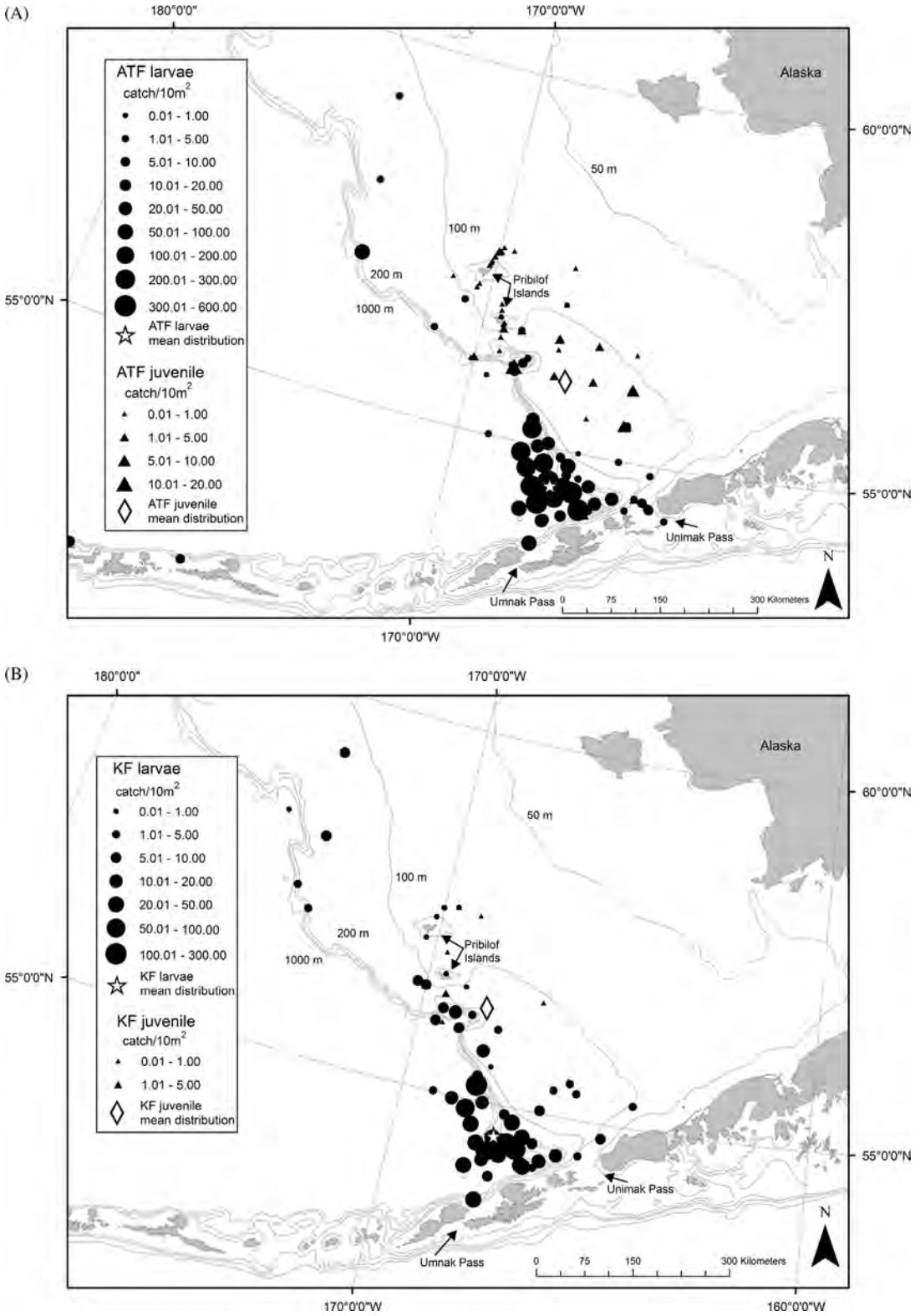

Fig. 2. Distribution of abundance (catch/10 m^2) for formalin preserved larval and juvenile *Atheresthes* identified to species using visual identification techniques: (A) arrowtooth flounder (ATF: *Atheresthes stomias*) and (B) Kamchatka flounder (KF: *A. evermanni*). In both maps, circles depict larvae (<25 mm SL), triangles depict juveniles (≥ 25 mm SL), stars depict calculation of mean distribution generated by ArcGIS software of larvae based on abundance, and diamonds depict calculated mean distribution of juveniles based on abundance. The size of circles and triangles is proportional to abundance.

Alaska have been described by Blood et al. (2007); however, efforts to conclusively identify larvae and juveniles in the Bering Sea have been confounded by the overwhelming physical similarities between arrowtooth and Kamchatka flounder.

4.1. Genetics

Genetic methods have proven to be useful tools in identifying unknown specimens to the species or family level using the

Table 2
Lengths of specimens used in condition analyses. Measurements are reported as mean ± standard error (number sampled). n/a indicates no specimens were available for condition analyses resulting in no length measurement.

Year	Stage	Arrowtooth flounder	Kamchatka flounder
2008	Larvae	14.4 ± 1.0 (6)	18.6 (1)
2009	Larvae	12.4 ± 0.3 (57)	14.5 ± 0.3 (20)
	Juveniles	37.2 ± 0.8 (9)	n/a (0)
2010	Larvae	11.9 ± 0.8 (11)	15.5 ± 0.6 (16)
	Juveniles	48.7 ± 0.5 (39)	49.2 ± 0.6 (20)

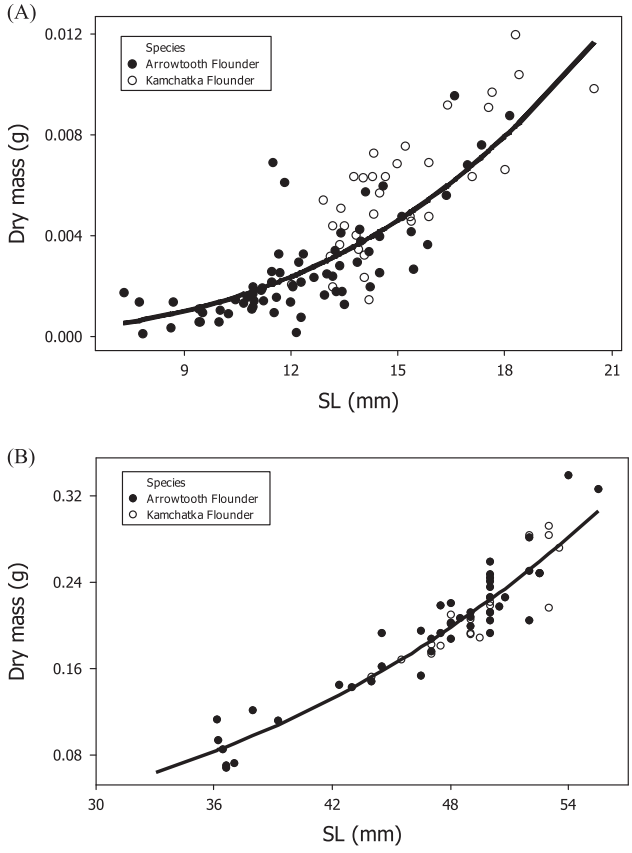

Fig. 3. Length–dry mass relationships for arrowtooth flounder (*Atheresthes stomias*) and Kamchatka flounder (*Atheresthes evermanni*) of larvae (A) and juveniles (B). Lines depict the least-squares relationships for all species combined.

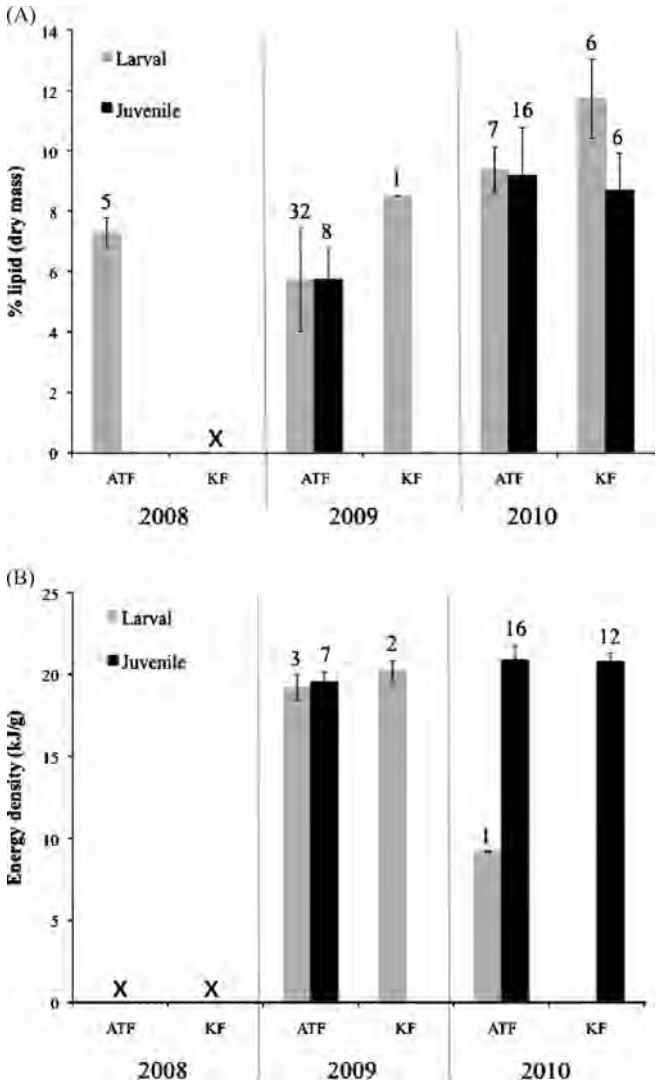

Fig. 4. Measures of condition for arrowtooth flounder (*Atheresthes stomias*) and Kamchatka flounder (*A. evermanni*) collected in June/July (larvae) and September (juveniles) 2008–2010: (A) % lipid (dry mass) and (B) energy density (kJ/g). Sample sizes are indicated above each bar. X indicates no specimens were available to be measured.

mtDNA gene COI (Hebert et al., 2002; Dawnay et al., 2007; Rocha et al., 2007). In Alaskan waters, Spies et al. (2006) also successfully used mtDNA COI to identify 15 different skate species. In this current study we have demonstrated that this genetic technique is valid for identifying specimens of *Atheresthes* to the species level. In addition, the technique developed in this study proved effective for use both in the laboratory and at sea aboard a research vessel. In particular, this ability to conclusively identify specimens to the species level while at sea is quite useful as it can enable a timely adjustment to sampling location or procedure in order to maximize collection of the target species.

4.2. Morphology

In the marine environment closely related species are often indistinguishable as larvae due to overlap in pigmentation and morphological characters. Prior to this study, all larval and early juvenile *Atheresthes* collected in the Bering Sea were identified only to the genus level. Despite numerous physical similarities, unique pigmentation and morphological differences were noted between the two *Atheresthes* species in the size ranges of 6.0–12.0 mm SL and ≥ 18.0 mm SL. In general, it appears that Kamchatka flounder acquire certain pigmentation characters at smaller sizes than arrowtooth flounder, thus the distinguishing characters noted in this paper can only be used for the specific size ranges to which they correspond. Specimens of 12.1–17.9 mm SL are indistinguishable at this time due because of a high degree of variability in pigment amongst individuals and a low number of genetically identified specimens in this size range. In addition to pigment, Kamchatka flounder larvae are stouter than arrowtooth flounder larvae (BD 12.0% SL vs. 9.8% SL) and have a slightly longer snout to anus length (36.3% SL vs. 35.1% SL). These are modest morphological differences and can be difficult to determine but can be helpful when used in conjunction with pigmentation characters to support species identification.

Using the pigment characteristics described in this study, two specimens illustrated by Blood et al. (2007; Fig. 13) should

be re-examined as both specimens were collected in the Bering Sea. The 13.4 mm SL specimen is most likely Kamchatka flounder, not arrowtooth flounder, based on the large amount of pigment present on the head and the pigment present on the dorsal midline between the two dorsal bands. While arrowtooth flounder do develop pigment on the crown of the head, the amount of pigment present at this size is more indicative of Kamchatka flounder. In addition, the presence of pigment on the dorsal midline between the two dorsal bands at this size can only be Kamchatka flounder as arrowtooth do not develop this pigment until approximately 25.0 mm SL. The 10.0 mm SL specimen (Blood et al., 2007; Fig. 12) may also be a Kamchatka flounder due to the large amount of pigment located on the crown of the head and within the two dorsal patches. However, complete identification is difficult from the illustrations alone; a close visual examination of the original specimens is needed.

4.3. Distribution

The larval distributions of arrowtooth flounder and Kamchatka flounder in the eastern Bering Sea are similar. Most of the larvae collected were located in the southern part of the eastern Bering Sea in water > 200 m along the shelf break (Fig. 2A and B). This may indicate that in the eastern Bering Sea both arrowtooth and Kamchatka flounder adults spawn in deep water, similar to that described for arrowtooth flounder in the Gulf of Alaska by Blood et al. (2007). The distribution of juveniles collected does appear to be different between the two species, but this result is tenuous due to the low number of juvenile Kamchatka flounder collected ($n=8$). However, this result may indicate that juvenile Kamchatka flounder are migrating to their adult habitat. In general, the majority of adult Kamchatka flounder are collected in deeper waters and farther to the west than adult arrowtooth flounder, which often occur in shallower waters to the east (Zimmerman and Goddard, 1996; Wilderbuer et al., 2011). One consideration for the low number of juvenile Kamchatka flounder collected is the limited sampling in deeper waters to the west of the shelf break.

4.4. Condition

Differences in the condition between arrowtooth flounder and Kamchatka flounder larvae collected in the summer may relate to differences in timing of development. For years in which sufficient numbers of larvae were collected for analysis, Kamchatka flounder larvae were significantly larger than arrowtooth flounder larvae in the summer. Comparison of the lengths of larvae sampled in the summer indicates that the bulk of arrowtooth flounder larvae were in the preflexion or flexion stages (Blood et al., 2007). Assuming stage designation is similar for Kamchatka flounder, the majority of Kamchatka flounder sampled in the summer were in the flexion and postflexion stages. The difference in developmental stage could account for the differences in the length adjusted dry mass of the two species and the trend towards increased lipid content in larval Kamchatka flounder. Energy allocation strategies can differ among developmental stages during the early life stages. This study suggests that postflexion larvae of *Atheresthes* may invest more energy accreting tissue mass than earlier stages. Comparison of the lengths of juveniles sampled indicates that the majority of the fish sampled from both species were in the transformation stage (Blood et al., 2007). Hence there were no differences in condition between juveniles of either species.

The results presented here are the first estimates of lipid and energy density in larval and juvenile arrowtooth flounder and Kamchatka flounder. Lipid content values of juveniles in this study are similar to those reported for Atlantic halibut (*Hippoglossus hippoglossus*) fed a diet that promoted growth and survival (Hamre et al., 2002). Energy densities of larvae were similar to those of juveniles and suggests no change in energy allocation strategy between these two stages. This is in contrast to walleye pollock which undergo significant changes in both lipid content and energy density between lengths of 20 and 60 mm (Siddon et al., 2013), which is when walleye pollock undergo and complete transformation to the juvenile stage (Brown et al., 2001). The only evidence of a shift in lipid content among both species of *Atheresthes* sampled here is associated with ontogeny in the larval stages.

4.5. Conclusion

This study has provided a method to genetically identify larval and early juvenile arrowtooth flounder and Kamchatka flounder both in the field and in the laboratory, and has provided morphological and pigmentation characters to visually identify these two species at small (6.0–12.0 mm SL) and large sizes (≥ 18.0 mm SL). Future sampling effort during June–August when arrowtooth flounder and Kamchatka flounder larvae 12.1–17.9 mm SL are in the water column could aid in completing the visual identification of these two species. Once all arrowtooth flounder and Kamchatka flounder between 6.0 mm SL to the juvenile stage can be identified, all historical samples of *Atheresthes* collected in 1991–2010 (19 years) by the AFSC from the eastern Bering Sea can be re-identified to the species level. This collection contains approximately 5065 individuals that, when identified to the species level, will greatly increase our knowledge of distribution and abundance for these two species. Additionally, increased sampling effort in the deeper water off the shelf break during summer and fall would help define the distribution of the larger sizes of these two species and determine if there is a difference in timing of development for larvae in the summer.

Acknowledgments

The authors would like to thank all the scientists that collected *Atheresthes* spp., larvae over the years and the officers and crews of the following ships: NOAA ship *Miller Freeman*, NOAA ship *Oscar Dyson*, R/V *Thomas G. Thompson*, USCGC *Healy*, and the R/V *Knorr*. We would also like to thank Dan Cooper for his help with genetic identification of specimens while on the May 2010 cruise and for reviewing a draft of this manuscript, Melanie Paquin for her help with genetic identification and sequencing in the laboratory, Ashlee Overdick for her illustrations of both species, and Debbie Blood for also reviewing a draft of this manuscript. This is BEST-BSIERP Bering Sea Project publication number 139 and NPRB publication number 488. This research is contribution EcoFOCI-0821 to NOAA's Fisheries-Oceanography Coordinated Investigations. The findings and conclusions in this manuscript are those of the authors, and do not necessarily represent the views of the National Marine Fisheries Service.

References

Aydin, K., Gaichas, S., Ortiz, I., Kinzey, D., Friday, N., 2007. A comparison of the Bering Sea, Gulf of Alaska, and Aleutian Islands large marine ecosystems through food web modeling. U.S. Department of Commerce, NOAA Technical Memorandum NMFS-AFSC-178, 298 pp.

Blood, D.M, Matarese, A.C., Busby, M.S. 2007. Spawning, egg development, and early life history dynamics of arrowtooth flounder (*Atheresthes stomias*) in the Gulf of Alaska. NOAA Professional Paper NMFS 7, 28 pp.

Brown, A.L., Busby, M.S., Mier, K.L., 2001. Walleye pollock *Theragra chalcogramma* during transformation from the larval to the juvenile stage: otolith and osteological development. Mar. Biol. 139, 845–851.

Dawnay, N., Ogden, R., McEwing, R., Carvalho, G.R., Thrope, R.S., 2007. Validation of the barcoding gene COI for use in forensic genetic species identification. Forensic Sci. Int. 173, 1–6.
Hebert, P.D.N., Cywinska, A., Ball, S.L., deWaard, J.R., 2002. Biological identifications through DNA barcodes. Proc. R. Soc. Lond. B 270, 313–321.
Hamre, K., Opstad, I., Espe, M., Solbakken, J., Hemre, G.I., Pittman, K., 2002. Nutrient composition and metamorphosis success of Atlantic halibut (*Hippoglossus hippoglossus*, L.) larvae fed natural zooplankton or *Artemia*. Aquac. Nutr. 8, 139–148.
Ianelli, J.N., Barbeaux, S., Honkalehto, T., Kotwicki, S., Aydin, K., Williamson, N., 2009. Assessment of the Walleye Pollock stock in the Eastern Bering Sea. Stock Assessment and Fishery Evaluation Report for the Groundfish Resources of the Bering Sea/Aleutian Islands Regions. North Pacific Fishery Management Council, USA.
Kendall Jr., A.W., Ahlstrom, E.H., Moser, H.G., 1984. Early life history stages and their characters. In: Moser, H.G., Richards, W.J., Cohen, D.M., Fahay, M.P., Kendall Jr., A.W., Richardson, S.L. (Eds.), Ontogeny and Systematic of Fishes. Special Publication 1 American Society of Ichthyologists and Herpetologists. Allen Press, Lawrence, KS, pp. 11–22.
Livingston, P.A., Jurado-Molina, J., 2000. A multispecies virtual population analysis of the eastern Bering Sea. ICES J. Mar. Sci. 57, 294–299.
Matarese, A.C., Blood, D.M., Picquelle, S.J., Benson, J.L., 2003. Atlas of abundance and distribution patterns of ichthyoplankton from the northeast Pacific Ocean and Bering Sea ecosystems based on research conducted by the Alaska Fisheries Science Center (1972–1996). NOAA Professional Paper NMFS 1, 281 pp.
Matarese, A.C., Kendall Jr., A.W., Blood, D.M., Vinter, B.M., 1989. Laboratory Guide to Early Life History Stages of Northeast Pacific Fishes. U.S Department of Commerce NOAA Technical Report NMFS 80, 652 pp.
Mecklenburg, C.W., Mecklenburg, T.A., Thorsteinson, L.K., 2002. Fishes of Alaska. American Fisheries Society, Bethesda, MD p. 1116.
Methot, R.D., 1986. Frame trawl for sampling juvenile fish. Calif. Coop. Oceanic Fish. Invest. Rep. 27, 267–278.
Ranck, C.L., Utter, F.M., Milner, G.B., Smith, G.B., 1986. Genetic confirmation of specific distinction of arrowtooth flounder, *Atheresthes stomias*, and Kamchatka flounder, *A. evermanni*. Fish. Bull. 84, 222–226.
Rocha, L.A., Craig, M.T., Bowen, B.W., 2007. Phylogeny and the conservation of coral reef fishes. Coral Reefs 26, 501–512.
Siddon, E.C., Heintz, R.A., Mueter, F.J., 2013. Conceptual model of energy allocation in walleye pollock (*Theragra chalcogramma*) from age-0 to age-1 in the southeastern Bering Sea. Deep-Sea Res. II 94, 140–149.
Spies, I.B., Gaichas, S., Stevenson, D.E., Orr, J.W., Canino, M.F., 2006. DNA-based identification of Alaska skates (*Amblyraja, Bathyraja* and *Raja*: Rajidae) using cytochrome *c* oxidase subunit I (col) variation. J. Fish. Biol. 69(B), 283–292.
Spies, I.B., Wilderbuer, T.K., Nichol, D.G., Aydin, K., 2011. Assessment of the Arrowtooth Flounder Stock in the Bering Sea/Aleutian Islands. North Pacific Management Council, pp. 727–744.
Tucker, G.H., 1951. Relation of fishes and other organisms to the scattering of underwater sound. J. Mar. Res. 10 (2), 215–238.
Van Handel, E., 1985. Rapid determination of total lipids in mosquitoes. J. Am. Mosq. Control Assoc. 1 (3), 302–304.
Vollenweider, J.J., Heintz, R., Schaufler, L., Bradshaw, R., 2011. Seasonal cycles in whole-body proximate composition and energy content of forage fish vary with water depth. Mar. Biol. 158, 413–427.
Wiebe, P.H., Burt, K.H., Boyd, S.H., Morton, A.W., 1976. A multiple opening/closing net and environmental sensing system for sampling zooplankton. J. Mar. Res. 34, 313–326.
Wilderbuer, T.K., Nichol, D.G., Lauth, R., 2011. Assessment of the Kamchatka flounder stock in the Bering Sea and Aleutian Islands. North Pacific Management Council, pp. 795–801.
Yang, M.S., 1988. Morphological differences between two congeneric species of pleuronectid flatfishes: arrowtooth flounder, *Atheresthes stomias*, and Kamchatka flounder, *A. evermanni*. Fish. Bull. 86, 608–611.
Yang, M.S., Livingston, P.A., 1986. Food habits and diet overlap of two congeneric species, *Atheresthes stomias* and *Atheresthes evermanni*, in the eastern Bering Sea. Fish. Bull. 82, 615–623.
Zimmerman, M., Goddard, P., 1996. Biology and distribution of arrowtooth, *Athersthes stomias*, and Kamchatka, *A, evermanni*, flounders in Alaskan waters. Fish. Bull. 94, 358–370.

Deep-Sea Research II 109 (2014) 190–203

Contents lists available at ScienceDirect

Deep-Sea Research II

journal homepage: www.elsevier.com/locate/dsr2

Effects of seasonal and interannual variability in along-shelf and cross-shelf transport on groundfish recruitment in the eastern Bering Sea

Cathleen D. Vestfals [a,*], Lorenzo Ciannelli [a,1], Janet T. Duffy-Anderson [b,2], Carol Ladd [c,3]

[a] College of Earth, Ocean, and Atmospheric Sciences, Oregon State University, 104 CEOAS Admin. Bldg., Corvallis, OR 97331-5503, USA
[b] NOAA Fisheries, Alaska Fisheries Science Center, Recruitment Processes Program, Resource Assessment and Conservation Engineering Division, 7600 Sand Point Way NE, Seattle, WA 98115-6349, USA
[c] NOAA Pacific Marine Environmental Laboratory, 7600 Sand Point Way NE, Seattle, WA 98115-6349, USA

ARTICLE INFO

Available online 4 October 2013

Keywords:
Bering Sea
Variability
Ocean currents
Slope
Along-shelf
Cross-shelf
Transport
Groundfish
Recruitment

ABSTRACT

The Bering Sea responds rapidly to atmospheric perturbations and over the past several decades has experienced extreme variability in both its physical and biological characteristics. These changes can impact organisms that inhabit the region, particularly marine fishes, as normal current patterns to which reproductive habits are tuned can be disrupted, which, in turn, may influence recruitment and population dynamics. To understand the influence of ocean circulation on groundfish recruitment in the eastern Bering Sea, we examined transport along and across the Bering Slope derived from 23 years (1982–2004) of simulations from a Regional Ocean Modeling System (ROMS) ocean circulation model. We expected that changes in the strength and position of the Bering Slope Current (BSC) would affect recruitment in selected species (Pacific cod, walleye pollock, Greenland halibut, Pacific halibut, and arrowtooth flounder), and that circulation features along and across the shelf edge would be strongly influenced by atmospheric forcing. Variability in along-shelf transport at three transects along the path of the BSC, cross-shelf transport across the 100 and 200 m isobaths, and transport through Unimak Pass were examined. Strong seasonal and interannual variations in flow were observed, with transport typically highest during fall and winter months, coinciding with timing of spawning activity in the five species. Significant correlations were found between transport, BSC position, and groundfish recruitment. Pacific cod, in particular, benefitted from decreased along-shelf and on-shelf flow, while Pacific halibut recruitment increased in relation to increased on-shelf transport through southern canyons. The results of this study improve our understanding of variability in circulation and associated effects on groundfish recruitment in the eastern Bering Sea.

1. Introduction

Numerous studies have shown that transport plays an important role in population regulation in marine fishes and have linked larval transport with variability in year-class strength (Parker, 1989; Van der Veer et al., 1998; Van der Veer and Witte, 1999; Wilderbuer et al., 2002; Mueter et al., 2006). Since adult spawning and juvenile settling locations are often geographically separated, early life history stages must rely on transport and retention features, as well as their own behavior, to move them toward or keep them within appropriate habitats for successful recruitment to the juvenile phase (Norcross and Shaw, 1984). Many species undergo a long dispersal stage from their source (e.g., fish spawning areas) to nursery locations (e.g., juvenile settling locations). During this period, eggs and larvae experience high mortality, which strongly influences recruitment variability (Cowen, 2002; Houde, 2008). Over time, organisms have likely adapted to optimize dispersal success and reduce mortality loss by taking advantage of local physical and biological conditions (Iles and Sinclair, 1982; Bailey and Picquelle, 2002; Bailey et al., 2008). Further, deviations from average conditions may be a source of population fluctuations (Bailey et al., 2005a, 2005b) when the normal current patterns to which reproductive habits are tuned are disrupted (Bakun, 1985).

A major source of transport in the eastern Bering Sea (EBS) is the Bering Slope Current (BSC). The BSC exists as either a series of eddies and meanders, or as a more uniform northwestward flowing current (Stabeno et al., 1999; Schumacher et al., 2003), with exchange across the shelf break likely dependent on which

* Corresponding author. Tel.: +1 541 737 3965; fax: +1 541 737 2064.
E-mail addresses: vestfals@coas.oregonstate.edu (C.D. Vestfals), lciannel@coas.oregonstate.edu (L. Ciannelli), janet.duffy-anderson@noaa.gov (J.T. Duffy-Anderson), carol.ladd@noaa.gov (C. Ladd).
[1] Tel.: +1 541 737 3142.
[2] Tel.: +1 206 526 6465.
[3] Tel.: +1 206 526 6024.

0967-0645/$ - see front matter © 2013 Elsevier Ltd. All rights reserved.
http://dx.doi.org/10.1016/j.dsr2.2013.09.026

flow pattern is dominant. Recent work by Ladd (2014) has shown that the BSC has a strong seasonal cycle and is typically not a continuous, cohesive feature outside of the winter months. On-shelf flow can also vary as a result of wind-driven advection, interaction of the BSC with topography, and the funneling effect of canyons (Springer et al., 1996; Stabeno and Van Meurs, 1999; Clement Kinney et al., 2009). Several large submarine canyons incise the EBS slope margin, including Bering Canyon to the south, which is long with a wide valley (> 400 km), and Pribilof and Zhemchug canyons to the north, which are steeper and have trough-shaped basins. These canyons are believed to enhance the flux of heat, salt, and water from the Aleutian Basin to the EBS shelf (Stabeno et al., 1999, 2008; Clement Kinney et al., 2009), and are thought to be important spawning locations for several species of marine fishes (Seitz et al., 2007; Sohn et al., 2010; Neidetcher et al., 2014).

Circulation in the EBS has been shown to vary with large-scale atmospheric features. In particular, the Arctic Oscillation (AO: Thompson and Wallace, 1998; Overland et al., 1999) and the Pacific Decadal Oscillation (PDO: Mantua et al., 1997) influence the distribution and intensity of winter storms, represented by the position and intensity of the Aleutian Low (AL: Wilderbuer et al., 2002). The AL influences surface winds in the EBS, which can affect advection (Ladd, 2014) and mixing of the upper ocean (Ladd and Stabeno, 2012), the production and advection of ice, and heat flux (Schumacher et al., 2003), as well as timing of the spring phytoplankton bloom, the degree of pelagic-benthic coupling, and the match-mismatch of prey production for larval fish (Napp et al., 2002). The El Niño-Southern Oscillation (ENSO) can also influence circulation through its positive correlation with the AL (Schumacher et al., 2003). Atmospheric circulation is an important determinant of water mass movement on the EBS shelf (Wespestad et al., 2000), with flows being highly sensitive to the surface forcing specific to each year (Hermann et al., 2002). Recent work by Ladd (2014) suggests that interannual variability of the BSC is wind-driven, with strong interannual variability in the strength of the BSC correlated with the North Pacific Index (NPI, Trenberth and Hurrell, 1994) and Multivariate ENSO Index (MEI, Wolter and Timlin, 1998). The extent of sea ice coverage over the shelf and timing of sea ice retreat are also believed to be important factors influencing transport and flow in the region (Stabeno et al., 2012).

The purpose of the present work is three-fold: (1) to investigate seasonal and interannual variations in hydrodynamic circulation in the EBS, (2) to relate observed transport variability to recruitment of slope- and shelf-spawning groundfish species, and (3) to discern the atmospheric features that modulate variation in flow. We characterized seasonal and interannual variability of along-shelf and cross-shelf transport in the EBS, along with changes in the position of the BSC, using 23 years of output from the Regional Ocean Modeling System (ROMS) ocean circulation model. We then compared results to recruitment indices of five groundfish species whose early life stages have shelf break crossings: age-0 Pacific cod (cod, *Gadus macrocephalus*), age-1 walleye pollock (pollock, *Gadus chalcogrammus*), age-1 Greenland halibut (*Reinhardtius hippoglossoides*), age-2 Pacific halibut (*Hippoglossus stenolepis*), and age-2 arrowtooth flounder (*Atheresthes stomias*) to determine the potential effects of oceanographic variability on recruitment. The species selected for this study are both commercially and ecologically important, and may be vulnerable to changes in circulation, as they spawn during winter months when storm activity is high (Stabeno et al., 1999) and have relatively long pelagic larval durations (3–4 months for cod and pollock; 5–8+ months for Greenland halibut, Pacific halibut, and arrowtooth flounder). Cod and pollock are largely considered shelf-spawners, though spawning may also occur along the outer continental shelf and slope region, while the three flatfish species are considered slope-spawners. Our analyses focus primarily on winter months to examine how recruitment in the different groundfish species varies in relation to transport during the various spawning seasons (cod: January–April (Bakkala, 1993; Neidetcher et al., 2014); pollock: February–April (Bacheler et al., 2010); Greenland and Pacific halibut: November–March (St-Pierre, 1984; Sohn et al., 2010); arrowtooth flounder: fall through winter (Blood et al., 2007, and references therein). Finally, we compared results from the circulation analysis to leading oceanic and atmospheric variables to resolve which climate variables are important to circulation-mediated recruitment.

2. Data and methods

2.1. Study area

The eastern Bering Sea consists of a broad (> 500 km), shallow shelf extending approximately 1000 km from the Alaska Peninsula north to Bering Strait, with a narrow continental slope adjoining the extensive Aleutian Basin. Patterns of wind and tidal energy divide the shelf into three domains during spring, summer, and fall: coastal (0–50 m depth), middle (50–100 m) and outer (100–200 m), each having its own characteristic hydrography, circulation, and assemblage of fauna and food webs (Coachman, 1986; Springer et al., 1996; Stabeno et al., 1998). In the winter and spring, a substantial portion of the shelf is covered by ice. The duration and extent of ice coverage is highly variable from year to year (Stabeno et al., 2012), which can strongly influence the timing of the spring bloom and transfer of energy to higher trophic levels (Hunt et al., 2002, 2011; Sigler et al., 2014).

Inflow from the Alaskan Stream through the Aleutian Islands feeds the cyclonic circulation pattern observed in the basin. Two currents dominate the eastern side of the Aleutian Basin, the Aleutian North Slope Current (ANSC), which flows eastward along the north side of the Aleutian Islands, and the BSC, which flows northwestward along the continental slope (Fig. 1). Before flowing northward into the BSC, the ANSC changes direction sharply in the southeast corner of the basin and accelerates, becoming unstable and generating eddies that can impinge upon the shelf (Stabeno and Van Meurs, 1999). Unimak Pass serves as the only major connection between the shelves of the North Pacific and the EBS, with inflow following the 50 and 100 m isobaths as it travels along the shelf (Reed and Stabeno, 1996; Stabeno et al., 2002). Cross-

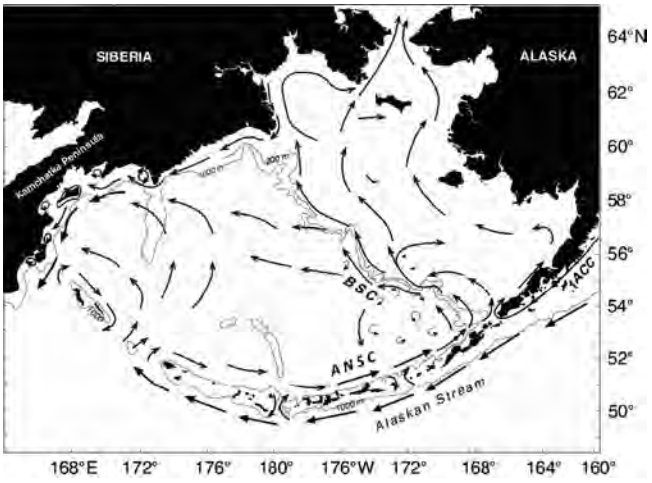

Fig. 1. Schematic diagram of flow in the Bering Sea at 40 m. BSC: Bering Slope Current, ANSC: Aleutian North Slope Current, ACC: Alaska Coastal Current. Modified from Stabeno et al. (1999).

shelf currents vary seasonally, with weakest flows during late spring and summer (< 0.5 cm s^{-1}) and stronger flows during the remainder of the year (1–2 cm s^{-1}) (Stabeno et al., 2012).

2.2. Modeled circulation

Output from the Regional Ocean Modeling System (ROMS) Northeast Pacific version 4 (NEP4) model from 1982–2004 was used to examine variation in transport along and across the EBS slope and shelf. ROMS is a state-of-the-art, free-surface, terrain-following, primitive equation model that is driven by atmospheric forcing, and has been widely used to examine the effects of climate and hydrography in the North Pacific and other oceans (Haidvogel et al., 2000; Curchitser et al., 2005; Shchepetkin and McWilliams, 2005; Di Lorenzo et al., 2008; Fiechter et al., 2009; Hermann et al., 2009). The NEP4 model, which includes the EBS, uses 10 km horizontal grid spacing with 42 levels in the vertical, and is nested in a larger, lower resolution North Pacific model. The model is forced with daily winds, heat, and freshwater fluxes, and includes a three-layer ice module. While the model is eddy-permitting, it cannot resolve the smallest eddies at this grid size and does not include tides. Despite these limitations, this circulation model generates the correct seasonal to interannual large-scale variability and represents the climatic signals of interest in the eastern Pacific Ocean (Curchitser et al., 2005).

2.2.1. Along-shelf analysis

Along-shelf transport was quantified across three transects placed perpendicular to the mean path of the BSC at 30 m depth, which represents the bottom of the wind-mixed surface layer. The mean path of the BSC was determined by averaging velocities over the 1995–2004 period. Transects were positioned north of Bering, Pribilof, and Zhemchug canyons (hereafter South, Central, and North transects, respectively) to examine how transport varied along the path of the BSC (Fig. 2). Each transect was subdivided into three sections, with Main sections bracketing mean flow greater than 0.02 m s^{-1}, Basin sections extending over the Aleutian Basin, and Shelf sections extending shelf-ward to approximately the 100 m isobath. Volume transport (in Sverdrups, Sv $= 10^6$ m^3 s^{-1}) was calculated for each entire transect and each section (Main, Basin, and Shelf) down to 500 m depth or the bottom, whichever was shallowest, and standardized to transect length in order to facilitate comparisons among transects. A general index (BSC Index) characterizing along-shelf flow was created by averaging standardized transport anomalies for the three BSC transects.

In addition to examining variation in the strength of the BSC, the three BSC transects were used to characterize the position of the BSC, defined by the location of the maximum current velocity from the ROMS output. In several cases, the maximum current velocity was found to occur close to the transect origin over the Aleutian Basin for the South and Central transects. Therefore, to represent positional changes in the main BSC flow closer to the shelf break, the location of maximum velocity along the South transect was calculated only in the region east of 168.55°W, and for the Central transect in the region east of 174°W. No restrictions were imposed for the North transect.

2.2.2. Cross-shelf analysis

Cross-shelf transport was characterized by analyzing transport across the 100 and 200 m isobaths (Fig. 2). The 100 and 200 m isobath transects were further divided into 7 and 12 sections, respectively, to explore finer scale variations in transport across the EBS shelf, and to examine variations in transport along each isobath. Sections followed the natural contour of each isobath along

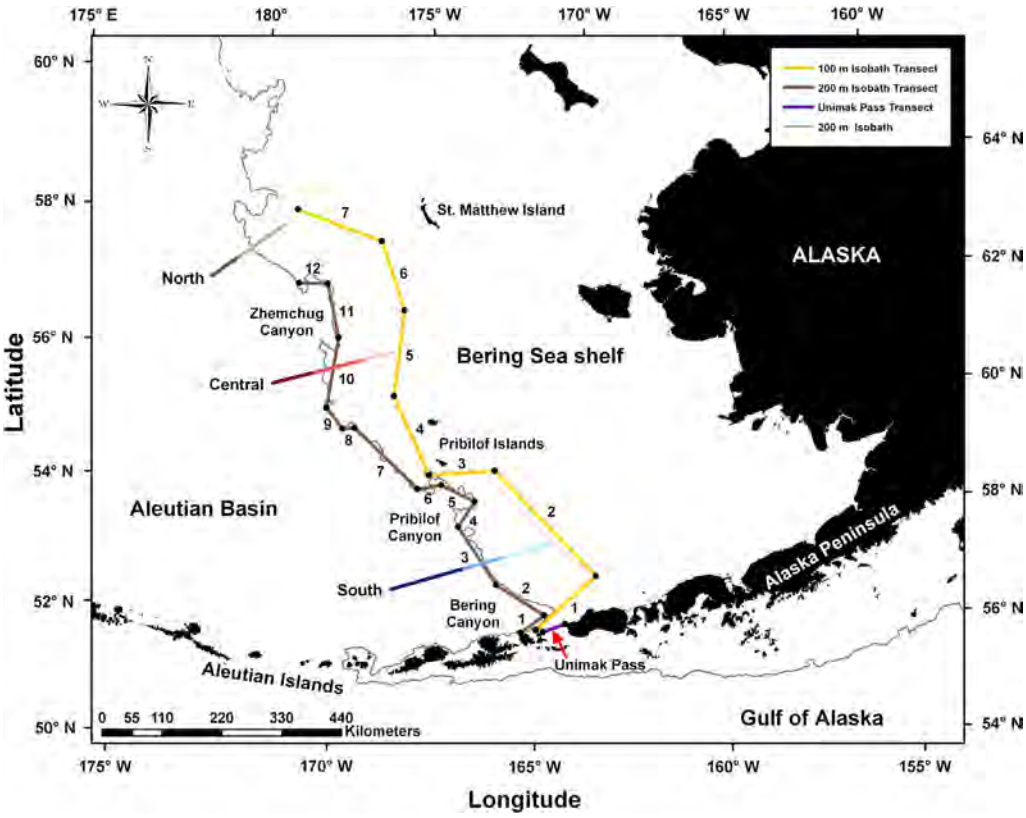

Fig. 2. Locations of the South, Central, and North BSC transects, the 100 and 200 m isobath transects, and the Unimak Pass transect used to examine variability in EBS circulation. Numbers denote 100 and 200 m isobath transect sections. Shading of BSC transects denotes Basin (dark), Main (medium), and Shelf (light) sections. The 200 m isobath is shown for reference.

the shelf to approximately 56–58°N. Sections were numbered consecutively, starting with Section 1 at the southernmost end of each isobath transect (Fig. 2). Cross-shelf transport was calculated over each section and standardized to section length and depth to facilitate comparisons between sections. General indices of cross-isobath flow were created by summing transport across all sections of each isobath transect for each year. Transport across the 200 m isobath was summed over Bering (Sections 1–2), Pribilof (Sections 4–6), and Zhemchug (Sections 10–12) canyons to create three canyon indices, as these canyons are known regions of shelf/slope exchange (Springer et al., 1996; Stabeno and Van Meurs, 1999; Clement Kinney et al., 2009) and were expected to be important to groundfish recruitment.

Transport through Unimak Pass (Fig. 2) was also calculated. Variability in the northward flow of the Alaska Coastal Current (ACC) onto the shelf through Unimak Pass was expected to strongly influence transport in the region.

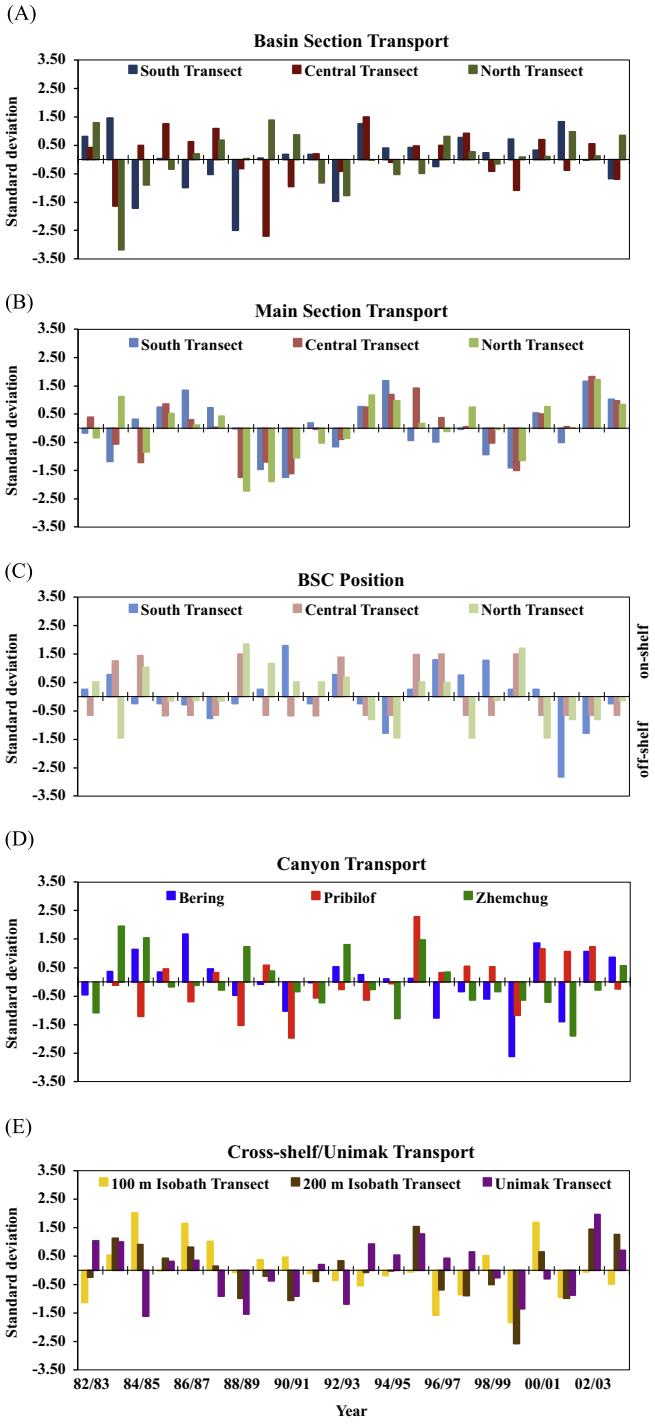

Fig. 3. December 1st–January 31st values from 1982/83 to 2003/04 used in the correlation analyses for (A) Basin transect transport, (B) Main transect transport, (C) BSC Position, (D) canyon transport, and (E) cross-shelf (100 and 200 m isobath) and Unimak transport indices. Anomalies are deviations from the mean transport or BSC position normalized by the standard deviation. Negative (positive) values for the BSC Position Index refer to an off-shelf (on-shelf) shift in the BSC.

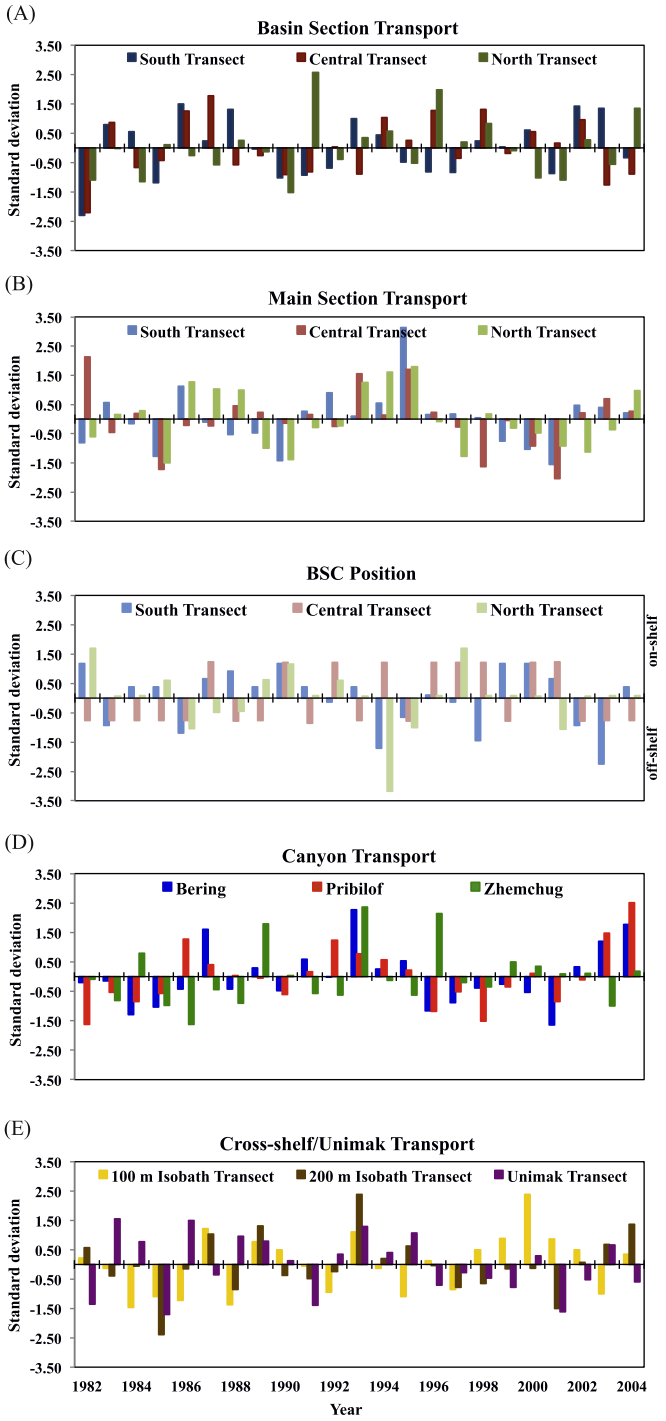

Fig. 4. February 1st–March 31st values from 1982 to 2004 used in the correlation analyses for (A) Basin transect transport, (B) Main transect transport, (C) BSC Position, (D) canyon transport, and (E) cross-shelf (100 and 200 m isobath) and Unimak transport indices. Anomalies are deviations from the mean transport or BSC position normalized by the standard deviation. Negative (positive) values for the BSC Position Index refer to an off-shelf (on-shelf) shift in the BSC.

2.2.3. Time periods evaluated

Annual and monthly transports were quantified for all transects to determine seasonal and interannual patterns. Winter transport, defined here as transport from Nov. 1st–Mar. 31st, was of particular interest as it coincides with timing of spawning activity and/or larval pelagic period of the selected groundfish species examined. Bi-monthly (Dec. 1st–Jan. 31st, Feb. 1st–Mar. 31st, and Apr. 1st–May 31st) transport indices were also derived to further resolve whether groundfish recruitment was influenced by circulation throughout the early life history stages, which can develop over the course of several months. Transport and BSC Position indices were developed from anomalies for each time period examined, and were calculated as deviations from the 1982–2004 mean transport (or mean position) normalized by the standard deviation (Fig. 3, December–January; Fig. 4, February–March; Fig. 5, April–May).

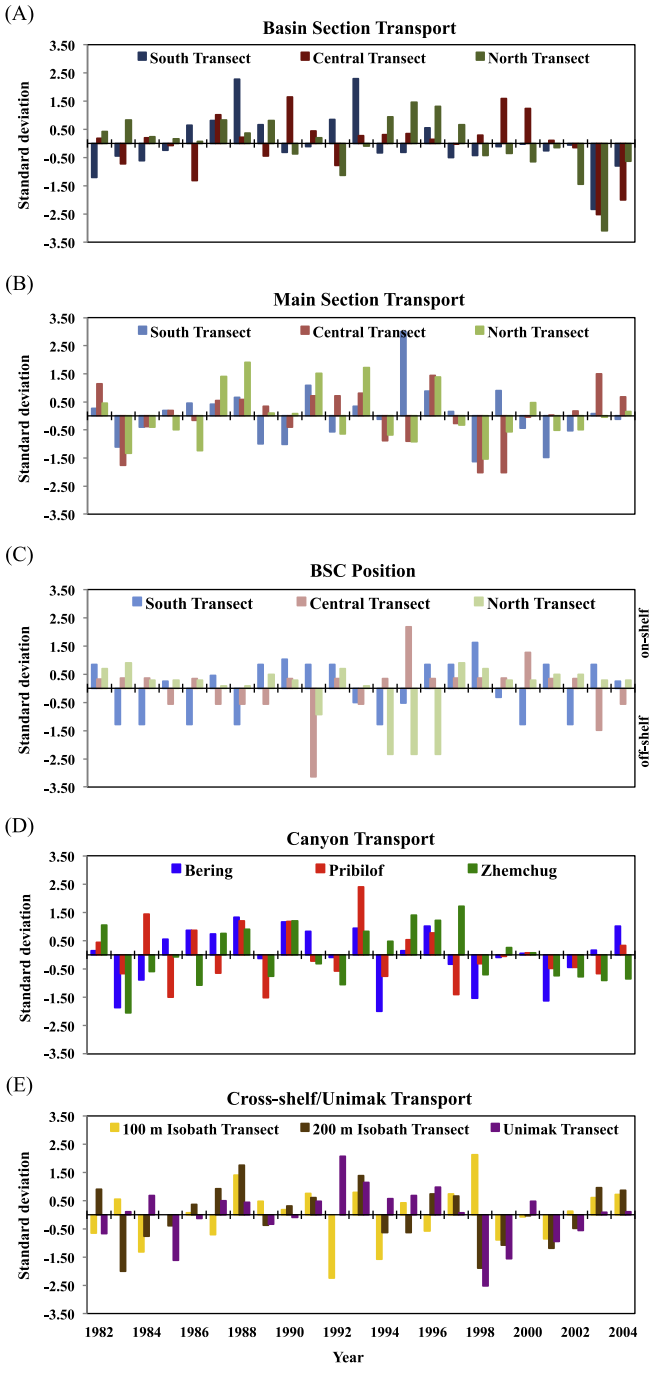

Fig. 5. April 1st–May 31st values from 1982 to 2004 used in the correlation analyses for (A) Basin transect transport, (B) Main transect transport, (C) BSC Position, (D) canyon transport, and (E) cross-shelf (100 and 200 m isobath) and Unimak transport indices. Anomalies are deviations from the mean transport or BSC position normalized by the standard deviation. Negative (positive) values for the BSC Position Index refer to an off-shelf (on-shelf) shift in the BSC.

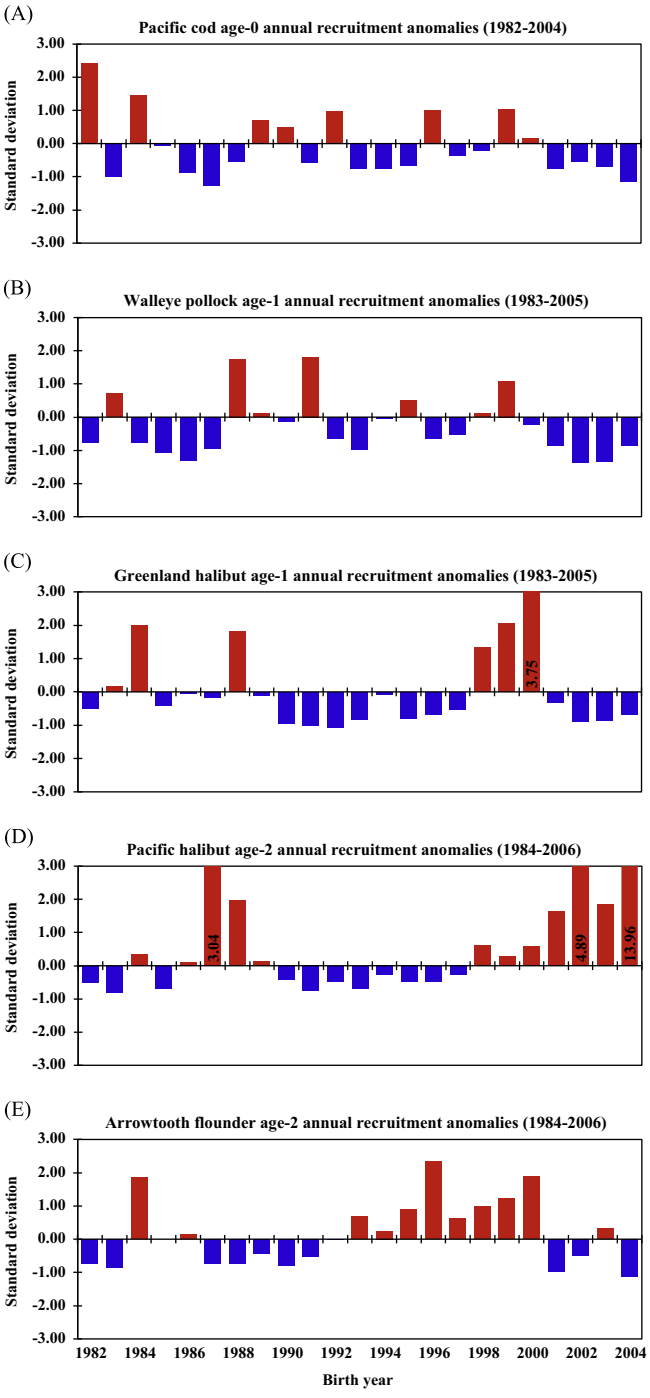

Fig. 6. Annual recruitment anomalies of (A) age-0 Pacific cod (1982–2004), (B) age-1 walleye pollock (1983–2005), (C) age-1 Greenland halibut (1983–2005), (D) age-2 Pacific halibut (1984–2006), and (E) age-2 arrowtooth flounder (1984–2006), with birth year shown on the *x*-axis (1982–2004). Recruitment anomalies are deviations from the mean normalized by the standard deviation. Values greater than three standard deviations from the mean are shown within their corresponding columns.

2.3. Correlations with groundfish recruitment

Recruitment indices for age-0 cod, age-1 pollock, age-1 Greenland halibut, and age-2 arrowtooth flounder (Fig. 6A–C and E) were obtained from NOAA's Bering Climate website, and are based on model estimates of the recruitment-at-age (millions) from the Alaska Fisheries Science Center's (AFSC) Stock Assessment and Fishery Evaluation (SAFE) Reports for each species. The recruitment anomalies are deviations from the mean value for the 1981–2000 period (1971–2000 for pollock) normalized by the standard deviation. Recruitment estimates for arrowtooth flounder in 2004–2006 are from estimates of abundance of fish less than 25 cm in length. Further information on the recruitment indices can be found at http://www.beringclimate.noaa.gov/data/index.php. The recruitment index for Pacific halibut (Fig. 6D) was derived from catch of age-2 fish (20–30 cm fork length (FL), Clark and Hare, 2006) in the AFSC's EBS bottom trawl shelf survey between 1982 and 2009, with recruitment anomalies as deviations from the mean value for the 1982–2000 period normalized by the standard deviation.

Groundfish recruitment indices were compared to selected indices representing flow along and across the EBS slope and shelf. Preliminary data analysis indicated that several transport indices were strongly correlated with each other. Thus, to reduce collinearity among covariates and the probability of making a Type I error, four transport indices were removed from the analysis. The BSC Index, which was strongly correlated with transport in the Main sections of all three transects, was removed, along with the three Shelf indices, which were strongly correlated with transport in their adjacent Main sections, as well as with transport through Unimak Pass. Along-shelf indices included in the analysis were the Basin, Main, and BSC Position indices for the North, Central, and South transects. Indices representing on-shelf flow were: transport over Bering, Pribilof, and Zhemchug canyons, and transport across the 100 and 200 m isobaths. Transport through Unimak Pass was also included in the analysis to account for inflow of larvae from the Gulf of Alaska and flow across Shelf sections. Correlations between groundfish recruitment indices and transport were calculated over bi-monthly time periods using Pearson's Product Moment Correlation, for a total of 15 comparisons per species per time period. Recruitment was lagged by one year for pollock and Greenland halibut (1983–2005), and two years for Pacific halibut and arrowtooth flounder (1984–2006) to correspond with transport at the time of spawning, while no lag was necessary for cod recruitment (1982–2004).

2.4. Correlations with oceanic, atmospheric, and climate indices

To determine possible mechanisms influencing groundfish recruitment, transport and position indices that were significantly correlated (here, $p < 0.1$) with recruitment were compared to atmospheric, oceanic, and climate indices thought to influence circulation in the EBS. Large-scale climatic drivers examined were the AL, represented by the NPI, ENSO, represented by the MEI, and the winter PDO. The Ice Cover Index (ICI) was selected to represent the influence of sea ice in the region and is a measure of the average ice concentration for January 1st–May 31st in a $2^\circ \times 2^\circ$ box (56–58°N, 163–165°W). All indices were obtained from NOAA's Bering Climate website (http://www.beringclimate.noaa.gov/data/index.php). To examine how surface winds influenced transport along and across the Bering Slope, along-shelf and cross-shelf wind indices were developed. Monthly mean u- and v- surface (0.995 sigma level) winds (NCEP/NCAR Reanalysis, Kalnay et al., 1996) were rotated in the along-shelf direction (blowing from the northwest, 315°) and averaged over the area 54.5–57.5°N, and 167.5°–175.0°W for each bi-monthly time period. Preliminary data analysis indicated that the winter PDO was strongly correlated with the MEI. To account for multiple comparisons and reduce the probability of making a Type I error, the PDO was removed from the analysis, which resulted in a total of 15 comparisons per index per time period.

3. Results

3.1. Along-shelf analysis

Analysis of flow across the South, Central, and North BSC transects revealed differences in average annual transport among transects and also among years. In the annual mean, transport across the South transect was more variable than transport across the Central and North transects (Table 1). Significant differences were found between mean transport across the South and Central transects (Welch's t test: $t_{(df=41.21)}=4.99$, $p \ll 0.001$) and the Central and North transects ($t_{(df=43.35)}=-5.70$, $p \ll 0.001$) but not between the South and North transects ($t_{(df=43.12)}=-0.24$, $p=0.81$).

Strong interannual variability in flow was observed in the Basin and Main sections of all three BSC transects, while lower variability was found across the Shelf sections (Table 1; Fig. 7). Transport was predominantly to the northwest (NW) across the Basin sections of the South and North transects, though directionality changed in some years (Fig. 7A). Annual transport across the Basin section of the South transect was to the southeast (negative) approximately 9% of the time, while for the North Basin transect, flow reversals occurred 30% of the time (Fig. 7A). The 1982–2004 mean direction of transport in the Central Basin section was southeastward (Table 1; Fig. 7A). Standardized flow across the Basin section of the Central transect differed significantly from Basin flow across the South ($t_{(df=38.11)}=4.64$, $p \ll 0.001$) and North ($t_{(df=43.97)}=-3.03$, $p < 0.01$) transects, which is likely due to higher mesoscale variability across the Central transect. Transport through the Main and Shelf sections of all three BSC transects was primarily northwestward (positive), however southeastward (negative) mean flow did occur in some years (Fig. 7B and C). Flow across the Main and Shelf sections differed significantly between all three transects ($p < 0.05$), with transport per km increasing as it flows to the NW through the Main sections. Transport along the adjacent shelf weakens from SE to NW, implying that BSC flow becomes more concentrated toward the north.

Strong seasonal variation in along-shelf flow was found across the Basin (not shown) and Main (Fig. 8A) sections of all three BSC transects, while little variation was observed across the Shelf sections (not shown). Transport in the BSC tended to be higher during fall and winter months (Table 1; Fig. 8A), as was also found from an analysis of surface currents derived from altimetry (Ladd, 2014). Winter, December–January, and February–March transport across the Central Basin section was to the NW, which contrasted with the mean annual southeastward flow (Table 1). Transport decreased drastically during April–May along all three transects, but especially across the Central transect (Table 1).

The position of the BSC was most variable across the South transect for all time periods examined (Table 2). Little variation was found in the BSC position across the Central and North transects. Winter and bi-monthly BSC positions were off-shelf of the mean annual position. The greatest variability in the position of the BSC was found during April–May, which is likely due to increased eddy activity in the region.

3.1.1. Cross-shelf analysis

Both the 100 and 200 m isobath transects exhibited net on-shelf transport, though off-shelf transport occurred across some sections (Table 1). On-shelf transport was highest across sections found on the north side of canyons (Sections 2, 6, and 12) for the 200 m isobath transect. For both isobath transects, flow was predominantly on-shelf

Table 1
Mean annual, winter (Nov. 1st–Mar. 31st), and bi-monthly (D–J=Dec. 1st–Jan. 31st, F–M=Feb. 1st–Mar. 31st, A–M=Apr. 1st–May 31st) volume transport (in Sv) for BSC (South, Central, and North), isobath (100 and 200 m), and Unimak Pass transects, with standard deviation shown in parentheses. Positive values represent northwestward/on-shelf transport; negative values represent southeastward/off-shelf transport.

Transect	Length (km)	Annual mean transport direction	Annual mean transport 1982–2004 (SD)	Winter mean transport (Nov. 1st–Mar. 31st) 82/83–03/04 (SD)	D–J mean transport (Dec. 1st–Jan. 31st) 82/83–03/04 (SD)	F–M mean transport (Feb. 1st–Mar. 31st) 1982–2004 (SD)	A–M mean transport (Apr. 1st–May 31st) 1982–2004 (SD)
BSC South	304.03	NW	2.62 (0.96)	4.48 (1.49)	4.67 (1.91)	5.17 (2.01)	3.02 (1.71)
Basin	137.00	NW	1.14 (1.05)	1.92 (1.26)	1.89 (1.79)	2.63 (1.27)	1.98 (1.29)
Main	80.00	NW	1.00 (0.51)	1.99 (0.68)	2.20 (0.88)	1.97 (1.11)	0.63 (0.91)
Shelf	87.03	NW	0.48 (0.07)	0.57 (0.11)	0.59 (0.15)	0.57 (0.17)	0.41 (0.13)
BSC Central	224.00	NW	1.36 (0.73)	3.55 (1.06)	4.28 (1.60)	3.32 (1.39)	0.29 (1.81)
Basin	75.00	SE	−0.36 (0.87)	1.18 (0.93)	1.64 (1.00)	1.09 (1.53)	−0.97 (1.88)
Main	95.00	NW	1.58 (0.35)	2.17 (0.51)	2.46 (0.80)	1.99 (0.81)	1.12 (1.04)
Shelf	54.00	NW	0.14 (0.02)	0.19 (0.05)	0.19 (0.06)	0.24 (0.07)	0.14 (0.05)
BSC North	194.24	NW	2.68 (0.83)	4.83 (0.98)	5.46 (1.50)	5.05 (1.76)	2.82 (2.09)
Basin	58.00	NW	0.32 (0.69)	0.77 (0.51)	1.03 (0.92)	0.56 (0.83)	0.74 (1.37)
Main	111.00	NW	2.27 (0.38)	3.96 (0.99)	4.34 (1.41)	4.37 (1.38)	1.98 (1.41)
Shelf	25.24	NW	0.09 (0.03)	0.10 (0.05)	0.09 (0.07)	0.13 (0.07)	0.11 (0.06)
100 m isobath	1144.45	On-shelf	0.24 (0.14)	0.38 (0.25)	0.40 (0.41)	0.31 (0.41)	0.20 (0.24)
1	151.55	Off-shelf	−0.51 (0.09)	−0.61 (0.13)	−0.65 (0.17)	−0.66 (0.19)	−0.51 (0.16)
2	261.56	On-shelf	0.24 (0.04)	0.32 (0.09)	0.36 (0.17)	0.32 (0.12)	0.20 (0.08)
3	116.73	On-shelf	0.39 (0.05)	0.51 (0.08)	0.53 (0.12)	0.51 (0.14)	0.36 (0.11)
4	157.87	Off-shelf	−0.17 (0.04)	−0.22 (0.05)	−0.25 (0.08)	−0.19 (0.09)	−0.12 (0.07)
5	163.57	Mixed On-/Off-shelf	−0.01 (0.03)	−0.06 (0.06)	−0.06 (0.11)	−0.10 (0.12)	0.02 (0.07)
6	134.42	On-shelf	0.04 (0.03)	0.05 (0.05)	0.05 (0.08)	0.03 (0.10)	0.04 (0.05)
7	158.75	On-shelf	0.26 (0.03)	0.39 (0.06)	0.42 (0.08)	0.40 (0.10)	0.22 (0.05)
200 m isobath	958.58	On-shelf	1.58 (0.21)	2.06 (0.32)	2.17 (0.47)	2.03 (0.43)	1.42 (0.43)
1	54.21	On-shelf	0.07 (0.02)	0.06 (0.03)	0.05 (0.04)	0.05 (0.04)	0.05 (0.04)
2	99.54	On-shelf	0.39 (0.09)	0.54 (0.11)	0.60 (0.16)	0.41 (0.17)	0.19 (0.16)
3	125.88	On-shelf	0.47 (0.12)	0.61 (0.15)	0.71 (0.20)	0.56 (0.24)	0.41 (0.24)
4	58.17	Off-shelf	−0.69 (0.18)	−0.87 (0.22)	−1.00 (0.29)	−0.78 (0.27)	−0.51 (0.33)
5	64.92	On-shelf	0.31 (0.07)	0.40 (0.07)	0.46 (0.11)	0.40 (0.08)	0.25 (0.12)
6	42.77	On-shelf	0.67 (0.14)	1.00 (0.23)	1.08 (0.27)	0.94 (0.35)	0.57 (0.33)
7	156.14	Off-shelf	0.20 (0.12)	−0.39 (0.14)	−0.44 (0.15)	−0.29 (0.24)	−0.13 (0.32)
8	21.45	On-shelf	0.24 (0.10)	0.42 (0.16)	0.46 (0.21)	0.41 (0.22)	0.19 (0.22)
9	46.07	Off-shelf	−0.27 (0.11)	−0.40 (0.11)	−0.40 (0.16)	−0.38 (0.18)	−0.25 (0.21)
10	135.46	Off-shelf	−0.35 (0.14)	−0.48 (0.18)	−0.59 (0.25)	−0.43 (0.25)	−0.23 (0.28)
11	102.60	Off-shelf	−0.04 (0.04)	−0.06 (0.07)	−0.07 (0.09)	−0.04 (0.10)	−0.02 (0.07)
12	51.37	On-shelf	0.99 (0.18)	1.22 (0.19)	1.31 (0.23)	1.18 (0.24)	0.90 (0.33)
Unimak	42.67	On-shelf	0.66 (0.10)	0.79 (0.14)	0.84 (0.18)	0.82 (0.21)	0.68 (0.17)

north of Bering Canyon (100 m isobath: Sections 2 and 3; 200 m isobath: Sections 1–3, 5, 6), off-shelf north of Pribilof Canyon (between 56 and 58°N; 100 m isobath: Sections 4 and 5; 200 m isobath: Sections 7, 9–11), and on-shelf north of Zhemchug Canyon (north of 58.5°N; 100 m isobath: Sections 6 and 7; 200 m isobath: Section 12) (Table 1; Fig. 2).

Cross-shelf transects exhibited strong seasonal signals along some sections, while transport across other sections remained fairly constant throughout the year (Fig. 8B). On-shelf transport was highest during the winter months (Table 1), while transport during April–May was lower than the other periods examined and highly variable. Transport direction remained consistent for each bi-monthly period examined (Table 1).

3.2. Correlations with groundfish recruitment

Results from the correlation analyses suggest seasonal differences in circulation may differentially affect recruitment in the five species examined (Table 3). The species most correlated with flow along and across the Bering Slope was cod, especially during the February–March period. In general, cod recruitment declined in relation to increased NW transport, specifically in the Basin sections of the South and Central transects, and the Main section of the North transect. The species least correlated with flow indices was pollock, with weakly significant correlations found only with along-shelf flow across the Central transect during April–May. Recruitment of pollock increased in relation to increased NW transport in the Basin Section, but decreased in relation to increased NW transport in the Main section. Similar results were found for Greenland halibut recruitment during the same time period. In contrast, Pacific halibut recruitment decreased as NW transport over the Central Basin section increased. Arrowtooth flounder recruitment was most strongly correlated with transport during December–January, with decreased recruitment associated with increased NW transport over the Basin section of the North transect (Table 3).

Cod recruitment increased with a more shelf-ward position of the BSC across the South and North transects. While Greenland halibut recruitment decreased in relation to a more shelf-ward position of the BSC across the South transect, arrowtooth flounder recruitment increased as the BSC moved closer to the shelf along the Central transect. Neither pollock nor Pacific halibut recruitment were associated with a shift in the BSC position (Table 3).

Cod recruitment was negatively correlated with increased on-shelf transport through Bering and Pribilof canyons. However, Pacific halibut showed the opposite trend, with recruitment increasing in relation to increased on-shelf transport through these canyons during February–March (Table 3). Over the same time period, recruitment in arrowtooth flounder was positively correlated with increased on-shelf flow through Zhemchug Canyon. Recruitment in Greenland halibut declined in relation to increased

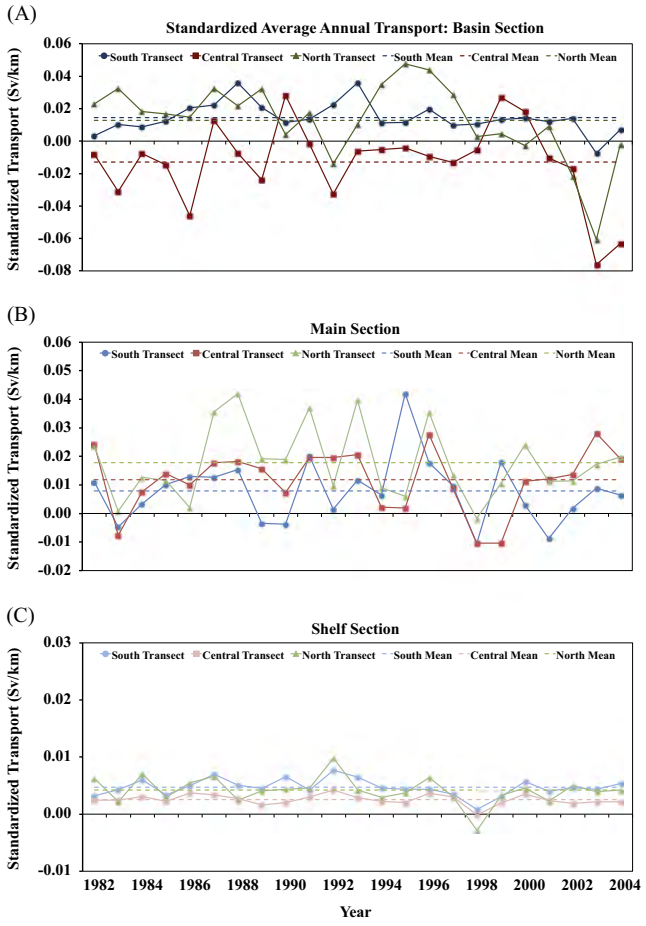

Fig. 7. Average annual transport in the BSC for the (A) Basin, (B) Main, and (C) Shelf sections of the South, Central, and North BSC transects. The 1982–2004 mean transport for each transect is also shown (dashed lines). Transport has been standardized to transect length (Sv/km) to facilitate comparison between transects. Positive values represent northwestward transport; negative values represent southeastward transport. Note different scales on vertical axes.

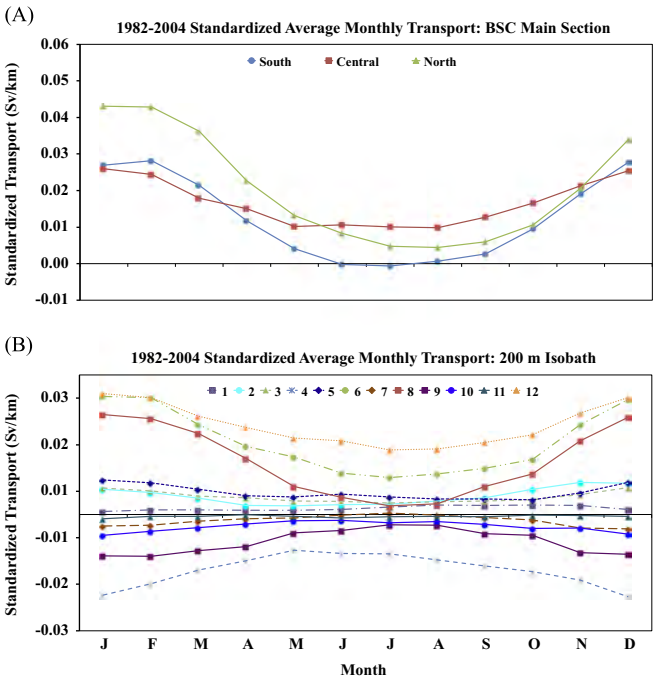

Fig. 8. Seasonal variation in (A) along-shelf and (B) cross-shelf transport. The 1982–2004 average monthly transport across Main sections of the three BSC transects (A) and the 200 m isobath transect (B) are shown. Transport has been standardized to transect length (Sv/km) to facilitate comparisons between transects. Positive values represent northwestward/on-shelf transport; negative values represent southeastward/off-shelf transport. Note different scales on vertical axes. Similar seasonal patterns were observed in other along-shelf sections and isobath transects.

on-shelf transport through Bering Canyon and across the 200 m isobath during December–January (Table 3), while cod recruitment decreased in relation to increased on-shelf transport across the 100 m isobath during April–May (Table 3). No significant correlations were found with pollock, Pacific halibut, or arrowtooth flounder recruitment and transport across either the 100 or 200 m isobaths. Similarly, no significant correlations were found with transport through Unimak Pass for any of the species examined (Table 3).

3.3. *Correlations with oceanic, atmospheric, and climate indices*

Indices representing environmental variability in the EBS were correlated (here, $p < 0.1$) with transport and BSC Position indices found to be important to groundfish recruitment. In general, the NPI was negatively correlated with NW along-shelf transport indices from December–March, while the MEI was positively correlated with increased NW along-shelf transport over the same time period (Table 4). Increased ice cover was negatively correlated with NW along-shelf transport, except during April–May across the Central Basin section, similar to the NPI. Increased northwesterly winds were associated with a decrease in NW transport in the Basin sections of both the South and Central transects, except during February–March for the Central Main section where transport increased. Similarly, along-shelf transport decreased in relation to increased southwesterly on-shelf winds between December–March (Table 4).

Positive correlations were found between the NPI and the South and North transect BSC Position indices, indicating a more shelf-ward position during a strong NPI (Table 4). The MEI was associated with shift in the BSC position towards the Aleutian Basin across both the South and Central transects, while ice cover showed no significant correlations with any of the BSC Position indices. In general, southeasterly along-shelf winds and southwesterly on-shelf winds were associated with a shelf-ward shift in the BSC position (Table 4).

The NPI showed mixed correlations with on-shelf transport through canyons, being negatively correlated with flow through Pribilof Canyon during December–January, but positively correlated with on-shelf flow through Zhemchug Canyon during April–May (Table 4). In contrast, the MEI was negatively correlated with on-shelf transport through Zhemchug Canyon. Ice cover was strongly and negatively correlated with on-shelf transport through Bering

Table 2
Mean location of maximum velocity in the BSC across the South, Central, and North transects, with transect length (in km) provided for reference. Locations are given as distances (in km) from the western origin of each transect, with standard deviation shown in parentheses. Mean locations were calculated over 1982–2004 (annual, Feb. 1st–Mar. 31st, Apr. 1st–May 31st) and 1982/83–2003/04 (winter, Dec. 1st–Jan. 31st).

Transect length (km)	South 304.24	Central 224.00	North 194.24
Annual	183.40 (8.96)	112.57 (2.87)	108.98 (4.16)
Winter (Nov. 1st–Mar. 31st)	168.72 (17.38)	109.48 (2.08)	106.95 (4.79)
Dec. 1st–Jan. 31st	174.22 (11.81)	109.49 (2.08)	105.93 (5.89)
Feb. 1st–Mar. 31st	162.22 (20.03)	109.84 (2.24)	104.53 (7.19)
Apr. 1st–May 31st	163.00 (31.32)	110.85 (4.87)	103.39 (19.10)

Table 3
Groundfish recruitment correlations with transport and BSC Position indices. D–J = Dec. 1st–Jan. 31st; F–M = Feb. 1st–Mar. 31st; A–M = Apr. 1st–May 31st. Positive along-shelf flow is toward the NW, while positive cross-shelf flow is on-shelf. Cell shading corresponds to significance of correlation (Dark gray: p-value ≤ 0.05, Light gray: $0.05 < p$-value ≤ 0.10, White: no significant correlation, p-value > 0.10). Bold font represents a significant correlation. Italicized font represents a significant negative correlation.

$p \leq 0.05$ $0.05 < p \leq 0.10$ $p > 0.10$

		Pacific cod		Pollock		Greenland halibut			Pacific halibut			Arrowtooth flounder		
	Transect	F-M	A-M	F-M	A-M	D-J	F-M	A-M	D-J	F-M	A-M	D-J	F-M	A-M
Along-shelf	**South**													
	Basin	*-0.49*	-0.13	-0.04	0.22	0.26	0.33	0.10	-0.07	0.15	-0.15	0.32	0.13	0.00
	Main	-0.31	-0.05	0.04	0.25	-0.29	-0.31	-0.14	0.32	0.00	-0.10	-0.29	0.16	0.25
	Central													
	Basin	*-0.40*	0.28	-0.07	**0.39**	-0.08	0.16	**0.39**	-0.08	-0.05	*-0.42*	-0.06	0.22	0.24
	Main	0.23	0.10	0.06	*-0.38*	-0.31	-0.28	*-0.42*	0.28	0.00	0.20	0.06	0.01	-0.15
	North													
	Basin	-0.26	0.06	0.32	0.35	-0.21	-0.24	0.02	0.27	0.20	-0.31	*-0.59*	0.07	0.08
	Main	*-0.41*	0.02	0.14	0.18	0.02	0.07	-0.04	0.29	0.16	0.07	0.18	0.10	-0.04
Position	**BSC**													
	South	**0.43**	0.22	0.22	-0.09	0.24	0.27	*-0.43*	-0.33	0.02	-0.03	0.26	-0.08	-0.15
	Central	0.00	0.20	-0.15	-0.17	0.20	0.06	0.28	-0.27	-0.15	-0.13	**0.54**	0.19	**0.37**
	North	**0.51**	0.10	-0.10	-0.22	0.01	-0.10	0.18	-0.19	-0.05	0.15	-0.06	-0.05	-0.35
Cross-shelf	**Canyon**													
	Bering	*-0.43*	0.03	-0.07	0.00	*-0.38*	-0.34	-0.19	0.21	**0.41**	0.19	-0.32	-0.28	-0.06
	Pribilof	*-0.52*	0.14	-0.19	0.03	-0.11	-0.23	0.14	0.08	**0.53**	0.01	0.21	-0.23	0.24
	Zhemchug	0.35	0.19	-0.10	0.12	0.00	0.04	-0.06	-0.07	-0.02	-0.23	0.29	**0.39**	0.25
	Isobath													
	100 m	-0.01	*-0.42*	-0.02	0.28	-0.15	0.25	0.03	-0.04	0.15	0.17	-0.30	0.01	-0.14
	200 m	-0.05	-0.03	-0.18	-0.13	*-0.39*	-0.18	-0.25	0.26	0.28	0.20	-0.06	0.02	-0.13
	Unimak	-0.23	-0.04	0.07	-0.02	-0.16	0.15	-0.21	0.12	-0.16	-0.05	0.21	0.14	0.11

Table 4
Environmental correlations with transport and BSC Position indices. D–J = Dec. 1st–Jan. 31st; F–M = Feb. 1st–Mar. 31st; A–M = Apr. 1st–May 31st. Positive along-shelf flow is toward the NW, while positive cross-shelf flow is on-shelf. Southeasterly along-shelf winds are positive, while southwesterly on-shelf winds are positive. Cell shading corresponds to significance of correlation (Dark gray: p-value ≤ 0.05, Light gray: $0.05 < p$-value ≤ 0.10, White: no significant correlation, p-value > 0.10). Bold font represents a significant correlation. Italicized font represents a significant negative correlation.

$p \leq 0.05$ $0.05 < p \leq 0.10$ $p > 0.10$

		NPI			MEI			ICI			Along-shelf wind			Cross-shelf wind		
	Transect	D-J	F-M	A-M	D-J	F-M	A-M	D-J	F-M	A-M	D-J	F-M	A-M	D-J	F-M	A-M
Along-shelf	**South**															
	Basin	-0.32	*-0.48*	0.07	0.18	0.25	0.02	0.22	-0.08	0.10	*-0.67*	0.18	-0.17	*-0.46*	*-0.41*	-0.24
	Main	*-0.37*	-0.29	0.19	**0.37**	**0.44**	-0.09	*-0.41*	0.09	0.13	0.02	0.24	-0.09	-0.14	*-0.42*	-0.27
	Central															
	Basin	*-0.40*	*-0.43*	**0.42**	0.28	0.20	-0.25	-0.17	-0.05	**0.41**	0.00	0.12	*-0.36*	-0.10	-0.19	-0.21
	Main	*-0.56*	0.25	0.18	**0.36**	0.04	-0.22	*-0.43*	-0.04	*-0.50*	-0.14	**0.41**	0.26	*-0.43*	-0.04	-0.05
	North															
	Basin	0.14	0.15	0.21	0.22	0.10	-0.10	-0.18	-0.10	0.02	-0.16	0.08	-0.27	-0.03	0.14	-0.28
	Main	*-0.54*	-0.31	0.34	0.30	**0.40**	-0.17	-0.23	-0.08	-0.29	-0.22	0.09	-0.03	*-0.48*	*-0.49*	-0.15
Position	**BSC**															
	South	0.09	**0.47**	0.17	-0.15	*-0.49*	0.05	0.28	0.17	-0.13	**0.37**	-0.08	0.21	0.04	0.26	**0.47**
	Central	0.26	-0.09	-0.17	*-0.55*	0.04	-0.05	0.07	-0.02	0.34	**0.53**	-0.04	0.05	0.21	-0.07	-0.17
	North	**0.41**	0.17	-0.24	-0.32	-0.14	0.05	0.09	0.21	0.13	**0.46**	0.22	**0.40**	**0.39**	0.28	**0.39**
Cross-shelf	**Canyon**															
	Bering	-0.27	0.04	0.27	0.23	0.35	-0.22	*-0.60*	-0.28	-0.09	0.28	**0.37**	0.26	0.08	0.09	0.06
	Pribilof	*-0.39*	-0.13	-0.05	0.05	0.14	0.01	-0.27	-0.23	0.03	-0.30	0.15	-0.01	-0.06	-0.33	-0.34
	Zhemchug	0.24	0.35	**0.48**	*-0.42*	*-0.41*	-0.26	-0.19	-0.13	0.09	**0.76**	**0.47**	0.00	0.19	0.20	-0.10
	Isobath															
	100 m	0.09	0.24	-0.04	-0.12	-0.24	0.28	-0.29	-0.06	-0.01	0.22	**0.42**	0.26	0.36	**0.55**	**0.51**
	200 m	-0.32	0.07	0.23	0.09	0.08	-0.16	*-0.64*	-0.25	-0.29	0.35	**0.70**	0.24	-0.16	0.01	-0.02
	Unimak	*-0.62*	*-0.40*	-0.07	**0.43**	**0.36**	0.13	-0.28	0.06	-0.15	-0.14	0.33	0.05	*-0.65*	*-0.67*	*-0.74*

Canyon ($r=-0.60$, $p<0.01$). On-shelf transport through Bering and Zhemchug canyons increased as southeasterly along-shelf winds increased, while no significant correlations were found between on-shelf canyon transport and cross-shelf winds. Southeasterly along-shelf winds were positively correlated with transport across both the 100 and 200 m isobaths, while southwesterly on-shelf winds were positively correlated with transport across the 100 m isobath (Table 4). Increased ice cover was negatively correlated with transport across the 200 m isobath ($r=-0.64$, $p<0.01$).

Transport through Unimak Pass, although not correlated with groundfish recruitment indices, decreased during a positive NPI, but increased during a positive MEI. Strong negative correlations were found between transport through Unimak Pass and increased southwesterly on-shelf winds for all bi-monthly time periods (Table 4), consistent with previous analyses showing enhanced northward transport through Unimak Pass during easterly wind anomalies along the Alaska Peninsula (Bond and Overland, 2005).

4. Discussion

We found that changes in the strength and position of the BSC were associated with changes in along-shelf and cross-shelf flow, which may differentially influence recruitment in the five EBS groundfish species examined. Additionally, we noted that changes in circulation were modulated by climate variability. Northern edges of canyons were identified as regions of increased on-shelf transport, in accordance with generalized canyon circulation, where upwelling typically occurs over the axis and downstream wall of the canyon (Hickey, 1995).

4.1. Transport variability and recruitment

In general, increased northwestward flow in the BSC during February–March was associated with decreased cod recruitment. Major spawning aggregations of cod are found north of Unimak Pass, southwest of the Pribilof Islands along the shelf (Shimada and Kimura, 1994), and at the shelf break near Zhemchug Canyon (Neidetcher et al., 2014). Spawning activity in cod occurs from January through April (Bakkala, 1993; Neidetcher et al., 2014), and takes place predominantly over the outer shelf, most often between 100 and 200 m depth (Neidetcher et al., 2014). Eggs sink to the bottom after fertilization, and are somewhat adhesive, in contrast to the pelagic eggs of the other species examined in this study. Reduced along-shelf transport during this time would likely further reduce northward dispersal of cod early life stages, which could potentially lead to enhanced connectivity with shelf nursery areas in the months following. While cod recruitment was negatively correlated with on-shelf flow from February through May, pelagic juveniles settle in shallow Alaskan coastal waters in July (Blackburn and Jackson, 1982; Laurel et al., 2007), which suggests that the transition to the shelf may occur in late spring or early summer, outside of the time periods examined in this study.

Spawning concentrations of pollock occur near Bogoslof Island, north of Unimak Island and the Alaska Peninsula, and around the Pribilof Islands, as suggested from egg distributions (Bacheler et al., 2010). Two major temporal pulses of eggs have been identified during February–March and April–May (Bacheler et al., 2010), and pollock eggs and larvae would likely be sensitive to flows during this time. Previous research that modeled dispersal of pollock eggs and larvae from a major spawning concentration near Unimak Pass found distinct differences in transport patterns between weak, strong, and average year classes (Wespestad et al., 2000). We found that pollock recruitment was weakly correlated with April–May along-shelf transport, but no other significant correlations were apparent. Flow through Unimak Pass showed no correlations with recruitment, which was surprising given its proximity to pollock spawning locations and its influence over flow on the shelf. The weak correlations with flow suggest that other factors likely influence pollock recruitment. For example, overwinter survival may be an important mechanism controlling their recruitment (Heintz et al., 2013).

For Greenland halibut in the EBS, spawning is believed to occur along the continental slope from Unimak Pass to as far north as Cape Navarin mainly between November and March (Musienko, 1970; Alton et al., 1988; Sohn et al., 2010). While Sohn et al. (2010) have suggested that Bering and Pribilof canyons are important conduits for transport of Greenland halibut larvae to shelf nursery areas, we found that on-shelf flow through Bering Canyon was associated with a decline in recruitment. Furthermore, Greenland halibut recruitment declined when the BSC shifted closer to the shelf south of Pribilof Canyon, which suggests that larvae may not connect with nursery areas via the southern shelf. Distributions of newly-settled age-0 individuals in the vicinity of St. Matthew Island support this conclusion (Sohn et al., 2010; Lauth, personal communication). Flow north of Pribilof Canyon may be important to Greenland halibut recruitment, and possibly to pollock recruitment as well. Eddy energy is known to be particularly strong in the spring near Zhemchug Canyon (Ladd et al., 2012). The opposing flow regimes observed there during April–May, which are indicative of meanders and eddies, could potentially enhance retention of larvae. Indeed, Greenland halibut and pollock larvae and juveniles recruit to these domains (Sohn et al., 2010; Smart et al., 2012).

For species with a long pelagic larval duration like Greenland halibut (Sohn et al., 2010), slowed northwestward transport may allow sufficient time for larval development prior to transitioning to nursery areas located on the shelf. Duffy-Anderson et al. (2013) showed that Greenland halibut connectivity could be negatively impacted by premature advection to the continental shelf. That study suggested that Greenland halibut could be advected to presumed nursery areas prior to the period of settlement competency, after which time larvae would not reconnect with suitable settlement habitat. Moreover, prolonged entrainment in the BSC reduces the exposure of vulnerable larvae to the variable thermal regimes and wind events over the shallower continental shelf in winter (Stabeno et al., 2012), providing some insulation from shelf-associated environmental stochasticity.

Spawning of Pacific halibut appears to be concentrated in relatively discrete winter spawning grounds near the edge of the continental shelf in the southeast Bering Sea to Pribilof Canyon (St-Pierre, 1984; Seitz et al., 2007). Juveniles settle along the northern Alaska Peninsula, near the Pribilof Islands, especially around St. Paul Island, and near St. Matthew Island (Skud, 1977; St-Pierre, 1989). Our results indicate that Pacific halibut larvae likely connect to shelf nursery areas through Bering and Pribilof canyons, and catches of age-0 individuals in the vicinity of the Alaska Peninsula and Unimak Island support this conclusion (Cooper, personal communication). Several studies have suggested that Pacific halibut larvae are transported into the Bering Sea via inflow of Gulf of Alaska coastal waters through island passes (Best, 1977; Skud, 1977; St-Pierre, 1984, 1989). If Pacific halibut spawned in the Gulf do indeed contribute to EBS recruitment, significant correlations between indices related to inflow from the Gulf of Alaska (e.g., Unimak Pass) and recruitment would be expected. Interestingly, we found no such correlations for any of the time periods examined, which suggests that most of the Pacific halibut in the recruitment index were spawned in the EBS and that delivery of larvae through the Aleutian Passes does not contribute meaningfully to their overall recruitment in the Bering Sea. However, Unimak Pass is narrow (16–35 km; Stabeno et al., 2002), and is not well-resolved by the ROMS model. A more accurate assessment of the relative importance of delivery of propagules through Unimak Pass to small-scale aggregations in the Unimak

vicinity might be a local index of Pacific halibut age-0s along the Alaska Peninsula.

Little is known about arrowtooth flounder spawning timing and location in the EBS, though several studies suggest that spawning occurs in deep waters along the outer continental shelf and slope during fall and winter months (Blood et al., 2007, and references therein). Our results suggest that arrowtooth flounder may connect with shelf nursery areas between Pribilof and Zhemchug canyons. Recruitment increased in relation to a more shelf-ward position of the BSC across the Central transect and on-shelf flow through Zhemchug Canyon, but decreased in relation to increased NW along-shelf flow north of Zhemchug Canyon. However, high numbers of juveniles ($\leq$100 mm FL) have also been found on the middle and outer shelves between Bering and Pribilof canyons (Cooper, personal communication), making it likely that arrowtooth flounder also connect to the shelf via southern locations.

4.2. Influence of atmospheric forcing on recruitment-relevant flow

The influence of the dominant modes of climate forcing on groundfish recruitment can be understood by examining their influence on EBS circulation. During a strong AL (negative NPI), warm air is pumped northward and sea ice extent is limited, which results in warmer than normal winters in the EBS (Hollowed and Wooster, 1995; Stabeno et al., 2001; Benson and Trites, 2002). A strong AL is associated with a strong sub-polar gyre, as evidenced by the increase in NW along-shelf transport found in our study, and gyre spin-up may generate more eddy activity in this region (Ladd et al., 2012). Eddies are believed to increase on-shelf transport while in the proximity of the shelf-break (Stabeno and Van Meurs, 1999; Mizobata et al., 2008; Clement Kinney et al., 2009). Eddies, which move downstream at slower rates than the mean currents, can aid in delivering retained larvae to nursery areas (Hinckley et al., 2001); however, they can also transport water from the outer shelf into the basin (Okkonen et al., 2004; Ladd et al., 2012). We found that a weak AL (positive NPI) was associated with a shelf-ward shift in the BSC position, likely due to a more uniformly flowing BSC with fewer eddies. On-shelf transport through Pribilof Canyon decreased, while that through Zhemchug Canyon increased, which again may be indicative of a more regular flow pattern during a positive NPI. Recruitment in cod was most closely associated with along-shelf and on-shelf transport patterns related to the NPI, ice cover, and wind indices. Areas of high intensity spawning have recently been identified for cod around the Pribilof Islands and along the shelf break near Zhemchug Canyon (Neidetcher et al., 2014). Strong northward advection of cod eggs and larvae away from these spawning areas would likely result in transport to unfavorable northern habitats, while a more shelf-ward position of the BSC would likely increase connectivity with nursery areas on the shelf.

Northwesterly along-shelf winds were associated with increased along-shelf transport across sections over the Aleutian Basin for the South and Central transects, while southeasterly winds were associated with increased transport in the main BSC north of Pribilof Canyon. Off-shelf Ekman transport during northwesterly winds may explain the increase in NW transport observed over the basin. However, a recent study of Bering Sea circulation by Danielson et al. (2012) found no evidence of increased off-shelf transport during northwesterly winds. Their study, which used the newer NEP6 ROMS model, found that southeasterly winds were associated with large on-shelf Ekman transport across most of the shelf break (Danielson et al., 2012). Similarly, we found that on-shelf transport through canyons and across isobaths increased when southeasterly along-shelf winds increased. Stronger on-shore flow over Bering Canyon and the shelf-break during winter may benefit a more southerly-distributed species, like Pacific halibut, while a more shelf-ward flow over Pribilof and Zhemchug canyons may benefit species like cod and arrowtooth flounder. In fact, stronger alongshore and cross-shelf winds during winter have been found to generate transport conditions favorable to survival of Pacific halibut, resulting in the production of strong year-classes (Parker, 1989).

Increased southeasterly along-shelf and southwesterly on-shelf winds were also associated with a more shelf-ward position of the BSC. Recent work by Ladd (2014) suggests that mesoscale variability is likely responsible for interannual shifts in BSC position. Large on-shelf Ekman transport generated by strong southeasterly winds may also be responsible for a more shelf-ward shift in BSC position, at least at the surface. Additionally, stronger on-shelf winds may push the BSC closer to the shelf break, and the resulting increased southeastward Ekman transport can potentially impede BSC flow at the surface, as evidenced by the reduced NW along-shelf flow found in our study.

Stronger flow close to the shelf-break during the winter has been observed from satellite altimetry (Ladd, 2014) and model results (Overland et al., 1994). However, we found that the BSC position shifted off-shelf of the mean annual position during the winter and spring. One possible explanation for this discrepancy is that the position calculation may be obscured by the prevalence of eddies in the summer, as the BSC is largely a system of eddies during this time and is not a particularly significant current (Ladd, 2014). Another explanation is that variability in BSC position may not be resolvable with our 10 km gridscale model output. Alternatively, satellite altimetry data measures surface currents, while our study examined changes in the BSC down to 500 m depth. Modeled maximum current velocities were often found at depth, sometimes as deep as 250 m. Interestingly, stronger and deeper flow in the BSC during winter may enhance vertical mixing at the shelf break, which may benefit deep water ($>$400 m), slope-spawning species like Greenland halibut, Pacific halibut, and arrowtooth flounder that require both vertical and horizontal connectivity with shelf nursery habitats.

High ice cover was associated with reduced along-shelf flow, likely because both ice and circulation are influenced by winds. Increased ice cover was also associated with reduced on-shelf transport through Bering Canyon and across the 200 m isobath, which would likely benefit species associated with the outer shelf (e.g., cod and Greenland halibut). Significant along-shelf transport was associated with warmer conditions on the Bering Sea shelf, namely a strong AL (negative NPI), and a positive MEI. Previous research has found that strong year classes of pollock occur during warm years when juveniles are transported inshore and away from cannibalistic adults in spring (Wespestad et al., 2000), though this was not confirmed by our results. Poor correlations between pollock and indices related to flow suggest that other factors may influence pollock survival (see Wespestad et al., 2000; Hunt et al., 2002, 2011; Mueter et al., 2006), and recent evidence suggests strong age-1 cohorts may be more the result of total energy condition at the end of their first summer (Heintz et al., 2013) than by transport conditions during the larval phase.

Atmospheric forcing largely controls the extent of sea ice over the EBS shelf, and sea ice extent and timing of retreat are believed to be important physical factors influencing circulation on the shelf (Stabeno et al., 2012). We expected stronger correlations between sea ice and modeled flow patterns, especially since preliminary data analysis indicated that ice cover was positively correlated with recruitment in all species, except for Pacific halibut. However, ice extent may not have much influence on BSC variability, and the link between sea ice and recruitment may be related to factors other than flow. For example, ice cover and extent can affect stratification of shelf waters and timing of the spring-phytoplankton bloom (Hunt and Stabeno, 2002; Hunt et al., 2002, 2011; Sigler et al., 2014), which can impact the match-mismatch of prey production for larval fish. Sea ice characteristics represent an integrated measure of winter atmospheric forcing (Schumacher et al., 2003) and clear relationships with indices related

to flow may be difficult to establish. Still, some speculation as to the relationship between sea ice and currents deserves mention. The freezing and melting of sea ice is known to influence baroclinic flow in the EBS (Stabeno et al., 1999), with circulation often opposing the direction of ice motion (Zhang et al., 2010). During years with high ice cover and strong, cold winds out of the north, the BSC could potentially be pushed off-shelf resulting in reduced along- and on-shelf flow, which may benefit species like cod and Greenland halibut.

4.3. Uncertainties

Despite the fact that strong correlations between flow and recruitment were not found for most of the species examined, except for cod, transport during the early life history stages still likely plays an important role in their recruitment variability. Transport has been shown to be important to year-class formation in Pacific halibut and arrowtooth flounder in the Gulf of Alaska (Bailey and Picquelle, 2002), while in the EBS, transport-mediated spatial separation of juvenile and adult pollock can influence year-class size (Wespestad et al., 2000; Mueter et al., 2006). Other studies have shown that strong year-classes of several flatfish species in the EBS, namely Pacific halibut, flathead sole (*Hippoglossoides elassodon*), northern rock sole (*Lepidopsetta polyxystra*), and arrowtooth flounder, occurred following periods of wind-driven on-shelf transport (Parker, 1989; Wilderbuer et al., 2002).

Recruitment in marine fishes is known to be highly variable, and is influenced by both biological and physical processes operating at changing spatial and temporal scales (Hollowed et al., 2001; Bailey et al., 2005a, 2005b). In addition, the relationships between climate forcing and marine biological responses at higher trophic levels are not as clear as those at lower trophic levels (Hollowed and Wooster, 1995; Hollowed et al., 2001). For example, climate can indirectly affect fish populations through changes in predator distribution and abundance (Bailey, 2000; Benson and Trites, 2002) and also through prey availability or prey quality (Hunt et al., 2002, 2011; Grebmeier et al., 2006; Heintz et al., 2013). Interestingly, we found that age-0 cod recruitment showed the strongest correlations with flow indices, while the correlations for other species were less pronounced. This may be a result of differences in reproductive strategies, as cod are semi-demersal spawners with negatively-buoyant semi-adhesive eggs that remain on or near the bottom (Hurst et al., 2009), while the other species are deep pelagic spawners with pelagic eggs (Doyle et al., 2009; Sohn et al., 2010). Additionally, attempting to correlate flow indices that affect larval abundances to recruitment at age-1 and age-2 may prove especially challenging, as survival to these ages can be influenced by many factors, such as temperature (Houde, 2008), ocean conditions at time of first feeding (Lasker, 1978, 1981), match-mismatch of prey (Cushing, 1974, 1990), predation (Leggett and Deblois, 1994; Wespestad et al., 2000; Mueter et al., 2006), as well as prey quality and quantity (Coyle et al., 2011; Hunt et al., 2011; Mueter et al., 2011). Indeed, it is widely understood that many processes act together over the early life stages and that recruitment variability is not controlled by a single process, mechanism, or factor (Houde, 2008). Another factor that makes it difficult to resolve underlying relationships between recruitment and transport are the recruitment indices themselves. The indices used in this study, except that for Pacific halibut, were derived from modeled estimates of recruitment-at-age. These are back-calculated from catches of older-aged individuals for which more data are available by assuming a constant mortality rate. However, mortality rates can change dramatically during the early life stages (Houde, 2002) and indices derived from older-aged fish may not represent true recruitment at the ages examined here. Similarly, the Pacific halibut recruitment index was derived from survey catch estimates of abundance and may not accurately reflect true recruitment, as smaller-sized Pacific halibut are not well-represented in the groundfish surveys. Finally, it is important to note that recruitment is often poorly correlated with measures of environmental variability, and is usually only significantly correlated for populations at the limit of a species' geographical range (Myers, 1998).

Biases inherent in the circulation model may also further obscure relationships between recruitment, transport, and drivers of environmental variability. While the NEP4 model captures the observed major current systems in the region and represents climatic signals of interest in the eastern Pacific Ocean (Curchitser et al., 2005), simulated currents are weaker and more topographically steered than observations, though current directions are in good agreement with observations (Duffy-Anderson et al., 2013). Another potentially confounding influence on transport estimates are eddies, which are prevalent in the Bering Sea (Stabeno and Van Meurs, 1999; Johnson et al., 2004; Clement Kinney et al., 2009). Since the ROMS model cannot fully resolve eddies at this grid size, on- or off-shelf transport resulting from eddy activity may be underestimated. These biases should be taken into consideration when interpreting the results of this study; however, future modeling efforts may improve upon our results, as the next generation of models under construction have finer spatial resolution.

5. Conclusion

Variability in ocean circulation patterns is likely a key factor in determining year-class strength of marine fishes (Van der Veer et al., 1998). Interannual variations in wind and current patterns may advect eggs and larvae in different directions, with substantial losses occurring when they are transported beyond typical habitat boundaries. Research into the causal relationships between environmental variability and recruitment in marine fishes has important practical and predictive applications (Norcross and Shaw, 1984), especially as climate change over the next century is expected to alter the dominant modes of climate variability and their influence upon circulation and biological processes in the Northeast Pacific (Capotondi et al., 2009; Overland et al., 2010). We found strong variations in the strength and position of the BSC. Changes in along-shelf and cross-shelf flow were associated with changes in recruitment in the groundfish species examined. Pacific cod, in particular, benefitted from decreased along-shelf and on-shelf flow, as did Greenland halibut to a lesser extent. In contrast, Pacific halibut recruitment benefitted from increased on-shelf transport through Bering and Pribilof canyons. Variability in transport and BSC position was strongly influenced by winds, ice cover, and large-scale climatic drivers. The present work aids in understanding how shifts in atmospheric and hydrographic forcing influences recruitment in several commercially and ecologically important groundfish species in the EBS, and may be informative when developing effective fishery management strategies that take a changing climate into account.

Acknowledgments

This research was supported by Grants from the National Science Foundation (NSF-CMG grant 0934961) and the North Pacific Research Board (Project 905). We are grateful to Kate Hedstrom and Enrique Curchitser, who were instrumental in creating the NEP ROMS circulation model and Al Hermann for discussions of circulation model results. The authors wish to acknowledge NPCREP and use of the Ferret program for analysis in this paper. Ferret is a product of NOAA's Pacific Marine Environmental Laboratory. We would like to thank E.D. Cokelet and Wei

Cheng for help with Ferret and the ROMS output, as well as Mary Hunsicker, Jeff Napp, Colleen Petrik, and three anonymous reviewers whose comments greatly improved this manuscript. This research is contribution EcoFOCI-0782 to NOAA's Fisheries-Oceanography Coordinated Investigations, NPRB publication number 445, and BEST-BSIERP Bering Sea Project publication number 114.

References

Alton, M.S., Bakkala, R.G., Walters, G.E., Munro, P.T., 1988. Greenland Turbot *Reinhardtius hippoglossoides* of the East Bering Sea and the Aleutian Islands Region. U.S. Dept. of Commerce, Seattle, WA p. 31. (NOAA Tech. Rep. NMFS 71).

Bacheler, N.M., Ciannelli, L., Bailey, K.M., Duffy-Anderson, J.T., 2010. Spatial and temporal patterns of walleye pollock (*Theragra chalcogramma*) spawning in the eastern Bering Sea inferred from egg and larval distributions. Fisheries Oceanography 19 (2), 107–120.

Bailey, K.M., 2000. Shifting control of recruitment of walleye pollock *Theragra chalcogramma* after a major climatic and ecosystem change. Marine Ecology Progress Series 198, 215–224.

Bailey, K.M., Abookire, A.A., Duffy Anderson, J.T., 2008. Ocean transport paths for the early life history stages of offshore spawning flatfishes: a case study in the Gulf of Alaska. Fish and Fisheries 9 (1), 44–66.

Bailey, K.M., Ciannelli, L., Bond, N.A., Belgrano, A., Stenseth, N.C., 2005a. Recruitment of walleye pollock in a complex physical and biological ecosystem: a new perspective. Progress in Oceanography 67, 24–42.

Bailey, K.M., Nakata, H., Van der Veer, H.W., 2005b. The planktonic stages of flatfishes: physical and biological interactions in transport processes. In: Gibson, R.N. (Ed.), Flatfishes: Biology and Exploitation. Blackwell Science Ltd., Oxford, UK, pp. 94–119.

Bailey, K.M., Picquelle, S.J., 2002. Larval distribution of offshore spawning flatfish in the Gulf of Alaska: potential transport pathways and enhanced onshore transport during ENSO events. Marine Ecology Progress Series 236, 205–217.

Bakkala, R.G., 1993. Structure and Historical Changes in the Groundfish Complex of the Eastern Bering Sea. NOAA Technical Report NMFS 114, 91pp.

Bakun, A., 1985. Comparative Studies and the Recruitment Problem: Searching for Generalizations. CalCOFI Report 26, pp. 30–40.

Benson, A.J., Trites, A.W., 2002. Ecological effects of regime shifts in the Bering Sea and eastern North Pacific Ocean. Fish and Fisheries 3 (2), 95–113.

Best, E.A., 1977. Distribution and Abundance of Juvenile Halibut in the Southeastern Bering Sea. International Pacific Halibut Commission, Scientific Report No. 62, 23p.

Blackburn, J.E., Jackson, P.B., 1982. Seasonal Composition and Abundance of Juvenile and Adult Marine Finfish and Crab Species in the Nearshore Zone of Kodiak Islands' Eastside during April 1978 through March 1979. Alaska Department of Fish and Game, Kodiak, Alaska. (Final Report 03-5-022-69).

Blood, D.M., Matarese, A.C., Busby, M.S., 2007. Spawning, Egg Development, and Early Life History Dynamics of Arrowtooth Flounder (*Atheresthes stomias*) in the Gulf of Alaska. NOAA Professional Paper NMFS 7, 28pp.

Bond, N.A., Overland, J.E., 2005. The importance of episodic weather events to the ecosystem of the Bering Sea shelf. Fisheries Oceanography 14, 97–111.

Capotondi, A., Combes, V., Alexander, M.A., Di Lorenzo, E., Miller, A.J., 2009. Low-frequency variability in the Gulf of Alaska from coarse and eddy-permitting ocean models. Journal of Geophysical Research 114, C01017, http://dx.doi.org/10.1029/2008JC004983.

Clark, W.G., Hare, S.R., 2006. Assessment and Management of Pacific Halibut: Data, Methods, and Policy. International Pacific Halibut Commission, Scientific Report No. 83, 104p.

Clement Kinney, J., Maslowski, W., Okkonen, S., 2009. On the processes controlling shelf-basin exchange and outer shelf dynamics in the Bering Sea. Deep-Sea Research Part II: Topical Studies in Oceanography 56 (17), 1351–1362.

Coachman, L.K., 1986. Circulation, water masses and fluxes on the southeastern Bering Sea shelf. Continental Shelf Research 5, 23–108.

Cowen, R.K., 2002. Larval dispersal and retention and consequences for population connectivity. In: Sale, P.F. (Ed.), Coral Reef Fishes, Dynamics and Diversity in a Complex Ecosystem. Academic, San Diego, CA, pp. 149–170.

Coyle, K.O., Eisner, L.B., Mueter, F.J., Pinchuk, A.I., Janout, M.A., Cieciel, K.D., Farley, E.V., Andrews, A.G., 2011. Climate change in the southeastern Bering Sea: impacts on pollock stocks and implications for the oscillating control hypothesis. Fisheries Oceanography 20, 139–156.

Curchitser, E.N., Haidvogel, D.B., Hermann, A.J., Dobbins, E.L., Powell, T.M., Kaplan, A., 2005. Multi-scale modeling of the North Pacific Ocean: Assessment and analysis of simulated basin-scale variability (1996–2003). Journal of Geophysical Research 110 (C11), C11021, http://dx.doi.org/10.1029/2005JC002902.

Cushing, D.H., 1974. The natural regulation of fish populations. In: Harden-Jones, P. F. (Ed.), Sea Fisheries Research. John Wiley and Sons, NY, pp. 399–412.

Cushing, D.H., 1990. Plankton production and year-class strength in fish populations: an update of the match/mismatch hypothesis. Advances in Marine Biology 26, 249–293.

Danielson, S., Hedstrom, K., Aagaard, K., Weingartner, T., Curchitser, E., 2012. Wind-induced reorganization of the Bering shelf circulation. Geophysical Research Letters 39 (8), L08601, http://dx.doi.org/10.1029/2012GL051231.

Di Lorenzo, E., Schneider, N., Cobb, K., Franks, P., Chhak, K., Miller, A., McWilliams, J., Bograd, S., Arango, H., Curchitser, E., Powell, T.M., Rivière, P., 2008. North Pacific Gyre Oscillation links ocean climate and ecosystem change. Geophysical Research Letters 35 (8), L08607, http://dx.doi.org/10.1029/2007GL032838.

Doyle, M.J., Piquelle, S.J., Mier, K.L., Spillane, M.C., Bond, N.A., 2009. Larval fish abundance and physical forcing in the Gulf of Alaska, 1981–2003. Progress in Oceanography 80, 163–187.

Duffy-Anderson, J.T., Blood, D.M., Cheng, W., Ciannelli, L., Matarese, A.C., Sohn, D., Vance, T.C., Vestfals, C., 2013. Combining field observations and modeling approaches to examine Greenland halibut (*Reinhardtius hippoglossoides*) early life ecology in the southeastern Bering Sea. Journal of Sea Research 75, 96–109.

Fiechter, J., Moore, A.M., Edwards, C.A., Bruland, K.W., Di Lorenzo, E., Lewis, C.V.W., Powell, T.M., Curchitser, E.N., Hedstrom, K., 2009. Modeling iron limitation of primary production in the coastal Gulf of Alaska. Deep-Sea Research Part II: Topical Studies in Oceanography 56 (24), 2503–2519.

Grebmeier, J.M., Overland, J.E., Moore, S.E., Farley, E.V., Carmack, E.C., Cooper, L.W., Frey, K.E., Helle, J.H., McLaughlin, F.A., McNutt, S.L., 2006. A major ecosystem shift in the northern Bering Sea. Science 311 (5766), 1461–1464.

Haidvogel, D.B., Arango, H.G., Hedstrom, K., Beckmann, A., Malanotte-Rizzoli, P., Shchepetkin, A.F., 2000. Model evaluation experiments in the North Atlantic Basin: simulations in nonlinear terrain-following coordinates. Dynamics of Atmospheres and Oceans 32 (3–4), 239–281.

Heintz, R.A., Siddon, E.C., Farley, Jr. E.V., Napp, J.M., 2013. Correlation between recruitment and fall condition of age-0 pollock (*Theragra chalcogramma*) from the eastern Bering Sea under varying climate conditions, Deep-Sea Research Part II: Topical Studies in Oceanography 94, 150–156.

Hermann, A.J., Hinckley, S., Dobbins, E.L., Haidvogel, D.B., Bond, N.A., Mordy, C., Kachel, N., Stabeno, P.J., 2009. Quantifying cross-shelf and vertical nutrient flux in the Coastal Gulf of Alaska with a spatially nested, coupled biophysical model. Deep-Sea Research Part II: Topical Studies in Oceanography 56 (24), 2474–2486.

Hermann, A.J., Stabeno, P.J., Haidvogel, D.B., Musgrave, D.L., 2002. A regional tidal/subtidal circulation model of the southeastern Bering Sea: development, sensitivity analyses and hindcasting. Deep-Sea Research Part II: Topical Studies in Oceanography 49 (26), 5945–5967.

Hickey, B., 1995. Coastal submarine canyons. In: Mueller, P., Henderson, D. (Eds.), Proceedings of the Hawaii Winter Workshop, January 17–10 Univ. Hawaii, pp. 95–100.

Hinckley, S., Hermann, A.J., Mier, K.L., Megrey, B.A., 2001. Importance of spawning location and timing to successful transport to nursery areas: a simulation study of Gulf of Alaska walleye pollock. ICES Journal of Marine Science: Journal du Conseil 58 (5), 1042–1052.

Hollowed, A.B., Hare, S.R., Wooster, W.S., 2001. Pacific Basin climate variability and patterns of Northeast Pacific marine fish production. Progress in Oceanography 49 (1–4), 257–282.

Hollowed, A.B., Wooster, W.S., 1995. Decadal-scale variations in the eastern subarctic Pacific. Part II. Response of Northeast Pacific fish stocks. In: Beamish, R.J. (Ed.), Climate Change and Northern Fish Populations. Canadian Special Publication of Fisheries and Aquatic Sciences, pp. 373–385.

Houde, E.D., 2002. Mortality. In: Fuiman, L.A., Werner, R.G. (Eds.), Fishery Science: The Unique Contributions of Early Life Stages. Blackwell Science, Oxford, UK, pp. 64–87.

Houde, E.D., 2008. Emerging from Hjort's shadow. Journal of Northwest Atlantic Fishery Science 41, 53–70.

Hunt, G.L., Coyle, K.O., Eisner, L.B., Farley, E.V., Heintz, R.A., Mueter, F., Napp, J.M., Overland, J.E., Ressler, P.H., Salo, S., Stabeno, P.J., 2011. Climate impacts on eastern Bering Sea foodwebs: a synthesis of new data and an assessment of the Oscillating Control Hypothesis. ICES Journal of Marine Science 68, 1230–1243.

Hunt, G.L., Stabeno, P., Walters, G., Sinclair, E., Brodeur, R.D., Napp, J.M., Bond, N.A., 2002. Climate change and control of the southeastern Bering Sea pelagic ecosystem. Deep-Sea Research Part II: Topical Studies in Oceanography 49 (26), 5821–5853.

Hunt, G.L., Stabeno, P.J., 2002. Climate change and the control of energy flow in the southeastern Bering Sea. Progress in Oceanography 55 (1), 5–22.

Hurst, T.P., Cooper, D.W., Scheingross, J.S., Seale, E.M., Laurel, B.J., Spencer, M.L., 2009. Effects of ontogeny, temperature, and light on vertical movements of larval Pacific cod (*Gadus macrocephalus*). Fisheries Oceanography 18, 301–311.

Iles, T.D., Sinclair, M., 1982. Atlantic herring: stock discreteness and abundance. Science 215 (4533), 627–633.

Johnson, G.C., Stabeno, P.J., Riser, S.C., 2004. The Bering Slope Current System Revisited. Journal of Physical Oceanography 34 (2), 384–398.

Kalnay, E., Kanamitsu, M., Kistler, R., Collins, W., Deaven, D., Gandin, L., Iredell, M., Saha, S., White, G., Woollen, J., Zhu, Y., Chelliah, M., Ebisuzaki, W., Higgins, W., Janowiak, J., Mo, K.C., Ropelewski, C., Wang, J., Leetmaa, A., Reynolds, R., Jenne, R., Joseph, D., 1996. The NCAR/NCEP 40-year reanalysis project. Bulletin of the American Meteorological Society 77, 437–471.

Ladd C., 2014. Variability of the Bering Slope Current, 109, 5–13, http://dx.doi.org/10.1016/j.dsr2.2013.12.005.

Ladd, C., Stabeno, P.J., 2012. Stratification on the eastern Bering Sea shelf revisited. Deep-Sea Research Part II: Topical Studies in Oceanography 65–70, 72–83, http://dx.doi.org/10.1016/j.dsr2.2012.02.009.

Ladd, C., Stabeno, P.J., O'Hern, J.E., 2012. Observations of a Pribilof eddy. Deep-Sea Research Part I: Oceanographic Research Papers 66, 67–76.

Lasker, R., 1978. The relations between oceanographic conditions and larval anchovy food in the California Current: identification of factors contributing

to recruitment failure. Rapports et Procès-Verbaux des Réunions du Conseil International pour l'Exploration de la Mer 173, 212–230.
Lasker, R., 1981. Factors Contributing to Variable Recruitment of the Northern Anchovy (*Engraulis mordax*) in the California Current: Contrasting Years, 1975 Through 1978. Rapports et Procès-Verbaux des Réunions du Conseil International pour l'Exploration de la Mer 178, 375–388.
Laurel, B.J., Stoner, A.W., Ryer, C.H., Hurst, T.P., Abookire, A.A., 2007. Comparative habitat associations in juvenile Pacific cod and other gadids using seines, baited cameras and laboratory techniques. Journal of Experimental Marine Biology and Ecology 351, 42–55.
Leggett, W.C., Deblois, E., 1994. Recruitment in marine fishes: is it regulated by starvation and predation in the egg and larval stages? Netherlands Journal of Sea Research 32 (2), 119–134.
Mantua, N.J., Hare, S.R., Zhang, Y., Wallace, J.M., Francis, R.C., 1997. A Pacific interdecadal climate oscillation with impacts on salmon production. Bulletin of the American Meteorological Society 78 (6), 1069–1079.
Mizobata, K., Saitoh, S., Wang, J., 2008. Interannual variability of summer biochemical enhancement in relation to mesoscale eddies at the shelf break in the vicinity of the Pribilof Islands, Bering Sea. Deep-Sea Research Part II: Topical Studies in Oceanography 55 (16), 1717–1728.
Mueter, F.J., Bond, N.A., Ianelli, J.N., Hollowed, A.B., 2011. Expected declines in recruitment of walleye pollock (*Theragra chalcogramma*) in the eastern Bering Sea under future climate change. ICES Journal of Marine Science: Journal du Conseil 68 (6), 1284–1296.
Mueter, F.J., Ladd, C., Palmer, M.C., Norcross, B.L., 2006. Bottom-up and top-down controls of walleye pollock (*Theragra chalcogramma*) on the Eastern Bering Sea shelf. Progress in Oceanography 68 (2), 152–183.
Musienko, L.N., 1970. Razmnozheine I razvitie ryb Beringova moray (Reproduction and development of Bering Sea fishes). Tr. Vses. Nauchno-issled. Inst. Morsk. Rybn. Koz. Okeanogr. In: Moiseev, P.A. (Ed.), Soviet Fisheries Investigations in the North Eastern Pacific, Pt. 5, vol. 70, pp. 161–224 (Avail. Natl. Tech. Info. Serv., Springfield, VA as TT 74-50127).
Myers, R.A., 1998. When do environment-recruitment correlations work? Reviews in Fish Biology and Fisheries 8, 285–305.
Napp, J.M., Baier, C.T., Brodeur, R.D., Coyle, K.O., Shiga, N., Mier, K., 2002. Interannual and decadal variability in zooplankton communities of the southeast Bering Sea shelf. Deep-Sea Research Part II: Topical Studies in Oceanography 49 (26), 5991–6008.
National Oceanic and Atmospheric Administration. Bering Climate: A Current View of the Bering Sea Ecosystem and Climate. ⟨http://www.beringclimate.noaa.gov/data/index.php⟩.
Neidetcher, S.K., Hurst, T.P., Ciannelli, L., Logerwell, E.A., 2014. Spawning phenology and geography of Aleutian Islands and eastern Bering Sea Pacific cod (*Gadus macrocephalus*). Deep-Sea Research Part II: Topical Studies in Oceanography 109, 204–214, http://dx.doi.org/10.1016/j.dsr2.2013.12.006.
Norcross, B.L., Shaw, R.F., 1984. Oceanic and estuarine transport of fish eggs and larvae: a review. Transactions of the American Fisheries Society 113 (2), 153–165.
Okkonen, S.R., Schmidt, G.M., Cokelet, E.D., Stabeno, P.J., 2004. Satellite and hydrographic observations of the Bering Sea 'Green Belt'. Deep-Sea Research Part II: Topical Studies in Oceanography 51 (10), 1033–1051.
Overland, J.E., Adams, J.M., Bond, N.A., 1999. Decadal variability of the Aleutian Low and its relation to high-latitude circulation. Journal of Climate 12 (5), 1542–1548.
Overland, J.E., Alheit, J., Bakun, A., Hurrell, J.W., Mackas, D.L., Miller, A.J., 2010. Climate controls on marine ecosystems and fish populations. Journal of Marine Systems 79 (3), 305–315.
Overland, J.E., Spillane, M.C., Hurlburt, H.E., Wallcraft, A.J., 1994. A numerical study of the circulation of the Bering Sea basin and exchange with the North Pacific Ocean. Journal of Physical Oceanography 24 (4), 736–758.
Parker, K.S., 1989. Influence of oceanographic and meteorological processes on the recruitment of Pacific halibut Hippoglossus stenolepis in the Gulf of Alaska. In: Beamish, R.J., McFarlane, G.A. (Eds.), Effects of ocean variability on recruitment and an evaluation of parameters used in stock assessment models, Canadian Special Publication of Fisheries and Aquatic Science 108, 221–237.
Reed, R.K, Stabeno, P.J, 1996. On the climatological mean circulation over the eastern Bering Sea shelf. Continental Shelf Research 16 (10), 1297–1305.
Schumacher, J.D., Bond, N.A., Brodeur, R.D., Livingston, P.A., Napp, J.M., Stabeno, P.J., 2003. Climate change in the southeastern Bering Sea and some consequences for biota. Large Marine Ecosystems of the World: Trends in Exploitation, Protection, and Research, 17–40.
Seitz, A.C., Loher, T., Nielsen, J.L., 2007. Seasonal movements and environmental conditions experienced by Pacific halibut in the Bering Sea, examined by pop-up satellite tags. International Pacific Halibut Commission, Scientific Report No. 84, 24pp.
Shchepetkin, A.F., McWilliams, J.C., 2005. The regional oceanic modeling system (ROMS): a split-explicit, free-surface, topography-following-coordinate oceanic model. Ocean Modelling 9 (4), 347–404.
Shimada, A.M., Kimura, D.K., 1994. Seasonal movements of Pacific cod, *Gadus macrocephalus*, in the eastern Bering Sea and adjacent waters based on tag-recapture data. Fishery Bulletin 92, 800–816.
Sigler, M.F., Stabeno, P.J., Eisner, L.B., Napp, J.M., Mueter, F.J., 2014. Spring and fall phytoplankton blooms in a productive subarctic ecosystem, the eastern Bering Sea, during 1995–2011. Deep-Sea Research Part II: Topical Studies in Oceanography 109, 71–83, http://dx.doi.org/10.1016/j.dsr2.2013.12.007.
Skud, B.E., 1977. Drift, Migration, and Intermingling of Pacific Halibut Stocks. International Pacific Halibut Commission, Scientific Report No. 63, 42pp.
Smart, T.I., Duffy-Anderson, J.T., Horne, J.K., Farley, E.V., Wilson, C.D., Napp, J.M., 2012. Influence of environment on walleye pollock eggs, larvae, and juveniles in the southeastern Bering Sea. Deep-Sea Research Part II: Topical Studies in Oceanography 65–70, 196–207.
Sohn, D., Ciannelli, L., Duffy-Anderson, J.T., 2010. Distribution and drift pathways of Greenland halibut (*Reinhardtius hippoglossoides*) during early life stages in the eastern Bering Sea and Aleutian Islands. Fisheries Oceanography 19 (5), 339–353.
Springer, A., McRoy, C., Flint, M., 1996. The Bering Sea Green Belt: shelf edge processes and ecosystem production. Fisheries Oceanography 5 (3–4), 205–223.
St-Pierre, G., 1984. Spawning Locations and Season for Pacific Halibut. International Pacific Halibut Commission Scientific Report No. 70, 46pp.
St-Pierre, G., 1989. Recent Studies of Pacific Halibut Postlarvae in the Gulf of Alaska and Eastern Bering Sea. International Pacific Halibut Commission Scientific Report No. 73, 31pp.
Stabeno, P., Moore, S., Napp, J., Sigler, M., Zerbini, A., 2012. Comparison of warm and cold years on the southeastern Bering Sea shelf. Deep-Sea Research Part II: Topical Studies in Oceanography 65–70, 31–45.
Stabeno, P.J, Van Meurs, P., 1999. Evidence of episodic on-shelf flow in the southeastern Bering Sea. Journal of Geophysical Research 104 (C12), 715–729.
Stabeno, P.J., Bond, N.A., Kachel, N.B., Salo, S.A., Schumacher, J.D., 2001. On the temporal variability of the physical environment over the south-eastern Bering Sea. Fisheries Oceanography 10 (1), 81–98.
Stabeno, P.J., Kachel, N., Mordy, C., Righi, D., Salo, S., 2008. An examination of the physical variability around the Pribilof Islands in 2004. Deep-Sea Research Part II: Topical Studies in Oceanography 55 (16), 1701–1716.
Stabeno, P.J., Reed, R.K., Napp, J.M., 2002. Transport through Unimak Pass, Alaska. Deep-Sea Research Part II: Topical Studies in Oceanography 49 (26), 5919–5930.
Stabeno, P.J., Schumacher, J.D., Davis, R.F., Napp, J.M., 1998. Under-ice observations of water column temperature, salinity and spring phytoplankton dynamics: Eastern Bering Sea shelf. Journal of Marine Research 56 (1), 239–255.
Stabeno, P.J., Schumacher, J.D., Ohtani, K., 1999. The physical oceanography of the Bering Sea. In: Loughlin, T.R., Ohtani, K. (Eds.), Dynamics of the Bering Sea. University of Alaska Sea Grant Publication AK-SG-99-03, Fairbanks, AK, pp. 1–28.
Thompson, D.W.J., Wallace, J.M., 1998. The Arctic Oscillation signature in the wintertime geopotential height and temperature fields. Geophysical Research Letters 25 (9), 1297–1300.
Trenberth, K.E., Hurrell, J.W., 1994. Decadal atmosphere-ocean variations in the Pacific. Climate Dynamics 9 (6), 303–319.
Van der Veer, H.W., Ruardij, P., Van den Berg, A.J., Ridderinkhof, H., 1998. Impact of interannual variability in hydrodynamic circulation on egg and larval transport of plaice *Pleuronectes platessa* L. in the southern North Sea. Journal of Sea Research 39 (1–2), 29–40.
Van der Veer, H.W., Witte, J.I.J., 1999. Year-class strength of plaice *Pleuronectes platessa* in the Southern Bight of the North Sea: a validation and analysis of the inverse relationship with winter seawater temperature. Marine Ecology Progress Series 184, 245–257.
Wespestad, V.G., Fritz, L.W., Ingraham, W.J., Megrey, B.A., 2000. On relationships between cannibalism, climate variability, physical transport, and recruitment success of Bering Sea walleye pollock (*Theragra chalcogramma*). ICES Journal of Marine Science: Journal du Conseil 57 (2), 272.
Wilderbuer, T.K., Hollowed, A.B., Ingraham, W.J., 2002. Flatfish recruitment response to decadal climatic variability and ocean conditions in the eastern Bering Sea. Progress in Oceanography 55 (1–2), 235–247.
Wolter, K., Timlin, M.S., 1998. Measuring the strength of ENSO events: How does 1997/98 rank? Weather 53 (9), 315–324.
Zhang, J., Woodgate, R., Moritz, R., 2010. Sea ice response to atmospheric and oceanic forcing in the Bering Sea. Journal of Physical Oceanography 40 (8), 1729–1747.

Deep-Sea Research II 109 (2014) 204–214

Contents lists available at ScienceDirect

Deep-Sea Research II

journal homepage: www.elsevier.com/locate/dsr2

Spawning phenology and geography of Aleutian Islands and eastern Bering Sea Pacific cod (*Gadus macrocephalus*)

Sandra K. Neidetcher [a,*], Thomas P. Hurst [b], Lorenzo Ciannelli [c], Elizabeth A. Logerwell [a]

[a] Fishery Interaction Team, Resource Ecology and Fisheries Management Division, Alaska Fisheries Science Center, National Marine Fishery Service, National Oceanic and Atmospheric Administration, 7600 Sand Point Way NE, Seattle, WA 98115, USA
[b] Fisheries Behavioral Ecology Program, Resource Assessment and Conservation Engineering Division, Alaska Fisheries Science Center, National Marine Fishery Service, National Oceanic and Atmospheric Administration, Hatfield Marine Science Center, Newport, OR 97365, USA
[c] College of Earth, Ocean, and Atmospheric Sciences, Oregon State University, Corvallis, OR, USA

ARTICLE INFO

Available online 25 December 2013

Keywords:
Pacific cod
Gadus macrocephalus
Reproductive maturity
Spawning grounds
Phenology
Aleutian Islands
Bering Sea

ABSTRACT

Pacific cod (*Gadus macrocephalus*) is an economically and ecologically important species in the southeastern Bering Sea and Aleutian Islands, yet little is known about the spawning dynamics of Pacific cod in these regions. To address this knowledge gap, we applied a gross anatomical maturity key for Pacific cod to describe temporal and spatial patterns of reproductive status over three winter spawning seasons: 2005, 2006, and 2007. Maturity status of female Pacific cod was assessed by fishery observers during sampling of commercial catches and used to construct maps showing spawning activity in the Bering Sea and Aleutian Islands. Most spawning activity was observed on the Bering Sea shelf and Aleutian Island plateaus between 100 and 200 m depth. Data for those days when a high percentage of spawning stage fish were observed were used to identify areas with concentrations of spawning fish. Spawning concentrations were identified north of Unimak Island, in the vicinity of the Pribilof Islands, at the shelf break near Zhemchug Canyon, and adjacent to islands in the central and western Aleutian Islands along the continental shelf. The spawning season was found to begin in the last days of February or early March and extend through early to mid-April. Variation in spawning time (averaging ~10 days between years) may have been associated with a change from warm (2005) to cold (2007) climate conditions during the study period. Our information on Pacific cod spawning patterns will help inform fishery management decisions, models of spawning and larval dispersal and the spatial structure of the stock.

Published by Elsevier Ltd.

1. Introduction

The timing and location of spawning are central components that define a species' reproductive strategy (Petitgas et al., 2010). The spawning site provides the initial conditions for development of early life stages. Spawning site features such as topography and bathymetry set the landscape in which recruitment processes unfold (Ciannelli et al., 2007), while meteorological and oceanographic cycles interacting with site features determine the physical conditions present during this critical period. The location and timing of spawning is assumed to be coupled, through natural selection, to ecological conditions beneficial for early life survival (Leggett, 1985) such as high concentration of prey and the dispersal potential of eggs or larvae (Cushing, 1969). Though the specific mechanisms determining the timing and location of marine fish spawning are poorly understood (Cury, 1994), recent experiments assessing interactions between environmental conditions and spawning found initial oocyte development aligned with the timing of earth's equinox and the progression of oocyte development related to ambient temperatures (Kjesbu et al., 2010; Olive et al., 1998). Knowledge of spawning patterns is also important for assessment of spawning migrations, identification of early life stage distribution and patters of dispersal to juvenile nurseries, and understanding of population structure (Hjort, 1926; Sinclair and Iles, 1988).

Pacific cod, *Gadus macrocephalus* range from the Sea of Japan across the North Pacific Rim to the California coast (Hart, 1973) and is an important groundfish species in Alaska. Pacific cod are predators of other demersal fishes (primarily walleye pollock, *Gadus chalcogrammus*) and crustaceans such as crab (Livingston and deReynier, 1996) and are prey for top predators, including endangered Steller sea lions (*Eumetopias jubatus*) (Sinclair and Zeppelin, 2002). Commercial Pacific cod catches from the Bering Sea and Aleutian Islands averaged 200,000 metric tons from 2001 to 2009 with an average annual value of US$120 million. Pacific cod catches in the Bering Sea and Aleutian Islands are second only to that of walleye pollock (Hiatt et al., 2011).

* Corresponding author. Tel.: +1 206 526 4521; fax: +1 206 526 6723.
E-mail address: Sandi.Neidetcher@noaa.gov (S.K. Neidetcher).

0967-0645/$ - see front matter Published by Elsevier Ltd.
http://dx.doi.org/10.1016/j.dsr2.2013.12.006

Table 1
Visual maturity stage descriptions for female Pacific cod.

Anatomical stage	Anatomical stage description
Immature	Small, pink or transparent, no oocytes visible to eye.
Developing	Small to ½ the length of the abdominal cavity, well-developed blood vessels, oocytes distinct and visible through ovary wall, coloration yellow to bright orange. Oocytes difficult to separate.
Prespawning	Ovaries are greater than ½ the abdominal cavity. The ovary surface is translucent and mottled grayish. Oocytes are opaque and less adhesive.
Spawning	Ova run under light pressure to the abdomen.
Spent	Gonads appear flaccid and watery. Ovaries may contain remnants of disintegrating ova and blood.
Resting	Ovaries are small and firm, may have black or silver coloration on surface. No oocytes are visible to eye.

In the Bering Sea and Aleutian Islands, Pacific cod inhabit the continental slopes and shelf, most often at depths to 300 m (Bakkala, 1984). Conventional mark and recapture efforts have demonstrated that adult Pacific cod are distributed across the continental shelf during summer and are found in dense spawning aggregations along the continental slope and shelf near Unimak Island and the Pribilof Islands during late winter (Shimada and Kimura, 1994). While several areas with large spawning aggregations have been identified, broad-scale surveys of spawning distribution have not been conducted in Alaskan waters, thus comprehensive information on the timing, locations, and depth of spawning are not well-described in the Bering Sea and Aleutian Islands regions. In Washington's Puget Sound, spawning was found to occur at depths of 40 to 265 m (Palsson, 1990), confirming earlier reports of spawning in shallow coastal areas (Karp, 1982). In British Columbia, Pacific cod have a short spawning season which occurs in the late winter and early spring (Foucher and Westrheim, 1990). Studies have suggested that spawning occurs slightly later at higher latitudes (Westrheim, 1996). Pacific cod stocks along the Asian coast also show variable spawning patterns related to latitude with migration patterns of northern stocks linked to local currents and temperature patterns (Savin, 2008). Northern stocks off the Russian coast move off-shore to spawn in warmer water at deeper depths in the late winter while the southern stocks off the Korean coast spawn in the seasonally warmer near-shore waters (Moiseev, 1960).

Pacific cod is a broadcast spawning species that releases approximately 1,000,000–1 mm diameter eggs per individual annually (Westrheim, 1996). Ovarian development is synchronous and eggs are released in a single batch (Stark, 2007; Sakurai and Hattori, 1996; Bowden et al., 1990). Because Pacific cod eggs are demersal (Thompson, 1963), they are rarely captured during ichthyoplankton surveys. Therefore, data from extensive annual ichthyoplankton surveys in the southeastern Bering Sea have not been used to infer spawning patterns in this species (Matarese et al., 2003; Smart et al., 2012). With these sampling limitations and a general lack of life history research effort focused on this species, little is known about the spawning patterns of adults or the distribution and movement patterns of early life stages (but see Hurst et al., 2012; Parker-Stetter et al., 2013).

Anatomical maturity keys characterize gross morphological changes of the ovaries to estimate reproductive maturity. Maturity keys are commonly used to study the onset and duration of the spawning season by determining the reproductive condition of adult fishes (Parenti and Grier, 2004; Hunter and Macewicz, 2003; West, 1990). However, maturity keys have been criticized for their subjectivity with key descriptions based on ovary characteristics such as color and relative size which may be interpreted differently among users. Additionally, because ovaries mature gradually, users often have difficulty in accurately identifying ovaries in transitional stages of development (West, 1990). Stark (2007) was critical of macroscopic maturity keys for Pacific cod because ovaries showing very early development can be classified as immature when examined visually. However, when validated against maturity stages based on histological examination of individual oocytes, maturity keys can provide a robust description of maturity states, and are especially useful in identifying later stages of maturity for single-batch spawning fishes. Further, through the application of an anatomical maturity key, researchers are able to assess significantly larger numbers of fish than would be practicable based on traditional histological analyses. Recent advances in applying shape analysis software to measure oocyte size show promising research in oocyte development (Thorsen and Kjesbu, 2001). However, these methods still require chemical fixation and laboratory processing, which makes them less practicable in some fishery-dependent sampling programs.

For this study we applied a maturity key developed specifically for Pacific cod. A complete description of the ovary characteristics and key development and validation are described in Neidetcher (2012). The key identifies changes in the gross appearances of ovaries (size, color, adhesion of oocytes in the ovary) that characterize changes that occur with the progression of the spawning season. The resulting gross anatomical maturity key for female Pacific cod includes the following stages: (1) Immature, (2) Developing, (3) Prespawning, (4) Spawning, (5) Spent and (6) Resting (Table 1).

The accuracy of the visual maturity key was evaluated against the staging of individual oocytes based on histological processing and microscopic examination. The comparison of observer-assigned maturity stages to histologically examined oocytes from within the same fish resulted in an overall misclassification rate of 43%. However, the mismatch is narrow with most misclassifications (95%) assigned to an adjacent stage. Further, most (59%) misclassifications occurred in the early stages of egg development (between the developing and prespawning stages). Only 10% of the fish histologically-determined to be in the developing or prespawning stages were misclassified as spawning or spent (Neidetcher, 2012). Therefore, we determined that the use of the maturity key was sufficiently robust to identify broad-scale temporal and spatial patterns in spawning of Pacific cod in the Bering Sea and Aleutian Islands. Various stages and stage combinations are used for mapping spawning locations and for determining spawning phenology. Misclassification rates associated with these stages are provided with each analysis.

The objectives of this research are to describe spatial and temporal spawning patterns of Pacific cod in the Bering Sea and Aleutian Islands. Gross anatomical maturity of female Pacific cod was assessed by fishery observers monitoring catch aboard commercial fishing vessels in the eastern Bering Sea and Aleutian Islands during three winter spawning seasons (2005–2007). Observers applied a visual maturity key developed for Pacific cod and validated against histological samples (Neidetcher, 2012). The broad spatial and temporal scale of sampling allowed for a comparison of spawning patterns from fished locations across

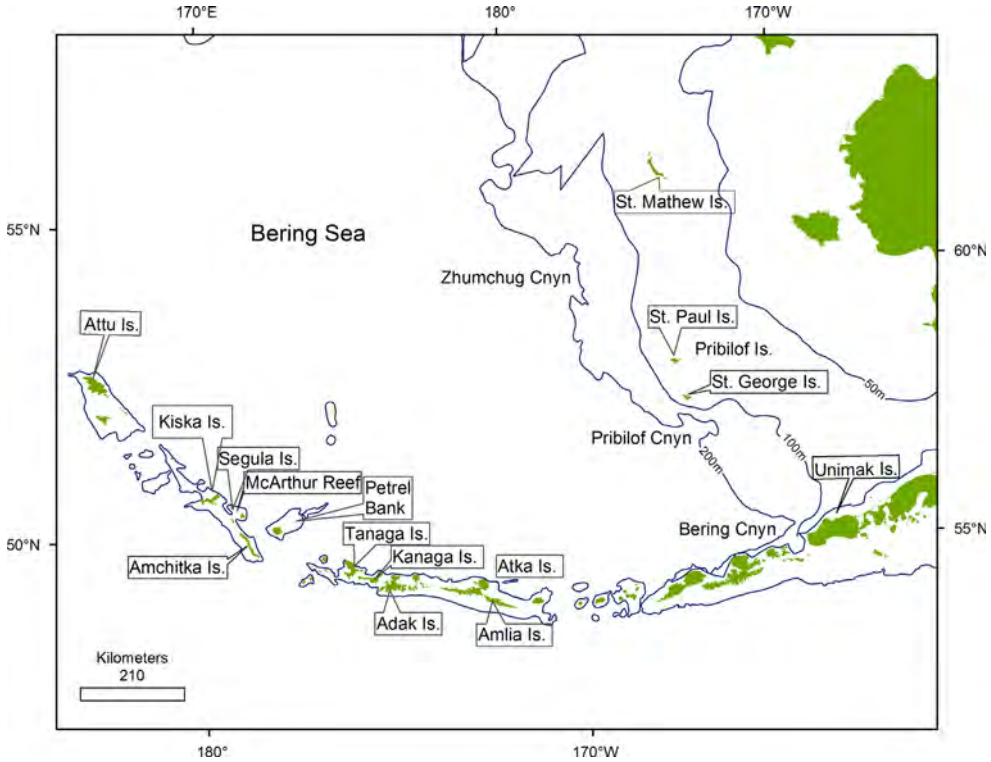

Fig. 1. Sampling locations in the eastern Bering Sea and Aleutian Islands where commercial fishery observers collected maturity information about Pacific cod.

the eastern Bering Sea and Aleutian Islands and over years with varying climate conditions.

2. Methods

2.1. Study area

The eastern Bering Sea slope separates the eastern Bering Sea diagonally from the southeast to the northwest into a shallow shelf and a deep-water basin (Fig. 1). The Aleutian Islands Archipelago is a string of volcanic islands separated by deep-water passes, marking the southern border of the Bering Sea. The island ridge, which intersects the slope at Unimak Island, is mostly comprised of a narrow continental shelf and steep slope. Conversely, the Bering Sea is dominated by a broad, flat continental shelf intersected by submarine canyons along the shelf break. The southernmost canyon, the Bering Canyon, breaches the slope at the intersection of the shelf and the Aleutian Island arc and Unimak Pass. The Pribilof Canyon cuts into the slope just south of the Pribilof Islands, while the Zhemchug Canyon is situated over 200 km to the northwest.

2.2. Data collection

Pacific cod maturity data were collected by fishery observers trained by the Alaska Fisheries Science Center's (AFSC) Fisheries Monitoring and Analysis Division (FMA). Observers used the maturity key to assess the maturity status of fish captured in fisheries specifically targeting Pacific cod and in fisheries that caught cod as incidental catch during operations directed to other species. The capture gear in the sampled fisheries included mid-water and bottom trawls, longlines, and pots. Prior to the at-sea operations, observers were trained in the use of the maturity key.

A random sampling protocol was used to select a subset of commercial catches (hauls) from which fish were selected for gender identification and measured for length. Most observers assessed the maturity of all fish specimens used for these gender and length collections. Additionally, some observers opportunistically sampled fish from hauls that were not assessed for biological characteristics when Pacific cod were available in those hauls. Random selection techniques were maintained in choosing individual fish for analysis from these additional hauls. Details concerning observer sampling protocols are available in the AFSC's North Pacific Groundfish Observer Manual (AFSC 2005–2007). To assess gonad maturity, the abdominal cavity was opened and characteristics of the surface of the ovaries and condition of individual oocytes were compared to descriptions and digital photographs provided in the maturity key. In addition to biological characteristics, observers recorded the date and location (latitude and longitude measured to degrees and minutes) of the fishing event. On vessels using trawl gear, capture locations recorded the point at which the gear is retrieved from fishing depth. For fixed-gears, the recovery location was typically the end of the gear string. Strings of pots and longlines of individual fishing hooks were often several kilometers in length.

Pacific cod maturity status was evaluated by fisheries observers through three winter spawning seasons: 2005, 2006, and 2007. In each spawning season, sampling began in early January and continued through April. Regional climate conditions varied markedly across the three sampling years: water temperatures were anomalously high in 2005, while 2006 was a year of transition to a colder regime (Rodionov et al., 2007). The sea ice extent for 2007 was one of the greatest on record reaching the outer Bering Sea shelf, the Pribilof Islands, and the Alaska Peninsula east of Unimak Island.

2.3. Data analysis

Using Geographic Information System (GIS) software, the catch locations for observer-assessed prespawning and spawning stage fish were plotted to display the locations of spawning Pacific cod

captured by the fishery. The prespawning stage occurs for a short period of time prior to egg hydration and spawning, therefore the location of fish at this stage is assumed to be in the vicinity of the spawning grounds. Pooling prespawning and spawning stages for this analysis reduced misclassification rates between histological analysis and visual assessment to 18%. Because rules of confidentiality apply to protect commercial fishing information, haul locations were binned according to a 20 × 20-km grid system. To avoid revealing catch locations for any given fishing vessel, data in grid cells with fewer than three vessels were excluded.

We identified concentrated spawning activity by: (1) identifying days when > 15% of fish sampled were classified as spawning; and (2) identifying locations where spawning fish were caught on those days. A daily percent spawning was calculated by dividing the number of spawning stage fish identified by observers by the number of fish examined each day over all geographical areas sampled that day. Days with 15% or greater spawning fish were identified as high spawning activity days. The maps show the capture locations during days when observers identified concentrated spawning. Because locations of concentrated spawning occurred in areas with high levels of sampling effort, rules of confidentiality did not prevent the public identification of these locations.

Temporal patterns in spawning were examined by grouping maturity stages to determine when oocyte maturation transitioned into, and past, the spawning stage. The fraction of fish determined to be in developing and prespawning stages were combined and plotted against the combined fraction of fish in the spawning and spent stages. The misclassification rate between these combined stages was only 3% (Neidetcher, 2012). Fish classified as immature or resting were omitted from this analysis. Collections from January 1 to April 30 were pooled into 5 day intervals to illustrate the general pattern over the spawning season. The beginning of the spawning season was defined as the time when the percent of spawning+spent stage fish reached 20% of sampled individuals; the end of the spawning season was defined as the time when this percentage reached 80%. Values between 40 and 60% defined the mid-spawning period.

3. Results

3.1. Observer-assessed maturity collections

Between 2005 and 2007, fishery observers determined the maturity status of 37,268 female Pacific cod (Table 2). This was accomplished through the use of an anatomical maturity key, applied by approximately 300 fishery observers aboard 152 commercial fishing vessels operating in the Bering Sea and Aleutian Islands over three years. Sampling levels were highest during 2005, remained high in 2006, and declined in 2007 because fewer observers participated in the project. In general, the proportion of fish assigned to each maturity stage was similar for the three study years, suggesting that there were no systematic differences in the interpretation of the maturity key by observers among years.

3.2. Spawning locations

Annual maps of the capture locations of prespawning and spawning stage Pacific cod indicated that spawning activity was widespread, occurring predominantly on the outer shelf of the eastern Bering Sea (outer shelf domain) most often between 100 and 200 m depth. Observer sampling effort in 2005 and 2006 identified widespread spawning along the northern outer shelf from southeast of the Pribilof Islands to west of St. Matthew Island. Despite minor differences in the spatial and temporal distribution of sampling in 2007, observers identified spawning activity in similar locations along the northern outer shelf. In all three years, additional spawning areas were identified in the southern Bering Sea from Unimak Pass to Amak Island, the central Aleutian Islands from Amlia Island to Tanaga Island, and the western Aleutian Islands from Petrel Bank to Attu Island (Fig. 2: see Fig. 1 for place names).

An examination of maturity stage assignments by fishing gear type from the same geographic region and time period shows reduced level of spawning stage assignments for longline gear. For example, comparison of maturity assignments from the Unimak area during peak spawning when all four gear types are deployed in this area shows 19% assignment to spawning stage by observers onboard bottom trawl vessels, but only 5% assignment to spawning stage onboard longline vessels (Fig. 3). Because longline is the primary gear type used along the northern outer shelf (Fig. 4), spawning locations in this area may be underrepresented by observer maturity assessments.

During the course of the study, spawning concentrations were identified along the Aleutian Islands, north of Unimak Island, near the Pribilof Islands, and the Bering Sea shelf edge along the 200 m isobaths (Fig. 5). Observers identified the highest percent spawning (> 35%) in 2005 in the western Aleutians at Attu Island, in the central Aleutians at Atka Island, and along the Bering Sea shelf north of Unimak Island, seaward of the Pribilof Islands and along the northern outer shelf. The percent of spawning stage fish sampled remained high at Atka and Unimak Island in 2006 (> 30%) (Fig. 5). Though observations of spawning stage fish in 2007 were low in many areas along the Bering Sea shelf break, concentrations of spawning stage fish were observed in these areas.

While spawning concentrations reoccur in the same general locations in the central and western Aleutian Islands and north of Unimak, their location around the Pribilof Island and along the outer shelf appeared to shift among years. Areas of concentrated spawning during 2005 occurred between the 100 and 200 isobaths seaward of the Pribilof Islands to the northern base of the Zhemchug Canyon, while these concentrations in 2006 occurred primarily east of St. George Island (southern Pribilof Island) and farther north along the shelf edge. Few spawning concentrations were detected either south or west of the Pribilof Islands in 2007, and only one area in the northern outer shelf was observed in the same year.

3.3. Spawning phenology

The timing of the spawning season for Pacific cod varied slightly over the three-year sampling period. Spawning typically

Table 2
Gross anatomical maturity stages for female Pacific cod assessed by observers from January 1–April 30 aboard commercial fishing vessels in the Bering Sea and Aleutian Islands.

Year	No. Obs.	Immature	Developing	Prespawn	Spawning	Spent	Resting	Total
2005	76	3352(23)	2947(20)	4875(33)	857(6)	1285(9)	1385(9)	14,703
2006	81	3505(26)	3080(23)	4927(37)	838(6)	408(3)	655(5)	13,413
2007	58	2005(22)	2104(23)	3034(33)	470(5)	894(10)	645(7)	9152

Parentheses show the percent of fish assigned to each maturity stage. No. Obs.=number of observers participating in the project.

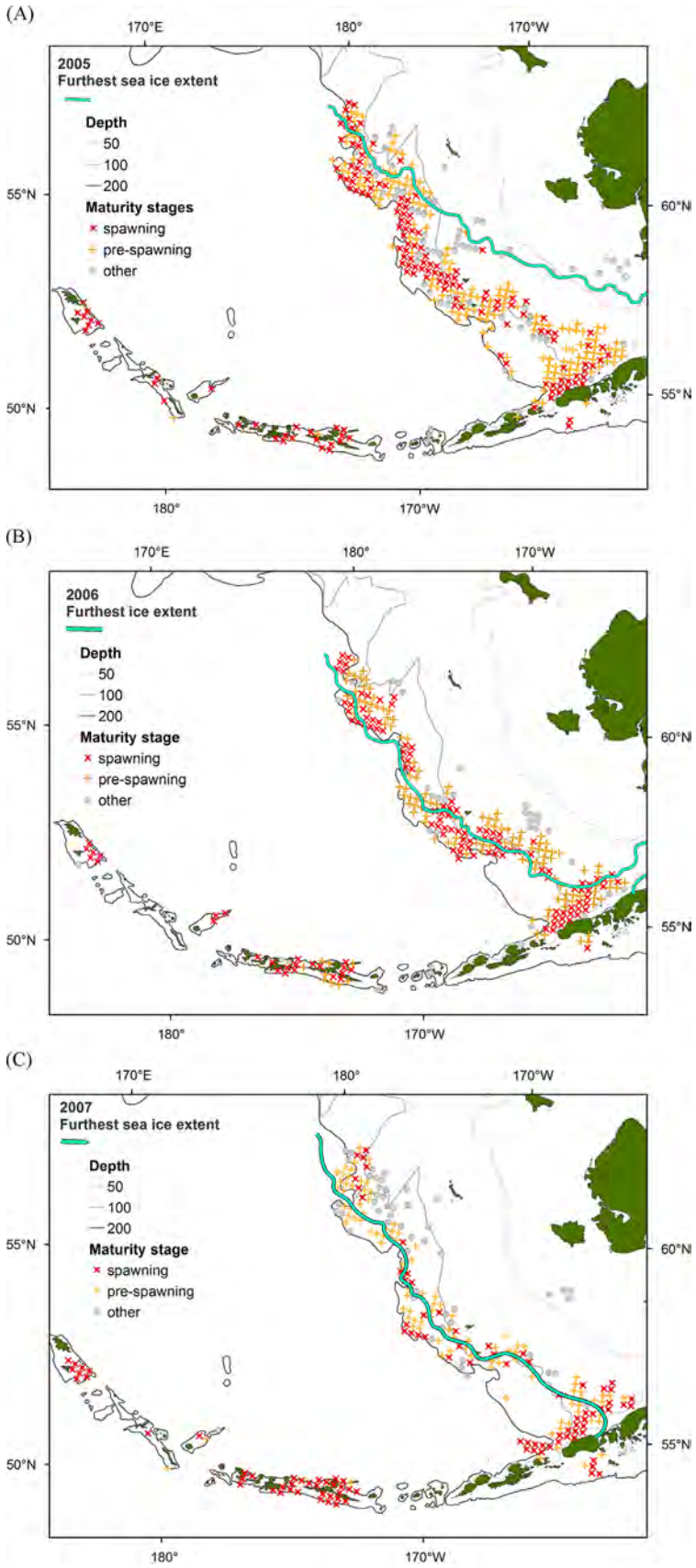

Fig. 2. Distribution of prespawning and spawning stages of female Pacific cod from maturity data in 2005–2007 (A–C) from January–April. To avoid revealing catch locations for any given fishing vessel, multiple vessel locations were merged into $20 \times 20\ km^2$ grid cells. The symbol x is used to indicate locations where observers identified spawning stage fish. The symbol + indicates locations where prespawning stage fish were observed in the absence of spawning stage fish. The locations of observed stages other than spawning and prespawning are indicated with circles.

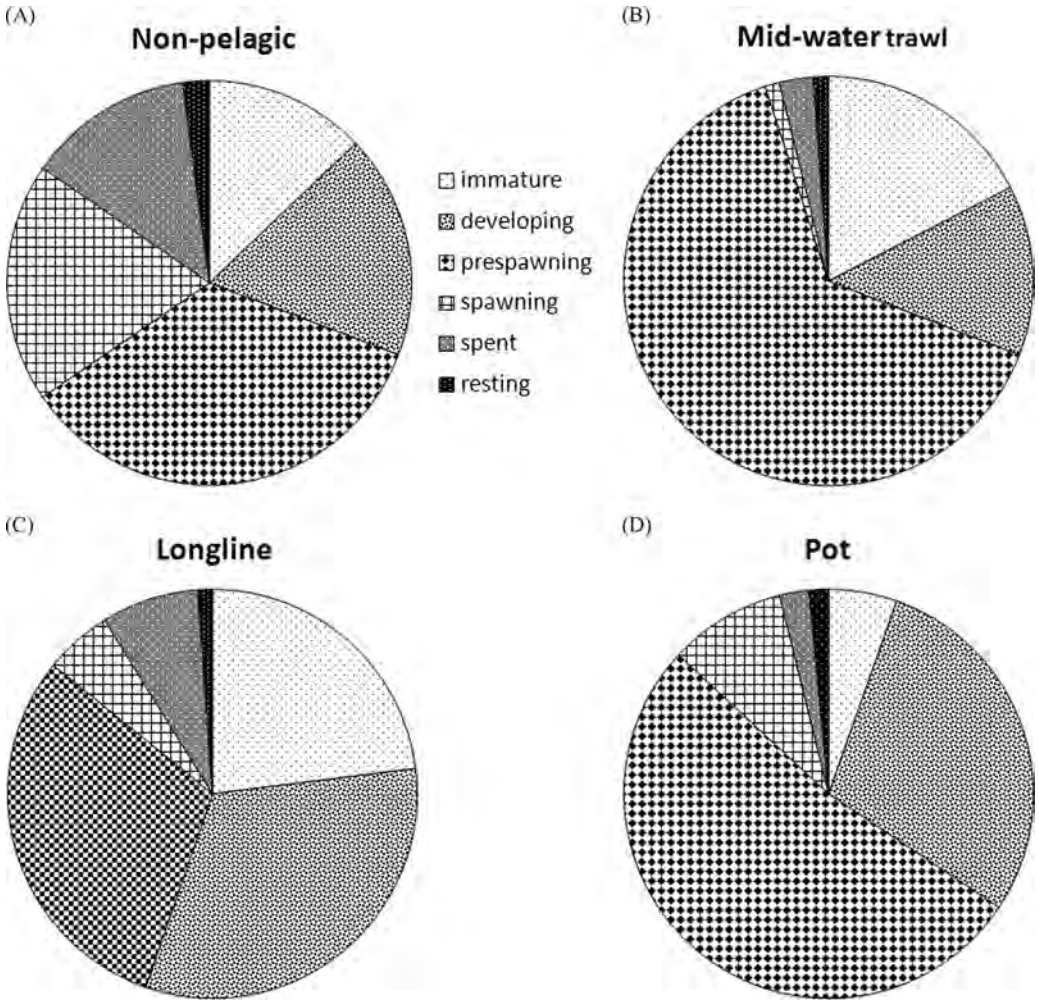

Fig. 3. Proportion of fish at each maturity stage from the Unimak Pass area by gear type.

began in early March and persisted through early April. In 2005, the fraction of spawning+spent stage fish increased to 20% by March 1. These numbers fell between 40 and 60%, for a short period during the last week of March, and reached 80% by April 1 (Table 3). Spawing+spent stage fish reached 20% a few days earlier in 2006 than 2005. Spawning+spent stages for 2006 reached 80% by the first week of April. In 2007, spawning+spent stages did not reach 20% until the second week in March but reached 40–60% for a short period early in the third week of March, then reached 80% by the end of the first week in April. The later date at which spawning+spent stage percentages reached 20% suggested a delayed initiation of spawning in 2007 (Fig. 6). During the third week of April in 2005, observers identified a significant number of fish that had not yet spawned. These results suggest the presence of a group of late-spawning fish, though sample sizes at this time were very low. Of interest is also the fluctuating pattern of 2006, which may indicate timing differences among spawning groups (Fig. 6).

4. Discussion

4.1. Using observer-assessed visual maturity keys to identify spawning patterns

Spawning activity in this species was found to be much more widely distributed than has generally been recognized. In addition to previously recognized spawning locations in the vicinity of Unimak Island and the Pribilof Islands, additional spawning concentrations were identified along the northern outer shelf and at sites along the Aleutian Islands. While our samples were limited to regions targeted by commercial fishing operations, it seems reasonable to assume that fishers are adept at locating harvestable fish aggregations because they are aided by advanced technologies and extensive knowledge of fish distributions. Thus our identified spawning areas likely represent broad patterns in spawning activity of Bering Sea and Aleutian Island Pacific cod. Pacific cod are most abundant on the shelf and are only rarely captured off the shelf at depths below 300 m (Bakkala, 1984). With the exception of the Bering Canyon, there was little fishing effort (and hence little sample coverage) off the slope at depths greater than 200 m, so it is unclear if Pacific cod are also spawning in the deepest parts of their range such as the outer canyons off the northern slope.

In addition, access to fishing areas on the middle shelf appears limited by sea ice cover during the winter spawning season in all but very low sea ice years. As a result, there were also few samples from shallow shelf areas of the Bering Sea in 2006 and 2007. During years with average sea ice coverage, access may be limited along the northern outer shelf, and during years with extensive sea ice coverage, sampling around the Pribilof Islands may be impacted. Sea ice coverage rarely reaches as far southeast as the Alaska Peninsula northeast of Unimak Pass (Stabeno et al., 2001). Although sampling did occur in the vicinity of the Pribilof Islands and along the shelf edge to the northwest in all three years, effort

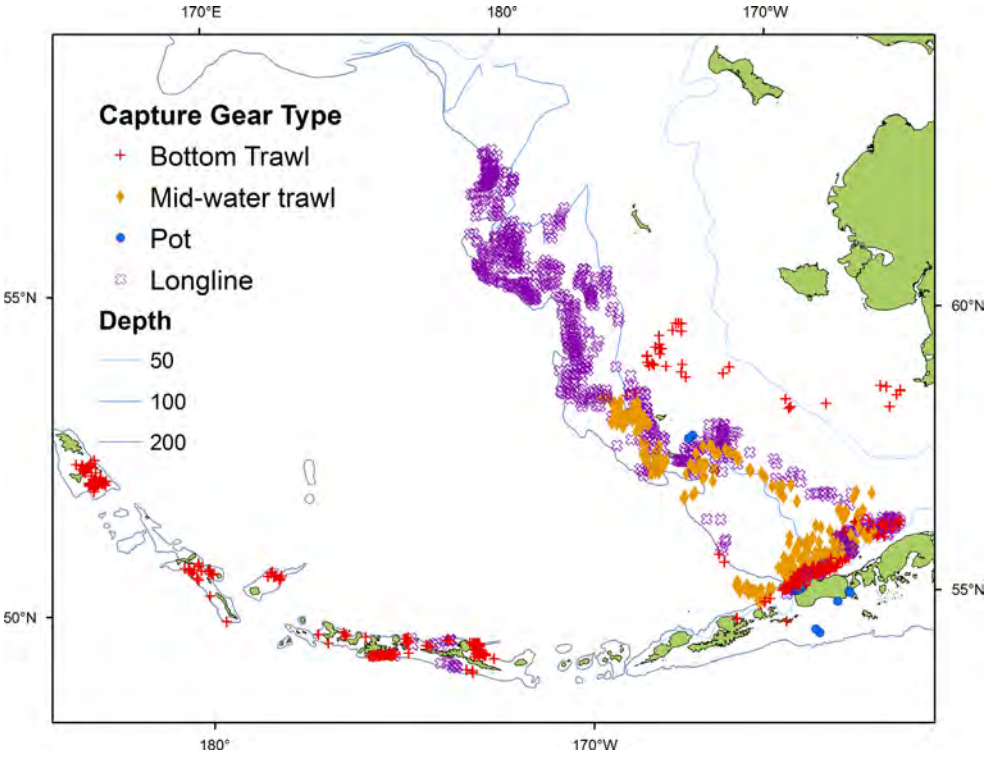

Fig. 4. Catch locations by gear type for maturity data assessed by observers aboard commercial vessels in the Bering Sea and Aleutian Islands.

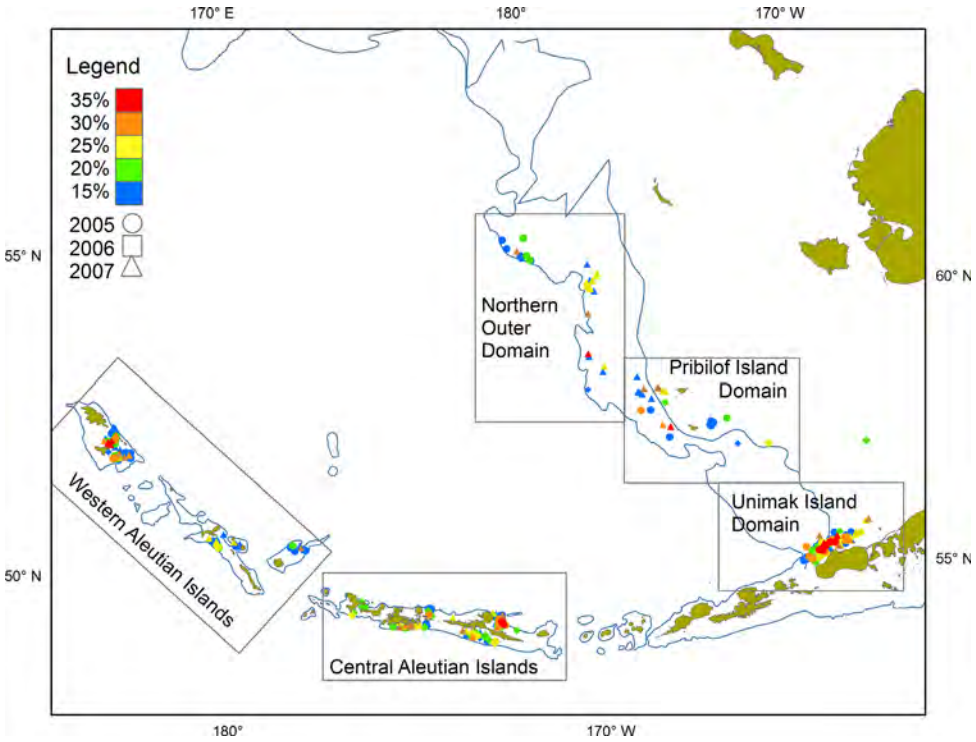

Fig. 5. Locations of concentrated spawning in the Bering Sea and Aleutian Islands for 2005–2007. Spawning concentrations locations are coded by color for daily percent spawning and by shape for sample year. Spawning stage data were plotted using unique colors for the different levels of percent spawning stage sampled, while unique shapes were used to represent sample year. (For interpretation of the references to color in this figure legend, the reader is referred to the web version of this article).

may have been reduced due to the presence, or predicted advance, of sea ice during the 2006 and 2007 spawning seasons. A decrease in fishing effort by longline vessels was reported by fishery managers in 2007 (Hiatt et al., 2008). This decrease was likely due to the extensive sea ice coverage and may explain the lack of sampling effort and the absence of spawning stage data for this location.

Table 3
Calendar dates when the percentage of observer sampled fish of spawning and spent stages combined reached 20, 40–60, and 80% for each of the study years.

Year	20%	40–60%	80%
2005	March 1	March 4	April 1
2006	February 4	March 4–April 1	April 1
2007	March 2	March 3	April 1

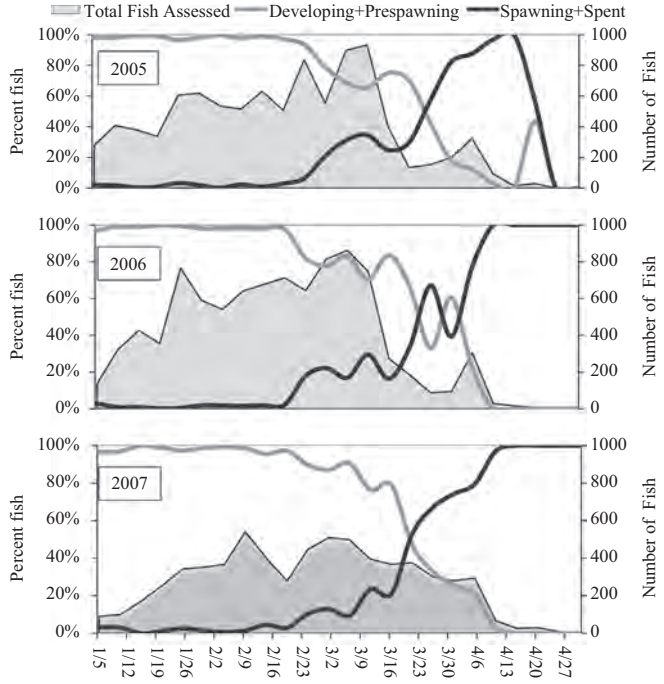

Fig. 6. Spawning phenology charts for the Bering Sea and Aleutian Islands from 2005 to 2007. The left *y*-axis is relevant to the chart lines and represents the percent spawning stage. The right *y*-axis is relevant to the gray shaded areas and represents observer sampling effort over time.

Reduced sampling may have reduced the chance of encountering spawning aggregations in the northern outer shelf in 2007.

There are gear-specific differences in fish catchability which may have had minor effects on the observed distribution of Pacific cod spawning. An examination of the proportion of fish assigned to each maturity stage per gear type from late February through early March from the Unimak Pass area found that bottom trawls captured the largest percentage of fish identified as spawning stage. Fixed gear types, such as longlines and pots rely on bait to attract fish to the gear. Diet research on Pacific cod found a high occurrence of empty stomachs during spawning suggesting reduced feeding activity (Poltev et al., 2012) which may result in lower catchability of spawning stage fish by these passive gear types. Interestingly, the lowest percentage of fish identified to spawning stage was found in mid-water trawls. As a result, these patterns suggest that spawning in the northern outer shelf may be more widespread than reflected in analyses of the presence of spawning fish in commercial catches.

The comparison of visual assessments to histological evaluation of oocyte development may indicate a high level of misclassification between some stages of development. Comparisons of visual maturity to the histological examination of oocytes within ovaries is an important exercise, although differentiating between stages of yolk development at both the macroscopic and microscopic scale can be subjective, particularly with transitioning stages of development. Aligning the markers for stage descriptions between the approaches is challenging and may account for a portion of the misclassifications (Neidetcher, 2012). Combining adjacent maturity stages for some analyses reduced the effective misclassification rates in this study. In addition, the large number of maturity assessments conducted during at-sea fishery sampling provides a robust tool for identifying the primary temporal and spatial patterns of spawning.

Despite these limitations of our study, the annual maps of the distribution of Pacific cod prespawning and spawning stages have increased our knowledge of spawning locations in the Bering Sea and Aleutian Islands. Previous conventional tagging studies describe Pacific cod spawning as large aggregations of fish over small spatial scales in areas near the shelf edge southwest of the Pribilof Islands and on the Bering Sea side of Unimak Pass, between Unimak and Unalaska Islands (Shimada and Kimura, 1994). More recently, archival tag studies have shown recoveries near the shelf edge in the vicinity of the Pribilof and Unimak Islands during the spawning season (Nichol et al., 2013). Russian trawl surveys have identified spawning and prespawning aggregations along the northern Bering Sea outer shelf, extending from Russian to US waters, in addition to areas in and around the Pribilof Islands and near Unimak Pass (Stepanenko, 1995). However, spawning activity of Pacific cod appears more widespread than suggested by those earlier surveys. Prespawning and spawning stage Pacific cod were found along the Bering Sea outer shelf (100 to 200 m depths), the shelf area between the Pribilof Islands and the slope, southeast of the Pribilof Islands closely associated with the 100 m isobath, and along the north side of Unimak Island inside of the 100 m isobath. Spawning concentrations were located near the heads of Zhemchug, Pribilof, and Bering canyons, around the shoaling isobaths of the Pribilof Islands, and among islands along the Aleutian archipelago.

4.2. Oceanographic conditions by regional spawning locations

Little is known about the behavioral mechanisms driving Pacific cod aggregation patterns which may be ephemeral in nature, forming and dispersing in accordance to environmental cues. Because cod spawn weeks before larvae begin feeding, a successful strategy for cod reproduction involves the anticipation of favorable feeding conditions and transport to suitable nursery areas (Brander, 1994). We hypothesize that the geophysical and hydrological characteristics of concentrated spawning locations provide an accumulation of conditions beneficial to Pacific cod productivity. While the identified spawning concentrations were located in areas of varying topography, current structure, and water column hydrology, they may each have characteristics which would enhance survival of offspring.

The oceanographic conditions of the three areas of consistent spawning activity identified in this study provide bio-physical mechanisms that enhance primary production and possibly larval feeding. The area off the north coast of Unimak Island is subject to the influence of currents and tidal flow from the Bering Sea Canyon; this flow provides high concentrations of nutrients observed near Unimak Pass (Schumacher and Stabeno, 1998), in turn increasing productivity and improving foraging conditions for cod larvae. Around the Pribilof Islands, tidally-driven clockwise circulation (Kowalik and Stabeno, 1999) enhances entrainment of nutrient-rich deep waters from the outer shelf and Pribilof Canyon (Stabeno et al., 2008). Additionally, seasonal frontal zone which forms around the islands may enhance the retention of organisms within the “Pribilof Domain” but may also limit productivity of surface waters later in the summer (Stabeno et al., 2008).

Spawning concentrations were observed with varying occurrence over the outer shelf seaward of the Pribilof Islands between the 100 and 200 isobaths, and near the north side of St. Paul Island, and east of St. George Island. Such variations may be attributed to changing conditions as a result of variation in circulation around the islands. In the northern outer shelf, a large saline front forms along the contour of the shelf edge transecting the Pribilof and Zhemchug Canyons (Stabeno and Reed, 1994). Although on-shelf flow has been identified primarily through tidal forcing, on-shore flow associated with eddies (Stabeno and Van Meurs, 1999) is thought to provide important nutrients for high levels of primary production seen along the shelf break area (Springer et al., 1996; Stabeno et al., 1999; McRoy et al., 2001). The high level of nutrients and the hydrographic structure in these areas may provide conditions beneficial for larval cod, such as higher levels of secondary production and concentration of prey in these fronts and eddies.

Observer-assessed maturity data provide the first documentation of discrete spawning sites along the Aleutian Islands. Spawning concentrations were located between the islands and in nearshore areas on both the Bering Sea and Pacific Ocean coasts of the eastern, central, and western Aleutian Islands. These areas are dominated by tidal activity and currents flowing along the island chain and in deep passes between island groups (Stabeno et al., 2005). The dominant northward flow through the passes intersects and mixes with the Aleutian North Slope Flow bringing warm, nutrient-rich waters which drive high productivity on the northern lee sides of islands (Schumacher and Stabeno, 1998; Ladd et al., 2005). Further, this current structure may provide important local retention features or transport cod larvae onto the Bering shelf (Lanksbury et al., 2007). Where hydrological structures may isolate Bering Sea stocks from the Aleutian Island stocks, deep water passes and water conditions through the passes may deter genetic exchange along the central and western Aleutian Islands. Recent tagging experiments (Seitz et al., 2011) and genetics research (Hauser et al., 2007; Nielsen et al., 2010) have pointed toward a more complex stock structure for Pacific halibut than the previously reported single stock in the Bering Sea and Aleutian Islands. Similarly, genetic analyses of Pacific cod have identified variation between the Gulf of Alaska, the Bering Sea, and among islands in the Aleutians (Spies, 2012; Cunningham et al., 2009).

4.3. Pacific cod spawning phenology

Stark (2007) found general trends in Pacific cod maturation and spawning to be seasonal and suggested that photoperiod may be the primary cue triggering reproduction in Pacific cod. These results are consistent with other studies throughout the distribution of Pacific cod. Southern stocks of Pacific cod along the west coast of North America spawn earlier than Alaska stocks. Peak spawning in the Bering Sea occurred in March during the three years of this study, consistent with observations in the Gulf of Alaska (Stark, 2007). Conversely, in Canadian stocks, peak spawning occurs in February and early March, and spawning along the west coast of the continental United States begins in December (Foucher and Westrheim, 1990). Pacific cod stocks of the western Bering Sea demonstrate a similar shift in spawning phenology with later spawning along the Russian coast (Savin, 2008; Rovnina et al., 1997) than in Japanese waters (Sakurai and Hattori, 1996; Hattori et al., 1992) or off the Korean coast (Cha et al., 2007). Though the mechanisms regulating these effects are still unknown, recent studies of Atlantic cod have linked initial oocyte maturation to the autumnal equinox and the rate of oocyte maturation to ambient water temperature (Kjesbu et al., 2010).

Pacific cod maturity data presented here indicates that spawning season in the Bering Sea and Aleutian Islands begins as early as the last week of February and extends to the first week of April, with shifts in timing of 10 days observed between the sample years. Ovary maturation was delayed in 2007 relative to 2005 and 2006 and the duration of the spawning season in 2006 was longer. Water temperatures were anomalously high in 2005, whereas 2006 was a year of transition to a colder regime and was marked with a high level of temperature fluctuation through the winter and early spring (Rodionov et al., 2007). 2007 was a cold year; the sea ice extent for that year was one of the greatest on record reaching the outer shelf, the Pribilof Islands, and the Alaska Peninsula east of Unimak Island. During high sea ice years, salinity stratification is stronger than in low sea ice years (Ladd and Stabeno, 2012). Coyle et al. (2008) suggests that years with weaker stratification are most favorable for summer production in the Bering Sea. Strong water column stratification in 2007 may have resulted in lower productivity or delayed production, and thus reduced prey resources for newly spawned cod larvae. The extended spawning observed in 2006 may have resulted from fluctuations in climate conditions during the winter months such that spawning cues varied across regions, expanding the spawning period.

5. Conclusion

Gross anatomical maturity keys provide an easily implemented tool for estimating reproductive maturation in fish. The application of maturity keys by fisheries observers aboard commercial fishing vessels allowed the collection of maturity data on broad spatial and temporal scales. Pacific cod spawning activity was found to be widely distributed across the outer Bering Sea shelf and among the Islands of the Aleutian Archipelago. Within this wide distribution, discrete spawning concentrations were observed associated with island topography such as that north of Unimak Island and along the Aleutian Chain, and along the outer Bering Sea shelf in each of the study years. Because collections are possible throughout the spawning season, these data provided fishery managers with estimates of the timing and location of spawning across regions and between years. The spawning season began during late February or early March and extended through early April. Slight variations ($\sim$10 days) in the average spawning time among years may have been associated with the transition from warm to cold climate conditions during the study period. Spawning patterns provide the initial points from which patterns in stock connectivity and larval dispersal may be inferred. These data will serve as a baseline for monitoring spawning patterns over time and varying climate conditions and to identify possible shifts associated with variations in recruitment and stock abundance (Ciannelli et al., 2013).

Acknowledgments

We thank the AFSC Observer Program and individual observers for their effort in data collections and for their valuable feedback from the field. Guidance in collection methods was provided by E. Connors, P. Munro, K. Rand, and D. Reece. LC acknowledges support from the NPRN BSIERP program (Project B60) and from NFS-CMG Grant 0934691. Helpful comments regarding content and editing was provided by G. Thompson, C. Ryer, and E. Dever. This research was supported in part by a Grant from the North Pacific Research Board (no. 618). We thank reviewers S. McDermott and J. Stark. The findings and conclusions in this paper are those of the authors and do not necessarily represent the views of the National Marine Fisheries Service. This is publication number 117 of the

BEST-BSIERP Bering Sea Project and publication number 453 of the North Pacific Research Board.

References

(AFSC) Alaska Fisheries Science Center, 2005 (2006, 2007). North Pacific Groundfish Observer Manual. North Pacific Groundfish Observer Program. AFSC, 7600 Sand Point Way N.E., Seattle, Washington, 98115 ⟨http://www.afsc.noaa.gov/FMA/Manual_pages/MANUAL_pdfs/manual2007.pdf⟩.

Bakkala, R.G., 1984. Pacific cod in the eastern Bering Sea. Int. North Pac. Fish. Comm. Bull. 42, 157–179.

Brander, K.M., 1994. Spawning and life history information for North Atlantic cod stocks. 1994. ICES Coop. Res. Rep. 205, 150.

Bowden, D.G., Foucher, R.P., Tyler, A.V., 1990. A guide to the ovarian histology of Pacific Cod. Canadian Technical Report of Fisheries and Aquatic Sciences No. 1723, Department of Fisheries and Oceans, Nanaimo, British Columbia, Canada.

Cha, H.K., Lee, S.I., Yoon, S.C., Kim, Y.S., Chun, Y.Y., Chang, D.S., Yang, J.H., 2007. Maturation and spawning of the Pacific cod, *Gadus macrocephalus* TILESIUS in East Sea of Korea. J. Korean Soc. Fish. Technol. 43, 320–328.

Ciannelli, L., Bailey, K.M., Chan, K.-S., Stenseth, N.C., 2007. Phenological and geographical patterns of walleye pollock *Theragra chalcogramma* spawning in the western Gulf of Alaska. Can. J. Fish. Aquat. Sci. 64, 713–722.

Ciannelli, L., Fisher, J.A.D., Skern-Mauritzen, M., Hunsicker, M.E., Hidalgo, M., Frank, K.T., Bailey, KM., 2013. Theory, consequences and evidence of eroding population spatial structure in harvested marine fishes. Mar. Ecol. Prog. Ser. 480, 227–243.

Coyle, K.O., Pinchuk, A.I., Eisner, L.B., Napp, J.M., 2008. Zooplankton species composition, abundance and biomass on the eastern Bering Sea shelf during summer: the potential role of water column stability and nutrients in structuring the zooplankton community. Deep Sea Res. II 55, 1755–1791.

Cunningham, K.M., Canino, M.F., Spies, I.B., Hauser, L., 2009. Genetic isolation by distance and localized fjord population structure in Pacific cod *Gadus macrocephalus*: limited effective dispersal in the northeastern Pacific Ocean. Can. J. Fish. Aquat. Sci. 66, 153–166.

Cury, P., 1994. Obstinate nature: an ecology of individuals. Thoughts on reproductive-behavior and biodiversity. Can. J. Fish. Aquat. Sci. 51, 1664–1673.

Cushing, D.H., 1969. The regularity of spawning season of some fishes. J. Cons. Int. Explor. Mer 33, 81–97.

Foucher, R.P., Westrheim, S.J., 1990. The spawning season of Pacific cod on the west coast of Canada. Can. Manuscript Rep. Fish. Aquat. Sci 2072, 25.

Hart, J.L., 1973. Pacific fishes of Canada. Bull. Fish. Res. Board Can. 180, 730.

Hattori, T., Sakurai, Y., Shimazaki, K., 1992. Maturation and reproductive cycle of female Pacific cod in waters adjacent to the southern coast of Hokkaido, Japan. Nippon Suisan Gakkaishi 58, 2245–2252.

Hiatt, T., Dalton, M., Felthoven, R., Fissel, B., Garber-Yonts, B., Haynie, A., Kasperski, S., Lew, D., Package, C., Sepez, J., Seung, C. Stock Assessment and Fishery Evaluation Report for the Groundfish Fisheries of the Gulf of Alaska and Bering Sea/Aleutian Island Area: Economic Status of the Groundfish Fisheries of Alaska, NPFMC, November, 2011.

Hiatt, T., Felthoven, R., Dalton, M., Garber-Yonts, B., Haynie, A., Lew, D., Sepez, J., Seung, C., the staff of Northern Economics, Inc. Stock Assessment and Fishery Evaluation Report for the Groundfish Fisheries of the Gulf of Alaska and Bering Sea/Aleutian Island Area: Economic Status of the Groundfish Fisheries off Alaska, NPFMC, November, 2008.

Hjort, J., 1926. Fluctuations in year classes of important food fishes. Cons. Int. Explor. Mer 1, 5–38.

Hauser, L., Newton, L., Loher, T., 2007. Microsatellite Variation in Spawning Adults of Pacific Halibut in the Gulf of Alaska and Bering Sea. Report of Assessment and Research Activities 2006, International Pacific Halibut Commission, Seattle, Wash.

Hunter, J.R., Macewicz, B.J. 2003. Improving the accuracy and precision of reproductive information used in fisheries. Kjesbu, O. S., Hunter, J. R., Witthames, P. R., (Eds,) Modern Approaches to Assess Maturity and Fecundity of Warm- and Cold-water Fish and Squids. Kjesbu. Fisken og havet 12, pp. 57–68.

Hurst, T.P., Moss, J.H., Miller, J.A., 2012. Distributional patterns of 0-group Pacific cod *Gadus macrocephalus* in the eastern Bering Sea under variable recruitment and thermal conditions. ICES J. Mar. Sci. 69, 163–174.

Karp, W.A. 1982. Biology and Management of Pacific cod Gadus macrocephalus Tilesius in Port Townsend, Washington (Ph.D. thesis). Univ. Washington, Seattle. 119 p.

Kjesbu, O.S., Righton, D., Krüger-Johnsen, M., Thorsen, A., Michalsen, K., Fonn, M., Witthames, P.R., 2010. Thermal dynamics of ovarian maturation in Atlantic cod Gadus morhua. Can. J. Fish. Aquat. Sci. 67, 605–625.

Kowalik, Z., Stabeno, P., 1999. Trapped motion around the Pribilof Islands in the Bering Sea. J. Geophys. Res. 104 (C11).

Ladd, C., Hunt Jr., G.L., Mordy, C.W., Salo, S.A., Stabeno, P.J., 2005. Marine environment of the eastern and central Aleutian Islands. Fish. Oceanogr. 14, 22–38.

Ladd, C., Stabeno, P.J., 2012. Stratification on the Eastern Bering Sea shelf revisited. Deep-Sea Res. II, 65–70.

Lanksbury, J.A., Duffy-Anderson, J.T., Mier, K.L., Busby, M.S., Stabeno, P.J., 2007. Distribution and transport patterns of northern rock sole, Lepidopsetta polyxystra, larvae in the southeastern Bering Sea. Prog. Oceanogr. 72, 39–62.

Leggett, W.C., 1985. The role of migrations in the life history evolution of fish. Contr. Mar. Sci. 27 (Suppl), 277–295.

Livingston, P.A., deReynier, Y., 1996. Groundfish Food Habits and Predation on Commercially Important Prey Species in the Eastern Bering Sea from 1990 to 1992. AFSC Processed Rep. 96-04, 214p. Alaska Fish. Sci. Cent., Natl. Mar. Fish. Serv., NOAA, 7600 Sand Point Way NE, Seattle, WA 98115-0070.

Matarese, A.C., Blood, D.M., Picquelle, S.J., Benson, J.L., 2003. Atlas of Abundance and Distribution Patterns of Ichthyoplankton from the Northeast Pacific Ocean and Bering Sea Ecosystems Based on Research Conducted by the Alaska Fisheries Science Center (1972–1996). U.S. Dep. Commer., NOAA Professional Paper, NMFS-1, 281 p.

McRoy, C.P., Mizobata, K., Nakanishi, S., Saito, S.I., 2001. Trends in ocean conditions and new production on the shelf of the southeastern BeringSea over the past twenty years. PICES Annual Meeting 2001, Victoria, British Columbia (Abstracts).

Moiseev, P., 1960. The behavior of the Pacific cod in different zoogeographical regions. Zool. Zh. 39, 558–562.

Neidetcher, S.K., 2012. Implementation of a Gross Anatomical Maturity key for the Study of Spawning Phenology and Geography of Pacific cod *Gadus macrocephalus* (Master's thesis). Oregon State University, Corvallis, OR, p. 116.

Nichol, D.G., Kotwicki, S., Zimmermann, M., 2013. Diel vertical migration of adult Pacific cod *Gadus macrocephalus* in Alaska. J. Fish Biol. 83, 170–189.

Nielsen, J.L., Graziano, S.L., Seitz, A.C., 2010. Fine-scale population genetic structure in Alaskan Pacific halibut *Hippoglossus stenolepis*. Conserv. Genet. 11, 999–1012.

Olive, P.J.W., Rees, S.W., Djunaedi, A., 1998. Influence of photoperiod and temperature on oocyte growth in the semelparous polychaete Nereis (Neanthes) virens. Mar. Ecol. Prog. Ser. 172, 169–183.

Palsson, W.A., 1990. Pacific cod *Gadus macrocephalus* in Puget Sound and Adjacent Waters: Biology and Stock Assessment. Wash. Dep. Fish. Tech. Rep. No. 112. Olympia, WA. p. 137.

Parenti, L.R., Grier, H.J., 2004. Evolution and phylogeny of gonad morphology in bony fishes. Integr. Comp. Biol. 44, 333–348.

Parker-Stetter, S.L., Horne, J.K., Farley, E.V., Barbee, D.H., Andrews III, A.G., Eisner, L.B., Nomura, J.M., 2013. Summer distributions of forage fish in the eastern Bering Sea. Deep-Sea Res. II: Top. Stud. Oceanogr..

Petitgas, P., Secor, D.H., Mcquinn, I., Huse, G., Lo, N., 2010. Stock collapses and their recovery: mechanisms that establish and maintain life-cycle closure in space and time. ICES J. Mar. Sci. 67, 1841–1848.

Poltev, Y.N., Mukhametov, I.N., Fatykhov, R.N., 2012. On the spawning of Pacific cod *Gadus macrocephalus* in the southeastern waters off Onekotan Island. J. Ichthyol. 52 (9), 671–675.

Rodionov, S.N., Bonda, N.A., Overland, J.E., 2007. The Aleutian Low, storm tracks, and winter climate variability in the Bering Sea. Deep-Sea Res. II 54, 2560–2577.

Rovnina, O.A., Klovach, N.V., Glabokov, A.I., Selyutin, A.P., 1997. On the biology of Pacific cod *Gadus macrocephalus* in the eastern part of the Sea of Okhotsk. J. Ichthyol. 37:21–26. Translated from Russian [1997 Voprosy Ikhti-ologii 37: 27-32] by Interperiodica Publishing, Russia.

Sakurai, Y., Hattori, T., 1996. Reproductive behavior of Pacific cod in captivity. Fish. Sci. 62, 222–228.

Savin, A.B., 2008. Seasonal distribution and Migrations of Pacific cod *Gadus macrocephalus* (Gadidae) in Anadyr Bay and adjacent waters. J. Ichythyol. 48, 610–621.

Schumacher, J.D., Stabeno, P.J., 1998. Continental shelf of the Bering Sea. In: Robinson, A.R., Brink, K.H. (Eds.), The Sea, vol. 11. John Wiley, pp. 789–822. (Chapter 27).

Shimada, A.M., Kimura, D.K., 1994. Seasonal movements of Pacific cod, Gadus macrocephalus, in the eastern Bering Sea and adjacent waters based on tag-recapture data. Fish. Bull. 92, 800–816.

Seitz, A.C., Loher, T., Norcross, B.L., Nielsen, J.L., 2011. Dispersal and behavior of Pacific halibut *Hippoglossus stenolepis* in the Bering Sea and Aleutian Islands region. Aquat. Biol. 12, 225–239.

Sinclair, M., Iles, T.D., 1988. Population richness of marine fish species. Aquat. Living Resour. 1, 71–83.

Sinclair, E.H., Zeppelin, T.K., 2002. Seasonal and spatial differences in diet in the western stock of Steller sea lions (*Eumetopias jubatus*). J. Mamm. 83, 973–990.

Smart, T.I., Duffy-Anderson, J.T., Horne, J.K., 2012. Alternating temperature states influence walleye pollock early life stages in the southeastern Bering Sea. Mar. Ecol. Prog. Ser. 455, 257–267.

Spies, I., 2012. Landscape genetics reveals population subdivision in Bering Sea and Aleutian Islands Pacific cod. Trans. Am. Fish. Soc. 141, 1557–1573.

Springer, A.M., McRoy, C.P., Flint, M.V., 1996. The Bering Sea green belt: shelf-edge processes and ecosystem production. Fish. Oceanogr. 5, 205–233.

Stabeno, P.J., Schumacher, J.D., Ohtani, K., 1999. The physical oceanography of the Bering Sea. In: Loughlin, T.R., Ohtani, K. (Eds.), Dynamics of the Bering Sea: A Summary of Physical, Chemical, and Biological Characteristics, and a Synopsis of Research on the Bering Sea. University of Alaska Sea Grant, AK-SG-99-03, North Pacific Marine Science Organization (PICES), Fairbanks, AK, pp. 1–28.

Stabeno, P.J., Bond, N.A., Kachel, N.B., Salo, S.A., Schumacher, J.D., 2001. On the temporal variability of the physical environment over the southeastern Bering Sea. Fish. Oceanogr. 10, 81–98.

Stabeno, P.J., Kachel, D.G., Kachel, N.B., Sullivan, M.E., 2005. Observations from moorings in the Aleutian passes: temperature, salinity and transport. Fish. Oceanogr. 14 (Suppl. 1), 39–54.

Stabeno, P.J., Kachel, N., Mordy, C., Righi, D., Salo, S., 2008. An examination of the physical variability around the Pribilof Islands in 2004. Deep-Sea Res. II 55 (16–17), 1701–1716.

Stabeno, P.J., Reed, R.K., 1994. Circulation in the Bering Sea basin observed by satellite-tracked drifters: 1986–1993. J. Phys. Oceanogr. 24 (4), 848–854.
Stabeno, P.J., Van Meurs, P., 1999. Evidence of episodic on-shelf flow in the southeastern Bering Sea. J. Geophys. Res. 104 (C12), 715–729. (720).
Stepanenko, M.K., 1995. Distribution, behavior and abundance of Pacific cod, *Gadus macrocephalus*, in the Bering Sea. J. Ichthyol. 35, 17–27.
Stark, J.W., 2007. Geographic and seasonal variations in maturation and growth of female Pacific cod *Gadus macrocephalus* in the Gulf of Alaska and Bering Sea. Fish. Bull. US 105, 396–407.
Thompson, J.A., 1963. On the demersal quality of the fertilized eggs of Pacific cod, *Gadus macrocephalus*. J. Fish. Res. Board Can. 20, 1087–1088.
Thorsen, A., Kjesbu, O.S., 2001. A rapid method for estimation of oocyte size and potential fecundity in Atlantic cod using a computer-aided particle analysis system. J. Sea. Res. 46 (3–4), 295–308.
West, G., 1990. Methods of assessing ovarian development in fishes: a review. Aust. J. Mar. Freshwater Res. 41, 199–222.
Westrheim, S.J., 1996. On the Pacific cod Gadus macrocephalus in British Columbia waters, and a comparison with Pacific cod elsewhere, and Atlantic cod (*G. morhua*). Can. Tech. Rep. Fish. Aquat. Sci. 2092, 390.

Deep-Sea Research II 109 (2014) 215–240

Contents lists available at ScienceDirect

Deep-Sea Research II

journal homepage: www.elsevier.com/locate/dsr2

Delineating ecological regions in marine systems: Integrating physical structure and community composition to inform spatial management in the eastern Bering Sea

Matthew R. Baker [a,b,*], Anne B. Hollowed [b]

[a] Joint Institute for the Study of the Atmosphere and Ocean, University of Washington, Seattle, WA 98105, United States
[b] Resource Ecology and Fisheries Management Division, Alaska Fisheries Science Center, NOAA Fisheries, 7600 Sand Point Way NE, Seattle, WA 98115, United States

ARTICLE INFO

Available online 19 March 2014

Keywords:
Biogeography
Community ecology
Ecoregions
Fisheries management

ABSTRACT

Characterizing spatial structure and delineating meaningful spatial boundaries have useful applications to understanding regional dynamics in marine systems, and are integral to ecosystem approaches to fisheries management. Physical structure and drivers combine with biological responses and interactions to organize marine systems in unique ways at multiple scales. We apply multivariate statistical methods to define spatially coherent ecological units or ecoregions in the eastern Bering Sea. We also illustrate a practical approach to integrate data on species distribution, habitat structure and physical forcing mechanisms to distinguish areas with distinct biogeography as one means to define management units in large marine ecosystems. We use random forests to quantify the relative importance of habitat and environmental variables to the distribution of individual species, and to quantify shifts in multispecies assemblages or community composition along environmental gradients. Threshold shifts in community composition are used to identify regions with distinct physical and biological attributes, and to evaluate the relative importance of predictor variables to determining regional boundaries. Depth, bottom temperature and frontal boundaries were dominant factors delineating distinct biological communities in this system, with a latitudinal divide at approximately 60°N. Our results indicate that distinct climatic periods will shift habitat gradients and that dynamic physical variables such as temperature and stratification are important to understanding temporal stability of ecoregion boundaries. We note distinct distribution patterns among functional guilds and also evidence for resource partitioning among individual species within each guild. By integrating physical and biological data to determine spatial patterns in community composition, we partition ecosystems along ecologically significant gradients. This may provide a basis for defining spatial management units or serve as a baseline index for analyses of structural shifts in the physical environment, species abundance and distribution, and community dynamics over time.

1. Introduction

Spatial classification of patterns in biogeography provide a practical approach to understand ecosystem dynamics. This has useful application to conservation (Lourie and Vincent, 2004; Spalding et al., 2007) and resource management (Marasco et al., 2007; Levin et al., 2009; Livingston et al., 2011; Link and Auster, 2011). Oceanographic processes, bathymetric structure and environmental conditions regulate system organization and productivity (Speckman et al., 2005) and influence competitive and predatory interactions (Kildaw et al., 2005). By recognizing and explicitly characterizing spatial heterogeneity in marine systems, we are able to define and better explain distinct regional patterns (Bailey, 1998).

There is an extensive history of classifying biogeographic patterns in the marine environment (Forbes, 1856; Ekman, 1953; Hedgepath, 1957a,b). Hierarchical approaches are often used, scaling from geographical realms (continental or oceanic scales), to provinces (seas or basins), ecosystems (self-contained systems), and regional-scale processes. To distinguish boundaries, classification systems have employed species endemism (Briggs, 1974), bathymetry (Allen and Smith, 1988), biogeochemical processes (Longhurst, 1998), oceanic production (Bailey, 1998), thermogeography (Adey and Steneck, 2001)

* Corresponding author at: Joint Institute for the Study of the Atmosphere and Ocean, University of Washington, Seattle, WA 98105, United States. Tel.: +1 206 794 7515.
E-mail addresses: Matthew.Baker@noaa.gov (M.R. Baker), Anne.Hollowed@noaa.gov (A.B. Hollowed).

http://dx.doi.org/10.1016/j.dsr2.2014.03.001
0967-0645/

and physiographic and oceanographic patterns (Piatt and Springer, 2007). Such classification systems have also used functional considerations such as utility and parsimony (Spalding et al., 2007). As part of this process, the concept of large marine ecosystems (LME) was established to define the continental margins according to ecological criteria (e.g. bathymetry, hydrography, productivity, and trophic relationships) and to facilitate transboundary and ecosystem-based management (Morgan, 1987; Sherman and Alexander, 1989; Sherman, 1991). LMEs are also widely used as distinct units of analysis in comparisons of marine systems (Branch et al., 2010; Pinsky et al., 2011). Due in part to the emphasis on Ecosystem-Based Fishery Management (EBFM) in the reauthorization of the Magnusson-Stevens Act, LMEs were also adopted by the US National Oceanic and Atmospheric Administration (http://www.lme.noaa.gov) and currently provide the basis for assessing and managing discrete fish stocks. While LMEs provide a robust and useful designation of distinct marine areas, there is increased interest in higher resolution understanding of ecosystem processes and regional phenomena relevant to both conservation (Dinerstein and Olson, 1997; Ford, 1998; Banks et al., 1999; Spalding et al., 2007) and natural resource management (Fogarty and Murawski, 1998; Fogarty and Keith, 2009; http://bsierp.nprb.org). This is recognized by international (UN FAO, 2003) and national authorities (Ecosystem Principles Panel, 1996; National Marine Fisheries Service, 1999; US Commission on Ocean Policy, 2004). As distinct units within LMEs, ecoregions serve this purpose. We define an ecoregion as an ecologically and geographically defined area characterized by distinct assemblages of biological communities and environmental conditions.

1.1. Purpose and intent

Both spatial and multispecies management approaches require robust methods to synthesize physical and biological data to identify regional structure within ecosystems, and determine the relative impacts of various environmental and biological drivers. We illustrate an approach to integrate data on species distribution with data on environmental variables and physical structure to distinguish regions with distinct biogeography and ecology (i.e. ecoregions).

1.2. Regional Delineation

LMEs are defined using broad-scale patterns of biodiversity, productivity and hydrographical features (Hempel and Sherman, 2003; Murawski, 2007). These boundaries distinguish ecosystem processes, food web and trophic interactions, and commercially exploited stocks. The criteria distinguishing ecoregions is less clear. Most approaches have been synthetic (consensus and expert opinion) and largely qualitative (Piatt and Springer, 2007; Ortiz, 2012). Past efforts to apply quantitative methods have typically focused on physical variables alone (Allen and Smith, 1988), used aggregate biomass without consideration of the composition of the ecological communities represented (Fogarty and Keith, 2009; Livingston et al., 1999; Pepin et al., 2010; Zwanenburg et al., 2010) or included anthropogenic and political considerations (Spalding et al., 2007).

Hard boundaries rarely exist in marine systems (Murawski, 2007). Ecological processes and species distributions fluctuate along gradients, often dictated by a relatively limited group of covariates (e.g. temperature, depth, salinity, stratification, nutrient availability, substrate type, productivity). Identifying how distinct biological communities organize across environmental gradients offers one means to differentiate ecoregions.

1.3. Study system: eastern Bering Sea

Our analyses focus on the eastern Bering Sea (EBS), a highly productive system that generates roughly half of US fish and shellfish landings and supports important populations of seabirds and marine mammals (National Research Council, 1996). It is characterized by a broad coastal shelf and a deep-sea basin, extending from the Alaska Peninsula to the Bering Strait. The Bering Sea shelf extends 800 km from Norton Sound to the

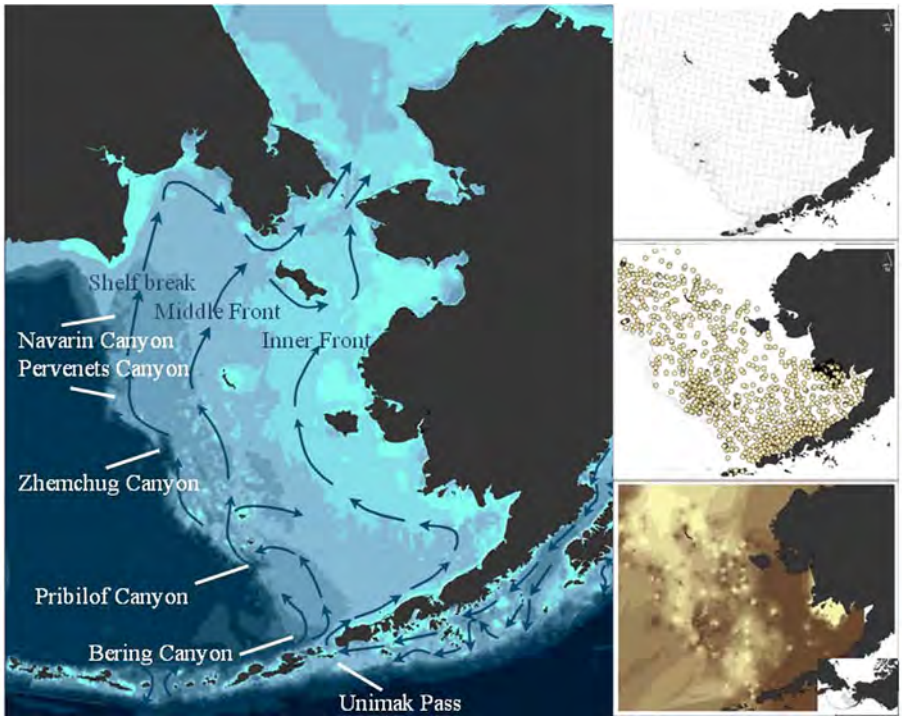

Fig. 1. Eastern Bering Sea shelf. Main panel displays depth, predominant currents, fronts and canyons. Side panels display fixed grid survey stations for survey biomass (top right), sampling locations for sediment (middle right) and inverse distance weighting of surficial sediments (darker shades indicate coarser substrates, bottom right).

continental slope and the Shelf Break extends 1200 km from Unimak Pass to Cape Navarin (Fig. 1). Patterns in productivity and energy flow are influenced by temperature, currents, annual cycles of sea ice formation (Napp and Hunt, 2001; Hunt et al., 2011, 2002) and multi-year climate regimes (Mantua and Hare, 2002; Bond et al., 2003). Temperature and hydrographic structure are dynamic, driven by terrestrial inputs, insolation, ice melt, tidal currents and wind events and are characterized by high inter-annual and spatial variability (Overland et al., 1999). These physical conditions influence localized production (Coyle and Cooney, 1993) and the distributions and interactions of commercially and ecologically important species (Coyle and Pinchuk, 2002; Ciannelli et al., 2004).

Depth gradients are often used to differentiate three bathymetric domains within the EBS: the coastal or inner domain (0–50 m), the middle domain (50–100 m) and the outer shelf (100–200 m) (Smith and Bakkala, 1982; Coachman, 1986) (Fig. 1). These domains are separated by hydrographic fronts, with inner, middle, and outer fronts located along the 50, 100 and 170-m isobaths, respectively (Coachman, 1986; Schumacher and Stabeno, 1998). In summer, the coastal domain is well mixed to weakly stratified, the middle domain is a strongly stratified two-layer system with a relatively warm wind-mixed surface layer overlaying a cold bottom layer, and the outer shelf has well mixed upper and lower layers separated by a zone of gradually increasing density. Profiles in all domains have high variability within and among years (Buckley et al., 2009). Despite strong structural fronts, cross-shelf transport does occur. Wind-driven circulation has important effects on nutrient flux and advection processes related to biological production and distribution (Stabeno et al., 2001; Danielson et al., 2012; Gibson et al., 2013) Canyon systems along the Shelf Break (Bering, Pribilof, Zhemchug, Pervenets, and Navarin) also play an important role in shelf/basin exchange (Stabeno et al., 1999; Kinney et al., 2009).

An extensive cold pool, defined as bottom temperatures ≤ 2 °C, forms as a legacy of sea ice melt (Wyllie-Echeverria and Wooster, 1998; Stabeno et al., 2012a,b) and persists until storm-induced mixing occurs in the fall (Ladd and Stabeno, 2012) (Fig. 2). The intensity and spatial extent of this cold pool is a dominant physical driver in the system, limiting nutrient transport and species distribution (National Research Council, 1996; Mueter and Litzow, 2008; Stabeno et al., 2012a,2012b). Stratification also influences nutrient transport and availability, primary and secondary production, larval survival and species interactions (National Research Council, 1996, Kachel et al., 2002). In concert, these oceanographic features influence inter-annual variability in species distribution (Lauth, 2012; Kotwicki and Lauth, 2013) and early life stage survival (Mueter et al., 2006, 2007), and constrain species overlap, predatory interactions, and cross-shelf distribution (Kotwicki et al., 2005; Ciannelli and Bailey, 2005, Spencer, 2008). Extensive research in this system, including the joint National Science Foundation Bering Sea Ecosystem Study (BEST) and North Pacific Research Board Bering Sea Integrated Ecosystem Research Program (BSIERP), suggests that depth, sediment type, prey distribution and spatial distribution of the cold pool define distinct core distributions for forage fish and flat fish species and structure distinct marine communities (Ciannelli and Bailey, 2005; Hollowed et al., 2012).

1.4. Previous regional classifications of the eastern Bering Sea

Several expert-based classification schemes have been applied to the EBS (Ford, 1998; Banks et al., 1999; Piatt and Springer, 2007; Sigler, 2011; Ortiz, 2012). While expert-derived qualitative divisions based large-scale oceanographic characteristics or published species–environment relationships are useful, environmental variables should be weighted proportional to their relative influence on biological patterns (Pitcher et al., 2012). Our analyses build on existing schemes to define biogeographical domains (ecoregions) that explicitly link environmental and biological data and identify statistically relevant breakpoints in biological community composition along distinct environmental gradients. We also highlight a method to project spatial shifts in these ecoregions as a function of dynamic physical variables, which fluctuate over time.

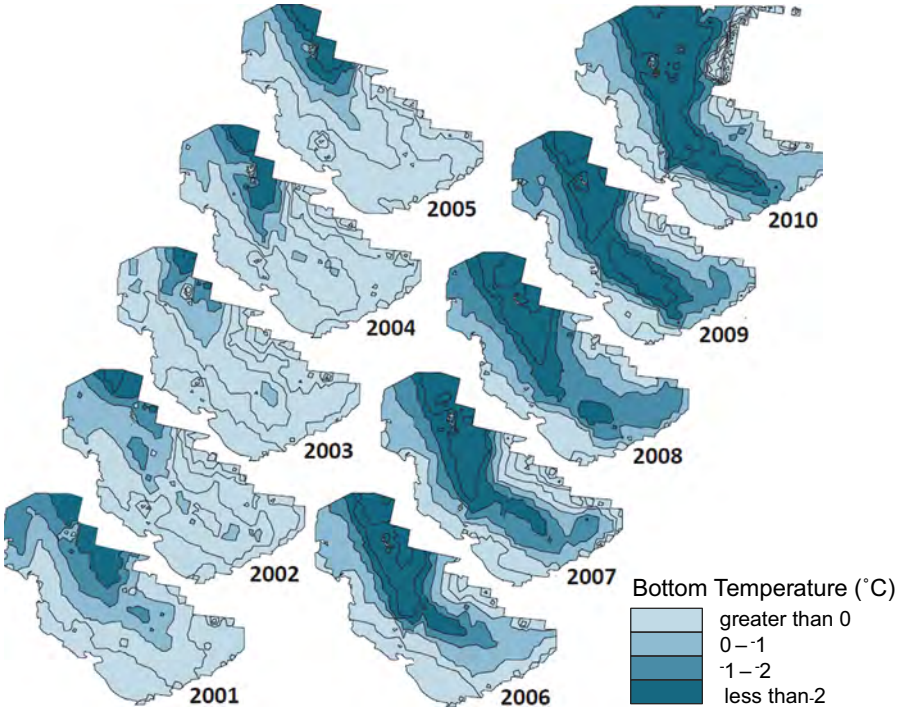

Fig. 2. Recent cold versus warm temperature regimes in the eastern Bering Sea. Maps of the cold pool extent (bottom temperature < 2 °C) are displayed for warm (2001–2005) and cold (2006–2010) years.

2. Materials and methods

2.1. Approach

Species distribution, abundance, and spatial patterns in community composition (or species turnover) are driven by multiple biological and physical factors, including threshold environmental tolerances and resource preferences, system connectivity, recruitment, climate shifts, and species interactions (McGlinn and Hurlbert, 2012). We apply the concept of turnover functions to delineate distinct ecoregions using random forest methods, specifically we: (1) quantify the extent to which environmental drivers (physical predictor variables) predict distribution patterns (biological abundance) for individual species; (2) assess the relative importance of predictor variables to species distributions; and (3) determine threshold values along the gradient of the predictor variable where species abundance shifts. To extend these methods to biological community assemblages, we then apply gradient forests to: (1) characterize the magnitude of change in the composition of biological communities along environmental predictor gradients and (2) identify critical values along the predictor gradients that correspond to threshold shifts in composition. A schematic of our overall approach is presented as a conceptual diagram in the appendix (Fig. A1)

We use random forest methods to recursively partition on species abundance, where splits are made at discrete values for a set of environmental predictor variables. The extent to which abundance shifts across partitions represents a metric for turnover in species abundance. By aggregating over species, weighting for relative predictor importance and goodness-of-fit for each species distribution model, we identify important environmental thresholds and produce functions that represent turnover in biological communities along each predictor gradient. Centroid-based clustering methods are then applied to partition the ecosystem into coherent spatial units (e.g. ecoregions) on the basis of distinct breakpoints in community composition. Finally, the persistence and inter-annual stability of ecoregion boundaries is evaluated. We use data across a time series of available bottom trawl surveys (1982–2012) to delineate ecoregions within the EBS LME and compare distinct temperature regimes within the time series (2000–2005, 2006–2011; Fig. 2).

2.2. Data

We used data collected by the Resource Assessment and Conservation Engineering (RACE) Division of the Alaska Fisheries Science Center, NOAA, which has conducted annual, standardized bottom trawl surveys since 1982 (Lauth, 2012). Each June–August, the EBS shelf (approximately 488,000 km^2) is systematically surveyed at depths ranging from 20 to 200 m. An 83–112 eastern otter trawl is deployed from chartered vessels at 376 standard stations in a sampling grid with 20×20 nautical mile cells (Fig. 1, top right). Species abundance data for each station were standardized to an index of catch per unit effort (CPUE), by dividing catch weight (kg) by area swept (ha), estimated as mean net width multiplied by distance towed (Alverson and Pereyra, 1969).

Depth, bottom temperature and surface temperature data were available for each tow and used to develop mean values per station across years. To further characterize temperature and hydrographic structure, we used data compiled from depth-temperature traces and digital bathythermograph recorders (BTR) attached to the headrope of the trawl net deployed in bottom trawl surveys (Buckley et al., 2009) to determine surface mixing and stratification within each depth-temperature profile. In the area of the shelf south of 60° N, temperature is the primary determinant of density (Stabeno et al., 1999; Stabeno et al., 2012a,b) and the most complete representation of physical structure of the water column (Kachel et al., 2002). Top layer depth (m) was calculated as the deepest of contiguous points within 1 °C of surface temperature. Bottom layer depth (m) was calculated as the shallowest of contiguous points within 1 °C of bottom temperature. Transition layer extent (m) was the difference between bottom layer and top layer depth. Mean, maximum, and minimum temperatures were calculated using data from all tows at a particular station. Thermocline depth was calculated as the depth of the maximum rate of decrease in temperature (as a function of increasing depth). The areal extent of the cold pool was calculated as the area (km^2) of bottom temperatures < 2 °C within the sampled shelf. The cold pool index is a standardized estimate of the fraction of the survey area covered by bottom water < 2 °C.

Sediments were assessed using the NOAA EBSSED database of surface sediments (Smith and McConnaughey, 1999), a compilation of historical (1934–1997) point-sample data ($N=2587$) from all available sources (Fig. 1, middle right). Data were used to develop standardized statistics characterizing grain size (phi, negative $\log_2$ diameter in mm), variation in grain size (sorting coefficient), percent composition by weight of various size grades (e.g. gravel, sand, mud, silt, clay), and a relative index of coarseness (percent sand and/or gravel). To link sediment type data to standardized trawl survey stations, we interpolated values using inverse distance weighting methods (Fig. 1, bottom right). We then related raster fields on sediment type to trawl stations via zonal statistics (ArcGIS v9.3).

2.3. Analytical methods

2.3.1. Assignment of species to functional group

Species were classified to functional groups on the basis of mean percent total weight of prey in the diet (http://access.afsc.noaa.gov/REEM/WebDietData/DietTableIntro.php). As per Garrison and Link (2000), we categorized fish as pelagic planktivores, benthivores, demersal piscivores, and pelagic piscivores based on pathway and content in the diet. Invertebrates were categorized by their use of habitat (Table 1). As per Mueter and Litzow (2008) arctic species were distinguished as those with > 50 percent total biomass in areas < 2 °C.

2.3.2. Criteria for inclusion of species in analyses

In most long-term bottom trawl surveys, there are discrepancies in precision of species identification over time. Some species aggregated to genus or family early in the time series are identified to species in later years. To ensure consistency over time we aggregated species to groups where necessary to ensure a common level of identification over time. To prevent errors in over-representing rare or inadequately sampled species, persistence plots were used to determine whether to include a given species or aggregated group in our analyses (Genner et al., 2004). The species ($n=126$) and aggregate groups ($n=57$) included in our analyses account for 99.89% of surveyed biomass in the EBS.

2.3.3. Contour plots of temperature and depth

To visualize how temperature and depth might shape the ecosystem, contour plots were developed. Contour plots of selected individual species were developed using mean weighted biomass (1982–2012).

2.3.4. Random forests

To assess importance of physical variables on individual species distributions, we applied random forest methods (package

Table 1
Functional guilds.

Planktivores
Pacific herring (*Clupea pallasi*), Arctic cod (*Boreogadus saida*), Saffron cod (*Eleginus gracilis*), Walleye pollock (*Gadus chalcogramma*), Eulachon (*Thaleichthys pacificus*), Capelin (*Mallotus villosus*), Rainbow smelt (*Osmerus mordax*), Prowfish (*Zaprora silenus*), Pacific ocean perch (*Sebastes alutus*), Dusky/dark rockfish (*Sebastes* spp.), Northern rockfish (*Sebastes polyspinis*), Yellow Irish lord (*Hemilepidotus jordani*), Butterfly sculpin (*Hemilepidotus papilio*)

Benthivores
Flathead sole (*Hippoglossoides elassodon*), Bering flounder (*Hippoglossoides robustus*), Rex sole (*Glyptocephalus zachirus*), Yellowfin sole (*Limanda aspera*), Longhead dab (*Limanda proboscidea*), Sakhalin sole (*Limanda sakhalinensis*), Starry flounder (*Platichthys stellatus*), Rock sole (*Lepidopsetta* spp.), Buttersole (*Isopsetta pleuronectes*), Alaska plaice (*Pleuronectes quadrituberculatus*), Sawback poacher (*Leptagonus frenatus*), Sturgeon poacher (*Podothecus accipenserinus*), Bering poacher (*Occella dodecaedron*), Searcher (*Bathymaster signatus*), *Gymnocanthus* sp., Threaded sculpin (*Gymnocanthus pistilliger*), Armorhead sculpin (*Gymnocanthus galeatus*), Spectacled sculpin (*Triglops scepticus*), Ribbed sculpin (*Triglops pingeli*), Spinyhead sculpin (*Dasycottus setiger*), Thorny sculpin (*Icelus spiniger*), Icelus species (*Icelus* spp.), Snailfish unident. (*Liparidae* spp.), Variegated snailfish (*Liparis gibbus*), Salmon snailfish (*Careproctus rastrinus*), Eelpoutt unident. (*Zoarcidae* spp.), Marbled eelpout (*Lycodes raridens*), Wattled eelpout (*Lycodes palearis*), Polar eelpout (*Lycodes turneri*), Shortfin eelpout (*Lycodes brevipes*)

Pelagic piscivores
Arrowtooth flounder (*Atheresthes stomias*), Kamchatka flounder (*Atheresthes evermanni*), Greenland turbot (*Reinhardtius hippoglossoides*), Pacific sleeper shark (*Somniosus pacificus*), Sablefish (*Anoplopoma fimbria*), Pacific sandfish (*Trichodon trichodon*), Chum salmon (*Oncorhynchus keta*)

Demersal piscivores
Pacific cod (*Gadus macrocephalus*), Alaska skate (*Bathyraja parmifera*), Pacific halibut (*Hippoglossus stenolepis*),Whitespotted greenling (*Hexagrammos stelleri*), Rougheye/Blackspotted rockfish, Bigmouth sculpin (*Hemitripterus bolini*), Bering wolffish (*Anarhichas orientalis*), Warty sculpin (*Myoxocephalus verrucosus*), Great sculpin (*Myoxocephalus polyacanthocephalus*), Plain sculpin (*Myoxocephalus jaok*)

Crab
Red King crab (*Paralithodes camtschaticus*), Blue king crab (*Paralithodes platypus*), Graceful decorator crab (*Oregonia gracilis*), Tanner crab (*Chionoecetes bairdi*), Circumboreal toad crab (*Hyas coarctatus*), Pacific lyre crab (*Hyas lyratus*), Snow crab (*Chionoecetes opilio*), Hybrid Tanner crab (*Chionoecetes* hybrid), Helmet crab (*Telmessus cheiragonus*), Hermit crab unident. (*Paguridae*), Sponge hermit (*Pagurus brandti*), Aleutian hermit (*Pagurus aleuticus*), Splendid hermit (*Labidochirus splendescens*), Knobbyhan hermit (*Pagurus confragosus*), Fuzzy hermit crab (*Pagurus trigonocheirus*), Alaskan hermit (*Pagurus ochotensis*), Longfinger hermit (*Pagurus rathbuni*), Hairy hermit crab (*Pagurus capillatus*)

Motile invertebrates
Seastars (15), Basket Star (*Gorgonocephalus eucnemis*), Brittlestars (3), Urchins (3), Common sand dollar (*Echinarachnus parma*), Sea cucumbers (2), Gastropods (26), Scyphozoa (5)

Benthic infauna
Clams (5), Blue mussel (*Mytilus* trossulus), Weathervane scallop (*Patinopecten caurinus*), Shrimp (4), Worms (6)

Sessile invertebrates
Anemones (9), Ascidians (9), Bryozoans (2), Corals (4), Sea Whips (2), Sponges (2)

randomForest, R Development Core Team 2011) to data on abundance (species biomass) at discrete sites (survey stations). Random forests (Breiman, 2001) are comprised of regression trees, where sample sites are partitioned into two groups such that species abundances at sites within each partition are as homogenous as possible. Partitioning occurs at a specific split value v for each predictor p (e.g. 0.2 °C for temperature), and at each partition, the split is selected to minimize impurity or the sum of squared deviations about the group mean. Partitions are recursively split until a partition becomes a terminal node. At each node in the tree, the importance of a split is measured as the reduction in impurity or the amount of variation explained by the partition.

A random forest aggregates results from an ensemble of regression trees to develop synthesized output with high classification accuracy, accounting for interactions among predictor variables (Liaw and Wiener, 2002; Cutler et al., 2007). Each tree is fit to an independent bootstrap sample of the data (resampling with replacement) and each partition within a tree is split on the best of a random subsample of the predictor variables. For each tree, data not selected in the bootstrap sample are termed the out-of-bag (OOB) data and used to provide a cross-validated estimate of generalization error. Random forests provide three relevant metrics: the goodness-of-fit R_s^2 for species s, the importance I_{sp} of each predictor p, and the raw importance value I_{spvt} for that predictor at each split value v in each tree t. Predictor importance I_{sp} quantifies the contribution of a predictor to the model goodness-of-fit by computing the prediction error of the model without the predictor and comparing it to the prediction error of the full model. Specifically, I_{sp} is estimated as the increase in OOB mean square prediction error when the predictor is randomly permuted while other variables in the model remain constant, effectively removing the predictor signal.

The goodness-of-fit R_s^2 (proportion of variance explained in a random forest) for species s is defined as

$$R_s^2 = 1 - \sum_i (X_{si} - \hat{X}_{si})^2 / (X_{si} - \overline{X}_s)^2 \quad (1)$$

where X_{si} is the ith abundance observation, $\hat{X}_{si}$ is the OOB prediction, and $\overline{X}_s$ is the mean abundance.

The goodness-of-fit R_s^2 for each random forest is partitioned among predictor variables in proportion to their importance I_{sp}, such that R_{sp}^2 (predictor p for species s) is calculated as

$$R_{sp}^2 = \frac{R_s^2 I_{sp}}{\sum_p I_{sp}} \quad (2)$$

The importance of a predictor variable for the entire biological community (R_p^2) is estimated by averaging R_{sp}^2 across all species, such that

$$R_p^2 = \frac{1}{N} \sum_s R_{sp}^2 \quad (3)$$

Correlation matrices were developed to examine multi-collinearity among environmental predictor variables (Figs. A2–A4). On this basis we removed minimum and maximum temperatures, as these closely mirrored top and bottom temperatures. To address correlations between remaining predictor variables, we applied a conditional permutation approach developed by Strobl et al. (2008), where values for each predictor were permuted only within data defined by splits on any other predictors that were correlated above a threshold of $r=0.5$ (Ellis et al., 2012).

2.3.5. Gradient forests

To establish where community composition changes occur along a given environmental gradient, we applied gradient forest

methods, which integrate results from individual random forest analyses over a suite of species. While random forest methods quantify the extent to which environmental variables predict species distribution patterns and the relative importance of each variable to the predictions, gradient forests quantify shifts in the composition of the aggregate biological community along environmental gradients and identify threshold values where important breakpoints occur. These methods develop flexible, non-parametric functions to quantify species turnover or threshold shifts in abundance for multiple species in response to physical predictors (R Package gradientForest, Ellis et al., 2012).

We developed a physical data matrix (sites-by-environment) and a log transformed biological abundance matrix (sites-by-species):

$$\log(y + \min(y, y > 0)) \quad (4)$$

where y is the abundance at the 334 survey stations and min $(y, y > 0)$ is the minimum positive abundance at each station.

Estimates of turnover in community composition along the gradient of each physical predictor p were generated by distributing R^2 values from all species among predictors in proportion to predictor importance I_{sp} and along the gradient of values for each predictor according to the density of raw importance values I_{spvt}. In random forests, the importance associated with a split value along a predictor gradient indicates the relative change in species abundance. Therefore, species turnover is reflected in split importance. For each predictor p, the split values v and importance values at each split I_{spvt} were assembled from every tree in random forests for each species s. For each species, importance values I_{spvt} were standardized by the density of observed values for each predictor p and normalized to sum to R^2_{sp}. Individual species turnover $F_{sp}(x)$ along a predictor gradient was defined as a monotonic function with minimum 0 and maximum R^2_{sp}, proportional to the importance of splits. This allowed us to depict cumulative shifts in species abundance along each predictor gradient and estimate the importance for any given predictor value x. Community composition turnover $F_p(x)$ or shifts in the assemblage of aggregate biological communities along each predictor variable was estimated as mean $F_{sp}(x)$ over all species (Pitcher et al., 2012). The derivative $f_p(x)$ of $F_p(x)$ is the compositional turnover rate at any given predictor value (Ellis et al., 2012). F_p provides a means to transform each physical predictor to biological units reflecting turnover in community composition. By applying this function to each predictor in sequence, we developed a spatial map of inferred biological community composition on the basis of multi-dimensional environmental data.

2.3.6. Ordination and projection of survey stations according to biological composition

Using cumulative functions to transform grid data layers of environmental data into a common biological scale, we applied F_p to quantify community responses along predictors. By taking the principle components of the transformed data we used ordination to represent the data as a biplot of survey stations where coordinate position represents different patterns in species composition, as associated with the predictors. The environmental variables were superimposed on this plot as vectors indicating the direction and magnitude of the most important environmental predictors.

2.3.7. Cluster analyses of sampling sites to delineate distinct ecoregions

We applied centroid-based approaches (partitioning around medoids, PAM, R package cluster; Kaufman and Rousseau, 1990) to identify survey stations that exhibited similar patterns in biological community composition on the basis of gradient forest output. We clustered stations in a manner that minimized the sum of dissimilarities. These clusters were used to define distinct ecoregions.

3. Results

3.1. Contour plots of species distribution by temperature and depth

The influence of the cold pool in the middle domain (50–100 m) is clearly evident in contour plot of the surveyed area (Fig. 3). Contour plots of select individual species also suggest the cold pool shapes and constrains species distributions (Fig. 3). Certain species (e.g. demersal piscivores, Pacific cod, Pacific halibut) appear to range across temperature and depth gradients, whereas other (e.g. pelagic piscivores, arrowtooth flounder, Greenland turbot) appear largely constrained by depth and temperature gradients. There are also important differences by age and life stage as demonstrated by walleye pollock (*Gadus chalcogramma*).

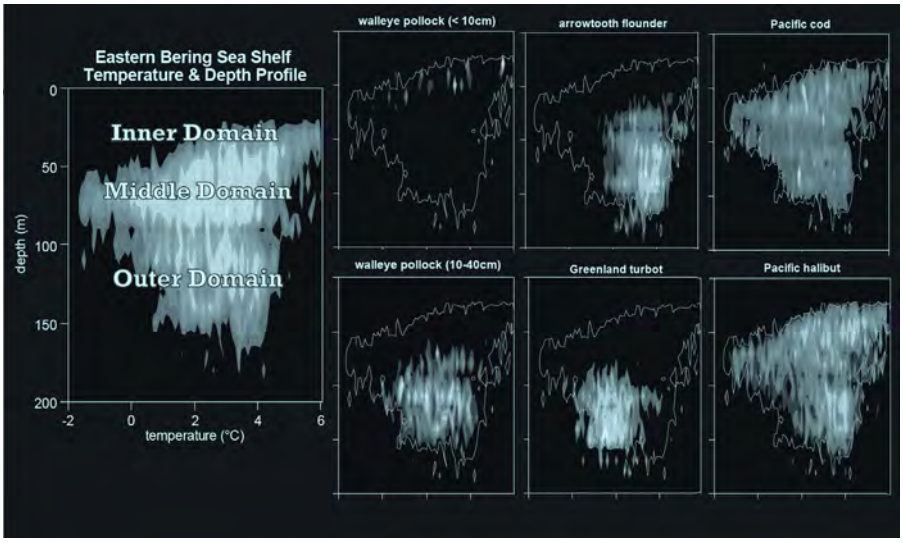

Fig. 3. Contour plots of relative species density (biomass) according to bottom temperature and depth (lighter areas indicate higher densities). A contour plot of the entire system outlines the three main domains of the eastern Bering Sea shelf (left). Distributions for select individual species are shown with an outline of the system-wide footprint superimposed on each species graph for reference.

Table 2
Model performance by species, R_s^2.

Functional guild	No. species	Mean R_s^2 (range)
Pelagic piscivore	7	0.77 (0.68–0.92)
Benthivore	34	0.70 (0.27–0.91)
Crab	18	0.69 (0.19–0.88)
Planktivore	13	0.68 (0.23–0.87)
Demersal piscivore	10	0.65 (0.44–0.85)
Motile invertebrates	56	0.55 (0.08–0.93)
Benthic infauna	17	0.49 (0.14–0.80)

3.2. Overall model performance and relative fit for individual species

Random forests tended to provide a better fit (Table 2) to species that had a strong response to dynamic predictor variables such as temperature. The most prevalent species also tended to drive observed patterns, such that the relationship between log species abundance and R_s^2 was significant ($R^2=0.27$, $P=0.024$). Overall, performance of random forests (R_s^2) was higher for upper trophic level species (fish, $R^2=0.68\pm0.20$ SE, $N=55$; in contrast to invertebrates, $R^2=0.55\pm0.21$, $N=135$). Distributions for pelagic piscivores ($R^2=0.82\pm0.04$, $N=5$) and benthic flat fish ($R^2=0.81\pm0.15$, $N=10$) were particularly well fit, reflecting relatively defined distributions that shift in extent and range over time in response to dynamic environmental variables, such as temperature. Demersal piscivores ($R^2=0.65\pm0.04$, $N=11$) and planktivorous forage fish ($R^2=0.56\pm0.08$, $N=13$) were not fit as well, reflecting broad habitat ranges, use of diverse prey resources, and relative insensitivity to dynamic environmental variables in the former, and highly variable patterns and poor sampling efficiency in the latter. As expected, the fit to distributions of motile invertebrates (crabs, $R^2=0.69\pm0.04$, $N=22$; gastropods, $R^2=0.59\pm0.03$, $N=27$; seastars and sea cucumbers, $R^2=0.55\pm0.06$, $N=20$; urchins, $R^2=0.48\pm0.06$, $N=3$; brittle and basket stars, $R^2=0.43\pm0.10$, $N=4$) reflected higher sensitivity to dynamic environmental variables than sessile invertebrates and benthic infauna (ascidians, $R^2=0.56\pm0.09$, $N=10$; corals and sea whips, $R^2=0.48\pm0.12$, $N=5$; bryozoans, $R^2=0.46\pm0.04$, $N=2$; anemones, $R^2=0.42\pm0.05$, $N=9$; sponges, $R^2=0.36\pm0.18$, $N=2$; worms, $R^2=0.58\pm0.08$, $N=5$; bivalves, $R^2=0.44\pm0.08$, $N=7$), suggesting sessile invertebrates may provide a good proxy for static habitat attributes, such as depth and substrate.

3.3. Cumulative importance of predictor variables for species and functional guilds

Cumulative plots display thresholds in species abundance and distribution to environmental factors (Fig. 4). Among benthivores, the ranges of individual species are distinguished from others in the guild by depth gradients (with a notable breakpoint at 100m) and by bottom temperatures (with notable breakpoints at −1 °C, 2 °C, 4 °C, and 6 °C). Rock sole species (*Lepidopsetta polyxystra*, *Lepidopsetta bilineata*) are also distinguished in associating with coarser substrates. Most demersal piscivores are generalists, ranging widely across depth gradients, temperatures and substrates, though Pacific halibut (*Hippoglossus stenolepis*) and skates (*Rajidae* spp.) demonstrate sensitivity to substrate coarseness and sculpins (*Myoxocephalus* spp.) to bottom temperature and depth. Among pelagic piscivores, individual species are largely distinguished by temperature gradients. Among planktivores, individual species are largely distinguished by bottom depth and mid-layer extent stratification, though most species are also sensitive to temperature.

3.4. Relative importance of predictor variables and important breakpoints along predictor gradients

Binned outputs from random forests on the location and importance of regression tree splits for species abundance on each environmental predictor gradient are depicted (Fig. 5). Breakpoints in biological communities and threshold shifts in the abundance of multiple species along a given physical gradients are identified at peak values (ratios >1) in the density plot of the splits standardized by the observations (Fig. 5). For kernel density plots of the splits and observations separately, see Figs. A5 and A6. Important breakpoints in aggregate community composition are noted at latitude (57°N, 60.5°N), longitude (−164°W, −168°W, −173°W), surface temperature (5.5 °C, 7.4 °C, 8.4 °C), bottom temperature (−1–0 °C, 1–2 °C, 3.5 °C), depth (40 m, 80 m, 100 m), and at four separate grades of substrate coarseness. Based on the eigenvalue or latent root, depth was the strongest explanatory physical predictor, followed sequentially by latitude, bottom temperature, longitude, range of temperature within the water column, bottom layer depth, surface temperature, mid-layer extent, and substrate coarseness and composition (R_p^2, Fig. 6, left).

3.5. Bioplot of species distribution and orientation of biological communities according to environmental predictors

Shifts in biological community composition along predictor gradients via cumulative functions were used to transform environmental data layers into biological scales. We present the transformed multi-dimensional biological space as a product of ordination (Table A1) presenting the first two dimensions (principle components) as a biplot (Fig. 6). The first two principle components account for 63% of total variance. Coordinate position represents inferred biological community compositions, as associated with the physical predictors variables (represented as vectors). To examine how individual species distribute across the system, we superimpose the weighted mean location of select species (Fig. 7). Planktivore species (Fig. 7, panel 1) range mostly in shallow areas; individual species within the guild vary by surface temperature, bottom temperature, temperature range and stratification. Pelagic piscivores (Fig. 7, panel 2) are generally found at depth and vary within the guild by temperature. Demersal piscivores (Fig. 7, panel 3) are relatively evenly spread across various physical predictor gradients. Benthivores (Fig. 7, panel 4) also range over most physical variables, but distinctions between species within the guild are noted according to depth, bottom temperature, and substrate coarseness. Snow (*Chionoecetes opilio*) and Tanner (*Chionoecetes bairdi*) crab distributions contrast by bottom temperature (Fig. 7, panel 5), whereas blue (*Paralithodes platypus*) and red (*P. camtschaticus*) king crab, as well as echinoderm taxa (Fig. 7, panels 6 and 7, plot 6) are distinguished by a combination of bottom temperature, substrate and depth. Sessile invertebrates (Fig. 7, panels 8 and 9), benthic infauna (Fig. 7, panel 9, plots 4 and 5), and bivalves (Fig. 7, panel 7, plots 1–3) are almost exclusively distinguished by substrate coarseness, sediment type, and depth and may therefore serve as viable proxies for static habitat features.

3.6. Delineation of EBS ecoregions

Using clustering (PAM) to aggregate survey stations based on similar community composition (Fig. 8), we define six distinct ecoregions within the EBS shelf (Table 3 and Fig. 9). We noted distinct trends moving from the inner to outer shelf and distinctions between latitudes at ~60°N. Across the time series, the inner shelf represents a consistent ecological region and a distinct region

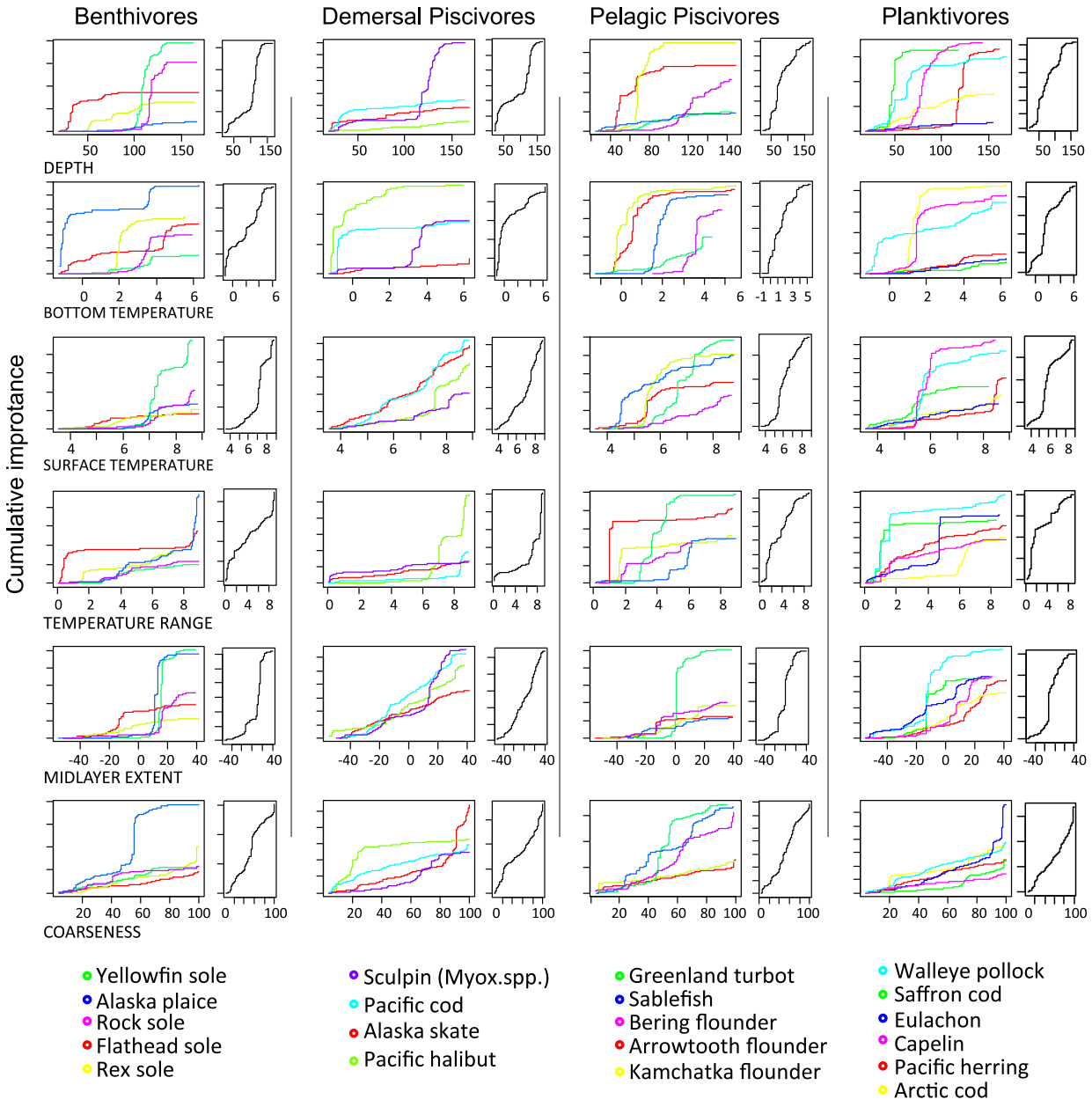

Fig. 4. Cumulative importance plots display cumulative shift (in R^2 units) of species abundance across the gradient of select environmental predictors. The common scale allows for the direct comparison of multiple species within each functional guild. Plots (colored, left) display prominent species from benthivore, pelagic planktivore, demersal piscivore and pelagic piscivore guilds. Plots (grayscale, right) display the aggregate response for each functional guild to a given environmental predictor. (For interpretation of the references to color in this figure caption, the reader is referred to the web version of this paper.)

is also identified along the outer shelf or slope. Within the middle domain and at island complexes, complex dynamics are observed, reflecting the dynamic nature of the environmental conditions and complex cross-shelf processes within these areas.

3.7. *Attributes of EBS ecoregions: physical structure and biological community*

Attributes of the individual ecoregions are summarized (Table 4). The inner shelf has an extensive spread along coastal areas with relatively warm and stable water temperatures and coarse substrates. The biological community in this ecoregion has relatively high concentrations of forage fishes, sessile invertebrates, and red king crab, with the notable absence of arctic species and pelagic piscivores (Fig. A7i and ii). A middle–inner domain spans relatively shallow depths between 40 and 70 m with relatively cold water temperatures and a broad range of species in the system with the notable exception of deepwater species (Fig. A7i and ii). A Southern domain spans the lower latitudes with moderate temperatures, fluctuating stratification patterns, and high substrate coarseness. This area has a relatively diverse assemblage of species (Fig. A7i and ii). A Northern domain occupies higher latitudes with the coldest water temperatures. This is the primary area for arctic species and capelin, corals, and blue king crab (Fig. A7i and ii); deep and warm water species are largely absent. A middle–outer domain encompasses consistently deep waters along an extensive latitudinal gradient with high variation in water temperatures and low substrate coarseness. This region contains high concentrations of both pelagic and demersal piscivores, echinoderms, and crab, but low abundance of sessile invertebrates (Fig. A7i and ii). The Shelf Break spans the entire shelf-slope interface and contains the

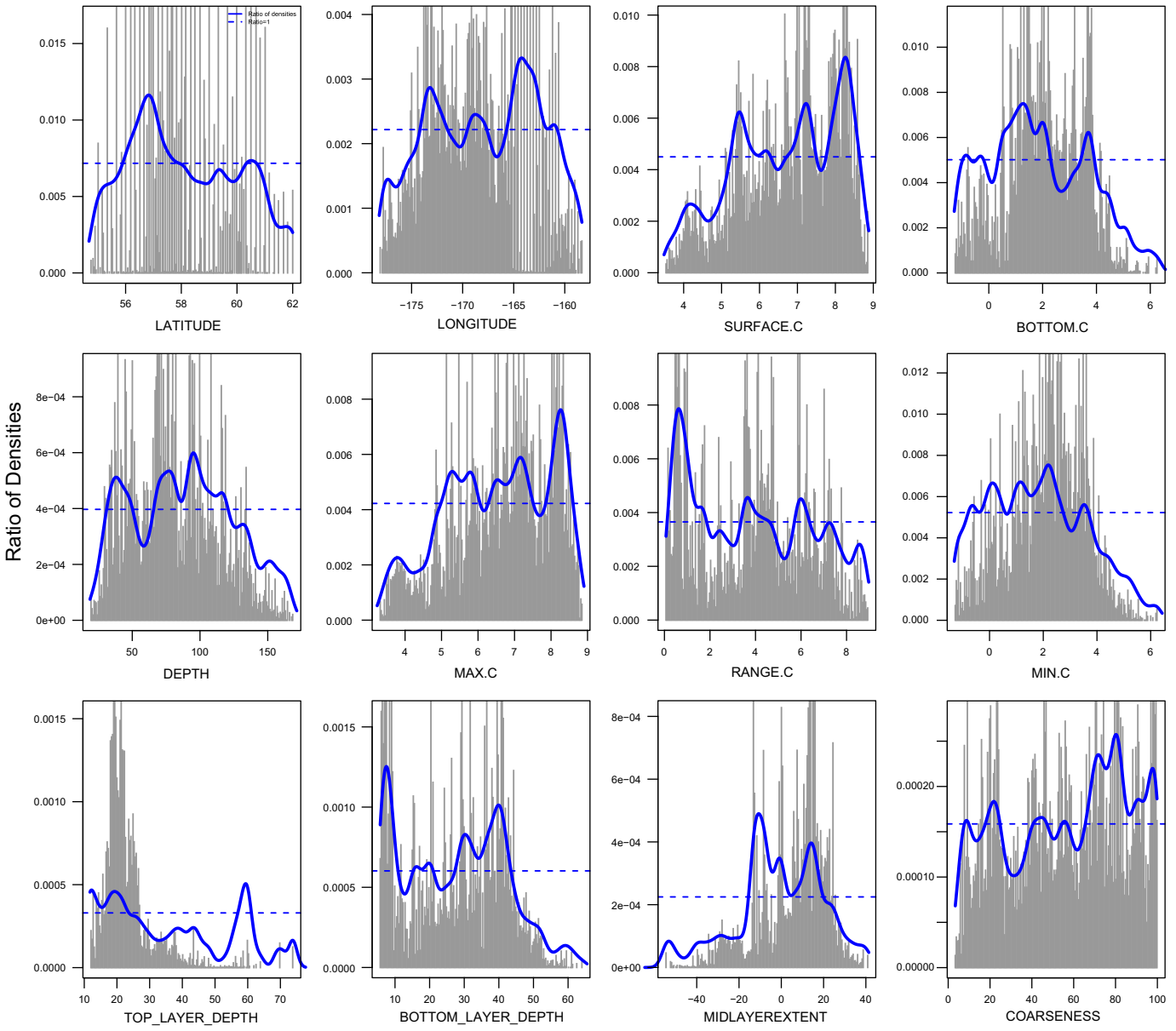

Fig. 5. Plots indicate threshold shifts in the abundance of multiple species along the gradient of a given environmental predictor, reflecting a rate of change in composition of the aggregate biological community. The gray histograms display the binned raw importance of splits from random forests for individual species relative to the environmental predictor variable on the horizontal axis. Density plots (lines) illustrate the estimated importance $f_p(x)$ or community turnover rate at any given predictor value, which is estimated as the ratio of the density of split importance (density of split values weighted by importance) to the density of observed predictor values along the predictor gradient. The horizontal dashed line indicates where the ratio is 1. Ratios >1 indicate locations of relatively greater change in community composition, such that peaks in the density plot indicate threshold values for each environmental predictor where community composition is expected to shift.

deepest areas as well as the widest range of depths in the system; temperatures are relatively stable. The Shelf Break is the exclusive habitat for some deepwater species and supports relatively high abundance of pelagic piscivore species. There is a notable absence of arctic species and low abundance of forage fishes and benthic flatfishes (Fig. A7i and ii).

3.8. *Climate fluctuations: evaluating the stability of ecoregion boundaries*

Results from gradient forests analyses of warm (2001–2005) and cold (2006–2010) periods were similar to each other (Figs. 9 and 10) and to results that integrated over the entire time series (Fig. 6). This suggests relatively stable structuring of the system over time. Still, there were important differences, mainly that the Northern domain extends southward in cold years and retracts northward in warm years. The expansion of the Northern domain seems to represent a constraint to subarctic species, but not an explicit benefit to arctic species, given the relationship between species abundance and cold pool extent (Fig. A8). Similar though non-significant trends were noted in indices for mean water column temperature, thermocline, and cold pool index (Fig. A8).

4. Discussion

We present a detailed overview of selected physical drivers influencing individual species distributions within the EBS and illustrate an approach to integrate biological and physical data to delineate ecoregions using statistical and geospatial analyses of biological community composition and physical habitat. Identifying ecologically significant units within LMEs is a necessary

and important step in defining units for spatial management and ecosystem approaches to management. Community ecology (which focuses on species diversity) and ecosystem ecology (which focuses on the physical processes that structure interactions) both offer insight into the ordering of complex ecosystems. Merging these perspectives is critical to holistic understanding of ecosystem functioning (Loreau, 2010).

4.1. Delineation and application of ecoregions

One element identified as an essential component of ecosystem-based approaches to fishery management is spatial resolution (National Marine Fisheries Service, 2000). This requires understanding population dynamic processes, species movement over time and space, stock structure, and habitat within a spatial

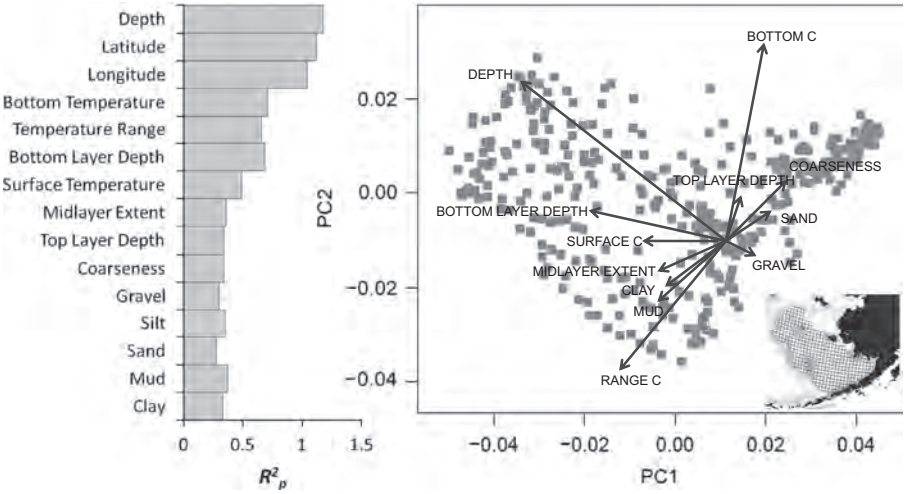

Fig. 6. Bar plot (left) of relative importance of environmental predictor variables weighted across species outputs (R^2_{sp}), where temperature is indicated as °C. Biplot of survey stations (right), where each individual point represents a sample station in the standard EBS bottom trawl survey. Coordinate position represents inferred community composition patterns, displayed as a biplot of the two principle components with all environmental variables used in the analysis displayed as vectors. Map of survey stations is provided as a reference (inset).

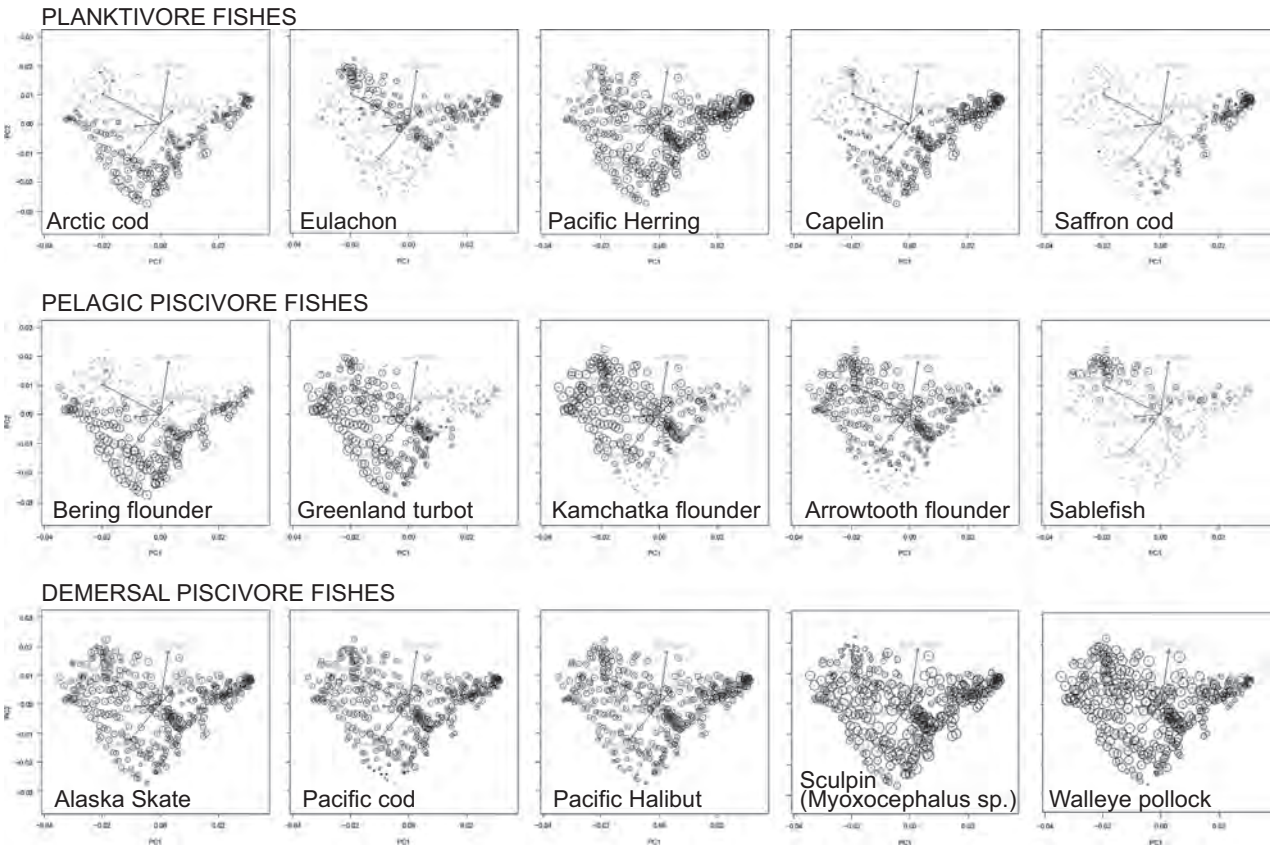

Fig. 7. Biplot of survey stations and environmental predictor vectors overlaid with weighted species abundance per station. Results demonstrate how individual species respond to multiple environmental variables and how individual species distributions compare to the system as a whole. Species are organized by function guild according to row. Note that invertebrates are integrated in random and gradient forest analyses as individual species, but aggregated in this figure to generalize trends. Trends for individual species within an aggregate group may differ.

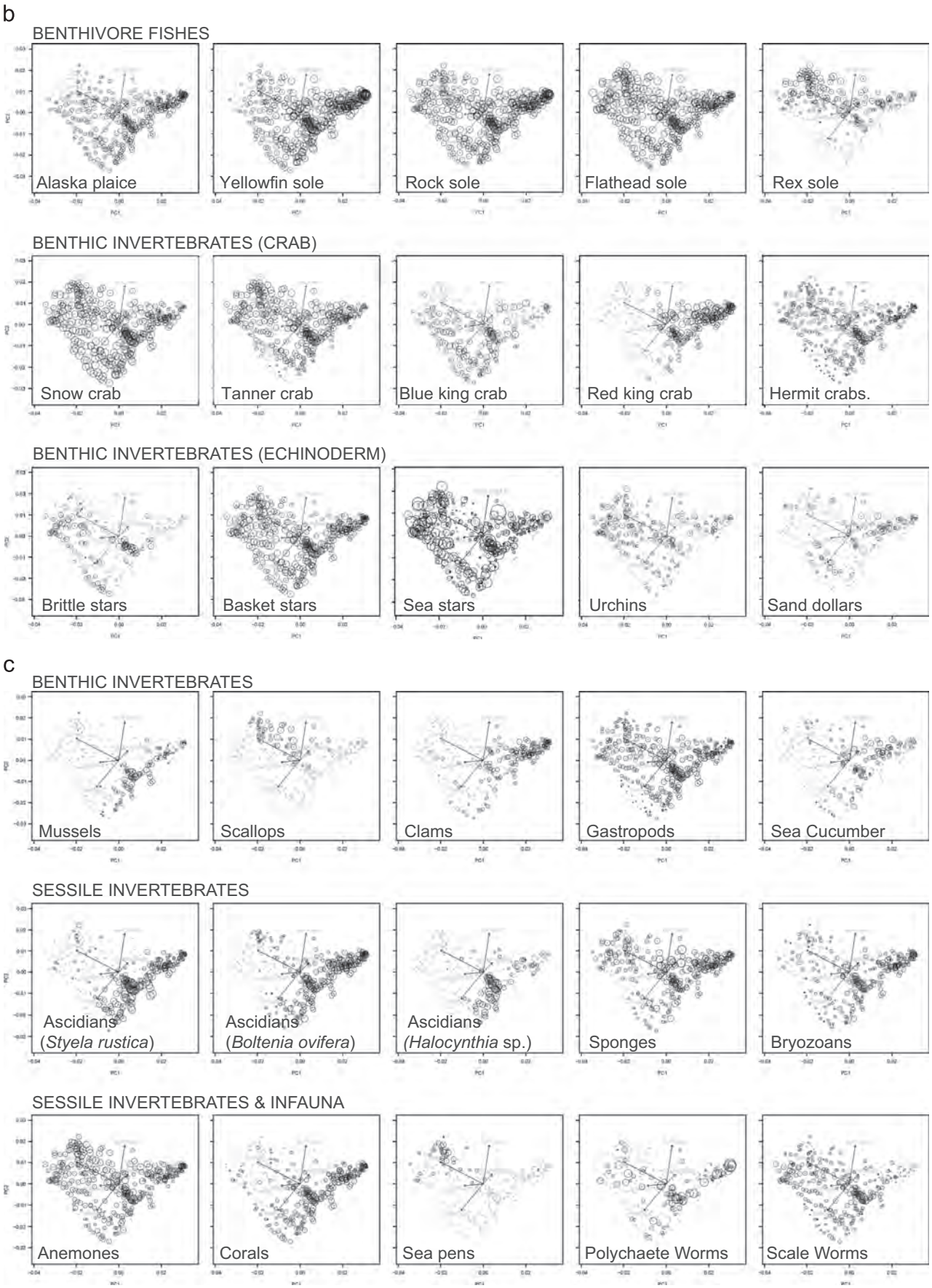

Fig. 7. (*continued*)

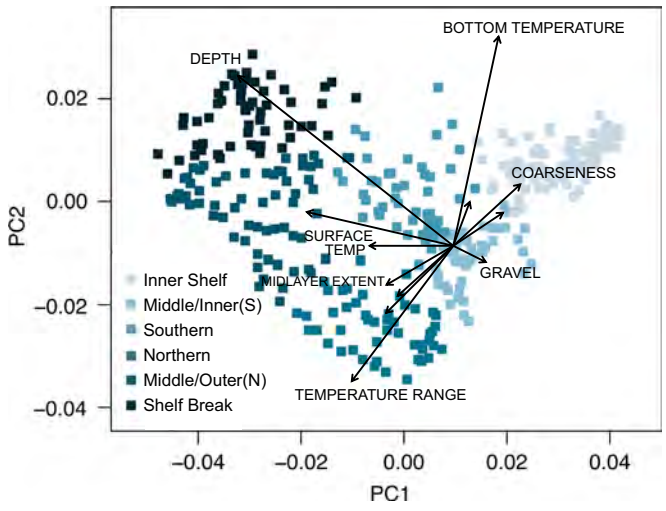

Fig. 8. Biplot of inferred community composition displays the results of the clustering (PAM) of survey stations, such that individual stations are grouped according to similarity in physical attributes (according to their relative position along the suite of environmental predictor vectors) and inferred species assemblages (species weighting associated with those vectors).

Table 3
Dissimilarity index for separation of survey stations into ecoregions. Isolation indicates relative distinctness between regions (the Northern region is most distinct).

Ecoregion	No. stations	Maximum dissimilarity	Mean dsissimilarity	Isolation
(1) Inner shelf	101	0.023	0.010	0.900
(2) Middle/inner (south)	48	0.019	0.009	0.965
(3) Southern	59	0.022	0.010	1.155
(4) Northern	50	0.027	0.011	2.057
(5) Middle/outer (north)	64	0.020	0.012	1.035
(6) Shelf break	54	0.018	0.009	0.949

context. The concept of ecoregions is useful in identifying key biological features and ecological processes that define unique areas and govern their dynamics (Piatt and Springer, 2007). Our results delineate regional habitats within the EBS LME on the basis of distinct ecological attributes. These outputs are intended to inform habitat assessment and valuation, inform analyses of potential interactions in multispecies models, and set the framework to better integrate spatially discrete environmental effects and species interactions into stock assessments.

4.2. Physical drivers and cross-shelf transport via wind advection

Several key drivers and forcing mechanisms structure the EBS shelf. Depth is a critical defining feature. While not necessarily the primary driver of species distributions, depth is often a convenient predictor (Levin and Dayton, 2009). Temperature is another critical predictor of species distribution in the EBS. Critical processes regulated by temperature control and thermal tolerance include survival and reproduction (Hutchins, 1947). Stratification within the water column also creates distinct environmental conditions and barriers to movement and was an important factor in our analysis. There is less consensus on the relative importance of physical features such as sediment (Levin and Dayton, 2009). While our analysis found sediment to have low relative influence on species distributions, in a broad shallow shelf system dominated by benthic and demersal pathways, sediment data may be informative; properties such as hardness, porosity, permeability, and displacement (none of which were examined here) influence the presence of fixed benthic invertebrates, prey availability, and predatory interactions.

Results of our analysis identified unique dynamics at island groups and distinct breakpoints between ecoregions along frontal boundaries. This suggests patterns consistent with studies of oceanographic processes that have revealed complex geostrophic currents at the Pribilof Islands and St Matthews Island (Stabeno et al., 2008) and the importance of frontal regions in concentrating prey resources (Lang et al., 2000; Coyle and Pinchuk, 2002; Stabeno et al., 2012a,b). We also noted cross-shelf patterns in the middle domain, possibly explained by wind-forced vectors that drive advection of nutrients and recruitment in this dynamic area. Circulation patterns in shelf flow alternate largely on the basis of wind direction, with northwesterly winds promoting off-shore transport and less frequent southeasterly winds associated with on-shelf transport across the shelf break (Danielson et al., 2012). Incorporating salinity data into future analyses (where available) may be instructive. In contrast to temperature gradients, which are predominantly along-isobath, salinity gradients are generally oriented cross-isobath (Danielson et al., 2011). Cross-isobath exchange has implications for both macronutrient (Whiteledge and Luchin, 1999) and micronutrient (Aguilar-Islas et al., 2007) transport and availability (Wespestad et al., 2000).

4.3. Comparison of EBS ecoregions to past biogeographic analyses of the system

Piatt and Springer (2007) define an ecoregion as an area distinguished from adjacent areas according to physiographic attributes (e.g. coastal, continental shelf, slope, basin) and bounded according to oceanographic processes (e.g. frontal boundaries and currents). Our results (arrived at through alternate means) reflect these attributes. Our delineation of ecoregions correspond to patterns recognized by previous classification schemes, which have divided the EBS along depth domains and latitudinal gradients. As in the previous studies (Stabeno et al., 2008; Hollowed et al., 2011; Ortiz, 2012), we also note unique patterns at canyons and island groups, related to recirculation patterns and topographic irregularities that create persistent oceanographic features and environments that support distinct fauna.

Integrating expert knowledge and previously established survey strata and ecological domains, Ortiz (2012) used the overarching structure of the conventional domains and applied regularly-spaced divisions along a North-South axis, designating several latitudinal divisions. Our analyses distinguishes only one (at approximately 60°N), which marks the approximate location of March minimum ice extent and corresponds to patterns in cross-shelf flow noted by Kinney et al. (2009) and Hollowed et al. (2012). Our analysis of discrete warm and cold phases, demonstrates how this boundary may shift based on climate and ice extent, such that the expansion of a Northern ecoregion is roughly associated with the extent of the cold pool. A workshop convened by the Nature Conservancy and World Wildlife Federation to distinguish biological features and ecological processes in the Bering Sea (Banks et al., 1999) identified four unique areas: (i) Bristol Bay; (ii) the Yukon-Kuskokwim Delta and Nunivak Island; (iii) the Golden triangle (bounded by Bogoslof Island, the Priblof Islands, and Izembek Lagoon); and (iv) the Bering Sea Shelf Break. The Inner, Southern and Shelf Break ecoregions defined in our analysis closely match the Bristol Bay, Golden Triangle and Bering Sea Shelf Break, respectively. Our Southern ecoregion is distinguished by physical processes such as tidal mixing, eddies and currents, which contribute to high levels of primary and secondary production. Our Shelf Break ecoregion is defined by the Bering Slope

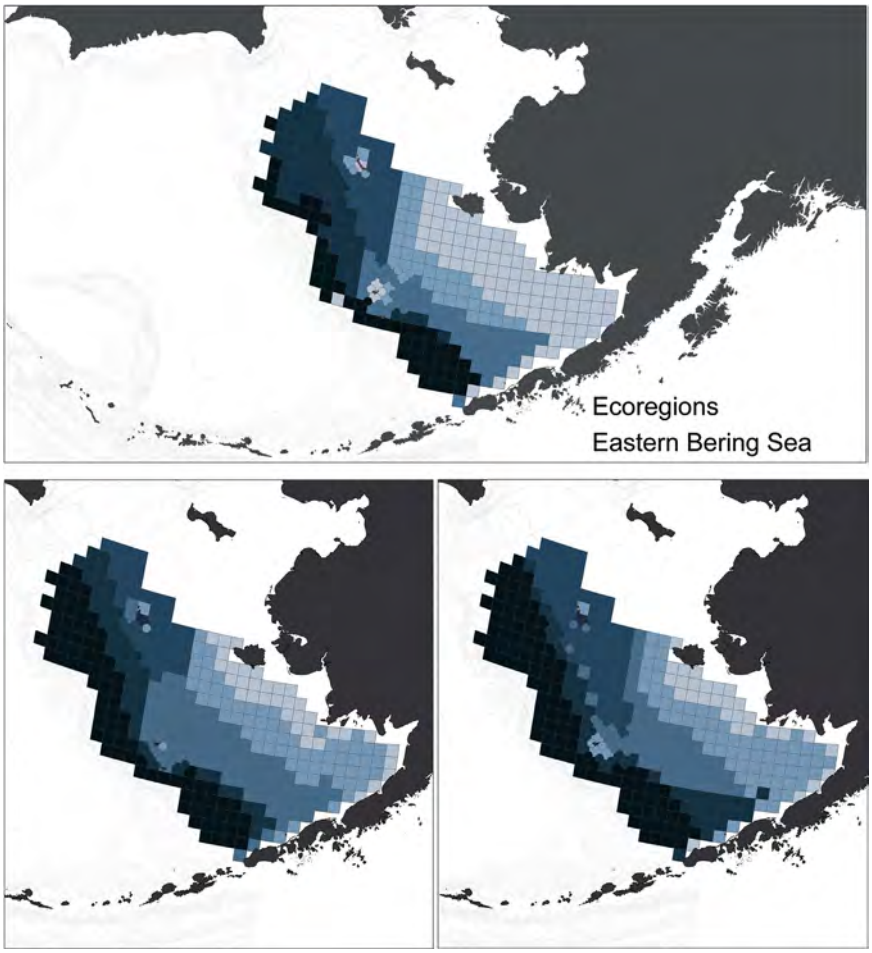

Fig. 9. Delineation of ecoregions based on the clustering of survey stations to represent distinct biological communities. Ecoregions are displayed for the entire time series (top graph) as well as for recent warm (2001–2005, bottom left) and cold (2006–2010, bottom right) years.

Current and marks the transition between basin and shelf dynamics, serving as a thermal refuge and area of enhanced biological productivity.

In general, our results support the conventional separation of the shelf according to major oceanographic boundaries, such as fronts associated with the 50 m and 100 m isobaths (Coachman, 1986), the Alaska Coastal Current, Bering Slope current, and circulation patterns in the southwestern Bering Sea (Stabeno et al., 1999). These domains are defined by relatively persistent bottom topography and current flow. However, we also recognize complex patterns in the inner and middle shelf, driven by a combination of substrate, temperature, and cross-shelf wind and geostrophic velocity vectors representing thermohaline circulation. While flow is generally along traditional frontal boundaries, advective corridors can transect the 100 m outer front and disrupt middle domain coherence, such that flow crosses from the outer to middle domain north of the Priblof Islands and continues towards northeast towards St. Matthew Island (Hollowed et al., 2012). This cross-shelf flow corresponds with the proximate outline of our latitudinal divide between northern and southern ecoregions and may explain shifting patterns in ecoregion boundaries in the middle domains between distinct time periods (Fig. 9). On the inner shelf, south of the Priblofs and landward of the 50 m isobaths, thermohaline flow is weak with areas of recirculation (Hollowed et al., 2012). This may explain the results of our composite analysis (across all years), which characterize the Inner Shelf as one large ecoregion. Conversely, shifts in the strength of thermohaline dynamics and recirculation patterns in distinct cold and warm periods may explain why our analyses on shorter time frames (cold and warm phases) characterize this area as two distinct ecoregions (Fig. 9).

4.4. Strength of approach

Recent species-specific analyses of how environmentally driven shifts (Spencer, 2008; Kotwicki and Lauth, 2013) and bioclimatic windows (Cheung et al., 2008) drive patterns in spatial distribution have provided important insights to marine ecology in the context of climate variability and change. Comprehensive analyses examining broad-scale community metrics, particularly in the Northwest Atlantic (Fogarty and Keith, 2009, Zwanenburg et al., 2010; Pepin et al., 2010) have also better informed our understanding of marine systems. Pepin et al. (2010) note that the use of variables such as biomass, diversity, and richness often aggregate areas that differ fundamentally in taxonomic diversity and in the functional communities represented in these areas. Our analyses address this by incorporating community composition within our approach to regional partitioning. With regard to the EBS, Piatt and Springer (2007) note that across-shelf boundaries are conspicuous and defined by persistent fronts or topographic gradients, whereas along shelf boundaries are more subtle and may be better resolved by patterns in biological characteristics. By integrating biological and physical data, we provide a more nuanced view of regional scale patterns.

Although we are able to integrate across a relatively extensive time series of data, we only have a snapshot of spring/summer

Table 4
Ecoregion characteristics.

Ecoregion	Latitude	Depth	Temperature	Stratification	Substrate
Physical characteristics					
Inner shelf	Extensive spread across latitude (55–60°N) and longitude (−158 to −170°W)	Shallow (range: 19–69 m) (mean = 42 ± 12 m SD)	Stable temperatures Relatively cold surface (5 ± 1 °C) and warm bottom (3 ± 1 °C) temperatures. Narrow range in min/max values (2–7 °C) and low variation within the water column (1 °C)	Extensive top layer depth extending mostly to seafloor	Coarse (mean = 80 ± 21%) Substrate entirely sand and gravel
Middle/ inner (south)	Middle latitudes (57–61°N)	Relatively shallow Consistent depths (range: 41–69 m) (mean = 61 ± 7 m SD)	Relatively cold surface 96 ± 1 °C) and bottom (1 ± 0 °C) temperatures. Considerable range in min/ max values (0–7 °C), and some variation within the water column (4 °C)	Extensive stratification (top layer depth 19 ± 3 m, bottom layer depth 22 ± 3 m) with minimal middle layer (3 ± 5 m)	Relatively coarse (mean = 56 ± 16%). Substrate largely sand with areas of mud and silt
Southern	Low latitude (55–58°N)	Mid-range (range: 67–96 m) (mean = 79 ± 8 m SD)	Moderate surface (7 ± 1 °C) and bottom (2 ± 1°C) temperatures Moderate range in min/ max values (2–8 °C), and some variation within the water column (4 °C)	Minimal, but variable middle layer (6 ± 12) (top layer depth 23 ± 8, bottom layer depth 29 ± 6)	Relatively coarse (mean = 68 ± 19%). Sand with extensive areas of mud and silt
Northern	High latitude (58–62°N)	Mid-range (range: 58–94 m) (mean = 75 ± 10 m SD)	Coldest bottom temperatures Warm surface (7 + 0 °C) and cold bottom (0 + 1 °C) temperatures Wide range in min/max values (0–9°C), and extensive variation within the water column	Even partition of water column (top layer depth 17 ± 2 m, bottom layer depth 32 ± 5 m, middle layer 15 ± 4 m)	Low coarseness (mean = 27 ± 15%). Substrate largely mud with areas of silt and clay
Middle/ outer (north)	High latitude (56–62°N)	Consistently deep (range: 94–148 m) (mean = 114 ± 15 m SD)	Moderate range temperatures (surface 8 ± 0 °C, bottom 2 ± 1 °C) Wide range in min/max values (−1–8 °C), and extensive variation within the water column (7 °C)	Highly stratified (top layer depth 21 ± 2 m, bottom layer depth 45 ± 5 m) with extensive middle layer 24 ± 6 m)	Low coarseness (mean = 23 ± 15%). Substrate mud, silt, and clay
Shelf break	Extensive spread across latitude (51–61°N)	Deep Wide range of depth, including deepest and shallowest areas sampled (range: 12–171 m) (mean = 131 ± 43 m SD)	Stable temperatures Relatively warm surface (8 °C) and bottom (4 °C) temperatures Moderate range in min/ max values (1–9 °C), and some variation within the water (4 °C)	Highly variable water column (top layer depth 28 ± 10 m, mid-layer depth 19 ± 24 m, bottom layer depth 47 ± 19 m)	Moderately coarse (mean = 48 ± 21) with high variation (3–100). Substrate equal mud, silt, sand
Biological characteristics					
Inner shelf	Relatively high concentrations of forage fish (saffron cod, capelin, eulachon, herring) and flat fish (yellowfin sole, Alaska plaice, rock sole). Arctic species (eelpout, snailfish) and pelagic piscivores (arrowtooth flounder, Kamchatka flounder, Greenland turbot) are absent. High abundance of fixed sessile invertebrates (e.g. ascidian, bryozoans, sponges, tube worms), sea cumber and red king crab				
Middle/inner (south)	Relatively uniform representation of fish species, with lower relative abundance of warm and deepwater species (e.g. rex sole, eulachon, sablefish, Kamchatka and arrowtooth founder, rockfish), demersal piscivore (e.g. Pacific halibut, Pacific cod, skates) and flat fish species (e.g. yellowfin sole, flathead sole, rock sole, Alaska plaice) and higher relative abundance of arctic species (e.g. arctic cod, snailfish, Bering flounder), fixed sessile invertebrates, and polychaetes				
Southern	Relatively low abundance of arctic species (e.g. arctic cod, snailfish, Bering flounder) and relatively high abundance of pelagic piscivores (e.g. Kamchatka and arrowtooth founder), scallop, sand dollar, sea cucumber, and sponge				
Northern	Predominant area for arctic species (e.g. arctic cod, snailfish, eelpout, Bering flounder) and also for populations of Greenland turbot, capelin, coral and blue king crab. Deepwater (e.g. sablefish, rockfish), or warm water and southern ranging species (e.g. Kamchatka flounder, arrowtooth flounder, eulachon) species are largely absent				
Middle/outer (north)	Relatively high abundance of pelagic piscivore (e.g. Greenland turbot, Kamchatka and arrowtooth flounder) and arctic fish species (e.g. arctic cod, snailfish, Bering flounder, eelpout), echinoderm (e.g. brittle star, basket star, sea star, urchin), crab (e.g. blue king crab, hermit, Tanner, snow), gastropod, and octopus. Also characterized be relatively low abundance of fixed sessile invertebrates (e.g. coral, ascidian, bryozoans) and benthic infauna				
Shelf break	Exclusive habitat of deepwater species (e.g. sablefish, rockfish) and high abundance for pelagic piscivores (Kamchatka and arrowtooth flounder). Also characterized by the absence of arctic species and low relative abundance of forage fishes and benthic flatfishes				

temperatures. Important interactions occur in other seasons that have critical influences in determining distribution (see Hunt et al., 2014). Additionally, our analyses examine ecoregions as static phenomena. It is clear, however, that as environmental gradients shift, climate regimes fluctuate, and relative species abundance vary within systems, boundaries may shift (Wang et al., 2010).

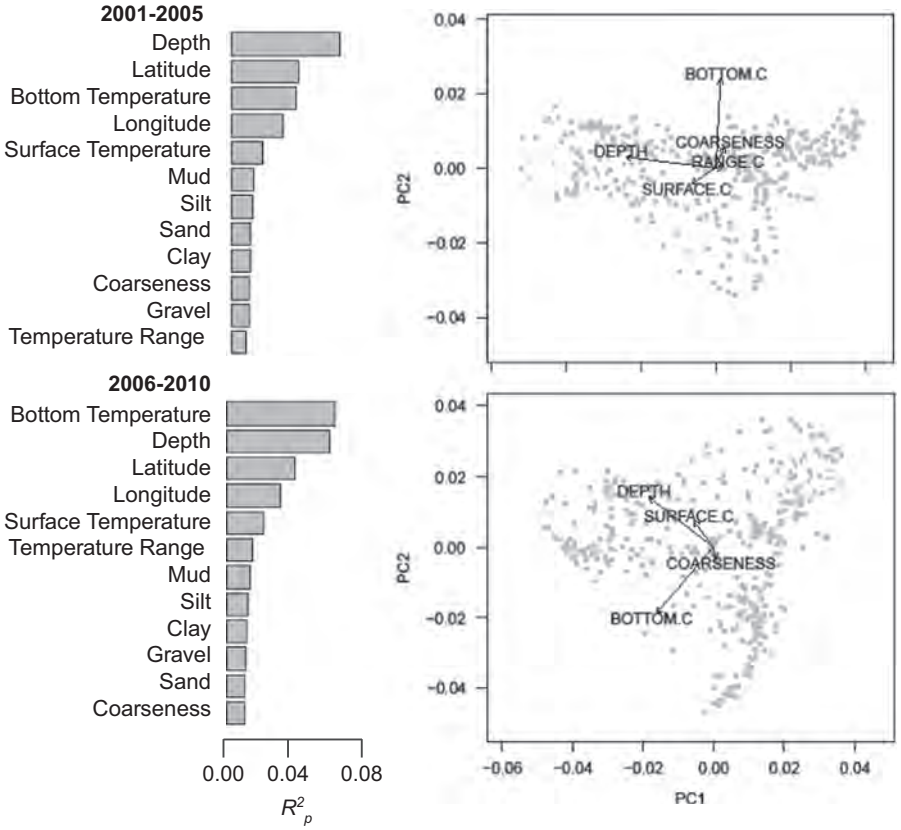

Fig. 10. Bar plot of relative predictor importance and projected biplots of survey stations according to predictor vectors for gradient forest outputs in warm (2001–2005) and cold (2006–2010) periods. Note that the relative importance of bottom temperature as a predictor variable differs across periods, ranking as the dominant variable in cold years, but third (behind depth and latitude) in warm years. Temperature range also ranks relatively higher as a predictor in cold years.

Climate variability and change will alter the volume of ecoregions within the EBS (Hollowed et al., 2012), resulting in shifts in interaction strength. We intend that our current results serve as a baseline against which to measure this phenomenon.

4.5. Practical applications

Our research approaches questions of broad-scale ecological interest in a manner that may inform practical understanding of species dynamics and their response to physical drivers. We highlight an analytical method that enables us to characterize unique regions on the basis of biological responses to physical processes and to project how the range and scope of such regions vary as a function of variables that shift in space over time. We use this method to delineate the EBS LME and to evaluate ecological dynamics at regional scales. We intend that our designation of ecoregions provide a framework for future analyses of the system, inform evaluations of ecological habitat, and serve as an important baseline for future analyses of the effects of climate change and fishing. Still, we note that ecosystem components overlap and interact at multiple scales (Levin et al., 2009); the appropriate scale of analysis will depend on the species, dynamics, and questions of interest. While our research investigates important drivers at relatively finite scales (20 nm × 20 nm scale of survey), processes that operate at broader ecosystem scales also drive patterns throughout the system. Moreover ecologically relevant boundaries may not correspond with boundaries appropriate to policy, viable to management, or relevant to resource allocation or regulation. With that in mind, our results are designed to distinguish regional patterns nested within a hierarchical system of spatial management.

Acknowledgments

We greatly appreciate the advice and guidance provided by R. Hilborn and M. E. Clarke in developing the ideas in this manuscript. We thank B. Lauth, J. Hoff, T. Buckley and L. Eisner for access to data and consultation, and acknowledge the efforts of the scientists and crew of NOAA survey vessels F/V *Aldebaran*, F/V *Northern Explorer*, F/V *Sea Storm* and F/V *Epic Explorer*. We thank K. Beame and A. Grieg for technical support. We also greatly appreciate the advice and counsel of R. Bell, T. Branch, J. Collie, T. Essington, K. Holsman, G. Hunt, S. Kotwicki, B. McConnaughey, F. Mueter, I. Ortiz, J. Overland, P. Spencer, and S. Zador, which contributed to the development and execution of these analyses. We also thank L. Ciannelli and three anonymous reviewers and guest editors J. Napp, P. Stabeno for significant insight and improvement to the final manuscript. This research was supported by a NOAA Comparative Analysis of Marine Ecosystem Organization (CAMEO) grant and partially funded by the Joint Institute for the Study of the Atmosphere and Ocean (JISAO) under NOAA Cooperative Agreement NA10OAR4320148, Contribution No. 2136. This publication also built on and contributed to BEST-BSIERP Bering Sea Project research (Publication No. 127) coordinated by

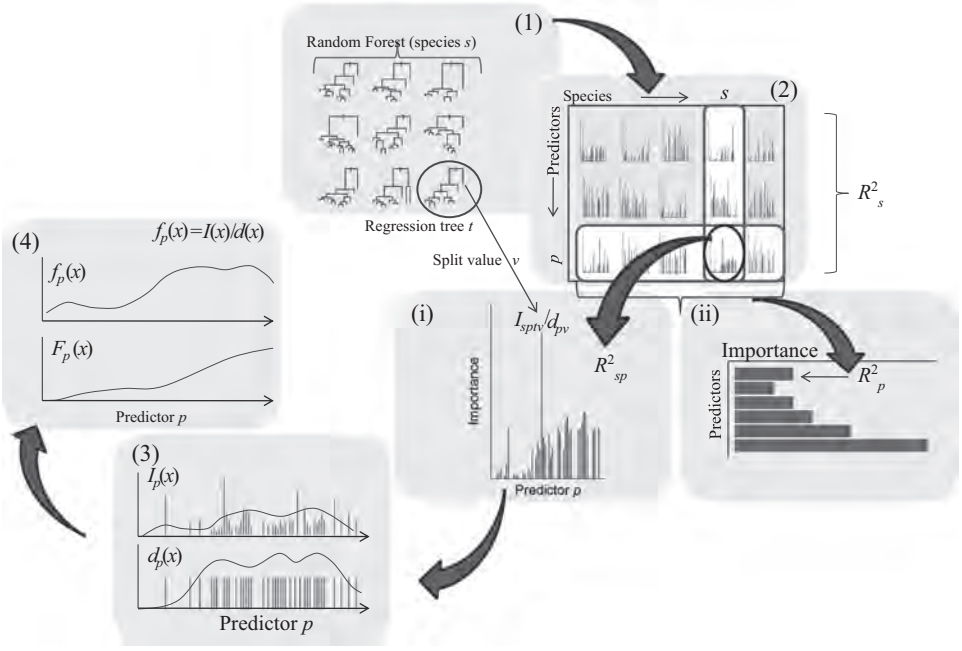

Fig. A1. Schematic of the analytical approach to random and gradient forest analyses. *Step I*. A random forest is generated for each species s, where the resulting model is a set of bifurcating trees (t) in which the nodes represent the predictor variables (environmental drivers) that split the response variable (species abundance) into partitions such that homogeneity within each partition is maximized (measured by the Gini index). Splitting continues until further partitioning does not reduce this index. The length of the branches following each partition indicates the relative importance of the partitioning variable as well as the predictor value at which the split occurs. Each random forest is an ensemble of regression trees, where bifurcations are selected from a set of best splits among a subset of environmental predictors. (Plot 1). *Step II*. The goodness of fit (R^2_s) of the random forest for each species is partitioned among the environmental predictors in proportion to their conditional importance (Plot 2, outlined column in table). This provides an estimate of the relative importance (R^2_{sp}) of each environmental predictor p for each species s (Plot 2, circled intersection of outlined row and column in Table 2). The overall importance (R^2_p) for an environmental predictor is determined as the mean across species (Plot 2, outlined row in table). *Step III*. For each predictor p in each random forest, the splits v and importances Isptv are gathered from every tree t in the forest. The importances are standardized by the density of the predictor split values and normalized to sum to R^2_s (Plot 2i). *Step IV*. For each predictor p the normalized importances are gathered across species, and a combined importance density Ip is computed for each predictor value x along the gradient of the predictor (Plot 3). A combined estimate of the compositional turnover rate fp(x) is estimated as the ratio I(x)/d (x) (Plot 4, top figure). A function for species turnover or shift in the composition of the biological community along the gradient of an environmental predictor variable Fp (x) is estimated as the integral of fp(x) (Plot 4, bottom figure).
Modified from Ellis et al. (2012).

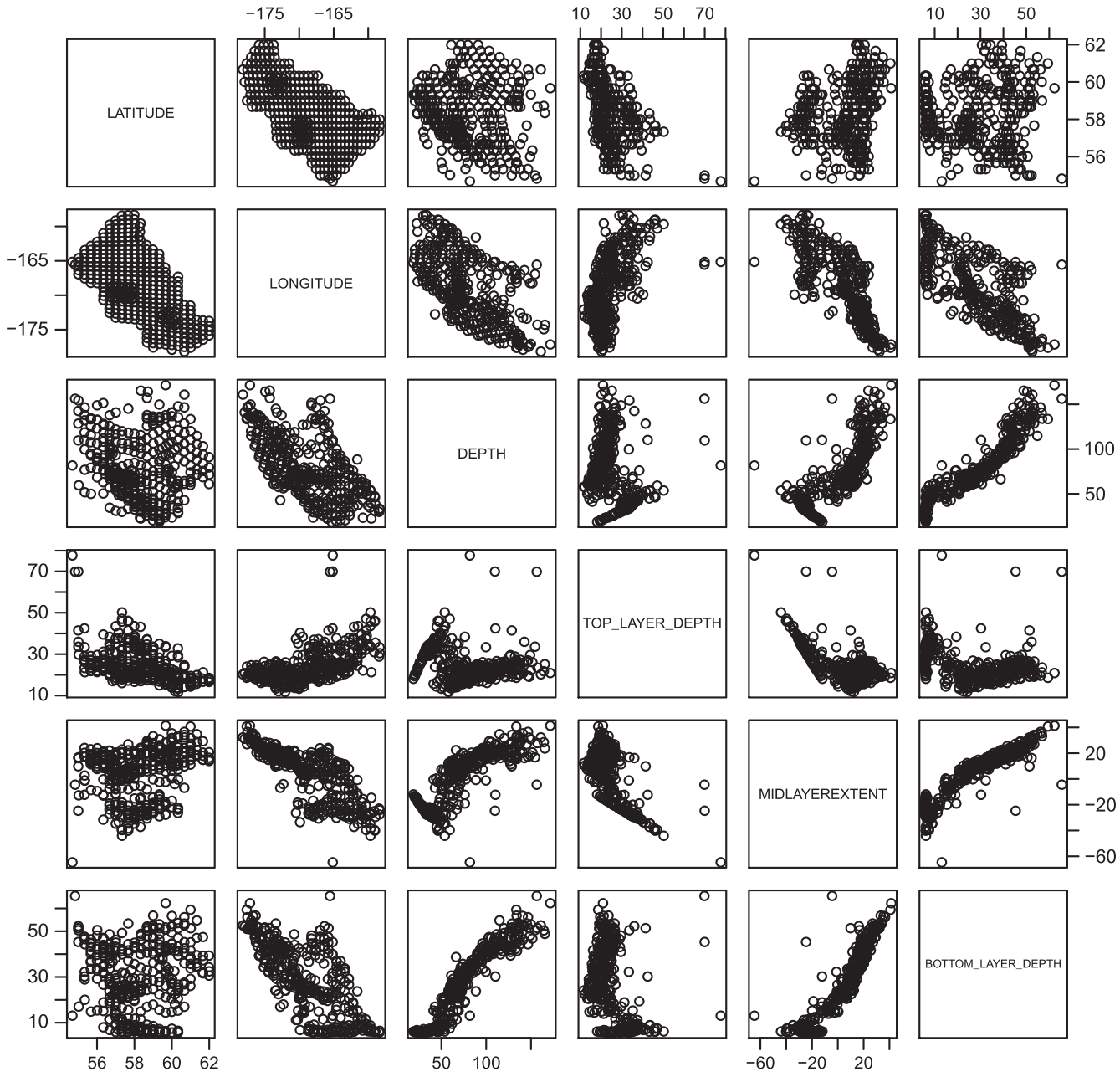

Fig. A2. Correlations between environmental predictor variables, including latitude, longitude, depth and stratification indices. Relationships between most predictor variables were significant (Pearson product-moment correlation, $P < 0.009$, Mean correlation, absolute value = 0.59). Those without significant correlation were depth-latitude, depth-bottom temperature, and latitude-bottomlayer.

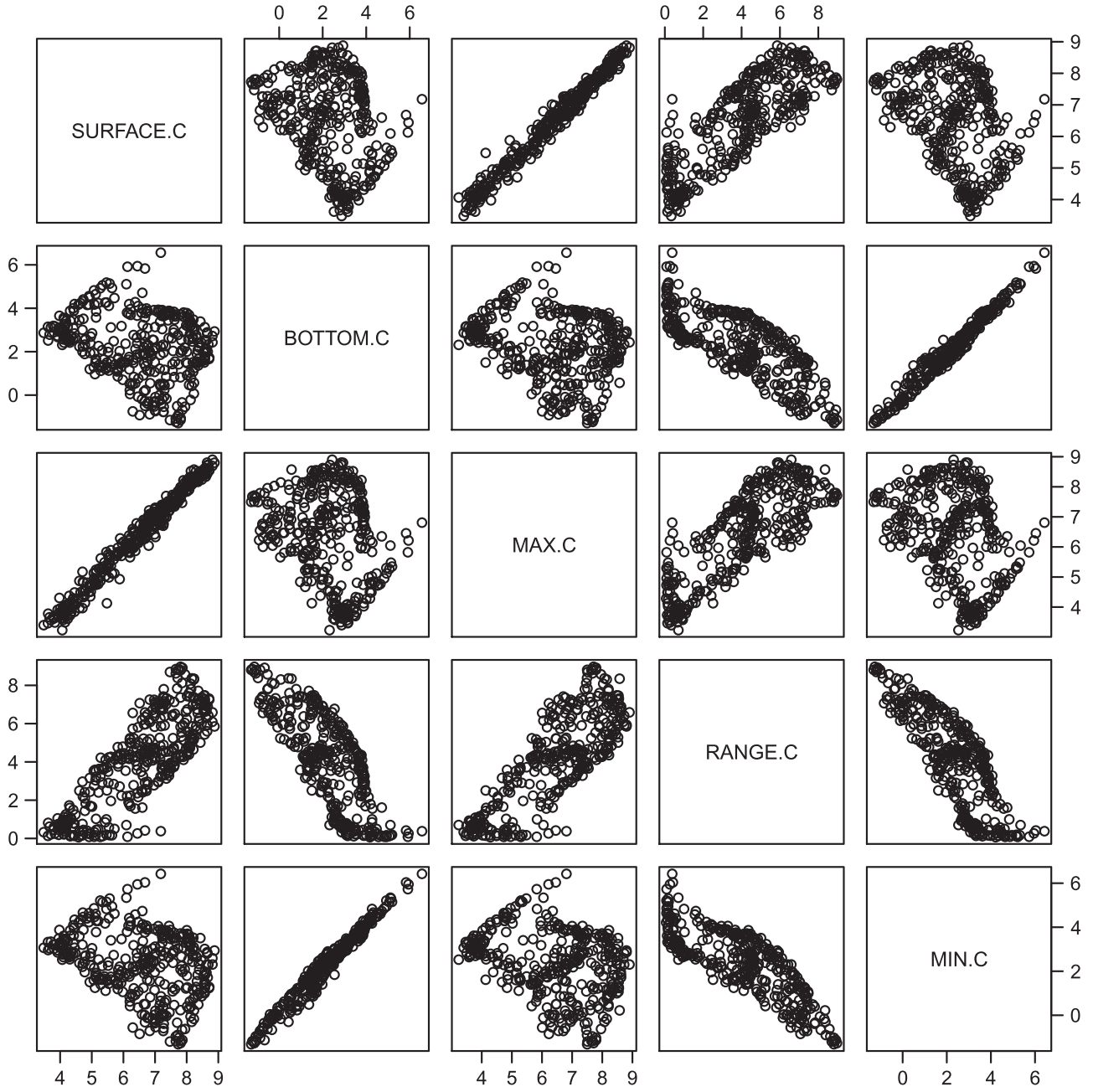

Fig. A3. Correlations between environmental predictor variables, including latitude, longitude, depth and water temperature indices. Relationships between most predictor variables were significant (Pearson product-moment correlation, $P < 0.009$, Mean correlation, absolute value = 0.59). Those without significant correlation were depth-latitude, depth-bottom temperature, and latitude-bottomlayer.

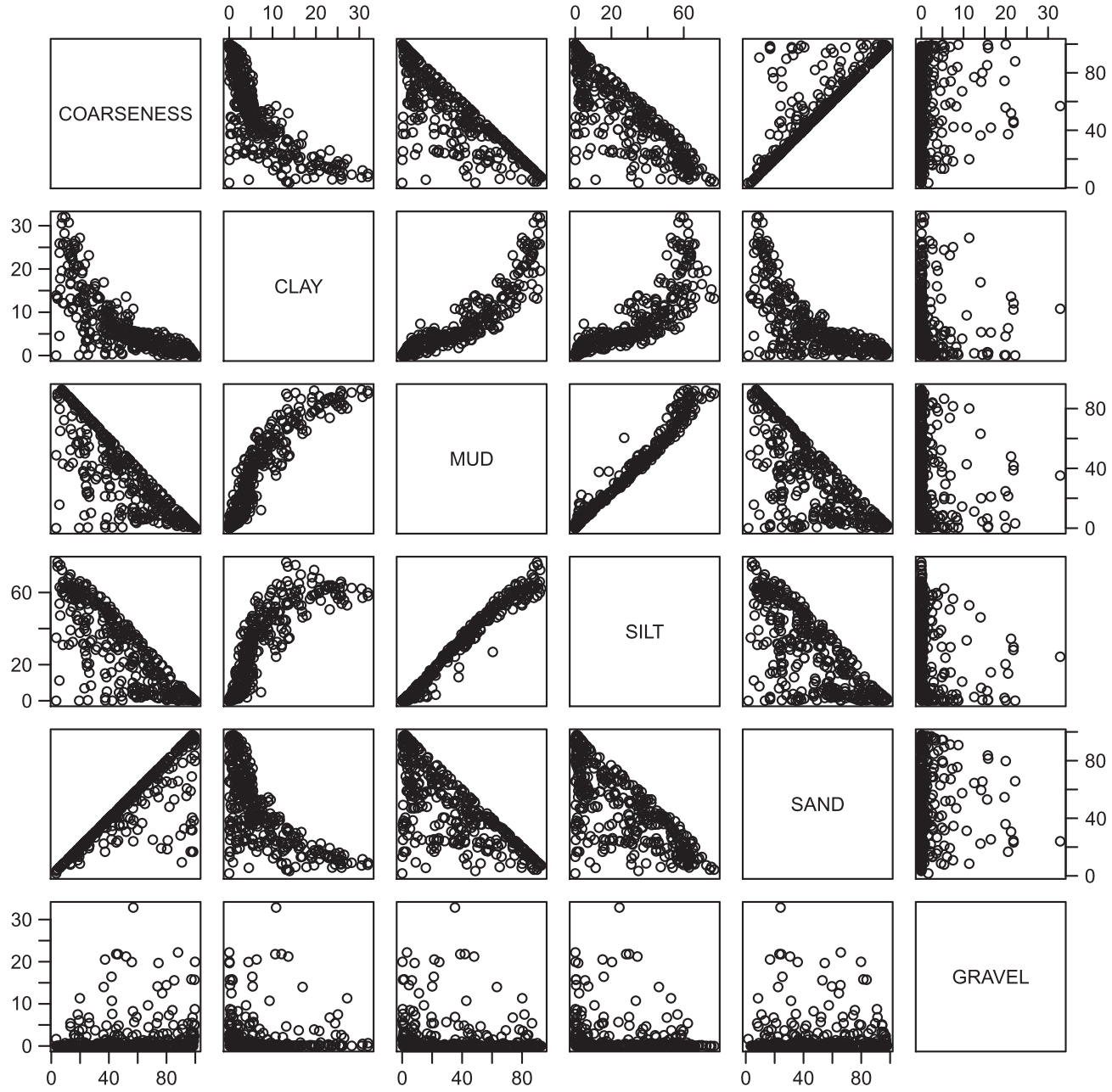

Fig. A4. Correlations between environmental predictor variables, including latitude, longitude, depth and sediment coarseness and substrate types. Relationships between most predictor variables were significant (Pearson product-moment correlation, $P < 0.009$, Mean correlation, absolute value = 0.59). Those without significant correlation were depth-latitude, depth-bottom temperature, and latitude-bottomlayer.

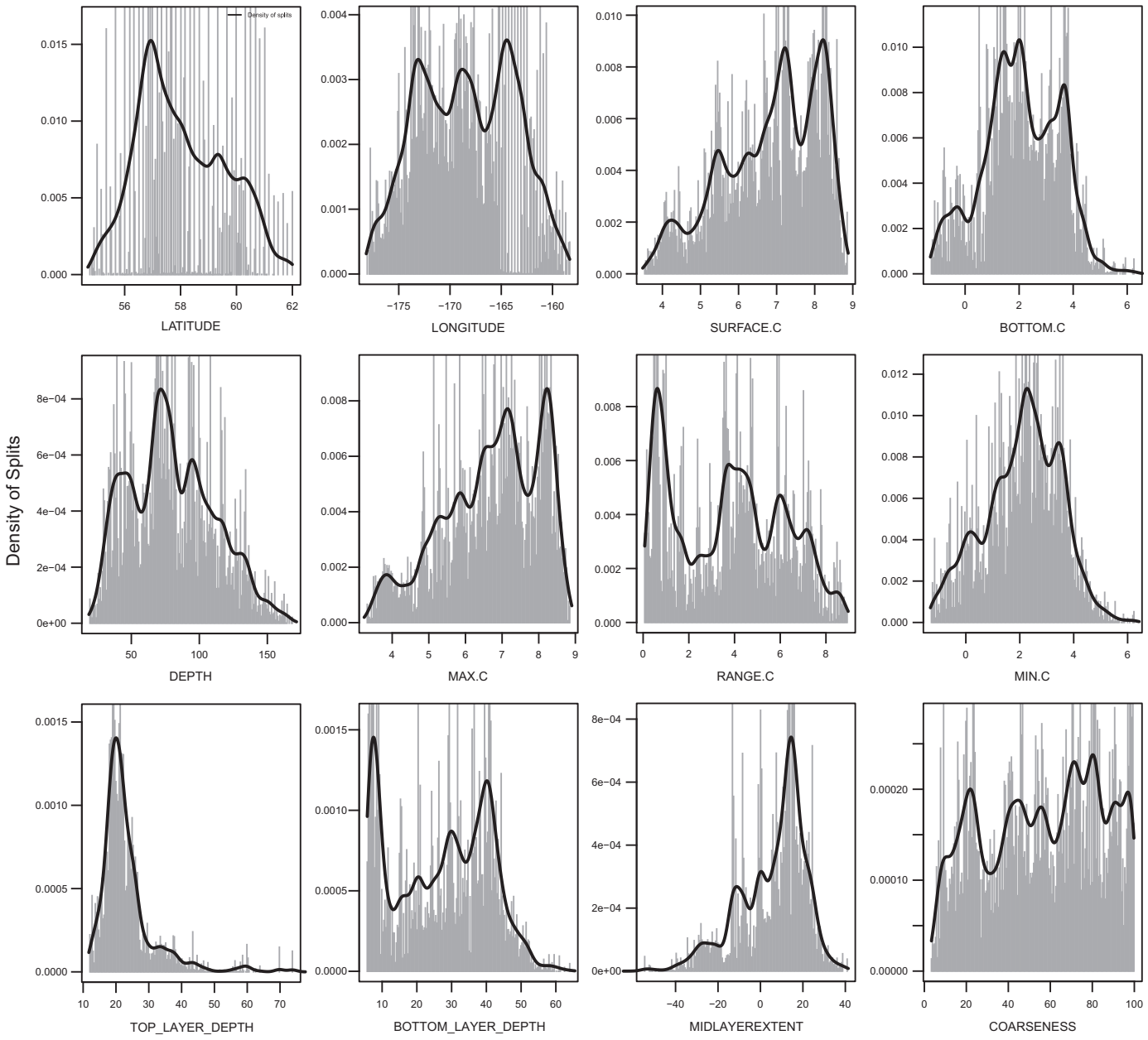

Fig. A5. Kernel density plot of the splits importance metrics from random forests of all species along each physical predictor gradient.

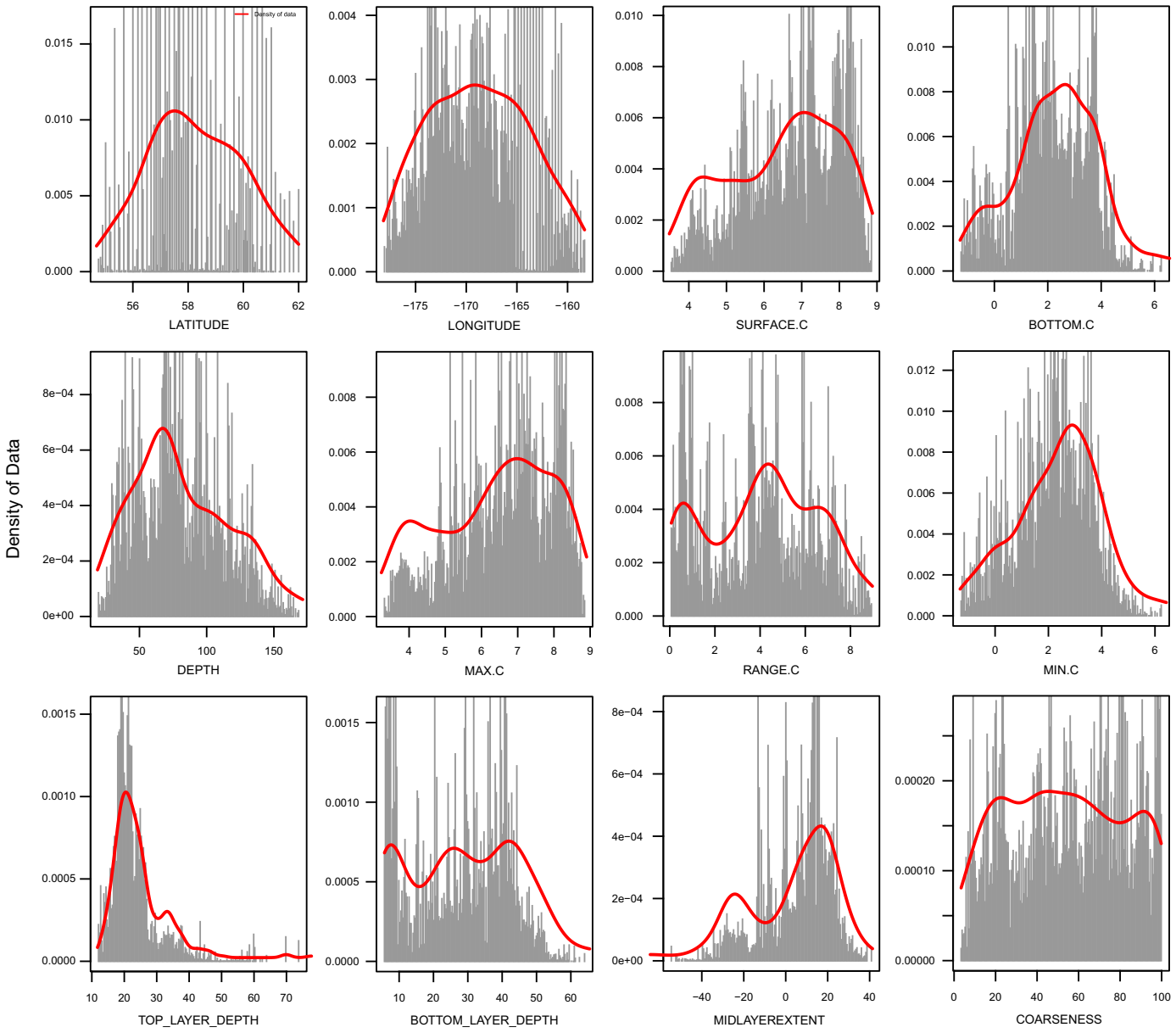

Fig. A6. Kernel density plot of the splits location from random forests of all species along each physical predictor gradient.

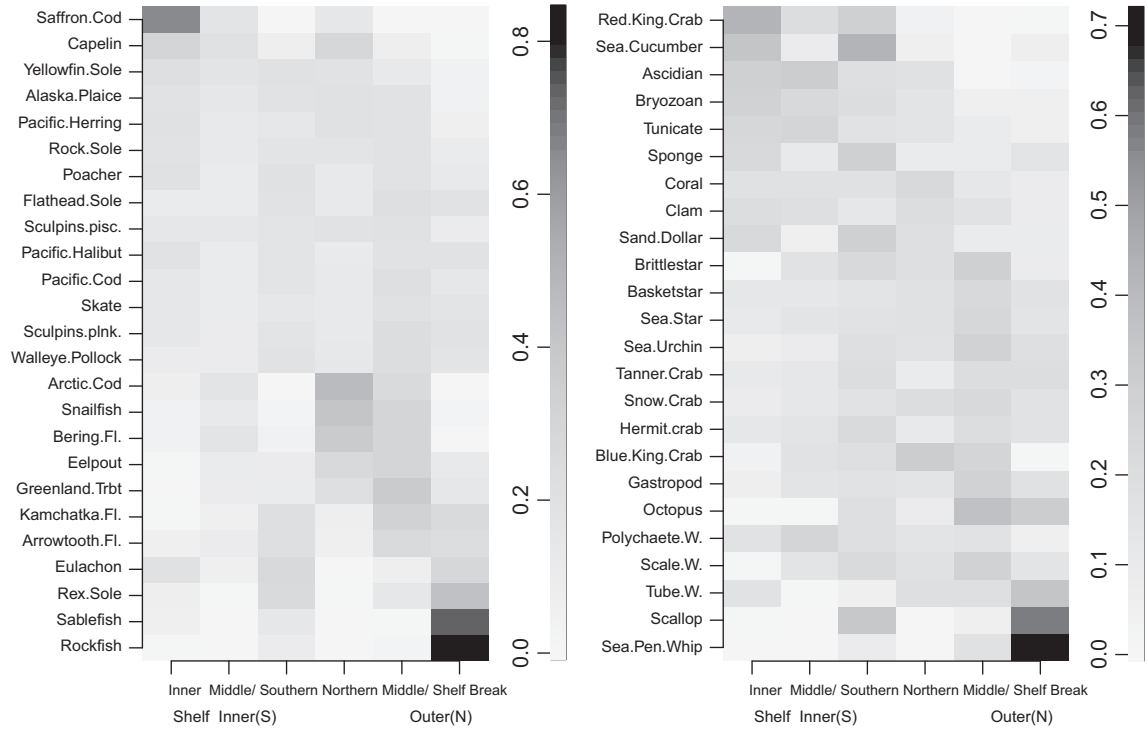

Fig. A7. Relative weighting of species abundance across ecoregions (vertebrates, i; invertebrates, ii). Darker colors indicate higher concentrations.

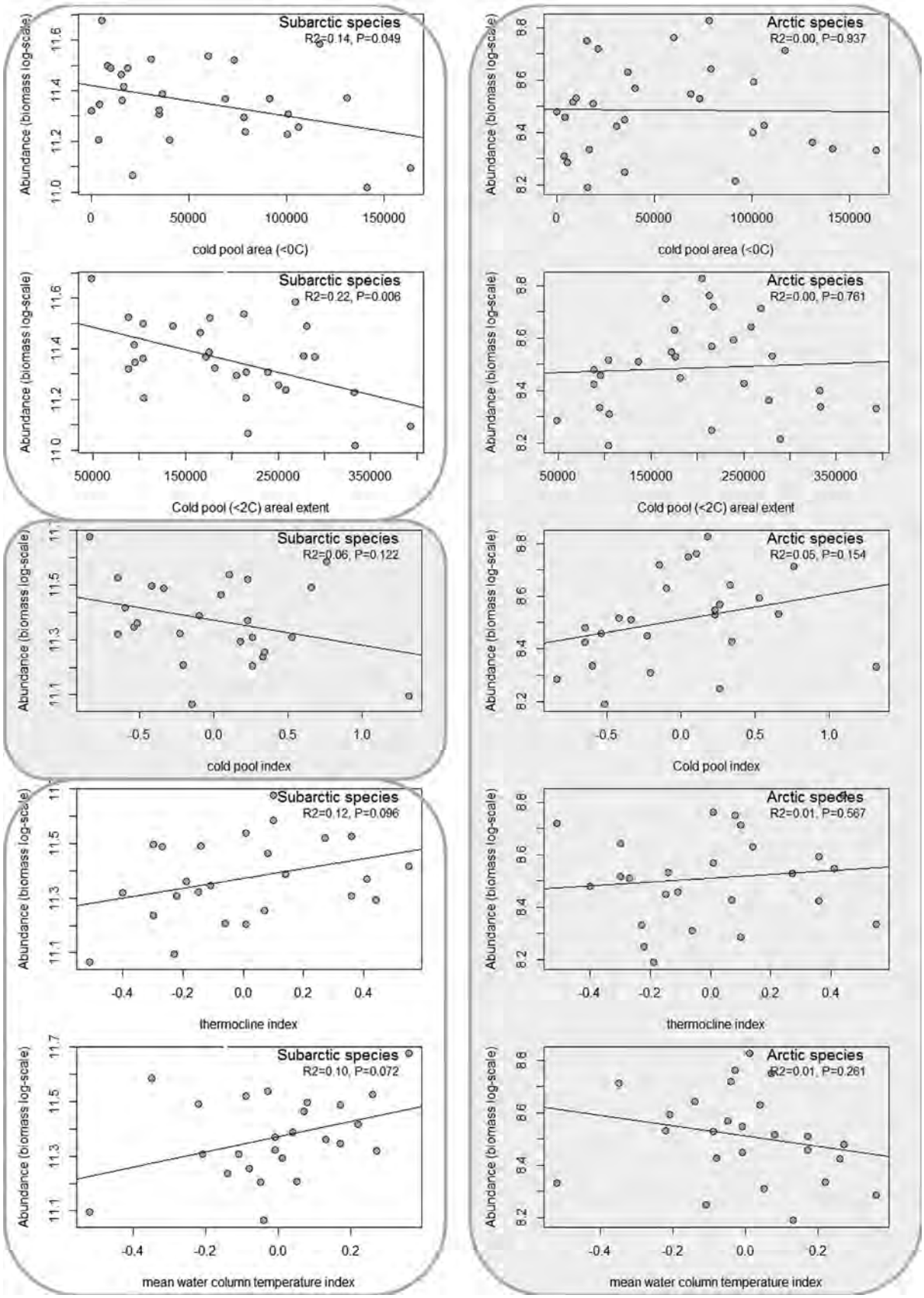

Fig. A8. Response of arctic species ($N=8$, right column) and subarctic species ($N=37$, left column) to the areal extent of the cold pool (0 °C, 2 °C), mean water column temperature, thermocline, and cold pool index. Plots with non-significant relationships are noted by shading. Note that subarctic species are negatively correlated with the areal extent of the cold pool and the cold pool index and positively correlated with thermocline and mean water column temperature indices. Arctic species demonstrate the reverse trends, though the relationships are not significant. These results extend analyses performed in Mueter and Litzow (2008) through recent years.

Table A1
Principle components output.

	PC1	PC2	PC3	PC4	PC5	PC6	PC7	PC8	PC9	PC10	PC11	PC12	PC13
Variance explained (%)	42	21	8	6	6	6	4	4	2	2	2	0	0
Rotation													
Depth	−6.2E−1	5.0E−1	−1.4E−1	−3.7E−1	2.2E−1	9.6E−2	−1.4E−1	−2.4E−1	7.3E−2	−2.6E−1	1.2E−2	2.8E−2	2.0E−2
Surface temperature	−2.8E−1	8.7E−3	−8.0E−2	6.5E−1	−1.1E−1	1.3E−1	−4.4E−1	−2.1E−1	−1.3E−1	1.3E−1	−4.4E−1	2.9E−2	5.6E−2
Bottom temperature	1.1E−1	6.6E−1	3.1E−1	4.1E−1	−1.7E−1	−2.6E−2	2.2E−2	7.6E−2	−9.9E−2	−2.5E−2	4.8E−1	−6.9E−2	−8.1E−2
Temperature range	−3.5E−1	−4.1E−1	−3.6E−1	1.3E−1	−1.4E−2	1.4E−2	−1.2E−1	−1.8E−2	−2.4E−1	6.5E−2	6.8E−1	−9.9E−2	−1.3E−1
Top layer depth	3.8E−2	1.4E−1	6.4E−2	−2.3E−1	1.7E−1	4.3E−2	−1.4E−1	5.7E−2	−3.5E−1	5.4E−1	−1.2E−1	1.1E−1	−6.5E−1
Bottom layer depth	−4.5E−1	1.2E−1	−7.6E−2	4.4E−2	−9.2E−2	−1.8E−1	4.0E−1	4.9E−1	1.2E−2	4.8E−1	−1.2E−1	−8.2E−2	2.9E−1
Mid-layer extent	−2.3E−1	−6.9E−2	−9.1E−2	2.2E−1	−2.2E−1	−1.4E−1	3.2E−1	1.2E−1	3.6E−1	−3.3E−1	−1.4E−1	1.3E−1	−6.5E−1
Substrate coarseness	1.5E−1	1.7E−1	−4.3E−1	−1.4E−1	−4.1E−1	3.2E−1	3.0E−2	3.4E−1	−4.8E−1	−3.1E−1	−1.5E−1	7.0E−2	2.6E−2
Mud	−2.2E−1	−1.7E−1	4.3E−1	−1.1E−1	−3.2E−1	1.5E−1	9.5E−2	−1.3E−1	−1.4E−1	3.4E−2	1.1E−1	7.2E−1	1.3E−1
Silt	−2.1E−1	−1.5E−1	4.2E−1	−1.6E−1	−3.3E−1	3.9E−2	1.9E−1	−2.6E−1	−3.1E−1	−9.3E−2	−1.4E−1	−6.2E−1	−9.4E−2
Clay	−1.3E−1	−1.4E−1	3.4E−1	−1.0E−1	−2.8E−2	3.9E−1	−4.7E−1	5.8E−1	3.1E−1	−7.0E−2	5.4E−2	−1.5E−1	−5.8E−2
Gravel	1.7E−2	−1.4E−2	−2.6E−2	2.0E−1	3.0E−1	7.8E−1	4.7E−1	−1.3E−1	8.5E−2	1.1E−1	2.7E−2	−4.8E−2	−2.4E−2
Sand	1.1E−1	1.2E−1	−2.6E−1	−2.0E−1	−5.9E−1	1.7E−1	−1.1E−1	−2.9E−1	4.6E−1	4.0E−1	9.9E−2	−8.7E−2	−1.5E−2
Medoids													
(1) Inner shelf	−2.0E−2	1.4E−2	9.3E−4	7.5E−4	−1.3E−3	−7.8E−4	1.0E−3	−1.4E−3	1.7E−4	−8.4E−4	7.6E−4	−3.2E−4	−1.4E−4
(2) Middle/inner (south)	2.9E−2	3.6E−3	−3.2E−5	−2.2E−3	4.8E−4	−1.3E−5	−1.2E−3	3.6E−4	5.7E−4	6.6E−4	−3.9E−5	−2.4E−4	2.9E−4
(3) Southern	5.3E−3	−1.1E−3	−7.5E−3	2.3E−3	−3.0E−3	−4.0E−4	−1.1E−3	−1.4E−5	6.6E−4	3.5E−4	1.4E−3	−4.6E−4	−3.6E−4
(4) Northern	5.0E−3	−9.7E−3	1.2E−3	−1.1E−3	−2.0E−3	−1.4E−3	1.7E−3	−1.8E−3	−2.0E−4	−1.3E−3	8.3E−4	−3.3E−4	3.5E−4
(5) Middle/outer (north)	−1.2E−2	−1.8E−2	5.8E−4	−1.9E−3	−9.0E−4	1.7E−3	−1.2E−4	7.8E−4	1.8E−4	−2.0E−4	−2.9E−4	−1.6E−4	−3.2E−4
(6) Shelf break	−3.0E−2	−8.2E−4	5.5E−3	1.1E−3	−1.4E−5	1.6E−3	−3.1E−3	1.4E−3	−2.0E−4	−6.7E−5	5.8E−4	−3.3E−5	−9.4E−5

Notes: Output of principle components analysis. Environmental predictor variables that loaded heavily ($< -4.0E-1$ or $> 4.0E-1$) on principle components (PC) are highlighted (negative=dark, positive=light). Ecoregions most influenced by each PC are also highlighted.

the North Pacific Research Board (Publication No. 469). The findings and conclusions of this paper are those of the authors and do not necessarily represent the views of the National Marine Fisheries Service.

Appendix A

See Figs. A1–A8 and Table A1.

References

Adey, W.H., Steneck, R.S., 2001. Thermogeography over time creates biogeographic regions: a temperature/space/time-integrated model and an abundance-weighted test for benthic marine algae. J. Phycol. 37, 677–698.

Aguilar-Islas, A.M., Hurst, M.P., Buck, K.N., Sohst, B., Smith, G.J., Lohan, M.C., Bruland, K.W., 2007. Micro-and macronutrients in the southeastern Bering Sea: insight into iron-replete and iron-depleted regimes. Prog. Oceanogr. 73, 99–126.

Allen, M.J., Smith, G.B., 1988. Atlas and Zoogeography of Common Fishes in the Bering Sea and NORTHEAST PACIFIC. US Department of Commerce, NOAA Technical Report NMFS 66, p. 151.

Alverson, D.L., Pereyra, W.T., 1969. Demersal fish explorations in the northeastern Pacific Ocean-an evaluation of exploratory fishing methods and analytical approaches to stock size and yield forecasts. J. Fish. Board Can. 268, 1985–2001.

Bailey, R.G., 1998. Ecoregions: The Ecosystem Geography of the Oceans and Continents. Springer, New York p. 192

Banks, D., Williams, M., Pearce, J., Springer A., Hagenstein R., Olson, D., 1999. Eco-region based conservation in the Bering Sea. In: Bering Sea Experts Workshop, Girdwood, Alaska, March 20–23, 1999.

Bond, N.A., Overland, J.E., Spillane, M., Stabeno, P., 2003. Recent shifts in the state of the North Pacific. Geophys. Res. Lett. 3023, 2183.

Branch, T., Watson, R., Fulton, E., Jennings, S., McGilliard, C., Pablico, R., Ricard, D., Tracey, S.R., 2010. The trophic fingerprint of marine fisheries. Nature 468, 431–435.

Breiman, L., 2001. Random forests. Mach. Learn. 451, 5–32.

Briggs, J.C., 1974. Marine Zoogeography. McGraw-Hill, New York

Buckley, T.W., Grieg, A., Boldt, J.L., 2009. Describing Summer Pelagic Habitat Over the Continental Shelf in the Eastern Bering Sea 1982–2006. NOAA Technical Memorandum NMFS-196.

Cheung, W.W., Lam, V.W.Y., Pauly, D., 2008. Modeling Present and Climate-Shifted Distributions of Marine Fishes and Invertebrates. University of British Columbia, Canada, Fisheries Centre Research Reports 16, pp. 5–50.

Ciannelli, L., Bailey, K.M., 2005. Landscape dynamics and underlying species interactions: the cod-capelin system in the Bering Sea. Mar. Ecol. Prog. Ser. 291, 227–236.

Ciannelli, L., Chan, K.S., Bailey, K.M., Stenseth, N.C., 2004. Non-additive effects of the environment on the survival of a large marine fish population. Ecology 85, 3418–3427.

Coachman, L.K., 1986. Circulation, water masses, and fluxes on the southeastern Bering Sea shelf. Cont. Shelf Res. 5, 23–108.

Coyle, K.O., Pinchuk, A.I., 2002. The abundance and distribution of euphausiids and zero-age pollock on the inner shelf of the southeast Bering Sea near the Inner Front in 1997–1999. Deep Sea Res. II 49, 6009–6030.

Coyle, K.O., Cooney, R.T., 1993. Water column sound scattering and hydrography around the Pribilof Islands, Bering Sea. Cont. Shelf Res. 13, 803–827.

Cutler, D.R., Edwards Jr, T.C., Beard, K.H., Cutler, A., Hess, K.T., Gibson, J., Lawler, J.J., 2007. Random forests for classification in ecology. Ecology 8811, 2783–2792.

Danielson, S., Eisner, L., Weingartner, T., Aagard, L., 2011. Thermal and haline variability over the central Bering Sea shelf: seasonal and interannual perspectives. Cont. Shelf Res. 31, 539–554.

Danielson, S., Hedstrom, K., Aagaard, K., Weingartner, T., Curchister, E., 2012. Wind-indiced regorganization of the Bering shelf circulation. Geophys. Res. Lett. 39, L08601–L08606.

Dinerstein, E., Olson, D., 1997. Ecoregion-based Conservation Planning: Identifying Priority Sites Within Ecorregions. World Wildlife Fund.

Ecosystem Principles Advisory Panel. Ecosystem-based Fishery Management. A Report to Congress as Mandated by the Sustainable Fisheries Act Amendments to the Magnuson-Stevens Fishery Conservation and Management Act 1996 ⟨http://www.nmfs.noaa.gov/sfa/EPAPrpt.pdf⟩.

Ekman, S., 1953. Zoogeography of the Sea. Sidgwick and Jackson, London

Ellis, N., Smith, S.J., Pitcher, C.R., 2012. Gradient forests: calculating importance gradients on physical predictors. Ecology 931, 156–168.

Fogarty, M.J., Murawski, S.A., 1998. Large scale disturbance and structure of marine systems: fishery impacst on Georges Bank. Ecol. Appl. 8, S6–S22.

Fogarty, M.J. Keith, C., 2009. Delineation of Regional Ecosystem Units on the US Northeast Continental Shelf. NESC Discussion Paper.

Forbes, E., 1856. Map of the distribution of marine life. In: Johnston, A.K., (Ed.). The Physical Atlas of Natural Phenomena, pp. 99–102 and plate 131.

Ford, G., 1998. Marine Ecoregions, Beringia. Prepared for World Wildlife Foundation, unpublished.

Garrison, L.P., Link, J.S., 2000. Dietary guild structure of the fish community in the northeast United States continental shelf ecosystem. Mar. Ecol. Prog. Ser. 202, 231–240.

Genner, M.J., Sims, D.W., Wearmouth, V.J., Southhall, E.J., Southward, A.J., Hawkins, S.J., 2004. Regional climatic warming drives long-term community changes of British marine fish. Proc. R. Soc. Lond. Ser. B: Biol. Sci. 271, 655–661.

Gibson, G.A., Coyle, K.O., Hedstrom, K., Curchitser, E.N., 2013. A modeling study to explore on-shelf transport of oceanic zooplankton in the Eastern Bering Sea. J. Mar. Syst. 121, 47–64.

Hedgepath, J.W., 1957a. Marine biogeography. Geol. Soc. Am. Mem. 67, 359–382.

Hedgepath, J.W., 1957b. Classification of marine environments. Geol. Soc. Am. Mem. 67, 17–28.

Hempel, G., Sherman, K., 2003. Large Marine Ecosystems of the World: Trends in Exploitation, Protection and Research. Elsevier, Amsterdam

Hollowed, A.B., Aydin, K.Y., Essington, T.E., Ianelli, J.N., Megrey, B.A., Punt, A.E., Smith, A.D., 2011. Experience with quantitative ecosystem assessment tools in the northeast Pacific. Fish Fish. 12, 189–208.

Hollowed, A.B., Barbeaux, S., Farley, E., Cokelet, E.D., Kotwicki, S., Ressler, P.H., Spital, C., Wilson, C., 2012. Effects of climate variations on pelagic ocean habitats and their role in structuring forage fish distributions in the Bering sea. Deep Sea Res. II 65–70, 230–250.

Hunt, G.L., Renner, M., Kuletz, K., 2014. Seasonal variation in the cross-shelf distribution of seabirds in the southeastern Bering Sea. Deep Sea Res. II 109, 266–281, http://dx.doi.org/10.1016/j.dsr2.2013.08.011.

Hunt, G.L., Coyle, K.O., Eisner, L.B., Farley, E.V., Heintz, R.A., Mueter, F., Napp, J., Overland, J.E., Ressler, P.H., Salo, S., Stabeno, P.J., 2011. Climate impacts on eastern Bering Sea foodwebs: a synthesis of new data and an assessment of the Oscillating Control Hypothesis. ICES J. Mar. Sci. 68, 1230–1243.

Hunt, G.L., Stabeno, P., Walters, G., Sinclair, E., Brodeur, R.D., Napp, J.M., Bond, N.A., 2002. Climate change and control of the southeastern Bering Sea pelagic ecosystem. Deep Sea Res. II 4926, 5821–5853.

Hutchins, L.W., 1947. The bases for temperature zonation in geographical distribution. Ecol. Monogr. 17, 325–335.

Kachel, N.B., Hunt, G.L., Salo, S.A., Schumacher, J.D., Stabeno, P.J., Whitledge, T.E., 2002. Characteristics and variability of the inner front of the southeastern Bering Sea. Deep Sea Res. II 49, 5889–5909.

Kaufman, L., Rousseau, P., 1990. Finding Groups in Data. John Wiley and Sons, New York

Kildaw, S.D., Irons, D.B., Nysewander, D.R., Buck, C.L., 2005. Formation and growth of new seabird colonies: the significance of habitat quality. Mar. Ornithol. 33, 49–58.

Kinney, J.C., Maslowski, W., Okkonen, S., 2009. On the processes controlling shelf-basin exchange and outer shelf dynamics in the Bering Sea. Deep Sea Res. II 56, 1351–1362.

Kotwicki, S., Buckley, T.W., Honkalehto, T., Walters, G., 2005. Variation in the distribution of walleye pollock with temperature and implications for seasonal migration. Fish. Bull. 103, 574–587.

Kotwicki, S., Lauth, R.R., 2013. Detecting temporal trends and environmentally driven changes in the spatial distribution of groundfishes and crabs in the eastern Bering Sea shelf. Deep Sea Res. II 94, 231–243.

Ladd, C., Stabeno, P.J., 2012. Stratification on the eastern Bering Sea shelf revisited. Deep Sea Res. II 65–70, 72–83.

Lang, G.M., Brodeur, R.D., Napp, J.M., Schabetsberger, R., 2000. Variation in groundfish predation on juvenile walleye pollock relative to hydrographic structure near the Pribilof Islands, Alaska. ICES J. Mar. Sci. 57, 265–271.

Lauth, R.R., 2012. Results of the 2012 Eastern Bering Sea Continental Shelf Bottom Trawl Survey of Groundfish and Invertebrate Resources. NOAA Technical Memorandum NMFSAFSC-181, Seattle, WA.

Levin, L.A., Dayton, P.K., 2009. Ecological theory and continental margins: where shallow meets deep. Trends Ecol. Evol. 24, 606–617.

Levin, P.S., Fogarty, M.J., Murawski, S.A., Fluharty, D., 2009. Integrated ecosystem assessments: developing the scientific basis for ecosystem-based management of the ocean. PLoS Biol. 7, 23–28.

Liaw, A., Wiener, M., 2002. Classification and regression by randomForest. R News 23, 18–22.

Link, J.S., Auster, P.J., 2011 The challenges of evaluating competition among marine fishes: contributed talk. In: 2011 International Mote Symposium: Species Interactions in Marine Communities.

Livingston, P.A., Low, L.L., Marasco, R.J., 1999. Eastern Bering Sea trends. In: Sherman, K., Tang, Q. (Eds.), Large Marine Ecosystems of the Pacific Rim: Assessment, Sustainability, and Management. Blackwell Science, Malden, MA, pp. 140–162

Livingston, P., et al., 2011. Alaska marine fisheries management: advancements and linkages to ecosystem research. In: Belgrano, A., Fowler, C. (Eds.), Ecosystem Based Management: An Evolving Perspective. Cambridge University Press, UK, pp. 113–152

Longhurst, A., 1998. Ecological Geography of the Sea. Academic Press, San Diego

Loreau, M., 2010. Linking biodiversity and ecosystems: towards a unifying ecological theory. Philos. Trans. R. Soc. Lond. B: Biol. Sci. 365, 49–60.

Lourie, S.A., Vincent, A.C.J., 2004. Using biogeography to help set priorities in marine conservation. Conserv. Biol. 18, 1004–1020.

Mantua, N.J., Hare, S.R., 2002. The Pacific decadal oscillation. J. Oceanogr. 581, 35–44.

Marasco, R.J., Goodman, D., Grimes, C.B., Lawson, P.W., Punt, A.E., Quinn II, T.J., 2007. Ecosystem-based fisheries management: some practical suggestions. Can. J. Fish. Aquat. Sci. 646, 928–939.

McGlinn, D.J., Hurlbert, A.H., 2012. Scale dependence in species turnover reflects variance in species occupancy. Ecology 93, 294–302.
Morgan, J.R., 1987. Large marine ecosystems: an emerging concept of regional management. Environment 29, 4–12.
Mueter, F.J., Boldt, J.L., Megrey, B.A., Peterman, R.M., 2007. Recruitment and survival of Northeast Pacific Ocean fish stocks: temporal trends, covariation, and regime shifts. Can. J. Fish. Aquat. Sci. 64, 911–927.
Mueter, F.J., Ladd, C., Palmer, M.C., Norcross, B.L., 2006. Bottom-up and top-down controls of walleye pollock (*Theragra chalcogramma*) on the Eastern Bering Sea shelf. Prog. Oceanogr. 68, 152–183.
Mueter, F.J., Litzow, M.A., 2008. Sea ice retreat alters the biogeography of the Bering Sea continental shelf. Ecol. Appl. 18, 309–320.
Murawski, S.A., 2007. Ten myths concerning ecosystem approaches to marine resource management. Mar. Policy 316, 681–690.
Napp, J.M., Hunt, G.L., 2001. Anomalous conditions in the south eastern Bering Sea 1997: linkages among climate, weather, ocean, and biology. Fish. Oceanogr. 10, 61–68.
National Marine Fisheries Service, 1999. Our Living Oceans. Report on the Status of U.S. Living Marine Resources. U.S. Department of Commerce, NOAA Technical Memorandum. NMFS-F/SPO-41, 1999.
NMFS (National Marine Fisheries Service), 2000. Ecosystem-based Fishery Management: A Report to Congress by the Ecosystem Principles Advisory Panel. U.S. Department of Commerce NOAA, Washington, DC.
National Research Council, 1996. The Bering Sea. National Academy Press, Washington, DC
Ortiz, I., 2012. The Bering Sea Project ⟨http://bsierp.nprb.org/⟩.
Overland, J.E., Salo, S.A., Kantha, L.H., Clayson, C.A., 1999. Thermal stratification and mixing on the Bering Sea shelf. In: Loughlin, T.R., Ohtani, K. (Eds.), Dynamics of the Bering Sea. University of Alaska Sea Grant Program (AK-SG-99-03), Fairbanks, AK, pp. 129–146.
Pepin, P., Cuff, A., Koen-Alonso, M., Ollerhead, N., 2010. Prelininary Analysis for the Delineation of Marine Ecoregions on the Newfoundland-Laborador Shelves. Northwest Atlantic Fisheries Organization Scientific Report Document 10/72.
Piatt, J.F., Springer, A.M., 2007. Marine ecoregions of Alaska. In: Spies, R.B. (Ed.), Longterm Ecological Change in the Northern Gulf of Alaska. Elsevier, Amsterdam
Pinsky, M.L., Olaf, P.J., Ricard, D., Palumbi, S.R., 2011. Unexpected patterns of fisheries collapse in the world's oceans. Proc. Natl. Acad. Sci. U.S.A. 108, 8317–8322.
Pitcher, C.G., Lawton, P., Ellis, N., Smith, S.J., Incze, L.S., Wei, C.L., Greenlaw, M.E., Wolff, N.H., Sameoto, J.A., Snelgrove, P.V.R., 2012. Exploring the role of environmental variables in shaping patterns of seabed biodiversity composition in regional-scale ecosystems. J. Appl. Ecol. 49, 670–679.
Schumacher, J.D., Stabeno, P.J., 1998. The continental shelf of the Bering Sea. In: Robinson, A.R., Brink, K.H. (Eds.), The Sea: The Global Coastal Ocean Regional Studies and Synthesis. John Wiley and Sons, New York, pp. 869–909
Sherman, K., Alexander, L.M., 1989. Biomass Yields and Geography of Large Marine Ecosystems. Westview Press, Boulder
Sherman, K., 1991. The large marine ecosystem concept: research and management strategy for living marine resources. Ecol. Appl. 1, 350–360.
Sigler, M.F., 2011. Fluxes, fins, and feathers. Oceanography 24, 250–265.
Smith, K.R., McConnaughey, R.A., 1999. Surficial Sediments of the Eastern Bering Sea Continental Shelf: EBSSED Database Documentation. U.S. Department of Commerce, NOAA Technical Memorandum. NMFS-AFSC-104 ⟨http://www.afsc.noaa.gov/Publications/AFSC-TM/NOAA-TM-AFSC-104.pdf⟩, 41p.
Smith, G.B., Bakkala, R.G., 1982. Demersal Fish Resources of the Eastern Bering Sea: Spring 1976. US Department of Commerce, National Oceanic and Atmospheric Administration, National Marine Fisheries Service.
Spalding, M.D., Fox, H.E., Allen, G.R., Davidson, N., Ferdana, Z.A., Finlayson, M., Halpern, B.S., Jorge, M.A., Lombana, A., Lourie, S.A., Martin, K.D., McManus, E., Molnar, J., Recchia, C.A., Robertson, J., 2007. Marine ecoregions of the world: a bioregionalization of coastal and shelf areas. BioScience 57, 573–583.
Speckman, S.G., Piatt, J.F., Minte-Vera, C.V., Parrish, J.K., 2005. Parallel structure among environmental gradients and three trophic levels in a subarctic estuary. Prog. Oceanogr. 66, 25–65.
Spencer, P.D., 2008. Density-independent and density-dependent factors affecting temporal changes in spatial distributions of eastern Bering Sea flatfish. Fish. Oceanogr. 17, 396–410.
Stabeno, P.J., Schumacher, J.D., Ohtani, K., 1999. The physical oceanography of the Bering Sea. In: Loughlin, T.R., Ohtani, K. (Eds.), Dynamics of the Bering Sea: A Summary of Physical, Chemical, and Biological Characteristics, and a Synopsis of Research on the Bering Sea. North Pacific Marine Science Organization (PICES), University of Alaska Sea Grant, Fairbanks, AK, pp. 1–28.
Stabeno, P.J., Bond, N.A., Kachel, K.B., Salo, S.A., Schumacher, J.D., 2001. Temporal variability in the physical environment over the southeastern Bering Sea. Fish. Oceanogr. 10, 81–98.
Stabeno, P.J., Kachel, N., Mordy, C., Righi, D., Salo, S., 2008. An examination of the physical variability around the Pribilof Islands in 2004. Deep Sea Res. II 55, 1701–1716.
Stabeno, P.J., Farley, E.V., Kachel, N.B., Moore, S., Mordy, C.W., Napp, J.M., Overland, J.E., Pinchuk, A., Sigler, M.F., 2012a. A comparison of the physics of the northern and southern shelves of the eastern Bering Sea and some implications for the ecosystem. Deep Sea Res. II 65–70, 14–30.
Stabeno, P.J., Kachel, N.B., Moore, S.E., Napp, J.M., Sigler, M., Yamaguchi, A., Zerbini, A.N., 2012b. Comparison of warm and cold years on the southeastern Bering Sea shelf and some implications for the ecosystem. Deep Sea Res. II 65–70, 31–45.
Strobl, C., Boulesteix, A., Kneib, T., Augustin, T., Zeileis, A., 2008. Conditional variable importance for random forests. BMC Bioinformatics 9, 307–317.
United Nations, FAO, 2003. Fisheries Management. The Ecosystem Approach to Fisheries. FAO Technical Guidelines for Responsible Fisheries, 4 Suppl. 2, p. 112.
U.S. Commission on Ocean Policy, 2004. An Ocean Blueprint for the 21st Century. Final Report. Washington, DC ⟨http://www.oceancommission.gov/⟩.
Wang, M., Overland, J.E., Bond, N.A., 2010. Climate projections for selected large marine ecosystems. J. Mar. Syst. 793, 258–266.
Wespestad, V.G., Fritz, L.W., Ingraham, W.J., Megrey, B.A., 2000. On relationships between cannibalism, climate variability, physical transport, and recruitment success of Bering Sea walleye pollock (*Theragra chalcogramma*). ICES J. Mar. Sci. 57, 272–278.
Whiteledge, T.E., Luchin, V.A., 1999. Summary of chemical distributions and dynamics in the Bering Sea, Dynamics of the Bering Sea, pp. 217–250
Wyllie-Echeverria, T., Wooster, W.S., 1998. Year-to-year variations in Bering Sea ice cover and some consequences for fish distributions. Fish. Oceanogr. 7, 159–170.
Zwanenburg, K., Horsman, T., Kenchington, E., 2010. Preliminary Analysis of Biogeographic Units on the Scotian Shelf. Northwest Atlantic Fisheries Organization Scientific Report Document 10/06.

Deep-Sea Research II 109 (2014) 241–250

Contents lists available at ScienceDirect

Deep-Sea Research II

journal homepage: www.elsevier.com/locate/dsr2

A cross-shelf gradient in $\delta^{15}N$ stable isotope values of krill and pollock indicates seabird foraging patterns in the Bering Sea

Nathan M. Jones [a,*], Brian A. Hoover [a], Scott A. Heppell [b], Kathy J. Kuletz [c]

[a] Moss Landing Marine Labs, Vertebrate Ecology Lab, 8272 Moss Landing Road, Moss Landing, CA 95616, USA
[b] Department of Fisheries and Wildlife, Oregon State University, 104 Nash Hall, Corvallis, OR 97331, USA
[c] United States Fish and Wildlife Service, Migratory Birds Management Office, 1011 East Tudor Road, MS 201, Anchorage, AK 99503, USA

ARTICLE INFO

Available online 29 April 2014

Keywords:
Isotopes
Shelf edge
Murre
Kittiwake
Rissa tridactyla
Uria lomvia
Food web
Habitat partitioning

ABSTRACT

Concurrent measurements of predator and prey $\delta^{15}N$ isotope values demonstrated that a cross-shelf isotopic gradient can propagate through a marine food web from forage species to top-tier predators and indicate foraging areas at a scale of tens of kilometers. We measured $\delta^{13}C$ and $\delta^{15}N$ in muscle tissues of thick-billed murres (*Uria lomvia*) and black-legged kittiwakes (*Rissa tridactyla*), and in whole body tissues of walleye pollock (*Gadus chalcogrammus*) and krill (*Thysanoessa* spp), sampled across the continental shelf break in the Bering Sea in 2008 and in 2009. We found significant basin-shelf differences at fine scales (<100 km) in $\delta^{15}N$ among murres but not kittiwakes, and no such differences in $\delta^{13}C$ in either seabird species at that scale. We then quantified the multi-trophic signal and spatial structure of a basin-shelf δ^{15}Nitrogen gradient in the central and southern Bering Sea, and used it to contrast foraging patterns of thick-billed murres and kittiwakes on the open ocean. Seabird muscle $\delta^{15}N$ values were compared to baselines created from measurements in krill and pollock tissues sampled concurrently throughout the study area. Krill, pollock, and murre tissues from northern, shallow, shelf habitat (<200 m) were enriched 1–2‰ in $\delta^{15}N$ relative to samples taken from deeper habitats (>200 m) to the south and west. Krill $\delta^{15}N$ baseline values predicted 35–42% of the variability in murre tissue values. Patterns between kittiwakes and prey were less coherent. The persistence of strong spatial autocorrelation among sample values, and a congruence of geospatial patterns in $\delta^{15}N$ among murre and prey tissues, suggest that murres forage repeatedly in specific areas. Murre isotope values showed distinct geospatial stratification, coincident with the spatial distribution of three colonies: St. Paul, St. George, and Bogoslof. This suggests some degree of foraging habitat partitioning among colonies.

1. Introduction

Differences among stable isotope baselines of invertebrate prey species can exist between shallow near shore and deep offshore habitats in the marine environment, and can be referenced to infer patterns in the diet and movement of predators that routinely forage across pelagic/shelf boundaries (Schell et al., 1998; Forero et al., 2004; Miller et al., 2008; Barnes et al., 2009; Olson et al., 2010; Jaeger et al., 2013). In general, cross-shelf patterns have proven most useful for inferring movement across very large distances (>100 km). Finer scale studies are less common because open ocean baseline sampling is often lacking or, at best, of limited resolution (Schell et al., 1998; Phillips et al., 2009; Quillfeldt et al., 2010; Jaeger et al., 2010, 2013). Fewer studies have used marine isoscapes and GIS techniques to elucidate food web linkages that describe foraging arenas of ocean predators at fine to medium (<100 km) scales (Barnes et al., 2009), and none have tested the multitrophic influence of an apparent cross-shelf gradient in the Bering Sea. In this study, we measured isotopic values from two pelagic seabirds, thick-billed murres (*Uria lomvia*) and black-legged kittiwakes (*Rissa tridactyla*), and two prey taxa (age-0 walleye Pollock, *Gadus chalcogrammus* and krill, *Thysanoessa* spp) in the Southeastern Bering Sea. We quantified the multi-trophic influence and spatial structure of a cross-shelf $\delta^{15}N$ isotopic gradient measured in krill and pollock, and used it to contrast the foraging patterns of the two seabird species. Measurements were developed from comparisons of $\delta^{15}N$ isotope values in seabird muscle tissues to baseline krill and pollock values obtained from isoscape mapping techniques.

Stable isotopes are useful in ecology because physical and geochemical processes are known to affect their values in predictable ways, and biophysical processes lead to their differential accumulation in the tissues of plants and animals that feed and grow within specific environments (Kelly, 2000; Post, 2002).

* Corresponding author.
E-mail address: njones@mlml.calstate.edu (N.M. Jones).

http://dx.doi.org/10.1016/j.dsr2.2014.04.008
0967-0645/

Isotopic values of new tissues reflect the diet and habitat use of an animal at the time of tissue synthesis. For example, among birds it has been shown that blood plasma and liver cellular turnover rates are quite rapid, representing tissue synthesis periods of a week or less, whereas red blood cell and muscle tissue turnover rates tend to range from four to seven weeks (Hobson and Clark, 1992; Bearhop et al., 2002; Cherel et al., 2005). Recent studies of both captive and wild seabirds have shown that isotopic values in blood, feather, and internal organ tissues can be used to infer long distance migratory movements (Quillfeldt et al., 2010), identify likely foraging habitat use (Phillips et al., 2009; Moreno et al., 2011; Roscales et al., 2011; Jaeger et al., 2013), and elucidate trophic relationships among birds and their prey (Hobson et al., 2002). Some of the most recent studies have made use of predictive isoscape techniques.

Predictive isoscape maps are theoretical isotopic landscapes to which researchers can compare focal species samples and infer movement patterns or assign a place of likely origin based on isotopic values (Hobson et al., 2007; Barnes et al., 2009; Bowen, 2010). Much isoscape work within the marine environment is based on coherent, cross-shelf patterns in $\delta^{13}C$ and $\delta^{15}N$ baseline values among shallow nearshore, and deep offshore systems (Goericke and Fry, 1994; Miller et al., 2008; Barnes et al., 2009; Kline, 2009; Quillfeldt et al., 2010). In broad scale studies of the Bering Sea, $\delta^{13}C$ and $\delta^{15}N$ values in euphausiids and copepods decreased from east (onshore, shallow, shelf system) to west (offshore, deep, pelagic system; Schell et al., 1998). Recently, Granger et al. (2011) measured a large cross-shelf gradient of $\pm 5‰$ in $\delta^{15}N$ of suspended sediments, and Morales et al. (2014) measured a similar gradient in phytoplankton, with the greatest values measured to the north and east of the Pribilof Islands over shallow, shelf waters. Copepods in the Gulf of Alaska display a similar cross-shelf gradient, and in the Atlantic differences in $\delta^{15}N$ were measured between coastal and pelagic fishes in the diet of the European shag, *Phalacrocorax aristotelis* (Kline, 2009; Moreno et al., 2011). Such cross-shelf patterns result from differences in the source pools of nutrients, the extent of vertical mixing and seasonal ice cover, the length of the food chain, and the products of phytoplankton physiology that result in differential uptake of nutrients between shelf and pelagic systems (Schell et al., 1998; Smith et al., 2002; Kline, 2009; Granger et al., 2011; Morales et al., 2014). Based on previous studies that measured a south-to-north, basin-to-shelf enrichment in $\delta^{15}N$ of suspended sediments (Granger et al., 2011), phytoplankton (Morales et al., 2014), and in euphausiids (Schell et al., 1998), we hypothesized that if breeding seabirds foraged preferentially and repeatedly in specific regions within the vicinity of their breeding colonies, they could acquire an isotopic signal positively correlated with that of basal prey species present in the same region, and yield related patterns in predator and prey isotopic values that might indicate that cross shelf gradients in isotopic baselines can be detected at multiple trophic levels (Kelly, 2000; Post, 2002; Bowen, 2010; Kline 2010; Olson et al., 2010).

Morales et al. (2014) demonstrated large cross-shelf differences in phytoplankton $\delta^{15}N$ values across our study area, so we expected that isotopic relationships between seabirds and prey at a relatively fine spatial scale (10's–100's of kms) could be heavily influenced by variation in $\delta^{15}N$. Variability in $\delta^{15}N$ can be greater than in $\delta^{13}C$ among predators, and is based on the trophic level of prey species present in the diet. This is because $\delta^{15}N$ values of predator tissues tend toward a greater average enrichment of 3.2–3.4‰ with each increase in trophic level, whereas $\delta^{13}C$ values change little with increasing trophic level, and are often less variable (approximately 1‰ with each level; (Kelly, 2000; Post, 2002). We therefore expected that any isotopic relationships based on correlations between prey base and predators could be more easily detected at fine scales in $\delta^{15}N$ than in $\delta^{13}C$. Characterizing the isotopic signal of primary producers at the biological base of an aquatic food web can be challenging because phytoplankton have short life spans, and individual generations can respond rapidly to transient conditions (Laws et al., 1995; Burkhardt et al., 1999; Rolff, 2000; Tamelander et al., 2009). Therefore, when building the prey $\delta^{15}N$ baseline isoscapes we chose to sample euphausiids (krill: *Thysanoessa* spp.) and age-0 walleye pollock (pollock: *G. chalcogrammus*) as proxies for the marine food web, because consumers at these levels integrate the more variable isotopic signal from phytoplankton and small zooplankton, in effect averaging short term conditions and reducing uncertainty in the estimation of the trophic position of consumers located higher in a given food web (Post, 2002; Barnes et al., 2009). These two prey types occur throughout the study region, they are among the dominant taxa of the eastern Bering Sea shelf in terms of biomass density (Aydin and Mueter, 2007), and they are commonly consumed by the focal seabird study species, thick-billed murres and black-legged kittiwakes (Sinclair et al., 2008; Renner et al., 2012; Paredes et al., 2012; Harding et al., 2014).

Thick-billed murres and black-legged kittiwakes use contrasting foraging methods (pursuit-divers versus plunging surface-feeders, respectively) that are widely employed by seabirds throughout the world, thus making them relevant templates for study. In the central and southern Bering Sea, the breeding season for both species spans the period from May through August (Byrd et al., 2008). During the breeding season these species function as central place foragers because both parents participate in territorial defense, egg incubation (~May–June), and the raising of young (~July–August), and therefore their foraging time and trip length are constrained by the need to return repeatedly to a nesting site at a central colony location (Paredes et al., 2012; Harding et al., 2014). Given such constraints, central place foraging seabirds are sensitive to local food availability (distribution, abundance, and density), and often demonstrate measurable patterns in foraging activity (specific diet or foraging site fidelity) that can appear as signals in isotopic measurements (Quillfeldt et al., 2005; Roscales et al., 2011; Jaeger et al., 2013). Isotopic signals in either (or both) species are influenced by diet specificity, however the pursuit-diving strategy of murres could necessitate a greater commitment to discrete foraging locations, so we suspected that their isotopic signal (if measureable) might be more noticeably enhanced by a local geospatial influence (Croll and McLaren, 1993; Gabrielsen et al., 1988; Byrd et al., 2008; Harding et al., 2014). It was therefore expected that any isotopic coupling between prey base and predator could be stronger among murres than among kittiwakes. In this context this study expanded on the spatiotemporal extent to which isotopic analysis can successfully inform foraging studies that link mobile marine predators to their dynamic prey base.

2. Methods

2.1. Study area

We conducted fine scale (20–100 km), simultaneous sampling of seabirds and their prey in waters within 185 km of the Pribilof Islands, St. George (56.60°N, 169.58°W) and St. Paul (57.19°N, 170.26°W), and extending southeastward to encompass all habitat within 185 km to the north of Bogoslof Island (53.93°N, 168.03°W; Fig. 1). The two Pribilof islands host large seabird breeding colonies that are functionally isolated (> 350 km to the nearest neighboring colonies) during the summer breeding season, and Bogoslof Island supports rapidly growing colonies of kittiwakes and murres (Kitaysky et al., 2000; Stephenson and Irons, 2003; Jahnke et al., 2008). Since Bogoslof and the Pribilof Island colonies

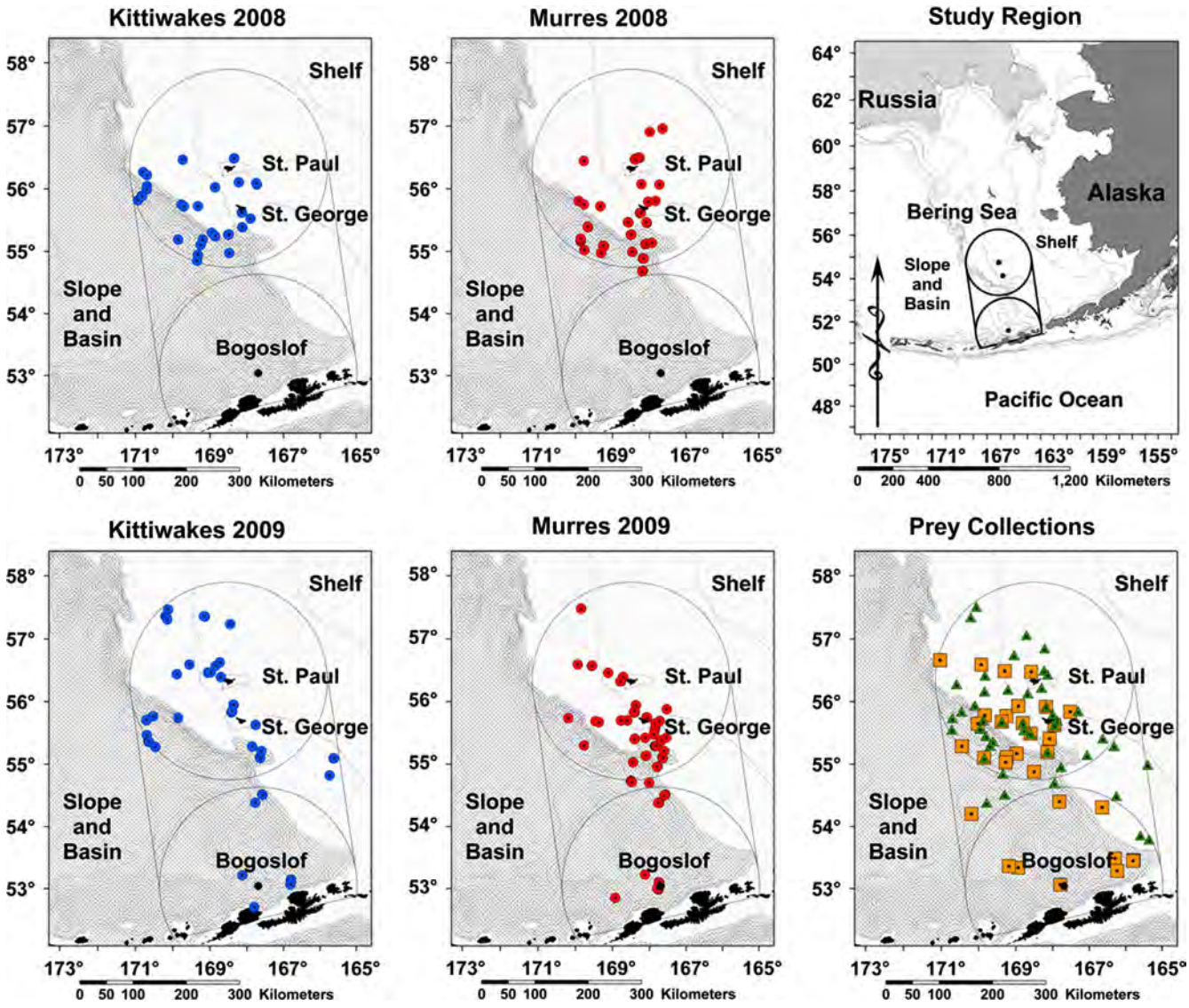

Fig. 1. Seabird, euphausiid and pollock collection locations.

are all relatively isolated, the sampling area was amenable to fine scale studies of foraging dynamics because birds collected near these islands were likely to have originated from those colonies and were using the local area specifically for foraging and breeding (Kitaysky et al., 2000; Stephenson and Irons, 2003; Byrd et al., 2008; Jahnke et al., 2008; Paredes et al., 2012; Harding et al., 2014). The portion of the North American continental shelf break encompassed by the study area is abrupt, and as such represents a discrete transition between oceanic basin and continental shelf habitats (Hunt et al., 2008). Broad scale, cross-shelf patterns in isotope baselines have been measured elsewhere, yet this environment offered an opportunity to study such phenomena on a more accessible scale than in many other ocean systems (Hunt et al., 2008; Miller et al., 2008; Jaeger et al., 2013).

2.2. Sample collections

2.2.1. Prey collections

Prey sampling was conducted at pre-determined, stratified, random 10 km transect survey (90%) locations, as well as adaptive 10 km transects (10%) that targeted prey patches discovered through acoustic measurements during the course of the study. In each location, prey specimens were collected using modified Marinovich trawls and Neuston nets targeted at prey patches that had been located with split-beam echo-sounders (38, 70, 120, and 200 kHz). Subsamples from net tows were collected, identified, and immediately frozen (-30 °C) for transport to laboratories onshore. Age-0 pollock were sampled in all cases, as well as the dominant krill species from each tow. However, prey patch compositions and locations varied throughout each year, and between years, and many net tows yielded neither krill nor pollock. Spatial coverage of intra-year krill and pollock sampling was too sparse to generate robust within-year isoscape maps. Therefore, we evaluated whether it was viable to pool samples from both years in order to achieve the greatest spatial coverage to create broadly predictive prey baselines. We were interested in looking at $\delta^{13}C$ and $\delta^{15}N$ individually to assess the potential of each as an independent tool in creating either $\delta^{13}C$ or $\delta^{15}N$ isoscapes that might be used to elucidate differences in habitat use among taxa. Data analyses indicated that $\delta^{15}N$ values could be combined appropriately to create baseline $\delta^{15}N$ models for prey taxa, but that $\delta^{13}C$ values were not amenable. Therefore, isotope values from repeat net tow sampling at a given location were averaged to generate a single $\delta^{15}N$ value for each prey type at each location. The resulting $\delta^{15}N$ datasets consisted of 33 sample locations for krill and 46 locations for pollock (Fig. 1). These sampling locations were used for discrete basin–shelf $\delta^{15}N$

comparisons, and in the generation of isotopic baselines for comparisons of patterns in baselines and predator tissue values.

2.2.2. Seabird collection

Adult thick-billed murres and black-legged kittiwakes were collected with a shotgun as they engaged in foraging activity on the open ocean (Fig. 1). All collected birds were in breeding condition, as verified by evidence of a brood patch. We also assessed subcutaneous fat deposits and pectoral muscle condition to ascertain that all were healthy and showed no signs of nutritional stress (Baduini et al., 2006). All collection locations were associated with randomly distributed net tow sampling and strip transects being undertaken by the research vessel, and therefore a thorough stratification of sampling was achieved to include all potential habitat types, in each week of data collection, for the duration of collection activities in both years. Birds were collected at all times of day between the hours of 0300–2340 h, AKDT. We preferentially targeted foraging birds that were within 25 m range of the ship and on the water surface, rather than in flight, because foraging and on-water birds could be linked directly to simultaneous prey base measurements and could be more clearly associated with the specified collection location. Some limitations to the sampling method were obvious, as the research vessel motoring at sea traveled at speeds of only 5–9 knots, while birds foraging in surrounding waters routinely traveled at multiples of that pace. Kittiwakes, in particular, are accomplished fliers, and both species are theoretically capable of traversing the entire study area, so it was not possible to know how long a particular bird had spent at a given location when it was targeted for collection (Paredes et al., 2012). Despite these limitations, spatial patterns resulting from at-sea collections were very likely indicative of foraging activity. Specifically, whereas each bird was collected at one random point during one single foraging trip, muscle isotope values reflected that bird's foraging activity integrated over a period of weeks. Therefore, if foraging birds collected randomly throughout the study area during a 30 day period were found to be regionally similar in isotopic composition, and to correlate with prey measurements taken in close proximity, then such coherent geospatial patterns were unlikely to have resulted from chance alone. We collected no more than 3 birds from any given location (within 500 m radius of initial take). The birds were retrieved from the water using a long-handled dip net, and then frozen (-30 °C) immediately onboard the ship for preservation (Barrett et al., 2007; Bugoni et al., 2008). Upon return, samples of left pectoral muscle were removed for stable isotope analyses. We collected 47 murres and 39 kittiwakes in 2008, and 78 murres and 66 kittiwakes in 2009. We initially combined samples from both years by species and divided them into two groups, "basin" (>200 m depth), and "shelf" (<200 m depth), for testing based on bathymetry associated with the collection site. Subsequently, samples were grouped by species in each year to make 2008 and 2009 comparisons to isotopic baselines.

2.3. Stable isotope analyses

Before testing, all samples were dried at 40 °C for 48 h, then ground into a fine powder and lipid-extracted using a methanol-chloroform mixture (Bligh and Dyer, 1959; Sotiropoulos et al., 2004; Kojadinovic et al., 2008). Seabird tissues were analyzed at the University of Alaska, Fairbanks. Fish and euphausiid tissues were analyzed at Northern Arizona University. Isotope values for $\delta^{13}C$ and $\delta^{15}N$ were measured with continuous-flow isotope-ratio mass spectrometry, using a Thermo-Electron Deltaplus Advantage gas isotope-ratio mass spectrometer interfaced with a Costech Analytical ECS4010 elemental analyzer. Internationally-accepted isotope elemental calibration standards were used to determine accuracy (acetanilide, cyclohexanone, cystine, methionine, nicotinamide, and sulfanilamide). Secondary isotopic reference materials included NIST bovine liver, and NIST mussel, as well as NIST pine needles, and NIST tomato leaves. Calibration runs were conducted frequently to check for run drift and linearity. Blanks were analyzed every twenty samples and Secondary isotopic reference materials were analyzed every ten samples. Precision of secondary isotope reference material ($n=82$) was $<0.25‰$ for both carbon and nitrogen. Twice a year the secondary isotopic reference materials from these labs are compared to NIST standards for quality assurance. The $\delta^{13}C$ and $\delta^{15}N$ values are expressed relative to Vienna-Pee Dee Belemnite limestone V-PDB for carbon, and to air for nitrogen. Stable isotopes are reported here in δ notation as the deviation from standards, in parts per thousand ($‰$), according to the following equation: $\delta X=[(R_{sample}/R_{standard})-1]$ where X is the isotope in question (^{15}N or ^{13}C) and R is the ratio of the heavier (e.g., ^{15}N) to the lighter (e.g., ^{14}N) isotope of the element (Fry, 2005).

2.4. Data analyses

2.4.1. Measuring isotopic differences between continental shelf and deep basin habitats

Our goal in basin-shelf comparisons was to identify whether there were detectable differences in either $\delta^{13}C$ or $\delta^{15}N$ that might indicate the existence of a cross-shelf pattern in isotopes. Analyses of 2008 and 2009 krill and pollock $\delta^{15}N$ isotopic values revealed no deviations from normality (Kolmogorov–Smirnov test), no differences in variance (Levene's test), and no statistical differences among means (Student's t-test, with Bonferroni corrections) between years within a given prey type, so $\delta^{15}N$ data from both years were pooled for each prey taxon to create two homogeneous prey baseline $\delta^{15}N$ datasets: one for krill and one for pollock. These were then used to compare basin and shelf habitats and to create $\delta^{15}N$ isoscapes. Inter-year analyses (Student's t-test, with Bonferroni corrections) of prey $\delta^{13}C$ isotope values indicated dissimilar mean values between years in both prey taxa, as well as significant differences (Levene's test) in variance among pollock samples between years. Therefore, prey $\delta^{13}C$ values from 2008 and 2009 were not pooled, and we did not create a homogeneous $\delta^{13}C$ baseline for comparison to seabird muscle values. Seabirds of a given species did not differ overall in $\delta^{13}C$ or $\delta^{15}N$ between years, so basin-shelf differences in $\delta^{13}C$ and $\delta^{15}N$ values in seabird muscle tissue were compared between habitat types using Student's t-tests (with Bonferroni corrections), because our interests lay specifically in assessing each isotope measure individually for its potential as a diagnostic tool in assessing habitat use. However, there were no overall basin-shelf differences in $\delta^{13}C$ values of seabird tissues ($p>0.5$ in both species), so further analysis focused on determining patterns of $\delta^{15}N$ isotope distribution across habitats and trophic levels. We performed these statistics using the R 2.14.0 statistical computing package (R: A Language and Environment for Statistical Computing. R Foundation for Statistical Computing http://www.r-project.org).

2.4.2. Spatial structure among isotope values of samples collected at sea

Given the likely muscle tissue turnover time ($\sim$48 days) in seabirds in the context of our 30 day sampling periods, we considered that significant isotope correlations between birds and prey would be indicative of 30–60 days of corresponding spatiotemporal similarities in the diet or foraging locations of the birds (Hobson and Clark, 1992). All datasets were standardized to Z-scores to account for the large differences in scale between

isotope values and distance measurements, and then we determined spatial structure (autocorrelation) by assessing the Moran's *I* statistic using the statistical program R 2.14.0 (Moran, 1950; Legendre and Legendre, 1998, R: A Language and Environment for Statistical Computing. R Foundation for Statistical Computing http://www.r-project.org).

2.4.3. Isoscape mapping and patterns in trophic relationships among taxa

Mapping and visualization were accomplished using ArcGIS v.9.3 (ESRI Corporation, Redlands, CA). Seabird, euphausiid, and pollock sampling locations did not always directly coincide, so it was necessary to map patterns for each taxon independently and then compare them to one another. To examine basic patterns in isotopic values across the study region, we used Inverse Distance^2 Weighted interpolations to generate a simple contour map of each isotopic dataset (δ^{15}N for tissues: krill, pollock, and seabird muscle (Fortin and Dale, 2005). Any resultant cross-shelf pattern that became evident for isotopic values of both prey and predators was then smoothed and modeled using a Local Polynomial Interpolation function in the Geostatistical Analyst toolkit of ArcGIS. In this process, the software generated predictive isoscape surfaces by repeatedly fitting a first order polynomial through prey sampling points (δ^{15}N of prey items captured in net tows) that fell within a pre-defined search neighborhood as it was passed across the entire study region. The search neighborhood parameters that were applied in the calculation (the shape, size, orientation, number of points included, and directional bias) were determined through an iterative process of variogram analysis and cross validation (ArcGIS v.9.3). The Local Polynomial Interpolation created two smoothed surfaces, one for krill and one for pollock, which were then used as templates to which seabird sample values were compared at their points of collection. This process yielded sets of values in triplicate (seabird tissue, predicted pollock tissue, and predicted krill tissue), and enabled the comparison of measured δ^{15}N values in seabird tissues to prey base δ^{15}N values that were derived from the contemporaneously-sampled prey items. Pearson's correlation statistics identified a strong relationship ($r \geq 0.95$; $p < 0.001$) between krill and pollock δ^{15}N baselines. Given this correlation, we focused our evaluation of the fundamental cross shelf gradient patterns using just the linear regression of krill prey baseline values on seabird δ^{15}N muscle values, with the assumption that working with pollock would yield similar results. Dependent variables were seabird values, with krill baseline δ^{15}N values as predictors (statistical program R 2.14.0).

3. Results

We measured significant differences in δ^{15}N values for three of our four taxa between deep and shallow habitats during the years 2008 and 2009. Euphausiid, pollock, and murre tissues sampled in shallow, continental shelf habitat had greater δ^{15}N values relative to tissues from samples taken over deeper basin habitats (Table 1). In contrast, we detected no differences in δ^{15}N between habitat types for kittiwakes. There were no detectable differences in δ^{13}C values of either murre or kittiwake muscle tissues sampled in 2008 and 2009, and sampling coverage was too sparse to enable robust intra-year comparisons of δ^{13}C in prey species.

Spatial structure (autocorrelation) was detected among δ^{15}N values of krill ($p = 0.017$) and pollock ($p = 0.0001$; Fig. 2), as well as murres ($p < 0.0001$ in both years; Fig. 3). Therefore, at scales of < 100 km, the δ^{15}N values of amimals collected in close proximity tended to be much more similar to one another than to δ^{15}N values in animals collected at greater distances. There was no spatial structure ($p > 0.20$) in δ^{15}N values of kittiwake muscle tissues in either year. Inverse Distance^2 Weighted mapping of δ^{15}N values in thick-billed murres and their prey yielded similar patterns at scales of < 100 km, suggesting fundamental differences between shallow, continental shelf habitat and deeper basin habitats. More specifically, the average δ^{15}N values of the tissues of murres, krill, and pollock increased with increasing latitude (north of St. Paul Island), and decreasing depth (continental shelf; Figs. 2and 3). Kittiwake isotope values exhibited no such spatial coherence with prey values in 2008, but demonstrated scattered clustering of like values in 2009, providing some suggestion of a basin-shelf dichotomy at least in that year (Fig. 3). Subsequent Local Polynomial Interpolation mapping effectively smoothed the prey data and generated krill and pollock predictive isoscapes that were both characterized by distinct, cross-shelf gradients in δ^{15}N values. Krill and pollock sampled over northern, shallower shelf habitat yielded values that were 1–2‰ greater than samples taken over deeper basin habitats to the south, at distances of only 20–100 km (Fig. 2), and predicted values of krill and pollock at seabird collection locations were highly correlated with one another in both years ($r \geq 0.95$, $p \leq 0.0001$), indicating a utility in choosing krill specifically to represent the prey base in subsequent testing (Table 2). Kittiwake muscle δ^{15}N values did not track krill and pollock δ^{15}N in 2008, however, in 2009 there were some average enrichment patterns across the study area, and weakly significant relationships between 2009 kittiwake muscle values and those of krill baselines, although the prey base values had virtually no predictive influence ($r^2 < 0.06$; Fig. 4, Table 2). In contrast, murre muscle δ^{15}N values tracked krill and pollock δ^{15}N more closely in both years, demonstrating more consistency among average ^{15}N enrichment trends throughout the study area (Fig. 4, Table 2). Krill baseline values predicted 35–42% of the δ^{15}N variability in murre muscle tissues (Table 2). These results reflected the concordance of spatial structure in δ^{15}N values of krill, pollock, and murre muscle tissue in both years; the Inverse Distance^2 Weighted maps and the regression plots demonstrated an increasing, basin-shelf trend in δ^{15}N values of murre tissues and their prey, with the greatest enrichment occurring N-NW of St. Paul Island over shallow shelf waters (Fig. 3). Relationships between kittiwakes and the prey base measures were less coherent.

Table 1
Differences in mean δ^{15}N values of seabirds and prey collected in basin (> 200 m depth) versus shelf (< 200 m depth) habitats in the southeastern Bering Sea Alaska, 2008 and 2009.

Taxon	Basin mean δ^{15}N value ± SE	Shelf mean δ^{15}N value ± SE	Test statistic	*p*-Value
Euphausiids	9.4 ± 0.1	10.4 ± 0.1	$T_{31} = 6.79$	< **0.0001**
Pollock	9.2 ± 0.2	11.2 ± 0.2	$T_{44} = 6.59$	< **0.0001**
Kittiwakes	12.9 ± 0.1	13.1 ± 0.1	$T_{103} = 1.18$	0.1300
Murres	11.9 ± 0.1	12.4 ± 0.1	$T_{123} = 4.38$	< **0.0001**

Samples were collected in the southeastern Bering Sea, Alaska, between July 15th–August 15th in two years: 2008 (within a 185 km radius of St. Paul Island), and 2009 (185 km radius of St. Paul Island and extending southward to within 185 km radius of Bogoslof Island). Dataset represents combined sampling effort from 2008 and 2009 after verification of statistical homogeneity (Kolmogorov–Smirnov and Levene's testing) between years. Bold indicates significance at $p < 0.0125$ after Bonferroni corrections were applied for multiple testing.

4. Discussion

Isotope values in murre and kittiwake pectoral muscle tissue represent a diet integrated over approximately 40–50 days, and our sampling periods were each ~30 days during the breeding seasons of 2008 and 2009 (Hobson and Clark, 1992; Bearhop et al., 2002; Cherel et al., 2005). Therefore, the degree of spatial structure (significance of Moran's *I* statistic), coupled with the

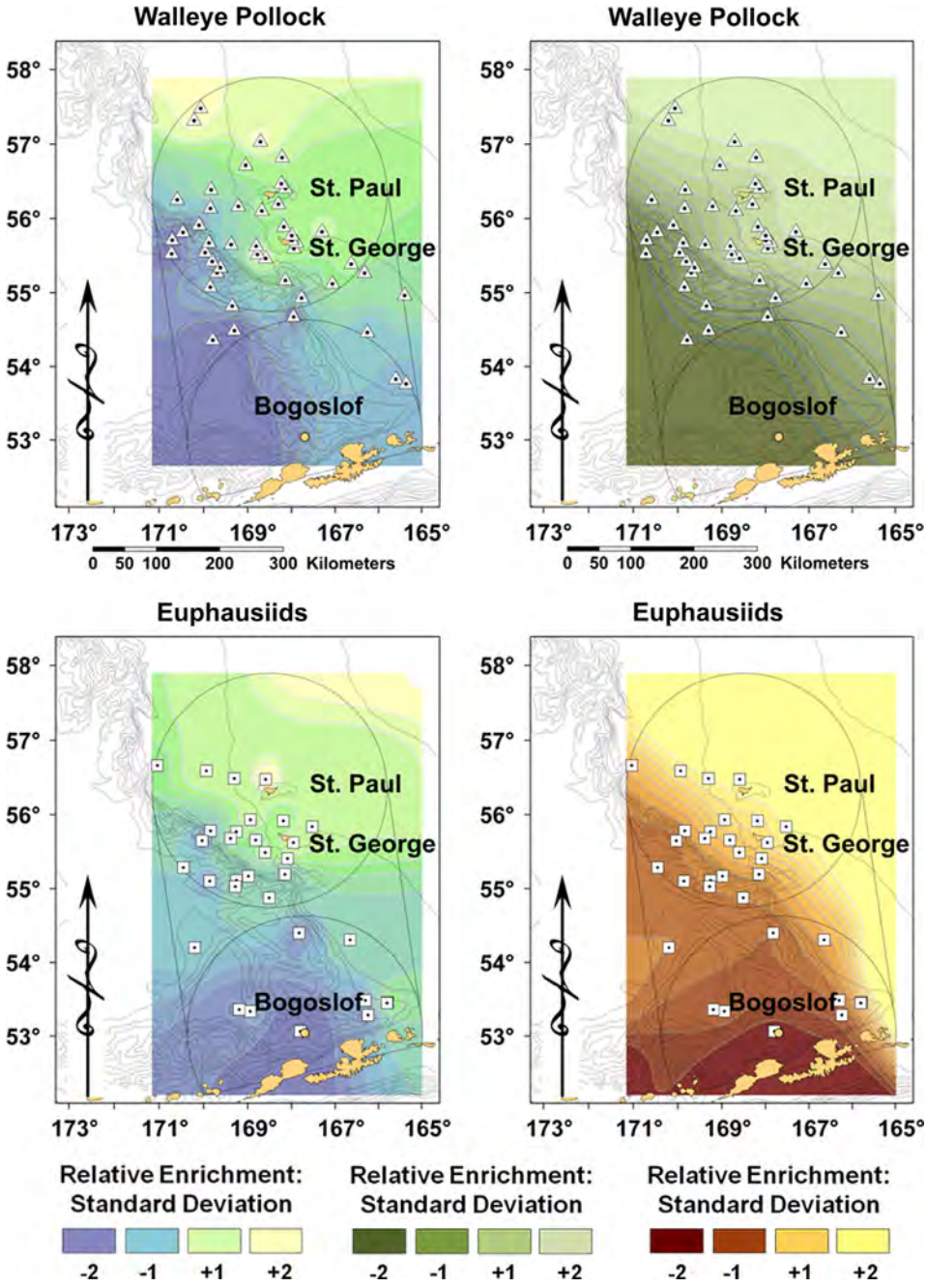

Fig. 2. Spatial autocorrelation patterns and predictive isoscape modeling of $\delta^{15}N$ values of seabird prey tissues.

strength of prey–predator linkage (magnitude and significance of regression r^2), could represent the degree to which birds foraged repeatedly in a given area during a given breeding season. Nitrogen values in murre muscle tissues yielded highly significant spatial structure in both years, and regression results indicated that prey baselines and murre tissue $\delta^{15}N$ values were spatially coupled throughout the entire sampling region in both years. This implied regional specificity, as well as intra-seasonal and inter-annual consistency, in murre choice of foraging areas during their breeding period. Patterns among kittiwake tissues were much less coherent. Differences in isotope patterns between the two bird species could reflect, in part, the physiological and morphological adaptations that accommodate the contrasting foraging strategies of pursuit-divers (murres) and plunging surface-feeders (kittiwakes).

Pursuit-diving murres have greater caloric needs (field metabolic rates) than surface-feeding kittiwakes (Gabrielsen et al., 1988; Croll and McLaren, 1993; Kitaysky et al., 2000), reflecting the greater energy demands of a sub-surface foraging strategy (e.g., immersion in cold water, periodic oxygen deprivation, and greater resistance to movement), and the increased flight costs of morphological adaptation to diving (greater body mass, increased fat layer, and small, stiff wings) that contribute to heavy wing-loading. Our results are consistent with the hypothesis that greater flight costs for murres should require them to be more selective or consistent in their foraging effort in specific areas, returning repeatedly to locations where prey species were previously encountered with greater frequency or in greater abundance or density (Paredes et al., 2012; Harding et al., 2014). In doing so they should acquire a more distinct isotopic signal related to isotope values of prey items eaten in the locations in which they foraged. Other studies in the Bering Sea have indicated that sub-surface foragers such as murres may require prey patches of

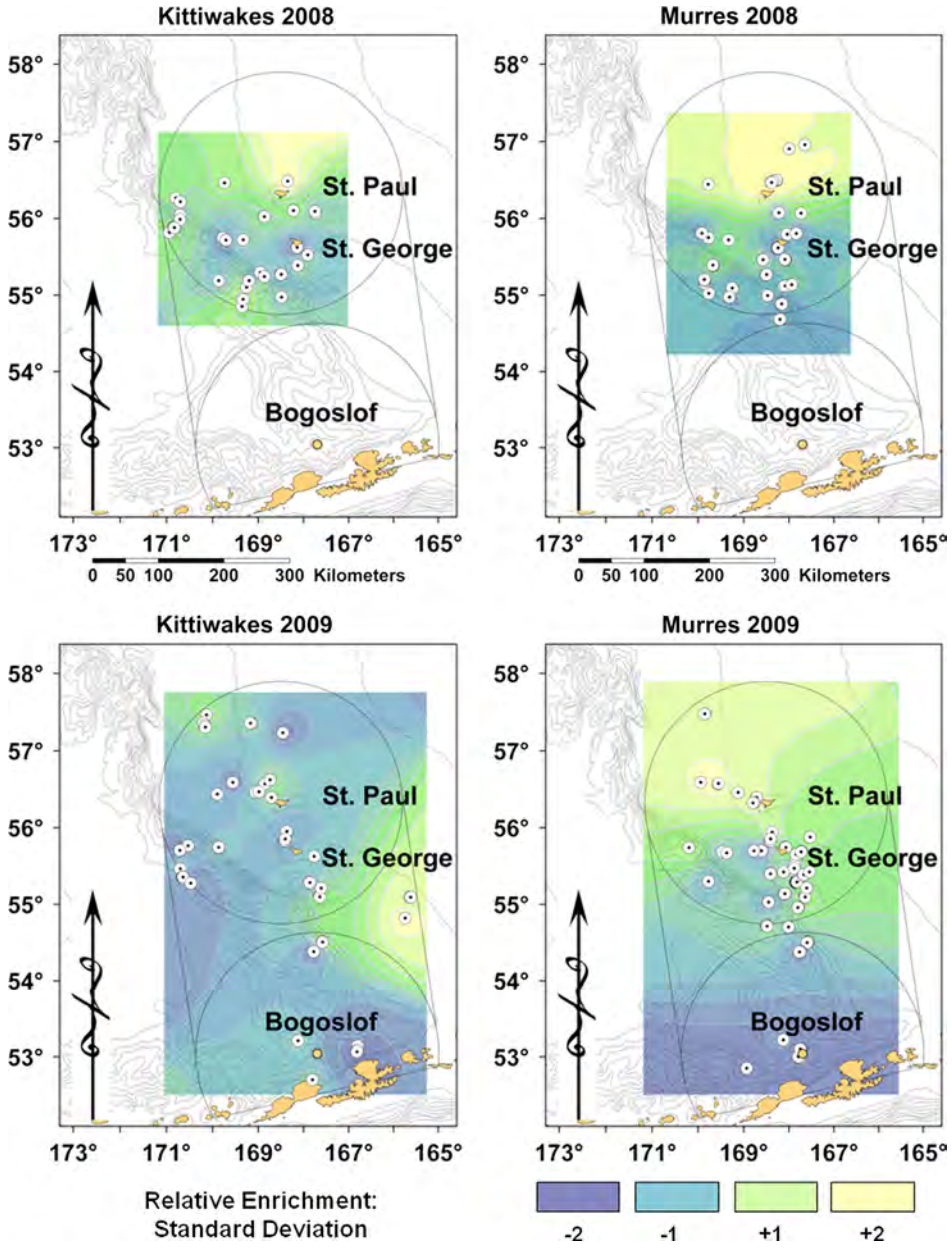

Fig. 3. Patterns in spatial autocorrelation of $\delta^{15}N$ values in seabird muscle tissues.

Table 2
Regression of $\delta^{15}N$ values in seabird liver and muscle tissues with those of predicted euphausiids (krill: *Thysanoessa* spp.) baseline tissues.

Seabird species	Year	Seabird tissue	β	t	R^2	F	p
Black-legged kittiwake	2008	Muscle	0.06	$t_{37}=0.27$	0.00	$F_{1,37}=0.07$	0.7910
Black-legged kittiwake	2009	Muscle	0.29	$t_{64}=2.09$	0.06	$F_{1,64}=4.36$	0.0410
Thick-billed murre	2008	Muscle	0.55	$t_{45}=5.71$	0.42	$F_{1,45}=32.63$	**0.0001**
Thick-billed murre	2009	Muscle	0.64	$t_{76}=6.34$	0.35	$F_{1,76}=40.22$	**0.0001**

Samples were collected in an area within a 185 km radius of St. Paul Island and extending southward to within 185 km radius of Bogoslof Island in the Bering Sea, July 15th–August 15th, 2008 and 2009. Krill values were chosen to represent the prey base, and were also strongly correlated (Pearson's $r \geq 0.95$; $p < 0.0001$) to pollock values. Krill values were obtained for each seabird sampling location from isoscape maps generated through Local Polynomial Interpolation (ArcGIS 9.3) of $\delta^{15}N$ values measured in actual prey items sampled concurrently from randomly placed net tows throughout the study area. Bold indicates significance at $p < 0.0125$ after Bonferroni corrections were applied for multiple testing. The regression coefficients and significance levels indicate stronger coupling between murre and prey base values throughout the area.

greater density and persistence than do surface-feeders such as kittiwakes, and that kittiwakes are indeed more widely dispersed at sea (Lovvorn et al., 2001; Hunt et al., 2005; Sigler et al., 2012). In contrast to murres, spatial structure and predator–prey regression results in the $\delta^{15}N$ values of kittiwakes were much weaker, which suggests that individual kittiwakes perhaps foraged more widely across the study region, and more frequently consumed prey from both shelf and basin habitats. Indeed, a recent broad scale study comparing persistent hotspots for the murres and kittiwakes in the Bering Sea came to similar conclusions, and a concurrent study

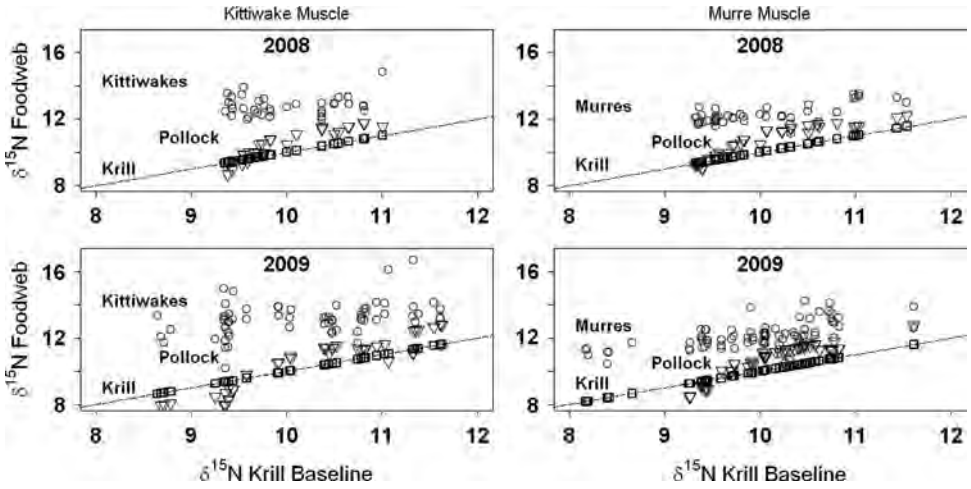

Fig. 4. Comparisons of δ^{15}N values in seabird muscle tissue and two measures of their prey base.

using tagged individual birds also found that kittiwakes foraged more widely across the eastern Bering Sea shelf (Paredes et al., 2012; Sigler et al., 2012).

There are other possible explanations for the lack of coherent isotope patterns among kittiwakes. Kittiwakes in the Gulf of Alaska and Bering Sea differ somewhat from thick-billed murres in their diet, and often consume larger proportions of myctophid fishes, the isotopic values of which might differ substantially from that of pollock (Sinclair et al., 2008; Renner et al., 2012). Myctophids are mesopelagic fishes and vertical migrators that inhabit deep water during the day, and may typically be underrepresented in survey trawls due to trawl avoidance behavior (Catul et al., 2011; Kaartvedt et al., 2012). Myctophids were infrequently collected during our sampling trawls, and the potential spatiotemporal mismatches between kittiwake foraging patterns, myctophid abundance and trawling effort made it difficult to assess the relationship of δ^{15}N in myctophid and kittiwake tissues. However, although our sampling yielded insufficient numbers of myctophids for isotope analyses, pollock nonetheless have been shown to constitute a consistent and important component of kittiwake diet in most years, and are commonly used as diagnostic tools in multi-year diet studies of predators in the Bering Sea (Sinclair et al., 2008; Renner et al., 2012). It is also likely there are differences in species composition among euphausiid communities between shelf and basin environments, although species-specific differences in isotopic values have not been thoroughly examined to date. Therefore, a greater breadth in foraging locations across the shelf break, coupled with differences in diet, could result in a more variable or diluted isotopic signal in kittiwake tissues, and weaker coupling to krill or pollock specifically.

The geospatial stratification of murre isotope values coincided in latitude with the three focal colonies (St. Paul, St. George, and Bogoslof). This suggests that the foraging habitat partitioning of individual tagged birds, measured by Harding et al. (2014) during the same time period, was likely representative of a much broader pattern. It could be expected that isotopes might identify a distinct foraging pattern for murres near Bogoslof, given its isolation from the Pribilof colonies. However, patterns in isotope values of murres collected within the Pribilof region also indicated the likelihood of con-specific habitat partitioning by colony, despite the close proximity (<75 km) of St. Paul to St. George. This suggests that these pursuit-diving seabirds might somehow be more closely linked to local patterns in resource availability than the wide-ranging, surface-feeding kittiwakes. Intra-specific habitat partitioning in the open ocean has been infrequently described in seabirds, however foraging site fidelity was inferred through analyses of stomach contents and stable isotope values in short-tailed shearwaters (*Puffinus tenuirostris*). The shearwaters were collected while foraging in several locations throughout Bristol Bay and the Eastern Bering Sea, and stable isotope values of organs indicated that groups of shearwaters were likely feeding for multiple weeks at a time in discrete locations, even though they were theoretically capable of foraging freely across a wide seascape while not breeding on a colony (Baduini et al., 2006). Elsewhere, Gremillet et al. (2004) demonstrated that foraging areas of cape gannets (*Morus capensis*) from two neighboring colonies overlapped very little, even though the two study colonies were well within (65–85%) the theoretical foraging range of one another, and Wiley et al. (2012) inferred habitat partitioning between two colonies of Hawaiian petrels (*Pterodroma sandwichensis*) in the Hawaiian Islands. Thus, it appears that habitat partitioning among con-specific marine birds may become an influential force affecting the delineation of a seasonal isotopic niche, the nature of which could be influenced by variations in habitat use as well as by differences in diet, although the relative importance of these two elements can be difficult to discern (Baduini et al., 2006; Newsome et al., 2007; Wiley et al., 2012).

Traditionally, δ^{13}C has been used as a diagnostic marker to infer latitudinal patterns in habitat use and distinguish between shallow, continental shelf and deep water, pelagic foraging areas, but in this study we found that δ^{15}N was also very useful in delineating predator habitat use, and at a fine scale (Hobson et al., 1994; Sydeman et al., 1997). For example, murres sampled over deep (>1000 m) Pribilof Canyon habitat were relatively depleted in ^{15}N compared to murres sampled just 25–75 km away over continental shelf habitat (<200 m depth) near St. Paul. On broader spatial scales, Forero et al. (2004) suggested isotope values of seabirds breeding along the Chubut coast of Argentine Patagonia reflected an enriched-depleted δ^{15}N cross-shelf gradient, Phillips et al. (2009) determined that stable nitrogen isotopes were useful markers for distinguishing wintering and pre-breeding habitat use by high latitude Atlantic procellariids, and Wiley et al. (2012) inferred habitat use of shearwaters in the central Pacific based on broad scale patterns in baseline δ^{15}N levels. We did not detect basin–shelf differences in δ^{13}C for either seabird species at the scale of our study, but Schell et al. (1998) detected a clear broad scale, cross-shelf pattern in δ^{13}C among copepods and krill. It is possible that a greater sampling effort, across a larger geographic area, would detect a similar cross-shelf pattern in δ^{13}C of our study species.

Isotope gradients in the Bering Sea appear to be persistent in time. The differences in basin/shelf δ^{15}N we measured for krill, pollock, and murres were similar in magnitude and spatial pattern to those measured by Schell et al. (1998) in copepods and

euphausiids in 1985–1995, and during our study we found no inter-annual differences in $\delta^{15}N$ isotope values within a given prey taxon. This corroborates assertions by some researchers that the measurement of isotope values in 1° and 2° consumers effectively integrates any seasonal variation present in the isotopic values of phytoplankton, smoothing variability to create a reliable baseline proxy (Post, 2002; Barnes et al., 2009). Cross-shelf gradients similar to what we found in murres and their prey have been measured elsewhere in other northern hemisphere systems that are characterized by seasonally well-mixed, shallow waters abutting abrupt shelf break and deep pelagic habitat (Bode and Alvarez-Ossorio, 2004; Miller et al., 2008; Olson et al., 2010). Recent food web modeling and meta analyses conducted for southern hemisphere marine communities have suggested that baseline signals could be transmitted upwards through the marine food web, manifesting in similar trends in $\delta^{13}C$ and $\delta^{15}N$ values of crustaceans and seabirds (Quillfeldt et al., 2005). Our results offer an empirical confirmation at fine scales through the simultaneous sampling of seabirds and their prey.

It is important to strive for an accurate understanding of baseline isotope values when applying stable isotope analyses in food web studies. Our results demonstrate that variations in baseline signals among habitats can propagate upward through food webs and affect multiple trophic levels. If regional variation is not accounted for, it can present potentially significant sources of error in estimates of predator diet composition and trophic level (Wiley et al., 2012; Solomon et al., 2008; Flaherty and Ben-David, 2010). In seabirds this phenomenon was also demonstrated by Moreno et al. (2011) in a contrast of two food webs including European shags on the coast of northwest Spain, where they found differences of 2.0‰ in $\delta^{15}N$ values of baseline mussel tissues between two study systems. Likewise, in the Bering Sea we found significant SW/NE, basin/shelf differences of approximately 2.0‰ in $\delta^{15}N$ values of age-0 pollock tissues, and approximately 1.0‰ in krill tissues, which represent sizeable sources of variation in trophic estimates, when considering that the average difference in $\delta^{15}N$ between an avian consumer and its prey in marine food webs is approximately 3.2‰ (Kelly, 2000).

Previous Bering Sea stable isotope research has successfully identified the long-distance migration routes and broad foraging habitats of fur seals (Kurle and Worthy, 2002), bowhead whales (Lee et al., 2005), and king eiders (Oppel and Powell, 2008). The habitat assignments of those studies were most successful at ecoregional scales (1000's km), whereas habitat studies based on isotopic signals at finer scales (<100 km) elsewhere have met with somewhat more mixed results (Szymanski et al., 2007). Our use of isoscapes to infer habitat use at fine scale was most informative when applied to murres, a species whose geospatial foraging patterns were more likely than kittiwakes to be constrained by physiological as well as ecological demands (for example, adaptations for pursuit diving, and obligate central place foraging during breeding). We were less successful at detecting an isotopic gradient in kittiwakes, a more wide-ranging predator species, and this lack of fine scale isotopic patterns may be more common in species with less spatially-constrained foraging behaviors. Nonetheless our study, which clearly demarcated a cross-shelf $\delta^{15}N$ gradient in a prey base shared by most top-tier predators in the region, may enable future researchers to increase the resolution at which it is possible to differentiate habitat use of multiple predators in the system.

Acknowledgments

This investigation made use of seabird tissues originally collected during the Patch Dynamics Study, which was a component of the North Pacific Research Board Bering Sea Integrated Ecosystems Research Program. Birds were collected with a shotgun under the auspices of the US Fish and Wildlife Service (USFWS/Migratory Bird collection permit #MB08537-1) and Alaska Department of Fish and Game (Fish and Game #08-134). Bird collection procedures were approved by the San Jose State University Animal Care and Use committee (IACUC Harvey#926), and the US Fish and Wildlife Service (IACUC #2008013). Prey species were collected under Oregon State University Animal Care and Use Protocol #3659, with Fish and Game collection permit #CF-09-094 from Alaska Department of Fish and Game. The study was funded by the North Pacific Research Board (BSIERP/Patch Dynamics Study Projects B67 and B77). This is BEST-BSIERP publication number 133, and NPRB publication number 476. We thank the captains and crew members of the F/V Frosti and F/V Gold Rush for their expert seamanship, commitment to safety, enthusiasm for science, and tireless efforts in support of the data collected at sea. We thank Luke Whitman for his help in data collection and logistics. We thank Larry Boyle (AK Fish and Game), David Irons (USFWS), and Dan Roby (OSU) for consulting on seabird collections activity; Kathy Turco for her expert prey I.D.; Michelle St. Peters (USFWS) for logistics support; Rick Doucett (NAU), Tim Howe (UAF), and Norma Haubenstock (UAF) for professional attention to detail and their truly exceptional generosity with time and lab resources; Larry Young for IACUC consulting at SJSU; Jim Harvey (MLML), and two anonymous reviewers for their generous time to review initial drafts of this manuscript; Dan Roby at OSU, and Hannah Nevins at California Fish and Game for providing seabird processing facilities, and to the students and technicians at Moss Landing Marine Labs and OSU for their time in processing collected seabirds.

References

Aydin, K., Mueter, F., 2007. The Bering Sea – a dynamic food web perspective. Deep-Sea Res. II 54, 2501–2525.
Baduini, C.L., Hunt, G.L., Pinchuk, A.I., Coyle, K.O., 2006. Patterns in diet reveal foraging site fidelity of short-tailed shearwaters in the southeastern Bering Sea. Mar. Ecol. Prog. Ser. 320, 279–292.
Barnes, C., Jennings, S., Barry, J.T., 2009. Environmental correlates of large-scale spatial variation in the $\delta^{13}C$ of marine mammals. Estuar. Coast. Shelf Sci. 81, 368–374.
Barrett, R.T., Camphuysen, K.C.J., Anker-Nilssen, T., Chardine, J.W., Furness, et al., 2007. Diet studies of seabirds: a review and recommendations. ICES J. Mar. Sci. 64, 1675–1691.
Bearhop, S., Waldron, S., Votier, S.C., Furness, R.W., 2002. Factors that influence assimilation rates and fractionation of nitrogen and carbon stable isotopes in avian blood and feathers. Physiol. Biochem. Zool. 75 (5), 451–458.
Bligh, E.G., Dyer, W.J., 1959. A rapid method of total lipid extraction and purification. Can. J. Biochem. Physiol. 37, 911–917.
Bode, A., Alvarez-Ossorio, M.T., 2004. Taxonomic versus trophic structure of mesozooplankton: a seasonal study of species succession and stable carbon and nitrogen isotopes in a coastal upwelling ecosystem. ICES J. Mar. Sci. 61, 563–571.
Bowen, G.J., 2010. Isoscapes: spatial pattern in isotopic biogeochemistry. Annu. Rev. Earth Planet. Sci. 38, 161–187.
Bugoni, L., McGill, R.A.R., Furness, R.W., 2008. Effects of preservation methods on stable isotope values in bird tissues. Rapid Commun. Mass Spectrom. 22, 2457–2462.
Burkhardt, S., Riebesell, U., Zondervan, I., 1999. Stable carbon isotope fractionation by marine phytoplankton in response to day length, growth rate, and CO_2 availability. Mar. Ecol. Prog. Ser. 184, 31–41.
Byrd, G.V., Sydeman, W.J., Renner, H.M., Minobe, S., 2008. Responses of piscivorous seabirds at the Pribilof Islands to ocean climate. Deep-Sea Res. II 55, 1856–1867.
Catul, V., Gauns, M., Karuppasamy, P.K., 2011. A review on mesopelagic fishes belonging to family Myctophidae. Reviews in Fish Biol. Fish. 21 (3), 339–354.
Cherel, Y., Hobson, K.A., Weimerskirch, H., 2005. Using stable isotopes to study resource acquisition and allocation in procellariiform seabirds. Oecologia 145, 533–540.
Croll, D.A., McLaren, E., 1993. Diving metabolism and thermoregulation in common and thick-billed Murres. J. Comp. Physiol. B 163, 160–166.
Flaherty, E.A., Ben-David, M., 2010. Overlap and partitioning of the ecological and isotopic niches. Oikos 119, 1409–1416.
Forero, M.G., Bortolotti, G.R., Hobson, K.A., Donazar, J.A., Bertelloti, M., et al., 2004. High trophic overlap within the seabird community of Argentinean Patagonia: a multiscale approach. J. Anim. Ecol. 73, 789–801.

Fortin, M.J., Dale, M.R.T., 2005. Spatial Analysis: A guide for Ecologists, VII ed. Cambridge University Press p. 365.
Fry, Brian, 2005. Stable Isotope Ecology, III ed. Springer Science Media, p. 308.
Gabrielsen, G.W., Mehlum, F., Karlsen, H.E., 1988. Thermoregulation in four species of arctic seabirds. J. Comp. Physiol. B 157, 703–708.
Goericke, R., Fry, B., 1994. Variations of marine plankton $\delta^{13}C$ with latitude, temperature, and dissolved CO_2 in the world ocean. Global Biogeochem. Cycles 8 (1), 85–90.
Gremillet, D., Dell'Omo, G., Ryan, P.G., Peters, G., Ropert-Coudert, Y., Weeks, S.J., 2004. Offshore diplomacy, or how seabirds mitigate intra-specific competition: a case study based on GPS tracking of Cape Gannets from neighboring colonies. Mar. Ecol. Prog. Ser. 268, 265–279.
Granger, J., Prokopenko, M.G., Sigman, D.M., Mordy, C.W., Morse, Z.M., et al., 2011. Coupled nitrification–denitrification in sediment of the eastern Bering Sea shelf leads to ^{15}N enrichment of fixed N in shelf waters. J. Geophys. Res. 116, C11006.
Harding, A., Paredes, R., Suryan, R., Roby, D., Irons, D., Orben, R., Renner, H., Young, R., Barger, C., Dorresteijn, I., Kitaysky, A., 2014. Does location really matter? An inter-colony comparison of seabirds breeding at varying distances from productive oceanographic features in the Bering Sea. Deep-Sea Res. II, 109.
Hobson, K.A., Clark, R.G., 1992. Assessing avian diets using stable isotopes I: turnover of $\delta^{13}C$ in tissues. Condor 94 (1), 181–188.
Hobson, K.A., Piatt, J.F., Pitocchelli, J., 1994. Using stable isotopes to determine seabird trophic relationships. J. Anim. Ecol. 63 (4), 786–798.
Hobson, K.A., Gilchrist, G., Falk, K., 2002. Isotopic investigations of seabirds of the North Water Polynya: contrasting trophic relationships between Eastern and Western Sectors. Condor 104 (1), 1–11.
Hobson, K.A., Wilgenburg, S.V., Wassenaar, L.I., Moore, F., Farrington, J., 2007. Estimating origins of three species of neotropical migrant songbirds at a gulf coast stopover site: combining stable isotope and GIS tools. Condor 109, 256–267.
Hunt, G.L., Drew, G.S., Jahncke, J., Piatt, J., 2005. Prey consumption and energy transfer by marine birds in the Gulf of Alaska. Deep-Sea Res. II 52, 781–797.
Hunt, G.L., Stabeno, P.J., Strom, S., Napp, J.M., 2008. Patterns of spatial and temporal variation in the marine ecosystem of the southeastern Bering Sea, with special reference to the Pribilof Domain. Deep-Sea Res. II 55, 1919–1944.
Jaeger, A., Lecomte, V.J., Weimerskirch, H., Richard, P., Cherel, Y., 2010. Seabird satellite tracking validates the use of latitudinal isoscapes to depict predators' foraging areas in the Southern Ocean. Rapid Commun. Mass Spectrom. 24, 3456–3460.
Jaeger, A., Jaquemet, S., Phillips, R.A., Wanless, R.M., Richard, P., Cherel, Y., 2013. Stable isotopes document inter- and intra-specific variation in feeding ecology of nine large southern Procellariiformes. Mar. Ecol. Prog. Ser. 490, 255–266.
Jahnke, J., Vlietstra, L.S., Decker, M.B., Hunt, G.L., 2008. Marine bird abundance around the Pribilof Islands: a multi-year comparison. Deep-Sea Res. II 55, 1809–1826.
Kaartvedt, S., Staby, A., Aksnes, D.L., 2012. Efficient trawl avoidance by mesopelagic fishes causes large underestimation of their biomass. Mar. Ecol. Prog. Ser. 456, 1–6.
Kelly, J.F., 2000. Stable isotopes of carbon and nitrogen in the study of avian and mammalian trophic ecology. Can. J. Zool. 78, 1–27.
Kitaysky, A.S., Hunt, G.L., Flint, E.N., Rubega, M.A., Decker, M.B., 2000. Resource allocation in breeding seabirds: responses to fluctuations in their food supply. Mar. Ecol. Prog. Ser. 206, 283–296.
Kline, T.C., 2009. Characterization of carbon and nitrogen stable isotope gradients in the northern Gulf of Alaska using terminal feed stage copepodite-V *Neocalanus cristatus*. Deep-Sea Res. II 56, 2537–2552.
Kline, T.C., 2010. Stable carbon and nitrogen isotope variation in the northern lampfish and *Neocalanus*, marine survival rates of pink salmon, and meso-scale eddies in the Gulf of Alaska. Prog. Oceanogr. 87, 49–60.
Kojadinovic, J., Richard, P., Le Corre, M., Cosson, R.P., Bustamante, P., 2008. Effects of lipid extraction on δ13C and δ15N values in seabird muscle, liver and feathers. Waterbirds 31, 169–178.
Kurle, C.M., Worthy, G.A.J., 2002. Stable nitrogen and carbon isotope ratios in multiple tissues of the northern fur seal *Callorhinus ursinus*: implications for dietary and migratory reconstructions. Mar. Ecol. Prog. Ser. 236, 289–300.
Laws, E.A., Popp, B.N., Bidigare, R.R., Kennicutt, M.C., Macko, S.A., 1995. Dependence of phytoplankton carbon isotopic composition on growth rate and $[CO_2]_{aq}$: theoretical considerations and experimental results. Geochim. Cosmochim. Acta 59 (6), 1131–1138.
Lee, S.H., Schell, D.M., McDonald, T.L., Richardson, W.J., 2005. Regional and seasonal feeding by bowhead whales *Balaena mysticetus* as indicated by stable isotope ratios. Mar. Ecol. Prog. Ser. 285, 271–287.
Legendre, P., Legendre, L., 1998. Numerical Ecology. Elsevier Science BV, Amsterdam (2nd English ed.).
Lovvorn, J.R., Baduini, C.L., Hunt, G.L., 2001. Modelling underwater visual and filter feeding by planktivorous shearwaters in unusual sea conditions. Ecology 82 (8), 2342–2356.
Miller, T.W., Brodeur, R.D., Rau, G.H., 2008. Carbon stable isotopes reveal relative contribution of shelf-slope production to the northern California Current pelagic community. Limnol. Oceanogr. 53 (4), 1493–1503.
Morales, L.V., Granger, J., Sigman, D.M., Prokopenko, M., Plessen, B., Chang, B.X., 2014. Elevated $^{15}N/^{14}N$ in particulate organic matter, zooplankton, and diatom frustules-bound nitrogen in the ice covered water column of the Bering Sea eastern shelf. Deep-Sea Res. II, 109, 100–111, http://dx.doi.org/10.1016/j.dsr2.2014.05.008.
Moran, P.A.P., 1950. Notes on continuous stochastic phenomena. Biometrika 37, 17–23.
Moreno, R., Jover, L., Velando, A., Munilla, I., Sanpera, C., 2011. Influence of trophic ecology and spatial variation on the isotopic fingerprints of seabirds. Mar. Ecol. Prog. Ser. 442, 229–239.
Newsome, S.D., Martinez del Rio, C., Bearhop, S., Phillips, D.L., 2007. A niche for isotopic ecology. Front. Ecol. Environ. 5 (8), 429–436.
Olson, R.J., Popp, B.N., Graham, B.S., López-Ibarra, G.A., Galván-Magaña, F., Lennert-Cody, C.E, Bocanegra-Castillo, N., Wallsgrove, N.J., Gier, E., Alatorre-Ramírez, V., Ballance, L.T., Fry, B., 2010. Food-web inferences of stable isotope spatial patterns in copepods and yellowfin tuna in the pelagic eastern Pacific Ocean. Prog. Oceanogr. 86, 124–138.
Oppel, S., Powell, A.N., 2008. Assigning king eiders to wintering regions in the Bering Sea using stable isotopes of feathers and claws. Mar. Ecol. Prog. Ser. 373, 149–156.
Paredes, R., Harding, A.M.A., Irons, D.B., Roby, D.D., Suryan, R.M., Orben, R.A., Renner, H., Young, R., Kitaysky, A., 2012. Proximity to multiple foraging habitats enhances seabirds' resilience to local food shortages. Mar. Ecol. Prog. Ser. 471, 253–269.
Phillips, R.A., Bearhop, S., McGill, R.A.R., Dawson, D.A., 2009. Stable isotopes reveal individual variation in migration strategies and habitat preferences in a suite of seabirds during the nonbreeding period. Oecologia 160, 795–806.
Post, D.M., 2002. Using stable isotopes to estimate trophic position: models, methods, and assumptions. Ecology 83 (3), 703–718.
Quillfeldt, P., McGill, R.A.R., Furness, R.W., 2005. Diet and foraging areas of Southern Ocean seabirds and their prey inferred from stable isotopes: review and case study of Wilson's Storm Petrel. Mar. Ecol. Prog. Ser. 295, 295–304.
Quillfeldt, P., Masello, J.F., McGill, R.A.R., Adams, M., Furness, R.W., 2010. Moving polewards in winter: a recent change in the migratory strategy of a pelagic seabird? Front. Zool. 7 (1), 15.
Renner, H.M., Mueter, F., Drummond, B.A., Warzybok, J.A., Sinclair, E.H., 2012. Patterns of change in diets of two piscivorous seabird species during 35 years in the Pribilof Islands. Deep-Sea Res. II: Top. Stud. Oceanogr. v65–70, 273–291.
Rolff, C., 2000. Seasonal variation in $\delta^{13}C$ and $\delta^{15}N$ of size-fractionated plankton at a coastal station in the northern Baltic proper. Mar. Ecol. Prog. Ser. 203, 47–65.
Roscales, J.L., Gómez-Díaz, E., Neves, V., González-Solís, J., 2011. Trophic versus geographic structure in stable isotope values of pelagic seabirds breeding in the northeast Atlantic. Mar. Ecol. Prog. Ser. 434, 1–13.
Schell, D.M., Barnett, B.A., Vinette, K.A., 1998. Carbon and nitrogen isotope ratios in zooplankton of the Bering, Chukchi and Beaufort seas. Mar. Ecol. Prog. Ser. 162, 11–23.
Sigler, M.F., Kuletz, K.J., Ressler, P.H., Friday, N.A., Wilson, C.D., Zerbini, A.N., 2012. Marine predators and persistent prey in the southeast Bering Sea. Deep-Sea Res. II 65–70, 292–303.
Sinclair, E.H., Vlietstra, L.S., Johnson, D.S., Zeppelin, T.K., Byrd, G.V., Springer, A.M., Ream, R.R., Hunt, G.L., 2008. Patterns in prey use among fur seals and seabirds in the Pribilof Islands. Deep-Sea Res. II 55, 1897–1918.
Smith, S.L., Henrichs, S.M., Rho, T., 2002. Stable C and N isotopic composition of sinking particles and zooplankton over the southeastern Bering Sea shelf. Deep-Sea Res. II 49, 6031–6050.
Solomon, C.T., Carpenter, S.R., Rusak, J.A., Vander Zanden, M.J., 2008. Long-term variation in isotopic baselines and implications for estimating consumer trophic niches. Can. J. Fish. Aquat. Sci. 65, 2191–2200.
Sotiropoulos, M.A., Tonn, W.A., Wassenaar, L.I., 2004. Effects of lipid extraction on stable carbon and nitrogen isotope analyses of fish tissues: potential consequences for food web studies. Ecol. Freshw. Fish 15, 155–169.
Stephenson, S.W., Irons, D.B., 2003. Comparison of colonial breeding seabirds in the eastern Bering and Gulf of Alaska. Mar. Ornithol. 31, 167–173.
Sydeman, W.J., Hobson, K.A., Pyle, P.P., McLaren, E.B., 1997. Trophic relationships among seabirds in Central California: combined stable isotope and conventional dietary approach. Condor 99, 327–336.
Szymanski, M.L., Afton, A.D., Hobson, K.A., 2007. Use of stable isotope methodology to determine natal origins of Mallards at a fine scale within the Upper Midwest. J. Wildl. Manag. 71 (4), 1317–1324.
Tamelander, T., Kivimae, C., Bellerby, R.G.J., Renaud, P.E., Kristiansen, S., 2009. Baseline variations in stable isotope values in an Arctic marine ecosystem: effects of carbon and nitrogen uptake by phytoplankton. Hydrobiologia 630, 63–73.
Wiley, A.E., Welch, A.J., Ostrom, P.H., James, H.F., Stricker, C.A., Fleischer, R.C., Gandhi, H., Adams, J., Ainley, D.G., Duvall, F., Holmes, N., Hu, D., Judge, S., Penniman, J., Swindle, K.A., 2012. Foraging segregation and genetic divergence between geographically proximate colonies of a highly mobile seabird. Oecologia 168, 119–130.

Deep-Sea Research II 109 (2014) 251–265

Contents lists available at ScienceDirect

Deep-Sea Research II

journal homepage: www.elsevier.com/locate/dsr2

Reproductive success of kittiwakes and murres in sequential stages of the nesting period: Relationships with diet and oceanography

Heather M. Renner [a,*], Brie A. Drummond [a], Anna-Marie Benson [b], Rosana Paredes [c]

[a] Alaska Maritime National Wildlife Refuge, US Fish and Wildlife Service, 95 Sterling Hwy, Suite 1, Homer, AK 99603, USA
[b] National Wildlife Refuge System, US Fish and Wildlife Service, 101 12th Ave, Fairbanks, AK 99701, USA
[c] Department of Fisheries and Wildlife, 104 Nash Hall, Oregon State University, Corvallis, OR 97331-3803, USA

ARTICLE INFO

Available online 19 March 2014

Keywords:
Marine birds
Diets
Black-legged kittiwake
Thick-billed murre
Reproductive success
Pribilof Islands
Bering Sea
Alaska
USA

ABSTRACT

Reproductive success is one of the most easily-measured and widely studied demographic parameters of colonial nesting seabirds. Nevertheless, factors affecting the sequential stages (egg laying, incubation, chick-rearing) of reproductive success are less understood. We investigated the separate sequential stages of reproductive success in piscivorous black-legged kittiwakes (*Rissa tridactyla*) and thick-billed murres (*Uria lomvia*) using a 36-year dataset (1975–2010) on the major Pribilof Islands (St. Paul and St. George), which have recently had contrasting population trajectories. Our objectives were to evaluate how the proportion of successful nests varied among stages, and to quantify factors influencing the probability of nest success at each stage in each island. We modeled the probability of nest success at each stage using General Linear Mixed Models incorporating broad-scale and local climate variables, and diet as covariates as well as other measures of reproduction such as timing of breeding and reproductive output in the previous year and previous stage. For both species we found: (1) Success in previous stages of the breeding cycle and success in the prior year better explained overall success than any environmental variables. Phenology was also an important predictor of laying success for kittiwakes. (2) Fledging success was lower when chick diets contained oceanic fish found farther from the colonies and small invertebrates, rather than coastal fish species. (3) Differences in reproductive variables at St. Paul and St. George islands did not correspond to population trends between the two islands. Our results highlight the potential importance of adult condition and annual survival to kittiwake and murre productivity and ultimately, populations. Adult condition carrying over from the previous year ultimately seems to drive annual breeding success in a cascade effect. Furthermore, condition and survival appear to be important contributors to population dynamics at each island. Therefore, adult condition and survival prior to breeding, and factors that influence these parameters such as foraging conditions in the non-breeding season, may be important datasets for understanding drivers of seabird demography at the Pribilof Islands.

Published by Elsevier Ltd.

1. Introduction

Seabirds are widely touted as "indicator species" for the state of the marine ecosystem (Furness and Camphuysen, 1997; Montevecchi, 1993; Piatt et al., 2007). Several characteristics are proposed to make them useful indicators: they are top predators, they are conspicuous central place foragers during the breeding season, many species are widespread and common, and as a group they exploit different aspects of the marine system (i.e., fish vs. plankton, surface vs. depth, nearshore vs. offshore) (Einoder, 2009).

Reproductive success (chicks fledged per nest start) is one of the most easily-measured and widely studied demographic parameters of colonial nesting seabirds (e.g., Dragoo et al., 2012; Mavor et al., 2008) even though for long-lived species, its relative contribution to population trends is often minimal (Schmutz et al., 1997; Schmutz and Byrd, 2004). Variation in seabird breeding success is often used as an indicator of changes in the marine environment because success is widely assumed to be "mediated through the food web" (e.g., Ainley et al., 1995; Byrd et al., 2008a; Frederiksen et al., 2005). Proximate causes of success or failure during different stages of seabird nesting cycles differ, however, because these cycles extend over several months and energetic constraints vary over this period (Shaffer et al., 2003).

Reproductive failure may occur during any one of three separate sequential stages: the nest building period (for those species that build nests), the incubation period, and the chick-rearing period. Prior to egg laying, seabirds are not tied to the nest site and have only themselves to feed. Laying failure may be related to breeding experience of the individual (Coulson, 1966),

* Corresponding author. Tel.: +1 907 226 4623; fax: +1 907 235 7783.
E-mail address: heather_renner@fws.gov (H.M. Renner).

http://dx.doi.org/10.1016/j.dsr2.2014.03.006
0967-0645/Published by Elsevier Ltd.

climate conditions prior to incubation (Quillfeldt, 2001), or nutritional condition of the adult (Kitaysky et al., 2010), which could theoretically be influenced by either reproductive expenditure during the previous breeding season or foraging conditions leading up to egg production in the current season [or unavailability of habitat – e.g., auklets (Bedard, 1969); gannets (Nelson, 1980)]. During incubation and chick-rearing, in contrast, adult birds are constrained by incubation or chick-feeding duties and have both decreased foraging range and increased energetic demands to raise young (Golet et al., 2000). Egg loss can result from predation or abandonment by the parent, either because the egg was not viable or because of food supply limitations during the laying or incubation period (e.g., Hatch and Hatch, 1990; Wanless and Harris, 1992). Finally, chick loss may result from storm events, predation, or the adult's inability to provide sufficient food resources to the chick during this energetically intensive period (e.g., Baird, 1990; Gill and Hatch, 2002; Hatch and Hatch, 1990). Given success or failure during each nesting stage may be affected by different aspects of the marine environment, understanding when breeding loss occurs and how each stage of reproduction relates to environmental factors are crucial to using seabirds as bioindicators.

Relationships between seabird demography and local and regional climate variables are largely affected by life history traits and colony location (review by Sydeman et al., 2012). Accordingly, the degree in climatic responsiveness of seabirds may reflect different tradeoffs between survival and reproduction (Coulson, 2002). For instance, although many studies have found relationships between climate variables and seabird productivity (Sydeman et al., 2012), others are weak (Satterthwaite et al., 2012), and population trajectories do not necessarily match patterns in reproductive success (Murphy et al., 1991). Some seabird species are more flexible in that they can adapt foraging in response to changes in the environment, masking effects on some breeding parameters (Piatt et al., 2007). For instance, kittiwakes can compensate for low food supply by increasing foraging range and effort, resulting in low interannual variation in chick growth rates despite variable foraging conditions (Kitaysky et al., 2000). Similarly, murres can increase foraging effort or feeding rates to maintain relatively constant levels of fledging success when facing low prey density (Harding et al., 2007) or a handicapped mate (Paredes et al., 2005). Of course, seabirds' ability to compensate for low food availability is limited; in extremely poor food years (i.e., El Nino events in the Southeastern hemisphere; Duffy, 1990), nest failure can occur at any stage of reproduction, leading to very low or zero reproductive success.

In general, though, changes in ocean conditions often correlate with seabird productivity and prey availability in a variety of marine habitats (Byrd et al., 2008a; Wolf et al., 2009; Watanuki and Ito, 2012); therefore changes in climatic variables (e.g., SST, PDO) are expected to affect seabird demography via food supply. Studies examining the relationships between prey availability and seabird productivity can use concurrent measures of foraging effort and prey abundance and distribution, but this is logistically a difficult task. Alternatively, seabird diets, which are a function of both prey availability and foraging effort, may be useful for exploring how the marine food web mediates seabird population processes (Connan et al., 2008).

We investigated the separate sequential stages of reproductive success in piscivorous black-legged kittiwakes (*R. tridactyla*) and thick-billed murres (*U. lomvia*) using a 36-year dataset (1975–2010) on the Pribilof Islands in the Bering Sea, Alaska. We had two primary objectives: (1) evaluate whether the proportion of successful nests varied among nesting stages and between islands, and (2) quantify factors influencing the probability of nest success at each stage. For the latter, we hypothesized that different stages would be responsive to different cues in the environment; we modeled three stages of nest success using (a) previous nesting stage reproductive output (assumed to be related to body condition which was not measured), (b) climate variables (broad-scale and local indices) likely to influence foraging conditions, and (c) seabird diet.

2. Study area and species

The Pribilof Islands are located in the Southeastern Bering Sea (~57°N, 169°W) near the edge of the continental shelf. St. Paul Island is approximately 65 km north of St. George Island and is closer to the southern extent of the winter sea ice, whereas St. George Island is closer to the edge of the continental shelf than St. Paul Island. The area along the shelf break is a region of high productivity that supports large numbers of forage fishes, marine mammals, and seabirds (Springer et al., 1996).

St. George and St. Paul Islands together comprise one of the largest breeding concentrations of marine birds in the North Pacific, estimated to exceed 2 million individuals (Hickey and Craighead, 1977). Both islands are approximately equal in size but St. George Island has more extensive cliff nesting habitat and an order of magnitude more ledge-nesting seabirds than St. Paul Island (Hickey and Craighead, 1977). Black-legged kittiwakes and thick-billed murres are the most abundant species of piscivorous seabirds on the Pribilofs, where they nest in mixed colonies with red-legged kittiwakes (*Rissa brevirostris*) and common murres (*Uria aalge*). The total population of black-legged kittiwakes at St. Paul (~15,000 individuals) and St. George (~72,000 individuals) for 2005 was calculated based on Hickey and Craighead (1977) counts and trend rates reported by Byrd et al. (2008b). The two islands also support substantially different numbers of breeding thick-billed murres: St. George=1,500,000, St. Paul=57,000 (Hickey and Craighead, 1977; modified using Byrd et al. (2008b)). Reproductive success of kittiwakes and murres at the Pribilof Islands is presumed to be related mostly to prey availability, as nest predation for ledge-nesting birds at both islands is minimal (Byrd et al., 2008a).

3. Materials and methods

3.1. Data collection

Reproductive success was estimated each year on St. Paul and St. George islands, 1975–2010, by recording the status (i.e., presence of nest structure, egg or chick) of nests on systematically-selected plots within the viewable population (see Byrd, 1989; Byrd et al., 2008a; Hunt et al., 1981). Prior to 1989 (except in 1984), nests monitored were not grouped into plots or plot-specific data were not available, and nests were treated as a simple random sample. In subsequent years plots were used as single-stage cluster samples, to more accurately represent the variance. Data collection consisted of photographing or drawing each plot and numbering nest sites on the photograph or drawing so individual sites could be identified and followed throughout the nesting cycle. For kittiwakes, nest sites were considered active only when new plant material was added within that season. Since murres do not build nests, the appearance of an egg constituted an active site (therefore, laying success could not be estimated for murres as it was for kittiwakes). Numbered sites typically were checked every three to five days throughout the incubation and chick-rearing periods to estimate loss of reproductive potential during the laying (kittiwakes only), egg, and chick stages of the nesting cycle. Nests were monitored until chicks departed the cliffs (fledged). Hatch dates were estimated as the mid-points between the date the egg was last seen and the date the chick was first observed. Nests were monitored in the same areas each year, with substantial overlap in individual nests and plots, but

Table 1
Sample sizes used for analyses of seabird reproductive success and diets of black-legged kittiwakes (BLKI) and thick-billed murres (TBMU) from the Pribilof Islands, 1975–2010. Numbers of nests are those with a known fate (successful or laying, egg or chick loss) at the end of the season. Diet samples represent those collected during the chick-rearing period only and exclude years with <6 samples.

Year	Species	St. George Island		St. Paul Island	
		Reproductive success (# nests)	Diet (# samples)	Reproductive success (# nests)	Diet (# samples)
1975	BLKI	–	–	185	118
1975	TBMU	–	–	–	–
1976	BLKI	34	31	127	55
1976	TBMU	–	6	47	17
1977	BLKI	110	60	157	129
1977	TBMU	51	21	102	20
1978	BLKI	229	52	203	70
1978	TBMU	90	23	114	16
1979	BLKI	146	–	158	23
1979	TBMU	–	–	–	–
1980	BLKI	106	–	–	–
1980	TBMU	–	–	–	–
1981	BLKI	102	10	–	–
1981	TBMU	88	–	–	–
1982	BLKI	–	–	–	–
1982	TBMU	–	–	–	–
1983	BLKI	–	–	–	–
1983	TBMU	–	–	–	–
1984	BLKI	49	67	92	29
1984	TBMU	55	31	27	20
1985	BLKI	154	12	428	–
1985	TBMU	253	–	360	–
1986	BLKI	155	38	554	–
1986	TBMU	388	–	624	–
1987	BLKI	126	–	506	23
1987	TBMU	377	11	792	–
1988	BLKI	85	28	204	48
1988	TBMU	195	36	317	12
1989	BLKI	59	–	351	–
1989	TBMU	326	–	346	–
1990	BLKI	95	–	369	–
1990	TBMU	286	–	325	–
1991	BLKI	99	–	–	–
1991	TBMU	269	–	–	–
1992	BLKI	98	65	511	7
1992	TBMU	360	–	475	–
1993	BLKI	113	11	–	8
1993	TBMU	318	–	–	–
1994	BLKI	113	–	–	–
1994	TBMU	322	–	–	–
1995	BLKI	57	–	–	–
1995	TBMU	269	–	–	–
1996	BLKI	95	–	280	–
1996	TBMU	243	–	356	–
1997	BLKI	105	9	301	30
1997	TBMU	297	–	293	–
1998	BLKI	75	39	299	30
1998	TBMU	160	–	246	–
1999	BLKI	76	13	290	–
1999	TBMU	243	–	434	–
2000	BLKI	110	9	289	–
2000	TBMU	364	–	546	–
2001	BLKI	95	–	360	–
2001	TBMU	382	38	482	–
2002	BLKI	113	–	343	–
2002	TBMU	371	–	265	–
2003	BLKI	121		349	22
2003	TBMU	418	19	425	–
2004	BLKI	158	–	425	–
2004	TBMU	310	7	386	–
2005	BLKI	161	7	543	–
2005	TBMU	590	–	177	–
2006	BLKI	255	–	479	9
2006	TBMU	574	52	316	–
2007	BLKI	67	–	483	–
2007	TBMU	729	18	627	–
2008	BLKI	179	36	388	33
2008	TBMU	327	75	337	355
2009	BLKI	169	24	422	22
2009	TBMU	307	237	351	193
2010	BLKI	199	51	366	35
2010	TBMU	363	200	370	77

varying enough to achieve desired sample sizes. Sample sizes of nests and diet samples in each year are shown in Table 1.

Kittiwake diet samples were collected from captured or shot adults attending the cliff breeding colonies or from chicks handled in their nests. Adult and chick diets were combined as in previous studies (e.g., Decker et al., 1995; Hunt et al., 1996; Renner et al., 2012; Sinclair et al., 2008) because it is not possible to distinguish between the two, given kittiwakes store prey in their crops for several hours before regurgitating it to the young. For both species, we only included diet data collected during the chick-rearing period (21 June–22 September) because our previous analysis and others (Hunt et al., 1981; Renner et al., 2012) have indicated significant differences across different stages of the breeding period and because we only had data from outside the chick period in a few years. We used the same samples analyzed in Renner et al. (2012) with two exceptions: (1) we eliminated years with less than six samples (Duffy and Jackson, 1986), resulting in the exclusion of two years data at each island for each species, and (2) we included samples collected in 2005 and 2010, which became available after the former analysis was conducted. Because sample collection, prey processing and identification for kittiwake samples were identical to Renner et al. (2012), we have not repeated the details here.

Murre chick diet samples were obtained from bill loads or ledge drops by adult murres and regurgitations by chicks. Bill load samples included actual collections as well as observations made through spotting scopes during either formal nest observations or incidental observations while monitoring nests for reproductive success data. For collected bill loads, ledge drops, and chick regurgitations (1975–1978, 1984, 1987, 1988), samples were preserved, and identified in the laboratory following procedures used for kittiwake samples (Renner et al., 2012). For bill load observations (1999–2010), prey items were identified visually in the field to the lowest taxonomic level possible by the observer as adults carrying bill loads arrived at nest sites to feed chicks. When identifications could not be made or were in question for any reason, prey were classified as “unknown fish”, “unknown invertebrate”, or “unknown prey”. All entirely unknown prey were excluded from further analysis.

3.2. Data analysis

3.2.1. Diet datasets

Because the diet data used in this paper were not collected and analyzed consistently in all years (e.g., biomass data collected in some but not all years, some prey items identified to species while others only to genus or family, etc., and some murre bill loads identified only by field observation), we were limited in our diet data metric to either numerical abundance (how many individuals of a prey type were in each sample) or frequency of occurrence (how many samples contained a given prey type, regardless of quantities). Both measures have potential biases: abundance data underemphasize the importance of fish and other larger diet items (a bird may eat only a few larger fish but many smaller invertebrates), whereas frequency of occurrence does not account for

differences in the quantities of prey items across samples (a sample containing a single individual is treated the same as a sample containing hundreds of individuals) and thus may underemphasize the importance of more numerous diet items. Fortunately, the measures are identical for murre chick samples, because adults carry only one prey item to the chick. Our previous analyses with this dataset (Renner et al., 2012) indicated consistent conclusions with both measures. We used frequency of occurrence for this study because it simplified the analysis and our ability to reclassify prey groupings; also, more years of diet data were available in this format.

Prior to the analyses, prey items were grouped into nine taxonomic groups representing the major prey types [walleye pollock (*Theragra chalcogramma*), Pacific sandlance (*Ammodytes hexapterus*), myctophids (family Myctophidae), capelin (*Mallotus villosus*), all fish combined, squid, amphipods, euphausiids, and all invertebrates combined]. All unidentified gadids were assumed to be walleye pollock, as the only other identified gadid (Pacific cod *Gadus macrocephalus*) occurred in just two years and in $<1\%$ of samples. It would have been preferable to further separate all invertebrate prey to the species level, as euphausiids, amphipods and squid are known to have species-specific distributional differences (Sinclair et al., 1999; Benoit-Bird, pers. comm.) but species identification of invertebrates were not available in all years, especially for murre chick diet.

3.2.2. Climate datasets

Details of the final climate, reproductive and diet variables chosen as fixed effects in our models are shown in Table 2. For climatic variables, we considered a wide range of local and regional variables that could affect prey availability and thus nesting success of seabirds. While atmospheric variability is believed to drive primary production, secondary production, forage fish recruitment, and ultimately, predator demographic parameters in the Bering Sea (see Renner et al., 2012 for detailed discussion), this can happen through direct and indirect effects on predators, and there is increasing decoupling at each sequential level of the food chain. As apex predators, seabirds are several steps removed from physical climate variables, and the marine system is complex enough that we had little a *priori* means to choose specific variables to investigate. Therefore, as in Renner et al. (2012), we cast a wide net of available climate time series, but then we reduced these by evaluating for multicollinearity and when two or more variables were highly correlated ($r \geq 0.60$; e.g., multiple datasets for sea surface temperature were considered), we removed the variables with the most missing data. We further limited our selection to those shown by previous studies to be correlated with seabird productivity (e.g., sea surface temperature and ice retreat index), as well as those for which we could hypothesize a direct mechanistic link to seabird demography (e.g., wind mixing would affect prey distribution on a short time scale, and strong wind events could directly destroy nests or kill chicks). We had two major limitations in our choice of climate variables. First, almost all of the available climate datasets are measured/integrated at an annual scale, which is not ideal for our intent to understand seabird processes occurring at a less-than-annual time scale (e.g., within a season). Second, in spite of having what is viewed widely as a tremendously long-term dataset, statistical power considerations severely limited our ability to test multiple variables in our very complicated model sets and we were forced to limit the scope of this paper. While climate variables may

Table 2
Environmental (or climatic), reproductive and diet variables, and their abbreviations, used in analyses of reproductive success of black-legged kittiwakes and thick-billed murres at the Pribilof Islands.

Variable		Description
Climate		
Summer wind mixing index	WM	Defined as mean daily wind speeds cubed at 10 m height at 57°N, 169°W (just east of the Pribilof Islands), averaged over the period 1 June-31 August (data from the NOAA Bering Climate website, http://www.beringclimate.noaa.gov).
Strong wind event index	WS	Defined as the number of days with wind speeds in excess of 9 m/s (same location/time period as wind mixing; data from the NOAA Bering Climate website).
Regional summer SST	SST	Longer time series for regional index of average sea surface temperature over the Eastern Bering Sea shelf during the summer breeding season (June through August), based on NOAA's extended reconstructed SST data over the approximate trawl survey region (inshore of approximately 200 m depth contour between 55°N and 61°N).
Spring ice retreat index	IRI	Defined as the number of days with ice cover after 15 March in the vicinity of Mooring 2 site (56.9°N, 164.1°W) as a proxy for the timing of ice retreat from the southeast Bering Sea shelf (data from the NOAA Bering Climate website, http://www.beringclimate.noaa.gov).
Pacific Decadal Oscillation Index (PDO)	PDO	November–March large-scale index related to climate variability in the eastern Bering Sea. Monthly values obtained from the Joint Institute of the Atmosphere and Oceans, University of Washington (http://jisao.washington.edu/pdo/PDO.latest).
Arctic Oscillation Index (AO)	AO	January-March large-scale index related to climate variability in the eastern Bering Sea. Monthly values obtained from NOAA, National Weather Service, Climate Prediction Center (http://www.cpc.ncep.noaa.gov/).
Reproductive		
Laying success	LS	The proportion of nest starts that had at least one egg laid for a given plot at each island each year. Variable used only for black-legged kittiwake models predicting hatching success.
Hatching success	HS	The proportion of nests with eggs that had at least one egg hatch for a given plot at each island each year. Variable used for thick-billed murre and black-legged kittiwake models predicting fledging success.
Fledging success	FS	The proportion of nests with chicks that had at least one chick fledge for a given plot at each island each year.
Previous year success	PYS	The proportion of successful nests (at least one chick fledged) in the previous year for a given plot at each island each year.
Timing	TIM	Annual mean hatch date at each island by Julian date.
Diet		
Pollock	POLL	Frequency of occurrence of pollock in chick (murres) and adult/chick (kittiwakes) diet.
Sandlance	SAND	Frequency of occurrence of sandlance in chick (murres) and adult/chick (kittiwakes) diet.
Myctophid	MYCT	Frequency of occurrence of myctophids in chick (murres) and adult/chick (kittiwakes) diet.
Capelin	CAPE	Frequency of occurrence of capelin in chick (murres) and adult/chick (kittiwakes) diet.
All fish	FISH	Frequency of occurrence of all fish combined in chick (murres) and adult/chick (kittiwakes) diet.
Squid	SQD	Frequency of occurrence of squid in chick (murres) and adult/chick (kittiwakes) diet.
Amphipod	AMPH	Frequency of occurrence of amphipods in chick (murres) and adult/chick (kittiwakes) diet.
Euphausiids	EUPH	Frequency of occurrence of euphausiids in chick (murres) and adult/chick (kittiwakes) diet.
NMDS axis 1	NMDS	Axis 1 from NMDS ordination of adult/chick diet of kittiwakes from Renner et al. (2012).

influence success of top predators with a time lag as their effects may be mediated through lower trophic levels, we chose not to investigate these relationships because they were recently explored in another publication (see Zador et al., 2013).

3.2.3. Statistical methods

We modeled the probability of success at each nesting stage with a separate model for each stage. We evaluated the effects of several variables: (1) prior reproductive output (previous colony-wide stage and year success) and timing of nesting, (2) environmental variables likely to influence foraging conditions (Table 1), and (3) diet sampled during the chick period. We used Generalized Linear Mixed Models (GLMM) to compare the importance of several variables for predicting the response (nest success or failure) at 3 stages in the nesting cycle for kittiwakes and in 2 stages for murres. Our candidate models took the form of

$$\Pr(y_i = 1) = logit^{-1}(\alpha_{01jk[i]} + \alpha_{02h[i]} + \beta_0 + \beta_1 X_{1[i]} + \beta_2 X_{2[i]} + \ldots \beta_n X_{n[i]} + \varepsilon_{[i]})$$

for $i = 1,\ldots n$ nests,

The response, $\Pr(y_i = 1)$, i.e., the probability of nest success, was modeled as a binomial random variable with a logit link for 3 responses: laying success (the probability of at least one egg being laid; kittiwakes only), hatching success (the probability of at least one egg hatching), and fledging success (the probability of at least one chick fledging successfully). The errors, $\varepsilon_{[i]} \sim N(0, \sigma^2)$, had independent normal distributions with mean zero and standard deviation σ. The random intercepts $\alpha_{01} \sim N(\mu = 0, \sigma^2{}_{jk})$, for $j = 1,\ldots, n$ plots in $k = 2$ islands, and $\alpha_{02} \sim N(\mu = 0, \sigma^2{}_h)$, for $h = 1,\ldots, n$ years were used to model the nonindependence of nests within plots, subset i.e., statistically nested, within two islands, crossed with year effects. For fixed effects, we estimated coefficients $(\beta_1,\ldots,\beta_n)$ for several ocean and diet variables $(X_1 \ldots X_n$; Table 1) to quantify the importance of these variables for predicting the mean response $\Pr(y_i = 1)$.

For many years some or all covariate data were not available, so data from these years had to be eliminated. Because climate data were available for most of the years when we had reproductive success data, but diet data were available for fewer (and different) years, we ran climate and reproductive parameters in the same model sets and diet separately.

We followed Bolker et al. (2009) and Grueber et al. (2011) procedures for fitting GLMMs. For variables that were not normally distributed (IRI and SST), we attempted several data transformations to improve the distribution. Additionally, we used models with nonlinear splines for these covariates; neither approach improved the distribution or fit of models with IRI and SST.

We centered all covariates to improve interpretation of the relative strength of parameter estimates (Grueber et al., 2011). Centering changed the interpretation so that the intercepts were no longer the expected value when the predictor = 0 on the original scale, but the expected value when the covariate was at its mean. For some variables, e.g., Julian date, there was no meaningful zero point (Julian hatch dates ranged from 181 to 230), which was another reason for centering variables.

For the climate and reproductive parameter modeling, we formulated 51–60 candidate models a priori to obtain balanced model sets. We model-averaged parameter estimates to account for model uncertainty (Bolker et al., 2009; Burnham and Anderson, 2002) using the natural-average method, where a parameter estimate for each predictor is averaged only over the models in which that predictor appears and is weighted by the summed weights of these models (Burnham and Anderson, 2002). The relative importance of variables was determined by summing the Akaike weights across all models in which the variable occurs (Burnham and Anderson, 2002). We also evaluated confidence intervals for model-averaged parameter estimates; we considered variables with 90% confidence intervals that did not overlap with zero to be significant predictors of the response.

We ran univariate diet models because we were interested in whether individual diet variables predicted nest success. Because diet data were limited to the chick-rearing period, we used diet parameters to model only fledging success for both species. Detailed results of all model selection and model-averaged parameter estimates are included in online supplementary appendices (Tables A.1–A.14).

We evaluated between-island differences in total nest success, with a univariate model using Island only as a fixed effect, where

$$\Pr(y_i = 1) = logit^{-1}(\alpha_{01j[i]} + \alpha_{02h[i]} + \beta_0 + \beta_1 \text{Island})$$

To test whether success stages on both islands was correlated, we used Pearson correlations.

All analyses were conducted using program R (R Development Core Team, 2012).

4. Results

4.1. Thick-billed murre

During the 36 years of the study, the proportion of successful murre nests was higher on St. George Island (prop. success = 0.512) than on St. Paul Island (prop. success = 0.442, $n = 18{,}465$ nests, $Z = 9.52$, $p < 0.001$). The proportion of successful nests varied among stages with most loss occurring during the egg period (Figs. 1 and 2).

4.1.1. Hatching success

The probability of hatching success was lower on St. Paul Island ($P_{success} = 0.560$, 90% CI = 0.542–0.579) than on St. George Island ($P_{success} = 0.617$, 90% CI = 0.583–0.649), and 90% confidence intervals do not overlap indicating this difference was significant. In addition, hatching success was significantly correlated between islands ($r_s = 0.466$, $p = 0.016$).

For the climate and reproductive parameter models ($n = 26$ years with complete data), several models tied for the best models ($\Delta AIC < 2$). Previous year success was the most important predictor of hatching success of thick-billed murres: it occurred in all competing models and was the only statistically significant fixed effect (Table 3). Higher hatching success followed higher success in the previous year. No climate variables were significant predictors of murre hatching success.

4.1.2. Fledging success

The probability of fledging success was not significantly different on St. Paul Island ($P_{success} = 0.818$, 90% CI = 0.802–0.832) than on St. George Island ($P_{success} = 0.847$, 90% CI = 0.820–0.871). Fledging success was not correlated between islands ($r_s = -0.183$, $p = 0.372$).

Timing of nesting and hatching success were the most important predictors of fledging success for the climate and reproductive parameter models showing high importance values and statistical significance (Table 3). Fledging success was higher with higher hatching success and earlier timing of breeding. Although the best model for fledging success also included the strong wind event index, wind index was not a significant predictor.

Hatching success was included in all diet models predicting fledging success because it was a significant predictor in climate and reproductive modeling. The best diet model also included myctophids, which was a significant negative predictor of fledging

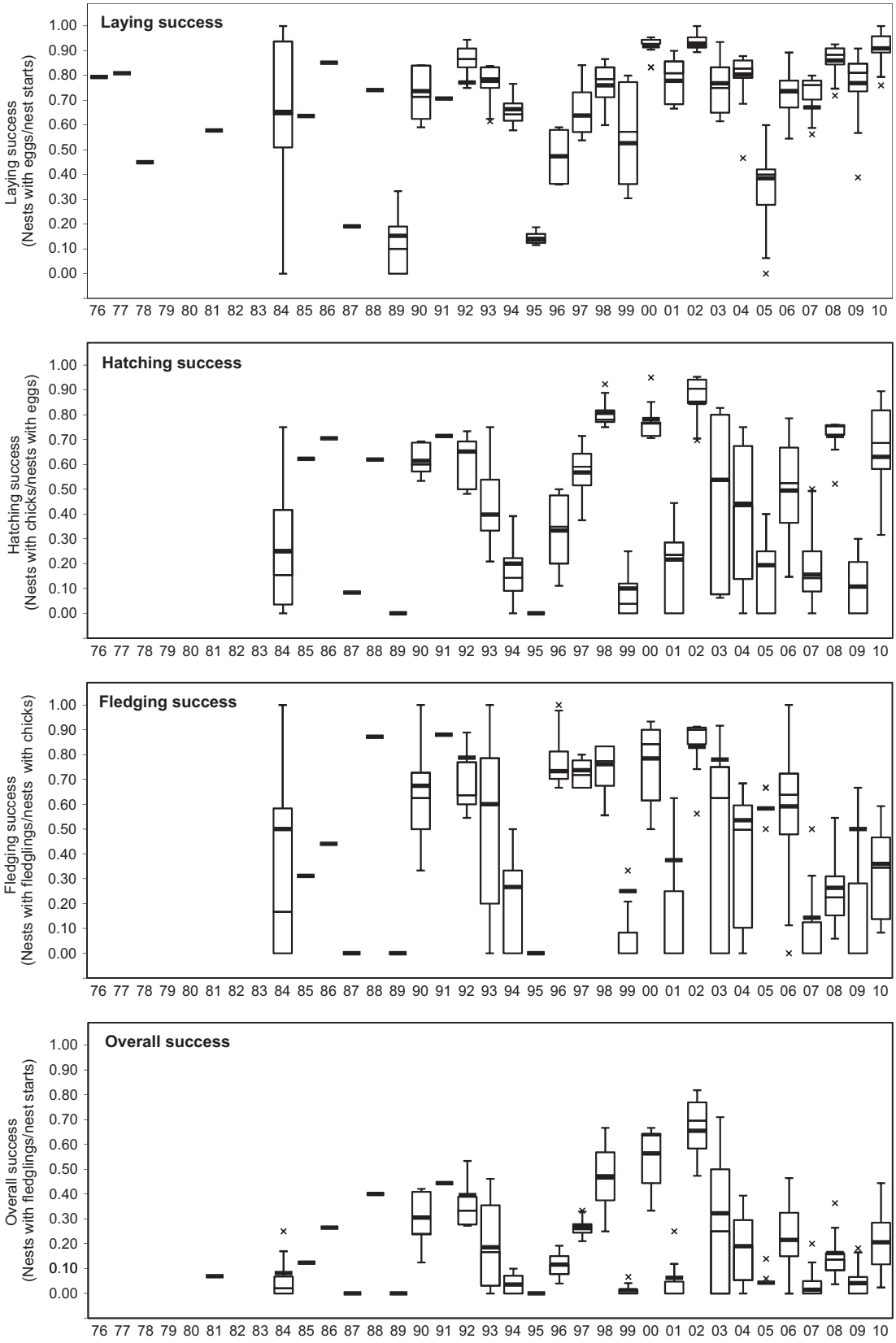

Fig. 1. Success of black-legged kittiwakes at St. George Island, Alaska in 1976–2010. Thick horizontal lines represent total annual success calculated across all nests each year. Box plots are calculated using annual success rates in each plot as the sample unit: boxes represent first and third quartiles, whiskers are 1.5x the interquartile range (IQR), and "x" shows outlier plots beyond 1.5xIQR. Years with no data for individual plots have no box plots.

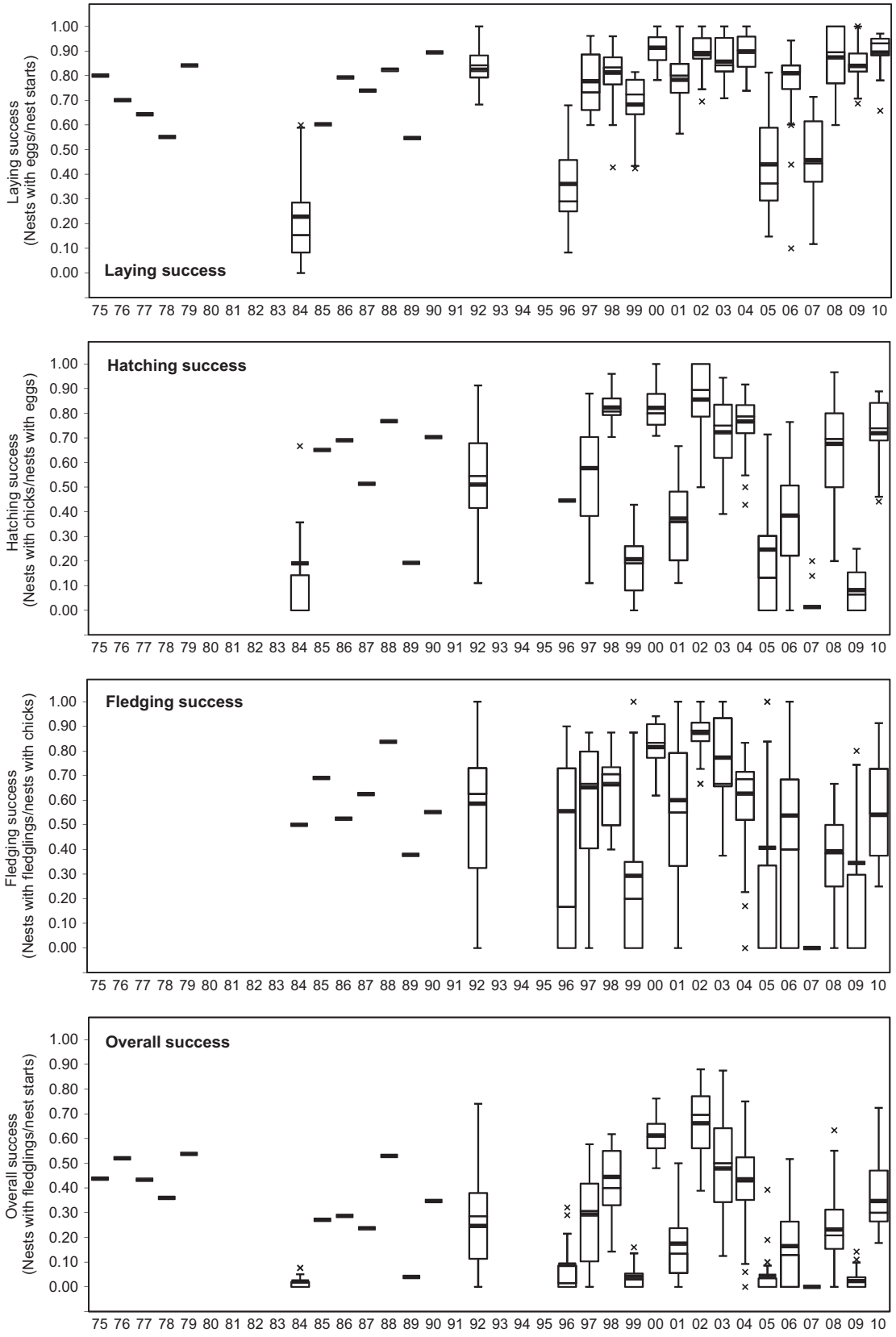

Fig. 2. Success of black-legged kittiwakes at St. Paul Island, Alaska in 1975–2010. Thick horizontal lines represent total annual success calculated across all nests each year. Box plots are calculated using annual success rates in each plot as the sample unit: boxes represent first and third quartiles, whiskers are 1.5x the interquartile range (IQR), and "x" shows outlier plots beyond 1.5xIQR; years with no data for individual plots have no box plots.

Table 3
Significant predictors of laying, hatching and fledging success of thick-billed murres and black-legged kittiwakes at St. Paul and St. George Islands, Alaska. Results are based on presence in top models (ΔAIC < 2), high relative importance based on AIC weights and model-averaged parameter estimates with 90% confidence intervals not overlapping with zero.

Reproductive stage	Thick-billed murre	Black-legged kittiwake
Laying success	*No data*	Timing (−)
Hatching success	Previous year success (+)	Previous year success (+) Laying success (+)
Fledging success	Hatching success (+) Timing (−) Myctophid (−)	Hatching success (+) Amphipod (−)

success (Table 3). These results may be spurious, however, because myctophids were rarely found in murre chick diets in the Pribilofs (only in one year for St. George Island and two years for St. Paul Island).

4.2. Black-legged kittiwake

During the 36 years of the study, the proportion of successful kittiwake nests was higher on St. Paul Island (prop. success = 0.234) than on St. George Island (prop. success = 0.1696; $n = 13{,}212$, $Z = 8.22$, $p < 0.001$). Most of the nests were lost in the first two stages, but in contrast to murres, even in the fledging stage, a high proportion of the remaining nests failed (Figs. 3 and 4).

We analyzed data from 27 years in climate and reproductive parameter models of black-legged kittiwakes and 22 years in diet models. Years with missing covariate data were excluded.

4.2.1. Laying success

The probability of laying success was not significantly different on St. Paul Island ($P_{success} = 0.677$, 90% CI = 0.651–0.702) than on St. George Island ($P_{success} = 0.611$, 90% CI = 0.532–0.684). Laying success was significantly correlated between islands ($r_s = 0.723$, $p < 0.001$).

In climate and reproductive models, timing of breeding occurred in the top two competing models (and all models with an AIC weight > 0) and was the only significant predictor of laying success (Table 3). Timing and laying success were inversely related, with a higher probability of laying success in years with earlier nest initiation dates. No climate variables were significant predictors of laying success.

4.2.2. Hatching success

The probability of hatching success was not significantly different on St. Paul Island ($P_{success} = 0.454$, 90% CI = 0.415–0.493) than on St. George Island ($P_{success} = 0.410$, 90% CI = 0.311–0.527). Hatching success was significantly correlated between islands ($r_s = 0.812$, $p < 0.001$).

In climate and reproductive models, laying success and previous year success were both important variables for predicting hatching success of black-legged kittiwakes. The two variables comprised the single top model that had 98% of the weight of the model set and both were statistically significant predictors of hatching success (Table 3). Hatching success was high in years when laying success was high and when overall reproductive success in the previous year had been high.

4.2.3. Fledging success

The probability of fledging success was not significantly different on St. Paul Island ($P_{success} = 0.610$, 90% CI = 0.564–0.651) than on St. George Island ($P_{success} = 0.522$, 90% CI = 0.438–0.604). Fledging success was significantly correlated between islands ($r_s = 0.700$, $p < 0.001$).

Because laying success and hatching success were positively correlated ($r = 0.576$, $p < 0.0001$), we included only hatching success in our fledging model set. In climate and reproductive models, hatching success was the most important variable for predicting fledging success: it appeared in all models with an AIC weight > 0 and was a statistically significant predictor of fledging success (Table 3). Higher fledgling success was predicted by higher hatching success. A number of other climate and reproductive variables appeared in competing models predicting fledging success but none were significant.

In diet models, hatching success was included in all models because it was a significant predictor of fledging success in climate and reproductive models. The best model also contained frequency of amphipods in diet, which was a significant predictor of kittiwake fledging success (Table 3). Fledging success was higher when frequency of amphipods in diets was lower.

5. Discussion

5.1. Reproductive stages for each species

Our findings for both kittiwakes and murres suggest that annual reproductive outcome is most strongly related to conditions occurring prior to the nesting season. Colony-wide probability of success in the earlier stages was always the best predictor for those individuals proceeding to the next sequential stage: colony-wide laying success predicted individual hatching success, and colony-wide hatching success predicted individual fledging success. In addition, previous year's success was the single most important predictor for hatching success. This pattern indicates a cascade effect, in which overall breeding success is dictated by success early in the season, which in turn is driven by success in the previous year. This temporal autocorrelation, likely a function of adult condition, could be explained by two not mutually exclusive hypotheses. First, a relationship between adult condition in year zero and year one could be due to autocorrelation in environmental and foraging conditions (e.g., Zador et al., 2013). Second, costs associated with reproductive output in one year may determine future reproductive output. If high success in year one was due to good foraging conditions, whereby the adults incurred little stress, they should be in good condition for year two. We could also predict the opposite relationship if merely the effort of reproduction is a great cost. Life-history theory assumes costs associated with reproduction, and that these costs should be seen in a trade-off between current-year reproductive effort and future reproductive success (e.g., Bell and Koufopanou, 1986; Charnov and Krebs, 1974; Lessells, 1991; Reznick, 1985; Stearns, 1989; Williams, 1966). Reproductive costs may be incurred in any of the three sequential stages, egg production, incubation or chick-rearing (Monaghan and Nagar, 1997). High costs in one or more of these stages in a given year should decrease survival or reproductive performance (in subsequent stages in the same year or in subsequent years). For example, Milonoff et al. (2004) showed goldeneyes that reared chicks had lower productivity the following year than those that failed during incubation. Indeed, in reduced food conditions, kittiwakes and murres at the Pribilofs Islands appear to accept potential long-term costs (e.g., adult survival) to successfully rear chicks (Harding et al., 2013; Paredes et al., 2014). In addition, the cost of breeding in a year with poor food supply may also carry over to the following year, thereby diminishing reproductive performance in the next year for surviving birds (Kitaysky et al., 2000; Moss et al., 2009). For seabirds with only 1–2 eggs, this often leads to nest failure;

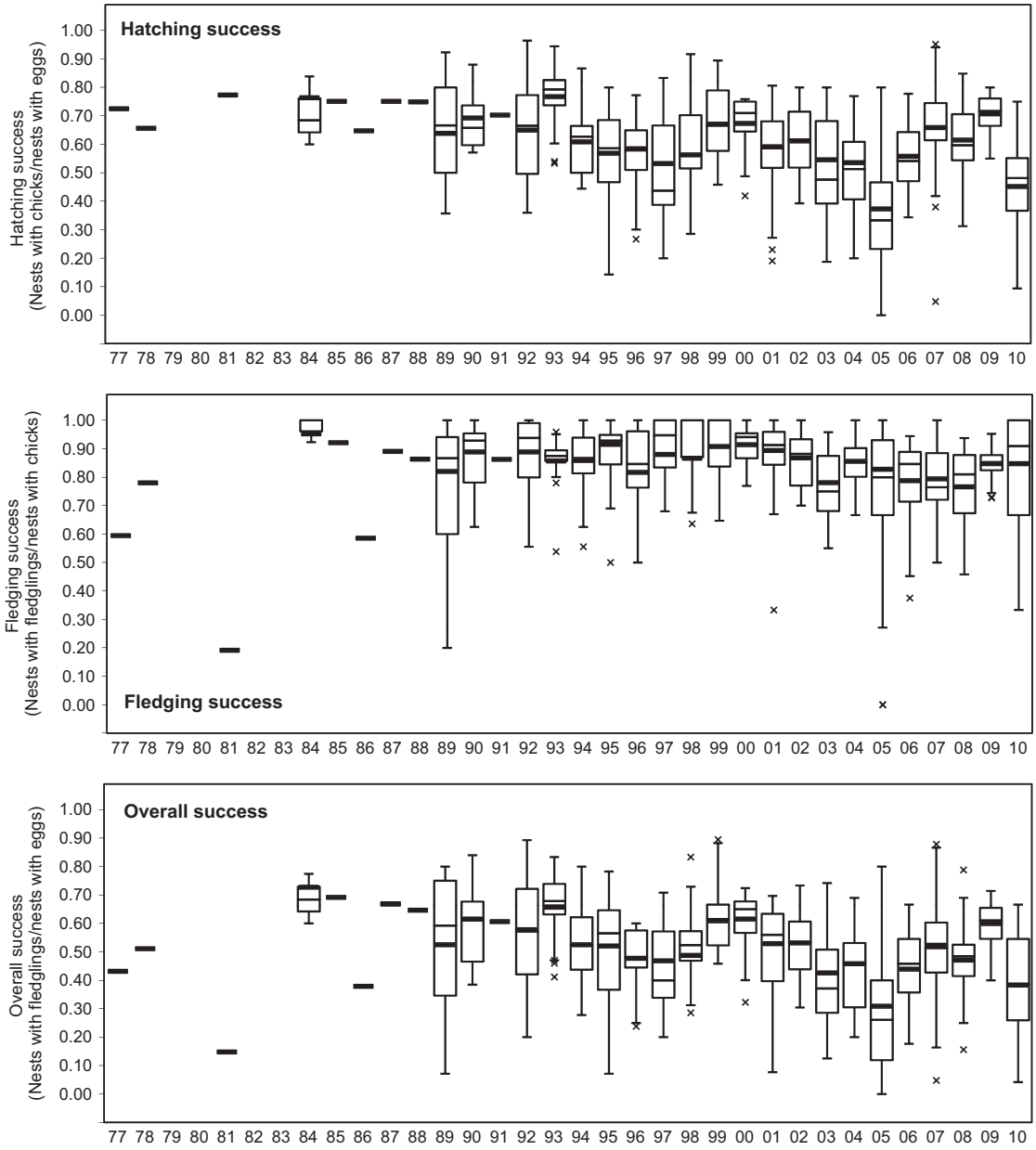

Fig. 3. Success of thick-billed murres at St. George Island, Alaska in 1977–2010. Thick horizontal lines represent total annual success calculated across all nests each year. Box plots are calculated using annual success rates in each plot as the sample unit: boxes represent first and third quartiles, whiskers are 1.5x the interquartile range (IQR), and "x" shows outlier plots beyond 1.5xIQR; years with no data for individual plots have no box plots.

unlike e.g., most waterfowl species, which can adjust clutch size in relation to body condition or stress (e.g., Erikstad et al., 1993), seabirds will forego a breeding attempt, or abandon a breeding attempt once initiated, if the consequences (presumably to adult condition/survival) are too great (e.g., Chastel et al., 1995).

Alternatively, environmental variation on the scale of the whole summer (which is all we have available for climate variables) may be most relevant to seabird reproductive success, which would imply that whole summers are good or bad for reproductive success. If this is the case, we would expect that hatching success would be a good predictor of fledging success, for example, because both components would be experiencing the same condition. Correlation with prior year also may not connote carryover effects, but instead could simply mean that if the conditions are the same between years, then reproductive success is about the same. Variation in environmental and reproductive parameters may not be continuous, but instead change may occur after a threshold is crossed from one relatively stable environmental state to another (e.g., a regime shift, Mantua et al., 1997).

5.2. Timing

Timing of breeding was the most important predictor of laying success for kittiwakes. Similarly, Shultz et al. (2009) found timing explained 78% of variability in laying success and 94% of the variability in total reproductive success in kittiwakes in the Gulf of Alaska. Many studies have shown that across a wide range of bird families, individuals breeding earlier do better than individuals breeding later in a given season (e.g., Hipfner, 1997). Better body condition in adult birds likely leads to both earlier breeding and higher laying success (Faivre et al., 2001).

Elevated stress levels (as measured by corticosterone, CORT) may result in a delayed time of breeding (Schoech et al., 2009) or reduced return rate of individuals (Goutte et al., 2010 for

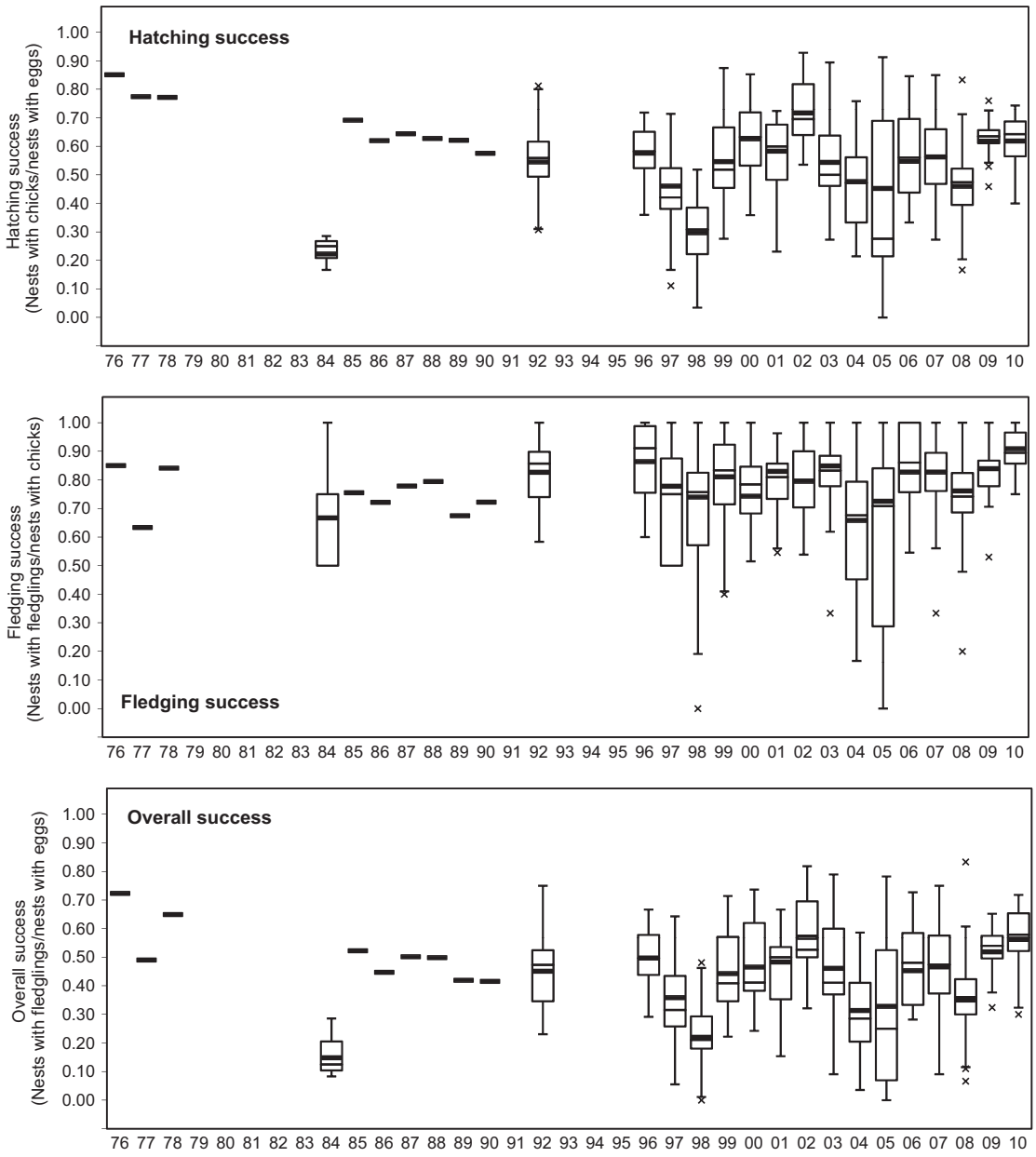

Fig. 4. Success of thick-billed murres at St. Paul Island, Alaska in 1976–2010. Thick horizontal lines represent total annual success calculated across all nests each year. Box plots are calculated using annual success rates in each plot as the sample unit: boxes represent first and third quartiles, whiskers are 1.5x the interquartile range (IQR), and "x" shows outlier plots beyond 1.5xIQR; years with no data for individual plots have no box plots.

kittiwakes) the following breeding season. Similarly, delayed egg-laying can be associated with high stress during the incubation stage and low laying success (Kitaysky et al., 2010) and overall productivity (Verhulst and Nilsson, 2008). Shultz et al. (2009) indicated that in the Gulf of Alaska, timing of breeding in kittiwakes was driven by amount of pre-lay food availability rather than timing of peak food, suggesting that timing of nest initiation was dictated by energetic constraints early in the season rather than anticipation of future food supplies (see also Sorensen et al., 2009).

For murres, although we found no relationship between timing and hatching success (the earliest stage measured in this study), timing was a good predictor of fledging success. This suggests that pre-egg laying food conditions appear to have little effect on the timing of breeding of murres. Instead, murre timing may be driven by conditions later in the breeding season that favor chick survival. Regular et al. (2009) found that breeding chronology in common murres in the Atlantic was related to food availability for chicks, such that hatching coincided with peak capelin abundance. There might be some advantages to chick survival to hatch earlier (that were not seen in the egg stage) such as seasonal variation in food conditions (Shultz et al., 2009). Alternately, it is possible that we did not detect an effect in hatching success because the ratio of noise to signal was too high (especially given we had no measure of laying success). Variation in murre timing was half that of kittiwakes, both in our study and in the Gulf of Alaska (Shultz et al., 2009). An alternative explanation is that such low variation in murre timing may be due to social reasons, such as selection pressure to synchronize with neighbors (Benowitz-Fredericks and Kitaysky, 2005).

We found no strong correlations between timing of either species and any of the regional or local environmental variables in our models. Shultz et al. (2009) found that kittiwake timing and laying success were related to sea surface temperature, with

earlier laying and higher laying success in colder years when forage fish were more abundant. In the Pribilofs, Byrd et al. (2008a) indicated that *detrended* kittiwake timing was inversely correlated with sea ice extent and winter sea surface temperature (neither of the two detrended). Detrending is typically used when a variable distorts or masks a variable of interest and Byrd et al. (2008a) suggested it was useful to emphasize high frequency interannual variability over interdecadal variability. We feel it was not warranted here because timing was not correlated with any of the other climate covariates, and because when timing was removed from our model, the other variables did not improve the fit. Further, Byrd et al. (2008a) found no relationships between timing and other measures of sea ice or temperature, leading us to infer what they found was a weak relationship.

5.3. Environmental variables

We found little evidence that any local or regional current-year climate variables were useful predictors of reproductive output at any stage. Although the top models ($\Delta AIC < 2$) occasionally contained an inconsistent suite of climate variables, all had parameter estimates with 90% confidence intervals overlapping zero. This is an apparent contradiction to previous studies (Table 4), which all used different subsets of the data and different analytical techniques. However, several lines of reasoning suggest to us that relationships described earlier were either weak or spurious. First, they are sometimes contradictory. Satterthwaite et al. (2012) found a *weak positive* relationship between sea surface temperature and overall reproductive success of kittiwakes in the Pribilofs using these same datasets. Using two different subsets of years, Springer (1992) and Byrd et al. (2008a) both reported a *negative* relationship with sea surface temperature. Using yet another subset of the same data, Decker et al. (1995) and Lloyd (1985) reported none at all with current-year sea surface temperature. Second, most earlier studies ran simple correlations on point estimates of mean reproductive success (but see Satterthwaite et al., 2012 and Zador et al., 2013). We were able to reproduce some of these earlier findings by running multiple simple correlations on our expanded dataset (Table 4), but not many others after adding more years. In fact, these relationships completely "go away" using our single-model approach accounting for individual nest and plot level effects, as well as all of the possible interacting reproductive and environmental variables. Our results strongly suggest that the outcome of previous year success was a better predictor of each stage of reproductive success than any environmental variables. Clearly changes in the environment are likely to affect foraging conditions and effort allocation in seabirds but relationships with fertility do appear to be straightforward. We propose that the condition of adults at the end of a breeding attempt might carry on across sequential nesting stages, masking any weak relationship with environmental variables in a given year.

Our modeling approach has two points of caution that may have lessened our precision in detecting relationships with environmental variables. First, model averaging increases standard error estimates for parameters to account for model uncertainty. This would make us less likely to call a variable "significant" based on its confidence interval overlapping with zero (if parameter estimates were not averaged across the entire model suite). Second, our modeling approach requires data to be present for every variable for each year, so 9 years with incomplete data for one or more climate variables were discarded, mostly earlier in the dataset.

A major difficulty in modeling ecological data and trying to define climatic predictors is the huge suite of time series with potentially weak mechanistic links (see Renner et al., 2012 for discussion). Our model sets were very large for even a 36-year study. Therefore we were forced to limit our models to include only climatic variables from the current year. Zador et al. 2013 found lagged effects (up to two years) of environmental forcing mechanisms with indices of Pribilof seabird productivity combined across species, and Lloyd (1985) found that kittiwake success on St. George Island was negatively correlated with sea surface temperature lagged one and two years.

Table 4
Literature review of relationships between climatic variables and breeding success of black-legged kittiwakes and thick-billed murres at the Pribilof Islands. Sources and specifics of climate datasets vary among studies (i.e., Byrd et al., 2008 and Satterthwaite et al., 2012 use different datasets for "Spring SST"). Positive (+) and negative (−) signs show significant positive and negative relationships, respectively; signs with "SG" or "SP" indicate a relationship found only for St. George or St. Paul. All studies use correlation analysis except Satterthwaite et al. (2012). Results from this study are pairwise Spearman rank correlations ($P < 0.1$) shown for comparison with other similar analyses.

Species	Source	Years	Success parameter	Annual SST	Winter SST	Spring SST	Summer SST	Ice	PDO	Wind speed
Black-legged	Satterthwaite et al., 2012	1985–2009	Overall			+	None	−	+	
Kittiwake	Byrd et al., 2008a	1975–2005	Overall		None	−SG[a]	None	+SG		
	Springer, 1998	1976–1995	Overall	+SG[b]						
	Decker et al., 1995	1975–1990	Overall	None						
	Springer, 1992	1976–1990	Overall	−						
	Springer, 1991	1976–1990	Overall	−						
	Lloyd, 1985	1976–1984	Overall	NoneSG			NoneSG			−SG
	This study (correlations)	1975–2010	Laying		None	None	None	None	None	None
	This study (correlations)	1975–2010	Hatching		None	None	+	None	None	None
	This study (correlations)	1975–2010	Fledging		+	+	+	−	+SP	+SG
	This study (correlations)	1975–2010	Overall		None	+SP	+	None	None	None
Thick-billed	Byrd et al., 2008a	1975–2005	Overall		None	−SG	−	None		
Murre	Decker et al., 1995	1975–1990	Overall	−						
	Lloyd, 1985	1976 – 1984	Overall	NoneSG			NoneSG			NoneSG
	This study (correlations)	1975–2010	Hatching		None	None	None	None	None	None
	This study (correlations)	1975–2010	Fledging		None	−SG	−SP	None	None	+SP
	This study (correlations)	1975–2010	Overall		None	−SG	None	None	None	None

[a] Detrended dataset only.
[b] Analysis is divided into two atmospheric regimes based on low pressure state (1976–1989) or high pressure state (1990–1995); in each state, seabird productivity is higher in warmer years.

5.4. Diet variables

Success of murres and kittiwakes was associated with prey in a few model sets. Murre fledging success was higher when they fed their chicks fewer myctophids (which represented 0.97 of the signal in all offshelf prey items), in spite of the relatively high energy content of that prey type (Van Pelt et al., 1997). These results may be spurious, however, because myctophids were rarely found in murre chick diets in the Pribilofs. Myctophids are a deep-water fish occurring beyond the shelf edge; if this is a real result, it suggests that murre fledging success was best when they were able to find food on the shelf, rather than when they had to travel further to the basin for myctophids. None of the shelf-based prey species (pollock, sandlance, or capelin) predicted fledging success, however, indicating that murres may switch readily among prey types and proximity of foraging resources is more important than any one prey type. Kittiwakes had lower fledging success when they fed their chicks more amphipods (which were correlated 0.5 with total invertebrates and −0.6 with total fish). This pattern suggests that fish of any type are preferred to zooplankton for chick feeding, likely due simply to their larger size. Optimal foraging predicts that individuals tend to feed chicks with larger prey than for themselves (Davoren and Burger, 1999).

While we assume that foraging conditions are among the primary drivers of stress and ultimately demographic parameters, we have few data about food availability in most systems. Shultz et al. (2009), who did have a short-term dataset including food availability in the Gulf of Alaska, found that for kittiwakes, pre-laying food availability explained variation in kittiwake laying success and clutch size while murre reproductive success was best explained by food availability during chick-rearing. Although both frequency of occurrence and number of individuals of prey types in seabird diet may somewhat reflect food availability (as described in Renner et al. (2012)), they may need to be paired with foraging studies to determine foraging effort that can be linked to breeding success (Burke and Montevecchi, 2009; Suryan et al., 2002).

Analysis of seabird diet data and breeding success is also biased by collection constraints as well as temporal variation in sampling methods. Most available diet information is obtained during the chick-rearing period, which differs from diet collected at other times of the breeding season (Renner et al., 2012). Murres are more constrained in chick provisioning by their need to deliver single, large prey items they can carry in their bill, while they often use smaller, more abundant crustaceans during incubation when they feed for self-provisioning (Ito et al., 2010). Regurgitated kittiwake chick and adult diet samples often cannot be separated, but are assumed to be more similar (Renner et al., 2012).

5.5. Differences between St. Paul and St. George islands – local-scale implications

Probabilities of success in each stage were correlated between islands, except for murres during the chick-rearing period. Fledging success may relate more to local foraging conditions, as birds are tied to the nest and restricted to make shorter foraging trips to meet chick-feeding rates (Gaston et al., 2007; Orians and Pearson, 1979). Fittingly, tracking data from murres during the chick period in 2008–2010 indicated no overlap in foraging areas between the two islands (Harding et al., 2013), suggesting birds on different islands were subject to different foraging conditions. Laying and hatching success, in contrast, appear set up by conditions earlier in the season (prior to laying or the previous year), when birds can forage widely. Although we have no information on foraging range prior to the chick period, we would predict more foraging overlap earlier in the nesting cycle when adults are not tied as closely to the nest, resulting in more similar conditions for birds on each island. That fledging success was correlated for kittiwakes (which can fly farther than murres) may be due to occasional overlap in foraging locations between islands (Paredes, pers. comm. data).

Murres had higher reproductive success on St. George Island than on St. Paul Island, mostly coming from strong differences in the egg period. Presumably St. George Island's location closer to the continental shelf break means more regular access to high quality prey (see Renner et al., 2012, indicating strong diet differences between the two islands). In contrast, kittiwake productivity did not differ significantly between islands, during which time the overall population of kittiwakes on St. Paul Island has declined but the population on St. George Island has remained stable (Byrd et al., 2008b). Seabird productivity may have a relatively low contribution to population change (Schmutz and Byrd, 2004), and other factors such as adult survival require further investigation in each locality. A recent tracking study indicated that both kittiwakes and murres at St. Paul Island increased foraging effort to cope with food shortages on the middle shelf, successfully raising chicks but at a cost of higher adult nutritional stress in some years. Birds at St. George Island, in contrast, may have been buffered from the lack of quality prey on the shelf by closer proximity to shelf-edge resources, leading to lower stress levels of piscivorous seabirds on St. George Island compared to St. Paul Island (Benowitz-Fredericks et al., 2008). High stress levels may lead to higher adult mortality or to higher chick mortality after fledging (Goutte et al., 2010; Kitaysky et al., 2010). Preliminary analysis using four years of resighting data suggests adult survival/permanent emigration may be lower at St. Paul Island than at St. George Island for both seabird species (AMNWR, unpubl. data); however larger data sets are required for conclusive results. Further efforts to measure adult survival, and other variables such as colony-age structure ("experience"), recruitment rates, and movements between colonies are needed for a better understanding of causes affecting population processes (Wooller et al., 1992).

5.6. Implications for seabird monitoring

We expected to find that each sequential stage of reproductive success was reflective of different climate conditions in the marine environment. Instead, we found that climate effects were strongly trumped by success in the previous year or previous stage and, for kittiwakes, timing of breeding. This suggests adult condition (going into the breeding season or going into each successive stage) plays a strong role in success for kittiwakes and murres at the Pribilof Islands. Given that both species, particularly murres, appear to work hard to raise their chicks at the cost of high nutritional stress in poor years (Benowitz-Fredericks et al., 2008; Satterthwaite et al., 2010) fledging rates may not reflect adult condition unless local food conditions are above or below certain thresholds. We currently have no consistent time series on body condition or stress during any part of the year in the Pribilof Islands. Data on body condition of banded birds at the beginning and end of the breeding season in successive years would be valuable for relating breeding performance to condition at the individual level and understanding differences at the population level.

Although prey availability earlier in the season or at the end of the prior season appear important drivers of breeding success, we lack much data on fall, winter, and early spring foraging conditions for seabirds. Diet data from seabirds are important as a proxy of prey quality and amount (biomass) that can be used to explain differences in breeding success (e.g., Suryan et al., 2002 for kittiwakes). Data on foraging behavior, available from an increasing number of GPS tracking studies, can be used in conjunction with diet data for a better picture of foraging effort (e.g., Paredes et al., 2014) and possible predictor of body condition or physiological

stress. However, most diet and tracking data are collected during the chick period (e.g., Barrett et al., 2007; Burger and Shaffer, 2008) and we have little understanding of food resources the rest of the year. Given the period prior to the breeding season seems to play an important role in determining reproductive output, some index of winter food availability seems critical.

Winter foraging conditions may also be critical for the transition between good years (high breeding success) and bad years (low breeding success). Food availability regardless of the mechanisms behind its variability is ultimately the driving force affecting foraging effort, adult condition, nutritional stress and at in many circumstances reproductive success. Given that hatching or laying success along with previous year breeding success were good predictors of breeding success within a year suggest food conditions prior to chick-rearing are critical. If previous year's success determines the following year's laying and/or hatching success (which is in turn a predictor of fledging success), then success would presumably continue to be always good or always bad until something breaks the cycle. We know that overall success of kittiwakes and murres fluctuates among years (see Figs. 1–4) so foraging conditions might override the influence of previous year's success. Unfortunately, the lack of enough data in seabird diets (proxy of prey quality/amount) at early stages of the reproduction precluded us to determine its influence in laying or hatching success. Likewise, foraging conditions during the non-breeding season may be also an important missing link to understanding what drives reproductive success at the Pribilof Islands.

5.7. Conclusions

Using a 36-year dataset of reproductive success for black-legged kittiwakes and thick-billed murres at the Pribilof Islands, we modeled sequential stages of success using reproductive, climatic, and diet variables. We found: (1) Success in previous stages and the previous year were more important predictors of overall success than any environmental variables. Timing was also an important predictor of laying success for kittiwakes. These relationships suggest a cascade effect, in which adult condition carrying over from the previous year plays a large role in reproductive success. (2) An increase of oceanic prey (mediated by distance traveled) and small invertebrates in diets negatively affects fledging success, which may indicate low availability of high quality prey near the colonies. (3) Differences in reproductive variables at St. Paul and St. George islands do not completely match population trends between the two islands, suggesting adult survival and condition may be important contributors to population dynamics. (4) Adult condition and foraging conditions during the non-breeding season may be important datasets for understanding drivers of kittiwake and murre reproductive success at the Pribilofs.

Acknowledgments

We are grateful to the many researchers who contributed productivity and diet data from the Pribilof Islands: M.S.W. Bradstreet, D.E. Dragoo, G.L. Hunt, M. Ito, D. Lloyd, A.M. Springer, and the University of Alaska Fairbanks. Countless field workers have worked through rain, wind, and fog to collect these data. Our BSIERP collaborators, especially D.B. Irons, N. Jones, A.S. Kitaysky, K. Kuletz, R. Orben, R. Paredes, and D.D. Roby, have provided invaluable contributions, support, and advice throughout this project. We thank J. Reynolds for substantial statistical advice on this project, J. Warzybok for three years of data collection and compilation, and J. Schmutz, M. Romano, M. Renner, and an anonymous reviewer for reviews of earlier versions of this manuscript. G.V. Byrd developed and tirelessly guided this project at every stage as well. Field work in 2008–2010 were funded by the North Pacific Research Board as part of BSIERP project B65. Data collected by the authors were within the scope of a current IACUC permit. This is BEST-BSIERP Bering Sea Project publication number 131 and NPRB publication number 474. The findings and conclusions in this article are those of the authors and do not necessarily represent the views of the United States Fish and Wildlife Service.

Appendix A. Supporting information

Supplementary data associated with this article can be found in the online version at http://dx.doi.org/10.1016/j.dsr2.2014.03.006.

References

Ainley, D.G., Sydeman, W.J., Norton, J., 1995. Upper trophic level predators indicate interannual negative and positive anomalies in the California Current food web. Mar. Ecol. Prog. Ser. 118, 69–79.

Baird, P.H., 1990. Influence of abiotic factors and prey distribution on diet and reproductive success of three seabird species in Alaska. Ornis. Scand. 21, 224–235.

Barrett, R.T., Camphuysen, C.J., Anker-Nilssen, T., Chardine, J.W., Furness, R.W., Garthe, S., Hüppop, O., Leopold, M.F., Montevecchi, W.A., Veit, R.R., 2007. Diet studies of seabirds: a review and recommendations. ICES J. Mar. Sci. 64, 1675–1691.

Bedard, J., 1969. The nesting of crested, least and parakeet auklets on St. Lawrence Island, Alaska. Can. J. Zool. 47, 1025–1050.

Bell, G., Koufopanou, V., 1986. The cost of reproduction. In: Dawkins, R., Ridley, M. (Eds.), Oxford Surveys in Evolutionary Biology, vol. 3. Oxford University Press, Oxford, pp. 83–131.

Benowitz-Fredericks, Z.M., Kitaysky, A.S., 2005. Benefits and costs of rapid growth in common murre chicks *Uria aalge*. J. Avian Biol. 36 (4), 287–294.

Benowitz-Fredericks, Z.M., Shultz, M.T., Kitaysky, A.S., 2008. Stress hormones suggest opposite trends of food availability for planktivorous and piscivorous seabirds in 2 years. Deep-Sea Res. II 55, 1868–1876.

Bolker, B.M., Brooks, M.E., Clark, C.J., Geange, S.W., Poulsen, J.R., Stevens, M.H.H., White, J.S., 2009. Generalized linear mixed models: a practical guide for ecology and evolution. Trends Ecol. Evol. 24, 127–135.

Burger, A.E., Shaffer, S.A., 2008. Perspectives in ornithology application of tracking and data-logging technology in research and conservation of seabirds. Auk 125, 253–264.

Burke, C.M., Montevecchi, W.A., 2009. The foraging decisions of a central place foraging seabird in response to fluctuations in local prey conditions. J. Zool. 278, 354–361.

Burnham, K.P., Anderson, D.R., 2002. Model Selection and Multimodel Inference: A Practical Information – Theoretic Approach, 2nd ed. Springer, New York

Byrd, G.V., 1989. Seabirds in the Pribilofs Islands, Alaska: Trends and Monitoring Methods (M.S. thesis). Univ. Idaho, Moscow (95 pp)

Byrd, G.V., Sydeman, W.J., Renner, H.M., Minobe, S., 2008a. Responses of piscivorous seabirds at the Pribilof Islands to ocean climate. Deep-Sea Res. II 55, 1856–1867.

Byrd, G.V., Schmutz, J.A., Renner, H.M., 2008b. Contrasting population trends of piscivorous seabirds in the Pribilof Islands: a 30 year perspective. Deep-Sea Res. II 55, 1846–1855.

Charnov, E.L., Krebs, J.R., 1974. On clutch size and fitness. Ibis 116, 217–219.

Chastel, O., Weimerskirch, H., Jouventin, P., 1995. Influence of body condition on reproductive decision and reproductive success in the Blue Petrel. Auk 112, 964–972.

Connan, M., Mayzaud, P., Trouve, C., Barbraud, C., Cherel, Yves., 2008. Interannual dietary changes and demographic consequences in breeding blue petrels from Kerguelen Islands. Mar. Ecol. Prog. Ser. 373, 123–135.

Coulson, J.C., 1966. The influence of pair-bond and age on the breeding biology of the kittiwake gull *Rissa tridactyla*. J. Anim. Ecol. 35, 269–279.

Coulson, J.C., 2002. Why do adult kittiwakes survive so long but breed so poorly in the Pacific? J. Avian Biol. 33, 111–112.

Davoren, G.H., Burger, A.E., 1999. Differences in prey selection and behaviour during self-feeding and chick provisioning in rhinoceros auklets. Anim. Behav. 58, 853–863.

Decker, M.B., Hunt Jr., G.L., Byrd, G.V., 1995. The relationships among sea-surface temperature, the abundance of juvenile walleye pollock (*Theragra chalcogramma*), and the reproductive performance and diets of seabirds at the Pribilof Islands, southeastern Bering Sea. In: Beamish, R.J. (Ed.), Climate Change and Northern Fish Populations, vol. 121. Canadian Special Publication of Fisheries and Aquatic Sciences, pp. 425–437.

Dragoo, D.E., Renner, H.M., Irons, D.B., 2012. Breeding Status, Population Trends and Diets of Seabirds in Alaska, 2009. U.S. Fish and Wildlife Service. Report AMNWR 2012/01. Homer, Alaska.

Duffy, D.C., Jackson, S., 1986. Diet studies of seabirds: a review of methods. Colon. Waterbirds 9, 1–17.
Duffy, D.C., 1990. Seabirds and the 1982–1984 El Niño/southern oscillation. In: Glynn, P.W. (Ed.), Global Ecological Consequences of the 1982/83 El Niño Southern Oscillation. Elsevier, pp. 395–415
Einoder, L.D., 2009. A review of the use of seabirds as indicators in fisheries and ecosystem management. Fish. Res. 95, 6–13.
Erikstad, K.E., Bustnes, J.O., Moum, T., 1993. Clutch-size determination in precocial birds: a study of the common eider. Auk 110, 623–628.
Faivre, B., Préault, M., Théry, M., Secondi, J., Patris, B., Cézilly, F., 2001. Breeding strategies and morphological characters in an urban population of blackbirds, *Turdus merula*. Anim. Behav. 61, 969–974.
Frederiksen, M., Wright, P.J., Heubeck, M., Harris, M.P., Mavor, R.A., Wanless, S., 2005. Regional patterns of kittiwake *Rissa tridactyla* breeding success are related to variability in sandeel recruitment. Mar. Ecol. Prog. Ser. 300, 201–211.
Furness, R.W., Camphuysen, K.C.J., 1997. Seabirds as monitors of the marine environment. ICES J. Mar. Sci. 54 (4), 726–737.
Gaston, A.J., Ydenberg, R.C., Smith, G.E.J., 2007. Ashmole's halo and population regulation in seabirds. Mar. Ornithol. 35, 119–126.
Gill, V.A., Hatch, S.A., 2002. Components of productivity in black-legged kittiwakes *Rissa tridactyla*: response to supplemental feeding. J. Avian Biol. 33, 113–126.
Golet, G.H., Irons, D.B., Costa, D.P., 2000. Energy costs of chick rearing in black-legged kittiwakes (*Rissa tridactyla*). Can. J. Zool. 78, 982–991.
Goutte, A., Antoine, E., Weimerskirch, H., Chastel, O., 2010. Age and the timing of breeding in a long-lived bird: a role for stress hormones? Funct. Ecol. 24, 1007–1016.
Grueber, C.E., Nakagawa, S., Laws, R.J., Jamieson, I.G., 2011. Multimodel inference in ecology and evolution: challenges and solutions. J. Evol. Biol. 24, 699–711.
Harding, A.M.A., Piatt, J.F., Schmutz, J.A., Shultz, M., Van Pelt, T.I., Kettle, A.B., Speckmann, S.G., 2007. Prey density and the behavioural flexibility of a marine predator: the common guillemot (*Uria aalge*). Ecology 88, 2024–2033.
Harding, Paredes, Suryan, Roby, Irons, Orben, Renner, Young, Barger, Dorresteijn, Kitaysky, 2013. Does location really matter? An inter-colony comparison of thick-billed murres (*Uria lomvia*) breeding at varying distances from productive oceanographic features in the Bering Sea. Deep Sea Res. II 94, 178–191.
Hatch, S.A., Hatch, M.A., 1990. Components of breeding productivity in a marine bird community: key factors and concordance. Can. J. Zool. 68 (8), 1680–1690.
Hickey, J.J., Craighead, F.L., 1977. A census of seabirds on the Pribilof Islands. Environmental Assessment of the Alaskan Continental Shelf. Final Reports of Principal Investigators, vol. 2. BLM/NOAA/OMPA, Boulder, pp. 96–195.
Hipfner, J.M., 1997. Fitness-related consequences of relaying in an Arctic seabird: survival of offspring to recruitment age. Auk 118 (4), 1076–1080.
Hunt Jr., G.L., Eppley, Z., Burgeson, B., Squibb, R., 1981. Reproductive ecology, foods, and foraging areas of seabirds nesting on the Pribilof Islands, 1975–1979. Environmental Assessment of the Alaskan Continental Shelf. Final Reports of Principal Investigators, vol. 12. BLM/NOAA/OMPA, Boulder, pp. 1–250.
Hunt Jr., G.L., Decker, M.B., Kitaysky, A., 1996. Fluctuations in the Bering Sea ecosystem as reflected in the reproductive ecology and diets of kittiwakes on the Pribilof Islands, 1975–1990. In: Greenstreet, S.P.R., Tasker, M.L. (Eds.), Aquatic Predators and Their Prey. Fishing News Books, Oxford, pp. 142–153
Ito, M., Takahashi, A., Kokubun, N., Kitaysky, A.M., Watanuki, Y., 2010. Foraging behavior of incubating and chick-rearing thick-billed murres *Uria lomvia*. Aquat. Biol. 8, 279–287.
Kitaysky, A.S., Hunt, G.L., Flint, E.N., Rubega, M.A., Decker, M.B., 2000. Resource allocation in breeding seabirds: responses to fluctuations in their food supply. Mar. Ecol. Prog. Ser. 206, 283–296.
Kitaysky, A.S., Piatt, J.F., Hatch, S.A., Kitaiskaia, E.V., Benowitz-Fredericks, Z.M., Shultz, M.T., Wingfield, J.C., 2010. Food availability and population processes: severity of nutritional stress during reproduction predicts survival of long-lived seabirds. Funct. Ecol. 24 (3), 625–637.
Lessells, C.M., 1991. The evolution of life histories. In: Krebs, J.R., Davies, N.B. (Eds.), Behavioural Ecology: An Evolutionary Approach. Blackwell, Oxford, pp. 32–68
Lloyd, D.S., 1985. Breeding Performance of Kittiwakes and Murres in Relation to Oceanographic and Meterologic Conditions Across the Shelf of the Southeastern Bering Sea (M.S. thesis). University of Alaska, Fairbanks (106 pp)
Mantua, N.J., Hare, S.R., Zhang, Y., Wallace, J.M., Francis, R.C., 1997. A Pacific decadal climate oscillation with impacts on salmon. Bulletin of the American Meteorological Society 78, 1069–1079.
Mavor, R.A., Heubeck, M., Schmitt, S., Parsons, M., 2008. Seabird Numbers and Breeding Success in Britain and Ireland, 2006. UK Nature Conservation. No. 31. Joint Nature Conservation Committee, Peterborough.
Milonoff, M., Pöysä, H., Runko, P., Ruusila, V., 2004. Brood rearing costs affect future reproduction in the precocial common goldeneye *Bucephala clangula*. J. Avian Biol. 35 (4), 344–351.
Monaghan, P., Nagar, R.G., 1997. Why don't birds lay more eggs? Trends Ecol. Evol. 12 (7), 270–274.
Montevecchi, W.A., 1993. Birds as indicators of change in marine prey stocks. In: Furness, R.W., Greenwood, D.J. (Eds.), Birds as Monitors of Environmental Change. Chapman & Hall, London, pp. 217–266
Moss, J.H., Farley, E.V., Feldmann, A.M., Ianelli, J.N., 2009. Spatial distribution, energetic status, and food habits of Eastern Bering Sea age-0 Walleye Pollock. Trans. Am. Fish. Soc. 138, 497–600.
Murphy, E.C., Springer, A.M., Roseneau, D.G., 1991. High annual variability in reproductive success of kittiwakes (*Rissa tridactyla L.*) at a colony in Western Alaska. J. Anim. Ecol. 60, 515–534.
Nelson, B., 1980. Seabirds: Their Biology and Ecology. Hamlyn, UK (224 pp).
Orians, G.H., Pearson, N.E., 1979. On the theory of central place foraging. In: Horn, D.J., Mitchell, R.D., Stairs, G.R. (Eds.), Analysis of Ecological Systems. Ohio State University Press, Columbus, pp. 154–177
Paredes, R., Jones, I.L., Boness, D.J., 2005. Reduced parental care, compensatory behaviour and reproductive costs experienced by female and male thick-billed murres (*Uria lomvia*) equipped with data loggers. Anim. Behav. 69, 197–208.
Paredes, R., Harding, A.M.A., Irons, D.B., Roby, D.D., Suryan, R.M., Orben, R.A., Renner, H.M., Young, R., Kitaysky, A., 2014. Proximity to multiple foraging habitats enhances seabirds' resilience to local food shortages. Mar. Ecol. Prog. Ser. 471, 253–269, http://dx.doi.org/10.3354/meps10034.
Piatt, J.F., Sydeman, W.J., Wiese, F., 2007. Introduction: a modern role for seabirds as indicators. Mar. Ecol. Prog. Ser. 352, 199–204.
Quillfeldt, P., 2001. Variation in breeding success in Wilson's storm petrels: influence of environmental factors. Antarct. Sci. 13, 400–409.
R Development Core Team, 2012. R: A language and environmentfor statistical computing. R Foundation for Statistical Computing, Vienna, Austria, http://www.R-project.org, (ISBN 3900051 07 0).
Regular, P.M., Shuhood, F., Power, T., Montevecchi, W.A., Robertson, G.J., Ballam, D., Piatt, J.F., Nakashima, B., 2009. Murres, capelin and ocean climate: inter-annual associations across a decadal shift. Environ. Monit. Assess. 156, 293–302.
Renner, H.M., Mueter, F., Drummond, B.A., Warzybok, J.A., Sinclair, E.H., 2012. Patterns of change in diets of two piscivorous seabird species during 35 years in the Pribilof Islands. Deep-Sea Res. II 65–70, 273–291.
Reznick, D.N., 1985. Cost of reproduction: an evaluation of the empirical evidence. Oikos 44, 257–267.
Satterthwaite, W.H., Kitaysky, A.S., Hatch, S.A., Piatt, J.F., Mangel, M., 2010. Unifying quantitative life history theory and field endocrinology to assess prudent parenthood in a long-lived seabird. Evol. Ecol. Res. 12, 779–792.
Satterthwaite, W.H., Kitaysky, A.S., Mangel, M., 2012. Linking climate variability, productivity and stress to demography in a long-lived seabird. Mar. Ecol. Prog. Ser. 454, 221–235.
Schmutz, J.A., Byrd, G.V., 2004. Modeling the influence of productivity, survival, and meta- population dynamics on trends of kittiwakes and murres at the Pribilof Islands, Alaska. Final Report to the U.S. Fish and Wildlife Service. Alaska Maritime National Wildlife Refuge. USGS Alaska Science Center, Anchorage, 59 pp.
Schmutz, J.A., Rockwell, R.F., Petersen, M.R., 1997. Relative effects of survival and reproduction on the population dynamics of Emperor Geese. J. Wildl. Manag. 61, 191–201.
Schoech, S.J., Rensel, M.A., Bridge, E.S., Boughton, R.K., Wilcoxen, T.E., 2009. Environment, glucocorticoids, and the timing of reproduction. Gen. Comp. Endocrinol. 163, 201–207.
Shaffer, S.A., Costa, D.P., Weimerskirch, H., 2003. Foraging effort in relation to the constraints of reproduction in free-ranging albatrosses. Funct. Ecol. 17, 66–74.
Shultz, M.T., Piatt, J.F., Harding, A.M., Kettle, A.B., Van Pelt, T.I., 2009. Timing of breeding and reproductive performance in murres and kittiwakes reflect mismatched seasonal prey dynamics. Mar. Ecol. Prog. Ser. 393, 247–258.
Sinclair, E.H., Balanov, A.A., Kubodera, T., Radchenko, V.I., Fedorets, Y.A., 1999. Distribution and ecology of mesopelagic fishes and cephalopods. In: Loughlin, T.R., Ohtani, K. (Eds.), Dynamics of the Bering Sea: A Summary of Physical Chemical and Biological characteristics, and a Synopsis of Research on the Bering Sea. North Pacific Marine Science Organization (PICES), University of Alaska Sea Grant AK-SG-99-03, Fairbanks, pp. 485–508
Sinclair, E.H., Vlietstra, L.S., Johnson, D.S., Zeppelin, T.K., Byrd, G.V., Springer, A.M., Ream, R.R., Hunt Jr., G.L., 2008. Patterns in prey use among fur seals and seabirds in the Pribilof Islands. Deep-Sea Res. II, 55; , pp. 1897–1918.
Sorensen, M.C., Hipfner, J.M., Kyser, T.K., Norris, D.R., 2009. Carry-over effects in a Pacific seabird: stable isotope evidence that pre-breeding diet quality influences reproductive success. J. Anim. Ecol. 78, 460–467.
Springer, A.M., 1991. Seabird relationships to food webs and the environment: examples from the North Pacific Ocean. In: Montevecchi, W.A., Gaston, A.J. (Eds.), Studies of High-latitude Seabirds. 1. Behavioral, Energetic, and Oceanographic Aspects of Seabird Feeding Ecology. Canadian Wildlife Service, Ottawa, pp. 39–48
Springer, A.M., 1992. A review: walleye Pollock in the North Pacific – how much difference do they really make? Fish. Oceanogr. 1, 80–96.
Springer, A.M., 1998. Is it all climate change? Why marine bird and mammal populations fluctuate in the North Pacific. In: Holloway, G., Muller, P., Henderson, D. (Eds.), Proceedings of the 10th 'Aha Huliko'a Hawaiian Winter Workshop on Biotic Impacts of Extratropical Climate Variability in the Pacific, January 26 – 30, 1998. SOEST Special Publication, Honolulu, pp. 121–125.
Springer, A.M., McRoy, C.P., Flint, M.V., 1996. The Bering Sea Green Belt: shelf-edge processes and ecosystem production. Fish. Oceanogr. 5, 205–223.
Stearns, S.C., 1989. Trade-off in life-history evolution. Funct. Ecol. 3, 259–268.
Suryan, R.M., Irons, D.B., Kauffman, M., Benson, J., Jodice, P.G.R., Roby, D.D., Brown, E.D., 2002. Short-term fluctuations in forage fish availability and the effect on prey selection and brood-rearing in the black-legged kittiwake (*Rissa tridactyla*). Mar. Ecol. Prog. Ser. 236, 273–287.
Sydeman, W.J., Thompson, S.A., Kitaysky, A., 2012. Seabirds and climate: roadmap for the future. Mar. Ecol. Prog. Ser. 454, 107–117.
Van Pelt, T.I., Piatt, J.F., Lance, B.K., Roby, D.D., 1997. Proximate composition and energy density of some north Pacific forage fish. Comp. Biochem. Physiol. 118A (4), 1393–1398.

Verhulst, S., Nilsson, J.-A., 2008. The timing of birds' breeding seasons: a review of experiments that manipulated timing of breeding. Philos. Trans. R. Soc. B 363 (1490), 399–410.
Wanless, S., Harris, M.P., 1992. Activity budgets, diet and breeding success of kittiwakes *Rissa tridactyla* on the Isle of May. Bird Study 39, 145–154.
Watanuki, Y., Ito, M., 2012. Climatic effects on breeding seabirds of the Northern Japan Sea. Mar. Ecol. Prog. Ser. 454, 183–196.
Williams, G.C., 1966. Natural selection, the cost of reproduction, and a refinement of Lack's principle. Am. Nat. 100, 687–690.
Wolf, S.G., Sydeman, W.J., Hipfner, J.M., Abraham, C.L., Tershy, B.R., Croll, D.A., 2009. Rangewide reproductive consequences of ocean climate variability for the seabird Cassin's auklet. Ecology 90, 742–753.
Wooller, R.D., Bradley, J.S., Croxall, J.P., 1992. Long term population studies of seabirds. Trends Ecol. Evol. 7, 111–114.
Zador, S., Hunt Jr., G.L., TenBrink, T., Aydin, K., 2013. Combined seabird indices show lagged relationships between environmental conditions and breeding activity. Mar. Ecol. Prog. Ser. 485, 245–258.

Deep-Sea Research II 109 (2014) 266–281

Contents lists available at ScienceDirect

Deep-Sea Research II

journal homepage: www.elsevier.com/locate/dsr2

Seasonal variation in the cross-shelf distribution of seabirds in the southeastern Bering Sea

George L. Hunt Jr.[a,*], Martin Renner[b], Kathy Kuletz[c]

[a] School of Aquatic and Fishery Sciences, Box 355020, University of Washington, Seattle, WA 98195, United States
[b] Tern Again Consulting, 388 E. Bayview Ave., Homer, AK, United States
[c] U.S. Fish and Wildlife Service, 1011 E. Tudor Rd., Anchorage, AK 99503, United States

ARTICLE INFO

Available online 5 September 2013

Keywords:
Bering Sea
Hydrographic domains
Marine birds
Multivariate tree analysis
Seabird assemblages
Bathymetry

ABSTRACT

We tested the hypothesis that the distribution of seabird species' associations across the southeastern Bering Sea shelf reflects the underlying ecology of four bathymetrically-defined hydrographic domains: the Inner or Coastal Shelf Domain (depth (Z) < 50 m), the Middle Shelf Domain (50 m < Z < 100 m), the Outer Shelf Domain (100 m < Z < 200 m), and the Shelf-Slope Domain (200 m < Z < 3000 m). The domains differ in stratification, which intensifies from winter to summer and breaks down in the fall. To examine seabird distributions with respect to these domains in multiple seasons, we quantified the cross-shelf distribution of species with respect to water depth using a 37-year database. We then used a multivariate tree analysis to group species with similar depth-use distributions, and mapped these clusters against the hydrographic domains. There were three patterns of seabird depth use: an inshore, shallow-water group in summer and fall, but not winter and spring, which conformed roughly to the Inner Shelf Domain; a group of species that were distributed widely across the Middle and Outer Shelf Domains, and a third group of species that occupied the outer portion of the Outer Shelf Domain and the Shelf-Slope Domain. The multivariate tree analysis revealed close correspondence between the seabird-derived domains and the bathymetrically-defined Outer Shelf and Shelf-Slope domains in spring and to a lesser extent in summer. In summer and fall, and to a lesser extent in spring, the seabird groupings showed a differentiation between the Inner Shelf Domain and the Middle Shelf Domain. Seabird-derived differentiation between the Shelf-Slope Domain and the Outer Shelf Domain was strongest in spring and summer. These seasonal patterns likely reflected the seasonal variation in the hydrographic differentiation of the bathymetrically-defined domains. Cross-validation of the multivariate tree analysis showed that the portion of seabird distribution patterns explained by the tree analysis was smallest in winter (when there is no stratification on the middle and inner shelves) and greatest in summer (when stratified water columns result in hydrographically defined domains), as would be expected under our hypothesis. We also examined hypotheses predicting why pursuit diving seabirds most often forage in shallow water whereas surface-foraging (surface-seizing) seabirds are more common over deep offshore waters. The hypothesis for regionally enhanced primary production as a driving factor was not supported for the inshore foraging seabirds but was supported for those foraging over shelf-slope waters.

1. Introduction

The distribution and abundance of seabirds have been linked to a wide variety of marine phenomena at spatial scales from those of ocean basins to small-scale tidal fronts a few hundred meters in width. Hunt and Schneider (1987) reviewed the marine ornithological literature available, and found that the examples of the distribution and abundance of seabirds at the scale of 100 km to 1000 km (meso-scale) were mostly drawn from upwelling systems during those seasons known for calm weather. Much less attention had been paid to how seabird communities might vary across broad expanses of continental shelf, or in winter, spring, or fall, when inclement weather may be a challenge (but see Renner et al., 2008).

Studies of seabird use of continental shelf ecosystems have taken two tacks. In the one, there has been an emphasis on the depth of water in which different foraging types prefer to seek prey. For example, Wynne-Edwards (1935), Joiris (1978, 1983), and Stone et al. (1995) suggested that seabirds that pick their prey from the surface (surface-seizing) forage farther offshore than do species that dive and pursue their prey underwater (pursuit-divers) in northwestern Atlantic and North Sea shelf systems. In the other, seabird foraging habitats have been related to waters with different mixing regimes, which in turn were tied to different depth ranges (Iverson et al., 1979; Kessel, 1979; Hunt et al., 1981b). The seasonally changing

* Corresponding author. Tel.: +1 206 441 6109; fax: +1 360 378 6748.
E-mail address: geohunt2@UW.edu (G.L. Hunt Jr.).

0967-0645/$ - see front matter © 2013 Elsevier Ltd. All rights reserved.
http://dx.doi.org/10.1016/j.dsr2.2013.08.011

conditions in the Bering Sea allow the separation of depth effects from oceanographic effects on seabird habitat use. Schneider (1997) explored some of the reasons why these foraging preferences might exist, and we address these hypotheses in Section 4.

In the eastern Bering Sea, early analyses showed that seabird species tended to be associated with specific depth ranges; over the outer shelf and slope, surface-seizing species predominated whereas in relatively shallow waters, pursuit-diving species predominated (Iverson et al., 1979; Kessel, 1979; Hunt et al., 1981b). The depth ranges corresponded to the then recently described hydrographic structure of eastern Bering Sea shelf waters (Kinder and Schumacher, 1981). Later work showed that there were significant spatial differences in the amount of surface-caught and sub-surface-caught prey obtained by seabirds over the southeastern Bering Sea shelf, with more subsurface-prey consumed in shallow waters and more surface-prey consumed in the outer portion of the shelf and shelf-slope (Schneider and Hunt, 1982; Schneider et al., 1986).

In this paper we test the hypothesis that seabird communities vary across the broad expanse of the southeastern Bering Sea shelf as a function of the location of the different hydrographic domains there. As these domains are seasonal phenomena, driven by thermal stratification built up by insolation in the warmer months, we predicted that seabird communities would also show stronger cross-shelf patterns during summer, when stratification is stronger, than during winter, when the water column over much of the shelf is well mixed (Stabeno et al., 2001; Hermann et al., 2002). Using a broader range of species than Schneider and Hunt (1982) and Schneider et al. (1986), we also examined the hypothesis that pursuit-diving seabirds prefer shallower waters and that surface-seizing seabirds prefer deeper waters. Ornithological studies have continued over the southeastern Bering Sea Shelf and have provided a rich data set. We take advantage of these new data to ask a series of new questions:

1) Do seabird species differ by bathymetry in their use of the southeastern Bering Sea shelf?
2) If one clusters seabird species by the depth intervals over which they forage, do these clusters define "domains" across the southeastern Bering Sea shelf that are similar to the bathymetrically-defined hydrographic domains?
3) Does the relationship of seabird distributions to bathymetry vary seasonally depending on stratification?
4) Is there a consistent pattern of surface-seizing seabirds predominating in the outer shelf and slope regions and the pursuit-diving seabirds occurring predominately in the Inner Shelf Domain?

We sought answers to these questions by using a 37-year data set of pelagic observations of seabirds obtained in the southeastern Bering Sea between 1975 and 2012.

2. Methods

2.1. Study area

2.1.1. The southeastern Bering Sea shelf

The southeastern Bering Sea continental shelf stretches from the shores of western Alaska to the shelf edge (depth ~200 m), which is almost 500 km distant. In summer, the shelf is characterized by

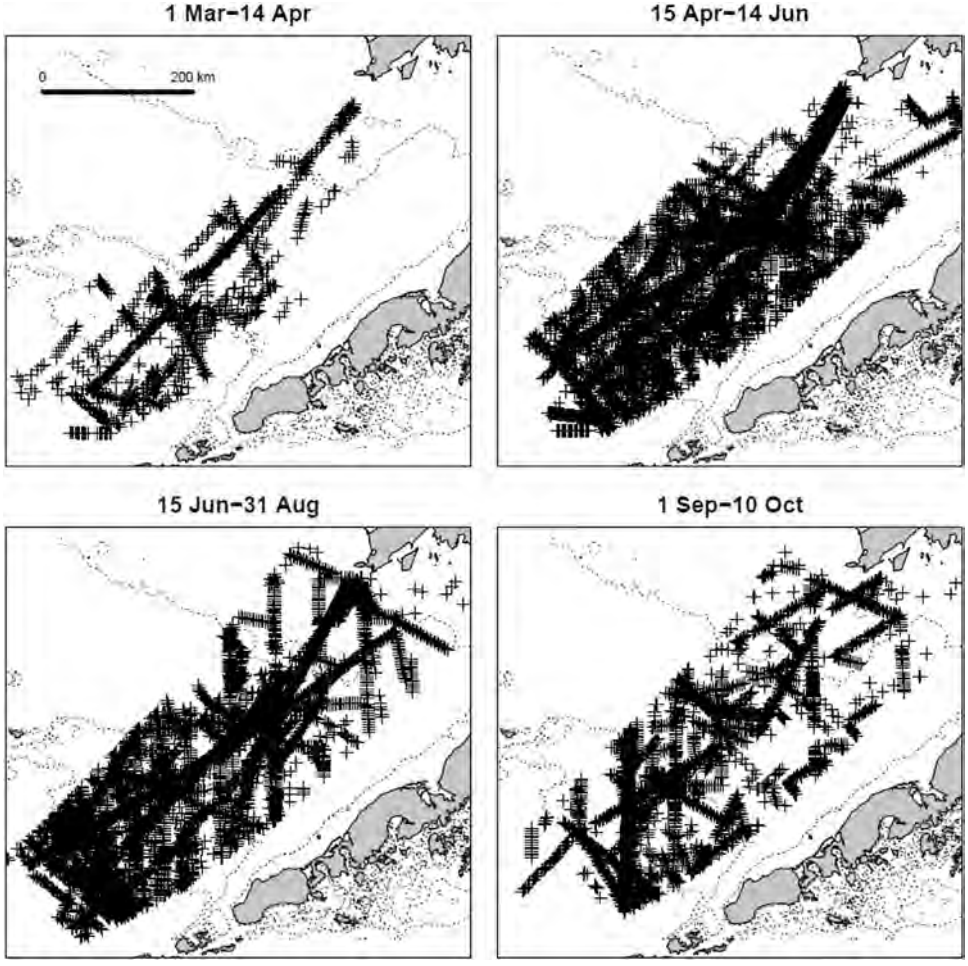

Fig. 1. Distribution of seabird counts, by season, on the southeast Bering Sea shelf. Each cross represents a 3 km-long transect segment.

having three hydrographic domains: the Inner Shelf Domain (depth (Z) < ~50 m), which is well mixed, the Middle Shelf Domain (~50 m < Z < ~100 m), which is strongly stratified with two layers in summer, and the Outer Shelf Domain (~100 m < Z < ~200 m), which is stratified with three layers (Kinder and Schumacher, 1981; Coachman, 1986). For comparison, we also included a Shelf-Slope Domain, which we define here as waters between 200 m and 3000 m depth (Fig. 1). The Inner Shelf Domain is separated from the Middle Shelf Domain by a structural front – the Inner Front (Schumacher et al., 1979, Kachel et al., 2002). In winter, the eastern Bering Sea is well mixed to 70 m or more (Stabeno et al., 2001), and there is no distinction in vertical structure between the Inner Shelf Domain and the Middle Shelf Domain, though there remains a front in terms of other chemical properties (Coachman, 1986). There is a broad transition between the Middle Shelf Domain and the Outer Shelf Domain, with a sub-surface salinity front separating the two domains (Coachman, 1986). This transition region is present year around. There is also a front at the shelf break that separates the Outer Shelf Domain from the deeper waters of the Shelf-slope Domain and Aleutian Basin, which is also present year around (Coachman, 1986).

Although the southeastern Bering Sea shelf is dominated by tidal currents rather than cross-shelf flows, there are important flows that help to define the differences between the domains (Coachman, 1986). Flows entering the Bering Sea through Unimak Pass bifurcate, with a portion turning eastward and flowing along the 50 m isobath coincident with or just offshore of the Inner Front (Stabeno et al., 1999, 2001). The remainder of the flow from Unimak Pass goes northwestward along the 100 m isobath (Stabeno et al., 2001, 2002). On-shelf flows of water from the Aleutian North Slope Current moving up Bering Canyon also add to the flux of nutrients and zooplankton along the 100 m isobath. Along the shelf edge, eddies in the Bering Slope Current (Kinder et al., 1975; Gregory et al., 2004) occasionally bring water from the Aleutian Basin onto the shelf as far as the 100 m isobath, thereby enriching nutrient supplies and the biomass of oceanic zooplankton there (Stabeno and van Meurs, 1999; Okkonen, 2001; Okkonen et al., 2004; Mizobata and Saitoh, 2004; Mizobata et al., 2006, 2008). Thus, the Outer Shelf Domain is influenced by the deeper waters of the basin.

As a result of these on-shelf flows, the Outer Shelf Domain is characterized as having a zooplankton fauna dominated by oceanic copepod species such as *Neocalanus plumchrus*, *N. flemengeri*, *N. cristatus, and Eucalanus bungii bungii* (Cooney and Coyle, 1982; Smith and Vidal, 1986; Vidal and Smith, 1986; Coyle et al., 2008). In contrast, the zooplankton fauna of the Middle Shelf and the Inner Shelf Domains is numerically dominated by small neritic copepod species, such as *Pseudocalanus* spp, *Arcatia longiremis*, and *Oithona similis*, though the larger, lipid-rich *Calanus marshallae*, accounts for a major portion of the copepod biomass. Euphausiids are present all across the shelf, with *Thysanoessa inermis* dominating in the Outer Shelf Domain and across the shelf slope, and *T. raschii* dominating in shelf waters shallower than 100 m (Smith and Vidal, 1986; Smith, 1991).

Because the *Neocalanus* copepods and the euphausiids *T. inermis* and *T. longipes* are present in the upper water column early in spring, they are efficient at grazing the nascent spring bloom over the Outer Shelf Domain and slope region (Walsh and McRoy, 1986). They thereby limit the bloom and capture much of the spring primary production for circulation in a pelagic food web in the upper water column (Cooney and Coyle, 1982; Smith and Vidal, 1986, Walsh and McRoy, 1986). In contrast, in the Middle and Inner Shelf Domains, there is a partial decoupling of the spring bloom from the grazers, with the zooplankton able to graze only a small portion of the bloom, much of which settles to the benthos (Walsh and McRoy, 1986). Although the numbers of copepods in the Middle and Inner Shelf Domains exceed those in the Outer Shelf and Shelf-Slope Domains, the biomass of copepods is much greater in the Outer Shelf and Shelf-Slope domains due to the greater size of the copepods there. Euphausiids are generally more abundant over the Outer Shelf and Shelf-Slope Domains (primarily *T. inermis* and *T. longipes*) than is the case over the Middle Shelf and Inner Shelf Domains (primarily *T. raschii*) (Smith, 1991, Pinchuk and Coyle, 2008), though in the Inner Shelf Domain and in the vicinity of the Inner Front, *T. raschii* form massive swarms that are fed upon by shearwaters (for Latin names of all bird species, see Table 2) (Hunt et al., 1996; Coyle and Pinchuk, 2002; Jahncke et al., 2005b).

Table 1
Effort (area [km^2] sampled) by cross-shelf domain (modified from Schneider et al., 1986) and season.

Domain	1 Mar.–14 Apr.	15 Apr.–14 June	15 June–31 Aug.	1 Sept.–10 Oct.	Total
Inner	70	633	682	467	1852
Middle	232	3121	1682	1018	6053
Outer	449	2615	1908	1158	6130
Slope	255	753	1238	272	2517
Total	1006	7122	5510	2914	16,552

The strong seasonal primary and secondary productivity of the southeastern Bering Sea supports some of the largest seabird colonies in the Northern Hemisphere, and the species richness and density of seabirds over the southeastern shelf are both high (Hunt et al., 1981b; Schneider and Shuntov, 1993). During the PROBES (Processes and Resources of the Bering Sea Shelf, McRoy et al., 1986) study, Schneider and Hunt (1982) and Schneider et al. (1986), recorded the distribution and abundance of seabirds throughout the PROBES area (Fig. 1) and estimated carbon flux to seabirds in each of the four hydrographic domains. In their analyses, Schneider et al. (1986) focused on the most abundant seabird species and found that four surface-seizing species or species groups, northern fulmar, fork-tailed storm-petrel, black-legged kittiwake, and large gulls had their greatest densities over deep water, whereas the pursuit-diving murres and shearwaters had their greatest numbers over the mixed waters of the Inner Shelf Domain. In contrast another subsurface forager, the tufted puffin, was fairly evenly distributed across the whole width of the shelf, except in 1981 when it was seldom observed in the Inner Shelf Domain. These findings fit well with the findings at lower trophic levels that the outer shelf is dominated by a pelagic food web, whereas in the middle shelf, a greater portion of the primary production is exported to the benthic food web (Schneider et al., 1986; Walsh and McRoy, 1986).

Other factors bring seasonal change to the southeastern Bering Sea shelf. Although in summer the Middle Shelf Domain is well stratified, in winter shelf waters are well mixed to 70 m depth or more, and many of the zooplankton species of importance to seabirds are at depths where they are inaccessible to seabirds (Smith and Vidal, 1986; Smith, 1991). Thus, we hypothesized that, if hydrography is the defining feature differentiating the domains for the seabirds, then seabird foraging distribution patterns relative to bathymetry should be weak in winter, when there is no hydrographic differentiation between the inner and middle shelves, somewhat stronger in spring, with summer being the period with the strongest correspondence between the seabird-defined domains and the hydrographically-defined domains. We also expected that correspondence between the seabird-defined domains and hydrographically defined domains would relax in fall, when early storms break down the stratification of the Middle Shelf Domain.

We selected a 134,868 km^2 cross-section of the southeastern Bering Sea shelf from the coast near Cape Newenham to the 3000 m isobath beyond the shelf break (Fig. 1). This region was the subject of the PROBES project (Hood, 1999), and there was good to

Table 2
Seabird species names, four letter codes, preferred foraging "mode", after Ashmole (1971), and weighted mean depth of occurrence over all seasons.

Common name	Latin name	Four letter code	Foraging mode	Mean depth ± SE
Laysan Albatross	*Phoebastria immutabilis*	LAAL	Surface seizing	829 ± 115
Short-tailed Albatross	*Phoebastria albatrus*	STAL	Surface seizing	992 ± 89
Black-footed Albatross	*Phoebastria nigripes*	BFAL	Surface seizing	570 ± 115
Northern Fulmar	*Fulmarus glacialis*	NOFU	Surface seizing	542 ± 103
Un. Dark Shearwater	*Puffinus spp.* (mostly *P. tenuirostris*)	UNSH	Pursuit diving	177 ± 60
Mottled Petrel	*Pterodroma inexpectata*	MOPE	Surface seizing	834 ± 113
Fork-tailed Storm-petrel	*Oceanodroma furcata*	FTSP	Surface seizing	706 ± 94
Leach's Storm-petrel	*Oceanodroma leucorhoa*	LESP	Surface seizing	1107 ± 106
Double-crested Cormorant	*Phalacrocorax auritus*	DCCO	Pursuit diving	89 ± 7
Pelagic Cormorant	*Phalacrocorax pelagicus*	PECO	Pursuit diving	153 ± 66
Red-faced Cormorant	*Phalacrocorax urile*	RFCO	Pursuit diving	116 ± 18
Red Phalarope	*Phalaropus fulicarius*	REPH	Surface seizing	273 ± 79
Red-necked Phalarope	*Phalaropus lobatus*	RNPH	Surface seizing	336 ± 111
Parasitic Jaeger	*Stercocarius parasiticus*	PAJA	Surface seizing/pirate	362 ± 57
Pomarine Jaeger	*Stercocarius pomarinus*	POJA	Surface seizing/pirate	262 ± 67
Long-tailed Jaeger	*Stercocarius longicaudus*	LTJA	Surface seizing/pirate	1186 ± 124
Ivory Gull	*Pagophila eburnea*	IVGU	Surface seizing	105 ± 2
Glaucous Gull	*Larus hyperboreus*	GLGU	Surface seizing	349 ± 80
Glaucous-winged Gull	*Larus glaucescens*	GWGU	Surface seizing	897 ± 177
Herring Gull	*Larus argentatus*	HEGU	Surface seizing	270 ± 94
Thayer's Gull	*Larus thayeri*	THGU	Surface seizing	91 ± 6
Slaty-backed Gull	*Larus schistisagus*	SLGU	Surface seizing	133 ± (NA)
Mew Gull	*Larus canus*	MEGU	Surface seizing	45 ± 3
Bonaparte's Gull	*Larus philadelphia*	BOGU	Surface seizing	101 ± NA
Sabine's Gull	*Xema sabini*	SAGU	Surface seizing	231 ± 73
Black-legged Kittiwake	*Rissa tridactyla*	BLKI	Surface seizing	296 ± 103
Red-legged Kittiwake	*Rissa brevirostris*	RLKI	Surface seizing	971 ± 125
Arctic Tern	*Sterna paradisaea*	ARTE	Surface seizing	299 ± 68
Aleutian Tern	*Onychoprion aleutica*	ALTE	Surface seizing	52 ± 6
Common Murre	*Uria aalge*	COMU	Pursuit diving	86 ± 39
Thick-billed Murre	*Uria lomvia*	TBMU	Pursuit diving	927 ± 119
Black Guillemot	*Cepphus grylle*	BAGU	Pursuit diving	86 ± 2
Pigeon Guillemot	*Cepphus columba*	PIGU	Pursuit diving	804 ± 171
Horned Puffin	*Fratercula corniculata*	HOPU	Pursuit diving	247 ± 79
Tufted Puffin	*Fratercula cirrhata*	TUPU	Pursuit diving	542 ± 99
Rhinoceros Auklet	*Cerorhinca monocerata*	RHAU	Pursuit diving	210 ± 15
Crested Auklet	*Aethia cristatella*	CRAU	Pursuit diving	244 ± 44
Whiskered Auklet	*Aethia pygmaea*	WHAU	Pursuit diving	308 ± (NA)
Least Auklet	*Aethia pusilla*	LEAU	Pursuit diving	238 ± 56
Parakeet Auklet	*Aethia psittacula*	PAAU	Pursuit diving	106 ± 35
Cassin's Auklet	*Ptychoramphus aleuticus*	CAAU	Pursuit diving	125 ± 32
Marbled Murrelet	*Brachyramphus marmoratum*	MAMU	Pursuit diving	34 ± 8
Kitlitz's Murrelet	*Brachyramphus brevirostris*	KIMU	Pursuit diving	33 ± 1
Ancient Murrelet	*Synthliboramphus antiquum*	ANMU	Pursuit diving	57 ± 25

excellent seabird survey effort there from the mid-1970s to the 2010s in all seasons (Fig. 1, Table 1, see also Schneider and Hunt, 1982; Schneider et al., 1986). The study area extended along a bathymetry gradient in the southeast Bering Sea, closely following that used by Schneider et al. (1986) (Fig. 2). The bathymetry gradient is unusually smooth in this area, ranges from the shallow coastal waters of Bristol Bay (starting at 10 m), and gradually increases in depth to the edge of the continental shelf. We also included the continental slope and rise down to 3000 m depth (Fig. 2a). These characteristics permitted us to work with a study area in which the isobaths were approximately perpendicular to the long axis of the study area, thereby allowing an examination of the effects of bathymetry and the associated hydrographic domains on seabird distribution. We assumed that, within our study area, this ecosystem is largely homogeneous along isobaths, and that the main ecological gradient is related to depth (see Schneider et al., 1988). We therefore based our analysis on bathymetry and regarded multiple samples along an isobath as replicates. To minimize influences from the foraging activities of breeding seabirds, we constrained the area on its north side to stay approximately 50 km from the Pribilof Canyon, a deep indentation into the shelf and 100 km from the Pribilof Islands, where over a million seabirds breed (Hunt et al., 1981a, see also Jahncke et al., 2008). We constrained the study are on the south to stay 50 km north of the Alaska Peninsula and an area locally known as the "Slime Banks" where waters from Unimak Pass, Bering Canyon and the shelf mix.

2.2. Species selection

We included all species of seabirds recorded in the study area, regardless of rarity, with the following exceptions. As did Schneider et al. (1986) and Schneider and Shuntov (1993), we excluded from our selection of seabird species all species of loons, grebes and ducks, as they were all migrants and rarely, if ever, foraged in the pelagic waters that we studied. Likewise, with the exception of phalaropes, we excluded all shorebirds and songbirds encountered, again because they were passage migrants that were not foraging in the marine environment.

2.3. Data sources and observation methods

We used data from the North Pacific Pelagic Seabird Database (NPPSD, Drew and Piatt, 2005). We excluded aerial surveys contained within the NPPSD. The sampling unit that we used, a transect segment, was a strip survey 300 m wide and about 3 km long (about 1 km^2) within which the numbers, behavior, and

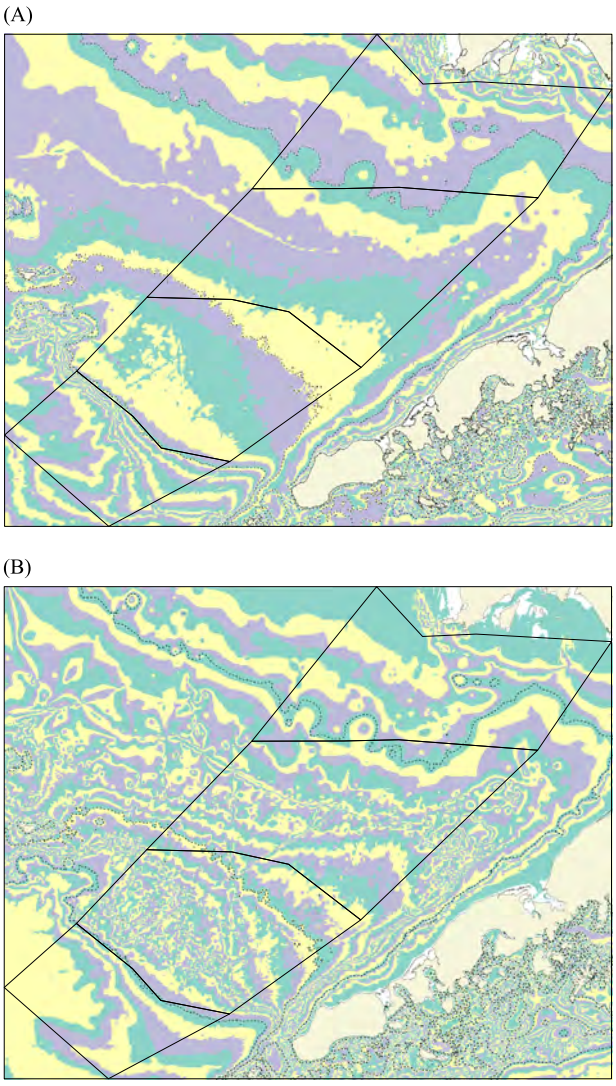

Fig. 2. Maps of the bathymetry bands used for the multivariate tree analyses of seabird species assemblage distribution. (A) The width of the bathymetry bands used for the cross-shelf distribution of individual species was determined such that bathymetry bands would be evenly spaced on a log-scale and the bounding isobaths would each be 1.15 times deeper than the previous respective isobath. (B) Bathymetry bands used for the species assemblage analysis were chosen so that all bands had an equal number of transect segments. The map shown is for summer (June 15–August 31). Outlines of boxes (solid black lines) indicate the Inner Shelf Domain, Middle Shelf Domain, Outer Shelf Domain and Shelf Slope Domain as used in Schneider and Hunt (1982) and Schneider et al. (1986). In both maps, a thin black line in the upper third of the map follows the 50 m contour.

species of seabirds present were recorded. The data set selected provided excellent spatial coverage within seasons (Fig. 1, Table 1), as well as strong coverage across most depth ranges within each season (Fig. 3). The weakest coverage was in winter (March 1–April 14), particularly in the Inner Shelf Domain with only 70 km^2 of effort (equivalent to about 70 transect segments, Table 1). However, there was a core of survey effort along the main study axis of the PROBES program, which conducted a full cross-shelf oceanographic survey at regular intervals from early March through mid-June. Survey efforts in the 1990s and 2000s also frequently covered all or part of this line. We did not attempt to analyze seabird distributions between October 16 and March 1, as data during that period were extremely sparse.

Birds were counted on standard 300 m strip transects. All surveys counted birds on the water continuously, but counting of flying birds used two approaches. Recent surveys, since 2007, have used the

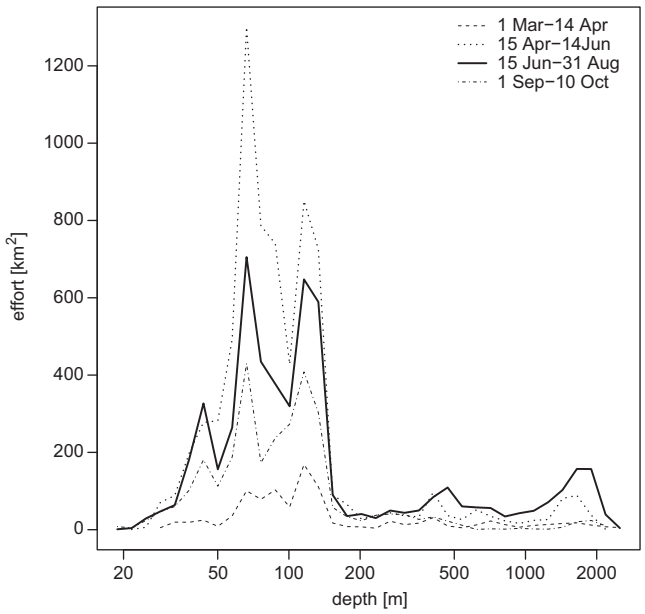

Fig. 3. Distribution of survey effort (km^2) by season and depth

snapshot method, in which observers, at set intervals that depend on ship speed, make an instantaneous scan or snapshot to count flying birds (Tasker et al., 1984; Gould and Forsell, 1989), thereby addressing the issue of biases from the motion of flying birds relative to the ship. The snapshot is a simple method for minimizing over estimation of flying birds and allows calculation of densities (birds km^{-2}) without further manipulation of the data. Many Bering Sea seabird surveys pre-2007 counted flying birds continuously, which leads to an inflated density estimate, if not corrected. Thus, a correction factor was required to make the pre- and post-2007 data comparable. For surveys in which all flying birds were counted, we corrected for flux as described in Renner et al. (in press) and listed in Appendix 1. We applied a correction factor that accounted for the bird's speed of flight (van Franeker, 1994; Spear and Ainley, 1997). We merged density data from the NPPSD from the two different methods applied to flying birds.

Known biases remain. Vessel attraction and avoidance can be a significant issue (Borberg et al., 2005), but should not have changed over time or between surveys. Birds attracted to the ship were noted on first observation but otherwise ignored. We also made no correction for detectability, causing estimates of density to be lower than the true density, especially for the smaller, less conspicuous species (Spear et al., 2004). However, we have no reason to believe that these biases changed over time or across our study area.

2.4. Data analysis

2.4.1. Unidentified birds

Birds identified only to higher taxonomic levels were prorated into their component species. If an unidentified bird could belong to species A, B, or C, we modeled the relative proportion of species A within the sum of identified individuals of species A, B, C with a GAM as a smooth function of bathymetry, month and year using a binomial error distribution with a logistic link-function and no interactions, thereby controlling for differences in species' proportions that might be affected by these variables. The level of smoothing was determined through generalized cross-validation (Wood, 2008). Prorating was applied sequentially, first to the smallest groups of unidentified species and then to more inclusive groups, as detailed in Appendix 2. We aggregated short-tailed and sooty shearwaters

sighting records into "unidentified dark shearwater (UNSH)" because reliable criteria for field identification of birds at a distance were not available until recently. We assumed that the vast majority of these birds in our study area were short-tailed shearwaters, based on distribution patterns of the two shearwater species and collections made over the years of study (Hunt, unpublished data).

2.4.2. Treatment of extreme values

To avoid having a small number of extreme observations unduly affect the analysis, we applied the following procedure to deal with outliers. To be considered an extreme value, a record needed to satisfy two conditions: first, over 1000 individuals of that particular species had to be observed and second, the observation had to be over ten standard deviations above the mean for that particular species. Extreme values were not removed, but rather their value was set to the maximal value observed within the remaining records of that species. This procedure affected 1 transect segment with fork-tailed storm-petrels, 14 with glaucous-winged gulls, 2 with black-legged kittiwakes, 27 with red-legged kittiwakes, 8 with common murres, 1 with thick-billed murres, 32 with parakeet auklets, and 33 with ancient murrelets out of a total of 16,552 transect segments in the entire data set.

2.4.3. Definition of seasons

We used 14 years of depth-temperature profiles collected at mooring 2 (located in the Middle Shelf Domain at 56. 9°N, 164. 1°W and 70 m water depth) to define four seasons: winter, March 1–April 14, when the water column was always mixed; spring, April 15–June 14, a transition period with some years showing stratification and other years showing a mixed water column; summer, June 15–August 31, when the water column is always stratified; and fall, September 1–October 15, when, in some years the water column of the middle shelf is still stratified, whereas in other years the stratification is in the process of being broken down by fall storms. We disregarded data outside of these dates.

2.4.4. Bathymetry bands

Bird species' assemblage data were collected in small, 1 km^2 transect segments. To improve the signal to noise ratio of the species assemblage data, we aggregated these small transect segments into groups of transect segments that were from a similar geographic area. Because the study area was selected to be homogeneous along isobaths, we aggregated seabird data over intervals of bathymetry. The bathymetry data were extracted from Seth Danielson's Alaska Region Digital Elevation Model (http://mather.sfos.uaf.edu/~seth/bathy/ accessed January 30, 2013).

From northeast to southwest, the ocean floor is gently down-sloping over much of the study area, but then drops rapidly at the continental slope (Fig. 2a). We considered two factors when defining the bathymetry bands within which to aggregate transect bins. The bathymetry bands should reflect natural, biologically justified intervals, and each band should contain a somewhat similar sample size. This created a trade-off between sufficient samples within each bathymetry band and spatial resolution. A logarithmic division of bathymetry was chosen, rather than linear intervals, because, with the inclusion of the shelf break, there were areas with rapid change in bathymetry as well as areas with very gradual change in bathymetry over the shelf as a whole. Sampling effort, however, was quite uneven when using these divisions (Fig. 3). Therefore, instead of applying one set of bathymetry bands to our entire analysis, we tailored the bathymetry bands to have the most appropriate divisions for each analysis (See Sections 2.4.5 and 2.4.6).

2.4.5. Cross-shelf distributions of individual species

To illustrate the cross-shelf distribution of individual seabird species within the study area in each of these four seasons, we defined bathymetry bands to be evenly spaced on a log-scale so that the bounding isobaths would each be 1.15 times deeper than the previous respective isobath (Fig. 2A). This method illustrated the often spiky nature of the distributions of individual species, as well as where the center of distributions of the species were located. We also plotted the cumulative frequency distributions of relative abundance of each species within seasons. This method showed clearly which species tended to have most of their population inshore or offshore and provided a means of assessing where they had sharp increases in their numbers and whether the locations of these increases were stable across seasons.

2.4.6. Multivariate tree analysis of seabird species assemblage distribution

To examine whether the seabirds recognized the same oceanographic domains as those delineated in terms of their hydrographic structure, we used the distributions of clusters of species, based on their observed depth distributions, to develop seabird-defined domains. This can be done in at least three different ways: (1) the use of hierarchical clustering, which joins nearest neighbors and thereby works from the leaves to the root of a clustering tree (2) the use of *k*-means clustering, which finds k groups that minimize the within-group variance and (3) because the study area is set-up along a 1-dimensional gradient (bathymetry), the use of multivariate regression tree analysis to find clusters of bathymetry bands (see Fig. 2B for the bands used) from the root to the leaves. We used the third approach because it has two advantages: it is intuitive to go from larger to smaller divisions and it is spatially constrained. The constraint has the effect that sites within one cluster are always spatially adjacent, eliminating the problem of outliers from noisy data. To visualize the spatial arrangement of the seabird species assemblage, we projected the seabird-derived clusters of bathymetry bands back onto the map.

To develop the multivariate tree analysis of seabird species assemblage distribution with respect to depth, we divided the shelf into bands of bathymetry such that, within each of the seasons analyzed, each band had an equal number of transects. This approach was necessary as, in preliminary analysis, even-width depth bands resulted in some bands with very small sample sizes. Having equal sample sizes in each band resulted in each band having an equal weighting in the analysis. However, it also resulted in bands of somewhat unequal width as a result of variable survey effort. The irregularity of the bands also reflects the small-scale variations in the bathymetry (Fig. 2, B).

3. Results

The cross-shelf distribution of most seabird species was "spiky", reflecting not only hotspots where seabirds might aggregate to forage on a regular basis, but also the occurrence of occasional large aggregations of foraging birds at ephemeral concentrations of prey (Fig. 4). Plots of cumulative frequency distributions showed that there were three general patterns of bird species' distributions: species that were concentrated over waters less than or equal to 50 m, those that were found primarily in waters deeper than 200 m, and those that were fairly uniformly distributed across all depths surveyed (Fig. 5, Table 2). Four of the commonest species with mean summer distributions < 50 m depth were pursuit divers, and of the 5 species with mean summer distributions > 200 m, 4 were surface seizing seabirds (Fig. 5, Table 2). Examples of species preferring the shallowest waters included common murre, marbled murrelet, ancient murrelet, and horned puffin, whereas species that

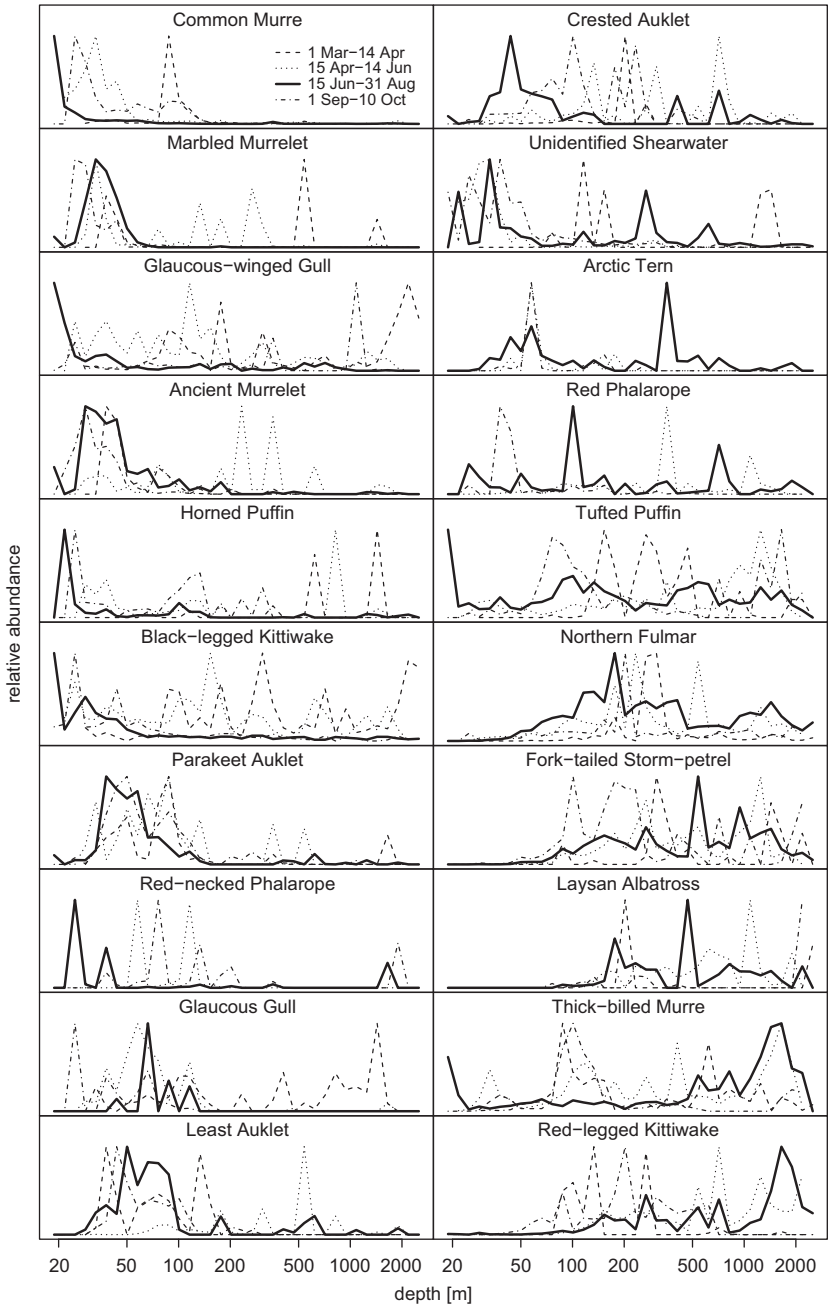

Fig. 4. Cross-shelf distribution of the 20 most abundant seabird species, standardized within species and season to the highest count for that species. Thus, the counts reflect variability in cross-shelf distribution for a given species and within a given season.

preferred deeper waters included red-legged kittiwake, Laysan albatross, thick-billed murre, and fork-tailed storm-petrel. In contrast, species such as tufted puffin and northern fulmar showed little evidence for a preferred depth range within the study area in summer.

Most species that had their center of distribution in shallow water shifted their distributions to deeper water in winter and, in many cases, in spring as well (e.g., common murre, marbled murrelet, glaucous-winged gull, ancient murrelet, horned puffin and black-legged kittiwake) (Fig. 5). In fall, some inshore species shifted their distributions farther inshore (e.g., marbled murrelet, ancient murrelet), whereas others shifted offshore in fall (common murre, glaucous-winged gull, horned puffin). Most offshore species shifted their distributions to shallower water in fall (e.g., red-legged kittiwake, thick-billed murre, fork-tailed storm-petrel), and in a number of cases were found over shallower waters in late winter (e.g., red-legged kittiwake, thick-billed murre, Laysan albatross) (Fig. 5). In winter, many of the migratory species were absent (e.g., red phalarope, red-necked phalarope, Arctic tern), though shearwaters were present in all seasons.

In all seasons but spring, seabirds that foraged by surface seizing were found over deeper water than seabirds that foraged by pursuit diving (Table 3). An interesting exception was the thick-billed murre, a pursuit-diving species that had its highest numbers over the shelf-slope in summer (Fig. 5). Most surface seizing seabirds were found at their shallowest in spring and shifted their distribution seaward in summer and back toward shallower water in fall. In contrast, pursuit divers were found at their deepest in spring, and moved toward shallower waters in summer and in fall.

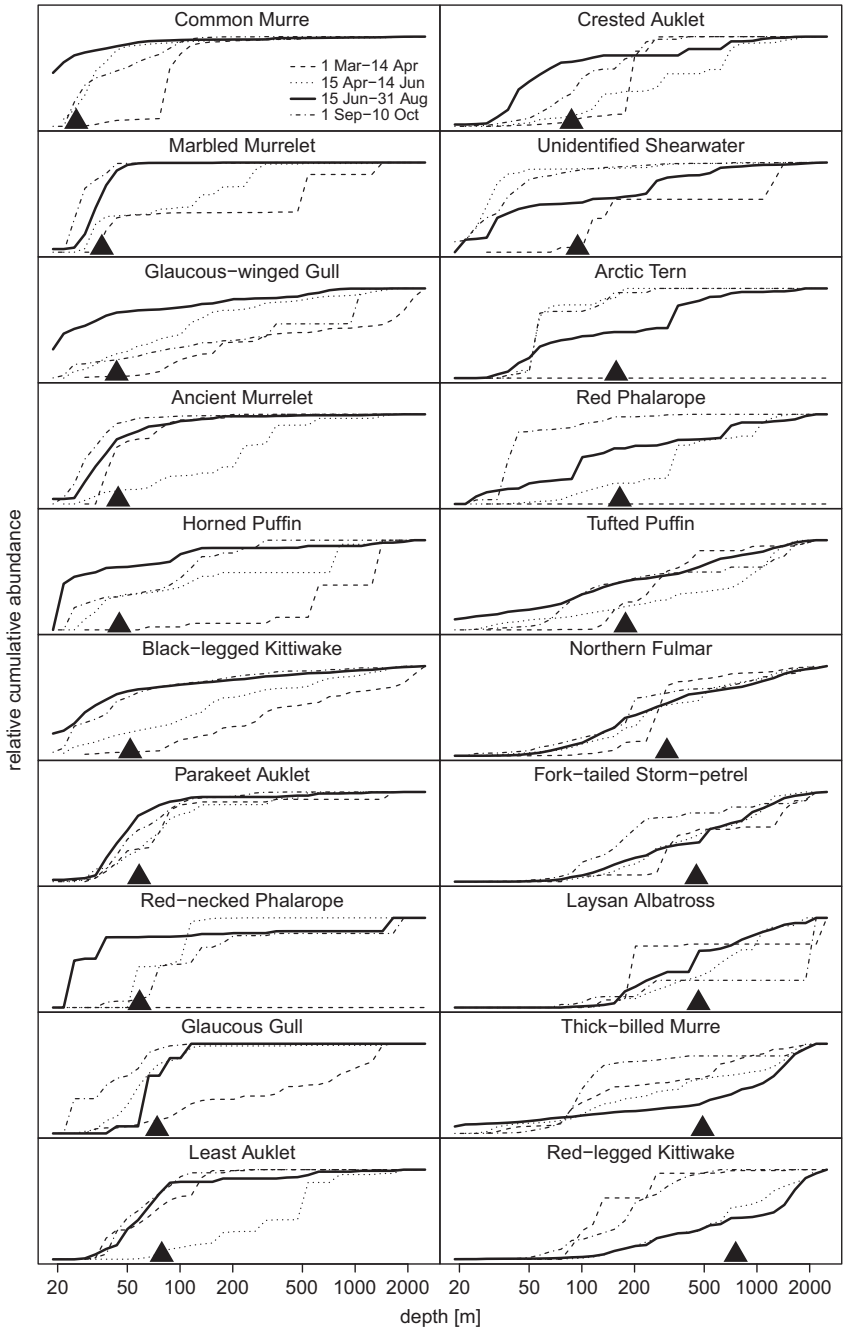

Fig. 5. Cumulative frequency distribution of the 20 most abundant seabird species, standardized within species and season to the total for that species. Thus, the cumulative distributions reflect variability in cross-shelf distribution for a given species and within a given season. Triangle represents the mean depth of the species' distribution during summer, solid line, 15 June–31 August.

Table 3
Mean of depths (m) used by surface-seizing and pursuit diving seabirds by season.

Foraging type	Winter	Spring	Summer	Fall
Surface seizing species	464 ± 71	341 ± 75	545 ± 84	454 ± 97
Pursuit diving species	257 ± 61	418 ± 110	213 ± 69	131 ± 34

We clustered depth bands according to their seabird faunas using a multivariate tree analysis and found that the patterns of clustering differed considerably among seasons (Fig. 6). In summer (June 15–August 31) and fall (September 1–October 15), the strongest differentiation (first node in the tree) was between the seabird-defined middle shelf and the seabird-defined inner shelf (depth bands < 61 m (summer) or < 57 m (fall) versus depth bands at greater depths). Summer and fall differed in that in fall, the next most important node was at 126 m whereas in summer, differences between the Outer Shelf Domain and the Shelf-Slope Domains and between two regions of the Inner Shelf Domain were about equally strong. In spring, the most important division was at 99 m depth. Secondarily, in spring (April 15–June 14) there was a division at 38 m depth and another equally strong division at 200 m depth. In winter (March 1–April 14) the most important difference was at 88 m depth, with a secondary division at 112 m depth. In winter, there was no evidence of a division within waters < 88 m deep.

When mapped, the clusters identified in the multivariate tree analysis of depth intervals with similar seabird faunas closely resembled the hydrographic domains of the southeastern Bering

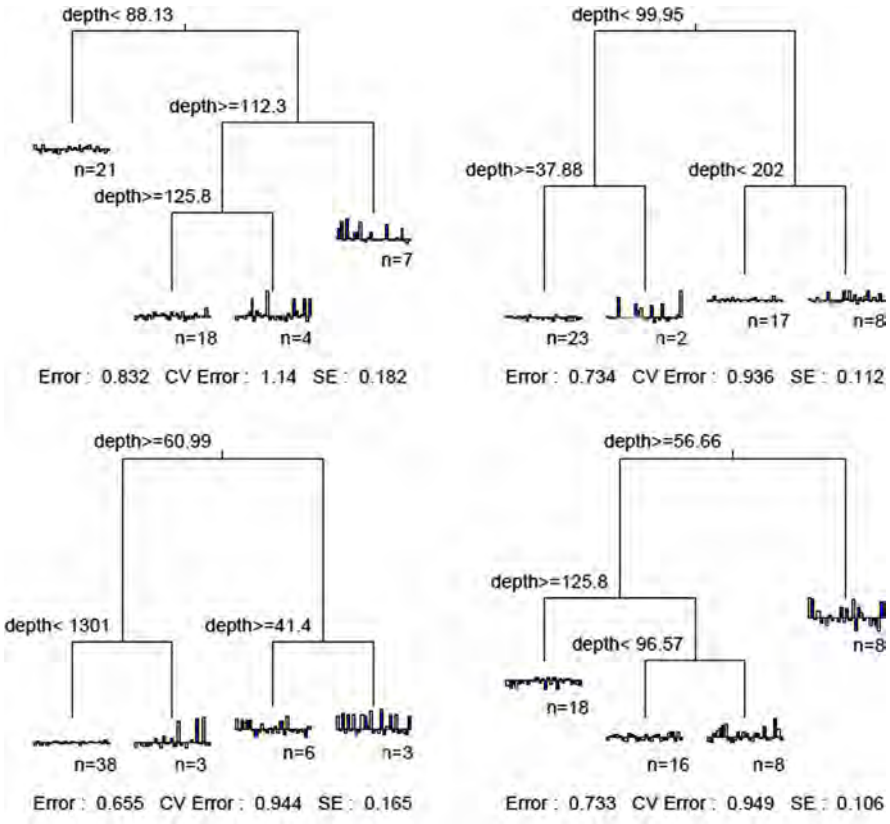

Fig. 6. Results of multivariate tree analysis of the clustering of depth bands based on seabird species composition within the depth bands, by season. Results were constrained to four clusters in each of four seasons: (A): March 1 to April 14; (B): April 15 to June 14; (C): June 15 to August 31; (D): September 1 to October 15. At each node, we labeled the rule for the left branch. n=the number of depth bands in the cluster.

Sea (Fig. 7). In all but winter, there was a differentiation between the Inner Shelf Domain and the Middle Shelf Domain between 49 and 59 m depth, although in both spring and summer there was also a seabird-defined domain at depths shallower than 38 m (spring) and 41 m (fall). In spring, the seabird-defined domains were remarkably close to the depth contours used to define the boundaries between the Middle Shelf Domain and the Outer Shelf Domain and the Outer Shelf Domain and the Shelf-slope Domain. However, as the seasons progressed, the seabird-defined Outer Shelf Domain expanded seaward to encompass the entire Shelf-Slope Domain. Analysis of multivariate tree cross-validated error over seasons showed that in winter the seabird communities did not fit well to the model of four bird-defined domains (Fig. 8). Model fit improved as stratification developed in spring and summer.

No strong patterns were evident in a multidimensional clustering of seabird species for most seasons and domains (Fig. 9). In spring there was a grouping of species that preferred the off-shelf, deep waters (Fig. 9B, right side), as well as a group of species that occurred primarily nearshore (Fig. 9B, upper left). In summer, there were two fairly distinct groups of species, an off-shelf group in the lower left of Fig. 9C, and an inshore group on the right side of Fig. 9C. Finally, in the fall, there was a group of inshore species in the lower right of Fig. 9D and an off-shelf group in the upper left of Fig. 9D. The species groups that occupied the Middle and Outer Shelf Domains were generally poorly differentiated, suggesting that these species groupings were not distinct.

4. Discussion

The data set on which we relied for this analysis is not only immense (16,552 transect segments), it is also heterogeneous. Methods for recording flying birds have changed over the course of the 35 year time period of the study, and seasonal and spatial coverage varied greatly across the shelf by season. We have addressed the first issue by using the methods of van Franeker (1994) and Spear and Ainley (1997) to correct for the known systematic bias introduced by the continuous count method (see also Renner et al., in press). In the present study, with these corrections, the change in methods of counting flying birds is unlikely to have influenced our results.

The lack of systematic surveys and resulting uneven spatial coverage of the shelf were addressed in three ways. First, we restricted the study area to that portion of the southeastern Bering Sea shelf that had the most consistent and thorough coverage over the study period. Second, rather than using raw numbers from the surveys to construct average distributions, we used calculations of density for each transect segment, and then averaged these. Third, in the multivariate tree analysis, we varied the width of the depth bands used such that all bands had the same number of transect segments within them, thereby giving each transect segment equal weight in the analysis.

In this study, we show that the pattern of use of the southeastern Bering Sea shelf by seabirds was variable among seasons, and that in seven of twelve instances the seabird-defined domains reflected the cross-shelf domains as defined by hydrography (Fig. 7). The strongest differentiation by seabirds in winter and spring was between the outer edge of the Middle Shelf Domain and the deeper waters of the outer shelf, and in summer and fall, between the Middle Shelf Domain and the Inner Shelf Domain (Fig. 7). In winter, there was a lack of seabird differentiation of the Inner Shelf and Middle Shelf Domains, possibly because the middle shelf is well mixed in winter, although our small sample size in winter reduces confidence in this result. In winter, there remain differences in the chemistry of the Inner Shelf and Middle Shelf Domains (Coachman, 1986), although there is no structural front present (Kinder and Schumacher, 1981; Coachman, 1986). There was

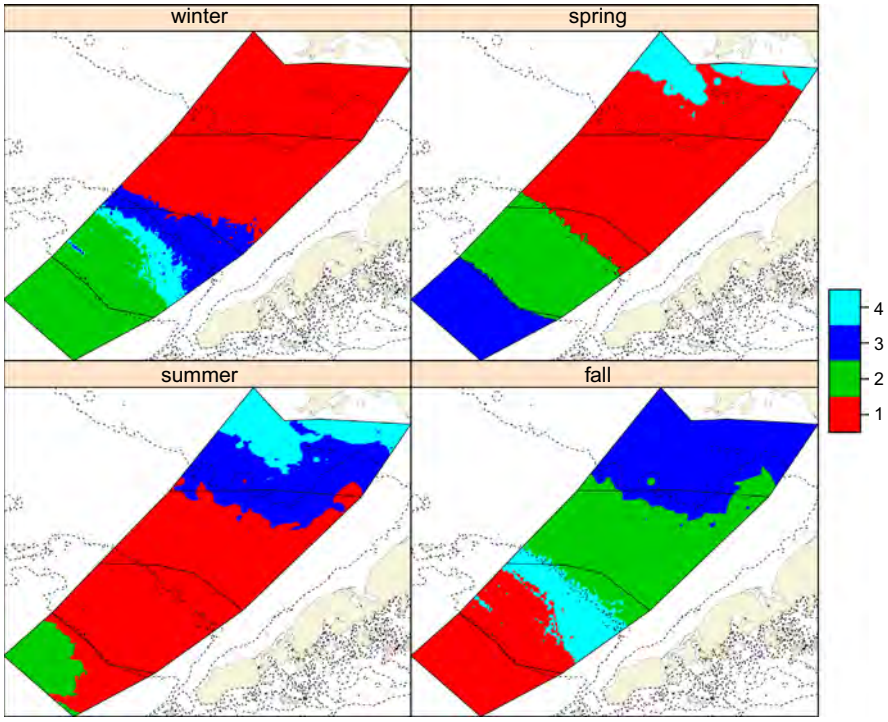

Fig. 7. Maps of the locations of the clusters, defined in Fig. 6, by season. Colors indicate the order in which the nodes of the tree were determined. Outlines of boxes (solid black lines) indicate the Inner Shelf Domain, Middle Shelf Domain, Outer Shelf Domain and Shelf Slope Domain as used in Schneider and Hunt (1982) and Schneider et al. (1986). Note, birds do not recognize inner/middle shelf separation in winter; in all seasons, the slope was differentiated from outer shelf and outer shelf was differentiated from middle shelf. Seasons are: Winter—March 1 to April 14; Spring—April 15 to June 14; Summer—June 15 to August 31; Fall – September 1 to October 15. The fine dotted lines represent the 50, 100 and 200 m isobaths.

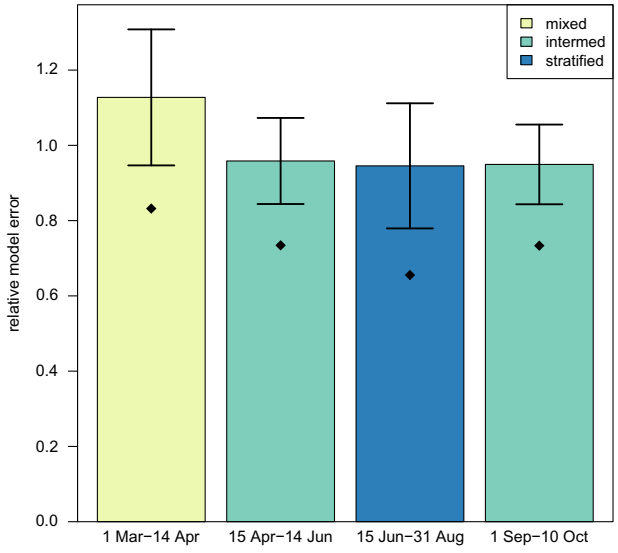

Fig. 8. Estimates of relative residual error using cross validation with standard errors of the CV indicated by the black lines. Simple errors are indicated by the diamonds, being equivalent to $1-r^2$. Color shading indicates the degree of stratification in each season.

a strong alignment of the seabird-defined boundaries between the Outer Shelf Domain and the Middle Shelf Domain and the Shelf-Slope Domain in spring and between the seabird-defined Outer Shelf Domain and the Middle Shelf Domain in fall.

Instances where the seabird-defined domains did not correspond with known hydrological differences are intriguing as they may indicate spatial differences in the shelf ecosystem that heretofore have not been identified (Fig. 7). In both spring and summer, there was a shallow, inshore seabird-defined region in waters < 38 m (spring) and < 41 m (summer). In neither season did seabirds strongly differentiate this area from the deeper portions of the Inner Shelf Domain, and it may represent the presence of foragers constrained by distance from their breeding sites. For example, common murres were concentrated in these shallow waters in both spring and summer, as were Arctic terns, both of which nest on the nearby capes (Fig. 5). However, for many other species, their concentration in these shallow waters was found in only one of these seasons, suggesting that there was a factor other than distance-to-breeding-site at play. For instance, shearwaters were highly concentrated in these shallow waters in spring and fall (Fig. 5). In spring, these Southern Hemisphere-breeding birds were observed foraging inshore on euphausiids and sand lance (*Ammodytes hexapterus*) and in fall on euphausiids and, somewhat farther offshore, on age-0 walleye pollock (*Theragra chalcogramma*) associated with elevated levels of production near the inner front (Hunt et al., 2002, Jahncke et al., 2005b; Kachel et al., 2002).

Another unexpected result was the lack of seabird differentiation of the outer shelf domain from the shelf-slope domain in summer, and even more so in fall and winter, even though there is believed to be strong differentiation between these two hydrographic domains throughout the year (Coachman, 1986). These seabird-derived amalgamations of the Shelf-slope Domain and the Outer Shelf Domain do not correspond with any of the traditionally-defined hydrographic domains. They may reflect the on-shelf extent of the influence of basin waters in fall and winter. Although the data set for spring was robust, thus lending credence to the results for spring, the small sample size in winter requires caution in the interpretation of winter results.

The differentiation of the Inner Shelf Domain from the Middle Shelf Domain was the second strongest seabird-derived division in spring (at 38 m), and the strongest division in both summer (at 60 m) and fall (at 57 m). We are reluctant to ascribe much significance to the apparent seasonal differences in the cut-off depths for the bird-defined Inner Shelf Domain, as the depth at which the Inner Front is

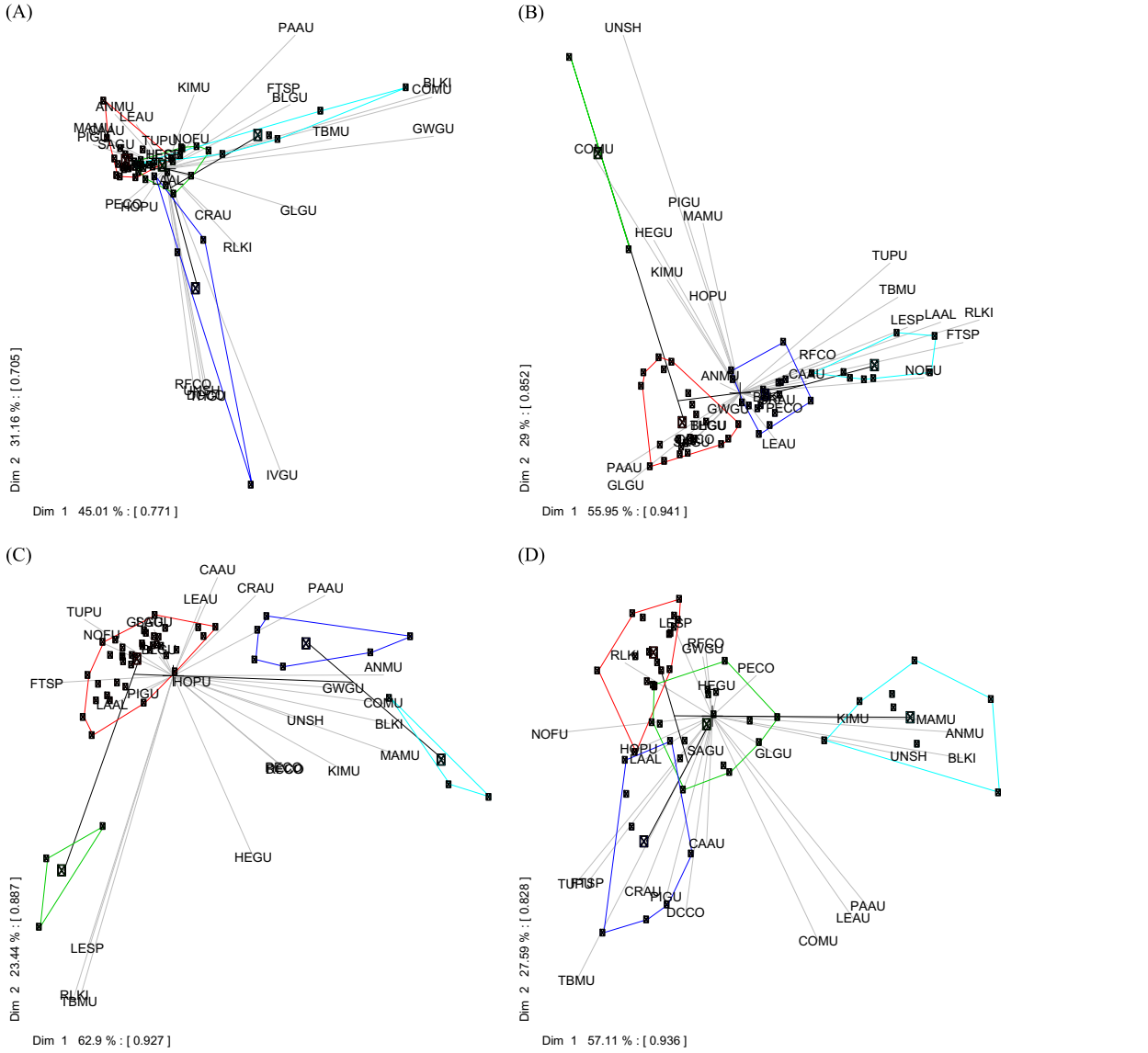

Fig. 9. Multidimensional clustering of species within seasons. Seasons were: (A): March 1 to April 14; (B): April 15 to June 14; (C): June 15 to August 31; (D): September 1 to October 15. In spring, a group of species associated with deep water can be seen in the right hand side of the panel (LAAL, NOFU, LESP, FTSP, RLKI, TBMU, TUPU). In summer, there is a clear cluster of species associated with deep water (lower left grouping, LESP, RLKI, TBMU), and another associated with the Inner Shelf Domain (grouping on right side of panel, UNSH, GWGU, BLKI, COMU, ANMU, MAMU). A group associated with the Inner Shelf Domain is also apparent in fall in the lower right side of the panel (UNSH, BLKI, ANMU, KIMU, MAMU). Species codes are provided in Table 2; colors, indicating clustering nodes, match those in Fig. 7.

located is known to move about considerably as a function of stratification of the Middle Shelf Domain, wind mixing and the phase of the lunar tide cycle (Kachel et al., 2002; Jahncke et al., 2005b). These interacting factors all operate at different time scales, from that of seasonal heating, to fortnightly tide cycles to episodic storm events, and the location of the Inner Front responds accordingly.

Although the multivariate tree analysis resulted in assignments of bird-determined domains similar to those described for spring, summer and fall by oceanographers, there remains a great deal of unexplained variance in the seabird distributions. Much of this may represent the chance encounters of different species in the 1-km^2 transect segments into which we aggregated our raw data. It would be of interest to investigate the dependence of our results on the spatial scale of aggregation of the data. This is similar to the scale-dependency of the relationship of seabird abundance at sea and the abundance of their prey (e.g., Hunt et al., 1992).

Overall, our data support the hypothesis that pursuit-diving seabirds prefer to forage in shallow water and surface-seizing seabirds prefer to forage over deep water. Of the 27 species that utilize waters with mean depths > 200 m, 19 were surface-seizing species and 8 were subsurface foragers (Table 2). Of the subsurface foragers over deep water, two species, pigeon guillemot and whiskered auklet were rare stragglers, and were in a habitat that was atypical for the species. In contrast, of the 9 seabird species centered in waters with mean depth distributions of < 100 m, 6 were pursuit-diving species. Of the 3 surface-seizing species in shallow water, two, mew gull and Thayer's gull, were relatively rare migrants.

One notable exception to the above pattern was the high abundance of thick-billed murres in the Shelf-Slope Domain. Examination of murre data by decade (Hunt et al., unpublished) suggests that the presence of a high percentage of thick-billed murres over deep water is something unique to years since 2000. It seems unlikely that murres over the outer shelf and the shelf-slope would have been overlooked for three decades of observations if they had been common there. A possible explanation is that there has been a shift in the foraging grounds of thick-billed murres such that they now forage over deeper water than was formerly the case (Jahncke et al., 2008; Benoit-Bird et al., 2013).

A number of hypotheses have been suggested to account for the preference of pursuit-diving seabirds to forage in shallow water and surface-seizing seabirds to prefer deeper waters (Schneider, 1997). These included: (1) distance to colony, (2) differences in primary productivity, and (3) "topographic anchoring" such that differences in bottom contours (or depth) result in alterations in near-surface flow fields, thereby affecting the concentration of prey in near-surface waters. Examination of our data suggests instances in which each of these hypotheses may play a role.

One hypothesis for explaining seabird preferences for shallow or deep water reviewed by Schneider (1997) is that seabirds partition food resources around their colonies by foraging at different distances from the colony (see also Cody, 1973). Bédard (1976) showed that the competition argument was unlikely to be true because one does not find a series of species-specific rings at different distances from a colony. It is also possible that pursuit-divers, with heavier wing loading, are forced by energetic constraints to forage closer to their colonies than surface-seizing seabirds, which generally have much lighter wing loading (Wynne-Edwards, 1935; Stone et al., 1995). As Schneider (1997) pointed out, species do forage within characteristic ranges from colonies (see also Pearson, 1968; Weimerskirch et al., 1988), and some of these differences undoubtedly relate to the costs of flight. In the southeastern Bering Sea, Sigler et al. (2012) concluded that thick-billed murres, with their greater travel costs, were more restrained by colony location and thereby restricted in their response to persistent prey concentrations than were the wide-ranging black-legged kittiwakes.

In our study, all of the pursuit-divers that occurred at an average depth of <100 m over the course of the study were species that nested on the mainland of Alaska adjacent to our study area. Likewise, one of the three species of surface-seizing seabirds (Aleutian tern) with a preference for shallow water nested on the nearby mainland. Other species (e.g., black-legged kittiwake, common murre, and tufted puffin) with an overall preference for moderate water depths are known to have large breeding populations on nearby Cape Peirce and Cape Newenham (USFWS, 2004). Thus, the high relative abundances of these species in the inshore waters in spring and summer (Fig. 4) may well be the result of foraging birds dispersing from their breeding colonies. Significantly, between spring and summer, the guild of pursuit-diving seabirds moved to shallower waters (Table 3). Additionally, several species (e.g., black-legged kittiwake, glaucous gull, Arctic tern and ancient murrelet) shifted their distributions inshore in fall, which presumably was in response to the availability of prey there, as at that time they were no longer restricted in foraging range by a need to return to their colonies. Thus, although proximity to their colonies likely was a factor in their choice of water depth for foraging, their choice of breeding site was also undoubtedly affected by the nearby availability of abundant prey (Schneider, 1991; Springer et al., 1996a,1996b; Hunt et al., 1999).

The use of inshore waters by pursuit-diving shearwaters was not influenced by colony location, as they breed during the austral summer in the Southern Hemisphere. In early spring, shearwaters foraged very close inshore on euphausiids and sand lance, and moved offshore as the spring progressed and the euphausiids became scarce in inshore waters (Hunt et al., 2002, Jahncke et al., 2005b). The shearwaters, when foraging on euphausiids, utilized dense patches which they harvested by filter-feeding (Lovvorn et al., 2001). Many of these patches were associated with the Inner Front (Jahncke et al., 2005b). Thus, the shearwaters provide an excellent example of a species whose foraging habitat preferences are strongly affected by topographic anchoring (Schneider, 1997). This may be a general pattern for the shearwaters, as in most cases where large foraging flocks were feeding on euphausiids, there were nearby fronts that enhanced local primary production, or shallows where mixing was enhanced (Hunt et al., 1996; Ladd et al., 2005; Jahncke et al., 2005a; Vlietstra et al., 2005).

Although the location of subsurface foraging by pursuit-divers may have been influenced by prey that were aggregated near the Inner Front, or in shallow, well mixed waters with elevated levels of primary production, the overall shelf-wide preference of pursuit divers for shallow water cannot be explained on the basis of differences in primary production between inshore and off shore waters. There is now an extensive body of literature that demonstrates that the waters of the Outer Shelf Domain and the Shelf-Slope Domain are the most productive in the eastern Bering Sea, with the highest levels of primary production (Springer et al., 1996a; Sambrotto et al., 2008; Brown et al., 2011) and the greatest standing stocks of large crustacean zooplankton (Cooney and Coyle, 1982; Smith and Vidal, 1986; Vidal and Smith, 1986; Coyle, 2005; Smith, 1991; Pinchuk and Coyle, 2008).

Between spring and summer, the guild of surface-seizing seabirds moved offshore (Table 3). The principal offshore subsurface-forager, the thick billed murre, moved farther offshore, from the Outer Shelf Domain to the deep waters of the Aleutian Basin in summer, contrary to what would have been expected if its foraging were dependent on topographic anchoring. The thick-billed murre eats small fish, squid, and large crustacean zooplankton (Sinclair et al., 2008), and these may be more reliably encountered in the well-stratified waters of the basin (Benoit-Bird et al., in review). To our knowledge, there is no seasonal time series of forage fish, squid, or large crustacean zooplankton that could be used to test this hypothesis of seasonally varying prey availability over the outer shelf and basin. To the extent that seabirds have the option of foraging over the "green belt" (Springer et al., 1996a), the high levels of productivity there, particularly in summer when productivity of Middle Shelf Domain waters declines due to nutrient exhaustion in the upper mixed layer, would make these shelf-edge waters most attractive.

In summary, our study has shown that seabird-defined domains are similar to the shelf domains defined by hydrographers in spring, summer and fall. In winter, the seabirds did not discriminate between the Inner Shelf Domain and the Middle Shelf domain, as would be expected from the hydrography, as in winter both the region of the Middle Shelf Domain and the Inner Shelf Domain are well mixed throughout the water column. Moreover, we found seasonal variation in the amount of variance explained by the seabird-defined domains, with explained variance poorest in winter when the hydrographic domains are least strongly defined. To our knowledge, this is the first instance in which the distribution and abundance of seabirds have been used to define the ecological partitioning of a marine shelf ecosystem. Since the seabird-defined domains are based on the bathymetry over which we encountered the birds, we explored the relationship between foraging types – surface-seizing and sub-surface pursuit-foragers, water depth and productivity. We found that the preponderance of pursuit divers in shallow water could not be explained by higher primary production there, though topographic anchoring of the Inner Front did provide a region of enhanced production and predictable concentrations of forage fish and euphausiids, and was likely the result of closeness of colonies. Our study provides strong support for the topographic anchoring hypothesis of Schneider (1997), support for a proximity to colony effect, and some support for the productivity hypothesis, in that the highly productive shelf-slope system was important for thick-billed murres and some other pursuit divers. The fact that the boundaries of the seabird-defined domains shifted seasonally suggests that the seabirds are more attuned to variations in the hydrographic structure or water masses present than they are to depth, per se. We look forward to further work with this data set examining inter-annual to decadal-scale changes in seabird use of the southeastern shelf and north-south variability in seabird use along the shelf from the Alaska Peninsula to Bering Strait.

Acknowledgments

We thank John Piatt for his foresight in establishing the North Pacific Pelagic Seabird Database, Gary Drew for his many years of effort in editing and organizing the database, and Elizabeth Labunski for coordinating recent surveys and her work on the database. We thank the legions of observers who have contributed the data on which we have relied. Without the hard work of these individuals, this study would not have been possible. Seth Danielson and Edward Cokelet pointed out that the bathymetry that we used originally was flawed for use in shallow water, and Seth provided us with access to the updated bathymetry that he has developed. We thank the three anonymous referees and David Ainley for their very helpful comments on the manuscript. GLH thanks the Office of Polar Programs at the National Science Foundation for the many years of support over which he gathered data, and for Grant ARC 0908262 that supported the analyses and writing of this paper. Kathy Kuletz was supported by the North Pacific Research Board (Projects 637 and B64) the Bureau of Ocean Energy Management (IA No. M10PG00050) and the U.S. Fish and Wildlife Service for the collection of pelagic seabird data since 2006. This is NPRB publication 439 and BEST/BSIERP publication 107.

Appendix

See Tables A1–A3.

Table A1
Conversion factors for each seabird species, using direct flying speeds from Pennycuick (1989) and travel speeds, including the zig-zag course from Spear and Ainley (1997).

Species	Spear speed (ms^{-1})	Conversion factor
ALTE	6.467184	2.471744
ANMU	11.33424	4.192677
ARTE	6.467184	2.471744
BFAL	8.133984	3.050330
BLKI	7.867296	2.959366
CAAU	10.70086	3.966513
COMU	12.33432	4.553430
CRAU	11.33424	4.192677
DCCO	10.16748	3.773632
FTSP	5.267088	2.067420
GLGU	7.600608	2.867131
GWGU	7.600608	2.867131
HEGU	7.600608	2.867131
HOPU	11.33424	4.192677
IVGU	6.867216	2.616855
KIMU	11.33424	4.192677
LAAL	8.133984	3.050330
LEAU	10.70086	3.966513
LESP	5.267088	2.067420
LTJA	8.300664	3.116016
MAMU	11.33424	4.192677
MOPE	6.967224	2.651604
NOFU	8.3340	3.122403
PAAU	10.70086	3.966513
PAJA	8.300664	3.116016
PECO	10.16748	3.773632
PIGU	12.33432	4.553430
POJA	8.300664	3.116016
PRCO	10.16748	3.773632
REPH	6.933888	2.628614
RFCO	10.16748	3.773632
RHAU	11.33424	4.192677
RLKI	7.867296	2.959366
ROGU	6.867216	2.616855
SAGU	6.867216	2.616855
SBGU	7.600608	2.867131
SOSH	8.233992	3.086300
STAL	8.133984	3.050330
STPE	6.200496	2.374994
STSH	8.233992	3.086300
TBMU	12.33432	4.553430
TUPU	11.33424	4.192677
UALB	8.133984	3.050330
UNAU	11.33424	4.192677
UNCO	10.16748	3.773632
UNGU	7.867296	2.959366
UNJA	8.300664	3.116016
UNKI	7.867296	2.959366
UNML	11.33424	4.192677
UNMU	12.33432	4.553430
UNPH	6.933888	2.628614
UNSH	8.233992	3.086300
UNSP	5.267088	2.067420
UNTE	6.467184	2.471744
UNTN	6.467184	2.471744
WHAU	10.70086	3.966513

Table A2
Unidentified species to which pro-ratings were applied.

Unidentified group	Taxonomic species included	Proportion of unidentified birds (%)
Unidentified storm-petrel – UNSP	LESP, FTSP	0.15
Unidentified petrel – UNPE	LESP, FTSP, MOPE	0.25
Unidentified procellariiform – UNPR	NOFU, UNSH	0.57
PRCO	PECO, RFCO	28.1
Unidentified cormorant – UNCO	DCCO, PECO, RFCO	69.6
Unidentified phalarope – UNPH	RNPH, REPH	17.0
Unidentified Jaeger – UNJA	LTJA, PAJA, POJA	27.7
Unidentified Kittiwake – UNKI	BLKI, RLKI	12.7
Unidentified Tern – UNTE	ARTE, ALTE	21.7
Unidentified Murre – UNMU	TBMU, COMU	58.5
Unidentified Guillemot – UNGI	PIGU, BLGU	1.77
Unidentified Puffin – UNPU	TUPU, HOPU	0.18
Unidentified Auklet – UNAU	PAAU, CRAU	19.3
Unidentified *Brachyrhamphus* Murrelet – BRMU	MAMU, KIMU	7.25
Unidentified Murrelet – UNML	ANMU, MAMU, KIMU	8.19
Unidentified small dark auk – USDA	CRAU, PAAU, CAAU, ANMU, MAMU, KIMU	14.7

Table A3
Densities (birds km^{-2}) of marine bird species by season, shelf wide, ordered from most abundant to least abundant.

Species code	1 Mar.–14 Apr.	15 Apr.–14 Jun.	15 Jun.–31 Aug.	1 Sep.–10 Oct.
UNSH	0.0046 ± 0.0025	6.8 ± 1.3	16 ± 2.8	7 ± 1.3
COMU	20 ± 6.7	0.74 ± 0.066	0.6 ± 0.039	0.76 ± 0.034
NOFU	2.1 ± 0.79	1.2 ± 0.064	4.4 ± 0.55	3.7 ± 0.66
BLKI	0.65 ± 0.063	0.51 ± 0.024	0.6 ± 0.04	2.9 ± 0.89
GWGU	2.5 ± 0.31	0.6 ± 0.065	0.047 ± 0.011	0.5 ± 0.066
FTSP	0.04 ± 0.013	0.31 ± 0.019	2.2 ± 0.17	1 ± 0.3
TBMU	1.3 ± 0.34	0.52 ± 0.039	0.64 ± 0.029	0.51 ± 0.033
TUPU	0.045 ± 0.0077	0.075 ± 0.0046	0.42 ± 0.015	0.73 ± 0.032
REPH	0 ± 0	0.073 ± 0.01	0.15 ± 0.057	0.42 ± 0.086
ANMU	2.9e − 05 ± 1.4e − 05	0.008 ± 0.0019	0.27 ± 0.024	0.34 ± 0.04
PAAU	0.18 ± 0.053	0.028 ± 0.0031	0.06 ± 0.0055	0.17 ± 0.016
LEAU	0.16 ± 0.05	0.049 ± 0.008	0.082 ± 0.011	0.12 ± 0.01
MAMU	0.0027 ± 0.00048	0.003 ± 0.00075	0.097 ± 0.0092	0.16 ± 0.022
RLKI	0.018 ± 0.01	0.038 ± 0.0041	0.095 ± 0.012	0.091 ± 0.012
GLGU	0.14 ± 0.016	0.066 ± 0.0056	0.0011 ± 0.00039	0.012 ± 0.002
CRAU	0.12 ± 0.028	0.025 ± 0.0078	0.02 ± 0.0035	0.048 ± 0.0058
IVGU	0.11 ± 0.026	0 ± 0	0 ± 0	0 ± 0
RNPH	0 ± 0	0.0012 ± 0.00072	0.0087 ± 0.0029	0.096 ± 0.043
HOPU	0.0077 ± 0.0028	0.02 ± 0.0022	0.024 ± 0.0023	0.045 ± 0.0056
ARTE	0 ± 0	0.0029 ± 0.0011	0.055 ± 0.0085	0.026 ± 0.005
CAAU	0.0027 ± 0.0016	0.00039 ± 0.00017	0.034 ± 0.0041	0.042 ± 0.0068
POJA	0 ± 0	0.01 ± 0.0015	0.024 ± 0.0022	0.026 ± 0.0031
LAAL	0.0072 ± 0.0025	0.014 ± 0.0014	0.0084 ± 0.0011	0.0038 ± 0.001
PECO	0.0042 ± 0.003	0.0038 ± 0.0011	0.00027 ± 0.00025	0.017 ± 0.0048
KIMU	3e − 17 ± 7.9e − 18	0.00039 ± 0.00026	0.0038 ± 0.0014	0.023 ± 0.0077
PAJA	0 ± 0	0.0015 ± 0.00038	0.0083 ± 0.0018	0.0071 ± 0.0016
SAGU	0.00033 ± 0.00033	0.00039 ± 2e − 04	0.0074 ± 0.0012	0.0081 ± 0.0016
BLGU	0.014 ± 0.014	0.00012 ± 0.00011	0.00029 ± 0.00029	0 ± 0
DCCO	0.013 ± 0.013	0.00071 ± 0.00055	2e − 05 ± 2e − 05	1.8e − 05 ± 1e − 05
RHAU	0 ± 0	2.7e − 05 ± 2.7e − 05	0 ± 0	0.011 ± 0.0022
HEGU	3e − 04 ± 3e − 04	0.0029 ± 0.00069	0.00044 ± 0.00025	0.0063 ± 0.0014
LTJA	0 ± 0	0.00087 ± 0.00026	0.0077 ± 0.0015	0.00044 ± 0.00029
BFAL	0 ± 0	7.5e − 05 ± 7.5e − 05	0.0011 ± 0.00039	0.0064 ± 0.0014
PIGU	0.0012 ± 0.00091	0.00061 ± 0.00031	0.004 ± 0.003	0.00082 ± 0.00047
LESP	8.6e − 06 ± 8.6e − 06	0.0012 ± 0.00035	0.0038 ± 0.00075	0.0011 ± 0.00054
ALTE	0 ± 0	7.9e − 05 ± 3.8e − 05	0.0027 ± 0.00076	0.0022 ± 0.0019
MOPE	0 ± 0	0.00036 ± 2e − 04	0.00059 ± 0.00029	0.0023 ± 0.00078
UNPA	0 ± 0	0.0014 ± 0.00046	0.00044 ± 0.00033	0.00081 ± 0.00047
STAL	0 ± 0	0 ± 0	0.00073 ± 0.00033	0.00054 ± 0.00038
THGU	0.00087 ± 0.00087	0.00011 ± 0.00011	0 ± 0	0 ± 0
MEGU	0 ± 0	0.00069 ± 0.00032	0 ± 0	0 ± 0
RFCO	4.3e − 18 ± 4e − 18	2.2e − 7 ± 2.2e − 7	0.00019 ± 0.00015	0.00035 ± 0.00028
TUFU	0 ± 0	0 ± 0	0.00044 ± 0.00033	0 ± 0
BASW	0 ± 0	0 ± 0	0.00029 ± 0.00021	0 ± 0
PEFA	0 ± 0	0 ± 0	0 ± 0	0.00027 ± 0.00027
BOGU	0 ± 0	0.00011 ± 0.00011	0 ± 0	0 ± 0
SBGU	0 ± 0	0.00011 ± 0.00011	0 ± 0	0 ± 0
WHAU	0 ± 0	0.00011 ± 0.00011	0 ± 0	0 ± 0

References

Ashmole, N.P., 1971. Sea bird ecology and the marine environment. In: Farner, D.S., King, J.R. (Eds.), Avian Biology, vol. 1. Academic Press, New York and London, pp. 223–286.

Bédard, J., 1976. Coexistence, coevolution and convergent evolution in seabird communities: a comment. Ecology 57, 177–184.

Benoit-Bird, K.J., Battaile, B.C., Heppell, S.A., Hoover, B., Irons, D., et al., 2013. Prey patch patterns predict habitat use by top marine predators with diverse foraging strategies. PLoS ONE 8 (1), e53348, http://dx.doi.org/10.1371/journal.pone.0053348.

Benoit-Bird, K.J., McIntosh, N.E., Heppell, S.A., 2013. Nested scales of spatial heterogeneity of juvenile walleye pollock (*Theragra chalcogramma*) in the southeastern Bering Sea. Mar. Ecol. Prog. Ser., 484, 219-238.

Borberg, J., Ballance, L.T., Pitman, R., Ainley, D.G., 2005. A test for bias due to seabird avoidance of ships when conducting surveys in the tropical Pacific. Mar. Ornithol. 33, 173–179.

Brown, Z.W., van Dijken, G.L., Arrigo, K.R., 2011. A reassessment of primary production and environmental change in the Bering Sea. J. Geophys. Res. 116, C08014, http://dx.doi.org/10.1029/2010JC006766.

Coachman, L.K., 1986. Circulation, water masses, and fluxes on the southeastern Bering Sea shelf. Continental Shelf Res. 5, 23–108.

Cody, M.L., 1973. Coexistence, coevoluation and convergent evolution in seabird communities. Ecology 54, 31–44.

Cooney, R.T., Coyle, K.O., 1982. Trophic implications of cross-shelf copepod distributions in the southeastern Bering Sea. Mar. Biol. 70, 187–196.

Coyle, K.O., Pinchuk, A.I., 2002. The abundance and distribution of euphausiids and age-0 pollock on the inner shelf on the inner shelf of the southeast Bering Sea near the inner front in 1997–1999. Deep-Sea Res. II 49, 6009–6030.

Coyle, K.O., Pinchuk, A.I., Eisner, L.B., Napp, J.M., 2008. Zooplankton species composition, abundance and biomass on the eastern Bering Sea shelf during summer: the potential role of water-column stability and nutrients in structuring the zooplankton community. Deep-Sea Res. II 55, 1775–1791.

Drew, G.S., Piatt, J.F., 2005. North Pacific Pelagic Seabird Database (NPPSD): compiling datasets and creating an archive, accessible database, and pelagic seabird atlas. Final Report for the North Pacific Marine Research Institute Project #: NPMRI 18 (T2110), U.S. Geological Survey, Anchorage, AK.

Gould, P.J., Forsell, D.J., 1989. Techniques for Shipboard Surveys of Marine Birds. U.S. Department of the Interior, Fish and Wildlife Service, Washington, D.C., U.S.A.. (Fish and Wildlife Technical Report).

Gregory, G.C., Stabeno, P.J., Riser, S.C., 2004. The Bering Slope Current system revisited. J. Phys. Oceanogr. 34, 384–398.

Hermann, A.J., Stabeno, P.J., Haidvogel, D.B., Musgrave, D.L., 2002. A regional tidal/subtidal circulation model of the southeastern Bering Sea: development, sensitivity analyses and hindcasting. Deep-Sea Res. II 49, 5945–5967.

Hood, D.W., 1999. PROBES: Processes and resources of the eastern Bering Sea shelf. In: Loughlin, T.R., Ohtani, K. (Eds.), Dynamics of the Bering Sea: A Summary of Physical, Chemical, and Biological Characteristics, and a Synopsis of Research on the Bering Sea. North Pacific Maine Science Organization (PICES) and University of Alaska Sea Grant, Fairbanks, Alaska, pp. 697–711.

Hunt Jr., G.L., Schneider, D.C., 1987. Scale dependent processes in the physical and biological environment of marine birds. In: Croxall, J. (Ed.), Seabirds: Feeding Biology and Role in Marine Ecosystems. Cambridge U. Press, Cambridge, pp. 7–41.

Hunt Jr., G.L., Coyle, K.O., Hoffman, S., Decker, M.B., Flint, E.N., 1996. Foraging ecology of short-tailed shearwaters near the Pribilof Islands, Bering Sea. Mar. Ecol. Prog. Ser. 141, 1–11.

Hunt Jr., G.L., Eppley, Z., Drury, W.H., 1981a. Breeding distribution and reproductive biology of eastern Bering Sea marine birds. In: Hood, D.W, J.A. Calder, J.A. (Eds.), The Bering Sea Shelf: Oceanography and Resources. Office of Marine Pollution Assessment, NOAA, Seattle, pp. 649–687. (Distributed by University of Washington Press).

Hunt Jr., G.L., Gould, P., Forsell, D.J., Peterson, H., 1981b. Pelagic distribution of marine birds in the eastern Bering Sea. In: Hood, D.W., Calder, J.A. (Eds.), The Bering Sea Shelf: Oceanography and Resources. Office of Marine Pollution Assessment, NOAA, Seattle, pp. 689–718. (Distributed by University of Washington Press).

Hunt Jr., G.L., Heinemann, D., Everson, I., 1992. Distributions and predator–prey interactions of macaroni penguins, Antarctic fur seals and Antarctic krill near Bird Island, South Georgia. Mar. Ecol. Prog. Ser. 86, 15–30.

Hunt Jr., G.L., Mehlum, F., Russell, R.W., Irons, D., Decker, M.B., Becker, P.H., 1999. Physical processes, prey abundance, and the foraging ecology of seabirds. In: Adams, N.J., Slotow, R. (Eds.), Proceedings of the 22nd International Ornithological Congress. BirdLife South Africa, Durban, Johannesburg, pp. 2040–2056.

Hunt, G.L., Jr., Stabeno, P., Walters, G., Sinclair, E., Brodeur, R.D., Napp, J.M., Bond, N. A. 2002. Climate change and control of the southeastern Bering Sea pelagic ecosystem. Deep-Sea Res. II 49, 5821–5853.

Iverson, R.L., Coachman, L.K., Cooney, R.T., English, T.S., Goering, J.J., Hunt Jr., G.L., Macauley, M.C., McRoy, C.P., Reeburgh, W.S., Whitledge, T.E., 1979. Ecological significance of fronts in the southeastern Bering Sea. In: Livingston, R.J. (Ed.), Ecological Processes in Coastal and Marine Systems. Plenum Press, New York, pp. 437–466.

Jahncke, J., Coyle, K.O., Hunt Jr., G.L., 2005a. Seabird distribution, abundance and diets in the central and eastern Aleutian Islands. Fish. Oceanogr. 14 (Suppl. 1), 160–177.

Jahncke, J., Hyrenbach, K.D., Baduini, C.L., Coyle, K.O., Hunt Jr., G.L., 2005b. Distribution of foraging shearwaters with respect to the inner front of the southeastern Bering Sea. Mar. Ecol. Prog. Ser. 305, 219–233.

Jahncke, J., Vlietstra, L.S., Decker, M.B., Hunt Jr., G.L., 2008. At-sea distributions of marine birds around the Pribilof Islands: a multi-year comparison of temporal and spatial trends. Deep-Sea Res. II 55, 1809–1826.

Joiris, C., 1978. Seabirds recorded in the northern North Sea in July: the ecological implications of their distribution. Le Gerfaut 68, 419–440.

Joiris, C., 1983. Winter distribution of seabirds in the North Sea: an oceanographical interpretation. Le Gerfaut 73, 107–122.

Kachel, N.B., Hunt Jr., G.L., Salo, S.A., Schumacher, J.D., Stabeno, P.J., Whitledge, T.E., 2002. Characteristics and variability of the inner front of the southeastern Bering Sea. Deep Sea Res. Part II 49, 5889–5909.

Kessel, B., 1979. Avian habitat classification for Alaska. Murrelet 60, 86–94.

Kinder, T.H., Schumacher, J.D., 1981. Hydrographic structure over the continental shelf of the southeastern Bering Sea. In: Hood, D.W., Calder, J.A. (Eds.), The Eastern Bering Sea Shelf: Oceanography and Resources, vol. 1. US. Government Printing Office, Washington, D.C, pp. 31–52.

Kinder, T.H., Coachman, L.K., Galt, J.A., 1975. The Bering Slope Current system. J. Phys. Oceanogr. 5, 231–244.

Ladd, C., Jahncke, J., Hunt Jr., G.L., Coyle, K.O., Stabeno, P.J., 2005. Hydrographic features and seabird foraging in the Aleutian Passes. Fish. Oceanogr. 14 (Suppl. 1), 178–195.

Lovvorn, J.R., Baduini, C.L., Hunt Jr., G.L., 2001. Modeling underwater visual and filter feeding by planktivorous shearwaters in unusual sea conditions. Ecology 82, 2342–2356.

McRoy, C.P., Hood, D.W., Coachman, L.K., et al., 1986. Processes and Resources of the Bering Sea Shelf (PROBES) – the development and accomplishments of the project. Continental Shelf Res. 5, 5–21.

Mizobata, K., Saitoh, S-I., 2004. Variability of Bering Sea eddies and primary productivity along the shelf edge during 1998–2000 using satellite multisensor remote sensing. J. Mar. Syst. 50, 101–111.

Mizobata, K., Saitoh, S-I., Wang, J., 2008. Interannual variability of summer biochemical enhancement in relation to mesoscale eddies at the shelfbreak in the vicinity of the Pribilof Islands, Bering Sea. Deep-Sea Res. II 55, 1717–1728.

Mizobata, K., Wang, J., Saitoh, S-I., 2006. Eddy-induced cross-slope exchange maintaining summer high productivity of the Bering Sea shelf break. J. Geophys. Res. 111, C10017, http://dx.doi.org/10.1029/2005JC00335.

Okkonen, S.R., 2001. Altimeter observations of the Bering Slope Current eddy field. J. Geophys. Res. 106, 2465–2476.

Okkonen, S.R., Schmidt, G.M., Cokelet, E.D., Stabeno, P.J., 2004. Satellite and hydrographic observations of the Bering Sea 'Green Belt'. Deep-Sea Res. II 51, 1033–1051.

Pearson, T.H., 1968. The feeding biology of sea-bird species breeding on the Farne Islands, Northumberland. J. Anim. Ecol. 37, 521–552.

Pennycuick, C., 1989. Bird Flight Performance: A Practical Calculation Manual. Oxford University Press, Oxford.

Pinchuk, A.I., Coyle, K.O., 2008. Distribution, egg production and growth of euphausiids in the vicinity of the Pribilof Islands, southeastern Bering Sea, August 2004. Deep-Sea Res. II 55, 1792–1800.

Renner, M., Hunt Jr., G.L., Piatt, J.F., Byrd, G.V., 2008. Seasonal and distribution patterns of seabirds along the Aleutian Archipelago. Mar. Ecol. Prog. Ser. 357, 301–311.

Renner, M., Parrish, J.K., Piatt, J.F., Kuletz, K.J., Edwards, A.E., Hunt Jr., G.L., 2013. Modeling the distribution and abundance of a pelagic seabird to disentangle the roles of climate change and commercial fisheries. Mar. Ecol. Prog. Ser.. (in press).

Sambrotto, R.N., Mordy, C., Zeeman, S.I., Stabeno, P.J., Macklin, S.A., 2008. Physical forcing and nutrient conditions associated with patterns of Chl *a* and phytoplankton productivity in the southeastern Bering Sea during summer. Deep-Sea Res. II 55, 1745–1760.

Schneider, D.C., 1991. The role of fluid dynamics in the ecology of marine birds. Oceanogr. Mar. Biol.: Annu. Rev. 29, 487–521.

Schneider, D.C., 1997. Habitat selection by marine birds in relation to water depth. Ibis 139, 175–178.

Schneider, D.C., Hunt Jr., G.L., 1982. Carbon flux to seabirds in waters with different mixing regimes in the southeastern Bering Sea. Mar. Biol. 67, 337–344.

Schneider, D.C., Shuntov, V.P., 1993. The trophic organization of the marine community in the Bering Sea. Rev. Fish. Sci. 1, 311–335.

Schneider, D.C., Duffy, D.C., Hunt, G.L., Jr., 1988 Cross-shelf gradients in the abundance of pelagic birds. In: Oulet, H. (Ed.), Acta XIX Congressus Internationalis Ornithologici Ottawa, Canada. 22–29 VI 1986. vol. 1, pp. 976–981.

Schneider, D.C., Hunt Jr., G.L., Harrison, N.M., 1986. Mass and energy transfer to seabirds in the southeastern Bering Sea. Continental Shelf Res. 5, 241–257.

Schumacher, J.D., Kinder, T.H., Pashinski, D.J., Charnell, R.L., 1979. A structural front over the continental shelf of the eastern Bering Sea. J. Phys. Oceanogr. 9, 79–87.

Sigler, M.F., Kuletz, K J, Ressler, P.H., Friday, N.A., Wilson, C.D., Zerbini, A.N., 2012. Marine predators and persistent prey in the southeast Bering Sea. Deep Sea Res. II 65–70, 292–303.

Sinclair, E.H., Vlietstra, L.S., Johnson, D.S., Zeppelin, T.K., Byrd, G.V., Springer, A.M., Ream, R.R., Hunt Jr., G.L., 2008. Patterns in prey use among fur seals and seabirds in the Pribilof Islands. Deep-Sea Res. II, 55; , pp. 1897–1918.

Smith, S.L., 1991. Growth, development and distribution of the euphausiids *Thysanoessa raschii* (M. Sars) and *Thysanoessa inermis* (Kroyer) in the southeastern Bering Sea. In: Sakshaug, E., Hopkins, C.C.E., Oritsland, N.A. (Eds.), Proceeding of the Pro Mare Symposium on Polar Marine Ecology, pp. 461–478.

Smith, S.L., Vidal, J., 1986. Variations in the distribution, abundance, and development of copepods in the southeastern Bering Sea in 1980 and 1981. Continental Shelf Res. *5*, 215–239.
Spear, L.B., Ainley, D.G., 1997. Flight speed of seabirds in relation to wind speed and direction. Ibis 139, 238–251.
Spear, L.B., Ainley, D.G., Hardesty, B.D., Howell, S.G.N., Webb, S.W., 2004. Reducing biases affecting at-sea surveys of seabirds: use of multiple observer teams. Mar. Ornithol. 32, 147–157.
Springer, A.M., McRoy, C.P., Flint, M.V., 1996a. The Bering Sea green belt: shelf-edge processes and ecosystem production. Fish. Oceanogr. 5, 205–223.
Springer, A.M., Piatt, J.F., Van Vliet, G.B., 1996b. Seabirds as proxies of marine habitats and food webs in the western Aleutian arc. Fish. Oceanogr. 5, 45–55.
Stabeno, P.J., van Meurs, P., 1999. Evidence of episodic on-shelf flow in the southeastern Bering Sea. J. Geophys. Res. 104 (C12), 29715–29720.
Stabeno, P.J., Bond, N.A., Kachel, N., Salo, S.A., Schumacher, J.D., 2001. On the temporal variability of the physical environment over the south-eastern Bering Sea. Fish. Oceanogr. 10, 81–98.
Stabeno, P.J., Reed, P.K., Napp, J.M., 2002. Transport through Unimak Pass, Alaska. Deep-Sea Res. II 49, 5919–5930.
Stabeno, P.J., Schumacher, J.D., Ohtani, K., 1999. The physical oceanography of the Bering Sea. In: Loughlin, T.R., Ohtani, K. (Eds.), Dynamics of the Bering Sea: A summary of Physical, Chemical, and Biological Characteristics, and a Synopsis of Research on the Bering Sea, North Pacific Marine Science Organization (PICES), University of Alaska Sea Grant, AK-SG-99-03, Fairbanks, Alaska, USA, pp. 1–28.
Stone, C.J., Webb, A., Tasker, M.L., 1995. The distribution of auks and Procellariiformes in northwestern European waters in relation to depth of sea. Bird Study 42, 50–56.
Tasker, M.L., Jones, P.H., Dixon, T., Blake, B.F., 1984. Counting seabirds at sea from ships: a review of methods employed and a suggestion for a standardized approach. Auk 101, 567–577.
USFWS, 2004. Beringian Seabird Colony Catalog (2004). ⟨http://seamap.env.duke.edu/dataset/270⟩. (accessed June 12.06.13).
van Franeker, J.A., 1994. A comparison of methods for counting seabirds at sea in the Southern Ocean. J. Field Ornithol. 65, 96–108.
Vidal, J., Smith, S.L., 1986. Biomass, growth, and development of populations of herbivorous zooplankton in the southeastern Bering Sea during spring. Deep-Sea Res. 33, 523–556.
Vlietstra, L.S., Coyle, K.O., Kachel, N.B., G.L. Hunt Jr, G.L., 2005. Tidal front affects the size of prey used by a top marine predator. Fish. Oceanogr. 14 (Suppl. 1), 196–211.
Walsh, J.J., McRoy, C.P., 1986. Ecosystem analysis in the southeastern Bering Sea. Continental Shelf Res. 5, 259–288.
Weimerskirch, H., Bartle, J.A., Jouventin, P., Stahl, J.C., 1988. Foraging ranges and partitioning of feeding zones in three species of southern albatrosses. Condor 90, 214–219.
Wood, S.N., 2008. Fast stable direct fitting and smoothness selection for generalized additive models. J. R. Stat. Soc.: Ser. B (Stat. Methodol.) 70, 495–518.
Wynne-Edwards, V.C., 1935. On the habits and distributions of birds on the North Atlantic. Proc. Boston Soc. Nat. Hist. 40, 233–346.

Deep-Sea Research II 109 (2014) 282–292

Contents lists available at ScienceDirect

Deep-Sea Research II

journal homepage: www.elsevier.com/locate/dsr2

Changes in the distribution and abundance of albatrosses in the eastern Bering Sea: 1975–2010

Kathy J. Kuletz [a,*], Martin Renner [b,1], Elizabeth A. Labunski [a], George L. Hunt Jr. [b]

[a] US Fish and Wildlife Service, 1011 E. Tudor Road, Anchorage, AK 99503, USA
[b] School of Aquatic and Fishery Sciences, University of Washington, Box 355020, Seattle, WA 98195, USA

ARTICLE INFO

Available online 21 May 2014

Keywords:
Decadal-scale changes in marine ecosystems
Bering Sea
Phoebastria
Seabird distribution
Laysan albatross
Black-footed albatross
Short-tailed albatross

ABSTRACT

A number of marine species are showing poleward shifts in their distributions in response to climate warming. Three albatross species frequent the Bering Sea, the Laysan (*Phoebastria immutabilis*), the black-footed (*Phoebastria nigripes*), and the endangered short-tailed albatross (*Phoebastria albatrus*). To determine if albatrosses changed their distribution or abundance in the eastern Bering Sea between 1975 and 2010, we examined at-sea survey data using the North Pacific Pelagic Seabird Database. Within our study area, all three species of albatross occurred most frequently in the waters of the Aleutian Islands. In the eastern Bering Sea, all three species were most abundant near the shelf break, and in particular in the vicinity of the major submarine canyons in the shelf slope. Starting in the 1990s, population densities increased for all three albatross species, with a marked increase in the 2000s. In the 2000s, there was also an increase in the frequency at which albatrosses were recorded in the central and northern Bering Sea. Both black-footed and short-tailed albatrosses shifted the centers of their Bering Sea distributions northward. The Laysan albatross center of distribution shifted southward due to increased numbers along the southern shelf break, but densities also increased northward. We suggest that the observed changes in distribution and abundance of the three albatross species in the eastern Bering Sea may have been responses to an increase in the availability of squid, their primary prey, there. Additionally, the expansion of the distribution of the short-tailed albatross in the eastern Bering Sea may represent the reclamation of its previous range, now that the population is beginning to recover from near extinction caused by over harvesting. We suggest that predicted increases in ocean temperatures and northward movement of prey could result in albatrosses and other marine apex predators foraging farther north along the Bering Sea shelf and staying later in fall.

Published by Elsevier Ltd.

1. Introduction

In the north temperate and sub-arctic seas, there is considerable evidence for the poleward shift of fish species' distributions in response to warming conditions (e.g., Loeng and Drinkwater, 2007; Mueter and Litzow, 2008; Portner and Peck, 2010; Simpson et al., 2011), which is likely to be reflected in the diets of marine birds (Gaston et al., 2003, Montevecchi and Myers, 1992, 1997). The eastern Bering Sea marine ecosystem has responded to climate variability with changes in food web structure (e.g., Hunt et al., 2011) and shifts in the distribution of fish species (e.g. Hollowed et al., 2012; Mueter and Litzow, 2008). Additionally, spatial shifts in commercial fisheries in the Bering Sea (Ianelli et al., 2012) could potentially influence distribution of seabird species that follow fishing vessels as a source of food (Renner et al., 2013). It would thus seem likely that seabirds foraging in the eastern Bering Sea might have shifted their distributions in response to shifts in the distributions of their food resources.

During the summer breeding season, seabirds may not be able to track broad-scale changes in the prey base because most seabird species are constrained by colony location. Breeding seabirds are obligate central place foragers and, because they must guard nest sites and mates, incubate eggs, and raise chicks, their foraging range while breeding is limited (Coulson, 2002). Even non-breeding individuals of the population may restrict their foraging range during the breeding season to prospect for mates and nest sites (Coulson, 2002). However, in Alaska, nearly half of the estimated numbers of seabirds present in summer have arrived solely to forage in the rich waters of the Bering Sea (USFWS, 2009). Among the estimated 30 million visiting seabirds, three species of albatrosses frequent Alaska waters- the Laysan

* Corresponding author. Tel.: +1 907 786 3453; fax: +1 907 786 3641.
E-mail addresses: Kathy_Kuletz@fws.gov (K.J. Kuletz), mrenner@gmx.com (M. Renner), Elizabeth_Labunski@fws.gov (E.A. Labunski), geohunt2@UW.edu (G.L. Hunt Jr.).
[1] Current address: Tern Again Consulting, 308 E. Bayview Ave., Homer, AK 99603, USA.

http://dx.doi.org/10.1016/j.dsr2.2014.05.006
0967-0645/Published by Elsevier Ltd.

(*Phoebastria immutabilis*), the black-footed (*Phoebastria nigripes*), and the short-tailed albatross (*Phoebastria albatrus*). Adults of these albatross species breed on islands near Japan (all three species) or the Hawaiian Archipelago (Laysan and black-footed), and travel to the Bering Sea primarily during their non-breeding season, which is principally June through September (Hyrenbach et al., 2002; Tickell, 2000). Non-breeding birds and immature birds may remain in northern waters throughout the year. Because these albatrosses do not breed in Alaska and are not tied to colonies during most of the summer, they can track prey without the limitations of being central place foragers. Thus their pelagic distributions should be good indicators of broad-scale changes in the eastern Bering Sea ecosystem.

Highly visible apex predators, seabirds are indicators of ecosystem change because individuals and populations respond at various spatial and temporal scales to alterations in their marine food base (Frederiksen et al., 2007; Piatt et al., 2007; Springer et al., 2007). The distribution of wide-ranging seabirds like albatrosses can be influenced by large-scale patterns of atmospheric circulation (Suryan et al., 2008), but also reflect ocean properties that concentrate fish, squid, and other invertebrates near the ocean surface (Piatt et al., 2006; Suryan et al., 2006). In this paper, we examined the pelagic distribution of the three North Pacific albatross species in the Aleutian Islands and the eastern Bering Sea. We sought to determine if the distributions of these apex predators have changed since the 1970s, when pelagic surveys of seabirds were initiated there. We focused on albatrosses because (1) they are not central place foragers in Alaska and thus should not be limited in tracking prey by the need to return to their colonies; (2) they are large, easily detected birds that are not typically clumped in distribution, which make counts at sea more precise and less affected by sea conditions; and (3) albatrosses in the Bering Sea are at the northern fringes of their ranges, thus increasing the likelihood of a detectable response to environmental change (Maggini et al., 2011; Worm and Tittensor, 2011). To determine if albatross species show evidence of shifts in their distributions in the eastern Bering Sea, and to determine their current distribution, we examined at-sea survey data from June through September spanning four decades, from 1975 to 2010.

2. Methods

2.1. Study area

The study area encompassed the eastern Bering Sea, from the Bering Strait to the Aleutian Archipelago (Fig. 1). The eastern Bering Sea comprises a 500 km wide, shallow shelf (average depth 70 m) and a deep basin with depths in excess of 4000 m. The eastern Bering Sea shelf is characterized by three sub-regions, defined by bathymetry and hydrographic fronts, with the greatest definition of the latter occurring in summer (Coachman, 1986; Kachel et al., 2002). The most coastal of these sub-regions, the Inner Domain (with depths <50 m and well mixed), is separated by the Inner Front from the Middle Domain (depths $\sim$50–100 m, more stratified), which in turn is separated from the Outer Domain (depths$\sim$100–180 m) by the Middle Transition Zone. A rapid change in depth occurs along the shelf break, referred to as the shelf slope. The shelf slope, which begins at about 200 m depth, is bisected by a number of large submarine canyons, which are the sites of significant on-shelf fluxes of water and biota (Gibson et al., 2013). Along-shelf flows predominate in the southeastern Bering Sea, with strong flows along the shelf slope in the Bering Slope Current (Johnson et al., 2004), the 100 m isobath, and weaker

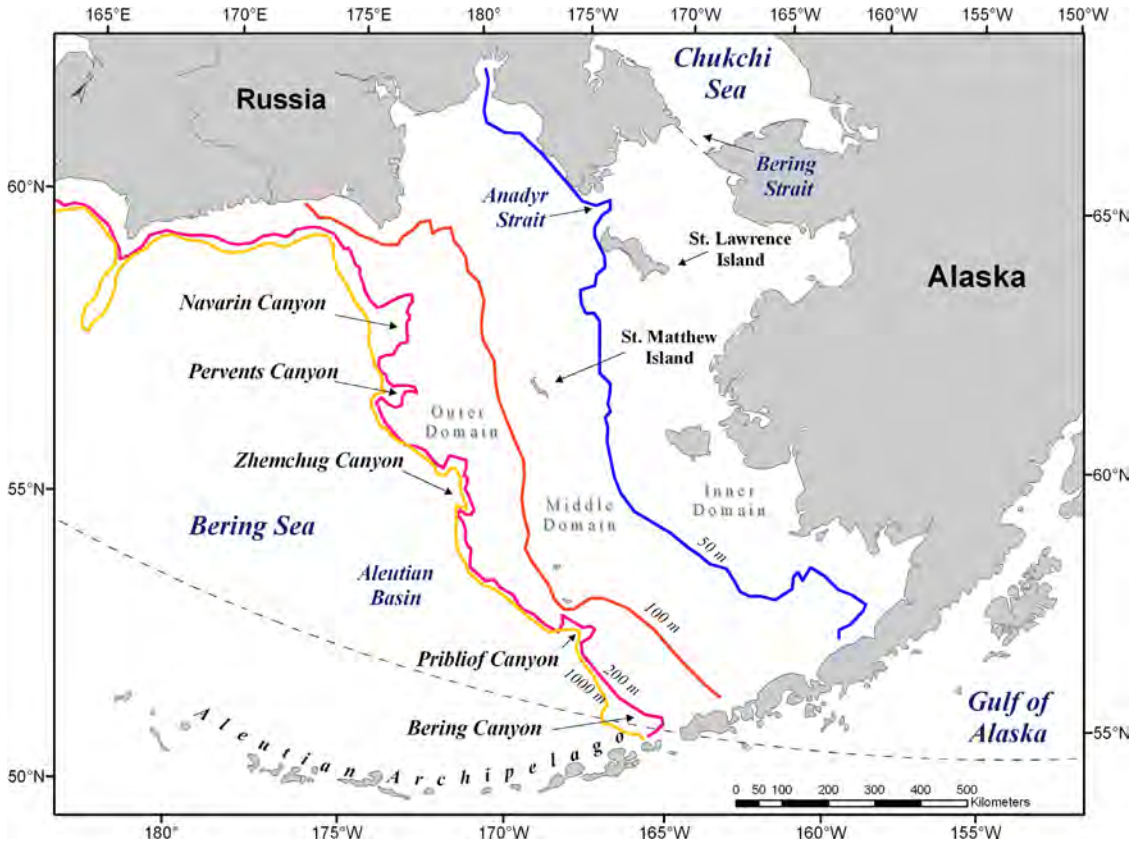

Fig. 1. The Bering Sea study area, with major bathymetric contours and locations of Bering Sea submarine canyons. The dashed line follows the 54.5°N latitudinal line and denotes the latitude within the Bering Sea northward of which we examined changes in albatross distribution and abundance.

flows along the Inner Front north of Bristol Bay (Stabeno et al., 2001, 2007). Cross-shelf fluxes in the southeastern Bering Sea are generally weak and are predominately influenced by tidal forces (Coachman, 1986), though there are important on-shelf flows from Bering Canyon along the Inner Front north of the Alaska Peninsula, as well as north of the Pribilof Islands (Stabeno et al., 2007, 2008). The shelf slope and 100 m isobath flows carry nutrients and plankton, originating in the south, northward along the slope, resulting in a highly productive outer shelf and slope region referred to as the "Green Belt" (Springer et al., 1996).

The Aleutian Archipelago is a 2000 km-long chain of islands separated by both shallow and deep passes. Water from the Gulf of Alaska, traveling southwestward in the Alaska Coastal Current and the Alaskan Stream enters the Bering Sea through the passes of the eastern and central Aleutian Islands (Ladd et al., 2005a). These waters then turn eastward north of the Aleutian Islands forming the Aleutian North Slope Current (Hunt and Stabeno, 2005; Stabeno et al., 2005). Tidal currents in the Aleutian passes are strong, and they result in the upwelling of nutrients, creating regions of high primary production, and frontal systems where seabirds forage on concentrations of zooplankton, squid, and fish (Jahncke et al., 2005; Ladd et al., 2005b; Mordy et al., 2005; Vlietstra et al., 2005).

2.2. Data source and collection methods

We obtained data from the North Pacific Pelagic Seabird Database (NPPSD) v3 (www.absc.usgs.gov/research/NPPSD). Most of these data came from three major periods of research effort. The first surge in data collection occurred from 1975 to 1985 during the Outer Continental Shelf Environmental Assessment Program (OCSEAP) when observers were put on many ships of opportunity, and there was coverage of most of the shelf and slope regions (Fig. 2). A second source of data was surveys conducted by GLH and others on process studies from the 1980s to 2004, as well as data collected by the Alaska Maritime National Wildlife Refuge (Renner et al., 2008). These efforts, while more focused on seabirds, were spatially concentrated, and large portions of the shelf and slope went unsurveyed (Fig. 2). The third period of data collection occurred from 2006 through 2010, prior to and during the Bering Sea Project (North Pacific Research Board and National Science Foundation; KJK); these surveys, also on ships of opportunity, occurred in conjunction with other research projects and coverage of the shelf and slope was thorough (Fig. 2).

During all decades of survey, the standard observation protocol consisted of a single observer on the bridge recording all birds within 300 m ahead of the ship's bow in a 90° arc to one side, using strip transect methodology (Gould and Forsell, 1989; USFWS, 2008a). During a number of the process studies in the 1980s and 1990s, the observer was aided by another person serving as recorder, as these surveys were in regions with exceptionally high seabird densities, particularly of small auklets. Occasionally weather conditions, especially fog, reduced the transect window to 200 m or 100 m, and densities were calculated accordingly. A single observer is susceptible to missing small species, but larger species such as albatrosses can be reliably detected by a single observer from large vessels at least out to 300 m (Spear et al., 2004).

During all surveys, all birds on the water or foraging (including birds actively foraging from the air, i.e., hovering and surface plunging) were recorded continuously. Methods for recording flying birds, however, varied among projects. Many surveys pre

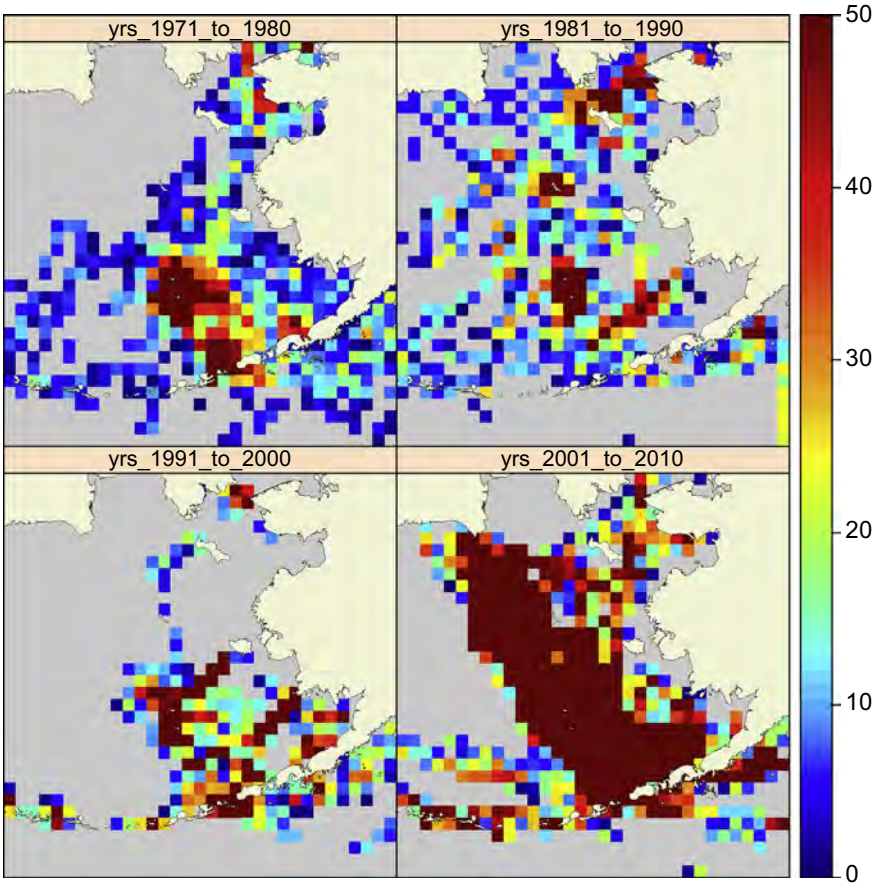

Fig. 2. Survey effort by decade over a 50 km × 50 km grid, measured as area surveyed [km^2] per grid cell. The scale is capped at 50 transects km^{-2}.

2007 counted flying birds continuously, but otherwise observers used the instantaneous scan, or 'snap-shot' of the 300 m transect window (Gould and Forsell, 1989). The snap-shot is a simple method for minimizing over-estimation of flying birds and it allows calculation of densities (birds $\cdot$ km^{-2}) without further manipulation of the data. Scan intervals varied with ship speed, and in our post-2006 surveys generally occurred every 37–65 s. Birds were recorded on first observation but otherwise ignored if they followed the ship. From 2007 to 2010, all flying birds were recorded using the snap-shot method and required no correction factor. For earlier surveys that counted flying birds continuously, we applied a correction factor of 0.2 (van Franeker, 1994).

Counting albatrosses from ships can be complicated by their tendency to be attracted to and follow ships, which can result in overestimation of their abundance (Hyrenbach, 2001). Likewise, albatrosses may aggregate near fishing vessels (Weimerskirch et al., 2000). However, our surveys were typically not conducted near fishing operations, and 94% of the 2175 observations in our database consisted of single birds. While acknowledging the potential for overestimating abundance, we have no reason to think that the tendency for albatrosses to move towards and follow a survey vessel varied over the decades, which could have created a bias in the analyses of trends in relative density.

In most years, observers also noted the occurrence of albatrosses outside of the 300 m transect window to record the presence of these relatively rare birds. These "off transect" observations were not used for calculating the densities of the albatrosses or the centers of their distribution. For maps of the current distribution of short-tailed albatross, we show both on and off transect observations made during surveys as a means of showing the distribution of this particularly rare albatross in the eastern Bering Sea during a period of unusually broad and thorough survey coverage (2006–2010). We did not use the USGS/USFWS database for short-tailed albatross sightings (Piatt et al., 2006; Zador et al., 2008a), which is separate from the NPPSD and mostly consists of opportunistic sightings from a variety of sources, with no measure of effort.

Prior to 1984, data were recorded by hand on paper forms in 10-min time segments, with each 10-min transect providing a start and end location. Since the mid-1980s, data have been recorded directly into laptop computers. The initial data entry programs recorded position and time at intervals, and then the positions of sightings were determined by interpolation. Since 2006, data on time and position were logged with each bird observation using a Global Positioning System connection.

2.3. Data Analyses

We selected data obtained between 1 June and 30 September of each year. To standardize historic and recent data spatially, all transects were binned into 3-km segments to calculate densities (birds $\cdot$ km^{-2}). For decadal comparisons and mapping densities by decadal period, we used only observations recorded within the 300 m transect window (on transect). Raster calculations were performed on a 50 km $\times$ 50 km grid in the standard Alaskan Albert Equal Area projection.

To examine the distribution of albatrosses, we included all waters around the Aleutian Islands and to the north. However, because of the much higher densities of albatrosses near the Aleutian Islands, for analysis of changes in distribution along the eastern Bering Sea shelf, we used only survey effort and observations north of 54.5°N, which excluded the Aleutian Islands. For each species, all density indices north of this latitude were combined into 0.5° latitudinal bands. Years were then combined into decades.

To evaluate changes in the latitudinal distribution across decades of each albatross species, while accounting for the heterogeneity of the dataset, we followed Renner et al. (2013), using the following process: (1) We averaged annual densities (from 3-km segments) over the 50 km $\times$ 50 km grid (Fig. 2). (2) Grid cells that were not surveyed in any one year were linearly interpolated through time (but not space) using the two nearest surveyed years. Rather than extrapolating a trend, we used the nearest known value for years beyond the surveyed range. In effect, we impute the missing values, but instead of using a long-term mean, we use a local mean. (3) The now complete matrix was analyzed for changes in latitude (center of gravity) by using mean density per grid cell as weights in a regression of latitude (of grid cell) over time. The annual proportion of missing cells varied among years, ranging from 57% to 99.5%. This proportion of missing cells may appear high, however, it is important to note that the interpolation procedure does not introduce a bias and that the total number of grid cells, not the annual values, are our sampling units.

We used a Generalized Additive Model (GAM) to model the changes in latitudinal distribution over time, allowing for non-linear effects, and adjusting the smoothing parameter through generalized cross-validation (Wood, 2000). Where the GAM did not differ from a simple linear regression, we reported the latter for simplicity.

We used R (R Development Core Team, 2011) for most calculations. GRASS GIS (Neteler and Mitasova, 2008) in conjunction with the R packages sp, and spgrass6 were used for all GIS operations. Models were fit using R with the packages mgcv (GAM).

3. Results

3.1. Decadal comparisons

All three species of albatross increased in abundance over the study period, though the increase was most marked in the most recent period (2000–2010) (Fig. 3A–C). The Laysan albatross was the most abundant species in all four decades, with the greatest increase occurring between about 54°N and 56°N (Fig. 4), i.e., the southern portion of the Bering Sea shelf and along the Aleutian Islands (Fig. 3A). The black-footed albatross increased primarily between 55°N and 56°N (Fig. 4). The first two records of short-tailed albatrosses in the North Pacific Pelagic Seabird Database (NPPSD) occurred in the Aleutian Islands in the 1980s, with a few more records in the 1990s; otherwise all summer records for the Bering Sea shelf occurred in the 2000s (Figs. 3C, 4).

The spatial distributions of all three albatross species changed over the study period (Fig. 3A–C). In the 1970s, Laysan albatrosses were found primarily near the western Aleutian Islands (Fig. 3A). By the 1980s, they had spread northward along the shelf edge, with high densities observed during surveys near Russia. Coverage was less extensive in the 1990s, but over that portion of the Eastern Bering Sea shelf that was surveyed, Laysan albatross sightings increased compared to earlier decades. By the 2000s, relatively high densities were observed throughout the Aleutian Islands, and observations extended along most of the Eastern Bering Sea shelf slope (Fig. 3A). In the 1970s, black-footed albatrosses were not observed in the Southeastern Bering Sea, and relatively low densities were recorded along the Aleutian Islands (Fig. 3B). During the 1980s and 1990s, few observations were made in the Eastern Bering Sea, with the exception of two unusual records north of St. Lawrence Island, recorded in the 1980s. By the 2000s, relatively high densities of black-footed albatrosses were observed in the Eastern Aleutian Islands, and birds occurred along the shelf from Unimak Pass to Pribilof Canyon. Short-tailed albatrosses were not recorded during surveys of the Eastern Bering Sea shelf in the 1970s and 1980s, and at only at one location near Unimak Pass in the 1990s. Sightings of short-tailed albatrosses in the early 2000s were most often near the head of Bering Canyon, or a short distance north of there in the Outer

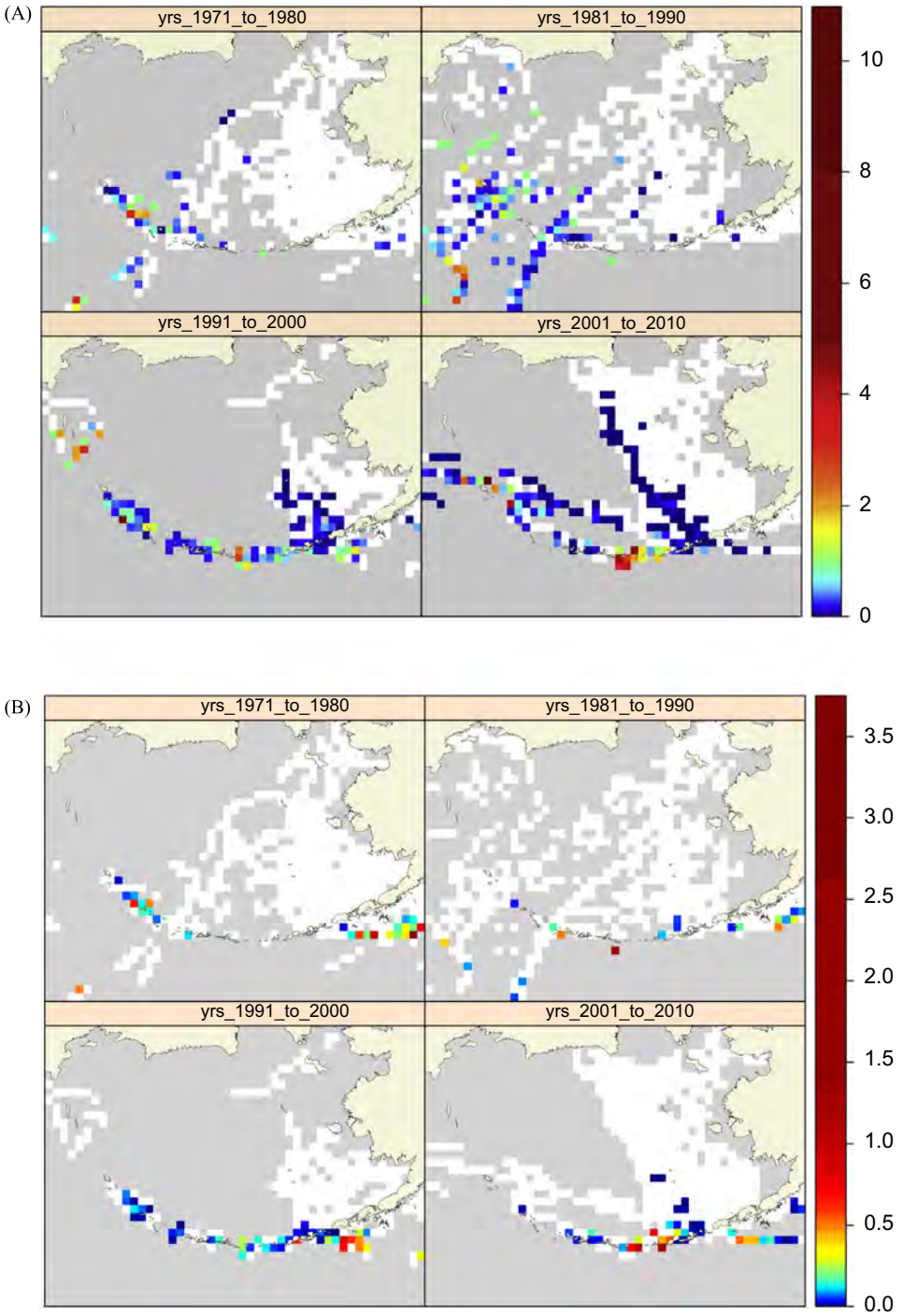

Fig. 3. Albatross densities (birds · km^{-2})in the Bering Sea (in 3-km segments), averaged per 50 km × 50 km cell within decades for Laysan (A), black-footed (B) and short-tailed (C) albatrosses. White areas had survey coverage within the decade, gray areas did not. Warm colors denote higher density indices, cool colors denote lower values.

Domain (Fig. 3C). As the number of short-tailed albatross observations increased, so did their occupation of the northern areas of the Outer Domain and the shelf slope region (Fig. 3C).

The centers of distribution for both black-footed and short-tailed albatrosses shifted significantly northward (Fig. 4; parameter estimates ± SE = 0.27 +/− 0.13 km year^{-1} and 16.75 +/− 2.87 km year^{-1}, respectively). In contrast, the center of distribution of Laysan albatrosses shifted southward (Fig. 4; −5.22 ± 0.65 km year^{-1}) due to the substantial increase in the number of birds observed near the southern terminus of the shelf break and Bering Canyon. That said, there were also more Laysan albatrosses at the northern edge of their range in the Bering Sea (Fig. 3A). A cross-validated, weighted temporal GAM of Laysan albatross distribution did not differ from a straight line, suggesting that a straight line is the best predictor supported by the data.

3.2. Current distribution

During the 2006–2010 surveys we had extensive coverage of the eastern Bering Sea shelf (Fig. 2), but nearly all albatrosses were observed near the shelf break or in the waters of the Aleutian Islands (Fig. 5A–C). Laysan albatrosses were abundant throughout

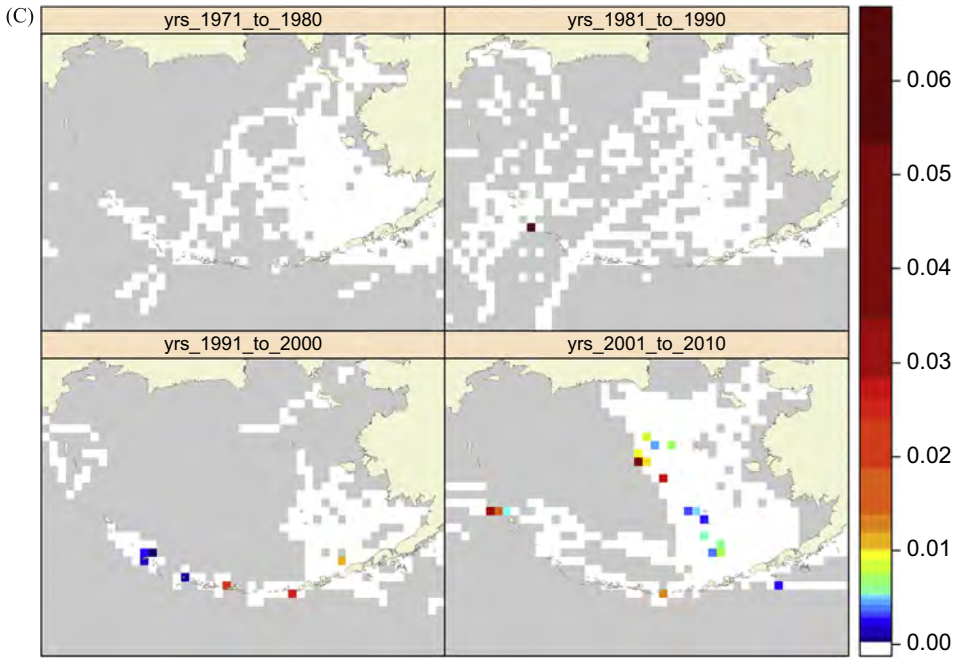

Fig. 3. Continued

the Aleutian Islands, and were regularly observed along the length of the eastern Bering Sea shelf, primarily the Outer Domain and shelf slope (Fig. 5A). They were also occasionally observed over the Middle Domain. We recorded relatively high densities of Laysan albatrosses near Bering Canyon at the south end of the Bering Sea shelf, and at Zhemchug Canyon in the north, but the highest densities in the eastern Bering Sea were in the vicinity of Pribilof Canyon (Fig. 5A). We found black-footed albatrosses primarily along the Aleutian Islands and the southeastern corner of the eastern Bering Sea (near Bering Canyon), with the northern-most observations near the head of the Pribilof Canyon (Fig. 5B). Short-tailed albatrosses were consistently recorded along the Outer Domain, and to a lesser degree, the Middle Domain, with proportionately more observations north of Zhemchug Canyon compared to the other two species (Fig. 5C).

4. Discussion

4.1. Decadal changes in abundance indices

We demonstrate that there has been an increase in albatross sightings during at-sea surveys in the eastern Bering Sea between 1975 and 2010. Numbers of recorded Laysan albatrosses began to increase in the 1980s, with what appears to have been accelerating rates of increase in the 1990s and 2000s. Black-footed albatross sightings also increased in the 1980s, but it was not until the 2000s that they were regularly encountered near the southwestern corner of the eastern Bering Sea shelf. In contrast, short-tailed albatrosses were rarely reported before 2000 during at-sea surveys, after which sightings increased substantially. It is apparent from distribution maps (e.g., Fig. 3A–C), and from the consistent sightings in the most recent decade (Fig. 5A–C), that albatrosses of all three species are comparatively common now along the Outer Domain of the eastern Bering Sea shelf, where they rarely were encountered in the past.

These changes in distribution of such far-ranging species suggest broad-scale ecosystem changes in the Bering Sea. However, linking changes in the distribution of seabirds to ecosystem change is complicated by a variety of ecological factors, including human activities (Ainley and Hyrenbach, 2010). While we found clear evidence of changes in albatross distribution, it is less clear which aspects of the marine system drove albatrosses to expand their distributions to the north.

Population increases in albatrosses may in part account for the increase in sightings in the eastern Bering Sea, as populations of all three species have increased on their southern breeding grounds since the mid-twentieth century (Naughton et al., 2007; USFWS, 2008b). Following decimation of many colonies by feather hunters in the early 1900s and by harassment during World War II, the Laysan albatross, and to lesser degree the black-footed albatross, increased at their northwestern Hawaiian Islands breeding sites between the 1970s and 1990s (Naughton et al., 2007). These two species continued to increase at these key breeding sites between the 1990s and 2005, and during this period they also re-colonized other breeding sites in the central Pacific (Awkerman et al., 2008, 2009).

The short-tailed albatross population at breeding colonies off Japan has been growing at 7% per annum since the 1990s (USFWS, 2008b; Zador et al., 2008a), and the increase in sightings in the Bering Sea is likely a result of increasing numbers and a re-occupation of their former range. The occurrence of short-tailed albatross bones in middens and historic records suggest that this species at one time occupied the northernmost regions of the Bering Sea shelf (Causey and Loring, 2010; Tickell, 2000). The very high rate of estimated movement north ($\sim$17 km year^{-1}) is probably inflated by the lack of sightings in the 1970s and 1980s (Fig. 3C). With numbers of birds estimated to have been in the hundreds during these decades (USFWS, 2008b), the probability of encountering birds that were in the Bering Sea would have been low regardless of survey effort.

4.2. Decadal changes in distribution

Accompanying the increase in albatross sightings in the southeastern Bering Sea, there has been an increased occupation of Outer Domain and shelf slope waters farther north. Laysan albatrosses were occasionally observed north of 58°N in the early decades, and recently they have increased throughout the Bering Sea. However, this increase

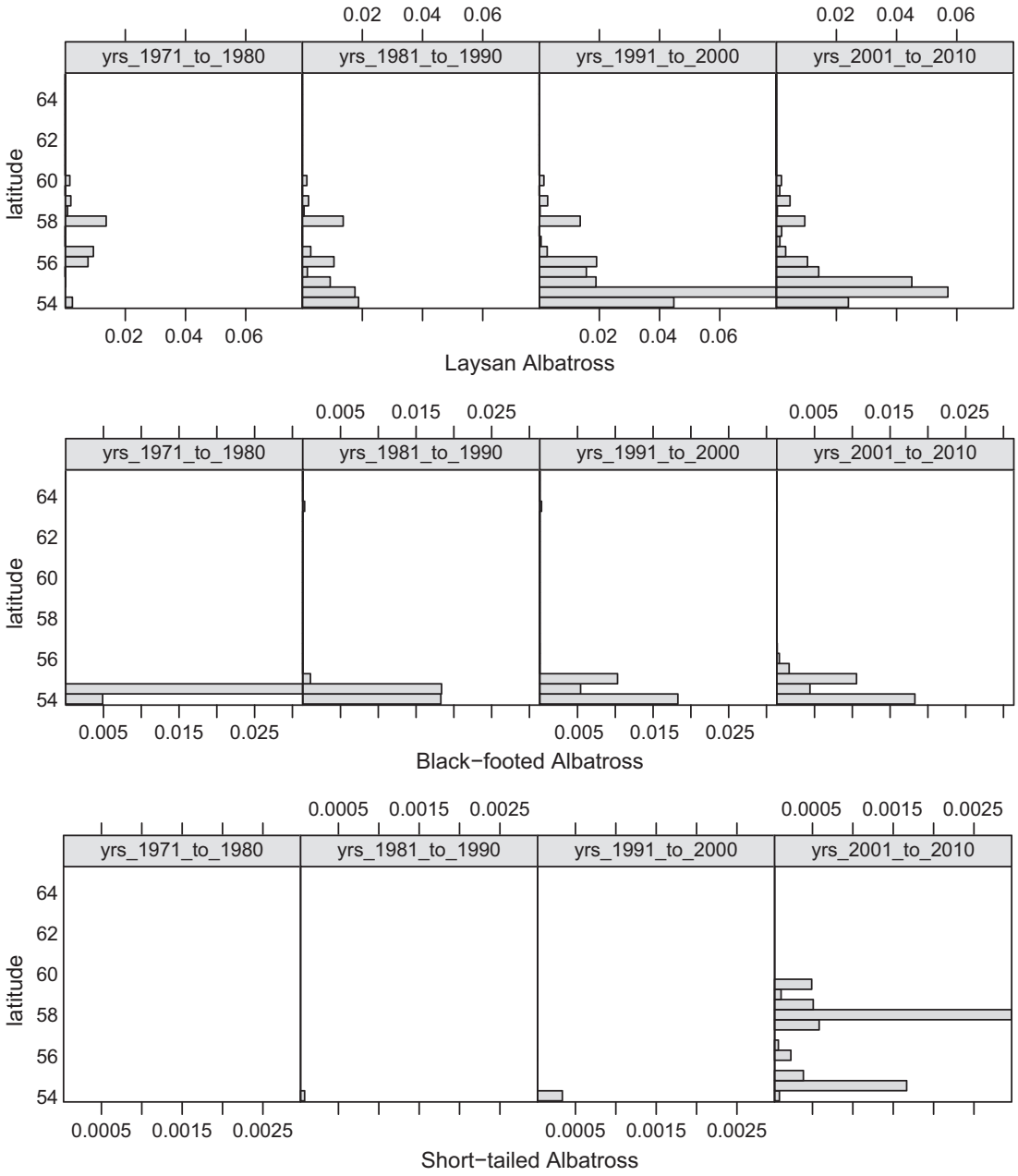

Fig. 4. Densities (birds · km^{-2}) of Laysan (top), black-footed (middle), and short-tailed (bottom) albatross in the eastern Bering Sea (not including the Aleutian Islands), by latitude and decade. Densities from the 3-km segments were averaged over the 50 km × 50 km grid, and cells that were not surveyed in any one year were interpolated with values of the closest neighbor in time. An analysis for changes in latitude (center of gravity) used mean density per grid cell as weights in a regression of latitude (of grid cell) over time.

has been more pronounced in the southeastern Bering Sea and the Aleutian Islands, thus the shift of center of their distribution southward (Fig. 4) despite more observations in the north over time (Fig. 3A). Shuntov (1999) reported that Laysan albatrosses occurred along the Siberian coast off the Kamchatka Peninsula, consistent with NPPSD records from the western Bering Sea (Fig. 3A), and it is likely that this species has entered the Bering Sea both through the passes of the Aleutian Islands and through the major passes connecting the western North Pacific Ocean and Bering Sea.

The black-footed albatross has typically been associated with the Gulf of Alaska and central North Pacific Ocean (Awkerman et al., 2008; Hyrenbach et al., 2002; Naughton et al., 2007), and their recent occurrence as far north as Pribilof Canyon represents a significant northward range expansion. However, their occurrence in the southeastern Bering Sea appears to be most frequent near the Aleutian Islands, where they were occasionally observed in earlier decades (Hunt et al., 1981). Most of the black-footed albatrosses recorded in the 2000s in the Bering Sea have been sighted in late summer and fall, with highest density indices in September (KJK, unpublished data), when water temperatures are at their highest in the Bering Sea.

There are two records in the NPPSD from the 1980s of black-footed albatrosses north of St. Lawrence Island at nearly 64°N. These are the only observations of black-footed albatrosses north of 57.5°N of which we are aware, and we suggest that they were misidentified juvenile short-tailed albatross; the juveniles have all dark plumage that looks similar to that of adult black-footed albatrosses.

The first Eastern Bering Sea sighting of a short-tailed albatross in the late 20th century of which we know was of an immature

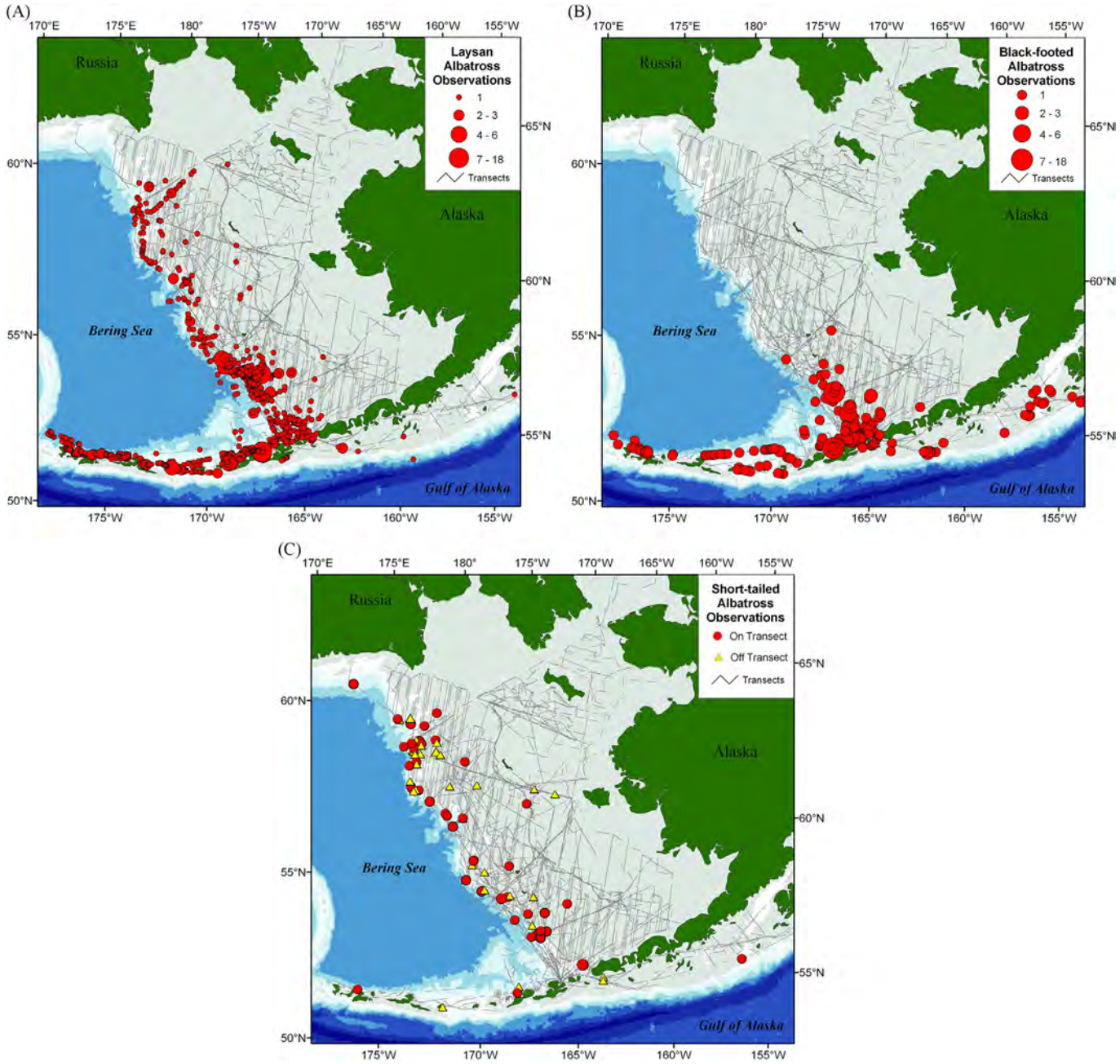

Fig. 5. Distribution of sightings of Laysan (A), black-footed (B), and short-tailed (C) albatrosses in the Bering Sea and Aleutian Islands, Alaska, based on surveys during 2006–2010. Colored dots show albatross distribution and numbers per sighting, gray lines show survey effort during those years. The Laysan and black-footed albatross maps show only sightings made within the 300-m transect window. The short-tailed albatross map includes observations from outside the transect window (> 300 m from vessel; yellow triangles), as well as those within it (red circles). (For interpretation of the references to color in this figure legend, the reader is referred to the web version of this article.)

bird on August 8, 1988, at 56° 36′N and 170° 26′W (GLH, unpublished data, R/V *Alpha Helix* bridge log). This observation was near the head of Pribilof Canyon. The distribution of short-tailed albatrosses during recent surveys (Fig. 5C) closely matches the opportunistic incidental sightings from 1988 to 2005 (Piatt et al., 2006; Zador et al., 2008b) and the movement patterns of satellite-tagged short-tailed albatrosses (Suryan et al., 2006, 2007). Zador et al. (2008b) found that the incidental sightings of short-tailed albatrosses increased in spring and summer and expanded north and west as the season progressed. Thus our June to September sample period reflects this summer peak in their abundance and their seasonally progressive northwestern shift in distribution.

4.3. Influences on albatross distribution

In Alaskan waters, the Aleutian Archipelago remains the primary albatross 'hotspot'. This island chain spans > 2000 km and has a narrow shelf, which brings upwelled waters close to the archipelago along its length. Currents running through the many passes of the Aleutian Islands offer a wealth of foraging habitat at canyon heads and associated tidal fronts. Zooplankton and forage fish are concentrated in these fronts, which in turn, attract high densities of foraging seabirds (Jahncke et al., 2005; Ladd et al., 2005b).

For all three albatross species in the eastern Bering Sea, their preferred marine habitat is the outer portion of the Outer Domain

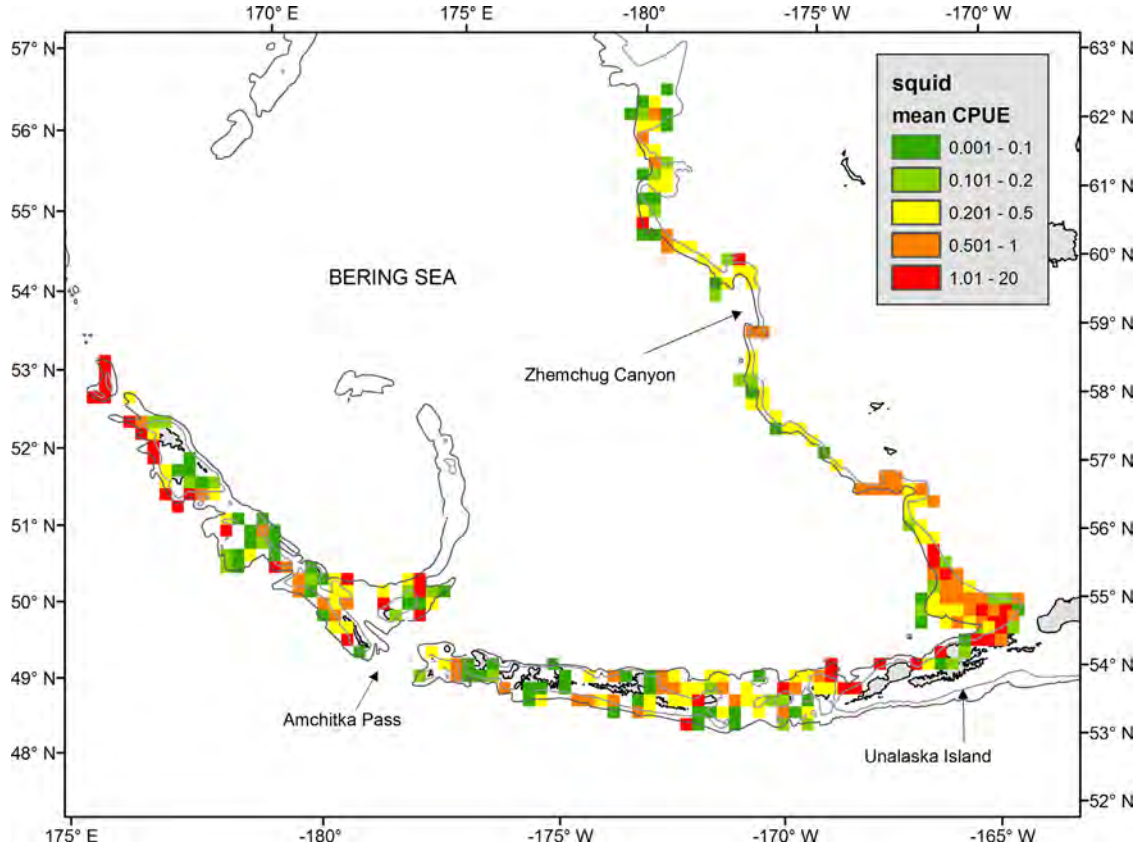

Fig. 6. Mean Catch Per Unit Effort (CPUE) of all squid species taken in NOAA trawl surveys, 2000–2012, in 20 km × 20 km cells. Reprinted with permission from Ormseth, 2012.

and shelf slope (the 'Green Belt'; Springer et al., 1996), especially the heads of major submarine canyons. This finding is consistent with other studies indicating the importance to albatrosses of shelf slope sites of upwelling and undersea canyons (Piatt et al., 2006; Suryan et al., 2006; Zador et al., 2008b). In particular, Pribilof and Bering Canyons in the southeastern Bering Sea are now regularly used by all three albatross species (Fig. 5A–C).

One of the primary prey groups for all three albatross species is squid (Awkerman et al., 2008, 2009; Croxall and Prince, 1994; Gould et al., 1997; Hunt et al., 2000; Tickell, 2000). Although squid and fish associated with fisheries are also common diet items for albatrosses (Harrison et al., 1983), juvenile squid is the most common natural diet component (Croxall and Prince, 1994; Pitman et al., 2004). The higher abundance of albatrosses in the Aleutians compared to the Bering Sea mirrors the relative density of squid in those regions (Ormseth, 2012). While there are no reliable direct biomass estimates for squid in Alaskan waters, mass balance ecosystem models (Aydin et al., 2007) suggest that approximately one million metric tons of squid are consumed by predators in the eastern Bering Sea annually, with total squid biomass density (in tons per square km) roughly seven times higher in the Aleutian Islands (Ormseth, 2012).

At least 15 species of squid occur in the Bering Sea, although more is known about adults of benthic species associated with the seafloor than is known about juveniles or the more pelagic species (Ormseth, 2012) on which albatrosses likely feed. There is presently no directed fishery for squid in Alaska, although squid are taken as bycatch in Alaska's commercial groundfish fisheries. Squid are also captured during NOAA stock assessment trawl surveys. NOAA trawl surveys find squid throughout the narrow shelf of the Aleutian Archipelago and along the eastern Bering Sea shelf slope, particularly near Bering Canyon (Fig. 6). In addition, squid bycatch in the Bering Sea Pollock fishery shows a consistently high biomass of squid taken near Zhemchug, Pribilof, and Bering Sea canyons, regardless of shifts in fishery locations (Ormseth, 2012). When large foreign fishing fleets were active in Alaska, squid harvests reached nearly 9000 t annually. After these foreign fisheries were stopped in 1986, squid bycatch in the groundfish fisheries increased, suggesting an increase in squid biomass between 1987 and 2008; these bycatch estimates were highly variable and an overall increase in squid biomass in the eastern Bering cannot be confirmed (Ormseth, 2012). Nonetheless, the spatial distribution of squid caught during NOAA trawl surveys (Fig. 6) and of bycaught squid, closely matches that of the albatrosses (Fig. 3A–C) throughout the Bering Sea Outer Domain and associated canyons. Although we cannot test for a link between albatross and squid distribution in the eastern Bering Sea given the lack of biomass data for squid, we propose that albatrosses have been and continue to be influenced by the distribution of this important prey group.

The presence of albatrosses in more northerly areas could also be, in part, a response to temporary increases in fishing activity there. Albatrosses are known to approach fishing vessels in search of food in the form of discharges of offal and discards, and they attempt to steal bait from longline fisheries as the lines are being set (Gonzalez-Zevallos and Yorio, 2006; Hyrenbach and Dotson, 2003; Weimerskirch et al., 2000). Suryan et al. (2007) concluded that the short-tailed albatross had the greatest potential overlap with fisheries in Alaska, and incidental observations of short-tailed albatrosses suggest that this species aggregates in the vicinity of fishing vessels (Piatt et al., 2006). Zador et al. (2008b) found that the distribution of short-tailed albatrosses overlapped most with Alaska trawl fisheries during summer and fall. Likewise, the increased sightings of Laysan and black-footed albatrosses in the

southeastern Bering Sea could increase their interactions with fisheries there.

Due in part to recent shifts in the distribution of fish stocks (Hollowed et al., 2012; Mueter and Litzow, 2008), and regulations that shifted fisheries operations to the northwest for brief periods (particularly in 2008–2010; Ianelli et al., 2012), since the early 2000s there has been more fishing activity along the northern Outer Domain of the eastern Bering Sea than was the case earlier. Although the albatross sightings made during surveys in the 2000s were not associated with fishing activity nor with the presence of fishing vessels, it is possible that the albatrosses were in the vicinity of our survey vessels because of fishing activity in the general area over the course of the summer. Nonetheless, commercial fishing activity also occurred in earlier decades, and during the 1970s and early 1980s it was much more intense due to huge foreign fisheries operating in U.S. waters (Ormseth, 2012). Despite this high level of fishing activity, there were few albatross sightings then.

4.4. Future considerations

Climate warming is expected to continue and to result in a reduced maximum extent of sea ice over the southeastern Bering Sea shelf (Overland et al., 2008; Serreze and Francis, 2006). Less extensive ice cover and longer ice-free summers are predicted to affect the southeastern Bering Sea shelf more dramatically than the northern shelf, with a hydrographic transition zone at about 60°N (Stabeno et al., 2012). While the differences in biophysical patterns between the northern and southern shelf may result in different trajectories for prey species, these impacts mainly apply to the Middle Domain (Stabeno et al., 2012). Since albatrosses primarily forage in the Green belt of the Outer Domain and shelf slope (Fig. 5A–C), the potential changes in the Middle Domain are less likely to impact albatrosses directly.

In the future, more open water along the Bering Sea shelf, particularly in the southern region, may be available to seabirds in spring (March–April). However, most albatrosses are still at their southern breeding grounds and raising young in the spring (Awkerman et al., 2008, 2009). Thus the earlier availability of open water along the Bering Sea shelf (Stabeno et al., 2012) is not likely to be a primary influence on the distribution of albatrosses. However, the ice-free season has also lasted longer into late summer and fall, and is predicted to continue to do so (Grebmeier et al., 2010; Wang and Overland, 2009), which could increase foraging opportunities in the northern Bering Sea Green Belt during a time when albatrosses are most likely to be present.

Delayed ice formation in the fall (Comiso, 2012), if accompanied with high prey abundance, could benefit immature albatrosses which do not need to return early to southern colonies. Indeed, an immature short-tailed albatross was recorded in the Chukchi Sea in August 2012 – a first record for any albatross species north of the Bering Strait (Day et al., 2013). Alternatively, if prey becomes less available in the southern Bering Sea or the Aleutian Islands, birds will have to travel farther north, potentially facing a net loss of energy in their search for prey while they prepare for migration back to their breeding grounds. In recent years, gray whales and humpback whales have been observed foraging later in fall, and farther north and east into the Beaufort Sea, perhaps due to the longer ice-free season (Moore, 2008; Stabeno et al., 2012).

The increase in albatross densities along the Aleutian Islands may partly reflect larger breeding populations of albatrosses taking advantage of rich summer foraging grounds. However, for these albatross species, the Bering Sea shelf has been the northern fringe of their ranges, and their increased use of this region in the last decade is likely another early indicator of changes among upper trophic levels in response to ecosystem changes.

Acknowledgments

We thank the crews of research vessels: *Healy, Tiglax, Miller Freeman, Oscar Dyson, Sea Storm, Sir Wilfrid Laurier* and the Principal Investigators who facilitated our surveys from 2006 to 2010: J. Duffy-Anderson, L. Eisner, M. Guttormsen, T. Honkalehto, J. Napp, P. Stabeno, N. Williamson, and T. Yasenak, C. Ashjian, L. Cooper, E. Farley, J. Grebmeier, R. Hopcroft, J. Lovvorn, R. Sambrotto. We also thank the many observers who collected the data. O. Ormseth generously provided information on Bering Sea squid and use of his figure of squid bycatch. J. Piatt contributed to the evolution of this manuscript, and we thank him and G. Drew for their work on the North Pacific Pelagic Seabird Database, which formed the basis of this study. This project was made possible by the support of U.S. Fish and Wildlife Service (Division of Migratory Bird Management) and Alaska Maritime National Wildlife Refuge (especially V. Byrd and J. Williams), USA; NOAA – Alaska Fisheries Science Center, USA; North Pacific Research Board (Project nos. 637 and BSIERP/B64 to KJK), USA; and National Science Foundation, USA; grants ARC – 0908262 and ARC – 1107250 to GLH. This is BEST-BSIERP Bering Sea Project publication number 134 and NPRB publication number 477.

References

Ainley, D.G., Hyrenbach, K.D., 2010. Top-down and bottom-up factors affecting seabird population trends in the California current system (1985–2006). Prog. Oceanogr. 84, 242–254.

Awkerman, J.A., Anderson, D.J., Causey Whittow, G., 2008. Black-footed Albatross (*Phoebastria nigripes*). In: Poole, A. (Ed.), The Birds of North America Online. Cornell Lab of Ornithology, Ithaca ⟨http://bna.birds.cornell.edu/bna/species/065⟩ (Retrieved from the Birds of North America Online).

Awkerman, J.A., Anderson, D.J., Causey Whittow, G., 2009. Laysan Albatross (*Phoebastria immutabilis*). In: Poole, A. (Ed.), The Birds of North America Online. Cornell Lab of Ornithology, Ithaca ⟨http://bna.birds.cornell.edu/bna/species/066⟩ (Retrieved from the Birds of North America Online).

Aydin, K., Gaichas, S., Ortiz, I., Kinzey, D., Friday, N., 2007. A comparison of the Bering Sea, Gulf of Alaska, and Aleutian Islands large marine ecosystems through food web modeling. NOAA Tech. Memo. (NMFS-AFSC-178).

Causey, D., Loring, S., 2010. Short-tailed Albatross (*Diomedea* [*Phoebastria*] *albatrus*). In: Corbett, D.G., West, D., Lefevre, C. (Eds.), The People at the End of the World: The Western Aleutians Project and the Archeology of Shemya Island, vol. 8. Alaska Anthropological Association Monograph Series, Aurora, Anchorage, pp. 99–105.

Coachman, L.K., 1986. Circulation, water masses, and fluxes on the southeastern Bering Sea shelf. Cont. Shelf Res. 5, 23–108.

Comiso, J.C., 2012. Large decadal decline of the Arctic multiyear ice cover. J. Clim. 25, 1176–1193.

Coulson, J.C., 2002. Colonial breeding in seabirds. In: Schreiber, Burger (Eds.), Biology of Marine Birds. CRC Press, New York, pp. 87–113.

Croxall, J.P., Prince, P.A., 1994. Dead or alive, night or day: how do albatrosses catch squid? Antarct. Sci. 6, 155–162.

Day, R.H., Gall, A.E., Morgan, T.C., Rose, J.R., Plissner, J.H., Sanzenbacher, P.M., Fenneman, J.D., Kuletz, K.J., Watts, B.H., 2013. Seabirds new to the Chukchi and Beaufort seas, Alaska: response to a changing climate? West. Birds 44, 174–182.

Frederiksen, M., Mavor, R.A., Wanless, S., 2007. Seabirds as environmental indicators: the advantages of combining data sets. Mar. Ecol. Prog. Ser. 352, 205–211.

Gaston, A.J., Woo, K., Hipfner, J.M., 2003. Trends in forage fish populations in northern Hudson Bay since 1981, as determined from the diet of nestling thick-billed murres *Uria lomvia*. Arctic 56, 227–233.

Gibson, G.A., Coyle, K.O., Hedstrom, K., Curchitser, E.N., 2013. A modeling study to explore on-shelf transport of oceanic zooplankton in the eastern Bering Sea. J. Mar. Syst. 121, 47–64.

Gonzalez-Zevallos, D., Yorio, P., 2006. Seabird use of discards and incidental captures at the Argentine hake trawl fishery in the Golfo San Jorge, Argentina. Mar. Ecol. Prog. Ser. 316, 175–183.

Gould, P., Forsell, D.J., 1989. Techniques for Shipboard Surveys of Marine Birds. U.S. Department of the Interior, Fish and Wildlife Service, Washington, DC. Fish and Wildlife Technical Report 25, 22pp.

Gould, P., Ostrom, P., Walker, W., 1997. Trophic relationships of albatrosses associated with squid and large-mesh drift-net fisheries in the North Pacific Ocean. Can. J. Zool. – Rev. Can. Zool. 75, 549–562.

Grebmeier, J.M., Moore, S.E., Overland, J.E., Frey, K.E., Gradinger, R., 2010. Biological response to recent Pacific Arctic sea ice retreats. EOS Trans. Am. Geophys. Union 91, 161–162.
Harrison, C.S., Hida, T.S., Seki, M.P., 1983. Hawaiian seabird feeding ecology. Wildl. Monogr. 85, 1–71.
Hollowed, A.B., Barbeaux, S.J., Cokelet, E.D., Farley, E., Kotwicki, S., Ressler, P.H., Spital, C., Wilson, C.D., 2012. Effects of climate variations on pelagic ocean habitats and their role in structuring forage fish distributions in the Bering Sea. Deep-Sea Res. II 65–70, 230–250.
Hunt Jr., G.L., Coyle, K.O., Eisner, L., Farley, E.V., Heintz, R., Mueter, F., Napp, J.M., Overland, J.E., Ressler, P.H., Salo, S., Stabeno, P.J., 2011. Climate impacts on Eastern Bering Sea food webs: a synthesis of new data and an assessment of the Oscillating Control Hypothesis. ICES J. Mar. Sci. 68, 1230–1243.
Hunt Jr., G.L., Gould, P.J., Forsell, D.J., Peterson, H., 1981. Pelagic distribution of marine birds in the Eastern Bering Sea. In: Hood, D.W., Calder, J.A. (Eds.), The Eastern Bering Sea Shelf: Oceanography and Resources, vol. 2. Distributed by Univ. Washington Press, Seattle, WA, pp. 698–718.
Hunt, G.L. Jr., Kato, H., McKinnell, S.M., (Eds.), 2000. Predation by Marine Birds and Mammals in the Subarctic North Pacific Ocean. PICES Scientific Report no. 14, 165p.
Hunt Jr., G.L., Stabeno, P.J., 2005. Oceanography and ecology of the Aleutian Archipelago: spatial and temporal variation. Fish. Oceanogr. 14 (s1), 292–306.
Hyrenbach, K.D., 2001. Albatross response to survey vessels: implications for studies of the distribution, abundance, and prey consumption of seabird populations. Mar. Ecol. Prog. Ser. 212, 283–295.
Hyrenbach, K.D., Dotson, R.C., 2003. Assessing the susceptibility of female black-footed albatross (*Phoebastria nigripes*) to longline fisheries during their post-breeding dispersal: an integrated approach. Biol. Conserv. 112, 391–404.
Hyrenbach, K.D., Fernandez, P., Anderson, D.J., 2002. Oceanographic habitats of two sympatric North Pacific albatrosses during the breeding season. Mar. Ecol. Prog. Ser. 233, 283–301.
Ianelli, J.N., Honkalehto, T., Barbeaux, S., Kotwicki, S., Aydin, K., Williamson, N., 2012. Assessment of the walleye pollock stock in the Eastern Bering Sea, Stock Assessment and Fishery Evaluation Report for the Groundfish Resources of the Bering Sea/Aleutian Islands Regions. North Pacific Fisheries Management Council, Anchorage, AK.
Jahncke, J., Coyle, K.O., Hunt Jr., G.L., 2005. Seabird distribution, abundance and diets in the eastern and central Aleutian Islands. Fish. Oceanogr. 14, 160–177.
Johnson, G.C., Stabeno, P.J., Riser, S.C., 2004. The Bering Slope Current system revisited. J. Phys. Oceanogr. 34 (2), 384–398.
Kachel, N.B., Hunt Jr., G.L., Salo, S.A., Schumacher, J.D., Stabeno, P.J., Whitledge, T.E., 2002. Characteristics and variability of the inner front of the Southeastern Bering Sea. Deep-Sea Res. II 49 (q26), 5889–5909.
Ladd, C., Hunt Jr., G.L., Mordy, C.W., Salo, S.A., Stabeno, P.J., 2005a. Marine environment of the Eastern and Central Aleutian Islands. Fish. Oceanogr. 14, 22–38.
Ladd, C., Jahncke, J., Hunt Jr., G.L., Coyle, K.O., Stabeno, P.J., 2005b. Hydrographic features and seabird foraging in the Aleutian Passes. Fish. Oceanogr. 14 (S1), S178–S195.
Loeng, H., Drinkwater, K., 2007. Climate variability and the ecosystems of the Barents and Norwegian Seas. Deep-Sea Res. II 54, 2478–2500.
Maggini, R., Lehmann, A., Kéry, M., Schmid, H., Beniston, M., Jenni, L., Zbinden, N., 2011. Are Swiss birds tracking climate change? Detecting elevational shifts using response curve shapes. Ecol. Modell. 222, 21–32.
Montevecchi, W.A., Myers, R.A., 1992. Monitoring Fluctuations in Pelagic Fish Availability with Seabirds. Canadian Atlantic Fisheries Scientific Advisory Committee (CAFSAC) Research Document, 92/94, 20.
Montevecchi, W.A., Myers, R.A., 1997. Centurial and decadal oceanographic influences on changes in northern gannet populations and diets in the north-west Atlantic: implications for climate change. ICES J. Mar. Sci. 54, 608–614.
Moore, S.E., 2008. Marine mammals as ecosystem sentinels. J. Mammol. 89, 534–540.
Mordy, C.A., Stabeno, P.J., Ladd, C., Zeeman, S., Wisegarver, D.P., Hunt Jr., G.L., 2005. Nutrients and primary production along the eastern Aleutian Island Archipelago. Fish. Oceanogr. 14 (S1), 55–76.
Mueter, F.J., Litzow, M.A., 2008. Sea ice retreat alters the biogeography of the Bering Sea continental shelf. Ecol. Appl. 18, 309–320.
Naughton, M.B., Romano, M.D., Zimmerman, T.S., 2007. A conservation Action Plan for Black-footed Albatross (*Phoebastria nigripes*) and Laysan Albatross (*P. immutabilis*). U.S. Fish and Wildlife Service, Washington, D.C..
Neteler, M., Mitasova, H., 2008. Open Source GIS: A GRASS GIS Approach, 3rd ed. Springer, New York, NY.
Ormseth, O.A., 2012. Assessment of the squid stock complex in the Bering Sea and Aleutian Islands, Stock Assessment and Fisheries Evaluation Report. North Pacific Fisheries Management Council, Anchorage, Alaska, pp. 1850–1886 ⟨http://www.afsc.noaa.gov/REFM/stocks/plan_team/BSAIsquid.pdf⟩.
Overland, J.E., Wang, M., Salo, S., 2008. The recent Arctic warm period. Tellus 60a, 589–597.
Piatt, J.F., Sydeman, W.J., Wiese, F., 2007. Introduction: a modern role for seabirds as indicators. Mar. Ecol. Prog. Ser. 352, 199–204.
Piatt, J.F., Wetzel, J., Bell, K., DeGange, A.R., Balogh, G.R., Drew, G.S., Geernaert, T., Ladd, C., Byrd, G.V., 2006. Predictable hotspots and foraging habitat of the endangered short-tailed albatross (*Phoebastria albatrus*) in the North Pacific: implications for conservation. Deep-Sea Res. II 53, 387–398.
Pitman, R.L., Walker, W.A., Everett, W.T., Gallo-Reynoso, J.P., 2004. Population status, foods and foraging of Laysan Albatrosses *Phoebastria immutabilis* nesting on Guadalupe Island, Mexico. Mar. Ornithol. 32, 159–165.
Portner, H.O., Peck, M.A., 2010. Climate change effects on fishes and fisheries: towards a cause-and-effect understanding. J. Fish Biol. 77, 1745–1779.
R Development Core Team, 2011. R: A Language and Environment for Statistical Computing. R Foundation for Statistical Computing, Vienna, Austria.
Renner, M., Hunt Jr., G.L., Piatt, J.F., Byrd, G.V., 2008. Seasonal distribution patterns of seabirds along the Aleutian Archipelago. Mar. Ecol. Prog. Ser. 357, 301–311.
Renner, M., Parrish, J.K., Piatt, J.F., Kuletz, K.J., Edwards, A.E., Hunt Jr., G.L., 2013. Modeled distribution and abundance of a pelagic seabird reveal trends in relation to fisheries. Mar. Ecol. Prog. Ser. 484, 259–277.
Serreze, M.C., Francis, J.A., 2006. The Arctic amplification debate. Clim. Change 76, 241–264.
Shuntov, V.P., 1999. Seabirds of the Western Bering Sea. In: Loughlin, T.R., Ohtani, K. (Eds.), Dynamics of the Bering Sea. University of Alaska Sea, Fairbanks, AK, pp. 651–682 (Grant, AK-SG-99-03).
Simpson, S.D., Jennings, S., Johnson, M.P., 2011. Continental shelf-wide response of a fish assemblage to rapid warming of the sea. Curr. Biol. 21, 1565–1570.
Spear, L.B., Ainley, D.G., Hardesty, B.D., Howell, S.G.N., Webb, S.W., 2004. Reducing biases affecting at-sea surveys of seabirds: use of multiple observer teams. Mar. Ornithol. 32, 147–157.
Springer, A.M., Byrd, G.V., Iverson, S.J., 2007. Hot oceanography: planktivorous seabirds reveal ecosystem responses to warming of the Bering Sea. Mar. Ecol. Prog. Ser. 352, 289–297.
Springer, A.M., McRoy, C.P., Flint, M.V., 1996. The Bering Sea Green Belt: shelf-edge processes and ecosystem production. Fish. Oceanogr. 5, 205–223.
Stabeno, P.J., Bond, N.A., Kachel, N.B., Salo, S.A., Schumacher, J.D., 2001. On the temporal variability of the physical environment over the South-Eastern Bering Sea. Fish. Oceanogr. 10, 81–98.
Stabeno, P.J., Bond, N.A., Salo, S.A., 2007. On the recent warming of the southeastern Bering Sea shelf. Deep-Sea Res. II 54, 2599–2618.
Stabeno, P.J., Farley, E., Kachel, N.B., Moore, S., Mordy, C.W., Napp, J.M., Overland, J. E., Pinchuk, A.I., Sigler, M.F., 2012. A comparison of the physics of the northern and southern shelves of the Eastern Bering Sea and some implications for the ecosystem. Deep-Sea Res. II 65–70, 14–30.
Stabeno, P.J., Kachel, D.G., Kachel, N.B., Sullivan, M.E., 2005. Observations from moorings in the Aleutian Passes. Fish. Oceanogr. 14 (S1), S39–S54.
Stabeno, P.J., Kachel, N., Mordy, C., Righi, D., Salo, S., 2008. An examination of the physical variability around the Pribilof Islands in 2004. Deep-Sea Res. II 55, 1701–1716.
Suryan, R.M., Anderson, D.J., Shaffer, S.A., Roby, D.D., Tremblay, Y., Costa, D.P., Sievert, P.R., Sato, F., Ozaki, K., Balogh, G.R., Nakamura, N., 2008. Wind, waves, and wing loading: morphological specialization may limit range expansion of endangered Albatrosses. PloS One 3 (12), e4016, http://dx.doi.org/10.1371/journal.pone.0004016.
Suryan, R.M., Dietrich, K.S., Melvin, E.F., Balogh, G.R., Sato, F., Ozaki, K., 2007. Migratory routes of short-tailed albatrosses: use of exclusive economic zone of North Pacific Rim countries and spatial overlap with commercial fisheries in Alaska. Biol. Conserv. 137, 450–460.
Suryan, R.M., Sato, F., Balogh, G.R., Hyrenbach, K.D., Sievert, P.R., Ozaki, K., 2006. Foraging destinations and marine habitat use of short-tailed albatrosses: a multi-scale approach using fist-passage time analysis. Deep-Sea Res. II 53, 370–386.
Tickell, W.L.N., 2000. Albatrosses. Yale University Press, New Haven, CT p. 448.
USFWS, 2008a. North Pacific Pelagic Seabird Observer Program Observer's Manual. U.S. Fish and Wildlife Service, Migratory Bird Management, Anchorage, AK (33pp).
USFWS, 2008b. Short-tailed Albatross Recovery Plan. U.S. Fish and Wildlife Service, Anchorage, AK (105pp).
USFWS, 2009. Alaska Seabird Conservation Plan. U.S. Fish and Wildlife Service, Migratory Bird Management, Anchorage, AK (136 pp).
van Franeker, J.A., 1994. A comparison of methods for counting seabirds at sea in the Southern Ocean. J. Field Ornithol. 65, 96–108.
Vlietstra, L.S., Coyle, K.O., Kachel, N.B., Hunt Jr., G.L., 2005. Tidal front affects the size of prey used by a top marine predator. Fish. Oceanogr. 14 (S1), S196–S211.
Wang, M., Overland, J.E., 2009. A sea ice free summer Arctic within 30 years? Geophys. Res. Lett. 36, L07502.
Weimerskirch, H., Capdeville, D., Duhamel, G., 2000. Factors affecting the number and mortality of seabirds attending trawlers and long-liners in the Kerguelen area. Polar Biol. 23, 236–249.
Wood, S.N., 2000. Modeling and smoothing parameter estimation with multiple quadratic penalties. J. R. Stat. Soc. Ser. B (Methodol.) 62, 413–428.
Worm, B., Tittensor, D.P., 2011. Range contraction in large pelagic predators. Proc. Natl. Acad. Sci. 108, 11942–11947.
Zador, S.G., Punt, A.I., Parrish, J.K., 2008a. Population impacts of endangered short-tailed albatross bycatch in the Alaskan trawl fishery. Biol. Conserv. 141, 872–882.
Zador, S.G., Parrish, J.K., Punt, A.I., Burke, J.L., Fitzgerald, S.M., 2008b. Determining spatial and temporal overlap of an endangered seabird with a large commercial trawl fishery. Endanger. Species Res., 2008, http://dx.doi.org/10.3354/esr00152 (Published online).

Deep-Sea Research II 109 (2014) 293–299

Contents lists available at ScienceDirect

Deep-Sea Research II

journal homepage: www.elsevier.com/locate/dsr2

Regular article

Connecting subsistence harvest and marine ecology: A cluster analysis of communities by fishing and hunting patterns

Martin Renner*, Henry P. Huntington

Tern Again Consulting, 388 E Bayview Ave, Homer, AK 99603, USA

ARTICLE INFO

Available online 19 March 2014

Keywords:
Alaska
Subsistence harvest
Community ecology
Fisheries
Cluster analysis

ABSTRACT

Alaska Native subsistence hunters and fishers are engaged in environmental sampling, influenced by harvest technology and cultural preferences as well as biogeographical factors. We compared subsistence harvest patterns in 35 communities along the Bering, Chukchi, and Beaufort coasts of Alaska to identify affinities and groupings, and to compare those results with previous ecological analyses done for the same region. We used hierarchical cluster analysis to reveal spatial patterns in subsistence harvest records of coastal Alaska Native villages from the southern Bering Sea to the Beaufort Sea. Three main clusters were identified, correlating strongly with geography. The main division separates coastal villages of western Alaska from arctic villages along the northern Chukchi and Beaufort Seas and on islands of the Bering Sea. K-means groupings corroborate this result, with some differences. The second node splits the arctic villages, along the Chukchi, Beaufort and northern Bering Seas, where marine mammals dominate the harvest, from those on islands of the Bering Sea, characterized by seabird and seal harvests. These patterns closely resemble eco-regions proposed on biological grounds. Biogeography thus appears to be a significant factor in groupings by harvest characteristics, suggesting that subsistence harvests are a viable form of ecosystem sampling.

1. Introduction

Subsistence hunting and fishing account for a large proportion of the food produced and consumed in rural Alaska (ADF&G, 2012). The types of fish, marine mammals, seabirds, invertebrates, and plants that are harvested reflect cultural preferences, access, harvest technology, and of course the underlying ecology of the surrounding land, freshwaters, and sea (e.g., Wolfe, 2004). In effect, we attempt to use subsistence harvests as a means of sampling the local environment, acknowledging that hunting and fishing practices depend on more than just the presence of potential prey species and that the existence of a potential prey species does not necessarily mean it will be harvested. Analyzing and comparing community-level harvests offered the prospect of insights into biogeographical patterns. By comparing our analysis to previous analyses done on the available fish and seabird fauna, we also hoped to be able to assess the degree to which cultural or other factors further influence subsistence harvest patterns, by identifying any anomalies that could not be explained by biogeographical factors.

The biogeographical contribution is implied in various regional characterizations of subsistence hunting in Alaska, for example showing that marine mammals are the largest category by weight of harvest in the region of the state designated as Arctic by the Alaska Department of Fish and Game (ADF&G), whereas fish occupy the top spot in all other regions of the state (Huntington et al., 1998). The reason for this difference is readily apparent. Bowhead whales (*Balaena mysticetus*), for example, occur and are harvested only in the Arctic, and Pacific walrus (*Odobenus rosmarus divergens*) are only taken in small numbers in southwestern Alaska in contrast to harvests of several hundred animals per year in several arctic communities (ADF&G, N.D.). A more detailed look at regional and community harvest patterns, however, has not previously been undertaken.

Although aspects of the ecology of subsistence harvests and similar local uses of plants and animals have been examined in depth in many parts of the world (e.g., Smith and Winterhalder, 1981; Hurtado and Hill, 1987; Smith, 1991; Lauer and Aswani, 2008), we are unaware of any studies that have looked at regional patterns. Here we use cluster analysis of the harvest patterns of Alaska Native communities to identify patterns across communities and regions.

We use subsistence harvest data from 35 Aleut, Yup'ik, St. Lawrence Island Yupik, and Iñupiaq communities on the coasts and islands of the Bering, Chukchi, and Beaufort Seas. First we

* Corresponding author. Tel.: +1 907 226 4672.
E-mail addresses: auklet@bigfoot.com (M. Renner), hph@alaska.net (H.P. Huntington).

http://dx.doi.org/10.1016/j.dsr2.2014.03.005
0967-0645/

analyze subsistence harvests on a community level, using all harvested species in the analysis.

We next compare regional affinities for eco-regions defined by Sigler et al. (2011) for similar analyses of data for small zooplankton, large zooplankton, bottom fish, surface fish, and seabirds in the southern Bering, central Bering, northern Bering, Chukchi, and Beaufort seas.

2. Methods

Harvest data were compiled from the ADF&G Community Subsistence Information System database (ADF&G, N.D.a), available online, which contains the results of the vast majority of the comprehensive subsistence harvest surveys conducted by the Department's Division of Subsistence since 1980. Methods for gathering these data are available from ADF&G, especially in the Division of Subsistence Technical Paper series (ADF&G, N.D.b), where most results were first reported. First, we identified the communities in the database that are located on or within a few kilometers of the coast of the Bering, Chukchi, or Beaufort Sea. Second, we examined all records for each community, identifying those that reported harvest results for all species. (Many records examined only a particular species or class, such as migratory birds, herring *Clupea pallasii*, or marine mammals.) Then, we extracted the harvest data, expressed as kg of prey species harvested per resident, for each of the communities and years for which the full records were available.

The available data (Table 1) included 35 communities with a total of 53 harvest survey years, spanning the period 1964–2007 (more recent results are not yet in the database), plus subsistence harvest surveys conducted in Akutan, Emmonak, and Togiak for the year 2008 and in Savoonga for the year 2009 (Bering Sea Project Data Archive, N.D.) as part of the Bering Sea Project (Wiese et al., 2012). For communities with more than one year reported, we took an average of the harvest for each species reported. While much of the harvest data is specific to species, most surveys also include some records only identified to higher taxonomic groups. To apply the same standards across sites, we aggregated harvest data to the smallest available common taxonomic group (see supplementary data).

We recognize that results spanning 45 years may also span considerable environmental change in the region (e.g., Mueter and Litzow, 2008; Hunt et al., 2011), along with changes in subsistence patterns due to cultural and social factors. For example, the harvest of ringed seals in Kivalina dropped by an order of magnitude from the two surveys in the 1960s to the four surveys done between 1982 and 2007. A likely factor is the replacement of dog teams by snowmachines as the primary means of winter transportation. The harvest of no other species shows such a clear pattern of directional change over time, which leads us to conclude that the basic patterns in each community appear reasonably consistent over time, even if the total harvest has changed (comparison of other data from Kivalina from 1964, 1965, 1982, 1983, 1992, and 2007; Fall et al., 2013). Unfortunately, there are too few communities in which harvest surveys have been repeated to allow a detailed analysis of changes over time; only four communities have harvest data separated by more than 10 years. Where time series data are available, the results typically indicate changes but no clear directional pattern (Fall et al., 2013) in either total harvest or the relative proportions of different species. We further note that the available data are predominantly from the 1980s, which may not reflect current ecological conditions. Our analyses and our ability to interpret our results are thus limited by the data that are available.

Table 1
Communities and years for which we used harvest data. Note that only four communities have harvest surveys separated by more than a decade and the predominance of studies are from the 1980s.

Community	Years with harvest data
Akutan	2008
Alakanuk	1980
Atka	1994
Barrow	1987, 1988, 1989
Brevig Mission	1989
Clark's Point	1989
Dillingham	1984
Egegik	1984
Emmonak	1980, 2008
False Pass	1998
Golovin	1989
Igiugig	1983, 1992
Kaktovik	1985, 1986, 1992
Kivalina	1964, 1965, 1982, 1983, 1992, 2007
Kotlik	1980
Kotzebue	1986, 1991
Manokotak	1985, 1999
Nelson Lagoon	1987
Nuiqsut	1985, 1993
Nunam Iqua	1980
Pilot Point	1987
Point Lay	1987
Port Heiden	1987
Quinhagak	1982
Savoonga	2009
Saint George	1994
Saint Paul	1994
Shishmaref	1989, 1995
Togiak	1999, 2008
Tununak	1986
Twin Hills	1999
Ugashik	1987
Unalaska	1994
Wainwright	1988, 1989
Wales	1993

To visualize harvest patterns among Alaskan coastal villages, we used non-metric multidimensional scaling (NMDS), with Manhattan distance (Minchin, 1987, Legendre and Legendre, 1998). This is an ordination technique similar to principal component analysis (PCA), reducing the high-dimensional space of distances between many villages and many prey taxa, to (in this case) two dimensions. These new axes are set up to capture a high proportion of the information within the entire dataset. In contrast to PCA, NMDS does not rely on linear relationships, and allows for an easy visual inspection of which harvested taxa were most associated with which group of villages.

To formally examine the natural groupings of subsistence harvests of Alaskan coastal villages, we applied two different algorithms (see Legendre and Legendre, 1998): hierarchical cluster analysis and k-means. For both cases we first standardized the data by expressing the harvest data as proportions of the total harvest per village, then calculated a Manhattan distance matrix based on the harvest data. For hierarchical clustering we used the Ward algorithm. Hierarchical clustering matches the closest neighbors from the leaves to the root. K-means on the other hand work without this hierarchy, looking for the k groups that minimize among group variance. To facilitate comparison with hierarchical clustering, we used the same number of groups (3) for the k-means analysis as we extracted from the hierarchical cluster analysis. To allow better comparisons of our results with those of Sigler et al. (2011), we also ran the cluster analysis after aggregating the data over six eco-regions, five as defined by Sigler et al. (2011), plus the Aleutian Islands (Fig. 1).

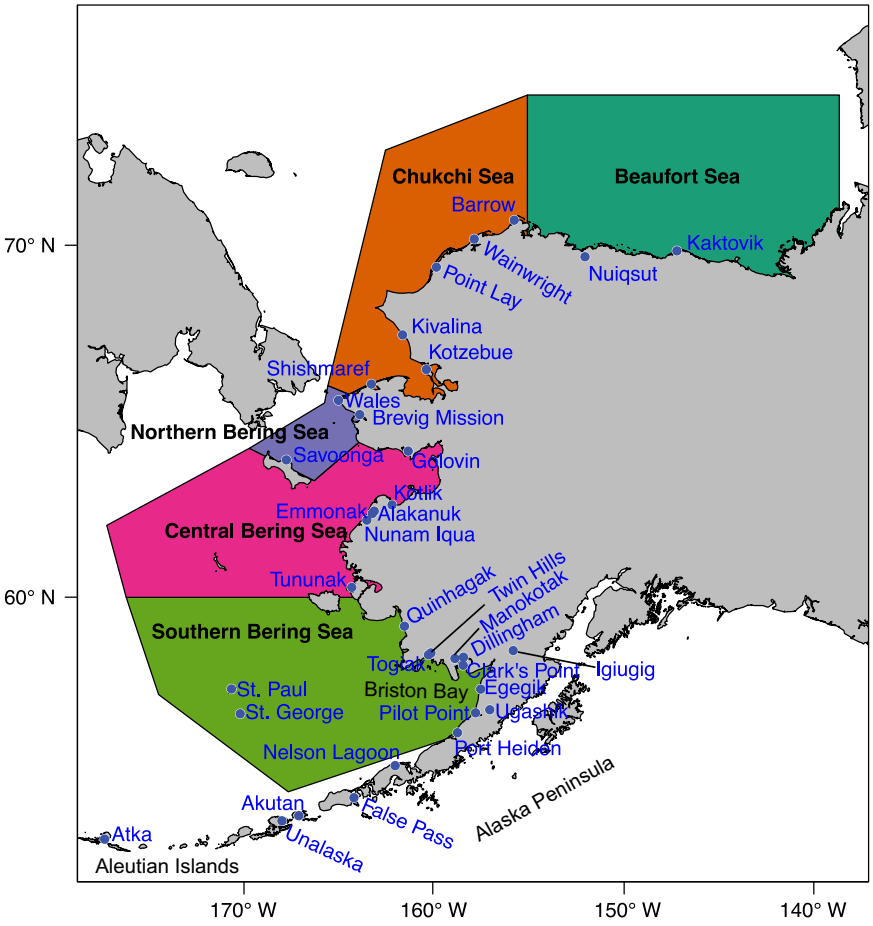

Fig. 1. Study area, location of villages and ecoregions described in Sigler et al. (2011) and also used here. We grouped the remaining villages along the Alaska Peninsula and in the Aleutian Islands as "Aleutian Archipelago".

3. Results

The first major axes of our non-metric multidimensional scaling reveal a tight cluster of villages on the low end of the NMDS1-axis (Fig. 2, left) and a loose cloud at high values (Fig. 2, right). The cluster on the left corresponds to villages in the Bristol Bay and Yukon-Kuskokwim-Delta region, which tend to harvest ducks and nearshore fish, including smelt, pike, and salmon. These villages are also in close geographic proximity (Fig. 1). On the opposite end of the primary axis (NMDS1) are villages on islands in the central and northern Bering Sea (St. George to Savoonga), which tend to harvest seabirds (like auklets, cormorants, and kittiwakes), pinnipeds and halibut. The second major axis (NMDS2) features villages in the far north on the Beaufort and Chukchi Sea coast (Point Lay to Kaktovik), associated with whale, polar bear, eider, and arctic fish (grayling, cisco, and whitefish). On the lower extreme are southern villages like Unalaska, and Tununak, associated with fish and other seafood (scallops, mussels, capelin, eel, wolfish, octopus,) and puffin.

The cluster analysis by village reveals three large groupings, separated by comparatively long branches (Fig. 3). Mapping these three clusters reveals strong geographic patterns (Fig. 4A). The first major division (Fig. 3) divides inshore coastal mainland villages from the Kotzebue Sound to Atka Island (left box). The remaining villages can be further grouped into arctic villages, from villages from Point Lay north on the Chukchi and Beaufort Seas on the one hand (middle box), and more oceanic and southern villages on islands of the Bering Sea and on the southern Chukchi Sea (right box, Figs. 3 and 4A).

Using k-means as an alternative approach, we find similar results (Fig. 4B). The northern and oceanic villages still form one group. The remaining villages were split into a group of villages on the Alaska Peninsula/southern Bristol Bay, and the remaining villages on the eastern coast of the Bering Sea. The one geographic outlier was Nuiqsut on the Beaufort Sea, oddly grouped with the villages on the Alaska Peninsula.

Aggregating the villages by the eco-regions defined by Sigler et al. (2011) prior to analyzing the harvest structure and applying a hierarchical cluster analysis to the aggregates, we find two main clusters (Fig. 5): an arctic group (northern Bering, Chukchi and Beaufort Seas) and a subarctic group (central Bering, southern Bering Seas, and Alaska Peninsula/Aleutian Islands). Within these two main groups, geographically adjacent regions were clustered together.

4. Discussion

Our analysis of village-by-village and regional patterns in the composition of subsistence harvests shows a predominantly geographical signal, likely reflecting ecological patterns. Hierarchical cluster analysis and groupings by k-means both find a major division in harvest patterns between the coastal villages of western Alaska and villages in on the Beaufort and Chukchi Seas and Bering Sea Islands. We can therefore observe a North–South division on the shore of mainland Alaska with a break point near Point Hope. By contrast, within the Bering and southern Chukchi Seas we find an East–West division. Our village-level analysis did

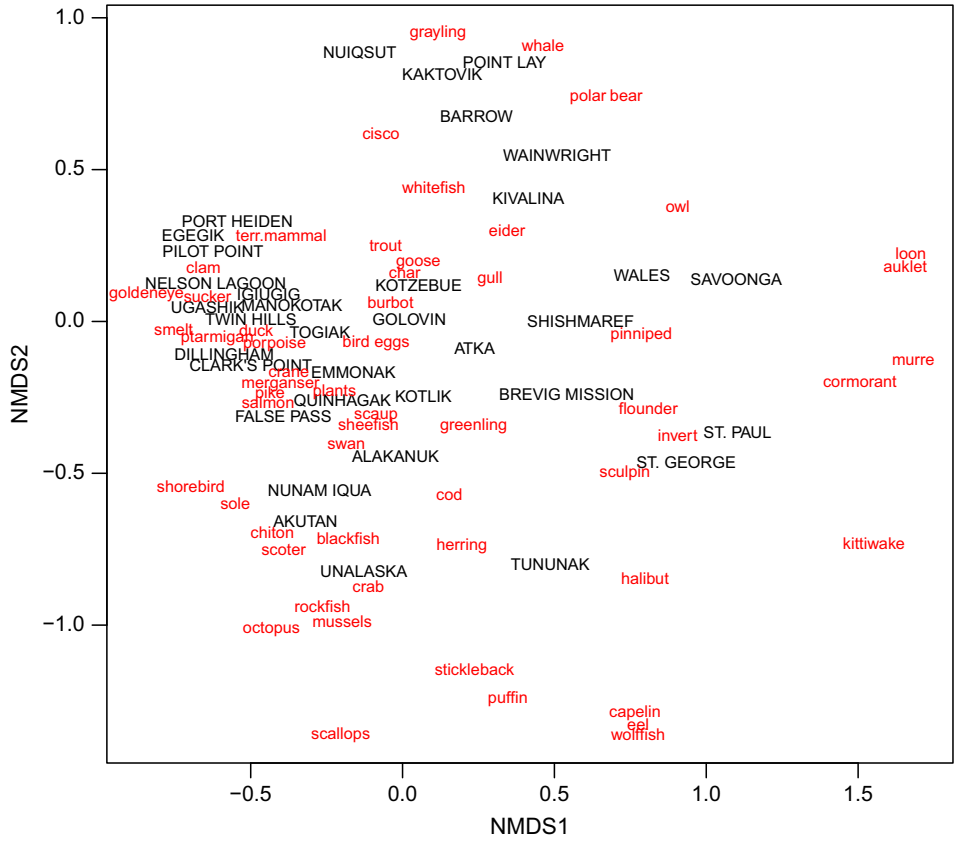

Fig. 2. The first two axes of a non-metric multidimensional scaling using Manhattan distances. Villages are shown in upper case black, harvested taxa in red. Harvested taxa close to a particular village does not indicate that those taxa are a dominant part of the harvest, but that they are relatively more commonly harvested there than elsewhere. The non-metric fit has a $R^2=0.985$, indicating that the analysis represents the multi-dimensional data well. Overlapping labels were moved slightly to make them legible. The full species names are given in the appendix. (For interpretation of the references to color in this figure caption, the reader is referred to the web version of this paper.)

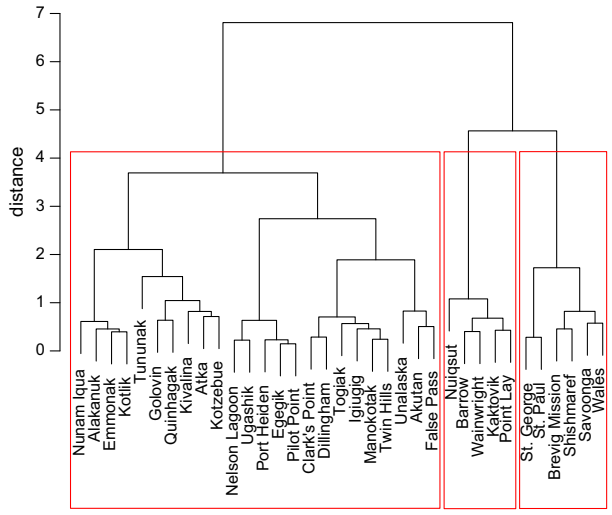

Fig. 3. Hierarchical clustering of communities by subsistence harvest characteristics. We used the Ward clustering algorithm on Manhattan distances. The boxes highlight the three most prominent, supported by long branch lengths, and also geographically coherent clusters.

not detect the North–South divisions within the Bering Sea, as proposed in Stabeno et al. (2012), although the regional analysis (Fig. 5) separates the northern Bering Sea from the central and southern Bering Sea.

The observed East–West division within the Bering Sea is a remarkably close match to ecoregions proposed by Piatt and Springer (2007). Both approaches found the major ecological division in the eastern Bering Sea to run East–West, instead of North–South. Both approaches also grouped the region around Kotzebue with inland waters farther south in the Bering Sea, rather than with those in the nearby Bering Strait, or places north along the Chukchi Sea. Our hierarchical cluster analysis detected a break point near Point Hope, also in agreement with the ecoregions proposed by Piatt and Springer (2007).

We also note that the patterns of subsistence harvests in northern Bering Sea are in general agreement with the East–West divisions one would predict based on physical and biological oceanography. Prevailing ocean currents in the Eastern Bering Sea run south to north (Coachman et al., 1975; Sigler et al., 2011). Several distinct, parallel currents flow through the area, each carrying characteristic water masses. The Alaska Coastal Current carries Alaska Coastal Water (ACW) over the shelf and through eastern Bering Strait (Coachman et al., 1975). ACW is poor in nutrients and large zooplankton (Kachel et al., 2002; Coyle et al., 2011). To the west of the ACW are the Bering Shelf Water and Anadyr Water (Sigler et al., 2011), both more saline and richer in nutrients and zooplankton than ACW. However, our data are not sufficient to resolve differences at such a fine scale.

Nuiqsut, on the Beaufort Sea coast, was the one disjunct outlier in the k-means analysis, being grouped with villages in Bristol Bay. Nuiqsut's harvest is characterized by a mix of marine mammals and fish rather than being dominated by marine mammals, as is the case for other North Slope villages. The inhabitants of Nuiqsut hunt bowhead whales, though they were not successful in every year surveyed (one out of two). Also, Nuiqsut is located in the delta of the Colville River, making it a favorable location for fishing.

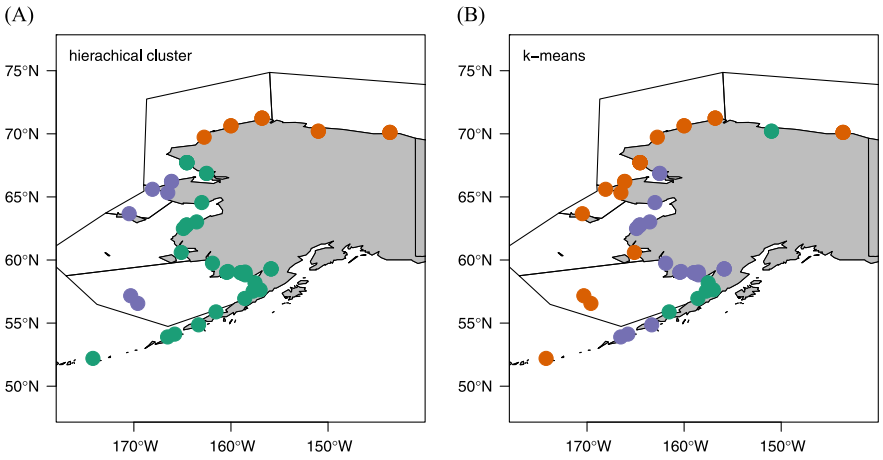

Fig. 4. Village locations indicating major cluster group by color for the two approaches used. (For interpretation of the references to color in this figure caption, the reader is referred to the web version of this paper.)

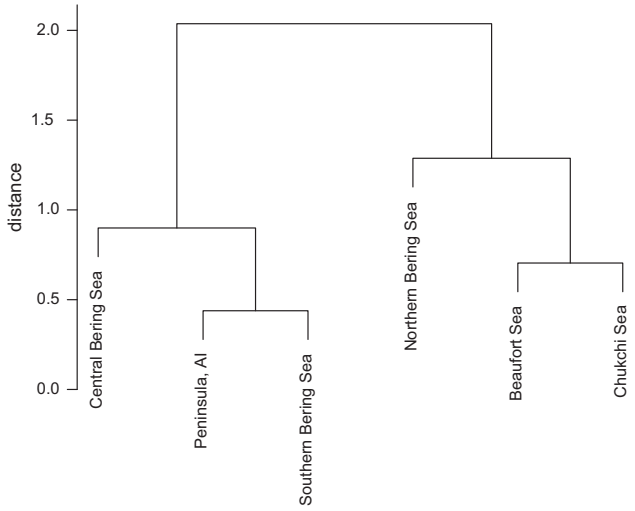

Fig. 5. Affinities of six oceanographic regions (from Sigler et al., 2011) according to subsistence harvest patterns. Details as in Fig. 3.

Thus, it may not be surprising that their harvest composition has greater balance between fish and marine mammals than do the communities in the northern cluster, which relied more exclusively on marine mammals. Within the hierarchical cluster analysis (Fig. 3), Nuiqsut is at the basal branch of the arctic cluster, indicating that it is somewhat distinct from the remaining villages, which is also supported by the NMDS analysis.

Many of the communities in the southeastern cluster, characterized by a predominance of fish, are concentrated around the greater Bristol Bay area, one of the richest salmon fishing areas in the world (Salomone et al., 2011). This group extends north to the Chukchi Sea coast and out the Aleutian Island chain, an affinity that is less obvious but likely reflects a common element of a substantial fish harvest. Communities on Bering Sea islands and the western Seward Peninsula make up the southwest cluster, characterized by a mix of fish and marine mammals. Salmon are not as abundant here as in the southeast region, but other fish such as Pacific halibut (*Hippoglossus stenolepsis*) and whitefish (*Coregonus* spp.) are caught in greater numbers. The non-metric multidimensional scaling analysis indicates that it was the harvest of seabirds, like murres and kittiwakes, as well as seals that set the harvest practices of these villages apart. The northern cluster is dominated by the production of marine mammals, including ice seals, walrus, bowhead whales, and beluga whales (*Delphinapterus leucas*).

The finer-scale clustering shown in Fig. 3 also shows a strong geographical signal. The Iñupiaq communities of Barrow and Wainwright are close in space, and close in the cluster diagram. St. Paul and St. George are the two Aleut communities on the remote Pribilof Islands, and are most closely affiliated with each other. Alakanuk, Kotlik, Emmonak, and Nunam Iqua are the four Yupik communities in the Yukon River delta, and they group tightly together. The Aleut communities of Unalaska, Akutan, and False Pass represent the Eastern Aleutian Islands and form one group in the cluster analysis. The villages of Brevig Mission, Savoonga, Shishmaref, and Wales are also tightly grouped. Brevig Mission, Shishmaref, and Wales are all Iñupiaq communities and have historical ties in addition to geographic proximity, so this grouping is not surprising. Savoonga is a St. Lawrence Island Yupik community, however, so its inclusion in this group appears to have little to do with culture or history.

By contrast, Kotzebue and Atka were paired with one another, despite great geographical separation (Arctic to Aleutian Islands, about 1750 km in a straight line) and being culturally distinct (Iñupiaq vs. Aleut). The NMDS plot (Fig. 2) shows both villages near the center of both major axes, indicating that the harvest patterns of both villages were close to the average. While this may indicate the clustering of these two villages to be spurious, both places share high harvest levels of terrestrial mammals, plants, marine mammals, and salmon.

We also examined results of the cluster analysis in terms of the cultural affiliation of the villages (Krauss, 1982). No pattern was apparent. The northern cluster (middle box in Fig. 3, orange dots in Fig. 4A) is homogenous, including only North Slope Iñupiaq communities. But not all Iñupiaq communities join this cluster. The southeast cluster (left box in Fig. 3, green dots in Fig. 4A) is largely Yup'ik (15 communities), with five Aleut communities along the Alaska Peninsula and at the base of the Aleutian Island chain, and three Iñupiaq communities, including two on the Chukchi Sea coast. The southwest cluster (right box in Fig. 3, purple dots in Fig. 4A) includes three Iñupiaq, one St. Lawrence Island Yupik, and two Aleut communities. While cultural patterns may contribute to some more subtle characteristics of the groupings (e.g., the proximity geographically and in the cluster analysis of the two Pribilof Island communities, and the similar proximity of Brevig Mission, Shishmaref, and Wales), any differences in subsistence practices and cultural food preferences appear to be modest in comparison with biogeography in determining the

groupings by subsistence harvest (e.g., the inclusion of Savoonga in the same small cluster as Brevig Mission, Shishmaref, and Wales).

The analysis of aggregated harvest data for six eco-regions (Fig. 5) allows a comparison with a similar analysis conducted by Sigler et al. (2011) on the clustering of biological communities of small zooplankton, large zooplankton, bottom fish, surface fish, and seabirds. Given that harvests include fish and seabirds but not small zooplankton and that only a few taxa that could be included in 'large zooplankton,' we may expect greater agreement between the results for harvest data and those for fish and seabird communities (Renner et al., 2012). In agreement with the cluster analyses of seabird, bottom fish, and large and small zooplankton communities, the harvest data clustered the southern and central Bering Seas together. The Chukchi and Beaufort Seas clustered together for the harvest data and also for bottom fish, but not for seabirds.

The topology of the cluster dendrogram in Fig. 5 differs from those presented in Sigler et al. (2011), where in four out of five cases, the northern Bering Sea clustered most closely with the Chukchi Sea, in contrast to the Beaufort-Chukchi cluster in the harvest data. This is not surprising in that Chukchi Sea water originates in the northern Bering Sea, passing through Bering Strait as several distinct water bodies (Hunt et al., 2013), blurring the biological distinction between the southern Chukchi and the northern Bering Sea. The greater affinity of the Chukchi Sea with the Beaufort Sea in the harvest clusters is consistent with the grouping of the northern cluster of communities in the village-level analyses. This may reflect the harvest of wide-ranging marine mammals, or be a cultural signal, or result from the fact that there are only two communities on the Beaufort Sea coast, making a limited sample for analysis. Note that Nuiqsut, one of the two Beaufort villages, joins a very different group in the k-means analysis, suggesting that its harvest pattern is not wholly consistent with that of other North Slope communities (all of which group together in both analyses).

While it may be tempting to invoke cultural factors for these differences, our analysis based on individual villages reveals more details: the main division in the southern Chukchi and northern Bering Seas does not run east–west but north–south, separating inshore waters (where fish and birds are primary targets of the harvest) and offshore waters, where marine mammal harvest is dominant. The regions used in Sigler et al. (2011) did not match the divisions that emerge from our village-based cluster analysis. This mismatch and the more pelagic sampling of the taxa used in Sigler et al. (2011) may be the primary causes of the mismatch in topologies.

In summary, our results indicate that people harvest what is available, and what is available depends on the biogeographical characteristics of their area. Thus, subsistence harvest data can broadly be regarded as ecological sampling data. The precise affinities among communities and regions are sensitive to the type of analysis being done and the characteristics in question. It is possible that greater differentiation of harvests at the species level, instead of aggregations of species groups due to lack of detailed harvest data, might reveal additional patterns that reflect the distributions of species within genera or other taxonomic classes. For example, a similar analysis could be done with more detailed data on subsistence harvests of waterfowl or salmon (much of which are available at ADF&G, N.D.a), though these datasets do not include the full range of subsistence species and thus correspond to sampling of a single taxon rather than an ecosystem. Nonetheless, the patterns are broadly consistent with other ecological analyses of the region, suggesting that subsistence harvests can serve as a useful proxy for ecological sampling. Future studies that document changing patterns in subsistence harvests, if supported by time series data for a sufficient number of villages, may also be able to shed light on ecological changes occurring in the Bering, Chukchi, and Beaufort Seas.

Acknowledgments

This paper uses data collected by scores of researchers, most notably those with the ADF&G Division of Subsistence, including many residents of the study communities. Thousands of individual hunters and fishers took part in the interviews that produced the data. We are grateful to all of them for their tireless work, persistence, and patience, without which this analysis would not have been possible. We especially note the pioneering work of Ernest S. Burch Jr. in the documentation of subsistence harvests, starting in Kivalina, Alaska, in the 1960s. For our analysis, Katie Royer compiled the subsistence harvest data on which the analyses were conducted, and we are grateful for her careful work. James Fall and Margaret Cunningham helped with the Latin names. Heather Renner's comments on an earlier version helped to improve manuscript. We thank the North Pacific Research Board for funding our work, and the leaders and researchers of Bering Sea Project for their encouragement and support. Finally, we thank James Magdanz and two anonymous reviewers for their constructive comments, and Tom Van Pelt for his fine editing. This is NPRB Publication no. 470. This project was part of the Bering Ecosystem Study – Bering Sea Integrated Ecosystem Research Program (the Bering Sea Project), and this paper is BEST-BSIERP Publication no. 128.

Appendix A. Supporting information

Supplementary data associated with this article can be found in the online version at http://dx.doi.org/10.1016/j.dsr2.2014.03.005.

References

ADF&G, 2012. Subsistence in Alaska: a Year 2010 update. Alaska Dept. of Fish& Game, Division of Subsistence, Anchorage, Alaska.
ADF&G, N.D.a. Community subsistence information system. ⟨http://www.adfg.alaska.gov/sb/CSIS⟩ (accessed 5 September 2012).
ADF&G, N.D.b. Technical Paper series. ⟨http://www.adfg.alaska.gov/sf/publications/⟩ (accessed 5 December 2012).
Bering Sea Project Data Archive, N.D. ⟨http://data.eol.ucar.edu/codiac/dss/id=245.B69-003⟩ (Akutan, Emmonak, and Togiak) and ⟨http://data.eol.ucar.edu/codiac/dss/id=245.B69-004⟩ (Savoonga).
Coachman, L.K., Aagaard, K., Tripp, R.B., 1975. Bering Strait: The Regional Physical Oceanography. University of Washington Press, Seattle p. 172
Coyle, K.O., Eisner, L.B., Mueter, F.J., Pinchuk, A.I., Janout, M., Cieciel, K., Farley, E., Andrews, A., 2011. Climate change in the southeastern Bering Sea: impacts on pollock stocks and implications for the oscillating control hypothesis. Fish. Oceanogr. 20, 139–156.
Fall, J.A., Braem, N.S., Brown, C.L., Hutchinson-Scarbrough, L.B., Koster, D.S., Krieg, T. M., 2013. Continuity and change in subsistence harvests in five Bering Sea communities: Akutan, Emmonak, Savoonga, St. Paul, and Togiak. Deep-Sea Res. II 94, 274–291.
Hunt Jr., G.L., Coyle, K.O., Eisner, L.B., Farley, E.V., Heintz, R.A., Mueter, F., Napp, J.M., Overland, J.E., Ressler, P.H., Salo, S., Stabeno, P.J., 2011. Climate impacts on eastern Bering Sea food webs: a synthesis of new data and an assessment of the oscillating control hypothesis. ICES J. Mar. Sci. 68, 1230–1243.
Hunt Jr., G.L., Blanchard, A.L., Boveng, P.L., Dalpadado, P., Drinkwater, K.F., Eisner, L., Hopcroft, R., Kovacs, K.M., Norcross, B.L., Renaud, P., Reigstad, M., Renner, M., Skjoldal, H.R., Whitehouse, A., Woodgate, R.A., 2013. The Barents and Chukchi Seas: comparison of two arctic shelf ecosystems. J. Mar. Syst. 109–110, 43–68.
Huntington, H.P., Mosli, J.H., Shustov, V.B., 1998. Peoples of the Arctic: characteristics of human populations relevant to pollution issues. In: AMAP. The AMAP Assessment Report: Arctic pollution issues. Arctic Monitoring and Assessment Program, Oslo. pp. 141–182.
Hurtado, A.M., Hill, K.R., 1987. Early dry season subsistence ecology of Cuiva (Hiwi) foragers of Venezuela. Hum. Ecol. 15, 163–187.
Kachel, N.B., Hunt Jr, G.L., Salo, S.A., Schumacher, J.D., Stabeno, P.J., Whitledge, T.E., 2002. Characteristics and variability of the inner front of the southeastern Bering sea. Deep Sea Res. II: Top. Stud. Oceanogr. 49, 5889–5909.
Krauss, M., 1982. Native peoples and languages of Alaska. Alaska Native Language Center, University of Alaska Fairbanks, Fairbanks.

Lauer, M., Aswani, S., 2008. Integrating indigenous ecological knowledge and multispectral image classification for marine habitat mapping in Oceania. Ocean Coast. Manag. 51, 495–504.
Legendre, P., Legendre, L., 1998. Numerical Ecology, 2nd English edition Elsevier, Amsterdam, Netherlands.
Minchin, P.R., 1987. An evaluation of relative robustness of techniques for ecological ordinations. Vegetatio 69, 89–107.
Mueter, F.J., Litzow, M.A., 2008. Sea ice retreat alters the biogeography of the Bering Sea continental shelf. Ecol. Appl. 18 (2), 309–320.
Piatt, J.F., Springer, A.M., 2007. Marine ecoregions of Alaska. In: Spies, R.B. (Ed.), Long-term Ecological Change in the Northern Gulf of Alaska. Elsevier, Amsterdam, Netherlands, pp. 522–526.
Renner, M., Arimitsu, M.L., Piatt, J.F., 2012. Structure of marine predator and prey communities along environmental gradients in a young fjord. Can. J. Fish. Aquat. Sci. 69, 2029–2045.
Salomone, P., Morstad, S., Sands, T., Jones, M., Baker, T., Buck, G., West, F., Krieg, T., 2011. 2010 Bristol Bay area annual management Report. Fishery Management Report No. 11-23. Alaska Department of Fish and Game, Anchorage. ⟨http://www.sf.adfg.state.ak.us/FedAidpdfs/FMR11-23.pdf⟩. (November 2011) (accessed 18 December 2012).
Sigler, M.F., Renner, M., Danielson, S.L., Eisner, L.B., Lauth, R.R., Kuletz, K.J., Logerwell, E.A., Hunt Jr., G.L., 2011. Fluxes, fins, and feathers: relationships among the Bering, Chukchi, and Beaufort Seas in a time of climate change. Oceanography 24 (3), 250–265 http://dx.doi.org/10.5670/oceanog.2011.77.
Smith, E.A., 1991. Inujjuamiut Foraging Strategies: Evolutionary Ecology of an Arctic Hunting Economy. Aldine De Gruyter, New York.
Smith, E.A., Winterhalder, B., 1981. New perspectives on Hunter-Gatherer socio-ecology. In: Smith, E.A., Winterhalder, B. (Eds.), Hunter-Gatherer Foraging Strategies: Ethnographic and Archeological Analyses. The University of Chicago Press, Chicago, pp. 1–12.
Stabeno, P.J., Farley, E., Kachel, N., Moore, S., Mordy, C., Napp, J.M., Overland, J.E., Pinchuk, A.I., Sigler, M.F., 2012. A comparison of the physics of the northern and southern shelves of the eastern Bering Sea and some implications to the ecosystem. Deep-Sea Res. II 65-70, 14–30.
Wiese, F.K., Wiseman, W.J., Van Pelt, T.I., 2012. Bering Sea linkages. Deep-Sea Res. II 65-70, 2–5.
Wolfe, R.J., 2004. Local traditions and subsistence: a synopsis from twenty-five years of research by the State of Alaska. Technical Paper 284. Juneau, Alaska: Alaska Dept. of Fish & Game, Division of Subsistence.